AD-A016 095

HIGH TEMPERATURE CORROSION OF AEROSPACE ALLOYS

ADVISORY GROUP FOR AEROSPACE RESEARCH
AND DEVELOPMENT

AUGUST 1975

KEEP UP TO DATE

Between the time you ordered this report—which is only one of the hundreds of thousands in the NTIS information collection available to you—and the time you are reading this message, several *new* reports relevant to your interests probably have entered the collection.

Subscribe to the **Weekly Government Abstracts** series that will bring you summaries of new reports *as soon as they are received by NTIS* from the originators of the research. The WGA's are an NTIS weekly newsletter service covering the most recent research findings in 25 areas of industrial, technological, and sociological interest—invaluable information for executives and professionals who must keep up to date.

The executive and professional information service provided by NTIS in the **Weekly Government Abstracts** newsletters will give you thorough and comprehensive coverage of government-conducted or sponsored research activities. And you'll get this important information within two weeks of the time it's released by originating agencies.

WGA newsletters are computer produced and electronically photocomposed to slash the time gap between the release of a report and its availability. You can learn about technical innovations immediately—and use them in the most meaningful and productive ways possible for your organization. Please request NTIS-PR-205/PCW for more information.

The weekly newsletter series will keep you current. But *learn what you have missed in the past* by ordering a computer **NTISearch** of all the research reports in your area of interest. dating as far back as 1964, if you wish. Please request NTIS-PR-186/PCN for more information.

WRITE: Managing Editor
5285 Port Royal Road
Springfield, VA 22161

Keep Up To Date With SRIM

SRIM (Selected Research in Microfiche) provides you with regular, automatic distribution of the complete texts of NTIS research reports *only* in the subject areas you select. SRIM covers almost all Government research reports by subject area and/or the originating Federal or local government agency. You may subscribe by any category or subcategory of our WGA **(Weekly Government Abstracts)** or **Government Reports Announcements and Index** categories, or to the reports issued by a particular agency such as the Department of Defense, Federal Energy Administration, or Environmental Protection Agency. Other options that will give you greater selectivity are available on request.

The cost of SRIM service is only 45¢ domestic (60¢ foreign) for each complete microfiched report. Your SRIM service begins as soon as your order is received and processed and you will receive biweekly shipments thereafter. If you wish, your service will be backdated to furnish you microfiche of reports issued earlier.

Because of contractual arrangements with several Special Technology Groups, not all NTIS reports are distributed in the SRIM program. You will receive a notice in your microfiche shipments identifying the exceptionally priced reports not available through SRIM.

A deposit account with NTIS is required before this service can be initiated. If you have specific questions concerning this service, please call (703) 451-1558, or write NTIS, attention SRIM Product Manager.

This information product distributed by

NTIS U.S. DEPARTMENT OF COMMERCE
National Technical Information Service
5285 Port Royal Road
Springfield, Virginia 22161

NORTH ATLANTIC TREATY ORGANIZATION

ADVISORY GROUP FOR AEROSPACE RESEARCH AND DEVELOPMENT

(ORGANISATION DU TRAITE DE L'ATLANTIQUE NORD)

AGARDograph No.200

HIGH TEMPERATURE CORROSION OF AEROSPACE ALLOYS

by

John F.Stringer

University of Liverpool
Liverpool, UK

This AGARDograph was sponsored by the Structures and Materials Panel of AGARD.

THE MISSION OF AGARD

The mission of AGARD is to bring together the leading personalities of the NATO nations in the fields of science and technology relating to aerospace for the following purposes:

- Exchanging of scientific and technical information;
- Continuously stimulating advances in the aerospace sciences relevant to strengthening the common defence posture;
- Improving the co-operation among member nations in aerospace research and development;
- Providing scientific and technical advice and assistance to the North Atlantic Military Committee in the field of aerospace research and development;
- Rendering scientific and technical assistance, as requested, to other NATO bodies and to member nations in connection with research and development problems in the aerospace field;
- Providing assistance to member nations for the purpose of increasing their scientific and technical potential;
- Recommending effective ways for the member nations to use their research and development capabilities for the common benefit of the NATO community.

The highest authority within AGARD is the National Delegates Board consisting of officially appointed senior representatives from each member nation. The mission of AGARD is carried out through the Panels which are composed of experts appointed by the National Delegates, the Consultant and Exchange Program and the Aerospace Applications Studies Program. The results of AGARD work are reported to the member nations and the NATO Authorities through the AGARD series of publications of which this is one.

Participation in AGARD activities is by invitation only and is normally limited to citizens of the NATO nations.

Published August 1975

533.65:669.018:620.193

Printed by Technical Editing and Reproduction Ltd
Harford House, 7–9 Charlotte St, London, W1P 1HD

REPORT DOCUMENTATION PAGE

1. Recipient's Reference	2. Originator's Reference	3. Further Reference	4. Security Classification of Document
	AGARD-AG-200		UNCLASSIFIED

5. Originator Advisory Group for Aerospace Research and Development
North Atlantic Treaty Organization
7 rue Ancelle, 92200 Neuilly sur Seine, France

6. Title High Temperature Corrosion of Aerospace Alloys

7. Presented at

8. Author(s) J.F.Stringer

9. Date August 1975

10. Author's Address University of Liverpool,
Liverpool, UK

11. Pages 610

12. Distribution Statement This document is distributed in accordance with AGARD policies and regulations, which are outlined on the Outside Back Covers of all AGARD publications.

13. Keywords/Descriptors

Aerospace engineering	Airframes	Reaction kinetics
Heat resistant alloys	Propulsion	Diffusion
High temperature tests	Alloys	Fade diagrams
Refractory materials	Corrosion	Thermodynamics
	Oxidation	

14. UDC 533.65:669.018:620.193

15. Abstract

As a result of increased operating temperatures being used in the design of aerospace propulsion systems and airframes, increased attention in recent years has been devoted to the subject of high temperature oxidation and corrosion of structural alloys. As a result of responses to an AGARD questionnaire, an effort was begun to collect into a single volume basic data on high temperature corrosion. Information contained in various places in the technical literature, in government and other similar reports, and information not yet published was gathered for inclusion in a comprehensive publication. This AGARDograph contains summary information on oxidation rates, diffusion, reaction kinetics, engineering information on practical alloys, and tests under simulated service conditions. The document is divided into a basic section and an applied section. The basic section contains data on phase diagrams, diffusion information and thermodynamic information. The applied section deals with data on superalloys and refractory metals. The AGARDograph is intended to provide information, save time and improve the efficiency of workers in the field of high temperature corrosion of aerospace alloys.

This AGARDograph was sponsored by the Structures and Materials Panel of AGARD.

FOREWORD

The Structures and Materials Panel of the Advisory Group for Aerospace Research and Development (AGARD) is comprised of scientists, engineers and technical administrators from industry, government and universities throughout NATO. They are concerned with advancing the status of aerospace research and development and with developing technical means and data for optimizing the vehicles and equipment of interest to NATO. The Panel, therefore, provides a discussion forum, a mechanism for exchange of information, and a means for stimulating, establishing and conducting cooperative technical efforts in selected areas.

The Panel has long recognized the advantage of increasing the allowable metal temperatures in the turbine section of aircraft gas turbines as a means of increasing turbine performance. It has recognized also the limitations of currently available alloys in resistance to hot corrosion at elevated temperatures both in gas turbines and in space vehicles and the importance of progress in these areas. The Panel formed a Working Group for detailed consideration of hot corrosion of aerospace alloys to aid in accelerating the needed progress.

The Working Group, with the assistance of Dr. R.I. Jaffee and Mr. Dana Moran of Battelle Memorial Institute, Columbus, Ohio and of Dr. A. Rahmel, Dechema Institute, Frankfurt, Germany made a survey of the NATO nations to identify the research and development work in progress in hot corrosion and the organizations and research workers concerned. The results of this survey, which included information collected by the Working Group on Corrosion by Hot Gases and Combustion Products of the European Federation of Corrosion, was published as AGARD Report 585-1. The Report lists 178 organizations and 240 names of workers in the field with a brief outline of the topics under investigation. By publication of this directory the AGARD Working Group intended to accelerate progress by improving communications among workers in the field.

It was then decided that a review of the state of knowledge in hot corrosion of aerospace alloys, an identification of gaps in knowledge and roadblocks to progress and identification of desirable goals and attractive approaches for future research work should be valuable in assisting research workers, managers and sponsoring organizations in planning future research efforts most effectively. In order to reach this objective the Working Group, with the assistance of Dr. R.I. Jaffee as Chairman of an Organizing Committee, planned and held a Specialists Meeting of experts in the field, drawn from the NATO nations, at Lyngby, Denmark, in April 1972. The results of this meeting which include the presentations and discussions at Lyngby and the resulting conclusions were published in the proceedings of the Lyngby conference, High Temperature Corrosion of Aerospace Alloys, AGARD-CP-120.

At the time the Directory of Organizations, Investigators and Programs was being prepared, a questionaire was sent to people active in hot corrosion research inviting comment on the desirability of collecting into one volume for ready availability basic data in hot corrosion that was in various places in the technical literature, in government and similar reports and information which had not been published. The response was predominantly in favor of such an effort. In view of the magnitude of the task the Working Group obtained, through AGARD channels, the assistance of Professor J. Stringer, University of Liverpool, himself an expert in hot corrosion. Professor Stringer, with his staff, assembled the volume that is presented here from the large number of sources indicated. It is hoped that this compilation will be effective in providing information, saving time, and thus improving the efficiency of research workers in the field of hot corrosion of aerospace alloys.

The Structures and Materials Panel notes with satisfaction this publication which completes the planned program of its Working Group. It is most pleased to acknowledge, with gratification, the contributions made to this, and to the preceeding publications in hot corrosion by the Chairman and Members of its Working Group, by Dr. R.I. Jaffee of the USA and Dr. A. Rahmel of Germany and by the Coordinator for this volume, Professor J. Stringer of the U.K. The Panel wishes to acknowledge also the important assistance of the members of the AGARD staff, Dipl. Ing. P.K. Bamberg, CDR E.R. Way, USN and Mlle A. Guerillot, in the program on hot corrosion and the help and advice of numerous experts in the NATO countries who contributed to this volume and to other parts of the program. We trust that the benefits derived will prove worthy of the efforts of these many individuals.

T. Gaymann
Chairman, Structures and Materials Panel

AGARD STRUCTURES AND MATERIALS PANEL

Panel Chairman	Dr-Ing Theodor Gaymann, Industrieanlagen, Betriebsgesellschaft, Munich, Germany
Panel Deputy Chairman	Mr. T.F. Kearns, Naval Air Systems Command, Washington, D.C., US
Chairman, Editorial Committee	Dr. B.P. Mullins, Royal Aircraft Establishment, Farnborough, UK
Chairman, Materials Group	Dr. rer. nat. W. Bunk, Deutsche Forschungs-und Versuchsanstalt für Luft-und Raumfahrt, Porz-Wahn, Germany
Chairman, Structures Group	Mr. G. Coupry, Office National D'Etudes et De Recherches Aerospatiales, Chatillon, France
Vice-Chairman, Materials Group	Dr. N.M. Tallan, Aerospace Research Laboratories, Wright Patterson Air Force Base, Ohio, US
Vice-Chairman, Structures Group	Mr. J.B. deJonge, National Aerospace Laboratory, NLR, Amsterdam, Netherlands

WORKING GROUP ON HIGH TEMPERATURE CORROSION OF AEROSPACE ALLOYS

Chairman	Mr. T.F. Kearns, Naval Air Systems Command, Washington, D.C., US
Members	Professor F. Bollenrath, Technische Hochschule, Aachen, Germany Professor A. Deruyttere, Instituut voor Metaalkunde Heverlee, Belgium Maj. Gen. A. Griselli, Ministero della Difesa Aeronautica, Rome, Italy Mr. H.V. Kinsey, Dept. of Energy, Mines and Resources, Ottawa, Canada Dr. P. Kofstad, Central Institute for Industrial Research, Oslo-Blindern, Norway Mr. H.P. Van Leeuwen, National Aerospace Laboratory NLR, Amsterdam Netherlands Mr. J.P. Poulignier, Office National D'Etudes et De Recherches Aerospatiales, Chatillon, France Mr. K.A. Rowland, British Aircraft Corp., Weybridge, Surrey, England Dr. N.M. Tallan, Aerospace Research Laboratories, Wright Patterson Air Force Base, Ohio, US

SPECIALISTS

Dr. R. I. Jaffee, Battelle Memorial Institute, Columbus, Ohio, US
Dr. A. Rahmel, DECHEMA, Frankfurt, Germany

CO-ORDINATOR

Prof. J. Stringer, University of Liverpool, Liverpool, England

SMP EXECUTIVE

CDR E. R. Way, USN

PANEL SECRETARY

Miss A. C. Guerillot

CONTENTS

The first page of each part lists the contents in more detail.

ACKNOWLEDGEMENTS

Thanks are due to Applied Science Publishers for permission to reproduce several illustrations from "Deposition and Corrosion in Gas Turbines", edited by A.J.B.Cutler and A.B.Hart, copyright 1973; to the American Society for Testing and Materials for permission to reproduce several illustrations from their Special Technical Publication No. 421, "Hot Corrosion Problems Associated with Gas Turbines", copyright 1967, and to the Metals and Ceramics Information Center for permission to reproduce several illustrations from their reports DMIC 123, Jan. 15, 1960, and DMIC 133, July 25, 1960. Thanks are also due to the Metallurgical Society of AIME for permission to reproduce a number of illustrations from their Conference Proceedings and Journals, and to the American Society for Metals for permission to reproduce illustrations from their journals. The publishers of Werkstoffe und Korrosion kindly gave permission for a number of illustrations to be reproduced, as did the Cobalt Information Center. Elsevier press are to be thanked for their permission to reproduce a number of figures from the Journal of Less-Common Metals. The sources of all Figures and Tables are, of course, referenced.

In the early part of the research for this Handbook I received helpful advice from a number of colleagues: these included Dr. M Brunetaud of SNECMA, France; Drs. P.Felix and E.Erdös of Sulzer Brothers, Switzerland; Dr. P.Kofstad of CIIR, Norway; Dr. C.Tedmon and a number of his colleagues at the G.E. Research and Development Laboratories; Mr. C.T.Sims and a number of his colleagues at the Gas Turbine Products Division of G.E., U.S.A.; Drs. W.Goward, F.S.Pettit, and E.J.Felten together with a number of colleagues at Pratt and Whitney Aircraft, U.S.A.; Drs. N.Bornstein and M.A.DeCrescente at United Aircraft Research Laboratories, U.S.A.; Dr. H.B.Probst and a number of his colleagues at NASA's Lewis Research Center, U.S.A.; Drs. S.A.Jansson, C.S.Spengler, W.E.Young and a number of their colleagues at the Westinghouse Research Laboratories, U.S.A.; Mr. W.L. Wheatfall of the Naval Ship Research and Development Laboratories, U.S.A.; Professor R.A.Rapp of Ohio State University, U.S.A.; Dr. I.G.Wright of Battelle's Columbus Laboratories, U.S.A.; and Mr. G.W.Meetham, Mr. G.Llewellyn and a number of their colleagues at Rolls-Royce (1971) Ltd., England. Many other people have offered advice and information, and I apologise for not naming them.

The draft manuscript was read by Dr. Pettit, Dr. Wright, Mr. Sims, and Dr. R.I. Jaffee of the Electric Power Research Institute, U.S.A., and I am grateful for their comments

I am particularly grateful to Mr. T.F.Kearns of the Naval Air Systems Command and Dr. N.M.Tallan of the Aerospace Research Laboratories for helping me to obtain copies of the relevant U.S. Government Reports, and for arranging clearance for those I wished to use.

I received invaluable assistance from the Metals and Ceramics Information Center at Battelle's Columbus Laboratories, and in particular from Mr. Stephen Rubin, who arranged for computer searches of the report literature. I am grateful to Battelle for the award of a Visiting Fellowship during the tenure of which I was able to complete the work.

The very considerable job of preparing the manuscript in its final form has been largely co-ordinated by Dr. M.E. El-Dahshan; the photography has been done by Mr. J. Gillies and the secretarial work by Miss Irene Grave, all of the Department of Metallurgy and Materials Science at the University of Liverpool. I am very grateful to them.

PART I. BASIC DATA

Basic data relevant to the high temperature oxidation and high temperature corrosion of aerospace alloys are presented in the following sections. The first section consists of tables of data, and this is followed by a section containing predominance diagrams. A section on the atmosphere in gas turbines is presented, and a summary of the vapor pressure and condensation of sodium sulphate. The final section is on diffusion data for systems of concern.

Contents

TABLE I.1 (i). HEATS OF FORMATION, STANDARD ENTROPIES, MELTING AND BOILING POINTS, AND STRUCTURES

The majority of the data in this table is from "Metallurgical Thermodynamics", 4th ed., O. Kubaschewski, E. Ll. Evans, and C. B. Alcock (Pergamon Press, Oxford, 1967). Some values have been updated from JANAF Thermochemical Tables, The Dow Chemical Company, Midland, Michigan, indicated by (J); and some additional data are included from W. J. Cooper and D. A. Scarpullo, Final Report SC-RR-66-67, Calley Chemical Co. to Sandia Corp. (January 1964), indicated by (C).

The values in parentheses are estimates.

Substance	ΔH_{298}^{o} K cal/mole	S_{298}^{o} cal/deg/mole	MP °C	BP °C	Structure
Al_2O_3	-400.0±1.5	12.2±0.1	2050	dec.	Cr_2O_3
Al_2S_3	-172.9±4.0	23(C)	1100	dec.	hexagonal
$Al_2(SO_4)_3$	-821.0±5.0	57.2±0.5	--	--	orthorhombic
CaO	-151.79±0.21(J)	9.133±0.03(J)	2927±50(J)	(3500)	NaCl
CaS	-113.5±0.5(J)	13.5±0.3	(2400)(J)	--	orthorhombic
$CaSO_4$	-342.4±3.5	25.5±0.4	(1400)	--	--
$CaCrO_4$	-329.6(C)	32(C)	2160(C)	--	
$CaMoO_4$	-369.5(C)	29.3(C)			
$CaWO_4$	-402.4(C)	30.2(C)			
$CoCl_2$	-74.7±0.3(J)	26.12±0.05(J)	740	1025	$CdCl_2$
CoO	-56.9±0.10(J)	12.67±0.08(J)	1805	dec.	NaCl
Co_3O_4	217.5±1.0(J)	27.32±1.0(J)	947dec. (J)		spinel
Co_9S_8	-197.0±12.0	(110)	(835)	--	--
$CoS_{0.89}$	-20.4±1.0	13.6±0.5	(834)	dec.	cubic
Co_3S_4	-75.0±3.0	--	(625)	--	--
CoS_2	-33.5±4.0	--	dec.	--	Pyrite
$CoSO_4$	-212.3±0.3(J)	28.05±1.00(J)	1400dec. (J)	--	--
$CoMoO_4$	(-246.6)(C)	(37.4)(C)			
$CoWO_4$	(-263)(C)	(32.70)(C)			
$CrCl_2$	-97.0±3.5	27.55±0.1	815	1300	orthorhombic
$CrCl_3$	-132.0±5.0	29.4±0.1	subl.	945	--
CrO_2Cl_2	-135.7±5.0	--	-95	117	--
Cr_2O_3	-270.0±2.5	19.4±0.2	(2400)	dec.	Cr_2O_3
CrO_2	-139.2±2.0	--	--	--	--
CrO_3	-138.5±2.5	17.5±2.5	185	dec.	--
CrS	--	--	1550(C)	--	--
FeCl	+45.0±9.0	57.5±2.5			
$FeCl_2$	-81.8±0.2	28.7±0.5	677	1012	$CdCl_2$
$FeCl_3$	-95.7±0.2	32.2±0.5	315	319	AsI_3

$FeO_{1.1}$	-63.2±0.3	14.05±0.2	1378	dec.	NaCl
Fe_3O_4	-266.9±1.0	36.2±0.6	1594	dec.	spinel
Fe_2O_3	-196.3±0.8	20.9±0.1	(1457)	--	
FeS	-22.8±0.3	16.1±0.3	1195	dec.	NiAs
FeS_2	-42.4±1.5	12.65±0.1	--	--	--
$FeSO_4$	-220.5±6.0	25.7±0.2	--	--	--
$FeAl_2O_4$	-10.0±1.0*	25.4±0.2	(1440)	--	spinel
Fe_2NiO_4	--	30.1±0.2	--	--	spinel
Fe_2CoO_4	--	32.2±0.2	--	--	spinel
$FeCo_2O_4$	--	30.0±0.2	--	--	--
$FeCr_2O_4$	-1.3±2.5*	34.9±0.5	2180	--	spinel
$FeMoO_4$	-257.5(C)		>1100(C)	--	--
$FeWO_4$	-274.1(C)	(35)(C)	--	--	--
HfO_2	-266.0±5.0	14.2±0.1	2900	--	monoclinic
MnO	-92.0±0.5	14.3±0.2	1875	dec.	NaCl
Mn_3O_4	-331.4±1.0	36.8±0.8	1565	--	tetragonal
Mn_2O_3	-228.7±1.2	26.4±0.5	dec.	--	Sc_2O_3
MnO_2	-124.3±0.5	12.7±0.1	dec.	--	orthorhombic
Mn_5O_8	-174.1±2.5	--	dec.	--	--
MnS	-49.0±0.5	18.7±0.3	1530	--	various
MnS_2	-49.5±2.5	--	--	--	pyrites
$MnMoO_4$	(-290.7)(C)	(34.7)(C)	--	--	--
$MnWO_4$	-312.5(C)				
$MnSO_4$	-254.2±1.0	26.8±0.3	700	--	--
$MoCl_5$	-90.8±2.5	65.0±5.0	194	268	$NbCl_5$
MoO_2	-140 0±0.9	13.0±2.0	dec.	--	monoclinic
Mo_4O_{11}	-680.3±2.5	--	disp.	--	orthorhombic
MoO_3	-178.2±0.5	18.6±0.3	795	1100	MoO_3 (orthorhombic)
Mo_2S_3	-92.5±4.0	28.5±2.0	--	--	hexagonal
MoS_2	-60.4±3.0	16.9±2.5	--	--	MoS_2 (hexagonal)
$NaAlO_2$	-270 84±0.17(J)	16.83(J)	>1650(J)	--	--
NaCl	-98.6±0.2	17.4±0.1	801	1456	NaCl
Na_2O	-99.9±1.0(J)	17.935(J)	1132(J)	dec.	CaF_2
Na_2O_2	-123.0±1.5	22.6±0.3	675	dec.	tetragonal
NaO_2	-62.5±1.0	27.7±0.3	dec.	--	KO_2
Na_2S	-92.4±2.0	23.5±2.5	950	--	CaF_2
Na_2S_2	-98.5±3.5	--	480	--	Na_2O_2
Na_2S_4	-101.0±3.5	--	285	--	--
Na_2SO_4	-333.5±2.0	35.73	884	--	orthorhombic

*from oxides

Na_2MoO_4	-350.4(C)	38.1(C)	686(C)	--	--
Na_2WO_4	-369.2±2(J)	38.32±0.5(J)	696(J)	--	--
NbO	-98.5±2.0	11.5±1.5	1935	--	hexagonal
NbO_2	-190.4±1.5	13.0±1.5	2080	--	c. rutile
Nb_2O_5	454.0±1.0(J)	32.82±0.3(J)	--	dec.	Ta_2O_5
NiCl	+55.0±9.0	57.5±2.5	--	--	--
$NiCl_2$	-73.0±0.5	23.35±0.2	subl.	987	$CdCl_2$
NiO	-57.5±0.5	9.1±0.1	1984	dec.	NaCl
Ni_3S_2	-47.5±2.5	32.0±0.2	(800)	--	--
NiS	-22.2±1.4	12.65±0.1	>800	dec.	NiAs
NiS_2	-34.0±4.0	--	dec.	--	--
$NiSO_4$	-212.5±5.0	(23.2)	675dec.(C)	--	--
$NiMoO_4$	(-251.5)(C)	(28.1)(C)	--		
$NiWO_4$	(-271.0)(C)	--			
Ta_2O_5	-488.5±1.0	34.2±0.4	1870	--	orthorhombic
TiO	-123.9±0.8	8.3±0.1	1760	--	NaCl
Ti_2O_3	-362.9±0.8	18.83±0.2	1820	--	Cr_2O_3
Ti_3O_5	-586.9±1.5	30.9±0.3	--	--	monoclinic
TiO_2	-225.5±1.0	12.0±0.05	1870	dec.	rutile
TiS_2	-(80.0)	18.73±0.2	--	--	CdI_2
WO_2	-140.9±1.5	16.0±2.5	disp.	--	monoclinic
W_2O_5	-543.5±4.0	--	disp.	--	monoclinic
WO_3	-201.4±0.7	19.9±0.2	1473	(1850)	monoclinic
WS_2	-48.4±4.0	20.0±3.0	dec.	--	MoS_2
ZrO_2	-259.5±1.5	12.1±0.1	2720	(4300)	monoclinic
ZrS_2	--	--	1650(C)	--	--
$Zr_2(SO_4)_3$	-597.4(C)	(24.1)(C)	--	--	--

TABLE I.1 (ii). STANDARD FREE ENERGY OF REACTION

$\Delta G_T^{\circ} = A + BT\log T + CT$

(from Kubaschewski et al., loc. cit.)

Reaction	ΔG° in cal			±	Temp. Range
	A	B	C	Kcal	°K
$Al_2O_3(s)=2Al(s)+1\frac{1}{2}O_2(g)$	400 810	3.98	-87.64	3	298-923
$Al_2O_3(s)=2Al(l)+1\frac{1}{2}O_2(g)$	405 760	3.75	-92.22	4	923-1800
$2CaO(s)=2Ca(s)+O_2(g)$	302 650	--	-47.32	3	298-1124
$2CaO(s)=2Ca(l)+O_2(g)$	307 100	--	-51.28	3	1124-1760
$2CaO(s)=2Ca(g)+O_2(g)$	380 200	--	-93.24	5	1760-2500
$2CaS(s)=2Ca(s,\alpha)+S_2(g)$	258 870	--	-45.62	2	298-673
$2CaS(s)=2Ca(s,\beta)+S_2(g)$	259 100	--	-45.92	2	673-1124
$2CaS(s)=2Ca(l)+S_2(g)$	263 560	--	-49.88	3	1124-1760
$2CaS(s)=2Ca(g)+S_2(g)$	336 710	--	-91.44	5	1760-2000
$CoCl_2(s)=Co(s)+Cl_2(g)$	78 700	6.9	-54.12	3	298-1000
$CoCl_2(l)=Co(s)+Cl_2(g)$	72 200	9.2	-54.52	4	1000-1323
$CoCl_2(g)=Co(s)+Cl_2(g)$	31 700	-13.8	+47.8	4	1323-1786
$2CoO(s)=2Co(s)+O_2(g)$	111 800	--	-33.8	2	298-1400
$Co_3O_4(s)=3CoO(s)+\frac{1}{2}O_2$	43 800	--	-35.4	3	298-1300
$\frac{1}{2}Co_2S_2(s)=\frac{2}{3}Co(s)+S_2(g)$	79 240	--	-39.81	2	298-1048
$\frac{1}{2}Co_2S_2(s)+S_2(g)=\frac{2}{3}Co_3S_4(s)$	-51 640	--	+34.03	3	600-750
$3CoS_2(s)=Co_3S_4(s)+S_2(g)$	50 160	--	-50.41	3	600-900
$CrCl_2(s)=Cr(s)+Cl_2(g)$	93 900	8.7	-55.0	3	298-1088
$CrCl_2(l)=Cr(s)+Cl_2(g)$	86 900	8.36	-47.5	3	1088-1577
$CrCl_2(g)=Cr(s)+Cl_2(g)$	27 700	-6.26	+37.0	5	1577-2100
$\frac{2}{3}CrCl_3(s)=\frac{2}{3}Cr(s)+Cl_2(g)$	87 400	7.42	-58.4	5	298-1200
$Cr_2O_3(s)=2Cr(s)+1\frac{1}{2}Cr(g)$	267 750	--	-62.1	4	298-2100
$FeCl_2(s)=Fe(s,\alpha)+Cl_2(g)$	82 770	6.98	-50.84	1	298-950
$FeCl_2(l)=Fe(s)+Cl_2(g)$	68 450	--	-15.22	1	950-1300
$FeCl_2(g)=Fe(s,\gamma)+Cl_2(g)$	25 250	-23.0	+89.65	4	1300-1812
$2FeCl_3(s)=2FeCl_2(s)+Cl_2(g)$	25 900	--	-38.7	1	400-500
$FeO(s)=Fe(s)+\frac{1}{2}O_2(g)$	62 050	--	-14.95	3	298-1642
$FeO(l)=Fe(l)+\frac{1}{2}O_2(g)$	55 620	--	-10.83	3	1808-2000
$Fe_3O_4(s)=3FeO(s)+\frac{1}{2}O_2(g)$	74 620	--	-29.9	3	298-1642
$3Fe_2O_3(s)=2Fe_3O_4(s)+\frac{1}{2}O_2(g)$	59 620	--	-33.62	8	298-1460
$2FeS(s,\alpha)=2Fe(s,\alpha)+S_2(g)$	74 320	--	-31.18	1	298-412
$2FeS(s\ \beta)=2Fe(s,\alpha)+S_2(g)$	71 820	--	-25.12	1	412-1179
$2FeS(s,\beta)=2Fe(s,\gamma)+S_2(g)$	72 140	--	-25.48	2	1179-1261
$2FeS_2(s)=2FeS(s)+S_2(g)$	86 700	--	-90.0	3	600-1100

$2Fe(s)+O_2(g)+2Cr_2O_3(s)=2FeCr_2O_4(s)$	-131 600	--	+24.2	3	1173-1700
$2Fe(s)+O_2(g)+2Al_2O_3=2FeAl_2O_4(s)$	-150 000	--	+41.8	8	1100-1400
$MnO(s)=Mn(s)+\frac{1}{2}O_2(g)$	91 950	--	-17.4	3	298-1500
$MnO(s)=Mn(l)+\frac{1}{2}O_2(g)$	95 400	--	-19.7	3	1500-2050
$MnS(s)=Mn(s,\alpha)+\frac{1}{2}S_2(g)$	64 000	--	-15.32	1.5	298-1000
$MnS(s)=Mn(s,\beta)+\frac{1}{2}S_2(g)$	64 540	--	-15.86	1.5	1000-1374
$MnS(s)=Mn(s,\delta)+\frac{1}{2}S_2(g)$	65 510	--	-16.56	1.5	1410-1517
$MnS(s)=Mn(l)+\frac{1}{2}S_2(g)$	69 010	--	-18.86	2	1517-1803
$MnS(l)=Mn(l)+\frac{1}{2}S_2(g)$	62 770	--	-15.40	2	1803-2000
$MoO_2(s)=Mo(s)+O_2(g)$	140 500	4.6	-55.8	6	298-1300
$MoO_3(s)=MoO_2(s)+\frac{1}{2}O_2(g)$	38 700	--	-19.5	3	298-1300
$\frac{2}{3}Mo_2S_3(s)=\frac{4}{3}Mo(s)+S_2(g)$	85 700	--	-36.41	2	1123-1473
$NaCl(s)=Na(l)+\frac{1}{2}Cl_2(g)$	99 000	--	-23.6	1.5	298-1073
$NaCl(l)=Na(l)+\frac{1}{2}Cl_2(g)$	114 300	--	-35.8	2	1183-1738
$Na_2S(s)=2Na(l)+\frac{1}{2}S_2(g)$	105 250	--	-31.45	5	371-1187
$2NbO(s)=2Nb(s)+O_2(g)$	198 700	11.5	-77.0	4	298-
$2NbO_2(s)=2NbO(s)+O_2(g)$	185 100	11.5	-79.5	4	298-
$2Nb_2O_5(s)=4NbO_2(s)+O_2(g)$	149 700	11.5	-68.9	5	298-
$NiCl_2(s)+H_2(g)=Ni(s)+2HCl(g)$	29 075	6.15	-58.53	0.8	298-1260
$NiO(s)=Ni(s)+\frac{1}{2}O_2(g)$	58 450	--	-23.55	2	298-1725
$NiO(s)=Ni(l)+\frac{1}{2}O_2(g)$	62 650	--	-25.98	3	1725-2200
$Ni_3S_2=3Ni(s)+S_2(g)$	69 960	--	-34.41	3	670-850
$Ta_2O_5(s)=2Ta(s)+2\frac{1}{2}O_2(g)$	491 000	20.7	-168.4	5	298-2000
$'TiO'(s)='Ti'(s)+\frac{1}{2}O_2(g)$	122 300	--	-21.3	4	600-2000
$Ti_2O_3(s)=2'TiO'(s)+\frac{1}{2}O_2(g)$	114 150	--	-19.05	4	298-2000
$2Ti_3O_5(s)=3Ti_2O_3+\frac{1}{2}O_2(g)$	88 500	--	-19.7	3	700-2000
$3TiO_2(s)=Ti_3O_5(s)+\frac{1}{2}O_2(g)$	73 000	--	-23.0	3	298-2123
$WO_2(s)=W(s)+O_2(g)$	138 500	--	-36.6	5	298-1500
$WO_3(s)=W(s)+1\frac{1}{2}O_2(g)$	201 500	10.2	-91.7	5	298-1400
$WS_2(s)=W(s)+S_2(g)$	62 360	--	-23.0	10	298-1400
$ZrO_2(s,\alpha)='Zr'(s,\alpha)+O_2(g)$	259 940	4.33	-59.12	4	298-1143
$ZrO_2(s,\beta)='Zr'(s,\beta)+O_2(g)$	260 200	6.44	-65.99	4	1478-2138

TABLE I.1 (iii). THERMODYNAMIC DATA FOR SPINELS

(from J. D. Tretjakow and H. Schmalzried, Berichte der Bunsengesellschaft, 69 (1965) 396)

$AO + B_2O_3 = AB_2O_4$

Spinel	ΔG^o, cals			
$FeCr_2O_4$	-13,750	+3.93T	(±200)	(1000-1500K)
$NiCr_2O_4$	-12,930	+5.17T	(±500)	(1000-1500K)
$CoCr_2O_4$	-19,360	+5.77T	(±200)	(1000-1500K)
Fe_3O_4	-4030	-2.76T	(±250)	(1100-1700K)
$CoFe_2O_4$	-5400	-3.20T	(±400)	(1173-1700K)
$NiFe_2O_4$	-4720	-1.00T	(±300)	(1173-1473K)

$NiAl_2O_4$

T K	1000	1100	1200	1300	1400	1500	
ΔG^o, cals	-10,200	-7000	-5200	-4000	-3250	-3000	(±400)

Thermodynamic Data for Reaction $AO+B_2O_3=AB_2O_4$
(ΔS in cal/deg, ΔH and ΔG in cal)

M		MCr_2O_4		MAl_2O_4		MFe_2O_4	
		T=298K	1273K	298K	1273K	298K	1273K
Fe	ΔS	-0.61	-3.93	-0.5	-4.0	-0.21	+2.76
	ΔH	-12,150±400	-13,750±200		-10,800±200	-6000±400	-4000±300
	ΔG	-12,000±400	- 8,750±200		- 5,700±200	-6100±400	-7500±250
Co	ΔS		-5.8		-2.7	-1.2±0.3	+3.2
	ΔH		-19,300±200		-10,700±400		-5400
	ΔG		-12,000±200		- 7,300±400		-9400
Ni	ΔS		-5.2		--	0.1±0.3	+1.0
	ΔH		-12,900±500		-10,500		-4720
	ΔG		- 6,400±500		- 4,400±400		-6000±300

TABLE I.1 (iv). PROPERTIES OF SULPHATES

(from "High Temperature Properties and Decomposition of Inorganic Salts: Part 1. Sulphates", K. H. Stern and E. L. Weise, NSRDS-NBS 7 (1966))

1. Dissociation of SO_3 · Free energy and equilibrium constants

T °K	ΔG_T^o KJ	log K	K
298.15	+70.88	-12.417	3.83×10^{-13}
400	61.26	- 7.999	1.00×10^{-8}
500	51.80	- 5.411	3.88×10^{-6}
600	42.35	- 3.687	2.06×10^{-4}
700	32.93	- 2.457	3.49×10^{-3}
800	23.56	- 1.538	2.90×10^{-2}
900	14.23	- 0.826	1.49×10^{-1}
1000	4.95	- 0.259	5.51×10^{-1}
1100	- 4.30	+ 0.204	1.60
1200	-13.50	0.587	3.87
1300	-22.67	0.911	8.15
1400	-31.82	1.187	15.4
1500	-40.92	1.425	26.6
1600	- 50.00	1.632	42.9
1700	-59.04	1.814	65.2
1800	-68.06	1.975	94.4
1900	-77.07	2.119	131.5
2000	-86.04	2.247	177

2. $Al_2(SO_4)_3(c) \rightleftarrows Al_2O_3(c) + 3SO_3(g)$ $\Delta H^o_{298.15}$ = 579.6 kJ, 138.5 kcal

$S^o_{298.15}$ = 339 J/mol/deg; 57.2 cal/mol/deg

$\Delta Hf^o_{298.15}$ = -3435 kJ/mol; -821.0 Kcal/mol

T °K	ΔG^o_T kJ	log K	K	Equilibrium pressures, atm. T	SO_2	O_2	SO_3	Total
298.15	+406.22	-71.165	6.84×10^{-72}	298.15	1.17×10^{-24}	5.83×10^{-25}	1.90×10^{-24}	3.65×10^{-24}
400	347.65	-45.394	4.04×10^{-46}	400	5.26×10^{-16}	2.63×10^{-16}	7.39×10^{-16}	1.53×10^{-15}
500	291.37	-30.437	3.66×10^{-31}	500	5.82×10^{-11}	2.91×10^{-11}	7.15×10^{-11}	1.59×10^{-10}
600	236.23	-20.564	2.73×10^{-21}	600	1.26×10^{-7}	6.29×10^{-8}	1.40×10^{-7}	3.29×10^{-7}
700	182.05	-13.583	2.61×10^{-14}	700	2.93×10^{-5}	1.46×10^{-5}	2.97×10^{-5}	7.36×10^{-5}
800	128.78	- 8.408	3.91×10^{-9}	800	1.69×10^{-3}	8.42×10^{-4}	1.58×10^{-3}	4.10×10^{-3}
900	76.32	- 4.429	3.72×10^{-5}	900	5.50×10^{-2}	2.75×10^{-2}	5.74×10^{-2}	1.40×10^{-1}
1000	+ 24.51	- 1.280	5.25×10^{-2}	1000	4.57×10^{-1}	2.29×10^{-1}	3.74×10^{-1}	1.06
1100	- 26.72	+ 1.269	18.6	1100	3.41	1.71	2.65	7.77

3. $CaSO_4(c) \rightleftharpoons CaO(c) + SO_3(g)$: $\Delta H^{\circ}_{298.15}$ = 401.9$_6$ kJ, 96.0$_7$ kcal.

$S^{\circ}_{298.15}$ = 106.$_7$ J/mol/deg; 25.5 cal/mol/deg.

$\Delta Hf^{\circ}_{298.15}$ = -1432.7 kJ/mol; -342.42 kcal/mol.

T °K	ΔG_T° kJ	log K	K	Equilibrium pressures, atm. SO_2	O_2	SO_3	Total
298.15	+345.39	-60.507	3.11×10^{-61}	3.49×10^{-49}	1.75×10^{-49}	3.11×10^{-61}	5.24×10^{-49}
400	326.18	-42.592	2.56×10^{-43}	2.59×10^{-34}	1.30×10^{-34}	2.56×10^{-43}	3.89×10^{-34}
500	307.44	-32.115	7.67×10^{-33}	1.31×10^{-25}	6.57×10^{-26}	7.67×10^{-33}	1.97×10^{-25}
600	288.74	-25.135	7.33×10^{-26}	8.19×10^{-20}	4.09×10^{-20}	7.33×10^{-26}	1.23×10^{-19}
700	270.20	-20.161	6.90×10^{-21}	1.11×10^{-15}	5.54×10^{-16}	6.90×10^{-21}	1.66×10^{-15}
800	251.96	-16.450	3.55×10^{-17}	1.34×10^{-13}	6.72×10^{-13}	3.55×10^{-17}	2.02×10^{-13}
900	234.18	-13.590	2.57×10^{-14}	3.22×10^{-10}	1.61×10^{-10}	2.57×10^{-14}	4.83×10^{-10}
1000	216.81	-11.324	4.74×10^{-12}	2.48×10^{-8}	1.24×10^{-8}	4.74×10^{-12}	3.73×10^{-8}
1100	199.91	- 9.491	3.23×10^{-10}	8.39×10^{-7}	4.19×10^{-7}	3.23×10^{-10}	1.26×10^{-6}
1200	183.43	- 7.984	1.037×10^{-8}	1.52×10^{-5}	8.64×10^{-5}	1.04×10^{-8}	2.29×10^{-5}
1300	167.36	- 6.724	1.888×10^{-7}	1.73×10^{-4}	6.73×10^{-4}	1.89×10^{-7}	2.60×10^{-4}
1400	151.75	- 5.662	2.18×10^{-6}	1.35×10^{-3}	3.89×10^{-3}	2.18×10^{-6}	2.02×10^{-3}

4. $Cr_2(SO_4)_3$ decomposes above 573°K. No thermodynamic data.

5. $CoSO_4(c) \rightleftharpoons CoO(c) + SO_3(g)$

$S^{\circ}_{298.15}$ = 113.$_4$ J/mol/deg; 27.1 cal/mol/deg

$\Delta Hf^{\circ}_{298.15}$ = -887.0 kJ/mol; -212.0 kcal/mol.

T °K	ΔG_T° kJ	log K	K	Equilibrium pressures, atm. SO_2	O_2	SO_3	Total
298.15	193.8$_9$	-33.966	1.08×10^{-34}	1.5×10^{-31}	7.5×10^{-32}	1.1×10^{-34}	2.3×10^{-31}
(900)	82.9$_3$	- 4.813	1.54×10^{-5}	2.2×10^{-4}	1.1×10^{-4}	1.5×10^{-5}	3.4×10^{-4}
1000	64.9$_4$	- 3.392	4.06×10^{-4}	4.6×10^{-3}	2.3×10^{-3}	4.1×10^{-4}	7.4×10^{-3}
1100	47.1$_1$	- 2.237	5.79×10^{-3}	5.6×10^{-2}	2.8×10^{-2}	5.1×10^{-3}	8.9×10^{-2}
(1200)	29.4$_6$	- 1.282	5.22×10^{-2}	4.3×10^{-1}	2.2×10^{-1}	5.2×10^{-2}	7.0×10^{-1}

6. $FeSO_4$ $S^{\circ}_{298.15}$ = 107.$_5$ J/mol/deg; 25.7 cal/mol/deg

$\Delta Hf^{\circ}_{298.15}$ = -922.6 kJ/mol; -220.5 kcal/mol

7. $Fe_2(SO_4)_3$ No data.

8. $MnSO_4$ $S^{\circ}_{298.15}$ = 112 J/mol/deg; 26.8 cal/mol/deg

$\Delta Hf^{\circ}_{298.15}$ = -1063.7 kJ/mol; -254.24 kcal/mol

$3MnSO_4(c) \rightleftharpoons Mn_3O_4(c) + 3O_2(g) + O_2(g)$

ΔH°_{298} = 914.1 kJ, 218.47 kcal

T °K	ΔG_T° kJ	log K	K	Equilibrium pressures, atm. SO_2	O_2	SO_3	Total
298.15	685.42	-120.076	8.40×10^{-121}	1.26×10^{-30}	4.20×10^{-31}	1.74×10^{-33}	1.68×10^{-30}
400	607.55	- 79.331	4.67×10^{-80}	1.94×10^{-20}	6.43×10^{-21}	1.35×10^{-22}	2.59×10^{-20}
500	532.00	- 55.573	2.67×10^{-56}	1.69×10^{-14}	5.57×10^{-15}	2.87×10^{-16}	2.27×10^{-14}
600	457.42	- 39.819	1.52×10^{-40}	1.47×10^{-10}	4.81×10^{-11}	4.50×10^{-12}	1.99×10^{-10}
700	384.01	- 28.653	2.22×10^{-29}	9.09×10^{-8}	2.96×10^{-8}	4.14×10^{-9}	1.25×10^{-7}
800	311.45	- 20.334	4.63×10^{-21}	1.09×10^{-5}	3.54×10^{-6}	6.63×10^{-7}	1.51×10^{-5}
900	239.90	- 13.922	1.20×10^{-14}	4.39×10^{-4}	1.41×10^{-4}	3.29×10^{-5}	6.13×10^{-4}
1000	169.28	- 8.841	1.44×10^{-9}	8.20×10^{-3}	2.61×10^{-3}	7.19×10^{-4}	1.15×10^{-2}
1100	99.46	- 4.722	1.90×10^{-5}	8.80×10^{-2}	2.79×10^{-2}	8.73×10^{-3}	1.25×10^{-1}
1200	31.72	- 1.381	4.16×10^{-2}	6.03×10^{-1}	1.90×10^{-1}	6.48×10^{-2}	8.57×10^{-1}

9. $NiSO_4$ $S^{\circ}_{298.15}$ - no data; $\Delta Hf^{\circ}_{298.15}$ = -870.7 kJ/mol; -208.1 kcal/mol

10. Na_2SO_4(V) $S^{\circ}_{298.15}$ = 149.5 J/mol/deg; 35.73 cal/mol/deg

$\Delta Hf^{\circ}_{298.15}$ = -1384.5 kJ/mol; -330.90 kcal/mol

Na_2SO_4(III) $S^{\circ}_{298.15}$ = 156.5 J/mol/deg; 37.4 cal/mol/deg

$\Delta Hf^{\circ}_{298.15}$ = -1381.4 kJ/mol; -330.16 kcal/mol

$Na_2SO_4(c) \rightleftharpoons Na_2O(c) + SO_3(g)$

from Na_2SO_4(III): $\Delta H^{\circ}_{298.15}$ = 570.3 kJ; 136.3 kcal

from Na_2SO_4(V): $\Delta H^{\circ}_{298.15}$ = 573.4 kJ; 137.0 kcal

T °K	ΔG_T° kJ	log K	K	Equilibrium pressures, atm. SO_2	O_2	SO_3	Total
298.15 (III)	518.74	-98.877	1.33×10^{-91}	1.98×10^{-69}	9.89×10^{-70}	1.33×10^{-91}	2.97×10^{-69}
400	501.27	-65.454	3.52×10^{-65}	1.49×10^{-49}	7.44×10^{-50}	3.52×10^{-66}	2.23×10^{-49}
500	484.61	-50.622	2.39×10^{-51}	6.03×10^{-38}	3.02×10^{-38}	2.39×10^{-51}	9.05×10^{-38}
514 (III-I)	482.48	-49.026	9.42×10^{-50}	1.07×10^{-36}	5.35×10^{-37}	9.42×10^{-50}	1.61×10^{-36}
600(I)	469.71	-40.889	1.29×10^{-41}	2.57×10^{-30}	1.29×10^{-30}	1.29×10^{-41}	3.86×10^{-30}
700	455.39	-33.979	1.05×10^{-34}	6.80×10^{-25}	3.40×10^{-25}	1.05×10^{-34}	1.02×10^{-24}
800	441.55	-28.828	1.49×10^{-29}	7.52×10^{-21}	3.76×10^{-21}	1.49×10^{-29}	1.13×10^{-20}
900	427.99	-24.838	1.45×10^{-25}	1.02×10^{-17}	5.11×10^{-18}	1.45×10^{-25}	1.53×10^{-17}
1000	414.83	-21.667	2.15×10^{-22}	3.16×10^{-15}	1.58×10^{-15}	2.15×10^{-22}	4.74×10^{-15}
1100	401.98	-19.085	8.22×10^{-20}	3.37×10^{-13}	1.69×10^{-13}	8.22×10^{-20}	5.06×10^{-13}

TABLE I.1 (v). MELTING AND BOILING POINTS

Some data are included in Table I.1(i). These additional values are from

"Molten Salts Handbook", G. J. Janz (Academic Press New York, 1967), whose principal sources were

"Selected Values of Chemical Thermodynamic Properties", F. D. Rossini, D. D. Wagman, W. H. Evans, S. Levine, and I. Jaffe, NBS Circ. 500 (1952),

"The Thermochemical Properties of Oxides, Fluorides, and Chlorides 1 - 2500K", A. Glassner, ANL Report 5750 (1959), and

"Compilation of the Melting Points of the Metal Oxides", S. J. Schneider, NBS Monograph 68 (1963).

Substance	Melting Point °C	Boiling Point °C	Substance	Melting Point °C	Boiling Point °C
LiCl	610	1382	$NaFeCl_4$	163	--
NaCl	808	1465	V_2O_5	670	2052
KCl	772	1407	V_2O_4	1542	3027
$MgCl_2$	714	1418	V_2O_3	1927	3027
$CaCl_2$	782	1627	VO	2077	3127
$AlCl_3$	192	180.1(s)	MoO_3	795	1155
$CrCl_2$	815	815 (s)	MoO_2	1927	d1977
$CrCl_3$	947	--	WO_3	1470	1827
$MoCl_2$	(d)	--	WO_2	1270	1852
$MoCl_3$	(d)	--	$MnCl_2$	649	
$MoCl_4$	(d 127)	--	MnO_2	(d 847)	--
WCl_2	(d)		MnO	1780	--
WCl_4	(d)		Mn_3O_4	1560	2627
WCl_5	248	276	SiO_2 quartz	1610	--
WCl_6	275	336.5	trydimite	1680	--
$MnCl_2$	650	1190	cristobalite	1728	--
$MnCl_3$	(587)	(627)	MgS	>2000	--
$CoCl_2$	724	1050	CaS	(2400)	--
CrS	1550	--			
MoS_2	1185	--			
FeS_2	1171	--			
$MgSO_4$	1127	--			
$CaSO_4$	1400	d.1149			
$Al_2(SO_4)_3$	770	d. 605			
$MnSO_4$	700	d. 755			
$CoSO_4$	--	d. 708			
$NiSO_4$	--	d. 675			
$FeSO_4$	--	d. 537			
Na_2SiO_3	1089	--			
Na_2SiO_5	874	--			
Na_2CrO_4	792	--			
$Na_2Cr_2O_7$	356.7	--			

TABLE I.1 (vi). CRYSTALLOGRAPHIC DATA FOR OXIDES

Oxide	System	Lattice Constants, nm a	b	c	c/a	
Na_2O	cubic					
Na_2O_2	hexagonal	0.622		0.447	0.718	
NaO_2	rhombic	0.426	0.554	0.344	0.819	
γAl_2O_3	hexagonal	0.4758	--	1.2991	2.72	
γAl_2O_3	cubic	0.790	--	--	--	
SiO_2 αquartz	hexagonal	0.3464	--	0.4382	1.27	
βquartz	hexagonal	0.4913	--	0.5405	1.10	
γtridymite	rhombic	0.988	1.71	1.63	1.65	
α ristobalite	tetragonal	0.4971	--	0.6918	1.39	
βcristobalite	cubic	0.718	--	--	--	
CaO	cubic (NaCl)	0.4799	--	--	--	
TiO	cubic	0.4162	--	--	--	
Ti_2O_3	hexagonal, γAl_2O_3	0.516	--	1.357	2.66	
Ti_3O_5	monoclinic	0.9757	0.3802	0.9452	--	β=93.11°
Ti_5O_9	triclinic	0.5369	0.7120	0.8865	--	α=97.55°
						β=112.34°
						γ=108.50°
TiO_2	tetragonal, rutile	0.4594	--	0.2958	0.644	
VO	cubic (NaCl)	0.4093	--	--	--	
V_2O_3	hexagonal, γAl_2O_3	0.543	--	--	--	(?)
VO_2	monoclinic	0.5743	0.4517	0.5375	--	β=122.6°
V_2O_5	hexagonal	1.151	0.3559	0.4371	--	
Cr_2O_3	hexagonal, γAl_2O_3	0.4950	--	1.3665	2.76	
CrO_3	rhombic	0.4789	0.8557	0.5743	--	
MnO	cubic (NaCl)	0.4444	--	--	--	
γMn_3O_4	tetragonal	0.576	--	0.944	1.638	
γMn_3O_4	cubic	0.87	--	--	--	
γMn_2O_3	tetragonal	0.885	--	0.995	1.12	
βMn_2O_3	cubic	0.9411	--	--	--	
βMnO_2	tetragonal, rutile	0.4398	--	0.2867	0.654	
γMnO_2	rhombic	0.4533	0.927	0.2866	--	

FeO	cubic, NaCl	0.4311	--	--	--	
Fe_3O_4	cubic	0.338	--	--	--	
γFe_2O_3	hexagonal, γAl_2O_3	0.509	--	0.441	0.866	
CoO	cubic, NaCl	0.42581	--	--	--	
Co_3O_4	cubic, $MgAl_2O_4$	0.8084	--	--	--	
Co_2O_3	hexagonal, γAl_2O_3	0.464	--	0.575	1.24	
NiO	cubic, NaCl	0.41769	--	--	--	
ZrO_2	monoclinic	0.517	0.526	0.530	--	$\beta=80^{\circ}10'$
	cubic	0.507	--	--	--	
NbO	cubic, NaCl	0.42013	--	--	--	
NbO_2	tetragonal	1.371	--	0.5985	0.43	
Nb_2O_5	monoclinic	2.134	0.3816	1.947	--	
	hexagonal	0.3607	--	0.3925	1.09	
	rhombic	0.619	0.365	0.394	--	
MoO_2	monoclinic	0.561	0.484	0.553	--	$\beta=119.6^{\circ}$
MoO_3	rhombic	0.39	1.38	0.37	--	
HFO_2	monoclinic	0.511	0.514	0.528	--	$\beta=99^{\circ}49'$
	tetragonal	0.514	--	0.525	1.02	
Ta_2O_5	rhombic	0.620	0.367	0.390	--	
WO_2	monoclinic, MoO_2	0.556	0.4884	0.5546	--	
WO_3	monoclinic	0.7285	0.7517	0.3835	--	$\gamma=90.90^{\circ}$
	tetragonal, ReO_3	0.5250	--	0.3915	0.746	

Data from "The Oxide Handbook", ed. G. V. Samsonov, translated by C. N. Turton and T. I. Turton (Plenum, New York; 1973).

TABLE 1.1 (vii). PROPERTIES OF SPINELS

Spinel	Color in Bulk	Color Under Microscope	Theoretical Density, g/cm³	Coefficient of Expansion, 25-900°C $°C^{-1} \times 10^{-6}$	Cell Size, A
$CoAl_2O_4$	ultramarine blue	bright blue	--	--	8.08
$FeAl_2O_4$	gray-green	pale green	4.392	9.0	8.12
$MnAl_2O_4$	dark cream	yellow	4.031	7.3	8.11 8.26
$NiAl_2O_4$	turquoise	pale blue	--	--	8.03 8.05
$CoCr_2O_4$	blue-green	deep blue	--	--	8.31 8.32
$FeCr_2O_4$	red-brown	deep red	5.058	8.5	8.34
$MnCr_2O_4$	pale green	none	4.900	8.9	8.41 8.49
$NiCr_2O_4$	olive green	deep green	--	--	8.30
Fe_3O_4	black	opaque	5.201	15.1	8.37 8.39
$MnFe_2O_4$	--	--	5.029	8.3	-- 8.55
$NiFe_2O_4$	purple brown	opaque	--	--	8.31 8.36
Co_2TiO_4	dark green	deep green	--	--	8.42 8.3
Fe_2TiO_4	purple brown	opaque	--	--	8.48 --
Mn_2TiO_4	red brown	orange red	--	--	8.63 --
Co_3O_4	black	--	--	--	-- 8.11
γAl_2O_3	white	none	--	--	-- 7.9
Mn_3O_4	black	deep red brown	--	--	8.14 --

From T. J. Gray, "Oxide Spinels", in "High Temperature Oxides - Part IV", ed. A. M. Alper, vol. 5 in "Refractory Materials", ed. J. L. Margrave (Academic Press, New York, 1971) 77.

J. D. Tretjakow and H. Schmalzried, Beichte der Bunsengesellschaft, 69 (1965) 396, list slightly different lattice parameters:

Spinel	a_o, A
$CoCr_2O_4$	8.332
$NiCr_2O_4$	8.248
$CoAl_2O_4$	8.105
$NiAl_2O_4$	8.046

G. C. Ulmer, "Chromite Spinels", in "High Temperature Oxides - Part I" (loc. cit) 251, also lists slightly different parameters:

Spinel	a_o, A
Fe_3O_4	8.397
$FeAl_2O_4$	8.153
$FeCr_2O_4$	8.381

TABLE I.1 (viii). VAPOR PRESSURES OF OXIDES

	T°C	P,N/m^2
Al_2O_3	1727	5.77×10^{-1}
	2050	46.263
	2351	1.013×10^{5}
SiO_2 cristobalite	1527	162.65×10^{-5}
	1627	1013.25×10^{-5}
CaO	1227	1.49×10^{-6}
	1727	7.19×10^{-2}
	2227	44.6
	2727	2.69×10^{3}
TiO_2	1576-1737	$\log p = 16.20 - 30361/T - 0.492 \times 10^{-3} T$
V_2O_5	700	4.49
	900	41.04
	1000	181.3
	1100	525.3
	1200	1195.9
FeO	750	213.582×10^{-17}
	950	198.65×10^{-11}
	2500	21.27×10^{-3}
Fe_2O_3	427	298.775×10^{-28}
Fe_3O_4	725	566.62×10^{-17}
NiO	25-1327	$\log p = 15.20 - 25500/T - 0.767 \times 10^{-3} T + 7.21 \times 10^{-9} T^2$
ZrO_2	1727	~0.1
	1800	0.015
	1927-2227	$\log p = 13.312 - 37421/T$
NbO_2	1665	0.0803
	1758	0.425
	1808	1.006
	1849	1.493
	1940-2120	$\log p = 14.54 - 30300/T$
Nb_2O_5	1380	11.47×10^{-4}
	1450	2.40×10^{-3}
MoO_3	25-793	$\log p = 32.81 - 16140/T - 5.53 \log T$
		$\log p = 14.077 - 15110/T + 1.46 \log T - 1.32 \times 10^{-3} T$ (over solid phase)
		$\log p = 35.5 - 11820/T - 7.04 \log T$ (over liquid phase)
	mp-bp	$\log p = 36.19 - 14560/T - 7.04 \log T$ (over liquid phase)
	25-mp	$\log p = 34.20 - 16150/T - 5.53 \log T$ (over solid phase)
	mp-bp	$\log p = 36.66 - 14110/T - 7.08 \log T$ (over liquid phase)

HfO_2	2667	3.039
WO_3	660	2.57
	753	27.46
	902	431
	980	1212
	1080	5480
	1187	19198
	727-mp	log p = 17.75 - 24600/T

Data from "The Oxide Handbook", ed. G. V. Samsonov, translated by C. N. Turton and T. I. Turton (Plenum, New York; 1973).

TABLE I.1 (ix). DENSITIES OF OXIDES

Oxide	Density, 10^{-3} kg/cm^3	Oxide	Density, 10^{-3} kg/cm^3
Na_2O	--	FeO	5.7
Na_2O_2	2.805	Fe_3O_4	5.0-5.4
NaO_2	--	Fe_2O_3	5.24
Al_2O_3	3.97	CoO	5.68
SiO_2 quartz	2.651	Co_3O_4	6.07
tridymite	2.26	Co_2O_3	5.18
cristobalite	2.32	NiO	7.45
CaO	3.40	ZrO_2 monoclinic	5.56
TiO	4.93-5.53	cubic	6.27
TiO_2	4.24	NbO	7.26
VO	5.2-5.758	NbO_2	5.98
V_2O_3	4.87	Nb_2O_5	4.95
VO_2	4.65	MoO_2	4.11
V_2O_5	3.32	MoO_3	4.69
Cr_2O_3	5.21	HfO_2 monoclinic	10.01
CrO_3	2.70	tetragonal	9.68
MnO	5.18	Ta_2O_5	8.73
Mn_3O_4	4.70	WO_2	11.4
Mn_2O_3	4.94	WO_3	6.47
MnO_2	5.026		

Data from "The Oxide Handbook", ed. G. V. Samsonov, translated by C. N. Turton and T. I. Turton (Plenum, New York; 1973).

TABLE 1.1 (x) LINEAR COEFFICIENT OF THERMAL EXPANSION, α, OF OXIDES

Oxide	α, $\times 10^6 deg^{-1}$	Temperature range, °K	
Al_2O_3	8.0	293-1273	
SiO_2	43	293-573	
	3.0	573-1373	crystalline
	0.5	293-1523	silica glass
CaO	13.7	293-1673	
TiO_2	8.0	293-873	
Cr_2O_3	9.6	293-1673	
MnO	11.0	above Neel point	
FeO	12.3	293-1073	
NiO	14	573-1073	
ZrO_2	8	343-1353	
HfO_2	6	523-1573	

Data from "The Oxide Handbook", ed. G. V. Samsonov, translated by C. N. Turton and T. I. Turton (Plenum, New York; 1973).

TABLE I.1 (xi). MODULUS OF NORMAL ELASTICITY OF OXIDES

Oxide	Temperature, °C	Modulus, GN/m^2
Al_2O_3	0	377
	500	358
	1000	314
	1250	265
	1500	160
SiO_2	20	66.7
TiO_2	--	88.3
FeO	800	1.079
		1.177
ZrO_2	20	168.68
	300	135.34
	465	127.49
	570	115.72
	850	113.76
	1050	113.76
	1225	104.93
	1360	94.15

Data from "The Oxide Handbook", ed. G. V. Samsonov, translated by C. N. Turton and T. I. Turton (Plenum, New York; 1973).

TABLE I.1 (xii). PHASE DIAGRAM INFORMATION FOR METAL-OXYGEN AND METAL-SULPHUR SYSTEMS

(a) Al-O: The only stable oxide appears to be Al_2O_3, and K. Torkar, H. Krischner, and H. Biegler, Monatsh. Chem. 94 (1963) 110, conclude that structures other than αAl_2O_3 (corundum) are stabilized by foreign atoms or radicals. The generally accepted melting point of Al_2O_3 is 2044 ± 4°C, but S. J. Schneider, Nat. Bur. Stand. (U.S.) Monograph 68 (1963) 31 pp, prefers the highest reported value of 2072°C. There is little information on the solubility of oxygen in Al: Hansen suggests it is probably close to 0.003 wt%.

(b) Al-S: Hansen considers that only one sulphide is stable, with a composition at room temperature of Al_2S_3. However, the homogeneity range at elevated temperatures is wide, including the composition AlS, at which there is a maximum in the melting point. Al_2S_3 melts at 1100 or 1130°C, and appears to have an allotropic transformation at about 1000°C from a low-temperature hexagonal form to a high-temperature form with a rhombohedral corundum structure.

(c) Co-O: There are three cobalt oxides, CoO, Co_3O_4, and Co_2O_3, the last of which appears to exist only as a hydrate, $Co_2O_3 . x H_2O$. At 900°C, Co_3O_4 decomposes to CoO. Both the lower oxides have a range of stability at lower temperatures: 56.7 - 58.5 at.% for Co_3O_4 and 50.0 - 51.7 at.% O for CoO; above 1000°C only stoichiometric CoO exists; it melts at 1810°C. The solubility of O in liquid Co is 0.20, 0.28, 0.38, and 0.52 wt% at 1550, 1600, 1650, and 1700°C, respectively.

(d) Co-S: There are five cobalt sulphides. Co_4S_3 is formed in a peritectic reaction at 935°C, and Co_9S_8 in a peritectoid at 830°C. A phase labelled CoS exists over a fairly wide homogeneity range, melting congruently at 1178°C. Co_3S_4 is stable up to about 670°C; lower values appear to be due to impurities. CoS_2 is formed by a peritectic reaction at approximately 950°C. There is a eutectic at 880°C between Co_4S_3 and Co. The solubility of sulphur in Co is very small.

(e) Cr-O: The only oxide in the range Cr-Cr_2O_3 is Cr_2O_3, with a melting point of 2424 ± 10°C and a rhombohedral structure. The solubility of oxygen in Cr is: 0.043 at.% O at 1500°C, 0.023 at.% O at 1400°C, 0.011 at.% O at 1300°C, 0.005 at.% O at 1200°C, and 0.0025 at.% O at 1100°C. CrO_3 decomposes at high temperatures, and a series of oxides intermediate between CrO_3 and Cr_2O_3 have been reported. Most important of these is the ferromagnetic, rutile structure, CrO_2.

(f) Cr-S: Several sulphides exist: CrS, Cr_7S_8, Cr_5S_6, Cr_3S_4, and two compositions near Cr_2S_3. There is a eutectic between CrS and Cr at 1350°C, 43.9 at.% S (32.5 wt% S). CrS melts at about 1565°C.

(g) Fe-O: Three oxides exist: FeO is formed by a peritectic reaction at 1424°C, and decomposes by a eutectoid reaction at 570°C. Fe_3O_4 melts at 1597°C, and Fe_2O_3 decomposes at 1457°C. The solubility of oxygen in Fe is very small. FeO has a relatively wide range of stability, from 51.2 to 52.9 at.% O at 1000°C.

(h) Fe-S: FeS has a fairly wide stability range and melts congruently at 1190°C. There is a eutectic between FeS and Fe at 988°C, 44 at.% S (31 wt%S). Fe S_2 exists in two modifications, marcasite at low temperatures, and pyrite at high temperatures; the transformation temperature is approximately 350°C. FeS_2 decomposes on heating, probably at about 740°C. δFe dissolves up to 0.31 at.% S at 1365°C; γFe dissolves a maximum of 0.09 at.% S at 1365°C; the maximum solubility in αFe is 0.035 at.% S at 913°C.

(j) Hf-O: Only one stable oxide is formed: HfO_2, which undergoes a transition from a low-temperature monoclinic form to a tetragonal form at 1450-1700°C (there is a wide variation in the results quoted in the literature). The oxide melts at about 2800°C. Hf dissolves a considerable amount of oxygen, which stabilizes the cph α modification; the maximum solubility in αHf is 21 at.% at 2180°C; the maximum solubility in βHf is 5 at.% at 2000°C.

(k) Hf-S: Several sulphides have been reported: HfS_3 (monoclinic), HfS_2 (hexagonal), Hf_2S_3 (hexagonal), HfS (cubic), Hf_2S (hexagonal), and $Hf_{\sim 8}S$ (not indexed).

(l) Mn-O: Several oxides have been reported: MnO, which has NaCl structure, and exists over a fairly wide homogeneity range from 50-53 at.% O; Mn_3O_4, which is face-centered tetragonal, related to the spinel structure at temperatures below 1160°C; Mn_2O_3, which has a bcc form and a tetragonal form; MnO_2, which exists in at least five different forms; MnO_3, whose existence is uncertain; and Mn_2O_7, which is a liquid at room temperature and pressure. MnO melts at about 1850°C; Mn_3O_4 melts at about 1570°C; Mn_2O_3 dissociates at about 880°C.

(m) Mn-S: Two sulphides, MnS and MnS_2 are formed. MnS has a stable NaCl structure, and two unstable forms are also reported; it melts at 1610°C. MnS_2 is isotypic with FeS_2.

(n) Mo-O: There are two principal oxides, MoO_2 and MoO_3, but in addition, there is a series of oxides extending from Mo_4O_{11} to $Mo_{20}O_{58}$. MoO_2 is monoclinic. MoO_3 is orthorhombic and melts at 795°C. The solid solubility of O in Mo is 0.018 at.% (0.003 wt%) at 1649°C.

(p) Mo-S: Several sulphides have been reported. MoS_3 is amorphous, and on heating above 200°C, it yields hexagonal $Mo_{0.93}S_2$. MoS_2 is hexagonal, and there is a very wide variation in opinion about its melting point, from 1185°C to over 1800°C, possibly as high as 2375°C. Mo_2S_3 is monoclinic, and does not appear to be stable below 605°C.

(q) Na-O: Several oxides are formed. Na_2O is fcc and melts at 920°C. Na_2O_2 is hexagonal below 512°C, where it transforms to a high-temperature modification; it melts at 675°C. Na_2O_3 is tetragonal. NaO_2 is fcc above -50°C. The ozonide, NaO_3, is body-centered tetragonal. The solubility of oxygen in liquid Na increases from a very small value at 200°C to 0.25 at.% O at 500°C.

(r) Na-S: Na_2S_3 melts at 230°C, and decomposes to $Na_2S_{1.9}$ on heating above 550°C. This sulphide melts at 460°C, and on heating above 1260°C dissociates to $Na_2S_{1.37}$, which solidifies over the range 650-830°C.

(s) Nb-O: There are three stable oxides: NbO is cubic (NaCl) and melts at 1945°C; NbO_2 is tetragonal, related to rutile, and melts at 1915°C; Nb_2O_5 is polymorphic, but it is possible that only one of these, a monoclinic structure, is stable; the others being either imperfectly crystallized or stabilized by impurities. Nb_2O_5 melts at 1491°C. The solubility of oxygen in Nb rises from 1 at.% O at 700°C to approximately 9 at.% O at 1915°C.

(t) Nb-S: NbS_3 is monoclinic. NbS_2 is rhombohedral below ~800°C, and hexagonal up to at least 1050°C. $Nb_{1+x}S_2$ (x = 0.12 - 0.25 at 1100°C, 0.12 - 0.5 at 800°C) is rhombohedral. $Nb_{1+x}S_2$ (x = 0.30 - 0.43) is hexagonal, stable above ~1000°C. $Nb_{2-x}S_2$ (x = 0.0 - 0.3), stable below 850°C, is hexagonal. NbS_{1-x} (x = 0.1 - ?) is hexagonal, NiAs-type.

(u) Ni-O: The principal oxide is NiO, which exists over a narrow homogeneity range with a NaCl structure above 200°C; it melts at 1984°C. There is a eutectic between NiO and Ni at 1438°C, 0.87 at.% O. The solubility of oxygen in Ni is 0.073 at.% O (0.020 wt%) at 600°C; 0.044 at.% O (0.012 wt%) at 1200°C. Ni_2O_3 has also been reported, although other authors have not been able to prepare it; and NiO_2 has been prepared under "high pressures".

(v) Ni-S: Several sulphides are formed. Below 550°C, a low-temperature rhombohedral form of Ni_3S_2 exists with a very narrow stability range; above this temperature, it transforms to a hexagonal form with a wide stoichiometry range (from about 36 at.% S to 44 at.% S) which is formed in a peritectic reaction at 806°C. There is a eutectic between this phase and Ni at 637°C, 33.4 at.% S. Ni_3S_2 transforms from a low-temperature orthorhombic (?) form to a low-symmetry form at 400°C; it decomposes at 573°C. The low-temperature rhombohedral form of NiS transforms to a NiAs structure at about 300°C, which melts at 992°C. Ni_3S_4 is fcc and decomposes at 303°C. NiS_2 is fcc, FeS_2-pyrite type, and melts at 982°C.

(w) Si-O: SiO_2 appears to be the only solid oxide, existing in four allotropic modifications: β-quartz to α-quartz at 573°C, to tridymite at 867°C, to cristobalite at 1470°C; the oxide melts at 1723°C. The lower three forms are all hexagonal; cristobalite is fcc. SiO exists as a vapor, but it is not well established that it is formed as a solid.

(x) Si-S: Two sulphides are formed. The sulphidation of Si always produces SiS_2, which melts at 1090°C and boils between 1100 and 1200°C. SiS can be prepared by reaction with SiS_2 and Si under vacuum at 850°C; it sublimes at about 960°C.

(y) Ta-O: There is only one stable oxide, Ta_2O_5, which is probably orthorhombic, and melts at 1870°C. There is a eutectic between this and tantalum at about 50 at.% O. The oxygen solubility of Ta is approximately 1 at.% O at 700°C, rising to 4 at.% at 1500°C; there are some discrepancies between the various authors.

(z) Ta-S: Several sulphides have been reported. $Ta_{\sim 1.8\text{-}1.95}S_2$ is hexagonal, and is in equilibrium with Ta. $Ta_{\sim 1.9}S_2$ is rhombohedral; $Ta_{\sim 1.15}S_2$ is also rhombohedral. Five compounds, all having the approximate composition TaS_2, have been reported. TaS_3 has been identified.

(aa) W-O: WO_2 is monoclinic, and decomposes at 1530°C to W + $W_{18}O_{49}$, which decomposes eutectoidally at 550°C to give WO_2 + $W_{20}O_{58}$; this latter oxide also decomposes eutectoidally at 420°C to WO_2 + WO_3. WO_3 exists in several allotropic modifications; it melts at about 1470°C.

(bb) W-S: WS_2 is usually hexagonal, but a rhombohedral form isotypic with rhombohedral MoS_2 can be prepared. It melts at about 1800°C or higher. WS_3 can be prepared by chemical means, but is always amorphous; it decomposes to WS_2 + S at 270-500°C, depending on the atmosphere.

(cc) Zr-O: There is only one stable oxide, ZrO_2, which transforms from a low-temperature monoclinic form to a tetragonal modification at 1000°C. It is possible that there is a further transition at 2285°C, possibly to fcc. The oxide melts at 2700°C. There is a eutectic between this oxide and the α-Zr solid solution at 1900°C, 41 at.% O. Oxygen stabilizes to cph α-Zr, which dissolves 33 at.% O; the maximum solubility in β-Zr is approximately 13 at.% O at 1940°C.

(dd) Zr-S: ZrS_3 is monoclinic, and disproportionates above 700°C. ZrS_2 is hexagonal, and melts at about 1550°C. There appears to be a phase existing over a fairly wide stoichiometry range about ZrS, with a structure based on NaCl.

The phase diagram information has been extracted from:

"Constitution of Binary Alloys", M. Hansen and K. Ancherko, 2nd Ed. (McGraw-Hill, New York; 1958).

"Constitution of Binary Alloys: First Supplement", R. P. Elliott (McGraw-Hill, New York; 1965).

"Constitution of Binary Alloys: Second Supplement", F. A. Shunk (McGraw-Hill, New York; 1969).

TABLE I.1 (xiii). PHASE DIAGRAM INFORMATION FOR SYSTEMS INVOLVING OXIDES, CHLORIDES, AND SULPHATES

(a) $CaO-Cr_2O_3$: There is a eutectic between $CaO.Cr_2O_3$ and $9CaO.4CrO_3.Cr_2O_3$ at about 54% Cr_2O_3, 1022°C.

(b) Na_2O-TiO_2: There is a eutectic between $Na_2Ti_3O_7$ and $Na_8Ti_5O_{14}$ at 985°C.

(c) $Na_2O-Nb_2O_5$: There is a eutectic between $3Na_2O.Nb_2O_5$ and $Na_2O.Nb_2O_5$ at 975°C, but to the Nb_2O_5 rich side of the diagram, no liquid is formed below 1220°C.

(d) Na_2O-MoO_3: There is a eutectic between $Na_2O.4MoO_3$ and MoO_3 at 510°C, and several low-melting point compounds are formed: $Na_2O.4MoO_3$ and $Na_2O.3MoO_3$ are formed in peritectic reactions at a little over 500°C; $Na_2O.2MoO_3$ melts at 610°C, and Na_2MoO_4 melts at 690°C.

(e) Na_2O-WO_3: $Na_2O.4WO_3$ is formed in a peritectic reaction at 785°C; $Na_2O.2WO_3$ melts at 730°C, and Na_2WO_4 melts at 700°C. There is a eutectic between $Na_2O.4WO_3$ and $Na_2O.2WO_3$ at 725°C, and one between $Na_2O.2WO_3$ and Na_2WO_4 at 625°C.

(f) $Na_2SO_4-CoSO_4$: Three intermediate compounds: $3Na_2SO_4.CoSO_4$, $Na_2SO_4.CoSO_4$, and $Na_2SO_4.3CoSO_4$ are found. $Na_2SO_4.CoSO_4$ is formed in a peritectic reaction at about 570°C.

(g) $Na_2SO_4-MgSO_4$: Three intermediate compounds with molar ratios 3:1, 1:1, and 1:3 are formed. There is a eutectic between the solid solution of $MgSO_4$ in Na_2SO_4 and $Na_2SO_4.3MgSO_4$ at about 660°C, 45 mol% $MgSO_4$.

(h) $Na_2SO_4-MnSO_4$: Two intermediate compounds with molar ratios 3:1 and 1:3. There is a eutectic between the extended solid solution of $MnSO_4$ in Na_2SO_4 and $3MnSO_4.Na_2SO_4$ at 650°C, 45 mol% Na_2SO_4.

(j) $Na_2SO_4-NiSO_4$: Three compounds are formed having molar ratios 3:1, 1:1, and 1:3. There is a eutectic between the extended solid solution of $NiSO_4$ in Na_2SO_4 and $NiSO_4.Na_2SO_4$ at about 670°C, 35 mol% $NiSO_4$.

(k) $NaCl-CoCl_2$: Eutectic at about 56% $CoCl_2$, 360°C. A compound $2NaCl.CoCl_2$ is reported which dissociates just below the eutectic temperature.

(l) $NaCl-MnCl_2$: $MnCl_2.4NaCl$ is formed by a peritectic reaction at 458°C. $MnCl_2.2NaCl$ is formed by a peritectoid at 437°C. $NaCl.MnCl_2$ is formed by a peritectic at 428°C, and $NaCl.2MnCl_2$ is formed by a peritectic reaction at 448°C. Between $2NaCl.MnCl_2$ and $NaCl.MnCl_2$ there is a eutectic at 420°C, 47 mol% NaCl.

(m) $NaCl-NiCl_2$: There is a eutectic at 50% NaCl, 560°C.

(n) $NaCl-MgCl_2$*: $NaCl.MgCl_2$ is formed by a peritectic reaction at 465°C, and $2NaCl.MgCl_2$ is formed by a peritectic reaction at 485°C. Between these two is a eutectic at 450°C, 47 mol% NaCl.

(o) $NaCl-Na_2SO_4$: There is a eutectic at about 65 mol% Na_2SO_4, 630°C.

(p) $NaCl-CoSO_4$: An intermediate compound, $NaCl.2CoSO_4$ is formed in a peritectic reaction at 650°C, and there is a eutectic between it and NaCl at 430°C.

(q) $Na_2SO_4-Na_2CrO_4-Na_2MoO_4$: A complete range of solid solutions is formed. The minimum on the liquidous surface is on the $Na_2SO_4-Na_2MoO_4$ binary at 30 mol% Na_2SO_4, 672°C.

(r) $Na_2SO_4-Na_2CrO_4-Na_2WO_4$: A complete range of solid solutions is formed. There is a minimum on the $Na_2SO_4-Na_2WO_4$ side at 25% Na_2SO_4, 655°C; and another on the $Na_2WO_4-Na_2CrO_4$ side at 15% Na_2CrO_4, 674°C.

(s) $Na_2SO_4-Na_2WO_4-Na_2MoO_4$: Complete range of solid solutions--valley connects to minima on the $Na_2SO_4-Na_2WO_4$ and $Na_2SO_4-Na_2MoO_4$ binary sides.

(t) $NaCl-CoSO_4$: $NaCl.2CoSO_4$ is formed in a peritectic reaction at 660°C, and there is a eutectic between this and Na_2Cl_2 at 53 mol% Na_2Cl_2, 430°C.

(u) $NaCl-NiSO_4$: $NaCl.2NiSO_4$ is formed in a peritectic reaction at 770°C, and there is a eutectic between this and Na_2Cl_2 at 60 mol% Na_2Cl_2, 500°C.

(v) $NaCl-Na_2CrO_4$*: There is a eutectic at 572°C, 78.5 equiv% Na_2CrO_4.

(w) $NaCl-Na_2MoO_4$*: An intermediate compound, $NaCl.Na_2MoO_4$ is formed. There are eutectics between this and NaCl at 628°C, 58 equiv% Na_2MoO_4 and between this and Na_2MoO_4 at 606°C, 81 equiv% Na_2MoO_4.

These data are mostly from "Phase Diagrams for Ceramists" and "Phase Diagrams for Ceramists - 1969 Supplement", E. M. Levin, C. R. Robbins, and H. F. MacMurdie (American Ceramic Society, Columbus, 1964 and 1969). The data marked with an asterisk (*) are from "Handbook of Solid-Liquid Equilibria in Systems of Anhydrous Inorganic Salts, Vols. 1 and 2", ed. N. K. Voskresenskaya, Akad. Nauk SSSR, Inst. Obshch. Neorg. Khim. im N.S. Kurnakova (1961) (Translated by Israel Program for Scientific Translations, Jerusalem, 1970).

SECTION 2. PREDOMINANCE DIAGRAMS

The following pages present a number of predominance phase diagrams which show thermochemical information relating to the stability of phases in a convenient graphical representation. It should be remembered that the solid and liquid phases are assumed to be at unit activity.

The sources for these diagrams are:

S. A. Jansson and E. A. Gulbransen, in "High Temperature Gas-Metal Reactions in Mixed Environments", ed. S. A. Jansson and Z. A. Foroulis, Proc. AIME Symposium, Boston (1972) 2.

J. M. Quets and W. H. Dresher, J. Materials, 4 (1969) 583.

T. R. Ingraham, Canad. Met. Quarterly, 3 (1964) 221.

J. A. Goebel, F. S. Pettit, and G. W. Goward, Met. Trans., 4 (1973) 261.

I. G. Wright, B. A. Wilcox and R. I. Jaffee, "Oxidation and Hot Corrosion of Ni-Cr and Co-Cr Base Alloys Containing Rare Earth Oxide Dispersions", Final Report to Naval Air Development Center on Contract N62269-73-C-0327 (April 1974).

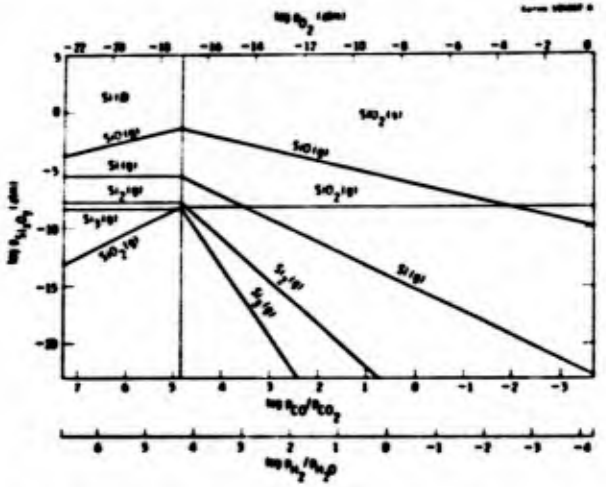

FIGURE I-2 (i) THERMOCHEMICAL DATA FOR Si-O SYSTEM AT 1800K (Janssgn and Gulbransen)

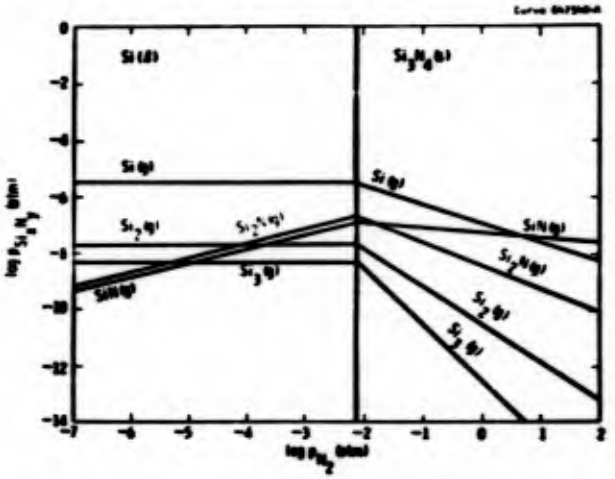

FIGURE I-2 (ii) THERMOCHEMICAL DATA FOR Si-N SYSTEM AT 1800K (Jansson and Gulbransen)

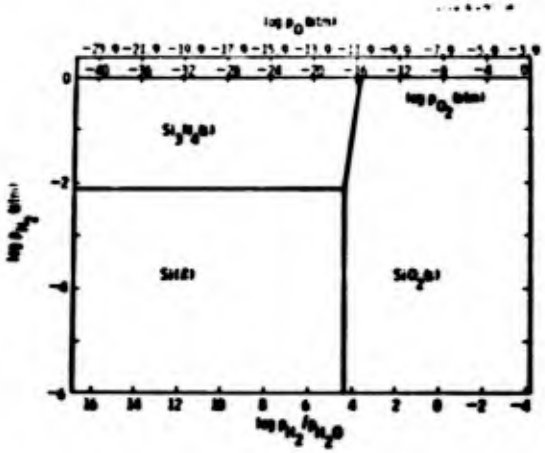

FIGURE I-2(iii). THERMOCHEMISTRY OF Si-O-N SYSTEM AT 1800K. Data for Si(ℓ), Si_3N_4(s), and SiO_2(s) were considered. (Janssen and Gulbransen)

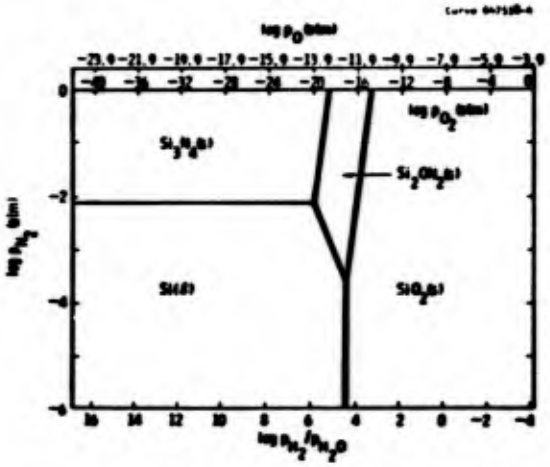

FIGURE I-2(iv). THERMOCHEMISTRY OF Si-O-N SYSTEM AT 1800K. Data for Si(ℓ), SiO_2(s), Si_3N_4(s), and Si_2ON_2(s) were considered. (Jansson and Gulbransen)

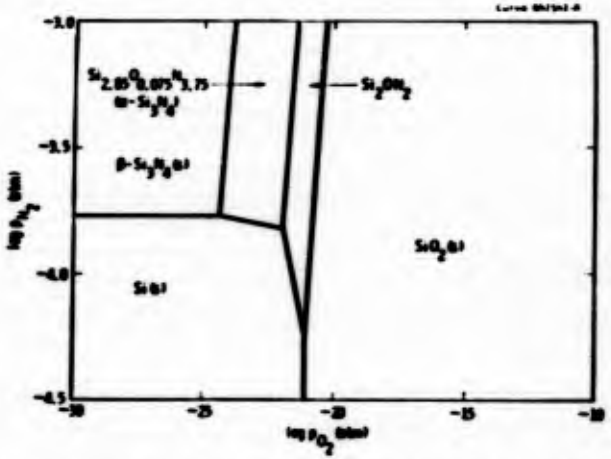

FIGURE I-2(v). THERMOCHEMISTRY OF Si-O-N SYSTEM AT 1567K BASED ON THE RESULTS OF GRIEVESON, JACK, AND WILD (Jansson and Gulbransen)

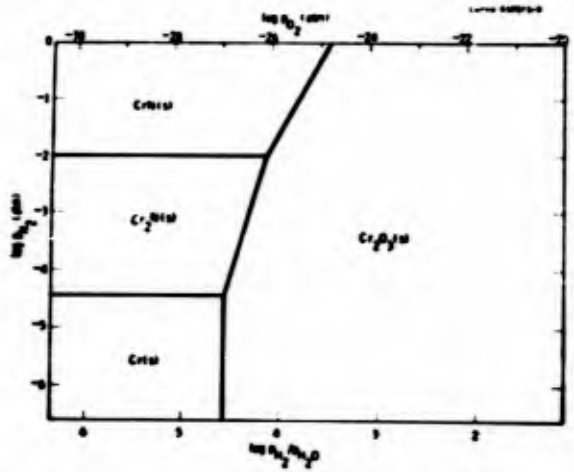

FIGURE I-2(vii). THERMOCHEMISTRY OF Cr-N SYSTEM AT 1100K (Jansson and Gulbransen)

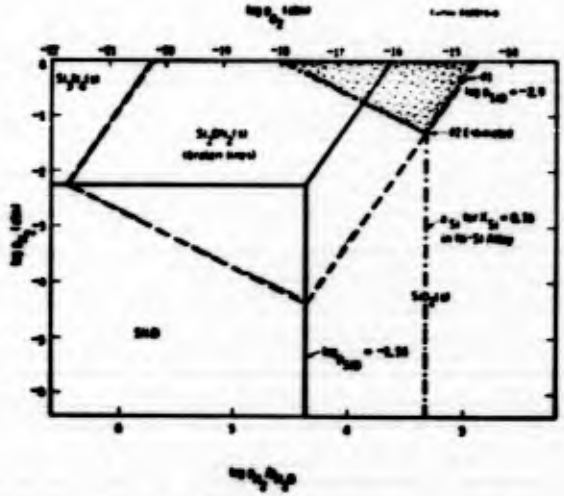

FIGURE I-2(vi). THERMOCHEMISTRY OF Si-O-N SYSTEM AT 1773K (1500°C). Experimental data of Ryall and Nuan are used to evaluate stability of Si_2ON_2(s) phase. (Jansson and Gulbransen)

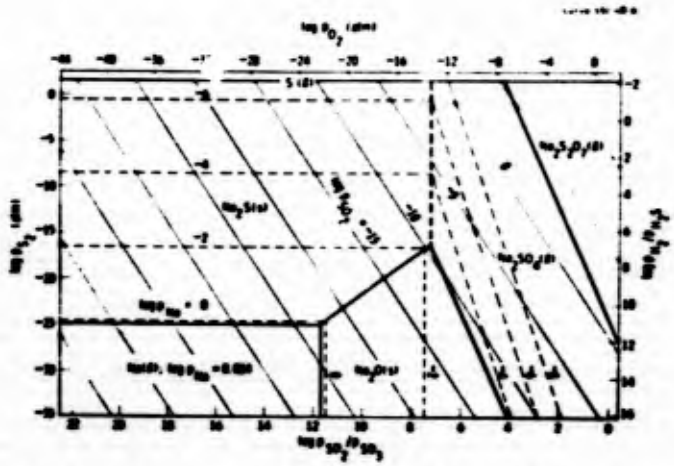

FIGURE I-2(viii). THERMOCHEMISTRY OF Na-O-S SYSTEM AT 1200K (Jansson and Gulbransen)

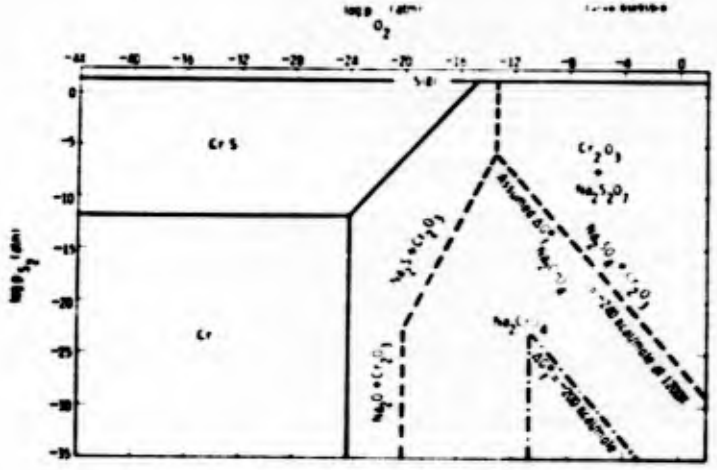

FIGURE 1-2(ix). THERMOCHEMISTRY OF Cr-O-S SYSTEM AT 1200K (solid lines) WITH AREAS FOR Na_2CrO_4(s) STABILITY (broken lines). Estimated free energy values for Na_2CrO_4(s) were used. (Janssen and Gulbransen)

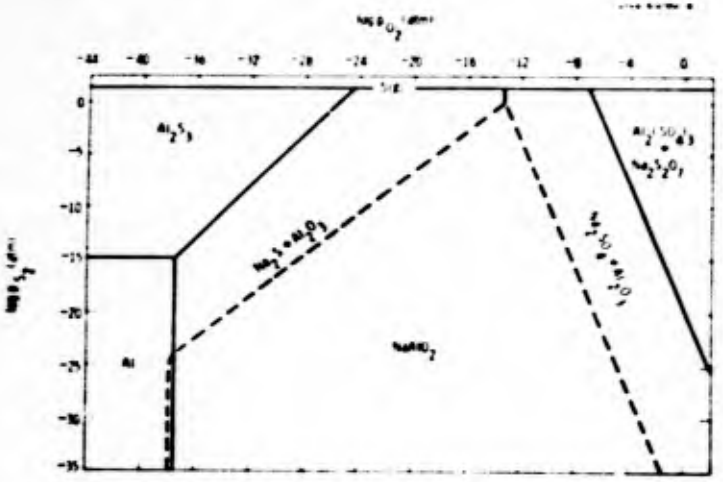

FIGURE 1-2(x). THERMOCHEMISTRY OF [illegible] WITH AREAS FOR [illegible]

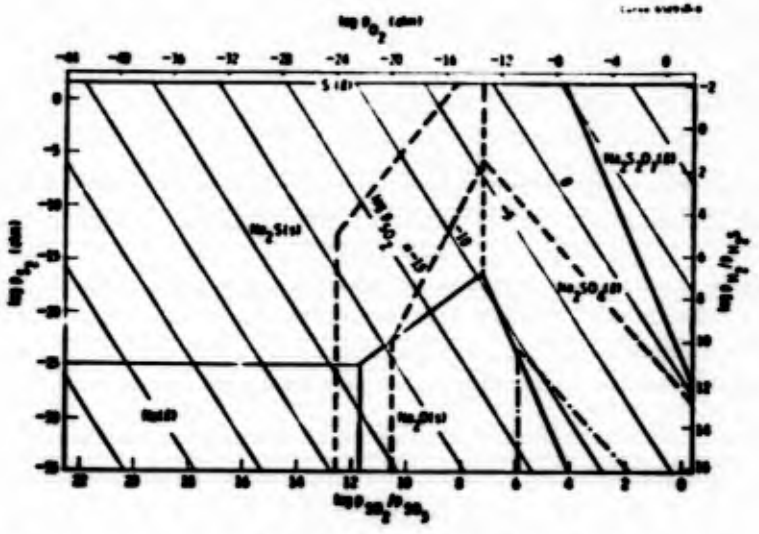

FIGURE 1-2(ix). STABILITY REGION FOR Cr_2O_3(s) (shaded area) IN 1200K Na-O-S THERMOCHEMICAL DIAGRAM (Janssen and Gulbransen)

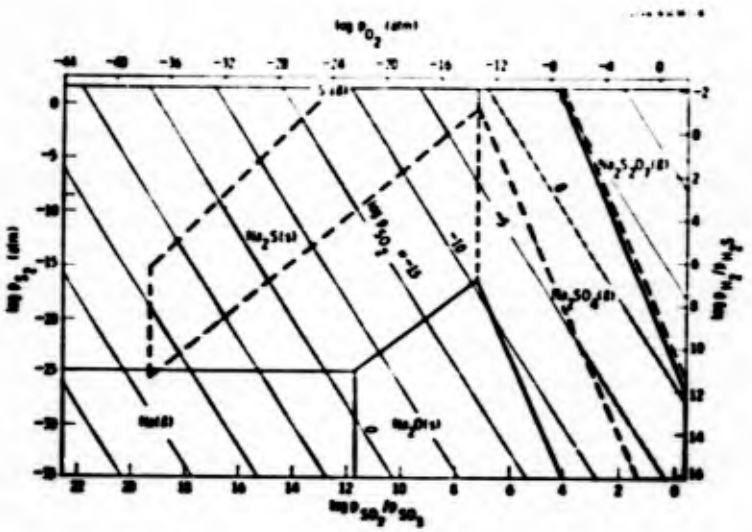

FIGURE 1-2(xi). STABILITY REGION FOR Al_2O_3(s) (shaded area) IN 1200K Na-O-S THERMOCHEMICAL DIAGRAM (Janssen and Gulbransen)

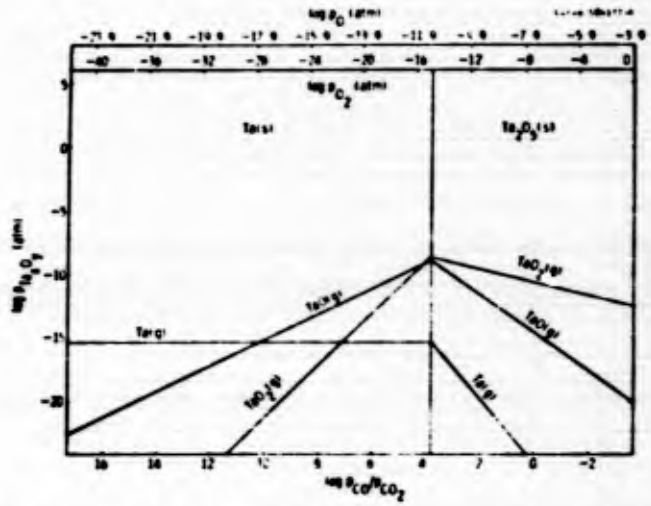

FIGURE I-2(xiii). THERMOCHEMICAL DATA FOR Ta-O SYSTEM AT 1800K
(Jansson and Gulbransen)

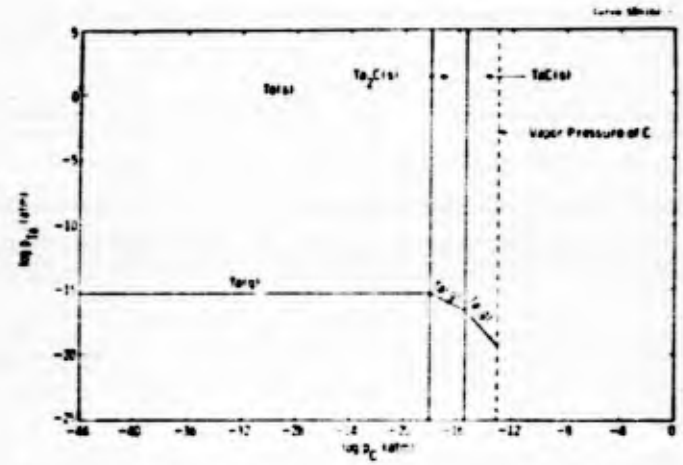

FIGURE I-2(xv). THERMOCHEMICAL DATA FOR Ta-C SYSTEM AT 1800K
(Jansson and Gulbransen)

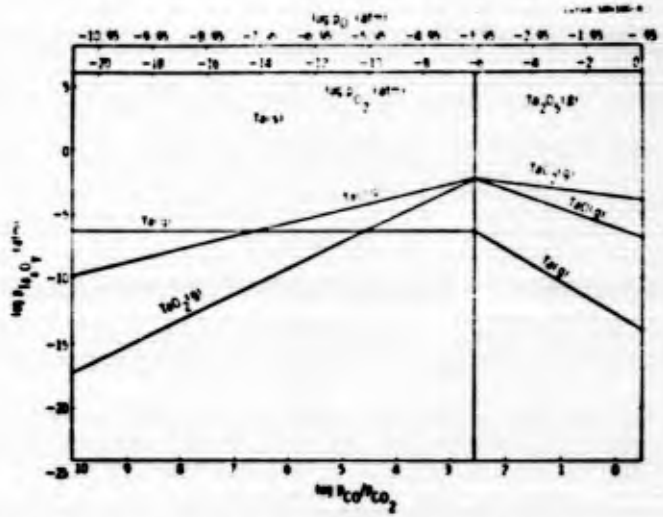

FIGURE I-2(xiv). THERMOCHEMICAL DATA FOR Ta-O SYSTEM AT 3000K
(Jansson and Gulbransen)

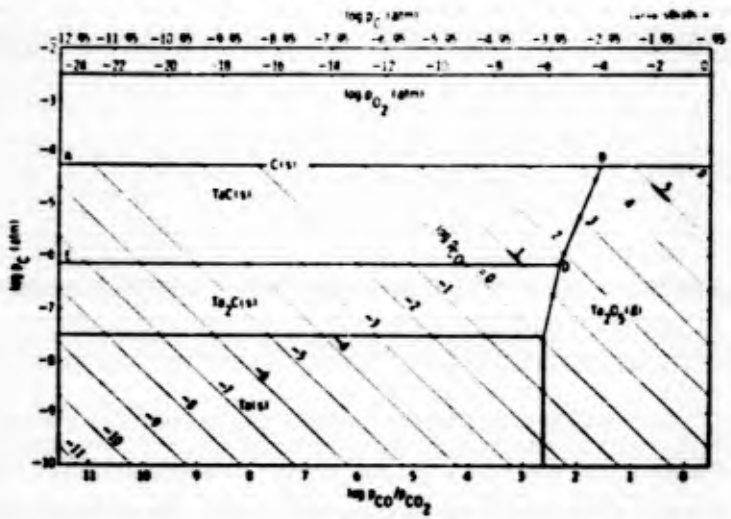

FIGURE I-2(xvi). THERMOCHEMISTRY OF Ta-O-C SYSTEM AT 3000K
(Jansson and Gulbransen)

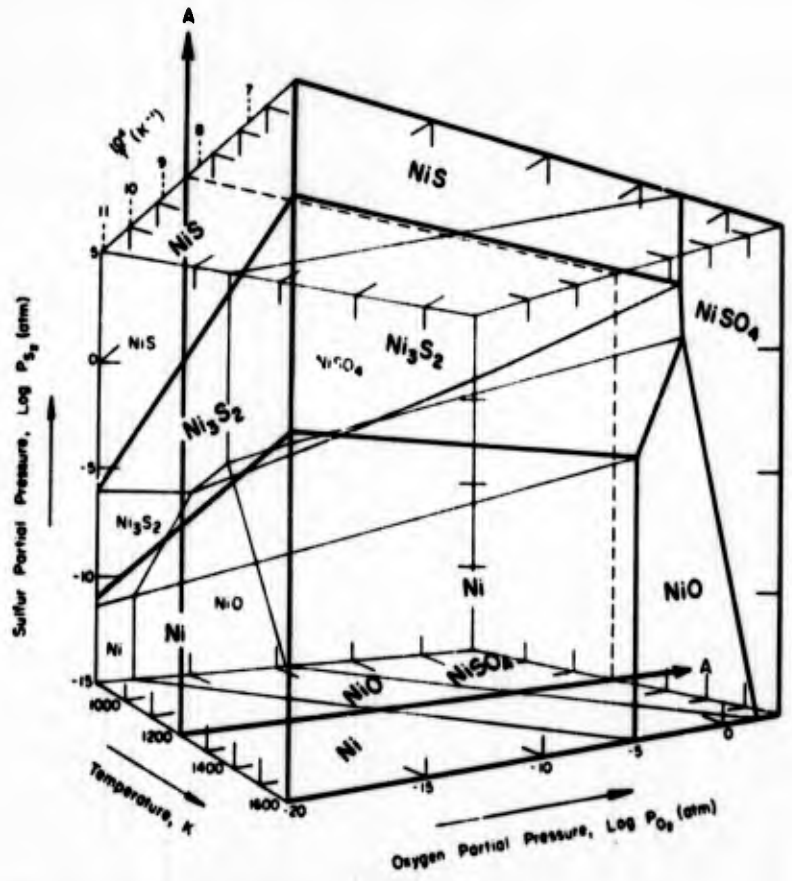

FIGURE I-2(xvii). PREDOMINANCE VOLUME DIAGRAM FOR Ni-S-O SYSTEM AT TEMPERATURES BETWEEN 900 AND 1600K (1160 and 2420 F) Section A-A appears as Figure I-2(xix) (Quets and Dresher)

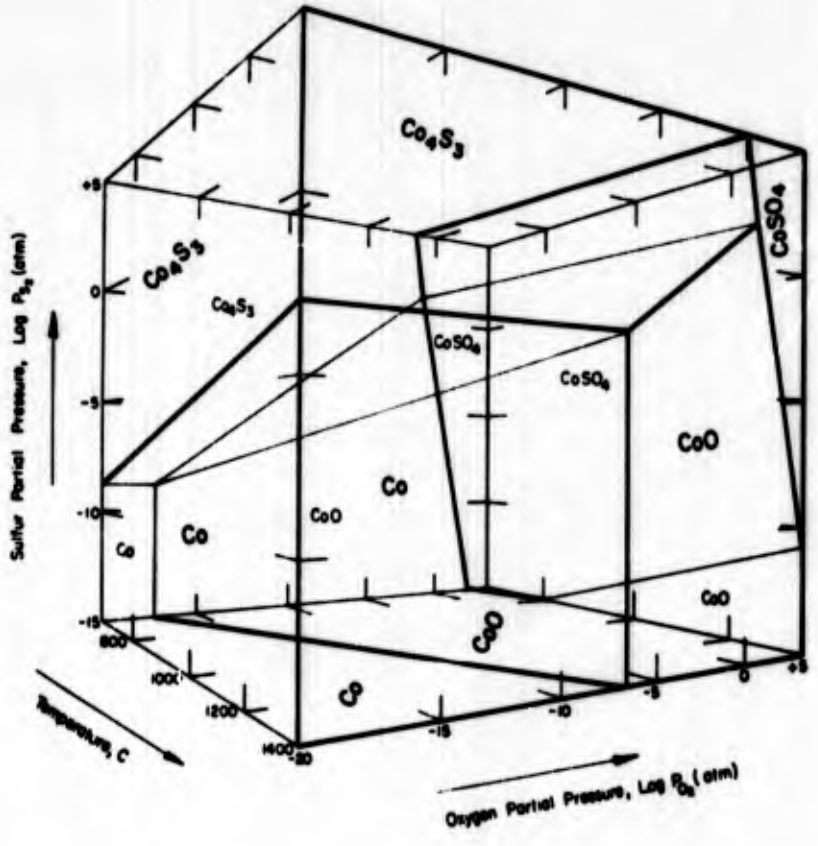

FIGURE I-2(xviii). PREDOMINANCE VOLUME DIAGRAM FOR Co-S-O SYSTEM AT TEMPERATURES BETWEEN 800 AND 1400 C (1472 and 2552 F) (from Ingraham)

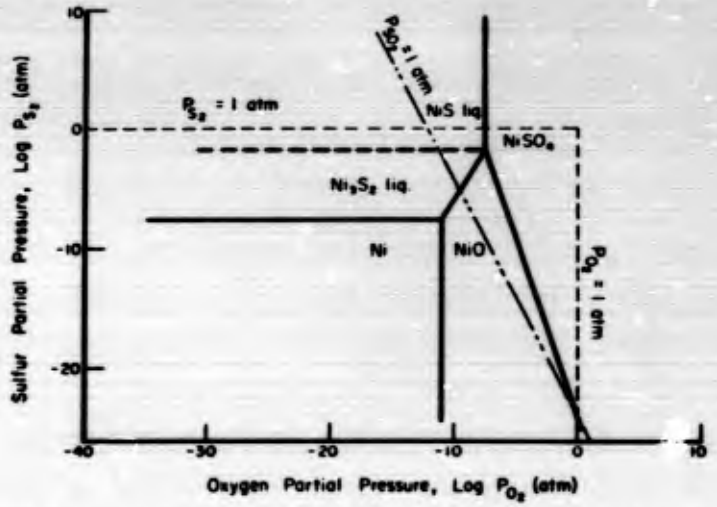

FIGURE I-2(xix). PREDOMINANT PHASE DIAGRAM FOR Ni-S-O SYSTEM AT 1200 K (1700 F) (Section A-A from Figure 1-2(xvii) (Quets and Dresher)

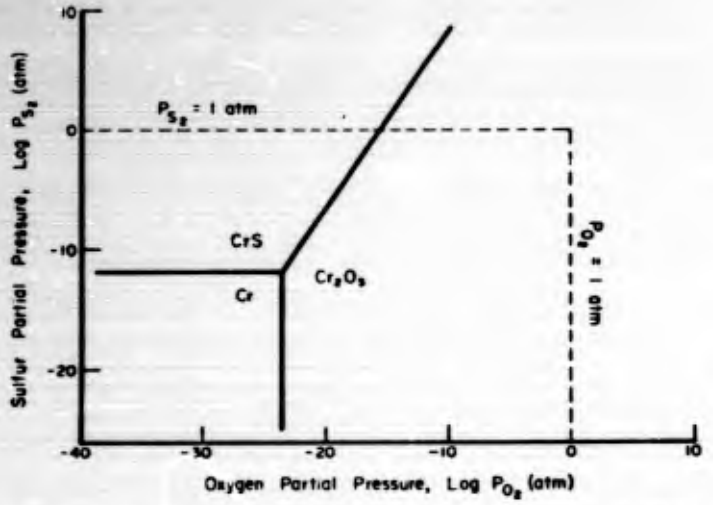

FIGURE I-2(xxi). PREDOMINANT PHASE DIAGRAM FOR Cr-S-O SYSTEM AT 1200K (1700F) (Quets and Dresher)

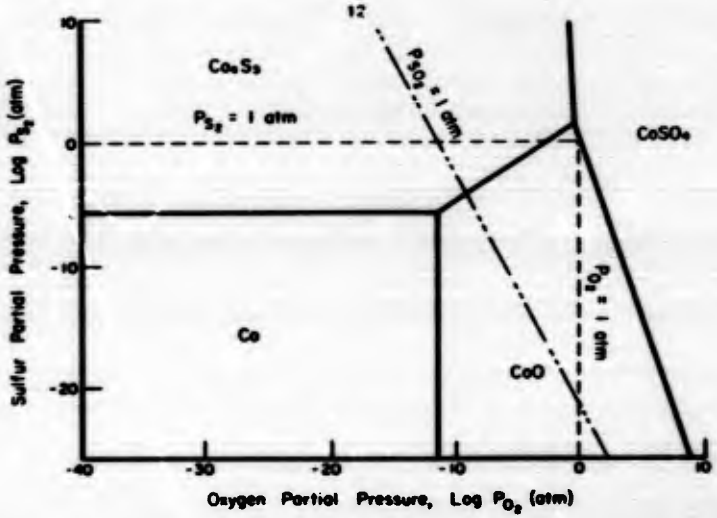

FIGURE I-2(xx). PREDOMINANT PHASE DIAGRAM FOR Co-S-O SYSTEM AT 1000 C (1832 F) (Section for Figure I-2(xviii) (from Ingraham)

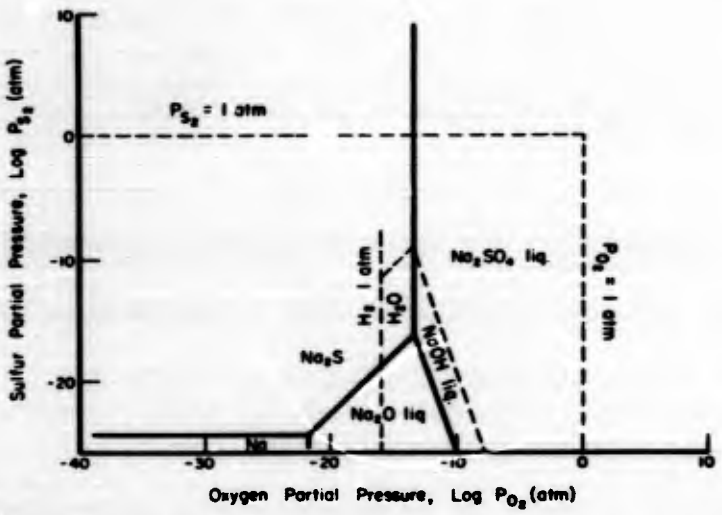

FIGURE I-2(xxii). PREDOMINANT PHASE DIAGRAM FOR Na-S-O SYSTEM AT 1200K (1700F) (Quets and Dresher)

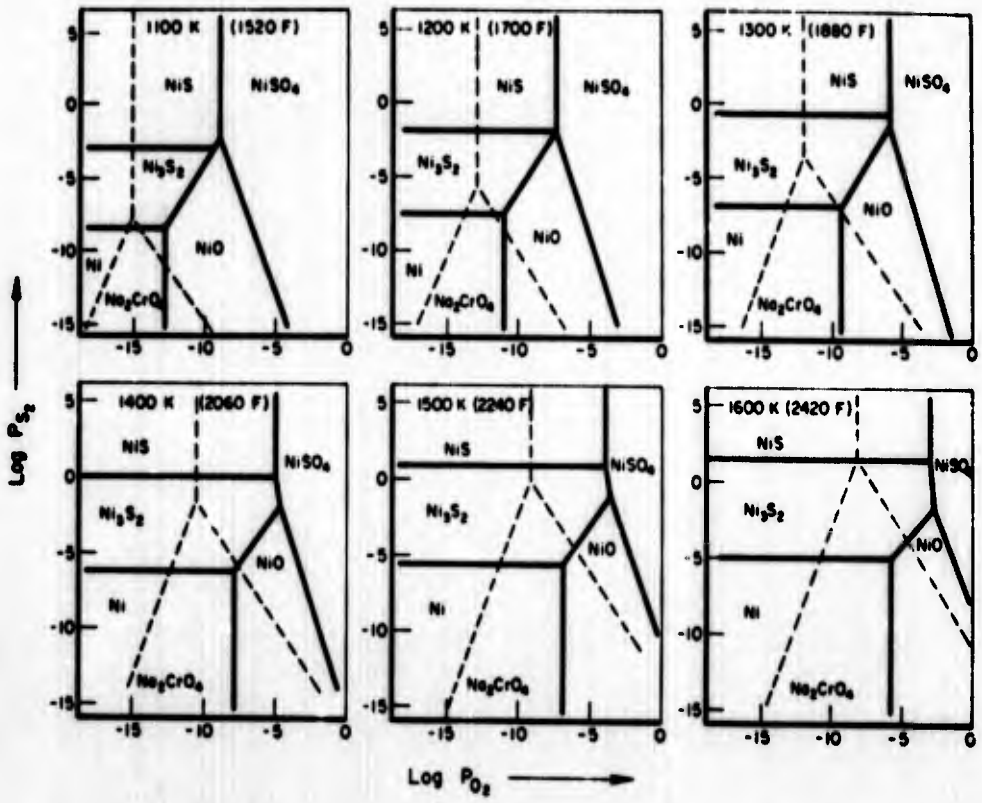

FIGURE I-2(xxiii). A COMPARISON OF THE PREDOMINANT PHASE DIAGRAMS OF THE SYSTEMS Ni-S-O AND Na-S-O UNDER THE CONDITION THAT Cr_2O_3 HAS REACTED WITH Na_2O (Quets and Dresher)

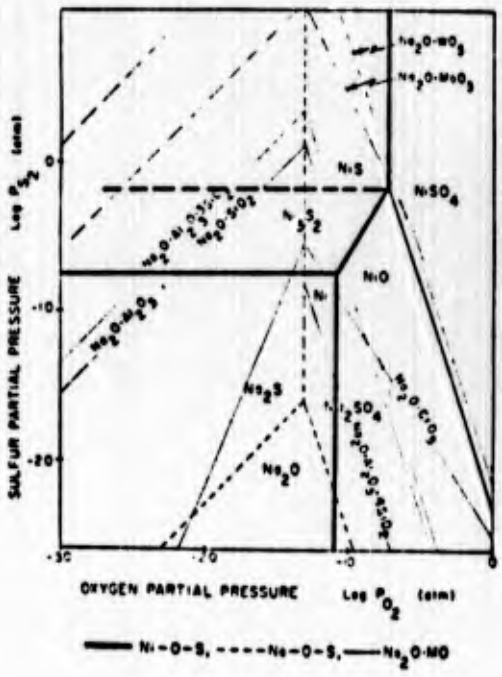

FIGURE I-2(xxiv). VARIATION OF Na_2O PHASE FIELD WITH ADDITION OF METAL OXIDES AT 1200K (Quets and Dresher)

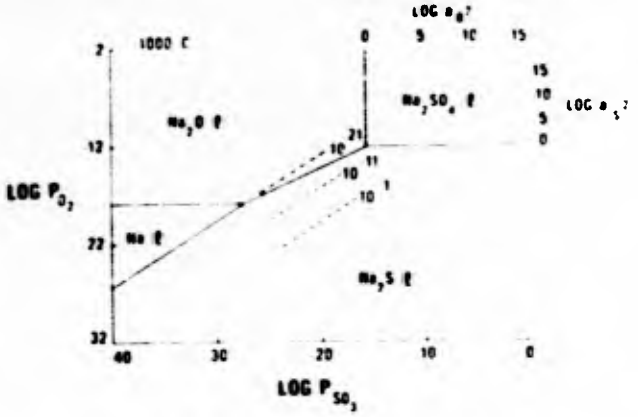

Figure I.2(xxv). Stability diagram for the Na-O-S system at 1000°C. The oxide ion and sulphide ion activity scales are for the Na_2SO_4 region of the diagram. The dashed lines are sulphur isobars (i.e.pS_2) and can be constructed for the entire diagram since $pS_2 = 10^{-20.6} p^2SO_3/p^3O_2$. (Goebel et al).

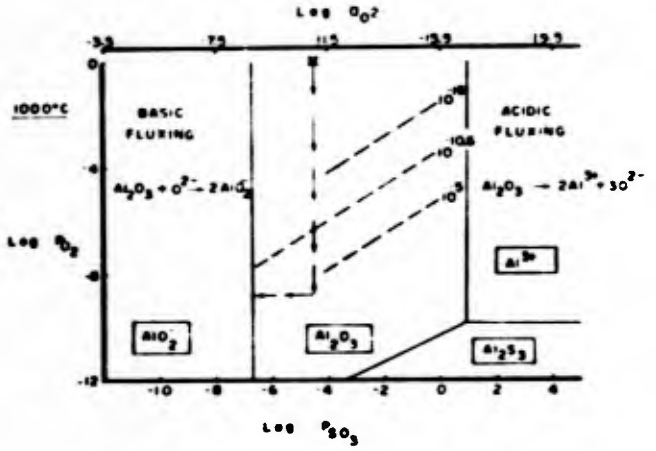

Fig. I.2(xxvi). Stability diagram showing the phases of aluminium that are stable in Na_2SO_4 at 1000°C. The arrows show how the composition of Na_2SO_4 can change because of removal of oxygen and sulphur. The dashed lines are sulphur isobars and the isobar of $10^{-10.6}$ is the sulphur pressure at which aluminium sulphide can be formed beneath an external Al_2O_3 scale on Ni-31Al. The diagram shows Al_2O_3 is stable in Na_2SO_4 with certain compositions and that Al_2O_3 reacts with Na_2SO_4 having either high or low oxide ion activities by what can be called basic or acidic fluxing reactions, respectively.
(Goebel et al).

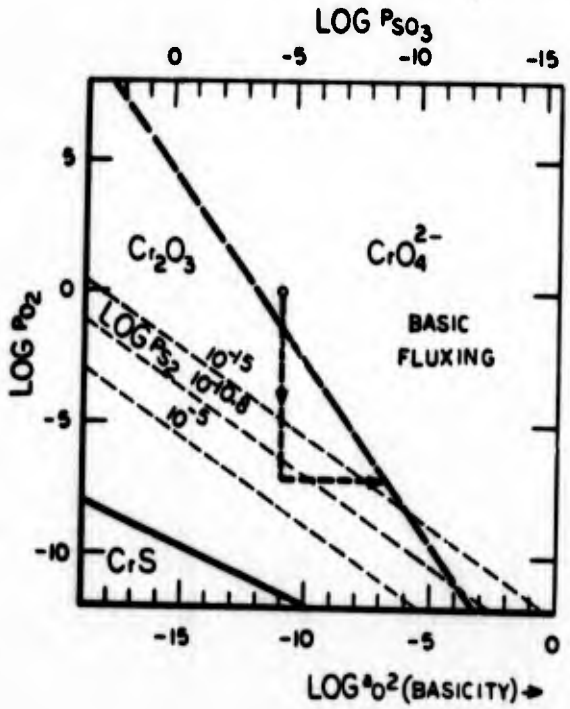

FIGURE I-2(xxvii). STABILITY DIAGRAM FOR Cr-O-S SYSTEM AT 1000°C (Wright, et.al.)

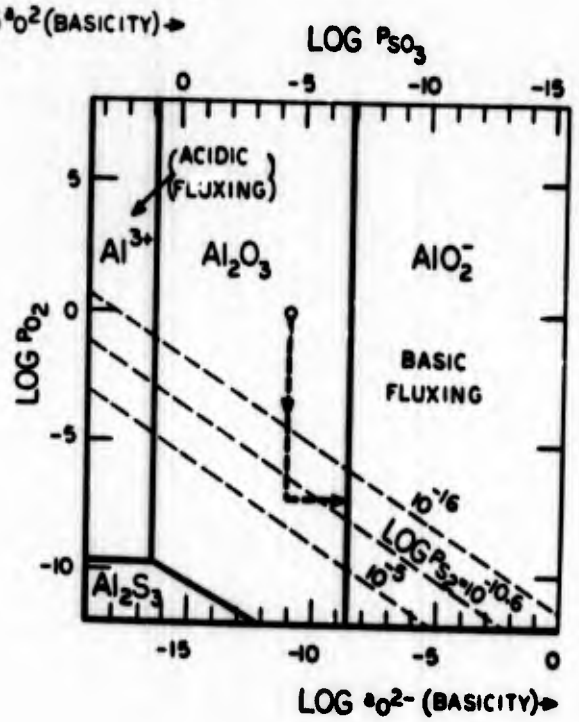

FIGURE I-2(xxviii). STABILITY DIAGRAM FOR Al-O-S SYSTEM AT 1000°C (Wright, et.al.)

SECTION 3. CONSTITUTION OF THE ATMOSPHERE IN THE GAS TURBINE

A calculation of the composition of the atmosphere in an aircraft gas turbine has been presented by J. G Tschinkel (Corrosion, 28 (1972) 161). The fuel was represented as $CH_{1.8}$, which is typical for a marine diesel fuel. It is remarked that the data on salt concentration in the air over the sea vary from 1.5 ppm measured at 20 feet above sea level to 0.01 ppm at several thousand feet.

Figure I-3(i) shows the calculated SO_3/SO_2 ratio as a function of the fuel-to-air ratio ϵ; the air inlet temperature to the combustor is assumed to be 600 F. Figure I-3(ii) shows the equilibrium flame temperature as a function of ϵ for air inlet temperatures of 400 and 600 F. Figure I-3(iii) shows the calculated equilibrium composition of the flame gas as a function of ϵ, assuming 0.5 wt% S in the fuel and 5 ppm NaCl in the air, the total pressure being 200 psia.

Actual analyses of turbine exhausts showed that the SO_3 content was much less than that expected, varying from less than 0.001 of theoretical for a low power setting with ϵ = 0.00640 to 0.004 of theoretical at a high power setting with ϵ = 0.01560.

Figure I-3(iv) shows the relative distribution of sulphur and sodium among their species as a function of temperature for the gas conditions shown in Figure I-3(iii).

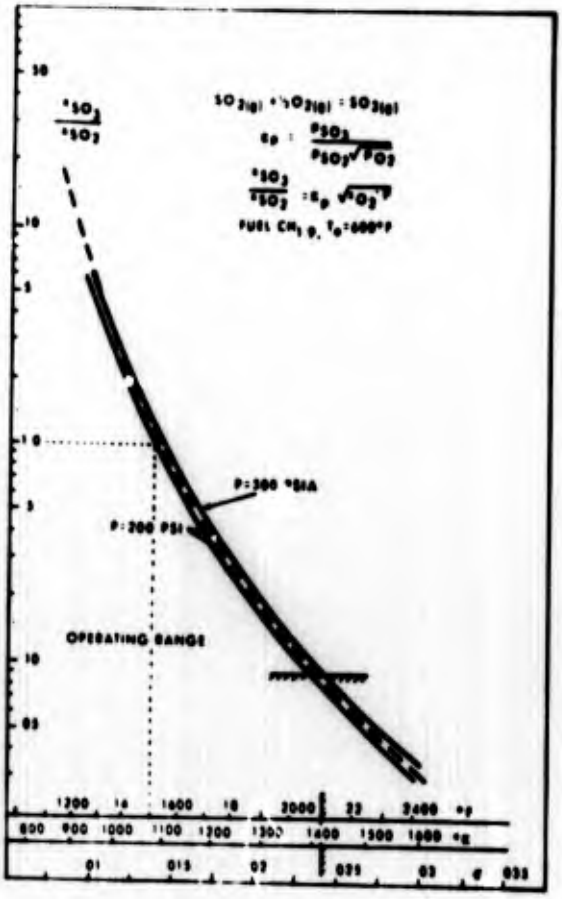

Figure I.3(i). SO_3/SO_2 mol ratio vs F/A ratio (ε). Full lines: machine computed, and dashed lines: hand calculated.

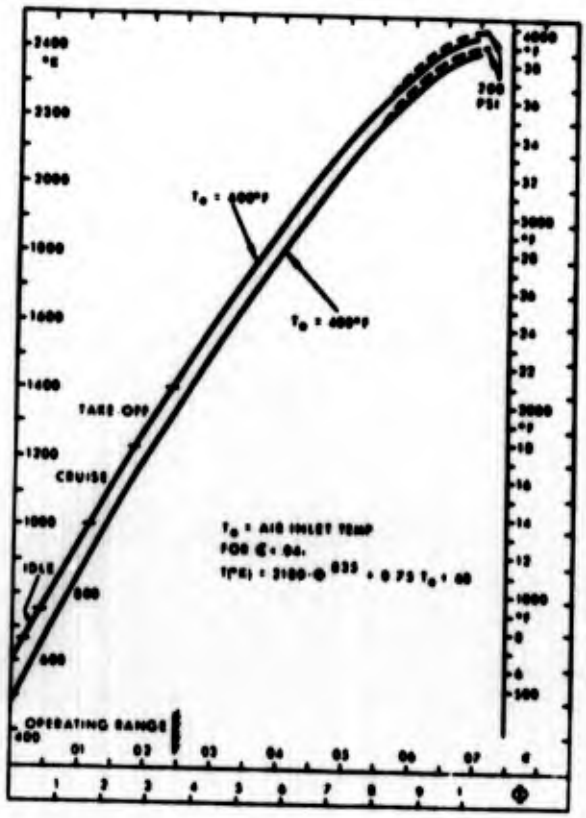

Figure I.3(ii). Equilibrium flame temperature vs F/A mass ratio (ε).

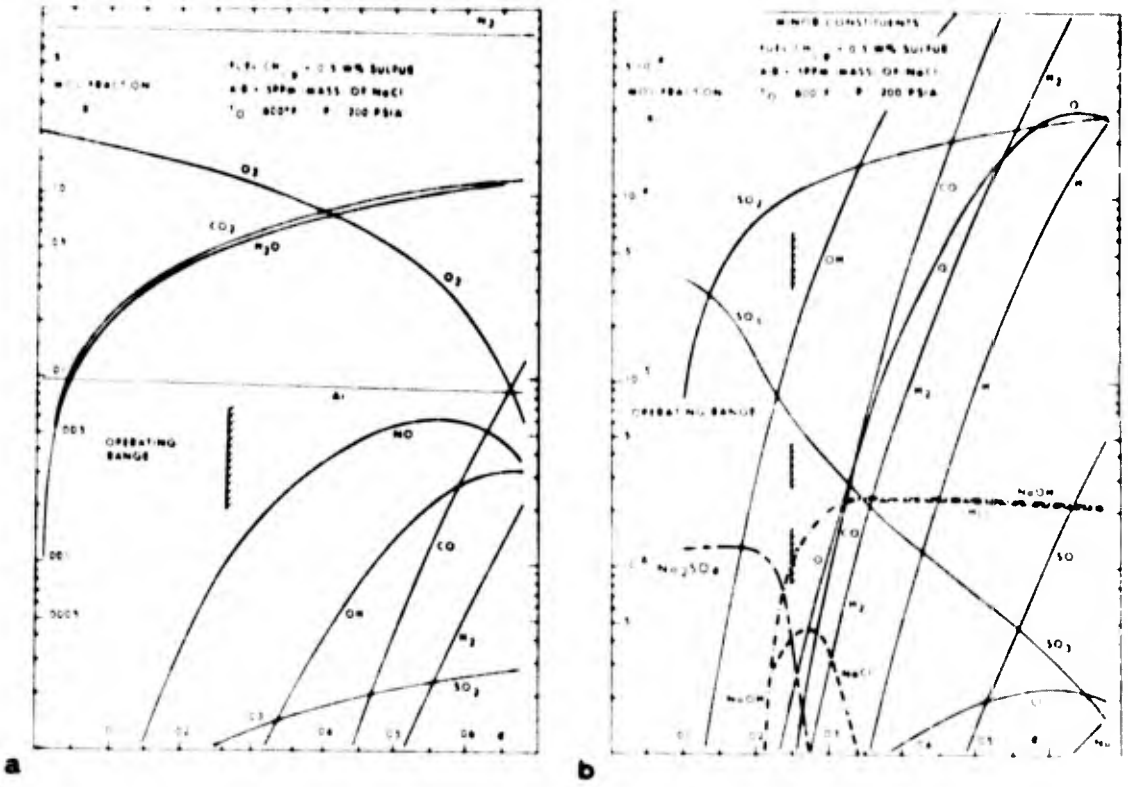

Figure I.3(iii). Equilibrium composition of flame gas vs F/A ratio.
(a) = major constituents, and
(b) = minor constituents.

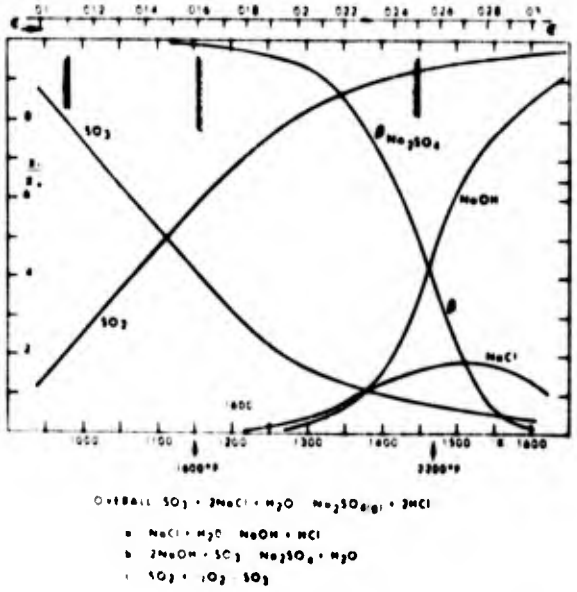

Figure I.3(iv). **Relative distribution of sulphur and sodium among their species as functions of temperature for the gas conditions shown in Figure I.3(iii). Ordinate: $x_{SO_3}/(x_{SO_3} + x_{SO_2})$; $x_{SO_2}/(x_{SO_3} + x_{SO_2})$ and $\beta = 2 \times Na_2SO_4 / x\ Na$; $xNaOH / x\ Na$; $x\ NaCl / x\ Na$; $x\ NaCl + 2 \times Na_2SO_4 + xNaOH$.**

SECTION 4. VAPOR PRESSURE AND CONDENSATION OF SODIUM SULPHATE

Since it is generally accepted that hot corrosion requires the presence of a condensed salt layer on the metal surface, the conditions under which this may be expected are clearly of importance. The actual composition of the salt varies somewhat with operation pattern: Table I-4(i) shows the results of the analysis of a number of components from Pratt and Whitney engines[1].

TABLE I-4(i). DEPOSITS ON TURBINE AIRFOILS FROM AIR LINES (Operating Time 1000 to 5000 Hours) (Tschinkel[1])

Source	Part Analyzed	Microgram Per Piece				
		SO_4	Ca	Na	Mg	Si
1	V	1900				
	B	900				
2	V	1750				
	V	1700				
	B	1570				
	V	410				
	B	720	200	500	20	250
	V	4000				
4	V	3200				
	B	800	200	250	20	20
5	V	1800				
	B	710	200	50	20	20
6	V	1000				
	B	300	300	50	20	
7	V	2270	500	165	60	
	B	540				
8	V	1250	350	150	50	
	B	600				
9	B	270		100		
	Coastal	350				
10	B	210		180		
		250				
		520		170		
		500				

1.2 meqv.cations	Cations, relative meqv.	
meqv.SO_4	Ca	57%
	Na	33%
	Mg	10%

However, it appears that sodium sulphate is the component responsible for the hot corrosion attack, and calculations have mainly been concerned with estimating the conditions under which this will condense: it is possible that the real condensation condition for the actual salt deposit may be different.

The problem seems to have been examined first by DeCrescente and Bornstein[2], who first calculated the dew point of NaCl, using the published vapor pressure data[3] (Figure I-4(i)) and concluded that in the hot section of the turbine NaCl would be in the vapor phase. Next, they pointed out that the sulphation reactions

$$2NaCl + SO_2 + 1/2\ O_2 + H_2O \rightarrow Na_2SO_4 + 2HCl$$

$$2NaCl + SO_3 + H_2O \rightarrow Na_2SO_4 + 2HCl$$

would go virtually to completion under the conditions encountered in the gas turbine, and calculated the dew point assuming complete conversion to Na_2SO_4 using the vapor pressure data of Liander and Olsson[4] and of Kroger and Stratmann[5]. The results are shown in Figure I-4(ii) in terms of the concentration of NaCl in the intake air.

As a check, six superalloy specimens were exposed in the Pratt and Whitney burner rig at 900 C, with a synthetic sea salt concentration of 3.5 ppm in the intake air for 157 hrs, and the deposits were analyzed for Na^+, $SO_4^=$, and Cl^-. The results are shown in Table I-4(ii) which indicates that sulphation did appear to have gone to completion, with very little chloride in the deposit.

TABLE I-4(ii). CHEMICAL ANALYSIS OF SULFIDATION BURNER RIG SPECIMENS (DeCrescente and Bornstein[2])

Specimen	Moles $Na^+ \times 10^5$	Moles $SO_4^= \times 10^3$	Moles $Cl^- \times 10^6$	Na/SO_4
1	0.675	0.313	0.745	2.16
2	0.348	0.178	0.653	1.96
3	0.387	0.207	3.34	1.88
4	0.457	0.228	0.453	2.00
5	0.424	0.219	0.653	1.94
6	0.457	0.238	0.607	1.92

Some experiments were performed for Pratt and Whitney Aircraft by Quigg and Schirmer using the Phillips Environmental Simulator to study the effect of pressure on the dew point and to examine the chemistry of the deposits on three nickel-base superalloys. The tests were for 100 hrs at 900 C, using 0.1 ppm synthetic sea salt in the air. The results are summarized in Table I-4(iii) from which it seems clear that there was condensation at 15 atm pressure but not at 1.5 atm. However, DeCrescente and Bornstein pointed out that in terms of their calculations, condensation should not have taken place under either of these conditions or indeed in the PWA burner test, and speculated that this might be due to inaccurate Na_2SO_4 vapor pressure data, temperature gradients in the specimens, irregular distribution of the salt in the flame, or a lowering of Na_2SO_4 vapor pressure by the formation of complex salts.

TABLE I-4(iii). CHEMICAL ANALYSIS OF SOLUBLE DEPOSITS
(DeCrescente and Bornstein[2])

Alloy	Time Hrs.	Temp. °C	Pressure Atm	Weight Loss[1] mg/cm²	Chemical Analyses (µg) Na^+	Ca^{++}	Mg^{++}	$SO_4^=$	Ca/Na[2] Molar Ratio
Waspaloy[3]	100	900	15	3.93	16	39	6	nil	(1.4)
U 700	100	900	15	2.98	-	-	-	-	-
B 1900	100	900	15	0.91	-	-	-	-	-
Waspaloy	87.5	900	15	10.48	1720	630	112	5380	0.21
U 700	87.5	900	15	6.44	890	225	100	2680	0.145
B 1900	87.5	900	15	17.0	815	107	28	1570	0.076
Waspaloy	100	900	15	11.3	-	-	-	-	-
U 700	100	900	15	30.2	-	-	-	-	-
B 1900	100	900	15	17.0	-	-	-	-	-

[1] Specimens cathodically descaled in fused NaOH.
[2] Ca/Na = 0.021 in synthetic sea salt

Figure I-4(iii) shows an extension of Quigg and Schirmer's study of the effect of pressure on condensation in the Phillips rig[6], from which it appears that the dew point for 10 ppm sea salt in the air at 15 atm pressure is about 1800 F (982 C), which is not inconsistent with DeCrescente and Bornstein. The dew point for 1 ppm sea salt is 1400-1500 F (760-816 C), which again, is not too far from the simple calculations. However, Figure I-4(iii) does not seem consistent with the data from the same rig quoted by DeCrescente and Bornstein and shown as Table I-4(iii).

Later, Quigg et al.[7] examined the effect of the fuel sulphur concentration on the deposit chemistry. Table I-4(iv) summarizes the results,

TABLE I-4(iv). SUMMARY OF ANALYSES FOR SOLUBLE SODIUM AND SULPHATE IONS IN SCALE COMPOSITES (Quigg et al.[7])

Fuel Sulphur, Wt %	Concentration in Scale Composite, wt %		Molar Ratio: Na/SO_4	
	Na^+	SO_4	Experimental	Theoretical for Na_2SO_4
0.0004	0.24	0.10	10.0	2.0
0.004	0.75	0.94	3.3	2.0
0.04	0.84	1.44	2.4	2.0

from which it appears that sulphation may be incomplete at very low fuel sulphur contents, but is substantially complete at realistic sulphur levels. The salt concentration was 1 ppm for these tests. Figure I-4(iv) presents the same data in graphic form.

Tschinkel[1] also considered the condensation of Na_2SO_4. Figure I-4(v) presents the vapor pressure data for NaCl and Na_2SO_4, and Tschinkel conducted some simple transpiration experiments, concluding that above 1000 C the data of Liander and Olsson[4] would become inaccurate due to dissociation of the Na_2SO_4 vapor, the effect depending on the atmosphere in which the test is conducted. Tschinkel recalculated the condensation conditions allowing for the dissociation, but continuing to use the former vapor pressure data, for lack of more reliable values. Figure I-4(vi) shows γ, the condensed fraction of the Na_2SO_4 present as a function of temperature, and hence as a function of fuel-to-air ratio ϵ (see previous section). He comments that condensation temperatures (dew points) are lower by 70 C at most than the intersection of these curves with the abscissa ($\gamma = 0$).

Condé[8] discussed both the conditions for condensation and the kinetics of sulphation and evaporation of sea salt aerosol particles. Tables I-4(v) and I-4(vi) present the dew point calculations for both NaCl, using the data of Zim and Mayer[9], Duffin[10], and Bishop et al.[11]; and Na_2SO_4, using the results of Liander and Olsson[4], Kroger and Stratmann[5], and values calculated from those of Bishop et al.: these last result in significantly lower dew points.

TABLE I-4(v). NaCl DEWPOINT TEMPERATURE DATA (Condé[8])

NaCl Concentration		Dewpoint Temperature °C		
mm Hg	ppm	(9)	(10)	(11)
0.25	660	775	749	760
0.11	290	747	705	793
0.005	145	718	676	707
3.8×10^{-4}	1	567		
3.8×10^{-5}	0.1	517		
3.8×10^{-6}	0.01	456		

TABLE I-4(vi). Na_2SO_4 DEWPOINT TEMPERATURE DATA (Condé[8])

Na_2SO_4 Concentration		Dewpoint Temperature °C		
mm Hg	ppm	(4)	(5)	Derived from (11)
1.53×10^{-2}	100	883	884	827
1.53×10^{-3}	10	727	814	687
1.53×10^{-4}	1	612	758	612
1.53×10^{-5}	0.1	514	707	492
1.53×10^{-6}	0.01	437	654	422

Condé also remarks that recent rig tests in the United Kingdom have shown that deposition can take place at a sea-salt concentration of 0.1 ppm at blade temperatures as high as 900 C at slightly above 1 atm system pressure. He points out that in practice deposits may also result from impaction of unevaporated salt particles as well as by condensation. Figure I-4(vii) shows the evaporation times measured by Samms[12] for NaCl and Na_2SO_4 droplets, and Figure I-4(viii) shows the kinetics of gas-phase sulphation of sodium chloride, from Hanby and Beer[13]. The residence time in the gas turbine is approximately 5 ms, so it is apparent that both processes may well be incomplete.

A further study of the vapor pressure of sodium sulphate using a Knudsen effusion technique in the temperature range 560-1000 C in vacuum has been published by Powell and Wyatt[14], who present Figure I-4(ix) comparing their results with references 4 and 5, and also data from Eyber[15], Terres[16], and Bruckner[17]. There are plainly some significant discrepancies, but Powell and Wyatt do not consider that dissociation processes can have played a significant part in their experiments.

Fryxell et al.[18] have also recently determined the vapor pressure of sodium sulphate in the temperature range 954-1204 C, using a transpiration method with air as the sweep gas. They, too, believe that Na_2SO_4 is essentially undissociated in this temperature range. However, they show evidence to suggest that reagent-grade anhydrous sodium sulphate contains significant amounts of an acid impurity, probably $NaHSO_4$, which could decompose easily at these temperatures. It also proved necessary to correct for weight loss of the platinum crucible. Figure I-4(x) shows their new results, which they regard as thermodynamically more probable than those of References 4 and 5, since the entropy of vaporization is 27.6 cal/deg. mole, as opposed to the 46.5 cal/deg. mole of Kroger and Stratmann and 7.06 cal/deg. mole of Liander and Olsson. Trouton's rule says that the entropy of vaporization should be 23.0 cals/deg. mole, and for most materials values between 21 and 24 cals/deg. mole are observed.

Bessen and Fryxell[19] have used this new vapor pressure data to calculate the dew point for Na_2SO_4, both under the condition where the NaCl in the sea salt is completely sulphated and under the condition where no sulphation takes place, and only the 1.2 percent Na_2SO_4 naturally present in sea salt is regarded as condensing. The results are shown in Figure I-4(xi) which represents very much higher dew points than those of the earlier authors. Recalling that condensation is observed at 1650 F, 1 atm. pressure with 0.1 ppm sea salt, it is plain that these curves are a great deal closer to experience than the previous results.

REFERENCES

1. J. G. Tschinkel, Corrosion, 28 (1972) 161.

2. M. A. DeCrescente and N. S. Bornstein, Corrosion, 24 (1968) 127.

3. Handbook of Chemistry and Physics, 46th Edition, p.D-101, Chemical Rubber Publishing Co., 1966.

4. H. Liander and G. Olsson, IVA, 4 (1937) 145.

5. C. Kroger and I. Stratmann, Glastechn. Ber., 34 (1961) 311.

6. H. T. Quigg and R. M. Schirmer, Final Report to Naval Air Systems Command on Contract N000 19-67-C-0275 (May, 1968).

7. H. T. Quigg, R. M. Schirmer and L. Bagnetto, Final Report to Naval Air Systems Command on Contract N000 19-70-C-0293 (January, 1971).

8. J.F.G. Condé, Proc. Gas Turbine Materials Conference, Naval Ship Engineering Centre, Washington, D C. (1972) 17.

9. B. H. Zim and J. E. Mayer, J. Chem. Phys., 12 (1944) 362.

10. H. C. Duffin, unpublished work, NGTE, 1960 (quoted by Conde[8]).

11. R. J. Bishop, K. R. Cliffe, and T. H. Langford, private communication to J.F.G. Conde, quoted in Ref. 8; R. J. Bishop and K. R. Cliffe, J. Inst. Fuel (July, 1969) 283.

12. J.A.C. Samms, unpublished report on U.K. MOD Contract (1971); quoted by Conde[8]).

13. V. I. Hanby and J. M. Beer, unpublished work under U.K. MOD Contract (1969-72) quoted by Conde[8]

14. D. G. Powell and P.A.H. Wyatt, J. Chem. Soc. A1971 3614.

15. G. Eyber, Glastechn. Ber., 33 (1960) 283.

16. E. Terres, Brennstoff Chemie, 35 (1954) 225.

17. R. Bruckner, Glastechn. Ber., 35 (1962) 93.

18. R. E. Fryxell, C. A. Trythall, and R. J. Perkins, G.E. Technical Information Series Report No. R73 AEG 111 (January, 1973) 20 pp.

19. I. I. Bessen and R. E. Fryxell, Proc. Gas Turbine Materials Conference, Naval Ship Engineering Center, Washington, D.C. (1972) 73.

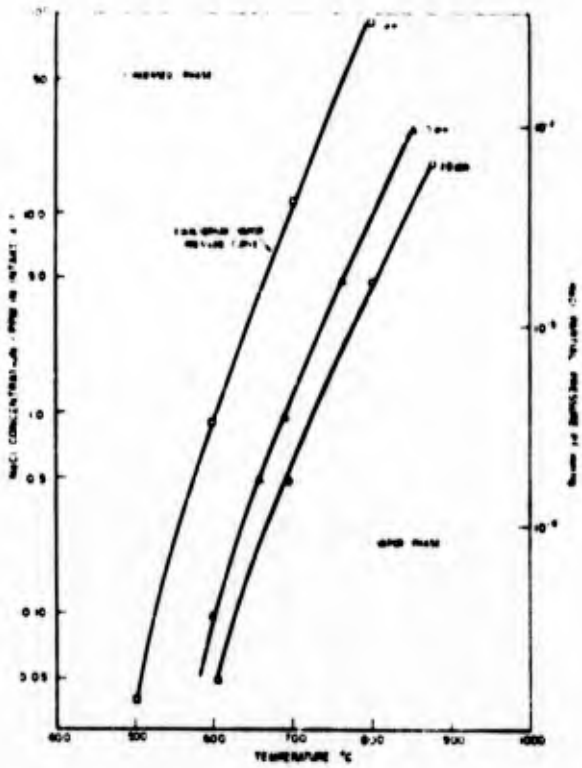

FIGURE I-4(i). THE DEW POINT OF NaCl AS A FUNCTION OF CONCENTRATION AND PRESSURE (DeCrescente and Bernstein[2])

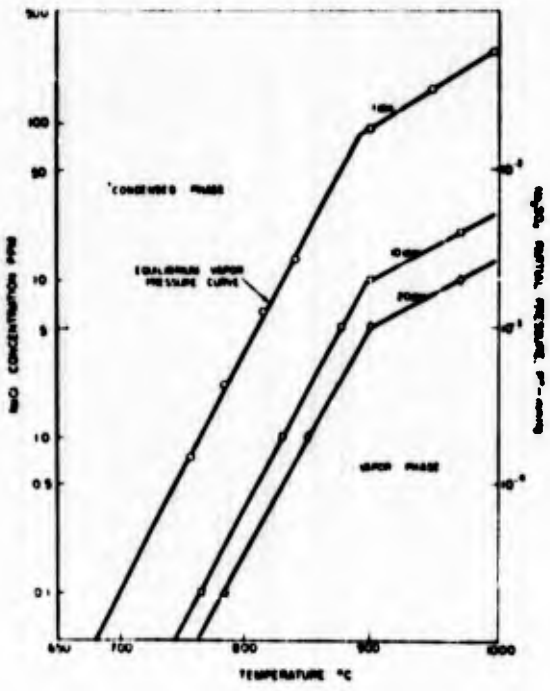

FIGURE I-4(ii). THE DEW POINT OF Na_2SO_4 AS A FUNCTION OF NaCl CONCENTRATION AND PRESSURE (DeCrescente and Bernstein[2])

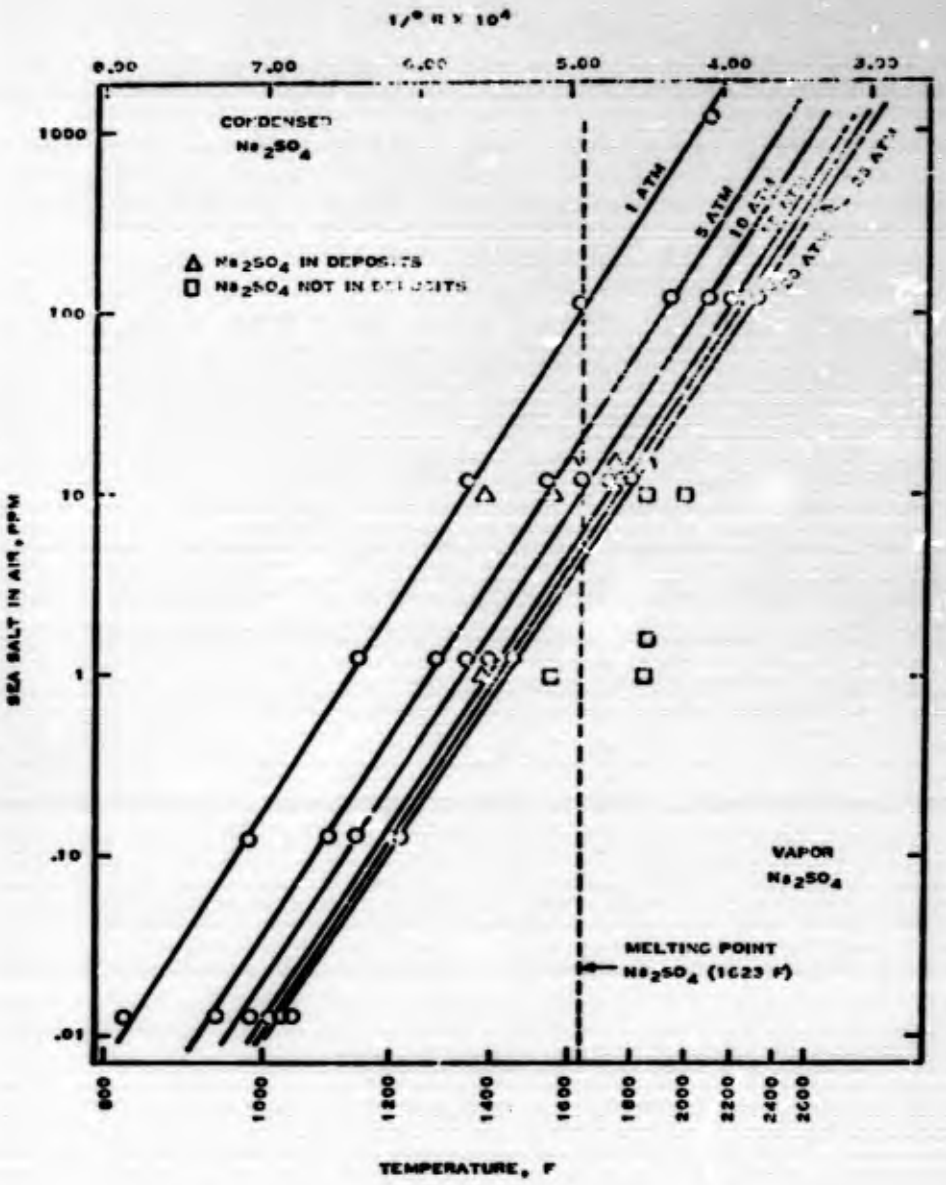

FIGURE I-4(iii). PHASE RELATIONSHIP FOR SODIUM SULPHATE (Quigg and Schirmer[6])

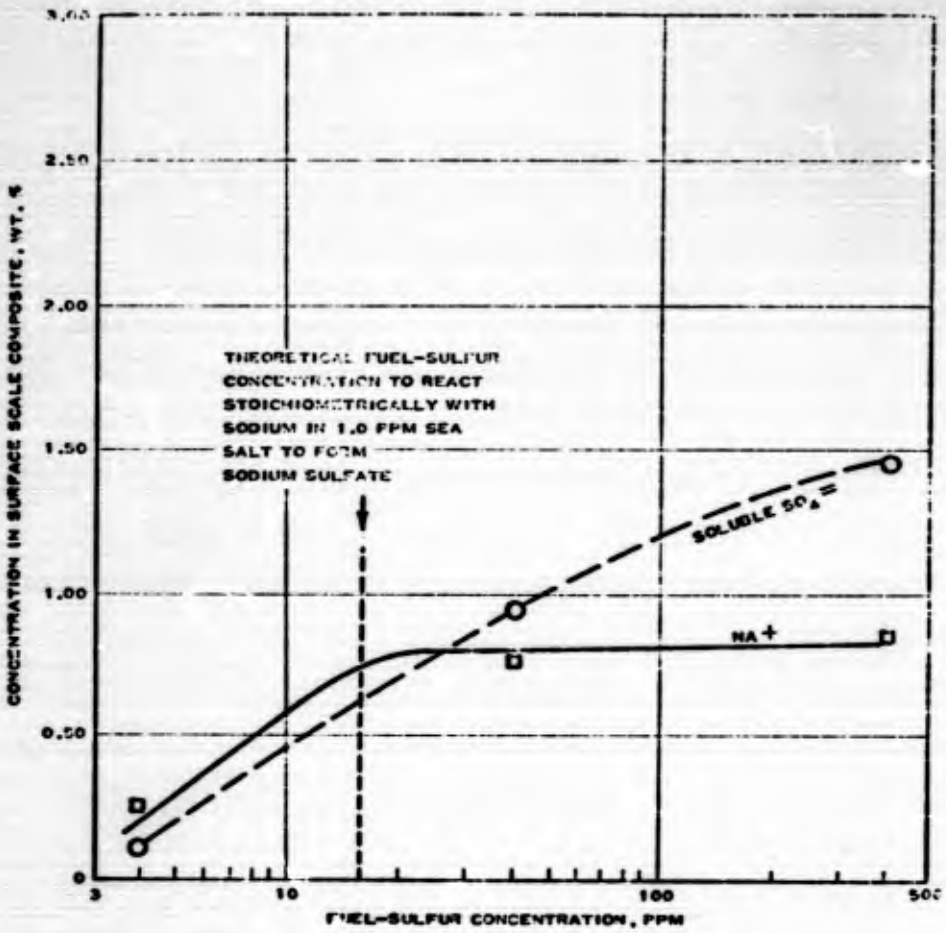

FIGURE I-4(iv). RELATIONSHIP OF SOLUBLE SODIUM AND SULPHATE IONS IN SURFACE SCALE TO FUEL-SULPHUR CONCENTRATION (Quigg et al.[7])

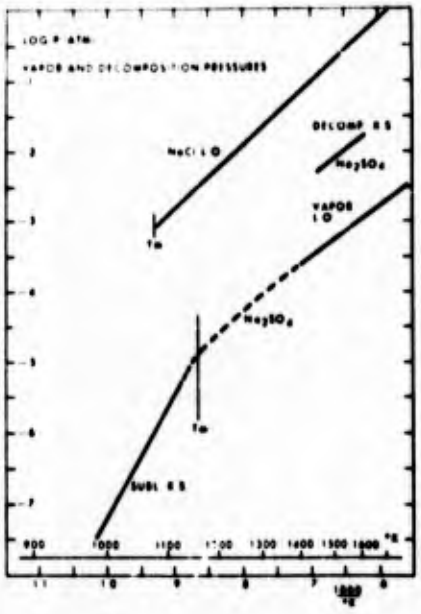

Figure I.4(v). Vapour pressure of Na_2SO_4 vs temperature. Measured by Liander and Olson [4] in 1937, and Kroger and Stratman [5] in 1961. Also: vapour pressure of NaCl, and measured decomposition pressure of Na_2SO_4. (Tschinkel [1]).

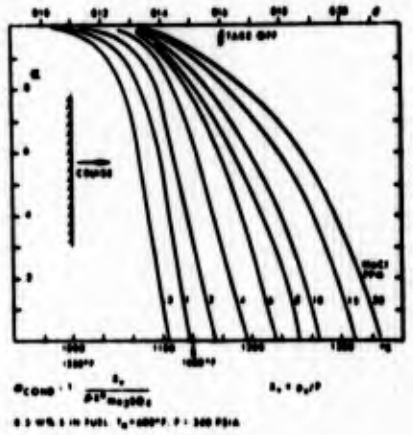

Figure I.4(vi). Condensed fraction of undissociated Na_2SO_4 vs temperature and NaCl (content in air). (Tschinkel [1]).

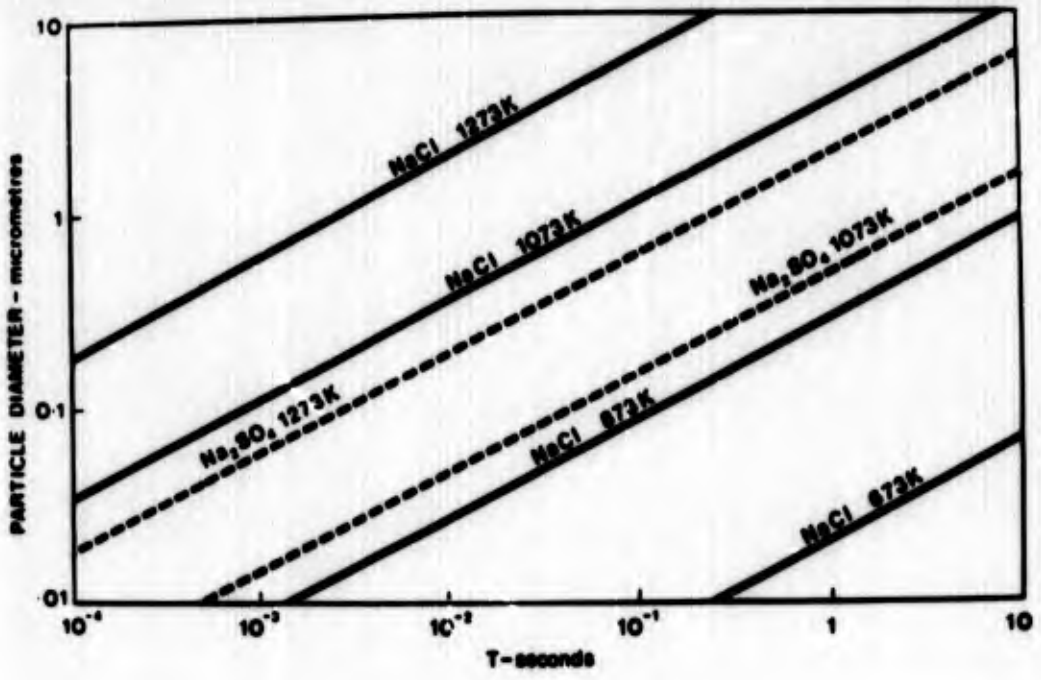

Figure 1-4.(vii). Evaporation times for NaCl and Na_2SO_4 droplets. (Ref. 12).

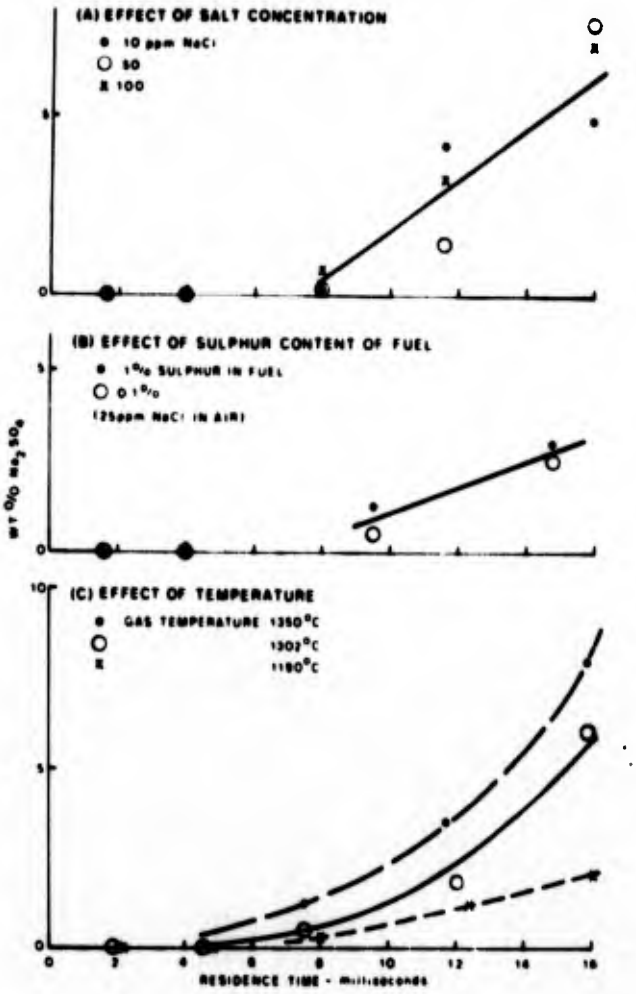

Figure 1-4(viii). Gas phase sulphation of sodium chloride (Ref. 13).

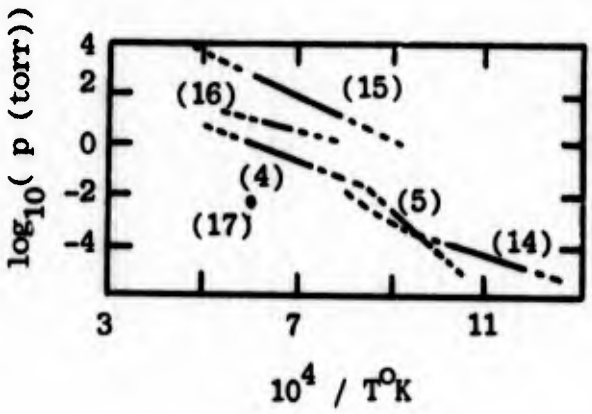

Figure 1.4(ix). Vapour pressure data for Na_2SO_4, compiled by Powell and Wyatt (14).

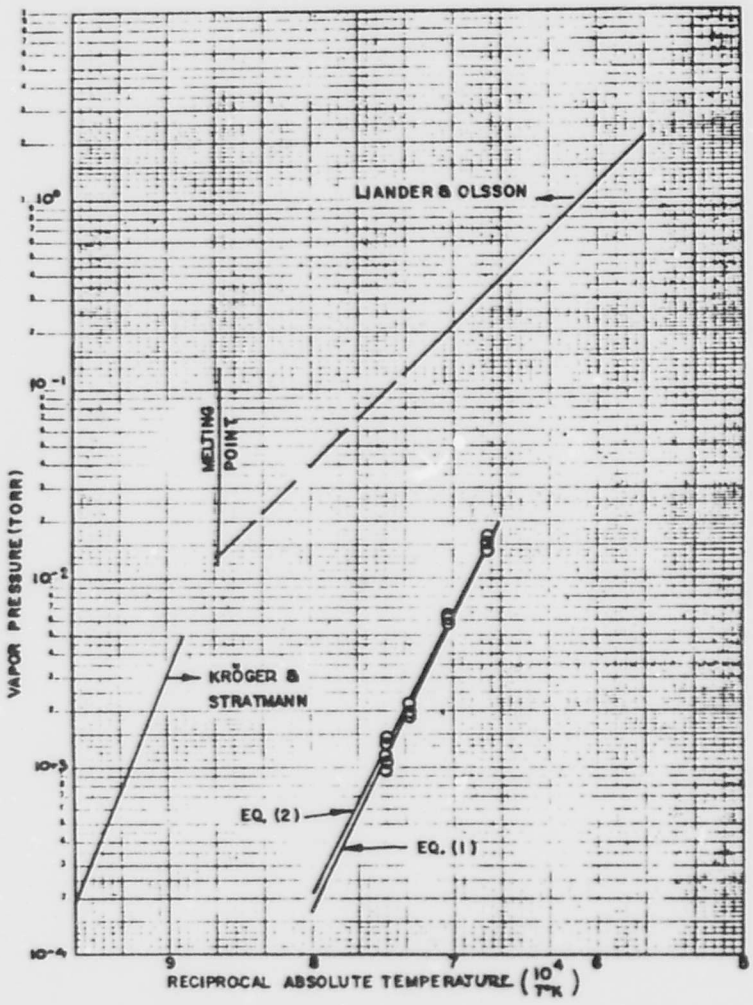

FIGURE I-4(x). VAPOR PRESSURE OF Na_2SO_4 AS A FUNCTION OF RECIPROCAL TEMPERATURE (Ref. 18)

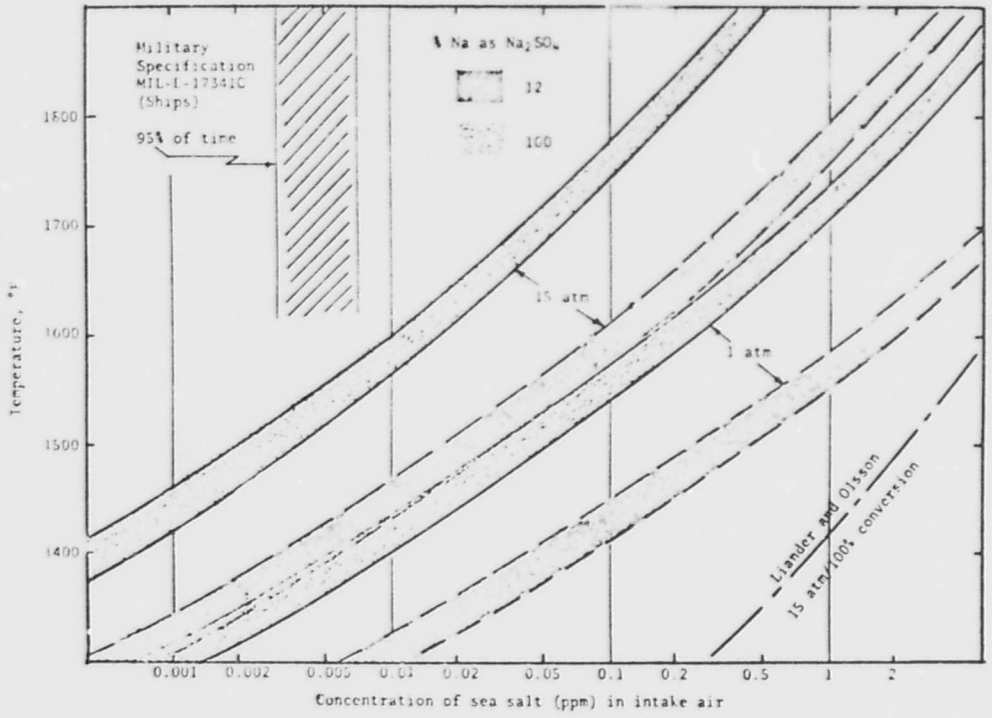

FIGURE I-4(xi). CONDENSATION TEMPERATURES FOR Na_2SO_4 AS FUNCTION OF CONCENTRATION AND PRESSURE (Ref. 19)

DIFFUSION DATA

The following section presents some diffusion data which may be relevant in the high-temperature oxidation and corrosion of aerospace alloys. The majority of the information presented has been extracted from Diffusion Data, with supplementary information in some more important cases. Most of the data have been published in the last ten years: the earlier literature has not been reviewed in detail, but again earlier data are presented for the more important systems.

DIFFUSION DATA I : METALS AND BINARY ALLOYS

MATERIAL	METHOD	TEMP. RANGE, °C.	D_0, $cm^2 s^{-1}$	D, $cm^2 s^{-1}$	Kcals $mole^{-1}$	Reference
Co in Co	residual activity, self diffusion	1120-1370	0.23		64.0	Badia, 1969.
Co in Co	sectioning technique, self-diffusion, Co^{60}.		$2.20^{+2.41}_{-1.13}$		70.5±2.1	Million and Kucera, 1969.
Co - Ni	Interdiffusion. Electronprobe micro-analysis. Above 1190°C, behaves as an ideal solid solution. Below 1145°C, it shows a maximum at 75% Ni, attributed to short range order.	880-1300	Values similar to those of Badia			Iijima and Hirano 1971.
Ni in Co	Impurity diffusion, microprobe.	900-1250	0.128		65.5±1.0	Badia and Vignes, 1967.
Ni in Co		1150-1400	1.25		72.1±1.4	MacEwan et al 1959.
Ni in Co		772-1048	0.34		64.3	
Ni in Co		1192-1297	0.10		60.2	Hirano et al 1962.
Ni in Co	Electron probe microanalysis Heterodiffusion at infinite dilution	1130-1370	0.4		67.4	Badia and Vignes 1969.
Ni in Co	Interdiffusion, microprobe; 5-95%Ni	1150-1300	D_n increases linearly with nickel content from 2.4×10^{-10} at 5% Ni to 6.1×10^{-10} at 95% Ni (1305°C); 0.8×10^{-10} to 2.5×10^{-10} (1245°C); 0.6×10^{-10} to 1.5×10^{-10} (1200°C) and 0.2×10^{-10} to 0.8×10^{-10} (1150°C).			Dorovskii et al 1967
Ni in Co	Interdiffusion, microprobe; 5-95%Ni	1136-1356	The interdiffusion coefficient shows a small positive deviation from a linear increase with increasing atom fraction of nickel. Typical values of D: 1136°C, x_{Ni} = 0, $D=1.5\times10^{-11}$ $cm^2 sec^{-1}$; $x_{Ni}=0.5$, $D=4\times10^{-11}$; $x_{Ni}=1$, $D=6\times10^{-11}$ 1356°C: $x_{Ni}=0$, $D=3.7\times10^{-10}$, $x_{Ni}=0.5$, $D=8.2\times10^{-10}$, $x_{Ni}=1$, $D=1.1\times10^{-9}$.			Badia 1969.
Ni-Ni-10%Cr	Interdiffusion. Microprobe analysis	1000-1300	0.604		61.4	Davin et al 1963.
Ni-Ni-15%V			0.287		59.2	
Ni-N-13.5%Mo			0.853		64.4	

Material	Method	Temp. Range, °C.	D_s, $cm^2 s^{-1}$	D, $cm^2 s^{-1}$	Q, Kcals $mole^{-1}$	Reference
Ni-N-14.6%W			0.862		70.4	
Ni in Co-40%Ni	Ni^{63} along edge dislocations in single crystals. Pipe radius 100 Å.	506-618	3.4		30.2	Baker et al 1967, 1968.
Ni in Co	tracer diffusion of Ni^{63}	1065-1290	$7.01^{+7.34}_{-3.59}$		74.3±2.0	Million and Kucera 1971
Co-3.7%Ni			$8.68^{+9.49}_{-4.53}$		74.6±2.1	
Co-7.1%Ni			$12.6^{+7.04}_{-4.52}$		75.6±1.3	
Co-10.3%Ni			$13.7^{+17.5}_{-7.70}$		75.8±2.4	
Co-30%Ni			$7.45^{+6.06}_{-3.34}$		73.3±1.7	
Co-49.3%Ni			$4.80^{+4.23}_{-2.25}$		71.7±1.8	
Co-69.7%Ni			$5.96^{+5.63}_{-2.90}$		71.4±1.9	
Co-73.7%Ni			$6.13^{+4.87}_{-2.72}$		71.6±1.7	
Co-80.1%Ni			$3.66^{+1.65}_{-1.13}$		70.2± 1.1	
Ni			$5.01^{+5.19}_{-2.55}$		70.3±2.0	

Material	Method	Temp. Range, °C.	D_0, $cm^2 s^{-1}$ / $D, cm^2 s^{-1}$	Q, Kcals $mole^{-1}$	Reference
Co in: Co	self -diffusion of Co^{60}; sectioning technique		$2.20^{+2.41}_{-1.13}$	70.5±2.1	Million and Kucera, 1969.
Co-3.7%Ni			$1.23^{+1.23}_{-0.61}$	67.7±2.0	
Co-7.1%Ni			$1.12^{+2.55}_{-0.61}$	66.9±3.4	
Co-10.3%Ni			$0.43^{+0.75}_{-0.28}$	63.9±3.0	
Co-30%Ni			$0.10^{+0.15}_{-0.06}$	58.9±2.7	
Co-49.3%Ni			$0.18^{+0.20}_{-0.09}$	60.2±2.1	
Co-69.7%Ni			$0.40^{+0.60}_{-0.25}$	61.8±2.8	
Co-73.7%Ni			$0.09^{+0.26}_{-0.07}$	57.4±3.8	
Co-80.1%Ni			$0.22^{+0.55}_{-0.16}$	59.9±3.6	
Ni in: Co	Microprobe	1136	13×10^{-11}		Sabatier and Vignes, 1967.
Co-30.2%Fe			11.5×10^{-11}		
Co-68.5%Fe			$8\text{-}8.8 \times 10^{-11}$		
Co-88.3%Fe			5×10^{-11}		
Fe			6×10^{-11}		
Co-Fe	Interdiffusion, microprobe	1136-.356	See graph		Bazia, 1969.

Material	Method	Temp. Range, ^{o}C.	D_o $cm^2 s^{-1}$ / $D, cm^2 s^{-1}$ / boundary width δ, μm.	Q Kcals $mole^{-1}$ / $D_{gb} \times \delta$ $cm^2 s^{-1}$	Reference
Co in Fe	Grain boundary diffusion in powders; spectrographic analysis.	850	0 - 30	1.77×10^{-14}	Fedorchenko et al 1969.
		1200	0 - 18	1.8×10^{-13}	
		1200	18 - 50	1.15×10^{-13}	
Fe in Co	Grain boundary diffusion in powders; spectrographic analysis.	850	0 - 55	1.27×10^{-14}	
		1200	0 - 25	1.53×10^{-13}	
		1200	25 - 60	3.04×10^{-13}	
	Grain boundary diffusion in cast metals				Aucouturier and Lacombe, 1965.
					James and Leak, 1965.
Fe in Co	Impurity diffusion, Microprobe	1100-1400	0.11	60.5	Vignes et al 1967
Fe in Co	Heterodiffusion at infinite dilution	950-1370	0.11	60.5	Badia and Vignes 1969.
Fe in Co-50%Ni	Fe^{59} impurity diffusion, sectioning technique	1000	1.15×10^{-11}		Guiraldeng and Poyet, 1970.
		1050	2.80×10^{-11}		
		1100	1.17×10^{-10}		
		1150	2.20×10^{-10}		
		1200	6.90×10^{-10}		
		1250	1.35×10^{-9}		
		1000-1250	125	76.5	
Fe in Co	Microprobe	1136	3.5×10^{-11}		Sabatier and Vignes, 1967.
Co-19.9%Ni			$4.8\text{-}5.2 \times 10^{-11}$		

Material	Method	Temp. Range, °C.	D_o, $cm^2 s^{-1}$	Q, Kcals $mole^{-1}$	Reference
			D, $cm^2 s^{-1}$		
Co-31.6%Ni			5×10^{-11}		
Co-56%Ni			$6.6\text{-}7.3 \times 10^{-11}$		
Co-69.3%Ni			9.2×10^{-11}		
Ni			1.1×10^{-10}		
Co - Pd	Mutual diffusion coefficient, microprobe	1150°C			Borovskii et al, 1966.
Co-10% Pd			1.39×10^{-10}		
Co-20% Pd			2.82×10^{-10}		
Co-30% Pd			7.07×10^{-10}		
Co-40% Pd			1.20×10^{-9}		
Co-50% Pd			1.45×10^{-9}		
Co-60% Pd			1.20×10^{-9}		
Co-70% Pd			5.5×10^{-10}		
Co-80% Pd		1150	2.56×10^{-10}		
Co-90% Pd			1.37×10^{-10}		
Co - Pt	Interdiffusion. Microprobe	1125-1300	D_m passes through a maximum at approx. 40 at % Pt. The concentration and temperature dependence of D_m is "highly peculiar" in the range 0-20 at % Pt.		Borovskii et al, 1967.
C in Co	Impurity diffusion. Thermogravimetry	950-1050	0.53	38.5	Lafitau, 1968.
Cr in Cr		1000-1350	--	76.0	Bokshtein et al, 1957

Material	Method	Temp. Range, ^{O}C.	D_o, $cm^2 s^{-1}$	D, $cm^2 s^{-1}$	Q Kcals $mole^{-1}$	Reference
Cr in Cr		1000-1350	120		86.0	Gruzin et al, 1959.
		1100-1250	45		85.0	quoted in Fedorov et al 1968
		1000-1250	1.15×10^{-4}		52.7	Paxton and Gondolf, 1959.
		1080-1320	1.65×10^{-3}		62.4	Bogdanov, 1960.
		1050-1400	6.47×10^{-2}		59.2	Ivanov et al, 1962.
		998-1600	0.28		73.2	Hagel, 1962.
		1000-1550	0.2		73.7	Askill and Tomlin, 1965.
	Residual activity. Electrolytic Cr	1050-1583	1.4×10^{-4}		52.7	Fedorov et al, 1968.
	Iodide Cr	1075-1583	3×10^{-2}		68.1	
	Note: Fedorov et al remark that below ~ 1000°C grain boundary diffusion becomes appreciable.					
Mo in Cr	Impurity tracer diffusion	1100-1420	2.7×10^{-3}		58.0	Borisov et al, 1968.
Cr-Pd	Interdiffusion. Electron probe micro-analysis. 0-40 at % Cr in Pd. The interdiffusion coefficient increases with increasing Cr content. The extrapolated Cr diffusion coefficient in Pd at	1200		3.5×10^{-10}		
C in Cr	Impurity trace diffusion	1200-1500	9.0×10^{-3}		26.5	Borisov et al, 1968.
C in Cr (H)	C^{14}. Serial sectioning, in the presence of hydrogen.	1200		0.57×10^{-6}		Zemskii and Pyakhin, 1967.
		1300		1.72×10^{-6}		
		1400		3.58×10^{-6}		
		1500		6.12×10^{-6}		
		1200-1500	0.4		39.0	
N in Cr	Internal friction, elastic after effect 10, 25, 80 ppm N.	65-190	1.6×10^{-2}		27.5	Klein, 1967.
C in Cr-0.5%Fe	Impurity tracer diffusion	1400-1600	4.5×10^{-2}		26.5	Borisov et al, 1968.
C in Cr-1%Fe	Impurity tracer diffusion	1400-1600	2.0×10^{-2}		24.0	Borisov et al, 1968.

Material	Method	Temp. Range, °C.	Do cm^2s^{-1} D, cm^2s^{-1}	Q Kcals mole $^{-1}$	Reference
C in Cr-18Ta	Impurity tracer diffusion	1300-1500	5.0×10^{-3}	28.8	Borisov et al, 1968.
Fe in alpha Fe	Sectioning technique: residual activity. Ferromagnetic		27.5	60.7	James and Leak 1966.
	Ferromagnetic		2.0	60.0	Buffington et al 1961.
	Paramagnetic		2.01	57.5	James and Leak 1966.
	Paramagnetic		1.9	57.2	Buffington et al 1961.
	Paramagnetic		2.0	57.3	Graham and Tomlins 1963.
	Paramagnetic		118	67.24	Borg and Birchenall 1960.
Fe in delta Fe			2.01	57.5	James and Leak 1966.
			1.9	57.0	Borg et al, 1962.
			6.8	61.7	Graham and Tomlin 1963.
			0 019	42.4	Steffanson and Birchenall, 1961.
			8.3	60.8	Price et al, 1964.
Fe in alpha Fe	Absorption method. 99.92% purity, 170-230 µm grain size.	809-889	5.4	60.3	Angers and Claisse 1968.
Fe in gamma Fe	Absorption method	950-1200	4.065	74.30	Ivantsov & Blinkin 1966.
Fe in gamma Fe	Residual activity measurement	-	0.5	68.0	Badia, 1969.
Fe in gamma Fe	Thin layer tracer technique	1000-1350	4.58	60.2	Kalinovich et al 1969.
Fe in gamma Fe	Serial sectioning	1171-1361	$0.49^{+0.38}_{-0.29}$	67.86 ± 1.45	Heumann and Imm 1968.
Co in Fe	Sectioning technique. alpha Fe, ferromagnetic.		7.19	62.2	James and Leak 1966.
	alpha Fe, paramagnetic		6.38	61.4	James and Leak 1966.
	ditto.,		9.5	62.3	Sato 1964.
	ditto.,		118	68.3	Borg and Lai 1962.
	delta Fe		6.38	61.4	James and Leak 1966.

Material	Method		Temp. Range, °C.	$D, cm^2 s^{-1}$	Q Kcals $mole^{-1}$	Reference
Co in Fe	Heterodiffusion at infinite dilution. Electron probe microanalysis.		1130-1360	1.0	72.1	Badia and Vignes 1969.
	Electron probe microanalysis		1100-1'00	0.17	67.0	Vigner et al, 1967.
Co in Fe-Ni	ditto.,	% Ni	1136			Sabatier and Givnes, 1967.
		0		0.6×10^{-11}		
		15.6		0.9×10^{-11}		
		31.6		$(1.5-1.6) \times 10^{-11}$		
		56		4×10^{-11}		
		69.3		$(4.8-4.9) \times 10^{-11}$		
		100		$(7.8-8) \times 10^{-11}$		
Cr in Fe	Microprobe analysis - gamma Fe		-	4.08	68.5	Bowen and Leak 1970
	Residual activity. gamma Fe		950-1400	$10.80^{+3.35}_{-2.56}$	69.7±1.7	
		alpha Fe	800-880	$8.52^{+3.20}_{-2.33}$	59.9±1.6	
Cr in Fe	Sectioning technique. Impurity diffusion of Cr^{51} in 99.95% pure polycrystalline alpha Fe					
	volume diffusion		775-875	2.53	57.5	Huntz et al, 1967.
	grain boundary diffusion		600-725	$D'=1.8 \times 10^{-4} cm^3 s^{-1}$	52.0	
Cr in Fe	Microprobe. Interdiffusion. Calculated Cr diffusivity in gamma Fe.		1300	3.6×10^{-10}		Hosoi et al, 1967.
Cr in Fe-15. and Fe-1.7%V	Cr Tracer diffusion, sectioning technique. For both alloys			2.0	57.0	Pavlinov et al, 1968.
Fe in Fe-Cr	Residual activity method, Fe^{59}					
	Fe-9.13%Cr		777-825	0.42	52.4	Ray and Sharma 1968
			575-726	9.27	55.1	
	Fe-15.22% Cr		726-777	0.27	51.5	
			595-677	1.25	54.1	
	Fe-19.75%Cr		690-825	0.18	49.7	
			575-646	0.65	51.9	

Material	Method	Temp. Range, °C.	D_0, $cm^2 s^{-1}$	D, $cm^2 s^{-1}$	Q Kcals $mole^{-1}$	Reference
Cr in Fe-Cr	Residual activity	800-1400				
	Fe-13% Cr		0.64		55.4	Bowen and Leak, 1970 (b)
	Fe-16% Cr		0.19		52.1	
	Fe-19% Cr		0.18		51.8	
Cr in Fe	Local spectroscopy	1250		1.1×10^{-10}		Krishtal and Mokrov, 1967.
		1300		0.9×10^{-9}		
Fe - Cr	Interdiffusion. Surface removal and X-ray fluorescence analysis. Work done on Fe- (0-50%) Cr- (0-7%)Al. Data shown are for Al-free alloys. Al additions up to 2% increase the Cr penetration rate; further additions retard it.	1100	at % Cr			
			25	15.5×10^{-10}		Demo, 1967.
			40	7.54×10^{-10}		
Mo in Fe-Cr	Sectioning technique. % Cr					
	11.83	728-833	0.14		50.4	Kucera et al, 1969.
	17.10	800-1343	0.074		48.5	
	25.80	1073-1329	0.059		47.?	

Material	Method		Temp. Range, °C.	D_0 $cm^2 s^{-1}$		Q Kcals $mole^{-1}$	Reference
					D, $cm^2 s^{-1}$		
V in Fe-Cr	Sectioning technique.	% Cr.					
		11.83	800-1316	0.086		48.6	Kucera et al 1969.
		17.10	1050-1300	0.061		46.2	
		25.80	1112-1313	0.46		52.4	
W in Fe-Cr		11.83	800-1344	0.030		47.1	
		17.10	1074-1330	0.041		48.6	
		25.80	1083-1342	0.066		50.4	
Mn in Fe	Residual activity		700-760	1.49		55.8	Nohara and Hirano, 1970.
			800-900	0.35		52.5	
			920-1280	0.16		62.5	
Mn in Fe	Local spectroscopy		1300		0.8×10^{-9}		Krishtal and Mokrov, 1967.
Mn in Fe	Mn from Fe-2Mn into Fe.		1050-1240	3.8×10^{-2}		59.0	Krishtal and Mokrov, 1967.
	Chemical diffusion. Layer by layer emission spectral analysis Mn from Fe-2 Cr-2Mn into Fe-2Cr.		1050-1290	0.23		65.0	
Mo in Fe	Mo from Fe-2 Mo into Fe.		1050-1280	4.3×10^{-2}		57.0	ditto.,
	Mo from Fe-2Mo-2Cr-2Mn-2Ti into Fe-2Cr-2Mn-2Ti		1050-1290	20.4		75.0	
Mo in Fe	Interdiffusion. Metallography		1090-1250	0.44		57.0	Krishtal and Mokrov, 1967 (b)
Mo in Fe	Local spectroscopy		1300		1.5×10^{-9}		Krishtal and Mokrov, 1967.
Fe-Mo	Interdiffusion. Displacement of interface between alpha and epsilon region, and by electron probe microanalysis.		790-1185	10		60	Pivot et al, 1969.
Ni in Fe	Heterodiffusion at infinite dilution.		1130-1360	3		75.0	Bauia and Vignes, 1969.
	Electron microprobe.		1140-1360	0.06		65.0	Badia and Vignes, 1967 (b)
	Impurity diffusion of Ni in Fe		1150-1400	6.92		77.6	MacEwan et al 1959.
			930-1050	0.77		67.0	Hirano et al, 1969.
			950-1130	0.344		67.5	Niemann and Shinyaev, 1953.

Material	Method	Temp. Range, °C.	Do cm^2s^{-1}	D, cm^2s^{-1}	Q Kcals $mole^{-1}$	Reference
Ni in Fe	Layer by layer spectral analysis and electron microscopy.					
	99.6% Fe	1000-1200	0.9		64.7	Krishtal et al, 1968
	99.98% Fe	1000-1200	1.25		67.7	
Ni in Fe	Electron probe microanalysis	1100-1400	0.6		62.6	Vignes et al, 1967
Ni in Fe-Ni	Microhardness measurements and local X-ray analysis F-(2.5-10)% Ni.	1000-1200	1.25		67.7	Krishtal et al, 1967
Ni in Fe-Ni	Residual activity method fcc alloys at % Ni					
	0.2		1.09		69.33±1.37	Hancock and Leak, 1967
	0.55		1.09		69.33±1.37	
	2.29		0.593		67.30±1.23	
	5.8		2.11		73.5	MacEwan et al, 1959
	9.21		0.497		66.40±1.52	Hancock and Leak,1967
	14.88		5.0		75.6	MacEwan et al, 1959
	19.34		0.409		65.41±0.78	Hancock and Leak, 1967
Fe-Ni	Mutual diffusion coefficient. Marker shift, at % Ni	1200				
	10			0.5×10^{-10}		Levasseur and Philibert 1967.
	25			1.0×10^{-10}		
	42			2.0×10^{-10}		
	55			3.0×10^{-10}		
	75			4.8×10^{-10}		
	90			4.0×10^{-10}		
N in Fe-Mn	Residual activity method fcc alloys, at % Mn.					
	0.42		0.495		67.46±1.45	Hancock and Leak, 1967
	1.26		0.364		66.83±2.53	
	4.60		0.144		64.61±1.07	
	9.7		0.132		63.90±1.85	

Material	Method	Temp. Range, °C.	Do $cm^2 s^{-1}$	Q Kcals $mole^{-1}$	Reference
			D, $cm^2 s^{-1}$		
Ni in Fe-Cr	Residual activity method. bcc and fcc alloys at % Cr				
	2.02 (fcc)		0.356	65.58±1.19	Hancock and Leak, 1967
	5.73 (fcc)		0.282	65.22±2.84	
	9.47 (fcc)		0.12	63.38±2.32	
	14.1 (bcc)		0.016	56.71±2.76	
	20.1 (bcc)		0.007	53.59±0.69	
Fe - Pd	Mutual diffusion. Microprobe analysis, at % Fe	950 and 1150	$Dx10^{11} cm^2 sec$ 950°C / 1150°C		Borovskii et al, 1966
	10		2.42 / 22.9		
	20		5.22 / 59.1		
	30		8.65 / 144		
	40		7.92 / 163		
	50		5.67 / 142		
	60		3.09 / 65.4		
	70		0.94 / 25.0		
	80		0.17 / 12.0		
	90		0.54 / 7.5		
Ti in Fe	Micrprobe analysis	1150 - 1300	$8.5x10^3$	90.0	Swisher, 1968.
Fe in Fe alloys	Sectioning technique at % solute.				
	4.8 Ge	900-1200	4.8	58.0±1	Lai and Borg, 1967
	2.5 Sb	896-1097	0.51	51.8±2	
	2.0 Ti	900-1200	2.8	57.8±1	
	5.7 Al	850-1185	3.7	58.7±1	
	1.8 V	900-1500	1.4	56.6±1	
	5.3 V	900-1193	1.87	57.4±1	
	4.7 Si	900-1460	1.63	55.5±1	
Al in Fe	Electronprobe microanalysis	800-1400	5.9	57.7±1	Vignes et al, 1967.
Fe - Al	Interdiffusion in bcc alapha phase. Electronprobe microanalysis.				Hirano and Hishinuma 1968.
	% Al				
	9 disordered phase	920-1210	$2.7x10^{-1}$	44.9	
	17 "	920-1210	$3.6x10^{-3}$	34.0	
	25 "	920-1210	$7.0x10^{-2}$	39.9	
	33 "	1100-1210	$7.3x10^{-3}$	31.0	
Fe - Al	33 ordered phase	800-1000	$2.1x10^4$	69.4	
	41 "	800-920	$1.5x10^5$	72.9	

Material	Method	Temp. Range, °C.	Do $cm^2 s^{-1}$ D, $cm^2 s^{-1}$	Q Kcals mole	Reference
Hf in gamma Fe	Residual activity	1110-1360	3600^{+1600}_{-1100}	97.3±2.6	Bowen and Leak, 1970
V in gamma Fe	ditto.	1120-1380	$0.28^{+0.16}_{-0.08}$	69.31±2.2	ditto.,
W in Fe	Interdiffusion. Metallography. Chemical diffusion of W in alpha Fe-W	1090-1250	25	71.0	Krishtal and Mokrov 1967 (b)
	Chemical diffusion of W in gamma Fe-W	1090-1250	460	81.0	
Si in Fe	Local spectroscopy	1300	2.7×10^{-9}		Krishtal and Mokrov 1967.
Fe in Fe-Si	Mössbauer effect.	850-1050	$0.20^{+0.65}_{-0.15}$	49.6±3.7	Lewis and Flinn 1969.
Si in Fe and alloys	Chemical diffusion. Layer by layer emission spectral analysis. Si from Fe-2Si into Fe	1050-1280	6.4×10^{-3}	49.0	Krishtal and Morova 1967.
	Si from Fe-2 Cr-2 Mn-2 Ti-2Si into Fe-2Cr-2Mn-2Ti	1050-1290	0.15	61.0	
Fe-Si	Chemical analysis, marker movements	1130-1220			Onishi and Mitani 1963.
	Chemical diffusion		1.8	50	
	Partial diffusion; Fe		5.6	54	
	Si		2.2	50	
S in Fe	Resistivity measurements				
	alpha Fe	780-880	2.7	49.0	Wang and Grable 1970
	gamma Fe	935-1025	0.5	50.0	
S in Fe	Residual activity. Gamma Fe	900-1250	1.7	53.0	Hoshino and Araki 1970
S in Fe	Surface residual activity grain boundary diffusion.	1100-1250	$D_o'\delta = 1.1 \times 10^{-5} cm^3 s^{-1}$	23.0	Hoshino and Araki 1971
S in Fe	Autoradiographym alpha Fe	800-900	1.07	40.2	Zemski et al 1970
	gamma Fe	1000-1200	2.46×10^{-3}	36.1	
S in Fe	Residual activity measurements. Effect of C and O contents of electrolytic iron on intergranular diffusion.				

Material	Method	Temp. Range, ^{o}C.	cm^2s^{-1} D, cm^2s^{-1}	$Kcals^{Q}mole^{-1}$	Reference
	200 ppm C, 20 ppm O, 20 ppm S	960-1090	$D_o' = 2.2 \times 10^{-6} cm^3 s^{-1}$	27.0	Aucouturier et al 1968
	20 ppm C, 800 ppm O, 100 ppm S	800-1200	1.5×10^{-6}	23.1	
S in Fe-Mn	Internal sulphidation of 0.19, 0.41, 0.87% Mn alloys	750-850	1.68	42.8	Herrnstein et al 1968.
S in Fe-Si	Sectioning, surface activity and autoradiography. Fe-3%Si-0.003%C-0.001%S-0.007%N				
	Volume diffusion	700-1200	1.7×10^{-2}	61.2	Gruzin et al 1971
	grain bonding diffusion	700-860	$D_o' = 4.1 \times 10^{-6} cm^3 s^{-1}$	35.7	
S in Fe-Si	Fe-3.25% Si	900-1300	2.68	49.7	Ainslie and Seybolt 1960
O in Fe	Internal oxidation, metallography	700-850	0.4 ± 0.1	39.9 ± 0.3	Barlow and Grundry 1969
N in Fe	Thermogravimetry during nitriding and denitriding alpha Fe		1.5×10^{-2}	19.1 ± 0.5	Bohnekamp 1967
	alpha Fe		6.6×10^{-3}	18.6	Fast and Verrijp (1954)
	gamma Fe		0.2	36.0	Bohnekamp 1967 and Fast and Verrijp (1954)
Mo in: Mo-0.1%W	Mo^{99}	1800-2400	1.42×10^{2}	112.0	Frantsevich et al, 1969
Mo-15%W		1400-2400	2.65×10^{2}	106.0	
Mo-20%W		1400-2400	1.46×10^{2}	102.0	
Mo-25%W		1400-2400	47	95.0	
Mo-35%W		1500-2400	28	92.0	
Mo-50%W		1700-2500	12	88.0	
Mo-65%W		1800-2600	1.3	86.0	
Mo-75%W		1800-2800	0.2	84.5	
Mo-80%W		1800-2800	0.11	82.0	
Mo-85%W		1800-2800	8.0×10^{-2}	80.0	
Mo-99.9%W		2200-2800	2.5×10^{-3}	78.0	
W in: Mo-0.1%W	W^{185}	1800-2400	8.5×10^{-3}	71.0	Frantsevich et al, 1969

Material	Method	Temp. Range, °C.	Do cm^2s^{-1}	Q Kcals $mole^{-1}$	Reference
			D, cm^2s^{-1}		
W in:					
Mo-15%W		1400-2400	1.4	73.0	
Mo-20%W		1400-2400	1.7	74.6	
Mo-25%W		1400-2400	2.2	77.0	
Mo-35%W		1500-2400	6.9	85.0	
W in:					
Mo-50%W		1700-2500	14	95.0	
Mo-65%W		1800-2600	16	102.0	
Mo-75%W		1800-2800	20	116.0	
Mo-80%W		1800-2800	22	119.0	
Mo-85%W		1800-2800	25	122.0	
Mo-99%W		2200-2800	24	130.0	
W in Mo	Radiotracer, serial sectioning	2075	$1.0x10^{-10}$		
		2180	$3.11x10^{-10}$		
		2260	$4.07-4.67x10^{-10}$		
		2075-2260	1.7	110.0	
W in Mo	Residual activity method	1700-2150	$4.5x10^{-4}$	77.5	Borisov et al, 1968,
Co in Mo	Residual activity method	1000-1500	6	77.5	Borisov et al, 1968.
Cr in Mo	Residual activity method	1000-1500	$2.5x10^{-4}$	54.0	Borisov et al, 1968.
Cr^{59} in Mo	Radioactive tracer technique.				
	Volume diffusion: sintered Mo	1000-1150	0.14	73.9±2.5	Mulyakaev et al, 1971
			0.18	74.9±2.0	
			1.88	81.8±4.8	
			D'δ, cm^3s^{-1}		
	grain boundary diffusion: sintered Mo	1000 1150	$7.62x10^{-10}$	40.0±5.3	
	vacuum melted Mo		$9.05x10^{-5}$	74.2±4.8	
Ta in Mo	Residual activity method	1700-2150	$3.5x10^{-4}$	83.0	Borisov et al, 1968.
w in Mo	Microprobe, metallography	1800-2200	140	136.0	Roux et al.

Material	Method	Temp. Range, °C.	Do cm^2s^{-1} D, cm^2s^{-1}	Q Kcals $mole^{-1}$	Reference
Mo - Nb	Interdiffusion. Incremental diffusion couples. Microprobe. Kirkendall shift.				Hartley et al, 1965
Mo in 100%Mo		1300-2160	40	115.0	
Nb-19.9%Mo			$1.4x10^3$	136.5	
Nb-16.2%Mo			$1.1x10^3$	134.6	
Nb			$9.2x10^2$	131.2	
Nb in: Mo			$1.0x10^3$	139.1	
Nb-19.9%Mo			$1.3x10^4$	139.9	
Nb			$1.9x10^3$	131.0	
Mo in Ta-rich Mo-Ta alloys	Microprobe. Diffusion couples.	1900-2300	$4.68x10^{-5}$	60.0	Ivanov et al, 1970.
Ta in Mo-rich Mo-Ta alloys			$4.16x10^{-5}$	56.0	
Mo-Ti	Interdiffusion. Incremental diffusion couples. Microprobe. Kirkendall shift.	820-1600			Hartley et al, 1965.
Mo in Ti-11.1%Mo			$1.0x10^{-2}$	48.7	
in ti			$2.5x10^{-2}$	47.0	
Ti in Ti-11.1%Mo			$1.8x10^{-3}$	38.4	
Ti in Mo			$6.3x10^{-6}$	50.5	
Ni in Ti-12%Mo	Autoradiography. Ni^{63}	820-1050	$4.0x10^{-1}$	43.5	Bokshtein et al, 1968
Mo-Ti	Interdiffusion. Microprobe	900-1500	D decreases more or less linearly with increasing Mo at all temperatures. At 900°C; 20% Mo, $D=2x10^{-12}$ cm^2s^{-1}. 40% Mo, $1.5x10^{-13}$. At 1500°C, 25% Mo, $D=3x10^{-10}$; 45% Mo, 10^{-11} cm^2s^{-1}		Fedotov et al, 1969.
N in Mo	$5x10^{-5}$ - 500 torr pressure	827-2227	$2.3x10^{-2}$	33.0	Frauenfelder, 1968.

Material	Method	Temp. Range, °C.	Do cm^2s^{-1} D, cm^2s^{-1}	Q Kcals $mole^{-1}$	Reference
N in Mo	Monitored gas release from N-containing specimens.	1500-2000	$3.0x10^{-3}$	40.3	Evans and Eyre, 1968, 1969.
N in Mo	Outgassing of gassed specimens	1300-2000	$4.3x10^{-3}$	26.0	Jehn and Fromm 1970.
C in Mo	Chem. analysis of carburised specimens.	1780-1970	$3.4x10^{-2}$	41.0	Rudman 1967.
C in Mo	Residual activity	1200-1600	$2.04x10^{-2}$	41.0	Nakonechnikov et al 1966.
C in Mo	Internal Friction	100-400	$2.8x10^{-4}$	166.5	Shchelkonogov et al, 1968.
O in Mo	Internal Friction	77	$3.46x10^{-16}$	22.0	
O on Mo	Internal Friction		$3.0x10^{-2}$	31.0±2.0	Baranova et al 1968.
Si in Mo	Chemical diffusion of silicon from various sources - Si, $MoSi_2$, SiO SiO_2.	1600-2200	At 1800°C, D varied from $2.5x10^{-7}$ cm^2s^{-1} to $3x10^{-8}$ cm^2s^{-1} for the different sources.		Lassner et al, 1968.
S in Mo	Sectioning technique. S^{35} in 99.9% + Mo	1947	$3.2-4.6x10^{-8}$		Vandyshev and Panov, 1968 (a)
		2007	$6.4-7.3x10^{-8}$		
		2067	$13-14x10^{-8}$		
		2127	$20-23x10^{-8}$		
		2197	$39x10^{-9}$		
		1947-2197	320	101.0	
P in Mo	Serial sectioning, p^{32}	2000	$4.8x10^{-9}$		Vandyshev and Panov, 1968 (b)
		2050	$6.1x10^{-9}$		
		2100	$8.1x10^{-9}$		
		2150	$1.3x10^{-8}$		
		2200	$2.1x10^{-8}$		

Material	Method	Temp. Range, °C.	Do $cm^2 s^{-1}$	Kcals $mole^{-1}$	Reference
			D, $cm^2 s^{-1}$		
P in Mo	Serial sectioning, P^{32}	2000-2200	0.19	80.5	
K in Mo	K^{42}, sectioning technique.				
	Polycrystals	800-1100	1.78×10^{-10}	13.7	Karpman et al, 1967; see also Dubinin et al 1969.
	single crystals		5.5×10^{-9}	25.0	
Na in Mo	Na^{24}, serial sectioning				
	Polycrystals	800-1100	4.2×10^{-10}	13.3	Dubinin et al, 1969
	Single crystals		2.95×10^{-9}	21.2	
Cr in Nb	Single crystals	953-1435	$0.30^{+0.28}_{-0.14}$	83.5±1.8	Pelleg, 1968.
	Polycrystals	947-1493	$0.13^{+0.12}_{-0.06}$	80.6±1.9	
Ti in Nb	Anodising/stripping technique, Ti^{44} in single crystals	994-1492	$(0.99^{+1.00}_{-0.50}) \times 10^{-1}$	86.9±2.2	Pelleg, 1970
V in Nb		1000	1.78×10^{-15}		Agarwala et al, 1968,
		1050	5.62×10^{-15}		
		1100	2.30×10^{-14}		
		1150	7.08×10^{-14}		
		1200	1.80×10^{-13}		
		1250	5.62×10^{-13}		
		1300	1.41×10^{-12}		
		1350	3.12×10^{-12}		
		1400	6.30×10^{-12}		
		1000 - 1400	2.21	85.0	
V in:	Incremental diffusion couples. Microprobe. Kirkendall shift.	1404 - 1505			
V-15%Nb			2.6×10^{-2}	59.0	Hartley et al, 1965.
V-20% Nb			4.2×10^{-2}	60.5	
Nb			2.9	96.8	

Material	Method	Temp. Range, °C.	D_0, cm^2s^{-1}	D, cm^2s^{-1}	Q, Kcals $mole^{-1}$	Reference
Nb in V			8.6×10^{-2}		65.7	
V-15%Nb			4.9×10^{-2}		66.4	
V-20%Nb			1.1×10^{-2}		61.4	
Nb-10%V	Microprobe of diffusion couples. Mutual diffusion coefficients.	1300°C		1.4×10^{-11}		Prokoshkin et al, 1967
Nb-90%V				2.3×10^{-10}		
Nb-10%Mo				8.75×10^{-12}		
Nb-90%Mo				1.67×10^{-12}		
Nb-10%Ta				1.58×10^{-13}		
Nb-90%Ta				2.76×10^{-14}		
Nb-10%W				1.39×10^{-14}		
Nb-90%W				3.75×10^{-15}		
Nb-10%Zr				1.75×10^{-11}		
Nb-90%Zr				2.5×10^{-10}		
Nb-10%Ti				3.48×10^{-11}		
Nb-90%Ti				3.9×10^{-10}		
Nb in: Nb	Sectioning, residual activity		28.18		113.0	Lyubimov et al, 1967.
Nb-5%W			2.334×10^{3}		130.0	
Nb-10%W			1.64×10^{2}		117.0	
Nb-30%W			2.57×10^{-2}		85.0	
Nb - Ti	Incremental diffusion couples. Microprobe. Kirkendall shift	1000-1588				Hartley et al, 1965.
Nb in Ti			3.8×10^{-3}		39.2	
Ti-18.9% Nb			2.2×10^{-3}		42.3	
Ti in Nb			5.0×10^{-4}		61.9	

Material	Method	Temp. Range, °C.	Do cm^2s^{-1} D, cm^2s^{-1}	Q Kcals $mole^{-1}$	Reference
Ti-18.9%Nb			1.7×10^{-3}	39.1	
Nb - Ti	Microprobe. Interdiffusion. At all temperature, D falls approximately with increasing Nb content.	900-1350	At 900°C, 10% Nb, $D=3\times10^{-11}$ cm^2s^{-1}; 60% Nb, 10^{-13} cm^2s^{-1}. At 1350°C, 40% Nb, 10^{-10} cm^2s^{-1}; 90% Nb, $2\times10^{-12}cm^2s^{-1}$		Fedotov et al, 1969
Nb - Zr	Incremental diffusion couples. Microprobe Kirkendall shift. Intrinsic diffusion.	870-1690			Hartley et al, 1965.
Nb in Zr			1.1×10^{-2}	45.6	
Zr-23%Nb			0.69	65.0	
Zr in Nb			2.2	99.2	
Zr-23%Nb			3.8×10^{-3}	44.2	
Co-Co-25%Cr	Interdiffusion. Microprobe analysis.	1000-1300	0.14	60.6	Green et al, 1973.
Co-Co-40% Cr	Interdiffusion. Sectioning and chemical analysis	1000-1360	0.44	63.6	Weeton 1952
Co-Co-15% Cr	Interdiffusion. Microprobe analysis	1000-1300	0.08	60.6	Davin et al 1963
Co-Co-15%V			0.021	53.0	
Co-Co-15% Mo			0.231	62.8	
Co-Co-15%W			0.008	56.9	
S in Nb	S^{35} in Nb single crystals	1097-1497	2.6×10^{3}	73.1	Vandyshev and Panov, 1968.
	In polycrystalline Nb, autoradiography shows that S diffuses along grain boundaries.				
C in Nb	Internal friction	50-140	0.015	27.0	Wert, 1950
C in Nb	Internal friction	130-280	0.004	33.2	Powers and Doyle, 1959
C in Nb		900-1100	1.09×10^{-5}	32.0	Gel'd and Iyubimov, 1961

Material	Method	Temp. Range, ^{o}C.	Do cm^2s^{-1}	Q_{mole}^{-1} Kcals	Reference
			D, cm^2s^{-1}		
C in Nb	Serial sectioning, C^{14} in 99.5%Nb	950-1800	0.033	37.9	Son et al, 1967
C in Nb	Decarburisation in low oxygen pressures	1500-2200	D is 10^{-5} cm^2sec^{-1} at 2200°C, approx. $3x10^{-6}$ at 1500°C.		Melchior, 1969.
C in Nb	C^{14}. Residual activity	1100-1400	$9.32x10^{-3}$	35.0	Nakonechnikov et al 1966.
C in Nb	Residual activity	800-1250	$1.09x10^{-5}$	32.0	Lyubimov et al, 1969
C in Nb-5%Mo	Residual activity		$1.12x10^{-11}$	7.0	Lyubimov et al, 1969
Nb-10%Mo			$1.2x10^{-8}$	15.5	
Nb-20%Mo			$7.9x10^{-8}$	18.0	
C in Nb-5%W			$3.0x10^{-11}$	4.8	
Nb-10%W			$4.45x10^{-9}$	10.2	
Nb-20%W			$8.05x10^{-9}$	10.6	
Nb-30%W			$3.0x10^{-9}$	10.9	
C in Nb-5%Ti			$3.0x10^{-9}$	8.9	
Nb-15.1%Ti			$1.40x10^{-9}$	7.7	
Nb-29.8%Ti			$3.00x10^{-10}$	5.1	
Nb-40.9%Ti			$1.10x10^{-10}$	2.9	
C in Nb-5%Zr			$1.99x10^{-7}$	11.7	
Nb-15.1%Zr			$2.24x10^{-7}$	10.5	
Nb-24.2%Zr			$5.63x10^{-10}$	9.5	
Nb-36.1%Zr			$1.5x10^{-10}$	8.4	
P in Nb	Serial sectioning, P^{32} in Nb single crystals	1300-1800	$5.1x10^{-2}$	51.5	Vandyshev and Panov. 1968
K in Nb	Sectioning technique, K^{42}.				
	single crystal Nb	900	$1.955x10^{-13}$		Karpman et al, 1967.
		1000	$3.875x10^{-13}$		See also Dubinin et al 1969

Material	Method	Temp. Range, ^{o}C.	Do cm^2s^{-1}	Q Kcals mole	Reference
			D, cm^2s^{-1}		
		1100	782×10^{-13}		
		900 - 1100	2.38×10^{-9}	22.1	
	Polycrystalline Nb	900	9.12×10^{-13}		
		1000	13.05×10^{-13}		
		1100	21.7×10^{-13}		
		900 - 1100	2.09×10^{-10}	13.6	
Na in Nb	Sectioning technique, Na^{24}				Dubinin et al 1969.
	Single crystal Nb	900	5.886×10^{-13}		
		1000	8.71×10^{-13}		
		1100	19.2×10^{-13}		
		900 - 1100	1.611×10^{-9}	18.6	
	Polycrystalline Nb	900	27.7×10^{-13}		
		1000	44.7×10^{-13}		
		1100	51.23×10^{-13}		
		900 - 1100	1.15×10^{-9}	10.0	
O in Nb-20.15wt%Ti	Microhardness	600 - 1000		20.0 $\pm$2.0	Perrin, 1971
Ni in Ni	Self diffusion in polycrystals	900 - 1200	2.22	69.2	Ivantsov 1966
			-	61.0 -65.0	Burgess and Smoluchowski 1955.
			1.27	66.8	Hoffman et al, 1956
			0.40	63.8	Reynolds et al, 1957
			0.48	65.9	Upthegrove & Sinnott 1958
			3.36	69.8	MacEwan et al 1959
			5.12	71.0	MacEwan et al 1959

Material	Method	Temp. Range, °C.	Do cm^2s^{-1}	Q Kcals/mole	Reference
			D, cm^2s^{-1}		
			1.00	66.7	Fedorov et al 1961
			2.59	69.5	Shinyaev 1963
		1000-1400	9.96	60.5	Kalinovich et al 1968
Ni in Ni		1100-1300	-	66.8	Swalin and Allan, 1956
	Residual activity	927-1327	1.27	67.2	Badia, 1969, also Mouma, 1964
			1.39	65.9	Hassner, 1962, Hassner and Lange, 1965.
	Single crystal results		2.59	70.1	Ivantsov 1966.
			5,8	69.7	Messner et al 1961
	Sectioning technique, Ni^{63} in 5N Ni	980-1400	Arrhenius plot is gradual curve. At 980°C, $D=2.4\times10^{-12}$, at 1200°C, 1.4×10^{-10}, at 1400°C, 2.3×10^{-9} cm^2s^{-1}		Bakker 1965
Ni-Ni-10%Cr	Interdiffusion. Microprobe analysis	1000-1300	0.604	61.4	Davin et al 1963
Ni-Ni-15%V			0.287	59.2	
Ni-Ni-13.5%Mo			0.853	64.4	
Ni-N-14.6%W			0.862	70.4	
Th in Ni	α-ray spectrometric techniques, as a function of oxygen pressure. In dry H_2.	1300		$1.11\pm0.16\times10^{-14}$	Alcock and Brown 1969
				$1.15\pm0.23\times10^{-14}$	
				$0.964\pm0.121\times10^{-14}$	
		1315		$2.85\pm0.56\times10^{-14}$	
		1350		$5.46\pm0.94\times10^{-14}$	
		1375		$7.86\pm1.37\times10^{-14}$	

Material	Method	Temp. Range, °C.	Do $cm^2 s^{-1}$	Q Kcals $mole^{-1}$	Reference
				$D, cm^2 s^{-1}$	
		1400		$3.73 \pm 0.75 \times 10^{-13}$	
	$I_{..}^{CO}/CO_2$: $P_{O_2} = 2 \times 10^{-14}$ atm	1340		$3.05 \pm 0.43 \times 10^{-14}$	
		1350		$4.35 \pm 0.86 \times 10^{-14}$	
Th in Ni		1370		$8.32 \pm 1.62 \times 10^{-14}$	
	2×10^{-10} atm	1295		$1.46 \pm 0.42 \times 10^{-14}$	
		1335		$5.25 \pm 1.05 \times 10^{-14}$	
		1354		$10.0 \pm 2.0 \times 10^{-14}$	
	2×10^{-9} atm	1320		$10.3 \pm 2.1 \times 10^{-14}$	
		1350		$32.3 \pm 3.7 \times 10^{-14}$	
		1380		$71.7 \pm 13.7 \times 10^{-14}$	
Fe in Ni	Impurity diffusion	1140-1360	0.28	60.5	Badia and Vignes, 1967
Fe in Ni	Impurity diffusion	950-1130	8.4×10^{-3}	51.0	Niemann and Shinyaev, 1953.
Fe in Ni	Heterodiffusion at infinite dilution	950-1370	0.22	60.4	Badia and Vignes, 1969 MacCoy and Murdock, 1963 Guiraldeng, 1964
Fe - Ni	Intrinsic diffusion coefficients. 31 - 33% Ni	1140-1360	1.6	72.5	Badia and Vignes, 1967 see also Borovskii et al 1967.
Ni in $FeNi_3$	Ni^{63} sectioning. Self diffusion is at a maximum at this composition; activation energy shows a sharp minimum:	814-1200			DeReca and Pampillo 1967
	At % Ni				
	65		16.7×10^{-3}	54.8	
	70		6.80×10^{-3}	51.9	
	73		1.95×10^{-3}	48.7	
	74		1.76×10^{-3}	47.7	
	80		7.19×10^{-3}	52.3	

Material	Method	Temp. Range, °C.	Do cm^2s^{-1}	Q Kcals $mole^{-1}$	Reference
			D, cm^2s^{-1}		
Fe in Ni	Serial sectioning technique. Impurity diffusion of Fe^{59}.	1020-1263	$7.4x10^{-2}$	58.6	Shinyaev, 1969
Ni in Ni-50%Fe	Serial sectioning. Self-diffusion of Ni^{63}.	1013-1235	66	77.0	Shinyaev, 1969.
Ni in Ni-20%Fe	Serial sectioning. Self-diffusion of Ni^{63}	1013-1235	418	68.4	Shinyaev, 1969.
Co in Ni	Impurity diffusion	1130-1360	0.16	60.2±1.0	Badia and Vignes 1967.
Co in Ni	Impurity diffusion	900-1250	1.46	68.3	Ruder and Birchenall 1951.
Co in Ni	Impurity diffusion	748-1192	0.75	64.7	Hirano et al 1962
Co in Ni	Impurity tracer diffusion of Co^{60} in electrolytic Ni	850-1200	$1.6x10^{-4}$	60.6	Borisov et al 1968.
Co in Ni	Heterodiffusion at infinite dilution	850-1370	0.59	64.4	Balia and Vignes 1969
Cu in Ni	Impurity diffusion. X-ray back reflection	650-890	$1.1x10^{-3}$	35.5	Matano, 1932
	lathe section	947-1054	$1.5x10^{-6}$	26.0	De Silva and Mehl, 1951
	X-ray	700-1000	0.5	56.5	Pines et al 1963.
	lathe section	1054-1359	0.57	61.7±2.2	Monma et al 1964.
	residual activity	850-1050	0.724	61.0	Anand et al 1965.
	thin film microprobe	775-1050	0.27±0.06	6.0±0.6	Helfmeir and Feller-Kniepmeier 1970.
	X-ray	1000		$\sim10^{-10}$	Mizuno et al 1954.
	microprobe	1000		$1.6x10^{-11}$	Hehenkamp 1968.
Mo in Ni	Impurity tracer diffusion, residual activity.	900 - 1200	$1.6x10^{-3}$	51.0	Borisov et al 1968.
Ni in Ni-20%Mo	Ni^{63}, in electric field	950 - 1300	0.19	48.8	Kalinovich et al 1969
Mo in Ni-8%Mo	Mo^{99}	1000 - 1400	1.31	54.9	Kalinovich et al 1968
Mo in Ni-23%Mo	Sectioning technique: Mo^{99}	1100		$2.94x10^{-9}$	Kalinovich et al 1970 (a)
		1125		$4.08x10^{-9}$	

Material	Method	Temp. Range, ^{o}C.	Do cm^2s^{-1}	D, cm^2s^{-1}	Q Kcals $mole^{-1}$	Reference
		1150		$5.58x10^{-9}$		
		1175		$7.58x10^{-9}$		
		1200		$1.00x10^{-8}$		
		1225		$1.34x10^{-8}$		
		1250		$1.76x10^{-8}$		
		1275		$2.29x10^{-8}$		
		1300		$2.92x10^{-8}$		
		1100 - 1300	0.20		49.5	
Mo in Ni-20%Mo		950		$2.95x10^{-10}$		Kalinovich et al 1970 (b,c)
		1000		$6.53x10^{-10}$		
		1050		$1.29x10^{-9}$		
		1100		$2.78x10^{-9}$		
		1150		$5.30x10^{-9}$		
		1200		$9.68x10^{-9}$		
		1250		$1.68x10^{-8}$		
		1300		$2.86x10^{-8}$		
		950 - 1300	0.25		50.3	
Ni in Ni-20.Mo	Sectioning technique: Ni^{63}	950		$4.05x10^{-10}$		Kalinovich et al 1970 (b,c)
		1000		$9.02x10^{-10}$		
		1050		$1.86x10^{-9}$		
		1100		$3.64x10^{-9}$		
		1150		$6.83x10^{-9}$		
		1200		$1.20x10^{-8}$		

Material	Method	Temp. Range, °C.	Do cm^2s^{-1}		Q Kcals $mole^{-1}$	REference
				D, cm^2s^{-1}		
		1250		$2.07x10^{-8}$		
		1300		$3.47x10^{-8}$		
		950 - 1300	0.19		48.8	
Ni in Ni-16%Mo		950		$3.45x10^{-10}$		
		1000		$7.98x10^{-10}$		
		1050		$1.72x10^{-9}$		
		1100		$3.47x10^{-9}$		
		1150		$6.83x10^{-9}$		
		1200		$1.26x10^{-8}$		
		1250		$2.31x10^{-8}$		
		1300		$3.93x10^{-8}$		
		1350		$6.51x10^{-8}$		
		950 - 1350	0.63		52.2	
		950		$2.62x10^{-10}$		
		1000		$6.31x10^{-10}$		
		1050		$1.42x10^{-9}$		
		1100		$3.05x10^{-9}$		
		1150		$6.07x10^{-9}$		
		1200		$1.16x10^{-8}$		
		1250		$2.12x10^{-8}$		
		1300		$3.70x10^{-8}$		
		1350		$6.44x10^{-8}$		
		950 - 1350	1.30		54.6	
Ni in Ni-8%Mo	Sectioning technique: Ni^{63}	1000		$7.77x10^{-10}$		Kazinovich et al 1970 (b,c)

Material	Method	Temp. Range, °C.	D_o cm^2s^{-1}	Q Kcals $mole^{-1}$	Reference
			D, cm^2s^{-1}		
		1050	1.36×10^{-9}		
		1100	3.10×10^{-9}		
		1150	6.37×10^{-9}		
		1200	1.21×10^{-8}		
		1250	2.27×10^{-8}		
		1300	4.18×10^{-8}		
		1350	7.16×10^{-8}		
		1400	1.21×10^{-7}		
		1000 - 1400	2.55	56.4	
Ni-Mo	Self diffusion. Ni^{63} and Mo^{99} Radioactive tracers,				
	at % Mo diffusing element				
	0 Ni		9.96	60.5	
	8 Ni		2.55	56.4	
	Mo		1.31	54.9	
	16 Ni		0.63	52.2	
	Mo		1.30	54.6	
	18 Ni		0.34	50.4	
	Mo		0.45	52.2	
	20 Ni		0.19	48.8	
	Mo		0.25	50.3	
	23 Ni		0.12	47.4	
	Mo		0.20	49.5	
W in Ni	Chemical diffusion. Microprobe		$4.2^{+8.3}_{-2.8}$	75.0 +3.0	Bergner, 1968
			0.86	74.0	Davin et al, 1963
			11.1	76.8	Swalin & Martin 1956.
Ce in Ni	Serial sectioning. Ce^{144}. Volume and grain boundary diffusion studied.				Paul and Agarwala, 1971
	Volume diffusion	700		$1.54, 1.60\times10^{-4}$	
		750		7.67×10^{-14}	
		800		3.16×10^{-13}	

Material	Method	Temp. Range, ^{o}C.	D_o cm^2s^{-1}	$Kcals^{Q}mole^{-1}$	Reference
			D, cm^2s^{-1}		
		850	$7.31x10^{-13}$		
		900	$2.46x10^{-12}$		
		950	$8.81x10^{-12}$		
		980	$1.81x10^{-11}$		
		1040	$6.20x10^{-11}$		
		1097	$1.22x10^{-10}$		
		700 - 1097	0.66±0.18	60,8 ±0.8	
Nd in Ni	Serial sectioning	700	$1.72,1.75x10^{-14}$		Paul and Agarwala 1971
		750	$9.73x10^{-14}$		
		800	$3.21x10^{-13}$		
		850	$7.46x10^{-13}$		
		900	$2.43x10^{-12}$		
		950	$9.28x10^{-12}$		
		1000	$2.19x10^{-11}$		
		1050	$6.73x10^{-11}$		
		1100	$1.59x10^{-10}$		
		700 - 1100	0.44±0.13	59.8±0.8	
Ni in Ni-1.2%Nb.	Serial sectioning Ni^{63} in single phase solid solution Ni(Nb) and in two phase Ni (Nb)+Ni_3Nb		0.12	60.8	Shinayaev, 1968
Ni-8%Nb			0.20	62.2	
Ni-10%Nb			1.80	67.1	

Material	Method	Temp. Range, °C.	Do cm^2s^{-1} D, cm^2s^{-1}	Q Kcals°mole^{-1}	Reference
Ni-Cr	Interdiffusion coefficient. Microprobe analysis of various couples.	1000-1300	Q rises from 54 kcals/mole at 100%Cr to 90 at 25%Cr: Fairly constant at 63 kcals/mole in Ni-base solutions up to 40%Cr. D_o is approx. 1.0 cm^2/sec at 0%Cr, rises to a maximum of 1.5 at 30%Cr. Rapid variation of D_o in Cr-rich solutions from $2x10^{-3}$ cm^2s^{-1} at 5%Ni to 10.0 at 20% Ni.		Ugaste, 1967.
Ni-Pt	Interdiffusion coefficient passes through a maximum at 35-40% Pt.	950-1300			Borovskii et al, 1967
Ni-Pd	Mutual diffusion coefficient, alloys containing 10-90% Ni.	859-1150	D is a maximum at 50%Ni for all temperatures. For this alloy, $D=2x10^{-11}$ cm^2sec^{-1} at 850°C, and $1.6x10^{-9}$ at 1150°C.		Borovskii et al, 1966
Ni-Pd	Microprobe. Interdiffusion coefficients.	1112	D is approximately $8x10^{-11}cm^2sec^{-1}$ for pure Pd, and 10^{-10} cm^2s^{-1} for pure Ni. There is a maximum at 50% Ni, with a value of 10^{-9} cm^2s^{-1}		Hirano and Ouchi, 1968
Ni - Ti	Reaction diffusion, metallography, microprobe followed growth of intermetallic layers.	500-900			Hirano and Ouchi, 1968
	$Ti Ni_3$		16.1		
	Ti Ni		27.2		
	Ti_2Ni		11.9		
C in Ni		1000(?)	$2.47x10^{-7}$		Lafitan et al 1966
			-	38.5	
		1000(?)	$0.72x10^{-7}$ (uncorrected) $1.3x10^{-7}$ (corrected)		Smithells & Ransley 1936.
		1000(?)	$3x10^{-7}$		Lander et al, 1952
		?	-	39.7	Seith, 1955
	cc pairs only		0.048	34.8	Diamond and Wert, 1967

Material	Method	Temp. Range, °C.	cm^2s^{-1}	Q Kcals $mole^{-1}$	Reference
			D, cm^2s^{-1}		
			0.13	34.5	Shovensin et al, 1965
			0.1	33.0	Gruzin et al, 1957
	single crystal	700	$0.75\pm0.25\times10^{-9}$		Walker et al 1968.
	polycrystal		$1.75\pm0.65\times10^{-9}$		
Ni - Al					Janssen and Rieck, 1967
Ni^{63} in Ni_3Al and $Ni_3(Al,Ti)$	Self-diffusion. Residual activity				
	Composition, at %				
	Ni Al Ti				
	76.20 23.80 -		4.41	73.16	
	74.71 25.29 -		4.41	73.16	
	73.20 26.80 -		1.00	72.40	
	74.95 19.92 5.13		3.11	71.73	
	74.16 20.83 5.01		0.055	62.79	
	73.03 21.84 5.13		0.039	62.02	
			0.085	63.74	
Ta - W	Mutual diffusion, Microprobe. Minimum at Ta-50%W.	2000	D is 5×10^{-11} cm^2s^{-1} at 10%W, 1×10^{-11} at 50%W, and 2×10^{-11} at 90%W.		Tregubov et al, 1968
	Interdiffusion. Microprobe	2100-2500			Ivanov et al, 1970
	W in Ta-rich alloys:		1.78	119.0	
	Ta in W-rich alloys:		4.16×10^{-2}	100.0	
Ta - Ti	Interdiffusion, microprobe.	900-1000	D falls approximately linearly with increasing Ta content. At 10% Ta, $D=3\times10^{-11}$ at 900°C, 6×10^{-11} at 1000°C. At 35% Ta, 6×10^{-13} and 3×10^{-12} cm^2s^{-1} respectively.		Fedotov et al, 1969
C in Ta	Internal friction	350		39.5 38.4	Powers and Doyle, 1957, 1959.
C in Ta	Residual activity	1200-1600	2.57×10^{-2}	43.0	Nakonechnikov et al 1966
C in Ta	Radiotracer, serial sectioning.	1450-2200	0.012	40.3	Son et al, 1966
C in Ta	Chemical diffusion. Microprobe. Grain size ~ 500 μm.	1600-1900	8.54×10^{-4}	52.5	Suzuki et al, 1969.

Material	Method	Temp. Range, °C.	D_o $cm^2 s^{-1}$	$D, cm^2 s^{-1}$	Q Kcals $mole^{-1}$	Reference
Mo in Ta	Impurity tracer diffusion, sectioning, residual activity	1750-2220	1.8×10^{-3}		81.0	Borisov et al, 1968
S in Ta	Impurity tracer diffusion, S^{35}, serial sectioning, residual activity. 99.0% Ta (0.85% Nb). Autoradiography showed that S collected manily on the Ta grain boundaries.	1970		1.8×10^{-6}		Vandyshev and Panov 1969.
		2030		3.2×10^{-6}		
		2050		3.5×10^{-6}		
		2110		6.0×10^{-6}		
		1970 - 2110	100		70.0	
W in W	Tracer diffusion, W^{188}, serial sectioning polycrystalline W, mean grain diameter ~25 μm.	2403		8.70×10^{-12}		Pawel and Lunay 1969
		2285		1.73×10^{-12}		
		2228		9.05×10^{-13}		
		2115		3.00×10^{-13}		
		2001		5.50×10^{-14}		
		1934		3.03×10^{-14}		
		1800		2.90×10^{-15}		
		1800 - 2403	1.88 ± 0.4		140.3 ± 7.2	
W in W	Review of data for surface diffusion, grain boundary diffusion, and volume diffusion. For this last, the recommended values are:	<0.8 Tm	4.64×10^{-2}		113.8	Neumann 1968
		>0.8 Tm	42.8		153.1	
N in W	Diffusion is extremely structure sensitive. Slow in recrystallised wires. relatively rapid in fibrous wires.	1200		$<1.1 \times 10^{-11}$		Friedmann and Brett, 1968.
Re in W	Radiotracter. Polycrystalline W	2100		0.36×10^{-11}		Larikov et al, 1967
		2200		1.3×10^{-11}		
		2300		3.0×10^{-11}		
		2400		11×10^{-11}		

Material	Method	Temp. Range, $^{o}C.$	Do $cm^{2}s^{-1}$	D, $cm^{2}s^{-1}$	Q Kcals $mole^{-1}$	Reference
		2100 - 2400	19.5		141.0	
Re in W-2/%W -0.2%Ti		2000		$1.63x10^{-11}$		
		2100		$4.1x10^{-11}$		
		2200		$6.6x10^{-11}$		
		2300		$12x10^{-11}$		
		2400		$25x10^{-11}$		
		2000 - 2400	$9.2x10^{-3}$		94.0	
Mo in W	Mo^{99}, sectioning. Single crystals	2000		$0.11x10^{-11}$		
		2100		$0.32x10^{-11}$		
		2200		$0.79x10^{-11}$		
		2400		$4.2x10^{-11}$		
		2000 - 2400	$5x10^{-2}$		121.0	
	Polycrystals	2100		$0.416x10^{-11}$		
		2300		$2.35x10^{-11}$		
		2400		$5.7x10^{-11}$		
		2100 - 2400	$3.7x10^{-3}$		110.0	
Mo in W-Mo	W-44% Mo	1900		$0.56x10^{-11}$		
		2000		$1.5x10^{-11}$		
		2100		$3.6x10^{-11}$		
		2200		$8.1x10^{-11}$		
		2300		$20x10^{-11}$		
		1900 - 2300	0.17		107.0	
	W-55% Mo	1900		$0.79x10^{-11}$		
		2000		$2.25x10^{-11}$		

Material	Method	Temp. Range, °C.	D_o cm^2s^{-1}		Q Kcals $mole^{-1}$	Reference
				D, cm^2s^{-1}		
		2200		$1.88x10^{-11}$		
		2300		$28.9x10^{-11}$		
		2400		$51.2x10^{-11}$		
		1900 - 2400	0.12		103.0	
	W-5% Mo	1900		$0.17x10^{-11}$		
	W-20% Mo	1900		$0.32x10^{-11}$		
	W-52% Mo	1900		$0.715x10^{-11}$		
	100% Mo	1900		$2.1x10^{-11}$		
Mo in W	Impurity trace diffusion	1700 - 2100	0.3		101.0	Borisov et al 1968
Nb in W	Nb^{95} in W-single crystals	1800		$(8.95-9.85)x10^{-15}$		Pawel and Lundy 1968
Nb in W	Nb^{95} serial sectioning, polycrystalline W, mean grain diameter ~ 25 μm	2367		$1.48x10^{-11}$		Pawel and Lundy 1969
		2311		$7.35x10^{-12}$		
		2272		$4.84x10^{-12}$		
		2187		$1.50x10^{-12}$		
		2139		$1.02x10^{-12}$		
		2020		$1.98x10^{-13}$		
		1993		$1.5x10^{-13}$		
		1903		$4.21x10^{-14}$		
		1798		$9.25x10^{-15}$		
		1710		$2.19x10^{-15}$		
		1597		$2.50x10^{-16}$		
		1501		$3.44x10^{-17}$		
		1399		$3.30x10^{-18}$		
		1305		$2.4x10^{-19}$		

Material	Method	Temp. Range, °C.	Do $cm^2 s^{-1}$	Q Kcals $mole^{-1}$	Reference
			D, $cm^2 s^{-1}$		
		1305 - 2367	3.01±0.1	137.6 ±0.7	
Ta in W	Ta^{128}, serial sectioning, poly-crystalline W, mean grain diameter ~ 25 μm	2375	9.38×10^{-12}		Pawel and Lundy 1969
		2211	1.57×10^{-12}		
		2180	8.93×10^{-13}		
		2038	1.60×10^{-13}		
		1939	4.88×10^{-14}		
		1799	5.97×10^{-15}		
		1708	1.30×10^{-15}		
		1598	1.24×10^{-16}		
		1502	1.45×10^{-17}		
		1417	2.08×10^{-18}		
		1400	1.60×10^{-18}		
		1305	1.30×10^{-19}		
		1305 - 2375	3.05±0.2	139.9±1.3	
W - Nb	Interdiffusion. analysis	Microprobe			
		Wt % W	2000-2500		
		10	81.45	105.0	Nechiporenko et al 1971
		20	22.2	100.0	
		30	1.97	89.9	
		40	1.4×10^{-2}	66.9	
		50	7.4×10^{-3}	65.0	
		60	3.0×10^{-3}	60.9	
		70	1.8×10^{-3}	59.1	
		80	1.0×10^{-4}	56.4	
		90	6.0×10^{-4}	54.5	
W - Mo	Interdiffusion. analysis	Microprobe	2000-2500		Nechiporenko et al 1971
		Wt % W			
		10	4.48	117.2	
		20	2.41	114.9	
		30	0.64	109.6	

Material	Method	Temp Range, °C.	D_o, $cm^2 s^{-1}$	Q, Kcals $mole^{-1}$	Reference
			D, $cm^2 s^{-1}$		
W - Mo	Interdiffusion. Microprobe analysis				
	Wt % W				
	40		0.48	109.3	
	50		0.30	107.7	
	60		0.17	105.4	
	70		0.14	104.7	
	80		0.08	102.7	
	90		0.05	100.8	
W - Ta	Interdiffusion. Microprobe analysis	2000-2500			Nechiporenko et al 1971
	Wt % W				
	10		7.0×10^{-4}	73.9	
	20		1.0×10^{-4}	72.1	
	30		1.22×10^{-5}	62.7	
	40		6.08×10^{-6}	60.6	
	50		3.34×10^{-6}	58.2	
	60		1.66×10^{-6}	55.2	
	70		1.5×10^{-6}	55.4	
	80		1.23×10^{-6}	54.8	
	90		2.2×10^{-7}	47.3	
O in W	Permeation cell	1965-2300	-	40.0±45.0	Aitken et al, 1967
N in W	Vacuum annealing of N-charged wires	1400-2200	2.4×10^{-3}	28.4	Jehn and Fromm, 1970.
N in W		827-2227	5.4	62.0	Frauenfelder, 1968
N in W		1200-1800	1.0×10^{-2}	41.5	Wagner, 1969.
C in W	Internal friction	100-400	3.15×10^{-3}	172.0±15.0	Shchelkonogov et al, 1968
C in W	Residual activity	1200-1600	8.9×10^{-2}	53.5	Nakonechnikov et al, 1966.

DIFFUSION DATA II: OXIDES, CARBIDES, SULPHIDES ETC.

Material	Diffusing Element	Method	Temp. Range, °C.	D_o, $cm^2 s^{-1}$	D, $cm^2 s^{-1}$	Q, Kcals $mole^{-1}$	Reference
Al_2O_3	Al		1100-1800	-		165.0	Coble, 1958
	Al		1700-1800	2.5×10^4		135.0	Kuczyski et al 1959
				5.0×10^{18}		230.0	
	Al	Sintering	1600-1800	-		130.0±20.0	Warshaw, 1961,1962.
	Al		1670-1905	28		114.0±15.0	Paladino and Kingery 1962
	Al	Calculated from ionic diffusion currents.	277	-		36.9	Christian and Taylor 1967
	Al?	Sintering	1300-1800	1×10^4		136.0±5.0	Vishnevskii et al, 1971.
	O		1200-1620	6.3×10^{-8}		57.6	Oishi and Kingery 1960
			1500-1700	0.9×10^3		152.0±15.0	
	O		170(?)		$(4.0 \pm 3.0) \times 10^{-11}$		Hayes et al 1963
	O?	Sintered Al_2O_3, doped with MgO, Mg Ti O_3. Measured strain rate under a stress of approx. 1000 psi, used Nabarro-Herring equation (so presumably oxygen diffusion). Addition of Mg Ti O_3 had little or no effect.					Hewson and Kingery 1967
		Impurity content / Grain size, µm / % Theor. Density					
		O / 100 / 98.12	1745		10.1×10^{-11}		
		O / 100 / 98.12	1830		38.6×10^{-11}		
		750 ppm MgO / 15 / 99.82	1641		0.599×10^{-11}		

Material	Diffusing Element	Method	Temp. Range, °C.	Do $cm^2 s^{-1}$	Q Kcals $mole^{-1}$	Reference
				D, $cm^2 s^{-1}$		
		Impurity content / Grain size, / % Theor. Density				
		750 ppm MgO / 15 µm / 99.82	1742		1.35×10^{-11}	
		1500ppm MgO / 18 / 99.80	1746		6.26×10^{-11}	
		500ppm $MgTiO_3$ / 20 / 99.74	1642		3.38×10^{-11}	
		20 / 99.74	1744		8.81×10^{-11}	
	O	Permeation and mass spectrometric analysis	1700		$\sim 10^{-7}$	Roberts & Robers 1967
Al_2O_3	Na^{22}	Thin layer deposition, sectioning, residual activity. Commercial purity Al_2O_3, 95% dense.	1223-1750	$(2.0 \pm 0.6) \times 10^{-2}$	50.0±2.0	Frischat, 1971
			1397		5.14×10^{-9}	
			1465		9.80×10^{-9}	
			1505		12.4×10^{-9}	
			1570		32.4×10^{-9}	
		Commercial Al_2O_3, nearly 100% dense	1392		0.152×10^{-9}	
			1489		1.02×10^{-9}	
		single crystal, parallel to C	1505		0.0158×10^{-9}	
			1505		0.0184×10^{-9}	
		single crystal, perpendicular to C	1568		0.0229×10^{-9}	
			1568		0.0123×10^{-9}	
	Ca^{45}	Commercial purity Al_2O_3, 95% dense	1397		3.10×10^{-9}	
Al_2O_3	Ta(?)	Movement of colour boundary in single crystal doped with Ta, in air.	1400-1800	430	80.0	Jones et al 1969
Al_2O_3-Cr_2O_3		Microprobe, Single crystal of Al_2O_3 embedded in Cr_2O_3 powder.	1490-1895			Nelson, 1967
		Mole % Al_2O_3				
		10		0.030	93,7	
		30		0.423	106.1	
		50		0.798	110.0	
		70		0.482	111.3	
		90		0.037	102,9	

Material	Diffusing Element	Method	Temp. Range, °C.	Do $cm^2 s^{-1}$	D, $cm^2 s^{-1}$	Q Kcals $mole^{-1}$	Reference
Al_2O_3-Cr_2O_3	Cr	Weight loss measurements of evaporation kinetics in ruby sinsters containing 10 mole % Cr_2O_3. Controlled by Cr diffusion.	955-1850	199		118,0 ± 20,0	Sasamoto & Satc,1971
Al_2O_3-Na_2O β-alumina		Ion exchange between single crystal β-alumina and molten salts, using radiotracers.	200-400				Yao and Kummer, 1967
		Ion					
		Na^+		$2.4x10^{-4}$		3,81	
		Ag^+		$1.65x10^{-4}$		4,05	
11 Al_2O_3-Na_2O β-alumina		K^+		$0.78x10^{-4}$		5.36	
		Rb^+		$0.34x10^{-4}$		7.18	
		Li^+		$14.5x10^{-4}$		8.71	
Al_2O_3	Pu^{239}	alpha absorption	1200-1450	$1.54x10^8$		142.2±6.0	Fiedler & Bobleter 1968
Al_2O_3	Am^{242}	" "	1200-1430	$4.94x10^6$		135.0±7.0	Fiedler & Bobleter 1968
Al_2O_3-Mn_xO	O?	Effect of Mn_xO on sintering kinetics of 5 μm alumina. Ascribed sintering to oxygen diffusion sintering data: specimen %MnO.					Keski and Cutler 1968
		0	1550		$1.1x10^{-12}$	155.0±17.0	
		0	1450-1650			155.0±17.0	
		0.1				158.0±90.0	
		0.2				180.0±17.0	
		0.3				187.0±21.0	
		0.4				179.0±26.0	
		0.5				185.0±22.0	
		0.6				182.0±16.0	
Al_2O_3-MgO		Electron microprobe analysis. Interdiffusion of single crystal MgO with single crystal or sintered Al_2O_3. Interdiffusion coefficient increases with increasing mole fraction of cation vacancies.					

Material	Diffusing Element	Method	Temp. Range, °C.	D_o cm^2s^{-1}	D, cm^2s^{-1}	Q Kcals $mole^{-1}$	Reference
		At 1 mole % Al_2O_3 in MgO	1565-1900	2.20		76.0	
CoO	Co	Self diffusion as a function of oxygen pressure. Radioactive tracer method (Carter) Fueki-Wagner method (Mrowec et al) calculated from parabolic oxidation constant (Mrowec). Data shown are those of Carter: the other two sets are very similar					
		PO_2, atm					
		0.04	1000		8.6×10^{-10}		
		0.07			10.2×10^{-10}		
		0.11			12.1×10^{-10}		
		0.21			15.1×10^{-10}		
		0.23			15.6×10^{-10}		
		0.29			16.9×10^{-10}		
		0.37			18.4×10^{-10}		
		0.43			19.4×10^{-10}		
		0.60			21.8×10^{-10}		
		1.00			26.0×10^{-10}		
	Co	Self diffusion, Co^{60} and Co55, serial sectioning. In air	963-1638	5.0×10^{-3}		38,4	Chen et al, 1969
	Co	Deduced from electrical conductivity changes at 1 atm O_2	800		1.39×10^{-8}		Price and Wagner 1966.
			900		4.07×10^{-9}		
			1000		9.06×10^{-10}		
			1100		3.91×10^{-10}		
	O	Isotope exchange. PO_2 = 0.21 atm. At constant T, $^2PO_2$, oxygen diffusivity increased when CoO doped with Li, decreased when doped with Al, suggesting vacancy mechanism.	1175-1560	50		95,0 ±5,0	Chen and Jackson 1969.
	O	Proton activation of O^{18}. Single crystal CoO. Much slower than data of Thompson, who used gaseous exchange.	1400		5×10^{-11}		Holt, 1967
							Thompson 1962.

Material	Diffusing Element	Method	Temp. Range, °C.	D_0, $cm^2 s^{-1}$	D, $cm^2 s^{-1}$	Q, Kcals $mole^{-1}$	Reference
	O	Calculated from Holt's data.	900-1400	7.9×10^{-5}		42,9	Hoch
CoO		Growth kinetics of grain boundary grooving in 99.999% pure polycrystalline CoO. Below 1100°C, surface diffusion controlled; above 1140°C, volume diffusion					
		(a) Assuming a surface free energy of 1000 ergs/cm^2	1144		2.29×10^{-9}		
			1309		8.7×10^{-9}		
			1353		1.22×10^{-8}		
			1407		2.07×10^{-8}		
		(b) assuming a surface free energy of 500 ergs/cm^2.	1144		4.58×10^{-9}		
			1309		1.75×10^{-8}		
			1353		2.43×10^{-8}		
			1407		4.14×10^{-8}		
			1144-1407	3.94×10^{-3}		38.42+2.11	
Co_3O_4	?		850	3×10^{-13}			quoted by Birchenall 1968 from Thompson 1962.
Co Al_2O_4	Co		1270-1500	8		85.0	Morkel and Schmalzried, 1962
Co Cr_2O_4	Co		1400-1600	10^{-3}		51.0	Sun 1958.
	Cr		1400-1600	2		70.0	Sun, 1958.
	Co		1100-1400	80		90.0	Morkel and Schmalzried, 1962
	Cr		1100-1400	300		85.0	Morkel and Schmalzried, 1962
Cr_2O_3	Cr		1000-1350	4×10^3		100.0	Lindner and Akerstrom, 1965

Material	Diffusing Element	Method	Temp. RAnge, °C.	D_o cm^2s^{-1}	D cm^2s^{-1}	Q Kcals $mole^{-1}$	Reference
	Cr		900-1100	4.29×10^{-8}		22.0	Ignatov et al, 1958
	Cr		1045-1550	0.137		61.1	Hagel and Seybolt, 1961
	Cr		1100		1.54×10^{-11}		Fedorchenko and Ermolovich, 1962.
			1150		4.55×10^{-11}		
			1200		1.52×10^{-10}		
			1250		3.63×10^{-10}		
			1100-1250	-		88.7	
	Cr		1300		5×10^{-10}		Walters and Grace. 1963, 1965
Cr_2O_3	O		1100-1450	15.9		101.0	Hagel, 1965
	O		1100-1450	440		109.9±7,3	
		Two interpretations.					Hagel et al, 1966
				3370		123,0±0.8	
	S	Sectioning technique S^{35} into 99.3% pure Cr_2O_3.	1000		1.5×10^{-10}		Seybolt, 1968
FeO	Fe	Reduction, oxidation kinetics in CO_2/CO mixtures.	1000				Fujii and Meussner 1967
		X in Fe_xO					
		0.952			1.1×10^{-7}		
		0.930			9.0×10^{-8}		
		0.909			7.0×10^{-8}		
	Fe	X in Fe_xO	1000				Levin (see F&M)
		0.952			1.4×10^{-7}		

Material	Diffusing Element	Method	Temp. RAnge, ^{o}C.	Do cm^2s^{-1}	Q Kcals $mole^{-1}$	Reference
				D, cm^2s^{-1}		
FeO	Fe	Reduction, oxidaton kinetics in CO_2/CO mixtures				
		x in Fe_xO				
		0.930		$8.0x10^{-7}$		
		0.909		$3.8x10^{-7}$		
	Fe	Chemical diffusion, thermogravimetric method	1050			Campbell, 1969
		$FeO_{1.07}$ (X=0.945)		$3.5x10^{-7}$		
		$F_eO_{1.13}$ (x=0.885)		$1.6x10^{-7}$		
			817-1055		~20.0	
	Fe	Fe^{55}, surface decrease method. O/Fe ratio(x)				Hembree and Wagner 1969
		1.062 0.940	1100	$1.03x10^{-7}$		
		1.078 0.928		$1.31x10^{-7}$		
		1.096 0.913		$1.54x10^{-7}$		
		1.112 0.900		$1.76x10^{-7}$		
		1.129 0.885		$1.99x10^{-7}$		
		1.146 0.872		$2.35x10^{-7}$		
Fe_3O_4	O	Self diffusion. Isotope exchange.	251	$(1.60\pm0.54)x10^{-20}$		Castle and Surman, 1967
			302	$(1.39\pm0.41)x10^{-20}$		
			349	$(3.65\pm0.23)x10^{-20}$		
			401	$(8.78\pm0.30)x10^{-20}$		
			455	$(1.72\pm0.46)x10^{-19}$		
			483	$(1.16\pm0.14)x10^{-18}$		
			498.5	$(5.90\pm0.50)x10^{-18}$		

Material	Diffusing Element	Method	Temp, Range. ^{O}C.	D_o cm^2s^{-1}	D, cm^2s^{-1}	Q Kcals $mole^{-1}$	Reference
Fe_3O_4	O	Self diffusion. Isotope exchange.	500		$(5.56\pm0.14)\times10^{-18}$		
			545		$(1.12\pm0.04)\times10^{-18}$		
			550		$(3.94\pm0.55)\times10^{-18}$		
			251-550	$(3.2\pm1.6)\times10^{-14}$		17.0 ± 1.65	
Fe_3O_4	O	Hetrogeneous Isotope exchange.	450-550	$D=1.80\times10^{-18}\left(\frac{PH_2}{PH_2O}\right)^{0.27}\exp$		$\frac{-17000}{RT}$	Castle and Surman, 1969
$Mg\ Al_2O_4$	?	Sintering kinetics	1050-1300	18.6		116.0	Bratton, 1969
$MgO.x\ Al_2O_3$	Ni	Electricprobe microanalysis Interdiffusion x=1 - 1.5. Diffusion coefficients varied linearly with the concentration of composition-dependent vacancies.					Yamaguchi et al 1969
$(Mg_{0.9}Ni_{0.1})O\ x\ Al_2O_3$	Ni						
		perfect spinels		-		106.0	
		defective spinels		-		70.0	
$MgO-Cr_2O_3$		Interdiffusion. MgO single crystals and Cr_2O_3 sintered pellets. Microprobe					Greskovich and Stubican. 1970.
		Mole % Cr_2O_3					
		D calculated by Wagner method. Boltzmann - Matano method gives slightly higher values	4.65 1640		2.0×10^{-9}		
			2.70 1520		1.1×10^{-10}		
			2.50 1465		8.3×10^{-11}		
			2.44 1465		8.4×10^{-11}		
			2.08 1410		3.0×10^{-11}		
			1.16 1360		9.0×10^{-12}		
MiO_{1+x}	Mn	Tracer diffusion of Mn^{54} using residual method. Also chemical diffusion using	850 - 1150			31.3	Price 1968.

Material	Diffusing Element	Method	Temp. Range, °C.	Do cm^2s^{-1}	D, cm^2s^{-1}	Q Kcals $mole^{-1}$	Reference
		change in electrical conductivity during equilibration with CO/CO_2.					
MnO_{1+x}	Mn	Tracer diffusion of Mn^{54} In low-pressure region, material exhibits apparent n-type behaviour. Graph of log D vs. log PO_2 at 1032°C has slope 1/5.4. Doubly ionised cation vacancies.					Price & Wagner, 1970
		PO_2, atm	1032				
		10^{-8}			$2,57x10^{-9}$		
		10^{-10}			$1.1x10^{-9}$		
		10^{-12}			$4.57x10^{-10}$		
		$10^{-13.4}$			$2.52x10^{-10}$		
		10^{-15}			$1.29x10^{-10}$		
		10^{-16}			$7.95x10^{-11}$		
		10^{-17}			$5.0x10^{-11}$		
		10^{-18}			$3.17x10^{-11}$		
Nb_2O_5	O	Gas-solid isotopic exchange. Near stoichiometric α Nb_2O_5. Single crystal particles, 80 - 230 µm dia.	850-1200	0.0172		49.4±3.3	Chen and Jackson 1967
		PO_2 = 0.23 atm					
		At const. temperature, D∝ PO_2 - 1/4.					
		Oxygen vacancy model.					
Nb_2O_5	O	Single crystals of αNb_2O_5 D is several hundred fold lower in oxide of large non-stoichiometry	680-965			2.2eV	Sheasby et al 1968

Material	Diffusing Element	Method	Temp. Range, °C.	Do $cm^2 s^{-1}$	D, $cm^2 s^{-1}$	Q Kcals $mole^{-1}$	Reference
		e.g.	909				
		PO_2 = 1 atm			1.82×10^{-6}		
		PO_2 = 2×10^{-16} atm			7.45×10^{-9}		
		Some results on γ Nb_2O_5 removed from oxidised specimen	628				
		PO_2 = 0.5 atm			7.65×10^{-5}		
		PO_2 = 10^{-6} atm			1.1×10^{-6}		
Nb_2O_5	O	O^{18} in single crystals, neutron reaction, autoradiography					Sheasby and Cox, 1968
		PO_2 = 10^{-17} atm, ∥ [010]	900		8.3×10^{-11}		
		⊥ [010]			1.4×10^{-12}		
		PO_2 = 10 torr, ∥ [010]	850		2.1×10^{-10}		
		⊥ [010]			1.1×10^{-12}		
NiO		Sintering of 1.6-2.1mm spheres of NiO formed by oxidising Grade A nickel plate at 1300°C. Volume diffusion. Sintering diffusion coefficients of green spheres to black NiO are much greater than those measured by conventional methods.	1100-1300	10^5		73.3	Jodlowski and Kuczynski, 1965.
NiO	Ni	Polycrystalline NiO equilibrated with different PO_2, measured transient electrical conductivity Used values for the vacancy concentration to derive self diffusion data:	800-1000	6.5×10^{-2}		48.8	Morlotti, 1969
		Po_2 atm 10^{-3}	1005		1.9×10^{-5}		
		10^{-2}			2.5×10^{-5}		
		10^{-1}			3.9×10^{-5}		

Material	Diffusing Element	Method	Temp. Range, °C.	Do cm^2s^{-1}		Q Kcals $mole^{-1}$	Reference
					D, cm^2s^{-1}		
		1			$4.7x10^{-5}$		
		$3.3x10^{-2}$	944		$3.0x10^{-5}$		
		$2.1x10^{-1}$			$3.2x10^{-5}$		
		1			$2.5x10^{-5}$		
		$3.3x10^{-2}$	885		$1.7x10^{-5}$		
		$2.1x10^{-1}$			$1.2x10^{-5}$		
		1			$5.3x10^{-6}$		
		10^{-1}	797		$4.0x10^{-6}$		
			797-1005	14		31.0	
NiO	Ni?	Electrical conductivity as a function of PO_2 to obtain chemical diffusion data.	993		$1x10^{-7}$		Deren et al, 1971
			1193		$6.3x10^{-7}$		
			993-1193			~1.46eV	
NiO	Ni		900-1000	$4.1x10^{-2}$		55.0	Moore, 1951
	Ni		1140-1400	$2.8x10^{6}$		119.5	Lindner and Akerstrom, 1956.
	Ni		1000-1400	$5.0x10^{-4}$		44.2±3.0	Shim and Moore, 1957
	Ni		1000-1400	$3.9x10^{-4}$		44.2±3.0	Shim and Moore, 1957
	Ni		700-1400	$1.7x10^{-2}$		56.0±1.3	Lindner and Akerstrom, 1957
	Ni		1300-1700	$8.0x10^{-4}$		53.5±3.0	Moore et al, 1960
	Ni		1000-1400	$1.83x10^{-3}$		45.6	Choi and Moore, 1962
	Ni		1190-1400	$4.8x10^{-4}$		48.4±2.0	Klotsman et al, 1962
	Ni		1100		$3.59x10^{-11}$		Price and Wagner, 1966
			1000		$1.12x10^{-11}$		
			900		$4.29x10^{-12}$		

Material	Diffusing Element	Method	Temp. Range, °C.	D_o, $cm^2 s^{-1}$	D, $cm^2 s^{-1}$	Q, Kcals $mole^{-1}$	Reference
			800		7.70×10^{-13}		
	Ni		276-723	1.26×10^{-5}		46.6	Wang, 1966
	Ni		1182-1762	4.8×10^{-2}		60.8	Volpe and Reddy, 1972
			1182-1762	2.1×10^{-2}		62.7	Volpe and Reddy, 1972
	Ni		800-1000	6.5×10^{-2}		48.8	Morlotti 1969
	O		1300		3.9×10^{-13}		Moore et al, 1960
	O		1100-1500	1.0×10^{-5}		54.0	O'Keefe and Moore 1961
	Cr		1300-1600	4×10^{-3}		55.0	Greskovich, 1970
	Co	Tracer sectioning. Co^{55} and Co^{60}, NiO single crystals in air.	1085-1 49	$(9.12 \pm 0.58) \times 10^{-3}$		54.163±0.465	Chen and Peterson 1972
$NiO-Al_2O_3$		Electronprobe microanalysis, and metallographic measurements of thickness of $NiAl_2O_4$. spinel layer. Authors consider that a complex of an aluminium ion and a nickel vacancy is the mobile species.	1440-1790	6.6×10^{-2}		54.0±3.0	Minford and Stubican 1973
$Nio-Fe_2O_3-al_2O_3$							Nicholas, 1967
$NiAl_2O_4$	Ni			3×10^{-5}		53.3	Linder and Akerstrom 1958
$NiCr_2O_4$	Ni		1130-1450	0.85		74.6	? 1956.
	Ni		950-1300	1.5×10^{-3}		61.400	Linder and Akerstrom 1958
	Cr		1130-1450	0.74		72.5	? 1956.
	Cr		1200-1500	2		100.0	? 1960.
	O		1200-1500	0.017		65.4	? 1960.
WO_3	O						Sikka and Rosa 1970

Material	Diffusing Element	Method	Temp. Range, °C.	Do cm^2s^{-1}	D, cm^2s^{-1}	Q Kcals $mole^{-1}$	Reference
Cr_xCy	C	Metallographic analysis of thickness of layers formed during carburisation of Cr.					
		Cr_7C_3	1200-1475	-		40	Fries et al 1967
		$Cr_{23}C_6$	"	-		40	
		Cr_3C_2	"	-		45	
Mo_2C	C	Ditto., for Mo. Change at 1415 related to the order/disorder transition in the C lattice.	1200-1415 1415-2100			114 68	
Mo_2C	C^{14}	Sectioning technique	1470-1730	80±20		91.5±4.5	Andrievskii et al, 1967
Mo_xC	C^{14}	"	1450-2000	300±60		95±5	
		Metallographic analysis	1270-2050	800+160		83±4	
Mo_2C	C	Reaction diffusion Metallographic and X-ray analysis	997-1777	810		83.0	Eremeev and Panov. 1968
		Self diffusion. Gruzin method. In cast Mo_2C	1467-1723	80		91.5	
		In Mo_2C produced by carburising Mo	1173-1723	300		95.0	
Mo_2C	C	Chemcial diffusion. Kinetics of carburisation	1550-2150	0.9		56.7	Fries et al 1968
HfC	C^{14}	Sectioning technique	1590-2000	$4.7x10^4$		128±6.5	Andrievskii et al 1967
HfC	C^{14}	Sectioning technique	220[illegible]-2800	63		130.3	Andrievskii et al 1969
NbC	C^{14}	" "	2200-2800	0.5		102	ditto.,
NbC	C	Layer growth kinetics	1700-2200	0.35		74.2	Fujikawa et al 1970
		-	1700-2300	7.6		88.2	Brizes et al 1966
		-	1900-2300	1.2		79.0	Resnick & Seigle 1966

Material	Diffusing Element	Method	Temp. Range, ^{o}C.	Do cm^2s^{-1}	D, cm^2s^{-1}	Q Kcals $mole^{-1}$	Reference
			1205-1816	0.102		72.7	Bornstein et al, 1965
NbC_x	C^{14}	Sectioning technique Carbide	2250-2650				
		(a) $Nb(C_{0.95}\ O_{0.01}\ N_{0.04})_{0.97}$		$0.11^{+0.03}_{-0.10}$		94±1.8	Amdrievskii et al, 1971
		(b) $Nb(C_{0.965}\ O_{0.03}\ N_{0.032})_{0.915}$		$0.21^{+0.18}_{-0.10}$		96.5±3.6	
		(c) $Nb(C_{0.998}\ O_{0.001}\ N_{0.001})_{0.915}$		$0.19^{+0.18}_{-0.16}$		95.5±3.6	
		(d) $Nb(C_{0.094}\ O_{0.004}\ N_{0.056})_{0.78}$		$1.47^{+0.52}_{-0.38}$		100±1.7	
	Nb^{95}	Same carbides: (a)		$0.11^{+0.28}_{-0.08}$		127±7	
		(b)		$0.11^{+0.28}_{-0.08}$		127±7	
		(d)		$0.11^{+0.28}_{-0.08}$		127±7	
Nb_2C	C	Layer growth kinetics	1700-2200	2.3×10^{-3}		39.9	Fujikawa et al 1970
NbC_x	C	Chemical analysis of carburised material. x=0.64-0.9	1827-2627	0.66		73.5	Vilk et al 1967
TaC	C^{14}	Sectioning technique	2360-2960	3.9		118.7	Andrievskii et al, 1969
TaC	C	Layer growth kinetics	2100-2650	2.0		90.7	Brizes, 1968.
		ditto.,	2200-2750	8.8		98.8	Fromm et al 1966.
Ta_2C	C	ditto.,	2100-2650	1000		115.0	Brizes, 1968
		ditto.,	2200-2750	2.70		85.0	Fromm et al 1966
		Chemical analysis of carburised material x =0.66-0.9	1827-2627	0.089		64.4	Vilk et al, 1967
W_2C	C	Kinetics of carburisation. Chemical diffusion	1550-2535	600		97±1.5	Fries et al 1968

Material	Diffusing Element	Method	Temp. Range, °C.	D_o cm^2s^{-1}	D, cm^2s^{-1}	Q Kcals $mole^{-1}$	Reference
ZrC_x	C	Chemical analysis of carburised material. x=0.56-1.0	1827-2627	0.34		69.0	Vilk et al 1967
ZrC	C^{14}	Sectioning technique	1600-2080	332±60		114±6	Ankrievskii et al, 1967
ZrC	C^{14}	ditto.,	1350-2150	132		113.2	Sarian and Criscione 1967
ZrC	C^{14}	ditto.,	2250-2740	56.4		124	Andrievskii et al 1969
ZrC_x	C^{14}	ditto.,	2250-2650				Andrievskii et al 1971
		Carbide					
		(a) $Zr(C_{0.966}\ O_{0.012}\ N_{0.022})_{0.97}$		$14.1^{+13.5}_{-12.7}$		108.9±6.1	
		(b) $Zr(C_{0.968}\ O_{0.011}\ N_{0.925})_{0.925}$		$19.5^{+40.5}_{-13}$		119.5±6.2	
		(c) $Zr(C_{0.88}\ O_{0.11}\ N_{0.02})_{0.88}$		$61.2^{+45.2}_{-54}$		127±12	
		(d) $Zr(C_{0.95}\ O_{0.01}\ N_{0.04})_{0.85}$		264^{+426}_{-163}		133±8.3	
		(e) $Zr(C_{0.96}\ O_{0.012}\ N_{0.028})_{0.84}$		316^{+880}_{-232}		137±7.6	
	Zr^{95}	For carbides (a) and (e)		1030^{+6030}_{-880}		172±10.7	
FeS	S	Sulphidation rate	400-480	3.4×10^{-5}		17.0	Gorev and Lifshits 1968.
$Ni_{1-x}S$	S	Sulphidation rate	450-600	3.2×10^{-4}		21.3	Fueki et al 1968
Cr_2N	N	Rate of growth of nitride in N_2/H_2 mixtures. Controlled by N^2 diffusion. Self diffusivity decreases with increasing nitrogen content, but intrinsic diffusivity virtually independent of nitrogen content.	1200		4.2×10^{-8}		Schwerdtfeger 1967

Diffusion Data - References

(A)

A - 1 R.P. Agarwala, S.P. Muraka and M.S. Anand, Acta. Met., 16 (1968) 61.

A - 2 N.G. Ainslie and A.U. Seybolt, J. Iron Steel Inst., 194 (1960) 341.

A - 3 E.A. Aitken, H.C. Brassfield, P.K. Conn, E.C. Duderstadt, and R.E. Fryxell, Trans. AIME, 239 (1967) 1565.

A - 4 C.B. Alcock and P.B. Brown, Metal. Sci. J., 3 (1969) 116.

A - 5 M.S. Anand, S.P. Muraka and R.P. Agarwala, J. Appl. Phys., 36 (1965) 3860.

A - 6 R.A. Andrievskii, V.S. Eremeev, V.N. Zagryazkin and A.S. Panov, Izv. Akad. Nauk SSSR, Neorg. Mat., 3 (1967) 2158.

A - 7 R.A. Andrievskii, Yu. F. Khromov and I.S. Alekseeva, Fiz., Metal. Metalloved., 32 (1971) 664.

A - 8 R.A. Andrievskii, V.V. Klimenko and Yu. F. Khormov, Fiz. Metal. Metalloved., 28 (1969) 298.

A - 9 R.A. Andrievskii, I.I. Spivak and A.E. Tsulin, Dokl. Akad. Nauk SSSR, 185 (1969) 792.

A - 10 R. Angers and F. Claisse, Canad. Met. Quart., 7 (1968) 73.

A - 11 J. Askill, Phys. Stat. Sol., 9 (1965) K167.

A - 12 J. Askill, Phys. Stat. Sol., 23 (1967) K21.

A - 13 J. Askill and D.H. Tomlin, Phil. Mag. 11 (1965) 467.

A - 14 M. Aucouturier, T. Araki, T. Rosso and P. Lacombe, Mem. Sci. Rev. Met., 65 (1968) 255.

A - 15 M. Aucouturier and P. Lacombe, Cobalt 28 (1965) 121.

(B)

B - 1 V.N. Babushkin and A.I. Borisenko, Zaschita Metallov., 4 (1968) 309.

B - 2 M. Badia, Doct. Diss., Univ. Nancy (France) 1969, 85 pp: Diff. Data 4 (1970) 36.

B - 3 M. Badia and A. Vignes, Compt. Rend. Acad. Sci., Paris, Ser. C, 264 (1967) 858.

B - 4 M. Badia and A. Vignes (b) Compt. Rend. Acad. Sci., Paris, Ser-C, 264 (1967) 1528.

B - 5 M. Badia and A. Vignes, Compt. Rend. Acad Sci., Paris Ser. C, 264 (1967) 1543.

B - 6 M. Badia and A. Vignes, Acta. Met., 17 (1969) 177.

B - 7 C. Baker, M. Wuttig and H.K. Birnbaum, Trans. Japan. Inst. Metals, Suppl. 9 (1968) 268.

B - 8 H. Bakker, Phys. Stat. Sol., 28 (1968) 569.

B - 9 V.I. Baramova, S.A. Golovin, M.A. Krishtal and M.I. Lerner, Fiz. Khim. Obrab. Mater., No. 2 (1968) 61: Diff. Data 3 (1969) 147.

B - 10 R. Barlow and P.J. Grundy, J. Mater. Sci., 4 (1969) 797.

B - 11 D. Bergner, Microchim. Acta., Suppl., No. 3, (1968) 19.

B - 12 C.E. Birchenall, in "Mass Transport in Oxides" ed. Wachtman and Franklin, NBS Publ. 296, (1968).

B - 13 N.A. Bogdonov, Izv. Akad. Nank SSSR, Met. i. Topl, No. 9 (1960) 39.

B - 14 K. Bohnekamp, Arch. Eisenhuttenw., 38 (1967) 229.

B - 15 S.Z. Bokshtein, M.B. Bronfin and S.T. Kishkin, "Diffusion Processes, Structures and Properties of Metals", Consultants Bureau, New York (1965) 16, 24.

B - 16 S.Z. Bokshtein et al., Zavod. Lab., 23 (1957) 316.

B - 17 S.Z. Bokshtein et al., Legk. Spalvy Metody Ikh. Obrab. (1968) 254.

B - 18 S.Z. Bokshtein et al., Metalloved. Term. Obrab. Metal., No. 1 (1969) 3.

B - 19 R.J. Borg and C.E. Birchenall, Trans. AIME, 218 (1960) 980.

B - 20 R.J. Borg and D.Y.F. Lai, U. Calif. Dept. No. UCRL 7123 (1962).

B - 21 R.J. Borg, D.Y.F. Lai and O.H. Krikorian, U. Calif. Dept. No UCRL 7124 (1962).

B - 22 N.S. Bornstein, E.C. Hirakis and L.A. Friedrich, Pratt and Whitney Report No. TIM - 927 (1965).

B - 23 E.V. Borisov. N.E. Garbuzova and P.L. Gruzin, Sb. Tr. Tsent. Nauch-Issled. Inst. Chem. Met., No. 59 (1968) 5.

B - 24 E.V. Borisov, P.L. Gruzin and S.V. Zemskii, Zashch. Pokryt. Metal., No. 2, (1968) 104.

B - 25 I.B. Borovskii, I.D. Marchukova and Yu. E. Ugaste, Fiz. Met. Metalloved., 24 (1967) 436: 22 (1966) 849.

B - 26 A.W. Bowen and G.M. Leak, Met. Trans., 1 (1970) 1695.

B - 27 A.W. Bowen and G.M. Leak, (b) Met. Trans. 1 (1970) 2767.

B - 28 R.J. Bratton, J. Am. Ceram. Soc., 52 (1969) 417.

B - 29 W.F. Brizes, J. Nucl. Mater. 26 (1968) 227.

B - 30 W.F. Brizes, L.H. Cadoff and J.M. Tobin, J. Nucl. Mater., 20 (1966) 57.

B - 31 F.S. Buffington, K. Hirano and M. Cohen, Acta. Meta., 9 (1961) 434.

B - 32 Ch. P. Bahsmer, Diss. Slate Univ., N.Y. (1968): Univ. Microfilms, Ann Arbor, Mich., No. 68-16, 616.

B - 33 C.P. Buhsmer and P.H. Crayton, J. Mater. Sci., 6 (1971). 981.

B - 34 H. Burgess and R. Smoluchowski, J. Appl. Phys., 26 (1955) 491.

(C)

C - 1 R.H. Campbell, Arizona State U. Thesis, (1969): Univ. Microfilm No. 69 - 5710.

C - 2 R. Carter and F. Richardson, Trans. AIME 200 (1954) 1244.

C - 3 J.E. Castle and P.L. Surman, J. Phys. Chem., 71 (1967). 4255: 73 (1969) 632.

C - 4 W.K. Chen and R.A. Jackson, J. Chem. Phys., 47 (1967) 1144.

C - 5 W.K. Chen and R.A. Jackson, J. Phys. Chem. Solids, 30 (1969) 1309.

C - 6 W.K. Chen and N.L. Peterson, J. Phys. Chem. Solids, 33 (1972) 881.

C - 7 W.K. Chen, N.L. Peterson and W.T. Reeves, paper presented at 1969 Spring Meeting of Met. Soc. of AIME, Pittsburgh Abstract in J. Met., 21 (1969) 50A:Phys. Rev. 186 (1969) 887.

C - 8 J.S. Choi and W.J. Moore, J. Phys. Chem., 66 (1962) 1308.

C - 9 J.H. Christian and H.L. Taylor, J. Appl. Phys., 38 (1967) 3843.

C - 10 R.L. Coble, J. Am. Ceram. Soc., 41 (1958) 55.

(D)

D - 1 L.C. DaSilva and R.F. Mehl, Trans. AIME, 191 (1951) 155.

D - 2 A. Davin, V. Leroy, D. Coutsouradis and L. Habraken, Cobalt, No. 19, (1963) 51.

D - 3 J.J. Demo, Trans. AIME, 239 (1967) 798.

D - 4 E.W. De Reca and C. Pampillo, Acta. Met., 15 (1967) 1263.

D - 5 J. Deren, Z.M. Jarzebski and S. Mrowec, Bull. Acad. Pol. Sci., Ser. Sci., Chim., 19 (1971) 153.

D - 6 S. Diamond and C. Wert, Trans AIME, 239 (1967) 705.

D - 1 D.V. Ignatov, I.L. Belokurova and I.N. Belgamin, Proc. Conf. on the Use of Radioactive and Stable Isotopes and Radiation in the National Economy and in Science (USSR, 1958) 326. U.S. AEC Dept. NP-tr-448 (1958) 256: Nucl. Sci. Abs. 14 1935 i.

D - 2 Y. Iijima and K. Hirano, Nippon Kinzoku Gakkaishi, 35 (1971) 511.

D - 3 A.N. Ivanov, G.B. Krasilnikova, and B.S. Mitin, Fiz. Metal. Metalloved., 29 (1970) 204.

D - 4 L. I. Ivanov et al, Izv. Acad. Nauk SSSR, O T N, No. 2, (1962) 104.

D - 5 I.G. Ivantsov. Fiz. Metal. Mettalloved., 22 (1966) 725.

D - 6 I. G. Ivantsov and A.M. Blinkin, Fiz. Metal. Metalloved., 22 (1966) 876.

D - 7 G.N. Dublinin, G.P. Benediktova, M.G. Karpman and G.V. Shcherbedinskii, Khim-Term, Obrab. Stali Splavov, No. 6 (1969) 129.

(E)

E - 1 V.P. Elyutin, Yu. A. Pavlov, A.V. Manukhin, and V.F. Melekhin, Izv. Vyssh. Ucheb. Zaved, Chem. Met., 13 (1970) 5.

E - 2 V.S. Eremeev and A.S. Panov, Sov. Powder Met., Metal Cerams., No. 4 (1967) 306.

E - 3 V.S. Eremeev and A.S. Panov, Izv. Akad. Nauk SSSR, Neorg. Mat., 4 (1968) 1507.

E - 4 W. Erley and H. Wagner, Phys. Stat. Sol. A6 (1971) 543.

E - 5 J.H. Evans and B.L. Eyre, Intl. Conf. Vacancies and Insterstitials in Metals, Julich, (1968) Vol. 2, 858: Acta Met., 17 (1969) 1109.

(F)

F - 1 J.D. Fast and M.B. Verrijp, J. Iron Steel Inst., 176 (1965) 24.

F - 2 I.M. Fedorchenko and Y.B. Ermolovich, Ukr. Chim. Zhur., 26 (1960) 429.

F - 3 I.M. Fedorchenko, I.I. Ivanova and O.I. Fushchich, Dopl. Akad. Nauk. Ukr. RSR, 33A (1969) 356.

F - 4 G.B. Fedorov et al, Metallurgy and Metal Physics of Pure Maths, No. 3 (1961) 201.

F - 5 G.B. Fedorov, F.I. Zhomov and E.A. Smirnov, Metal. Metalloved. Chist. Metal., (1968) 128.

F - 6 S.G. Fedotov, M.G. Chudinov and K.M. Konstantinov, Fiz. Metal. Metalloved., 27 (1969) 873: Diff. Data 4 (1970) 68.

F - 7 W. Fiedler and O. Bobleter, Atomkernenergie, 13 (1968) 57.

F - 8 E. Fitzer and K. Matthias, Paper No. 50 presented at 6 th Plansee Seminar, Reutte (Austria) 1968: High Temp. Sci., 3 (1971) 93.

F - 9 I.N. Frantsevich, D.F. Kalinovich, I.I. Kovenskii and M.D. Smolin J. Phys. Chem. Solids, 30 (1969) 947.

F - 10 I.N. Frantsevich, D.F. Kalinovich, I.I. Kovenskii and M.D. Smolin, Atomic Transport in Solids and Liquids (Proc. Europhys Conf.) eds. A. Lodding and T. Lagerwall (1971), 100.

F - 11 R. Frauenfelder, J. Chem. Phys. 48 (1968) 3966.

F - 12 S. Friedmann and J. Brett, Trans. AIME 242 (1968) 2121.

F - 13 R.J. Fries, J.E. Cummings, C.G. Hoffman and S.A. Daily Paper No. 36 presented at 6th Plansee Seminar, Reutte, Tyrol (Austria) 1968: U.S. AEC Report LA-3795 (1967) 32 pp.

F - 14 G.H. Frischat, Ber. Deut. Keram. Ges., 48 (1971) 441.

F - 15 E. Fromm, E. Gebhardt and U. Roy, Z. Metallk, 57 (1966) 808.

F - 16 K. Fueki, Y. Oguri and T. Mukaibo, Bull, Chem. Soc. Japan, 41 (1968) 569.

F - 17 C.T. Fujii and R.A. Meussner, Rep. Nav. Res. Lab. Progr., (1967) 27.

F - 18 Y. Fujikawa, P. Son, M. Miyake and T. Sano, Nippon Kinzoku Gakkaishi 34 (1970) 1259.

(G)

G - 1 P. Geld and V.D. Lyubimov, Izv. Akad. Nauk SSSR, OTN Met. Toplivo, No. 6, (1961) 119.

G - 2 K.V. Gorev and S.L. Lifshits, Vesti Akad. Navak. Belarus. SSR, Ser. Fiz. - Tekh Navak No. 2 (1968) 119.

G - 3 R.N. Goshtagore, J. Appl. Phys., 4 (1969) 4374.

G - 4 S. Goto and S. Koda, Nippon Kinzoku Gakkaishi 34 (1970) 319.

G - 5 S. Goto, K. Nomaki and S. Koda, J. Japan. Inst. Met., 31 (1967) 590.

G - 6 D. Graham adn D.H. Tomlin, Phil. Mag., 8 (1963) 1581.

G - 7 A. Green, D.P. Whittle and N. Swindells, Scripta Met., 7, (1973) 1079.

G - 8 C.D. Greskovich, J. Am, Ceram. Soc., 53 (1970) 498.

G - 9 C. Greskovich and V.S. Stubican, J. Am. Ceram. Soc., 53 (1970) 251.

G - 10 P.L. Gruzin, V.V. Mural and A.P. Fokin, Fiz. Metal. Metalloved., 32 (1971) 208.

G - 11 P.L. Gruzin, Yu. A. Policarpov, and G.B. Fedorov, Fiz. Metal. Metalloved., 4 (1957) 94.

G - 12 P.L. Gruzin, S.V. Zemskii and J.B. Rodina, Met. Metalloved. Chist. Metal., Sb. Nauchn. Rabot., 4 (1963) 243.

G - 13 P.L. Gruzin et al, Trudy In-ta Metal, in Baikova, 5 Izv. Akad. Nauk SSRR (1959) 155.

G - 14 P. Guiraldenq., Thesis, U. Paris, 1964: Met. Corros. Ind., 39 (1964) 347.

G - 15 P. Guiraldenq and P. Poyet, Compt. Rend. Acad. Sci., Paris, Ser. C. 270 (1970) 2116.

(H)

H - 1 W. Hagel, Trans. AIME, 224 (1962) 430.

H - 2 W.C. Hagel, J. Am. Ceram. Soc., 48 (1965) 70: Trans ASM. 56 (1963) 583.

H - 3 W.C. Hagel, P.J. Jargensen and D.S. Tomalin, J. Am. Ceram. Soc., 49 (1966) 23.

H - 4 W.C. Hagel and A.U. Seybolt, J. Electrochem. Soc., 108 (1961) 1146.

H - 5 G.F. Hancock, Phys. Stat. Sol. A, 7 (1971) 535.

H - 6 G.F. Hancock and G.M. Leak, Metal Sci., J., 1 (1967) 33.

H - 7 C.S. Hartley, J.E. Steedly and L.D. Parsons, "Diffusion in bcc Metals" ASM (1965).

H - 8 A. Hässner, Dissertation, Tech. Univ. Dresden (1962).

H - 9 A. Hässner, L. Ehrhardt. G, Ergelmann and B. Epler, Neue Hutle, 12 (1967) 286.

H - 10 A. Hässner and W. Lange, Phys. Stat. Sol. 8 (1965) 77.

H - 11 D. Hayes, D.W. Budworth and J.P. Roberts, Trans. Brit. Ceram. Soc. 62 (1963) 507.

H - 12 T. Hehenkamp, Z. Naturforsch., 23 (1968) 229.

H - 13 H. Helfmeier and M. Feller - Kniepmeier, J. Appl. Phys. 41 (1970) 3202.

H - 14 P. Hambree and J.B. Wagner, Jr., Trans. AIME, 245 (1969) 1547.

H - 15 W.H. Herrnstein, F.H. Beck and M.G. Fontana, Trans. AIME, 242 (1968) 1049.

H - 16 Th. Heumann and R. Imm, J. Phys. Chem. Solids, 29 (1968) 1613.

H - 17 C.W. Hewson and W.D. Kingery, J. Am. Ceram. Soc., 50 (1967) 218.

H - 18 K. Hirano, R.P. Agarwala, B.L. Averback and M. Cohen, J. Appl. Phys., 33 (1962) 3049.

H - 19 K. Hirano, M. Cohen and B.L. Averback, Acta. Met., 9 (1961) 440.

H - 20 K. Hirano and A. Nishinuma, Nippon Kinzoku Gakkaishi, 32 (1968) 516.

H - 21 K. Hirano and K. Ouchi, Nippon Kinzoku Gakkaishi, 32 (1968) 613.

H - 22 R.E. Hoffman, F.W. Pikus and R.A. Ward, J. Met., 8 (1956) 483.

H - 23 P.H. Holloway and G.P. Mohanty, J. Phys. Chem. Solids 32 (1971) 2656

H - 24 J.B. Holt, Proc. Brit. Ceram. Soc., No. 9 (1967) 157.

H - 25 A. Hoskino and T. Araki, Tetsu to Hagane 56 (1970) 252.

H - 26 A. Hoshino and T. Araki, Trans. Nat. Res. Inst. Metals, 13 (1971) 99.

H - 27 Y. Hosoi, S. Kondo, H. Okada and K. Inouye, Kinzoku Hyomen Gijutsu 18 (1967) 62.

H - 28 A.M. Huntz, M. Aucouturier and P. Lacombe, compt. Rend., Acad. Sci., Paris, Ser. c, 265 (1967) 554.

H - 29 A.M. Huntz, P. Guiraldenq, M. Aucouturier and P. Lacombe, Mem. Sci. Rev. Met., 66 (1969) 85: Diff. Data, 4 (1970) 205.

(J)

J - 1 D.W. James and G.M. Leak, Phil. Mag. 12 (1965) 117, 491.

J - 2 D.W. James and G.M. Leak, Phil. Mag., 14 (1966) 70.

J - 3 M.M.P. Janssen and G.D. Rieck, Trans. AIME, 239 (1967) 1372.

J - 4 D.W. James and G.M. Leak, Phil. Mag., 12 (1965) 117, 491.

J - 5 R.M. Jodlowski and G.C. Kuczynski, Proc - 2nd Intl. Conf. on sintering and Related Phenomena, 1965 (Publ. 1967) 553.

J - 6 H.A. Johansen, Paper No. 35 at 6th Plansee Seminar, Reutte (Austria) 1968.

J - 7 T.P. Jones, R.L. Cable and C.J. Mogab, J. Am. Ceram. Soc., 52 (1969) 331.

(K)

K - 1 D.F. Kalinovich, I.I. Kovenskii and M.D. Smolin, Ukrain, Fiz. Zh., 13 (1969) 340.

K - 2 D.F. Kalinovich, I.I. Kovenskii and M.D. Smolin, Ukr. Fiz. Zh., 13 (1968) 518: Fiz. Tverd. Tela., 10 (1968) 569: 29 (1970) 671.

K - 3 D.F. Kalinovich, I.I. Kovenskii, M.D. Smolin and V.M. Statsenko, Fiz. Tverd. Tela, 11 (1969) 1723, 2378.

K - 4 D.F. Kalinovich, I.I. Kovenskii, M.D. Smolin and V.M. Statsenko, Fiz. Khim. Metch. Mater., 6 (1970) 104: Fiz. Metal. Metalloved, 29 (1970) 653.

K - 5 M.G. Karpman, G.V. Shcherbedinskii, G.N. Dublinin and G.P. Bendediktova, Metalloved. Term. Obrab. Metal., No. 3, (1967) 46.

K - 6 M.J. Klein, A. Appl. Phys., 38 (1967) 167.

K - 7 S.M. Klotsmann, A.N. Timofeyev and I. Sh. Traktenberg, Phys. Met. Metallog., 14 (1962) 91.

K - 8 D.L. Kohlstedt, W.S. Williams and J.B. Woodhouse, J. Appl. Phys., 41 (1970) 4476.

K - 9 A. Kohn, J. Levasseur, J. Philibert and M. Wanin, Acta. Meta., 18 (1970) 163.

K - 10 Yu. V. Kornev and V.I. Shaidurov, Diffuz. Protesy Metal., (1968) 25.

K - 11 V. Ya. Kovarskii, I.T. Aleksanyan, U.E. Bondarenko and B.M. Orlov Fiz. Tverd. Tela, 10 (1969) 272.

K - 12 G.B. Krasilnikova and B.S. Mitin, Fiz. Metal, Metalloved., 29 (1970) 204.

K - 13 K.G. Kreidev and G. Bruggeman, Trans. AIME, 239 (1967) 1222.

K - 14 I.R. Kreski and I.B. Cutler, J. Am. Ceram. Soc., 51 (1968) 440.

K - 15 M.A. Krishtal and A.P. Mokrov, Zavod. Lab., 33 (1967) 827.

K - 16 M.A. Krishtal and A.P. Mokrov, Zashch. Pokryt. Metal., No. 1 (1967) 18 (b).

K - 17 M.A. Krishtal, A.P. Mokrov and O.V. Stepanova, Fiz. Metal. Metalloved., 24 (1967) 688.

K - 18 M.A. Krishtal, A.P. Mokrov, O.V. Stepanova and I.A. Goncharenk Zashch. Pokryt. Metal., No. 2 (1968) 209.

K - 19 M.A. Krishtal and A.M. Morova, Vch. Zap. Tul. Gos. Pedagog. Inst. Fiz. - Tekhn. Nauki, No. 1 (1967) 93.

K - 20 J. Kucera and B. Million, Z Metallk., 61 (1969) 160.

K - 21 J. Kucera, B. Million and K. Ciha, Kovove Mat., 7 (1969) 97: Diff. Data 4 (1970) 198.

K - 22 G.C. Kuczyski, L. Abernethy and J. Allan, "Kinetics of High Temp. Processes" Conf. Proc., (Wiley, N.Y., 1959) 163.

(L)

L - 1 H. Lafitau, Compt.Rend. Acad. Sci., Paris, Ser. C., 267 (1968) 132.

L - 2 H. Lafitau, P. Gendrel and L. Jaque, Compt. Rend. Acad. Sci., Paris, Ser. C., 263 (1966) 1033.

L - 3 D.Y.F. Lai and R.J. Borg, U.S. AEC Rept. UCRL-50314 (1967) 6 pp.

L - 4 J.J. Lander, H.E. Kern and A.L. Beach, J. Appl. Phys., 23 (1952) 1305.

L - 5 L.N. Larikov, V.M. Tyshkevich, and L.F. Chorna, Ukr. Fiz. Zh., 12 (1967) 983.

L - 6 E. Lassner, R. Püschel and F. Benesovsky, Planseeber, Pulvermet., 16 (1968) 91: Diff. Data 3 (1969) 28.

L - 7 J. Levasseur and J. Philibert, Compt. Rend. Acad. Sci., Paris Ser. C., 264(1967) 380.

L - 8 G. Levin, Osnovy Vakumnoi Tekhniki Izd. "Energia" (1969) (quoted by Zholobov and Malev: see Diff. Data 5 (1971) 605.

L - 9 R.L. Levin and J.B. Wagner, Jr., Trans. AIME, 233 (1965) 159.

L - 10 S.J. Lewis and P.A. Flinn, Appl. Phys. Lett., 15 (1969) 331.

L - 11 R. Lindner and A. Akerstrom, Z. Phys. Chem. 6 (1965) 162: Discuss. Farad. Soc., 23 (1957) 133: Z. Phys. Chem. 18 (1958) 303.

L - 12 V.D. Lyubimov, P.V. Geld. G.P. Shveikin and Yu. A. Sutina, Izv. Akad. Nauk SSSR, Metal., No. 2, (1967) 84.

L - 13 V.D. Lyubimov et al, Izv. Akad. Nauk SSSR, Metal., No. 3 (1969) 201.

(M)

M - 1 H.E. MacCoy and J.F. Murdock, Trans. ASM, 56 (1963) 11.

M - 2 J.R. MacEwan, J.V. MacEwan and L. Yaffe, Canad. J. Chem., 37 (1959) 1623, 1629.

M - 3 P.S. Mauya, W.K. Chen and N.L. Peterson, Met. Trans., 1 (1970) 801.

M - 4 C. Matano, Mem. Coll. Sci. Univ. Kyoto, 15 (1932) 351.

M - 5 M.A. Matosyan and V.M. Golikov, Izv. Akad. Nauk Arm. SSR, Fiz., 2 (1967).

M - 6 G. Melchior, J. Less-Common Metals, 17 (1969) 443.

M - 7 A. Messner, R. Benson and J.E. Dorn, Trans. ASM, 53 (1961) 227.

M - 8 B. Million and J. Kucera, Acta. Met., 17 (1969) 339.

M - 9 B. Million and J. Kucera, Czech. J. Phys., B 21 (1971) 161.

M - 9b W.J. Minford and V.S. Stubican, Report to U.S. Office of Naval Research on Contract No. N00014-A-0385-0011 (Dec. 1973).

M - 10 M. Miyake and T. Sano, Tech. Rep. Osaka Univ., 18 (1968) 317.

M - 11 J. Mizuno, S. Ogawa and T. Hirone, J. Phys. Soc. Japan 9 (1954) 961.

M - 12 K. Monma, J. Japan Inst. Met., 28 (1964) 188.

M - 13 K. Monma, H. Suto and H. Oikawa, J. Inst. Met., 28 (1964) 192.

M - 14 W.J. Moore, U.S. AEC Report ORO-78 (1951).

M - 15 W.J. Moore, J.J. Landnor, S.R. Logan, M. O'Keefe, J.S. Choi, Y. Ebisuzaki, S. Brown and D. Mitchell, U.S. AEC Rept. TID-11020 (1960).

M - 16 A. Morkel and H. Schmalzreid, Z. Phys. Chem., N.F., 32 (1962) 76.

M - 17 R. Morlotti, Z. Naturforschg., 24A (1969) 441.

M - 18 S. Mrowec, Bull. Acad. Pol. Sci., Ser. Sci. Chim., 15 (1967)373.

M - 19 S. Mrowec. Bull. Acad. Pol. Sci., Ser. Sci. Chim., 15 (1967) 521, 527.

M - 20 S. Mrowec, T. Walec and T. Werber, Corr. Sci., 6 (1966) 287.

M - 21 L.M. Mulyakaev. G.V. Shcherbedinskii and G.N. Dubinin, Metalloved, Term. Obrat, Metal., No. 8 (1971) 45.

(N)

N - 1 A.I. Nakonechnikov, L.V. Pavlinov, and V.N. Bykov., Phys. Met. Metallog., 22 (1966) 73: Diff. Data 4 (1970) 50.

N - 2 E.P. Nechiporenko, V.M. Krivoruchko, A.S. Mitrofanov, and V.I. Khotkevich, Fiz. Metal. Metalloved., 32 (1971) 604.

N - 3 R.P. Nelson, Acta Polytech. Scand., Chem, Met. Ser., No. 60 (1967) 31 pp.: Diff. Data 2 (1968) 331.

N - 4 G.M. Neumann, Paper No. 7, 6th Plansee Seminar, Reutee, Austria (1968).

N - 5 J. Nicholas, J. Phys. Chem. Solids 28 (1967) 847.

N - 6 M.B. Niemann and A.Y. Shinyaev, Dokl. Akad. Nauk SSSR, 91 (1953) 265.

N - 7 K. Nohara and K. Hirano, Proc. Intl. Conf. Tech. Iron Steel, Tokyo, 1970.

(O)

O - 1 Y. Oishi and W.D. Kingery, J. Chem. Phys. 33 (1960) 480.

O - 2 M. O'Keefe in "Sintering and Related Phenomena" ed. Kuczyinski, Hooton and Gibbon (Gordon and Breach, N.Y. 1967).

O - 3 M. O'Keefe and W.J. Moore, J. Phys. Chem. 65 (1961) 1438.

O - 4 M. Onishi and H. Mitani, Kinzoku Hyomen Gijutsu, 19 (1968) 146.

(P)

P - 1 A.E. Paladino and W.D. Kingery, J. Chem. Phys., 37 (1962) 957.

P - 2 A.R. Paul and R.P. Agarwala, Met. Trans., 2 (1971) 2471.

P - 3 L.V. Pavlinov, E.A. Isadzanov and V.P. Smirnov, Fiz. Metal. Metalloved., 25 (1968) 959.

P - 4 R.E. Pawel and T.S. Lundy, J. Electrochem. Soc., 115 (1968) 233.

P - 5 R.E. Pawel and T.S. Lundy, Acta. Met., 17 (1969) 979.

P - 6 H.W. Paxton and E.G. Gondolf, Arch. Eisenhutt., 30 (1959) 55.

P - 7 R.F. Peart, D. Graham and D.H. Tomlin, Acta. Met., 10 (1962) 519.

P - 8 J. Pelleg. paper presented to 1968 Fall Meeting of Met. Soc. OF AIME, Detroit: Abstract in J. Met., 20 (1968) 53.

P - 9 J. Pelleg. Phil. Mag., 21 (1970) 735.

P - 10 Ch. Perrin, Compt. Rend. Acad. Sci., Paris, Ser. C., 272 (1971) 1026.

P - 11 Yu. V. Piguzov, V.D. Verner, I. Ya. Rzhevskaya and Nguyon Ngoc Quin, Diffuz. Metal Splavakh, Tr. Vses. Kouf., 3rd (1968) 315.

P - 12 B. Ya. Pines, I.G. Ivanov and I.V. Smushkov, Sov. Phys. Solid State, 4 (1963) 7, 1380.

P - 13 B. Pines and I.V. Smushkov, Soviet Phys. - Techn. Phys., 28 (1958) 626.

P - 14 J.P. Pivot, A. van Craeynest, and D. Calais, J. Nucl. Mater., 31 (1969) 342.

P - 15 R.W. Powers and M.V. Doyle, J. Appl. Phys., 28 (1957) 255: 30 (1959) 514.

P - 16 J.B. Price, Thesis, Northwestern U. (1968): Univ. Microfilm. No. 69 - 6979. Diff. Data 4 (1970) 236.

P - 17 A.T. Price, H.A. Hall and A.P. Greenough, Acta. Met., 12 (1964) 49.

P - 18 J.B. Price and J.B. Wagner, Jr., Z. Phys. Chem., 49 (1966) 257.

P - 19 J.B. Price and J.B. Wagner, Jr., J. Electrochem. Soc., 117 (1970) 242.

P - 20 D.A. Prokoshkin, E.V. Vasileva and L.L. Vergasova, Fiz. Metal. Metalloved., 23 (1967) 1134: Metalloved. Term. Obrab. Metal. No. 3 (1967) 44.

(R)

R - 1 S.P. Ray and B.D. Sharma, Acta. Met., 16 (1968) 981.

R - 2 S.P. Ray and B.D. Sharma. Trans. Indian Inst. Metals 22 (1969) 17.

R - 3 R. Resnick and L. Seigle, Trans. AIME, 236 (1966) 1732.

R - 4 T.C. Reuther and M.R. Achter, Met. Trans. 1 (1970) 1777.

R - 5 J.E. Reynolds, B.L. Averback and M. Cohen, Acta. Met., 5 (1957) 29.

R - 6 E.W. Roberts and J.P. Roberts, Bull. Soc. Fr. Ceram., No. 77, (1967) 3.

R - 7 G.N. Ronami et al, Izv. Akad. Nauk SSSR, Neorg. Mater., 7 (1971) 1490.

R - 8 F. Roux, D. Ablitzer and A. Vignes, IEEE Conf. Record of 1970. Thermionic Conversion Specialist Conf., Florida, Oct 1970, 109.

R - 9 R.C. Ruder and C.E. Birchenall, J. Met., 3 (1951) 142.

R - 10 P.S. Rudman, Trans. AIME, 239 (1967) 1949.

R - 11 V.R. Ryabov and V.D. Duplyak, Svar. Proizrod., No. 8 (1968) 10.

(S)

S - 1 J.P. Sabatier and A. Vignes, Mem. Sci. Rev. Met., 64 (1967) 225.

S - 2 G.I. Samuel and M.M. Pavlyuchenko, Vest. Akad. Navuk Belarus, SSR, Ser. Khim. Navuk 1969 (4) 11 - 15.

S - 3 S. Sarian, J. Appl. Phys., 39 (1969) 5036.

S - 4 S. Sarian, J. Appl. Phys., 40 (1969) 3515.

S - 5 S. Sarian and J.M. Criscione, J. Appl. Phys., 38 (1967) 1794.

S - 6 T. Sasamoto and T. Sata, Kogyo Kagaku Zasshi 74 (1971) 832.

S - 7 K. Sato, Trans. Japan Inst. Met., 5 (1964) 91.

S - 8 K. Schwerdtfeger, Trans. AIME, 239 (1967) 1432.

S - 9 M.G. Seibel, Rev. Met. Mem, Sci., 61 (1964) 431.

S - 10 W. Seith, "Diffusion in Metallen" (2nd Ed.) Springer, Berlin, 1955.

S - 11 C.E. Sessions and T.S. Lundy, J. Nucl. Mater., 31 (1969) 316.

S - 12 A.U. Seybolt, Trans. AIME, 242 (1968) 752.

S - 13 V.Y. Shchelkonogov, L.N. Aleksandrov, V.A. Piterimov and V.S. Mordynk, Fiz. Metal. Metalloved., 25 (1968) 80.

S - 14 J.S. Sheasby and B. Cox, J. Less-Common Metals, 15 (1968) 129.

S - 15 J.S. Sheasby, W.W. Smeltzer and A.E. Jenkins, J. Electrochem. Soc., 115 (1968) 338.

S - 16 A.Y. Shinyaev, Fiz. Metal. Metalloved., 15 (1963) 100.

S - 17 A.Y. Shinyaev, Izv. Akad. Nauk SSRR, Metal, No. 4 (1969) 182.

S - 18 A.Y. Shinyaev, Izv. Akad. Nauk SSSR, Metal, No. 1. (1968) 203, Diff. Data 2 (1968) 142.

S - 19 M.T. Shim and W.J. Moore, J. Chem. Phys., 26 (1957) 802.

S - 20 V.K. Sikka and C.J. Rosa, U.S. Clearinghouse Fed. Sci. Sci. Techn. Info. Report No. AD-715006 (1970) 54pp.

S - 20(b) A.B. Shovensin, A.H. Minkevitch and G.B. Scherbinski, Izv., Vyssh. Uchebn. Zaved, Chem. Met., No. 1 (1965) 95.

S - 21 N.N. Sirota and S.N. Sokolov, Dokl. Akad. Nauk Beloruss, SSR, 15 (1971) 881.

S - 22 C.J. Smithells and C.E. Ransley, Proc. Roy. Soc., A 155 (1936) 195.

S - 23 P. Son, S. Ihara, M. Miyake and T. Sano, J. Japan. Inst. Met., 30 (1966) 1137.

S - 24 P. Son, S. Ihara, M. Miyake, and T. Sano, J. Japan Inst. Met., 31 (1967) 998.

S - 25 P. Son, M. Miyake and T. Sano, Tech. Rep. Osaka Univ., 18 (1968) 317.

S - 26 S. Steeb and R. Keppeler, Z. Naturforsch., 24A (1969) 1601.

S - 27 L.I. Steffansson and C.E. Birchenall, AFOSR Report (1961) 733.

S - 28 R. Sun, J. Chem. Phys., 28 (1958) 290.

S - 29 H. Suzuki, S. Kimura, T. Hase, and Y. Tsuchie, Bull. Tokyo. Inst. Technol., No. 90 (1969) 105.

S - 30 R.A. Swalin and M. Allan, J. Met., 8 (1956) 567.

S - 31 R.A. Swalin and A. Martin, J. Metals, 8 (1956) 567.

S - 32 J.H. Swisher, Trans. AIME 239 (1967) 110.

S - 33 J.H. Swisher, Trans. AIME 242 (1968) 2433.

(T)

T - 1 B.A. Thompson, Ph.D. Thesis, Resasselaer Polytech. Inst., (1961) (quoted by Holt (1967)).

T - 2 I.A. Tregubov, L.N. Kuzina and O.S. Ivanov, Dokl. Akad. Nauk SSSR, 180 (1968) 423 Diff. Data 2 (1968) 306.

T - 3 E.T. Turkdogan Trans AIME 242 (1968) 1665

(U)

U - 1 Yu. E. Ugaste, Fiz. Metal. Metalloved., 24 (1967) 442.

U - 2 Yu. E. Ugaste, Fiz. Metal. Metalloved., 30 (1970) 1107.

U - 3 W.R. Upthegrove and M.J. Sinnott, Trans. ASM, 50, (1958) 1031.

(V)

V - 1 B.A. Vankyshev and A.S. Panov, Fiz. Metal, Metalloved., 25 (1968) 321: 26 (1968) 517.

V - 2 B.A. Vandyshev and A.S. Panov, Izv. Akad. Nauk. SSSR, No. 1 (1968) 206.

V - 3 B.A. Vankyshev and A.S. Panov, Izv. Akad. Nauk, SSSR, Metal., No. 1 (1969) 244.

V - 4 M.V. Venzouskii and A.A. Oleinikov, Svar. Priozvod., No. 5 (1967) 16.

V - 5 A. Vignes, J. Philibert, M. Badia and J. Levasseur, Trans. 2nd Natl. Conf. Electron Microprobe Anal., Boston (1967) paper No. 20

V - 6 A. Vignes and J.P. Sabatier, Trans. AIME 245 (1969) 1795.

V - 7 Yu. N. Vilk, S.S. Nikolskii and R.G. Avarbe, Teplofiz. Vys. Temp., 5 (1967) 607.

V - 8 I.I. Vishnevskii, E.I. Akselrod, and N.D. Talyanskaya, Fiz. Tverd. Tela 13 (1971) 3446.

V - 9 M.L. Volpe and J. Reddy, J. Chem. Phys. (1972)

(W)

W - 1 R.L. Wagner, paper at 1969 Spring Meeting of Met. Soc. of AIME, Pittsburgh: abstract in J. Met., 21 (1969) 66A.

W - 2 B.F. Walker, V.A. Johnson, W.C. Hahn, Jr., and J.D. Wood, Trans. AIME, 242 (1968) 1233.

W - 3 L.C. Walters and R.E. Grace, J. Appl. Phys., 36 (1965) 2331: Jr. Electrochem. Soc. 110 (1963) 192.

W - 4 F.Y. Wang, J. Appl. Phys., 37 (1966) 929.

W - 5 S.J. Wang and H.J. Grabke, Z. Metallk., 61 (1970) 597.

W - 6 M. Wanin and A. Kohn, C.R. Acad. Sci., Paris, Ser. C, 267 (1968) 1558: Diff. Data 3 (1969) 401.

W - 7 S.I. Warshaw, Ph.D. Thesis, M.I.T., 1961: see A.E. Paladino and R.L. Cable, J. Am. Ceram, Soc., 46 (1963) 133.

W - 8 S.I. Warshaw and F.H. Norton, J. Am. Ceram. Soc., 45 (1962) 479.

W - 9 J.W. Weeton, Trans ASM, 44 (1952) 436.

W - 10 C.A. Wert, J. Appl. Phys. 21 (1950) 1196.

W - 11 W.P. Whitney and V.S. Stubican, J. Phys. Chem. Solids, 32 (1971) 305.

(Y)

Y - 1 G. Yamaguchi, M. Nakano and M. Tosaki, Bull. Chem Soc. Japan 42 (1969) 2801.

Y - 2 Y.F.Y. Yao and J.T. Kummer, J. Inorg. Nucl. Chem., 29 (1967) 2453.

(Z)

Z - 1 S.V. Zemskii, v.M. Gruzdeva and L.S. Lvov, Izh. Vyssh. Ucheb. Zaved., Chern. Met,. 13 (1970) 106.

Z - 2 S.V. Zemskii and B.P. Pyakhin, Fiz. Metal, Metalloved., 23 (1967) 913.

Z - 3 S.P. Zholobov and M.D. Malev, Zh. Tekh. Fiz., 41 (1971) 627: see Diff. Data 5 (1971) 605.

Z - 4 V.I. Zmii and A.S. Seryugina, Zashch. Pokryt. Metal., No. 2 (1968) 195.

Part 2. Oxidation and Hot Corrosion of Commercial Superalloys

The following section presents a summary of information on the oxidation and corrosion of commercial nickel and cobalt base superalloys. Many of the original papers present results for several superalloys, and in these cases the results have been described in detail under one alloy, with a cross-referencing under the others. However, where a Figure or a Table relates only to one alloy, it has been included under that alloy, even if the general summary of the work is elsewhere. So far as possible, all the original data have been presented, including metallographs of the attack since this is considered to be an important parameter in the case of hot corrosion. Mechanistic discussions have in general not been included, but any comments relating to practical in-service experience have been reproduced verbatim.

The nominal compositions of the alloys listed are presented in a Table preceding the text. The alloys included are:-

TABLE 0-1

COMPOSITION OF THE SUPER ALLOYS

Alloy	Nominal Composition, per cent															
	Ni	Co	Cr	Al	Ti	Mo	W	Ta	Nb	Fe	Mn	Si	Zr	B	C	Other
B 1900	bal	10.0	8.0	6.0	1.0	6.0	0.1 max	4.3	0.1 max	0.35max	0.2max	0.25max	0.08	0.015	0.10	
B 1910	bal	10.0	10.0	6.0	1.0	3.0	-	7.0	-	0.35max	-	-	0.10	0.015	0.10	
FSX 414	10.5	bal	29.5	-	-	-	7.0	-	-	2.0	1.0	-	-	0.01	0.35	
FSX 418	10.5	bal	29.5	-	-	-	7.0	-	-	2.0	1.0	-	-	0.01	0.05	0.15V
G 64	bal	-	11.0	6.0	-	3.0	3.5	-	2.0	5.0max	0.4	0.5	-	0.25	0.12	
GMR 235	bal	-	15.5	3.0	2.0	5.25	-	-	-	10.0	0.25max	0.60max	-	0.06	0.15	
Hastelloy X	bal	1.5	22.0	-	-	9.0	0.6	-	-	18.5	0.5	0.5	-	-	0.10	
IN 100	bal	15.0	10.0	5.5	4.7	3.0	-	-	-	-	-	-	0.06	0.015	0.15	1.0V
IN 587	bal	20.0	28.5	1.2	2.3	-	-	-	0.7	-	-	-	0.05	0.003	0.05	
IN 589	bal	-	50	-	-	-	-	-	-	-	-	-	1.50	-	0.04	
IN 597	bal	20.0	24.5	1.5	3.0	1.5	-	-	1.0	-	-	-	0.05	0.012	0.05	
IN 700	bal	28.5	15.0	3.0	2.2	3.75	-	-	-	0.7	0.10	0.30	-	-	0.12	
713C	bal	-	12.5	6.1	0.80	4.2	-	-	2.0	2.5max	0.25max	0.50max	0.10	0.012	0.12	
713LC	bal	-	12.0	5.9	0.60	4.5	-	-	2.0	0.5max	0.25max	0.50max	0.10	0.01	0.05	
IN 717	bal	9.5	11.0	7.7	1.0	3.5	-	-	2.4	-	-	-	0.10	0.013	0.10	
IN 718	bal	-	19.0	0.50	0.90	3.05	-	-	5.13(+Ta)	18.5	0.18	0.18	-	-	0.04	
IN 728NX	bal	10.0	17.0	6.25	-	1.5	2.0	2.0	1.0	-	-	-	0.10	0.02	0.05	
IN 738	bal	8.5	16.0	3.4	3.4	1.75	2.6	1.75	0.9	0.50max	0.20max	0.30max	0.10	0.01	0.17	
IN 750	bal	-	15.5	0.70	2.50	-	-	-	0.95 (+ Ta)	7.0	0.50	0.25	-	-	0.04	
IN 751	bal	-	15.5	1.20	2.30	-	-	-	0.95 (+ Ta)	7.0	0.50	0.25	-	-	0.05	
K 2	bal	15.0	21.0	2.0	0.5	3.0	1.0	-	1.0 (+ Ta)	-	-	-	-	0.015	0.03	
L 605	10.0	bal	20.0	-	-	-	15.0	-	-	-	1.50	0.50	-	-	0.10	
Mar-M 200	bal	10.0	9.0	5.0	2.0	-	12.5	-	1.0	-	-	-	0.05	0.015	0.15	
Mar-M 246	bal	10.0	9.0	5.5	1.5	2.5	10.0	1.5	-	-	-	-	0.05	0.015	0.15	
M 252	bal	10.0	19.0	1.0	2.6	10.0	-	-	-	-	0.50max	0.50max	-	0.005	0.15	
Mar-M 302	-	bal	21.5	-	-	-	10.0	9.0	-	-	-	-	0.20	0.005	0.85	
Mar-M 421	bal	9.5	15.8	4.25	1.75	2.0	3.8	-	2.0	-	-	-	0.05	0.015	0.15	
Mar-M 432	bal	20.0	15.5	2.8	4.3	-	3.0	2.0	2.0	0.50max	0.10max	0.10max	0.05	0.015	0.15	
Mar-M 509A	10.0	bal	24.0	-	0.20	-	7.0	3.5	-	-	-	-	0.50	-	0.60	
Nicrotung	bal	10.0	12.0	4.0	4.0	-	8.0	-	-	-	-	-	0.05	0.05	0.10	
Nimonic 75	bal	-	20	-	0.4	-	-	-	-	5.0max	1.0max	1.0max	-	-	0.01	
Nimonic 80A	bal	2.0max	18/21	0.5/1.8	1.8/2.7	-	-	-	-	5.0max	1.0max	1.0max	-	-	0.1max	
Nimonic 81	bal	-	30	0.9	1.7	-	-	-	-	-	-	-	0.05	0.003	0.04	
Nimonic 90	bal	15/21	18/21	0.8/2.0	1.8/3.0	-	-	-	-	5.0max	1.0max	1.0max	-	-	0.13max	

Nimonic 100	bal	18/22	10/12	4.0/6.0	1.0/2.0	4.5/5.5.	-	-	-	2.0max	-	0.5max	-	-	0.3max	
Nimonic 105	bal	18/22	13.5/16	4.2/4.8	0.9/1.5	4.5/5.5	-	-	-	1.0max	1.0max	1.0max	-	-	0.2max	
Nimonic 115	bal	15	15	5	4	3.5	-	-	-	-	-	-	-	-	0.2max	
PDRL 161	bal	-	17.0	6.5	1.0	1.0	-	-	2.0	-	-	-	0.10	0.02	0.12	
PDRL 162	bal	-	10.0	6.5	1.0	4.0	2.0	2.0	1.0	-	-	-	0.10	0.02	0.18	
PDRL 163	bal	-	17.0	6.3	0.1	1.6	2.0	1.9	1.0	-	-	-			0.05	
RA 333	bal	3.0	25.0	-	-	3.0	3.0	-	-	18.0	1.5	1.25	-	-	0.05	
Rene 41	bal	11.0	19.0	1.5	3.1	10.0	-	-	-	-	-	-	-	0.010 max	0.09	
Rene 80	bal	9.5	14.0	3.0	5.0	4.0	4.0	-	-	-	-	-	0.03	0.015	0.17	
S 816	20.0	bal	20.0	-	-	4.0	4.0	-	4.0	3.0	1.20	0.40	-	-	0.38	
SEL	bal	22.0	15.0	4.4	2.4	4.5	-	-	-	1.0	0.3	0.5	-	0.015	0.08	
SEL15	bal	14.5	11.0	5.4	2.5	6.5	1.5	-	0.5	0.5 max	0.3 max	0.5 max	-	0.015	0.07	
TRW 1800	bal	-	13.0	6.0	0.6	-	9.0	-	1.5	-	-	-	0.07	0.07	0.09	
TRW 1900	bal	10.0	10.3	6.3	1.0	-	9.0	-	1.5	-	-	-	0.10	0.03	0.11	
U 500	bal	18.0	19.0	2.9	2.9	4.0	-	-	-	4.0 max	0.75 max	0.75 max	-	0.005	0.08	
U 520	bal	12.0	19.0	2.0	3.0	6.0	1.0	-	-	-	-	-	-	0.005	0.05	
U 700	bal	18.5	15.0	4.25	3.5	5.2	-	-	-	1.0 max	-	-	-	0.05 max	0.15 max	
U 710	bal	15.0	18.0	2.5	5.0	3.0	1.5	-	-	-	-	-	-	0.20	0.07	
Unitemp 1753	bal	7.2	16.2	1.9	3.2	1.6	8.4	-	-	9.5	0.05	0.10	0.06	0.008	0.24	
Waspaloy	bal	13.5	19.5	1.4	3.0	4.3	-	-	-	2.0max	0.5max	0.5max	0.09	0.006	0.07	0.03max5
WI52	1.0 max	bal	21.0	-	-	-	11.0	-	2.0	2.0	0.50 max	0.50 max	-	-	0.45	
X40	10.5	bal	25.5	-	-	-	7.5	-	-	2.0	1.0	0.5	-	0.01	0.50	
X45	10.5	bal	25.5	-	-	-	7.5	-	-	2.0	1.0	-	-	0.01	0.25	
21 D4																

B 1900

L. D.Graham, J. D. Gadd and R. J. Quigg, Hot Corrosion Problems Associated with Gas Turbines, ASTM Special Technical Publication, STP 421, 1967, 105.

See 713C for details. B 1900 is very bad in both the PWA burner rig at 1800°F (982°C) and a crucible test in 99% Na_2SO_4, 1% NaCl at 1650°F (900°C): 1.6g loss in crucible, 4.5g loss in rig test. Far and away the worst of alloys tested - much worse than 713C, Mar M 302 and TRW 1900 were ranked overall marginally worse, Mar M 200 marginally better, at 1800°F (982°C). Rate of attack of B 1900 increased progressively with temperature in this range.

Authors remark that corrosion products (imply that it was the same on all the heavily corroded material) contained NiO and Ni_3S_2, together with nickel metal. Specimens of B 1900 coated with Al/Cr) also tested - good resistance.

J. J. Walters, (AVCO/Lycoming Division) Technical Report to the Air Force Materials Laboratory, Wright-Patterson Air Force Base AFML-TR- 67-297 (September 1967).

Several alloys evaluated (713C, 713LC, TRW 1800, B 1900, B 1910, Mar-M 200, PDRL 161, PDRL 162, IN 738X, U 700, U 710 and X 40). Rig tested airfoil-shaped specimens with 120h at peak specimen metal temperatures of 1600 and 1750°F (871 and 955°C) with salt/combustor inlet air ratios of 4 and 8 ppm and fuel sulphur levels of 0.03 wt % (JP-4) and 0.16 wt % (JP-4R). An additional test was run with JP-5 fuel (0.16 wt % S). A second phase of the programme involved rig testing specimens for 120, 240 and 360h at peak metal temperatures of 1600° and 1750°F with a salt/air ratio of 4 ppm and fuel sulphur content of 0.03 wt % (JP-4). The alloys were prepared by vacuum induction melting and casting into shell moulds. The temperature distribution across the specimens was determined using inserted pins. The rig used was the Lycoming environmental test rig, having a combustor capable of generating a high velocity (700 ft per second) gas stream to which artificial sea water is added. The specimens were fixed in a holder mounted on a water-cooled shaft rotating at 1000 rpm. After 10 min at temperature the specimens were cycled out of the combustion gas stream and allowed to air cool; this cycle was repeated until the required total time at temperature had been completed. The air/fuel ratio was maintained on the oxidising side of stoichiometry, varying between 25/1 and 34/1.

After the test each specimen was visually examined for the extent, nature and location of sulphidation. Depth of attack measurements were made on sections cut at 0.25, 1.0 and 1.5 in from the tip of the specimens. The comparisons were made at the points where the sections intersect the temperature isotherms plotted at 25°F intervals. In the evaluation of the 1600°F test, the ¼ in. section intersected the 1450, 1475 and 1500°F isotherms; the 1 in section crosses the 1525, 1550, 1575, and 1600°F and the 1¼ in section intersects the 1475, 1500, 1525 and 1550°F isotherms. For the 1750°F test, the equivalent contours intersected were 1700, 1725 and 1750°F at ¼ in; 1675, 1700, 1725 and 1750°F at 1¼ in. The scales were identified by X-ray techniques, and the alloys were also subjected to microprobe analysis; three areas were looked at on each alloy: (1) Initial attack - oxidation had taken place and a very narrow depleted zone containing only a few sulphides had been generated; (2) Mild attack - oxides, sulphides and a depleted zone have been formed, but the depth to which the attack has penetrated is shallow; (3) Gross attack - the attack has penetrated to a much greater depth.

Testing at 1600°F caused the corrosion to be located in the hotter portions of the air foils while the cooler areas tended to be corrosion-free. Exposure at 1750°F peak metal temperature resulted in corrosion-free areas in the hotter sections of the specimens while the cooler areas were susceptible to attack. From the measurements of alloy corrosion versus temperature, graphs were constructed. The "total corrosion" was reported as the area under these curves. These exhibited a lower threshold temperature below which there was no corrosion, and an upper terminal temperature above which there was no attack. It was suggested that this upper temperature was associated with the vaporization temperature of the salt. The salt deposit on the specimens was sodium sulphate and magnesium sulphate: the chloride ion was not detected. Depth of penetration measurements were also made.

The alloys were grouped in four sets: B 1900, together with B 1910 Mar M 200 and IN 100 had very poor resistance. 713 C, 713 LC, PDRL 161 and PDRL 162 had poor resistance. U 700, IN 728 X and TRW 1800 had relatively good resistance, and X-40 had excellent resistance (no attack). B 1900 was the worst of all. The corrosion resistance correlated quite well with chromium content (Fig. 1.1).

Table 1.I. lists the results of tests at 1600 and 1750°F peak temperature using JP-4 and JP-4R fuel with 4 ppm salt; Table 1.II with 8 ppm salt. Table 1.III compares the relative performance of the alloys under various test conditions. Table 1.IV lists the threshold and terminal temperatures after 120 and 360h using JP-4 fuel and 4 ppm salt: for B 1900 the temperatures were not given. Table 1.V lists the corrosion products on the trailing edge determined by X-ray diffraction after 40h. For B 1900 a spinel with lattice spacing 8.17 Å, NiO and Al_2O_3 were detected, in that order. After 120h, a further unknown phase with d-spacings 3.88, 3.29, 2.74, 1.94, 1.67, 1.65 and 1.38 was detected. (Table 1.VI) Table 1.VII lists the corrosion products found in powders removed from areas which had undergone sulphidation corrosion after 120h of testing. For B 1900, a spinel with spacing 8.25, NiO, and an unknown phase with d-spacings 3.33, 2.54 and 1.73 were present. Table 1-VIII lists the results of a microprobe analysis of the depletion zone areas. B 1900 - 84.2% Ni, 0.5% Cr, 4.0% Mo, 2.7% Al, 0% Ti, 5.9% Co and 1.5% Ta.

Figure 1.2 shows the corrosion as a function of temperature for B 1900 using JP-4 fuel, 8 ppm salt. Fig. 1.3, 4 ppm salt. Fig. 1.4, JP-4R fuel, 8 ppm salt. Fig. 1.5, 4 ppm salt. Fig. 1.6, JP-5 fuel (0.16% S), 8 ppm salt. Figure 1.7 shows a bar diagram comparing the "total corrosion" of all the alloys (B 1900 was the worst). Figure 1.8 shows the threshold temperature as a function of chromium content. Table 1.IX compares the relative performance of the alloys in the various conditions.

J. R. Johnston and R. L. Ashbrook NASA Technical Note TN D-5376 (August 1969).

Uncoated specimens of a number of commercial nickel and cobaltbase alloys were cyclically tested in the NASA high velocity test rig for times up to 100 h at temperatures ranging from 1700 to 2000°F (927 to 1093°C). Natural gas was used in the burner. The specimens were 10 cm x 2.5 cm x 0.63 cm, with one long edge tapered. 8 of these were mounted in a holder, each positioned radially with the tapered edge outwards. The holder was rotated in the exhaust from the burner at 900 rpm for 1 n, then lowered into a cold gas stream for 3 min - this constituting 1 cycle. The velocity of both the hot and the cold gas was Mach 1. These were the standard conditions - three variations were used: Mach 0.7, shutdowns every 10h, without forced air cooling; and cooling at the standard rate, but only at 1200°F (649°C) before heating.

At intervals of 20h of testing the specimens were removed from the apparatus, weighed, photographed and inspected for cracks with fluorescent dye penetrant. Prior to further testing they were again degreased. In most cases, one specimen was removed for metallographic examinations after 20h, and another after 60h of testing.

The authors note that the difference between alloys is much greater in high velocity tests than in the static tests. The ranking of alloys is also quite different in the two types of test.

The oxides on the materials oxidised in the high-velocity tests were determined by X-Ray diffraction. For B 1900, after 100h at 1800°F, only Al_2O_3 was present- this was also true after 100h at 1900°F. After 20h at 2000°F Al_2O_3 and a spinel with a_o = 8.05 Å were detected. After 60h and 100h, Al_2O_3, monoxide (NiO) and a spinel with a_o = 8.10 Å.

Figure 1.9 reports the weight loss data for all the alloys, and Figure 1.10 summarises the weight loss data for the alloys in terms of a bar diagram. B 1900 was one of the best alloys tested. Fairly severe thermal fatigue cracks developed in the tapered leading edge of B 1900 specimens. Figure 1.11 shows the surface recession of a number of alloys, including B 1900,and Figure 1.12 summarises the surface recession data after 100h at 2000°F (1093°C) as a bar graph. Figure 1.13 shows the microstructure of the edge after 100h test at 2000°F (1093°C), Figure 1.14 shows the specimens after various times and temperatures for B 1900, Mar.M 509 A and TD Ni Cr.

V.S. Moore, and A.R. Stetson, Final Report on NASC Contract No. N00019-68-C-0532, Solar Research Division Report RDR 1626.5 (December 1970) (see also progress reports: RDR-1626 1,2,3, and 4).

This research was primarily concerned with the hot corrosion of coated superalloys, and in particular with the selection of the best coating procedure for each alloy. However, some tests were performed on the uncoated alloys. The specimens were paddle-shaped to simulate blades, the actual blade length being 2 in, width 1 in, tested in the Solar turbine enviromental simulator. This involved a combustion chamber similar to that used in Solar's small commercial gasturbine. Eight specimens were mounted in a holder rotated at 1725 rpm. JP -5 fuel was used for all tests. 35 parts per million of synthetic sea salt were added to the combustion gases. Specimens were tested at 1650°F (899°C) and 1800°F (982°C) for the nickel-base alloys, and 1800°F (982°C) and 2000°F (1093°C). The nozzle exit gas velocity was maintained at Mach 0.85 minimum. One hour thermal cycles were used for a total of 150h maximum. Initially, specimens were removed at the end of each 20h exposure for visual examination, cleaning and weighing: later this period was extended to 30h for the coated specimens, but shortened to 10 to 20h for most of the uncoated specimens because of early failures. The temperature distribution over the blades was determined by means of imbedded thermocouples in model specimens for each of the test temperatures. The sulphur content of the fuel ranged between 0.02 to 0.10 wt %, averaging 0.08 wt %, much less than the maximum of 0.4% allowable in JP-5.

Curves of cumulative weight change versus exposure time are presented. Photographs were taken of the specimens after light glass bead blasting. The specimens were then sectioned and examined metallographically, the section being through the hottest part of the blade.

Uncoated B 1900 failed after only 20h at 1650F (899°C.) Figure 1.5 shows the cross-sections of the specimen.

B 1900 was the least corrosion resistant of the alloys tested: SEL 15 was next worst.

The weight changes are listed in Table 1-X and 1-X1. For B 1900 at 1650°F after 10h the weight change for two specimens were + 17.4 mg and + 54.6 mg. At 1800°F the change after 10h was -363 and -387mg. After 17h the figures were -1470 and -1610 mg.

H.T. Quigg, R.M. Schirmer and L. Bagnetto, Final Report to NASC on Contract N00019-69-C-0221 (Phillips Petroleum Company Research and Development Report 5732-70) July 1970.

See 713C for details.

P.E. Hamilton, K.H. Ryan and E.S. Nichols, Hot Corrosion Problems Associated with Gas Turbines, ASTM Special Technical Publication STP 421, 1967, 188.

See 713C for detailed summary. Figure 10-75 shows the performance of B 1900 in a test stand engine with and without salt injection: B 1900 was worse than 713C under both circumstances, about the same as Mar-M 200 with salt but rather worse without. With salt, TRW 1900 and IN 100 are rather worse than B 1900.

H.T. Quigg, R.M. Schirmer and L. Bagnetto, Final Report to Naval Air Systems Command on Contract N00019-70-C-0293 (Phillips Petroleum Company Research and Development Report 5903-71) Jan. 1971.

See 713C for details. Figure 1.16 shows a section of a B1900 specimen after 15h in a 2000F (1093°C) cyclictest with 1.0 ppm sea salt in the air and 0.04 wt % S in the fuel. Figure 1.17 shows a specimen corroded under the same circumstances with 100 ppm benzotriazole added to the fuel.

N.S. Bornstein, M.A. DeCrescente and H.A. Roth, in "Deposition and Corrosion in Gas Turbines", A.B. Hart and A.J.B. Cutler (eds.) (Applied Science Publishers, London, 1973) 70.

Figure 1.18 compares the oxidation of B 1900 at 900°C (a) uncoated, (b) coated with 1 mg/cm^2 Na_2SO_4, and (c) coated with 1 mg/cm^2 of a mixture of Na_2SO_4 and Cr_2O_3. In the last case, no accelerated oxidation is observed: it is stated that the same is true if SnO_2 is added to the Na_2SO_4. Figure 1.19 compares the oxidation at 900°C coated with (a) 1 mg/cm^2 each of Na_2SO_4 and MoO_3, and (b) 1 mg/cm^2 each of Na_2SO_4 and Cr_2O_3. Figure 1.10 shows that the oxidation of a specimen coated with 1 mg/cm^2 each of Na_2SO_4 and SiO_2 is slow, approximately the same as simple oxidation; but if the specimen is thermally shocked, a rapid oxidation, similar to that with just Na_2SO_4 ensues.

Specimens coated with 1 mg/cm^2 each of SiO_2 and Na_2SO_4 were after 1000 min exposure at 1000°C, washed and the solution chemically analysed. Only trace quantities of Na_2SO_4 were found. The surface of the specimen was coated with a glossy scale believed to be a sodium aluminium silicate. Specimens similarly coated and exposed 300 min at 900°C were also washed: the solutions were found to contain soluble sodium and silicon. The silicon was inferred to be present as the water-soluble $Na_2Si_2O_5$.

A number of B1900 coupons coated with mixtures, of Na_2SO_4 and various metal oxides and oxidised at 900°C for up to 6h are shown to show the relation between the attack and the melting point of the salt. The additional oxides and the melting points of the mixtures were (a) V_2O_5, 690°C; (b) MoO_3, 795°C; WO_3, 1473°C; and Cr_2O_3, 1990°C. The first two, and pure Na_2SO_4, produced characteristic hot corrosion attack; the last two produced light, adherent scales resembling simple oxidation.

V.S. Moore and A.R. Stetson, Final Report to Naval Air Propulsion Test Center on Contract N00156-71-C-1020, July 1973.

See 713C for details.

N.S. Bornstein, M.A. DeCrescente and H.A. Roth, Annual Report to the Office of Naval Research on Contract N00014-70-C-0234, June 1973.

Shows a section of a B1900 blade from an industrial engine showing severe hot corrosion. The blade was originally coated, and was uncooled.

C.E. Lowell and R.V. Miner, NASA Technical Memorandum TM X-68191, Jan. 1973.

Describes the improvement in the cyclic oxidation resistance of B1900 produced by the addition of 1% silicon. The alloys were tested in cyclic oxidation at 1000° and 1100°C in air for 700 and 200 hr for the 1% Si and 0% Si alloys respectively. Each cycle consisted of 6 minutes in the furnace hot zone and 9 minutes cooling. The oxidation was measured by metallography and specific weight change. The same oxide formed on both alloys, so the effect was presumably due to improved oxide adherence.

The oxides detected by X-ray diffraction were NiO; a spinel with a_o = 8.21 Å (probably $Ni(Cr,Al)_2O_4$); a spinel with a_o = 8.08 Å (probably $NiAl_2O_4$), a tapiolite, presumably $NiTa_2O_6$ with other refractory metals substituting for Ta, and Al_2O_3.

Figure 1.21 shows the weight change for both alloys at 1000°C and Figure 1.22 that at 1100°C. Figure 1.23 shows the reduced thickness of the depleted zone in the 1% Si alloy after 2000 cycles at 1100°C.

N.S. Bornstein, M.A. DeCrescente and H.A. Roth, Gas Turbine Materials Conference Proceedings, Naval Air Systems Command, Washington (1972) 3.

It is shown that a coating of 1 mg/cm^2 Na_2SO_4 greatly accelerates the oxidation of B1900 at 900°C for times up to 800 min. The additions of Cr_2O_3 to the salt reduces the rate almost to the value with no salt at all. The additions of 1 mg/cm^2 of MoO_3 to the sulphate produces a further considerable acceleration. A coating of 1 mg/cm^2 each of Na_2SO_4 and SiO_2 results in a slow corrosion rate, but if such a specimen is thermally shocked by removing from the hot zone of the furnace and replacing, rapid oxidation ensues. V_2O_5 accelerates the rate, but SnO_2 and (surprisingly) WO_3 reduce it (the figures are similar to 1.18, 1.19 and 1.20). The authors present calculation of the relative ranking of the oxides in terms of their lowering the oxygen ion content of Na_2SO_4: WO_3 comes between MoO_3 and V_2O_5. It is suggested that the higher melting point of the oxide may be significant.

D.A. Spera and S.J. Grisaffe, Gas Turbine Materials Conference Proceedings, Naval Air Systems Command, Washington (1972) 102.

Describes testing procedures in use at N.A.S.A. Figure 1.24 shows the weight change of B 1900 specimens during cyclic burner rig oxidation compared with cyclic furnace behavior.

Data relating to this alloy will also be found in the following figures:
10.67, 10.68, 10.75, 10.84 10.123, 10.124,
and Tables:
10-XVII, 10-XXV, 10-XXVI

TABLE 1-I

RESULTS OF TESTING AT 1600°F AND 1750°F PEAK TEMPERATURES USING JP-4 AND JP-4R FUEL WITH A 4 PPM SALT/AIR RATIO (WALTERS)

ALLOY	HEAT NO.	FUEL TYPE	SULFUR (w/o)	THRESHOLD TEMP. (°F)	TERMINAL TEMP. (°F)	TEMP. OF MAX. ATTACK (°F)	MAX. DEPTH OF ATTACK (mils)	TOTAL ** CORROSION
Inco 713C	RW 113	JP4R	0.16	1475	1700	1575	13	4.8
Inco 713C	RW 113	JP4	0.02	1500	1725	1625	3	.9
Inco 713LC	RW 153	JP4R	0.16	1450	1700	1625	8	3.3
Inco 713LC	RW 153	JP4	0.02	1500	1700	1650	3	1.3
TRW 1800	X2832	JP4R	0.16	1525	1625	1600	3	.5
TRW 1800	X2832	JP4	0.02	1525	1675	1625	2	.6
B 1900	X2833	JP4R	0.16	1450	1700	1575	18	7.2
B1900	X2833	JP4	0.02	1450	1700	1625	9	5.1
B1910	84V4819	JP4R	0.16	1440*	1700	1525	15	6.0
B1910	84V4819	JP4	0.02	1450	1700	1550	4	1.9
MAR-M200	RL088	JP4R	0.16	1475	1725	1550	19	5.5
MAR-M200	RL088	JP4	0.02	1450	1725	1525	11	2.5
PDRL-161	X2834	JP4R	0.16	1500	1675	1600	13	3.4
PDRL-161	X2834	JP4	0.02	1500	1625	1575	2	.3
PDRL-162	VD698	JP4R	0.16	1575	1700	1625	10	2.2
PDRL-162	VD698	JP4	0.02	1600	1675	1650	4	.4
IN728X	21325	JP4R	0.16	1600	1760	1700	2	.6
IN728X	21325	JP4	0.02	1650	1750	1750	2	.4
X40	MA460	JP4R	0.16	NO VISIBLE CORROSION			0	0
X40	MA460	JP4	0.02	NO VISIBLE CORROSION			0	0
U700	64156	JP4R	0.16	1600	1750	1750	4	1.0
U700	64156	JP4	0.02	NO VISIBLE CORROSION			0	0
IN100	RV 134	JP4R	0.16	1550	1700	1625	11	2.8
IN100	RV 134	JP4	0.02	1600	1750	1650	8	1.7

* Extrapolated

** Area under the corrosion vs. temperature curve (square inches)

TABLE I-II

RESULTS OF TESTING AT 1600° AND 1750°F PEAK TEMPERATURES USING JP-4 AND JP-4R FUEL WITH A 8 PPM SALT/AIR RATIO (WALTERS)

ALLOY	HEAT NO.	FUEL TYPE	SULFUR (w/o)	THRESHOLD TEMP. (°F)	TERMINAL TEMP. (°F)	TEMP. OF MAX. ATTACK (°F)	MAX. DEPTH OF ATTACK (mils)	TOTAL ** CORROSION
Inco 713C	RW113	JP4R	0.16	1650	1725	1600	16.	7.8
Inco 713C	RW113	JP4	0.02	1650	1750	1600	4.	1.8
Inco 713LC	RW153	JP4R	0.16	1650	1725	1675	21.	7.7
Inco 713LC	RW153	JP4	0.02	1650	1725	1600	5.	2.4
TRW 1800	X2832	JP4R	0.16	1500	1725	1600	5.	1.6
TRW 1800	X2832	JP4	0.02	1650	1725	1550	2.	.8
B1900	X2833	JP4R	0.16	1630*	1750	1650	20.	11.3
B1900	X2833	JP4	0.02	< 1650	1750	1600	17.	> 9.8
B1900	04V4819	JP4R	0.16	< 1650	1750	1650	16.	> 8.4
B1900	04V4819	JP4	0.02	1675	1725	1550	7.	2.4
MAR-M200	RL008	JP4R	0.16	1650	1750	1600	20.	9.7
MAR-M200	RL008	JP4	0.02	1650	1750	1575	12.	6.7
PDRL 161	X2834	JP4R	0.16	1500	1725	1600	20.	9.9
PDRL 161	X2834	JP4	0.02	1550	1725	1600	6.	1.6
PDRL 162	VD698	JP4R	0.16	1675	1725	1625	12.	4.5
PDRL 162	VD698	JP4	0.02	1675	1625	1550	3.	.7
IN728X	21325	JP4R	0.16	1550	1700	1650	7.	1.4
IN728X	21325	JP4	0.02	1625	1750	1700	2.	.4
X40	MA660	JP4R	0.16	No	Visible	Corrosion	0	0
X40	MA660	JP4	0.02	No	Visible	Corrosion	0	0
U700	64156	JP4R	0.16	1625	> 1750	1700	10	> 2.0
U700	64156	JP4	0.02	1600	> 1750	***	1	> .3
IN100	RV134	JP4R	0.16	1675	1770*	1625	22	10.8
IN100	RV134	JP4	0.02	1650	> 1750	1550	15.	> 6.2

*Extrapolated

**Area Under the Corrosion vs. Temperature Curve (Square Inches)

***Amount of Corrosion too Little to Determine Temperature of Maximum Attack

TABLE 1-III

RELATIVE PERFORMANCE OF ALLOYS TESTED UNDER VARIOUS TEST CONDITIONS (WALTERS)

RANK	0.16% S/8 PPM SALT ALLOY	TOTAL CORR.*	0.16% S/4 PPM SALT ALLOY	TOTAL CORR.*	0.02% S/8 PPM SALT ALLOY	TOTAL CORR.*	0.02% S/4 PPM ALLOY	TOTAL CORR.*
1	X40	0	X40	0.	X40	0.	X40	0.
2	IN728X	1.4	TRW 1800	0.5	U700	> 0.3	U700	0.
3	TRW 1800	1.6	IN728X	0.6	IN728X	0.4	PDRL161	0.3
4	U700	>2.0	U700	1.0	PDRL162	0.7	PDRL 162	>0.4
5	PDRL162	4.5	PDRL162	2.2	TRW 1800	0.8	IN 728X	0.4
6	PDRL161	5.9	IN100	2.8	PDRL161	1.6	TRW1800	0.6

7	Inco713LC	7.7	Inco 713LC	3.3	Inco 713C	1.8	Inco 713C	0.9
8	Inco713C	7.8	PDRL161	3.4	Inco 713LC	2.4	Inco 713LC	1.3
9	B1910	>8.4	Inco713C	4.8	B1910	2.4	IN100	> 1.7
10	MAR-M200	9.7	MAR-M200	5.5	IN100	> 6.2	B1910	1.9
11	IN100	10.8	B1910	6.0	MAR-M200	6.7	MAR-M200	2.5
12	B1900	11.3	B1900	> 7.2	B1900	> 9.8	B1900	> 5.1

* Area Under Depth of Penetration vs. Temperature Curve.

TABLE 1-IV

THRESHOLD AND TERMINAL TEMPERATURES AFTER 120 and 360 HOURS TESTING USING JP-4 FUEL AND A SALT-TO-AIR RATIO OF 4 PPM (WALTERS)

	THRESHOLD		TERMINAL	
	120 Hours °F	360 Hours °F	120 Hours °F	360 Hours °F
Inco 713C	1475	1450	1700	1750
TRW1800	1500	1475	1600	1635
B1910	1450	1450	1625	1650
IN728X	1675	1600	1750	1750
IN728X HT	1650	1575	1750	1750
U700	1625	1600	1750	1750

TABLE 1-V

SUMMARY OF CORROSION PRODUCTS FOUND ON THE TRAILING EDGE
AFTER 40 HOURS OF RIG TESTING (WALTERS)

ALLOY	CORROSION PRODUCTS
X40	Co Matrix (fcc) + CoO + $CoCr_2O_4$
IN 728	Ni_3Al[(b)] + Spinel (a_o = 8.27) + NiO + Cr_2O_3 + Unknown
TRW 1800	Ni_3Al[(b)] + Spinel (a_o = 8.24) + NiO + $NiWO_4$ (trace) + Al_2O_3 (trace)
U700	Ni_3Al[(b)] + NiO + Spinel (a_o = 8.32)
PDRL 162	Ni_3Al[(b)] + Spinel (a_o = 8.15) + NiO + Al_2O_3 (trace) + Unknown
PDRL 161	Ni_3Al[(b)] + NiO + Spinel (a_o = 8.24) + Al_2O_3 + Cr_2O_3 (trace)
INCO 713	Ni_3Al[(b)] + NiO + Spinel (a_o = 8.17) + Al_2O_3 (trace) + Cr_2O_3 (trace)
B1910	Ni_3Al[(b)] + Spinel (a_o = 8.27) + NiO + Unknown (a major phase d = 3.90, 3.30, 2.75) + Al_2O_3 (trace)
M200	Ni_3Al[(b)] + NiO + Spinel (a_o = 8.26) + $NiWO_4$ (trace)
IN 100	Ni_3Al[(b)] + NiO + Spinel (a_o = 8.34)
B1900	Ni_3Al[(b)] + Spinel (a_o = 8.17) + NiO + Al_2O_3

(a) Phases listed in order of decreasing quantities as indicated by X-ray intensities.

(b) This phase is the γ' phase from the base alloy and is used as a reference for the patterns.

TABLE 1-VI

SUMMARY OF CORROSION PRODUCTS FOUND ON THE TRAILING EDGE
AFTER 120 HOURS TESTING (WALTERS)

ALLOY	CORROSION PRODUCTS
X 40	Co (Matrix) (fcc) + CoO + $CoCr_2O_4$
IN 728	Ni_3Al[(b)] + Spinel (a_o = 8.27) + NiO + Cr_2O_3 Unknown
TRW 1800	Ni_3Al[(b)] + Spinel (a_o = 8.24) + NiO + $NiWO_4$ (trace) Al_2O_3 (trace)
U 700	Ni_3Al[(b)] + NiO + Spinel (a_o = 8.32)

PDRL 162	Ni_3Al [(b)] + Spinel (a_o = 8.15) + NiO + Al_2O_3 + Cr_2O_3 + Unknown
PDRL 161	Ni_3Al [(b)] + NiO + Spinel (a_o = 8.24) + Al_2O_3 + Cr_2O_3
INCO 713	Ni_3Al [(b)] + NiO + Spinel (a_o = 8.17) + Unknown + Al_2O_3 (trace + Cr_2O_3 (trace)
B 1910	Ni_3Al [(b)] + Spinel (a_o = 8.27) + NiO + Unknown (a major phase d = 3.90, 3.30, 2.75)
M 200	Ni_3Al [(b)] + NiO + Spinel (a_o = 8.26) + $NiWO_4$ Unknown (d = 2.11, 2.63, 1.93, 1.86)
IN 100	Ni_3Al [(b)] + NiO + Spinel (a_o = 8.34)
B1900	Ni_3Al [(b)] + Spinel (a_o = 8.17) + NiO + Al_2O_3 + Unknown (d = 3.88, 3.29, 2.74, 1.94,1.67, 1.65, 1.38)

(a) Phases presented are listed in order of decreasing quantities as indicated by X-ray intensities.

(b) This phase is the phase from the base alloy and is used as a reference for the pattern.

TABLE 1-VII

SUMMARY OF CORROSION PRODUCTS FOUND IN POWDERS REMOVED FROM AREA WHICH HAS UNDERGONE SULFIDATION CORROSION FOR 120 HOURS OF TESTING (WALDERS)

ALLOY	CORROSION PRODUCTS
X 40	No oxides removed, too thin and adherent
IN 728	Spinel (a_o = 8.24) + NiO + Unknown
TRW 1800	Spinel (a_o = 8.20) + NiO + $NiWO_4$
U 700	NiO + Spinel (a_o = 8.32)
PDRL 162	Spinel (a_o = 8.20) + NiO + Unknown (d = 3.40, 2.34)
PDRL 161	NiO + Spinel (a_o = 8.20) + Unknown (d = 3.33, 1.76, 1.72)
INCO 713	NiO + Spinel (a_o 8.24) + Al_2O_3 (trace) + Cr_2O_3 (trace) + Unknown
B1910	Spinel (a_o = 8.27) + NiO + Al_2O_3 + Unknown (d = 3.36)
M200	NiO + Spinel (a_o 8.27) + $NiWO_4$
IN 100	NiO + Spinel (a_o = 8.27)
B1900	Spinel (a_o = 8.25) + NiO + Unknown (d = 3.33, 2.54, 1.73)

(a) Phases listed in order of decreasing quantities as indicated by X-ray intensities.

TABLE 1-VIII

MICROPROBE ANALYSIS OF DEPLETION ZONE AREAS (WALTERS)

ALLOY	Ni	Cr	Mo	Al	Ti	Cb	S	W	Co	Ta
INCO 713C	75.0	0.30	3.5	3.0	0.01	0.2	-	-	-	-
TRW 1800	90.5	0.5	-	2.0	0.08	1.0	-	6.6	-	-
IN 728	80.3	0.4	1.2	2.0	-	0.1	-	1.5	13.7	1.1
PDRL 161	95.5	0.8	0.7	2.8	0.02	0.1	-	-	-	-
PDRL 162	94.2	0.4	0.9	2.4	0	-	-	1.3	0	1.0
U700	76.2	0.9	3.6	2.3	0.12	-	-	-	15.0	-
B1900	84.2	0.5	6.0	2.7	0	-	-	-	5.9	1.5
IN100	74.0	0.4	1.0	1.4	0.03	-	-	-	3.0	-
M200	80.5	0.5	-	1.9	0	0	-	7.0	10.0	-
B1910	83.0	2.0	1.9	3.3	.05	-	-	-	8.2	4.3

0 Indicates complete depletion of element
- Indicates element not present in original alloy.

TABLE 1-IX

RELATIVE PERFORMANCE OF ALLOYS TESTED UNDER VARIOUS CONDITIONS (WALTERS)

RANK	0.1% S/8 PPM SALT ALLOY	TOTAL CORR.*	0.1% S/4 PPM SALT ALLOY	TOTAL CORR.*	0.02% S/8 PPM SALT ALLOY	TOTAL CORR.*	0.02% S/4 PPM ALLOY	TOTAL CORR.*
1	X40	0	X40	0.	X40	0.	X40	0.
2	IN728X	1.4	TRW 1800	0.5	U700	> 0.3	U700	0.
3	TRW 1800	1.6	IN728X	0.6	IN728X	0.4	PDRL161	0.3
4	U700	> 2.0	U700	1.0	PDRL 162	0.7	PDRL 162	> 0.4
5	PDRL162	4.5	PDRL162	2.2	TRW 1800	0.8	IN728X	0.4
6	PDRL161	5.9	IN100	2.8	PDRL161	1.6	TRW1800	0.6
7	Inco713LC	7.7	Inco 713LC	3.3	Inco 713C	1.6	Inco 713C	0.9
8	Inco713C	7.8	PDRL161	3.4	Inco 713LC	2.4	Inco713LC	1.3
9	B1910	> 8.4	Inco713C	4.8	B1910	2.4	IN100	> 1.7
10	MAR-M200	9.7	MAR-M200	5.5	IN100	> 6.2	B1910	1.9
11	IN100	10.8	B1910	6.0	MAR-M200	6.7	MAR-M200	2.5
12	B1900	11.3	B1900	> 7.2	B1900	> 9.8	B1900	> 5.1

*Area Under Depth of Penetration vs. Temperature Curve

TABLE 1-X

WEIGHT CHANGE DURING HOT-CORROSION TEST (MOORE AND STETSON)

1650°F MAXIMUM TEST TEMPERATURE

35ppm SEA SALT

UNCOATED NICKEL ALLOYS

Exposure Time (Hours)	Cumulative Weight Change (mg)											
	Specimen Number											
	B1	B2	I1	I2	S1	S2	C1	C2	U1	U2	R1	R2
10	+17.4	+54.6	+6.9	-14.0	-0.4	-7.2	+ 4.9	+ 8.9	+ 7.4	+ 8.1	+3.3	- 2.6
20	-	-	-	-	-	-	+ 6.4	+ 11.8	+10.6	+ 8.9	3.7	- 2.5
30	-	-	-	-	-	-	+ 7.2	+ 11.6	+11.0	+ 9.7	+3.4	- 2.7
40	-	-	-	-	-	-	+12.8	+ 18.2	+20.4	+23.7	+8.0	- 7.9
50	-	-	-	-	-	-	+12.8	- 17.6	+19.4	+19.5	+3.4	- 1.0
60	-	-	-	-	-	-	+14.9	-104.7	+19.7	+20.7	-4.3	- 8.2
70	-	-	-	-	-	-	-	-	+19.8	+20.9	-6.3	-10.3
80	-	-	-	-	-	-	-	-	+22.1	+22.5	-4.7	-10.1
90	-	-	-	-	-	-	-	-	+20.0	+21.4	-8.2	-10.4
100	-	-	-	-	-	-	-	-	+12.9	+23.2	-8.0	- 9.7
110	-	-	-	-	-	-	-	-	+10.6	+ 3.2	-6.7	- 9.3
120	-	-	-	-	-	-	-	-	-	-	-	-7.6	- 8.4
150	-	-	-	-	-	-	-	-	-	-	-	-9.3	-11.4

TABLE 1-XI

WEIGHT CHANGE DURING HOT-CORROSION TEST (MOORE AND STETSON)

1800°F MAXIMUM TEST TEMPERATURE

35ppm SEA SALT

UNCOATED NICKEL ALLOYS

Exposure Time (Hours)	Cumulative Weight Change (mg)							
	Specimen Number							
	C3	C4	B29	B30	I24	I25	S3	S4
10	-418	-81.3	- 363	- 287	- 777	- 960	-	-
17	-	-	-1478	-1610	-1960	-2280	-	-
20	-	-	-	-	-	-	-4895	-3673

Exposure Time (Hours)	Cumulative Weight Change (mg)			
	Specimen Number			
	R3	R4	U3	U4
10	-	-	+15.2	+ 5.3
20	-16.9	-16.4	+14.4	+21.8
30	-	-	+20.8	+42.4
40	-39.0	-37.0	+20.4	+43.2
50	-55.0	-52.4	+20.7	+24.4
70	-77.8	-53.0	+25.1	+21.9
80	-	-	+19.0	+17.6
100	-	-	+18.9	+17.6
120	-	-	+24.4	+17.4
140	-	-	+25.2	+12.0
150	-	-	+25.0	+25.7

Note: - denotes weight loss

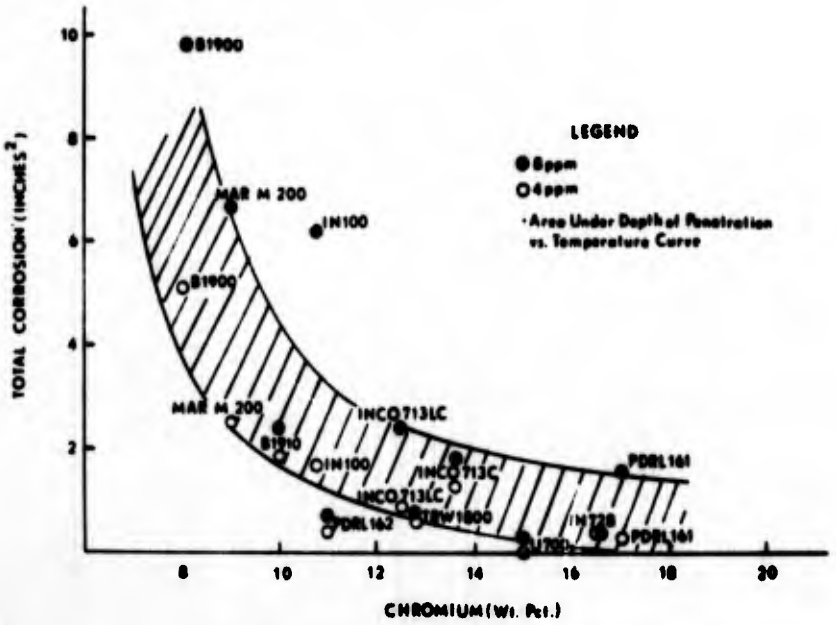

Figure 1.1. Total Corrosion as a Function of Chromium Content for Alloys Tested Using JP-4R Fuel. (Walters).

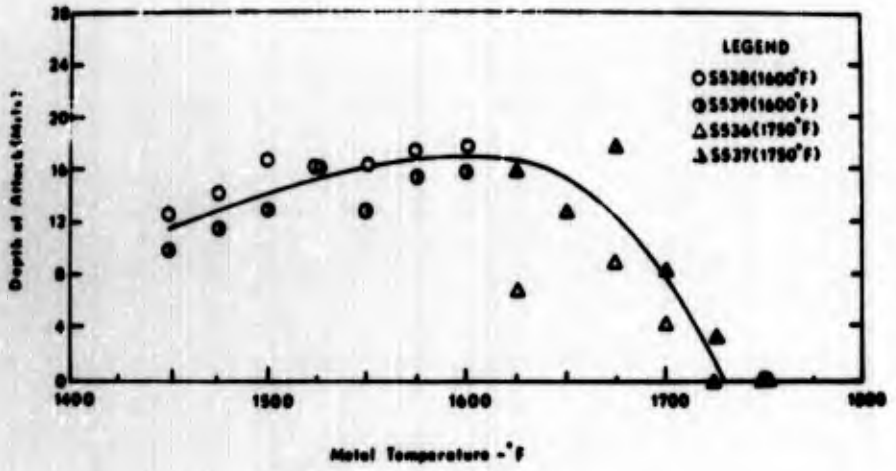

Figure 1.2. Corrosion as a Function of Temperature for B1900 Tested Using JP-4 Fuel with a Salt/Air Ratio of 8 ppm. (Walters).

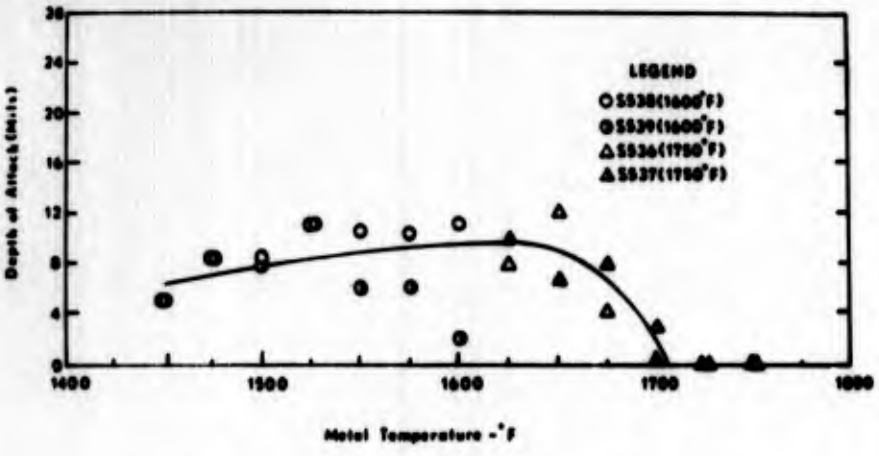

Figure 1.3. Corrosion as a Function of Temperature for B1900 Tested Using JP-4 Fuel with a Salt/Air Ratio of 4 ppm. (Walters).

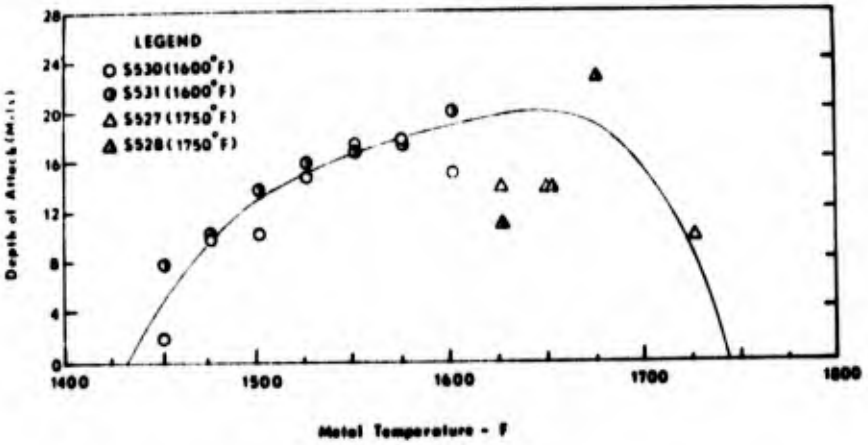

Figure 1.4. Corrosion as a Function of Temperature for B1900 Using JP-4R Fuel with a Salt/Air Ratio of 8 ppm. (Walters).

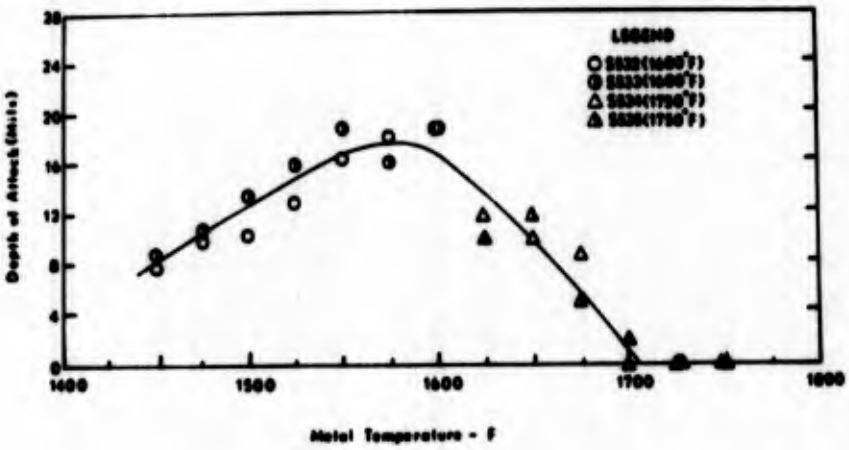

Figure 1.5. Corrosion as a Function of Temperature for B1900 Using JP-4R Fuel with a Salt/Air Ratio of 4 ppm (Walters).

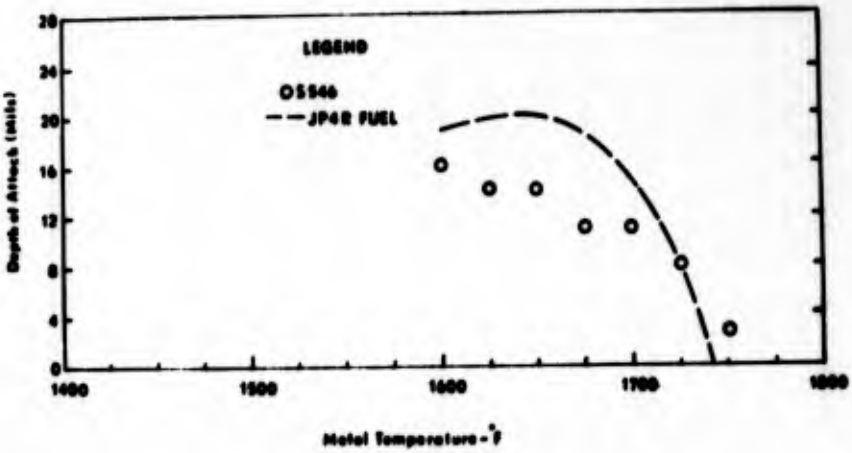

Figure 1.6. Corrosion as a Function of Temperature for B1900 Tested Using JP-8 Fuel (0.16%S) with a Salt/Air Ratio of 8 ppm. (Walters)

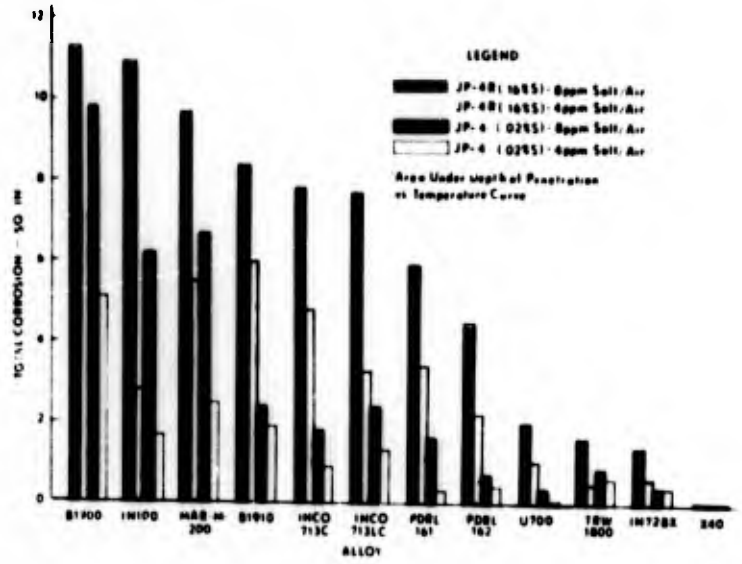

Figure 1.7. Bar Graph Showing Variation in Total Corrosion of Alloys Tested with JP-4 and JP-4R Fuels Using 4 and 8 ppm Salt/Air Ratios. (Walters).

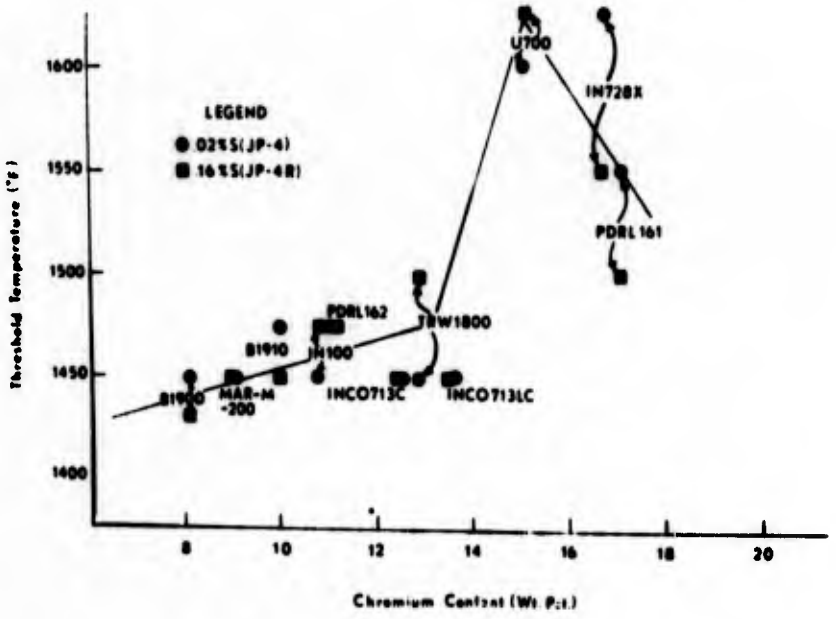

Figure 1.8. Threshold Temperature as a Function of Chromium Content for Alloys Tested Using a Salt/Air Ratio of 8 ppm. (Walters).

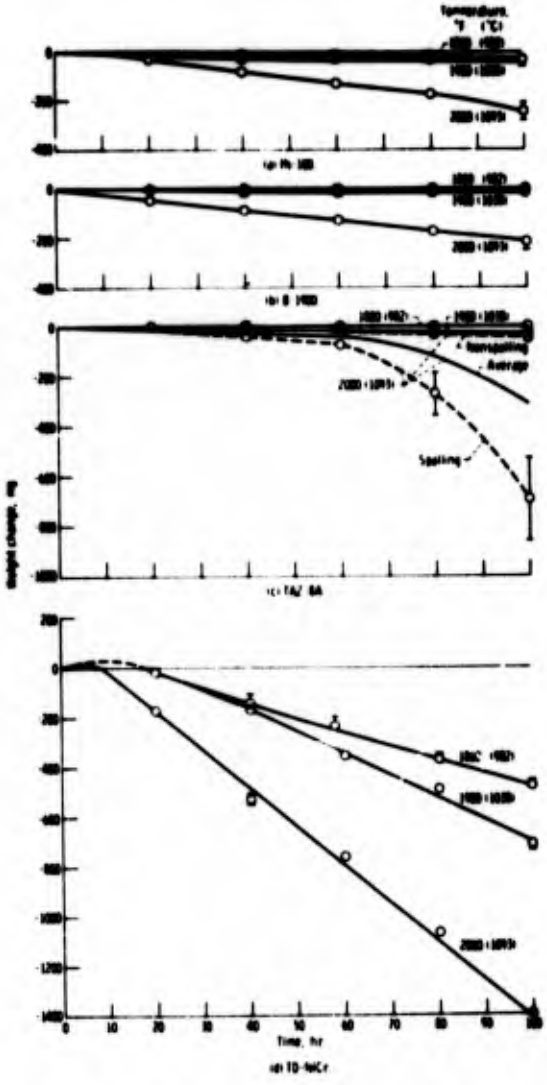

Figure 1.9. Weight change of materials at various temperatures during exposure to high-gas-velocity oxidation apparatus. Test cycle: 1 hour at test temperature, 3 minutes at room temperature. (Johnston and Ashbrook).

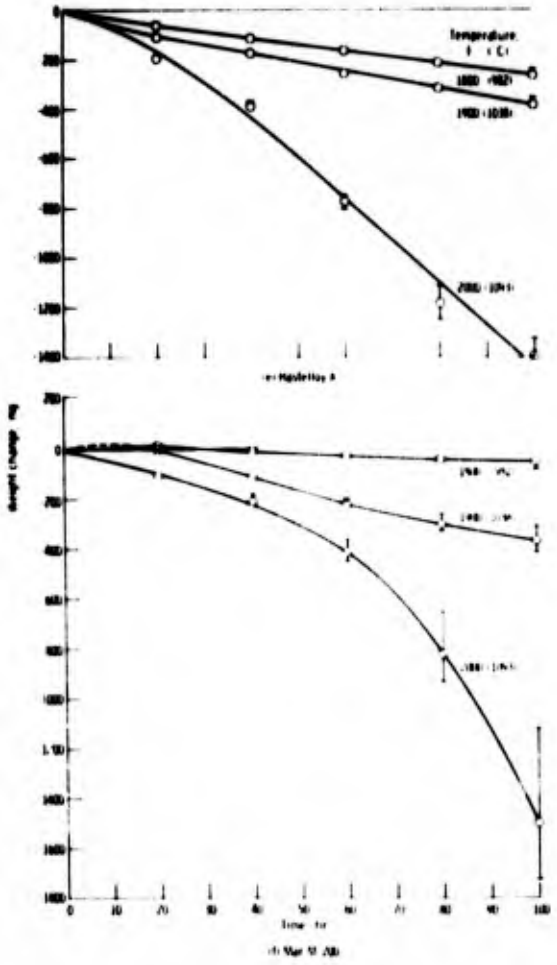

Figure 1.9. - Continued.

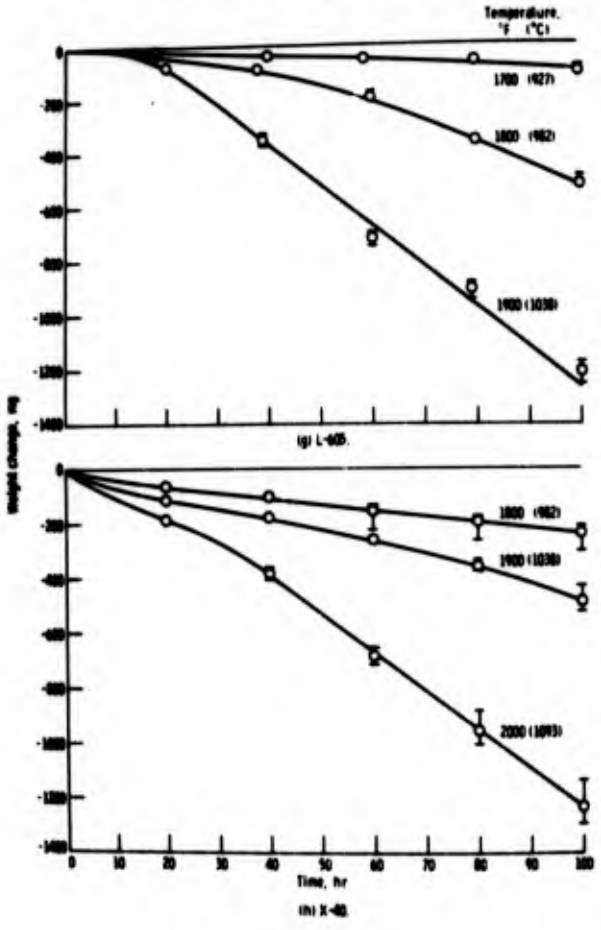

Figure 1.9. - Continued.

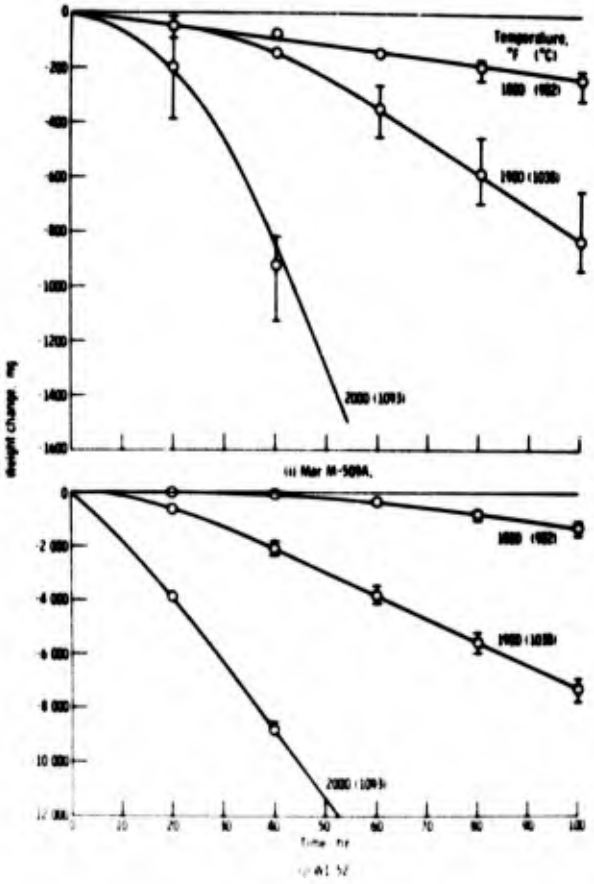

Figure 1.9. - Continued.

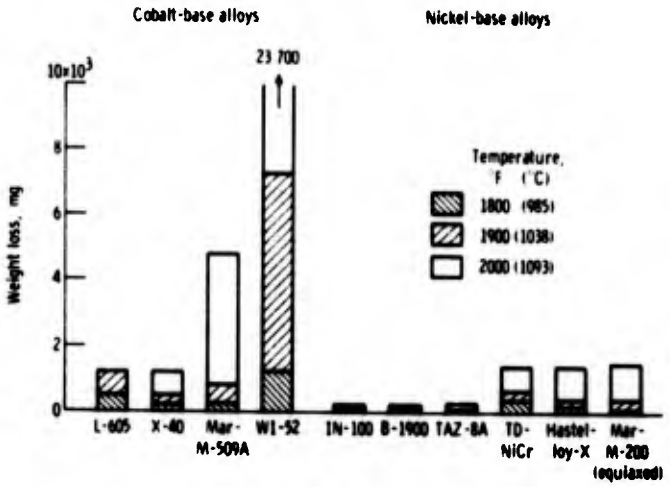

Figure 1.10. Summary of weight loss data for materials exposed 100 hours to high-gas-velocity oxidation apparatus. (Johnston and Ashbrook).

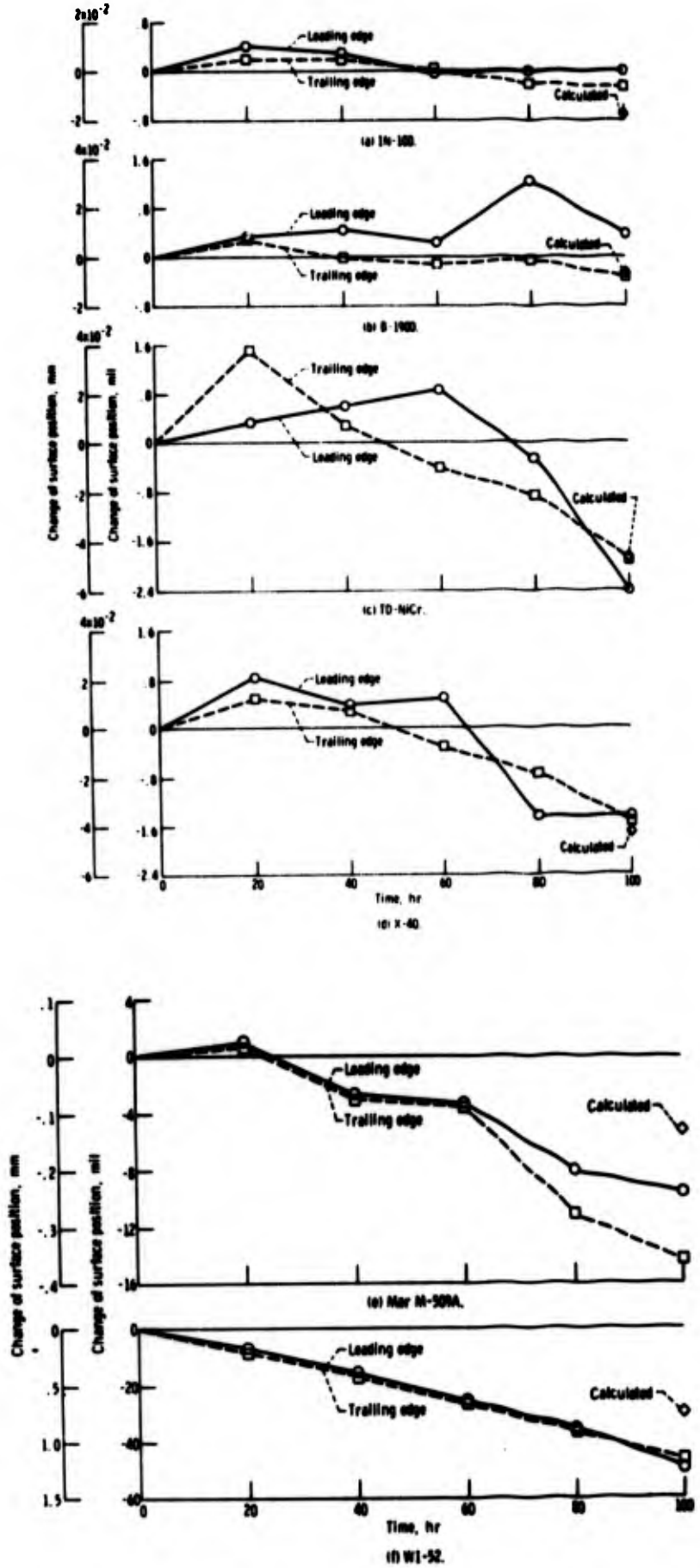

Figure 1.11. Surface recession of oxidation specimens. Standard cycle; maximum temperature, 2000°F (1093°C). (Johnston and Ashbrook).

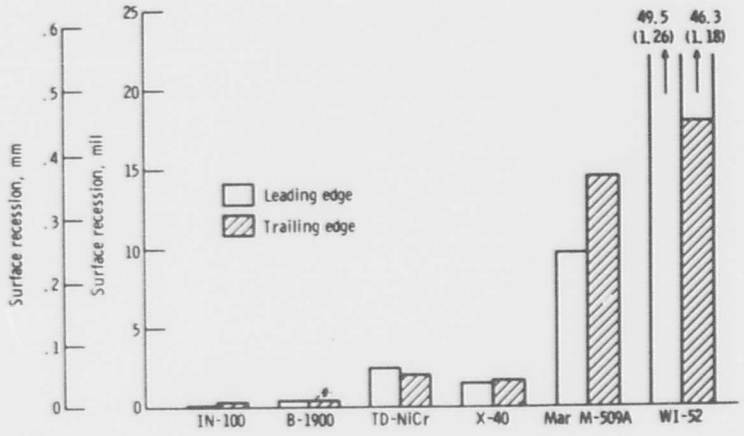

Figure 1.12. Summary of surface recession measurements after 100 hours at 2000°F (1093°C) using standard cycle. (Johnston and Ashbrook).

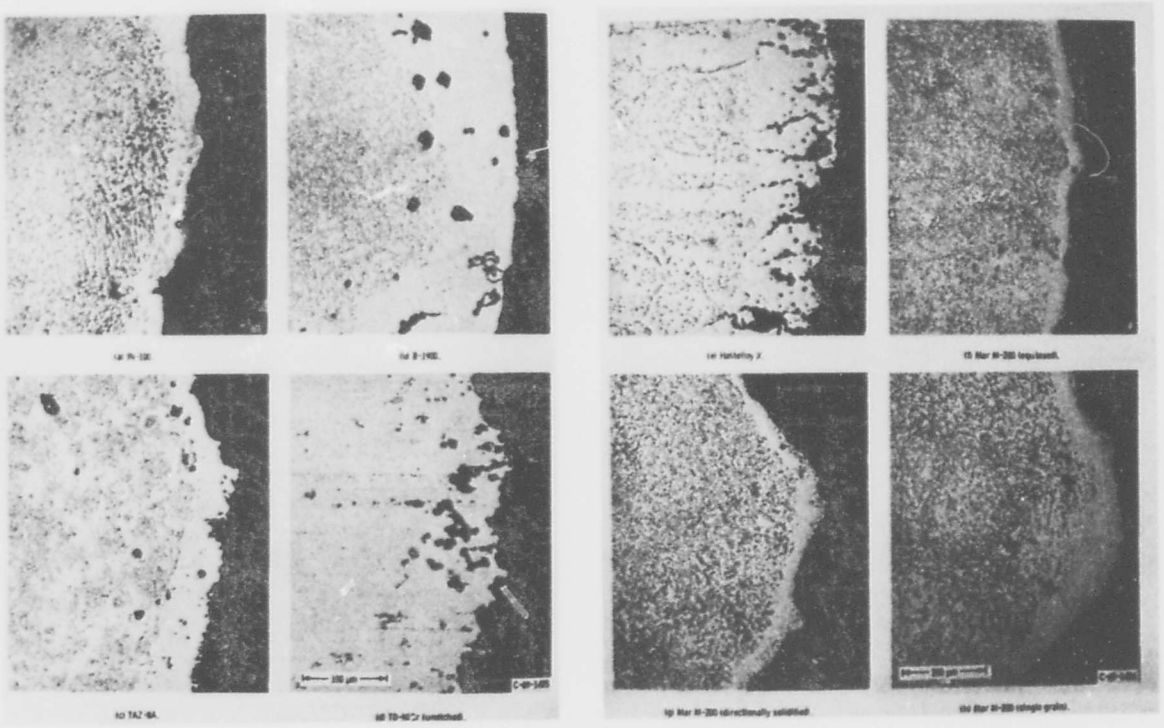

Figure 1.13. Microstructures of materials after exposure to standard cycle for 100 hours at 2000°F (1093°C). X 250 (Johnston and Ashbrook).

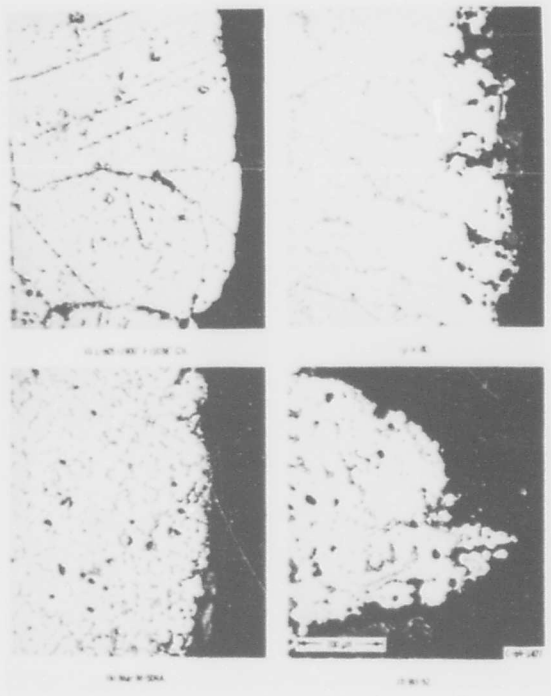

Figure 1.13. - Continued.

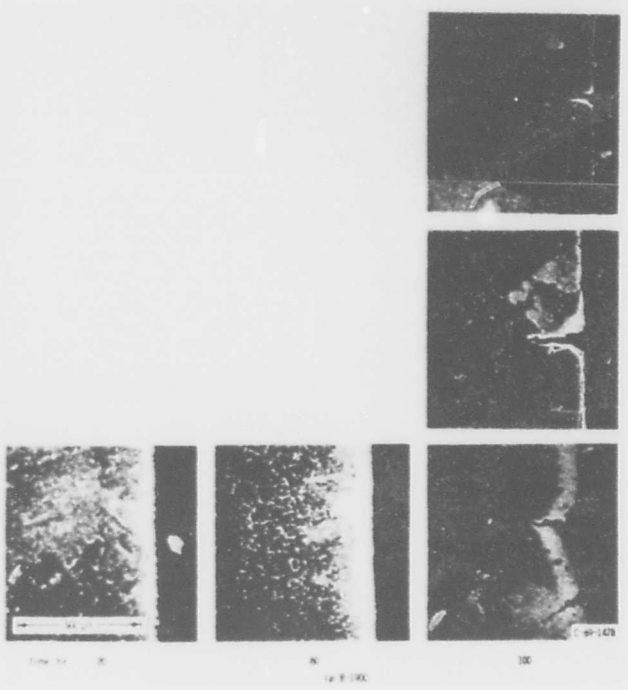

Figure 1.14. Specimens after exposure for various times and temperatures using standard cycle. (Johnston and Ashbrook).

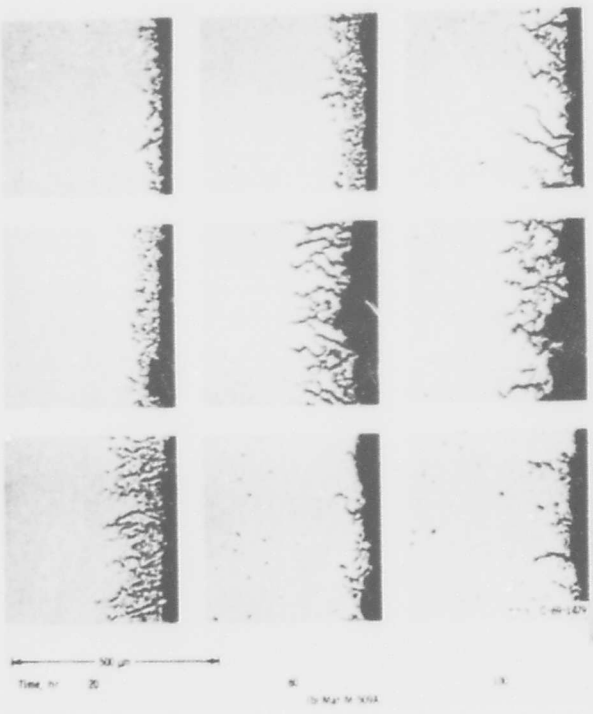

Figure 1.14. - Continued.

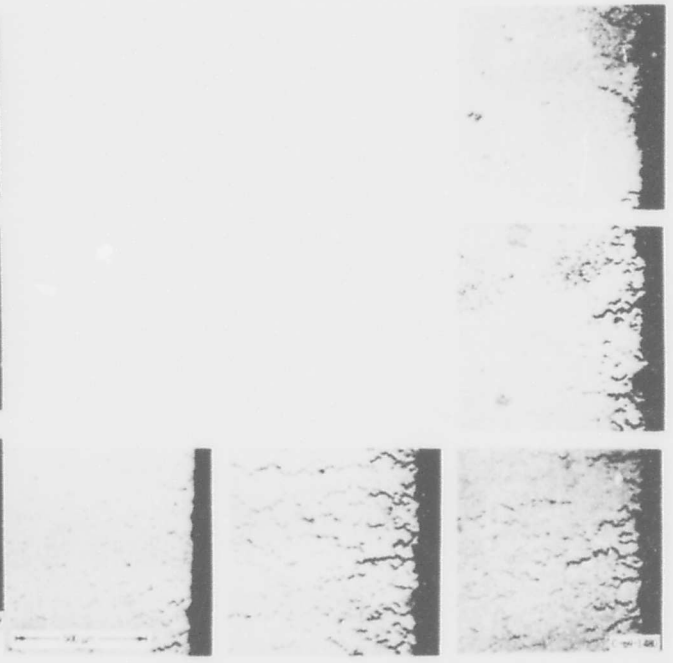

Figure 1.14. - Concluded.

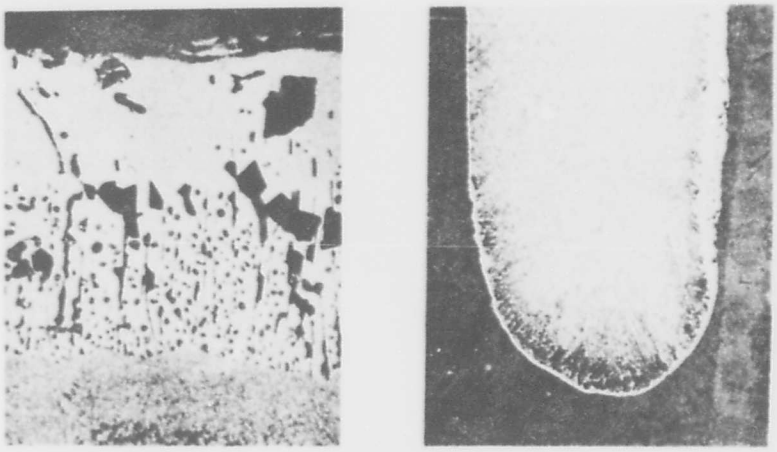

Magnification: 1000X Specimen B 26 Magnification: 40X

Figure 1.15. Microstructure of Uncoated B1900 Alloy after Hot Corrosion Tests at 1650°F for 20 hours. (Moore and Stetson).

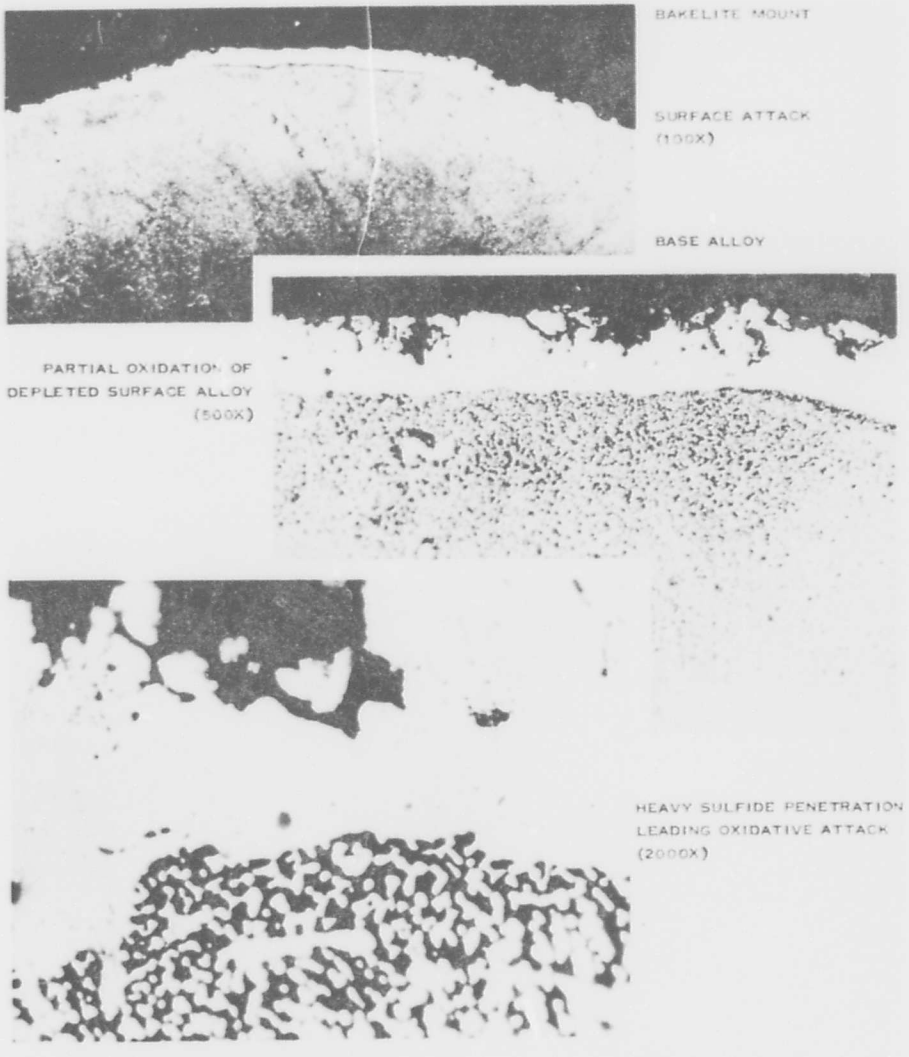

Figure 1.16. Hot Corrosion of Bare B1900 Specimen after 15 hours (Base-Line Test) (Quigg et al).

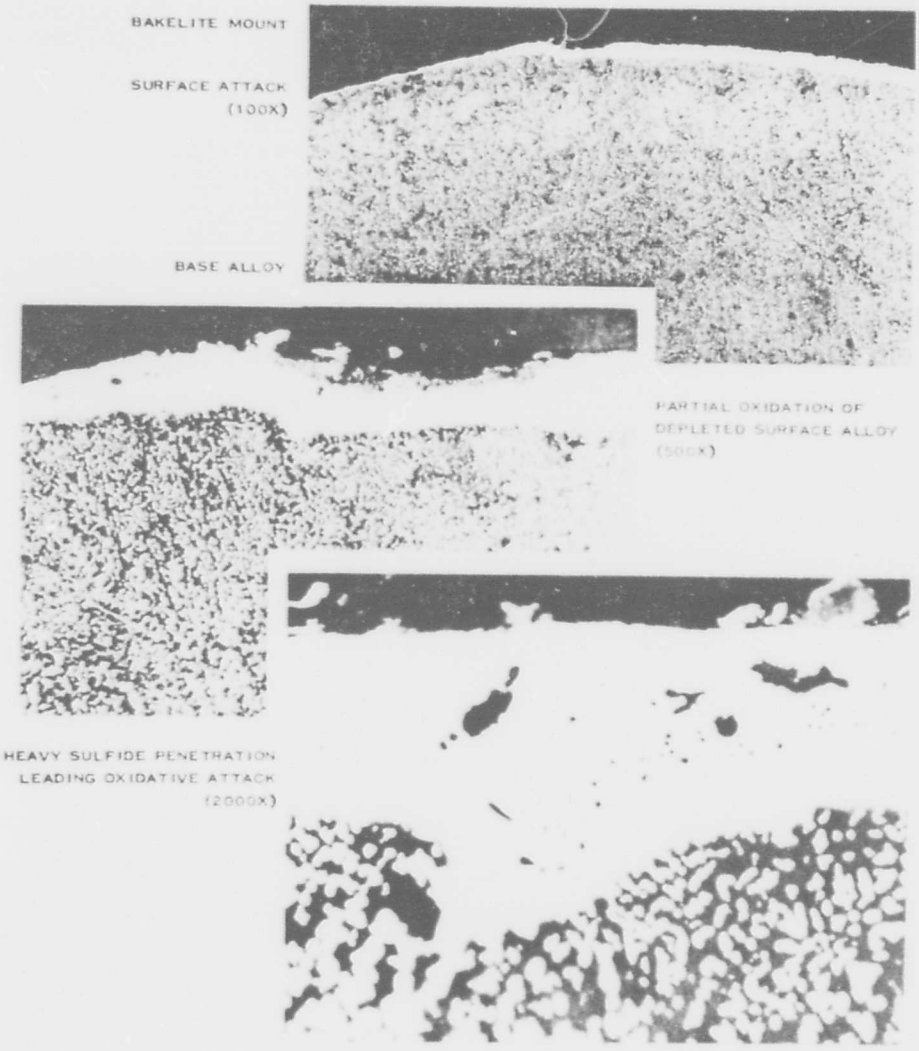

Figure 1.17. Hot Corrosion of Bare B1900 Specimen after 15 hours (Test with Benzotriazole in Fuel) (Quigg et al).

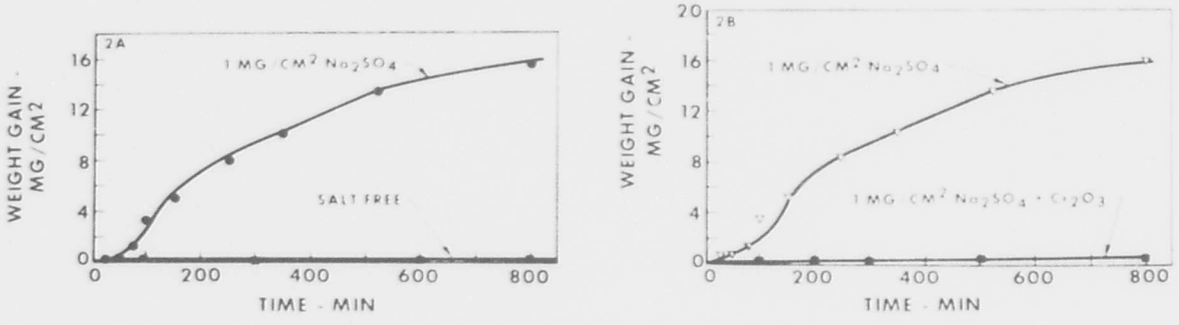

Figure 1.18. Oxidation of B-1900 alloy at 900°C.(Bornstein et al).

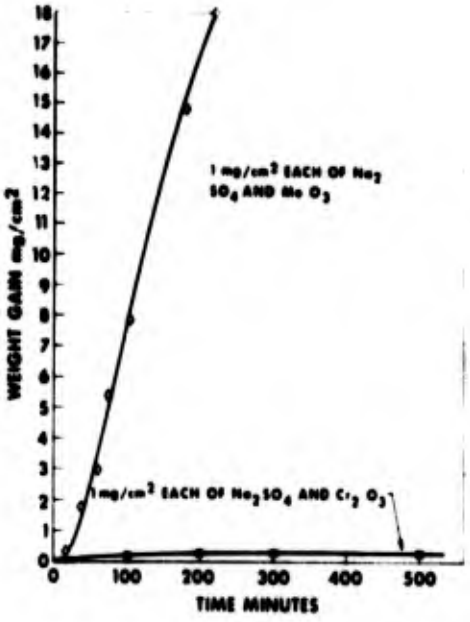

Figure 1.19. Oxidation of salt-coated B-1900 at 900°C. (Bornstein et al).

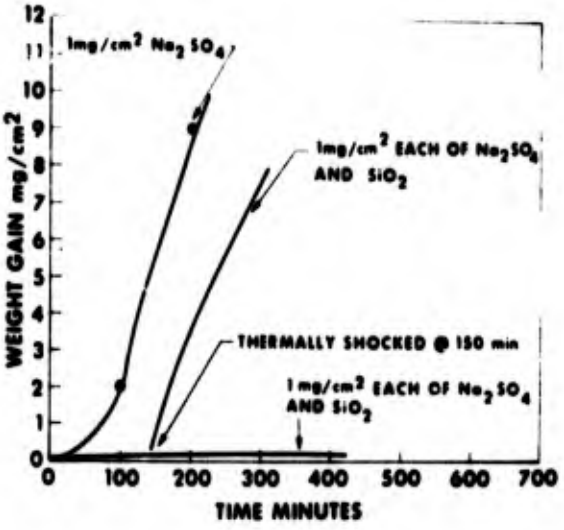

Figure 1.20. Oxidation of salt-coated B-1900 at 900°C. (Bornstein et al).

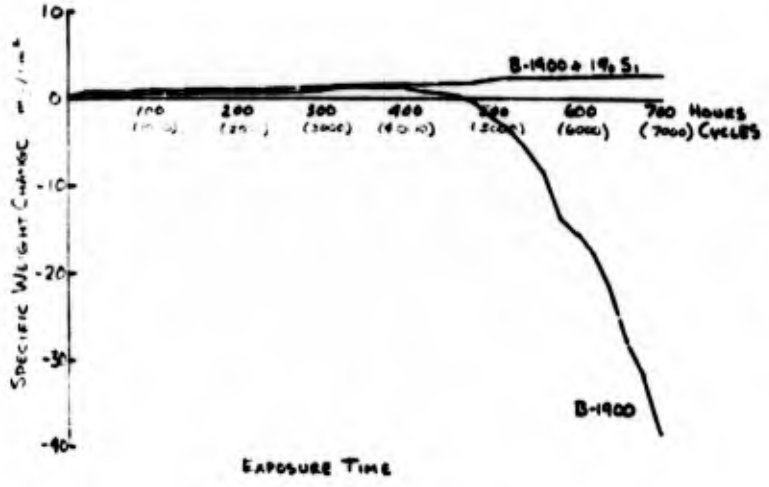

Figure 1.21. The Effect of Si on the Resistance to Cyclic Oxidation of B1900 at 1000°C. Cycle consists of 6 minutes in the furnace and 9 minutes cooling. (Lowell and Miner).

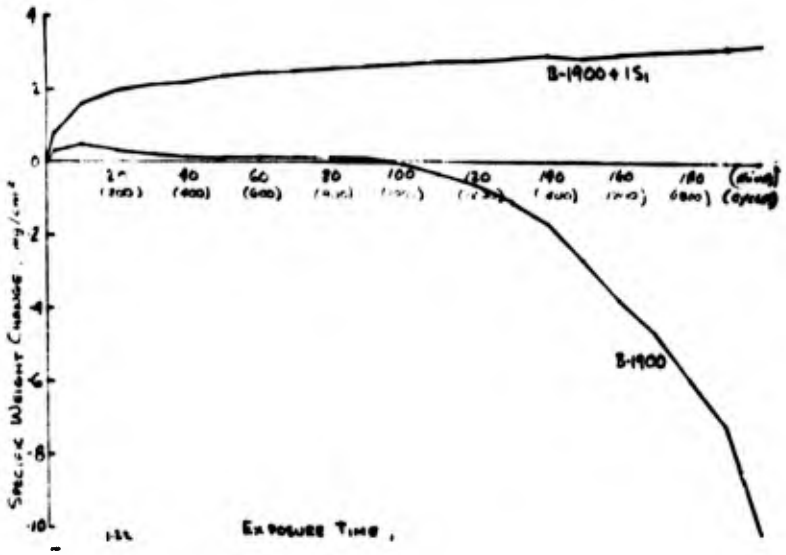

Figure 1.22. The Effect of Si on the Cyclic Oxidation Resistance of B1900 at 1100°C. Cycle consists of 6 minutes in the furnace and 9 minutes cooling. (Lowell and Miner).

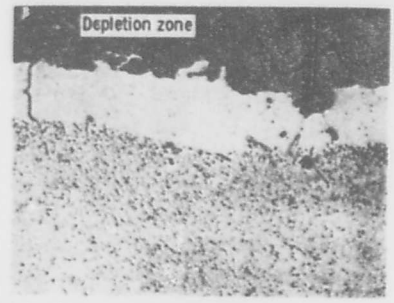

(a) B-1900.

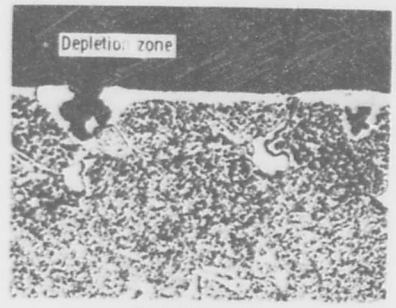

(b) B-1900 + 1 Si.

Figure 1.23. Microstructural effects of Si on thermal cycling of B1900 during oxidation at 1100°C. 2000 cycles (200 hours at temperature). Etched with 33 acetic acid, 33 nitric acid, 33 water, and 1 hydrofluoric acid. X 250. (Lowell and Miner).

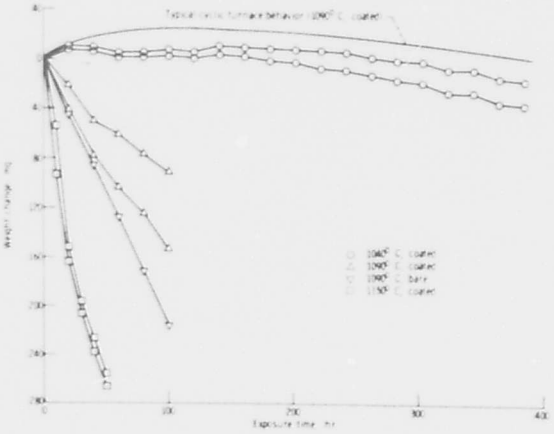

Figure 1.24. Weight change of B1900 specimens during cyclic burner-rig oxidation compared with cyclic furnace behaviour. Minimum temperature, 20°C; 1 cycle per hour. (Spera and Grisaffe).

B 1910

J.J. Walters (AVCO/Lycoming Division) Technical Report to the Air Force Materials Laboratory, Wright-Patterson Air Force Base AFML-TR-67-297 (Sept. 1967).

Extended summary in B1900. B 1910 was one of a group of alloys described as having "very poor resistance to attack" - the others in this group were B 1900, Mar-M 200 and IN 100. Of this group, B 1910 was the best. The threshold and terminal temperatures after 120 and 360h testing using JP-4 fuel and a salt-to-air ratio of 4 ppm, for B 1910, were 1450 and 1625°F; and 1450 and 1650°F (788 and 885°C; 788 and 899°C). X-ray analysis of corrosion products found on the trailing edge after 40h rig testing for B 1910 in order of predominance were a spinel with a_o = 8.27 Å, NiO, an unknown phase with d = 3.90, 3.30, 2.75 Å, and a trace of Al_2O_3. The products after 120h testing were the same as at the shorter time, except that no Al_2O_3 was detected.

The corrosion products detected in powder removed from an area of a B 1910 specimen which had undergone sulphidation corrosion for 120h, in order of predominance were a spinel with a_o = 8.27 Å, NiO, Al_2O_3, and an unknown phase with d = 3.34 Å. A microprobe analysis of the depleted metal zone in B 1910 was 83% Ni, 2.0% Cr, 1.9% Mo, 3.3% Al, 0.05% Ti, 8.2% Co and 4.3% Ta.

Figure 2.1 shows the attack on B 1910 tested using JP-4 fuel and a salt/air ratio of 8 ppm as a function of temperature. Figure 2.2 - JP -4, 4 ppm salt. Figure 2.3, JP-4R, 8 ppm salt. Figure 2.4, JP-4R, 4 ppm salt. Figure 2.5, JP-5, 8 ppm salt. Figure 2.6 shows the corrosion as a function of temperature for JP-4 fuel, 4 ppm salt, for three test times: 120, 240 and 360h.

Data relating to this alloy will also be found in the following Figures:
1.1, 1.7, 1.8, 10.13, 10.14;
and Tables:
1-I, 1-II, 1-IV, 1-V, 1-VI, 1-VII, 1-VIII, 1-IX.

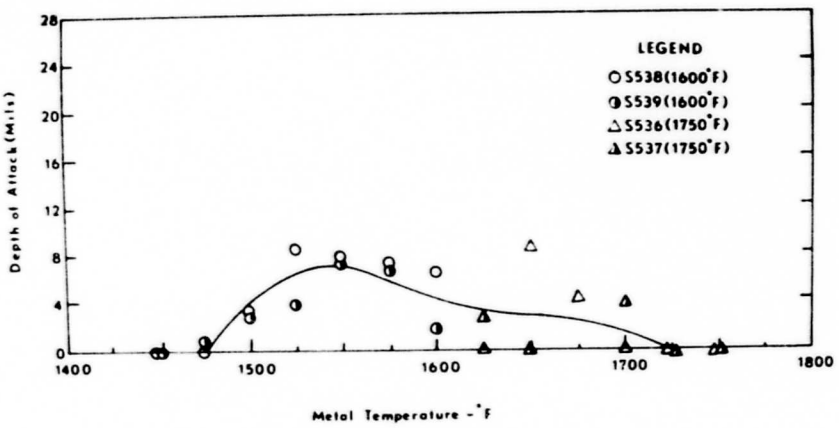

Figure 2.1. Corrosion as a function of Temperature for B1910 tested using JP-4 fuel with a Salt/Air Ratio of 8 ppm. (Walters).

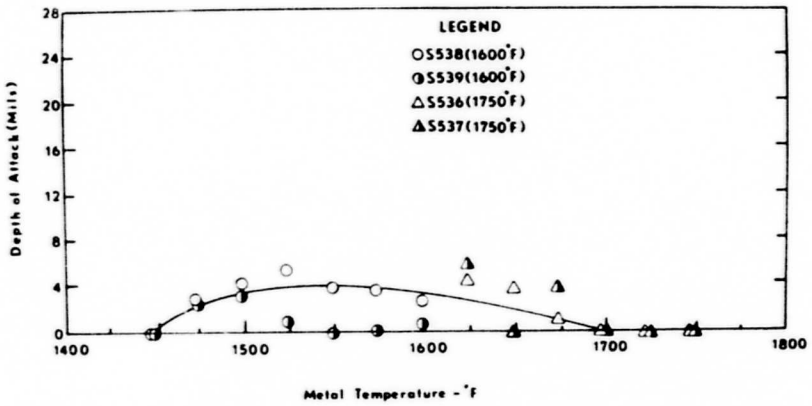

Figure 2.2. Corrosion as a function of Temperature for B1910 Tested using JP-4 fuel with a Salt/Air Ratio of 4 ppm. (Walters).

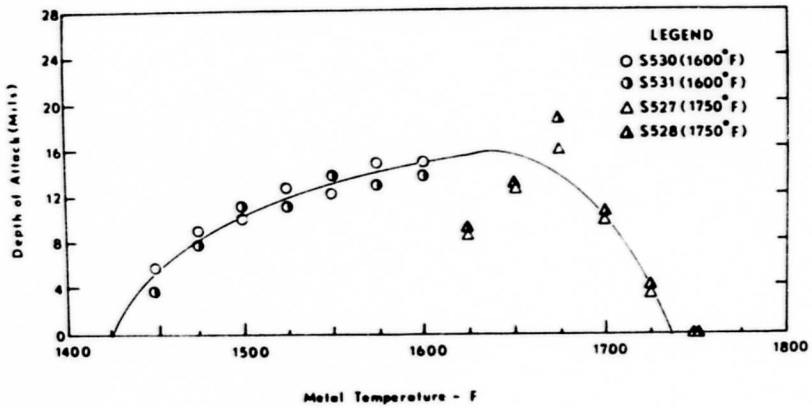

Figure 2.3. Corrosion as a function of temperature for B1910 using JP-4R fuel with a Salt/Air Ratio of 8 ppm. (Walters).

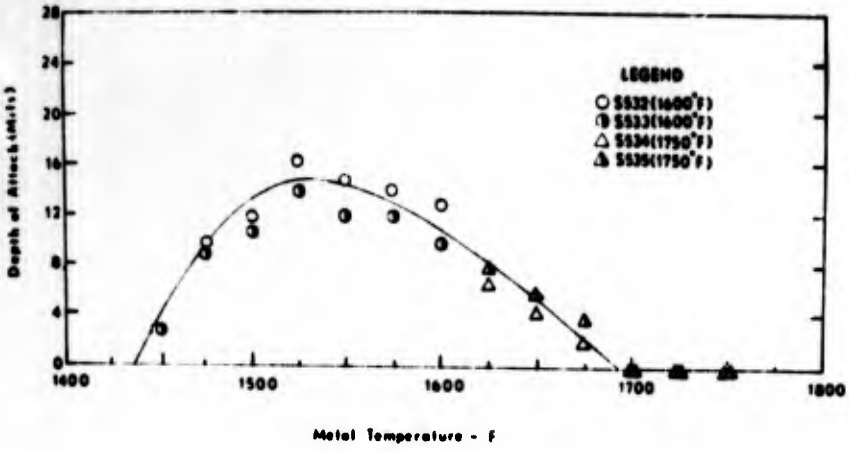

Figure 2.4. Corrosion as a function of temperature for B1910 Using JP-4R Fuel with a Salt/Air Ratio of 4 ppm. (Walters).

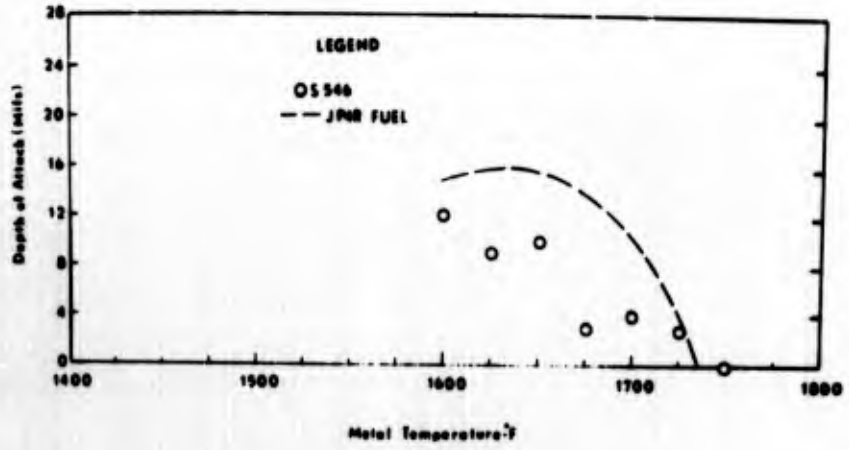

Figure 2.5. Corrosion as a function of temperature for B1910 tested using JP-5 Fuel (0.16%S) with a Salt/Air Ratio of 8 ppm. (Walters).

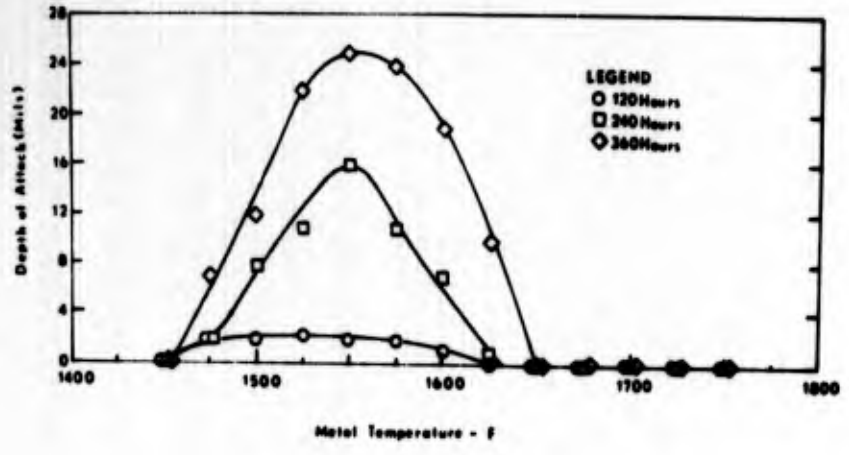

Figure 2.6. Corrosion as a function of temperature for B1910 tested using JP-4 fuel with a Salt/Air Ratio of 4 ppm. (Walters).

FSX 414, 418

A. M, Beltran, Cobalt No. 46, 1970, 3.

See X-40 for details. The good oxidation resistance of 414 at 2000°F (1093°C), and the even better oxidation resistance of 418 at 1600, 1800 and 2000°F (871, 955 and 1093°C) is shown.

The hot corrosion resistance of a group of alloys in a burner rig using 3% S residual oil containing 325 ppm NaCl (= 5 ppm NaCl in the air), 600h tests at 1600°F (871°C) is compared. For both alloys the maximum penetration was 0.04 mm per side.

The oxidation resistance of several alloys in 5000h tests is shown: FSX 414 and 418 compare very well withNi-base alloys - a little worse than Rene 77, but appreciably better than U 500 C.

Data relating to these alloys will also be found in the following Figures:
32.10, 52.10, 52.14.

G 64

G. Llewellyn, Hot Corrosion Problems Associated with Gas Turbines, ASTM Special Technical Publication, (STP 421) 1967, p1.

See Nimonic 100 for details. Figure 4.1 shows severe attack of uncoated blades after 500h running.

Threshold temperature in 6hr cycle, intermittent SO_3 and air at 45 min intervals 850°C; 830°C in contact with carbon: 980°C pack aluminised 910°C pack aluminised in contact with carbon. Reduced by holding: thus, after 500h at 900°C the threshold temperature for the pack aluminised material was reduced to 940°C.

Figure 4.2 is a section through coating showing deterioration after 3000h.

K. Page and R. J. Taylor, in "Deposition and Corrosion in Gas Turbines" A. B. Hart and A. J. B. Cutler (eds.), (Applied Science Publishers, London 1973) 350.

See Nimonic 105 for details. Nimonic 105 and G64 blades from an industrial Proteus engine are compared: the G64 performed surprisingly well.

Data relating to this alloy will also be found in the following Figure:
32.13;
and Table:
31-I

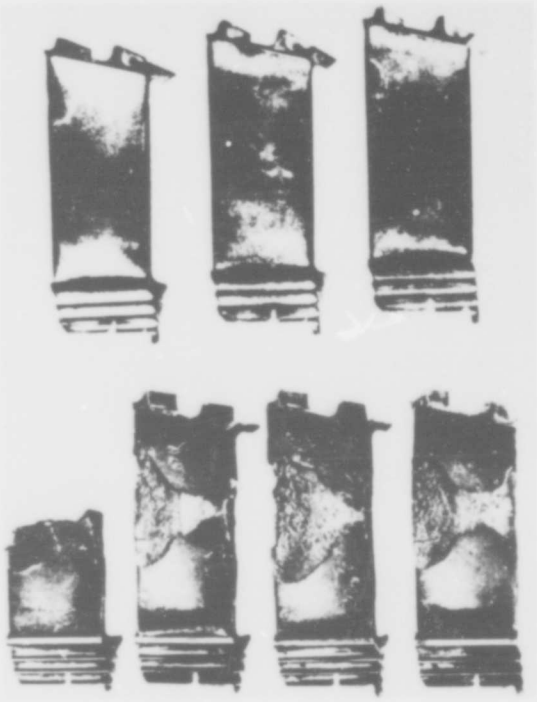

Figure 4.1. G.64 turbine rotor blades showing sulphur attack. Top row: Pack aluminized blades. Bottom Row: Standard blades. (Llewellyn).

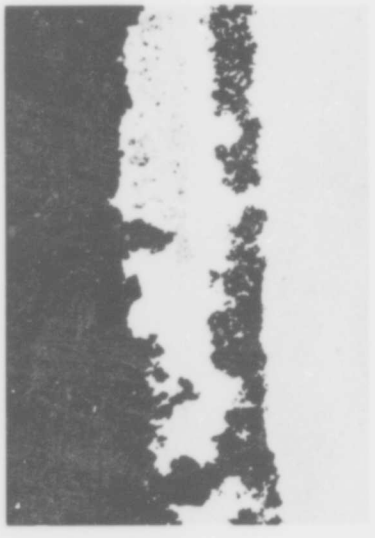

Figure 4.2. Deterioration of aluminized coating on a G.64 turbine rotor blade after 3000 hr running. (Llewellyn).

GMR-235

K. H. Ryan, J. R. Kildsig and P. E. Hamilton (Allison Division of General Motors) Technical Report to Wright-Patterson AFB, Air Force Materials Laboratory AFML-TR-67-306 (Aug. 1967).

A detailed summary of the procedure used in this report is given under PDRL-163. GMR-235 is the second worst of the alloys studied: Mar-M 246 is worse (the others are PDRL-163, IN 728 NX, 713C, 713C+Cr, 713C+Cr+Y, Mar-M 421, IN 100 and Inco 717). Figure 5.1 shows the volume loss from the as cast and heat-treated GMR-235 as a function of temperature. The corrosion of the heat-treated alloy was faster than that of the as-cast material (with most of the alloys there was no difference). Figure 5.2 compares the measured volume loss and that predicted by the regression equation (see PDLL 163).

The microstructure of all the alloys could be described in terms of three zones: (1) an outer layer of continuous oxide on the surface which gradually graded into an area of mixed metal and oxide; (2) a layer of depleted metal; (3) globular sulphide particles. The depleted zone in GMR-235 contained a high iron content which the authors considered may have contributed to its relatively poor corrosion resistance. Figure 5.3 shows the microprobe traverse for an 1800°F cyclic test on GMR-235.

R. Viswanathan, Corrosion 24 (1968) 359.

See 713C for details. GMR-235 was one of the best alloys tested, comparable to PDRL 163 and Waspaloy. After 150h at 1500°F (816°C) the specimen had lost 3.2 mg/cm^2 (after descaling); 98.0% of the alloy was unaffected.

Data relating to this alloy will also be found in the following Figures:
31.3, 31.4, 31.6, 36.1, 36.2, 36.3, 36.4, 36.5, 36.6, 36.7.

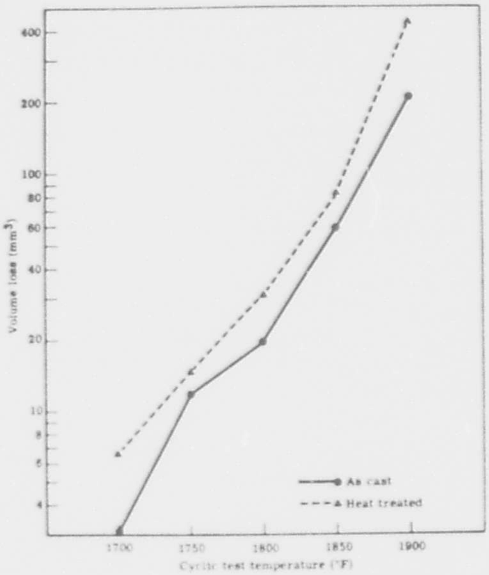

Figure 5.1. As-cast versus heat treated GMR-235 at each cyclic test temperature. (Ryan et al).

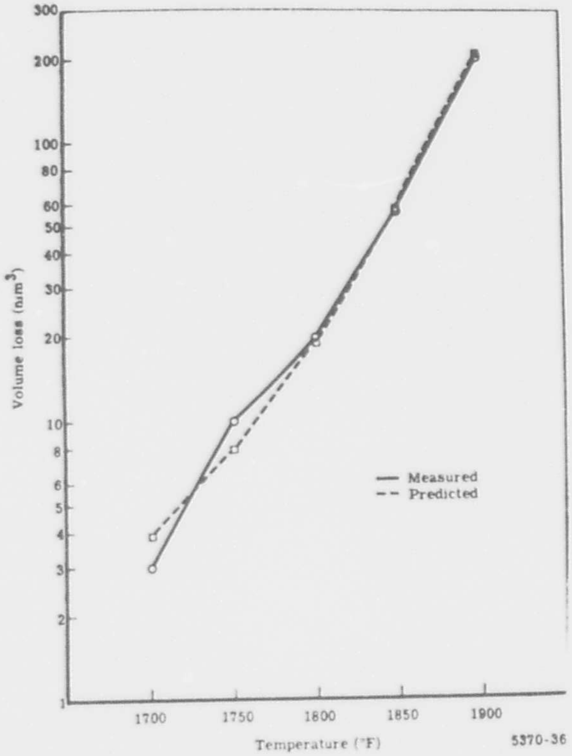

Figure 5.2. Comparison of the measured volume loss and the loss predicted by the regression equation for GMR-235 (Ryan et al).

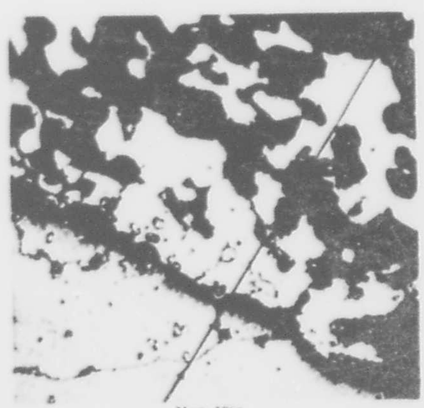

Magn 500×

Microprobe traverse on GMR-235 - 1800°F cyclic test

Relative composition

Location on traverse	Depletion zone α→β	Oxide sulfides β→γ	Sulfide γ	Depletion zone γ→δ	Sulfide δ	Matrix
Element						
Iron*	10	[illegible]	3	8-10	8	10.4
Nickel	76-85	10-[illegible]	26	[illegible]	60	58
Sulfur**	2-3	3-59	45	1-2 (peak to 40)	42	1
Chromium*	1 1/2-2	[illegible] 2-18	10	1 1/2	[illegible]	15.5
Titanium	1-1 1/2	4-30	15	1-3	4	[illegible]
Aluminum*	7	2-17	17	2	2 1/2	2.8
Molybdenum*	6-8	3-14	37	[illegible]	8	4.2

* Approximate weight percent

** X-ray intensity — compare with matrix

Figure 5.3. Microprobe traverse across corrosion area of GMR-235 after 1800°F cyclic test. (Ryan et al).

Hastelloy X

P.A. Bergman, C.T. Sims and A.N. Beltran, Hot Corrosion Problems Associated with Gas Turbines, ASTM Special Technical Publication, STP 421, 1967, 38.

See 713C for details. Attack at 1750°F (954°C) in burner rig, 100h, 200 ppm salts shown. Loss of surface (diameter) 2 mils; maximum penetration 9 mils. Most resistant alloy in this programme (a little better than U 500, but basically very similar). Some grain boundary attack.

P.A. Bergman, Corrosion 23 (1967) 72.

See S E L for an extended summary and the principal results. Hastelloy X was tested at 920°C and 980°C with 200ppm salt in the air : the corrosion resistance was good at both these temperatures. Figure 6.1 shows a Hastelloy X test fixture subject to hot corrosion: there appears to be preferential oxidation of large grey (sulphide?) particles. All the nickel-base alloys studied at 913 - 1093°C with 200 ppm salt formed nickel oxide and spinels with lattice parameters in the range 8.16 - 8.34 Å and usually in the range 8.28 - 8.33 Å : these latter were identified as $NiCr_2O_4$.

R. Viswanathan, Corrosion 24 (1968) 359.

See 713C for details. Hastelloy X was one of the better alloys tested, comparable to U-500 and U-520. After 150h test at 1500°C (816°C) the alloy had lost 3.5 mg/cm^2.

J.R. Johnston and R.L. Ashbrook, NASA Technical Note TN D-5376 (August 1969).

See B 1900 for details, and a list of the general figures and tables. The weight changes in 50h tests at 2000°F (1093°C) in high gas-velocity cyclic tests (19.5 mg/cm^2) and static oxidation tests (2.0mg/cm^2) are compared. The oxides determined by X-ray diffraction on Hastelloy X exposed to high gas-velocity oxidation were: 100h at 1800°F (982°C) produced Cr_2O_3, monoxide (NiO) and a spinel with a_o = 8.30 Å. The same time at 1900°F (1038°C) and 2000°F (1093°C) produced Cr_2O_3 and a spinel with a_o = 8.25 Å.

The mean weight loss after 100h at 2000°F (1093°C) was 1450 mg; about the same as Mar-M 200; a lot worse than IN 100 or B 1900.

W.L. Wheatfall, in "High Temperature Corrosion of Aerospace Alloys" J. Stringer, R.I. Jaffee and T.F. Kearns (eds.), AGARD Conference Proceedings No. 120, (March 1973) 235.

See 713 for details.

Data relating to this alloy will also be found in the following Figures:
1.9, 1.10, 1.13, 10.58, 10.105, 10.106, 38.14, 41.2 ;
and Tables:
10-XXX, 18-IV, 38-I, 38-II.

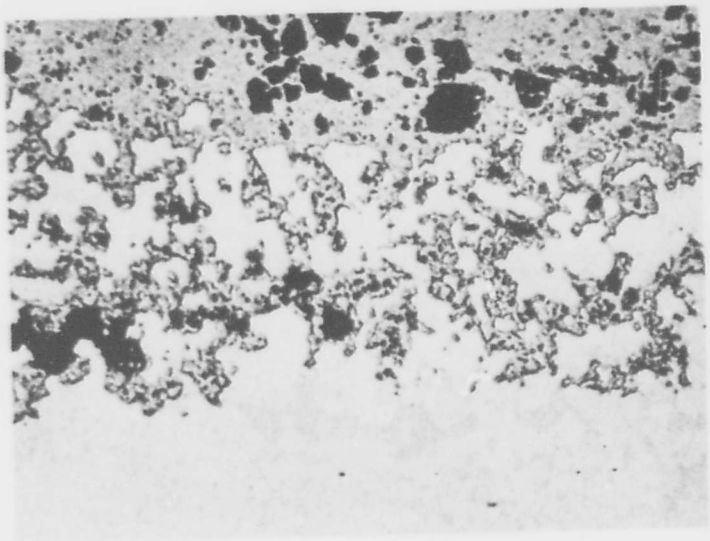

Figure 6.1. A Hastelloy X test fixture subject to hot corrosion. There is a preferential oxidation of the large grey particles. Unetched. 500 x. (Bergman).

IN 100

J.J. Walters (AVCO/Lycoming Division) Technical Report to the Air Force Materials Laboratory, Wright-Patterson Air Force Base AFML-TR-67-297 (Sept. 1967)

Extended summary in B 1900. IN 100 was one of a group of alloys described as having "very poor resistance to attack" - the others in this group were B 1900, B 1910 and Mar M 200. The phases found on the trailing edge of IN 100 specimens after 40h testing in order of predominance were NiO and a spinel with a_o = 8.34 Å. After 120h the products were the same as at the shorter time. The corrosion products found in powders removed from an area which had undergone hot corrosion in a 120h test were NiO and a spinel with a_o = 8.27 Å. A microprobe analysis of the depletion zone in the metal, for IN 100 was 94% Ni, 0.4% Cr, 1.0% Mo, 1.4% Al, 0.03% Ti and 3.0% Co.

Figure 7.1 shows the corrosion of IN-100 as a function of temperature tested using JP-4 fuel with 8 ppm salt in the air. Figure 7.2 - JP-4, 4 ppm salt. Figure 7.3 - JP-4R fuel, 8 ppm salt. Figure 7.4, JP-4R, 4 ppm salt. Figure 7.5 JP-5, 8 ppm salt.

P. A. Bergman, Corrosion 23 (1967) 72.

Describes the use of the GE "small burner rig" to evaluate super-alloys. JP-5 referee fuel containing 0.25% S was used at an air/fuel ratio of 30/1 (stoichiometric is 15/1). Both natural and artificial sea water were used, 0, 2 and 200 ppm salt being added to the air. All tests were for 50h. The principal method of evaluation was metallographic measurement of loss in diameter. Two data points are shown for the corrosion of IN 100 with 200 ppm salt, at 910°C and 982°C: the loss in diameter is greater than 70 mils in both cases. See SEL for a summary of some of the general results.

K.H. Ryan, J.R. Kildsig and P.E. Hamilton (Allison Division of General Motors) Technical Report to Wright-Patterson Air Force Base, Air Force Materials Laboratory AFML-TR-67-306 (August 1967).

A detailed summary of the procedure and of the general results is given under PDRL-163. IN 100 was one of a middle group of alloys (the others in this group were Mar-M 421, 713C, and Inco 717). Figure 7.6 shows the volume loss as a function of temperature in the range 1700 - 1900°F (927 and 1038°C) for both as-cast and heat-treated IN 100.

Figure 7.7 compares the measured volume loss with that predicted by the equation derived by regression analysis (see PDRL 163) for IN-100.

H. T. Quigg and R. M. Schirmer (Phillips Petroleum Company Research Division)Progress Report No. 4 to Naval Air Systems Command Contract NO_w65-0310-d (August 1966) Phillips Petroleum Company Report 4411-66R.

See 713 C for details.

R. M. Schirmer and H. T. Quigg, Progress Report on NASC Contract NO_w65-0310-d. Phillips Petroleum Company Research Division Report 4370-66R (June 1966).

See 713 C for details.

Figure 7.8 shows the mean weight loss for IN-100 under the various conditions. IN 100 was rather worse than 713C, rather better than W1-52.

The effect of the various conditions on the weight loss for IN 100 were analysed. The conclusions are: a significant decrease in metal weight loss was found for an increase in temperature from 1400° to 1600°F at 0.40 wt % S; no significant effect at lower sulphur contents, little systematic effect at other temperatures. Increasing sea-salt increased the corrosion under most conditions. The effect of fuel sulphur content was very variable.

Figure 7.9 shows the oxidised sample after 5h at 2200°F, no sea salt, 0.0002 wt % S. Figure 7.10 shows sulphidation after 5h at 1400°F, no sea salt, 0.40 wt % S. Figure 7.11 shows hot corrosion after 5h at 1600°F, 10 ppm sea salt, 0.0002 wt % S. Figure 7.12 shows a surface pit formed under the same conditions. Figure 7.13 shows hot corrosion after 5h at 1800°F, 10 ppm salt, 0.0002 wt % S. Figure 7.14 shows hot corrosion after 5h at 2200°F, 10 ppm salt, 0.0002 wt % S.

H. von E. Doering and P. A. Bergman Naval Ship Research and Development Centre Materials Laboratory Research and Development Report No. 2844 (March 1969).

See 713C for details. In a 100h test at 1750°F (955°C) with 200 ppm salt and in a 1000h test with 5 ppm salt the specimen was completely destroyed. SEL-15 was as bad- 713C rather better.

R. Field, D. J. Fisk and H. von E. Doering, Naval Ship Research and Development Centre Materials Laboratory, Research and Development Report 2833 (January 1969).

See 713C.

J. R. Johnston and R. L. Ashbrook, NASA Technical Note TN D-5376 (August 1969).

See B 1900 for details. The weight changes in high gas velocity cyclic tests and in static oxidation tests at 2000°F (1093°C) were compared: the dynamic weight loss for IN 100 was 3.7 mg/cm^2 is 50h, the best of the 7 alloys listed; the static weight gain in the same time was 2.8 mg/cm^2, the fourth of the alloys. Like B 1900, Mar. M. 200and TAZ-8A the thermal fatigue resistance was poor.

The oxides detected on IN 100 exposed in the high velocity apparatus were: at 1800°F (982°C) after 100h, Al_2O_3 and monoxide (NiO); at 1900°F (1038°C) after 100h, Al_2O_3 and a spinel with a_o = 8.30 Å; at 2000°F (1093°C) after 20h, monoxide and two spinels with a_o = 8.10 and 8.30 Å; after 60h, Al_2O_3 was also present; after 100h, Al_2O_3 monoxide, and the spinel with a = 8.30 Å.

Curiously, IN 100 lost significantly more in a Mach 0.7 test than in a Mach 1.0 test. The average weight loss in a 100h test at 2000°F (1093°C) was 250 mg (B 1900, 216 mg was the best; IN 100 was the second best).

V.S. Moore and A.R. Stetson, Final Report on NASC Contract No. N00019-68-C-0532 (Solar Research Division Report RDR 1626-5) (Dec. 1970),

See B 1900 for details.

Figure 7.15 shows the microstructure of a specimen after 20h at 1650°F. Figure 7.16 shows that of a specimen after 17h at 1800°F. The alloy failed after 20h at 1650F and 17h at 1800F. The hot corrosion of the alloy was poor, better than but comparable with SEL 15 and B 1900.

Two specimens tested for 10h at 1650F changed by +6.9 and -14.0 mg. 10h at 1800°F: -777 and -860 mg; 17h at 1800°F: - 1960 and -2280 mg.

H. T. Quigg and R. M. Schirmer, Progress Report No. 3 on NASC Contract No. N00019-68-C-0252 (Phillips Petroleum Company Research and Development Report 5423-69) July 1969.

See 713C for details. This report is principally concerned in testing the ASTM "Round Robin" group of alloys in the Phillips Turbine Environmental Simulator using a cyclic test in which the specimen is heated to 1600, 1800 or 2000°F (871, 982 or 1093°C) for 8 min and cooled to 1000°F (583°C) producing an attack approximately six times more severe than the isothermal routine used in the earlier tests. After 44h at a maximum of 2000°F, IN 100 had lost 372 mg/cm^2, the surface loss was 56 mils, the maximum penetration 56 mils, the worst of the alloys tested. The exposure time required to result in a loss of 127 mg/cm^2 was 11h. The data are presented in various tables (see 713C).

ASTM Round Robin Test organised by the Hot Corrosion Task Force of the Gas Turbine Panel, 1970.

See 713C. IN 100 usually ranked worst of the six alloys tested - 713C was nearly as bad, U 700 was a little better. Figure 7.16 shows the metal loss reported by the participants.

H.T. Quigg, R.M. Schirmer and L. Bagnetto, Final Report to NASC on Contract No. N00019-69-C-0221 (Phillips Petroleum Company Research and Development Report 5732-70) July 1970.

See 713C for details.

M.J. Donachie, Jr., R.A. Sprague, R.N. Russell, K.G. Bolt, and E.F. Bradley, Hot Corrosion Problems Associated with Gas Turbines, ASTM Special Technical Publication, STP 421, 1967, 85.

See 713C for details. The test conditions for IN 100 were: (a) JP-5R fuel with 0.4% S; 3.5 ppm sea salt in air; 1650°F (899°C); 100h; and (b) Marine Diesel fuel with 1.0% S; 3.5 ppm sea salt in air; 1650°F; 50h; according to one of the Tables , although the other Tables imply that other conditions were used as well. After 50h test at 2000°F (1093°C) in 1% S diesel fuel and 3.5 ppm salt IN 100 had lost 0.27g. With 3.5 ppm salt at 1650°F after 50h; 1.0% S, -1.35g; 0.4% S, -0.85g: after 100h, 1.0%S, -3.25g; 0.4%S, -2.70g. At 1650°F with JP-5R fuel and 3.5 ppm salt as a function of time up to 120h, IN 100 is much worse than the other alloys shown (713, U 700, Waspaloy). An example is shown of IN 100 specimen tested at 2000°F (1093°C) which had no Cr_2S_3 formed at the hot-spot on the wedge specimen; rather, the Cr_2S_3 was predominantly formed at the extremities of the hot spot where temperatures were about 1750 to 1800°F (953° to 982°C).

L. D. Graham, J. D. Gadd and R. J. Quigg, Hot Corrosion Problems Associated with Gas Turbines, ASTM Special Technical Publication STP 421, 1967, 105.

See 713C for details. Fine grain IN 100 appreciably better than coarse grain in crucible test for 1h at 1800°F (982°C); both better than 713C, comparable with PDRL 163.

P.E. Hamilton, K.H. Ryan and E.S. Nichols, Hot Corrosion Problems Associated with Gas Turbines, ASTM Special Technical Publication STP 421, 1967, 188.

See 713C for details. IN 100, together with TRW 1900, were the worst two alloys tested.

R. M. Schirmer and H. T. Quigg, Hot Corrosion Problems Associated with Gas Turbines, ASTM Special Technical Publication STP 421, 1967, 270.

See 713C for details. This paper is based on reports abstracted above, and describes experiments in the Phillips Environmental Simulator in the temperature range 1400 - 2200°F (760 - 1204°C), with 0.0002, 0.040 and 0.40% S in JP-5, 0, 1.0 and 10.0 ppm sea salt in the air. Figure 7.17 shows the corrosion of IN 100 as a function of temperature and test conditions. Table II shows the relative durability of the alloys: IN 100 is poor, comparable with WI 52 and SM 200, appreciably worse than 713C.

D.L. Deadmore, NASA Technical Memorandum TM X-2195, March 1971 (Lewis Research Center).

Isothermal and cyclic oxidation tests on IN 100 and WI 52 at 1900 and 2000°F (1038 and 1093°C). Tests included exposure cycles of 1, 2, 5, 20 and 170h for total oxidation times of up to 340h. Oxidation was evaluated by weight and thickness change measurements. Coupon specimens 1 x 1 x 0.11 inch (2.5 x 2.5 x 0.27 cm) were cut and ground to 600 g to a final thickness of 0.1 inch (0.25 cm). Initially, the specimens were placed in alumina boats, but the IN 100 specimens reacted extensively with the boat (WI 52 specimens did not) so later specimens were suspended by platinum wire in a vertical furnace.

Figure 7.18 shows a specimen after 45 2h cycles at 2000°F (1038°C). There is a thin surface scale, with some protrusions into the metal, and a depleted zone in the alloy beneath this. Isothermal and cyclic oxidation weight change data are shown in Figures 7.19 and 7.20; the isothermal data are compared with those from G.E. Wasiewlewski, Interim Rept. No. 2, General Electric Co., June 30, 1966 (work done under Contract AF33(615)-2861). Data are also available in W. J. Waters and J.C. Freche, NASA TN D-3597, 1966 at 1038°C: 0.96 mg/cm^2 at 64h, 4.0 mg/cm^2 at 112h and 9.76 mg/cm^2 at 304h. These are rather larger than the results in the present study, but the authors think this may be due to the fact that Waters and Freche used a technique which would retain any scale which spalled at temperature. The isothermal weight gain for IN 100 is less than that of WI 52 at both temperatures. For example, IN 100 gained 1.8 mg/cm^2 in 100h at 1093°C while WI 52 gained about 7 mg/cm^2.

The spalling in the cyclic test was quite small. The greater the cycle frequency, the greater the spalling, which is reflected in a smaller weight gain. IN 100 is more spall resistant than WI 52. Metal thickness loss is presented in Figure 7.21 for 1093°C.

Since so little spall developed from the IN-100 tests only in-situ surface diffraction was made on this material. The results are presented in Table 7-I for the specimen given sixty 2h cycles at 1093°C, which includes data from J. R. Johnston and R.L. Ashbrook, NASA TN D-5376, 1969 for 60 1h cycles in a high-velocity burner rig at 1093°C.

H.T. Quigg, R.M. Schirmer and L. Bagnetto, Final Report to Naval Air Systems Command on Contract N00019-70-C-0293 (Phillips Petroleum Company Research and Development Report 5903-71) Jan. 1971.

See 713C for details.

K. Page and R.J. Taylor in "Deposition and Corrosion in Gas Turbines" A.B. Hart and A.J.B. Cutler (eds.), (Applied Science Publishers, London, 1973) 350.

See Nimonic 105 for details. One or two graphs show data for IN 100.

D.L. Deadmore NASA Technical Note TN D-6842 (July 1972).

The report describes the cyclic oxidation of IN 100 and VI A in the NASA high gas-velocity oxidation apparatus, fuelled with natural gas. The maximum specimen temperature was 1093°C and the gas velocity Mach 1. The specimens were plates 10 x 0.6 x 2.5 cm, with a wedge section along one edge, and were mounted on a holder rotated at 900 rpm. The specimens were heated in 1 min, held for 1h, then cooled to room temperature in 3 min by a cold air blast, again at Mach 1. The majority of the tests were on coated specimens, but some tests were performed on uncoated materials. Figure 7.22 shows the weight change as a function of time, and compare the results with those of J. R. Johnston and R. L. Ashbrook, NASA TN D 5376, 1969 and W.A. Sanders, C.A. Barrett and H.B. Probst, NASA TN D-6400, 1971.

W.L. Wheatfall in "High Temperature Corrosion of Aerospace Alloys" J. Stringer, R.I. Jaffee and T.F. Kearns (eds.), AGARD Conference Proceedings No. 120 (April 1972) 235.

See 713 for details.

Data relating to this alloy will also be found in the following Figures :
1.1, 1.7, 1.8, 1.9, 1.10, 1.11, 1.12, 1.13, 10.51, 10.53, 10.68, 10.75, 10.84, 10.105, 10.106, 10.117, 10.123, 10.124, 32.19, 32.20, 36.1, 36.2, 36.3, 36.4, 36.5, 36.6, 36.7, 41.2, and Tables :
1-I, 1-II, 1-V, 1-VI, 1-VII, 1-VIII, 1-IX, 1-X, 10-I, 10-VI, 10- VIII, 10-XI, 10-XIII, 10-XV , 10-XVI, 10-XVII, 10-XVIII, 10-XIX, 10-XXI, 10-XXV, 10-XXVI, 10-XXX, 31-I.

TABLE 7-I

IN SITU X-RAY DIFFRACTION RESULTS

FOR IN-100 TESTED AT 2000°F (1093°C) (DEADMORE)

FOR 60 HOURS

Furnace test (2-hr cycles)	Burner rig test[a] (1-hr cycles)
Spinel, a_o = 8.1Å ($NiAl_2O_4$)	α - Al_2O_3
Spinel, a_o = 8.3Å ($NiCr_2O_4$)	Monoxide (probably NiO)
α - Cr_2O_3	Spinel, a_o = 8.10Å
α - Al_2O_3	Spinel, a_o = 8.3Å
TiO_2	

a Data from Johnston and Ashbrook

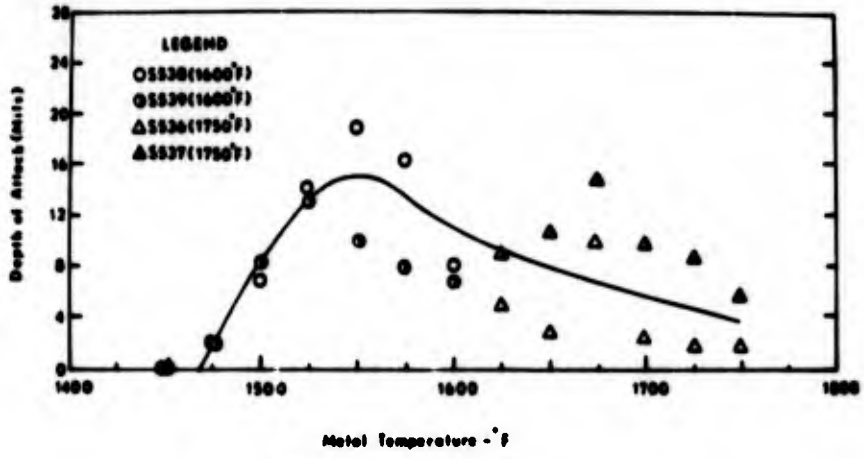

Figure 7.1. Corrosion as a function of temperature for IN100 tested using JP-4 fuel with a Salt/Air Ratio of 8 ppm. (Walters).

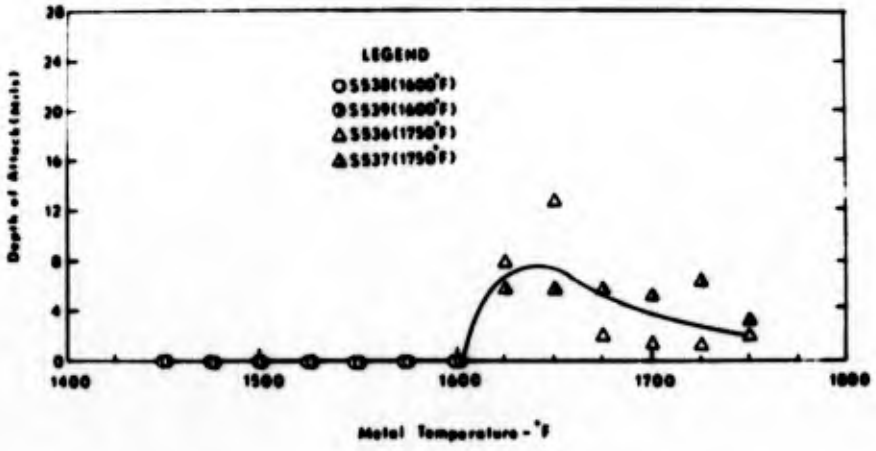

Figure 7.2. Corrosion as a function of temperature for IN100 tested using JP-4 fuel with a Salt/Air Ratio of 4 ppm. (Walters)

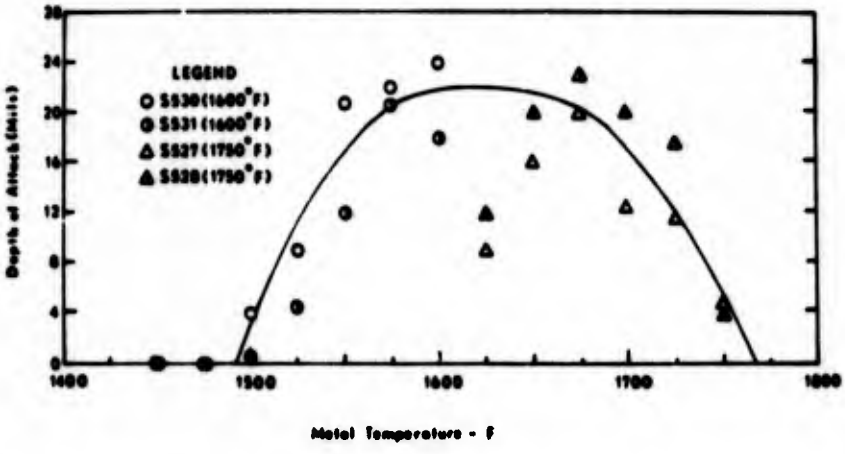

Figure 7.3. Corrosion as a function of temperature for IN100 using JP-4R fuel with a Salt/Air Ratio of 8 ppm. (Walters).

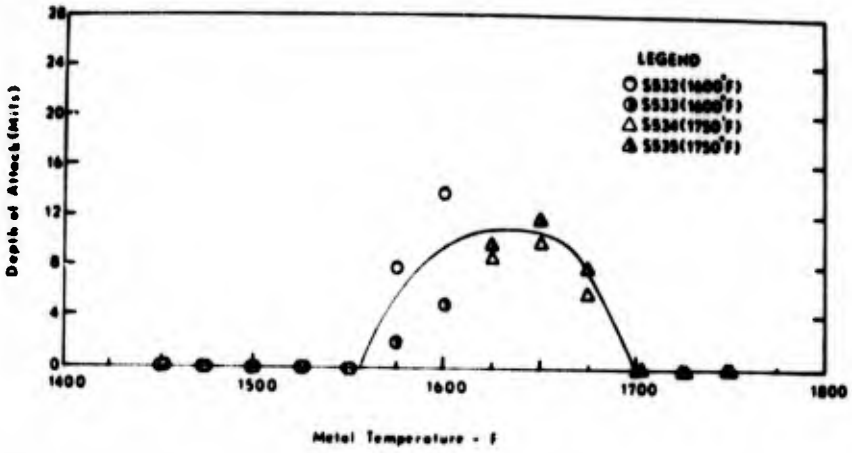

Figure 7.4. Corrosion as a function of temperature for IN100 using JP-4R fuel with a Salt/Air Ratio of 4 ppm. (Walters).

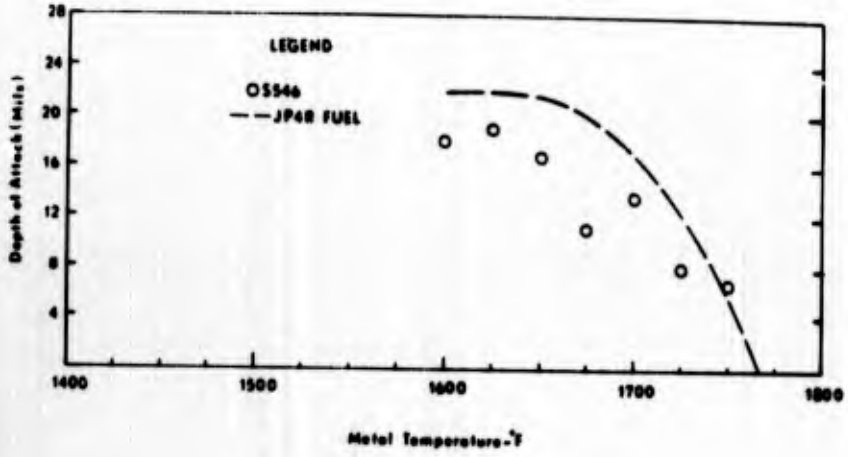

Figure 7.5. Corrosion as a function of temperature for IN100 tested using JP-5 fuel (0.16%S) with a Salt/Air Ratio of 8 ppm. (Walters).

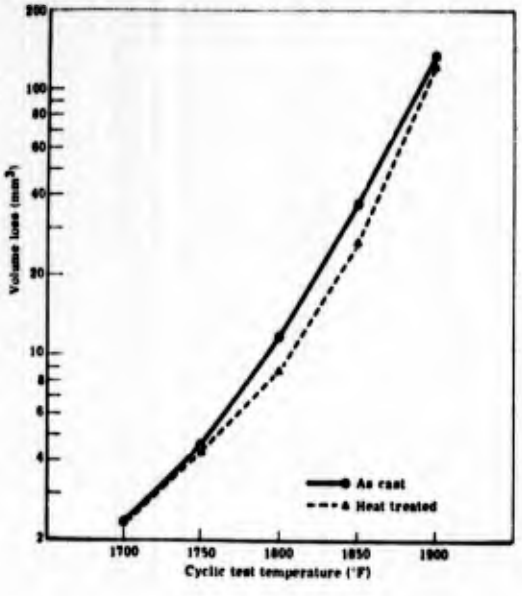

Figure 7.6. As-cast versus heat treated IN-100 at each cyclic test temperature. (Ryan et al).

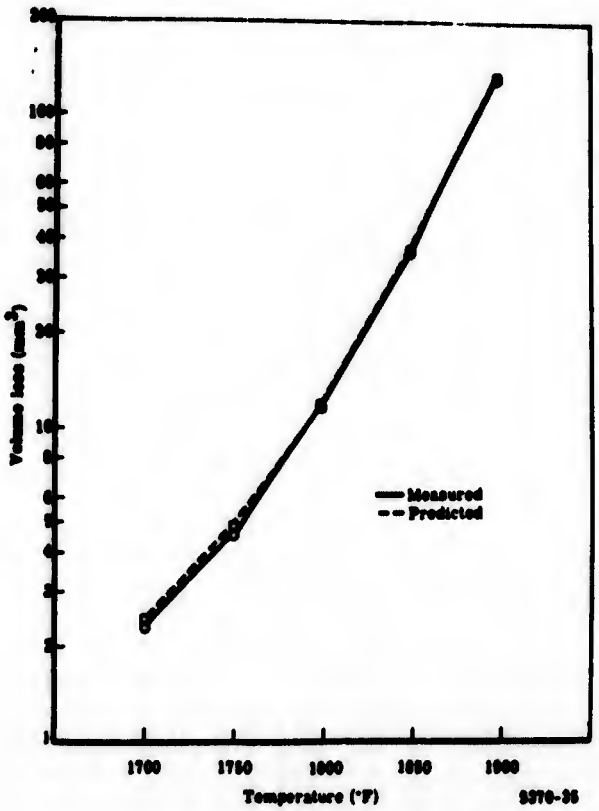

Figure 7.7. Comparison of the measured volume loss and the loss predicted by the regression equation for IN-100. (Ryan et al).

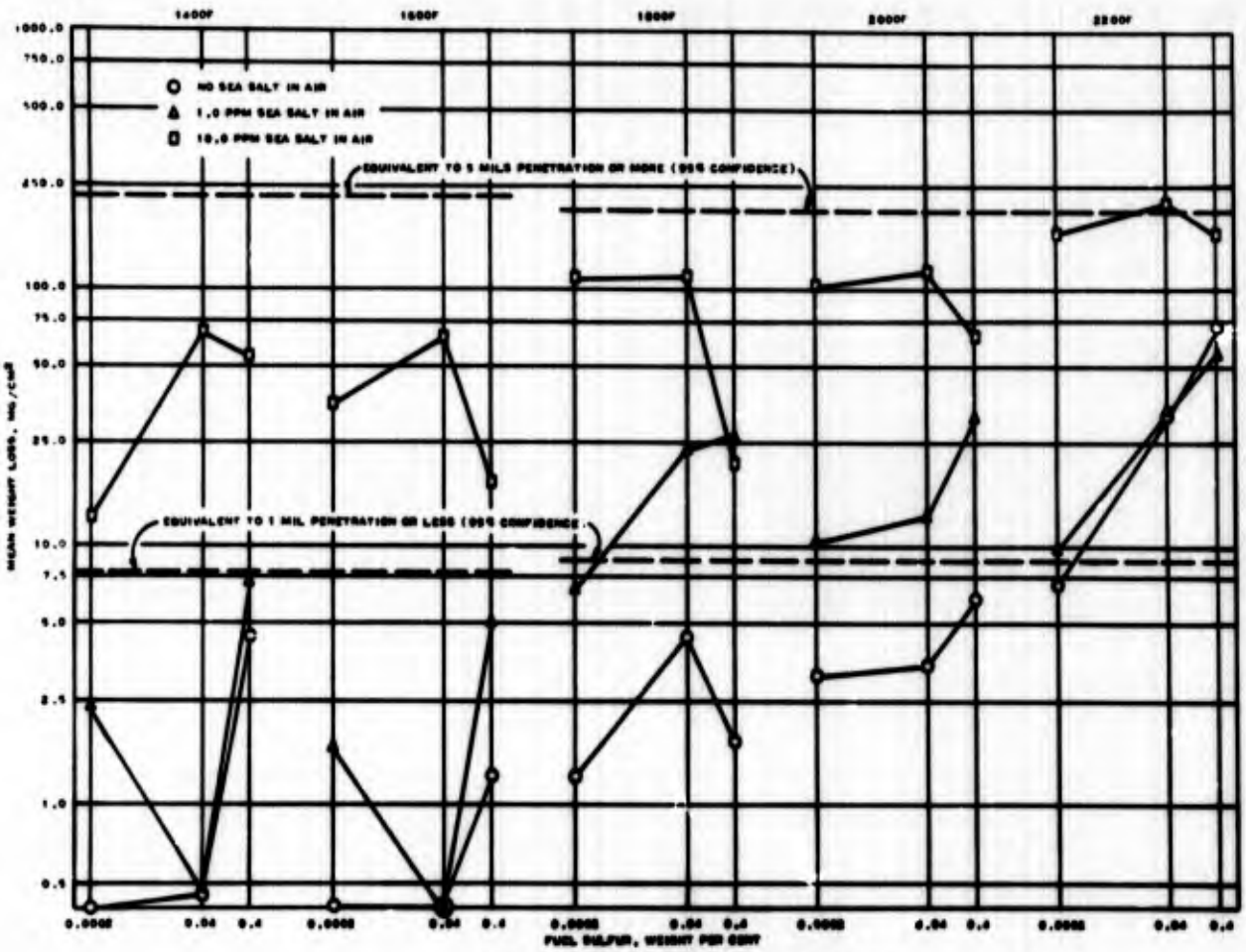

Figure 7.8. Effect of fuel sulphur, sea salt in air and gas temperature on metal loss of IN-100 test specimens (Schirmer and Quigg).

UNIFORM
SURFACE ATTACK

BASE METAL
UNETCHED
200X

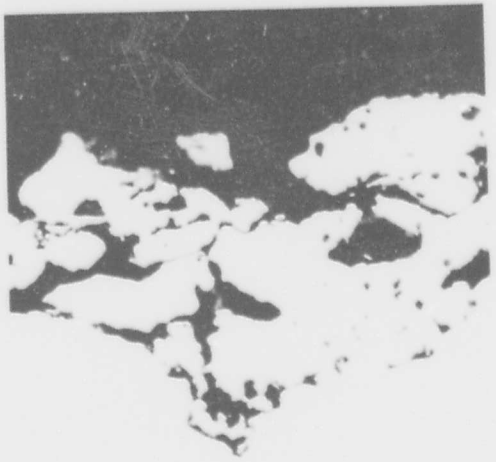

INTERDENDRITIC OXIDATION

BASE METAL
UNETCHED
200X

Figure 7.9. Oxidation of IN-100 in Phillips Rig. (Schirmer and Quigg).

5 hours exposure at 2200 F test condition with no sea salt in air and 0.0002 wt % sulphur in fuel.

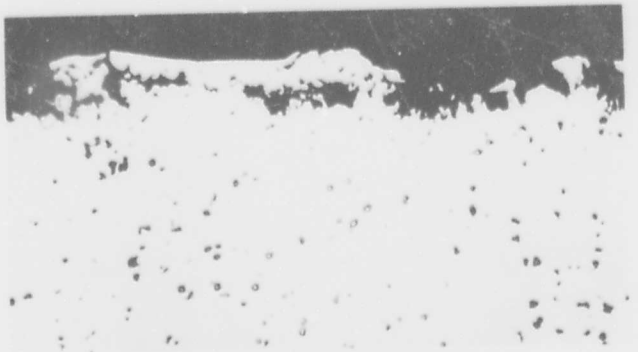

VARIABLE
SURFACE ATTACK

BASE METAL
UNETCHED
200X

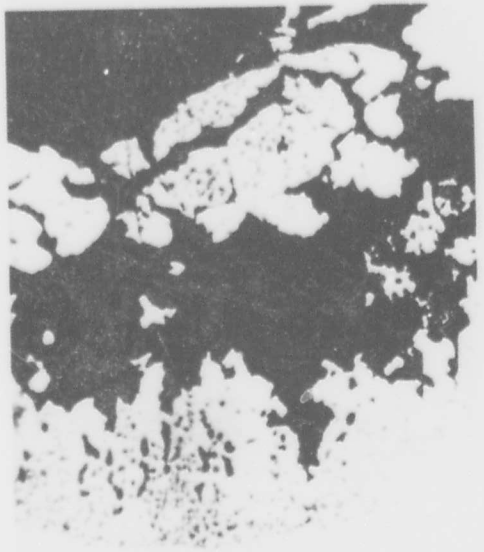

HEAVY SULFIDE PENETRATION

UNETCHED
1500X

Figure 7.10. Sulfidation of IN-100 in Phillips Rig. (Schirmer and Quigg).

5 hours exposure at 1400 Ftest condition with no sea salt in air and 0.40 wt % sulphur in fuel.

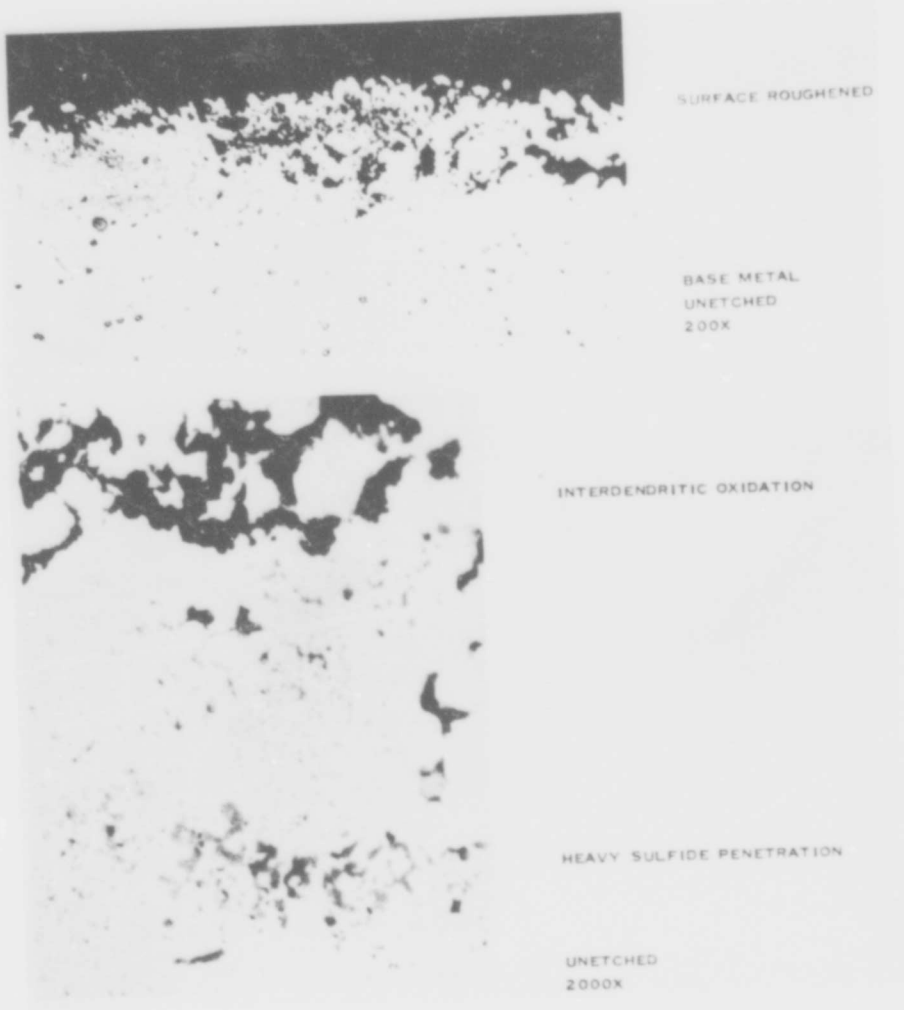

Figure 7.11. Hot Corrosion of IN-100 in Phillips Rig. (Schirmer and Quigg).

5 hours exposure at 1600 F test condition with 10 ppm sea salt in air and 0.0002 wt % sulphur in fuel.

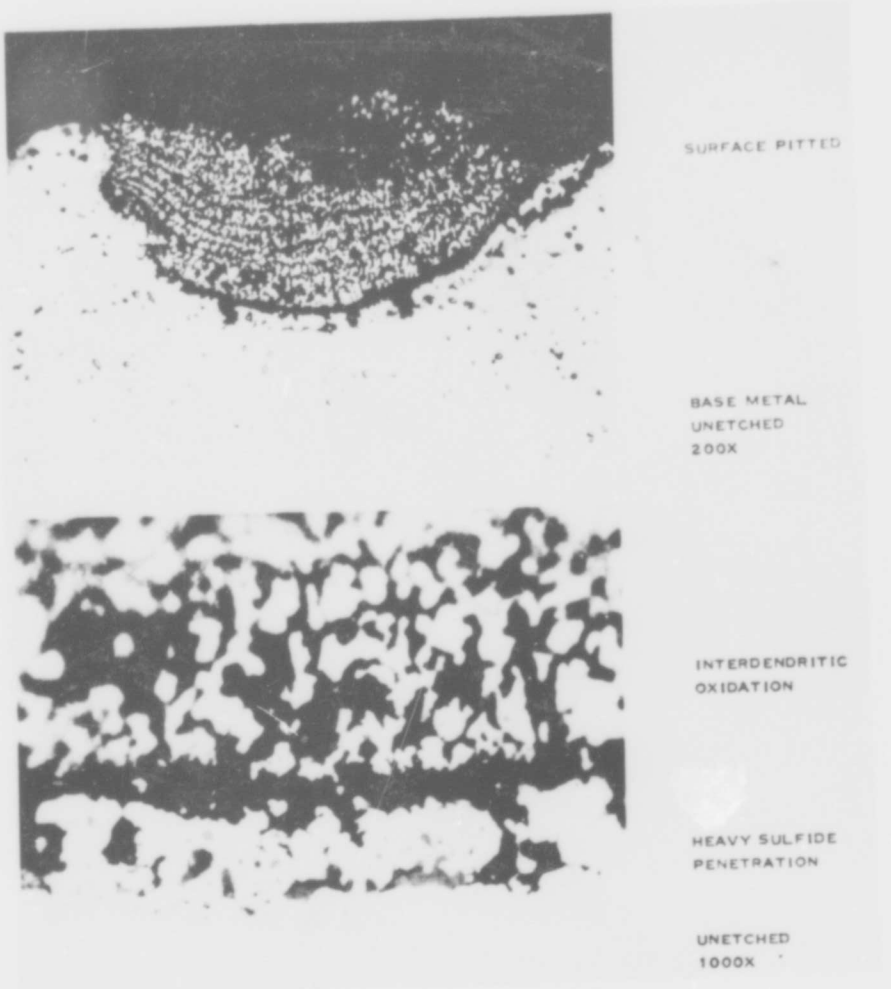

Figure 7.12. Hot Corrosion of IN-100 in Phillips rig. (Schirmer and Quigg).

5 hours exposure at 1600 F test condition with 10 ppm sea salt in air and 0.0002 wt % sulphur in fuel.

SURFACE ROUGHENED

BASE METAL
UNETCHED
200X

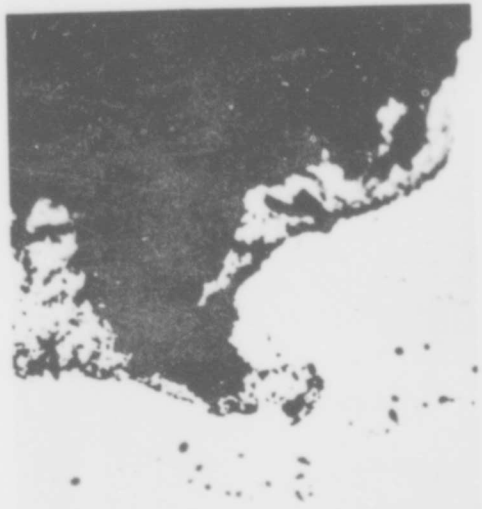

SULFIDE PENETRATION

BASE METAL
UNETCHED
2000X

Figure 7.13. Hot Corrosion of IN-100 in Phillips rig. (Schirmer and Quigg).

5 hours exposure at 1800F test condition with 10 ppm salt in air and 0.0002 wt % sulphur in fuel.

SURFACE ROUGHENED

BASE METAL
UNETCHED
200X

GROSS OXIDATION
CLOSELY FOLLOWING
SULFIDE PENETRATION

BASE METAL
UNETCHED
2000X

Figure 7.14. Hot Corrosion of IN-100 in Phillips rig. (Schirmer and Quigg).

5 hours exposure at 2200 F test condition with 10 ppm sea salt in air and 0.0002 wt % sulphur in fuel.

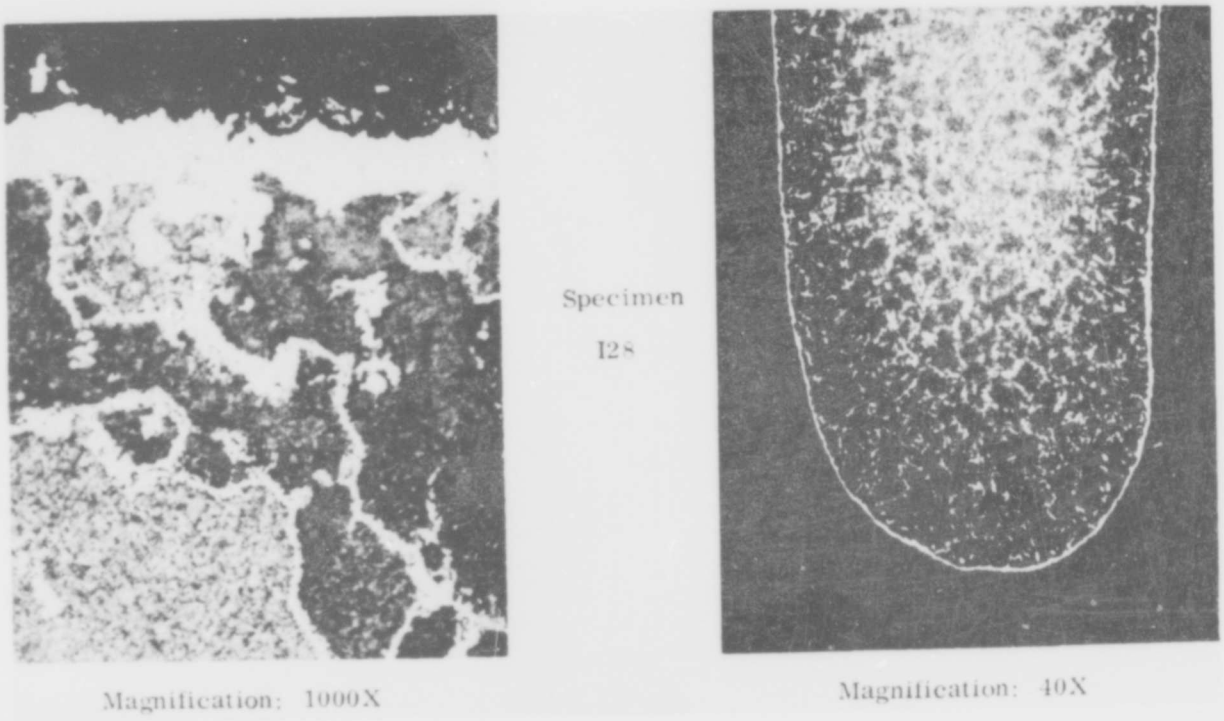

Figure 7.15. Microstructure of uncoated IN-100 alloy after hot corrosion tests at 1650°F for 20 hours. (Moore and Stetson).

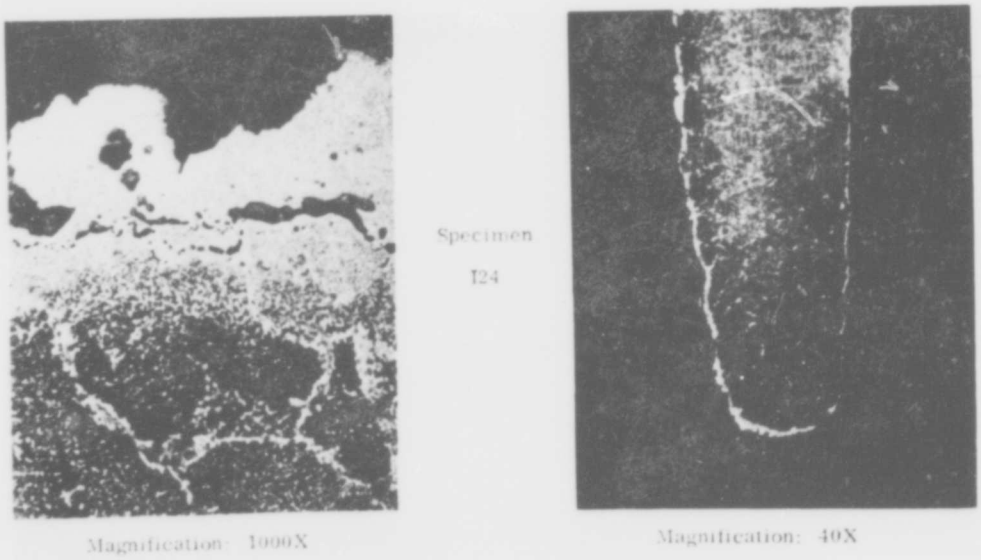

Figure 7.16(a). Microstructure of uncoated IN-100 alloy after hot corrosion tests at 1800°F for 17 hrs. (Moore and Stetson).

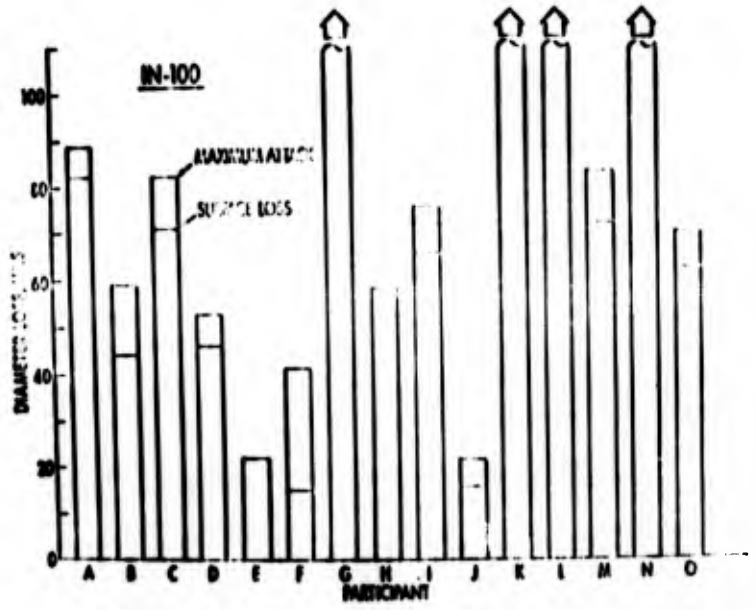

Figure 7.16(b).
Results of ASTM Round Robin tests for IN 100.

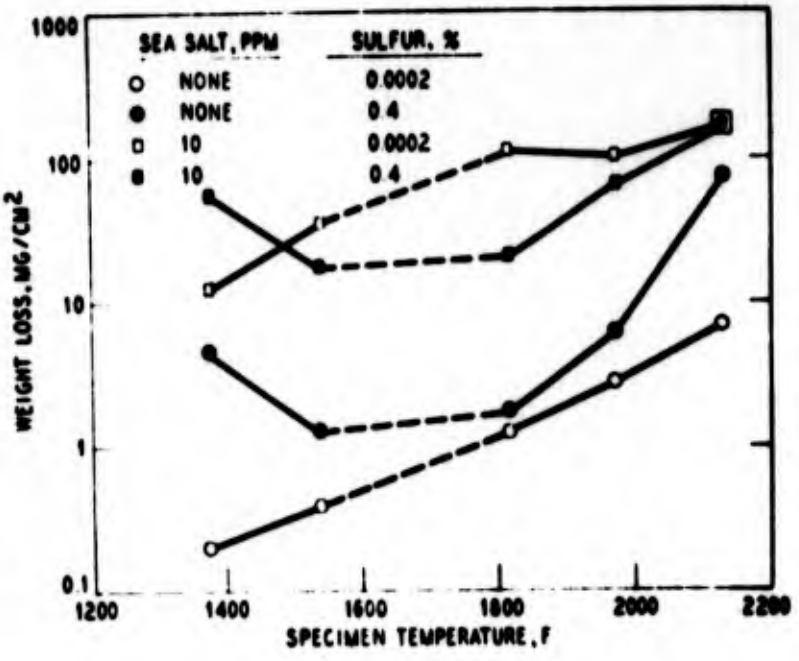

Figure 7.17. Hot corrosion of IN-100 (Schirmer and Quigg).

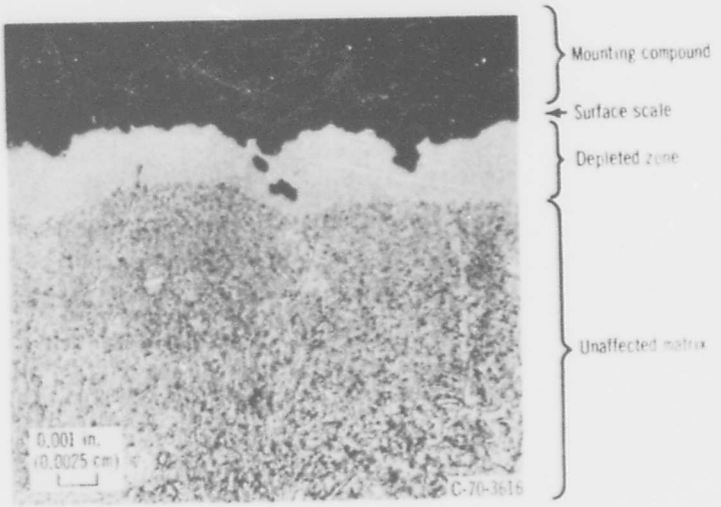

Figure 7.18. IN-100 after forty-five 2-hour cycles at 2000°F (1038°C). X250. (Deadmore).

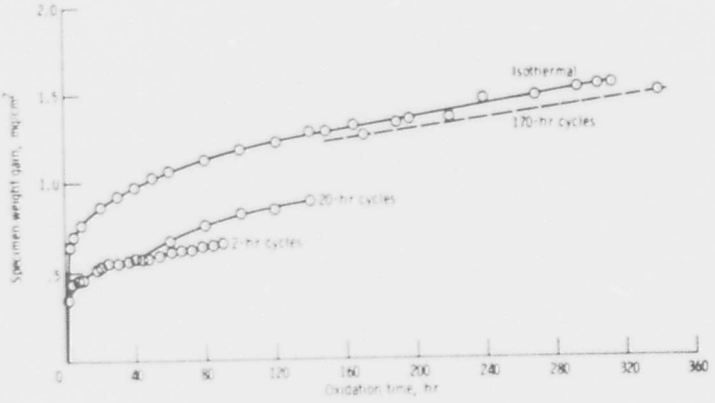

Figure 7.19. Effect of cyclic and isothermal oxidation on weight gain of IN-100 at 1900°F (1038°C). (Deadmore).

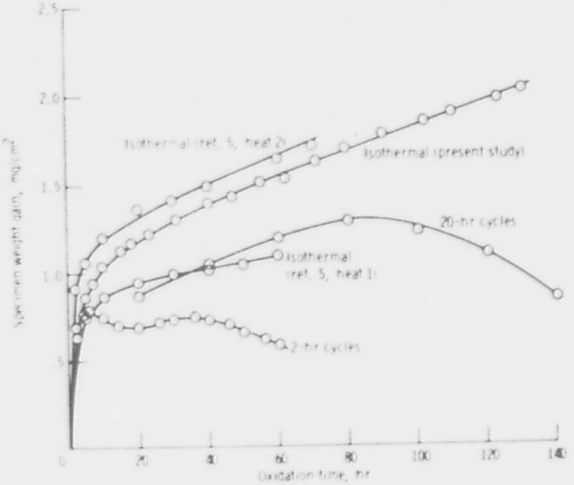

Figure 7.20. Effect of isothermal and cyclic oxidation at 2000°F (1093°C) on weight gain of IN-100. (Deadmore).

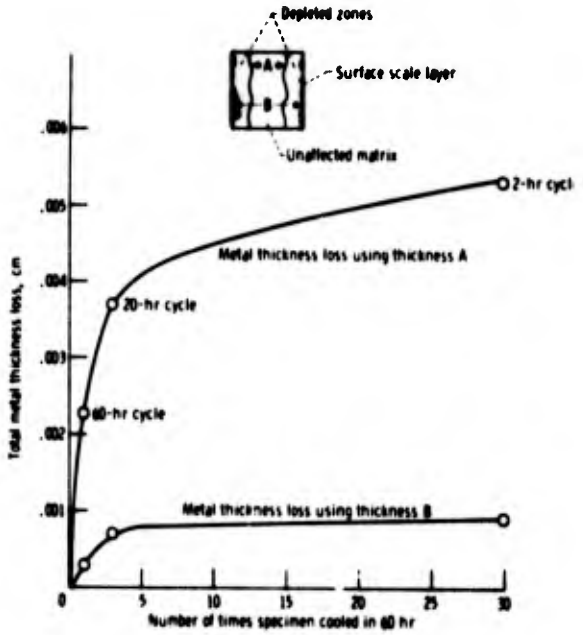

Figure 7.21. Effect of cyclic oxidation on total metal thickness loss of IN-100 at 2000°F (1093°C). Original metal thickness, 0.25 centimeter. (Deadmore).

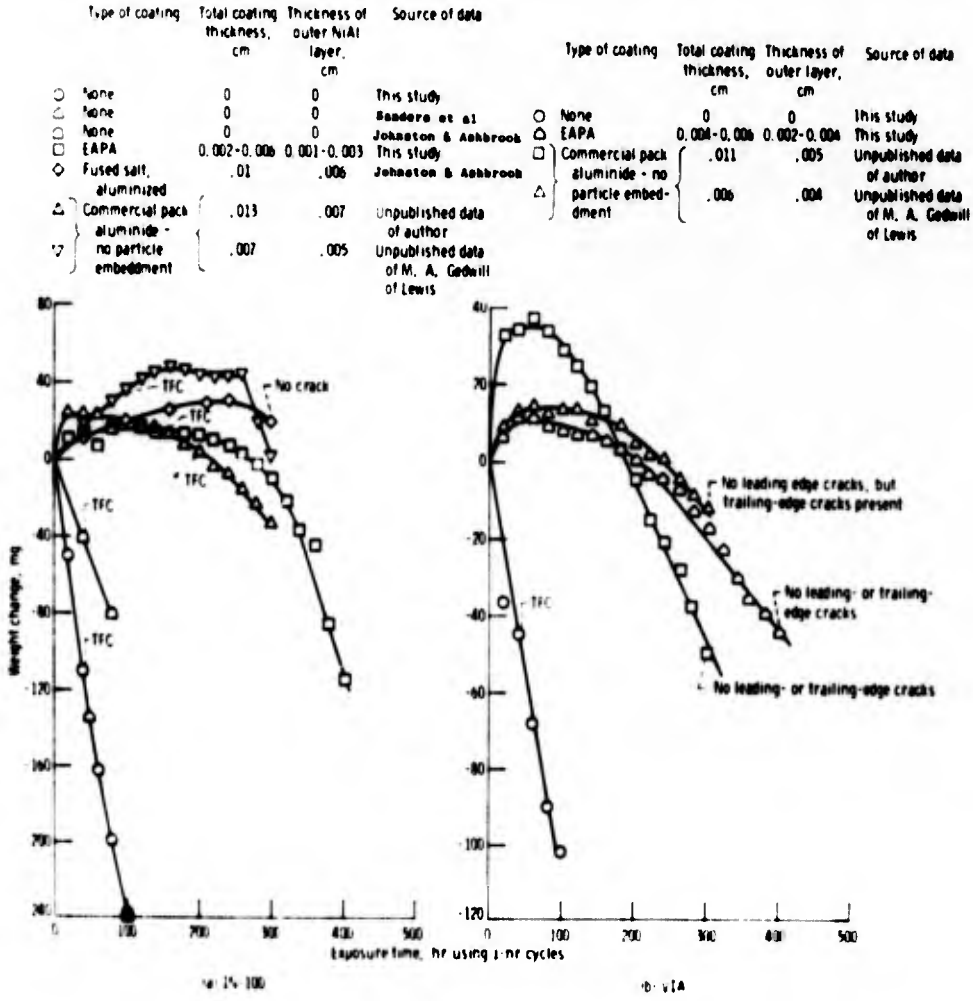

Figure 7.22. High-gas-velocity cyclic oxidation weight-changes of coated and bare IN-100 and VIA at 1093°C (2000°F). All specimens were Lewis wedge bars. Note: TFC indicates that a thermal fatigue crack was observed. (Deadmore).

IN 587, 589, 597.

P. L. Norman and J. D. Harston, in "Deposition and Corrosion in Gas Turbines" A. B. Hart and A. J. B. Cutler (eds.) (Applied Science Publishers, London, 1973) 260.

See Nimonic 80A. The corrosion of several nickel-base alloys in a salt-spray test using 75% Na_2SO_4, 25% NaCl at 700, 800 and 900°C is compared using weight loss after descaling as a measure of the corrosion. 587 and 597 are fairly similar, with quite good resistance at 700°C, intermediate resistance at 800°C comparable with IN 738, and quite good resistance at 900°C.

P. C. Felix, in "Deposition and Corrosion in Gas Turbines" A. B. Hart and A. J. B. Cutler (eds.), (Applied Science Publishers, London, 1973) 331.

See 713C for details. (587, 597).

Data relating to these alloys will also be found in the following Figures:
10.92, 14.8, 14.9, 14.10, 32.6, 32.10.

Inconel 700

R. Viswanathan, Corrosion 24 (1968) 359.

See 713C for details. Inco 700 was one of the worst alloys tested. Only U-700 was as bad. After 10h at 1500°F (816°C) the alloy had lost 6.2 mg/cm^2; after 150h 196 mg/cm^2 (after descaling). In the latter case none of the alloys was unaffected by the corrosion. The attack was very irregular, some regions being virtually unattacked, others being completely penetrated.

The effect of two different sulphur trioxide levels in the gas stream was tested: 6 ppm and 150 ppm. For Inco 700 the weight losses in a 150h test at 1500°F were 7.40 and 196 mg/cm^2 respectively. The authors consider that the SO_3 stabilised the sulphate salt coating on the specimens.

L. D. Graham, J. D. Gadd and R. J. Quigg, Hot Corrosion Problems Associated with Gas Turbines, ASTM Special Technical Publication STP 421, 1967, 105.

See 713C for details. Inconel 700 was one of the best two alloys tested (the other was Waspaloy) in a crucible test. Order of magnitude better than U 700, PDRL 163, 713C.

F. J. Wall and S. T. Michael, Hot Corrosion Problems Associated with Gas Turbines ASTM Special Technical Publication STP 421, 1967, 223.

See 713C for an extended summary. Specimens of several commercial alloys were coated with 50% Na_2SO_4/50% $MgSO_4$ and oxidised in a simulated combustion gas at 1250, 1350 and 1450F (677, 732, 788°C) for times up to 1000h. The alloys were identified only by number and by approximate compositions, but alloy No. 17 appears to be Inconel 700. Figure 9.1 shows the kinetics of the corrosion at the three temperatures. The corrosion resistance was rate "poor" (the same as U 700 (?), Nicrotung (?)and 713C (?)). Waspaloy (?) and U500(?) were rated "good".

C. J. Spengler, S. Y. Lee and W. E. Young in "Deposition and Corrosion in Gas Turbines" A. B. Hart and A. J. B. Cutler (eds.) (Applied Science Publishers London, (1973) 294.

See U500 for details.

C. E. Hussey, S. Y. Lee and W. E. Young, paper presented to ASTM Annual Meeting, Symposium on Gas Turbine Fuel Requirements, Handling and Quality Control, June 1972.

See U500 for extended summary. Figure 9.2 shows an example of a First stage Inco 700 rotor blade.

Data relating to this alloy will also be found in the following Figures:
10.67, 10.68, 45.38.

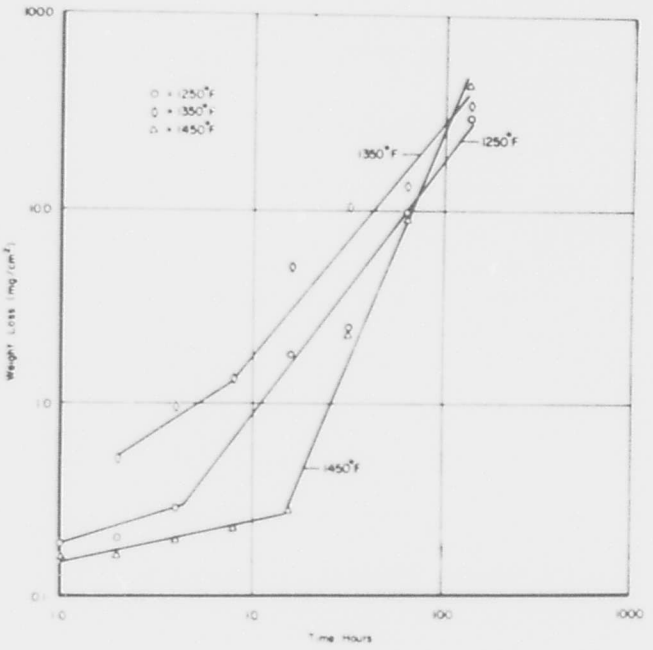

Figure 9.1. Weight loss of Ni-15 Cr-3 Al alloy after exposure to 1250, 1350, and 1450 F. (Wall and Michael).

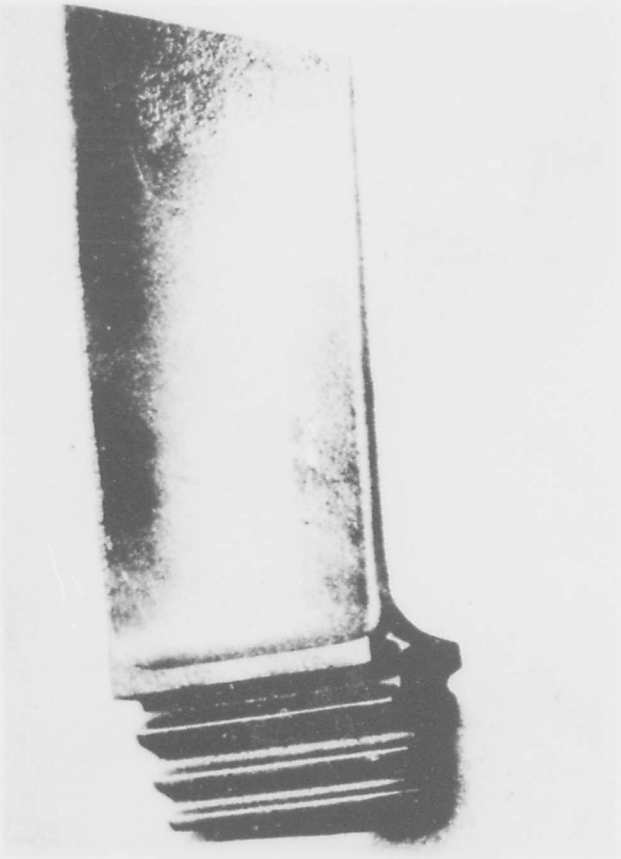

Figure 9.2. First-stage Inco 700 rotating blade, 1965-66. (Hussey et al).

713 C and 713 LC

J.J. Walters (AVCO/Lycoming Division) Technical Report to the Air Force Materials Laboratory, Wright-Patterson Air Force Base, AFML-TR-67-297 (September 1967).

The author remarks that AVCO Lycoming's experience with hot corrosion began with the discovery, at engine overhaul, of corrosion on an uncoated 713C T53 gas producer nozzle vanes after they had been in service in Vietnam. About the same time, the U.S. Navy returned a T53-L-11 engine from Patuxent River because of premature turbine failure, which again turned out to be due to hot-corrosion of uncoated 713C nozzle guide vanes. A similar attack was observed on uncoated 713C hardware from AVCO Lycoming's marine engines (LVS, LVH) which were being developed during this period. The AVCO Lycoming environmental test rig was built, and Figure 10-1 shows good correlation between the 120h tests in this rig with 6ppm salt in the air with engine tests in T53-L-II engines with 1ppm salt in the air (60 and 90h tests) for four alloys, including 713C. See B 1900 for a summary of the test procedure in the present programme.

713C was one of a group of alloys described as having "poor resistance to attack" - the others in this group were PDRL 161 and PDRL 162. The results of testing at 1600 and 1750°F (871 and 955°C) peak metal temperature using JP-4 and JP-4R fuel with 4 and ppm salt in the air are shown under B 1900. The threshold and terminal temperatures after 120 and 360h testing using JP-4 fuel with 4 ppm salt in the air for 713C are 1475 and 1700°F; and 1450 and 1750°F (802 and 927°C, and 788 and 955°C). The X-ray analysis of the corrosion products found on the trailing edge after 40h testing for 713C in order of predominance showed NiO, a spinel with a_o = 8.17 Å, a trace of Al_2O_3 and a trace of Cr_2O_3. The products after 120h testing for 713C were the same as at the shorter time except that in addition there were small amounts of an unknown phase. The corrosion products found in powder removed from an area of a 713C specimen which had undergone hot corrosion in a 120h test were NiO, a spinel with a_o = 8.24 Å, a trace of Al_2O_3, a trace of Cr_2O_3 a trace of Al_2O_3, and an unknown phase. A microprobe analysis of the depleted metal zone was 95% Ni, 0.3% Cr, 3.5% Mo 3.0% Al, 0.01% Ti and 0.2% Nb.

Figure 10.2 shows the attack of 713C as a function of temperature tested using JP-4 fuel with 8 ppm salt in the air. Figure 10.3 shows the same for 713LC. Figure 10.4 - 713C, JP-4, 4 ppm. Figure 10.5 the same for 713LC. Figure 10.6 - 713C, JP-4R, 8ppm salt. Figure 10.7, the same for 713 LC. Figure 10.8 - 713C, JP-4R, 4 ppm salt. Figure 10.9, the same for 713 LC. Figure 10.10; 713C, JP-5, 8 ppm salt. Figure 10.11, the same 713 LC. Figure 10.12 shows the corrosion as a function of temperature for 713 C using JP-4 fuel with 4 ppm salt, for three test times - 120, 240 and 360h.

Figure 10.13 compares the total corrosion for several alloys, including 713C, tested in JP-4 fuel with 4 ppm salt in the air for three times - 120, 240, and 360h. Figure 10.14 shows the depth of attack as a function of time at 1550°F (844°C) for three alloys, including 713 C.

K.H. Ryan, J.R. Kildsig and P.E. Hamilton (Allison Division of General Motors) Technical Report to Wright-Patterson Air Force Base, Air Force Materials Laboratory AFML-TR-67-306 (August 1967).

A detailed summary of the procedure and the overall results is given under PDRL-163. 713 C was one of a middle group of alloys (the others in the group were Mar-M 421, IN-100 and Inco 717). The effect of heat-treatment is small for 713C, and for 713C + 2% Cr, and 713 C + 2% + Y. Figure 10.15 shows the volume loss as a function of temperature in the range 1700 - 1900°F for both as-cast and heat-treated samples of 713C. Figure 10.16 is the same for 713C + 2% Cr. Figure 10.17 is the same for 713C + 2% Cr + Y.

A regression analysis was performed for the corrosion in terms of temperature and the alloy composition:

$$\log_{10}(\text{volume loss}) = 5.85238 \times 10^{-9} T^3 - 1.33860 \times 10^{-5} T^2 + 6.32837 \times 10^{-2} \text{ w/o W} + 8.63834 \times 10^{-2} \text{ w/o Mo} - 6.77702 \times 10^{-2} \text{ w/o Cr} - 8.982 \times 10^{-2} \text{ w/o Al} + 11.2807$$

Figure 10.18 compares the volume loss measured experimentally and that calculated from the above equation. Figure 10.19 is the same for 713 C + 2% Cr; Figure 10.20 the same for 713 C + 2% Cr + Y.

Figure 10.21 shows light and electron micrographs of corrosion on 713 C after 1900 and 2000°F cyclic tests (1038° and 1093°C). Figure 10.22 shows the microstructure, and the microprobe analysis of 713C after 1800°F cyclic test (982°C). Figure 10.23 is the same for a 1900°F (1038°C) cyclic test. Figure 10.24 shows the same for 713C + 2% Cr after an 1800°F (982°C) cyclic test.

H.T. Quigg and R.M. Schirmer (Phillips Petroleum Company, Research Division) Progress Report No. 4, Naval Air Systems Command Contract NOw 65-0310-d August 1966, Phillips Petroleum Company Report 4411 - 66R.

This report is concerned with the effect of manganese and lead-containing additives in the fuel on hot corrosion. The manganese is contained in a smoke-supressant additive; the lead was present at one time in fuel used for carrier-based operations. Tests were in the Phillips 2 in combustor at 1400, 1600, 1800 and 2000°F, (760, 871, 982, and 1093°C), 0 and 10.0 ppm salt in the air, 0.0002 and 0.40 wt % S in the fuel. Manganese was tested at 15.14 ml of the additive CI-2 per gallon, and lead at 15.33 ml of the additive TEL per gallon of fuel. The weight loss data are shown in Tables 10-I. At most temperatures there is relatively little difference in attack: in some particular cases the attack is much more rapid or much slower with the additives. Table 10-II shows apartial analysis by X-ray diffraction of deposits from specimens exposed to TEL, and Table 10-III and 10-IV show partical analysis by X-ray fluorescence of deposits from both tests.

H.T. Quigg and R.M. Schirmer. Progress Report No. 3 NASC Contract NO$_w$66-0263-d. Phillips Petroleum Company, Research Division Report 4706-67R. (April 1967).

Phillips 2 in combustor, 2000°F, (1093°C), < 0. 0040, 0.040 and 0.40 wt % S in the fuel; 0 and 1 ppm sea salt in the air, test duration up to 55h; 15 atm pressure, 745 ft per second gas velocity, 60/1 air / fuel ratio. Most of the tests were on MISCO-coated (packed aluminised) 713C, but some tests were run on uncoated alloys. On the coated alloy, NiO was identified as the major scale component, Ni(Al,Cr)$_2$O$_4$ as the minor components. Na_2SO_4 was not detected. X-ray fluorescence detected S and K, but not Cl. Weight loss was evaluated in terms of an exponential growth curve:

$$W = A\ B^x$$

where w is the weight loss per unit area, A,B are constants, and x is the exposure time. With no salt, A = 6.6 and B = 1.052; with 1.0 ppm salt and 0.004%S, A = 14.7 and B = 1.069, with the higher sulphur contents, the equation was written $W = A\ B^x\ C^S$, where S is the sulphur content of the fuel; A = 10.29, B = 1.118 and C = 8.092. For these equations, W is mg/cm^2 x is in h, and S is in wt %. Figure 10.25 shows the data for uncoated 713C with no sea salt in the air, and Figure 10.26 shows the data with 1.0 ppm sea salt.

Figure 10.27 shows a section of a hot corroded 713C turbine blade from a Navy scrap heap. Figure 10.28 shows a specimen exposed for 25h. at 2000°F (1093°C) with 1.0 ppm sea salt and 0.4 wt % S in the fuel.

The experimental data are in Table 10-V.

R.M. Schirmer and H.T. Quigg, Progress Report on NASC Contract NO$_w$ 65-0310-d. Phillips Petroleum Company Research Division Report 4370 - 66 R. (June 1966).

Phillips 2 in combustor, 15 atmospheres pressure, 565 - 805 ft per second gas velocity, 5h cyclic test. 1400, 1600, 1800, 2000 and 2200°F (761, 871, 982, 1093, 1204°C); 0.0002, 0.040 and 0.40 wt % S in the fuel; 0, 1.0 and 10.0 ppm sea salt in the air.

Figure 10.29 shows the weight loss (after descaling) of 713C specimens for various test conditions. Table 10-VI shows the weight loss for specimen in 5h tests under various conditions in different stages of the apparatus. Table 10-VII shows the measured sulphide penetration and penetration from weight loss of the test specimen: for 713C at 2000°F, 0.040 wt % S, 10.0 ppm salt, the penetration from weight loss was 0.9 mils in 5h; the sulphide penetration was 9.8 mils in 5h. The durability of the alloys was compared on the basis of cross-sectional area measurements: 713C appeared to be similar to U 500, and a lot better than IN-100.

Figure 10-30 shows a cross section of a 713C turbine blade operated in the South Pacific for 600h. Figure 10-31 shows a 713C specimen corroded in the Phillips rig for 5h at 2000°F, 10 ppm salt in the air and 0.0002% S in the fuel. Figure 10-32 shows an electron microprobe of the same specimen.

Increasing the temperature from 1400 to 1600°F (760 to 871°C) decreased metal weight loss significantly, at 0.40 wt % S, but had no significant effect at the two lower sulphur contents. Increasing the temperature from 2000 to 2200°F (1093°C to 1204°C) significantly increased the weight loss at all three levels of sea salt.

Metal weight loss was significantly higher at 10.0 ppm salt than at 0. or 1.0 ppm for the range 1400 - 1600°F. Increasing salt content increased the metal loss in most cases at the higher temperatures.

Metal weight loss was significantly higher at 0.40 than at 0.040 wt % S at both 1400 and 1600°F. Further reduction to 0.0002 wt % S had an effect at 1400°F, but was not significant at 1600°F. At higher temperatures there was no difference between loss at 0.40 and 0.040 wt % S, but both were higher than at 0.0002 wt % S.

The report also studied 713C with a MDC-1 pack aluminised coating - the attack was slight under all conditions.

Figure 10.33 shows the oxidised alloy after 5h at 2200°F, no sea salt, 0.0002 wt % S. Figure 10.34 shows sulphidation of the alloy after 5h at 1400°F, no sea salt, 0.40 at % S. Figure 10.35 shows hot corrosion after 5h at 1600°F, 10 ppm salt, 0.0002 wt % S. Figure 10.36 shows hot corrosion after 5h at 1800°F, 10 ppm salt, 0.0002 wt % S. Figure 10.37 shows hot corrosion after 5h at 2200°F, 10 ppm salt, 0.0002 wt % S.

R. Viswanathan Corrosion 24 (1968) 359.

Westinghouse swirl furnace. No. 2 diesel fuel contaminated with 6% sulphur. Gas passed over platinised ceramic catalyst to give large content of sulphur trioxide. Typical gas analysis 12% CO_2; 3.2% O_2; 1500 ppm SO_2; 150 ppm SO_3; remainder nitrogen. Cylindrical hollow specimens, ½ in OD, 3/8 in ID, and ½ in long. Cleaned specimens coated with salt by dipping into a molten mixture of equal parts sodium and magnesium sulphates. Testing at 1500°F (816°C) for times of 10 - 200h. The corrosion was estimated by metallographic measurements of the thickness of "unaffected metal", the weight loss after descaling was also measured.

713-C lost 0.6 mg/cm^2 after 10h, 242 mg after 150h; similar results on Inco 700, U-700 and Inco 751 suggest the existence of an incubation period. After 150h, 32.2% of the metal was unaffected. 713-C was one of the poorest alloys tested, about the same as Nicrotung, rather better than U-700. Figure 10.38 shows the alloy after 150h: intense localised attack occured. The author remarks that formation of grey sulphide occurs below the outer oxide scale, and at considerable depth in some cases. Preferential oxidation along paths of prior sulphidation.

The effect of two different levels of sulphur trioxide in the gas stream: 6 ppm and 150 ppm. For 713C, the weight losses in 150h test were 4.30 and 242 mg/cm^2 respectively. The author considers that the SO_3 stabilises the sulphate coating.

H. von E. Doering and P.A. Bergman, Naval Ship Research and Development Centre Materials Laboratory Research and Development Report No. 2844, March 1969.

The burner rig facility is described in some detail: fuel is injected through a nozzle, atomised, and burnt in the forward sections of a ceramic flame tube. Sea salt or other soluble contaminants are atomised and injected into the combustion area. The gases and salts are thoroughly mixed by the swirl action of air entering through tangential slots in the combustion tube. The test specimens are mounted in a fixture rotating at 20 rpm downstream of the combustor; they are partly heated by the flame and partly by auxiliary resistance heaters, permitting operation between 1500° and 2100°F (816 and 1149°C). Air/fuel ratios vary from 15/1 (approximately stoichiometric) through at least 60/1. Diesel and high distillate fuels (JP4 and JP5) have been used. Sulphur can be added as ditertiary butyl sulphide. Tests can be run up to 1000h.

The test stand held 8 specimens, ½ in diameter, 3 in long. Sometimes, up to 48 smaller specimens - 1/8 in diameter, 1½ in long - could be tested simulaneously. The specimen fixtures were made of Hastelloy X. Corrosion was evaluated metallographically, determining surface loss and maximum penetration.

Tests were run in this programme on 9 alloys; the designation in the paper are non-standard, but comparison with the nominal compositions tabulated show them to be 713C, Hastelloy X, U-500, IN-100, SEL, SEL-15, SM-200, X40 and L605. Tests at 0.5, 5.0 and 200 ppm sea salt were run, mostly the latter two. The low-salt runs were for 500 and 1000h, the 200 ppm salt tests for 100h. Comparison with corroded sections in practice suggests that the 0.5 ppm salt level is more realistic, giving more oxidation and less sulphidation. The specific ranking of the alloys depended on test conditions, and a summary is shown in Table 10-VIII.

Figure 10.39 shows severe hot corrosion on 713C 1st stage nozzle guide vanes. Figure 10.40 shows a section of the leading edge, and Figure 10.41 shows a detail of the metal/corrosion interface, showing the sulphides. Figure 10.41 shows a 713C specimen tested at 1550°F (844°C) for 1000h with 0.5 ppm sea salt, and Figure 10.42 shows a specimen tested at 1600°F (871°C) for 1000h with 5 ppm sea salt.

In general, the alloys showed no corrosion below a certain temperature, and little above another temperature. For 5 ppm salt, 1000h, the temperature range for hot corrosion was 1525 - 1800°F (the upper temperature is alloy dependent, but no more data are given). For 220 ppm salt, 100h, it is 1625 - 1900°F. The authors consider that the lower temperature would certainly be reduced if the tests were continued for a longer time (implying the existence of an incubation period).

713C is one of the poorer alloys, poorer than SEL but better than IN-100 in the lower salt tests, with the higher salt concentration the alloy was completely destroyed in the test.

H.T. Quigg and R.M. Schirmer, Final Summary Report on NASC Contract N00019-C-67-0275. Phillips Petroleum Company Research Division Report 5058-68R (May 1968).

The report is mainly concerned with coated 713C and Mar-M 200 in the Phillips 2 in combustor at 15 atm and 2000°F (1093°C); 0.4, 0.04 and <0.004 per cent sulphur in the fuel, and 0 and 1.0 ppm sea salt in the air. In addition, tests were done with 0.4% S in JP-5 fuel, 0 and 1.0 ppm salt in the air, and 1.0 or 3.8 ppm V in the fuel.

Figure 10.44 shows a section of a specimen oxidised in salt-free gas at 2000°F for 55h: sulphur content had no particular effect. Figure 10.45 shows a specimen exposed for 25h with 1.0 ppm sea salt in the air. Table 10.IX lists the weight loss in the tests.

Table 10.X lists the weight loss and deposit weight data for the 713C specimens in the vanadium tests. Figure 10.45 shows a cross-section of a 713C specimen after 55h, at 2000°F with 0.017 ppm V in the air. Figure 10.46 shows a specimen after the same time with 0.063 ppm V in the air. Figure 10.47 shows a specimen after 20h at 2000°F with 1.0 ppm sea salt and 0.063 ppm V in the air. Figures 10.48 and 10.49 show the hot corrosion data in graphical form.

The phase relationships for Na_2SO_4, were calculated and compared with the analysis of deposits on Misco MDC-9 coated 713C exposed for 45h at 1400, 1600 and 1800°F (see earlier section). The authors conclude that condensation of sodium sulphate is not a requisite for hot corrosion.

H.T. Quigg and R.M. Schirmer, Proc. of the Eighth Annual National Conference on Environmental Effects of Aircraft and Propulsion Systems (1968?).

Covers essentially the same ground as the previous report,

R. Field, D.J. Fisk and H. von E. Doering, Naval Ship Research and Development Centre. Materials Laboratory Research and Development Report 2833 (January 1969).

The report extends the method of statistical analysis described in the report by Ryan, Kildsig and Hamilton abstracted above to a total of 137 alloys tested in the small burner rig, including 17 commercial nickel-base superalloys. The test temperatures ranged from 1600 to 2125°F (871 - 1163°C), times from 86 to 100h with 200 ppm salt and from 489 to 1100h with 5 ppm salt. A total of 969 tests were examined in the regression analyses. The alloys tested included IN-100, SM-200, 713C, Rene 41, U-500, U-700, SEL. SEL-15, PDRL 163.

V.S. Moore and A.R. Stetson, Final Report On NASC Contract No. N00019-68-C-0532 (Solar Research Division Report RDR 1626-5) (December 1970).

See B 1900 for details. Figure 10.50 shows the microstructure of a specimen exposed for 60h at 1650°F.

Figure 10.51 compares the ranking of the alloys tested: 713C is better than Mar-M-246 but not as good as Rene 41. Table in Appendix II lists the cumulative weight change on the alloys: two specimens of 713C were tested at 1650°F.

weight change:	Specimen 1	+4.9	+6.4	+7.2	+12.8	+12.8	+14.9
mg.	Specimen 2	+8.9	+11.8	+11.6	+18.2	-17.6	-104.7
Exposure time, hours.		10	20	30	40	50	60

Two specimens were tested for 10h at 1800°F: the weight changes were -4.18 and -81.3 mg respectively.

H.T. Quigg and R.M. Schirmer, Progress Report No. 3 on NASC Contract No. N00019-68-C-0252 (Phillips Petroleum Company Research and Development Report 5423-69) July 1969.

This report is concerned with the use of the Phillips Turbine Simulator using a cyclic temperature procedure. The conditions 15 atm. pressure, 1.0 ppm sea salt in the air, 0.04 wt % S in the fuel at nominal exhaust-gas temperatures cycled from 1000° to a maximum of 2000°F (538°-1093°C). The cyclic testing was halted at 11h intervals to allow visual inspection of specimens. The 713C tested in the earlier programme was tested in this, together with the alloys of the ASTM Round Robin programme. After exposure the specimens were weighted with the scale and deposit in place, then electrocleaned and weighed again, the difference being the "deposit weight" expressed as per unit area.

The data for the ASTM alloys are shown in Table 10.XI and Table 10.XII shows a listing for the 713C tested in the earlier programme. The data are subjected to statistical analysis, and a "time to produce a weight loss of 127 mg/cm^2" calculated:

Superalloy	Source	Exposure time for 127 mg/cm^2, hours.
IN-100	ASTM	11
U-700	ASTM	35
713C	ASTM	37
Mar M421	ASTM	42
IN-738	ASTM	55
U-500	ASTM	81
713C	Misco	48

Figure 10.52 shows the weight loss of bare and coated 713C as a function of time, and Figure 10.53 shows the same for all the ASTM alloys.

Table 10.XIII shows the penetration data for the ASTM alloys,

This test was approximately six times more severe than that in the earlier tests.

Figure 10.54 shows the attack of the ASTM alloys after 44h 2000°F cyclic test, Figure 10.55 shows the attack for a 713C specimen in a similar test, and Figure 10.56 shows a detail of the interface on the same specimen.

The cycle time was 8 min at 1600, 1800, and 2000°F, 2 min at 1000°F.

In a 44h test with a maximum gas temperature of 2000°F (1093°C) the weight loss of 713C was 200 mg/cm^2, the surface loss 31 mils and the maximum attack 32 mils. This was significantly worse than U-700, but much better than IN-100.

ASTM Round Robin Test organized by the Hot Corrosion Task Force of the Gas Turbine Panel, 1970.

A group of six alloys (713C, IN-100, U-700, Mar-M 421, IN-738, and U-500) were tested by 15 participants. Table 10-XIV lists the participants' test conditions. Table 10-XV shows the ranking of the alloys by the participants - 713C was one of the worst two in everybody's test, the other usually being IN-100. Table 10-XVI shows the attack in 100h tests at 1650F - for 713C the mean surface loss was 41.0 mils, the median 31.0 mils; the mean maximum attack is 53.1 mils, the median 41.3 mils. Figure 10-57 shows the loss in diameter for 713C reported by the various participants.

H.T. Quigg, R.M. Schirmer and L. Baguetto, Final Report on NASC Contract No. N00019-60-C-0221 (Phillips Petroleum Company Research and Development Report 5732-70) July 1970.

This is an extension of the earlier studies to determine whether a further lowering of the sulphur content of the fuel to 0.0004 wt % would reduce hot corrosion. Again the Phillips Turbine Simulator was used, operating at 15 atm pressure with the gas temperature and velocity at the test specimens cycled from 1000 - 2000°F (538 - 1093°C) and 163 - 275 ft/ sec by control of the fuel flow. Sea salt was added to the inlet air at a concentration of 1 ppm. On the basis of visual ratings made at the end of each 5h period, specimens were removed from test after exposures of 5 - 165 h.

After it was removed from the specimen holder after exposure each specimen was weighed. A sample of surface scale was removed by scraping with a spatula, and the specimen was then electrocleaned. The difference between the weight after test and the weight after electrocleaning was recorded as the weight of surface scale. Table 10-XVII shows the results: Test 1 is with 0.040 wt % S inthe fuel, Test 2 with 0.0004 wt % S. For uncoated 713C after 10h there seems little difference. The Table also lists the weight loss data for all the experiments. With 0.0004% S in the fuel 713C, U-700, U-710 and IN-738 are fairly similar; with 0.040% S 713C is very much worse than the other three.

P.A. Bergman, C.T. Sims and A.N. Beltran, in "Hot Corrosion Problems Associated with Gas Turbines" ASTM Special Technical Publication STP 421 (1967) 38.

This paper describes work designed to develop a nickel-base alloy for turbine blade application at 1600F (871°C) with the strength and reliability of 713 and a cobalt-base alloy for vane service at 1900°F (1038°C) with mechanical properties equivalent to WI-52. These alloys had to be capable of 5000h in a 1% S in diesel fuel combusted with air containing 1 ppm by weight sea salt. The alloys were tested in a small burner rig. They included a number of experimental alloys, and the commercial alloys WI-52, SM-302, X-45, SEL, Inco 713, SM-200, U-700, U-500 and Hastelloy X for comparison. The evaluation of the corrosion was by metallographic measurement of the surface loss and the maximum penetration. The rig burnt a diesel fuel containing 1% S, and added 200 ppm sea salt to the air. All tests were run for 100h. 713C was used in all tests as an example of an alloy with poor hot-corrosion resistance: SEL was included as an example of mid-range hot-corrosion resistance.

At 1750°F (955°C) 4 tests of 713C produced a range of maximum penetration of 34 to 49 mils. Figure 10-58 compares the hot-corrosion of the commercial alloys on a bar-diagram. 713C seems the worst of the nickel-base alloys at 1600°F (871°C), but is better than SEL, SM-200 and U-700 at 1750°F (955°C).

M.J. Donachie, Jr., R.A. Sprague, R.N. Russell, K.G. Boll and E.F. Bradley, Hot Corrosion Problems Associated with Gas Turbines, ASTM Special Technical Publication STP 421, 1967, 85.

This paper reports investigations using the Pratt and Whitney burner test rig using (a) a marine diesel oil with 1% S or (b) JP-5R fuel with 0.4% S. Sea salt was injected in to the combustion gases, at a level of 3.5, 7 or 35 ppm. The test temperatures were 1450, 1650 and 2000F (788, 899 and 1093°C) and the test durations were 50 or 100h. The specimens were wedge-shaped, to simulate an airfoil section, and were rotated in the gas stream. The specimens were removed and weighed every 20h or so. At the end of the test they were descaled and the metal loss measured. Metallographic examination of transverse section was performed. In addition, some early crucible tests are described.

Figure 10.59 shows a section through a 713 blade from a turbo prop engine showing light-grey Cr_2S_3 (?) phase ahead of the oxidation front. Figure 10.6o shows a section of a specimen tested in a 90/10 Na_2SO_4 /NaCl mixture in a crucible test at 1650°F (899°C).

Table 10-XVIII lists the test conditions used in the burner rig. For 713C, they were (a) JP-5R; 0.4% S; 3.5 ppm salt, 1650°F (899°C); 100h. (b) Marine diesel; 1.0% S; 3.5 ppm salt; 1650F; 50h. (c) Marine diesel; 1%S; 7 ppm salt; 1650F; 50h (d) Marine diesel; 1%S; 35 ppm salt; 1650F; 50h; and (e) Marine diesel; 1%S; 35 ppm salt; 2000°F (1093°C); 50h.

The weight change data are listed in Tables 10-XIX a, b, and c; Table 10-XIX d also shows the thickness change. Figure 10-61 compares the weight loss of 713C, Mar-M 302 and AMS 5382 (X-40) on a bar diagram. 713 is very similar to Mar-M 302 at both 1650 and 2000F. (no salt concentrations, fuel type or times given for this diagram). Figure 10.62 shows the effect of salt concentration on the attack of 713, U-700, Mar-M 302 and X-40 (no temperature or fuel quoted) - the nickel-base alloys are much more susceptible to salt concentration than the cobalt-base.

Figure 10.63 shows the weight change of U-700, Waspalloy, IN-100, and 713, as a function of time at 1650°F with JP-5R fuel and 3.5 ppm salt. 713 seems about the same as cast U-700, much better than IN-100. Wrought U-700 and Waspalloy were much better.

Figure 10.64 shows a section of a 713 specimen after 26h at 1800°F (982°C) in burner rig (no fuel type, salt concentration given).

Figure 10.65 shows the difference between 50h with 35 ppm salt and 500h with 3.5 ppm salt tests at 1650°F using 1% S diesel fuel. The longer test is more severe for all the alloys tested (713, U-700, Mar-M 302 and X-40) but whereas the nickel alloys appear about the same as each other and much worse than the cobalt-base alloys after the shorter test, after the longer one U-700 is about the same as the cobalt-base alloys and 713 is very considerably worse. Fig. 10.66 shows the variation of the weight change with time in these tests.

L.D. Graham, J.D. Gadd and R.J. Quigg, Hot Corrosion Problems Associated with Gas Turbines, ASTM Special Technical Publication STP 421, 1967, 105.

Eleven commercial alloys - 713C, Inconel 700, IN-100, Waspalloy, U-700, PDRL 163, Mar-M 200, B 1900, TRW 1900, WI-52, and Mar-M 302 were tested in a crucible test: 99% Na_2SO_4, 1% NaCl in a 30mil silica crucible. 1600, 1700, 1800, 1900 and 2000°F (871, 927, 982, 1038, and 1093°C); 1, 2, 5 and 25h. After corrosion, scale removed by cathodic descaling, corrosion reported as weight loss. Some specimens examined metallographically without descaling. Scale mechanically removed from some alloys and examined by X-ray diffraction.

Figure 10.67 compares the results for an 1800°F crucible test with the Pratt and Whitney burner rig at 1650°F (899°C) for five of the alloys- B 1900, 713C, PDRL 163, U-700 and Inconel 700 showing a reasonable correlation. Figure 10.68 ranks the alloys in terms of the 1800°F, 1h crucible test. Mar-M 302, TRW 1900, B 1900, and Mar-M 200 are together very bad, losing about 2g. 713C, IN-100 (coarse grain) and PDRL 163 are next, losing 0.3g. IN-100 (fine grain) is rather better, losing less than 0.2g. U-700 and WI-52 are quite good, losing about 0.1g, and Waspalloy and Inconel 700 are the best, losing less than 0.01g. (This order is really a little suspect, in view of later information).

Attack increased with temperature for 713C in the range 1600 - 1800°F, but diminished at 2000°F.

R.S. Bartocci, Hot Corrosion Problems Associated with Gas Turbines, ASTM Special Technical Publication STP 421, 1967, 169.

Figure 10.69 shows the corrosion of a 713C nozzle diaphragm which operated in a marine environment for only 250h. The paper is principally concerned with hot corrosion testing of coated alloys, but some results are presented for uncoated alloys. The GE small burner rig was used, burning JP fuel. The air/fuel ratio was 40/1. Salt was injected at 100ppm of the air. The corrosion was evaluated in terms of weight change. Figure 10.70 shows the results: at 1675, 1800 and 1875 (913, 982 and 1024°C) the specimens gained weight rapidly, "erupting" (meaning not defined) after 14h or less. At 2000°F (1093°C) the specimen lost weight continuously.

P.E. Hamilton, K.H. Ryan and E.S. Nichols, Hot Corrosion Problems Associated with Gas Turbines, ASTM Special Technical Publication, STP 421, 1967, 188.

Remark that Allison Division of General Motors have observed distress from hot corrosion on several nickel bearing materials operating in a variety of environmental parameters, but the most extensive experience has been with 713C turbine blades in the following types of service :

(a) Aircraft engines using JP-4 and JP-5 fuel both inland and sea coastal service.
(b) Stationary engines using natural gas fuel, inland locations.
(c) Engines in Indianapolis test stands using JP-4 fuel with no intentional sulphur contamination.

Figure 10.71 shows a "typically appearing" turbine blade which has undergone hot corrosion attack: there is heavy corrosion on the concave surface with grey globular sulphide particles in the metal ahead of the oxidation front. Figure 10.72 shows the transverse cross section of six turbine blades operated in the same engine for 2700h. Two show severe distress, while the others show only minor effects of attack. Figure 10.73 shows a group of blades which operated almost entirely over the ocean using air fields at sea-coast locations. "Marine atmosphere exposure appears to drastically accelerate the sulphidation attack as is indicated by these parts shown at first teardown, with considerably less service than the blades in Figs. 10.71 and 10.72".

To date, the authors had seen isolated cases of hot corrosion of Waspalloy, Inco 901, A 286 and 16-25-6 materials after long time service as turbine wheel or spacer components which should normally operate at temperatures below 1400F (760°C).

Electron microprobe traces of a corroded 713C surface, demonstrated that the sulphides were chromium-rich.

20 blades showing gross oxidation and 20 showing only slight oxidation were taken from a single rotor. There was a better correlation of the attack with the (chromium and aluminium) content than with chromium content along.

Three tests were used: some specimens were run in the Phillips Turbine Environmental Simulator at 1500 and 2000°F (816 and 1093°C); 0.0002% and 0.40% S in the fuel; 10 ppm sea salt added to the inlet air. First stage turbine blades were used as specimens. A second test was an engine test, using a T56 turboprop test stand engine modified to inject synthetic sea water through the fuel nozzle, while burning JP-5 fuel. The salt content was 0.75 ppm of the air. 30 cycles each of 30 min at a turbine inlet temperature of 1780°F (971°C) were used. Micro-structural examination of a bare 713C blade after 30 cycles of testing in the test engine indicates this corrosion is identical to that observed on the turbine blades returned from flight service. Figure 10.74 shows four alloys (Inco 717, 713C, TRW 1900, and SM 200) subjected to a test at 1880F (1027°C) with 15 ppm salt injection: this test was regarded as untypically severe. The third test was a modified thermal fatigue apparatus. A cycle consisted of heating 8 rotating (1800 rpm) standard turbine blade test specimens in the furnace area to 1750°F (955°C) in 1.5 min by means of a city gas-air burner, at which time the entire rotating unit was retracted into a cooling chamber where it was sprayed with a sodium sulphate or sodium chloride - deionized water solution, or both, for 0.5 min. A complete test consisted of 500 cycles. Again, the microstructural characteristics of the corrosion produced in the laboratory rig were very similar to the hot corrosion in service engines. The corrosion was assessed by

determining the weight loss after descaling.

Figure 10.75 compares the performance of five alloys, four in a stationary engine using natural gas fuel at an inland location, 2000h service (Inco 717, TRW 1900, Mar-M 200 and 713C) and two in a test-stand engine, JP-5 fuel, 570h service (713C and B 1900). In addition, the relative performance of the same five alloys together with IN-100 in the test stand engine with salt injection is shown.

Figure 10.76 compares the performance of four alloys in the cyclic salt spray test: 713C was the worst, PDRL 163 next, then MAR-M 211M and best of all PDRL 163 with 10% cobalt.

W.L. Wheatfall, H. Doering and G.J. Danek, Jr. Hot Corrosion Problems Associated with Gas Turbines, ASTM Special Technical Publication STP 421, 1967, 206.

The effect of molten salts - Na_2SO_4, NaCl and mixtures - on the behaviour at 1650F (899°C) of two superalloys, AMS 5391A, which appers to be 713LC, and AMS 5384, which appears to be U-500. One series of tests used an electrochemical technique measuring the electrode potential of the alloy in the molten salt versus a platinum electrode, with either still air or argon atmospheres. In addition, oxidation experiments for times up to 250h in air were conducted.

Table 10-XX shows the results, and Figure 10.77 shows a potential/time curve for 713LC.

F.J. Wall and S.T. Michael, Hot Corrosion Problems Associated with Gas Turbines ASTM Special Technical Publication STP 421, 1967, 223.

This paper is concerned with corrosion in industrial turbines burning natural gas: it is noted that corrosion was first observed in a 1350F (732°C) inlet gas temperature turbine located in Japan. The rotating blade alloy was a nickel-base precipitation hardening alloy containing about 15 per cent chromium (U-700?). The natural gas contained an abnormally high amount of hydrogen sulphide (10-13%) and the turbine was located near the sea coast. The next sign of corrosion attack when burning natural gas occurred in a 1450°F inlet gas temperature turbine located in a Canadian prairie. The attack occurred on first stage stationary vanes made of a nickel-base, precipitation hardened alloy containing about 13% Cr (713C?). However, in this case the level of hydrogen sulphide was so low that it could not be detected by chromatographic or mass spectrometric techniques. Isolated attack on stationary diaphragms with vanes of the same alloy was observed under various conditions ranging from burning distillate oils to low level hydrogen sulphide natural gas and from atmospheres associated with isolated sea coasts to those associated with highly industrialised areas. Figure 10.78 shows an example.

An apparatus was constructed which allowed a controlled atmosphere to be passed over specimens in a furnace. The atmosphere was selected to simulate the combustion of a natural gas containing 10% H_2S. The gas composition was typically 77.7% nitrogen, 16.7% oxygen, 2.13% carbon dioxide, 3.33% water, and 0.14% sulphur dioxide. Samples of Ni-13 Cr-6 Al (a model of 713C) and Ni-15 Cr-1Al (a model of no very obvious alloy) were exposed to the gas at 1450°F for 100h with no visual signs of attack. Subsequent analysis of turbine operating experience indicated that corrosion was most likely associated with ash deposit, so specimens were coated with various salt mixtures. A representative deposit, of 50% Na_2SO_4 + 50% $MgSO_4$ was selected: this is a eutectic mixture with a melting point of about 1250°F (677°C). A standard test consisted of coating specimens with this mixture and exposing them to the simulated combustion gas for 100h at 1450°F. Specimens of 25 commercially available alloys were tested: these are listed in terms of major constituents, but are not named. Identification is not absolutely certain; but included are X-40, WI-52, Hastelloy X, S 816, Waspaloy, U-500, U-700, Nicrotung, 713C, and Mar-M 200, in decreasing order of corrosion resistance.

Corrosion rate tests were performed at 1250, 1350 and 1450°F (677, 732 and 786°C) corroded for various times. Four nickel-base alloys (apparently 713C, Inconel 700, U-500, and Ra 333), a cobalt-base alloy (apparently X-40) and an iron-base alloy (a 20 Ni 25 Cr steel) were included in these tests. Figure 10.79 shows the results for 713C(?). The amount of sulphur in the gas stream played a minor part in the corrosion.

Overall analysis suggested that there is an "incubation time" at each temperature during which attack is negligible. The length depends on temperature and alloy composition. For example, at 1450°F, alloys with 25% Cr exhibit an incubation period in excess of 1000h.

Specimens of 713C(?) and U-500(?) were subject to electron probe microanalysis. Figure 10.80 shows the result for 713C exposed for 90h at 1450°F. The internal sulphides had the $FeCr_2S_4$ crystal structure, and contained Cr, Al, Ti, Mo and S.

Many of the alloys were attacked at 1250°F, and even at 1750F, but were resistant at 1450°F.

R.M. Schirmer and H.T. Quigg, Hot Corrosion Problems Associated with Gas Turbines, ASTM Special Technical Publication STP 421, 1967, 270.

This paper is based on the reports abstracted above. Figure 10.81 shows 713C turbine blades from a U.S. Navy aircraft turbine, and Figure 10.82 shows a section of the metal/scale interface on one of the same blades. Tests are reported in the Phillips Environmental Simulator at 1400, 1600, 1800, 2000 and 2200F (760, 871, 982, 1093 and 1204°C); JP-5 fuel with 0.0002, 0.040 and 0.40% S; 0, 1.0 and 10.0 ppm sea salt in the air. The alloys tested were 713C, uncoated and with an MDC-1 pack aluminised coating, IN-100, SM-200, U-500 and WI-52. Weight loss data is presented in Table 10-XXI. The relative durability of the alloys was compared: coated 713C was best, followed by U-500: 713C was only a little worse. The remaining alloys were quite significantly worse.

In discussion, the authors quote experiments at 2000°F using the very low sulphur fuel, and injecting (a) 15 ppm sea salt, (b) 9 ppm sodium or (c) no salt. The weight losses were 0.2% with no salt, 8.7% with sea salt, and 14.2% with NaCl (see also SM-200, which shows that NaOH is even worse).

S.Y. Lee and W.E. Young, in Combustion and Heat Transfer in Gas Turbine Systems, Cranfield Symposium No. 11, E.R. Norster (ed) (Pergamon, Oxford 1971) 253.

Describes a simple small burner test involving specimens mounted on a table rotated at 2000 rpm: this was heated in a furnace for 1h, then withdrawn and cooled by a 2 min air blast. The holder accommodated 24 ¼ in diameter pins. A standard test run was 1000 cycles with frequent removal of the specimens for weighing. In addition, a high-pressure rig designed around an actual gas turbine combustor is described. It simulates the pressure, temperature, gas velocity and flow as found in a turbine, and will handle a wide variety of fuels with and without contaminants.

Corrosion was evaluated by descaling, measuring the weight loss and determining the surface roughness using a modified Brush surface analyser.

The first series of tests in the high-pressure rig were 50h duration, doing a 7h day using normal start-up and shut down cycling. Gas stream velocity at the test section was 500 ft/sec. Natural gas or diesel oil (Gulf Dieselect) was used. Sulphur was introduced by mixing the appropriate amount of ditertiary butyl disulphide in the diesel oil. Contaminants could be added either into the fuel or the air: in the latter case a water solution of NaCl and $MgCl_2$ was sprayed directly into the air stream just ahead of the combustor. Table 10-XXII lists the test conditions.

Table 10-XXIII summarises the deposits and corrosion products on the specimen surface. Table 10-XXIV lists the weight loss (after descaling) data.

It appeared that the presence of an extremely small amount of sodium (less than 0.5 ppm in the fuel) was enough to form sodium sulphate and to form a deposit on the specimen surface. However, when natural gas which contains no sulphur was used (in test 10) no evidence of sulphidation was found on the specimen although other contaminants such as particular sulphates of sodium and magnesium could be present in the atmospheric air and ingested through the compressor intake.

Figure 10.83 shows the effect of pressure on the oxidation rate of four alloys in a 150h test at 1800°F (982°C): at 1 atm pressure the oxidation of X-45, IN-738X, U-500 and 713C is roughly the same, with 713C the best, and X-45 next. At 3 atm pressure, 713C is still the best, but the other three are quite a bit worse, and X-45 is the worst of all.

S.Y. Lee, S.M. DeCorso and W.E. Young, J. Engineering for Power (Trans ASME) July 1971, 313.

Paper is mainly concerned with a comparison of U-500 and X-45, but one or two graphs include data for 713C. See U-500 for details.

H.T. Quigg, R.M. Schirmer and L. Bagnetto, Final Report to Naval Air Systems Command on Contract N00019-70-C-0293 (Phillips Petroleum Company Research and Development Report 5903-71) January 1971.

An extension of the earlier studies, using the Phillips Turbine Simulator, to determine the effect of fuel sulphur on the corrosion of turbine blade materials. This part was aimed at discovering if there is a "threshold" level of sulphur below which there is no corrosion. Specimens were cycled from 2000 to 1000°F (1093 to 538°C) with gas velocities from 275 to 163 ft/sec at a presssure of 15 atm. Sea water was added at a concentration equivalent to 1 ppm sea salt in the inlet air. 13 different superalloys (713C, B1900, Mar-M 246, Mar-M 200, IN-100, U-700, IN-738, U-710, WI-52, Mar-M 509, Mar-M 302, X-40 and AiResist 215) and 20 different superalloy/coating combinations were exposed from 5 to 165 h using a fuel containing 0.0040 wt % S in an experiment designed to allow comparison with the earlier tests using fuels containing 0.040 and 0.0004 wt. % S.

Table 10-XXV shows the weight of surface scale the weight loss after descaling, and the visual estimation of the attack, for all the specimens, and includes the data for 0.0004 and 0.04% S from the earlier tests. Table 10-XXVI shows the X-ray diffraction analysis of the scale products. Interestingly, Na_2SO_4 was only occasionally identified. The principal products for all the alloys were monoxides and spinels. Sodium sulphate was also analysed by wet chemical methods on powdered scale from three tests: the sample represented all the scale from all exposed test specimens at a particular sulphur level. Soluble sodium and sulphate were present in all cases, and the amount increased with increasing sulphur content. At the lowest sulphur content, there was five times as much sodium present as is required to tie up the sulphur, so presumably other sodium salts were present. At the highest sulphur content, most of the sodium will have been present as sodium sulphate.

The visual appearance of the cleaned specimens followed the following general principles:

(i) The low-chromium superalloys (B1900, Mar-M 246, Mar-M 200, and IN 100) appeared smooth and bright.

(ii) The high chromium nickel-base superalloys (U-710 and IN-738) and the cobalt-base superalloys (WI-52, Mar-M 509, Mar-M 302 and X-40) have porous and dirty surfaces.

Figure 10.84 (a) presents the effect of sulphur content of the fuel on hot corrosion for four uncoated superalloys including 713C, which is noticeably worse than the others (U-700, U-710, IN1738) at the highest sulphur content; little difference between them all at lower sulphate contents.

Figure 10.84 (b) presents similar data for the remaining four superalloys which all corrode at approximately the same rate: the data are plotted for four different times.

E. Erdös in "Deposition and Corrosion in Gas Turbines", A.B. Hart and A.J.B. Cutler (eds.) (Applied Science Publishers, London 1973) 115.

This paper describes experiments to determine the composition and crystallographic structure of sulphides formed in the process of sulphidation of several nickel-base alloys: Nimonic 75, Nimonic 80A, Nimonic 90, Nimonic 105, IN-738 and 713LC. Samples were heated in an evacuated quartz capsule containing either elemental sulphur, or Ni_3S_2. In the case of 713LC specimens were also studied after corrosion in a gas turbine burning natural gas, after corrosion in a pilot plant, and corroded in a molten mixture of sulphates. The sulphides were determined using a powder X-ray diffraction technique; metallography using the zinc selenide interference technique was also helpful in identifying particular products. The sulphide phases, their colour with ZnSe, their shape and their location on the corrosion layers are listed.

In some cases a stratified sulphide scale was found (see Nimonic 90) with an outer layer composed of NiS + $(Co,Ni)_3S_4$, or sometimes Ni_3S_2 + $(Co,Ni)_9S_8$; a middle layer of Cr_3S_4 and Cr-Al-S with enhanced nickel and cobalt; and an adherent inner layer of Cr_3S_4. This sort of arrangement was found with Nimonic 90, Nimonic 105, IN-738, and 713LC. In other cases evidence of liquid sulphide phases was found (see IN-738). Table 10-XXVII shows quantitative electron-probe microanalysis of sulphides in situ for Nimonic 80A, Nimonic 105, and 713LC.

The author comments that the stratified scale-type is hardly encountered while the molten sulphide type is not infrequent, and the crystallising of $NiCr_2S_4$ in a matrix of Ni_3S_2 has also been observed (E. Erdös, P. Brezina and R. Scheidegger, Werkstoffe u. Korrosion, 22 (1971) 148).

With sulphidation over Ni_3S_2 in vacuum the same morphology was generally obtained as in hot corrosion. Figure 10.85 shows the internal sulphides formed in 713LC after 168h at 800°C over Ni_3S_2 in vacuum. Figure 10.86 shows the sulphides in a vane from a gas turbine burning natural gas with 2 - 4% H_2S with Ca and Na impurities in the air, 1 year at 700 - 750°C. Figure 10.87 shows a specimen corroded for 300h at 850°C in a pilot plant burning gas oil containing 0.4% S, 15 ppm Na and 5 ppm V. Figure 10.88 shows a specimen corroded for 112h at 800°C in a molten salt mixture consisting of 53 mole % Na_2SO_4, 40 mole % $MgSO_4$ and 7 mole % $CaSO_4$. The formation of sulphides was basically the same with all the environments. Only the frequency of the Cr-Al-S phase varies considerably. This phase was observed after sulphidation with elemental sulphur in all the aluminium bearing alloys. After sulphidation over Ni_3S_2 it was found "markedly" in 713LC at 800°C; traces were found in IN 738 at 850°C; at 900°C only faint traces were visible in 713LC. The phase has been observed sporadically in actual hot corrosion of gas turbine 713LC vanes, often in the neighbourhood of precipitates of Ni_3S_2 (see Fig. 10.86). It was also formed in 713LC corroded at 800°C in the sulphate mixture. MX_2 phase was extracted from 713LC sulphidised over Ni_3S_2 for 96h at 800°C, and crystallographic data for this phase is listed. This phase was also detected in actual hot corrosion.

A final section of the paper describes the oxidation of 713LC after presulphidation. Figure 10.89 shows the oxidation of 713LC in oxygen at 1 atm pressure at 900°C for up to 24h as cast, and sulphidised by one of the following treatments: 0.23 mg/cm² S, 16h at 900°C; 6.0 mg/cm² S sulphidised over Ni_3S_2 in vacuum for 96h at 900°C; and 5.3 mg/cm² S sulphidised over Ni_3S_2 in vacuum for 96h at 800°C. The first treatment produced little acceleration, but the latter two produced a large increase. Figure 10.90 shows the same curves extended to 190h. Table 10-XXVIII lists the phases identified. Figure 10.91 shows oxidation at 800°C for times up to 24h for specimens presulphidised over Ni_3S_2 in vacuum for 96h at 800 and 900°C to produce 6.2 and 6.8 mg/cm² respectively. As at the higher oxidation temperature, the lower temperature sulphidation produced the greater acceleration. The higher temperature sulphidation seemed to result in a short "incubation period" after which the rate accelerated.

While the sulphide formation in hot corrosion could be reproduced by presulphidation and oxidation there was a difference in the oxide scale obtained. Hot corroded samples of 713LC contained a spinel phase with a_o = 8.19Å, whereas in sulphidised/oxidised samples the spinel had a_o = 8.31Å. However, pretreatment of 713LC with a 0.14 N aqueous solution of Na_2SO_4 or Na_2CO_3 prior to oxidation for 24h at 900°C produced exactly the same spinel as in hot corrosion or in rig tests.

P.L. Norman and J.D. Marston, in "Deposition and Corrosion in Gas Turbines" A.B. Hart and A.J.B. Cutler (eds.) (Applied Science Publishers, London, 1973) 260.

See Nimonic 80A for details. The hot corrosion behaviour of a number of nickel-base superalloys was examined in a salt-spray test at 800°C, using 75% Na_2SO_4, 25% NaCl spray. 713C was much the worst of the alloys tested.

C.J. Spengler, S.Y. Lee and W.E. Young, in "Deposition and Corrosion in Gas Turbines" A.B. Hart and A.J.B. Cutler (eds.) (Applied Science Publishers, London 1973) 294.

See U500 for details. Several experiments include results for 713C, mostly reported in earlier papers from Westinghouse group (see above).

P.C. Felix, in "Deposition and Corrosion in Gas Turbines" A.B. Hart and A.J.B. Cutler (eds.) (Applied Science Publishers, London 1973) 331.

This paper describes the use of a simulator rig test to determine the corrosion resistance of several alloys.

The rig burnt extra light fuel oil at atmospheric pressure in the temperature range 700 - 1000°C. The fuel contained 0.40% S; 15 ppm sodium and 5ppm vanadium were added. Corrosion was evaluated by metallographic determination of the unaffected metal. The standard test was for 300h at 850°C. Figure 10.92 shows the corrosion behaviour: in order of increasing corrosion resistance the alloys were 713LC, EPD 16, Mar-M 246, Nimonic 105, Mar-M 421, IN-738, Mar-M 432, Nimonic 80A, IN 587 and IN 597, and finally Nimonic 90. The corrosion is then correlated with chromium content (Figure 10.93), aluminium content (Figure 10.94), Al/Cr ratio (Figure 10.95), titanium content (Figure 10.96) Al/Ti ratio (Figure 10.97) and Al/Ti Cr^3 (Figure 10.98). Generally 713LC performs much worse than would be expected in terms of the other alloys.

Table 10-XXIX shows the corrosion rates of six of the alloys (Nimonic 80A, Nimonic 105, 713LC, IN-738, Mar-M 421 and Mar-M 246) at 750, 850 and 950°C. The data are plotted as log corrosion rate versus the reciprocal of temperature in Figures 10.99 and 10.100. Figure 10.101 shows the corrosion rate as a function of chromium content at the three temperatures, and Figure 10.102 shows the rate as a function of Al/Ti Cr^3 for all three temperatures.

Specimens of 713LC from the test rig and from operating turbines were compared using microprobe analysis and X-ray investigations. The turbine operated at 710°-740°C, 7 atm, natural gas 2.8% H_2S for 8800h, the air containing desert dust with sodium salts. Figure 10.103 shows the test sample (dark means high concentrations) and Figure 10.104 shows the corroded vane material. There are some similarities, but some noticeable differences.

K.H. Ryan, Technical Report to Air Force Materials Laboratory, Wright Patterson Air Force Base, AFML-TR-71-173 (Detroit Diesel Allison, Division of General Motors) Vols. 1 and 2 (Jan. 1972).

This report is concerned with the evaluation of coated alloys - 713, IN 100, IN 738, U 700, U 710, Mar-M 246, AF2N, VIA, X-40, WI 52. There are no data for the uncoated alloys.

W.L. Wheatfall in "High Temperature Corrosion of Aerospace Alloys". J. Stringer, R.I. Jaffee and T.F. Kearns (eds.) AGARD Conference Proceedings No. 120, (April 1972) 235.

Table 10-XXX shows the results of hot-corrosion burner rig tests on commercial nickel and cobalt superalloys, taken from P.A. Bergman et al. "Development of Hot-Corrosion Resistant Alloys for Marine Gas Turbine Service" NEL-Sponsored Report 2437, Final Report under Contract N600 (61533) 65661 with the General Electric Co. Oct. 1967. The alloys were SEL, 713C, SEL 15, IN 100, Mar-M 200, U 500, U 700, Rene 41, Hastelloy X, X-40, Mar-M 302, Mar-M 509, WI-52 and L-605. The tests were presumably in the GE small burner rig, and used 5 ppm sea salt in the air with 9 - 18 thermal cycles. Figures 10-105 and 10-106 present the same data as bar graphs: the second shows the corrosion of the nickel-base alloys as a function of chromium content.

H. Huff and F. Schreiber, Werkstoffe and Korrosion 5 (1972) 370.

This paper describes the hot corrosion of 713C (called 713V), Mar-M 246, and Nimonic 90 in a simulator rig. The combustion gas contained 6% CO_2 and 11% O_2, and the gas velocity at the specimens was 250 m/s. Between 0 and 30 ppm synthetic sea salt were added to the hot gases. The specimens could be stressed at the same time, and stresses between 80 and 350 N/mm^2.

Figure 10.107 shows the influence of corrosion on the time to rupture at stresses in the range 10 - 25 kp/mm^2 of 713C at 900°C. Combustion gases reduce the strength compared to air, but a larger reduction, particularly at the lower stress levels, is produced by the addition of sea salt to the atmosphere. Figure 10.108 shows the influence of salt concentration, in the range 0.085 - 36 ppm, on the time to failure at a stress of 140 N/mm^2. Figure 10-109 shows the variation in the time to rupture at a stress of 140 N/mm^2 in air, combustion gases, and combustion gases with 31 ppm salt. Figure 10-110 shows the creep strain versus time of 713C at a stress of 140 N/mm^2 at 900°C in air, and in combustion gases with 0.085, 0.85 and 31 ppm.

The corrosion was estimated in terms of the general loss of metal and the maximum local penetration, expressed as a rate by dividing by the exposure time. Figure 10-111 shows the corrosion of 713C as a function of the applied stress: as one might expect, at high stresses, the local corrosion rate increases markedly.

The 100h rupture strength at 900°C was 270 N/mm^2 in air, 210 N/mm^2 in combustion gases without salt, and 140 N/mm^2 with 30 ppm sea salt.

S.Y. Lee, W.E. Young and C.E. Hussey, J. Eng. for Power (Trans. ASME) 1972, 149.

This paper describes the use of the Westinghouse facility. All the figures have appeared in papers summarised above.

L.M. Maas and C.L. Miller, ASME Paper 72-GT-77, presented at the Gas Turbine and Fluid Engineering Conference and Products Show, March 1972.

The paper describes a 3000h durability test of a modified Allison Model 501-K 15 engine operating on Navy distillate fuel, with salt water ingestion. Preliminary selection involved an accelerated test with a non-air cooled 501-K14 engine with 0.75 ppm salt in the air. During the first 2000h of the test the fuel was No. 2 diesel fuel with 0.45% S. During this period the engine was not air cooled, and the first stage vanes were X-40, the first stage blades Alpak coated 713, and the nominal turbine inlet temperature was 1660°F (905°C). Sulphidation was evident on ten blades following 1000h operation. Testing of the air-cooled 501-K15 engine was then initiated using No. 2 diesel fuel. The air cooled first stage blades were Alpak coated 713, IN 738, U 710 and Mar M 246. After 1012 h testing the Alpak/IN 738 were in excellent shape with no evidence of corrosion. The Alpak/Mar-M 246 were in good condition except for isolated areas where the coating was too thin. The Alpak/U 710 blades exhibited some regions of surface corrosion. The Alpak/713 blades were in the least desirable condition, with hot corrosion evident along the leading and trailing edges. Alpak coated first stage vanes of 713, IN 738 and U 710 were tested during the same 1012h. Again, IN 738 was superior to the others: the Alpak/713 segments suffered severe blistering.

At the start of the evaluation using Navy distillate fuel, first stage blades of Alpak/IN 738 and first stage vanes of Alpak/X-40 were incorporated. After 1000h testing, both were in good condition, although Alpak/713 second stage vanes were severely corroded. Hot corrosion had proceeded to the point that the leading edges had split. It is likely, according to the authors, that the coating was degraded by combustor carbon erosion and corrosion. In the next stage of the test these vanes were replaced by Alpak/X-40 segments, which were in good condition after a further 568h testing.

The test schedule consisted of 21h cycles with a 3h shutdown period. During each down period, three starts were accomplished, the third being the start of the next 21h operating cycle. The test cycle is presented in Table 10-XXXI. Table 10-XXXII shows the salt concentration and droplet size.

Prior to cleaning, all four stages of turbine blades had heavy deposits on the airfoils. A spectrographic qualitative analysis was conducted on deposit samples. A major portion consisted of sulphates of the alloying metals from each blades component (Ni, Mn, Cr, Co, Mo and W).

I.I. Bessen and R.E. Fryxell, General Electric Technical Information Report R72AEG317, (Nov. 1972); paper presented at the Gas Turbine Materials Conference, Naval Ship Engineering Center, Oct. 1972.

See Rene 80 for details.

V.S. Moore and A.R. Stetson, Final Report to Naval Air Propulsion Test Center on Contract N00156-71-C-1020, July 1973.

The report is principally concerned with the development and application of aluminide coatings to nickel-base superalloys, but a limited amount of information on uncoated specimens is quoted. The alloys studied were B1900, IN 100, 713C, IN 738, Mar M 200, Mar M 246 or TRW VI A.

Oxidation is slowly moving air of uncoated 713C at 2000°F (1093°C) produced the following weight changes :

exp.time(h)	40	105	176	248	265	320	391	444	507
wt.gain(mg)	+1.7	-23.9	-38.0	-50.2	-52.6	-60.0	-66.9	-73.9	-89.9

At the end of the test, the alloy had a depleted layer some 80 μm thick.

Hot corrosion tests were performed in the Solar environmental simulator burning JP5 fuel with 35 ppm synthetic sea salt in the air. Specimens were tested at 1650 and 1800°F (899 and 982°C) in a holder rotated at 1725 ppm. The minimum gas velocity was Mach 0.85. One-hour thermal cycles were used until specimen failure. The specimens were removed at the completion of each 30 to 40h exposure for visual examination, cleaning and weighing. At the end of 40h at 899°C corrosion was just starting on 713C, and the weight loss was 8 mg, whereas B 1900 was severely hot corroded, with a weight loss of 330 mg. Both alloys showed severe hot corrosion after 20h at 982°C. 713C losing 212 mg and B 1900 388 mg.

C.C. Clark and W.R. Hulsizer, Gas Turbine Materials Conference Proceedings Naval Air Systems Command, Washington (1972) 35.

Cyclic (24 or 100h) tests were conducted at 1100°C in a slowly moving atmosphere containing 0.1, 5 and 10% water vapour for 400 to 1000h. Oxidation was measured by weight loss, both undescaled after each cycle and descaled at the end of each test. The results are presented in Figures 10-112 - 10-122 for a range of alloys, including 713C : there is a significant increase in the weight loss with water vapour, but the effect is even more noticeable with some other alloys. The authors suggest that

(possibly) the higher the refractory metal content, the greater the effect of water vapour.

A.R. Stetson and V.S. Moore, Gas Turbine Materials Conference Proceedings Naval Air Systems Command, Washington (1972) 43.

A number of alloys (including 713C) were tested in the Solar gas turbine environmental simulator with JP-5 fuel (0.04 - 0.12%) and 35 ppm synthetic sea salt injected into the combustion gases. Nickel-base alloys were tested at 1650 and 1800°F (899 and 983°C); cobalt alloys were tested at 1800 and 2000°F (983 and 1093°C). One hour thermal cycles were used for a total of 150h maximum. Samples were removed periodically for visual examination, cleaning and weighing.

Figure 10-122 shows the test results for uncoated nickel-base alloys. Here, B=1900, C=713C, I=IN100, M=Mar-M246, R=Rene 41, S=SEL 15, U=U-700, D=U-710, W=WI-52 and X=X-40.

Neither the equivalent chromium parameter used (Cr + ½ Al - ½ Mo) nor the Lewis and Smith nor the Rentz equivalents gave very good correlations at 1800°F.

Both uncoated cobalt-base alloys suffered extremely rapid attack at both test temperature; X-40 was more resistant than WI-52. At the comparable temperature of 1800°F (983°C) the cobalt-base alloys were marked by inferior to Rene 41, U 700 and U 710. Figure 10-124 summarises the data for all the alloys.

Rolls-Royce (1971) Ltd.,

Figures 10.125 and 10.126 show hot corrosion data for 713C, Nimonic 105 and Nimonic 115 at 870°C and 1050°C respectively, in a small burner rig test with 4 ppm sea salt in the air.

Data relating to this alloy can also be found in the following Figures :
1.1, 1.7, 1.8, 14.9, 36.1, 36.2, 36.3, 36.4, 36.5, 36.6, 36.7, 41.1, 41.2, 41.6, 41.7, 45.33, 45.37, 52.15;

and Tables :
1.I, 1.II, 1.IV, 1.V, 1.VI, 1.VII, 1.VIII, 1.IX, 1.X, 31.I.

TABLE 10-I

METAL LOSS DATA (MG/CM^2) FOR TEST SPECIMENS (QUIGG AND SCHIRMER)
(5 hours Test Duration)

Temperature, °C	Sea Salt in Air, ppm	Sulfur in Fuel wt %	Superalloy	Weight Loss, mg/cm^2		
				Base (a)	CI-2	TEL
760	0	0.0002	Inco 713C	0.2	0.3	0.1
			Inco 713C + MDC-1	0.4	1.9	1.4
			IN-100	0.2	0.3	0.7
			SM-200	0.6	0.5	0.6
			U-500	0.3	0.8	1.8
			WI-52	0.8	1.1	3.2
760	0	0.40	Inco 713C	1.4	7.3	2.2
			Inco 713C + MDC-1	1.6	5.4	3.2
			IN-100	4.5	5.8	6.0
			SM-200	3.7	5.3	3.3
			U-500	3.9	8.6	3.2
			WI-52	5.4	12.3	7.3
760	10.0	0.0002	Inco 713C	3.1	2.6	2.2
			Inco 713C + MDC-1	3.1	3.6	4.7
			IN-100	12.8	4.0	8.0
			SM-200	2.6	2.6	4.4
			U-500	24.1	6.8	16.4
			WI-52	13.3	7.1	53.8
760	10.0	0.40	Inco 713C	86.0	44.7	78.5
			Inco 713C + MDC-1	1.8	5.0	2.2
			IN-100	54.7	40.6	55.0
			SM-200	11.6	5.0	4.6
			U-500	19.5	26.9	60.0
			WI-52	5.4	13.4	8.0
872	0	0.0002	Inco 713C	0.5	1.6	1.7
			Inco 713C + MDC-1	1.4	1.6	0.6
			IN-100	0.4	0.6	6.7
			SM-200	1.2	2.7	6.1
			U-500	0.7	1.8	2.8
			WI-52	1.1	2.5	18.8
872	0	0.40	Inco 713C	0.5	0.3	0.6
			Inco 713C + MDC-1	0.9	1.3	1.6
			IN-100	1.3	0.3	0.8
			SM-200	1.6	0.4	0.8
			U-500	1.1	1.0	0.6
			WI-52	2.2	1.0	1.1
872	10.0	0.0002	Inco 713C	5.8	2.8	3.1
			Inco 713C + MDC-1	0.4	1.8	5.0
			IN-100	35.6	4.7	36.9
			SM-200	22.8	10.4	13.4
			U-500	38.1	7.3	13.3
			WI-52	3.6	9.8	24.6
872	10.0	0.40	Inco 713C	11.2	6.3	11.4
			Inco 713C + MDC-1	1.2	7.9	6.9
			IN-100	17.8	16.6	7.6
			SM-200	78.0	3.4	5.1
			U-500	3.6	2.5	4.8
			WI-52	2.6	10.6	11.1
982	0	0.0002	Inco 713C	1.1	1.0	5.7
			Inco 713C + MDC-1	1.5	2.2	1.8
			IN-100	1.3	1.0	16.8
			SM-200	2.5	4.0	117.5
			U-500	2.4	0.9	4.7
			WI-52	3.4	2.1	131.9

(a) Geometric mean weight loss of three values.

982	0	0.40	Inco 713C	1.1	16.0	19.3
			Inco 713C + MDC-1	1.0	1.4	1.0
			IN-100	1.8	36.8	40.7
			SM-200	2.8	39.5	104.4
			U-500	2.4	4.6	11.1
			WI-52	3.4	12.6	284.2
982	10.0	0.0002	Inco 713C	55.8	10.1	6.6
			Inco 713C + MDC-1	1.2	0.9	3.2
			IN-100	110.9	84.6	50.3
			SM-200	141.5	99.9	82.1
			U-500	7.0	56.0	17.3
			WI-52	20.1	20.4	90.2
982	10.0	0.40	Inco 713C	37.0	6.3	5.4
			Inco 713C + MDC-1	2.5	1.6	1.5
			IN-100	21.1	33.0	88.8
			SM-200	24.1	34.8	2.4
			U-500	4.2	20.2	13.8
			WI-52	11.9	26.5	30.3
1093	0	0.0002	Inco 713C	1.6	4.8	25.0
			Inco 713C + MDC-1	2.5	0.5	1.8
			IN-100	2.8	21.8	20.4
			SM-200	10.1	83.5	89.9
			U-500	4.3	16.2	7.1
			WI-52	8.5	42.1	211.7
1093	0	0.40	Inco 713C	2.2	18.9	93.5
			Inco 713C + MDC-1	1.7	0.1	4.1
			IN-100	6.2	64.0	157.3
			SM-200	15.3	44.8	476.6
			U-500	4.5	17.0	35.5
			WI-52	17.5	27.7	266.6
1093	10.0	0.0002	Inco 713C	31.0	39.0	43.0
			Inco 713C + MDC-1	1.7	2.0	1.8
			IN-100	102.5	92.7	98.8
			SM-200	235.4	146.3	487.4
			U-500	72.1	82.4	55.8
			WI-52	80.4	54.8	213.2
1093	10.0	0.40	Inco 713C	76.6	258.1	7.6
			Inco 713C + MDC-1	1.7	1.1	2.3
			IN-100	66.0	88.9	68.8
			SM-200	19.0	20.4	79.1
			U-500	8.6	11.6	8.9
			WI-52	28.9	27.3	92.8

(a) Geometric mean weight loss of three values.

TABLE 10-II

PARTIAL ANALYSIS BY X-RAY DIFFRACTION OF DEPOSITS FROM TEST SPECIMENS EXPOSED TO TEL IN FUEL (QUIGG AND SCHIRMER)

Temp., °C	Sea Salt in Air, ppm	Sulfur in Fuel, Wt. %	Superalloy	Weight Loss, mg/cm^2	Relative Intensities			
					NaCl	Na_2SO_4	PbO, $PbSO_4$	$PbSO_4$
760	0.0	0.40	Inco 713C	2.2			W	S
	0.0	0.40	WI-52	7.3			W	S
	10.0	0.0002	Inco 713C	2.2	S	M		
	10.0	0.40	Inco 713C	78.5		S		?VW
	10.0	0.40	WI-52	8.0		S		M
872	0.0	0.0002	Inco 713C	1.7			VW	
	0.0	0.0002	IN-100	6.7			M	
	0.0	0.0002	SM-200	6.1			VW	
	0.0	0.0002	U-500	2.8			M	
	0.0	0.0002	WI-52	18.8			VW	
	0.0	0.40	Inco 713C	0.6			S	S
	0.0	0.40	Inco 713C+ MDC-1	1.6			S	S
	0.0	0.40	IN-100	0.8			S	S
	0.0	0.40	SM-200	0.8			S	S
	0.0	0.40	U-500	0.6			S	S
	0.0	0.40	WI-52	1.1			S	S
	10.0	0.0002	Inco 713C	3.1	M	M		
	10.0	0.0002	WI-52	24.6		M		
	10.0	0.40	Inco 713C	11.4		S		
	10.0	0.40	Inco 713C+ MDC-1	6.9		S		
	10.0	0.40	WI-52	11.1		S		

Relative Intensities S = Strong; M = Medium; W = Weak; VW = Very Weak; ? = Pattern not positively identified.

TABLE 10-III

PARTIAL ANALYSIS BY X-RAY FLUORESCENCE OF DEPOSITS FROM TEST SPECIMENS EXPOSED TO CI-2 IN FUEL (QUIGG AND SCHIRMER)

Temp °C	Sea Salt in Air, ppm	Sulfur in Fuel, Wt. %	Superalloy	Weight Loss mg/cm^2	Wt. % in Deposits (a)			
					Mn	Cr	Ni	Co
760	10.0	0.0002	Inco 713C	2.6	12.0	0.6	< 0.4	< 0.4
	10.0	0.0002	Inco 713C+MDC-1	3.6	13.0	0.5	< 0.4	< 0.4
	10.0	0.0002	IN-100	4.0	16.0	0.5	< 0.4	< 0.4
	10.0	0.0002	SM-200	2.6	14.0	< 0.4	< 0.4	< 0.4
	10.0	0.0002	U-500	6.8	18.0	0.7	< 0.4	< 0.4
	10.0	0.0002	WI-52	7.1	18.0	0.8	< 0.4	1.5
	10.0	0.40	Inco 713C	44.7	10.0	2.4	10.0	< 0.06
872	10.0	0.0002	Inco 713C	2.8	35.0	1.4	< 0.4	< 0.06
	10.0	0.40	Inco 713C	6.3	19.0	< 0.4	< 0.2	< 0.2
	10.0	0.40	Inco 713C+MDC-1	7.9	20.0	< 0.4	0.3	< 0.2
	10.0	0.40	IN-100	16.6	20.0	< 0.4	0.4	< 0.2
	10.0	0.40	SM-200	3.4	19.0	< 0.4	< 0.2	< 0.2
	10.0	0.40	U-500	2.5	20.0	< 0.4	< 0.2	< 0.2
	10.0	0.40	WI-52	10.6	23.0	0.8	< 0.2	2.0
982	10.0	0.0002	Inco 713C	10.1	51.0	1.0	1.1	< 0.06
	10.0	0.40	Inco 713C	6.3	51.0	0.5	1.0	< 0.06
1093	10.0	0.0002	Inco 713C	39.0	50.0	1.6	8.7	< 0.1
	10.0	0.40	Inco 713C	258.1	12.0	5.2	25.0	0.2

(a) ± 20% of amount present.

TABLE 10-IV

PARTIAL ANALYSIS BY X-RAY FLUORESCENCE OF DEPOSITS FROM TEST SPECIMENS EXPOSED TO TEL IN FUEL (QUIGG AND SCHIRMER)

Temp. °C	Sea Salt in Air, ppm	Sulfur in Fuel, Wt, %	Superalloy	Weight Loss, mg/cm^2	Wt. % in Deposits (a)				
					Pb	Br	Cr	Ni	Co
760	0.0	0.40	Inco 713C	2.2	57.0	<0.2	<0.3	<0.4	<0.06
760	10.0	0.40	Inco 713C	78.5	4.7	0.6	2.9	10.0	<0.6
872	10.0	0.40	Inco 713C	11.4	2.9	<0.2	1.0	3.2	<0.06

(a) ± 20% of amount present.

TABLE 10-V

SUMMARY OF SPECIMEN WEIGHT LOSS DATA, 1093°C (QUIGG AND SCHIRMER)

Salt in Air ppm	Exposure Time, h	Total Specimen Weight Loss, mg/cm^2		
		<0.0040%S	0.040%S	0.40%S
0	5	3.78	5.07	5.65
	10	8.88	10.05	13.76
	15	15.30	17.91	15.52
	20	18.35	25.38	24.71
	25	23.08	42.58	30.92
	25	-	24.81	-
	30	42.24	30.35	46.82
	35	46.90	21.12	31.55
	40	91.13	35.64	68.92
	45	43.35	68.16	48.35
	50	74.81	67.61	80.93
	55	62.63	-	81.67
1.0	5	8.67	15.41	27.67
	5	-	15.64	28.63
	5	-	-	41.85
	5	-	-	66.14
	10	21.63	47.52	73.10
	10	-	19.72	132.31
	15	57.03	85.91	146.88
	15	67.66	70.72	134.69
	20	71.97	95.84	182.85
	20	72.40	115.74	199.50
	25	100.93	242.25	366.48
	25	114.50	220.54	299.46
	30	93.40	203.15	-
	35	130.37	-	-
	40	127.11	-	-

TABLE 10-VI

WEIGHT LOSS DATA FOR TEST SPECIMENS UNDER VARIOUS TEST CONDITIONS

(SCHIRMER AND QUIGG)

Temp. °C	Fuel Sulphur %	Salt in Air ppm	Time h	Weight Loss mg/cm² Stage 1	Stage 2	Stage 3	
760	0.0002	0	5	0.1	0.5	0.1	713C
		1.0		0.3	0.5	0.7	
		10.0		1.7	4.2	4.2	
	0.040	0		0.1	0.2	0.5	
		1.0		0.2	0.4	0.2	
		10.0		5.3	4.6	13.8	
	0.40	0		1.9	2.6	0.6	
		1.0		5.6	0.9	1.3	
		10.0		100.4	58.8	107.8	
872	0.0002	0		0.4	0.3	0.8	
		1.0		0.9	0.4	0.8	
		10.0		3.4	10.9	5.2	
	0.040	0		0.2	0.4	0.4	
		1.0		0.2	0.1	0.2	
		10.0		18.0	4.8	8.6	
	0.40	0		1.4	0.3	0.3	
		1.0		1.6	1.3	1.2	
		10.0		50.7	46.7	0.6	
760	0.0002	0	5	0.1	0.2	0.8	IN 100
		1.0		3.0	1.0	4.5	
		10.0		4.1	18.0	27.2	
	0.040	0		0.9	0.5	0.2	
		1.0		0.3	0.3	1.2	
		10.0		25.7	102.9	116.9	
	0.40	0		1.7	6.6	8.0	
		1.0		9.8	13.0	3.0	
		10.0		49.9	63.6	51.5	
872	0.0002	0		0.8	0.4	0.2	
		1.0		0.7	4.0	1.7	
		10.0		26.8	40.8	41.3	
	0.040	0		0.5	0.3	0.4	
		1.0		0.3	0.3	0.3	
		10.0		41.8	83.2	79.5	
	0.40	0		0.3	6.5	1.2	
		1.0		3.8	7.5	4.5	
		10.0		12.9	8.5	51.1	
760	0.0002	0	5	0.4	0.2	2.5	SM-200
		1.0		2.9	0.8	1.0	
		10.0		2.2	2.5	3.2	
	0.040	0		1.1	0.4	0.8	
		1.0		0.2	0.3	0.8	
		10.0		1.9	2.8	3.2	
	0.40	0		1.4	5.8	6.2	
		1.0		4.8	5.9	3.8	
		10.0		14.4	15.9	6.8	
872	0.0002	0		1.2	1.6	0.9	
		1.0		0.7	3.0	1.9	
		10.0		18.8	17.2	36.5	
	0.040	0		0.8	0.2	1.3	
		1.0		2.3	2.3	0.8	
		10.0		37.5	49.3	31.5	
	0.40	0		0.7	3.3	1.7	
		1.0		1.8	3.4	2.5	
		10.0		70.0	103.4	65.5	

760	0.0002	0	5	0.9	0.1	0.2	U 500
		1.0		1.3	5.8	1.4	
		10.0		21.0	34.5	19.4	
	0.040	0		0.4	1.4	0.5	
		1.0		0.6	0.6	0.6	
		10.0		8.3	32.8	27.2	
	0.40	0		6.8	1.3	6.8	
		1.0		18.6	5.0	6.7	
		10.0		5.6	40.7	32.5	
872	0.0002	0		0.4	1.0	1.1	
		1.0		1.7	1.5	1.8	
		10.0		35.4	52.0	30.0	
	0.040	0		0.7	0.9	0.4	
		1.0		0.8	0.8	0.5	
		10.0		64.6	41.8	94.1	
	0.40	0		1.2	0.7	1.7	
		1.0		1.9	1.0	0.5	
		10.0		5.0	3.1	3.0	
760	0.0002	0	5	1.4	0.4	0.8	WI 52
		1.0		1.3	7.1	1.5	
		10.0		11.9	15.8	12.5	
	0.040	0		0.5	2.0	2.2	
		1.0		0.8	0.6	1.1	
		10.0		6.5	11.4	8.9	
	0.40	0		10.1	2.2	7.2	
		1.0		10.2	5.4	2.9	
		10.0		3.9	7.6	5.3	
872	0.0002	0		0.8	1.7	1.1	
		1.0		2.6	2.6	2.4	
		10.0		2.4	6.0	3.2	
	0.040	0		1.5	1.2	1.5	
		1.0		0.6	0.7	0.7	
		10.0		1.7	3.8	5.0	
	0.40	0		1.7	1.4	4.8	
		1.0		12.0	9.2	6.9	
		10.0		2.2	3.2	2.5	

TABLE 10-VII

MEASURED SULFIDE PENETRATION AND PENETRATION FROM WEIGHT LOSS OF TEST SPECIMENS (SCHIRMER AND QUIGG)

Temp., °F	Fuel Sulfur, Wt. %	Sea Salt in Air, ppm	Superalloy	Penetration, from Weight Loss, mils/5 hr.	Sulfide Penetration, mils/5 hr.
2000	0.040	10.0	Inco 713C	0.9	9.8
2000	0.040	10.0	Into 713C + MSC-1	0.1	-
2000	0.040	10.0	IN-100	6.3	19.5
2000	0.040	10.0	SM-200	3.8	26.4
2000	0.040	10.0	Udimet 500	0.6	10.6
2000	0.040	10.0	WI-52	3.0	15.0
1800	0.0002	0	IN-100	0.1	5.1
1800	0.0002	10.0	IN-100	6.2	13.3
1800	0.40	10.0	IN-100	1.3	7.0
2200	0.0002	0	IN-100	0.3	7.2
2200	0.0002	10.0	IN-100	6.3	23.7
2200	0.40	10.0	IN-100	8.7	29.4

TABLE 10-VIII

BURNER RIG TEST RESULTS AT 1750°F (DOERING AND BERGMAN)

200 PPM/100 Hours		5 PPM/1000 Hours	
Alloy	Attack mils[1]	Alloy	Attack mils[1]
5384 (U500)	1.1/7.0	5382D	1.0/11.6
5382D (X-40)	0.6/9.2	5759D	5.5/15.3
PA1 (SEL)	15.9/26.4	5384	8.8/31.7
5759D (L605)	10.7/27.8	PA1	31.5/51.8
PA3 (SM 200)	14.4/44.5	5391A	59.0/77.1[2]
5391A (713C)	56.6/65.8	5397	130[3]
5397 (IN100)	130[3]	PA3	130[3]
PA2 (SEL15)	130[3]	PA2	130[3]

[1] Results given as surface loss/maximum penetration expressed as losses in diameter.

[2] At times, specimens of this alloy have been destroyed.

[3] Specimens destroyed.

TABLE 10-IX

TEST SPECIMEN WEIGHT LOSS DATA AT 1093°C

(QUIGG AND SCHIRMER, 1968)

Total Time, hours	Weight Loss, mg/cm²								
	Zero Sea Salt in Air			1.6 ppm Sea Salt in Air					
	Sulfur in Fuel, wt %			Sulfur in Fuel, wt %					
	<0.0040	0.040	0.40	<0.0040		0.040		0.40	
				Run 1	Run 2	Run 1	Run 2	Run 1	Run 2
				Inconel 713C					
5	3.78	5.07	5.65	8.67	-	15.41	-	27.67	41.85
5	-	-	-	-	-	15.64	-	28.63	66.14
10	8.88	10.05	13.76	21.63	-	47.52	-	73.10	-
10	-	-	-	-	-	19.72	-	132.31	-
15	15.30	17.91	15.52	57.03	-	85.91	-	146.88	-
15	-	-	-	67.66	-	70.72	-	134.69	-
20	18.35	25.38	24.71	71.97	-	95.84	-	182.85	-
20	-	-	-	72.40	-	115.74	-	199.50	-
25	23.08	42.58	30.92	100.93	-	242.25	-	366.48	-
25	-	24.81	-	114.50	-	220.54	-	299.46	-
30	42.29	30.35	46.82	93.40	-	203.15	-	-	-
35	46.90	21.12	31.55	130.37	-	-	-	-	-
40	91.13	35.64	68.92	127.11	-	-	-	-	-
45	43.35	68.16	48.35	-	-	-	-	-	-
50	74.81	67.61	80.93	-	-	-	-	-	-
55	62.63	-	81.67	-	-	-	-	-	-

TABLE 10-X

WEIGHT LOSS DATA DEPOSIT WEIGHT DATA FOR INCONEL 713C AT 1093°C (QUIGG AND SCHIRMER)

Sea Salt in Air, ppm	Exposure Time, hours	Total Specimen Weight Loss mg/cm²		Deposit Weight (a) mg/cm²	
		0.017 ppm V in air (b)	0.063 ppm V in air (c)	0.017 ppm V in air (b)	0.063 ppm V in air (c)
0	5	6.69	31.18	7.34	6.44
	10	16.79	68.17	9.69	7.17
	15	27.16	81.02	11.62	8.26
	20	32.23	109.07	8.55	5.61
	25	23.62	192.82	11.32	7.15
	30	33.70	94.12	9.45	6.93
	35	23.09	110.81	8.02	7.53
	40	36.57	161.56	7.52	6.32
	45	129.52	199.29	8.28	7.28
	50	58.63	213.25	9.12	6.47
	55	94.26	249.90	9.16	7.38
1.0	5		34.73		14.09
	5		111.78		14.65
	10		219.34		27.27
	10		182.87		21.83
	15		327.90		24.94
	15		354.37		20.75
	20		384.03		19.55
	20		515.16		25.97
	20		439.06		24.94

(a) Obtained by difference between weight of specimen after test and weight of specimen after cleaning.

(b) Equivalent to 1.0 ppm vanadium in fuel at 1093 C conditions.

(c) Equivalent to 3.8 ppm vanadium in fuel at 1093 C conditions.

TABLE 10-XI

DEPOSIT AND WEIGHT LOSS DATA FOR ASTM SPECIMENS (QUIGG AND SCHIRMER)

Exposure Time, Hours	Deposits mg/cm²	Total Specimen Weight Loss mg/cm²
	IN-100	
11	11.13	125.92
22	17.18	229.72
33	19.17	308.96
44	6.42	371.58
	Inconel 713C	
11	8.40	63.98
11	10.59	52.47
22	12.83	117.57
22	9.81	45.94
33	12.50	163.97
33	20.85	59.42
44	15.48	200.07
44	20.58	177.98
	Udimet 700	
22	17.68	70.58
44	9.38	164.05
66	29.88	316.76
88	15.70	327.28
	Mar M 421	
22	14.68	69.20
44	17.34	126.15
66	28.72	236.88
88	26.57	288.39

	IN-738	
22	10.36	42.94
44	19.08	97.16
66	22.41	151.58
88	25.46	190.58
	Udimet 500	
44	5.93	56.13
44	8.43	20.39
77	9.74	137.88
77	30.37	118.31
110	26.89	226.97
110	17.15	226.84
143	37.30	430.38
143	18.21	411.68

TABLE 10-XII

DEPOSIT AND WEIGHT LOSS DATA FOR INCONEL 713C SPECIMENS (QUIGG AND SCHIRMER)

Exposure Time Hours	Deposits mg/cm^2	Total Specimen Weight Loss mg/cm^2	Exposure Time, Hours	Deposits mg/cm^2	Total Specimen Weight Loss mg/cm^2
	Block 1				
11	11.69	33.46	44	13.97	120.88
11	14.48	28.99	33	9.25	103.76
22	12.25	85.42	22	5.59	5.21
22	12.56	29.01	11	13.05	23.32
33	13.21	145.01	44	21.83	111.66
33	20.02	63.97	33	14.66	95.00
44	9.61	170.87	22	15.10	89.20
44	19.69	136.35	11	17.64	28.40
	Block 2			Block 6	
11	11.52	14.26	11	11.79	39.42
11	15.85	26.18	11	9.20	39.16
22	10.10	53.84	22	14.48	99.96
22	16.38	81.26	22	10.10	114.88
33	11.57	79.88	33	13.27	149.95
33	22.14	100.56	33	12.29	190.13
44	16.70	143.61	44	10.88	197.41
44	21.66	94.36	44	12.02	228.29
	Block 3			Block 7	
11	11.83	23.19	11	13.31	38.00
11	15.08	27.14	11	8.58	32.77
22	12.63	76.10	22	14.20	115.19
22	12.82	31.70	22	12.04	107.03
33	15.28	139.77	33	16.67	162.13
33	17.24	59.68	33	10.32	182.68
44	8.30	145.77	44	12.81	238.89
44	16.09	146.81	44	9.59	207.94
	Block 4			Block 8	
11	12.31	17.28	11	14.77	27.20
11	18.36	25.90	11	8.38	36.47
22	10.76	43.84	22	12.32	104.87
22	13.61	84.56	22	8.44	110.81
33	10.32	57.14	33	10.88	178.79
33	17.67	101.57	33	10.44	163.64
44	16.29	122.18	44	10.75	234.00
44	21.52	86.81	44	9.19	219.78
	Block 5				
			44	17.81	109.53
11	9.97	8.31	33	12.10	85.73
11	14.37	19.77	22	8.84	8.13
22	17.40	36.91	11	4.60	18.49
22	16.28	72.03			
33	8.94	78.51	44	22.18	82.42
33	15.95	98.19	33	20.28	65.96
44	16.26	119.40	22	21.82	57.39
44	22.58	104.30	11	12.89	20.54

	Block 8 (contd.)				
44	15.66	80.00	44	17.09	205.17
33	9.96	101.24	33	12.15	144.92
22	7.65	7.05	22	12.04	71.70
11	12.80	37.87	11	10.15	15.68
44	21.18	64.69	44	21.29	187.36
33	21.18	68.58	33	13.41	119.05
22	16.91	73.18	22	15.68	63.02
11	17.64	20.05	11	13.67	24.88
	Block 9				
			44	19.47	196.73
11	12.73	27.74	33	11.40	125.74
11	9.57	19.83	22	14.65	69.51
22	15.73	90.11	11	7.99	20.20
22	9.21	83.69			
33	12.99	117.61	44	14.86	189.41
33	13.14	150.32	33	11.65	148.34
44	11.64	186.46	22	14.08	67.94
44	10.48	163.11	11	10.68	13.98
			44	13.35	95.70
			33	19.33	68.22
			22	11.78	88.82
			11	12.99	23.80

TABLE 10-XIII

PENETRATION DATA FOR ASTM SPECIMENS (QUIGG AND SCHIRMER)

Spec. No.	Superalloy	Exposure Time hr	Surface Loss			Maximum Attack		
			Average Visual Attack, mils	Maximum Visual Attack, mils	Mean, mils	Average Visual Attack, mils	Maximum Visual Attack, mils	Mean, mils
45	IN 100	11	19 & 21 (B)	21 & 23 (B)	21	20 & 21 (B)	21 & 23 (B)	21
46	IN 100	22	37 & 38 (B)	39 & 40 (B)	38	37 & 38 (B)	39 & 40 (B)	38
47	IN 100	33	43 & 45 (B)	49 & 53 (B)	48	43 & 45 (B)	49 & 53 (B)	48
48	IN 100	44	53 & 56 (B)	57 & 58 (B)	56	53 & 56 (B)	57 & 58 (B)	56
25	Inco 713C	11	9 & 13 (B)	12 & 13 (B)	12	9 & 15 (B)	12 & 13 (B)	12
26	Inco 713C	22	20 & 22 (B)	20 & 23 (B)	21	22 & 23 (B)	23 & 23 (B)	23
27	Inco 713C	33	24 & 30 (B)	28 & 35 (B)	29	24 & 30 (B)	28 & 35 (B)	29
28	Inco 713C	44	30 & 30 (B)	32 & 32 (B)	31	30 & 32 (B)	32 & 32 (B)	32
76	Inco 713C	11	6 & 9 (B)	9 & 11 (-)	9	6 & 9 (B)	9 & 11 (B)	9
75	Inco 713C	22	7 & 11 (B)	10 & 10 (B)	10	7 & 12 (B)	10 & 10 (B)	10
74	Inco 713C	33	6 & 12 (B)	9 & 10 (B)	9	7 & 12 (B)	9 & 10 (B)	10
73	Inco 713C	44	24 & 30 (B)	29 & 34 (B)	29	24 & 30 (B)	29 & 34 (B)	29
33	Udimet 700	22	7 & 7 (B)	11 & 15 (B)	10	10 & 11 (B)	12 & 16 (B)	12
34	Udimet 700	44	18 & 18 (B)	18 & 19 (B)	20	18 & 19 (B)	23 & 25 (B)	21
35	Udimet 700	66	18 & 33 (B)	44 & 46 (B)	35	19 & 35 (B)	47 & 48 (B)	37
36	Udimet 700	88	37 & 43 (B)	45 & 47 (B)	43	38 & 45 (B)	47 & 51 (B)	45
41	Mar M421	22	10 & 10 (B)	12 & 15 (B)	12	13 & 15 (B)	17 & 18 (B)	16
42	Mar M421	44	19 & 19 (B)	21 & 22 (B)	20	20 & 21 (B)	22 & 24 (B)	22
43	Mar M421	66	32 & 34 (B)	37 & 37 (B)	35	35 & 35 (B)	37 & 37 (B)	36
44	Mar M421	88	33 & 38 (B)	38 & 46 (B)	39	33 & 38 (B)	40 & 46 (B)	39

Notes : (B) = Attack on both sides of cross-sectioned area.

TABLE 10-XIV

PARTICIPANT'S TEST CONDITIONS (ASTM ROUND ROBIN TEST)

Participant	Air/Fuel Ratio	Gas Velocity (ft/sec)	Salt Conc. (ppm)	Temp. (°F)	Time (hrs.)	Fuel	Fuel Sulfur Content (%)	Pressure (atm)	Cycling
A	30/1	700	5	1650	100	JP-4R	0.2	1	yes
B	30/1	(a)	5	1650	100	JP-5	(a)	1	No
C	(a)	700	5	1650	100	Jet A	0.4	1	yes
D	54/1	200	5	1650	100	JP-4	0.16	1	Yes
E	(a)	(a)	(b)	1800	104	Natural Gas	(a)	1	Yes
F	(a)	(a)	5	1600	100	Kerosene	0.95	1	No
G	(c)	-	-	1650	100	-	-	1	No
H	62/1 to 106/1	163 to 275	1	2000(d)	44	JP-5	0.04	15	Yes
I	30/1	4.45 SCFM	100	1650	100	Diesel	0.86	1	No
J	(a)	(a)	5	1650	100	JP-4R	(a)	1	No
K	(e)	-	-	1700	-	-	-	-	-
L	30/1	(a)	100	1650	100	(a)	(a)	1	No
M	17/1	6.71 SCFM	100	1650	100	2 Diesel	0.15	1	Yes
N	(a)	MACH 1	5	1650	100	JP-5	(a)	1	Yes
O	30/ 1	700	5	1650	100	JP-4R	0.16	1	Yes

(a) not reported
(b) salt solution (1% sulfate ion, water solution) sprayed on specimens during cooling cycle
(c) static rig, specimens coated with Na_2SO_4 - NaCL (50/50) mixture exposed to 0.15% SO_2, 2.25% CO_2 air and water vapor mixture
(d) maximum gas temperature
(e) crucible tests, 90% Na_2SO_4 - 10% NaCl@1700°F

TABLE 10-XV

ASTM ROUND ROBIN TEST

Alloy	Ranking of Alloys By Participant															Average Rank	Order of Alloys by Avg. Rank	No. of Participant Ranking Alloy					
	A	B	C	D	E	F	G	H	I	J	K	L	M	N	O			1	2	3	4	5	6
U-500	1	2	2	2	1	3	1	1	3	3	3	3	1	3	1	2.00	1	6	3	6	0	0	0
IN-738	2	1	1	3	3	2	3	2	2	2	1	2	3	1	2	2.00	1	4	7	4	0	0	0
MM-421	3	3	3	4	4	1	2	4	1	5	2	1	2	2	3	2.67	3	3	4	4	3	1	0
U-700	4	4	4	1	2	4	4	3	4	1	4	4	4	4	4	3.40	4	2	1	1	11	0	0
IN-713C	5	6	5	5	6	5	5	5	5	6	6	5	5	5	5	5.27	5	0	0	0	0	11	4
IN-100	6	5	6	6	5	6	6	6	6	4	5	6	6	6	6	5.67	6	0	0	0	1	3	11
No. of Alloys Not Ranked According to Average	1	3	1	4	5	3	2	3	3	[illegible]	4	3	2	2	1								
Total No. of Places Removed From Average	1	3	1	7	7	3	3	3	5	11	5	5	3	3	1								

TABLE 10-XVI

ASTM ROUND-ROBIN TESTS

Mean and Median Values of Surface Loss and Maximum Attack for 1650°F, 100 hr. Burner Rig Tests

	Surface Loss(mils)		Maximum Attack (mils)	
Alloy	Mean	Median	Mean	Median
U-500	8.5	2.5	12.4	4.5
IN-738	8.0	5.3	17.5	15.0
MM-421	8.8	5.5	21.1	15.5
U-700	27.3	20.5	39.6	30.0
IN-713C	41.0	31.0	53.1	41.3
IN-100	84.9	68.0	119.4	78.5

Participants A, B, C, D, G, I, J, L, M, N, O only

TABLE 10-XVII

SUMMARY OF VISUAL RATINGS VS WEIGHT LOSS FOR TEST SPECIMENS (QUIGG ET ALL)

Test 1 with 0.040 wt % Sulfur and Test 2 with 0.0004 wt % Sulfur in Fuel

		Test 1		Test 2		Weight of Surface Scale, mg/cm^2	
Superalloy	Exposure Time, hrs.	Visual Rating	Weight Loss, mg/cm^2	Visual Rating	Weight Loss, mg/cm^2	Test 1	Test 2
B-1900	5	7	6.10	9	1.02	5.46	1.06
B-1900	5	8	4.18	9	5.41	4.91	4.74
B-1900	5	8	9.78	8	2.26	6.43	2.64
B-1900	5	7	15.39	6	3.43	8.44	2.91
B-1900	5	9	3.44	7	2.51	3.63	2.32
B-1900	5	9	1.96	9	0.94	2.54	1.22
B-1900	10	7	21.04	8	1.87	8.93	2.22
B-1900	15	6	102.95	7	12.81	16.26	7.05
B-1900	15	6	93.32	9	2.32	7.98	2.63
B-1900	15	7	73.56	6	4.82	8.23	4.82
B-1900	15	6	95.19	8	2.46	8.21	2.74
B-1900	15	6	68.18	7	6.39	14.57	4.57
B-1900	15	8	52.30	7	1.28	6.25	1.43
B-1900	20	7	132.64	7	4.97	23.09	5.01
Mar M-246	5	6	35.75	7	10.46	13.45	6.96
Mar M-246	5	7	31.00	7	1.65	5.62	1.89
Mar M-246	5	7	22.90	6	6.17	5.58	4.68
Mar M-246	5	7	24.24	7	15.90	13.85	6.80
Mar M-246	5	7	37.47	6	6.95	11.78	6.74
Mar M-246	5	8	13.49	9	4.43	8.03	5.36
Mar M-246	10	7	43.19	6	15.53	9.78	7.81
Mar M-246	15	5	124.32	5	81.26	15.05	16.20
Mar M-246	15	5	149.34	5	35.50	10.18	7.37
Mar M-246	15	6	154.66	5	73.06	27.41	15.14
Mar M-246	15	6	126.28	5	30.26	9.20	6.89
Mar M-246	15	7	83.70	6	11.43	14.81	9.44
Mar M-246	15	6	80.82	6	24.41	16.29	7.73
Mar M-246	20	6	143.64	7	23.92	20.94	10.08
Mar M-200	5	8	22.34	7	9.44	12.02	6.92
Mar M-200	5	6	37.54	6	20.44	15.50	8.16
Mar M-200	5	7	31.64	6	16.94	16.96	8.87
Mar M-200	5	7	29.61	7	10.35	11.58	11.00
Mar M-200	10	6	44.04	6	9.08	13.08	8.53
Mar M-200	15	6	150.80	5	90.72	22.20	17.01
Mar M-200	15	6	153.27	6	36.66	17.20	10.44
Mar M-200	15	5	151.11	5	39.17	30.53	11.51
Mar M-200	15	6	117.08	6	29.02	12.77	8.05

Mar M-200	15	7	132.67	6	60.53	27.76	13.07
Mar M-200	15	8	110.57	6	14.73	16.57	13.21
Mar M-200	20	8	142.38	7	8.53	14.26	10.45
IN-100	5	7	21.58	7	1.51	5.59	1.79
IN-100	5	7	16.08	9	3.68	5.40	4.75
IN-100	5	7	10.26	9	4.54	5.98	5.73
IN-100	5	8	22.54	8	6.95	4.33	6.75
IN-100	5	6	29.79	9	3.54	10.41	4.74
IN-100	5	8	6.86	7	1.38	5.30	1.82
IN-100	10	7	45.33	6	14.19	12.80	12.20
IN-100	15	6	114.50	6	10.64	8.53	8.63
IN-100	15	6	118.07	6	7.19	11.48	6.48
IN-100	15	6	102.30	6	8.17	10.97	9.54
IN-100	15	6	52.38	7	7.16	1.04	8.25
IN-100	15	6	93.78	7	10.28	14.96	10.22
IN-100	15	8	73.17	7	5.08	10.28	5.84
IN-100	20	7	130.94	8	4.03	9.84	4.56

Note: remaining data in this Table duplicated in Jan. 1971 Table.

TABLE 10-XVIII

TEST CONDITIONS EMPLOYED (DONACHIE ET AL)

Alloy	Alloy Condition	Fuel	Sulfur Content, %	Salt* Content, ppm	Temperature, deg F	Total Test Time, hr
Waspaloy	wrought	JP-5R	0.4	0.5	1650	100
U-700	wrought	JP-5R	0.4	0.5	1650	100
U-700	cast	JP-5R	0.4	0.5	1650	100
IN-713	cast	JP-5R	0.4	0.5	1650	100
IN-100	cast	JP-5R	0.4	0.5	1650	100
AMS 5382	cast	marine diesel	1.0	0.5	1450	50
Waspaloy	wrought	marine diesel	1.0	0.5	1650	50
U-700	wrought	marine diesel	1.0	0.5	1650	50
IN-713	cast	marine diesel	1.0	0.5	1650	50
IN-100	cast	marine diesel	1.0	0.5	1650	50
AMS 5382	cast	marine diesel	1.0	0.5	1650	50
MAR-M 302	cast	marine diesel	1.0	0.5	1650	50
WI-52	cast	marine diesel	1.0	0.5	1650	50
U-700	wrought	marine diesel	1.0	1.0	1650	50
AMS 5382	cast	marine diesel	1.0	1.0	1650	50
MAR-M 302	cast	marine diesel	1.0	1.0	1650	50
IN-713	cast	marine diesel	1.0	1.0	1650	50
U-700	wrought	marine diesel	1.0	5.0	1650	50
AMS 5382	cast	marine diesel	1.0	5.0	1650	50
MAR-M 302	cast	marine diesel	1.0	5.0	1650	50
IN-713	cast	marine diesel	1.0	5.0	1650	50
IN-713	cast	marine diesel	1.0	0.5	2000	50
MAR-M 302	cast	marine diesel	1.0	0.5	2000	50

* Synthetic sea salt. Nominal concentration, for actual, multiply by 7.

TABLE 10-XIX

RESULTS OF HOT CORROSION TESTS (DONACHIE ET AL)

(a) Effect of temperature on weight change after 50-hr test in 1 per cent sulfur diesel fuel and 0.5 ppm nominal salt/air ratio.

Alloy	Weight Change at Temperature Indicated, g[a]			
	1450 F		1650 F	2000 F
Waspaloy	-0.06	(0.10)		
WI-52	-0.12	(0.25)		
AMS 5382	-0.13	(0.23)	-0.08	
U-700 (W)			-0.05	
MAR-M 302			-0.08	-0.20
IN-713			-0.04	-0.17
IN-100				-0.27

[a]Numbers in parentheses indicate 100-hr data.

(b) Effect of salt concentration on weight loss after 50-hr rig test in 1 per cent sulfur diesel fuel at 1650 F.

Alloy	Weight Change at Salt Concentration[a] Indicated, g		
	0.5 ppm	1.0 ppm	5.0 ppm
AMS 5382	-0.08	-0.13	-0.11
NAR-M 302	-0.08	-0.16	-0.44
IN-713	-0.04	0.00	-1.55
U-700 (W)	-0.05	-0.03	-1.30

[a]Nominal concentration, for actual, multiply by 7.

(c) Effect of sulfur concentration on weight loss after 50 and 100-hr tests at 0.5 ppm nominal salt/air ratio at 1650 F.

Alloy	Weight Change at Indicated (Fuel) Sulfur Concentration and Time, g			
	50 hr		100 hr	
	MD-1% S	JP-5 R-0.4%S	MD-1% S	JP-5 R-0.4% S
MAR-M 302	-0.10	-0.10	-0.20	-0.25
Waspaloy	-0.10	-0.03	-0.17	-0.06
AMS 5382	-0.15	-0.04	-0.20	-0.10
WI-52	-0.30	-0.25	-0.80	-0.65
IN-100	-1.35	-0.85	-3.25	-2.70
IN-713	-0.04	-0.10		
U-700 (W)	-0.05	-0.03		

(d) Weight and thickness changes of alloys after 1650 F burner rig sulfidation testing.

Alloy	Salt Concentration, ppm	50 Hr		500 Hr	
		Weight Loss, g	Metal Loss, %	Weight Loss, g	Metal Loss, %
U-700 (W)	0.5	-0.05	-0.88	-2.32	-8.89
MAR-M 302	0.5	-0.08	-0.40	-1.76	-3.95
IN-713	0.5	-0.04	-0.08	-7.94	-18.32
U-700 (W)	5.0	-1.30	-3.35		
MAR-M 302	5.0	-0.44	-0.56		
IN-713	5.0	-1.55	-4.24		

TABLE 10-XX

RESULTS OF EXPOSURES OF ALLOYS TO MOLTEN SALTS (WHEATFALL ET AL)

Experiment No.	Alloy	Preoxidation Time	Electrolyte	Atmosphere	Initial[a] Potential, v[c]	Max[b] Potential, v[c]	Time to Start of Sustained Potential Rise, hr	Total Time of Exp., hr	Scale Thickness (in.) or Oxide Penetration, μ	Rate of Scale Formation, in./hr[f]	Figure No.
1	Nickel	24 hr	Na_2SO_4	air	0.15	0.50	1	50	[e]	[e]	4
2	Alloy A (AMS 5391A)	5 min	Na_2SO_4	air	0.26	0.92	4	74	0.030 in.	7.1×10^{-4}	2
3		2 hr	Na_2SO_4	air	0.12	0.90	14	101	0.055 in.	6.3	2
4		2 hr	Na_2SO_4	argon	0.14	0.83	18	46	0.012 in.	4.3	
5		5 min	Na_2SO_4-NaCl	air	0.87	0.85	0	121	0.170 in.	14.0	2, 5
6		2 hr	Na_2SO_4-NaCl	air	0.09	0.65	8	92	0.100 in.	11.9	
7		2 hr	Na_2SO_4-NaCl	argon	0.12	1.10	24	41	0.030 in.	17.6	
8	Alloy B (AMS 5384)	5 min	Na_2SO_4	air	0.05	0.11	[d]	131	10μ	[e]	3, 7
9		2 hr	Na_2SO_4	air	0.07	0.10	[d]	328	17μ	[e]	6, 7
10		5 min	Na_2SO_4	argon	0.32	0.40	[d]	41	7μ	[e]	7
11		2 hr	Na_2SO_4	argon	0.02	0.30	[d]	238	20μ	[e]	6, 7
12		5 min	Na_2SO_4-NaCl	air	0.10	0.66	100	160	[e]	[e]	3, 8
13		2 hr	Na_2SO_4-NaCl	air	0.06	0.28	[d]	245	[e]	[e]	3, 8
14		2 hr	Na_2SO_4-NaCl	air	0.04	0.95	282	471	[e]	[e]	

[a] Minimum value after initial rise and descent.
[b] Maximum value after initial rise and descent.
[c] Potential versus platinum electrode.
[d] No sustained rise during experiment.
[e] Indicated measurement not applicable.
[f] Rate of scale formation = $\frac{\text{scale thickness}}{\left(\text{total time}\right) - \left(\text{time to sustained potential rise}\right)}$

TABLE 10-XXI

SUMMARY OF TEST SPECIMEN WEIGHT LOSS DATA (SCHIRMER AND QUIGG)

Temperature, deg F	Sulfur in Fuel, %	Sea Salt in Air, ppm	Geometric Mean Weight Loss, mg/cm^2					
			U-500	I-713C	IN-100	SM-200	WI-52	MDC-1
1400	0.0002	0	0.3	0.2	0.2	0.6	0.8	0.4
		1.0	2.2	0.5	2.4	1.3	2.4	0.8
		10.0	24.1	3.1	12.8	2.6	13.3	3.1
	0.040	0	0.6	0.2	0.4	0.7	1.3	0.3
		1.0	0.6	0.2	0.5	0.4	0.8	0.7
		10.0	19.5	7.0	67.6	2.6	8.7	2.6
	0.40	0	3.9	1.4	4.5	3.7	5.4	1.6
		1.0	8.5	1.9	7.3	4.8	5.4	1.9
		10.0	19.5	86.0	54.7	11.6	5.4	1.8
1600	0.0002	0	0.7	0.5	0.4	1.2	1.1	1.4
		1.0	1.7	0.7	1.7	1.6	2.5	0.4
		10.0	38.1	5.8	35.6	22.8	3.6	0.4
	0.040	0	0.6	0.3	0.4	0.6	1.4	0.3
		1.0	0.7	0.2	0.3	1.6	0.7	0.4
		10.0	63.3	8.8	65.2	38.8	3.2	1.5
	0.40	0	1.1	0.5	1.3	1.6	2.2	0.9
		1.0	1.0	1.4	5.0	2.5	9.1	1.5
		10.0	3.6	11.2	17.8	78.0	2.6	1.2
1800	0.0002	0	2.4	1.1	1.3	2.5	3.4	1.5
		1.0	4.5	2.2	6.8	39.5	17.9	1.1
		10.0	7.0	55.8	110.9	141.5	20.1	1.2
	0.040	0	2.7	2.5	4.4	5.2	4.2	1.2
		1.0	4.7	11.4	24.3	37.7	11.8	0.8
		10.0	5.8	45.9	113.3	104.4	15.3	1.7
	0.40	0	2.5	1.1	1.8	2.8	3.4	1.0
		1.0	4.0	16.8	26.9	24.4	7.7	2.0
		10.0	4.2	37.0	21.1	24.1	11.9	2.5
2000	0.0002	0	4.3	1.6	2.8	10.1	8.5	2.5
		1.0	6.7	2.9	10.6	74.7	53.3	1.4
		10.0	72.1	31.0	102.5	235.4	80.4	1.7
	0.040	0	4.3	1.5	3.5	7.2	11.3	0.6
		1.0	8.0	5 5	13.1	41.3	29.3	2.7
		10.0	25.0	20.2	118.7	76.2	47.8	1.7
	0.40	0	4.5	2.2	6.2	15.3	17.5	1.7
		1.0	6.7	5.6	32.3	37.7	28.4	1.4
		10.0	8.6	76.6	66.0	19.0	28.9	1.7
2200	0.0002	0	6.7	3.7	7.2	42.7	127.7	1.3
		1.0	7.9	6.0	9.8	73.4	129.7	0.8
		10.0	80.0	60.2	166.8	685.5	387.0	2.1
	0.040	0	6.5	10.2	32.6	82.2	115.2	1.2
		1.0	10.4	9.5	34.1	153.6	164.6	2.7
		10.0	8.7	111.1	220.2	591.0	376.3	2.1
	0.40	0	5.3	19.5	72.5	155.9	173.2	1.3
		1.0	12.4	10.6	58.2	184.4	216.3	1.6
		10.0	60.1	61.9	165.5	193.6	241.6	2.6

TABLE 10-XXII

SUMMARY OF TEST CONDITIONS (LEE AND YOUNG)

		Cooled tests									Uncooled tests			
											Cylinders		Paddles	
	Test Number	2	3	4	5	6	7	9	10	12	8	14	In 738X test	U-500 test
CONTAMINANTS	(Sulfur (% in fuel	1	1	1	1	1	1	1	0	0	1	1	1	0†
	(Sodium (ppm in (fuel	45	18.5	18.5	5	5	5	0.5‡	0	0	5	5	5	0.5‡
	(Magnesium (ppm in (fuel	30	2.2	2.2	0.6	0.6	0.6	less than 0.1	0	0	0.6	0.6	0.6	less than 0.1
	(Chlorine (ppm in (fuel	0	0	0	8.6	0	8.6	0	0	0	8.6	0	0	0
	(Others	-	-	-	-	Water on back surface	-	-	-	Water on back surface	-	-	-	-
	(Total sea (salt in (air, ppm	3.6	1	1	0.25	0.25	0.25	0.02	0	0	0.25	0.25	0.25	0.02
	(Added to	Fuel	Fuel	Fuel	Air	Fuel	Fuel	-	-	-	Air	Fuel	Fuel	-
Metal temperature (°F)		1100-1250	1100-1450	1100-1500	1200-1600	1300-1600	1300-1600	1300-1600	1300-1600	1300-1600	1400-1500	1400-1500	1400-1500	1400-1500
Nominal gas temperature (°F)		1450	1750	1750	1750	1750	1750	1750	1750	1750	1450	1450	1450	1450
Specimen used		In 713C (2)	In 713C (2)	X-45 U-500	X-45 U-500	X-45 U-500	X-45 U-500	X-45 U-500	X-45 U-500	U-500 (2)	X-45 U-500	X-45 U-500	X-45 U-45 In 738 x (2)	U-500 (4)

† Small amount of sulfur (less than 0.1%) present in fuel.
‡ This amount originally present in fuel.

TABLE 10-XXIII

DEPOSIT AND CORROSION PRODUCTS ON SPECIMEN SURFACE (LEE AND YOUNG)

Test number	Specimen	Amount of deposit, g	Visual observation	X-Ray diffraction analysis
2	In 713C		Very heavy deposit No visible scales	
3	In 713C	1.861	Very heavy corrosion products Heavy scale	
4	X-45	0.698	No molten Na_2SO_4 Heavy scale on front surface	
4	U-500	0.638	Molten Na_2SO_4 on front and back surface mixed with corrosion products	
5	X-45	0.400	Patches of molten Na_2SO_4 on front Corrosion product on back	Na_2SO_4, $NiCr_2O_4$
5	U-500	0.514	Some molten Na_2SO_4 patches on front and back Corrosion product on all surfaces	Na_2SO_4, $NiCr_2O_4$ MgO·3NiO
6	X-45	0.118	Smaller amount of deposit than test 5 White water marks on back	White water marks are $CaSO_4$
6	U-500	0.119	Smaller amount of deposit than test 5 White water marks on back	MgO·3NiO $NiCr_2O_4$ Na_2SO_4, $CaSO_4$
7	X-45	0.363	Flaky corrosion products on front Patches of molten Na_2SO_4 on back	Na_2SO_4, $NiCr_2O_4$ MgO·3NiO, $MgAl_2O_4$
7	U-500	0.438	Patches of molten Na_2SO_4 on front and back	Na_2SO_4, MgO·3NiO $MgCo_2O_4$
9	X-45	0.182	Moderate amount of deposit, less than test 5, 6 or 7	Na_2SO_4
9	U-500	0.205	Moderate amount of deposit	Na_2SO_4
10	X-45	0.081	Very fine powder-like deposit on both front and back	NiO, $NiCr_2O_4$ NiCoO
10	U-500	0.118	Light-colored fine powder on both front and back	NiO, $NiCr_2O_4$
12	U-500	1.511 †	Powder-like deposit on front, heavy white water mark on back	NiO on front $CaSO_4$ on back
8	X-45	0.319	Very light deposit	$NiCr_2O_4$, Na_2SO_4 MgO·3NiO
8	U-500	0.168	Very light deposit	Na_2SO_4, $NiCr_2O_4$ MgO·3NiO
14	X-45	0.163	Light deposit	
14	U-500	0.172	Light deposit	
In 738 test	In 738 (A)	0.106		MgO·3NiO
	In 738 (B)	0.104		Na_2SO_4, $NiCr_2O_4$ MgO·3NiO
In 738 test	X-45	0.090		MgO·3NiO, $NiCr_2O_4$ Na_2SO_4
	U-500	0.076		Na_2SO_4, MgO·3NiO
U-500 test	U-500	0.027	Very light deposit	Na_2SO_4 $NiCr_2O_4$ MgO·3NiO

† Large due to water mark.

TABLE 10-XXIV

WEIGHT LOSS DATA (LEE AND YOUNG)

Test number	Specimen	Total weight loss, mg.	% Weight change	Specific weight loss, mg/cm^2	Modified specific weight loss, mg/cm^2	Visual observation	Metallographic examination
2	In 713C	-	-	-	-	Loss of metal on all surfaces. Some pits on sides. Moderate uniform attack on front.	
3	In 713C	2079.1	2.09	45.8	-	Deep concentrated attack on front. Uniform attack on back.	
4	X-45	726.8	0.69	15.9	13.1	Severe uniform attack on front. Moderate irregular attack on back.	
	U-500	438.4	0.44	9.6	6.6	Severe non-uniform attack on back.	
5	X-45	280.1	0.27	6.1	3.3	Non-uniform attack on front and back.	
	U-500	433.8	0.46	9.5	6.5	Uniform attack on all surfaces.	
6	X-45	268.9	0.26	5.9	3.1	Severe uniform attack on front. Moderate irregular attack on back.	
	U-500	247.4	0.25	5.4	2.5	Uniform moderate attack on front. Moderate irregular attack on back.	
7	X-45	398.8	0.41	8.7	5.9	Moderate uniform attack on front. Almost no attack on back.	
	U-500	532.8	0.55	11.7	8.7	Moderate uniform attack on all surfaces.	
9	X-45	346.7	0.33	7.6	4.8	Slight attack on all surfaces.	Sulphidation on outside. Oxidation on inside.
	U-500	498.7	0.51	10.9	8.0	Slight uniform attack on most surfaces. Some pits.	Sulphidation on outside. Oxidation on inside.
10	X-45	300.4	0.29	6.6	3.8	Very slight uniform attack on all surfaces.	Oxidation on all surfaces.
	U-500	315.3	0.33	6.9	3.9	Very slight uniform attack on all surfaces.	Oxidation on all surfaces.
12	U-500	131	0.14	2.9	-	Very slight uniform attack on front. Some pits on back.	Oxidation front. Sulphidation on back.

8	X-45	205.8	0.20	4.5	2.6	Slight attack on front and back	Outside sulphidation. Inside oxidation.	
	U-500	60.1	0.06	1.3	0.8	Slight attack on all surfaces.	Outside sulphidation. Inside oxidation.	
14	X-45	136.3	0.13	3.0	1.7	Slight attack on all surfaces.	Outside sulphidation. Inside oxidation.	
	U-500	434.4	0.47	9.5	5.4	Slight attack on all surfaces.	Outside sulphidation. Inside oxidation.	
738 test	In 738X (A)	63.6	0.19	2.5	2.5			
	In 738X (B)	58.6	0.17	2.3	2.3			
	X-45	66.5	0.21	2.6	2.6			
	U-500	47.4	0.14	1.8	1.8			
U-500 test	U-500 (A)	56.0	0.17	2.2	2.2			
	(B)	59.8	0.18	2.3	2.3			
	(C)	51.8	0.16	2.0	2.0			
	(D)	38.8	0.12	1.5	1.5			

TABLE 10-XXV

SUMMARY OF WEIGHT OF SURFACE SCALE VISUAL RATINGS AND WEIGHT LOSS (QUIGG ET AL)

Superalloy	Exposure Time, hrs.	Weight of Surface Scale, mg/cm^2 (b) 0.0004% S	(c) 0.004% S	(d) 0.04% S	Visual Rating and Weight Loss (b) 0.0004% S Rating	mg/cm^2	(c) 0.004% S Rating	mg/cm^2	(d) 0.04% S Rating	mg/cm^2
B-1900	5	2.32	7.11	3.63	7	2.51	7	11.25	9	3.4
B-1900	5	1.22	3.38	2.54	9	0.94	7	2.77	9	1.9
B-1900	10	2.22	7.52	8.93	8	1.87	5	13.49	7	21.0
B-1900	15	4.57	14.93	14.57	7	6.39	5	63.18	6	68.1
B-1900	15	1.43	12.82	6.25	7	1.28	5	48.95	8	52.3
B-1900	20	5.01	18.90	23.09	7	4.97	5	77.77	7	132.6
Mar M-246	5	6.74	11.88	11.78	6	6.95	5	24.72	7	37.47
Mar M-246	5	5.36	9.20	8.03	9	4.43	6	22.10	8	13.49
Mar M-246	10	7.81	18.39	9.78	6	15.53	5	32.64	7	43.19
Mar M-246	15	9.44	21.22	14.81	6	11.43	5	87.35	7	83.70
Mar M-246	15	7.73	21.56	16.29	6	24.41	4	73.84	6	80.82
Mar M-246	20	10.08	42.11	20.94	7	23.92	3	85.15	6	143.64
Mar M-200	5	8.87	13.71	16.96	6	16.94	6	49.13	7	31.64
Mar M-200	5	11.00	11.75	11.58	7	10.35	6	18.26	7	29.61
Mar M-200	10	8.53	20.97	13.08	6	9.08	5	45.90	6	44.04
Mar M-200	15	13.07	23.97	27.76	6	60.53	5	96.50	7	132.67
Mar M-200	15	13.21	19.24	16.57	6	14.73	6	74.15	8	110.57
Mar M-200	20	10.45	29.33	14.26	7	8.53	5	99.92	8	142.38
IN-100	5	4.74	5.44	10.41	9	3.54	6	10.18	6	29.79
IN-100	5	1.82	6.62	5.30	7	1.38	5	11.56	8	6.86
IN-100	10	12.20	10.71	12.80	6	14.19	6	43.37	7	45.33
IN-100	15	10.22	9.48	14.96	7	10.28	6	37.95	6	93.78
IN-100	15	5.84	9.07	10.28	7	5.08	6	26.42	8	73.17
IN-100	20	4.56	15.67	9.84	8	4.03	5	71.90	7	130.94
Inconel 713C	10	4.08	7.96	10.06	8	3.56	6	7.34	6	26.22
Inconel 713C	10	3.81	9.19	11.86	9	3.36	7	8.02	7	27.92
Inconel 713C	20	8.05	7.72	9.66	6	11.33	7	7.20	6	68.39
Inconel 713C	20	4.23	16.40	12.06	9	4.90	5	40.55	7	74.25
Inconel 713C	30	10.40	9.02	10.45	7	14.42	5	49.37	6	130.81
Inconel 713C	30	16.26	15.27	14.66	6	17.60	4	85.07	6	165.11
Inconel 713C	40	12.00	8.40	9.72	6	30.17	4	53.16	5	180.16
Inconel 713C	40	12.78	14.69	11.43	6	33.36	4	123.86	5	219.68
Udimet 700	10	3.79	8.56	5.46	9	3.68	6	7.95	9	5.13
Udimet 700	10	3.45	4.51	5.03	9	3.42	7	4.03	9	4.30
Udimet 700	20	6.76	11.57	10.12	8	6.29	6	19.32	6	36.84
Udimet 700	20	5.18	10.17	10.53	8	5.26	6	23.19	8	29.44
Udimet 700	30	7.85	6.75	18.94	6	28.49	5	30.69	6	109.47
Udimet 700	30	8.72	13.58	13.58	6	12.40	5	62.10	6	86.07
Udimet 700	40	9.87	11.20	20.26	5	63.52	4	62.84	6	139.38
Udimet 700	40	8.39	16.60	16.71	6	23.62	4	110.51	6	145.84
IN-738	10	2.50	5.90	6.33	9	2.63	9	5.49	9	5.88
IN-738	20	6.31	17.56	10.80	8	5.84	6	25.81	8	12.96
IN-738	30	8.05	24.21	11.24	6	12.73	5	29.04	7	31.14
IN-738	40	8.43	20.81	12.11	7	13.65	5	44.03	7	56.67
IN-738	60	12.85	38.36	18.47	6	39.96	5	94.12	6	156.49
Udimet 710	10	4.78	5.67	5.46	8	6.25	7	5.48	9	5.41
Udimet 710	20	8.79	9.97	8.66	7	10.26	5	12.33	7	14.28
Udimet 710	30	6.57	18.28	11.82	8	6.29	5	34.25	7	19.66
Udimet 710	40	8.88	14.72	24.72	6	30.29	3	59.33	7	65.41
Udimet 710	60	10.59	13.70	27.11	6	52.65	4	69.65	6	108.94
Udimet 710	80	12.06	22.50	22.74	6	61.32	4	145.05	6	190.60

WI-52	20	8.93	15.57	15.53	6	57.73	5	53.52	7	27.14
WI-52	25	9.47	17.25	21.20	6	48.39	4	79.45	7	47.37
WI-52	40	9.91	24.37	24.43	5	55.23	4	121.53	7	89.07
WI-52	55	8.44	25.66	27.70	5	102.04	4	147.31	6	103.32
WI-52	70	12.62	30.78	32.37	4	175.60	4	160.95	6	125.52
Mar M-509	20	15.02	15.80	9.03	5	14.64	6	13.86	9	9.34
Mar M-509	25	18.47	20.67	23.16	8	17.42	7	23.55	9	20.70
Mar M-509	40	19.23	19.74	17.82	6	21.62	6	26.78	7	22.95
Mar M-509	40	21.84	20.26	18.40	6	29.17	7	18.99	8	21.78
Mar M-509	55	22.70	26.66	21.57	7	27.54	6	39.12	7	31.89
Mar M-509	55	23.85	18.84	17.38	6	35.64	6	24.75	8	33.85
Mar M-509	70	22.96	33.45	19.32	7	29.04	5	52.46	6	38.16
Mar M-509	70	20.49	19.01	20.93	7	29.66	5	41.65	7	53.35
Mar M-302	20	4.61	16.69	13.04	8	5.06	6	16.65	8	12.13
Mar M-302	25	4.08	16.65	17.98	7	4.43	6	28.76	8	21.18
Mar M-302	40	18.49	18.99	22.10	7	22.80	6	37.34	8	34.83
Mar M-302	55	20.20	22.87	26.91	6	28.71	6	39.46	7	41.52
Mar M-302	70	23.43	19.77	20.66	6	34.02	5	35.78	7	53.84
X-40	20	9.55	14.88	12.76	7	10.33	5	17.83	9	12.25
X-40	25	11.52	12.71	12.40	8	12.64	7	19.17	9	11.49
X-40	55	18.70	22.36	16.89	6	26.75	5	39.14	7	27.52
X-40	85	19.05	23.49	24.69	6	34.29	5	55.63	6	53.40
X-40	115	20.26	35.62	44.00	6	58.49	4	90.38	6	89.36
Ai-Resist	15	5.95	3.43	5.14	6	5.10	7	3.22	9	4.65
Ai-Resist	40	8.32	15.04	15.76	7	6.96	5	12.78	8	14.14
Ai-Resist	45	10.45	16.94	18.59	7	8.66	6	14.07	8	16.89

(b) 1 ppm sea salt in air.
0.0004 weight per cent sulfur in fuel.

(c) 1 ppm sea salt in air.
0.004 weight per cent sulfur in fuel.

(d) 1 ppm sea salt in air.
0.04 weight per cent sulfur in fuel.

TABLE 10-XXVI

SUMMARY OF X-RAY DIFFRACTION ANALYSES OF SCALE RESULTING FROM HIGH-TEMPERATURE EXPOSURE OF SUPERALLOY TEST SPECIMENS TO DIFFERENT FUEL-SULFUR CONCENTRATIONS (QUIGG ET AL)

		X-Ray Diffraction Results for Scale Composites[a]											
		Bunsenite (NiO)			Mixed Spinel Structures			Unidentified Patterns			Other Patterns Indicated		
Super-alloy	Coating	S_0	S_1	S_2	S_0	S_1	S_2	S_0	S_1	S_2	S_0	S_1	S_2
B-1900	None	S	S	S	S^b	W^b	S^b	S	W^g	S	NiF_2	NiF_2	NiF_2
MM-246	None	S	S	S	S^b	S^b	S^b		W^g	S	NiF_2	NiF_2	
MM-200	None	S	S	S	S^b	S^b	S^b	S	$?^f, W^g$	S		NiF_2	
IN-100	None	...	S	S	...	S^b	S^b	...		W	...	Na_2SO_4	
I-713C	None	S	S	S	S^b	S^b	S^b	S	W^g	S		NiF_2	NiF_2
U-700	None	S	S	S	S^d	S^b	S^b			W		Na_2SO_4	
IN-738	None	S	S	S	S^d	$?^c$	$S^c, ?^b$		W^g	S		NiF_2	
U-710	None	S	W	S	S^d	S^b	$S^c, ?^b$	S		W	NiF_2		
WI-52	None				S^d	W^b	S^b		W^g		CoO	CoO	CoO
MM-509	None				S^d	W^b	W^b	S	W^g	W	$CoNiO_2$, Na_2SO_4(?)	CoO	CoO

MM-302	None		W^b	S^b		S^g	S	$CoNiO_2$, Na_2SO_4(?)	CoO	CoO
X-40	None		S^d	W^b	W^b	S	W	S	$CoNiO_2$	CoO	CoO
AR-215	None	...		...		...		W	...	CoO	CoO

(a) Samples analyzed represent a composite of the loosely-adhering scale from all exposed test specimens (i.e., for all time periods) in a given superalloy-coating system
b Unidentified cubic structure
c Nickel chromite ($NiCr_2O_4$)
d Cobalt chromite ($CoCr_2O_4$)
e Nickel Aluminite ($NiAl_2O_4$)
f Possibly sodium tungstate dihydrate ($Na_2WO_4 \cdot 2H_2O$)
g Possibly sodium cobalt (II) fluoride
S_0 Fuel containing 4 ppm sulfur
S_1 Fuel containing 40 ppm sulfur
S_2 Fuel containing 400 ppm sulfur

Response Designation:
S = Strong pattern observed
W = Weak pattern observed
? = Pattern not positively identified
(...) = Analysis not performed due to insufficient sample

TABLE 10-XXVII

QUANTITATIVE ELECTRON-MICROPROBE ANALYSIS OF SULPHIDES IN SITU (ERDOS)

Phase	*Alloy*	*Sulphidation procedure*	*Analysis in at %* Ni	Co	Cr	Ti	Al	Mo	Nb	Ta	S
Cr_2S_3	Nim 80A	S_2 780 168 h	7.4		30.0	3.1	0.0				59.4
Cr_2S_3	Nim 105	S_2 800 96 h	6.8	5.5	24.9	5.9	0.0	2.4			54.4
Cr Al S	Nim 105	S_2 800 96 h	6.8	1.9	20.9	0.1	7.7	5.8			56.7
Cr Al S	IN 713 LC	diphatic melt* 800 168 h	9.3		19.7	0.3	9.1	2.2	0.5		58.8
NiS	IN 713 LC	S_2 850 15 h	8.5		3.6	0.6	0.0	4.6	24.3	0.6	57.7
$CrS_{(x)}$	IN 713 LC	N_2S 900 96 h	5.1		26.7	2.1	0.3	2.3	1.8		61.7

Analyses are confirmed by semiquantitative microprobe analysis of various alloys of Table 1

Composition of sulphatic melt: 53 Mole % Na_2SO_4
40 Mole % $MgSO_4$
7 Mole % $CaSO_4$

Atmosphere above the melt: air

TABLE 10-XXVIII

SUBSEQUENT SULPHIDATION AND OXIDATION OF IN 713 LC

X-RAY DIFFRACTION ANALYSIS (ERDOS)

Treatment	*Identifiable phases*
as cast + 24 h 900 C O_2	Cr_2O_3, α-Al_2O_3 'Rutile', $NiMoO_4$
0.23 mg cm^{-2} S 16 h 900 C	Cr_2S_3, CrS? + Ni
+ 24 h 900 C O_2	Cr_2O_3, trace α-Al_2O_3, 'Rutile'
+ 168 h 900 C air	Cr_2O_3, $NiCr_2O_4$, NiO, α-Al_2O_3, 'Rutile', $NiMoO_4$
96 h 800 C, N_2S_2 in vacuum	Cr_2S_3, Cr Al S
+ 24 h 900 C O_2	NiO, $NiCr_2O_4$, Cr_2O_3, trace α-Al_2O_3, 'Rutile', $NiMoO_4$
+ 168 h 900 C air	NiO, $NiCr_2O_4$, trace Cr_2O_3, trace α-Al_2O_3, 'Rutile', sometimes trace Ni_3S_2, $NiMoO_4$
96 h 900 C, N_2S_2 in vacuum	Cr_2S_3, sometimes traces of α-Al_2O_3
+ 24 h 900 C O_2	NiO, Cr_2O_3, $NiCr_2O_4$, α-Al_2O_3, 'Rutile', sometimes Ni_3S_2, $NiMoO_4$
+ 168 h 900 C air	the same as above

Remarks: $NiCr_2O_4$: a spinelphase with a_0 = 8.30–8.33 Å. 'Rutile' a phase of Rutile structure, tetragonal, P 4$_2$/mnm, a = 4.67 Å, c = 3.01 Å, c/a = 0.645

TABLE 10-XXIX

CORROSION RATES AS A FUNCTION OF TEMPERATURE (FELIX)

Material	750 C (μm/300 h)	850 C (μm/300 h)	950 C (μm/300 h)
Nim 80A	55	80	135
Nim 105	10	230	113
IN-713 LC	68	1 040	1 600
IN-738	30	120	200
M-421	36	130	428
M-246	210	330	580

TABLE 10-XXX

RESULTS OF HOT-CORROSION BURNER-RIG TESTS ON COMMERCIAL NICKEL AND COBALT SUPERALLOYS*† (WHEATFALL)

Alloy Class	*Item No.*	*Alloy*	*Loss in Diameter (Surface loss/max. penetration (mils))*			
			1600°F/500 hr.	*1600°F/1000 hr.*	*1750°F/1000 hr.*	*1800°F/1000 hr*
Nickel-base	1	SEL	22.7/45.8	62.3/69.3	31.5/51.8	2.1/11.4
	2	Inco 713C	130 + **	–	59.0/77.1 to 130 + **	130 + **
	3	SEL-15	130 + **	–	130 + **	–
	4	IN-100	130 + **	–	130 + **	–
	5	Mar-M200	38.4/64.4	–	130 + **	–
	6	Udimet 500	1.3/7.6	2.7/12.4	8.8/31.7	5.5/29.3
	7	Udimet 700	39.6/66.0 to 130 + **	–	45.9/63.9	–
	8	René 41	2.6/10.3	–	–	6.8/30.8
	9	Hastelloy X	–	1.3/8.5	1.8/12.0	1.3/15.2
Cobalt-base	10	X-40	0.6/4.2	–	1.0/11.6	–
	11	Mar-M302	0.8/5.4	–	3.5/10.0	–
	12	Mar-M509	–	–	2.1/10.9	–
	13	WI-52	15.6/21.4	–	6.6/18.2	–
	14	L-605	–	1.0/8.6	5.5/15.3	1.8/11.3

* Data from Bergman et al

† Test Conditions: 5 ppm sea salt (in air); 30/1 air/fuel ratio (by wt);

** Specimen completely penetrated.

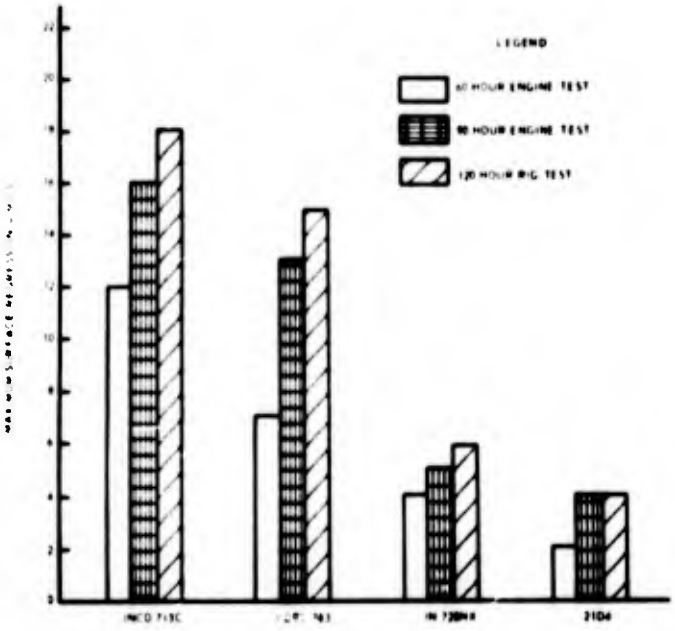

Figure 10.1. Relative performance of superalloys investigated in engine (Salt/Air ratio: 1 ppm) and rig (Salt/Air ratio: 6 ppm) tests. (Walters).

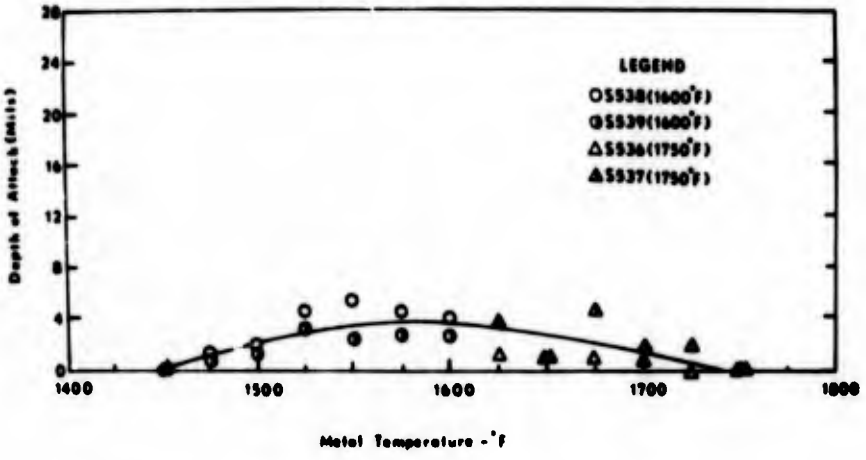

Figure 10.2. Corrosion as a function of temperature for Inco 713C tested using JP-4 fuel with a Salt/Air ratio of 8 ppm. (Walters).

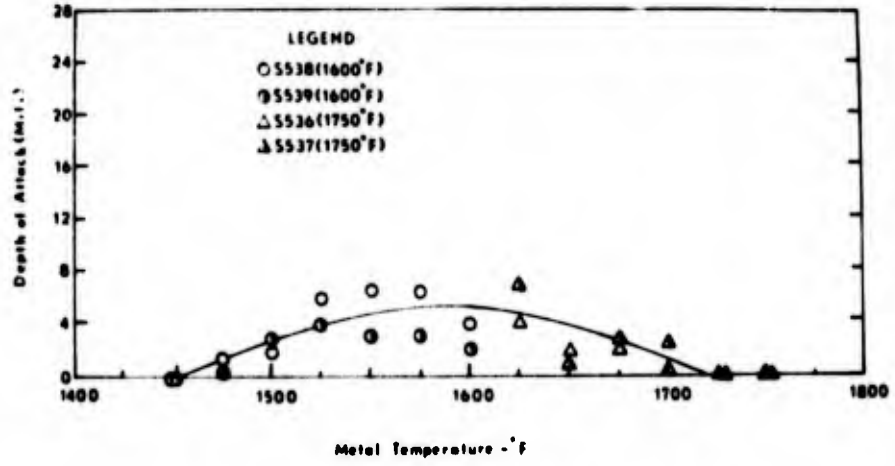

Figure 10.3. Corrosion as a function of temperature for Inco 713LC tested using JP-4 fuel with a Salt/Air ratio of 8 ppm. (Walters).

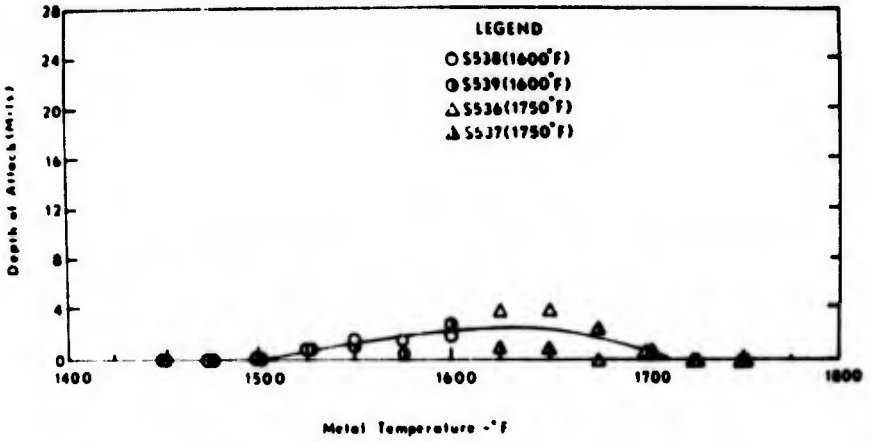

Figure 10.4. Corrosion as a function of temperature for Inco 713C tested using JP-4 fuel with a Salt/Air Ratio of 4 ppm. (Walters).

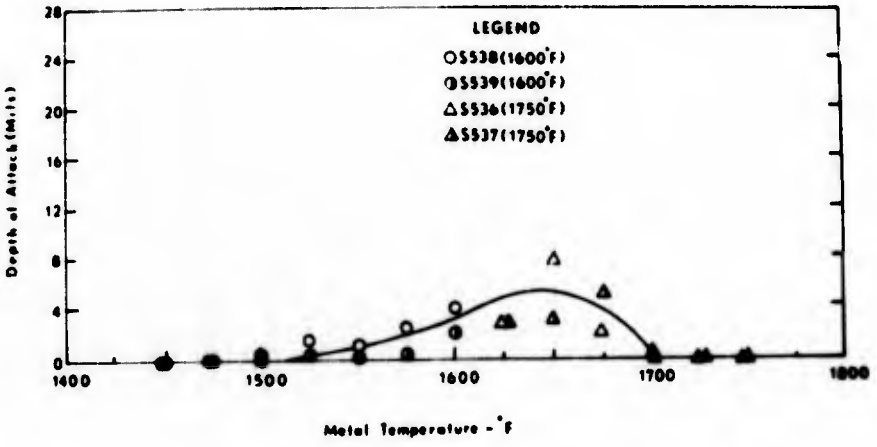

Figure 10.5. Corrosion as a function of temperature for Inco 713LC tested using JP-4 fuel with a Salt/air Ratio of 4 ppm. (Walters).

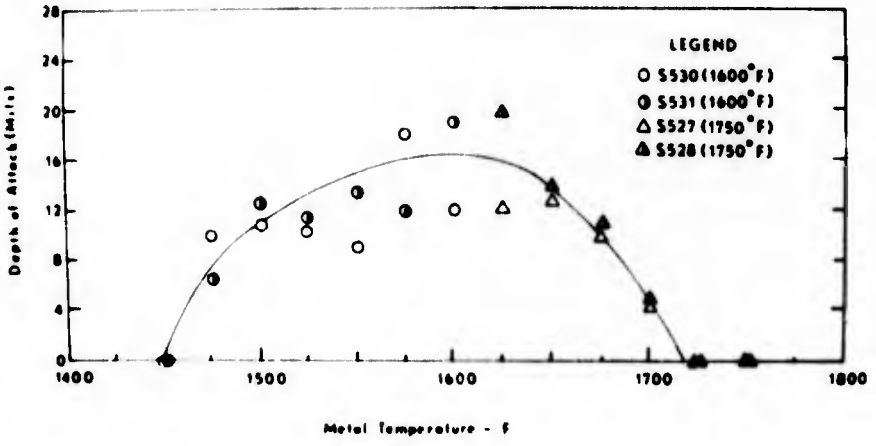

Figure 10.6. Corrosion as a function of temperature for Inco 713C using JP-4R fuel with a Salt/ Air Ratio of 8 ppm. (Walters).

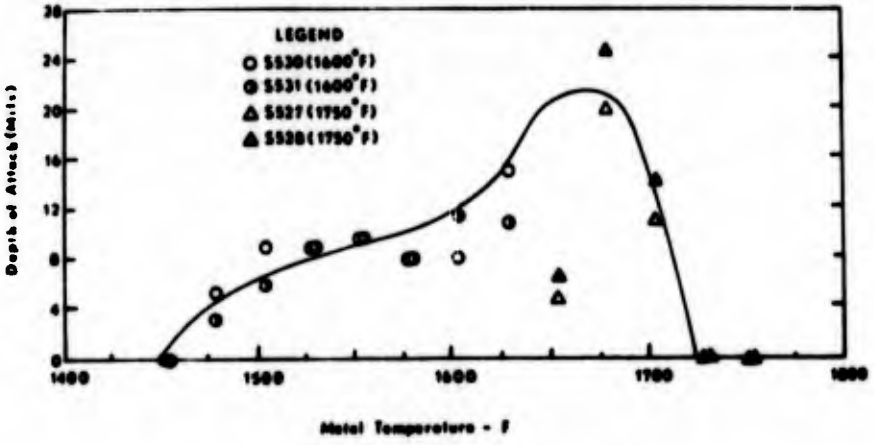

Figure 10.7. Corrosion as a function of temperature for Inco 713LC using JP-4R fuel with a Salt/ Air Ratio of 8 ppm. (Walters).

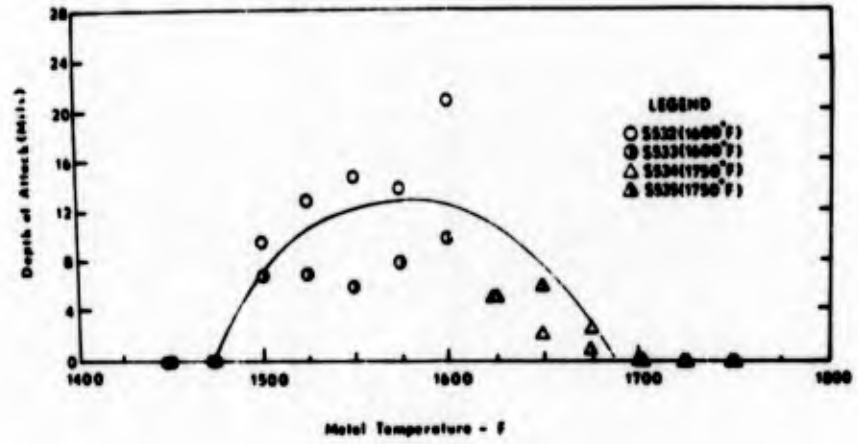

Figure 10.8. Corrosion as a function of temperature for Inco 713C using JP-4R fuel with a Salt/ Air Ratio of 4 ppm. (Walters).

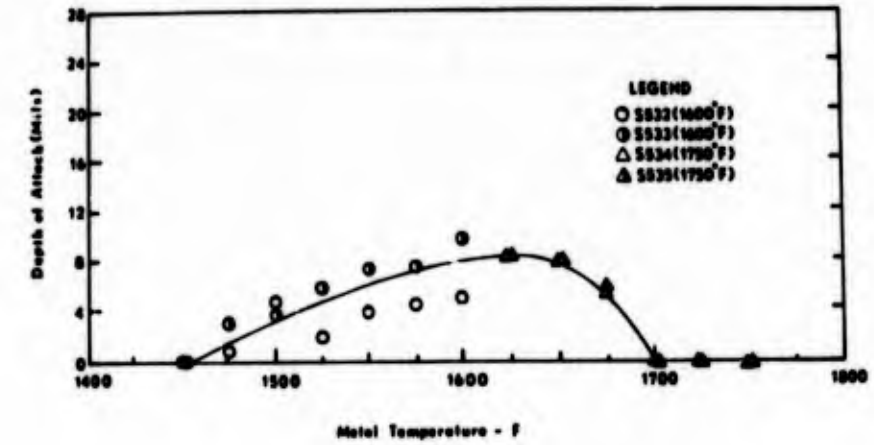

Figure 10.9. Corrosion as a function of temperature for Inco 713LC using JP-4R fuel with a Salt/ Air Ratio of 4 ppm. (Walters).

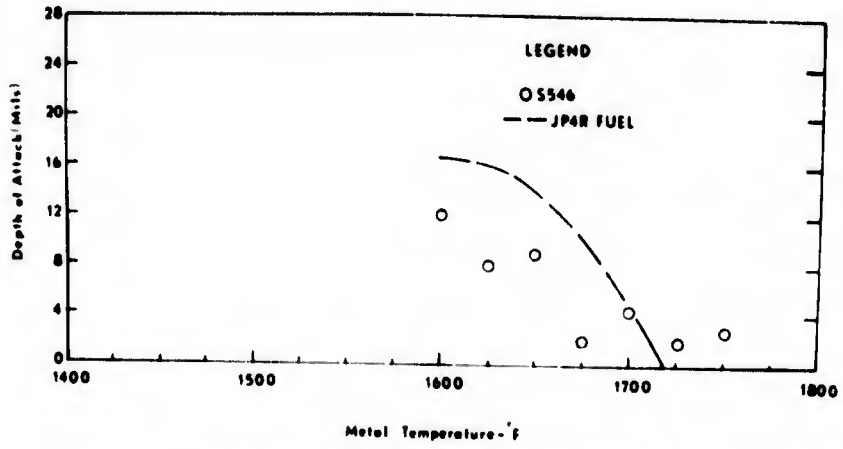

Figure 10.10. Corrosion as a function of temperature for Inco 713C tested using JP-5 fuel (0.16%S) with a Salt/Air Ratio of 8 ppm. (Walters).

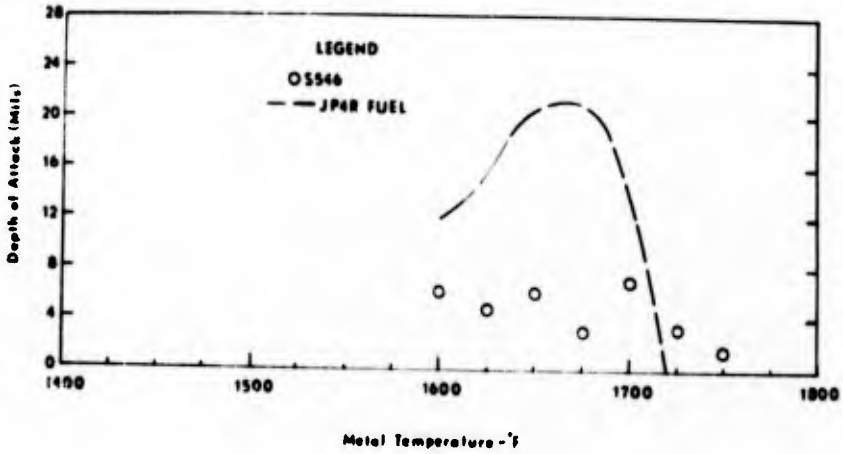

Figure 10.11. Corrosion as a function of temperature for Inco 713LC tested using JP-5 fuel (0.16%S) with a Salt/Air Ratio of 8 ppm. (Walters).

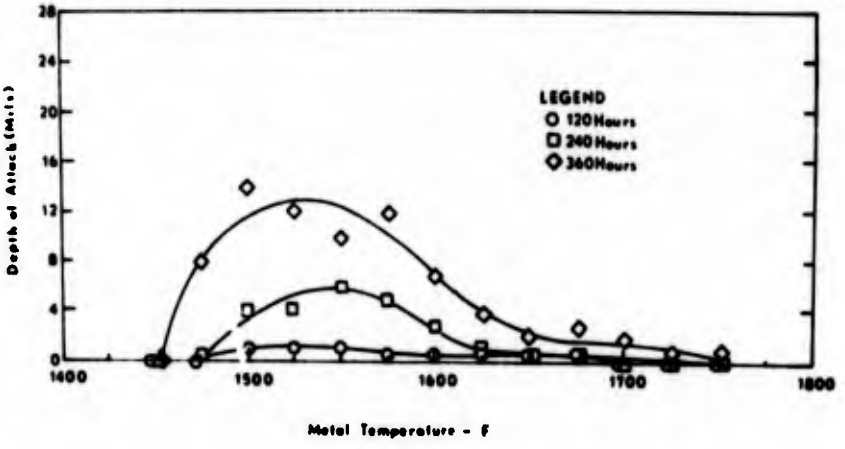

Figure 10.12. Corrosion as a function of temperature for Inco 713C tested using JP-4 fuel with a Salt/Air Ratio of 4 ppm. (Walters).

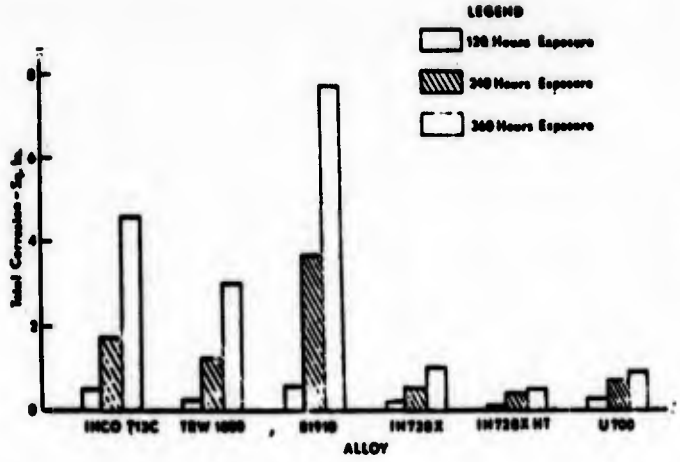

Figure 10.13. Variation of Total corrosion with time for alloys tested using JP-4 fuel and a Salt/ Air Ratio of 4 ppm. (Walters).

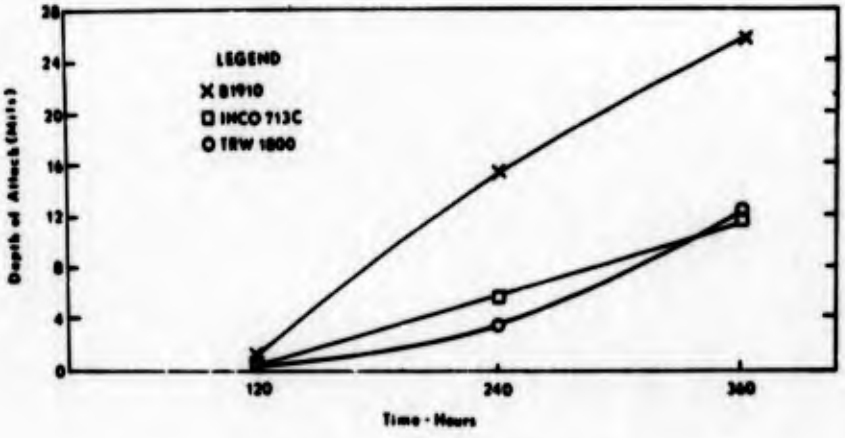

Figure 10.14. Depth of Attack at 1550°F as a function of time of exposure. (Walters).

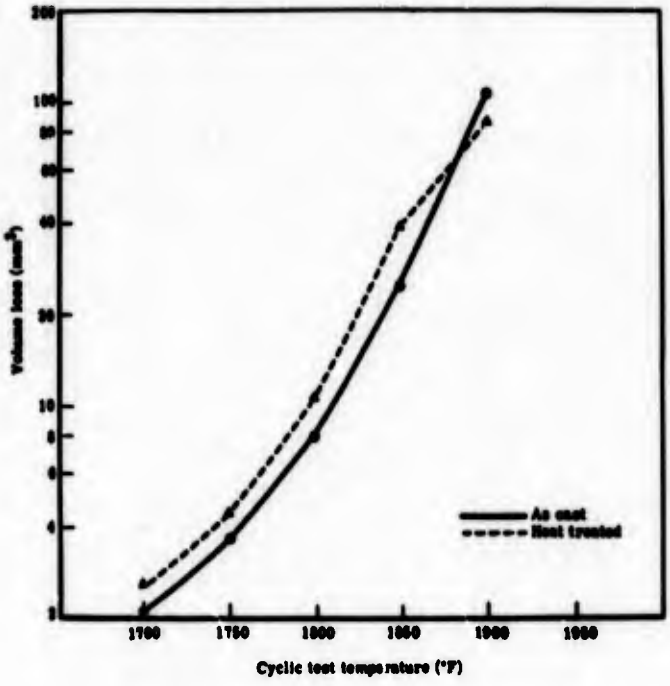

Figure 10.15. As-cast versus heat treated Alloy 713C at each cyclic test temperature. (Ryan et al).

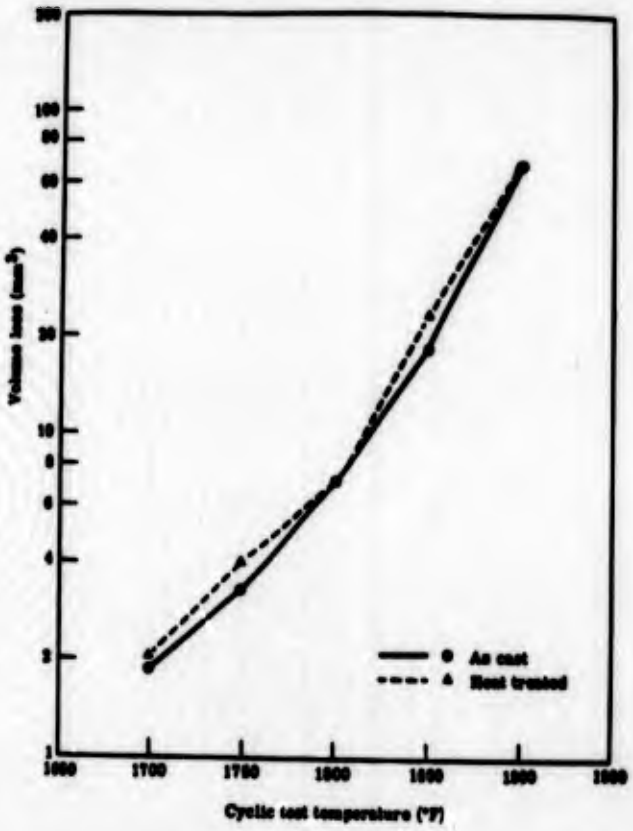

Figure 10.16. As-cast versus heat treated Alloy 713C + 2% Cr at each cyclic test temperature. (Ryan et al).

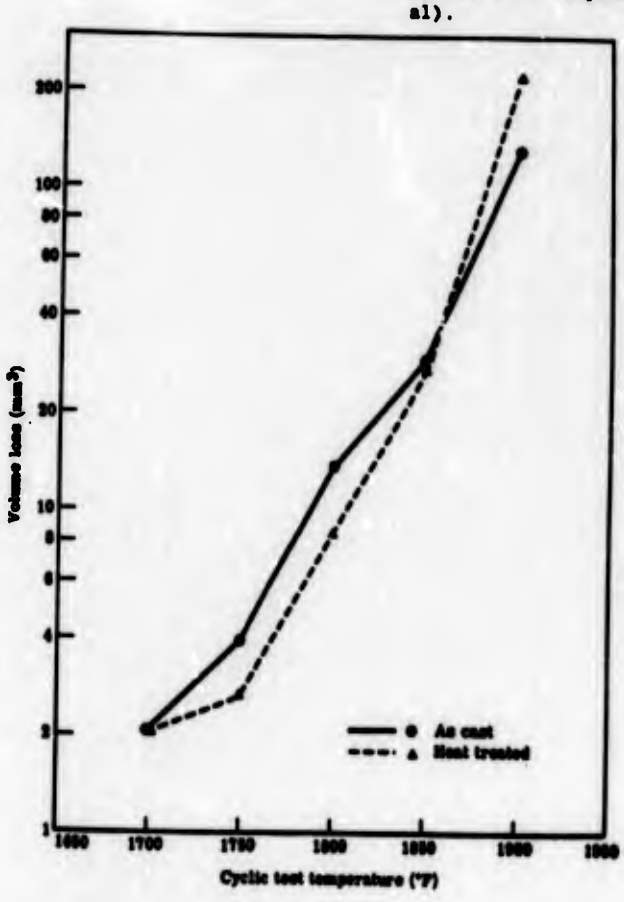

Figure 10.17. As-cast versus heat treated Alloy 713C + 2% Cr + Y at each cyclic test temperature. (Ryan et al).

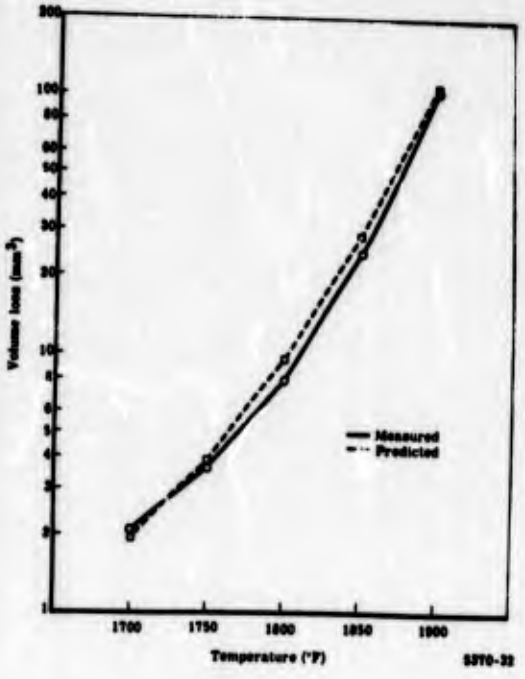

Figure 10.18. Comparison of the measured volume loss and the loss predicted by the regression equation for Alloy 713C. (Ryan et al).

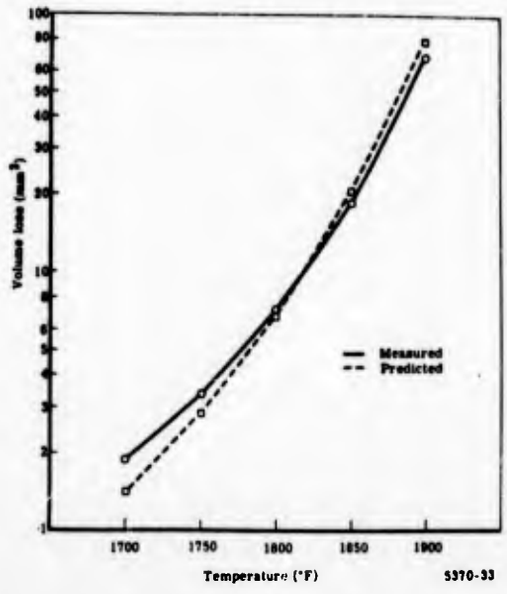

Figure 10.19. Comparison of the measured volume loss and the loss predicted by the regression equation for Alloy 713C + 2% Cr. (Ryan et al).

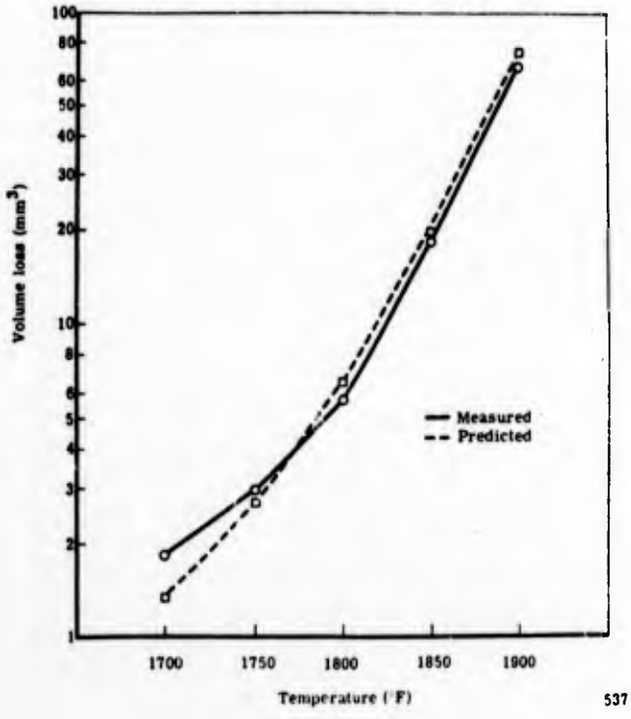

Figure 10.20. Comparison of the measured volume loss and the loss predicted by the regression equation for Alloy 713C + 2% Cr + Y. (Ryan et al).

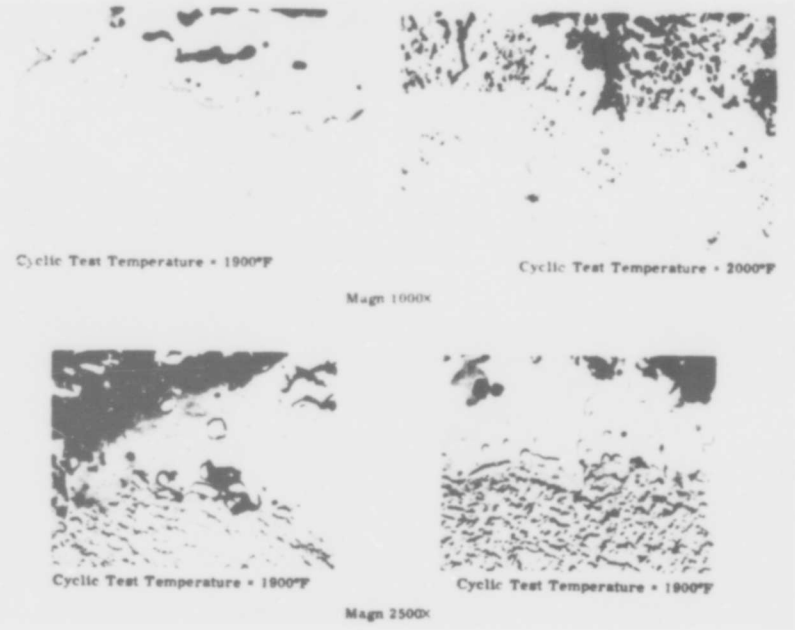

Figure 10.21. Light and electron micrographs of corrosion on Alloy 713C after 1000 and 2000°F cyclic tests. (Ryan et al).

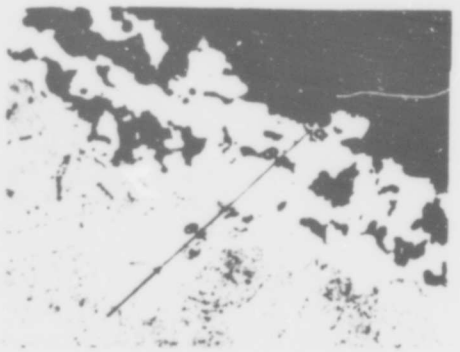

Microprobe traverse on Alloy 713C – 1800°F cyclic test

Location on traverse	Oxide → α	Depletion zone α→β→γ	Sulfide γ	Depletion zone sulfides γ→β	Matrix interface β	Matrix
Element	Relative composition					
Nickel*	51-81	78-92	28	65-91	72	72
Chromium*	1-6	1	2*	1-12	12	13.2
Sulfur**	2-5	1-4	93	2-23	1	1
Aluminum*	9-26	2 (β 14)	2	2-3	4-5	6-3
Molybdenum*	4 1/2-6	2 1/2-4	2 1/2	2 1/2-3	4	4 1
Niobium**	3-7	2-3	4	3	5	5
Titanium**	1-7	1	1 1/2	1/2	2	2 1/2

*Approximate weight percent
**X ray intensity – compare with matrix

Figure 10.22. Microprobe traverse across corrosion area of Alloy 713C after 1800°F cyclic test. (Ryan et al).

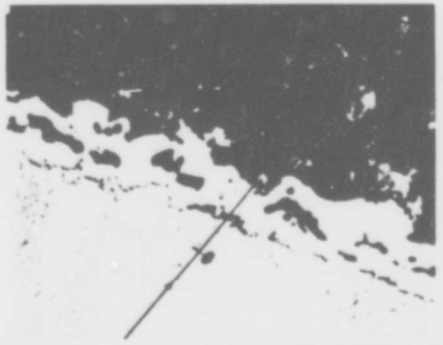

Magn 500× Etchant: ferric chloride No. 2

Microprobe traverse on Alloy 713C – 1900°F cyclic test.

Location on traverse	Oxide α	Depletion zone β→γ	Sulfide γ	Interface γ→	Matrix
Element	Relative composition				
Nickel*	30-60	86-88	22	72	72
Chromium*	4-18	1-2	27	12	13.2
Sulfur**	2-15	2-3	77	1 1/2	1 1/2
Aluminum*	5-32	2-3	2	6	6.3
Molybdenum*	1 1/2	4-5	3 1/2	4 1/2	4.7
Niobium**	1-3		1 1/2	1 1/2	1 1/2
Titanium**	2-10	1-2	8	5	5

* Approximate weight percent

** X-ray intensity – compare with matrix

Figure 10.23. Microprobe traverse across corrosion area of Alloy 713C after 1900°F cyclic test. (Ryan et al).

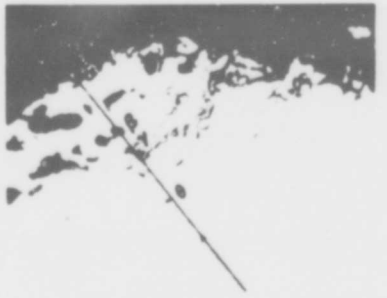

Magn. 500× Etchant: ferric chloride No. 2

Microprobe traverse on modified chromium alloy 713C

Location on traverse	Oxide →α	Depletion zone α→β	Oxide β	Depletion zone β→	Sulfide γ	Matrix θ
Element	Relative Composition					
Nickel*	20-45	84-87	59	68-86	35	70
Sulfur**	2 1/2-4	2-4	2	2	80	2
Titanium**	20-40	3-4	3	2 1/2	10	12 1/2
Chromium*	7-16	1 1/2-2	1 1/2	1 1/2-2	23	15.7
Molybdenum*	2	4-7	4	3-4	4	4.7
Niobium**	2-11	2-2 1/2	2	2-3	3	4
Aluminum*	10-35	2	8	3	2 1/2	5.9

* Approximate weight percent

** X-ray intensity – compare with matrix

Figure 10.24. Microprobe traverse across corrosion area of Alloy 713C + 2% Cr after 1800°F cyclic test. (Ryan et al).

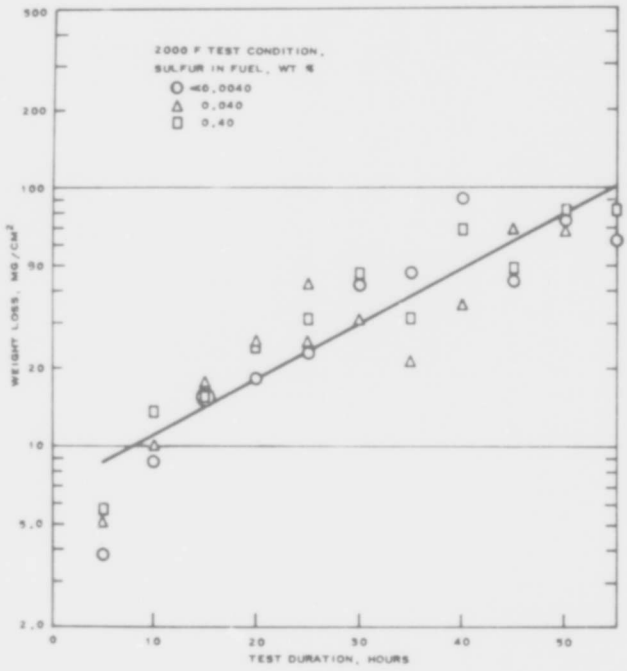

Figure 10.25. Hot Corrosion of Inconel 713C with zero sea salt in air (Quigg and Schirmer).

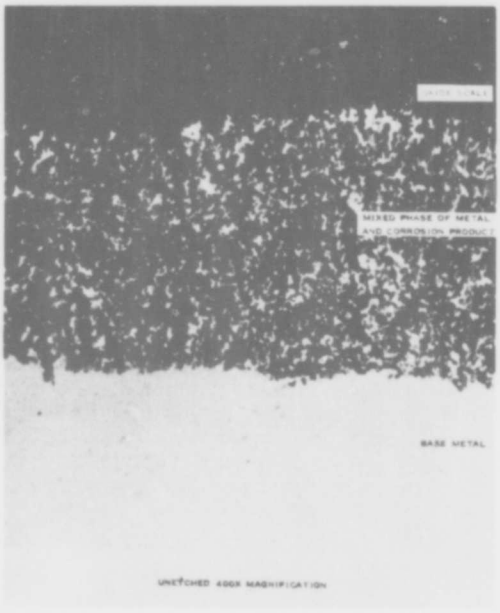

Figure 10.27. Hot Corrosion of Inconel 713C turbine blade. (Quigg and Schirmer).

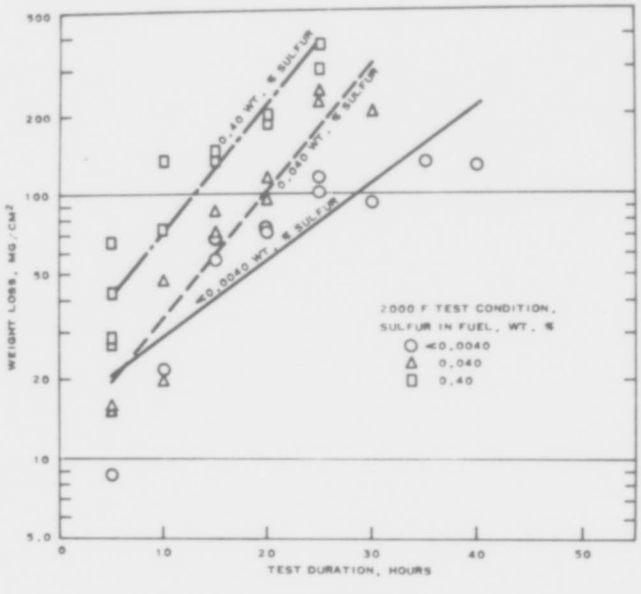

Figure 10.26. Hot Corrosion of Inconel 713C with 1.0 ppm sea salt in air (Quigg and Schirmer).

Figure 10.28. Hot Corrosion of Inconel 713C Specimen (Quigg and Schirmer).

25 hours at 2000F test condition with 1.0 ppm sea salt and 0.4 wt % sulphur Marble's reagent etch. 4000 X Mag.

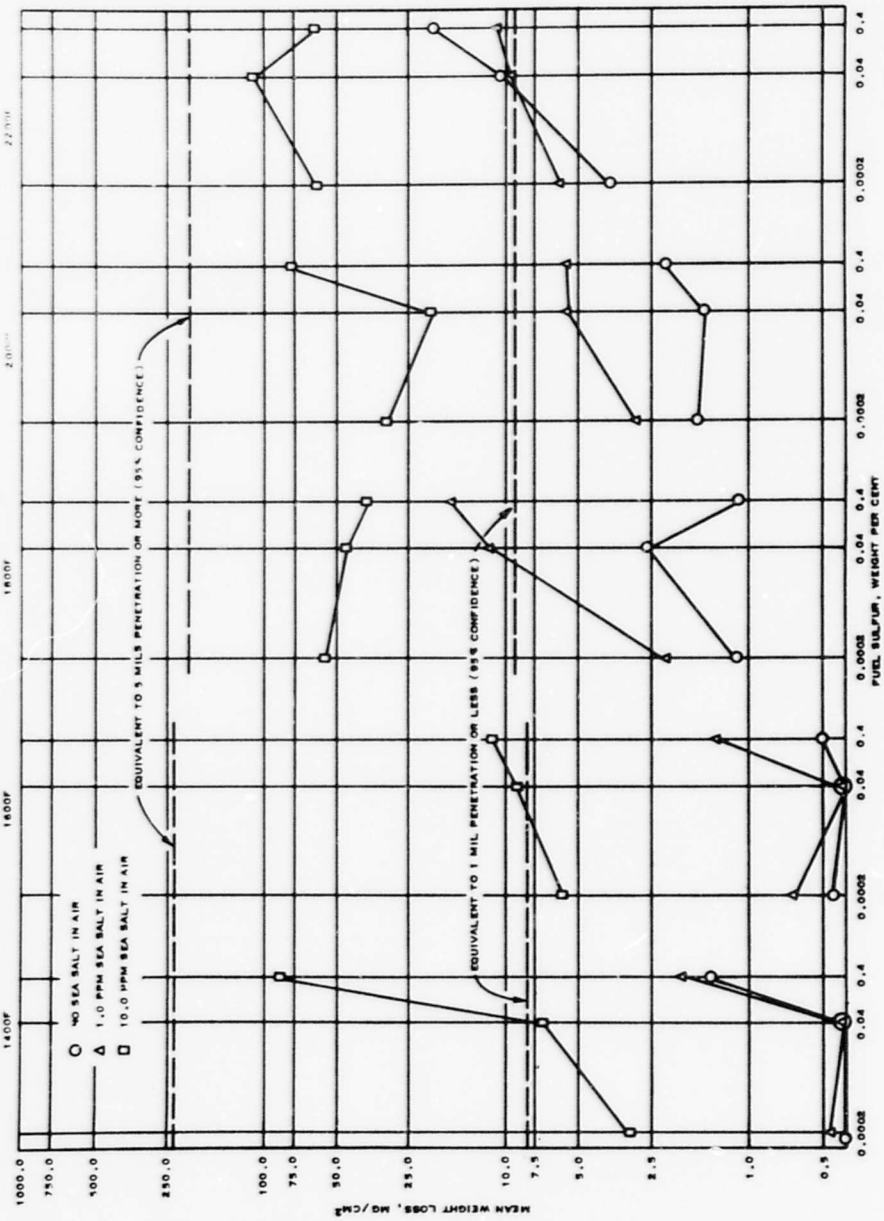

Figure 10.29. Effect of fuel sulphur sea salt in air and gas temperature on metal loss of Inco 713C test specimens. (Schirmer and Quigg)

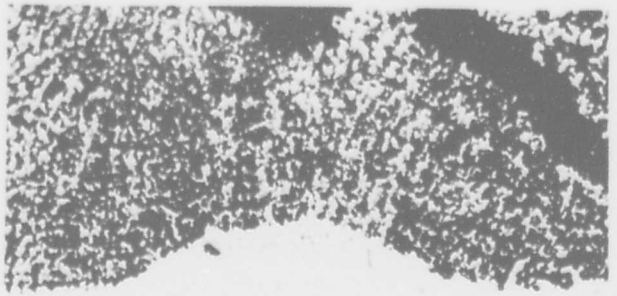

SURFACE ROUGHENED

BASE METAL
UNETCHED
200X

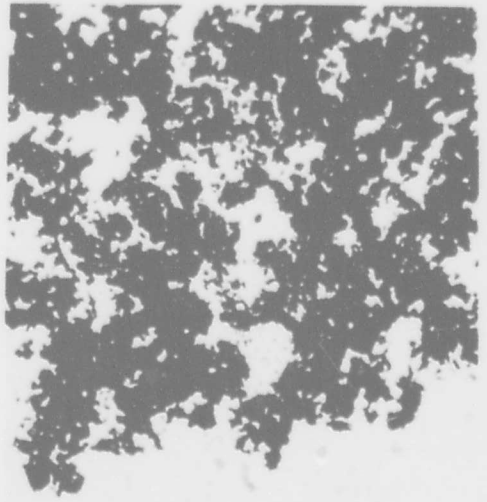

INTERDENDRITIC OXIDATION

HEAVY SULFIDE PENETRATION

UNETCHED
2000X

Figure 10.30. Hot Corrosion of Inco 713C turbine blade operated in South Pacific for 600 hours. (Schirmer and Quigg).

SURFACE ROUGHENED

BASE METAL
UNETCHED
200X

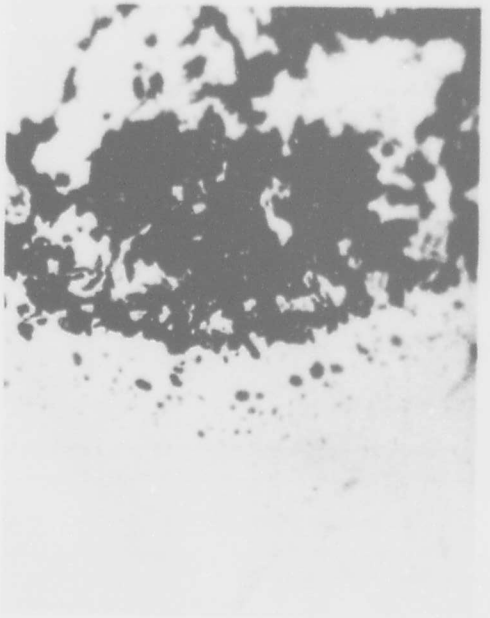

INTERDENDRITIC OXIDATION

HEAVY SULFIDE PENETRATION

BASE METAL
UNETCHED
2000X

Figure 10.31. Hot Corrosion of Inco 713C in Phillips Rig. (Schirmer and Quigg).

5 hours exposure at 2000F test condition with 10 ppm sea salt in air and 0.0002 wt % sulphur in fuel.

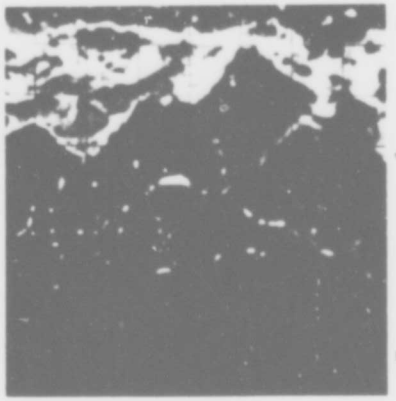

SPECIMEN CURRENT OF SECTION X1776
(LOW MOLECULAR WEIGHT MATERIAL IS LIGHT)

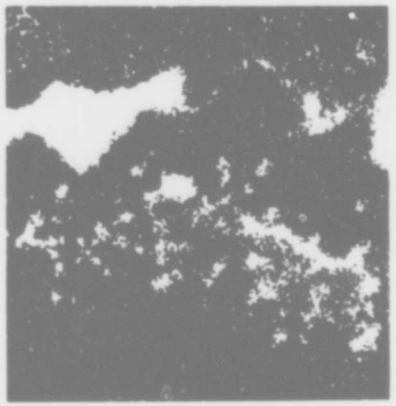

SULFUR K_α X – RAY OF SECTION X1776
(SULFIDES ARE LIGHT)

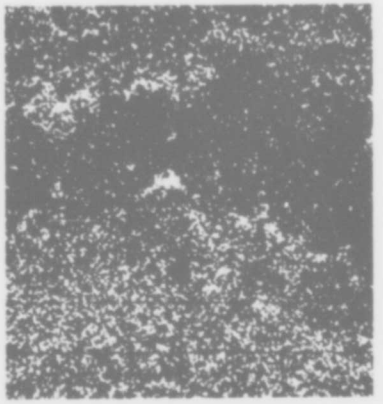

CHROMIUM K_α X – RAY OF SECTION X 1776
(CHROMIUM DEPLETED AREA IS DARK)

Figure 10.32. Electron microprobe analysis at corrosion interface of Figure 10.31 test specimen showing hot corrosion attack. (Schirmer and Quigg).

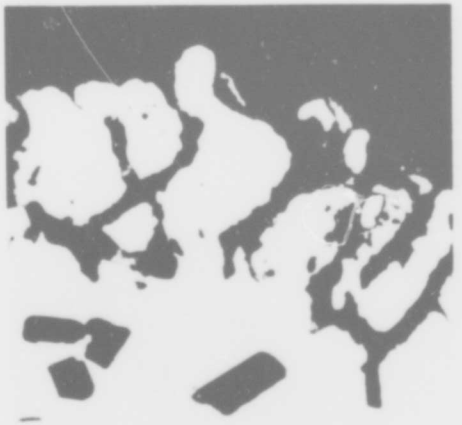

Figure 10.33. Oxidation of Inco 713C in Phillips Rig. (Schirmer and Quigg).

5 hours exposure at 2200 F test condition with no sea salt in air and 0.0002 wt % sulphur in fuel.

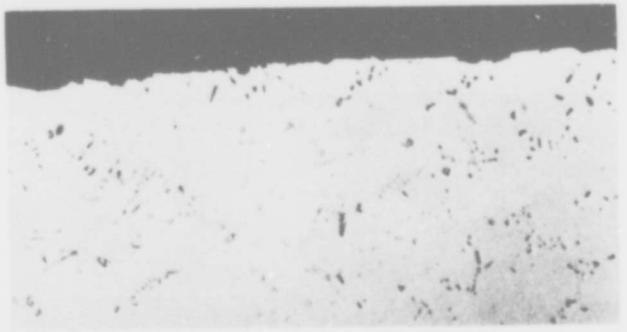

VARIABLE
SURFACE ATTACK

BASE METAL
UNETCHED
200X

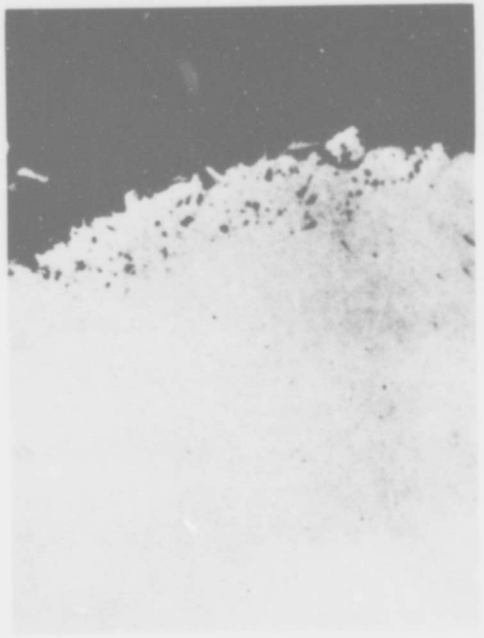

SULFIDE PENETRATION

5 hours exposure at
1400F test condition with
no sea salt in air and
0.40 wt % sulphur in fuel.

BASE METAL
UNETCHED
2000X

Figure 10.34. Sulphidation of
Inco 713C in Phillips Rig.
(Schirmer and Quigg).

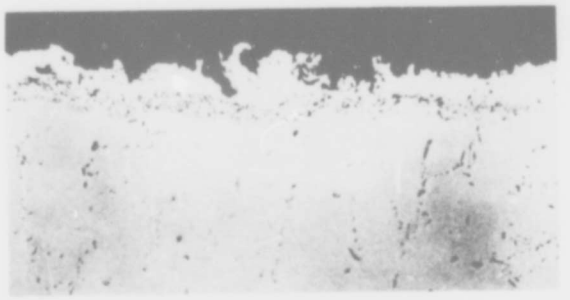

Surface roughened.

Base Metal
Unetched
200 X.

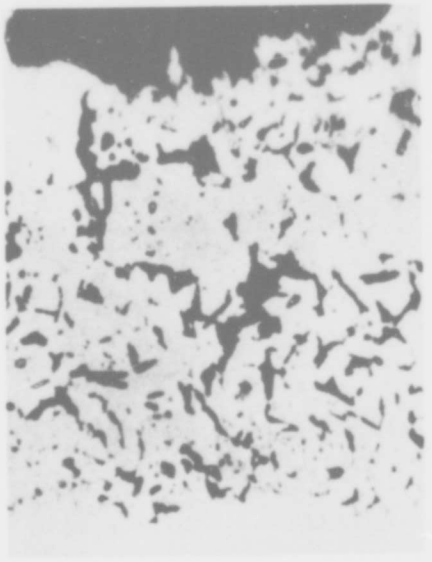

INTERDENDRITIC OXIDAT
CLOSELY FOLLOWING
SULFIDE PENETRATION

UNETCHED
2000X

Figure 10.35. Hot Corrosion of
Inco 713C in Phillips Rig.
(Schirmer and Quigg).

5 hours exposure at
1600F test condition with
10 ppm sea salt and
0.0002 wt % sulphur in fuel.

Figure 10.36. Hot Corrosion of Inco 713C in Phillips Rig. (Schirmer and Quigg).

5 hours exposure at 1800 F test condition with 10 ppm sea saltin air and 0.0002 wt % sulphur in fuel.

Figure 10.37. Hot Corrosion of Inco 713C in Phillips Rig. (Schirmer and Quigg).

5 hours exposure at 2200 F test condition with 10 ppm sea salt in air and 0.0002 wt % sulphur in fuel.

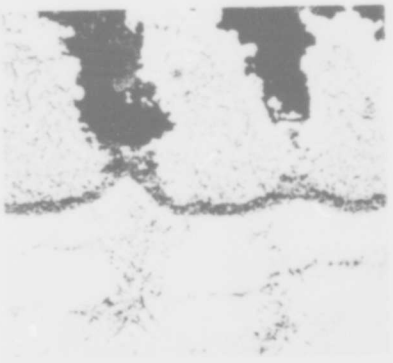

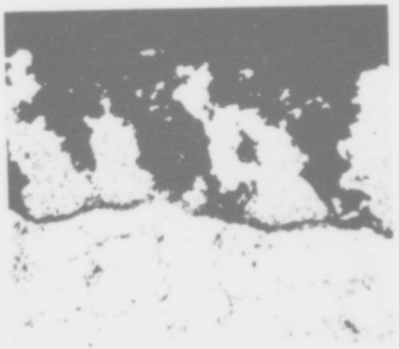

Figure 10.38. Inco 713C after 150 hours of testing at 1500 F. Top photo is 6.24 magnifications, centre photo is 200 magnifications, and the bottom photo is 100 magnifications. (Viswanathan).

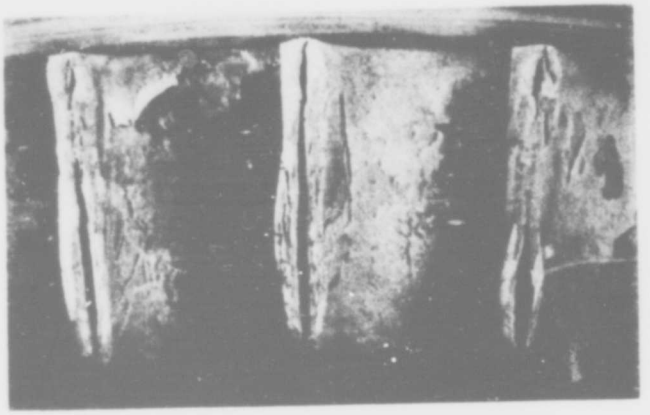

Figure 10.39. Severe hot corrosion on AMS5391A (713C) (Doering and Bergman).

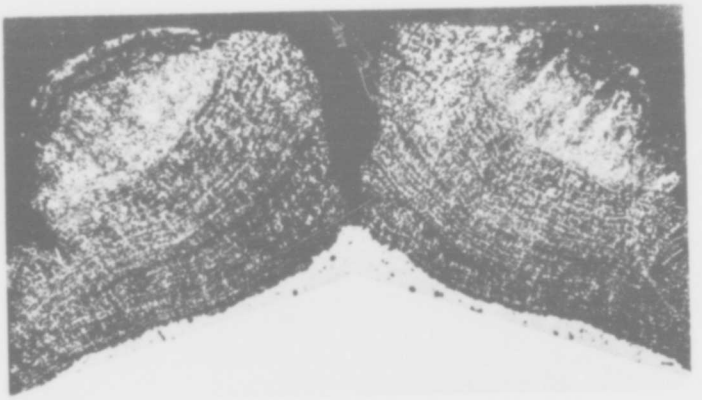

Figure 10.40. Photomicrograph of cross-section area of the leading edge of a corroded AMS5391A (713C) nozzle vane. (Unetched, 60x). (Doering and Bergman).

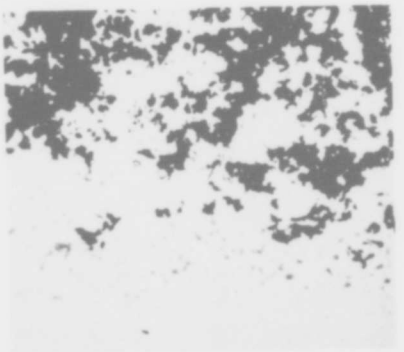

Figure 10.41. Photomicrograph of the AMS5391A (713C) nozzle vane illustrating the small grey globular phase at the interface of the oxides and base matrix (Unetched 1000x) (Doering and Bergman).

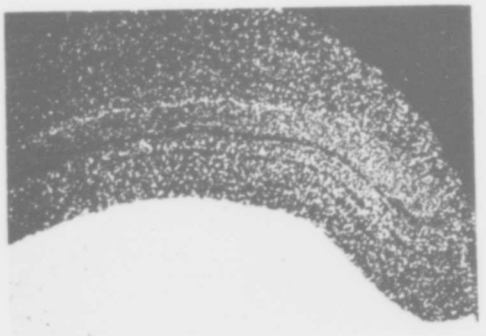

Figure 10.42. Photomicrograph of cross-section area of an AMS5391A (713C) specimen tested at 1550°F for 1000 hours with 0.5 ppm sea salt (Unetched, 50X). (Doering and Bergman).

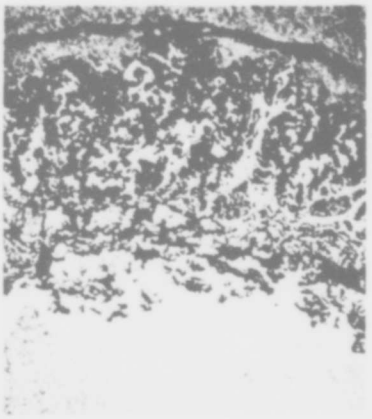

Figure 10.43. Photomicrograph of cross-section area of an AMS5391A (713C) specimen tested at 1600°F for 1000 hours with 5 ppm sea salt (Unetched, 80x) (Doering and Bergman).

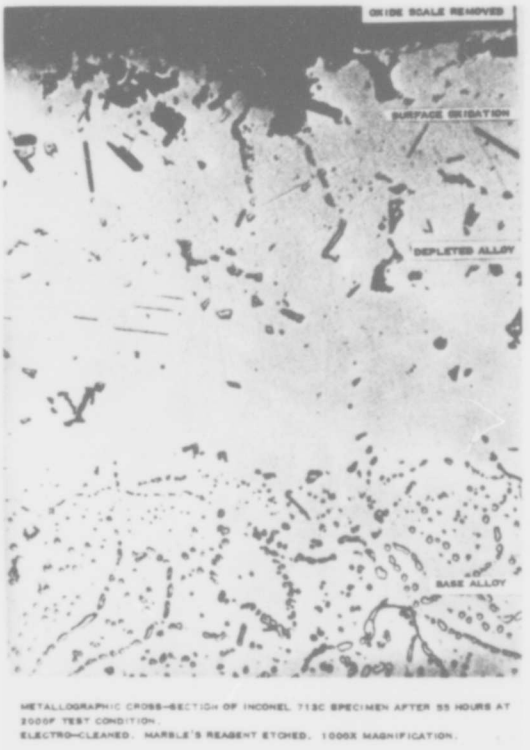

Figure 10.44. Surface oxidation (Quigg and Schirmer).

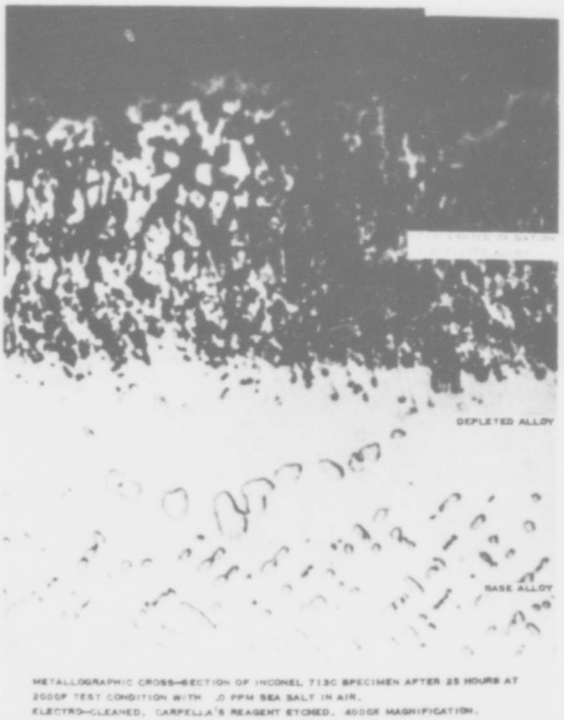

Figure 10.45. Accelerated surface oxidation (Quigg and Schirmer).

Figure 10.46(a). Surface oxidation with vanadium penetration. (Quigg and Schirmer).

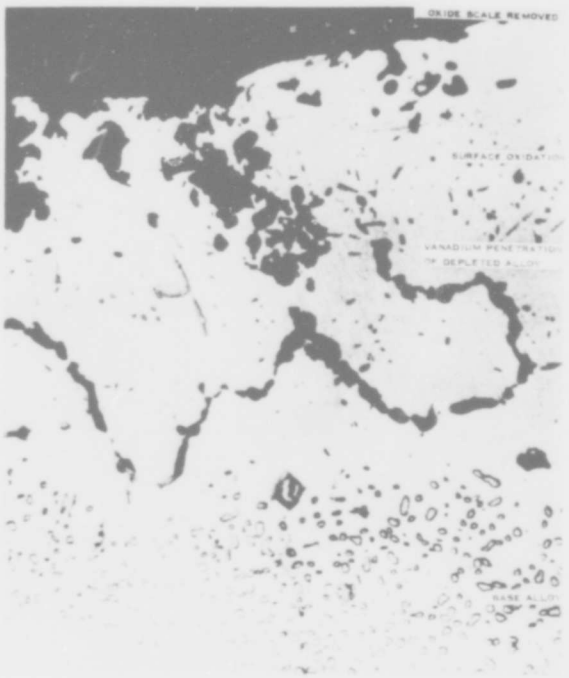

METALLOGRAPHIC CROSS-SECTION OF INCONEL 713C SPECIMEN AFTER 55 HOURS AT 2000F TEST CONDITION WITH 0.063 PPM VANADIUM IN AIR. ELECTRO-CLEANED. MARBLE'S REAGENT ETCHED. 1000X MAGNIFICATION.

Figure 10.46(b). Surface oxidation with vanadium penetration. (Quigg and Schirmer).

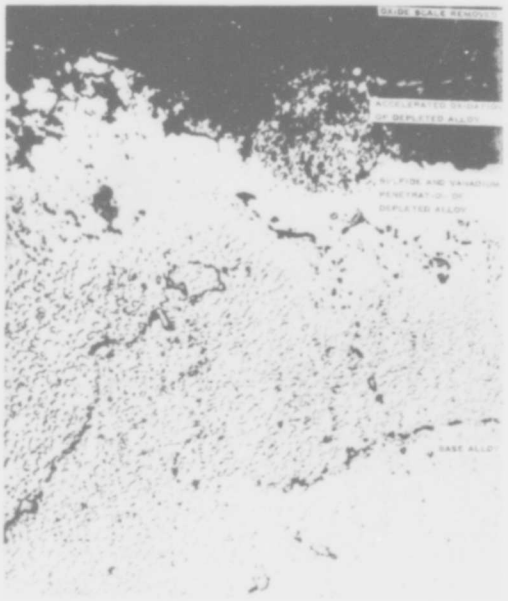

METALLOGRAPHIC CROSS-SECTION OF INCONEL 713C SPECIMEN AFTER 20 HOURS AT 2000F TEST CONDITION WITH 1.0 PPM SEA SALT AND 0.063 PPM VANADIUM IN AIR. ELECTRO-CLEANED. MARBLE'S REAGENT ETCHED. 1000X MAGNIFICATION.

Figure 10.47. Accelerated surface oxidation with vanadium penetration. (Quigg and Schirmer).

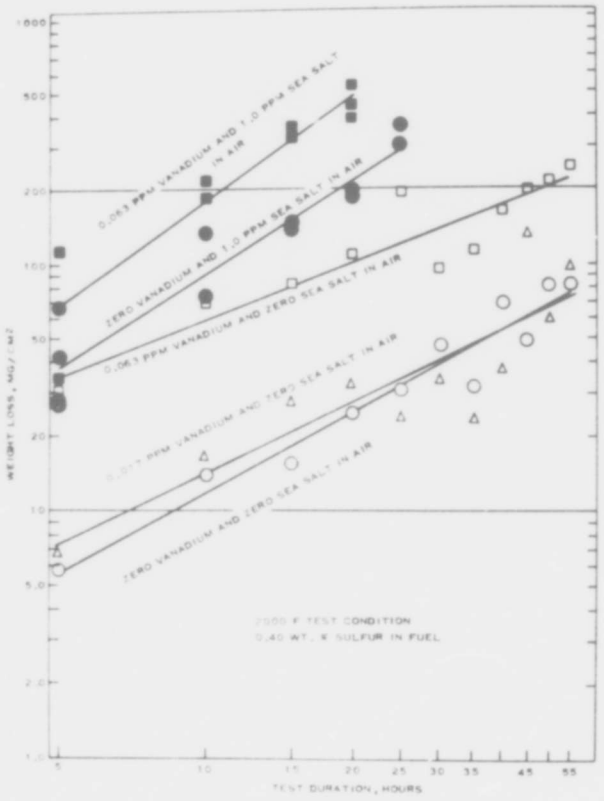

Figure 10.48. Hot corrosion of Inconel 713C. (Quigg and Schirmer).

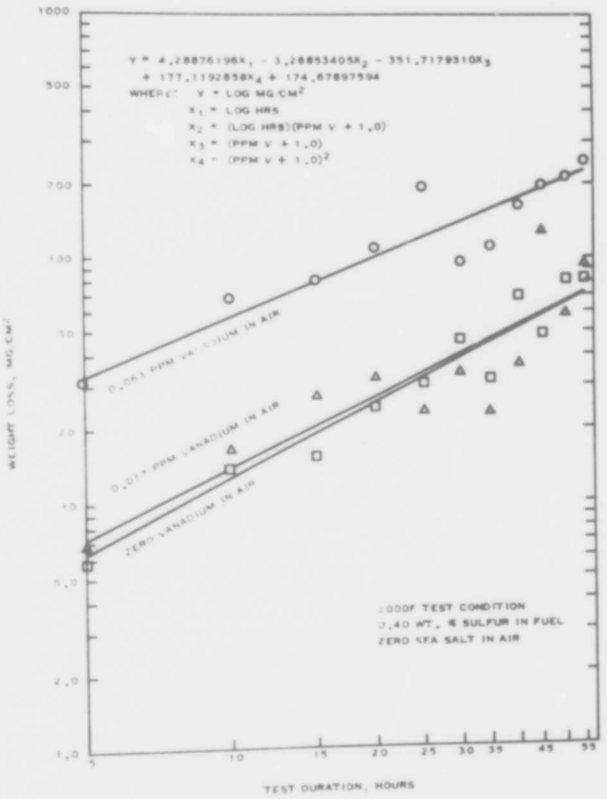

Figure 10.49. Hot corrosion of Inconel 713C. (Quigg and Schirmer).

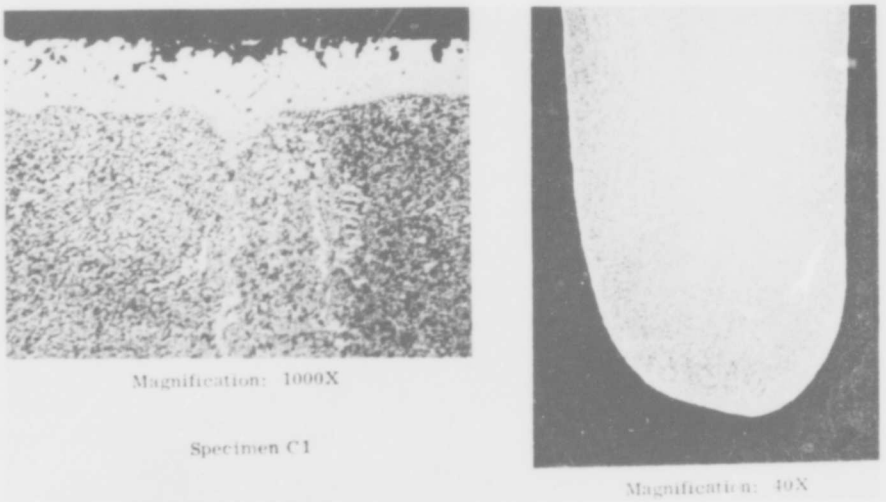

Figure 10.50. Microstructure of uncoated Inco 713C after hot corrosion tests at 1650°F for 60 hours. (Moore and Stetson).

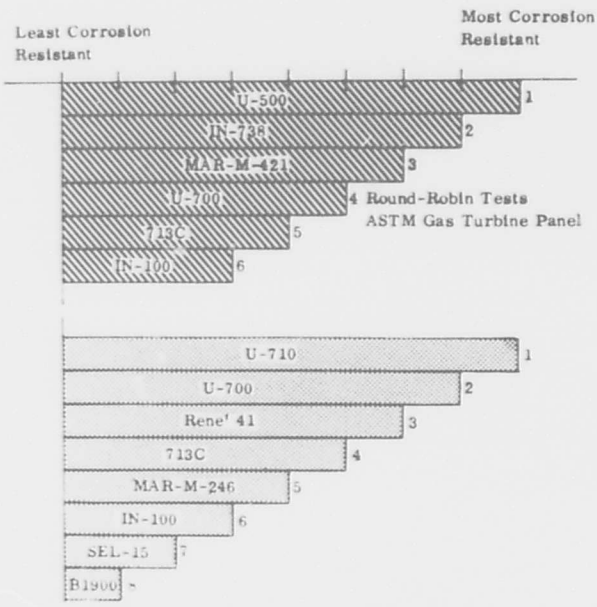

Figure 10.51. Ranking of uncoated nickel-base alloys. (Moore and Stetson).

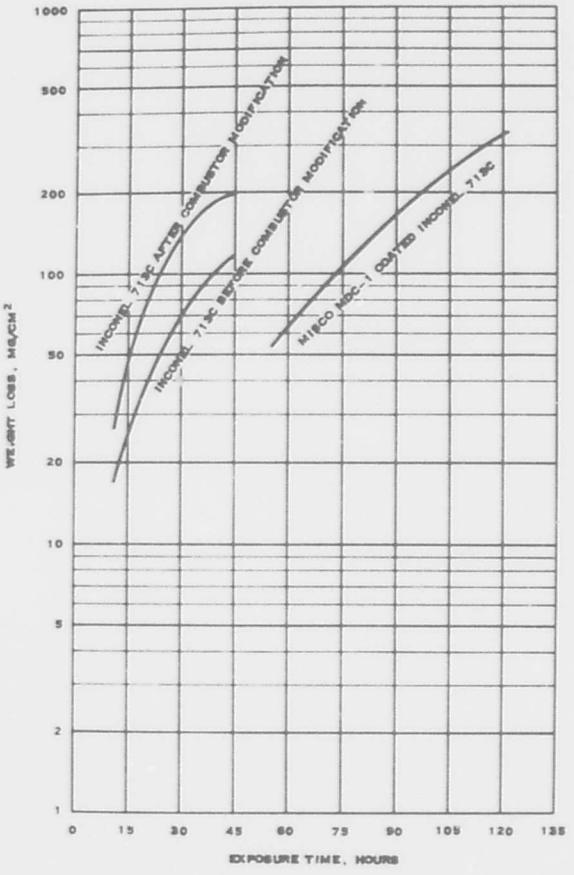

Figure 10.52. Relationship between weight loss and exposure time for bare and coated Inconel 713C. (Quigg and Schirmer).

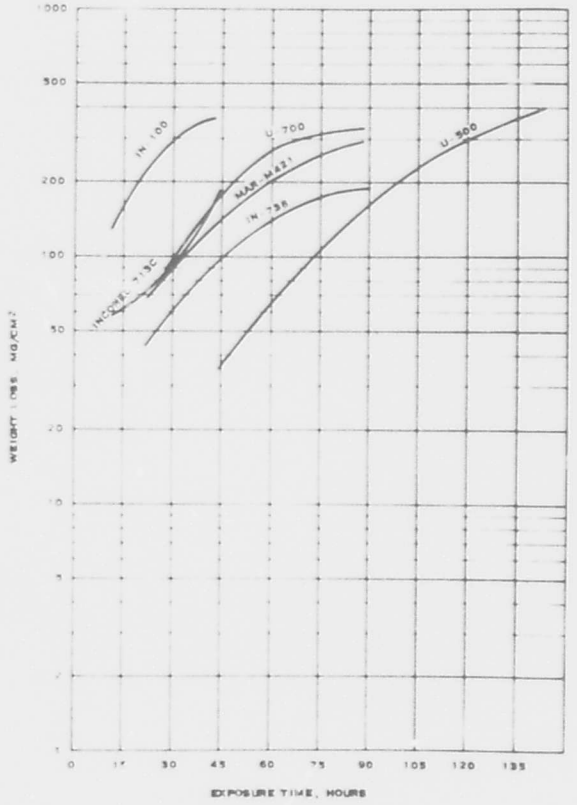

Figure 10.53. Relationship between weight loss and exposure time for superalloys in ASTM Program (Quigg and Schirmer).

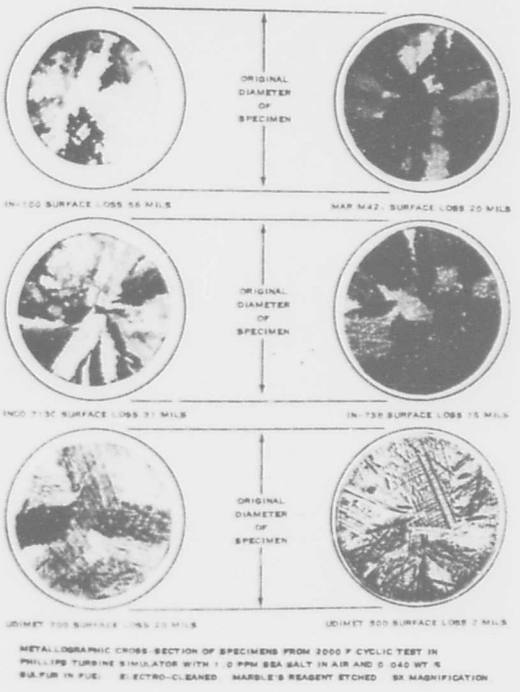

METALLOGRAPHIC CROSS SECTION OF SPECIMENS FROM 2000 F CYCLIC TEST IN PHILLIPS TURBINE SIMULATOR WITH 1.0 PPM SEA SALT IN AIR AND 0.040 WT % SULFUR IN FUEL. ELECTRO-CLEANED. MARBLE'S REAGENT ETCHED. 8X MAGNIFICATION

Figure 10.54. Hot corrosion of superalloys after 44 hours exposure. (Quigg and Schirmer).

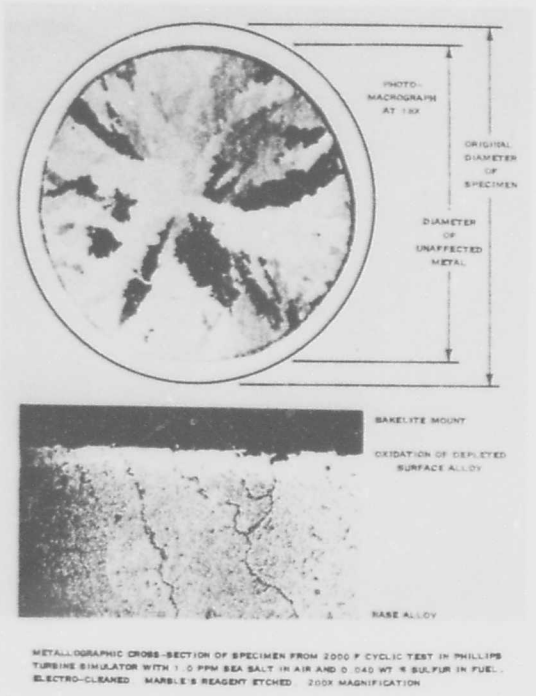

Figure 10.55. Hot corrosion of Inconel 713C specimen after 44hours. (Quigg and Schirmer).

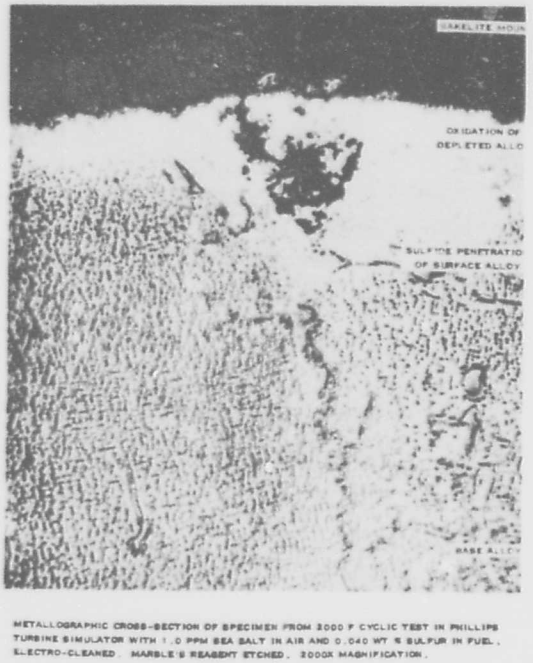

Figure 10.56. Accelerated surface oxidation of Inconel 713C specimen after 44 hours. (Quigg and Schirmer).

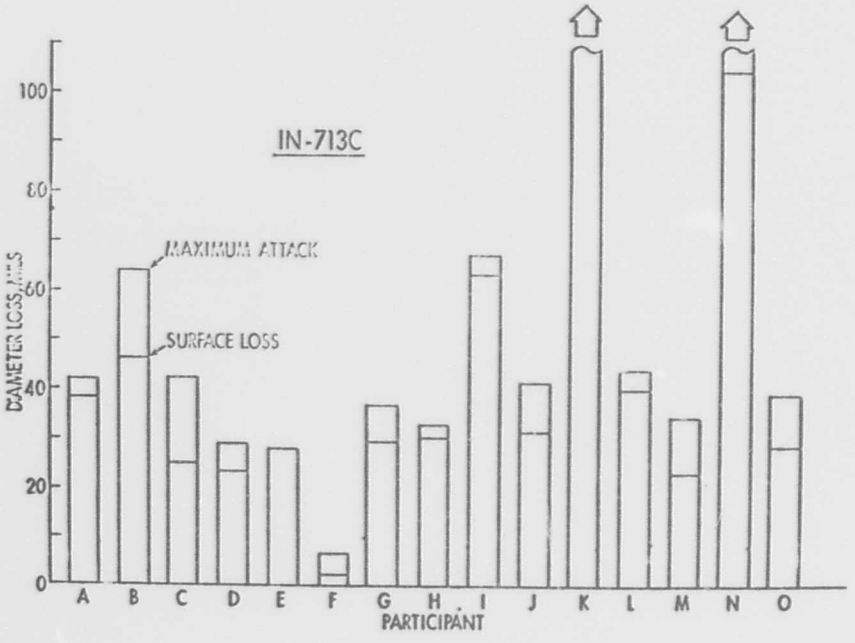

Figure 10.57. Result of the ASTM Round Robin tests for 713C.

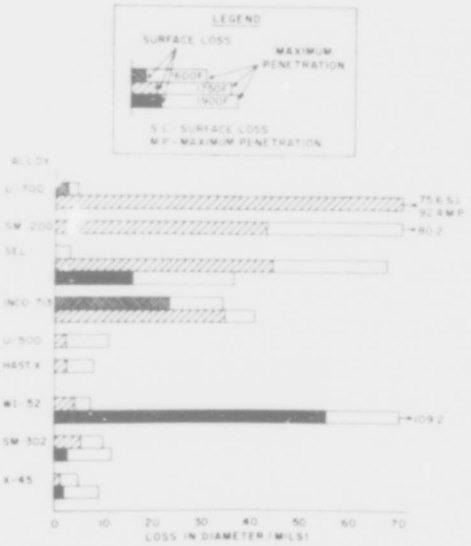

Figure 10.58. Hot-corrosion attack in commercial nickel-base and cobalt-base alloys. (Bergman et al).

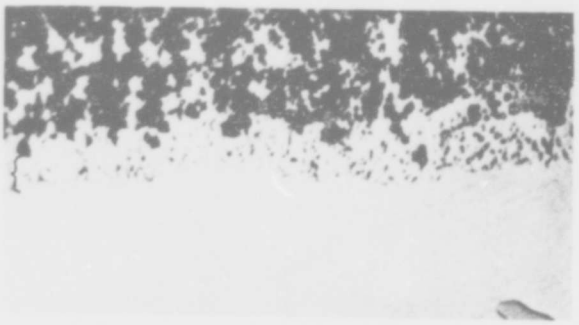

Figure 10.59. Section through IN - 713 blade airfoil of turboprop engine showing light gray Cr_2S_3 phase (bracket) preceding oxidation (x1300). Etchant: mixed acids. Reduced one third for reproduction. (Donachie et al).

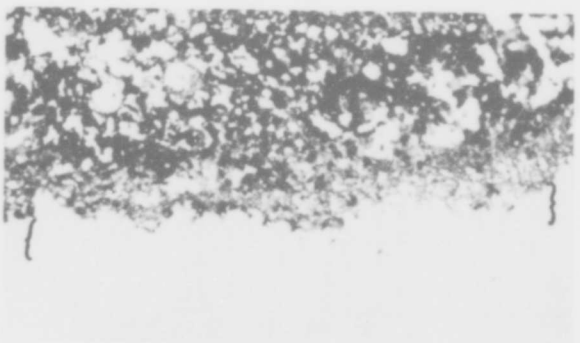

Figure 10.60. Section through IN-713 wedge specimen tested in 90/10 Na_2SO_4 NaCl mixture (Fig. 5) showing light gray Cr_2S_3 phase (bracket) similar to service experience of IN-100 and IN-713 in turboprop engines (x100). Unetched. Reduced one third for reproduction. (Donachie et al).

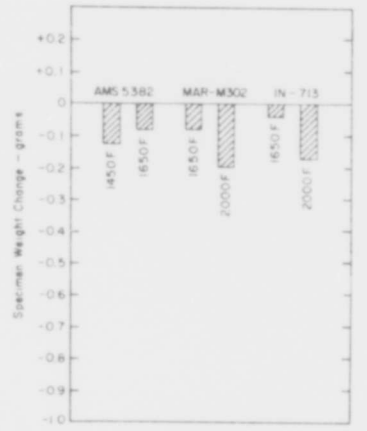

Figure 10.61. Effect of temperature on weight loss after sulphidation rig testing. (Donachie et al).

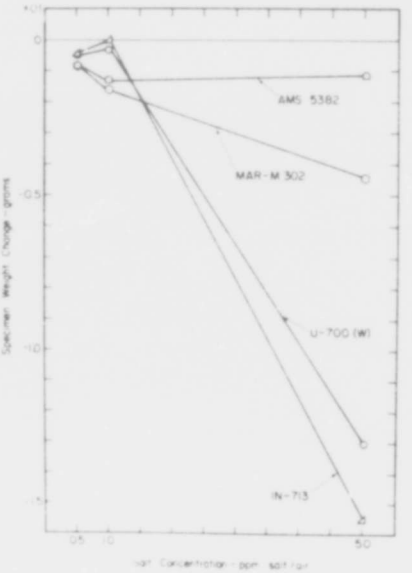

Figure 10.62. Effect of salt concentration on weight loss after sulphidation rig testing. (Donachie et al).

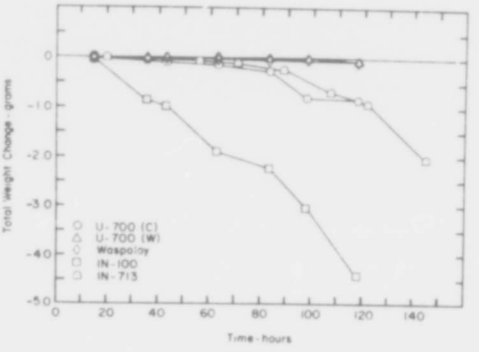

Figure 10.63. Sulphidation test results at 1650 F with JP-5R fuel and nominal 0.5 ppm synthetic sea salt. (Donachie et al).

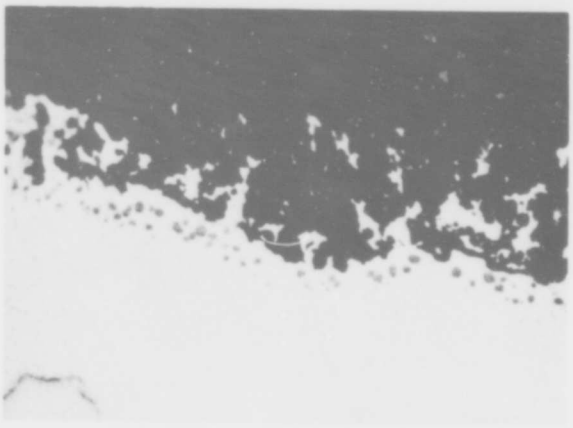

Figure 10.64. Section through IN-713 test specimen after 26 hr at 1800 F in sulphidation rig test. Note light gray Cr_2S_3 phase. (Donachie et al).

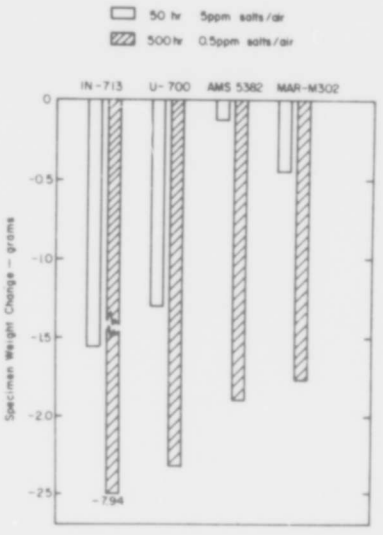

Figure 10.65. Effect of salt concentration and time on weight loss after 1650 F rig testing using 1 per cent sulphur marine diesel fuel. (Donachie et al).

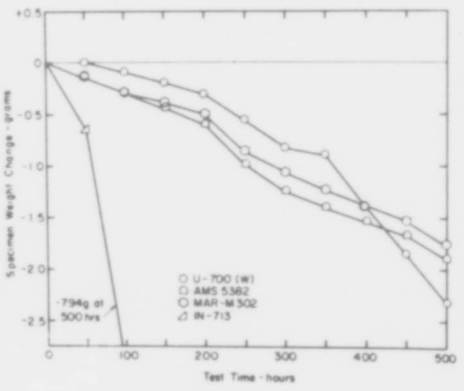

Figure 10.66. Specimen weight change during 1650 F - 500 hr. rig test using 1 per cent sulphur diesel fuel and 0.5 ppm salt:air ratio (Donachie et al).

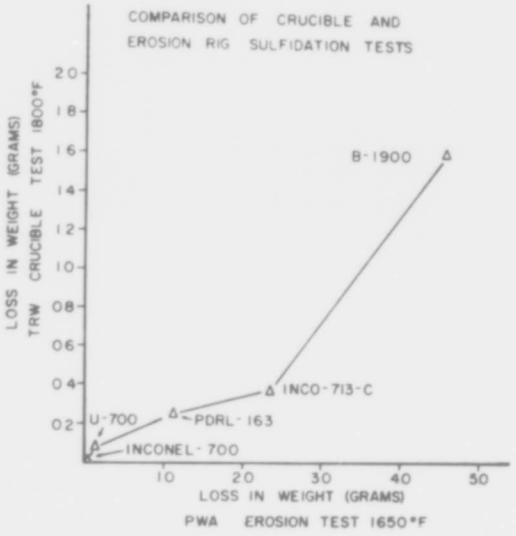

Figure 10.67. Comparison of crucible and erosion rig sulphidation test data. (Graham et al).

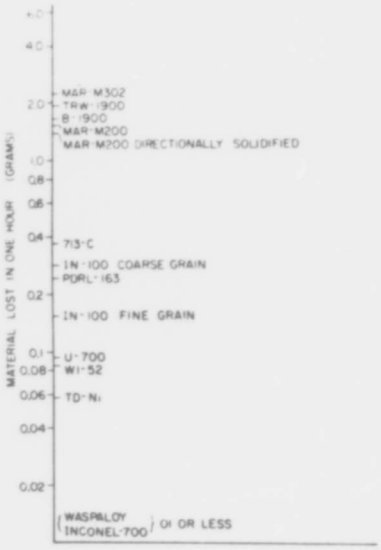

Figure 10.68. Comparison of sulphidation behaviour at 1800 F of commercial super-alloys as determined by crucible test. (Graham et al).

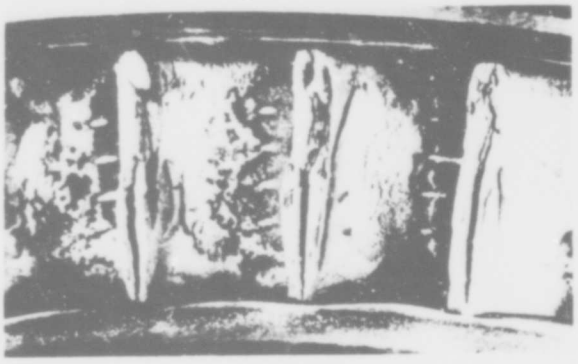

Figure 10.69. Engine-tested uncoated Inco 713 nozzle diaphragm. (Bartocci).

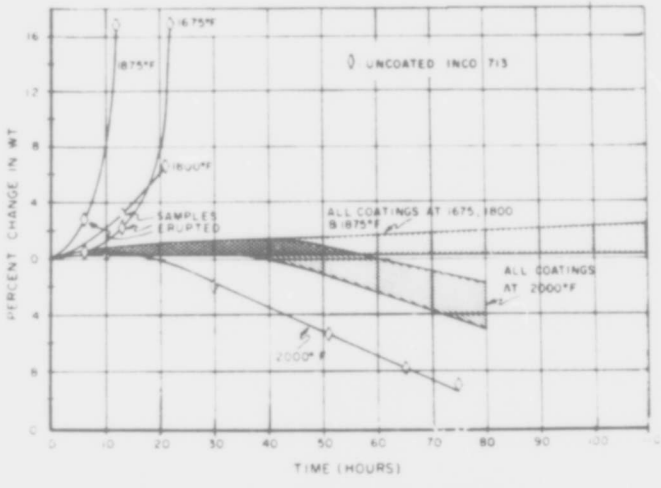

Figure 10.70. Effect of time and temperature on hot-corrosion resistance of coated and uncoated Inco 713. (Bartocci).

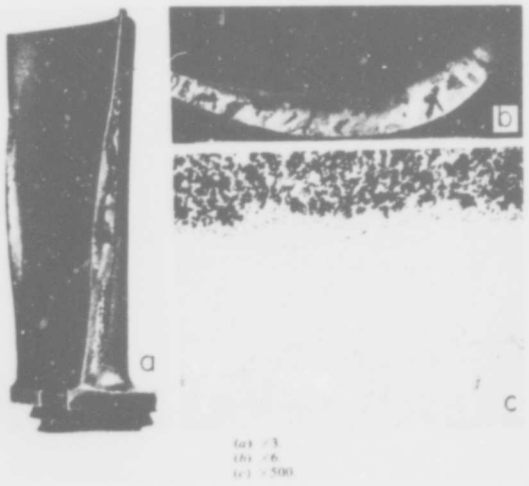

Figure 10.71. Typical corroded 713C turbine blade and details. (Hamilton et al).

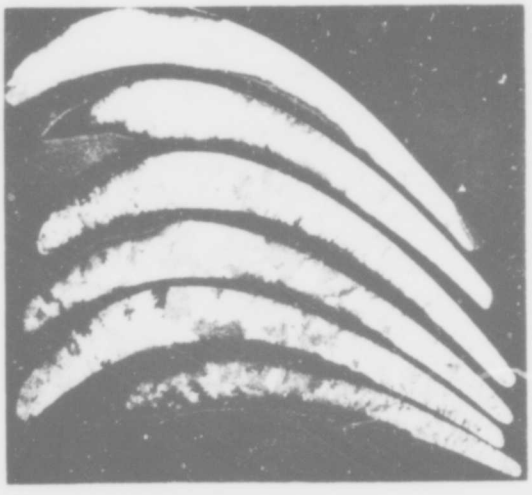

Figure 10.72. Transverse sections of airfoils from corroded turbine blades after 2700h operation (713C?) (Hamilton et al).

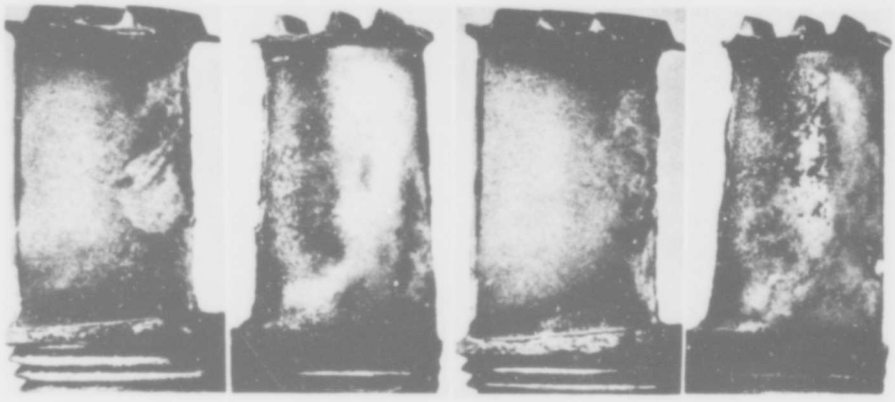

Figure 10.73. Corroded 713C turbine blades operated in a marine environment. (Hamilton et al).

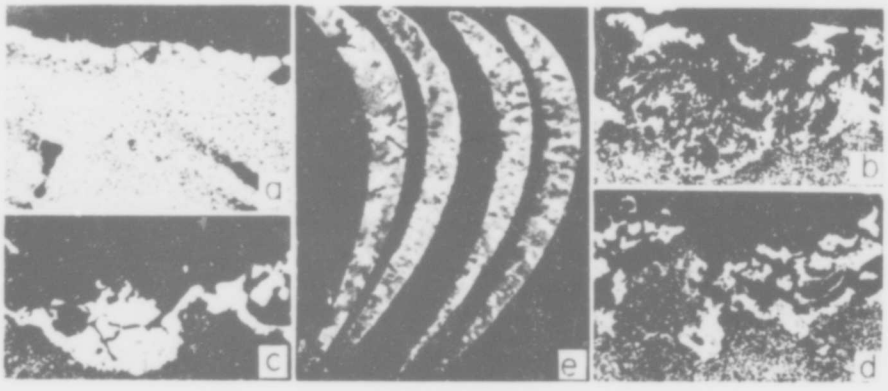

Figure 10.74. Accelerated engine tested alloys. (Hamilton et al).

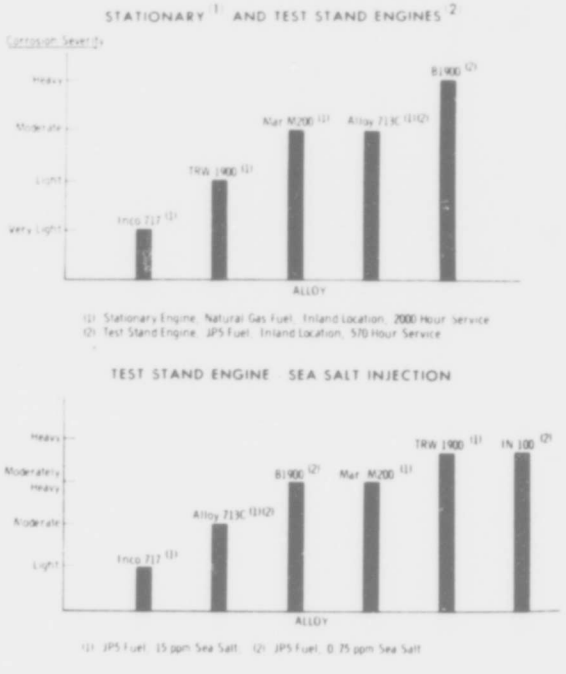

Figure 10.75. Hot corrosion of turbine blade alloys. (Hamilton et al).

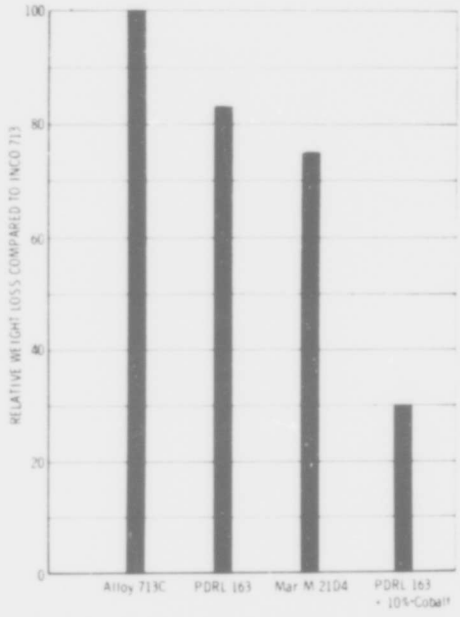

Figure 10.76. Relative weight loss compared to Alloy 713C material. (Hamilton et al).

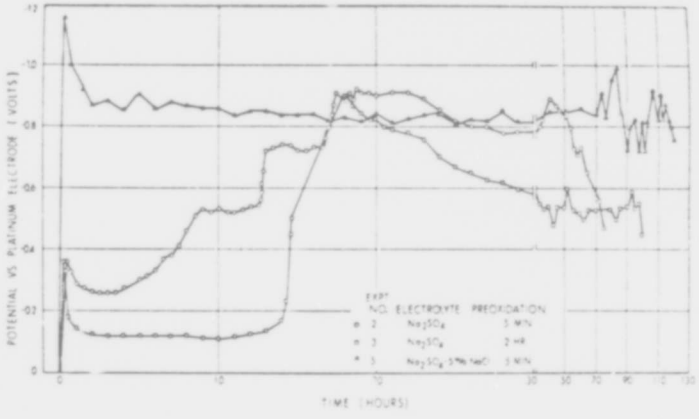

Figure 10.77. Potential-time curves of Alloy A (AMS 5391A) at 1650 F in molten salts under air. (Wheatfall et al).

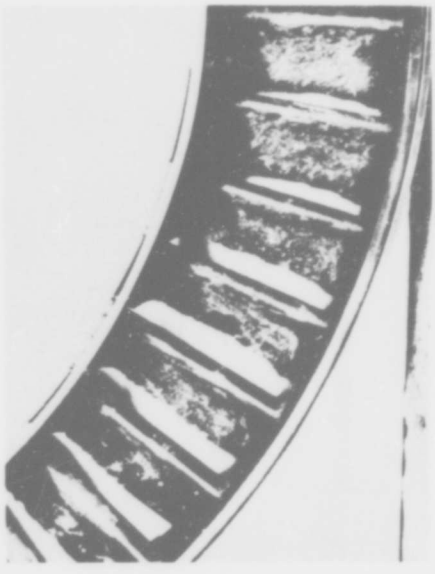

Figure 10.78. "Alloys containing about 13% Cr" - almost certainly 713C. (Wall and Michael).

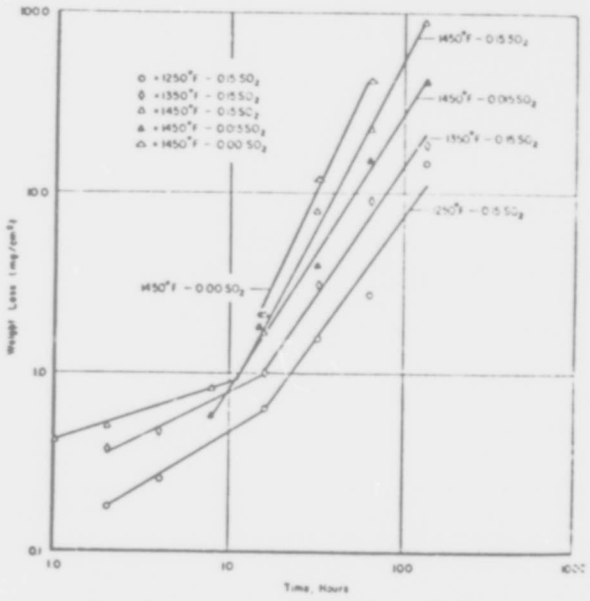

Figure 10.79. Weight loss of Ni-13 Cr-6 Al alloys after exposure to 1250, 1350, and 1450 F. (Wall and Michael).

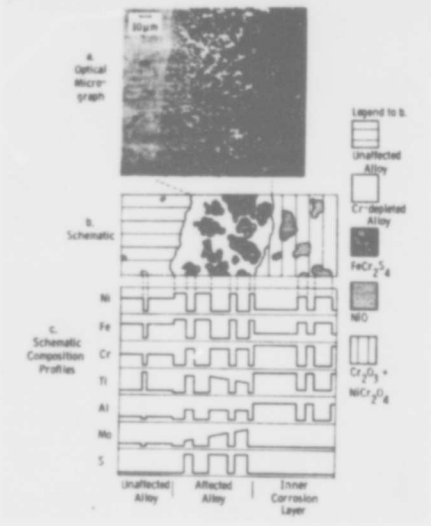

Figure 10.80. Composition profile of Ni-13 Cr-6 Al (713C) alloy exposed 90 hr at 1450 F. (Wall and Michael).

Figure 10.81. Turbine blades from navy aircraft engine. (Schirmer and Quigg).

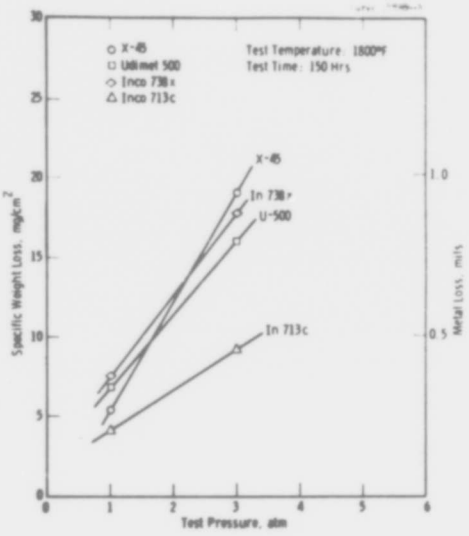

Figure 10.83. Effect of pressure on the oxidation rate of superalloys. (Lee and Young).

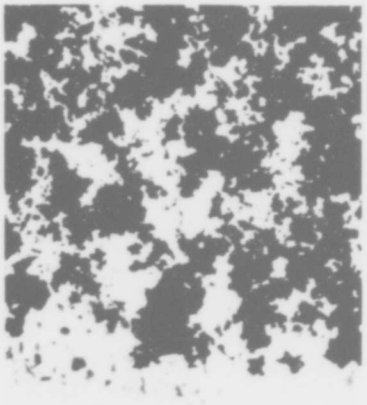

Figure 10.82. Hot corrosion of Inconel 713C turbine blade (x2000) (Schirmer and Quigg).

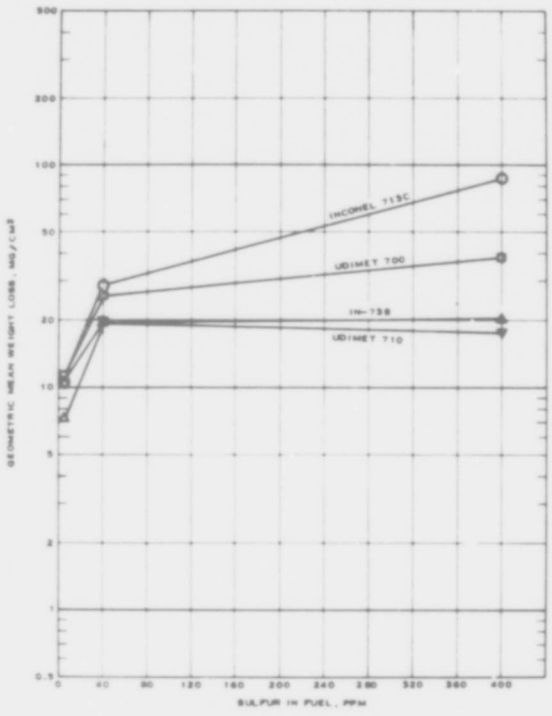

Figure 10.84(a). Effect of sulphur in fuel on hot corrosion of four bare superalloys. (Quigg et al).

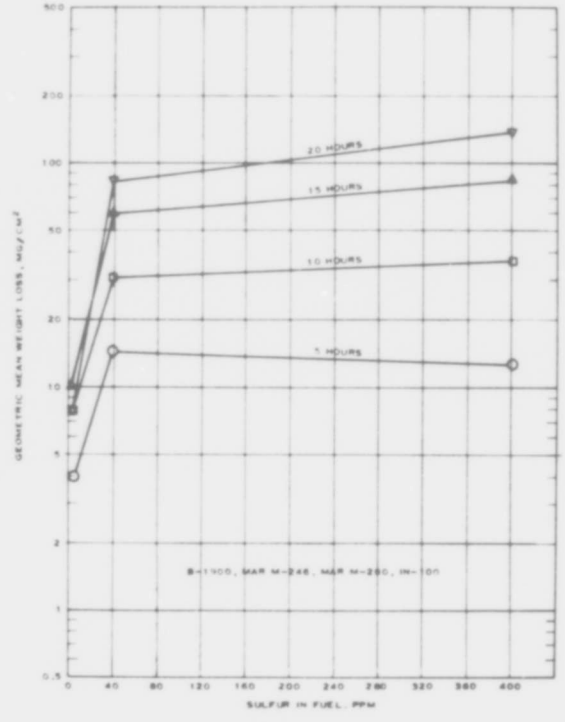

Figure 10.84(b). Effect of sulphur in fuel on hot corrosion of four bare superalloys (Quigg et al).

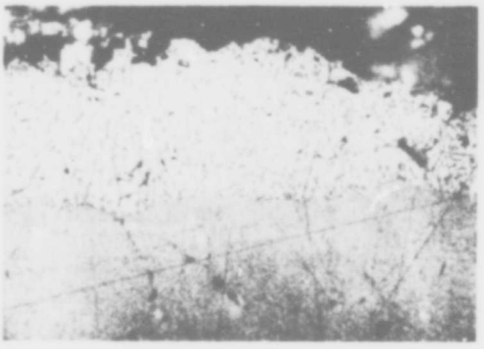

Figure 10.85. IN 713 LC 168 h/800°C/ Ni_3S_2 (Erdos).

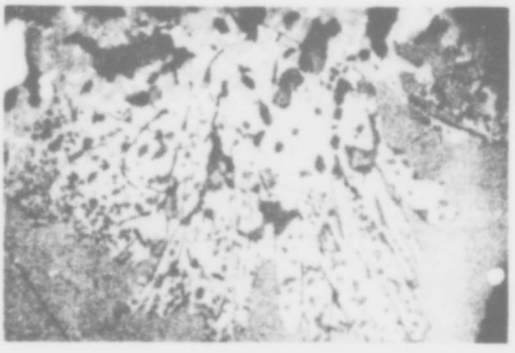

Figure 10.86. IN 713 LC Hot corrosion in gas turbine 1 year 700 - 750°C. (Erdos).

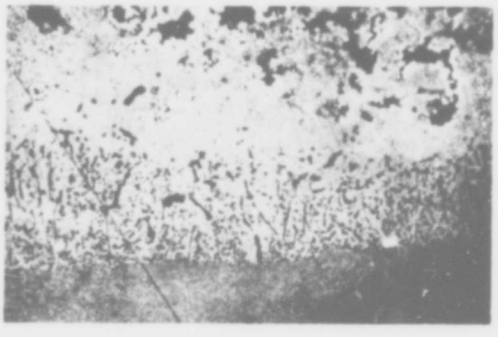

Figure 10.87. IN 713 LC in pilot plant 300 h/850°C (Erdos).

Figure 10.88. IN 713 LC in sulphatic salt melt 112 h/800°C (Erdos).

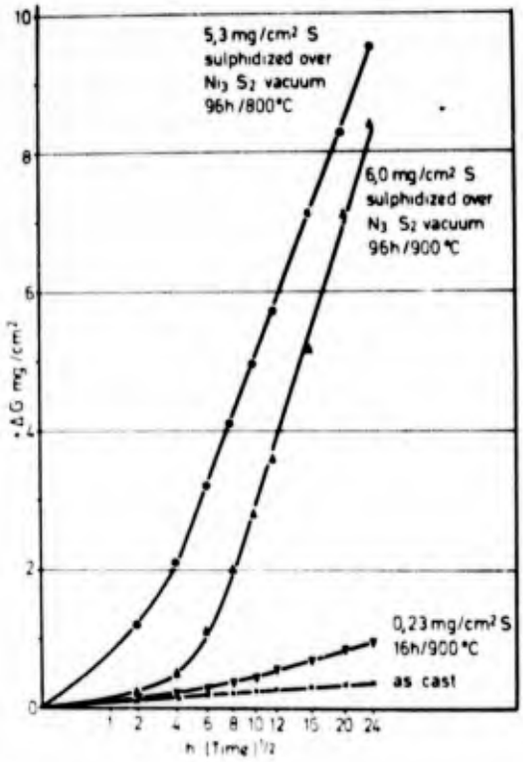

Figure 10.89. Oxidation rates of IN 713 LC in O_2 1 atm. 900°C. (Erdos).

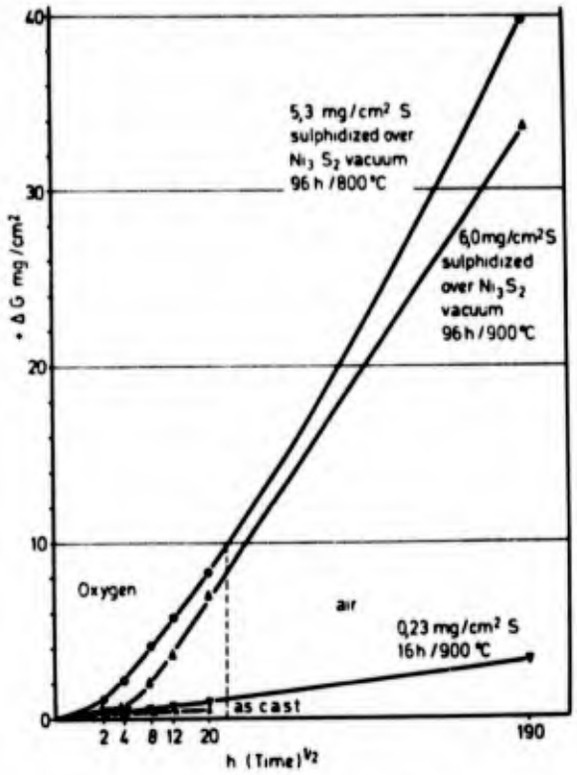

Figure 10.90. Oxidation rates of IN 713 LC in O_2 (air) 1 atm, 900°C. (Erdos).

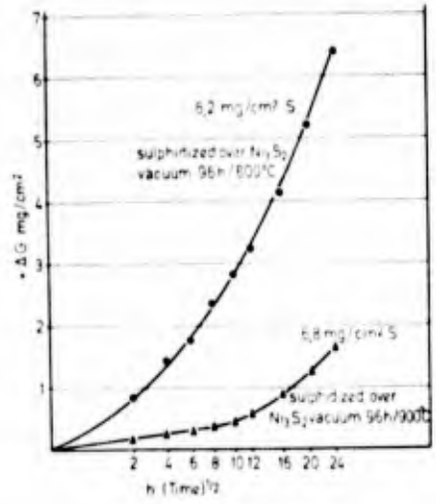

Figure 10.91. Oxidation rates of IN 713 LC in O_2 1 atm. 800°C. (Erdos).

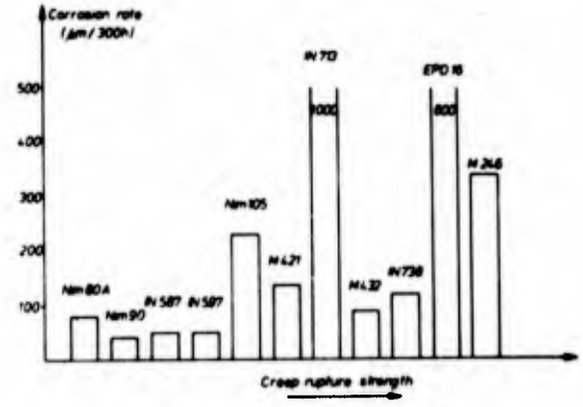

Figure 10.92. Corrosion behaviour of nickelbase superalloys. (Felix).

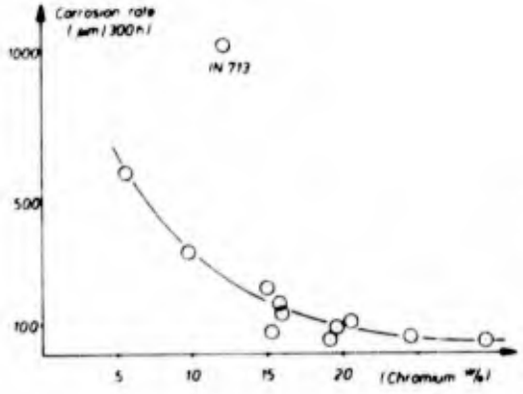

Figure 10.93. Effect of chromium on the hot corrosion of nickelbase alloys. (Felix).

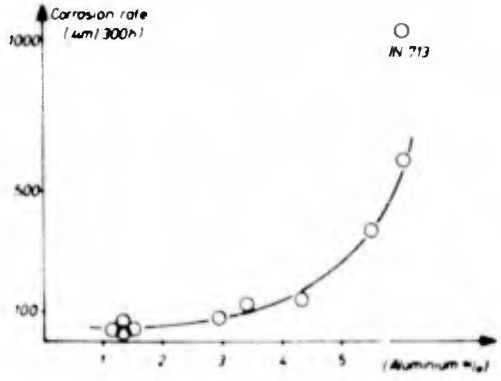

Figure 10.94. Hot corrosion effect of aluminium content in nickel alloys. (Felix).

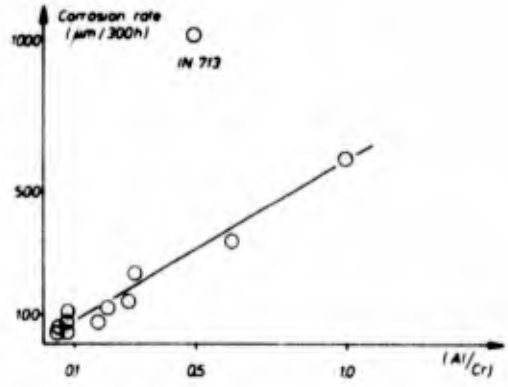

Figure 10.95. Effect of Al/Cr-ratio on the corrosion of nickel alloys. (Felix).

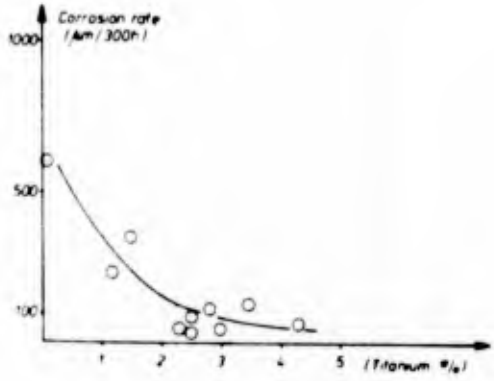

Figure 10.96. Corrosion effect of the titanium content in nickel alloys. (Felix).

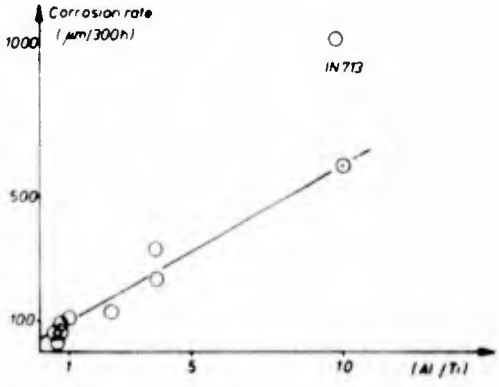

Figure 10.97. Effect of Al/Ti-ratio on the corrosion of nickel alloys. (Felix).

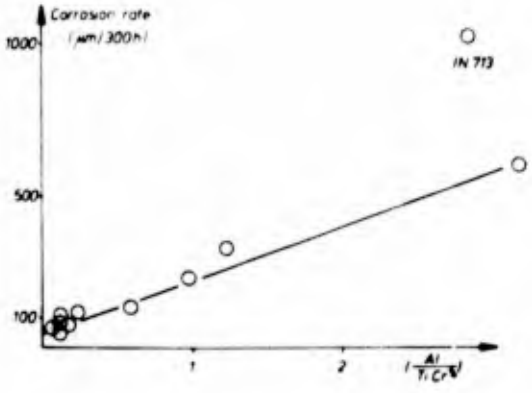

Figure 10.98. Corrosion effect of Al/Ti Cr^2 ratio in nickel alloys. (Felix).

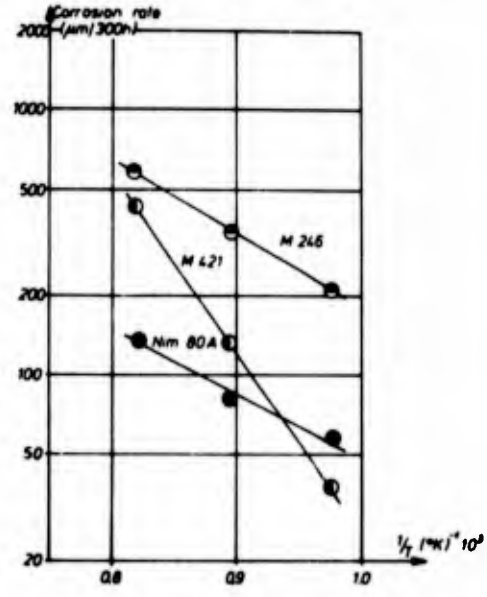

Figure 10.99. Arrhenius plot for the hot corrosion of nickel alloys (showing linear temperature dependence) (Felix).

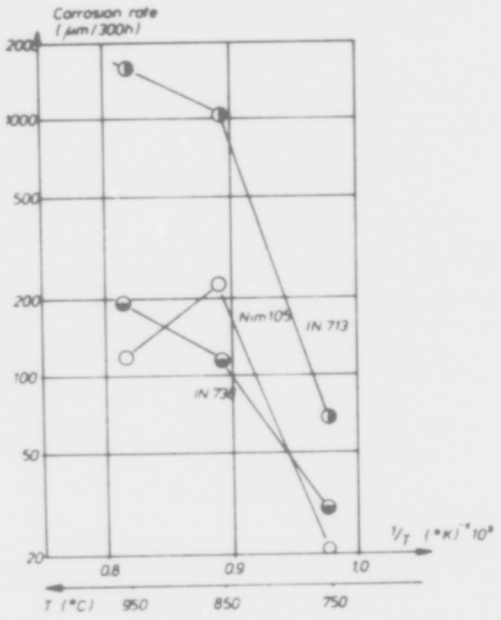

Figure 10.100. Arrhenius plot for the hot corrosion of nickel alloys (showing non linear temperature dependence) (Felix).

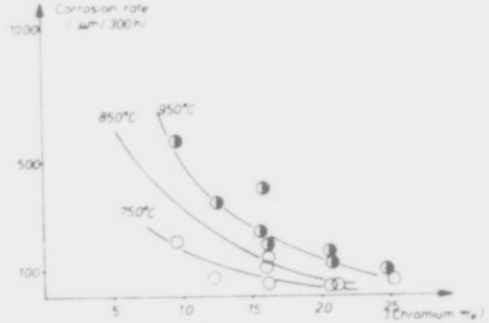

Figure 10.101. Effect of chromium on the corrosion of nickel alloys at different temperatures. (Felix).

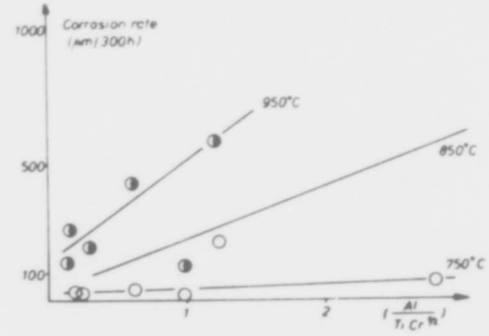

Figure 10.102. Corrosion rate as a function of Al/Ti $Cr^{\frac{1}{2}}$ ratio at different temperatures. (Felix).

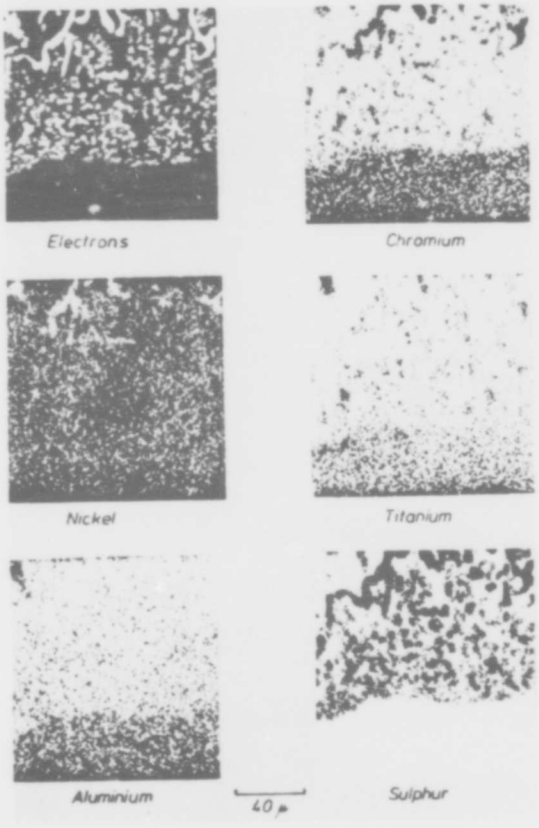

Figure 10.103. Microprobeanalysis of a corroded test sample, material IN 713 LC (Kα, 500 x) (dark means high concentration) (Felix).

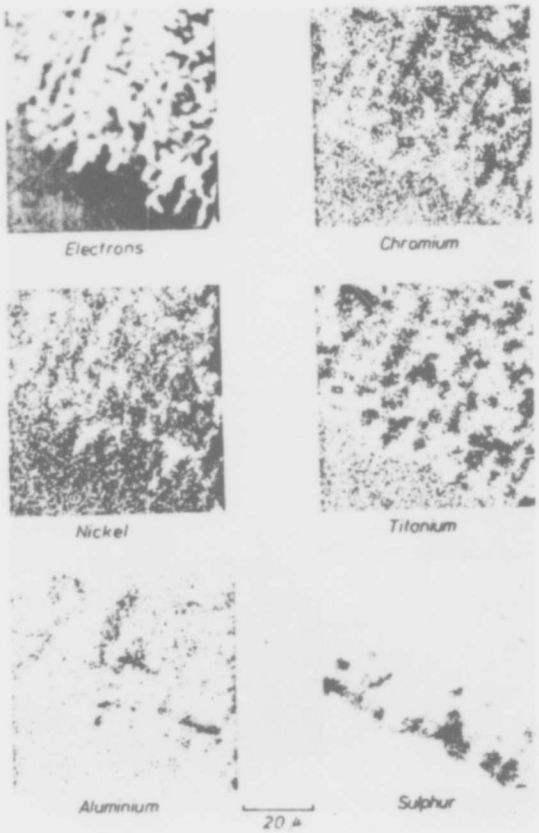

Figure 10.104. Microprobeanalysis of a corroded turbine vane, material IN 713 LC (Kα, 1000x) (dark means high concentration) (Felix).

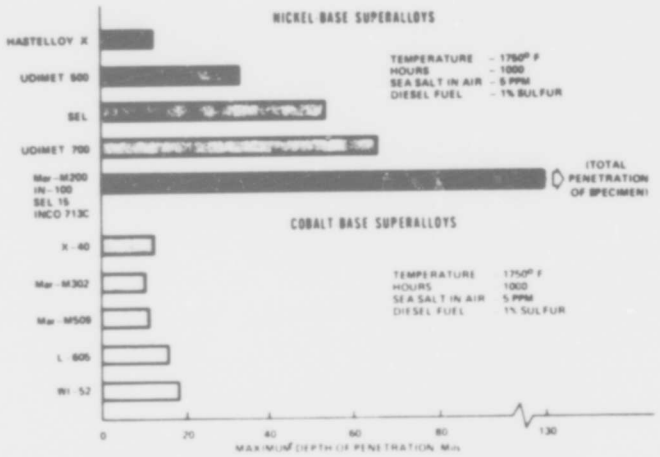

Figure 10.105. Hot-corrosion attack in nickel- and cobalt-base superalloys at 1750°F (Bergman et al, quoted by Wheatfall).

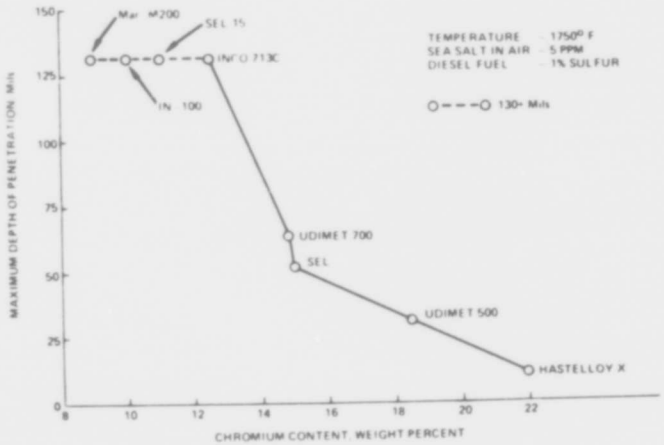

Figure 10.106. Maximum depth of penetration versus chromium content for nickel-base gas turbine superalloys in a hot-corrosion burner-rig test at 1750°F (Bergman et al quoted by Wheatfall).

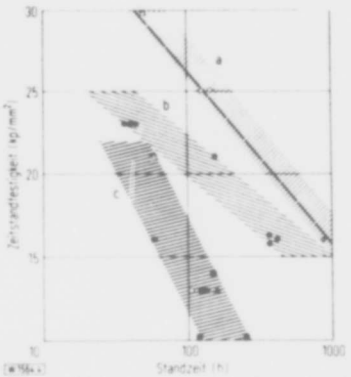

Abb. 4 Der Einfluß der Korrosion auf das Zeitstandverhalten der Nickelbasislegierung 713 V bei 900 °C Probentemperatur

a) in Luftatmosphäre
— — — n. Prospekt
b) im Heißgasstrom und
c) im Heißgasstrom mit künstlichem Meersalz nach DIN 52 900, jedoch trocken, 36 g/48 h

○ ohne Schutzschicht
◌ verdromt
● ohne Schutzschicht
■ ohne Schutzschicht
□ verdromt
△ LDC-2, Aluminid-Schutzschicht mit Pt
▲ Aluminid-Schutzschicht

Figure 10.107. The influence of corrosion on the creep behaviour of the nickel-base alloy 713V at 900°C.
(a) in air.
(b) in hot gas stream.
(c) in hot gas stream with synthetic sea salt according to DIN 50900 but dry. 36g/48h.

- ○ without protective coating.
- ◌ chromized.
- ● without protective coating.
- ■ without protective coating.
- □ chromized.
- △ LDC-2 aluminide coating with Pt.
- ▲ aluminide coating.

(Huff and Schreiber)

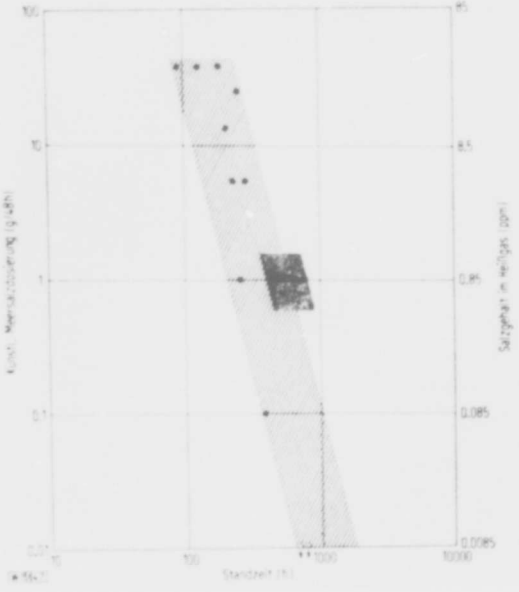

Figure 10.108. The influence of salt concentration on the fatigue life at 900°C, Nimocast 713V, 140 N/mm^2.

- ♀ without protective layer, and without salt.
- ● without protective coating, with salt.
- △ 50 µm thick protective coating LDC-2, with salt.
- □ 70 µm thick protective coating LDC-2, with salt.
- ♀ 50 µm thick protective coating LDC-2, without salt.
- ✗ with enamel coating.

(Huff and Schreiber)

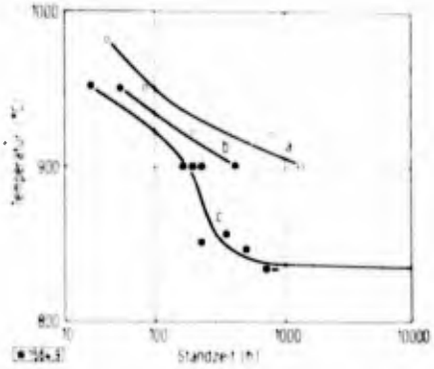

Figure 10.109. The influence of temperature on the creep behaviour of the nickel-base alloy Nimocast 713V at 140 N/mm^2.

(a) in air. ○
(b) in hot gas stream from JP4 fuel. ●
(c) in hot gas stream with synthetic sea salt according to DIN 50900, but dry, 36g/48h (31 ppm). ■

without protective coating.

(Huff and Schreiber).

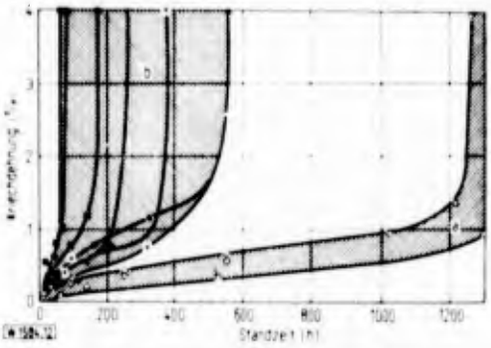

Figure 10.110. The influence of corrosion on the creep extension of the nickel-base alloy Nimocast 713C at a stress of 140 N/mm^2 at 900°C.

(a) in still air. ○
(b) in hot gas stream with synthetic sea salt according to DIN 50900 31 ppm ■, 0.95 ppm ▲, 0.085 ppm ×

(Huff and Schreiber).

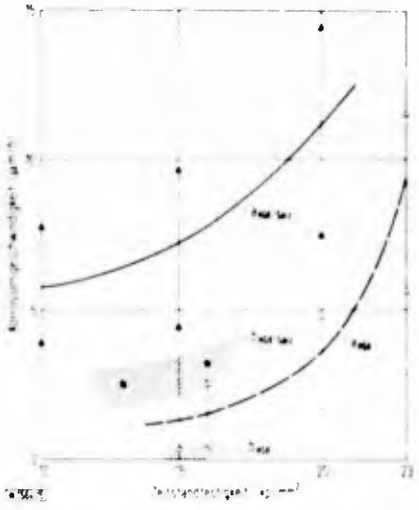

Figure 10.111. Localized and surface corrosion rates at different stresses, nickel-base alloy 713V, 900°C.

a_{HGK} localized corrosion rate in hot gas.
$a_{HCK/salz}$ localized corrosion rate in hot gas with synthetic sea salt 36g/48h.
b_{HGK} surface corrosion rate in hot gas.
$b_{HGK/salz}$ surface corrosion rate in hot gas with synthetic sea salt 36g/48h.

(Huff and Schreiber).

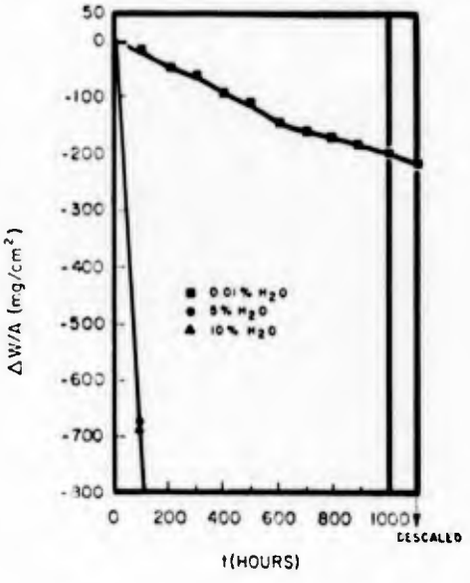

Fig. 1 .112. Effect of water vapour on the cyclic oxidation resistance of 304 SS at 1100°C in air. (Cycled every 100 hours). (Clark and Hulsizer).

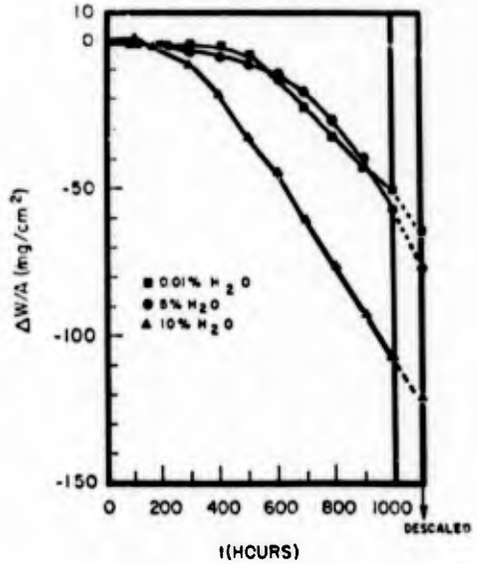

Fig. 10.113. Effect of water vapour on the cyclic oxidation resistance of alloy 600 at 1100°C in air. (Cycled every 100 hours). (Clark and Hulsizer).

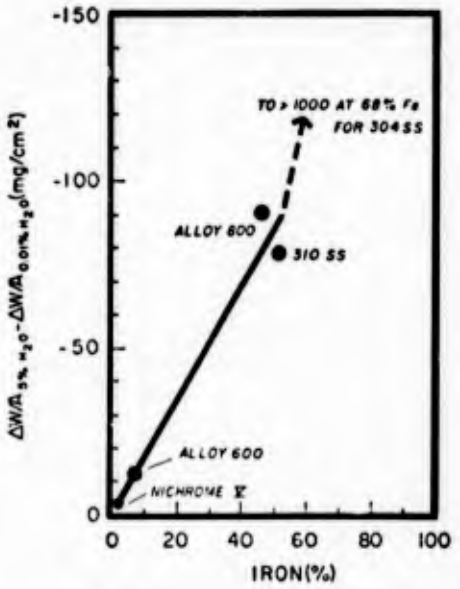

Fig. 10.114. Relationship between iron content and water vapour effect for Fe-Ni-Cr alloys after 1000 hours of cyclic oxidation at 1100°C. (Clark and Hulsizer).

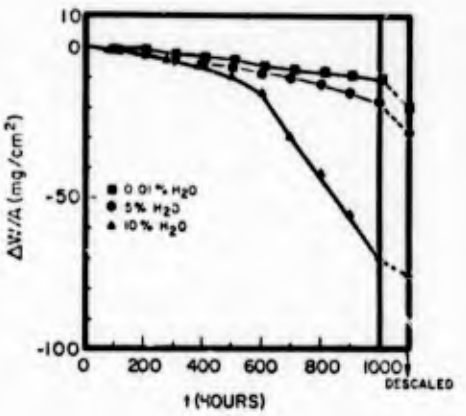

Fig. 10.115. Effect of water vapour on the cyclic oxidation resistance of Hastelloy alloy X at 1100°C in air. (Cycled every 100 hours). (Clark and Hulsizer).

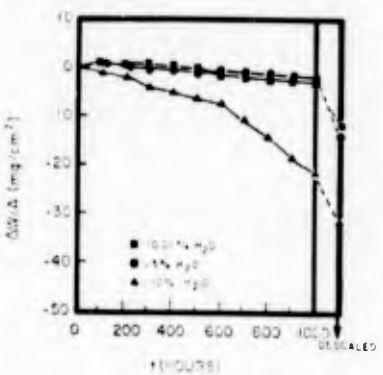

Figure 10.116. Effect of water vapour on the cyclic oxidation resistance of IN-586 at 1100°F in air. (Cycled every 100 hours). (Clark and Hulsizer).

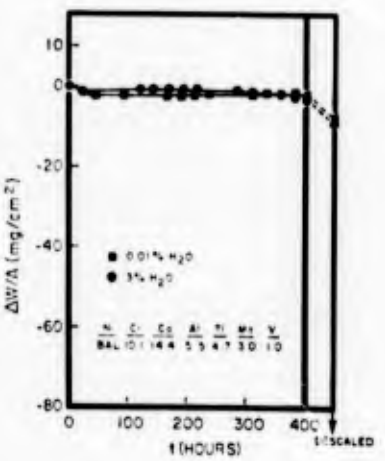

Figure 10.117. Effect of water vapour on the cyclic oxidation resistance of IN-100 at 1100°C in air. (Cycled 24 to 100 hours). (Clark and Hulsizer).

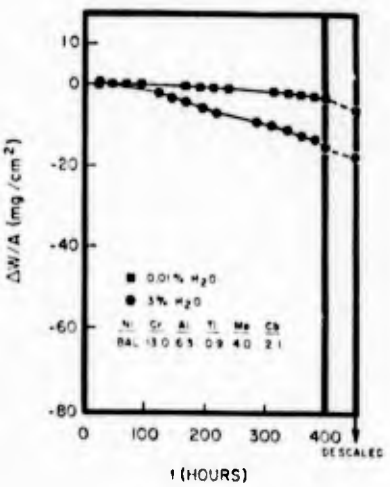

Figure 10.118. Effect of water vapour on the cyclic oxidation resistance of alloy 713C at 1100°C in air. (Cycled 24 to 100 hours). (Clark and Hulsizer).

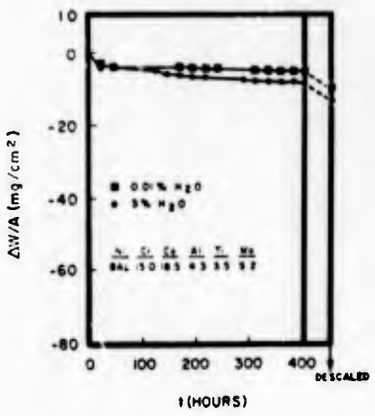

Figure 10.119. Effect of water vapour on the cyclic oxidation resistance of Udimet 700 at 1100°C in air. (Cycled 24 to 100 hours). (Clark and Hulsizer).

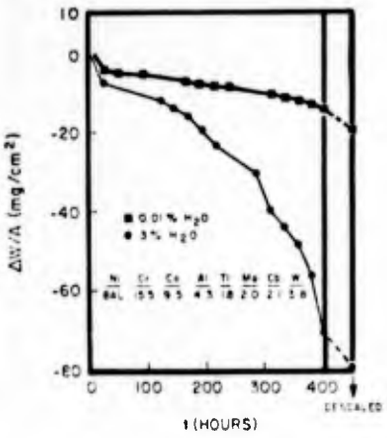

Figure 10.122. Effect of water vapour on the cyclic oxidation resistance of Udimet 500 at 1100°C in air. (Cycled 24 to 100 hours). (Clark and Hulsizer).

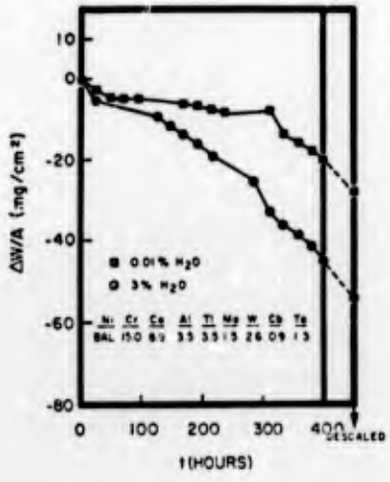

Figure 10.120. Effect of water vapour on the cyclic oxidation resistance of IN-738 at 1100°C in air. (Cycled 24 to 100 hours). (Clark and Hulsizer).

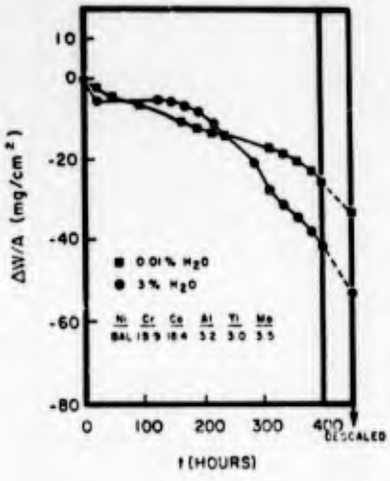

Figure 10.121. Effect of waver vapour on the cyclic oxidation resistance of Mar-M alloy 421 at 1100°C in air. (Cycled 24 to 100 hours). (Clark and Hulsizer).

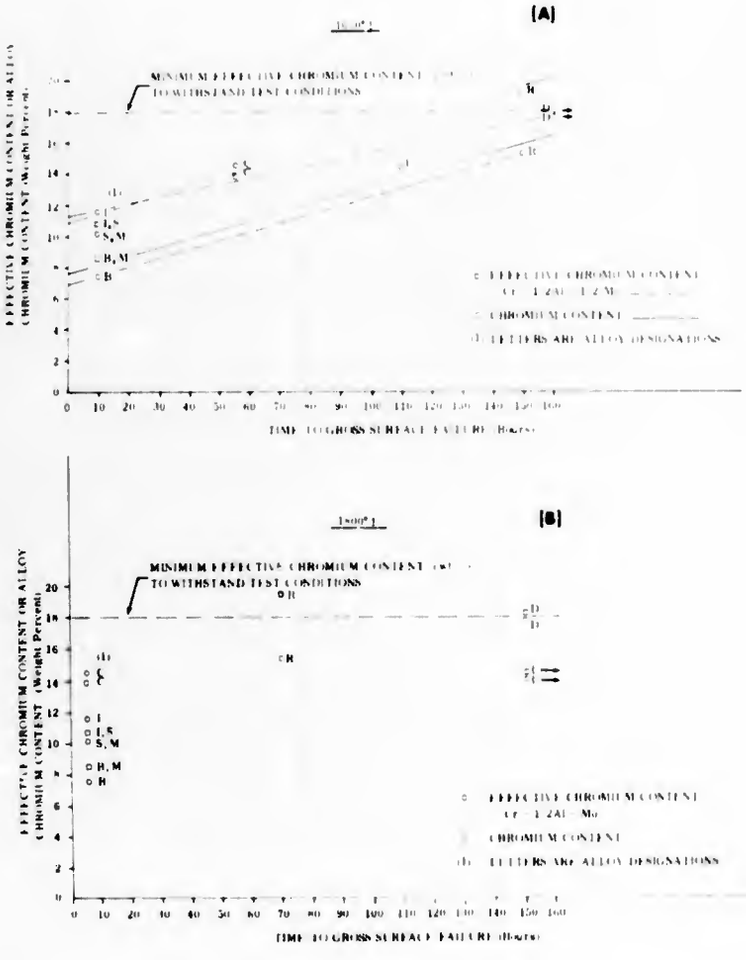

Fig. 1.123. Hot corrosion rig test results for uncoated nickel-base alloys. (Stetson and Moore).

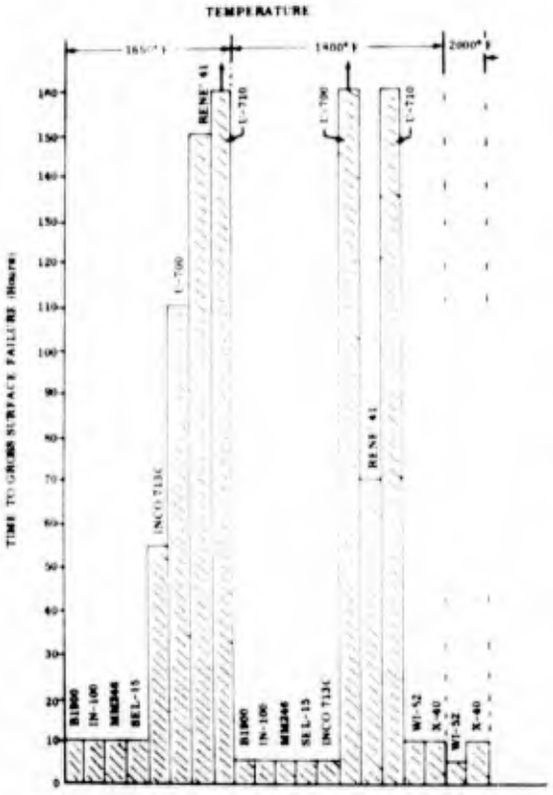

Figure 10.124. Summary of hot corrosion rig tests on uncoated nickel- and cobalt-base alloys. (Stetson and Moore).

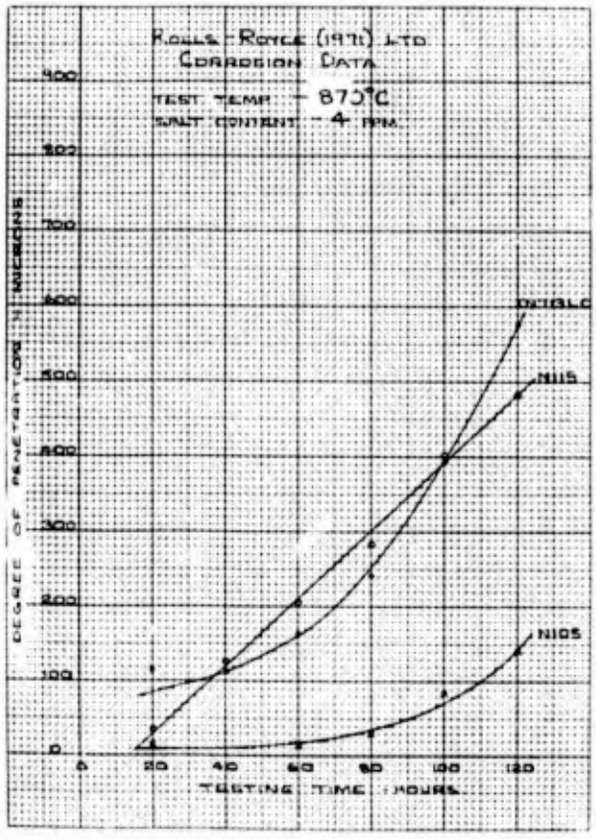

Figure 10.125. Hot corrosion data from Rolls-Royce (1971) Ltd.

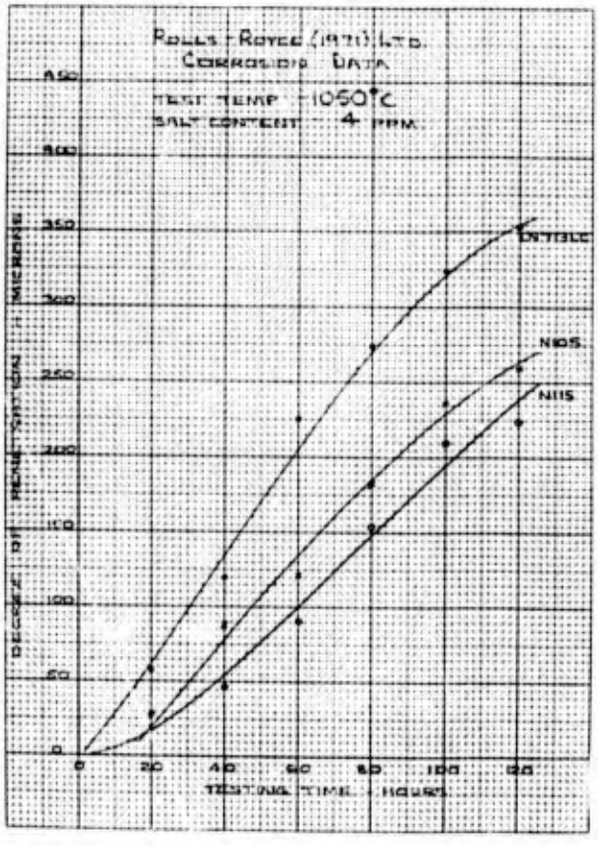

Figure 10.126. Hot corrosion data from Rolls-Royce (1971) Ltd.

Inco 717

K.H. Ryan, J.R. Kildsig and P.E. Hamilton (Allison Division of General Motors) Technical Report to Wright Patterson AFB, Air Force Materials Laboratory AFML-TR-67-306 (Aug. 1967).

A detailed summary of the procedure used in this report and the principal result is given under PDRL-163. Inco 717 is one of the middle group of alloys tested (the others were PDRL 163, IN 728 NX, 713C, 713C+Cr, 713C+Cr+Y, Mar-M 421, Mar-M246, IN 100, GMR 235; 717 was comparable with IN 100, 713C and Mar-M 421; GMR 235 and Mar-M 246 were considerably worse than this group). Figure 11.1 shows the volume loss as a function of temperature for both as-casted heat-treated specimens. Figure 11.2 compares the measured volume loss and that predicted by the regression equation (see PDRL 163).

The microstructure of all the alloys could be described in terms of three zones: (1) an outer layer of continuous oxide on the surface which gradually graded into an area of mixed metal and oxide; (2) a layer of depleted metal; (3) globular sulphide particles. Figure 11.3 shows the general appearance of the corrosion, and Figure 11.4 shows a microprobe traverse, and the relative analysed compositions.

P.E. Hamilton, K.H. Ryan and E.S. Nichols, Hot Corrosion Problems Associated with Gas Turbines, ASTM Special Technical Publication STP 421, 1967, 188.

See 713C for details. 717 seemed quite resistant, in comparison with the other alloys tested (713C, TRW 1900 and SM 200).

Data relating to this alloy will also be found in the following Figures :
10.74, 10.75, 36.1, 36.2, 36.3, 36.4, 36.5, 36.6, 36.7.

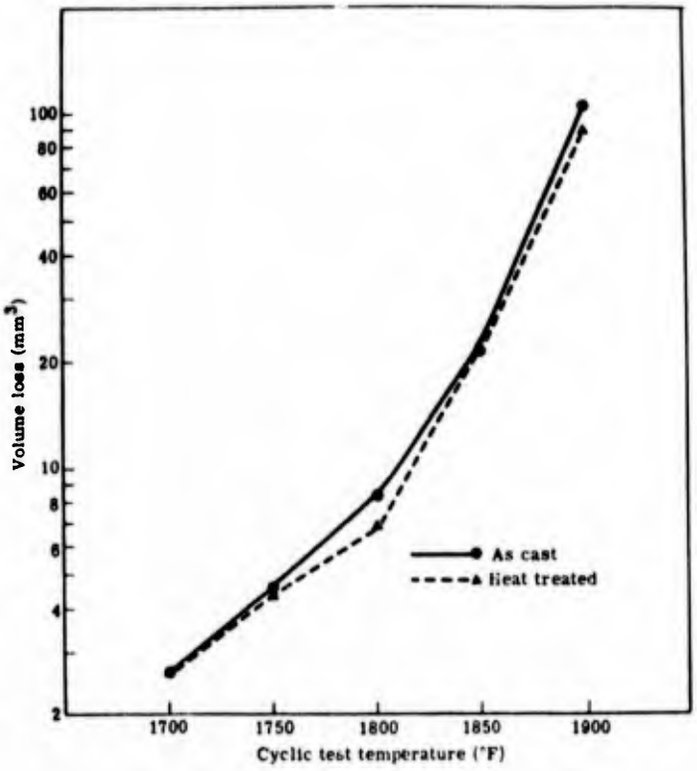

Figure 11.1. As-cast versus heat treated Inco 717 at each cyclic test temperature. (Ryan et al).

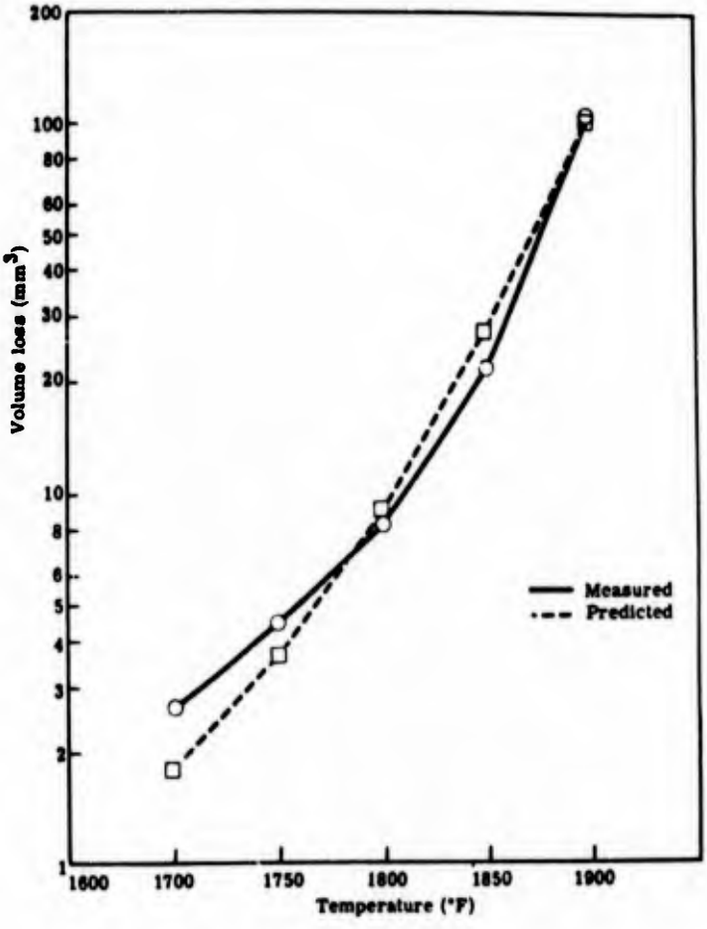

Figure 11.2. Comparison of the measured volume loss and the loss predicted by the regression equation for Inco 717 (Ryan et al).

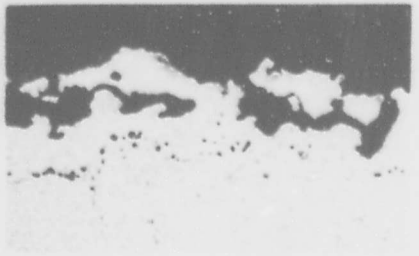

Magn 1000×

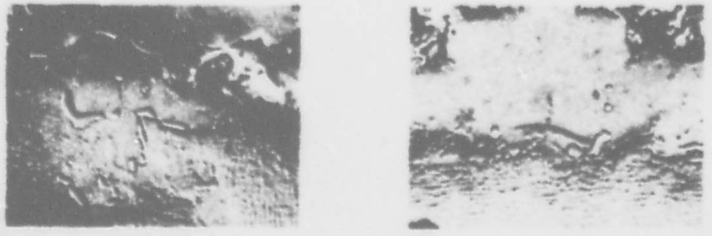

Magn 2500×

Figure 11.3. Light and electron micrograph of corrosion on Inco 717 after 1900°F cyclic test. (Ryan et al).

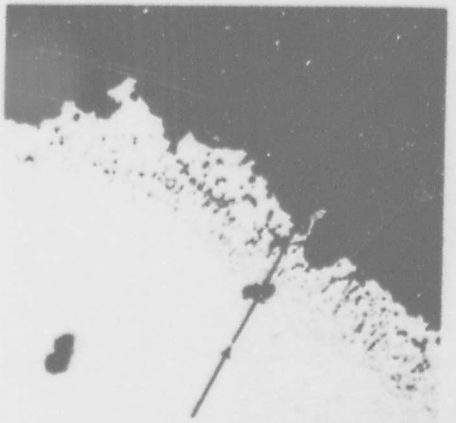

Magn 500× Etchant: ferric chloride No. 2

Microprobe traverse on Inco 717—1800°F cyclic test.

Location on traverse	Relative composition: Oxide scale α → β	Depletion zone β → γ	Sulfide γ	Depletion zone sulfides, γ - θ	Matrix Interface θ	Matrix
Element						
Nickel*	25-48	76-87	71	73-84	66	66
Cobalt*	3-12	7-11	8	8-9	10 1/2	10.5
Aluminum*	7-16	4-5	4	4 1/2-5	6	7.1
Sulfur**	8-15	16-21	76	25-77	10	10
Chromium*	4-8	2	6	3-3 1/2	12	12.6
Titanium**	16-65	3 5	6	4-12	18	20
Molybdenum*	1-1 1/2	2-4	4	3 1/2-4	3 1/2	4.2
Niobium**	3-15	2-3	2 1/2	2 1/2-7	5	5

*Approximate weight percent

**X-ray intensity—compare with matrix

Figure 11.4. Microprobe traverse across corrosion area of Alloy 717 after 1800°F cyclic test. (Ryan et al).

Inco 718

R. Viswanathan, Corrosion 24 (1968) 359.

Westinghouse swirl furnace, No. 2 diesel fuel contaminated with 6% sulphur. Gas passed over platinised ceramic catalyst to give large content of sulphur trioxide. Typical gas analysis: 12% CO_2 3.2% O_2, 1500 ppm SO_2, 150 ppm SO_3; remainder nitrogen. Cylindrical hollow specimens, ½ in. OD, ¼ in ID, 2½ in long. Cleaned specimen coated with salt by dipping in molten mixture of equal parts sodium and magnesium sulphates. Testing at 1500°F (816°) for times of 10 - 200h. Corrosion estimated by metallographic measurement of "unaffected metal" and by weight loss after descaling.

Inco 718 lost 8.5 mg/cm^2; 95.4% of the metal was unaffected in a 150h test. One of the better group of alloys tested, comparable with Hastelloy X and U-500.

The effect of two different sulphur trioxide levels in the gas stream was tested: 6 ppm and 150 ppm. For 718 the weight losses in a 150h test were 1.90 and 8.50 mg/cm^2 respectively. The author considers that SO_3 stabilises the sulphate coating.

Data relating to the alloy will also be found in the following Figure : 38.14;
and Table : 38-I.

IN 728 NX

K.H. Ryan, J.R. Kilsdig and P.E. Hamilton (Allison Division of General Motors) Technical Report to Wright-Patterson AFB, Air Force Materials Laboratory AFML-TR-67-306 (August 1967).

A detailed report of the procedure is given under PDRL-163. IN 728 NX was the second best alloy tested: (PDRL 163 is best; 713C + Cr is next). Figure 13.1 compares the volume loss of the as-cast and heat-treated alloy for all temperatures. Figure 13.2 compares the measured volume loss and that calculated from regression formula (see PDRL 163) for IN 728 NX. For all the alloys, the microstructure of the corrosion could be divided into three zones: (1) an outer layer of continuous oxide on the surface which gradually graded into an area of mixed metal and oxide; (2) a layer of depleted metal; (3) Globular sulphide particles. Pictures are shown of 713C, 717 and GMR-235; there are no sections of IN 728 NX shown.

J.J. Walters (AVCO/Lycoming Division) Technical Report to the Air Force Materials Laboratory, Wright-Patterson Air Force Base, AFML-TR-67-297 (September 1967).

Extended summary in B 1900. IN 728 NX is listed as one of a group of alloys with "relatively good resistance to attack". The others were U 700 and TRW 1800. X-ray analysis of the corrosion products found on the trailing edge after 40h of rig testing identified a spinel with a_o = 8.27 Å, NiO, Cr_2O_3, and an unknown phase. The phases after 120h were the same as at 40h. The products identified in powder removed from an area which had undergone sulphidation for 120h were a spinel with a_o = 8.24 Å, NiO and an unknown phase. A microprobe analyses of the depleted regions in the alloy showed 80.3% Ni, 0.4% Cr, 1.2% Mo, 2.0% Al, 0.1%Nb, 1.5%W, 13.7% Co and 1.1%Ta. The relative performance of four superalloys investigated in the engine for 60 and 90h with 1 ppm salt in the air and in the rig for 120h with 6 ppm salt in the air was compared (see 713C). The correlation seems quite good. IN 728 NX was considerably better than Alloy 713C and PDRL 163; slightly worse than 21 D4.

Figure 13.3 shows the corrosion as a function of temperature of IN 728 X tested using JP-4 fuel with 8 ppm salt in the air. Figure 13.4 - JP-4, 4 ppm salt. Figure 13.5 - JP-4R, 8 ppm salt. Figure 13.6 - JP-4R, 4 ppm salt. Figure 13.7 - JP-5; 8 ppm salt. Figure 13.8 shows the corrosion as a function of temperature using JP-4 fuel with 4 ppm salt, for 120, 240 and 360h tests. Figure 13.9 shows the same data for heat-treated IN 728 X samples.

Figure 13.10 shows a cross-section of a specimen oxidised for 360h at 1700°F (927°C). A needle phase develops after prolonged testing and the microprobe results for this are shown in Figure 13.11.

Rolls-Royce (1971) Ltd.

Hot corrosion data from a small burner rig is shown under X-40.

Data relating to this alloy will also be found in the following Figures :

1.1, 1.7, 1.8, 10.1, 10.13, 36.1, 36.2, 36.3, 36.4, 36.5, 36.6, 36.7, 52.28, 52.29;
and Tables :
1.I, 1.II, 1.IV, 1.V, 1.VI, 1.VII, 1.VIII, 1.IX.

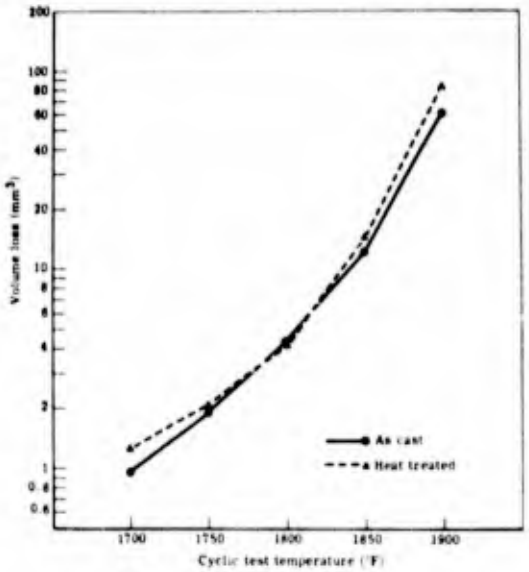

Figure 13.1. As-cast versus heat treated IN-728 NX at each cyclic test temperature. (Ryan et al).

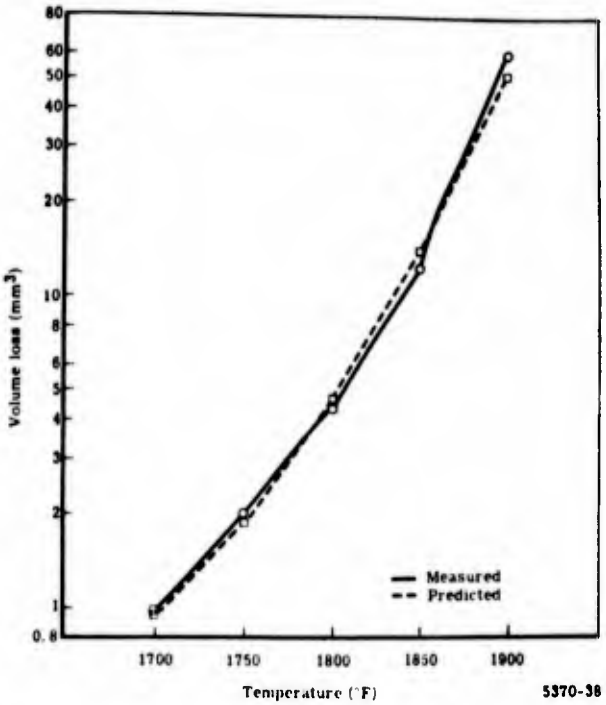

Figure 13.2. Comparison of the measured volume loss and the loss predicted by the regression equation for IN-728 NX. (Ryan et al).

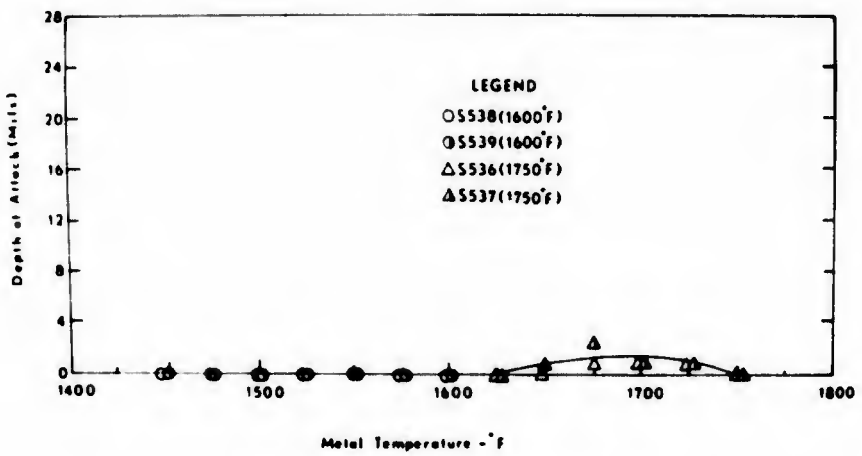

Figure 13.3. Corrosion as a function of temperature for IN 728 X tested using JP-4 fuel with a Salt/Air Ratio of 8 ppm. (Walters).

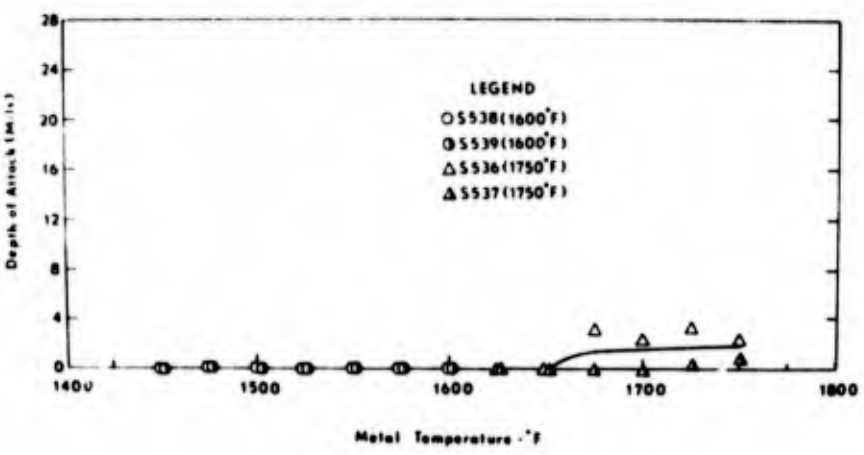

Figure 13.4. Corrosion as a function of temperature for IN728X tested using JP-4 fuel with a Salt/Air Ratio of 4 ppm. (Walters).

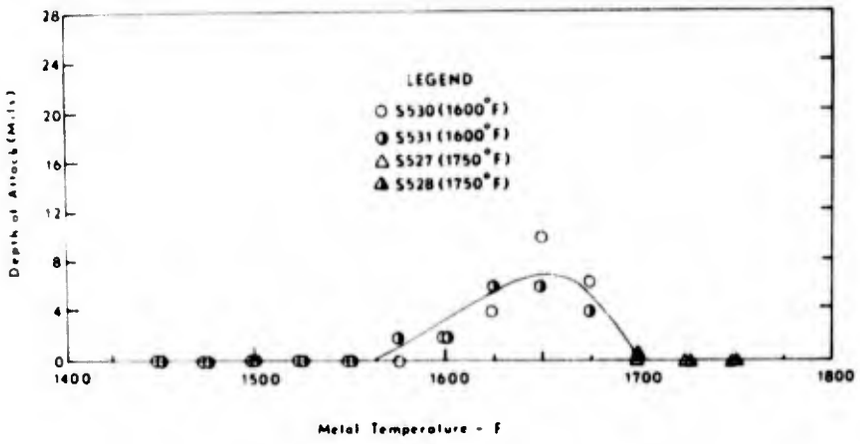

Figure 13.5. Corrosion as a function of temperature for IN 728 X using JP-4R fuel with a Salt/Air Ratio of 8 ppm. (Walters).

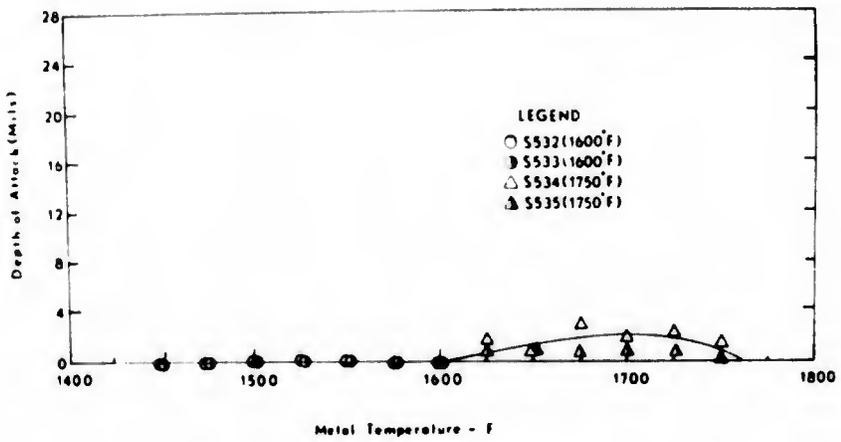

Figure 13.6 Corrosion as a function of temperature for IN 728 X using JP-4R fuel with a Salt/Air Ratio of 4 ppm. (Walters).

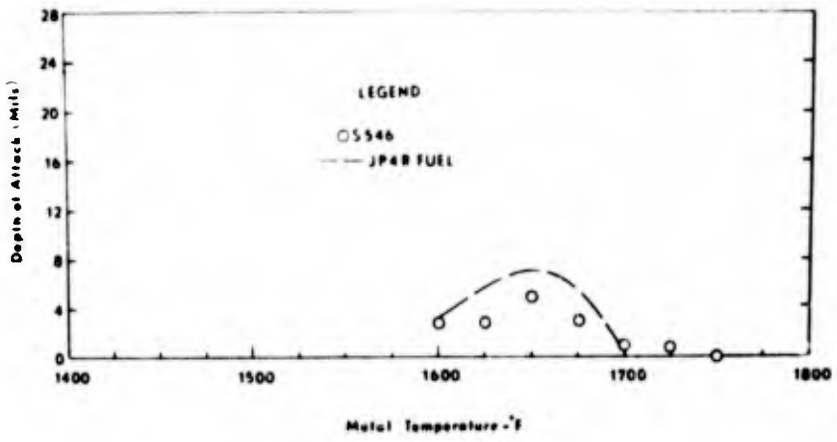

Figure 13.7. Corrosion as a function of temperature for IN 728 X tested using JP-5 fuel (0.16%S) with a Salt/Air Ratio of 8 ppm. (Walters).

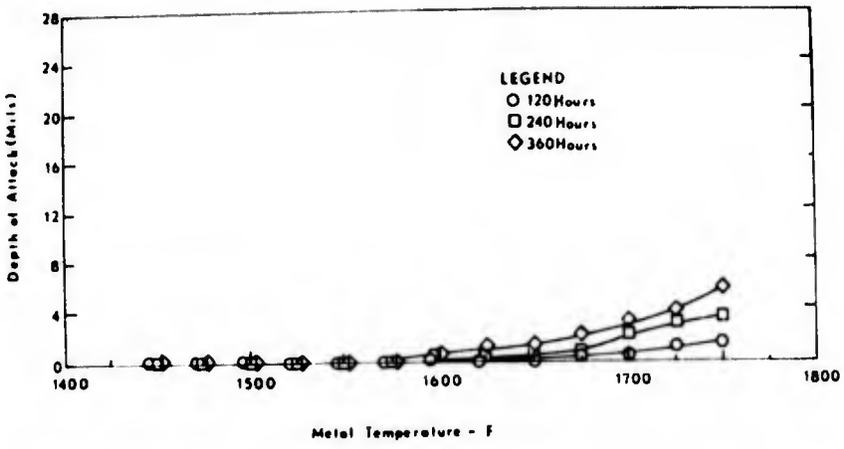

Figure 13.8. Corrosion as a function of temperature for IN 728 X tested using JP-4 fuel with a Salt/ Air Ratio of 4 ppm. (Walters).

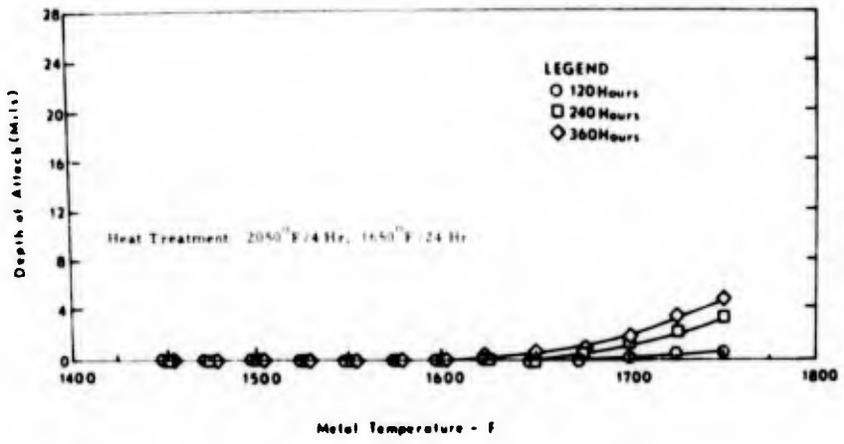

Figure 13.9. Corrosion as a function of temperature for IN728X HT tested using JP-4 fuel with a Salt/ Air Ratio of 4 ppm. (Walters).

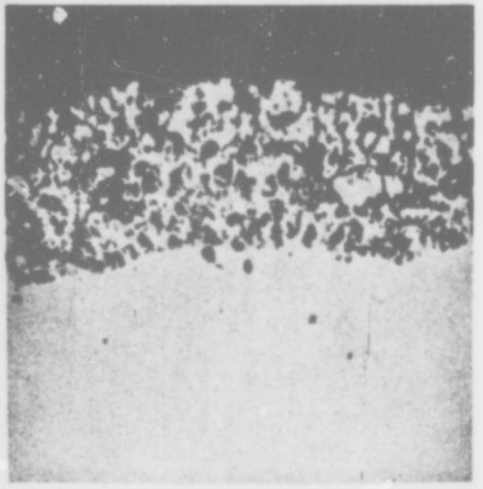

Figure 13.10. Oxidized surface of IN728X after 360 hours of testing at 1700°F. (Walters).

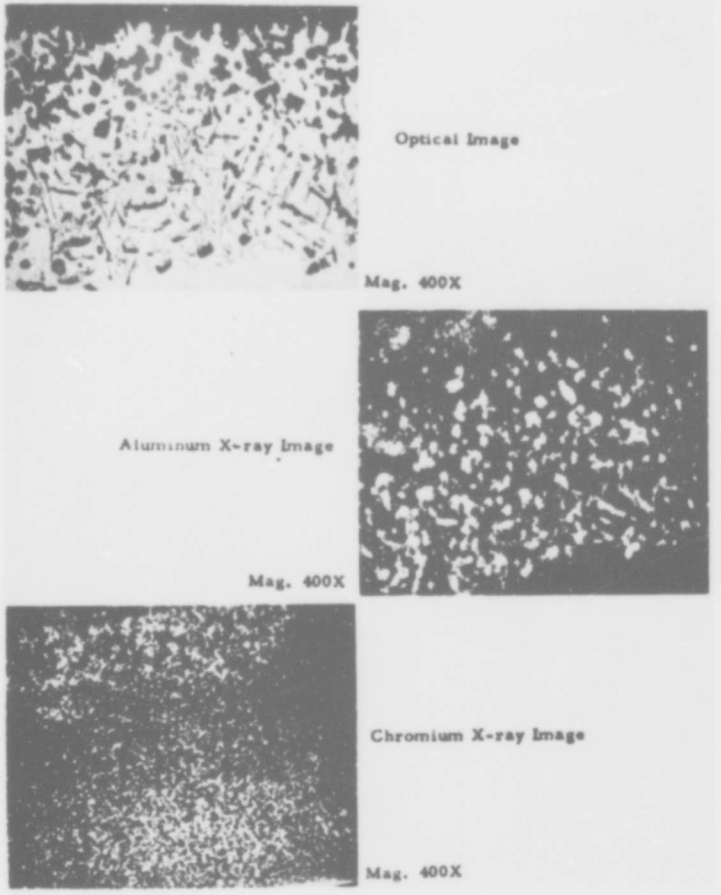

Figure 13.11. Optical and microprobe images of needle phase surface of IN728X after 360 hours of testing at 1750°F. (Walters).

H.T. Quigg and R.M. Schirmer, Progress Report No. 3 on NASC Contract No. N00019-68-C-0252 (Phillips Petroleum Company Research and Development 5423-69) July 1969.

See 713C for details. This report is principally concerned in testing the ASTM "Round Robin" group of alloys in the Phillips Turbine Environmental Simulator using a cyclic test in which the specimen is heated to 1600, 1800 or 2000°F (871, 982 or 1093°C) maximum temperature for 8 min followed by a cooling to 1000°F (538°C) for 2 min, producing an attack approximately six times more severe than the isothermal routine used in the earlier tests. After 44h at 2000°F max, IN 738 had lost 97 mg/cm^2, the surface loss was 15 mils and the maximum attack 16 mils. The alloy was the second best of those tested, better than Mar-M 421 but not as good as U 500. It was estimated that it would take 55h for the specimen to lose 127 mg/cm^2.

The data are presented in tables and graphs (see 713C).

ASTM Round Robin Test organised by the Hot Corrosion Task Force of the Gas Turbine Panel, 1970.

See 713C for details. IN 738 was one of the best two alloys tested, the other being U-500. Figure 14.1 shows the metal loss reported by the participants.

H.T. Quigg, R.M. Schirmer and L. Bagnetto, Final Report to NASC on Contract No. N00019-69-C-0221 (Phillips Petroleum Company Research and Development Report 5732-70) July 1970.

See 713C for details.

S.Y. Lee and W.E. Young in Combustion and Heat Transfer in Gas Turbine Systems; Cranfield Symposium No. 11, E.R. Norster (ed.) (Pergamon, Oxford 1971) 253.

See 713C for details. In 150h tests at 1800°F (982°C) for 738X the rate is approximately three times faster at 3 atm pressure than at 1 atm. U-500 and X-45 behave similarly; 713C is the same at the lower pressure, but the rate only doubles at the higher pressure.

H.T. Quigg, R.M. Schirmer and L. Bagnetto, Final Report to Naval Air Systems Command on Contract N00019-70-C-0293 (Phillips Petroleum Company Research and Development Report 5903-71) Jan. 1971.

See 713C for details. Figure 14.2 shows sections of a specimen after 60h in [illegible]00°F (1093°C) cyclic test with 1.0 ppm salt in the air and 0.0040 wt % S in the fuel, after electrolytic cleaning. Figure 14.3 shows a section of a specimen similarly tested with 0.0004 wt % S fuel.

E. Erdös, in "Deposition and Corrosion in Gas Turbines", A.B. Hart and A.J.B. Cutler (eds.) (Applied Science Publishers, London, 1973) 115.

See 713C for details. Figure 14.4 shows the sulphide phases in IN 738 preoxidised in air for 24h and sulphidised in S_2 vapour for 16h at 850°C, and Figure 14.5 displays the scanning analyses with the microprobe (dark means high concentration). Four different sulphides are visible; Ni_3S_2 (matrix), Cr-Ti-S (Cr_3S_4) globular, Cr-Al-S blocky, and $(Ta,Nb)S_2$ platelets. In addition, a trace of a carbide WC is detectable.

A.J.B. Cutler and C.J. Grant, in "Deposition and Corrosion in Gas Turbines",A.B. Hart and A.J.B. Cutler (eds.) (Applied Science Publishers, London, 1973) 178.

This paper reports experiments using an electrochemical method in which the corrosion current is determined from an analysis of the current potential function obtained when a transient perturbation is applied to the potential of the electrode. The corrosion rates of several superalloys - IN 738, Nimonic 90, Nimonic 105, Nimonic 115, Stellite 7, Stellite 8, and X-40 - in the ternary Li/Na/K eutectic sulphate melt at 1000°K. (727°C) under 1 atm oxygen and 3.23 x 10^{-4} atm SO_3. Figure 14.6 shows the corrosion data. IN 738 corrodes quite rapidly for 7 - 8 hours, but then the rate drops abruptly to a very slow value. Nimonic 90 is worst, Nimonic 115 next, then Nimonic 105; the cobalt alloys are just a little better than 105, but not quite as good as 738. Figure 14.7 shows repeat determinations for IN 738, showing that the drop in corrosion rate after a few hours is reproducible.

The sulphide concentration in the corrosion pits was appreciably greater than in the regions protected by the thin oxide layer.

P.L. Norman and J.D. Harston, in "Deposition and Corrosion in Gas Turbines" A.B. Hart and A.J.B. Cutler (eds.) (Applied Science Publishers, London, 1973) 260.

See Nimonic 80A for details. Figure 14.8 shows the hot-corrosion of various nickel-base alloys in a salt-spray test at 700°C using 75% Na_2SO_4, 25% NaCl spray, in terms of the weight loss after descaling. IN 738 does not show up very well, being with Nimonic 105, the worst alloy at least up to 100h, and much worse than Mar M 432 or Nimonic 90. Figure 14.9 shows similar data for a test temperature of 800°C. 738 is about the same as Nimonic 105 up to 50h, but at this time Nimonic 105 undergoes a great acceleration in rate; 738 shows no signs of an increase up to 100h. 713C and Nimonic 90 were much worse, Mar-M 432 was again better. Figure 14.10 shows the results at 900°C: 738 was now

appreciably better than Nimonic 90 or 105, and a little better than Mar M 432.

J.F.G. Conde and G.C. Booth, in "Deposition and Corrosion in Gas Turbines" A.B. Hart and A.J.B. Cutler (eds.) (Applied Science Publishers, London, 1973) 278.

See Nimonic 105 for details. Tests in the AML low pressure rig are described. At 850°C, 0.1 ppm salt, 200h tests, IN 738 was the worst of a group of four alloys, the other three in increasing order of resistance being Mar-M 432, Nimonic 90 and Nimonic 105. However, pack-aluminised 738 was very good.

C.J. Spengler, S.Y. Lee and W.E. Young, in "Deposition and Corrosion in Gas Turbines" A.B. Hart and A.J.B. Cutler (eds.) (Applied Science Publishers, London 1973) 294.

See U 500 for details. Some tests include IN 738 X, mostly reported in earlier papers.

P.C. Felix in "Deposition and Corrosion in Gas Turbines" A.B. Hart and A.J.B. Cutler (eds.) (Applied Science Publishers, London 1973) 331.

See 713C.

K. Page and R.J. Taylor, in "Deposition and Corrosion in Gas Turbines" A.B. Hart and A.J.B. Cutler (eds.) (Applied Science Publishers, London 1973) 350.

See Nimonic 105 for details. IN 738 is being evaluated as primary candidate as a blade material for Rolls-Royce industrial and marine turbines.

W.L. Wheatfall, in "High Temperature Corrosion of Aerospace Alloys" J. Stringer, R.I. Jaffee and T.F. Kearns (eds.), AGARD Conference Proceedings No. 120 (March 1973) 235.

See 713C for details. Figure 14.11 shows the relative hot corrosion resistance of 738, U 500, Mar-M 509 and X 40 and 1400, 1500 and 1600°F (760, 816, 871°C) in 300h tests with 35 ppm sea salt in the air, JP-5R fuel with 0.04%S. The data is taken from M. Gell, unpublished data from Pratt and Whitney.

L.M. Maas and C.L. Miller, ASME Paper 72-GT-77, presented to the Gas Turbine and Fluids Engineering Conference and Products Show, March 1972.

See 713C for details.

I.I. Bessen and R.E. Pryzell, General Electric Technical Information Report R72 AEG 317, (Nov. 1972), paper presented at the Gas Turbine Materials Conference Naval Ship Engineering Center, Oct. 1972.

See Rene 80 for details.

W.L. Wheatfall, S.J. Dapkunas and J. Sydavar, Naval Ship Research and Development Center, Materials Department, Research and Development Report 8 - 868 (August 1971).

Samples of this alloy and of Mar-M 432 were oxidised in flowing oxygen for 210h at 1650°F (899°C) and 235h at 1750°F (954°C). Results were compared with similar tests run on U 500. The extent of oxidation was measured in terms of oxide thickness, general penetration, and maximum depth of oxide penetration. For IN 738 the results were:-

	Surface oxide.	General penetration.	Maximum penetration (all mils)
210h at 899°C.	0.7	1.1	1.9
235h at 954°C.	1.5	2.5	4.2

U 500 was the most deeply oxidised alloy at 899°C, but had the lowest depth of attack at 954°C. The oxide scale on U 500 at 899°C was twice as thick as those on IN 738 and Mar M 432. Surface scales on U 500 were rough and uneven at both temperatures. At 899°C, IN 738 showed a slightly greater penetration than Mar-M 432. Grain boundary penetration of IN 738 was quite extensive at 954°C. Mar-M 432 was more resistant to oxidation than IN 738 at both temperatures. Suface scales were uniform on Mar-M 432, but fairly uneven on IN 738.

J.F.G. Conde Gas Turbine Materials Conference Proceedings, Naval Air systems Command, Washington (1972) 17.

Figure 14.12 shows a section of a pack aluminised IN 738 test specimen after 200h, 750°C, 1.0 ppm sea salt, in AML Low Pressure combustion test rig.

Data relating to this alloy will also be found in the following Figures :
10.51, 10.53, 10.54, 10.83, 10.84, 10.92, 10.100, 10.120, 32.17, 32.18, 32.19, 32.20, 45.33, 45.35, 45.37; and Tables :
10-XI, 10-XV, 10-XVI, 10-XXII, 10-XXIII, 10-XXIV, 10-XXV, 10-XXVI, 10-XXIX, 32-I, 39-I.

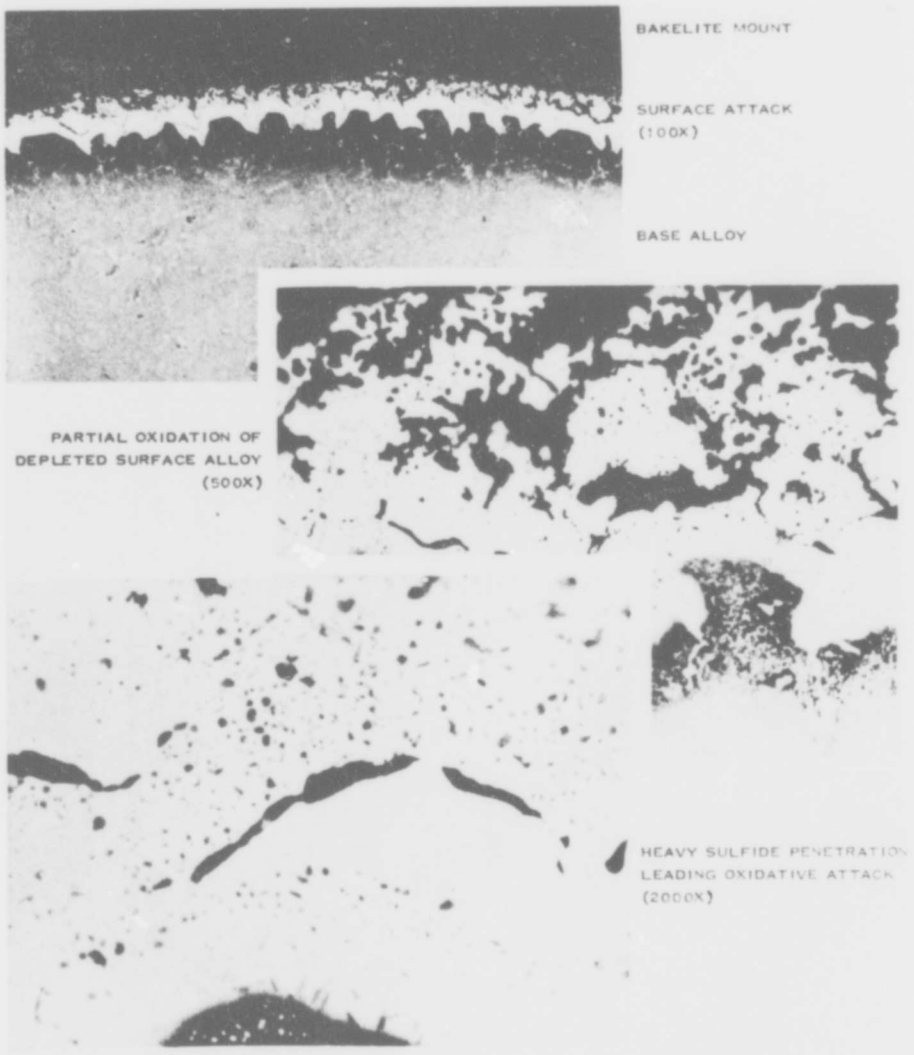

METALLOGRAPHIC CROSS-SECTION OF SPECIMEN FROM 2000 F CYCLIC TEST IN PHILLIPS TURBINE SIMULATOR WITH 1.0 PPM SEA SALT IN AIR AND 0.0040 WT % SULFUR IN FUEL. ELECTRO-CLEANED, 10% OXALIC ACID-ELECTROLYTIC ETCHED.

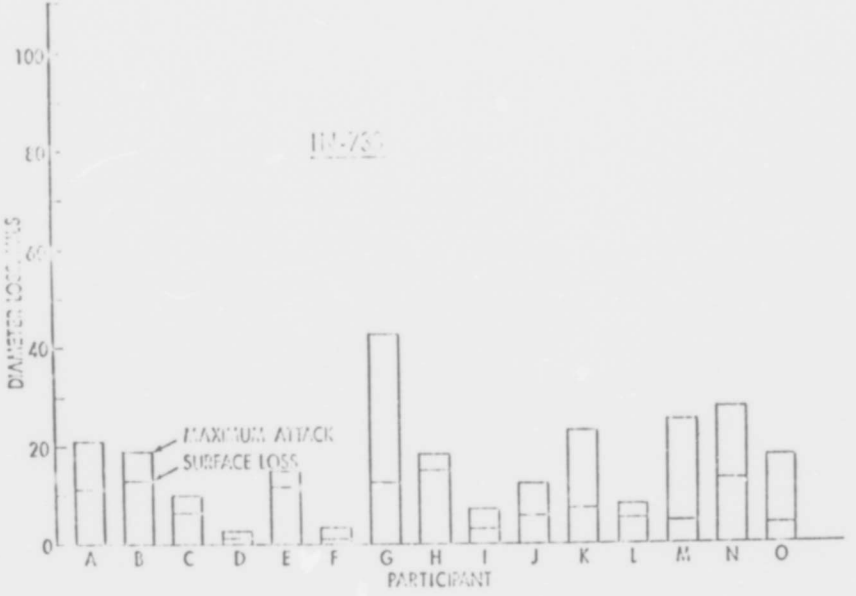

Figure 14.1. Results of ASTM Round Robin test for IN 738.

Figure 14.2. Hot corrosion of bare IN - 738 specimen after 60 hours (low sulphur fuel) (Quigg et al).

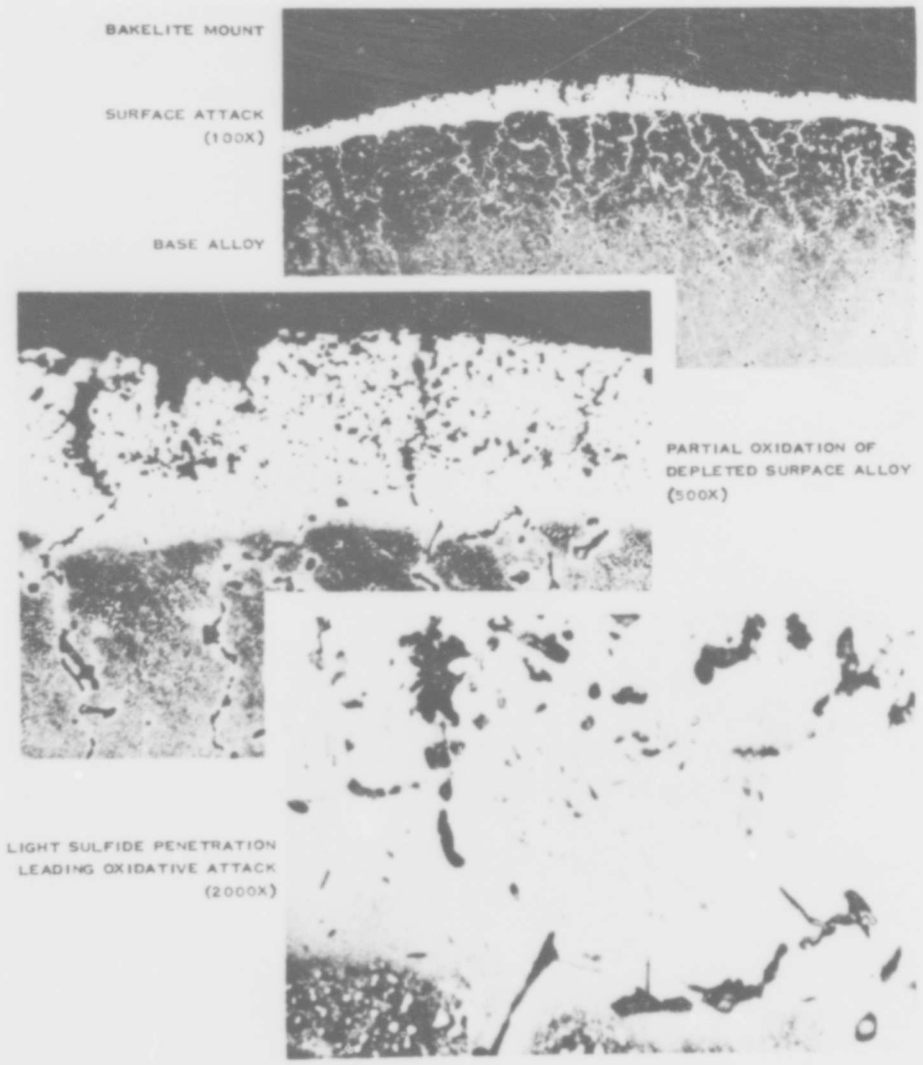

Figure 14.3. Hot corrosion of bare IN-738 specimen after 60 hours (very low sulphur fuel) (Quigg et al).

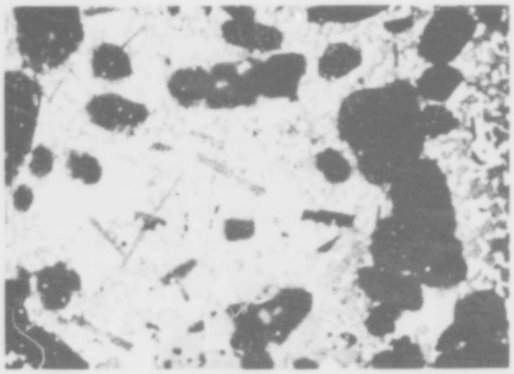

Figure 14.4. IN 738 preoxidized 16h/850^{o}C/S_2 (Ercos).

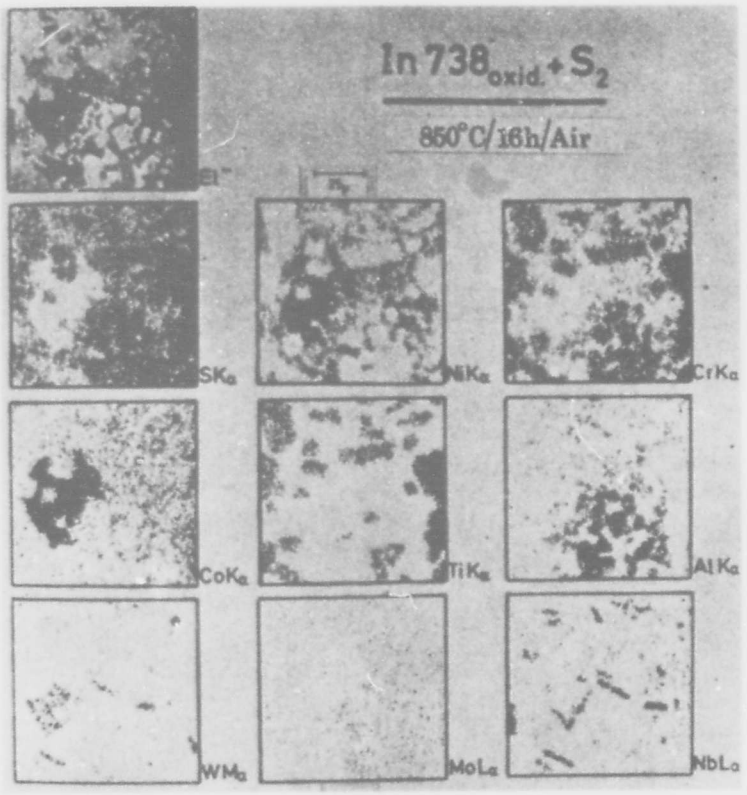

Figure 14.5. Electron microprobe pictures of IN 738 oxidised in air for 24h and sulphidised in S_2 vapour for 16h at 850°C. Dark means high concentration. (Erdos).

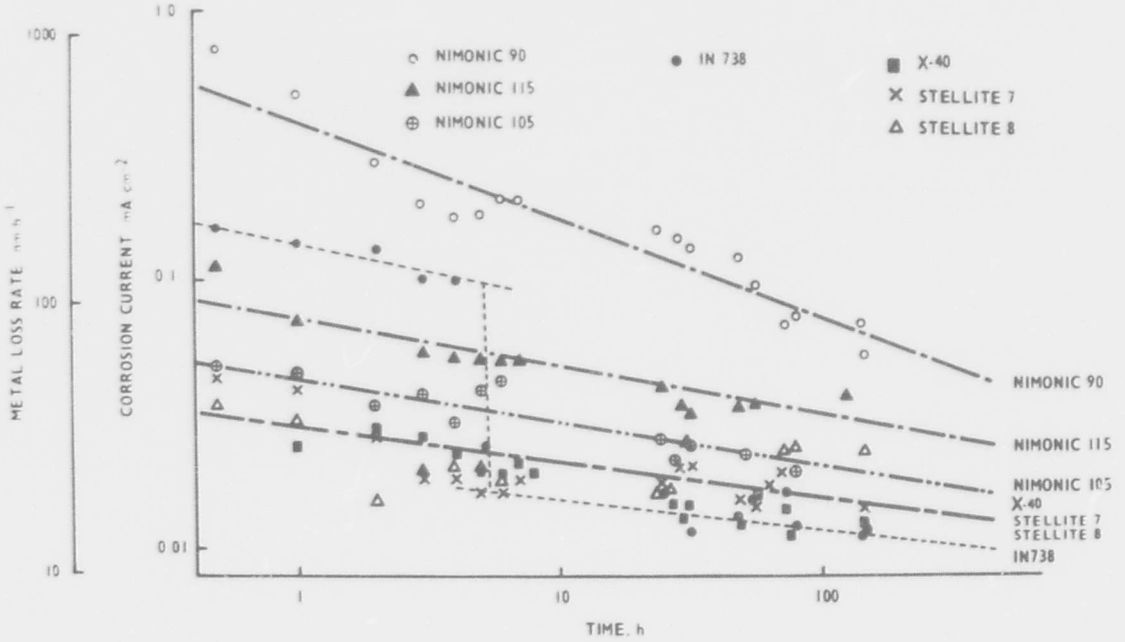

Figure 14.6. Corrosion data for gas turbine alloys in molten sulphate at 1000 K. (Cutler and Grant).

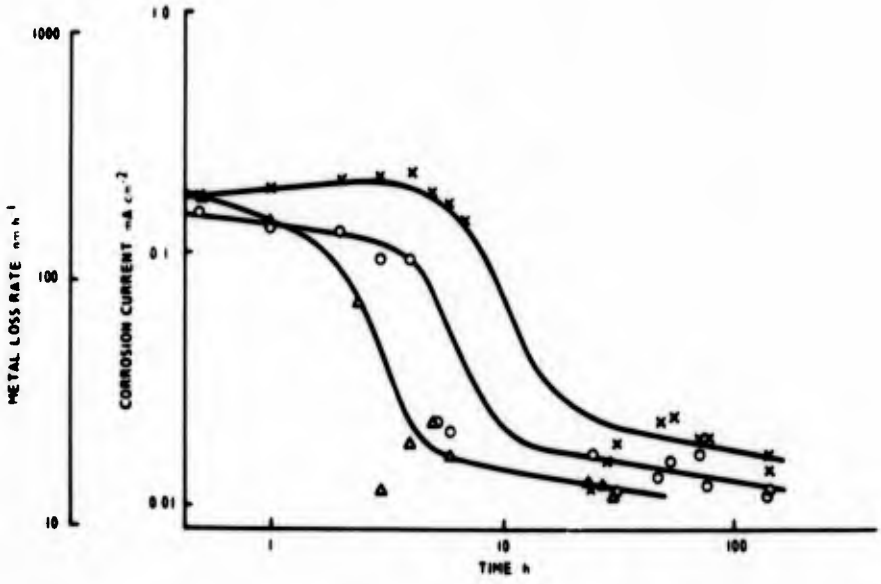

Figure 14.7. Corrosion data for IN 738 in molten sulphate at 1000 K. (Cutler and Grant).

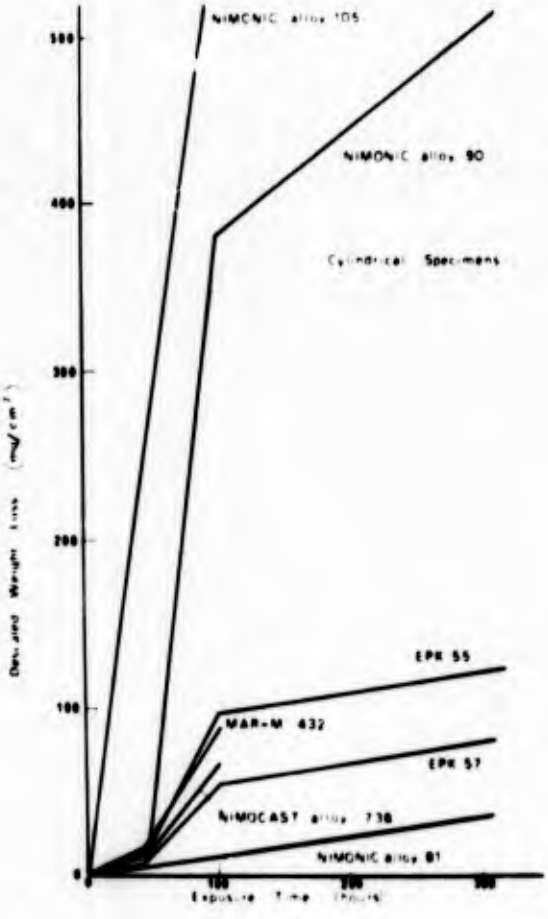

Figure 14.8. Hot corrosion of various Ni-base gas-turbine alloys in 75% Na_2SO_4-25% NaCl at 700°C. (Norman and Harston).

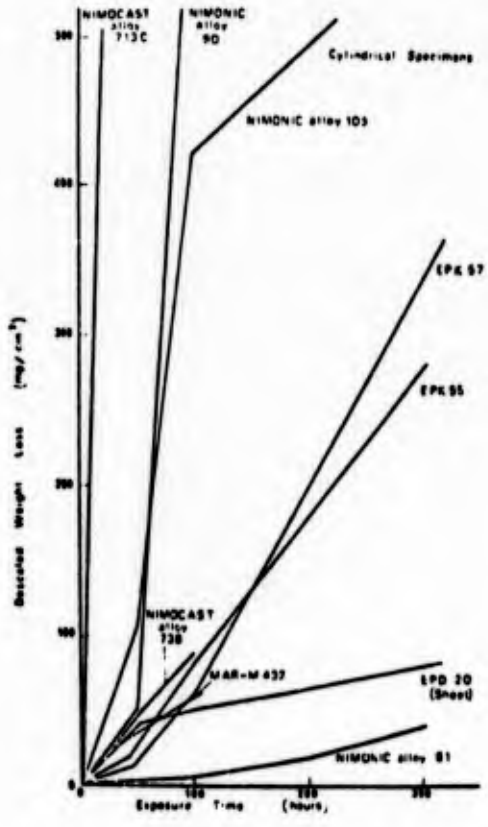

Figure 14.9. Hot corrosion of various Ni-base gas-turbine alloys in 75% Na_2SO_4 + 25% NaCl at 800°C. (Norman and Harston).

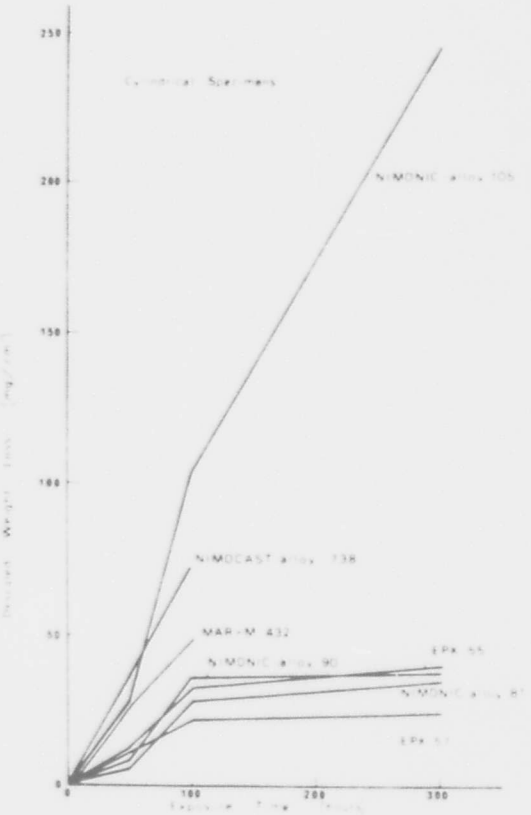

Figure 14.10. Hot corrosion of various Ni-base gas-turbine alloys in 75% Na_2SO_4 + 25% NaCl at 900°C. (Norman and Harston).

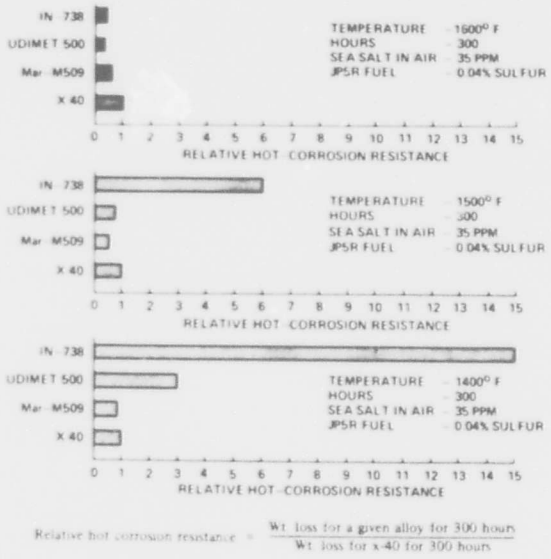

Figure 14.11. Relative hot-corrosion resistance of nickel- and cobalt-base superalloys as a function of temperature. (Wheatfall, quoting Gell).

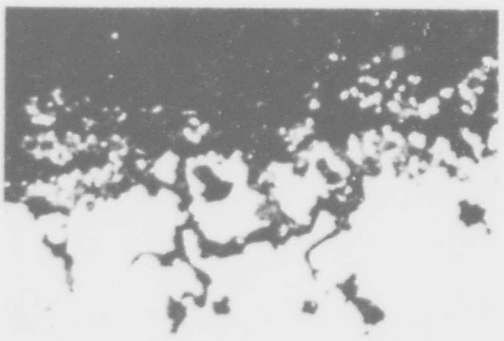

Figure 14.12. Pack-aluminised IN 738 test specimen after 200 h, 750°C, 1.0 ppm seasalt, in AML Low Pressure combustion test rig. X 375. (Conde).

Inco 750, Inco 751, K 2.

Inco 750

R. Viswanathan, Corrosion 24 (1968) 359.

See 713C for details. Weight loss after descaling, 7.0 mg/cm^2; 95.4% of metal unaffected, after 150h test at 1500°F (816°C). Comparable to Inco 751, not quite as good as 718, Hastelloy X.

Inco 751

R. Viswanathan, Corrosion 24 (1968) 359.

See 713C for details. Weight loss after descaling after 10h test at 1500°F, 0.6 mg/cm^2. After 150h, 27.5 mg/cm^2. 88.2% of metal unaffected. Moderate resistance, similar to that of 750, 718. Not as good as Hastelloy X.

K 2

P.A. Bergman, Corrosion 23 (1967) 72.

See SEL for a summary of the method and the results. At 982°C the rate in 50h tests with 200 ppm salt is about the same as SEL and 713; at 1020°C the resistance is better than the other two alloys. In spite of its high chromium content K2 was subject to deep intergranular attack.

Date relating to this alloy will also be found in Figure 41.2.

L 605

P.A. Bergman, Corrosion 23 (1967) 72.

See SEL for a summary of the method and some of the general results. L605 was severely corroded at 1020°C in 50h with 200 ppm salt in air, 0.25% S in the fuel. The alloy was subject to deep intergranular attack.

H. von E. Doering and P.A. Bergman, Naval Ship Research and Development Center Materials Laboratory Research and Development Report No. 2844 (March 1969).

See 713C for details. In a 100h test at 1750°F (955°C) with 200 ppm salt the surface loss was 10.7 mils and the maximum penetration was 27.8 mils: this was fairly similar to SEL, and a little better than SM-200. In a 1000h test with 5 ppm salt the figures were 5.5 and 15.3 mils respectively, better than U 500, not quite as good as X-40. The authors regard the low salt, long time test as better related to the real situation.

J.R. Johnston and R.L. Ashbrook, NASA Technical Note TN D-5376 (August 1969).

See B 1900 for details and the general figures and tables. The oxides were identified by X-ray diffraction on specimens exposed to high gas-velocity testing for 100h: at 1800°F (982°C) and at 1900°F (1038°C) they were a monoxide (presumably CoO) and a spinel with a_o = 8.30 Å.

S.T. Wlodek, Paper presented at the Atlantic City Meeting of the Electrochemical Society, October 1970.

Continuous weight-gain measurements in dry flowing air on sheet specimens 1.5 in x 0.4 in x 63 mil. Internal oxidation measurements were obtained on 1 in x 0.5 in diameter cylinders, static exposure followed by metallographic examination. The alloy was in the mill annealed condition (2225°F, 1218°C). All specimens were mechanically abraded through 600 paper and electropolished.

Figure 18.1 shows the weight gain versus time for temperatures between 1400 and 2200°F (760 - 1204°C). After 1000 min at 1700°F or 10 - 100 min at higher temperatures the rate was more or less parabolic. Figure 18.2 shows parabolic plots and Figure 18.3 shows an Arrhenius plot of the rate constants: the activation energy was approximately 42 ± 10 kcal/mole; a second parabolic rate at 2000°F and above having an activation energy of 50 ± 14 kcal/mole. Table 18-I lists the rate constants.

Areas of very localised attack were noted at 2200°F (1204°C). The scale on specimens tested above 1700°F cracked and exfoliated, usually along the metal/oxide interface.

Metallographic evidence showed that the erratic results obtained at or below 1600°F (871°C) could be associated with extremely heterogeneous scale distribution.

The internal oxidation of a specimen oxidised 100h at 1800°F (982°C) is shown in Fig. 18.4. The oxides are mainly associated with grain boundaries. The internal oxidation process was very heterogeneous and erratic. Figure 18.5 shows the relative penetration of specimens oxidised at 1600, 1800 and 2000°F (871, 982 and 1093°C) for 400h, and at 2200°F (1204°C) for 100h.

Figure 18.6 shows the general catastrophic attack of a specimen after 100h at 2200°F (1204°C). A low-melting point phase appears to have been produced: it is suggested that this is a mixture of $CoCr_2O_4$ + $CoWO_4$ and Co_3O_4.

Table 18.II summarises the oxidation products identified by X-ray and electron diffraction: the predominant oxide in most cases was $CoCr_2O_4$ (a_o in the range 8.27 - 8.35 Å). At 2200°F $CoWO_4$ was also detected in regions of catastrophic attack. Cr_2O_3 was present in most specimens in small amounts.

Chemical analysis of the oxide formed in the catastrophic oxidation showed that it contained 38% Co, 14% Cr, 12% W, 7.5% Ni, 1.5% Fe, 1% Mn, 0.5% Si and traces of other elements.

The internal oxides were identified by extraction techniques, and the results are summarised in Table 18.III. At 1600 and 1800°F, the principal product was probably amorphous SiO_2, with some $CoCr_2O_4$; at 2000 and 2200°F, the products were α - cristobalite and Cr_2O_3.

Microprobe traverses over specimens oxidised for 400h at 1600F and 1800F respectively indicate that the scale is more involved than implied by the X-ray diffraction results. On both specimens the scale was found to consist of two definite layers, with the outer layer possessing a concentration of some 5 - 15% Mn at 1600°F and 10 - 25% Mn at 1800°F: it seemed that the scale on the 1600°F specimen had an outer scale of the $Co(Cr,Mn)_2O_4$ type and an inner scale of $CoCr_2O_4$. At 1800°F the inner scale was Cr_2O_3, the outer probably $(CoNi)(CoCrMn)_2O_4$.

The author considers that the activation energy suggests that the rate controlling process is diffusion through a spinel layer. Figure 18-7 presents a schematic summary of the oxidation process, and Table 18-IV compares the behaviour of X-40 and L605 with the nickel-base alloys Rene 41, U 700 and Hastelloy X.

W.L. Wheatfall, in "High Temperature Corrosion of Aerospace Alloys". J. Stringer, R.I. Jaffee and T.F. Kearns (eds.), AGARD Conference Proceedings No.120, (March 1973) 235.

See 713C for details.

C.E. Lowell and D.L. Deadmore, Oxid. Metals, 7 (1973) 55.

Refers to the "anomalous weight increase" formed during the oxidation of L 605 by J.S. Wolf and G.D. Sandrock, NASA TN D-4715 (1968), in some tests with low Si or Mn contents, and attributed by those authors to failure of the metal under the growth stresses of the initially-formed Cr_2O_3 scale, exposing new metal. Lowell and Deadmore remark that other authors have attributed this acceleration in oxidation to the failure of the oxide rather than the metal. Their programme was intended to resolve the disagreement. Samples of the most-prone alloy tested by Wolf and Sandrock were oxidised at 1100°C for times up to 100h, with varying surface finish. A typical rate curve showed a slow initial parabolic rate, abruptly terminated by the oxidation rate increase of over 100 times; the rate then gradually diminished to a value close to the initial rate. The time at which the rapid acceleration took place increased with increasing surface deformation, and at a given surface roughness increased with decreasing moisture content; so for a 120 grit surface, the breakaway time was 15h with 2.5 ppm water, 10h with 8000 ppm water, and less than 15 minutes with 25,000 ppm water. The results correlate not with the surface roughness, but with the deformation introduced by the grinding as indicated by X-ray line broadening.

Cr_2O_3 was the only oxide formed before breakaway, while CoO, $CoCr_2O_4$, $CoW O_4$ were also present afterwards.

Lowell and Deadmore suggest that the Cr_2O_3 is formed under compressive stress, and blisters from the surface. Volatilisation of the oxide as CrO_3 causes greater thinning of the oxide where it is separated from the metal since "Cr would have to be vapour transported across the void, which must be a slower step". The oxide cracks at these thin places, allowing direct access of the oxidant to the chromium depleted metal. CoO forms rapidly, lifting off the poorly adherent Cr_2O_3. Si is considered to promote Cr_2O_3 formation, as does prior deformation.

Data relating to this alloy will also be found in the following Figures :
1.9, 1.10, 1.13, 10.105, 41.2, 52.12;
and Tables :
10-III, 10-XXX.

TABLE 18-I

RATE CONSTANTS FOR L-605 (WLODEK)

Temp °F	Heat	Rate Constatns Observed
1600	B	$K_p = 2.76 \times 10^{-5}$ (t > 200)
1700	A	$K_p = 1.15 \times 10^{-4}$ (t > 1000)
1800	A	$K_p = 2.02 \times 10^{-4}$ (t < 200)
1800	B	$K_p = 2.57 \times 10^{-4}$ (t < 200)
1900	A	$K_p = 4.88 \times 10^{-3}$ (t > 400)
2000	A	$K_{p1} = 9.90 \times 10^{-4}$ (2500< t > 200) $K_{p2} = 7.06 \times 10^{-4}$ (t > 2500)
	B	$K_{p1} = 7.42 \times 10^{-4}$ (2300 < t > 200) $K_{p2} = 5.68 \times 10^{-4}$ (t > 2300)
2100	A	$K_{p1} = 1.79 \times 10^{-3}$ (2000< t > 200) $K_{p2} = 1.54 \times 10^{-3}$ (t > 2000)
2200	A	$K_{p1} = 2.87 \times 10^{-3}$ (1000< t > 100) $K_{p2} = 2.54 \times 10^{-3}$ (2000 < t > 1000) K_L 9.70 x 10^{-2} (t < 2000)
	B	$K_{p1} = 3.23 \times 10^{-3}$ (800 < t > 200) $K_{p2} = 2.60 \times 10^{-3}$ (2200< t > 800) $K_L = 9.0 \times 10^{-2}$ (t > 2200)

K_p = $mg^2/cm^4/min.$, K_L = $mg/cm^2/min$

Figures in brackets indicate time interval in minutes during which each rate is operative.

TABLE 18-II

SURFACE REACTION PRODUCTS IDENTIFIED ON L-605 (WLODEK)

Exposure Temp °F	Hr.	Phases Identified
1600*	0.17	CoO + $Co\,Cr_2O_4$
1600**	1.0	CoO (a_o = 4.27Å) + Cr_2O_3
1600	53.0	$CoCr_2O_4$ (a_o = 8.32Å) + Cr_2O_3 + CoO (trace)
1600	100.0	$CoCr_2O_4$ (a_o = 8.27Å) + CoO (a_o = 4.28Å) + Cr_2O_3
1600	400.0	$CoCr_2O_4$ (a_o = 8.30Å) + Cr_2O_3
1800**	0.17	Cr_2O_3 + CoO (a_o = 4.24Å) + $CoCr_2O_4$ (a_o = 8.41)
1800	1.0	$CoCr_2O_4$ (a_o = 8.29Å) + Cr_2O_3 (trace)
1800	100.0	$CoCr_2O_4$ (a_o = 8.29Å) + Cr_2O_3 (trace)
1800	400.0	$CoCr_2O_4$ (a_o = 8.29Å) + Cr_2O_3
2000	0.17	Cr_2O_3 + $CoCr_2O_4$ (a_o = 8.42Å)
2000	1.0	$CoCr_2O_4$ (a_o = 8.30Å) + Cr_2O_3 (trace)
2000	400	$CoCr_2O_4$ (a_o = 8.33Å) + Cr_2O_3
2200	100	$CoCr_2O_4$ (a_o = 8.35Å) + Cr_2O_3 + CoO (a_o = 4.24Å) with Co_3O_4 (a_o = 8.16Å) and $CoWO_4$ in areas of catastrophic attack.

*Electron Diffraction on electrolytically stripped film

**X-ray diffraction film pattern on electrolytically stripped film

Order of listing at each exposure condition signifies abundance of phases.

TABLE 18-III

SUBSCALE REACTION PRODUCTS (WLODEK)

Alloy	Exposure Condition Temp °F	Exposure Condition Time Hr.	Phases Identified
L-605	1600	400	SiO_2 (?) amorph. + $CoCr_2O_4$
L-605*	1800	400	SiO (?) amorph. + $CoCr_2O_4$ + α-cristobalite (tr)
L-605	2000	100	α-cristobalite + Cr_2O_3
L-605**	2000	400	α-cristobalite + Cr_2O_3
X-40**	1800	400	Cr_2O_3 + α-cristobalite
X-40**	2000	400	α-cristobalite + Cr_2O_3

*Identified by extraction replica and electron diffraction as well as x-ray diffraction on first 2-3 mils of subscale residue.

**Identified only by x-ray diffraction extraction residue obtained on first 2-3 miles of subscale zone.

All others electron diffraction on extraction replica only.

TABLE 18-IV

COMPARISON OF THE OXIDATION BEHAVIOR OF COBALT AND NICKEL-BASE ALLOYS (WLODEK)

	1600°F		1800°F		2000°F		2200°F	
Alloy	*Kp	100 Hr. I.O. Mils/side	*Kp	100 Hr. I.O. Mils/side	*Kp	100 Hr. I.O. Mils/side	*Kp	100 Hr. I.O. Mils/side
X-40	-	0.5	-	1.5	-	3.1	-	3.7
L-605	2.8×10^{-5}	0.6	2.3×10^{-4}	1.3	6.4×10^{-4}	2.0	2.6×10^{-3}	3.9
Rene 41	1.0×10^{-4}	0.6	1.7×10^{-3}	1.2	1.28×10^{-2}	2.5		
Udimet 700	4.6×10^{-5}	0.0	4.6×10^{-4}	0.1	4.6×10^{-2}	1.2	-	-
Hastelloy X	-	0.0	4.9×10^{-6}	1.2	1.5×10^{-5}	3.0	7.6×10^{-5}	

*Kp = $mg^2/cm^4/min$

I.O. = depth of internal oxidation

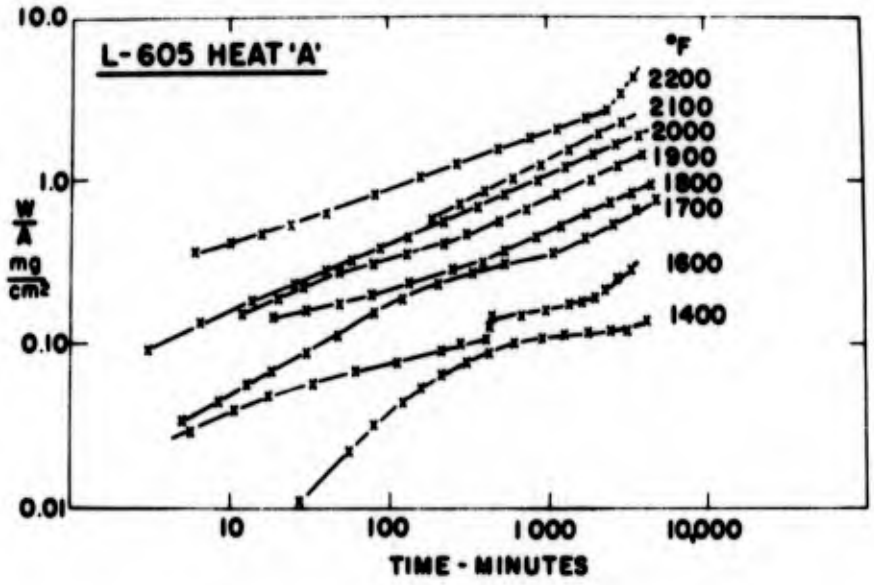

Figure 18.1. Log-log plot of weight gain data for L-605 (Heat A). Note irreproducible, mixed kinetics below 1700°F, parabolic behaviour (slope = ½) 1700 to 2200°F and beginning of linear rate (slope = 1) after prolonged exposure at 2200°F. (Wlodek).

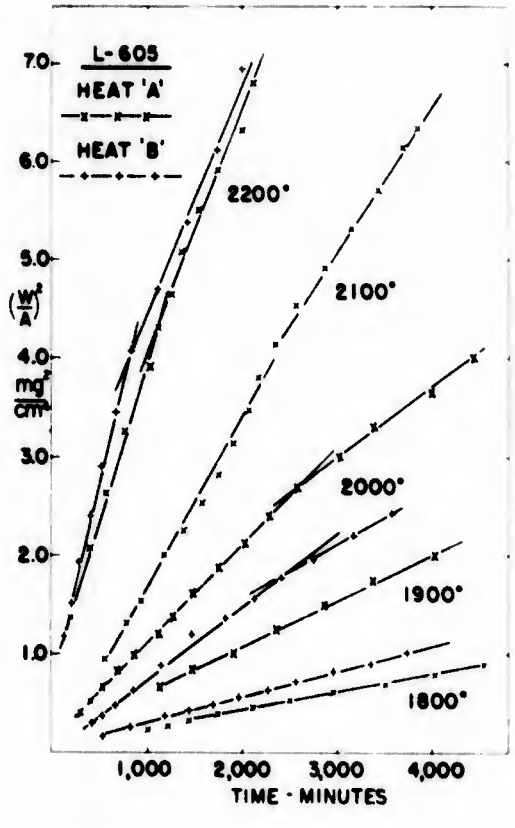

Figure 18.2. Parabolic scaling kinetics for Heats A and B of L-605. Note occurrence of two parabolic rates at 2000°F and above. (Wlodek).

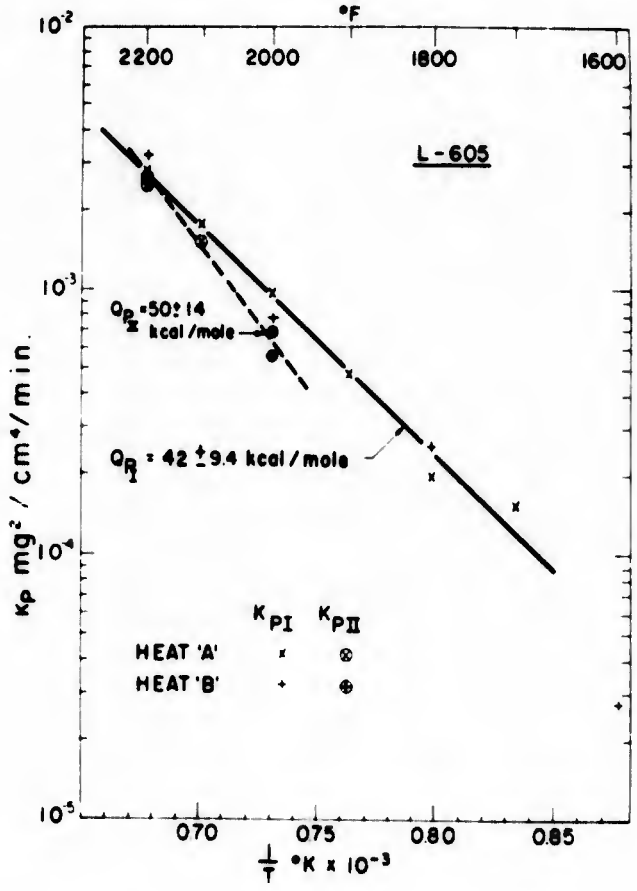

Figure 18.3. Arrhenius plot of L605 rate constants. An activation energy of about 42 ± 9.4 kcal/mole can be assigned to the first and 50 ± 14 kcal/mole to the second parabolic rate. (Wlodek).

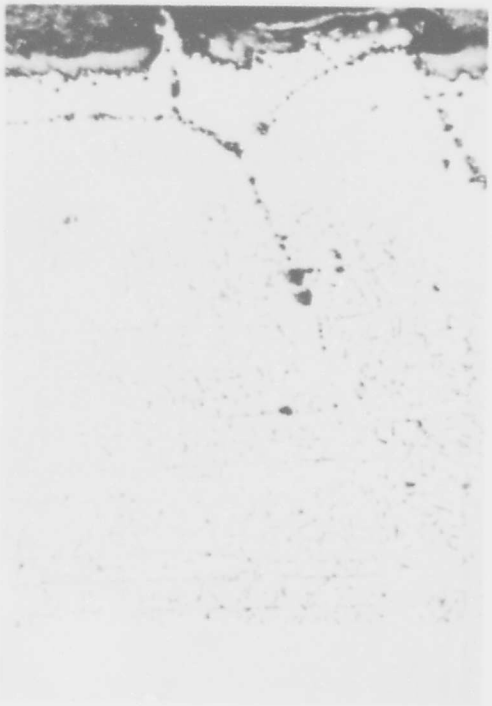

Figure 18.4. Microstructure of internal oxidation processes after 100h at 1800°F (982°C) in L605 (Wlodek) x 500. Taper section x 3.5

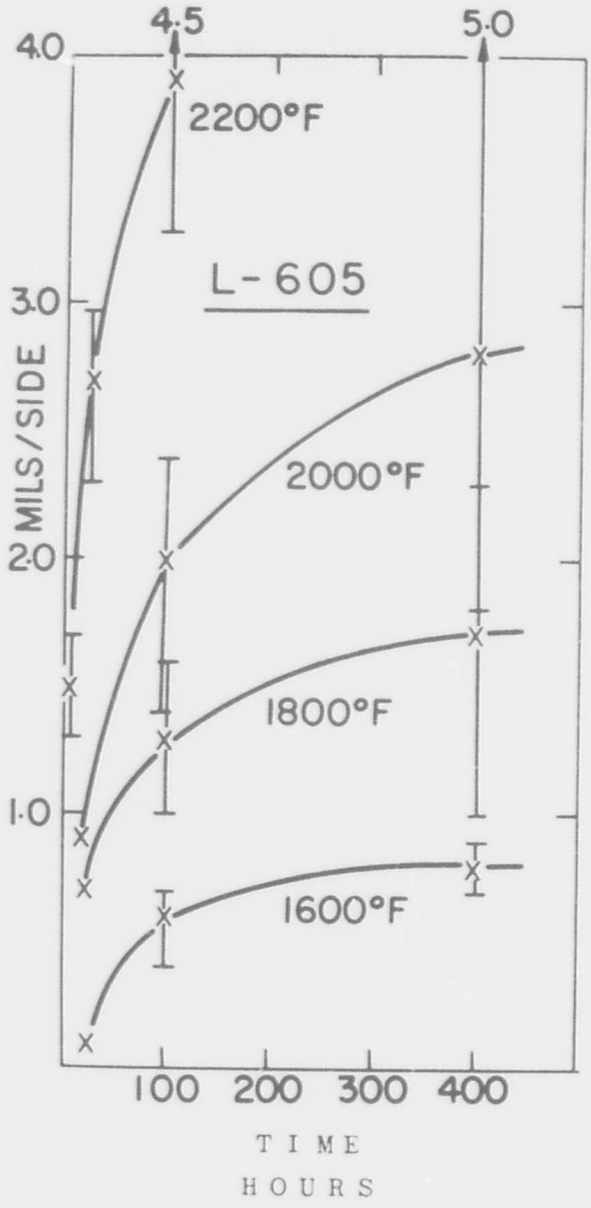

Figure 18.5 Extent of internal oxidation in L605. Results reflect five specimens and two heats. (Wlodek).

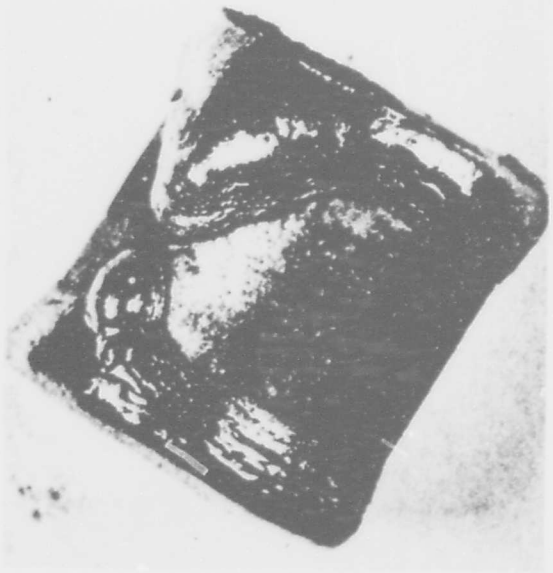

Figure 18.6. General catastrophic attack of L-605 after 100 hours at 2200°F. Formation of low melting point mixture of $CoCr_2O_4$+$CoKO_4$ +Co_3O_4 produces linear oxidation at 2200°F. (Wlodek) X4.

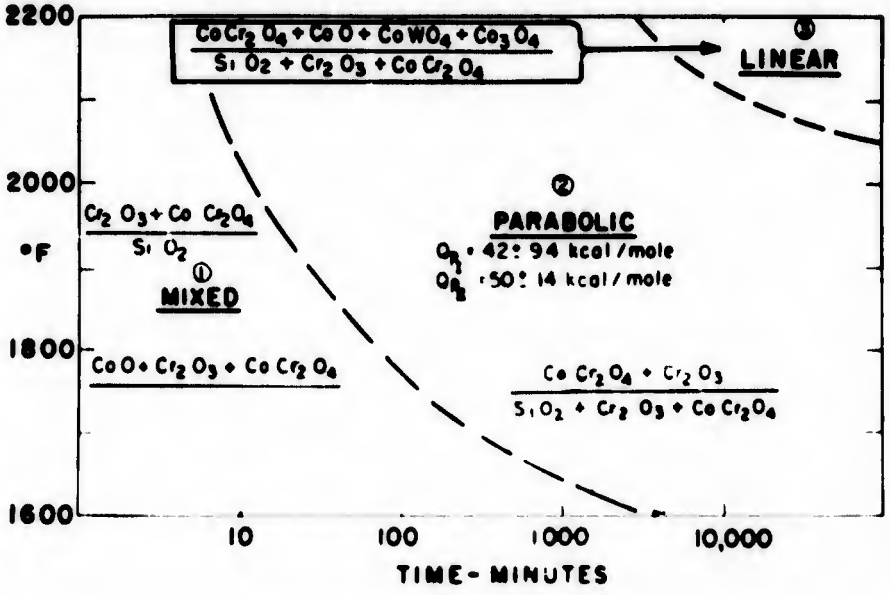

Figure 18.7. Schematic summary of L-605 oxidation process. Three definite regions: #1 mixed oxidation kinetics, #2 parabolic oxidation, #3 linear oxidation due to liquid reaction products, can be identified. In each region the reaction processes are presented as a quotient with the surface scale products in the numerator and the subscale products in the denominator. Use of formulae to identify reaction products not to be taken to indicate that phases are pure or stoichiometric. (Wlodek).

Mar-M 200

L.D. Graham, J.D. Gadd and R.J. Quigg, Hot Corrosion Problems Associated with Gas Turbines, ASTM Special Technical Publication, STP 421, 1967, 105.

See 713C for details. MAR-M 200 was one of the worst alloys tested, only marginally different from B 1900, TRW 1900 and MAR-M 302. The directionally solidified alloy is virtually the same as the randomly solidified. Graph of attack vs. temperature (Fig. 19.1) increases to 1900°F, then abruptly falls, increases again to 2100F. A photomicrograph of corroded sample is shown in Figure 19.2. Major scale products were NiO, Ni_3S_2, unreacted Ni (text does not mention specific alloy for this, implies that all heavily corroded alloys are the same).

J.J. Walters (AVCO/Lycoming Division) Technical Report to the Air Force Materials Laboratory, Wright-Patterson Air Force Base AFML-TR-67-297 (September 1967).

Extended summary in B 1900. Mar.M. 200 is listed as one of a group of alloys with very poor resistance to attack (the others are B 1900, B1910 and IN 100). X-ray analysis of corrosion products found on the trailing edge after 40h of rig testing identified NiO, a spinel with a_o = 8.26 Å, and a trace of $NiWO_4$. After 120h an unknown phase with d-spacings 2.11, 2.63, 1.93 and 1.86 Å was also present. In powder removed from an area which had undergone sulphidation corrosion for 120h, NiO, a spinel with a_o = 8.27 Å, and $NiWO_4$ were present. The microprobe analysis of the depletion zone in Mar-M 200 was 80.5% Ni, 0.5% Cr, 1.9% Al, 0% Ti, 0%Nb, 7.8% W and 10.8% Co.

Figure 19.3 shows the corrosion as a function of temperature using JP-4 fuel, 8 ppm salt. Figure 19.4 - JP-4, 4 ppm salt. Figure 19.5 - JP-4R, 8 ppm salt. Figure 19.6 - JP-4R, 4 ppm salt. Figure 19.7 - JP-5 fuel, 8 ppm salt.

H.T. Quigg and R.M. Schirmer Final Summary Report on NASC Contract N00019-C-67-0275. Phillips Petroleum Company Research Division Report 5058-68R (May 1968).

This report is concerned with hot corrosion of coated 713C and Mar-M-200. Although some details are given of uncoated 713C, there is nothing on uncoated Mar-M-200. See 713C for details.

J.R. Johnston and R.L. Ashbrook NASA Technical Note TN D-5376 August 1969.

See B 1900 for details, and the principal figures. In high velocity tests at 1093°C Mar-M 200 lost 10 mg/cm^2 in 50h, ranking second to IN-100. In the static test at the same temperature it lost 0.9 mg/cm^2 in 50h, the best of the 7 alloys tested. The equiaxed alloy had poor thermal fatigue resistance, but the directionally solidified and single crystal alloy were excellent. The oxides on materials exposed to high gas-velocity testing were determined by X-ray diffraction: (982°C), Cr_2O_3 and a spinel with a_o = 8.15 Å were detected; at 1900°F (1038°C) the same; at 2000°F (1093°C) a monoxide (NiO) and the same spinel.

Figure 19.8 compares the oxidation behaviour of the three microstructures: the equiaxed showed the smallest weight loss.

The average weight loss of the alloy after 100h at 1093°C was 1500mg; this is worse than Hastelloy X and X-40, but better than Mar-M 509A.

H.T. Quigg, R.M. Schirmer and L. Bagnetto, Final Report to NASC on Contract No. N00019 (Phillips Petroleum Company: Research and Development Report 5732-70) July 1970.

See 713C for details.

P.E. Hamilton, K.H. Ryan and E.S. Nichols, Hot Corrosion Probelms Associated with Gas Turbines, ASTM Special Technical Publication STP 421, 1967, 188.

See 713C for details. The results of test stand engine testing, with and without salt injection, are shown. Without salt, Mar-M 200 is worse than TRW 1900, and about the same as 713C. With salt, it is worse than 713C, about the same as B 1900, better than TRW 1900.

H.T. Quigg, R.M. Schirmer and L. Bagnetto, Final Report to Naval Air Systems Command on Contract N00019-70, C-0293 (Phillips Petroleum Company Research and Development Report 5903-71) Jan. 1971.

See 713C for details.

W.L. Wheatfall, in "High Temperature Corrosion of Aerospace Alloys" J. Stringer, R.I. Jaffee and T.F. Kearns (eds.), AGARD Conference Proceedings No. 120, (March 1973) 235.

See 713C for details.

P.A. Bergman, C.T. Sims and A.N. Beltran, Hot Corrosion Problems Associated with Gas Turbines; ASTM Special Technical Publication, STP 421, 1967, 38.

See 713C for details. Attack at 1750°F (954°C) in burner rig, 100h, 200 ppm salt is shown. Surface loss about 40 mils (in diameter) maximum penetration 80.2 mils. Worse than 713; not quite as bad as U-700 at this temperature.

R.M. Schirmer and H.T. Quigg, Progress Report No. 3 for NASC Contract NO_w65-0310-d; Phillips Petroleum Company Research Division Report 4370-66R (June 15, 1966).

See 713C for details. Figure 19.9 shows the effect of fuel sulphur, sea salt in air, and gas temperature on metal loss(after descaling). SM-200 seems to be relatively heavily attacked, worse than IN 100 or 713C. The metal durability in terms of penetration from cross-sectional area is the worse of the alloys studied (others are Inco 713C, U-500, IN-100, and WI-52).

A significant effect for sulphur content was found at low temperatures but not at high temperatures. Increasing temperature from 1400° to 1600°F significantly increased the attack with 10 ppm salt, but had little effect at lower salt concentrations. In most cases, increasing the temperature from 2000 to 2200°F increased metal weight loss in all salt concentrations. 1.0 ppm sea salt produces little increase in attack at either 1400 or 1600°F. Reducing fuel sulphur from 0.40 to 0.04 wt % reduced the metal weight loss at low temperatures; there is no effect of a further reduction to 0.0002 wt %. At high temperatures, sulphur content seemed to have very little effect.

Decreasing the salt from 10 ppm to 1 ppm reduced attack at 1600°F. Decreasing the temperature from 1600 to 1400°F in the presence of 10.0 ppm salt decreased attack. There was no significant effect of sea salt at these temperatures. At higher temperatures decreasing sea salt decreased attack in the majority of cases. Decreasing the temperature from 2200 to 2000°F decreased attack; a further decrease to 1800°F had less effect. Decreasing sulphur from 0.40 to 0.040 wt % did not decrease attack in any case, but in some cases increased it. Further decrease to 0.0002 wt % S had little effect.

Oxidation (no salt or sulphur) is relatively severe, which the authors consider is related to its high tungsten content (12.2%). There is also relatively severe attack in high sulphur fuel (no salt) which the authors consider to be due to the low chromium content.

Figure 19.10 shows the oxidation attack - 5h at 2200°F with no sea salt in air and 0.0002 wt % S in fuel. Figure 19.11 shows the heavy sulphide penetration after 5h, 1400°F, no sea salt, 0.40 wt % sulphur in the fuel. Figure 19.12 shows the hot corrosion after 5h at 1600°F with 10 ppm sea salt, 0.0002 wt % S in fuel. There is heavy sulphide penetration, followed by oxidation which appears to be "interdendritic". Further addition of sulphur in the fuel affected the hot corrosion very little. Figure 19.13 shows the attack after 5h at 1800°F with 10 ppm salt and 0.0002 wt % S in the fuel. Figure 19.14 shows the attack after 5h at 2200°F with 10 ppm sea salt in the air and 0.0002 wt % S in the fuel. Figure 19.15 shows the attack after 5h at 2200°F with 10 ppm sea salt and 0.40 wt % S.

H.T. Quigg and R.M. Schirmer, Progress Report No. 4 on NASC Contract NO_w65-0310-d; Phillips Petroleum Company Report 4411-66R August 1966.

See 713C.

H. von E. Doering and P.A. Bergman, Naval Ship Research and Development Centre, Materials Laboratory Research and Development Report No. 2844 (March 1969).

See 713C for details. In a 100h test at 1750°F (955°C) with 200 ppm salt the surface loss was 14.4 mils and the maximum penetration was 44.5 mils: appreciably worse than SEL, but quite a lot better than 713C. In a 1000h test with 5 ppm salt the specimen was wholly destroyed - rather worse than 713C, comparable with IN 100 and SEL 15.

R. Field, D.J. Fisk, H. von E. Doering, Naval Ship Research and Development Centre, Materials Laboratory Research and Development Report 2833 (Jan. 1969).

See 713C.

P.E. Hamilton, K.H. Ryan and E.S. Nichols, Hot Corrosion Problems Associated with Gas Turbines, ASTM Special Technical Publication STP 421, 1967, 188.

See 713C for details.

R.M. Schirmer and H.T. Quigg, Hot Corrosion Problems Associated with Gas Turbines, ASTM Special Technical Publication STP 421, 1967, 270.

See 713C for details. This paper is based on reports abstracted above, and describes experiments on the Phillips Environmental Simulator at temperatures in the range 1400 - 2200°F (760 - 1204°C); 0.0002, 0.040 and 0.40%S in JP-5 fuel; 0, 1.0 and 10.0 ppm sea salt in the air. Figure 19.16 shows the corrosion of SM-200 as a function of temperature and test condition. SM-200 was the worst of the alloys tested, but WI-52 and IN-100 were much the same.

In discussion, the authors presented results for the corrosion of SM-200 at 2000°F using 0.0002%S JP-5 fuel, with (a) no salt injection; (b) 15 ppm sea salt; (c) 9 ppm NaCl; and (d) 6 ppm NaOH. The relative weight losses were (a) 1.2%; (b) 42.7%; (c) 43.7%; and (d) 100%. The scale products for the last three were all the same: NiO, Na_2WO_4, and $Fe(Al,Cr)_2O_4$. From this they conclude that neither sulphur or chlorine is essential for hot corrosion, the important component being the sodium.

Data relating to this alloy will also be found in the following Figures :
1.1, 1.7, 1.8, 1.9, 1.10, 1.13, 10.58, 10.68, 10.74, 10.75, 10.84, 10.105, 10.106;
and Tables :
1-I, 1-II, 1-V, 1-VI, 1-VII, 1-VIII, 1-IX, 10-I, 10-VI, 10-VIII, 10-XVII, 10-XXI, 10- XXV, 10-XXVI, 10-XXX, 31-I.

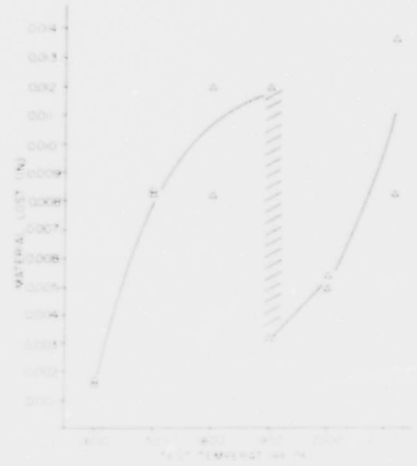

Figure 19.1. Effect of temperature on the sulphidation behaviour of Mar-M 200 (Graham et al).

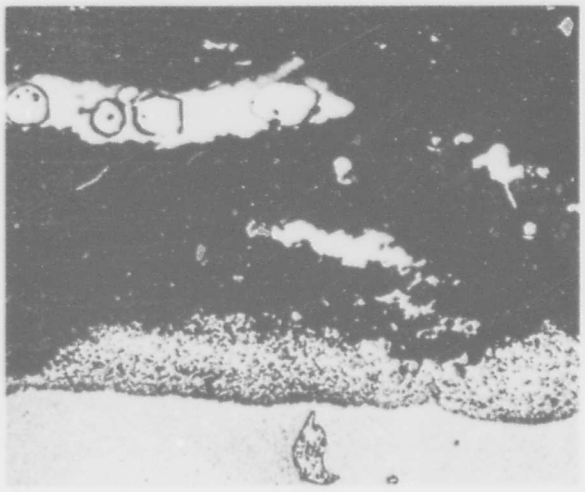

Figure 19.2. Photomicrograph of etched sample of Mar-M 200 corroded in 99% Na_2SO_4-1% NaCl showing metal-scale interface and two-phase inclusion in the scale. (Graham et al).

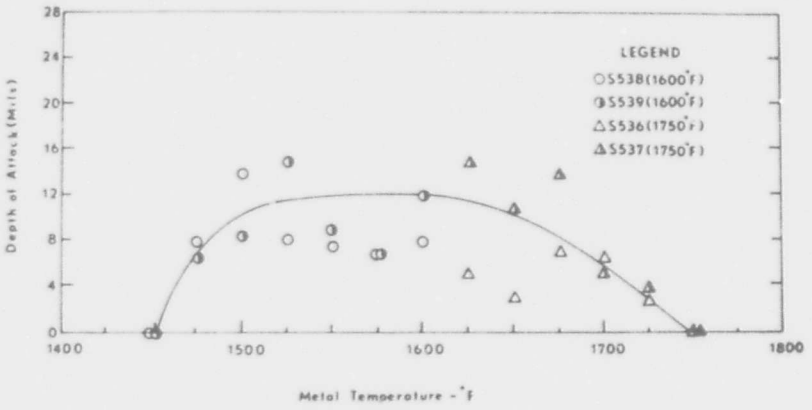

Figure 19.3. Corrosion as a function of temperature for Mar-M 200 tested using JP-4 fuel with a Salt/Air Ratio of 8 ppm. (Walters).

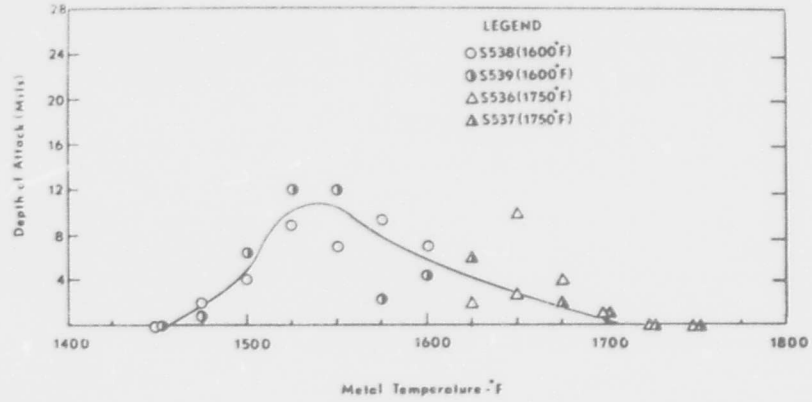

Figure 19.4. Corrosion as a function of temperature for Mar-M 200 tested using JP-4 fuel with a Salt/Air Ratio of 4 ppm. (Walters).

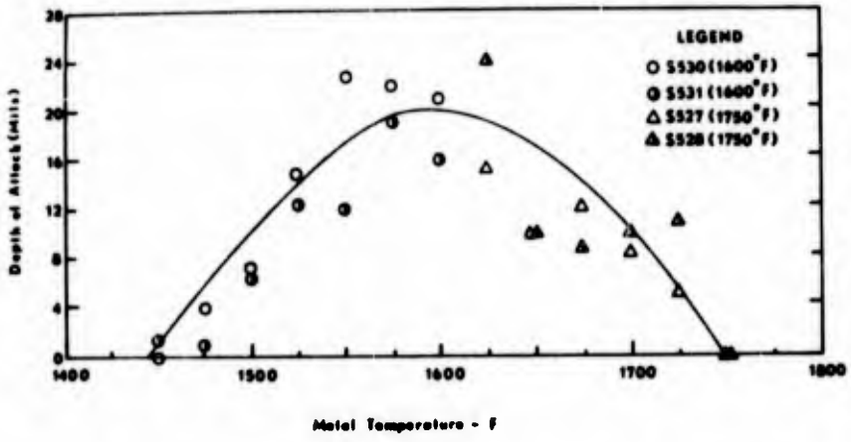

Figure 19.5. Corrosion as a function of temperature for Mar-M 200 using JP-4R fuel with a Salt/Air Ratio of 8 ppm. (Walters).

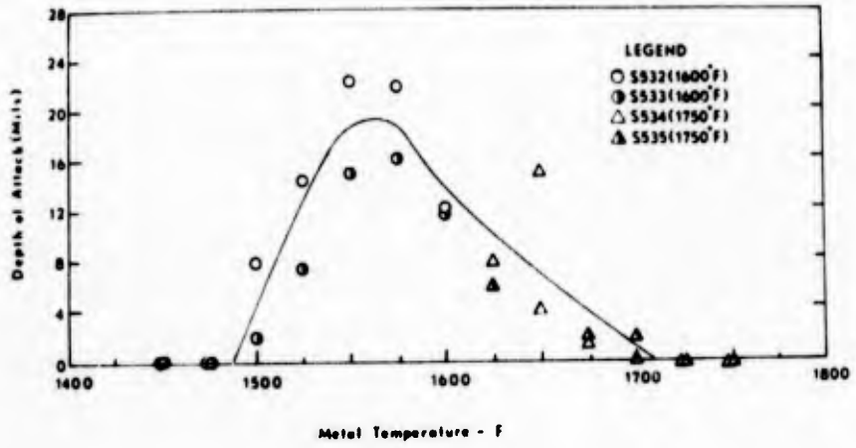

Figure 19.6. Corrosion as a function of temperature for Mar-M 200 using JP-4R fuel with a Salt/Air Ratio of 4 ppm. (Walters).

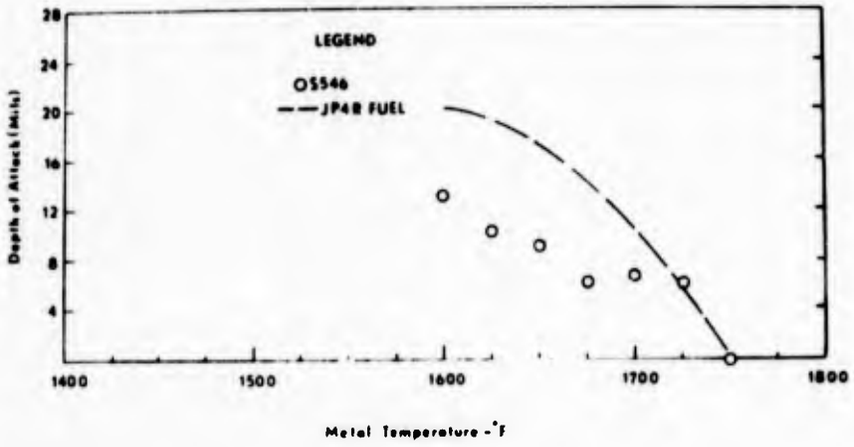

Figure 19.7. Corrosion as a function of temperature for Mar-M 200 tested using JP-5 fuel (0.16%S) with a Salt/Air Ratio of 8 ppm. (Walters).

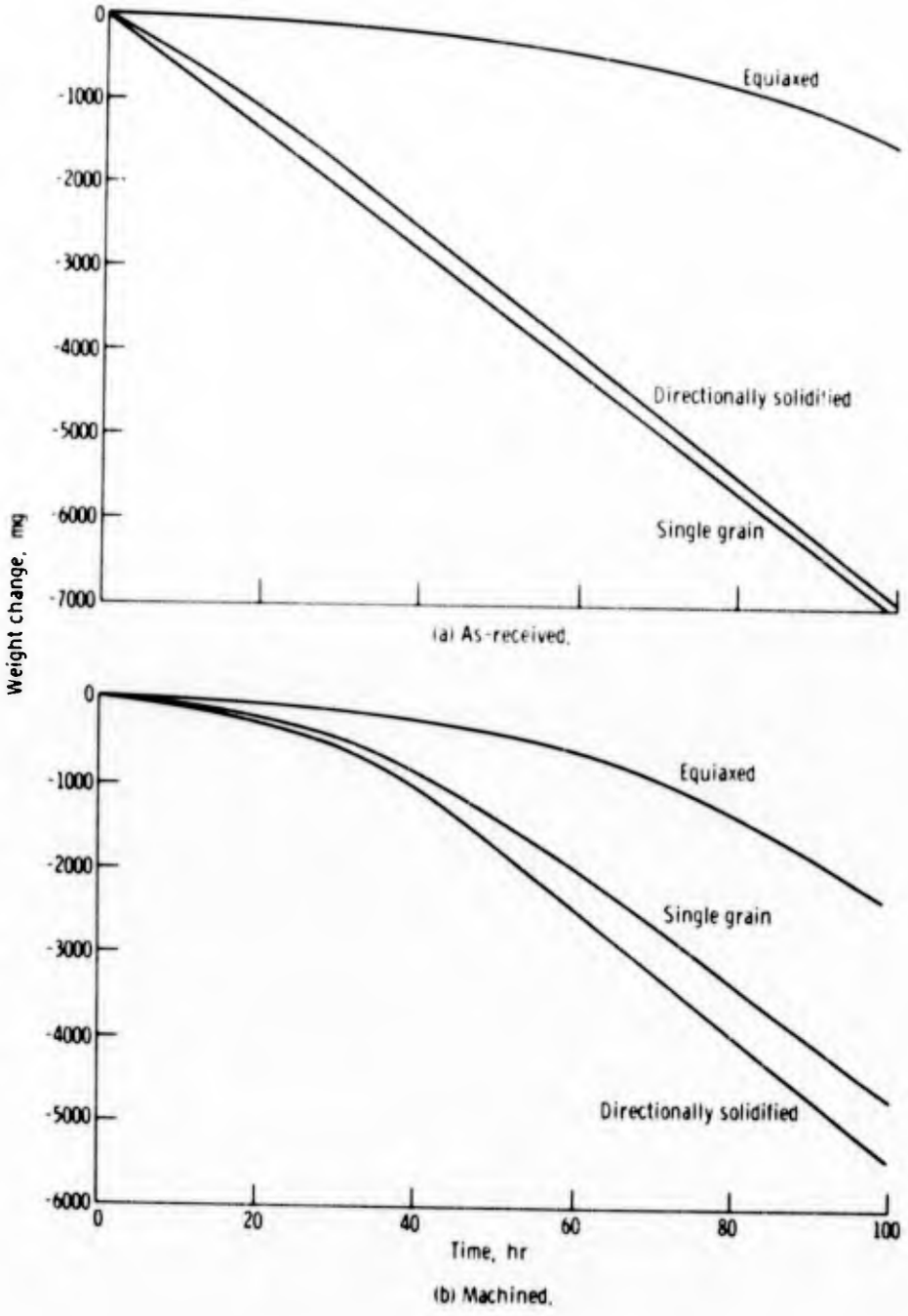

Figure 19.8. Comparison of high-gas-velocity oxidation behaviour of three macrostructures of Mar-M-200 after exposure to standard cycle at 2000°F (1093°C) maximum temperature. (Johnston and Ashbrook).

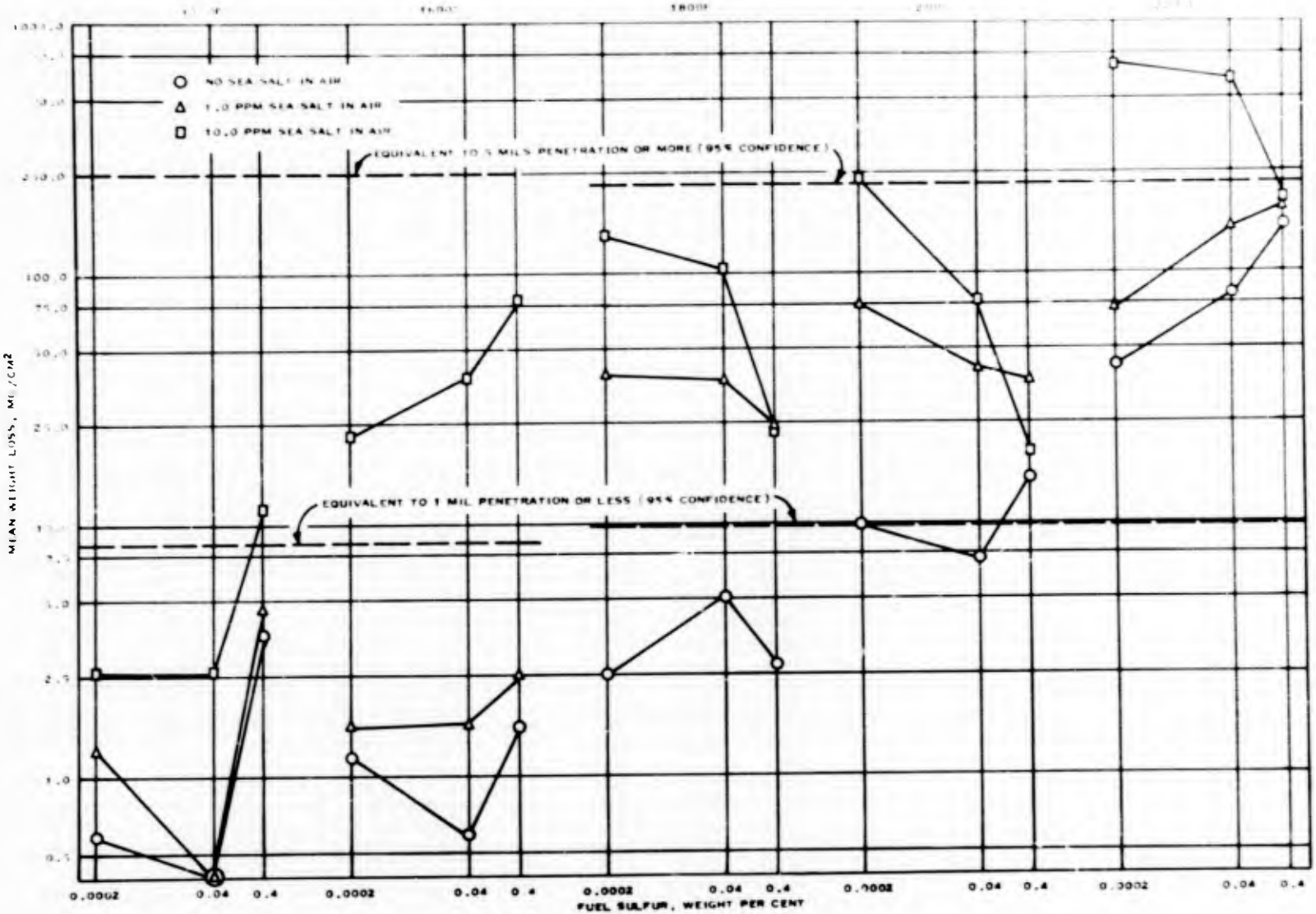

Figure 19.9. Effect of fuel sulphur, sea salt in air and gas temperature on metal loss of CM-200 test specimens (Schirmer and Quigg).

UNIFORM SURFACE ATTACK

BASE METAL
UNETCHED
200X

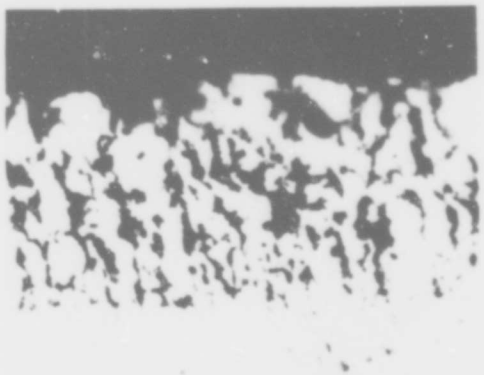

INTERDENDRITIC OXIDATION

BASE METAL
UNETCHED
2000X

Figure 19.10. Oxidation of SM-200 in Phillips Rig. (Schirmer and Quigg).

5 hours exposure at 2200 F test condition with no sea salt in air and 0.0002 wt % sulphur in fuel.

VARIABLE
SURFACE ATTACK

BASE METAL
UNETCHED
200X

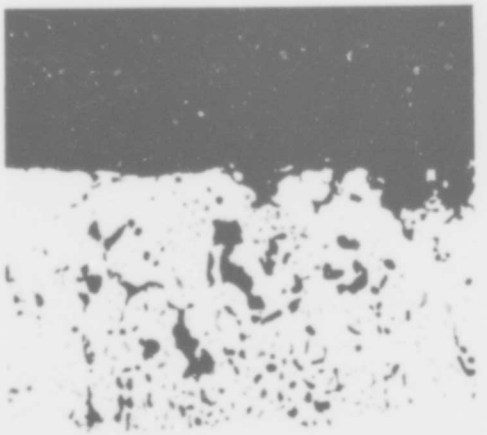

HEAVY SULFIDE PENETRATION

BASE METAL
UNETCHED
2000X

Figure 19.11. Sulphidation of SM-200 in Phillips rig.

5 hours exposure at 1400 F test condition with no sea salt in air and 0.40 wt % sulphur in fuel.

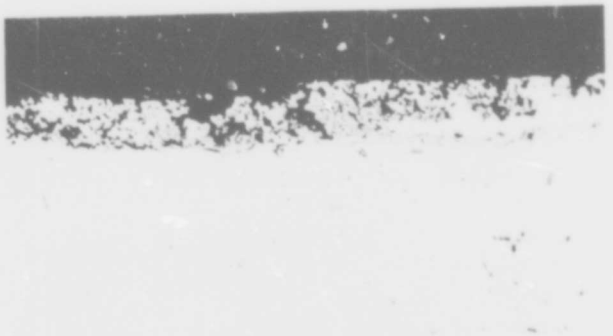

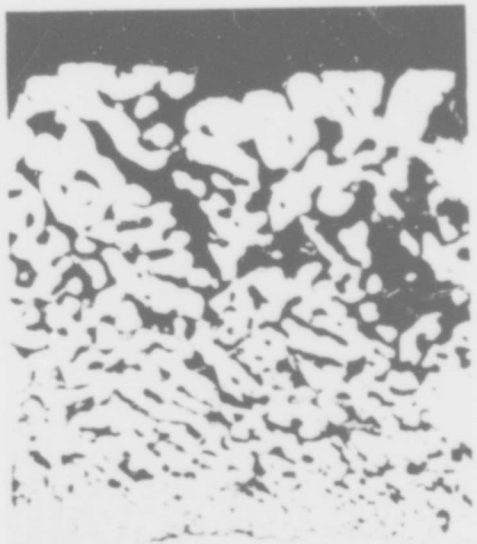

Figure 19.12. Hot corrosion of SM-200 in Phillips Rig. (Schirmer and Quigg).

5 hours exposure at 1600 F test condition with 10 ppm sea salt in air and 0.0002 wt % sulphur in fuel.

Figure 19.13. Hot corrosion of SM-200 in Phillips Rig. (Schirmer and Quigg).

5 hours exposure at 1800 F test condition with 10 ppm sea salt in air and 0.0002 wt % sulphur in fuel.

Figure 19.14. Hot corrosion of SM-200 in Phillips Rig. (Schirmer and Quigg).

5 hours exposure at 2200 F test condition with 10 ppm sea salt in air and 0.0002 wt % Sulphur in fuel.

Figure 19.15. Hot corrosion of SM-200 in Phillips Rig. (Schirmer and Quigg).

5 hours exposure at 2200 F test condition with 10 ppm sea salt in air and 0.40 wt % sulphur in fuel.

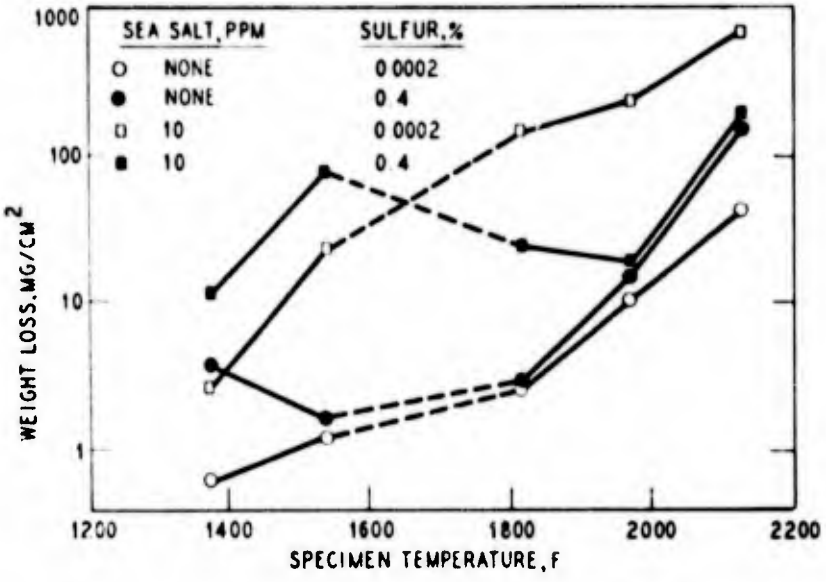

Figure 19.16. Hot corrosion of SM-200 (Schirmer and Quigg).

Mar-M 246

K.H. Ryan, J.R. Kildsig and P.E. Hamilton (Allison Division of General Motors) Technical Report to Wright-Patterson AFB, Air Force Materials Laboratory AFML-TR-67-306 (August 1967).

A detailed summary of the procedure used in this report is given under PDRL-163. Mar-M-246 was the worst of the alloys studied by a considerable margin (the others were PDRL 163, IN 728 MX, 713C + Cr, 713C + Cr+Y, Inco 717, 713C, Mar-M 421, IN 100 and GMR-235). Mar-M 246 held for 50h at 1550°F (844°C) corrodes nearly twice as much as the as-cast alloy (most of the other alloys show no effect of heat treatment). Figure 20.1 shows the volume loss for the as-cast and the heat-treated alloy at all temperatures. Figure 20.2 compares the measured volume loss and that predicted by the regression equation. The microstructure of all the alloys can be described in terms of three zones: (1) an outer layer of continuous oxide on the surface which gradually graded into an area of mixed metal and oxide; (2) a layer of depleted metal; and (3) globular sulphide particles. No pictures are shown of Mar-M 246.

V.S. Moore and A.R. Stetson, Final Report on NASC Contract No. N00019-68-C-0532 (Solar Research Division Report RDR 1626-5) December 1970.

See B 1900 for details. Figure 20.3 shows the microstructure of the attack on uncoated Mar-M 246 after 20h at 1650°F; the corrosion resistance was extremely poor, ranking with B 1900, IN 100 and SEL 15; much worse than 713C.

Table 20-I and 20-II give the cumulative weight change during the tests.

H.T. Quigg, R.M. Schirmer and L. Bagnetto, Final Report to NASC on Contract No. N00019-69-C-0221 (Phillips Petroleum Company Research and Development Report 5732-70) July 1970.

See 713C for details. Figure 20.4 shows a specimen of Mar-M 246 tested for 15h in a 2000°F (1093°C) cyclic test with 1.0 ppm salt in the air and 0.04 wt % S in the fuel. Figure 20.5 shows a specimen subjected to a similar test with 0.0004% S in the fuel.

H.T. Quigg, R.M. Schirmer and L. Bagnetto, Final Report to Naval Air Systems Command on Contract N00-019-70-C-0293 (Phillips Petroleum Company Research and Development Report 5903-71) January 1971.

See 713C for details. Figure 20.6 shows the general appearance of cross section of uncoated specimens corroded for 15h with 0.0040% and 0.0004% S in the fuel; MDC-1 coated specimens corroded for 80h with the same two fuels (in the higher sulphur content there is extreme local attack); and MDC-9 coated specimens corroded 110h in the same two fuels; (there is extreme local attack, particularly with the high sulphur content). Figure 20.7 shows a detail of a section of the uncoated specimen after 15h with the low sulphur fuel. Figure 20.8 shows a detail of the section of an uncoated specimen after 15h with the higher sulphur fuel. Under all circumstances uncoated Mar-M 246 was worse than uncoated B 1900.

P.C. Felix in "Deposition and Corrosion in Gas Turbines", A.B. Hart and A.J.B. Cutler (eds.) (Applied Science Publishers, London, 1973) 331.

See 713C for details.

H. Huff and F. Schreiber, Werkstoffe and Korrosion 5 (1972) 370.

See 713C for details. The paper describes experiments in a combustor rig which allowed the specimen to be simultaneously stressed. Most tests were conducted at 900°C, but some were in the range 850 - 980°C. Figure 20.9 shows the influence of the corrosion conditions on the time to rupture at stresses in the range 12 - 35 kp/mm^2. The conditions were: air, combustion gases, combustion gases with 31 ppm synthetic sea salt. Figure 20.10 shows the influence of salt concentration in the range 0.085 - 36 ppm on the time to rupture at a stress of 210 N/mm^2 at 900°C. Figure 20.11 shows the influence of temperature on the time to rupture at a stress of 210 N/mm^2 in various atmospheres, Figure 20.12 shows the creep extension as a function of time under a stress of 210 N/mm^2 and at 900°C, in air, combustion gases, and combustion gases with salt at 0.085, 0.85 and 31 ppm. Figure 20.13 shows the local and overall corrosion rate at 900°C as a function of stress in combustion gases with and without salt.

The 100h rupture strength at 900°C was 350 N / mm^2 in air, 300 N/mm^2 in combustion gases without salt, and 180 N/mm^2 with 30 ppm sea salt.

L.M. Maas and C.L. Miller, ASME paper No. 72-GT-77, presented at the Gas Turbine and Fluids Engineering Conference and Products Show, March 1972.

See 713C for details.

Data relating to this alloy will also be found in the following Figures :
10.51, 10.84, 10.92, 10.99, 10.123, 10.124, 36.1, 36.2, 36.3, 36.4, 36.5, 36.6, 36.7,
and Tables :
1-X, 10-XVII, 10-XXV, 10-XXVI, 10-XXIX.

TABLE 20-I

WEIGHT CHANGE DURING HOT-CORROSION TESTS (MOORE AND STETSON)

1650°F MAXIMUM TEST TEMPERATURE

35 ppm SEA SALT

MAR-M-246 ALLOY

Exposure Time (Hours)	Cumulative Weight Change (mg) Specimen Number							
	MA1	MA2	MG1	MG2	MJ1	MJ3	M1	M2
20	-	-	-18.3	-24.4	+ 4.8	+ 5.3	-16.1	-65.9
30	+3.8	+3.5	-	-	-	-	-	-
40	-	-	- 7.8	-65.9	+ 9.5	+ 9.1	-	-
60	+4.5	+5.2	-	-	+23.3	+19.4	-	-
80	-	-	-	-	+15.6	+18.4	-	-
90	+4.5	+5.8	-	-	-	-	-	-
100	-	-	-	-	+14.4	+19.7	-	-
120	+7.5	+6.7	-	-	+16.7	+24.6	-	-
140	-	-	-	-	+22.1	+26.0	-	-
150	+6.4	+8.2	-	-	+23.8	+28.0	-	-

Note: - denotes weight loss

TABLE 20-II

WEIGHT CHANGE DURING HOT-CORROSION TESTS (MOORE AND STETSON)

1800°F MAXIMUM TEST TEMPERATURE

35 ppm SEA SALT

MAR-M-246 ALLOY

Exposure Time (Hours)	Cumulative Weight Change (mg) Specimen Number									
	M4	M5	MA3	MA4	MA5	MG3	MG4	MJ2	MJ4	MJ5
20	+173	+109	-	-	-	-	-	-	-	-
30	-	-	+2.2	-599	-186	-0.3	+1.0	+ 4.4	+ 1.3	+ 4.3
60	-	-	+3.5	-	-	-0.4	+4.4	+ 8.2	+ 9.8	+10.8
90	-	-	+3.6	-	-	+3.3	+5.0	+10.1	+ 7.8	+10.6
120	-	-	+6.6	-	-	+5.5	+6.8	+10.4	+ 9.1	+11.5
150	-	-	-	-	-	+8.5	+9.8	-	+16.2	+13.7

Note: - denotes weight loss

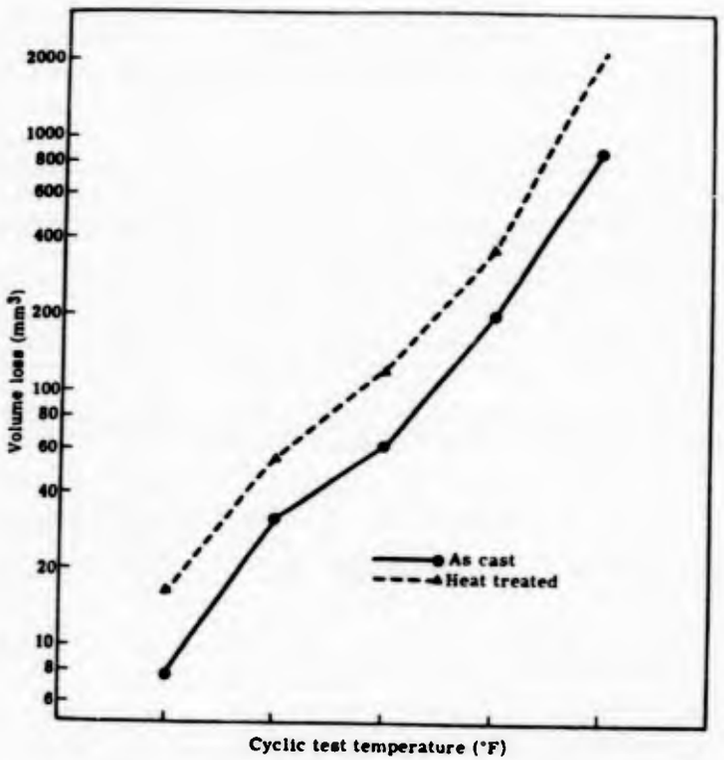

Figure 20.1. As-cast versus heat treated Mar-M 246 at each cyclic test temperature. (Ryan et al).

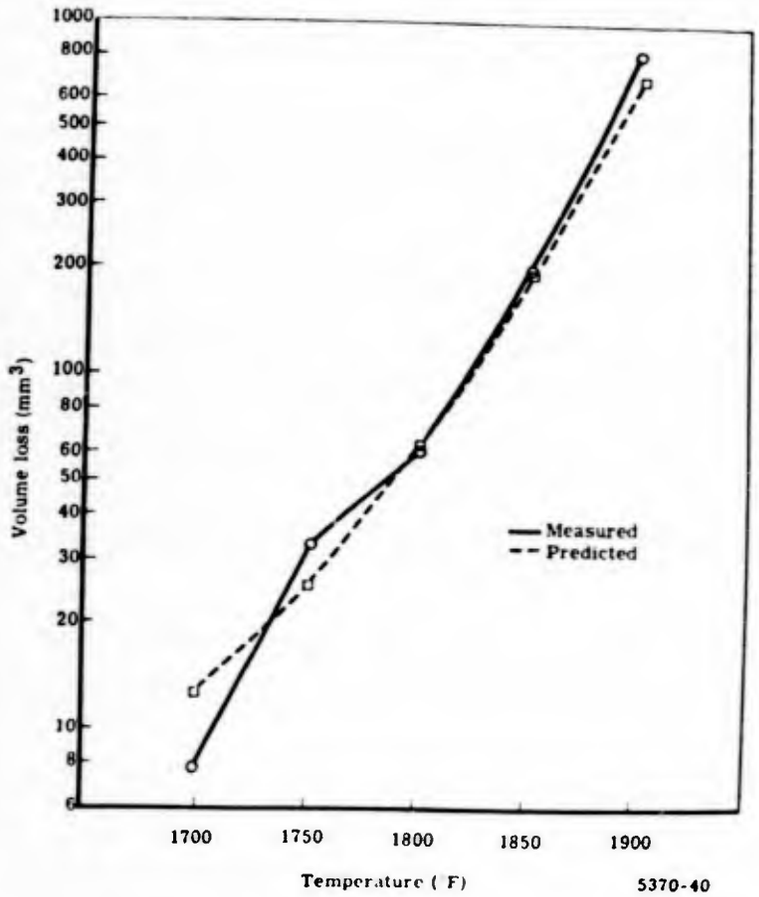

Figure 20.2. Comparison of the measured volume loss and the loss predicted by the regression equation for Mar-M 246. (Ryan et al).

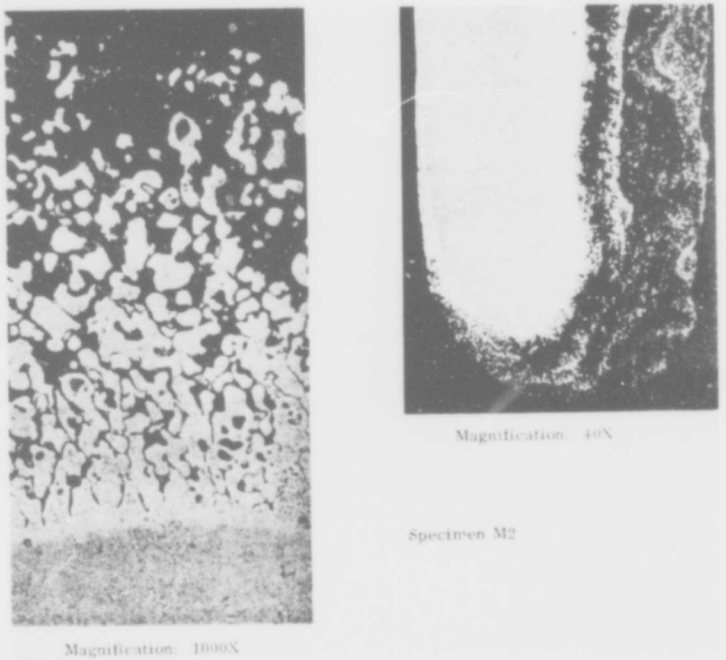

Figure 20.3. Microstructure of uncoated Mar-M-246 after hot corrosion tests at 1650°F for 20 hours. (Moore and Stetson).

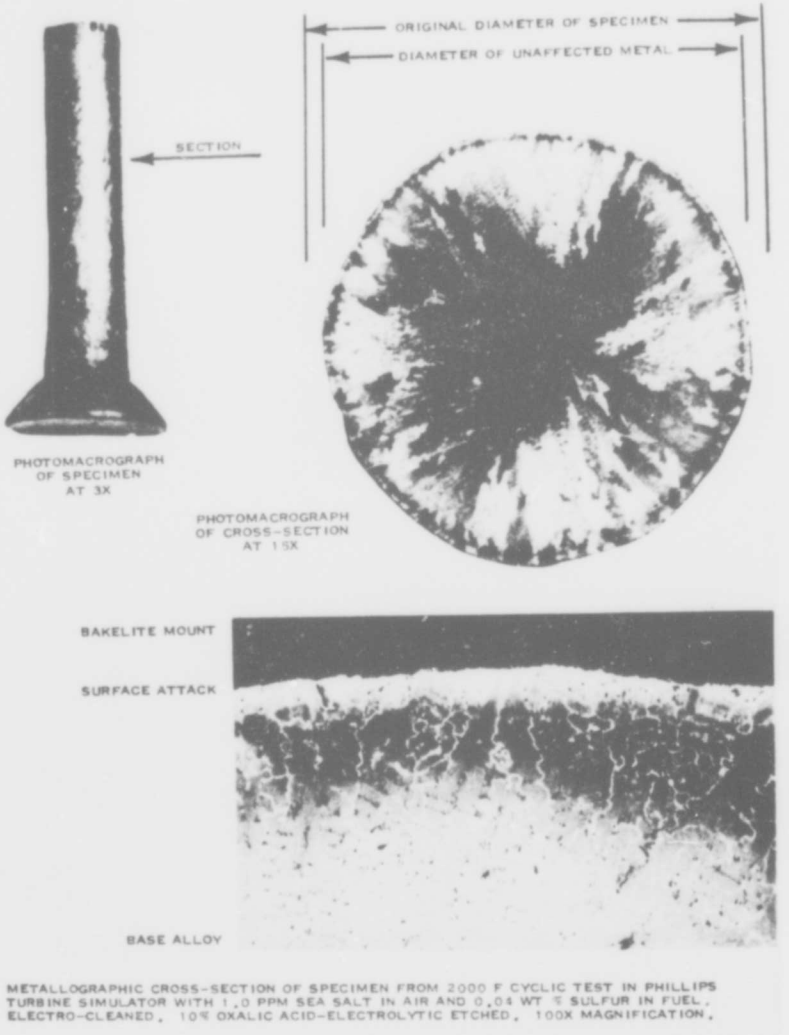

Figure 20.4. Hot corrosion of Mar-M-246 specimen after 15 hours with high-sulphur fuel (Quigg et al).

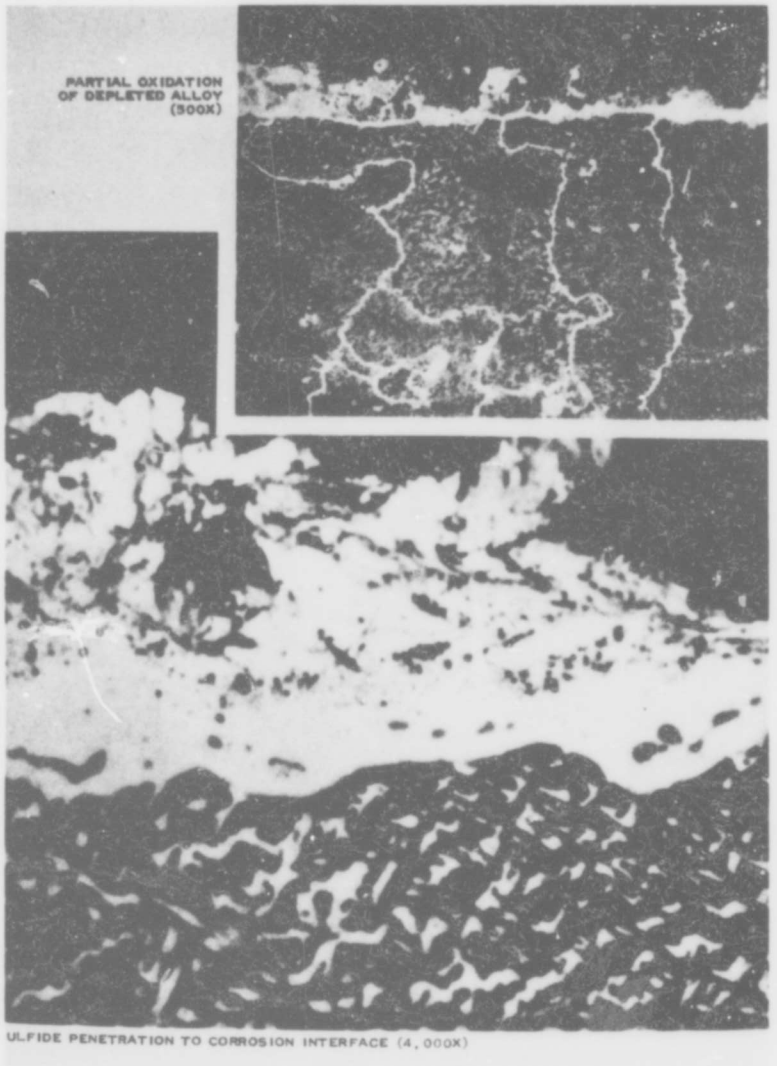

Figure 20.4. (continued).

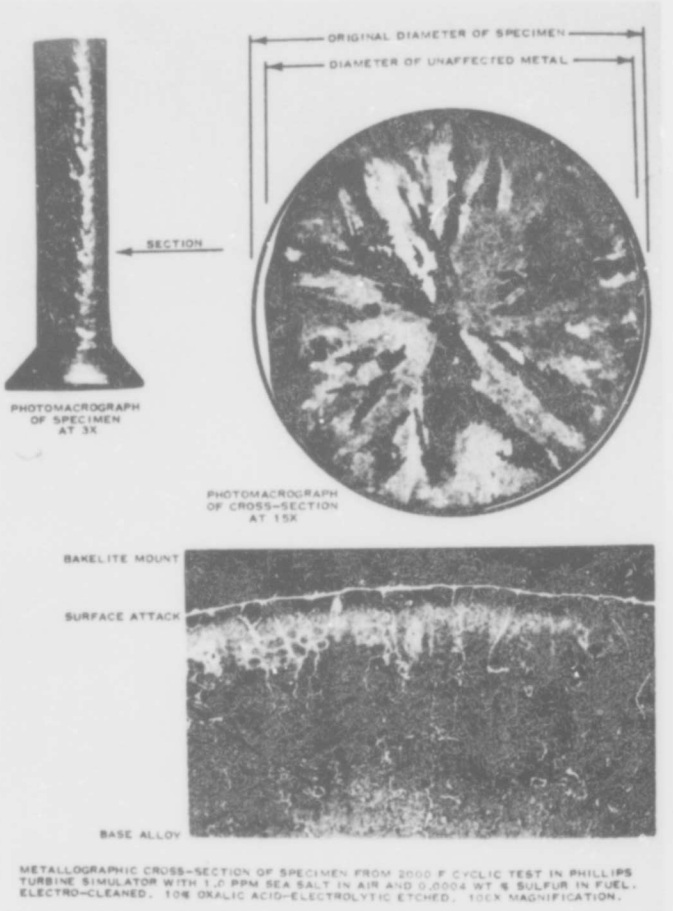

Figure 20.5. Hot corrosion of Mar-M-246 after 15 hours with low-sulphur fuel (Quigg et al).

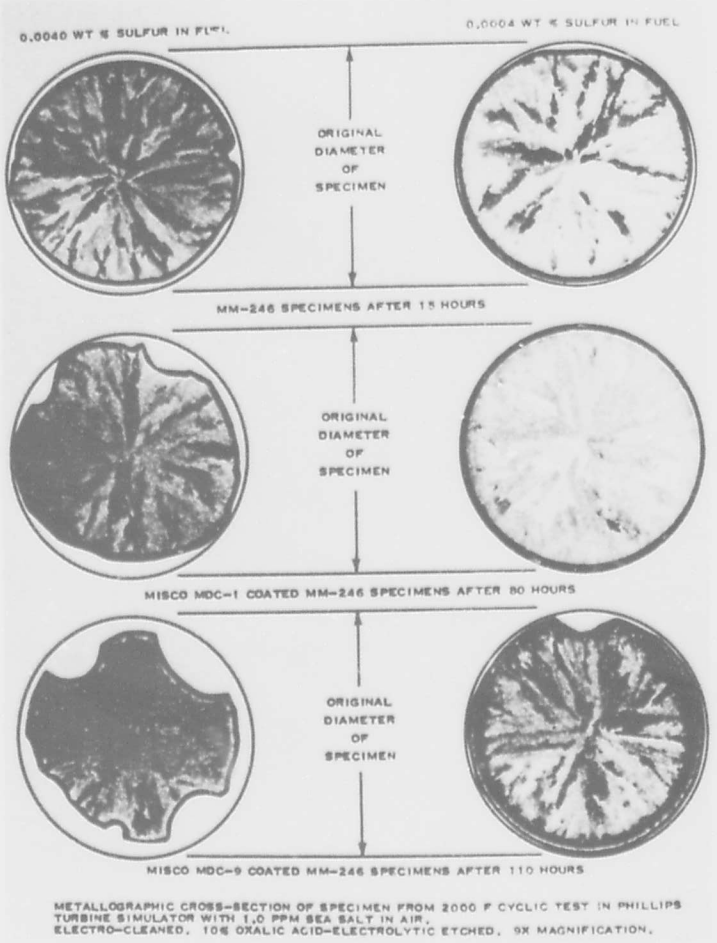

Figure 20.6. Hot corrosion of representative specimens (Quigg et al).

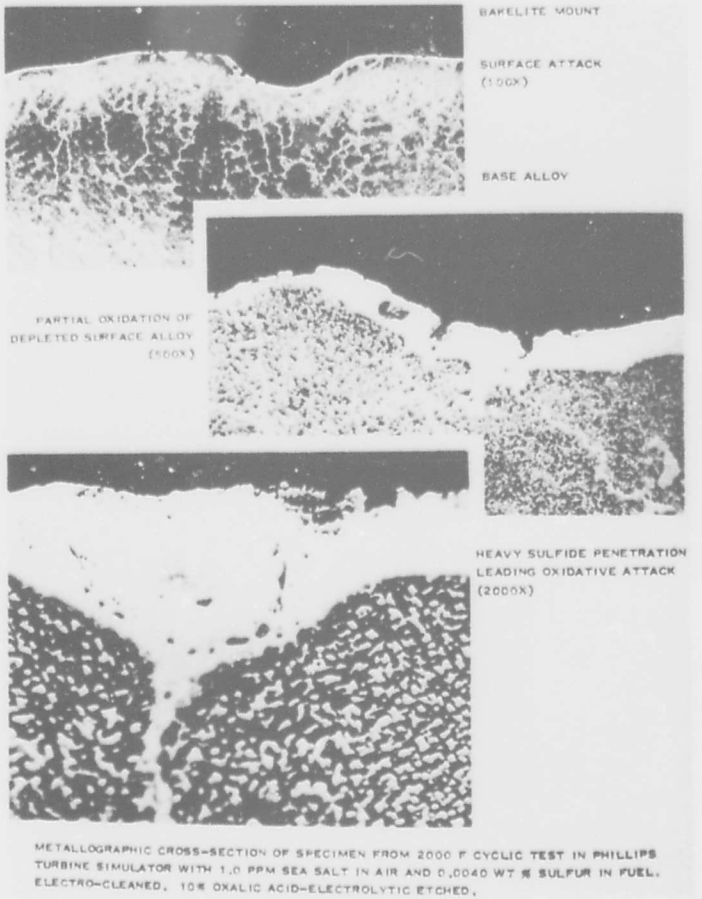

Figure 20.7. Hot corrosion of bare MM-246 specimen after 15 hours (low sulphur fuel) (Quigg et al).

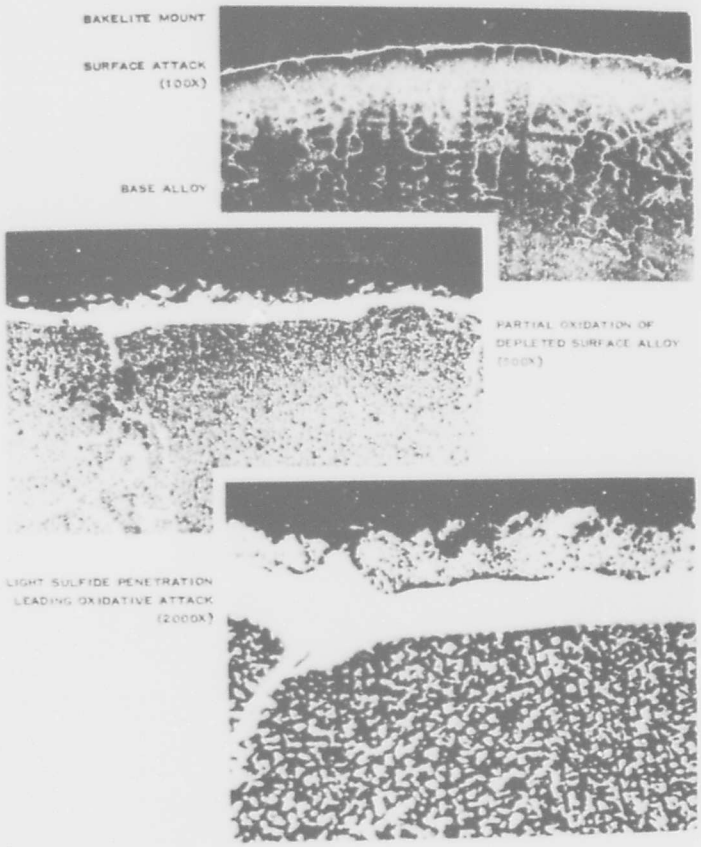

Figure 20.8. Hot corrosion of bare MM-246 specimen after 15 hours (very low sulphur fuel) (Quigg et al).

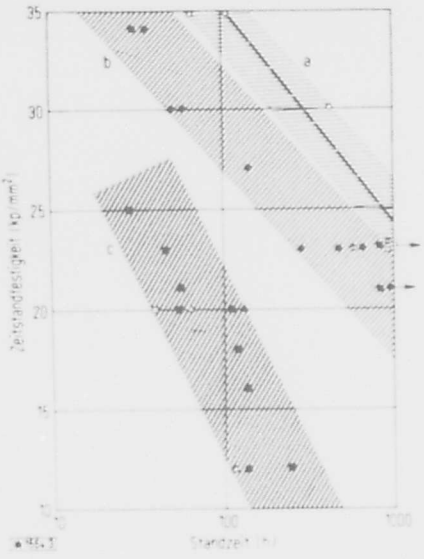

Figure 20.9. The influence of corrosion in the creep behaviour of the nickel-base alloy M 246 at 900°C.
(a) in air.
(b) in hot gas stream from JP4 fuel and
(c) in hot gas stream with synthetic sea salt according to DIN 50900, but dry. 36g/48h.

- ○ without protective coating.
- ⊖ chromized.
- ● without protective coating.
- ■ without protective coating.
- □ chromized.
- △ LDC2 aluminide coating with Pt.
- ▲ aluminide coating.

(Huff and Schreiber).

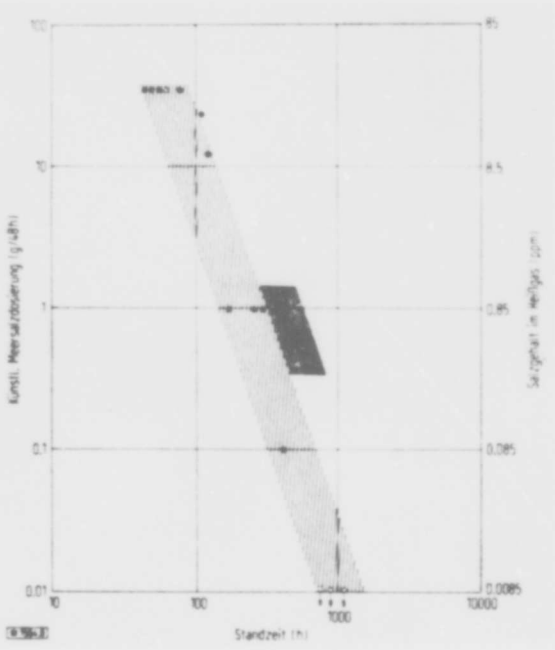

Figure 20.10. The influence of salt concentration of the life at 900°C, MAR-M 246, 210 N/mm^2.

- ♀ without protective coating, without salt.
- ● without protective coating with salt.
- △ 50 µm thick protective coating LDC-2, with salt.
- □ 70 µm thick protective coating LDC-2, with salt.
- ♀ 50 µm thick protective coating LDC-2 without salt.

(Huff and Schreiber).

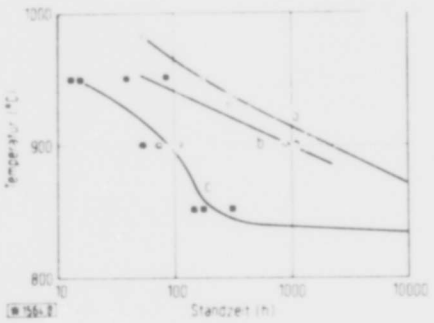

Figure 20.11. The influence of temperature on the creep behaviour of the nickel-base alloy MAR-M 246 at 210 N/mm^2.

(a) in air.
(b) in hot gas stream from JP4 fuel.
(c) in hot gas stream with synthetic sea salt according to DIN 50,900 36 g/48 h (31 ppm), dry.

- ○ without protective coating
- ● without protective coating
- ■ without protective coating

(Huff and Schreiber).

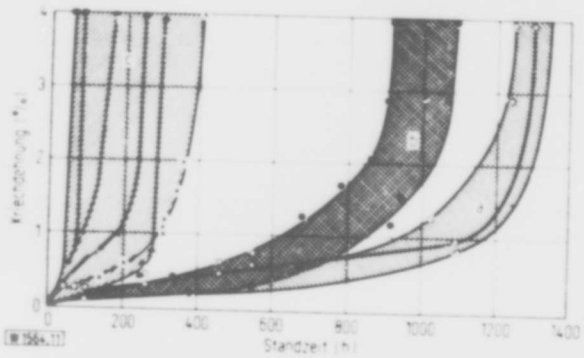

Figure 20.12. The influence of corrosion in the creep extension of the nickel-base alloy MAR-M 246 at a stress of 210 N/mm^2 and 900^{o}C.
(a) in still air. ○
(b) in hot gas stream and ●
(c) in hot gas stream with synthetic sea salt according to DIN 50900 (dry).

31 ppm	■
0.85	▲
0.085.	×

(Huff and Schreiber).

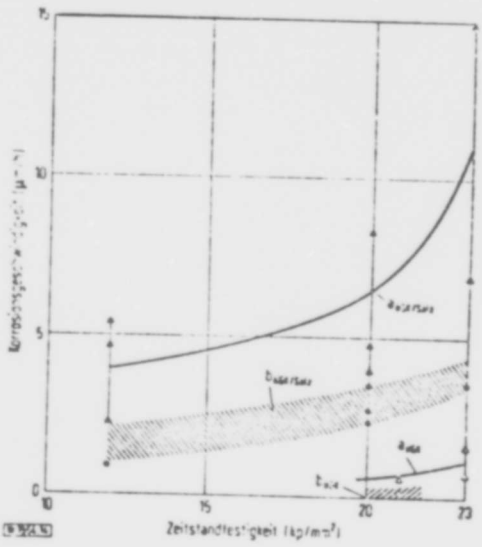

Figure 20.13. Localized and surface corrosion rates at different stresses, nickel-base alloy MAR-M 246, 900^{o}C.

a_{HGK} localized corrosion rate in hot gas.

$a_{HGK/salt}$ localized corrosion rate in hot gas with synthetic sea salt, 36g/48h.

b_{HGK} surface corrosion rate in hot gas

$b_{HGK/salt}$ surface corrosion rate in hot gas with synthetic sea salt 36g/48h.

(Huff and Schreiber).

M 252

B.O. Buckland, A.D. Foster and J.J. Treanor, presented at National Association for Corrosion Engineers, Annual Meeting (April 21, 1966) Miami, Florida.

See U-500 for a summary of the paper. Graph of total corrosion in a small burner rig operating with natural gas for a number of temperatures as a function of time is presented (Fig 21.1). The performance is not really very different from U-500 or X-45. Some parts taken from engines were examined (see U-500): buckets B-1, 12,700h. in residual oil, 29 shutdowns per 100h. Calculated metal temperature was 1280°F (693°C) but the corrosion (6 mils) was consistent with a temperature of 1570°F (854°C) in the small burner test. Bucket B3 was from a turbine running on crude oil after 15,937h; 0.4 shutdowns per 100h: calculated metal temperature 1330°F (721°C); corrosion 6 mils, so apparent temperature 1550°F (843°C). Bucket B5: natural gas: 32,500h: 0.2 shutdowns/100h; 1260°F (682°C); 0.75 mils; 1370°F (743°C). Bucket B6: natural gas; 9,000h; 0.2 shutdowns per 100h; 1340°F, 1 mil; 1430°F. Bucket B12: natural gas; 21,000h, 0.2 shutdowns per 100h; 1340°F, 1 mil; 1390°F.

Data relating to the alloy will also be found in Tables :
45-I, 45-II and 45-III.

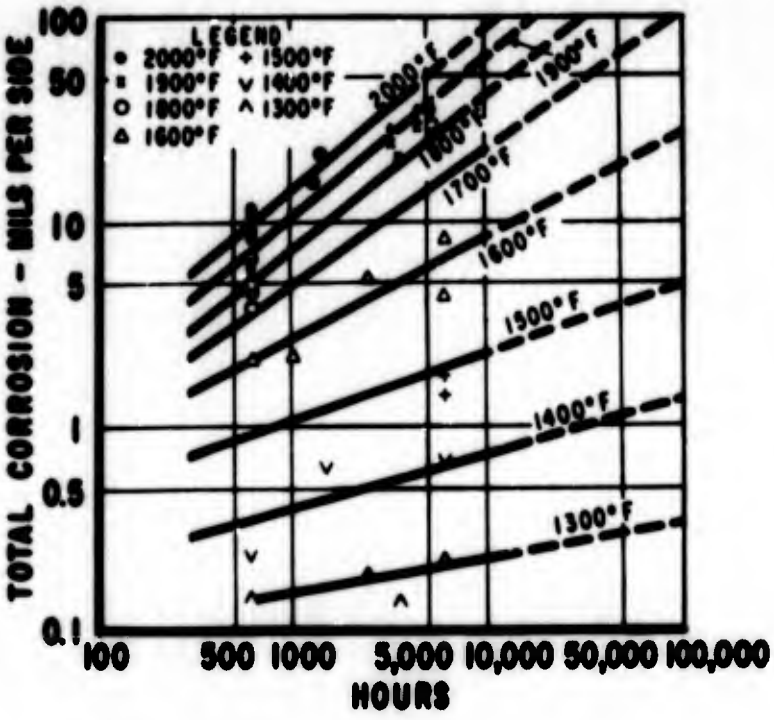

Figure 21.1. Total corrosion of alloy M252 with natural gas fuel as measured by the small burner test. (Buckland et al).

Mar-M 302 (SM 302)

P.A. Bergman, C.T. Sims and A.N. Beltran, Hot Corrosion Problems Associated with Gas Turbines, ASTM Special Technical Publication, STP 421, 1967, 38.

See 713C for details. Attack at 1750°F (954°C) and 1900°F (1093°C) in burner rig, 100h, 200 ppm salt, shown in bar diagram Mar-M 302 has good resistance; 2 - 4 mils loss on diameter (surface loss); max penetration <10 mils at both temperatures. Nearly as good as X-45. However, a note in the text suggests that other GE results in other test rigs show more difference.

L.D. Graham, J.D. Gadd and R.J. Quigg, Hot Corrosion Problems Associated with Gas Turbines, ASTM Special Technical Publication, STP 421, 1967, 105.

See 713C for details. MM 302 was the worst alloy tested, about the same as TRW 1900, B1900 and MM200. Authors suggest that high carbon content may be responsible. Much worse than WI-52, which didn't do at all badly in these tests.

A.R. Cox and R.J. Hecht, (Pratt and Whitney Aircraft, Florida Research and Development Center) Technical Report to the Air Force Materials Laboratory, Wright-Patterson AFB, AFML-TR- 70-273 (December 1970).

See WI-52 for a detailed summary. MM302 was about the same as MM509 in an oxidation/erosion test at 2200°F (1204°C), much better than WI-52; extensive internal oxidation of the carbide network. Accelerated cyclic hot corrosion tests with 35 ppm salt for 70h - again, Mar-M 302 is virtually the same as Mar-M 509, and very much better than WI-52. With 3.5 ppm, Mar-M 302 was appreciably better than 509.

N.T. Wagenheim, Cobalt 48, 1970, 129.

See X-40 for details. The corrosion data at the 5 ppm sea salt level is listed: 500h at 1600°F (871°C), surface loss 0.8 mils, maximum penetration 5.4 mils. 1000h at 1750°F (955°C): 3.5 and 10.0 mils. 1000h at 1900°F (1038°C): 8.5 and 23.1 mils. Not as good as X-40, but better than WI-52.

A.M. Beltran, Cobalt No. 46, 1970, 3.

See X-40 for details. Mar-M 302 seems relatively resistant to oxidation at 1093°C: very similar to 509. Mar-M 302 also seems quite good in oxidation at 1600, 1800 and 2000°F (871, 982 and 1093°C) in the natural gas burner rig: fairly similar to FSX 414. The relative hot corrosion resistance, of several alloys is shown in a burner rig burning 3% S residual oil, 325 ppm NaCl in the fuel (= 5 ppm salt in the air), 600h test at 1600F (871°C). The maximum penetration was 0.11 mm per side, the second "worst" of the alloys tested (X-45 was a little worse, but in fact all the alloys were resistant). In hot corrosion in 1% S diesel fuel, 5 ppm sea salt in the air, at 1600, 1750 and 1900°F (871, 955, 1039°C) for times of 500, 1000 and 1000h respectively, Mar-M 302 was the second best of the group of alloys, very similar to X-40. Mar-M 509 was a little worse, and L605 and WI-52 very much more so.

H.T. Quigg, R.M. Schirmer and L. Bagnetto, Final Report to NASC on Contract No. N00019-69-C-0221 (Phillips Petroleum Company Research and Development Report 5732-70) July 1970.

See 713C for details.

M.J. Donachie, Jr., R.A. Sprague, R.N. Russell, K.G. Boll and E.F. Bradley, Hot Corrosion Problems Associated with Gas Turbines, ASTM Special Technical Publication STP 421, 1967, 85.

See 713C for details. The test conditions for Mar-M 302 were: (a) Marine diesel fuel with 1.0% S; 3.5 ppm sea salt in the air; 1650°F (899°C); 50h; (b) 7 ppm salt, same conditions otherwise; (c) 35 ppm salt, same conditions otherwise; (d) 3.5 ppm salt, 2000°F (1093°C), otherwise the same. These conditions are listed in Table 2, but in fact the text makes it clear that other conditions were used as well. The cobalt-base alloys seem relatively insensitive to salt concentration. At the short time (50h) the cobalt-base alloys look good, but their performance becomes about the same as U-700 in the longer test (500h).

H.T. Quigg, R.M. Schirmer and L. Bagnetto, Final Report to Naval Air Systems Command on Contract N00019-70-C-0293 (Phillips Petroleum Company Research and Development Report 5903-71) Jan. 1971.

See 713C for details.

W.L. Wheatfall, in "High Temperature Corrosion of Aerospace Alloys" J. Stringer, R.I. Jaffee and T.F. Kearns, AGARD Conference Proceedings No. 120, (March 1973) 235.

See 713C for details.

E.J. Felton and R.A. Gregg, Trans. A.S.M., 57 (1964) 804.

Studied the oxidation of SM-302 using weight-gain technique; some thermobalance measurements as well. Temperature range 850 - 1200°C. Determined structure of oxide with X-ray diffraction: in situ for adherent scales, for spalled scales both spalled oxide and remaining adherent oxide examined. Some synthetic mixtures of oxides prepared, to determine likely compounds: these are shown in Table 22.I. Also measured carbon in exhaust gases to study degree of oxidation of carbides. Weight gain data are shown in Figure 22.1, and included are data from Martin Metals at 1093°C. In general, results obeyed the expression

$$\Delta W = Kt^{0.37 \pm 0.03}$$

A plot of the rate constant k versus $^1/_T$ is shown in Figure 22.2, and the "activation energy" is 13.3 kcal/mole between 850 and 1100°C; above 1100°C it is 41.0 kcal/mole.

Figure 22.3 shows thermobalance results; here, the curves can be described as $\Delta W = Kt^n$ where n increases with increasing temperature, approaching unity at the highest temperature. However, at 1200°C a value of n = 0.37 was obtained, as in the weight gain experiments.

Table 22.II shows the oxides found in contact with the metal. The carbide were selectively oxidised: Figure 22.4 shows selective oxidation of the MC carbides. The phase boundary between the carbide and the matrix was attacked initially, followed by a consumption of the carbide phase.

Table 22.III shows spectrographic analysis of the oxide spalled from specimens oxidised 2h at 1200°C. Figure 22.5 shows the variation in the tantatum content of the spalled oxide as a function of time, and Figure 22.6 shows the variations in tungstem contents. Table 22.IV lists the cobalt and chromium contents of the oxides. Table 22.V lists the analysis of the adherent oxide and the internal oxide. Table 22.VI shows the analysis of the inner and outer surface of an oxide layer which spalled intact from a specimen oxidised for 2h at 1300°C. Figure 22.7 is an electron-probe picture showing the chromium rich oxide layer adjacent to the metal surface.

Figure 22.8 shows the carbon evolution from the specimen: the polished specimens were first oxidised for approximately 55 min at 1150°C, then cooled and reheated to the same temperature, then cooled again, repolished, and reheated to 1150°C. Finally this last step was repeated.

Data relating to this alloy will also be found in the following Figures :
10.58, 10.61, 10.62, 10.65, 10.66, 10.68, 10.105, 51.7, 51.8, 51.9, 51.10, 51.11, 51.12, 52.8, 52.9, 52.11, 52.12;
and Tables :
10-XVIII, 10-XIX, 10-XXV, 10-XXVI, 10-XXX, 31-1.

TABLE 22-I

PREPARATIVE AND STRUCTURAL DETAILS OF SYNTHETIC OXIDES FOUND IN SM-302

Oxide composition	Firing temp., C	Firing time, hr	Product	Structural data
$CoO + Cr_2O_3$	1200	80	$CoCr_2O_4$	Cubic (spinel) a_0 = 8.332 A
$CoO + Ta_2O_5$	1400	20	$CoTa_2O_6$	Tetragonal (trirutile) a_0 = 4.738 A, c_0 = 9.170 A
				Pseudo-rutile cell a_0 = 4.738 A, c_0 = 3.057 A
$Cr_2O_3 + Ta_2O_5$	1315	80	$CrTaO_4$	Tetragonal (rutile) a_0 = 4.649 A, c_0 = 3.018 A
$CoO + WO_3$	1200	60	$CoWO_4$	Monoclinic (tungstate)

TABLE 22-II

OXIDES FOUND IN CONTACT WITH SM-302 AFTER HEAT TREATMENT (FELTEN AND GREGG)

Specimen number	Temp., C	Time, hr	Type of specimen	Oxides present
83	850	192	Metallic	Cr_2O_3 + spinel + weak rutile + trirutile
84	850	432	Metallic	Cr_2O_3 + spinel + weak rutile + trirutile
25	950	16	Metallic	Cr_2O_3 + spinel + trirutile + rutile + very weak CoO
9	1000	30	Metallic	Cr_2O_3 + spinel + rutile + trirutile
23	1000	360	Metallic	Spinel + Cr_2O_3 + rutile + trirutile + very weak CoO
32	1100	2	Metallic	Cr_2O_3 + rutile + spinel + trirutile + very weak CoO
13	1100	16	Metallic	Cr_2O_3 + spinel + rutile + trirutile + very weak CoO
35	1100	40	Metallic	Cr_2O_3 + spinel + rutile + very weak trirutile
89	1100	65	Spalled oxide	Cr_2O_3 + weak spinel + very weak rutile + trirutile
66	1150	4	Metallic	Spinal + Cr_2O_3 + rutile + trirutile + very weak CoO
69	1150	40	Metallic	Cr_2O_3 + spinel + weak rutile
69	1150	40	Spalled oxide	Cr_2O_3 + spinel + weak rutile + trirutile
70	1150	120	Spalled oxide	Cr_2O_3 + spinel + weak rutile
93	1200	2	Metallic	Cr_2O_3 + spinel + weak rutile + trirutile
90	1200	16	Spalled oxide	Cr_2O_3 + weak spinel + very weak rutile + trirutile
44	1200	16	Metallic	Spinel + Cr_2O_3 + very weak CoO
103	1200	48	Spalled oxide	Spinel + weak Cr_2O_3 + tungstate
104	1200	96	Spalled oxide	Spinel + weak Cr_2O_3 + tungstate
85	1250	1	Metallic	Spinel + tungstate
87	1250	1	Metallic	Spinel + tungstate + weak Cr_2O_3
87	1250	1	Spalled oxide	Spinel + tungstate
217	1250	22	Spalled oxide	Cr_2O_3 + spinel + CoO + weak tungstate
154	1260	4	Spalled oxide	Spinel + tungstate + CoO
215	1300	120	Spalled oxide	CoO + spinel + tungstate
155	1316	0.5	Metallic	CoO
155	1316	0.5	Spalled oxide	Spinel + CoO + weak tungstate

TABLE 22-III

SPECTROGRAPHIC ANALYSIS OF OXIDE FORMED ON SM-302 AFTER 2 HR AT 1200 C (FELTEN AND GREGG)

Specimen number	Content, %					
	Cr	Co	Ta	W	Co + Cr	Ta + W
243A	30.93	46.87	16.40	4.31	77.80	20.71
243B	43.26	36.05	13.70	4.97	79.31	18.67
243C	53.64	23.93	16.03	4.19	77.77	20.22
243D	50.75	29.02	12.77	5.37	79.77	18.14
243E	56.92	21.08	15.60	4.53	78.00	20.13
243F	57.16	19.71	16.95	4.04	76.87	20.99
Average	48.81	29.44	15.24	4.57	78.25	19.81
Standard deviation	±10.2	±10.4	±1.64	±0.51	±1.17	±1.31

TABLE 22-IV

COBALT AND CHROMIUM CONTENTS OF THE OXIDE FORMED ON SM-302 OXIDIZED BETWEEN 1000 AND 1300 C (FELTEN AND GREGG)

Oxidation temp., C	Firing time, hr	Content %		
		Co	Cr	Co + Cr
1000	.32	22.83	57.52	79.95
	64	15.54	70.58	86.11
	128	24.14	59.34	82.48
	256	14.52	72.62	87.14
	Average	18.9	65.0	83.9
1100	8	17.086	63.18	80.24
	16	11.53	72.07	83.60
	32	11.39	75.94	87.33
	128	10.83	72.18	83.01
	Average	12.7	70.9	83.6
1200	2	28.41	52.56	80.97
	4	50.65	32.92	83.57
	8	33.086	40.48	83.54
	16	42.64	41.36	84.00
	32	55.56	27.22	82.78
	Average	44.1	38.9	83.0
1300	0.25	62.79	19.32	82.11
	0.5	60.78	22.57	83.29
	1	53.16	26.58	79.74
	2	60.34	21.94	82.28
	4	63.54	17.11	80.95
	Average	60.1	21.5	81.6

TABLE 22-V

X-RAY FLUORESCENCE ANALYSIS OF THE ADHERENT OXIDE AND METAL MATRIX BELOW THE OXIDE FOR HEAT TREATED SM-302 SPECIMENS (FELTEN AND GREGG)

Characteristic x-ray radiation	Intensity of metal + oxide, $c/s \times 10^3$	Intensity of metal, $c/s \times 10^3$	Intensity ratio, metal/metal + oxide	Treatment*
CoKα	11.1	51.7	4.65	A
CrKα	23.7	9.9	0.42	A
WLβ	12.9	13.5	1.05	A
TaLβ	1.8	1.7	0.96	A
CoKα	12.4	47.5	3.82	B
CrKα	19.5	9.8	0.50	B
WLβ	12.9	13.2	1.02	B
TaLβ	1.9	2.4	1.24	B
CoKα	17.6	46.1	2.62	C
CrKα	19.1	10.5	0.55	C
WLβ	13.0	13.9	1.07	C
TaLβ	2.3	2.6	1.15	C
CoKα	21.6	41.6	1.93	D
CrKα	11.2	10.4	0.93	D
WLβ	14.7	14.3	0.97	D
TaLβ	2.1	1.9	0.74	D

* *Treatment: A, Heated 256 hr at 1000 C; B, heated 128 hr at 1100 C; C, heated 32 hr at 1200 C; D, heated 2 hr at 1300 C.*

TABLE 22-VI

X-RAY FLUORESCENCE ANALYSIS OF OXIDE WAFER FROM SM-302 OXIDIZED FOR 2 HR AT 1300 C (FELTEN AND GREGG)

Intensity of	Oxide at gas interface	Oxide in contact with metal
CoKα $c/s \times 10^3$	80.0	13.8
CrKα $c/s \times 10^3$	7.2	13.3
WLβ $c/s \times 10^3$	12.7	19.4
TaLβ $c/s \times 10^3$	Nil	2.9

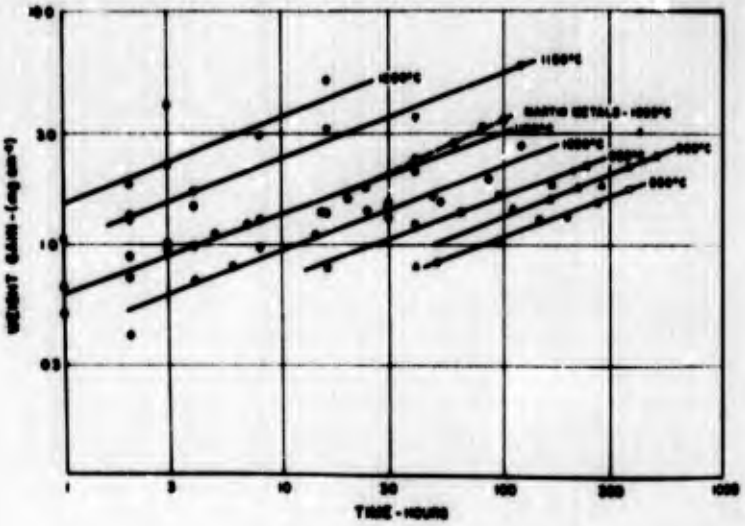

Figure 22.1. Static oxidation test data for SM-302 between 850 and 1200C. (Felten and Gregg).

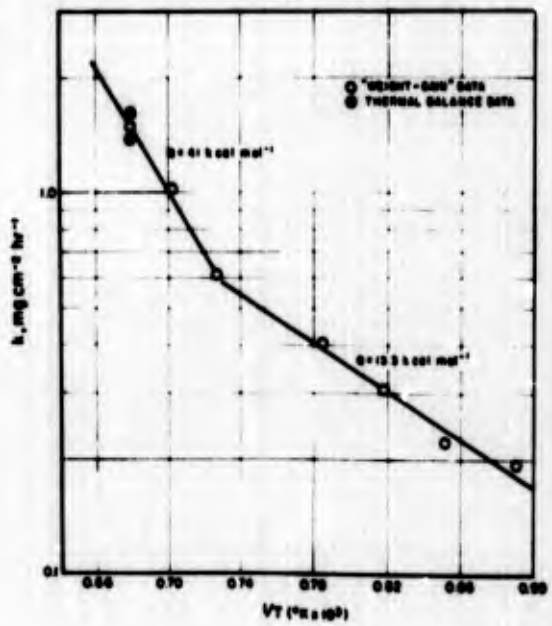

Figure 22.2. Arrhenius plot of oxidation data for SM-302 from 850 to 1200 C. (Felten and Gregg).

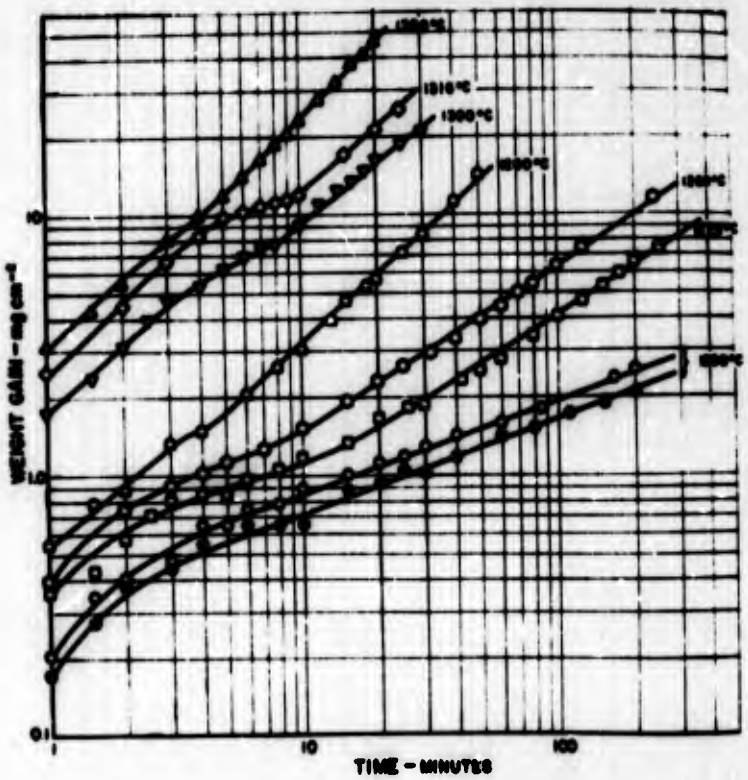

Figure 22.3. Thermal balance data for SM-302 in static air from 1200 to 1300 C. (Felten and Gregg).

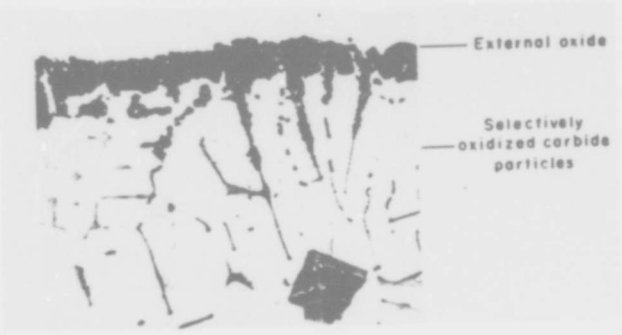

Figure 22.4. SM-302 oxidized 480 hr at 1000 C in air after etching: X500. (Felten and Gregg).

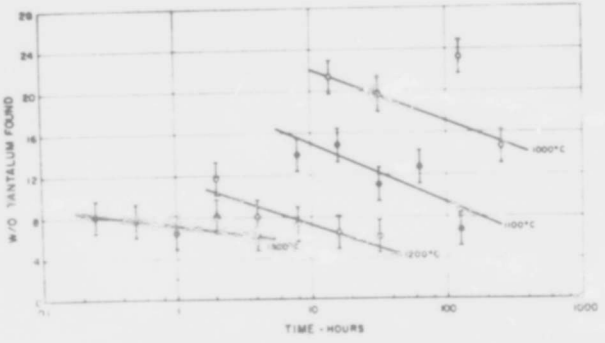

Figure 22.5. Tantalum concentration of spalled oxide from SM-302 between 1000 and 1300 C. (Felten and Gregg)

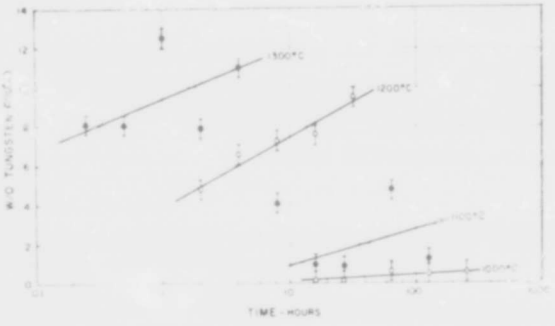

Figure 22.6. Tungsten concentration of spalled oxide from SM-302 between 1000 and 1300 C. (Felten and Gregg).

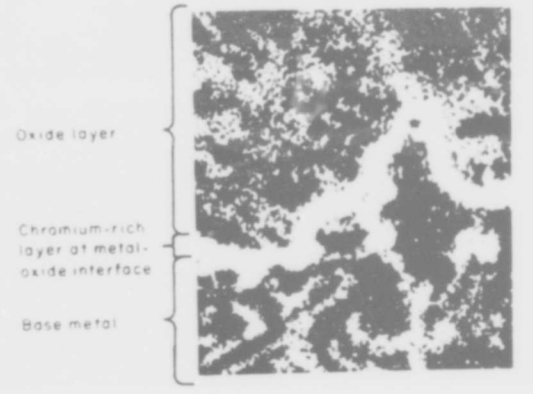

Figure 22.7. X-ray backscatter photograph showing chromium distribution at metal-oxide interface of SM-302. X800. (Felten and Gregg).

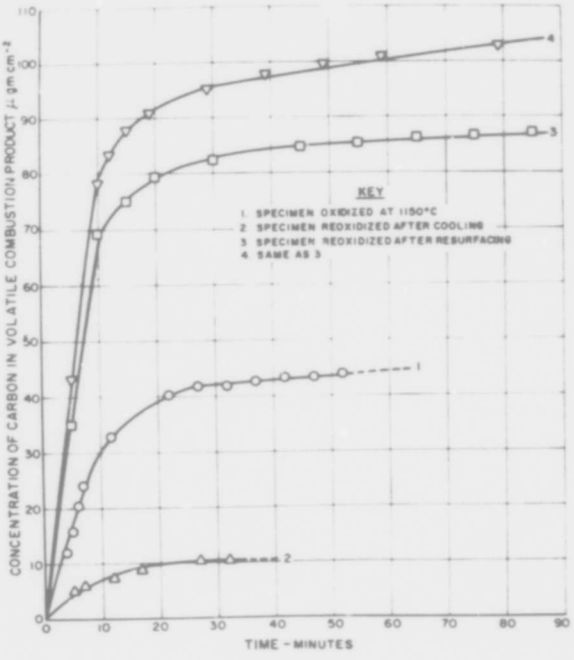

Figure 22.8. Carbon produced as a result of carbide combustion in SM-302 at 1150°C. (Felton and Gregg).

Mar-M 421

K.H. Ryan, J.R. Kildsig and P.E. Hamilton (Allison Division of General Motors) Technical Report to Wright-Patterson AFB, Air Force Materials Laboratory AFML-TR-67-306 (Aug. 1967).

A detailed summary of the procedure used in this report is given under PDRL-163. Mar-M 421 is one of the middle group of alloys; it is comparable to 713C, IN 100 and Inco 717. Figure 23.1 shows the volume loss for the as-cast and heat-treated Mar-M 421 as a function of temperature. Heat treatment has a negligible effect on the corrosion rate. Figure 23.2 compares the measured volume loss and that predicted by the regression equation, (see PDRL 163).

The microstructure of all the alloys could be described in terms of three zones: (1) an outer layer of continuous oxide on the surface which gradually graded into an area of mixed metal and oxide; (2) a layer of depleted metal; (3) globular sulphide particles.

H.T. Quigg and R.M. Schirmer, Progress Report No. 3 on NASC Contract No. N00019-68-C-0252 (Phillips Petroleum Company, Research and Development Report 5423-69) July 1969.

See 713C for details. This report is principally concerned in testing the ASTM "Round Robin" group of alloys in the Phillips Turbine Environmental Simulator using a cyclic test in which the specimen is heated to 1600, 1800 or 2000°F (871, 982 or 1093°C) maximum temperature for 8 min followed by a cooling to 1000°F (538°C) for 2 min producing an attack approximately six times more severe than the isothermal routine used on their earlier tests. After 44h at 2000°F max, Mar-M 421 had lost 126 mg/cm^2, the surface loss was 20 mils and the maximum penetration 22 mils. This was appreciably worse than IN 738, but a little better than U 700. The data are presented in tables and graphs (see 713C).

ASTM Round Robin Test organised by the Hot Corrosion Task Force of the Gas Turbine Panel 1970.

See 713C for details. Mar-M 421 was one of two alloys of intermediate resistance, rather better than the other, U-700. Not as good as U-500 or IN-738. Figure 23.3 shows the metal loss data reported by the participants.

P.C. Felix, in "Deposition and Corrosion in Gas Turbines" A.B. Hart and A.J.B. Cutler (eds.) (Applied Science Publishers, London, 1973) 331.

See 713C for details.

Data relating to this alloy will also be found in the following Figures :
10.51, 10.53, 10.54, 10.92, 10.99, 10.121, 36.1, 36.2, 36.3, 36.4, 36.5, 36.6, 36.7, 45.33, 45.35,
and Tables :
10-XI, 10-XIII, 10-XV, 10-XVI, 10-XXIX.

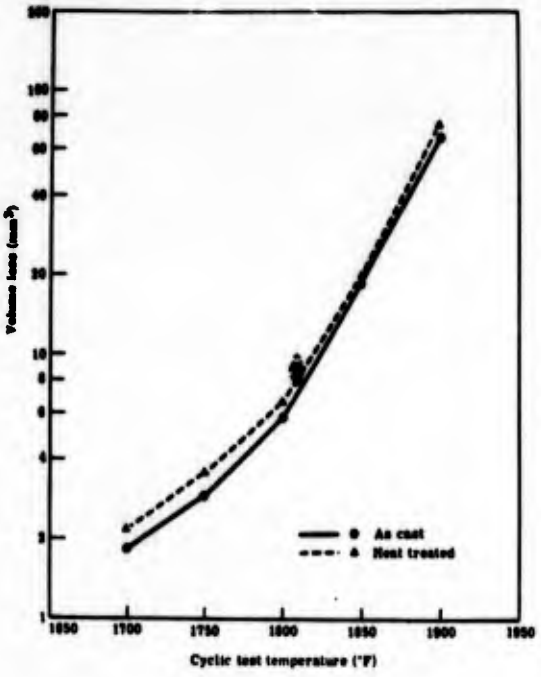

Figure 23.1. As-cast versus heat treated Mar-M 421 at each cyclic test temperature. (Ryan et al).

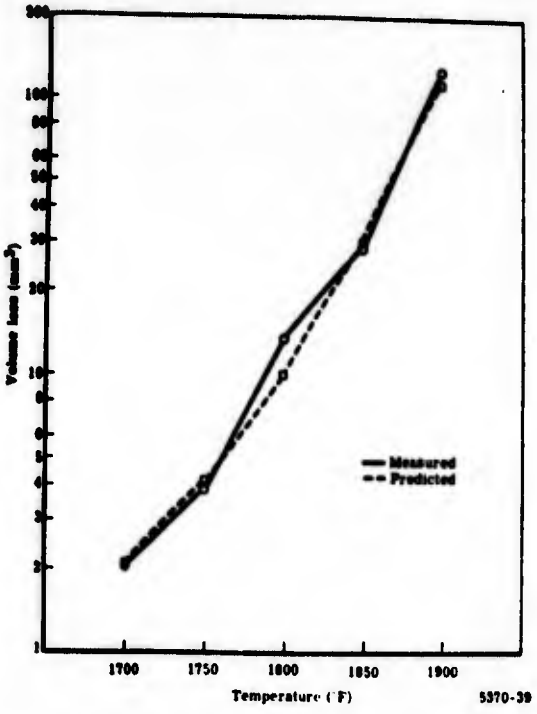

Figure 23.2. Comparison of the measured volume loss and the loss predicted by the regression equation for Mar-M 421. (Ryan et al).

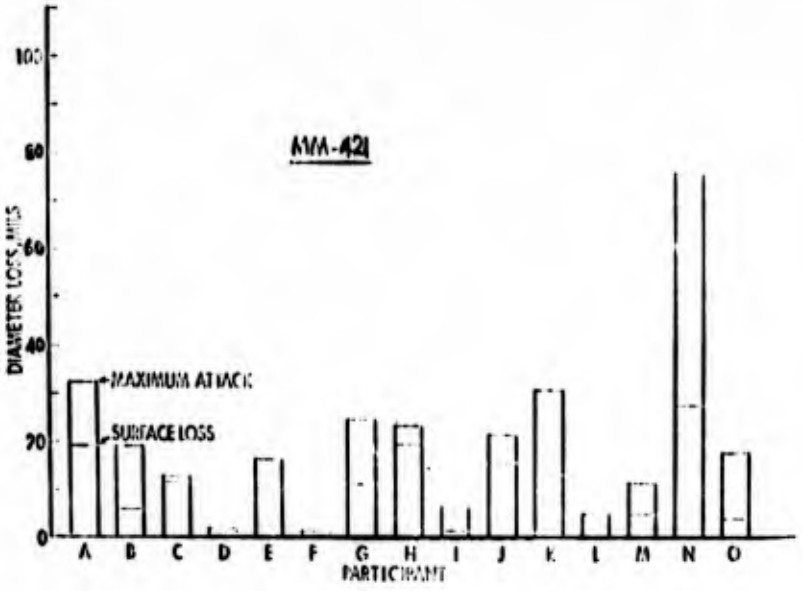

Figure 23.3. Metal loss data for Mar-M 421 reported by participants in ASTM Round Robin test.

Mar-M 432

P.L. Norman and J.D. Harston, in "Deposition and Corrosion in Gas Turbines" A.B. Hart and A.J.B. Cutler (eds.) (Applied Science Publishers London, 1973) 260.

See Nimonic 80A for details. Figure 24.1, 24.2 and 24.3 compare the hot corrosion of a number of nickel-base alloys in a salt-spray test using 75% Na_2SO_4, 25% NaCl at 700, 800 and 900°C, evaluating the corrosion in terms of weight-loss after descaling. Mar-M 432 appears to be a resistant alloy, better than IN 738 at the two lower temperatures, and about the same at the highest temperature.

J.F.G. Conde and G.C. Booth, in "Deposition and Corrosion in Gas Turbines" A.B. Hart and A.J.B. Cutler (eds.) (Applied Science Publishers, London, 1973) 278.

See Nimonic 105 for details. Tests in AML low pressure test rig: at 850°C with 0.1 ppm salt, 200h test, Mar-M 432 is not as good as Nimonic 90, but better than IN 738.

P.C. Felix, in "Deposition and Corrosion in Gas Turbines" A.B. Hart and A.J.B. Cutler (eds.) (Applied Science Publishers, London 1973) 331.

See 713C for details.

K. Page and R.J. Taylor, in "Deposition and Corrosion in Gas Turbines" A.B. Hart and A.J.B. Cutler (eds.) (Applied Science Publishers, London, 1973) 350.

See Nimonic 105 for details. Three alloys are being evaluated for Rolls-Royce industrial and marine turbines: IN 738 is the primary candidate, but Mar-M 432 is thought to be nearly as good.

W.L. Wheatfall, S.J.Dapkunas and J. Sydavar, Naval Ship Research and Development Center, Materials Department, Research and Development Report 8-868 (August 1971).

Samples of this alloy, IN 738 and U 500 were oxidised in flowing oxygen for 210h at 1650°F (899°C) and 235h at 1750°F (954°C). The extent of oxidation was measured in terms of oxide thickness, general penetration and mixiumum depth of oxide penetration. For Mar-M 432, the results were :

	Surface Oxide	General Penetration	Maximum Penetration (all mils.)
210h at 899°C	0.5	1.0	1.5
235h at 954°C	1.1	2.2	3.5

U 500 was the most deeply oxidised alloy at 899°C, but had the lowest depth of attack at 954°C. The oxide scale on U 500 at 899°C was twice as thick as that on IN 738 and Mar-M 432. The surface oxide on U 500 was rough and uneven at both temperatures. At 899°C, IN 738 showed a slightly greater penetration than Mar-M 432. Mar-M 432 was more resistant to oxidation than IN 738 at both temperatures. Grain boundary attack was moderate in Mar-M 432. Surface scales on Mar-M 432 were uniform at both temperatures.

Date relating to this alloy will also be found in the following Figures :
10.92, 14.8, 14.9, 14.10, 32.17, 32.18, 32.19, 32.20,
and in Table 32.I.

Mar-M 509A

J.R. Johnston and R.L. Ashbrook, NASA Technical Note TN D-5376, (August 1969).

See B 1900 for summary and list of the principal tables and figures. In the high velocity gas test at 2000°F (1093°C) the alloy lost 46 mg/cm^2 in 50h; in the static test the corresponding figure was 5.0 mg/cm^2. This was worse than X-40, but better than WI-52 in each case. The oxides determined by X-ray diffraction on materials exposed to high gas-velocity for various time and temperatures are listed; at 1800°F (982°C): 20h, Cr_2O_3; 60h, monoxide (CoO), a spinel with a_o = 8.30 Å; and $CoWO_4$; 100h, Cr_2O_3, CoO, spinel. At 1900°F (1038°C): 20h, Cr_2O_3, CoO, a spinel with a_o = 8.20 Å, a spinel with a_o = 8.30Å, and $CoWO_4$; 60h, CrO_3, CoO, a spinel with a_o = 8.15 Å, a spinel with a_o = 8.30 Å, and $CoWO_4$; 100h, Cr_2O_3, CoO, a spinel with a_o = 8.15 Å, a spinel with a_o = 8.20 Å and $CoWO_4$. At 2000°F (1093°C): 20h, Cr_2O_3, CoO, and a spinel with a_o = 8.25 Å; 60h, Cr_2O_3, CoO, a spinel with a_o = 8.35 Å, and $CoWO_4$; 100h, Cr_2O_3, CoO, a spinel with a_o = 8.25 Å, and $CoWO_4$.

The effect of variations in the operating conditions is shown: for Mar-M 509A, in the standard cycle of 100 1h cycles at 2000°F (1093°C) in Mach 1 with forced air cooling, the sample lost 4870 mg; with a free air cool and 10h cycles, the weight loss was only 795 mg.

Oxidation proceeds along the interdendritic carbides, at least in the early stages.

A.R. Cox and R.J. Hecht (Pratt and Whitney Aircraft, Florida Research and Development Center) Technical Report to the Air Force Materials Laboratory, Wright-Patterson AFB, AFML-TR-70-273 (December 1970).

See WI-52 for a detailed summary. Mar-M 509 very much better than WI-52, about the same as Mar-M 302, except in a low-salt (3.5 ppm) cyclic hot corrosion test, in which it was rather worse.

A.M. Beltran, Cobalt, No. 46, 1970, 3.

See X-40 for details. Mar-M 509 is quite resistant to oxidation at 1093°C, very similar to Mar-M 302. In hot-corrosion testing in 3% S residual oil with 325 ppm NaCl in the fuel (= 5ppm salt in the air), 600h tests at 1600°F (871°C), Mar-M 509 showed a maximum penetration of 0.08 mm per side, a little better than Mar-M 302. The relative hot-corrosion resistance of another group of alloys tested in 1% S diesel oil with 5 ppm salt in the air at 1600F (871°C), 1750°F (955°C) and 1900°F (1039°C) for 500, 1000, 1000h respectively is shown: Mar-M 509 seemed a little worse than Mar-M 302, especially at the highest temperature.

H.T. Quigg, R.M. Schirmer and L. Bagnetto, Final Report to NASC on Contract No. N00019-69-C-0221 (Phillips Petroleum Company Research and Development Report 5732-70) July 1970.

See 713C for details.

H.T. Quigg, R.M. Schirmer and L. Bagnetto, Final Report to Naval Air Systems Command on Contract N00019-70-C-0293 (Phillips Petroleum Company Research and Development Report 5903-71) Jan 1971.

See 713C for details.

W.L. Wheatfall, in "High Temperature Corrosion of Aerospace Alloys" J. Stringer, R.I. Jaffee and T.F. Kearns (eds.) AGARD Conference Proceedings No. 120, (March 1973) 235.

See 713C and IN 738 for details.

Data relating to this alloy will also be found in the following Figures :
1.9, 1.10, 1.11, 1.12, 1.13, 1.14, 10.105, 14.11, 51.7, 51.8, 51.9, 51.10, 51.11, 51.12, 52.8, 52.9, 52.11, 52.12, 52.14;
and Tables :
10-XXX, 31-I.

Nicrotung and Nimonic 75

R. Viswanathan, Corrosion 24 (1968) 359.

See 713C for details. Nicrotung was one of the poorer alloys studied. After 150h testing at 1500°F (816°C) the specimen had lost 15.6 mg/cm^2; 36.5% of the alloy was unaffected. Inco 751 was comparable; the weight loss on 713C was much higher, but the affected metal was about the same.

J.F.G. Conde, paper to Conference on Naval Materials: Current and Future Problems Royal Naval Engineering College, Manadon, July 1970.

Remarks that limited incidence of sulphidation corrosion has occured in Nimonic 75 combustion chambers on certain engines, but this has been overcome by redesign to permit better cooling and by pack aluminising. In the Allen 500 kW turbine, combustion chambers were failing by sulphidation after about 1200h, but improvements in design have resulted in a life in excess of 10,000h.

E. Erdös in Deposition and Corrosion in Gas Turbines" A.B. Hart and A.J.B. Cutler (eds.) (Applied Science Publishers, London 1973) 115.

See 713C for details.

Nimonic 80A

B.O. Buckland, A.D. Foster and J.J. Treanor, presented at National Association of Corrosion Engineers Annual Meeting (April 21, 1966) Miami, Florida.

See U 500 for a summary of the paper. A number of components were taken from service turbines and examined; some of these were Nimonic 80A.

Bucket B.7: from turbine operated on natural gas, after 60, 836h: turbine shutdown on average 0.2 times per 100h. Calculated metal temperature 1350°F (732°C). Corrosion 2 mils, which would be expected in this time from a metal temperature of 1420°F (771°C) as indicated by the small burner test.

Bucket B.8: natural gas, 32,850h, 0.2 shutdowns/100h; 1320°F (716°C) 2 mils, 1440°F (782°C).

Bucket B.13: natural gas, 40,000h, 0.2 shutdown/100h; 1320°F; 1 mil; 1390°F (754°C).

W. Möller, Paper B16 in 9th International Congress on Combustion Engines, CIMAC, Stockholm, 1971.

Corroded up to 1000h at 650 - 750°C and 60 m/s gas velocity in a test rig burning a distillate oil containing 0.3% S with additions of sulphur, sodium and vanadium. Six conditions were used: no additions (0.3% S), 2.2% S; 2.2% S + 7 ppm Na; 2.2% S + 28 ppm V; 2.2% S + 28 ppm V + 7 ppm Na; and 2.2% S + 37 ppm Na + 28 ppm V. Corrosion was determined by measuring the weight loss after descaling.

Figure 28.1 shows the scale formed by oxidation in air for 10,000h at 750°C. The chemical composition is shown in Table 28-I and the phases present as indicated by X-ray diffraction in Table 28-II. The scale is very irregular and in some places is up to 25 µm thick. It consists of Cr_2O_3, TiO_2 and a little NiO. No spinel was detected. The calculated weight loss from the measured scale thickness was 6.5 mg/cm^2 equivalent to a metal loss of 7.5 µm. The light-etching layer is depleted in Cr, Ti and Al, and is up to 65 µm thick.

Figure 28.2 shows the weight losses in the complexion atmospheres, and these are listed in Table 28-III. Figure 28.3 shows the scale formed after 400h in flue gas with sulphur. Figure 28.4 shows the heavy corrosion in S + V at 700°C; Figure 28.5 in S+V+Na at 750°C. Sulphur and sodium additions produce no change in the corrosion of Nimonic 80A.

E. Erdös in "Deposition and Corrosion in Gas Turbines" A.B. Hart and A.J.B. Cutler (eds.) (Applied Science Publishers, London 1973) 115.

See 713C for details.

W. Moller, in "Deposition and Corrosion in Gas Turbines" A.B. Hart and A.J.B. Cutler (eds.) (Applied Science Publishers, London 1973) 1.

Figure 28.6 shows the cross-section of the corrosion interface on Nimonic 80A after 27,000h service at 700 - 730°C in a turbine burning blast furnace gas.

P.L. Norman and J.D. Harston in "Deposition and Corrosion in Gas Turbines" A.B. Hart and A.J.B. Cutler (eds.) (Applied Science Publishers, London 1973) 260.

This paper describes the use of a new salt-shower test to evaluate the hot-corrosion resistance of superalloys. The alloys tested were Nimonic 80A, Nimonic 90, Nimonic 105, Nimonic 81, EPK 55, (IN 587), EPK 57, (IN 597), 713C, EPD 20, (IN 589), IN 738, and Mar-M 432. The specimens were inside a vertical tube furnace through which a coarse salt mixture was dropped using a vibratory feeder which operated for 5 min every hour. Tests were continued for 300h. The salt mixture was 75% sodium sulphate, 25% sodium chloride. After removal specimens were descaled and weighed, the corrosion being evaluated in terms of the weight loss.

Table 28-IV shows preliminary results for Nimonic 80A and 81. Table 28-V shows the results of half-immersion crucible tests on the same two alloys. The salt spray test was much more reproducible than the crucible test, and allowed the two alloys to be clearly distinguished.

P.C. Felix in "Deposition and Corrosion in Gas Turbines" A.B. Hart and A.J.B. Cutler, (eds.), (Applied Science Publishers, London 1973) 331.

See 713C for details.

Data relating to this alloy will also be found in the following Figures :
10.92, 10.99;
and Tables :
10-XXVII, 10-XXIX, 28-IV, 28-V, 31-II, 45-III.

TABLE 28-I

DISTRIBUTION OF THE ELEMENTS IN THE CORROSION LAYERS OF NIMONIC 80A (MULLER)

Matrix			Cr	Ni	Ti	Al	S					
		Weight %	19,3	75,2	2,6	1,4	n.b.					
		Intensity %	19...20	65...71	2,2...2,5	1,1...1,4	0,005...0,02					
Zone	µm		<-12	<-20	<-60		<-30	<-60	<-25	<-30	<-10	<-75
Run			Air annealed				H	N	O	←	O	→
Addition			-	-	-		S + V	S + V + Na		S + Na + V		
No. of Sample			303	307	314		165	256	284	306go	309go	329w
Temp.	°C		650	700	750		700	750	700	650	700	750
Time	h		10 000	10 000	9 260		1000	1000	1000	←	2000	→
Position							lee-side	luff-side	lee-side	luff-side	luff-side	lee-side
Subsurf. layer	µm		-12...-2	-20...-3	-60...-3		-30... 0	-60... 0	-25... 0	-30...-5	-20... 0	-75...-5
	% Cr		20...16	20...15	20...16	Int.-% Cr	20...11	19... 9	19...11	16... 9	21..12..24	-6... 3
	% Ni		75...83	84...86	75...81	" Ni	65...77	69...82	74...84	80...64	68...19	72...92
	% Ti		2,6..0,4	2,6..0,3	2,6..<0,4	" V	-	-	-	0...0,1	<0,05	-
	% Al		1,4..0,4	1,4..0,1	1,4..0,1..5	" S	ö.Sp.	0,01..1,3	0,02..0,6	<0,02	2...23	ö..20
Phase boundary = 0 µm												
Heterogeneous layer	µm											Pure scale
							0...10	5...15	5...20		5...20	5...15
						Int.-% Cr	9...21	25...27	23..13..28		32...19	20...38
						" Ni	68...56	50...14	47...32		12...40	57...10
						" V	0...9	0... 5	0... 2		<0.2	0,6...8
						" S	ö.Sp.	<0,04	<0,06		14... 2	<0.1
Scale inside	µm		0.,4.. 8	2.. 4.. 8	2.. 5.. 7		15..35..55	20..70..95	25...35*)	5...20	25...65	20...65
	% Cr		20..46.. 1	12..50..44	43..39..46	Int.-% Cr	25.. 3..10	23...2...7	33... 2	34...15	43..24..41	28...18
	% Ni		24.. 5.. 1	17.. 1..21	1..22.. 2	" Ni	20..33..20	14..26..22	14...34	11...22	12... 6	12
	% Ti		3..15 öA.	7..17.. 8	18..10.. 5	" V	10..18..15	12...17	4... 8	0,2...4	0,2..0,5	3...0,8
	% Al		<24 öA.	36..11.. 8	14..36.. 8	" S	n.b.	<0,06	<0,02	<0,2	1...0,1	<0,1..0,6
Scale outside	µm		12...16	20..27..30	12..18..24		60*)	115*)	40		75...110..	
	% Cr		29... 5	38.. 6..<1	50... 4	Int.-% Cr	<1	20	<1		1	
	% Ni		<1	<1	<1	" Ni	35	7	19		(61) 25..	
	% Ti		<2	18..13.. 1	15..48..<1	" V	23	2	19		(18) 1..	
	% Al		8...18	3..54.. 8	3..16.. 9	" S	n.b.	o,?	0,1		0,6	
						µm				35	..150..180 .	
						Int.-% Cr				1	1	
						" Ni				32	..59... 5	
						" V				5	.. 1... 0	
						" S				2	.. 2... 0	

ö = local , A. = enriched
Sp.= traces
*) = measured at several positions

TABLE 28-II

COMPOUNDS IDENTIFIED FROM X-RAY PATTERNS (MULLER)

Alloy	Run Addition	Air -	L S + Na	M S + V	N + O S+V+Na		Q S + Na + V	
	No. of sample Temp. °C	303,307,314 650...750	207 750	304 700	258 750	326,404,306 650	407 700	329,414,312 750
	Sp. 8,28 Å $NiCr_2O_4$		m	m	mst	s	mst	sst
	NiO	(s)	m		m	s?	?	ms
	Cr_2O_3	m	ss					
	$Ni_3V_2O_8$		?	sst	sst	mst	st	mst
	Na_2SO_4 5-0631		m	sss	ms	st	sst	st
	Na_2SO_4 8-31.		st		?	?	ms	st
	Ni	st	sst					
	Others	TiO_2 sst	Na_2CrO_4 ?				$Ni_2V_2O_7$ m?	

TABLE 28-III

WEIGHT LOSSES AFTER DESCALING IN mg/cm^2 (MULLER)

test time h		400	600	1000
run	temp. °C	N i m o n i c 80 A		
I	650	0.3	5.0	5.6
	700	0.8	5.7	4.0
	750	1.4	4.1	2.0
K+)	650	0.3	0.6	0.4
	700	0.4	0.4	0.4
	750	0.6	0.7	0.7
L	650	0.5	0.6	0.6
	700	0.6	0.7	0.8
	750	0.8	0.9	1.1
M	650	7.0	8.7	12.4
	700	10.5	14.7	19.7
	750	15.0	20.0	33.2
N	650	5.9	7.3	6.9
	700	8.5	10.0	12.7
	750	12.9	13.1	21.2
O	650	6.4	7.6	11.6
	700	9.1	12.2	15.0
	750	15.5	19.9	28.6
Q	650	-	-	7.8
	700	-	-	12.0
	750	-	-	30.7

TABLE 28-IV

PRELIMINARY RESULTS ON NIMONIC ALLOYS 80A and 81 INDICATING EXCELLENT AGREEMENT AND REPRODUCIBILITY AND THE TWO ALLOYS ARE EASILY DISTINGUISHED ON THE BASIS OF HOT-CORROSION RESISTANCE (NORMAN AND HARSTON)

Alloy	Temp. C	Time hours	Descaled wt loss (mg cm^2)			
			1	2	3	4
Nimonic alloy 80A	750	1	6·1	5·1	5·5	6·1
		3	40·8	37·7	33·8	37·3
		8	49·0	53·8	53·8	108·3
		24	69·3	68·3	59·6	74·9
	800	1	4·1	3·9	2·2	3·7
		3	19·6	27·3	25·2	23·8
		8	27·3	23·0	42·3	23·2
		24	79·6	77·0	103·2	93·7
	850	1	1·7	3·8	2·2	6·3
		3	20·2	20·3	19·1	29·2
		8	55·5	67·8	47·3	87·2
		24	72·8	71·1	90·3	59·6
Nimonic alloy 81	750	1	3·1	5·6	6·3	5·8
		3	3·6	3·2	4·7	3·9
		8	25·3	30·7	28·6	25·3
		24	27·6	29·8	27·2	31·5
	800	1	1·0	1·5	1·0	1·0
		3	6·3	7·8	7·5	7·5
		8	5·9	6·3	4·8	6·1
		24	n.d.	n.d.	n.d.	n.d.
	850	1	6·4	6·3	5·4	6·4
		3	11·7	10·0	10·7	7·4
		8	6·4	7·2	7·5	7·0
		24	13·8	20·1	17·6	17·5

n.d. Not determined.

TABLE 28-V

HALF IMMERSION CRUCIBLE TESTS ON NIMONIC ALLOYS 80A and 81, SALT-75% Na_2SO_4 + 25% NaCl (NORMAN AND HARSTON)

Alloy	Temp. C	Time hours	Descaled wt loss (mg cm^2)	
			1	2
Nimonic alloy 80A	700	50	7·6	12·7
		100	5·1	5·1
		300	5·0	7·6
	800	50	n.d.	7·6
		100	2·5	3·8
		300	35·1	129·3
	900	50	10·1	7·6
		100	12·7	149·3
		300	116·8	117·5
Nimonic alloy 81	700	50	7·6	n.d.
		100	2·5	n.d.
		300	5·1	12·7
	800	50	10·1	n.d.
		100	5·1	n.d.
		300	11·4	9·4
	900	50	12·7	n.d.
		100	15·2	n.d.
		300	20·3	n.d.

n.d. Not determined.

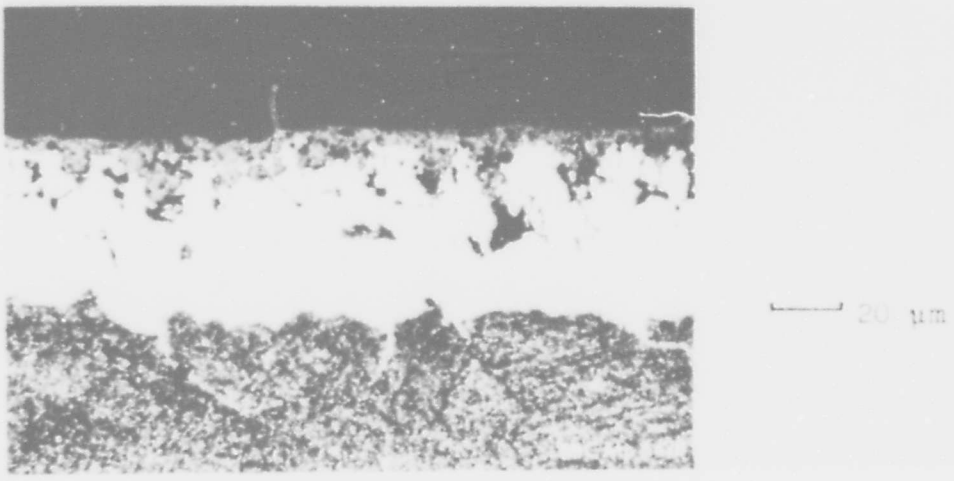

Figure 28.1. Structure of corrosion layers on Nimonic 80A after 10,000h at 750°C in air (Müller).

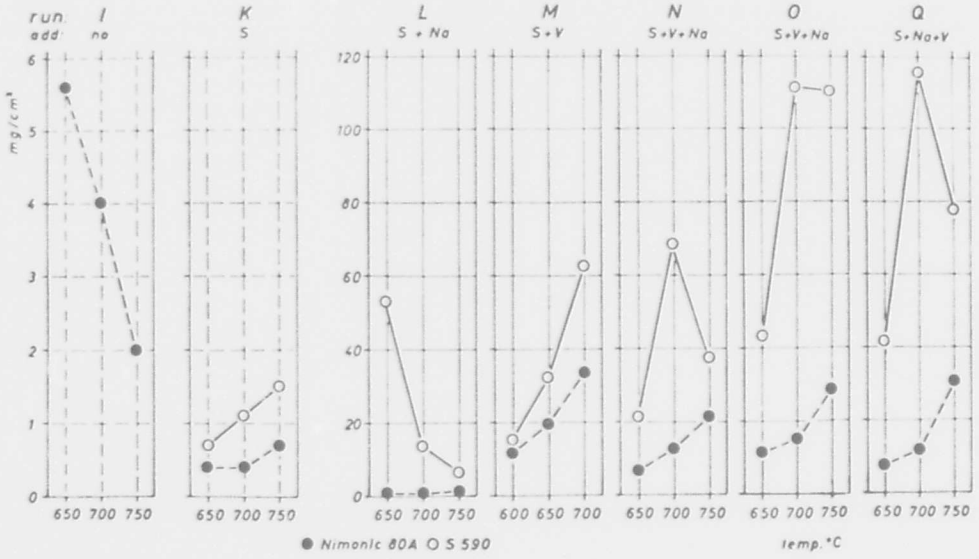

Figure 28.2. Weight losses of Nimonic 80A and S590 as function of test temperature (Müller).

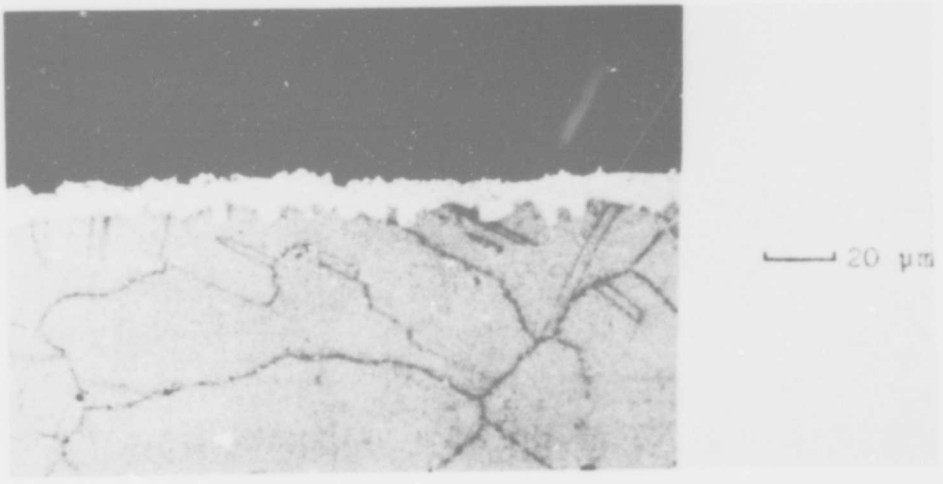

Figure 28.3. Structure of corrosion layers after 400h exposure at 750°C to flue gas with sulphur addition. (Müller).

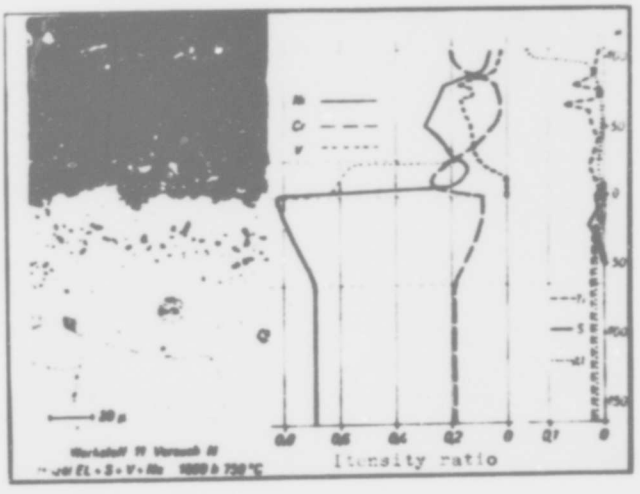

Figure 28.4. Structure of corrosion layers and distribution of elements after 1000h exposure at 700°C to flue gas with addition of sulphur and vanadium (Müller).

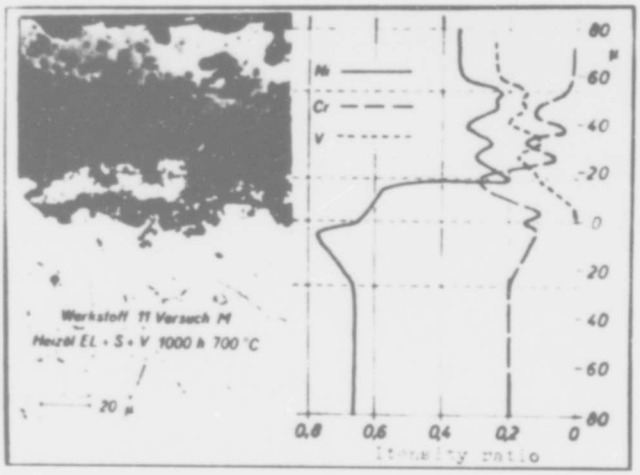

Figure 28.5. Structure of corrosion layer and distribution of elements after 1000h exposure to flue gas with additions of sulphur, vanadium and sodium. (Müller).

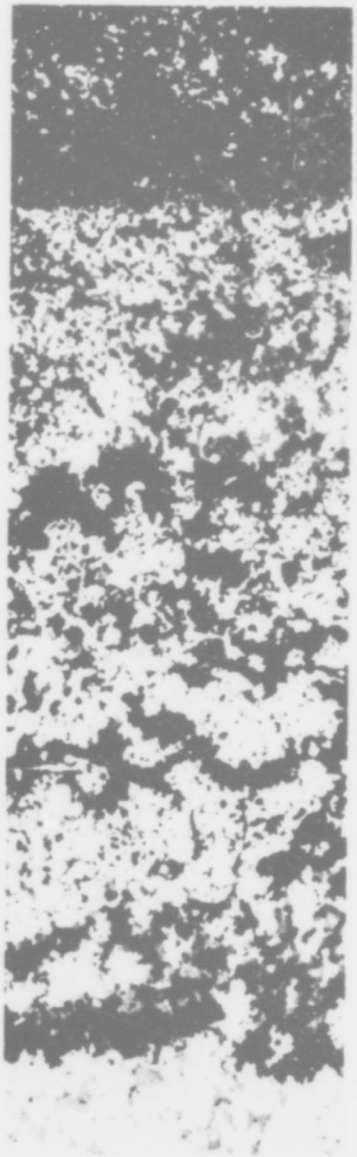

Figure 28.6. Example of sulphide-oxide attack after 27,000h service at 700-730°C exhaust blast furnace gas. Material Nimonic 80A. Magnification X120. (Müller).

Nimonic 81

P.L. Norman and J.D. Harston, in "Deposition and Corrosion in Gas Turbines" A.B. Hart and A.J.B. Cutler (eds.) (Applied Science Publishers, London 1973) 260.

See Nimonic 80A. Figure 29.1 shows the increase in hot corrosion of Nimonic 81 after 300h at 800°C in a salt-spray apparatus using 75% Na_2SO_4, 25% NaCl as a function of the surface area to volume ratio, the corrosion being evaluated in terms of weight loss after descaling. The corrosion of a number of nickel-base alloys at 700, 800 and 900°C is shown. Nimonic 81 is very resistant at all three temperatures, in general appearing to be the best of the alloys tested.

Data relating to this alloy will also be found in Figures :
14.8, 14.9, 14.10 and 32.6.

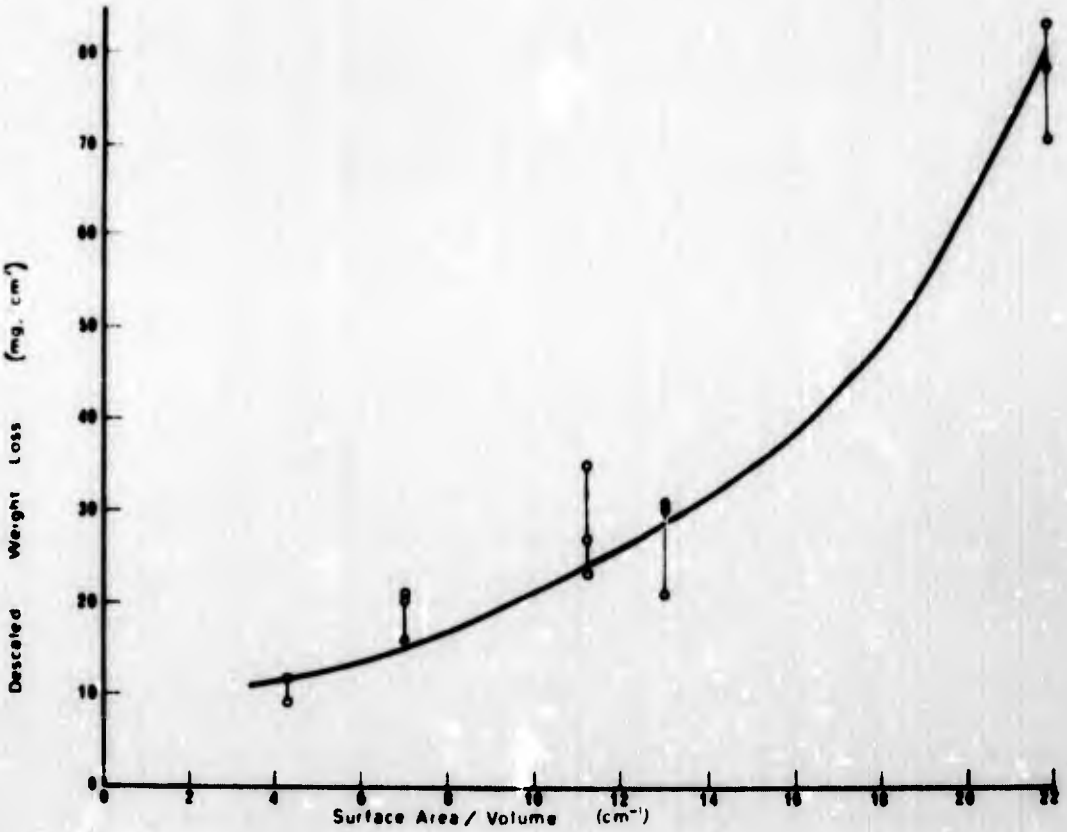

Figure 29.1. The increase in hot corrosion rate of Nimonic alloy 81 after 300h at 800°C with increase in surface area to volume ratio. (Norman and Harston).

Nimonic 90

G. Llewellyn, Hot Corrosion Problems Associated with Gas Turbines, ASTM Special Technical Publication, (STP 421) 1967, p.1.

See Nimonic 100. Threshold temperature in 6hr test, 45 min cycle, SO_2/air, 930°C; 920°C in contact with carbon, 1020°C pack aluminised 1000°C pack aluminised in contact with carbon.

J.F.G. Conde, paper to Conference on Naval Materials: Current and Future Problems, Royal Naval Engineering College, Manadon, July 1970.

Remarks that three separate failures of Nimonic 90 first stage nozzles in Allen 500 kW turbines (maximum temperature 735°C) in large vessels were related to heavy intake of sea water during rough weather in two instances and salt spray and diesel engine exhaust fumes in a further instance. The nozzles have been made from X-40 since 1965 with no sign of corrosion. Figure 30.1 shows a very severely corroded cast Nimonic 90 nozzle segment from a Proteus engine which had operated for 800 h in a Brave Borderer.

The overall effects of various concentrations of salt in air have been studied in a series of engine tests on a Proteus at the National Gas Turbine Establishment using a Nimonic 90 first stage nozzle segment as a corrosion monitor. The results have been summarised (by S.G. Morgan, A.W. Lamport and A.J.R. Smith "Gas Turbines in the Royal Navy" ASME Paper 70-GT-10, presented at the ASME Gas Turbine Conference and Products Show, Brussels, Belgium, May 1970) as follows:

> 0.5 ppm NaCl in the intake air, with turbine entry temperature in the range 650 - 750°C - corroded after 365 h
> 0.05 ppm NaCl, 660 - 780°C - corroded after 1000h
> 0.005 ppm NaCl, turbine entry temperature ranging to 780°C approx. on power cycle - no corrosion after 1400h of which 1000h were with salt ingestion.

E. Erdös in "Deposition and Corrosion in Gas Turbines" A.B. Hart and A.J.B. Cutler (eds.) (Applied Science Publishers, London , 1973) 115.

See 713C for details. Figure 30.2 shows a stratified scale on Nimonic 90 exposed to sulphur vapour for 118 h at 800°C. Three different layers developed: an outer layer of NiS + $(Co, Ni)_3S_4$, a middle layer of Cr_3S_4 + Cr-Al-S, and an inner adherent layer of Cr_3S_4.

R.C. Hurst, J.B. Johnson, M. Davies and P. Hancock, in "Deposition and Corrosion in Gas Turbines", A.B. Hart and A.J.B. Cutler (eds.), (Applied Science Publishers, London 1973) 143.

This paper describes a study of the effect of chloride and sulphate contamination on the oxidation of alloys in the temperature range 600 - 950°C, using a hot-stage microscrope. In addition, some experiments were performed using a vibration apparatus.

The effect of introducing sodium sulphate or sodium chloride after 100h on the resonant frequency of Nimonic 90, Nimonic 105, IN 597 and Brightray C was studied: sodium sulphate had no effect, but sodium chloride produced a very sharp drop, indicating loss of adhesion or cracking in the scale.

A.J.B. Cutler and C.J. Grant in "Deposition and Corrosion in Gas Turbines" A.B. Hart and A.J.B. Cutler (eds.) (Applied Science Publishers, London 1973) 178.

See IN 738 for details. Nimonic corroded significantly more rapidly (at 727°C in Li/Na/K sulphate mixture, in 1 atm O_2, 3.23×10^{-4} atm SO_3) than Nimonic 115 or 105. At the conclusion of the experiments with Nimonic 90 the molten sulphate had an intense blue coloration corresponding to an appreciable concentration of Co^{++} dissolved in the melt. The thick oxide layer formed on Nimonic 90 had a crystalline dendritic appearance. Microprobe analysis of the scale showed that there is a layer of chromium and nickel sulphides adjacent to the metal.

P.L. Norman and J.D. Harston in "Deposition and Corrosion in Gas Turbines" A.B. Hart and A.J.B. Cutler (eds.) (Applied Science Publishers, London 1973) 260.

See Nimonic 80A for details. Nimonic 90 is quite resistant to the salt-shower test at 700°C, better than Nimonic 105, IN 738 or Mar-M 432. However at 800°C and 900°C it is poor, comparable to 105, nearly as bad as 713C. Nimonic 90 goes through a maximum attack at 800°C.

J.F.G. Conde and G.C. Booth in "Deposition and Corrision in Gas Turbines" A.B. Hart and A.J.B. Cutler (eds.), (Applied Science Publishers, London 1973) 278.

See Nimonic 105 for details. Describes use of the AML low pressure simulator in testing alloys, principally at 750 and 830°C for 200h with 0.1 ppm sea salt. Nimonic 90 appers to be a very resistant alloy, comparable with X-40.

P.C. Felix in "Deposition and Corrosion in Gas Turbines" A.B. Hart and A.J.B. Cutler (eds.), (Applied Science Publishers, London 1973) 331.

See 713C for details.

K. Page and R.J. Taylor, in "Deposition and Corrosion in Gas Turbines" A.B. Hart and A.J.B. Cutler (eds.), (Applied Science Publishers, London 1973) 350.

See Nimonic 105 for details.

H. Huff and F. Schreiber, Werkstoffe and Korrosion 5 (1972) 370.

See 713C for details. The paper describes experiments in a combustor rig in which a stress can be applied to the specimen. Figure 30.3 shows the time to rupture at stresses in the range 8 - 17 kp/mm^2 in air at 815^o and 900^{o}C, in combustion gas at 900^{o}C and in combustion gas with 31 ppm salt at 900^{o}C. The 100h rupture strength at 900^{o}C was 170 N/mm^2 in air, the same in combustion gases without salt, and 80 N/mm^2 with 30 ppm sea-salt. Figure 30.4 shows the influence of temperature on the time to rupture at 120 N/mm^2 in air, combustion gas, and combustion gas with 31 ppm sea salt.

R.W. Archdale, paper to Inter-Service Metallurgical Research Council, Heat Resistant Metals Committee, ISMET 2805 HR 558 (November 1961).

Refers to a test carried out in 1955 on a Proteus engine with the object of determining the degree of corrosion to be expected under marine operating conditions. Salt was injected into the air intake at 1.07 ppm; the fuel contained 0.57 - 0.76% S. The running period was 225h, and it was necessary to increase the turbine entry temperature to achieve the specified power. This turned out to be due to the build up of a layer of anhydrous sodium sulphate on the first stage stator blades, reducing the throat gap. Severe corrosion of the stator blades had occurred in the form of mounds or tumours on the blade surface. In some cases parts of the trailing edges were corroded away. The maximum turbine entry temperature had been quoted as 872^{o}C, and the maximum operating temperature of the first stage stator blades was estimated to be in excess of 900^{o}C. Figure 30.5 shows the general appearance of a stator segment after 22h with 2% sea water in fuel.

The deposit was 93.6% water soluble, containing 4.91% calcium sulphate, 5.65% magnesium sulphate, balance sodium sulphate. The insoluble part contained the oxides of Cr, Ni, Co and Fe together with some carbonaceous matter. No chloride was detected. Nickel sulphide, Ni_3S_2 was detected by X-ray crystallographic methods in the inner zones of the corrosion mounds.

In the laboratory, sodium sulphate alone failed to give this form of attack on Nimonic 90, but mixtures of sodium sulphate and sodium chloride gave tumour-like corrosion products which were visually and metallographically similar to those found after the engine run. Subsequently it was observed that mixtures of sodium sulphate and carbon would also give this form of attack.

Archdale considers sulphidation, and in particular the formation of nickel sulphide, to be important in the reaction, but comments that the natural oxide film has some resistance to sulphur penetration and breakdown of this film tends to depend on the presence of a triggering agent such as the chloride ion.

The results of crucible tests at 900^{o}C sodium sulphate/sodium chloride tests are given in Table 30-I. In test A, the specimen is half immersed in powdered solid salt in a silica crucible and the entire assembly is heated until the salt is molten. In test B, the specimen is half immersed in the already molten salt.

A further test used a mixture of 95% magnesium sulphate with 5% carbon. This followed reports that "black plague" corrosion followed the use of water containing appreciable quantities of magnesium sulphate for compressor washing. Again the tests were conducted at 900^{o}C, for 72h.

Table 30-II results of magnesium sulphate/carbon crucible tests (Archdale).

Loss in weight, mg/cm; 72h in 95% $MgSO_4$ + 5% C.

Nimonic 90	13.4, 25.0
Nimonic 100	107.0, 93.5
Nimonic 105	45.0, 3.4
Nimocast 258	29.0, 3.1
G-64	76.0, 3.5
G-67	2.4, 1.7

Archdale considered that the low chromium alloys (Nimocast 258, Inconel 713, G64 and Nimonic 100) could suffer reaction without the presence of a triggering agent over a broad front. The high-chromium alloys, on the other hand, required triggering and so exhibited local attack at isolated points; however, once triggered, the attack could be catastrophic. The author regards Nimonic 105 as a borderline case.

Data relating to this alloy will also be found in the following Figures :
10.92, 14.6, 14.8, 14.9, 14.10, 32.6, 32.9, 32.10, 32.17, 32.18;
and Tables :
31-I, 31-II, 32-I.

TABLE 30-I

CRUCIBLE TEST RESULTS (ARCHDALE)

Test A, Loss in weight, mg/cm^2

Alloy	Na_2SO_4	0.5% NaCl	1% NaCl	10% NaCl	50% NaCl
	6h	1.5h	6h	6h	6h
Nimonic 90	1.18	0.80	2.06	14.30	5.50
Nimonic 100	0.45	1.25	288.00	436.00	1230.00
Nimonic 105	0.70	0.50	0.60	25.40	3.70
Nimocast 258	0.3 to 49.0	0.1-8.45	0.30	0.80-0.50	-
Inonel 713	1.60	7.40	46.00, 50.00	-	-
G-64	0.85 to 146	64.0-48.0	206.0-232.0	189.0-199.0	-
G-67	0.50	0.50	0.65	0.68	-
X-40	0.80	-	1.79, 1.33	80.5	-
W.I. 52	1.54	-	5.5, 110.9, 60.8	77.2	-

Test B, Loss in weight, mg/cm^2

Alloy	Na_2SO_4	1% NaCl	10% NaCl	50% NaCl
Nimonic 90	0.60	1.80	118.0	complete destruction
Nimonic 100	0.30	223.0	480.80	4.20, 1060.0
Nimonic 105	0.70	0.65	0.80	3.00 - 5.30
Nimocast 258	0.76-3.1	0.4-105.0	0.4, 0.3	-
G-64	0.7, 0.85	217, 234	396, 70	-

Figure 30.1. (a) Cast Nimonic 90 nozzle segment from Proteus engine after 800 hours in Brave Class Fast Patrol Boat.

(b) Cast X40 nozzle segment from Industrial Engine. (Conde).

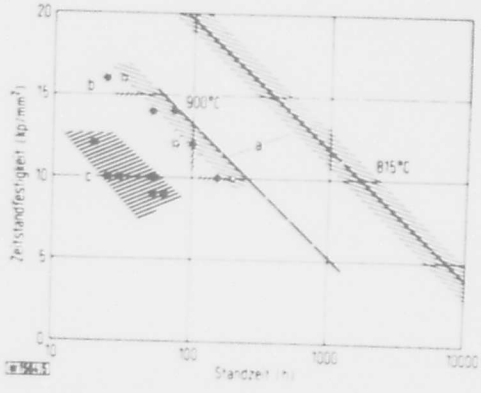

Figure 30.3. The influence of corrosion on the creep behaviour of the nickel base alloy Nimonic 90
(a) in air at 900°C and 813°C.
(b) in hot gas stream at 900°C.
(c) in hot gas stream at 900°C with synthetic sea salt according to DIN 50900, 36g/48 h.
(Huff and Schreiber)

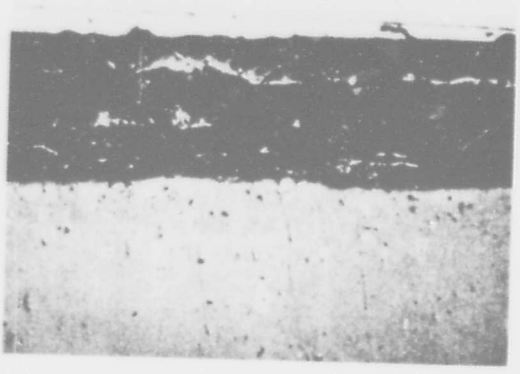

Figure 30.2. Nimonic 90 118h/800°C/ S_2 stratified sulphide scale. (Erdös).

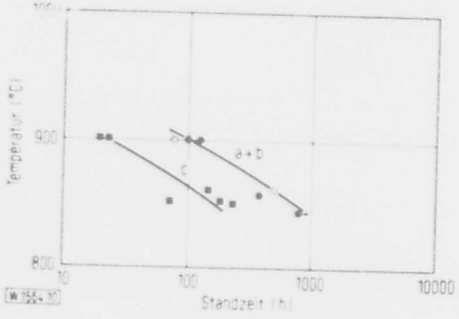

Figure 30.4. The influence of temperature on the creep behaviour of the nickel-base alloy Nimonic 90 at 120 N/mm^2.
(a) in air.
(b) in hot gas stream from JP4 fuel.
(c) in hot gas stream with synthetic sea salt according to DIN 50900, 36 g/48 h (31 ppm), dry.
(Huff and Schreiber)

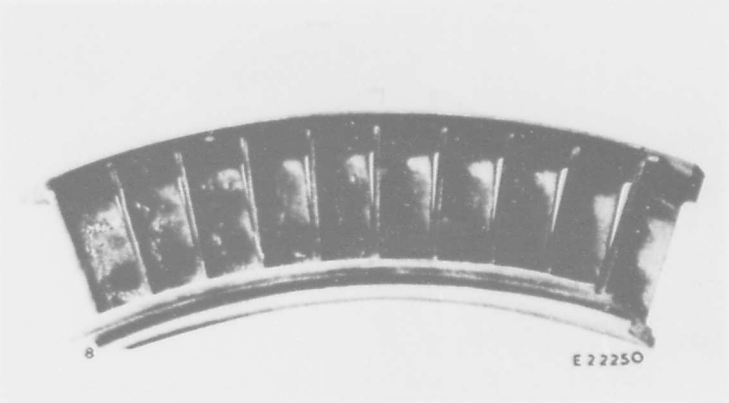

Figure 30.5. The general appearance of a Nimonic 90 stator segment from a Proteus engine after 22h running with 2% sea salt in the fuel. (Archdale).

Nimonic 100

G. Llewellyn, Hot Corrosion Problems Associated with Gas Turbines, ASTM Special Technical Publication, (STP 421) 1967, p.1.

A picture of corroded blade is shown in Fig. 31.1. "Sulphur attack is evident in the early stages by dark coloured blisters on the surface - formerly known as "black plague". In more severe cases blistering can cover the whole of the concave site of the hottest region of the blade. Cracks may then appear in the sulphur attack itself, for instance longitudinally on the leading edge or in a transverse direction at the trailing edge. The cracks are usually restricted to the attack with little or no penetration into the sound core material".

"Particles chipped from a corroded component are normally noticeably ferromagnetic, and there is evidence to show this is strongest in the intermediate zone where presumably the material is sufficiently nickel-rich to produce this effect."

"A remarkable feature ... blades have suffered severe attack without failure. This is because the attack tends to advance on a broad front rather than by preferential attack on the grain boundaries".

Figure 31.2 is a cross-section of a corroded specimen; material not indicated, but probably Ni 100. Corrosion product is (outer layer) NiO + $NiCr_2O_4$, notes report of Fe_2TiO_5, but unable to confirm this. Next, Cr_2O_3 + metal, then Cr sulphides in the metal.

Gives threshold temperature as determined by a test involving a 6hr cycle with intermittent SO_2 and air at 45 min intervals as 800°C; 780°C with the specimen in contact with C: relative performance of a number of alloys is shown in Table 31-I.

P.R. Belcher, R.J. Bird and R.W. Wilson, Hot Corrosion Problems Associated with Gas Turbines, ASTM Special Technical Publication (STP 421), 1967, p123.

The authors refer to the attack as "black plague" and remark that it was first observed on Ni 100 blades, quoting reference of C.A. Dalton in ASME Publication 65-GTP-7. No cases of black plague on Nimonic 100 blades have been reported unless they have been operated for at least 100h at 900°C. Figure 31.3 shows a number of corroded blades, including a Nimonic 100 blade after 1063h service; Figure 31.4 shows the cross-sections; Figure 31.5 and 31.6 shows details of the metal/scale interfaces. "Scale is very hard and adherent and is not disturbed when a blade is quenched into water from 900°C". Sulphur is always present in small amounts at the metal/scale interface. "On the Nimonic 100 blades the heterogeneous scale appears to be a disordered mixture". Always a narrow band of sulphide particles at the scale/metal interface with an occasional tendency for the sulphides to penetrate intergranularly. Electron probe pictures of blades are shown in Figures 31.7, 31.8 and 31.9. The scale products were various spinels, together with some NiO. Black plague-attacked Nimonic 100 blades were brittle, easily broken with a hammer. Uncorroded blades which had been in service for a time were also brittle, the brittle fracture being intergranular. The authors concluded that the brittleness was not connected with the corrosion. Tests were carried out in a full scale combustion chamber - air/fuel 45/1, aviation kerosine 0.13% S 923°C, 25h. No attack, either continuous or intermittent running. Added CCl_4 (66 ppm) in fuel - no effect. Added 100 ppm NaCl in fuel, got typical sulphidation attack: specimen coated with Na_2SO_4 and $NiCr_2O_4$; some $NiCo_2O_4$ and (Ni,Co) O detected by X-rays. Other tests 850 - 950°C, 100h (some extended to 500h). The test results are listed in Tables 31-II and 31-III. Old blades corrode more than new ones,

M.J. Donachie, Jr., R.A. Sprague, R.N. Russell, K.G. Boll and E.F. Bradley, Hot Corrosion Problems Associated with Gas Turbines, ASTM Special Technical Publication STP 421, 1967, 85.

See 713C for details. Figure 31.10 shows a Nimonic 100 first stage turbine blade from a turboprop engine, exhibiting severe attack: Figure 31.11 is a section of the same blade.

C.C. Smith, P. Dean, W.E. Laker and D. Jones, Bristol Siddeley Engines Laboratory Report No. 452, (August 1957).

Several Nimonic 100 first stage Olympus turbine blades were sent to the laboratory after 401h engine running. All had a black deposit on the leading edge and on the concave surface. Attack seemed most pronounced at the hottest regions of the blade (Figure 31.12). Figure 31.13 shows the general appearance of the attack in a badly affected region, and Figure 31.14 shows the detailed structure of the corrosion; Figure 31.15 shows the lighter-appearing phases in the metal ahead of the oxidation front. This darkened when etched in alkaline potassium permanganate, and a similar etching effect was observed on nickel sulphide formed by covering a Nimonic 100 specimen with sulphur and oxidising at 870°C (the approximate blade operating temperature) for two hours, renewing the sulphur every half hour. However, the morphology of the sulphides was felt to be different in the two cases.

Data relating to this alloy will also be found in Tables 30-I and 30-II.

TABLE 31-I

COMPARATIVE RESISTANCE OF VARIOUS ALLOYS, COATED AND UNCOATED, TO SULFUR ATTACK. (LLEWELLYN)

6 HOUR CYCLE, INTERMITTENT SO_2 AND AIR AT 45 MINUTE INTERVALS

MATERIAL IN GAS STREAM	THRESHOLD TEMP °C	MATERIAL IN CONTACT WITH CARBON
	770	M 21 VC
	780	N 105 N 100 EPK 34 (IN 100)
M 21 VC	790	
N 105 N 100 EPK 34 (IN 100)	800	
	810	
	820	
G 64 (HT DENUDED LAYER REMOVED)	830	INCO 713 G 64
INCO 713	840	
G 64	850	
	860	
	870	MAR M 200
	880	MAR M 302
MAR M 200	890	N 115
MAR M 302	900	
	910	G 64 (PA Ni_3Al COATING) 500 HOURS 900°C
	920	N 90 X 40
N 90 N 115	930	MAR M 509 MAR M 322
G64 (PA Ni_3 Al COATING) 500 HOURS 900°C	940	
MAR M 322 MAR M 509	950	W 52 M 21 VC PA
	960	G 64 PA
M 21 VC PA	970	MAR M 322 PA
W 52 G 64 PA X 40	980	X 40 PA W 52 PA
	990	MAR M 302 PA
INCO 713 PA N 105 PA X 40 PA EPK 34 (IN 100) PA	1000	N 105 PA EPK 34 PA N 90 PA
W 52 PA	1010	
N 90 PA	1020	MAR M 509 PA
	1030	
	1040	MAR M 200 PA
MAR M 302 PA MAR M 509 PA	1050	
MAR M 200 PA	1060	

PA - PACK ALUMINISED BY BRISTOL SIDDELEY PROCESS

TABLE 31-II

SMALL-SCALE COMBUSTION RIG TESTS. (BELCHER ET AL)

AIR/FUEL RATIO: 40/1

Test No	Temperature, deg C (deg F)	Test Duration, hr	Contaminant	Test Specimen	Results, Including X-ray Diffraction of Oxide Scales
AVIATION KEROSINE (AVTUR) (0.13 WEIGHT PER CENT SULFUR)					
5	900 (1650)	100	None	Nimonic 100 blades machined, electrolytically polished, aluminized, also Nimonic 80A and 90	no attack; NiO and spinels on Nimonic 100, Cr_2O_3 on Nimonic 80A and 90
6	900 (1650)	100	Avtur sprayed on blades while running 2 ml/min = 2.5 weight per cent of main fuel flow	Nimonic 80A, 90 and 100 blades	no attack
7	900 (1650)	100	Avtur with 4 weight per cent sulfur sprayed on blades as above	Nimonic 80A, 90 and 100 blades	no attack
8	950 (1740)	100	Avtur with 4 weight per cent sulfur sprayed on blades as above	Nimonic 80A, 90 and 100 blades	no attack
9	950 (1740)	100	1 ml/gal of tetraethyl-lead in fuel	Nimonic 80A, 90 and 100 blades	pale green color on blades; NiO-Cr_2O_3 spinel identified; no sulfide attack or unusual corrosion
10	950 (1740)	100	rig stopped hourly; blades immersed in Avtur	Nimonic 80A, 90 and 100 blades	a few superficial black spots on blades
11	950 (1740)	100	rig stopped hourly; blades immersed in Avtur + 1 weight per cent sulfur	Nimonic 80A, 90 and 100 blades	no attack
12	950 (1740)	100	blades sprayed with 12.1 weight per cent solution of NaCl at 2 ml/min = NaCl at 0.4 weight per cent of fuel flow	Nimonic 80A, 90 and 100 blades	severe sulfide corrosion and intergranular attack on all blades
13	950 (1740)	100	blades sprayed with 12.1 weight per cent solution of $CaCl_2$ at 2 ml/min = $CaCl_2$ at 0.4 weight per cent of fuel flow	Nimonic 80A, 90 and 100 blades	bulky white deposits and severe intergranular sulfide attack on all blades
WIDE CUT DISTILLATE (0.3 WEIGHT PER CENT SULFUR)					
14.....	950 (1740)	100	2.7 weight per cent aqueous NaCl solution sprayed into dilution air at 2 ml/min = (NaCl/fuel ratio of 100 ppm)	two used Nimonic 100 blades, one with black plague, one without	some dark areas of accelerated scaling—not typical of black plague
15.....	950 (1740)	100	rig stopped hourly; blades dipped in Avtur + 0.1 weight per cent residual fuel	two used Nimonic 100 blades, one with black plague, one without	no attack on good blade; no extension of attack on corroded blade
16.....	950 (1740)	100	none	two used Nimonic 100 blades, one with black plague, one without	no attack on good blade; no extension of attack on corroded blade
17.....	900 (1650)	100	none	two used Nimonic 100 blades, one with black plague, one without	slight intensification of attack on corroded blade

TABLE 31-III

SMALL-SCALE COMBUSTION RIG TESTS USING SODIUM CHLORIDE INJECTION IN DOWNSTREAM AIR. (BELCHER ET AL)

AIR/FUEL RATIO: 40/1

Test No	Temperature, deg C (deg F)	Test Duration, hr	Contaminant	Test Specimen	Results
AVIATION KEROSINE (0.13 WEIGHT PER CENT SULFUR)					
18	850 (1560)	100	2.7 weight per cent aqueous NaCl solution injected into downstream air at 2 ml/min = 100 ppm NaCl in fuel for 25 hr, then 75 hr with 0.27 weight per cent NaCl injection = 10 ppm NaCl in fuel	1 new Nimonic 100 blade; 1 Nimonic 100 blade after 1300 hr service without black plague	both blades scaled heavily; sulfide attack, see Fig. 13
19	850 (1560)	500	0.027 weight per cent aqueous NaCl solution injected into downstream air at 2 ml/min for first 200 hr	1 new Nimonic 100 blade; 1 Nimonic 100 blade after 1300 hr service without black plague	used blade showed signs of attack rather like black plague; traces of Na_2SO_4 on blades
20	850 (1560)	200	blades dipped in strong NaCl solution and allowed to dry before test	1 new Nimonic 100 blade; 1 Nimonic 100 blade after 1300 hr service without black plague	no attack; no sodium compounds detected
21	900 (1650)	500	0.027 weight per cent aqueous NaCl solution injected = 1 ppm NaCl in fuel	1 new Nimonic 100 blade; 1 Nimonic 100 blade after 1300 hr service without black plague	black plague attack reproduced on used blades, see Figs. 11 and 13; no sodium compounds deposited
22	900 (1650)	500	0.027 weight per cent aqueous NaCl solution injected = 1 ppm NaCl in fuel; rig stopped every 25 hr	5 bar specimens of Nimonic 100 and 105	black plague on Nimonic 100 specimens; no sodium compounds deposited
23	900 (1650)	500	0.027 weight per cent aqueous NaCl solution injected = 1 ppm NaCl in fuel, except salt injection for only 25 hr in every 100 hr	1 new Nimonic 100 blade; 1 used Nimonic 100 blade	scale on used blade similar to black plague, see Fig. 13; no sodium compounds deposited
24	950 (1740)	100	continuous injection of 0.027 weight per cent NaCl solution = 1 ppm NaCl in fuel	4 Nimonic 105 blades: (*a*) new; (*b*) heated at 950 C (1740 F) in air for 1000 hr; (*c*) heated at 1000 C (1830 F) in air for 100 hr; (*d*) 2052 hr service without black plague	see Fig. 12; no sodium compounds deposited

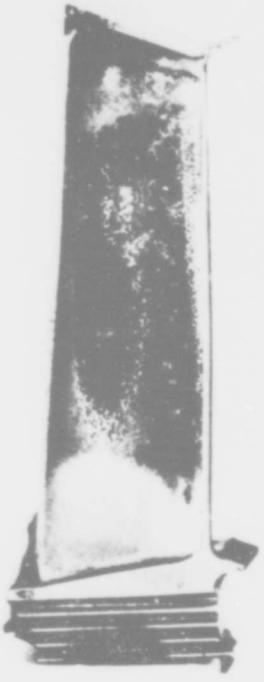

Figure 31.1. Distribution of sulphur attack on concave surface of a Nimonic 100-turbine rotor blade (full size). (Llewellyn).

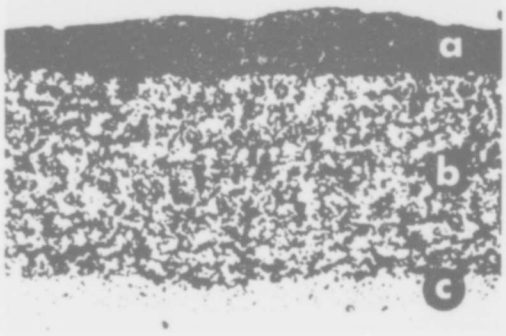

Figure 31.2. Transverse section of blade showing sulphur attack. (x250). (Llewellyn).

(a) Nimonic 105 blade after 2800 hr service.
(b) GMR 235 blade after 1605 hr service.
(c) Nimonic 105 blade after 3675 hr service.
(d) Nimonic 100 blade after 1063 hr service.

Figure 31.4. Cross section of blades with black plague (x2). (Belcher et al).

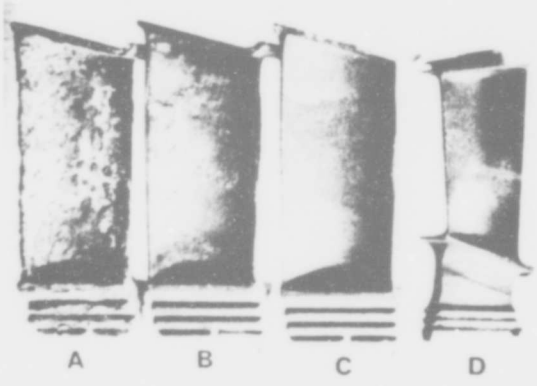

Figure 31.3. Typical corroded blades (x1). (Belcher et al).

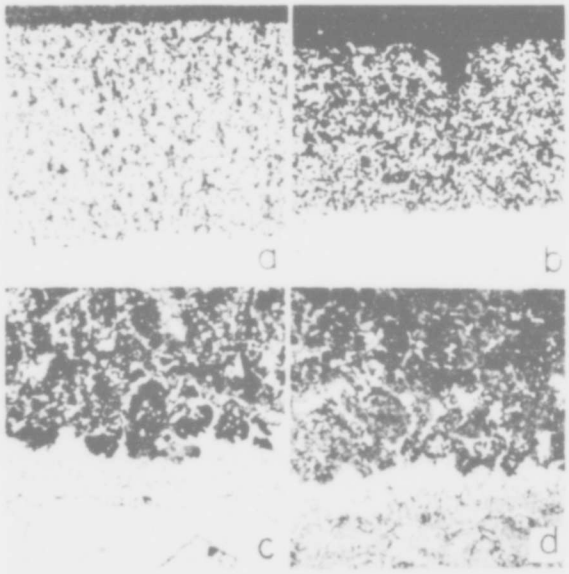

(a) Nimonic 100, unetched (×100).
(b) Nimonic 105, unetched (×100).
(c) Nimonic 100 etched, showing sulfides in white band (×500).
(d) Nimonic 105 etched, showing some sulfides in white band (×500).

Figure 31.5. Metallographic features of black plague scale. (Belcher et al).

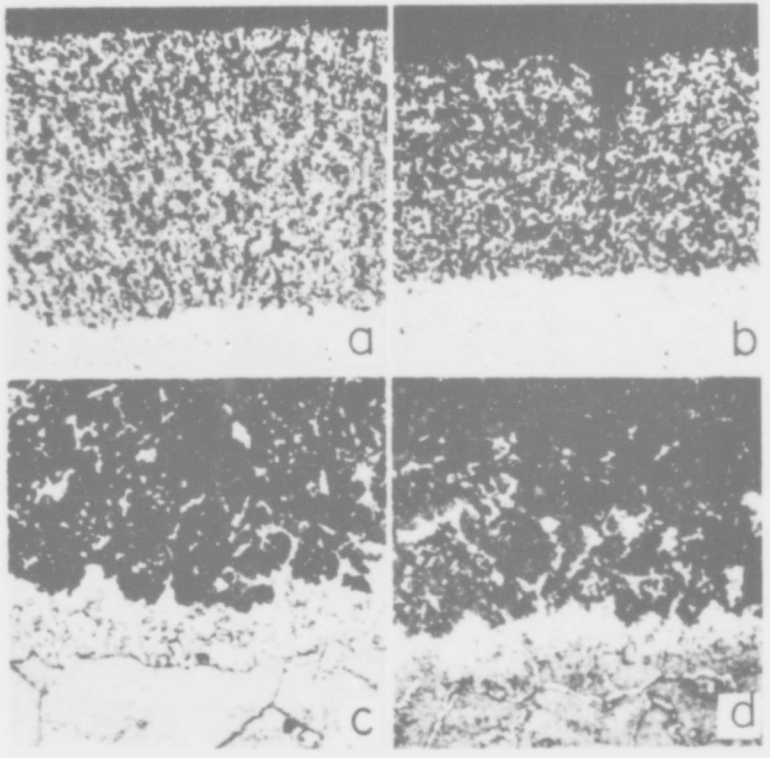

(*a*) Nimonic 100, unetched (×100).
(*b*) Nimonic 105, unetched (×100).
(*c*) Nimonic 100 etched, showing sulfides in white band (×500).
(*d*) Nimonic 105 etched, showing some sulfides in white band (×500).

Figure 31.6. Metallographic features of black plague scale. (Belcher et al).

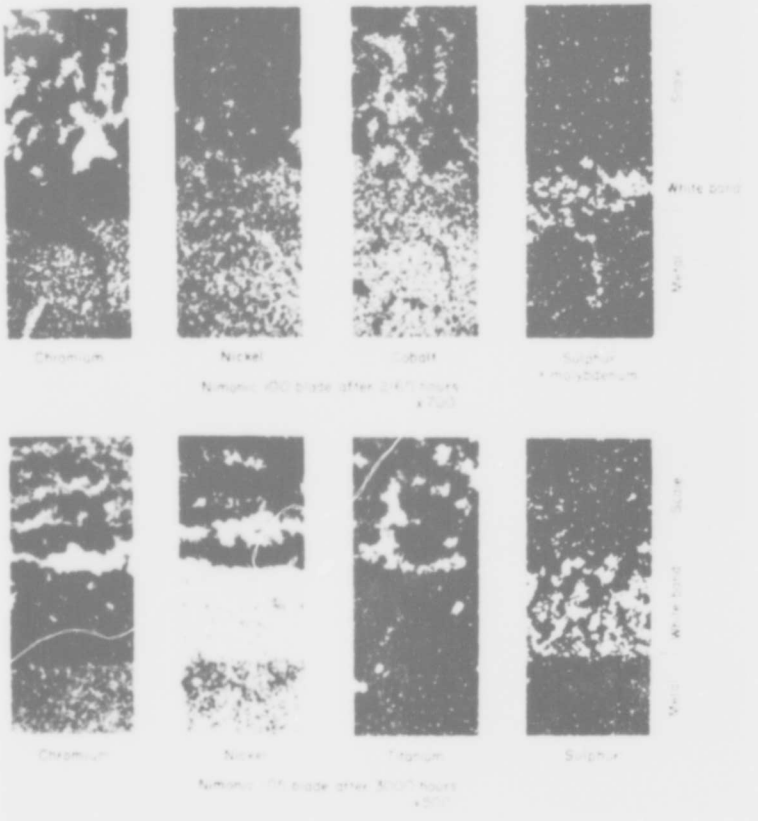

Figure 31.7. Electron-probe micrographs showing distribution of elements in Nimonic 100 and Nimonic 105 blades. (Belcher et al).

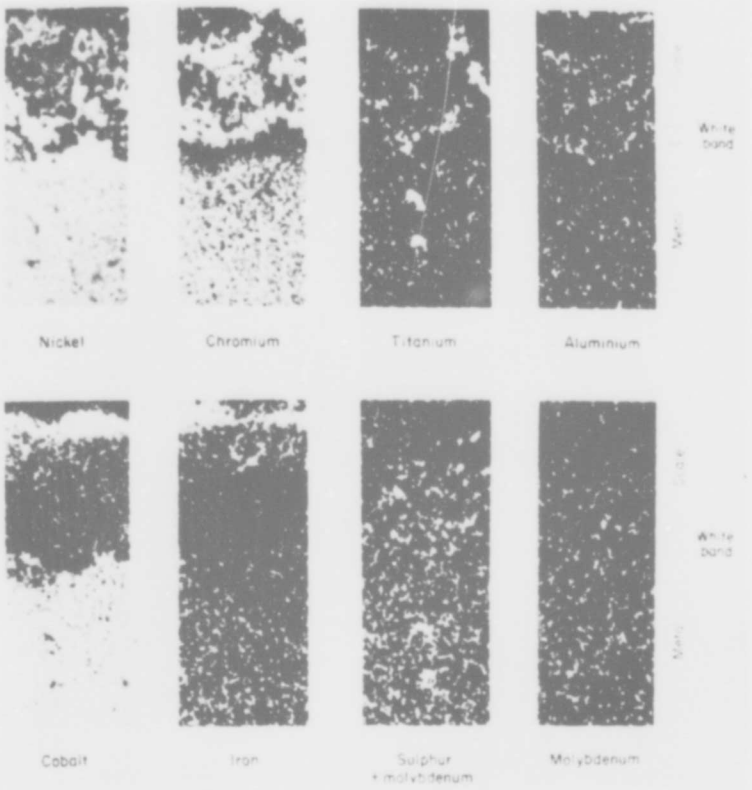

Figure 31.8. Electron-probe micrographs showing distribution of elements in black plague scale of Nimonic 105 blade after 2776 hr. (x350). (Belcher et al).

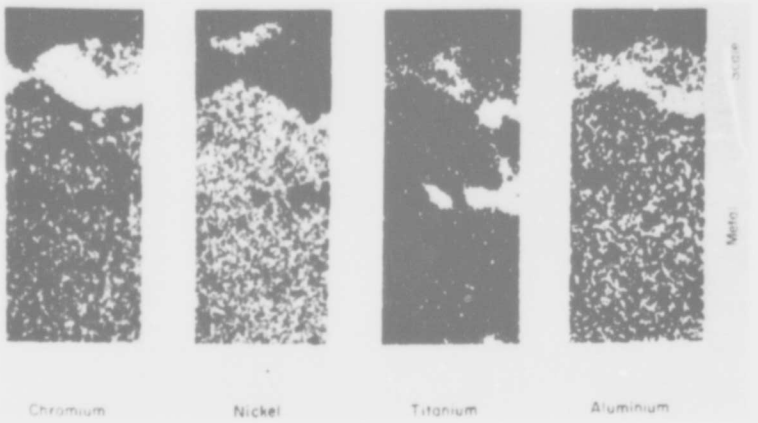

Figure 31.9. Electron-probe micrographs of Nimonic 105 blade shown in Fig. 5 (x800). (Belcher et al).

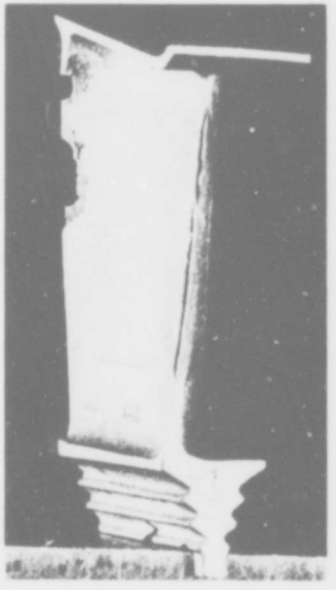

Figure 31.10. NI-100 first-stage turbine blade from turboprop engine showing deterioration due to sulphidation (Donachie et al).

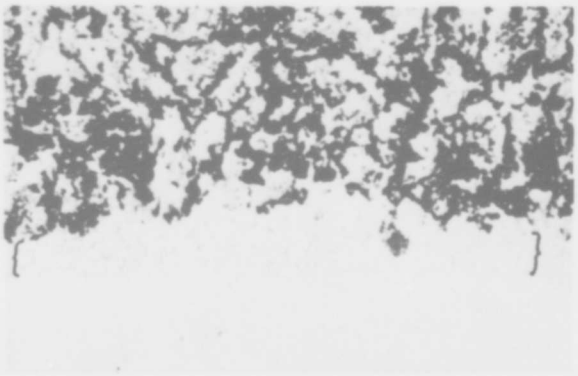

Figure 31.11. Section through NI-100 blade airfoil of Fig. 31.10. showing light gray Cr_2S_3 phase (bracket) preceding oxidation (x1000). Unetched. Reduced one third for reproduction. (Donachie et al).

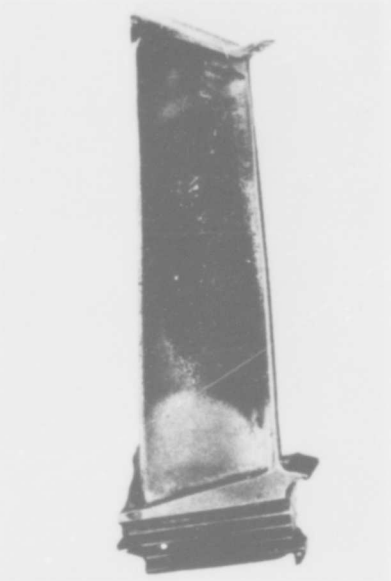

Figure 31.12. The corrosion on the concave surface of a Nimonic 100 first-stage turbine blade from an Olympus engine after 401 h running. (Smith et al).

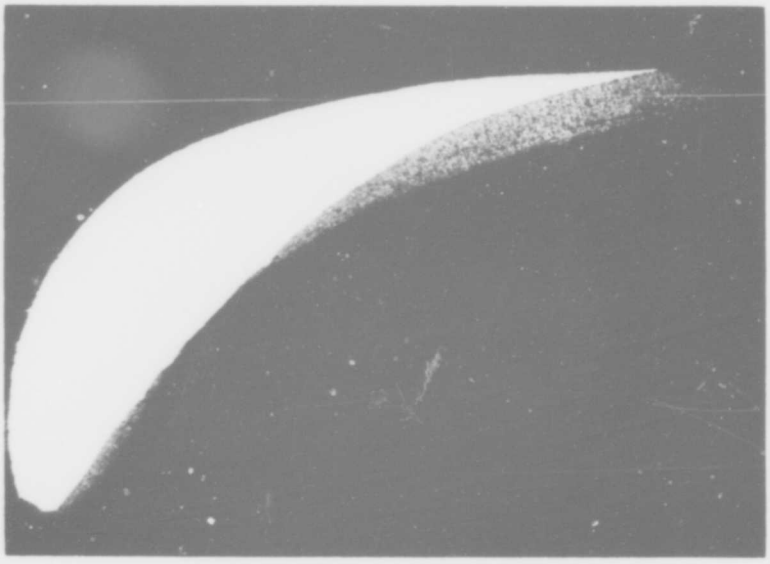

Figure 31.13. A section of a similar blade to that shown in Figure 31.12 showing the unetched structure in a badly affected region. (Smith et al).

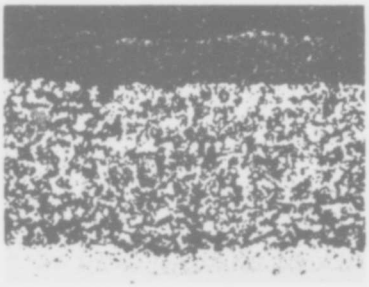

Figure 31.14. Part of the field shown in Figure 31.13. (x250).

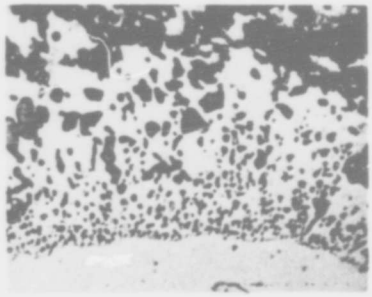

Figure 31.15. Innermost layer of compounds. (x1050).

Nimonic 105

G. Llewellyn, Hot Corrosion Problems Associated with Gas Turbines ASTM Special Technical Publication, STP 421, 1967, 1.

See Nimonic 100. Threshold temperature 6h test, alternate SO_2/air, 45 min cycle, 800°C; 780°C in contact with carbon; 1000°C Pack aluminised; unaffected by carbon.

P.R. Belcher, R.J. Bird and R.W. Wilson, Hot Corrosion Problems Associated with Gas Turbines, ASTM Special Technical Publication (STP 421) 1967, p123.

See Nimonic 100 for details. There appears to be an incubation period: for Nimonic 105 no blades show corrosion until they have been in service for 1000h at 900°C. Examples of corroded Nimonic 105 blades are included in the Figures shown under Nimonic 100: in particular, Figure 31.3 shows a blade corroded after 3675h service. This blade had been free from corrosion at 2800h. Whereas sulphur was always present at the interface on Nimonic 100 blades, it was present only in about half the corroded 105 blades. Attempts were made to analyse specific sulphides in a Nimonic 105 blade, although it is emphasized that these results must be treated with caution because of the small size of the particles. Nevertheless, the authors conclude that the amounts of chromium are insufficient to account for all the sulphur as chromium sulphide:

Inclusion :	1	2	3 (all wt%)
Sulphur	25	32	24
Chromium	18	14	13
Nickel	58	53	64

Table 31-III presents the results of a number of rig tests: test No. 24 was a number of Nimonic 105 blades : (a) new, (b) heated in air at 950°C for 1000h; (c) heated at 1000°C in air for 100h; (d) 2052h service without black plague. The test was with aviation kerosine containing 0.13 wt % S, at 950°C, for 100h with continuous injection of NaCl equivalent to 1 ppm in the fuel. No sodium compounds were deposited on the blades.

J.F.G. Conde, paper to Conference on Naval Materials: Current and Future Problems. Royal Naval Engineering College, Manadon, July 1970.

Figure 32.1 shows a "typical example" of a badly corroded pack aluminised Nimonic 105 first stage turbine blade after only 600h operation (in an industrial Proteus engine(?) text is not very clear), and compares it with a pack aluminised X-40 blade. Figure 32.2 shows the performance of pack aluminised Nimonic 105 first stage and plain uncoated Nimonic 105 second stage turbine blades in a test on a Proteus engine for 1000h with 0.01 ppm NaCl in the air.

Figure 32.3 illustrates the structure found on the trailing edge of a pack aluminised Nimonic 105 turbine blade. The attack is normally characterized by a deposit covering a heavy scale layer which overlies a part-oxidised layer containing some sulphide. The adjacent metallic zone contains a discrete grey globular phase which is usually identified as chromium sulphide. The surface deposits have usually been identified as sodium sulphate, and sodium chloride has only been positively established on rare occasions.

E. Erdös, in "Deposition and Corrosion in Gas Turbines", A.B. Hart and A.J.B. Cutler (eds.) (Applied Science Publishers, London 1973) 115.

See 713C for details. Figure 32.4 shows a section of a Nimonic 105 specimen sulphidised in S_2 vapour for 96h at 800°C, and Figure 32.5 shows the corresponding electron microprobe photographs (dark signifies high concentration). Two sulphides are present: Cr-Ti-S (Cr_3S_4) and Cr-Al-S.

R.C. Hurst, J.B. Johnson, M. Davies and P. Hancock, in "Deposition and Corrosion in Gas Turbines", A.B. Hart and A.J.B. Cutler (eds.), (Applied Science Publishers, London 1973) 143.

See Nimonic 90 for details.

A.J.B. Cutler and C.J. Grant, in "Deposition and Corrosion in Gas Turbines" A.B. Hart and A.J.B. Cutler (eds.) (Applied Science Publishers London, 1973) 178.

See IN 738 for details. Nimonic 105 corroded appreciably more slowly than Nimonic 115 or Nimonic 90, and only a little faster than X-40 (in Li/Na/K sulphate at 727°C).

P.L. Norman and J.D. Harston, in "Deposition and Corrosion in Gas Turbines" A.B. Hart and A.J.B. Cutler (eds.), (Applied Science Publishers, London, 1973) 260.

See Nimonic 80A. Nimonic 105 was one of the poorest alloys tested in the salt-spray test. Figure 32.6 compares the general behaviour of the alloys as a function of temperature: the corrosion of 105 increases progressively with temperature, unlike most of the other alloys which exhibit a maximum in attack at about 800°C.

J.F.G. Conde and G.C. Booth, in "Deposition and Corrosion in Gas Turbines" A.B. Hart and A.J.B. Cutler (eds.), (Applied Science Publishers, London, 1973) 278.

This paper describes the AML low-pressure test rig which burns fuel to DEF 2402 B with a sulphur content of 0.5%, and < 0.03 ppm chloride. Two specimen assemblies are used: one has blade-type specimens mounted in a cascade, and the second 6.35 mm cylinders 43.5 mm long in a rotating test chamber, in a test stand rotating at 16 rpm. Blade specimens are cooled to 300°C every 20h during the 200h test; rod specimens are cooled by switching off the rig every 25h. Specimens were removed at 50, 100, 150, and 200h, and the corrosion evaluated, usually by metallography, but also by descaling in some cases. The salt content was typically 0.1 ppm in the air, and the gas velocity at the test section was 365 m/sec.

Figure 32.7(a) shows a Nimonic 105 specimen corroded in the rig, exhibiting deep pitting-type corrosion; and Figure 32.7(b) shows a section of a Nimonic 105 blade from an engine with very similar form of attack. Figure 32.8 similarly compares two pack-aluminised Nimonic 105 specimens.

The attack was most severe on the leading edge and on the pressure surface near the trailing edge. The suction surface was glazed with a coating of sulphate with Na/Mg/Ca in the ratio 4/2/1 compared with the ratio 35/4/1 in sea-salt. The amount of the chloride was 10^{-3} of the sulphur present in the deposit. The authors comment that the dependence of attack on position suggests that the mechanism depends either on the impaction of solids or on thinning of the molten salt deposits by gas turbulence to aid reaction.

Table 32-I shows corrosion data at 850°C for uncoated 105, 90, Mar-M 432 and IN 738, and pack-aluminised IN 738, Nimonic 105, and Mar-M 432. Nimonic 105 was the best of the uncoated alloys, followed by Nimonic 90, Mar-M 432 and IN 738.

Figure 32.9 shows the results of a cyclic test at 750°C for 200h for rod specimens of X-40, Nimonic 90, and Nimonic 105. X-40 and Nimonic 90 were about the same, Nimonic 105 five times worse. Figure 32.10 shows a similar chart for several alloys tested at 830°C for 200h (X-40, Nimonic 90, Fulmer 2C, FSX 414, FSX 418, IN 597 and IN 853 or more or less in order of increasing corrosion.

P.C. Felix, in "Deposition and Corrosion in Gas Turbines" A.B. Hart and A.J.B. Cutler, (eds.), (Applied Science Publishers, London, 1973) 331.

See 713C for details.

K. Page and R.J. Taylor, in "Deposition and Corrosion in Gas Turbines", A.B. Hart and A.J.B. Cutler (eds.), (Applied Science Publishers, London, 1973) 350.

This paper describes Rolls Royce experience in engines in environments promoting corrosion. At the time when aero service engines were first adopted for marine service the most common blade material was Nimonic 105; the nozzle guide vanes were X-40 and C 242. All blades and vanes in the critical positions are pack aluminised to thickness limits of 0.0007 - 0.0015 in.

Figure 32.11 shows X-40 and Nimonic 105 blades from a Proteus test stand engine run 975h with 0.6 ppm salt in the fuel with a maximum blade metal temperature of 870°C. Figure 32.12 shows X-40 blades from a hovercraft Proteus after 1525h running with a blade metal temperature of 850°C max. and Nimonic 105 blades, also from a hovercraft Proteus after 1260h operation at the same temperature - the nickel alloy is much more heavily attacked than the cobalt alloy. Figure 32.13 compares Nimonic 105 and G64 blades after operation for 2000h in an industrial Proteus in a salt environment with a maximum turbine inlet temperature of 875°C. The G 64 blades are much less heavily corroded than the Nimonic 105.

Figure 32.14 compares the fairly general attack of the concave surface observed in marine applications (610h) with the "wart-like growths" in land-based industrial applications (1022h). Blade maximum temperature 850°C.

Although the corrosion often increases with increasing temperature profiles on the blades, Figure 32.15 shows that this is not always so on Nimonic 105 blades from a Proteus industrial engine after 576h.

The authors state that where salt levels in the fuel have exceeded 0.6 ppm sodium in industrial applications, sulphidation of turbine blading has been severe. On marine shore trials where salt is introduced into the engine at 0.01 ppm salt in the air (equivalent to 0.25 ppm sodium in the fuel) the corrosion has been less severe.

Figure 32.16 shows further examples of severe attack on pack aluminised Nimonic 105 blades from a Hovercraft Proteus after 1260h operation with maximum blade metal temperature of 850°C.

Present philosophy is to use cast cooled blades made from materials with a reasonable corrosion resistance and with the surface metal temperature limited to a maximum of 825°C. The blade material selected on the basis of laboratory and corrosion rig tests is IN 738, with Mar-M 432 as an alternative.

At Derby, a low-pressure combustor rig was used, with 7 mm diameter rod specimens mounted in an assembly rotated at 1300 rpm in the gas stream. 4 ppm sea salt sprayed into the air before combustion. Fuel was a medium gas oil to BSS 2869. IN 738, Mar-M 432 and U 700 were the candidate materials with Nimonic 90 and Nimonic 105 included as comparators. Figure 32.17 and 32.18 show the results for 820 and 870°C. Curiously, at the lower temperature the coated alloys were generally more heavily attacked than the uncoated: at the higher temperature all the coated alloys were very resistant. Uncoated Nimonic 105 was much more severely attacked than the other alloys at both temperature. Figure 32.19 shows the results of earlier tests with aviation kerosine as the fuel with 4 ppm salt injection at 870°C: these were quite different, with a much greater attack, and with U 700 appearing very poor, Nimonic 105 very good. Figure 32.20 shows data from the same series of experiments as a function of temperature.

The authors consider that in the newer tests Nimonic 105 appeared to exhibit an incubation period of 100h or so, and that the temperature of maximum attack was rather less than 870°C.

At Bristol, the principal objective has been testing coatings for Nimonic 105, but other materials are being evaluated as well. The test consists of threee furnace cycles of 18h each at 850°C on specimens that are first washed and weighed and then coated with 1 mg/cm^2 Na_2SO_4 prior to each cycle. This is followed by 72h at 850°C and finally cleaning by blasting with fine alumina abrasive. The cycle is repeated until the coating shows signs of failure. Additional furnace tests at 850°C have been carried out using an alternative procedure in which the application of sodium chloride replaces erosion as the means of removing the protective scale. Low pressure burner rigs using 10 ppm salt in the air have also been conducted. The results of the programme are listed in Table 32.II. Figure 32.21 shows cross-sections of specimens from the tests.

The third series of tests were performed at AML in a low pressure combustion rig using Diesofuel and with 0.1 ppm sea salt injected in the air. The gas velocity was 1200 ft/sec, and tests were at 850°C for 200h. The average weight loss for uncoated specimens was: IN 738, 0.297g; Mar-M 432, 0.122g; Nimonic 90, 0.094g; Nimonic 105, 0.091g.

Rolls-Royce Laboratory Report M 13092 (Dec. 1963)

This reports an examination of first-stage turbine blades from a Spey engine after 387 h of an attempted 1000h service simulation run. The blades were subjected to high temperatures (trailing edge 950-1000°C) due to a blocked burner after 256h. There was a considerable loss of section at the leading edge - estimated to be at least 0.005 in. The maximum thickness of oxide at this point was 0.004 in. The trailing edge (concave side) had also suffered considerable damage: 0.007 in of oxide remained. Because of the unusual severity of corrosion, atmospheric influence noted at the bottom of Report M 13496 is probably involved.

Rolls-Royce Laboratory Report M 13496 (Aug. 1964).

A similar report of blades from a Spey engine after 622 h of a 1000 h simulated Trident flight test. This test consisted of 60 cycles at 984°C flame temperature, 234 cycles at 1029°C, and 40 cycles at 1165°C flame temperature. Cross-sections showed an outer layer of oxide, an inner layer of mixed oxide and metal, and finally a chromium depleted, white layer in the metal. Detailed examination of this showed severe intergranular attack containing particles of chromium sulphide. The structure of the nimonic itself suggested that the blade temperature had not been significantly above 950°C. The depth of corrosion remaining on the leading and trailing edges was about 0.013 in., and approximately 0.013 in metal had apparently been removed. Because of the relatively low temperature, it is thought that the cyclic conditions were important in inducing the corrosion. The source of the sulphur is believed to be chemical fertiliser used by farmers in fields adjacent to the test establishment.

Rolls Royce Laboratory Report M 13300 (March 1964)

This reports corrosion on HP blades from Tyne engines after 2750 and 3400h aircraft operations. The corrosion was predominantly at the leading edge on both upper and lower surfaces, and again the form of attack involved grain boundary penetration of the depleted layer with associated chromium sulphides.

E.G. Roberts, Rolls-Royce Laboratory Report LE 71/18 (Jan. 1971).

Shows corrosion of Nimonic 105 rotor blades from an Olympus industrial/marine turbine. Notes that attack is more prevalent in the 750-900°C range. Figure 32.22 shows a typical blade after service exposure in a sulphate and chloride containing atmosphere, a local area of heavy scale being apparent at the concave trailing edge. Figure 32.23 shows a microsection of this, with a chromium sulphide containing layer adjacent to the unaffected metal. The author notes that once formed this sulphide layer is self-sustaining, and will advance through the metal at temperature without further sulphate/chloride exposure. Generally corrosion takes the form of heavy local scaling of the concave form, but in the most aggressive environments the concave form can develope wart-like growths, which is where a low-melting point "flux" has been formed. Figure 32.24 shows Proteus blades exhibiting this form of attack.

Cobalt-base X-40 stators are generally much more resistant, hot corrosion has been observed as selective oxidation of the carbides. (Figure 32.25).

E. G. Roberts, Rolls-Royce Laboratory Report LE 71/11 (April 1971).

This report discusses the corrosion of pack aluminised Nimonic 105 blades and pack aluminised X.40 vanes from a Proteus marine engine run on a test bed at Pyestock for a total of 692h. Salt had been added to the fuel (amount not given) and this had resulted in catastrophic "crater-flux" type sulphidation, with metal removal to a depth of the order of 0.040 in on both concave and convex forms and disintegration of the trailing edge in the worst cases. The author notes that this type of attack has been experience on land-based sets (e.g. Las Palmas) whereas marine environments have produced less catastrophic "sulphur assisted oxidation" although the Hovercraft may prove the exception. He considers that the crater-flux attack requires the formation of the low melting point Ni - Ni_3S_2 eutectic. The X-40 segments suffered little attack, apart from preferential carbide oxidation after the aluminised coating had gone. The author notes that on the Nimonic 105 blades "It was possible to see on some blades how corrosion progressed with quite distinct 'flux' fingers running towards the shroud obviously under centrifugal influence". Figure 32.26 shows a characteristic "sulphidation" (hot-corrosion) morphology. Figure 32.27 shows "complete local envelope breakdown under a small bridge of flux, which is probably the Ni - Ni_3S_2 eutectic."

J. F. G. Conde, Gas Turbine Materials Conference Proceedings, Naval Air Systems Command, Washington (1972) 17.

Figure 32.28 shows a section of a pack aluminised Nimonic 115 first stage turbine blade run for 951 h with, for the last 409h, 0.01 ppm salt in the air and 0.6 ppm sodium in the fuel. The peak temperature was 870°C.

Rolls-Royce (1971) Ltd.

Corrosion data from a small burner rig is shown under 713C.

Data relating to this alloy will also be found in the following Figures:
10.92, 10.100, 10.125, 10.126, 14.6, 14.8, 14.9, 14.10, 31.3, 31.4, 31.5, 31.6, 31.7, 31.8, 31.9; and Tables:
10-XXVII, 10-XXIX, 30-I, 30-II, 31-I, 31-III.

TABLE 32-I

RESULTS ON AEROFOIL SECTIONS 850°C 0.1 PPM SALT (CONDE AND BOOTH)

Uncoated material	Weight loss, g	Average
Nimonic 105	0.066, 0.052, 0.044	0.05
Nimonic 90	0.093, 0.066	0.08
Mar M432	0.114, 0.102	0.11
IN 738	0.480, 0.211, 0.202, 0.122, 0.103	0.22

Note: In this experiment the Nimonic 105 did not suffer from pitting attack.

Pack-aluminised material	
IN 738	Coating attacked but not penetrated
Nimonic 105	Two isolated penetrations of coating
Mar M432	Coating lost over 12 mm length

TABLE 32-II

ROLLS ROYCE BRISTOL LABORATORY WORK. MERIT RATING OF MATERIALS/COATINGS FROM RESULTS TO DATE (PAGE AND TAYLOR)

Material coating 1·5–2·0 thou	*Sodium sulphate/ erosion 850 C coating life h*	*Sodium sulphate/ sodium chloride 850°C coating life h*	*BED burner rig (10 ppm salt)* 870°C depth of penetration in 400 h thou*
N105 Pt-Al (LDC 2)	1 500		
X.40 P.Al	1 500	125	
X.40 Cr-Al (H.1.15)	1 250	375+	
N105 Ta-Cr-Al	1 250–1 500	375	
IN 587 P.Al.	1 250	125	
N105 Cr-Al (H.1.15)	1 250	250	
IN 738 P.Al	1 000–1 250	125	0·8
N105 CoCrAlY (Vac. Hyd slurry)	500–1 000		
N105 (Cr) Al (MDC 701)	875–1 000		
M432 P.Al	875–1 000	125	1·1
N105 Cr-Mn-Al	875		
N105 Mn-Si-Al	750–875		
N105 P.Al	500–625		1·4
N115 P.Al	500		1·2

* Injected as Portland sea water supplied by the Admiralty Materials Laboratory.

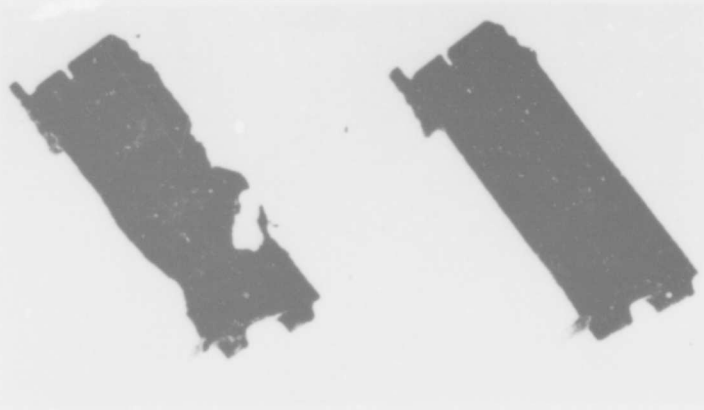

Figure 32.1. (a) Corroded pack aluminised Nimonic 105 first stage turbine blade after 600 hrs. operation.
(b) Experimental pack aluminised Cast X40 first stage turbine blade from test engine after 1,000 hrs. with 0.01 ppm NaCl in air. (Conde).

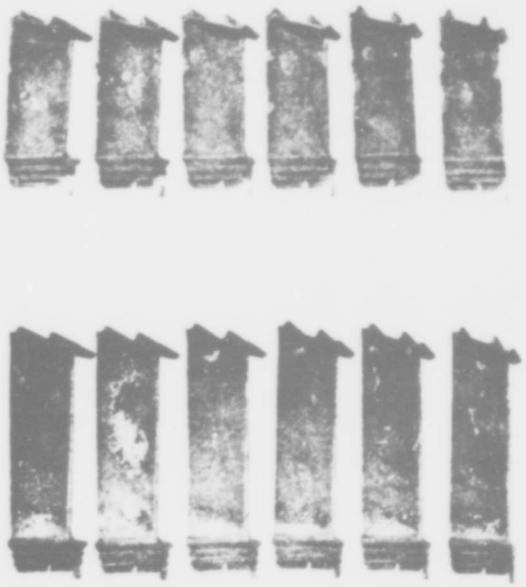

Figure 32.2. Corroded first row (a) and second row (b) turbine blades from Proteus engine test after 1,000 hrs. with 0.01 ppm NaCl in air

(a) Pack aluminied Nimonic 105.
(b) Nimonic 105.
(Conde).

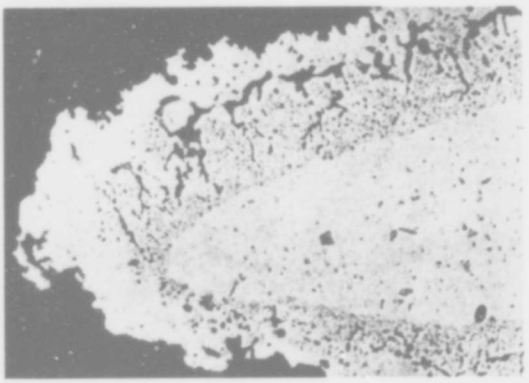

Figure 32.3. Metallographic features of hot corrosion on pack aluminised Nimonic 105 turbine blade trailing edge. (Conde).

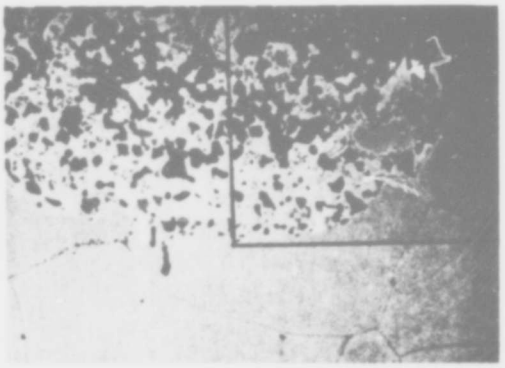

Figure 32.4. Nimonic 105 96 h/ $800^{\circ}C/S_2$. (X400). (Erdoes).

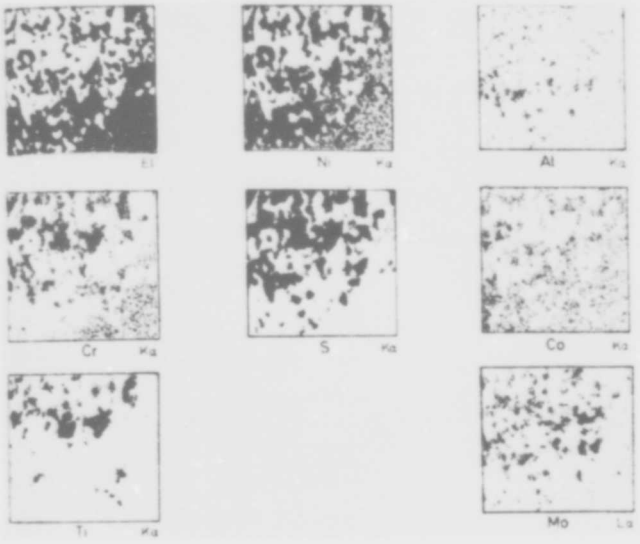

Figure 32.5. *Nimonic* 105 + S_2 800°C 96 h water (all × 300) (Erdös)

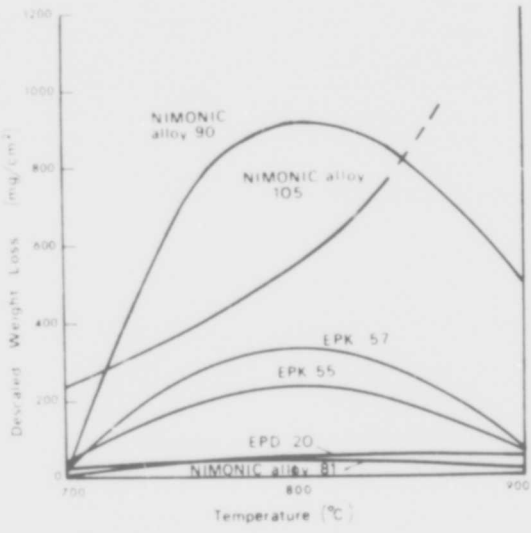

Figure 32.6. Weight loss measurements recorded on various alloys after exposure for 300 h. in the salt shower test. (Norman and Harston).

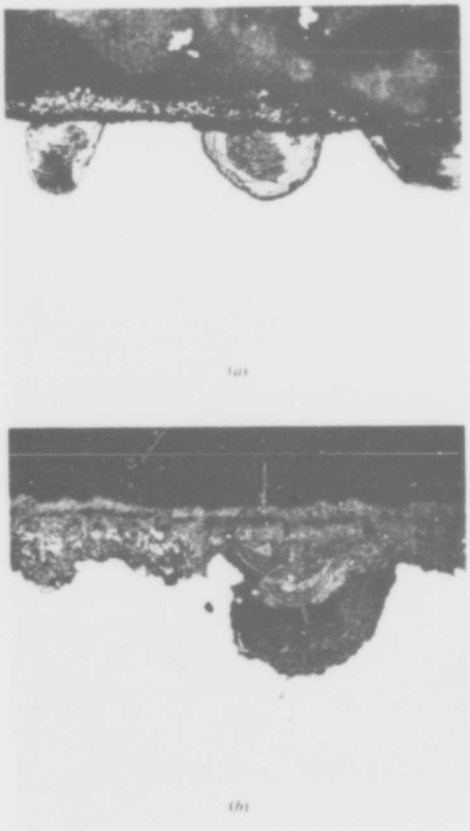

Figure 32.7. (a) Section of N105 specimen from the AML rig (x280). (b) Section of N105 blade from an engine (X240). (Conde and Booth).

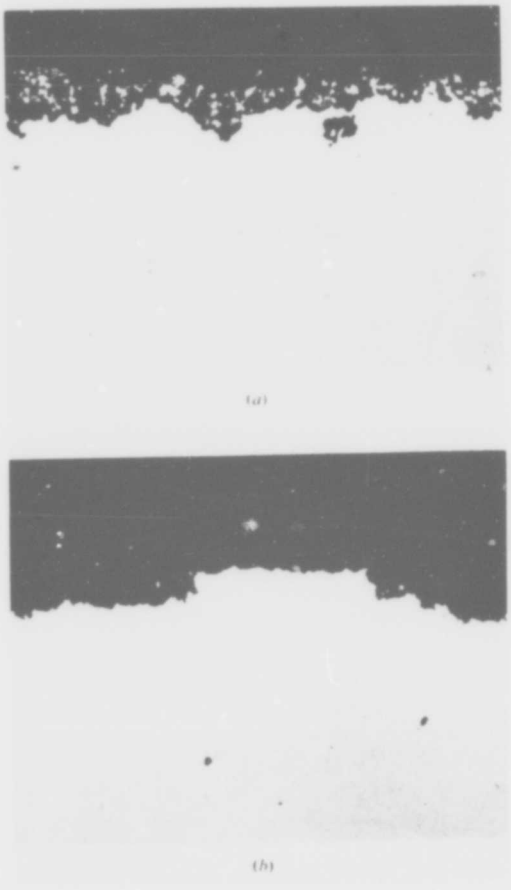

Figure 32.8. (a) Section of a pack-aluminised N105 specimen from the AML test rig (x400). (b) Section of a pack-aluminised N105 blade from an engine (x400). (Conde and Booth).

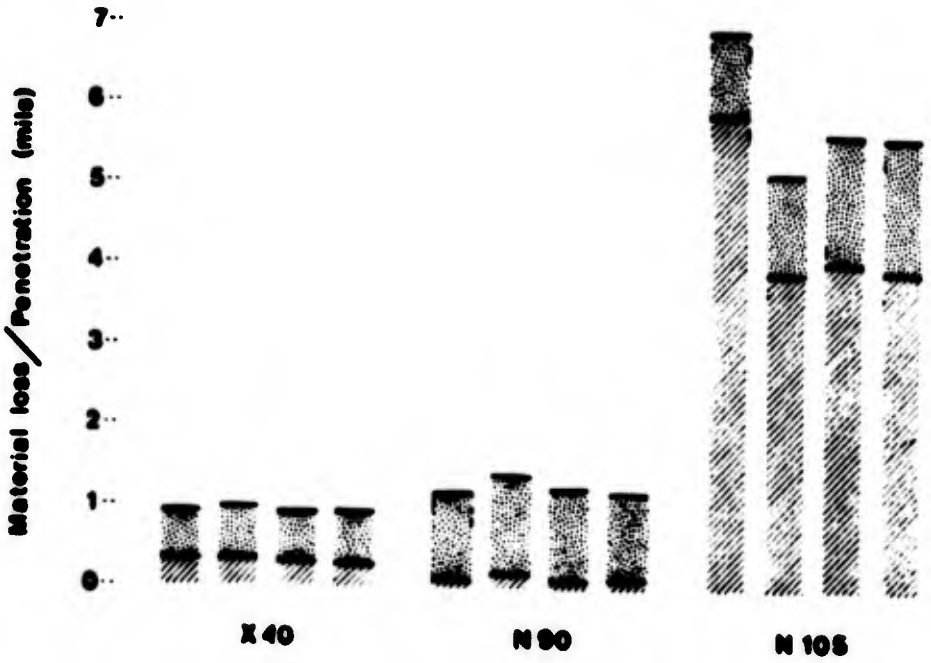

Figure 32.9. Histogram showing results of a cyclic test carried out at 750°C for 200 hr. (Conde and Booth).

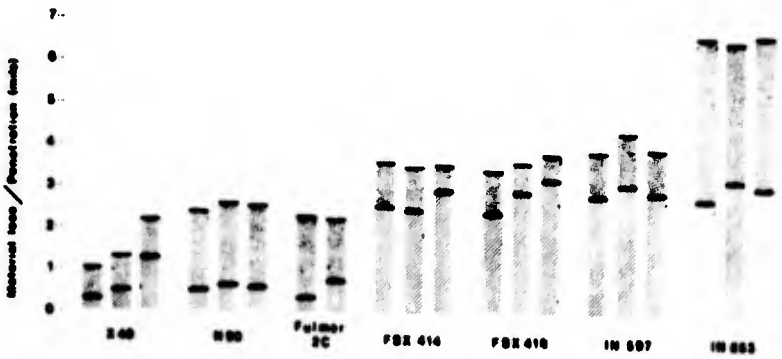

Figure 32.10. Histogram showing results of a cyclic test carried out at 830°C for 200 h. (Conde and Booth).

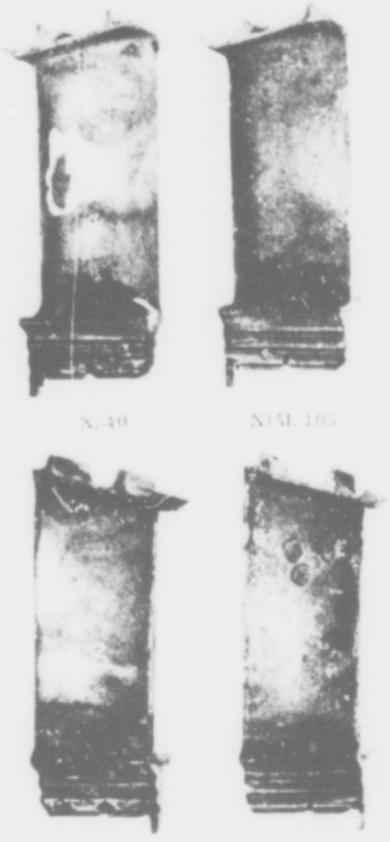

X.40 NIMONIC 105

X.40 NIMONIC 105

COMPARATIVE CORROSION ATTACK ON NIMONIC 105 AND X40 MATERIAL (PACK ALUMINISED) HP ROTOR BLADING TRIALS EVALUATION AT N.G.T.E. PYESTOCK.

Figure 32.11. Proteus engine - HP blades in X40 and N105 pack aluminised - 1000 h shore trials - maximum turbine entry temperature 1180°K (Page and Taylor).

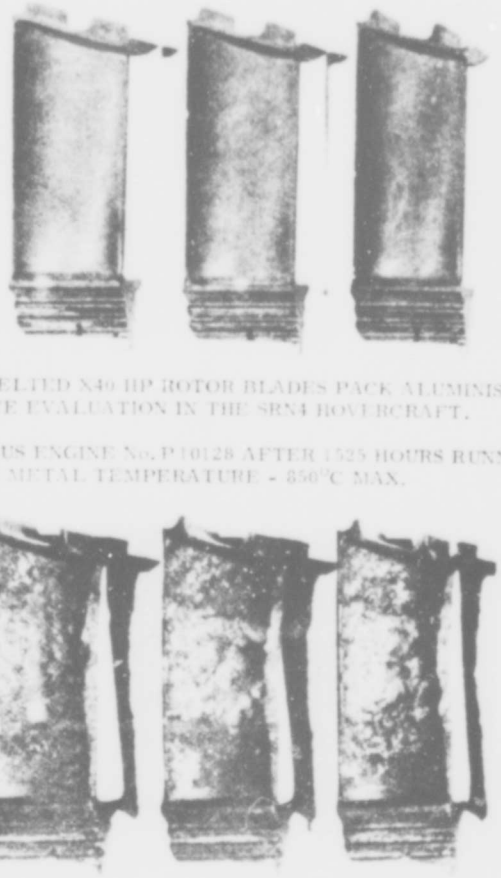

VAC MELTED X40 HP ROTOR BLADES PACK ALUMINISED - SERVICE EVALUATION IN THE SRN4 HOVERCRAFT.

PROTEUS ENGINE No. P10128 AFTER 1525 HOURS RUNNING BLADE METAL TEMPERATURE - 850°C MAX.

NIMONIC 105 MATERIAL HP ROTOR BLADES PACK ALUMINISED SHOWING SEVERE CORROSION ATTACK AFTER 1260 HOURS RUNNING IN THE SRN4 MARINE HOVERCRAFT

Figure 32.12. Proteus engine - HP blades in X40 and N105 pack aluminised - 1500 h Hovercraft operation - maximum turbine entry temperature 1145°K. (Page and Taylor).

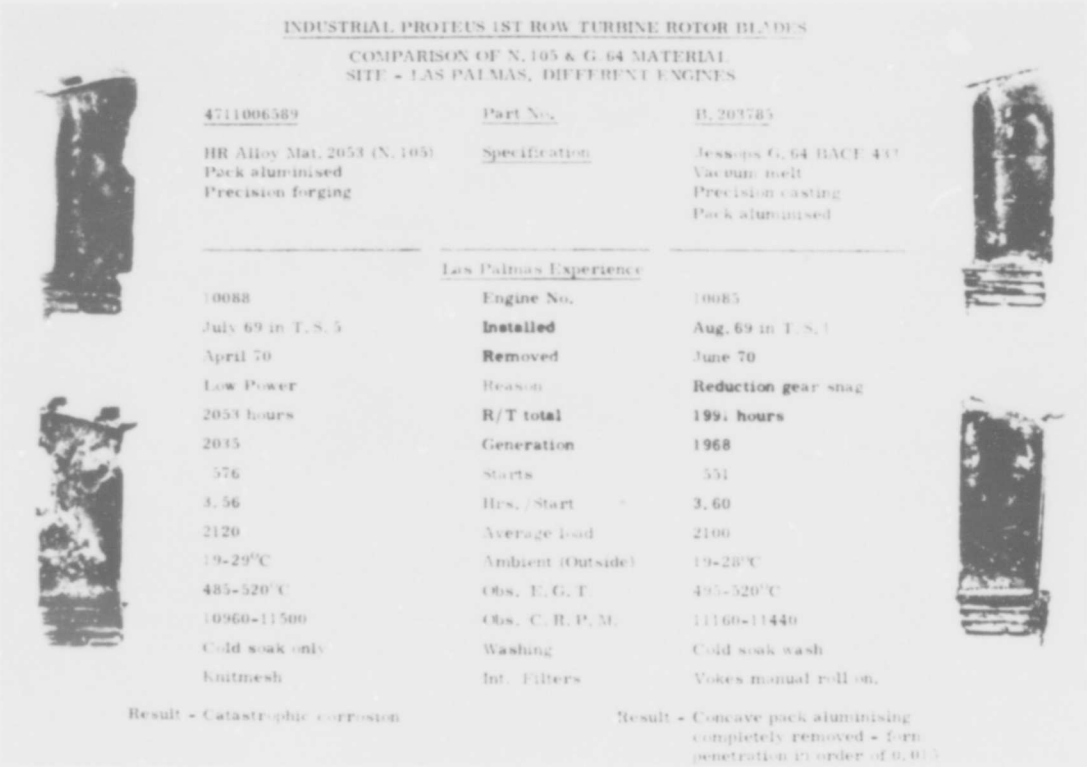

Figure 32.13. Proteus engine HP blades after 2000 h in salt environment with a maximum turbine inlet temperature of 875°C. (Page and Taylor).

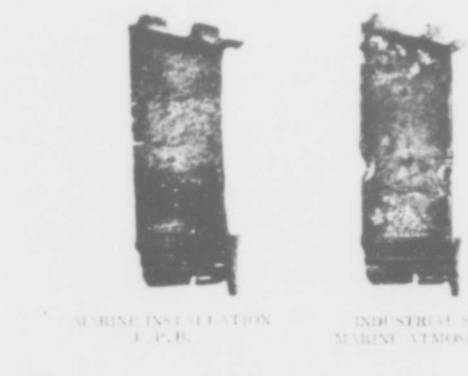

Figure 32.14. Proteus engine - comparison of 'marine' and 'industrial' corrosion on HP turbine blading - 1500 h. (Page and Taylor).

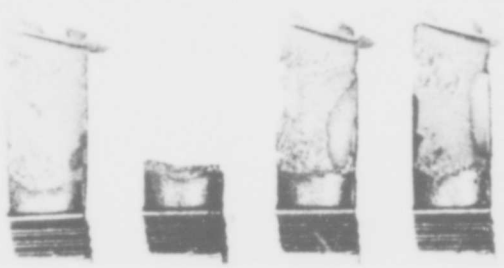

Figure 32.15. Proteus engine - HP blade N105 corroded remote from maximum temperature profile on blade aerofoil - industrial operation. (Page and Taylor).

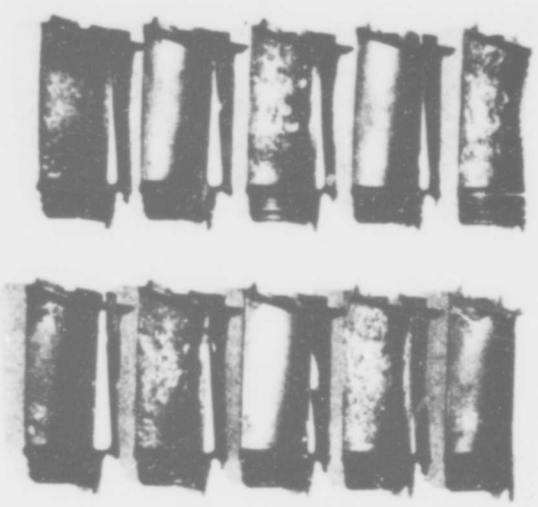

NIMONIC 105 PACK ALUMINISED HP BLADES SHOWING SEVERE CORROSION ATTACK ON 0,0007 INCH THICK PACK ALUMINISED BLADES.

Figure 32.16. Proteus engine - further evidence of effect of pack aluminising layer thickness on Proteus engine Hovercraft application, 1500 h - 1145°K. (Page and Taylor).

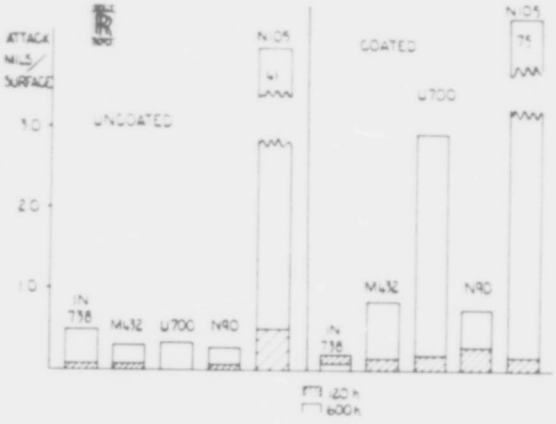

Figure 32.17. Corrosion resistance of materials, uncoated, pack aluminised - 820°C - combustion rig. (Page and Taylor).

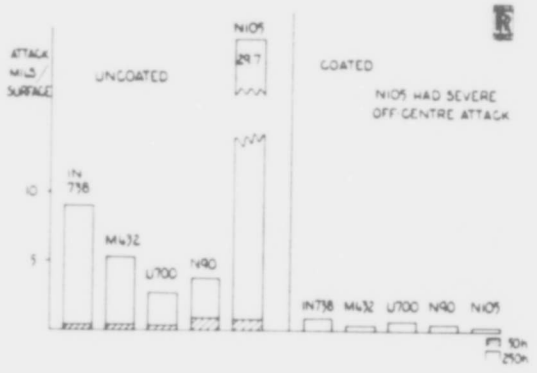

Figure 32.18. Corrosion resistance of materials, uncoated, pack aluminised - 870°C - combustion rig. (Page and Taylor).

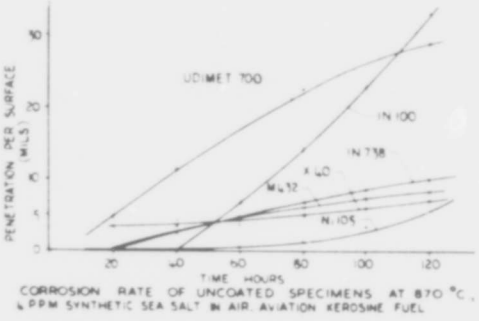

Figure 32.19. Corrosion resistance of materials, uncoated, relative to time and over a range of temperatures, combustion rig. (Page and Taylor).

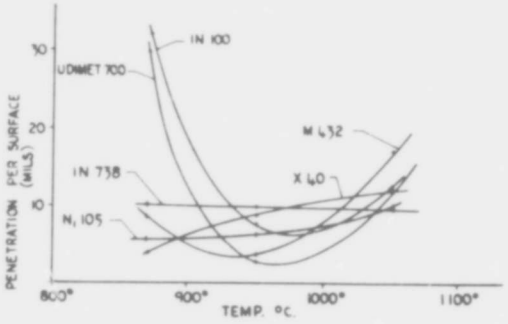

Figure 32.20. Corrosion resistance of materials, uncoated, relative to time and over a range of temperatures, combustion rig. (Page and Taylor).

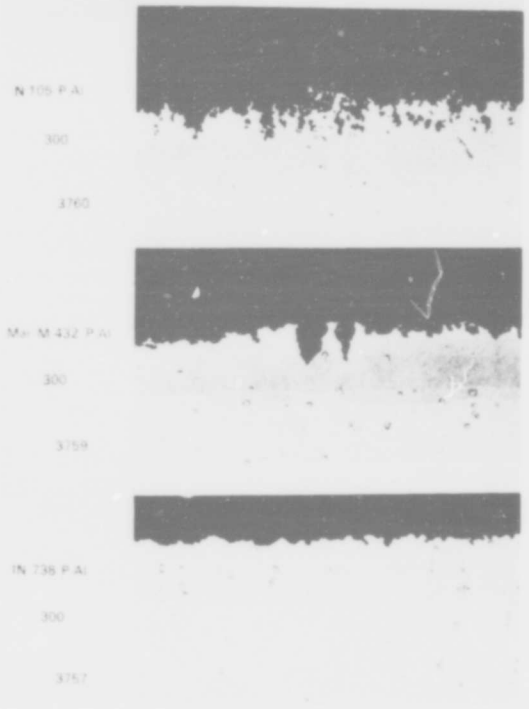

Figure 32.21. Micro sections of pack aluminised N105, M432, IN 738 - RR Bristol Laboratory Low Pressure Burner Rig 850°C - 10 ppm salt. (Page and Taylor).

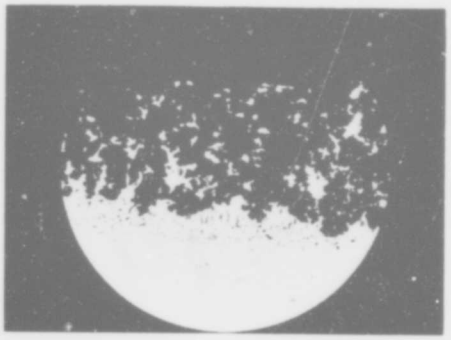

Figure 32.23. A section of the blade shown in Figure 32.33, showing chromium sulphides. (X400). (Roberts).

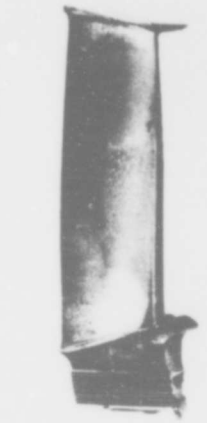

Figure 32.22. A pack-aluminised Nimonic 105 blade from an Olympus engine exhibiting hot corrosion. (Roberts).

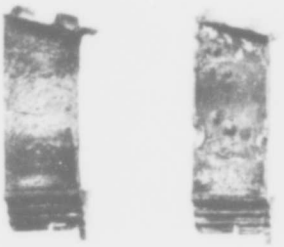

Figure 32.24. Wart-like growths on Nimonic 105 Proteus blades. (Roberts).

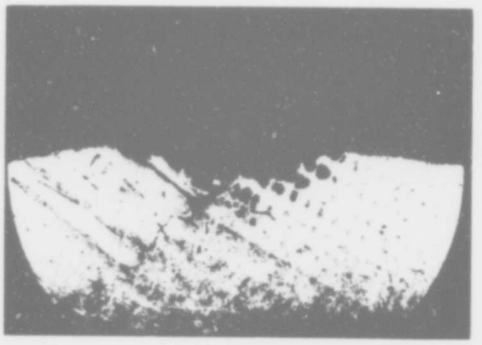

Figure 32.25. Oxidation of carbides in an X-40 stator blade from an Olympus engine. (Roberts).

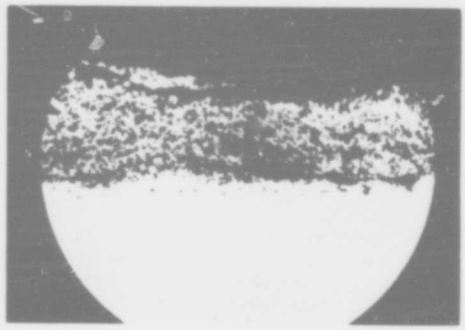

Figure 32.26. A section of a pack-aluminised Nimonic 105 blade from a marine Proteus after 692h running with salt in the fuel. There was catastrophic crater-flux type attack; this section shows chromium sulphides in the metal. (X120). (Roberts).

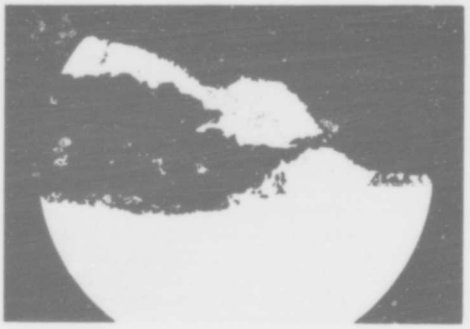

Figure 32.27. A section from the same blade as that shown in Figure 32.26, through a "finger" extending from a crater, showing complete local envelope breakdown under a small bridge of flux, which is probably the Ni-Ni_3S_2 eutectic.

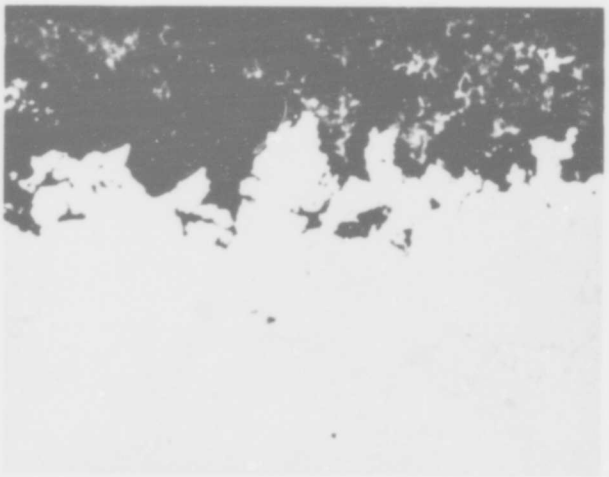

Figure 32.28. Pack-aluminised Nimonic 115. 1st stage. Turbine blade run for 951 h with last 409 h 0.01 ppm salt in air and 0.6 ppm sodium in fuel. Peak temperature 870°C. x 375. (Conde).

Nimonic 115

A.J.B. Cutler and C.J. Grant, in "Deposition and Corrosion in Gas Turbines" A.B. Hart and A.J.B. Cutler (eds.), (Applied Science Publishers, London, 1973) 78.

See IN 738 for details. Nimonic 115 corroded slower than Nimonic 90, but more rapidly than Nimonic 105 in Li/Na/K sulphates at 727°C in 1 atm O_2 + 3.23 x 10^{-4} atm SO_3. Figure 33.1 shows the protection afforded by an aluminised coating to 115.[2] Nimonic 115 specimens formed a relatively thick layer of corrosion product on the ends of the rectangular (10 x 3 x 2 mm^3) specimens, but a relatively thin layer over the rest of the specimen.

J. Billingham, J. Lauridsen, R.E. Lawn and M. A. P. Dewey, in "Deposition and Corrosion in Gas Turbines" A. B. Hart and A. J. B. Cutler (eds.), (Applied Science Publishers, London, 1973) 229.

This paper is concerned with the optimisation of the Ti/Al ratio in a nickel-base superalloy. The basis composition appears identical with Nimonic 115- the Ti content is varied from 1.5 to 8.3 (base composition 4%) and the Al from 1.7 and 7.5% (base composition 5%), the total being 9% for five alloys, 10% for two. The corrosion resistance was evaluated over the temperature range 800 - 950°C using a simple laboratory salt-spray test. The resistance to hot-salt corrosion attack increases as the Ti/Al ratio increases in the range 0.5 - 5.0.

K. Page and R. J. Taylor in "Deposition and Corrosion in Gas Turbines" A. B. Hart and A. J. B. Cutler (eds.), (Applied Science Publishers, London, 1973) 350.

See Nimonic 105 for details. Figure 33.2 shows pack aluminised Nimonic 115 blades from an industrial Avon engine after 1900 running hours with a maximum operating turbine entry temperature of 900°C with high levels of salt in the fuel showing the "wart-like growths" characteristic of industrial turbine corrosion. Figure 33.3 shows pack aluminised Nimonic 115 blades from a marine Olympus engine after 951h shore trials, 409h with salt injection: 0.01 ppm salt in the air plus 0.6 ppm salt in the fuel. The blade metal temperature was 880°C max (turbine entry temperature 950°C).

Rolls-Royce (1971) Ltd.

Hot corrosion data from a small burner rig is shown under 713C.

Data relating to this alloy will also be found in the following Figures:
10-125, 10.126, 14.6;
and in Table 31-I.

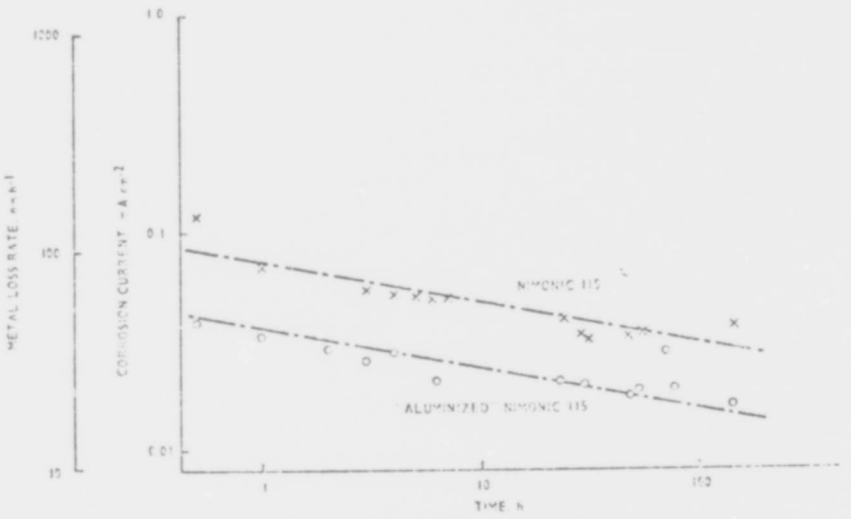

Figure 33.1. Corrosion data for Nimonic 115 and 'Aluminised' Nimonic 115 in molten sulphate at 1000K. (82.5% of the surface area of the aluminised sample was covered by the aluminising layer.) (Cutler and Grant).

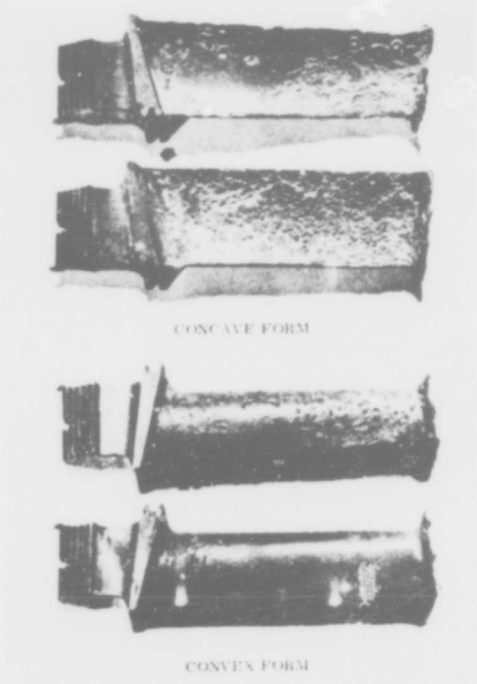

Figure 33.2. Industrial Avon - corrosion at 1900 h on N115 HP blade, pack aluminised with high levels of salt in fuel - maximum operating entry temperature 1170°K. (Page and Taylor).

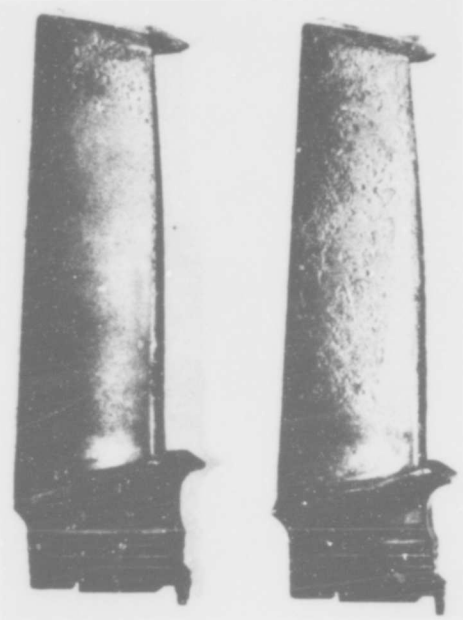

Figure 33.3. Olympus engine - marine shore trials at 1225°K turbine entry temperature. Corrosion at 1000 h, with comparison between thin and thick pack aluminising (0.0007 in to 0.0015 in) respectively. Material N115. (Page and Taylor).

PDRL 161

J.J. Walters (AVCO/Lycoming Division) Technical Report to the Air Force Materials Laboratory, Wright-Patterson Air Force Base AFML-TR-67-297 (Sept. 1967).

Extended summary in B1900. PDRL 161 is one of a group of alloys described as having "poor resistance to attack" - the others in this group were 713C, 713LC and PDRL 162. This poor performance of PDRL 161 is rather surprising in view of its high chromium content. X-ray analyses of the corrosion products found on the trailing edge after 40h rig testing for PDRL 161 showed in order of predominance NiO, a spinel with a_o = 8.24 Å, Al_2O_3 and a trace of Cr_2O_3. The products after 120h testing were the same as at the shorter time except that there was a little more Cr_2O_3. The corrosion products found in powder removed from an area that had undergone sulphidation attack in a 120h test were NiO, a spinel with a_o = 8.20 Å, and an unknown phase with d = 3.33, 1.76 and 1.72 Å. Microprobe analysis of the depleted metal zone was 95.5% Ni, 0.8% Cr, 0.7% Mo, 2.8% Al, 0.02% Ti and 0.1% Nb.

Figure 34.1 shows the corrosion of PDRL 161 tested using JP-4 fuel and a salt-to-air ratio of .8 ppm as a function of temperature. Figure 34.2, JP-4, 4 ppm salt. Figure 34.3 ; JP-4R, 8 ppm salt. Figure 34.4; JP-4R, 4 ppm salt. Figure 34.5; JP-5, 8 ppm salt.

Data relating to this alloy will also be found in the following Figures:
1-1, 1-7, 1-8;
and Tables:
1-I, 1-II, 1-V, 1-VI, 1-VII, 1-VIII, 1-IX.

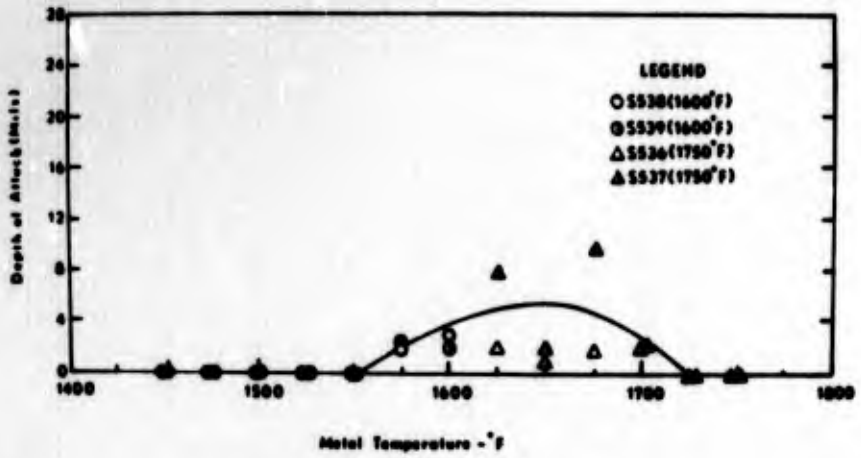

Figure 34.1. Corrosion as a function of temperature for PDRL 161 tested using JP-4 fuel with a Salt/Air Ratio of 8 ppm. (Walters).

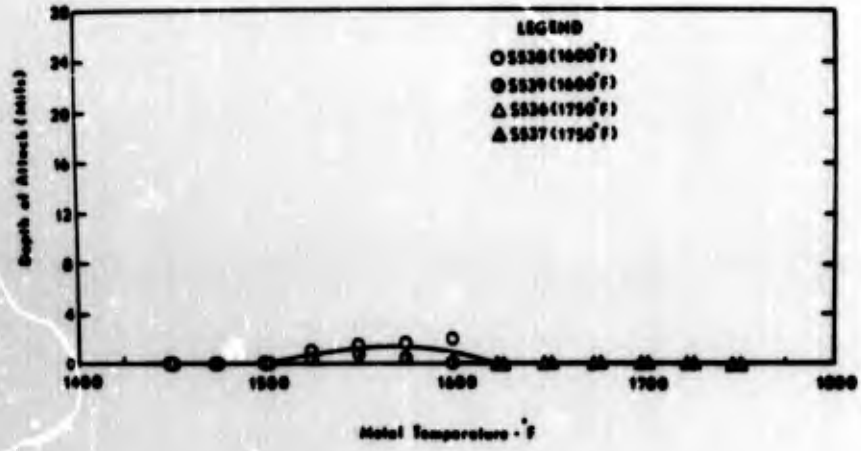

Figure 34.2. Corrosion as a function of temperature for PDRL 161 tested using JP-4 fuel with Salt/Air Ratio of 4 ppm. (Walters).

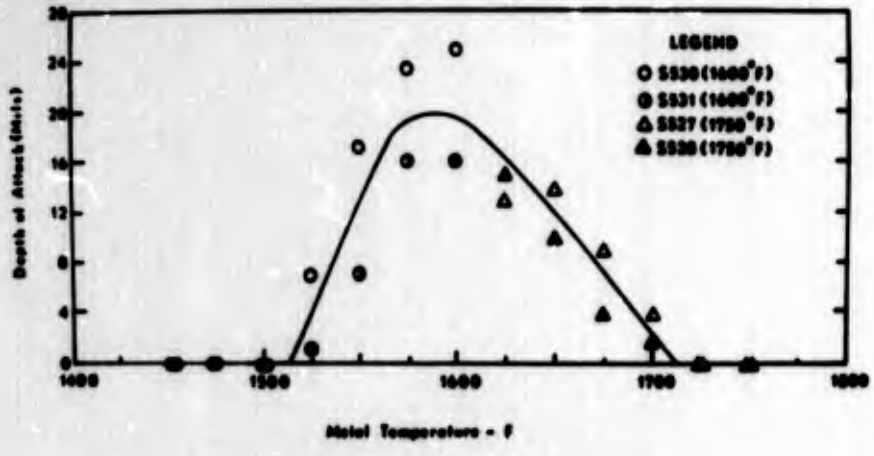

Figure 34.3. Corrosion as a function of temperature for PDRL 161 using JP-4R fuel with a Salt/Air Ratio of 8 ppm. (Walters).

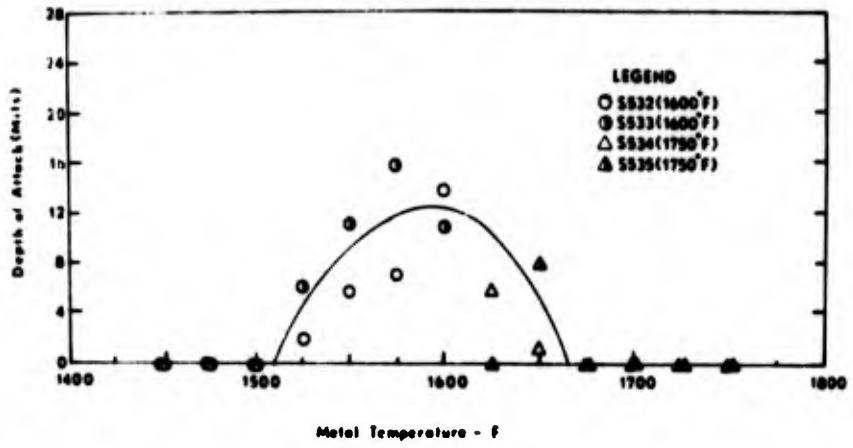

Figure 34.4. Corrosion as a function of temperature for PDRL 161 using JP-4R fuel with a Salt/Air Ratio of 4 ppm. (Walters).

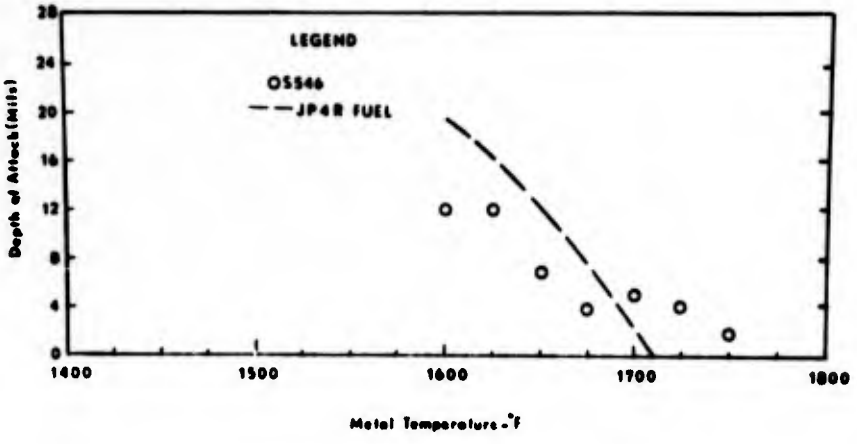

Figure 34.5. Corrosion as a function of temperature for PDRL 161 tested using JP-5 fuel (0.16%S) with a Salt/ Air Ratio of 8 ppm. (Walters).

PDRL 162

J. J. Walters (AVCO/Lycoming Division) Technical Report to the Air Force Materials Laboratory, Wright-Patterson Air Force Base AFML-TR-67-297 (September 1967).

Extended summary in B1900. PDRL 162 is one of a group of alloys described as having "poor resistance to attack" - the others in this group were 713C, 713LC and PDRL 162. X-ray analysis of the corrosion products found on the trailing edge after 40h rig testing detected for PDRL 162, in order of predominance, a spinel with a_o = 8.15 Å, NiO, a trace of Al_2O_3, plus an unknown phase. The phases present after 120h testing were the same spinel, NiO, Al_2O_3, Cr_2O_3, plus an unknown phase. The phases present in powder removed from an area which had undergone sulphidation attack in a 120h test were a spinel with a_o = 8.20 Å, NiO, plus an unknown phase with d = 3.40, 2.34 Å. A microprobe analysis of the depleted region in the metal was 94.2% Ni, 0.4% Cr, 0.9% Mo, 2.4% Al, 0% Ti, 1.3% W, 0% Co and 1.0% Ta.

Figure 35.1 shows the corrosion of PDRL 162 as a function of temperature using JP-4 fuel with 8 ppm salt in the air. Figure 35.2; JP-4, 4 ppm salt. Figure 35.3; JP-4R, 8 ppm salt. Figure 35.4; JP-4R, 4 ppm salt. Figure 35.5; JP-5, 8 ppm salt.

Data relating to this alloy will also be found in the following Figures:
1.1 and 1.7
and Tables:
1-I, 1-II, 1-V, 1-VI, 1-VII, 1-VIII, 1-IX.

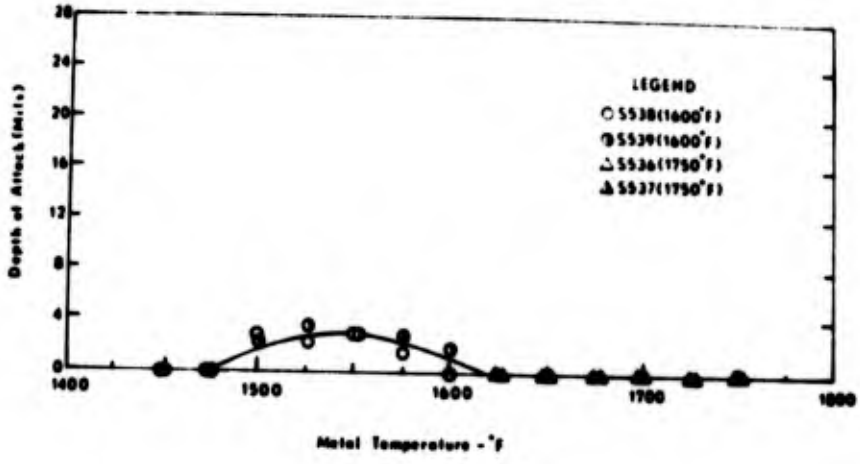

Figure 35.1. Corrosion as a function of temperature for PDRL 162 tested using JP-4 fuel with a Salt/Air Ratio of 8 ppm. (Walters).

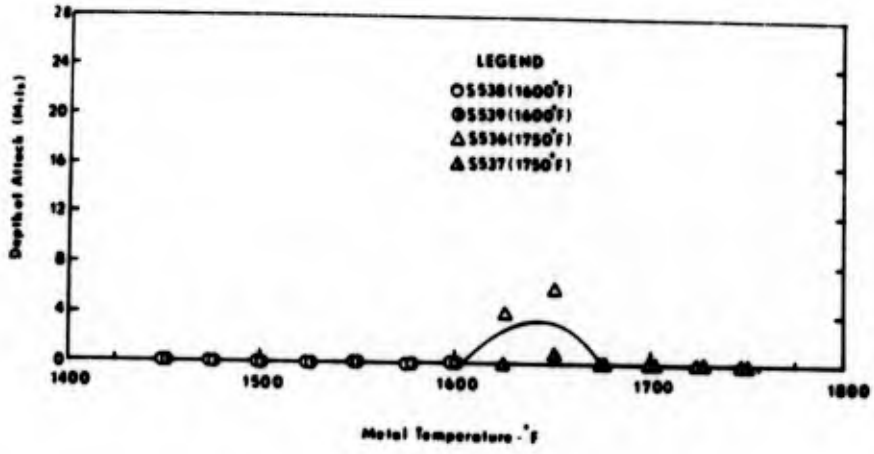

Figure 35.2. Corrosion as a function of temperature for PDRL 162 tested using JP-4 fuel with a Salt/Air Ratio of 4 ppm. (Walters).

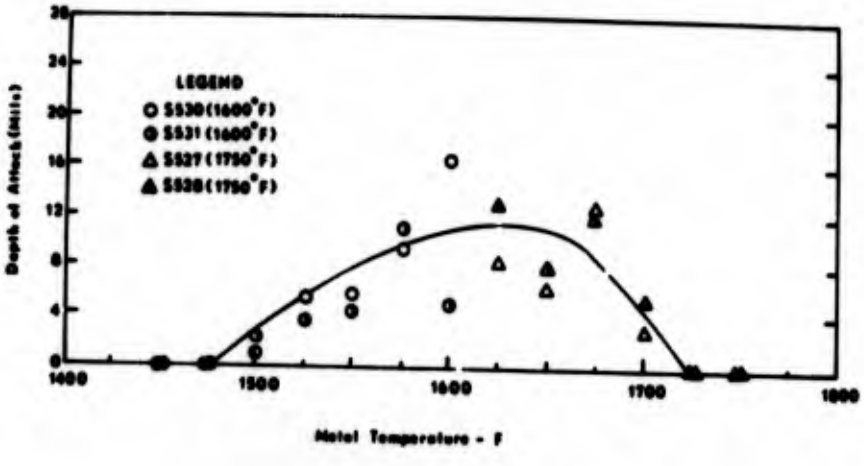

Figure 35.3. Corrosion as a function of temperature for PDRL 162 using JP-4R fuel with a Salt/Air Ratio of 8 ppm. (Walters).

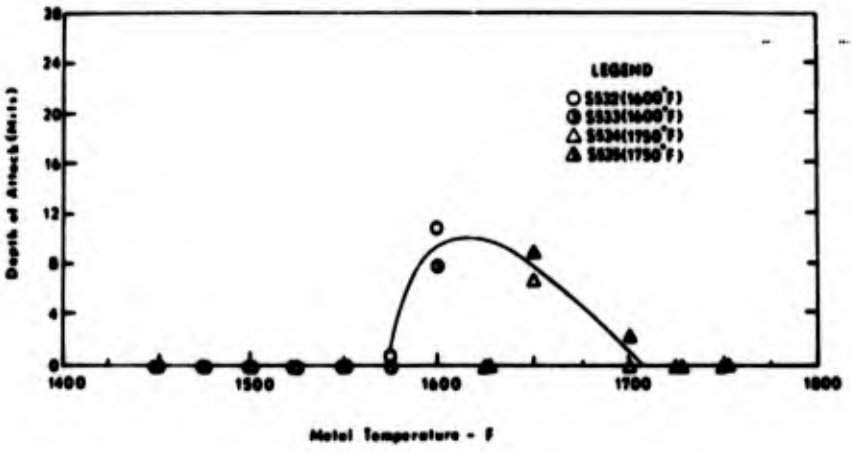

Figure 35.4. Corrosion as a function of temperature for PDRL 162 using JP-4R fuel with a Salt/Air Ratio of 4 ppm. (Walters).

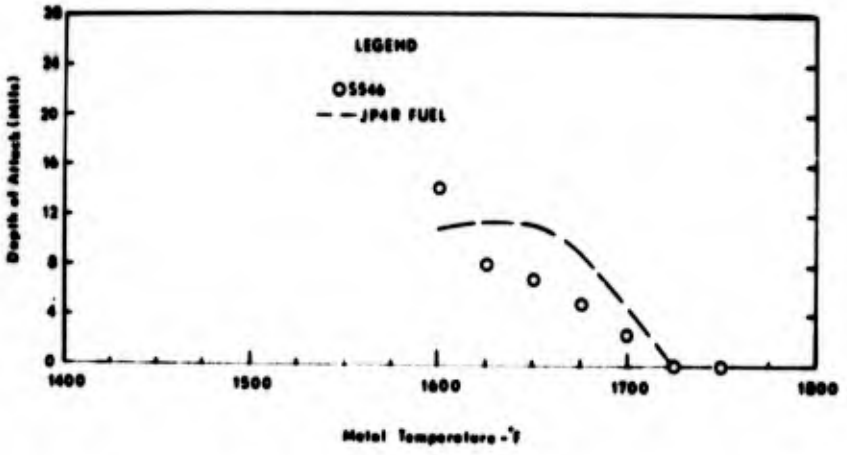

Figure 35.5. Corrosion as a function of temperature for PDRL 162 tested using JP-5 fuel (0.16%S) with a Salt/Air Ratio of 8 ppm. (Walters).

PDRL 163

L. D. Graham, J. D. Gadd and R. J. Quigg, Hot Corrosion Problems Associated with Gas Turbines, ASTM Special Technical Publication, STP 421, 1967, 105

See 713C for details. PDRL 163 loses approx. 0.3g in crucible test at 982°C, 1.2g in PWA rig test at 900°C. Comparable, but not as bad as 713C. Ranking makes it worse than U-700, better than 713C, comparable to IN 100. Attack is increased for 1600 to 1800F, decreased 1800 to 2000F.

K. H. Ryan, J. R. Kilsdig and P. E. Hamilton (Allison Division of General Motors) Technical Report to Wright-Patterson AFB, Air Force Materials Laboratory AFML-TR-67-306 (August 1967).

The alloys were tested in the as-cast condition, and as heat-treated by the following procedure: held for 2h at 2100F in vacuum, cooled rapidly, followed by 4h at 1950°F in vacuum followed by rapid cooling, and finally 16h at 1400°F, air cool. The alloys were cast into test specimens the same shape as a T56 turbine blade. The test consisted of heating 16 blades, rotating at 1800 rpm in a furnace to a pre-selected temperature, after which the entire unit was retracted into a cooling chamber. Here it was sprayed with an aspirated solution of deionised water and 1% sulphate ion supplied as water soluble sodium sulphate. A cycle consisted of 1.5 min heating time and 0.5 min cooling. A standard test consisted of 500 cycles. The exhaust gas in the furnace was relatively low in oxygen, varying from 6-10% at 1700°F to 0 - 1% at 2000°F. Test temperatures were 1700, 1750, 1800, 1850, 1900 and 2000°F (927, 955, 982, 1010, 1038 and 1093°C). Temperature patterns as a function of position on the blade and time in the heating cycle were determined by a variety of techniques. Blades were weighed prior to testing and cathodically cleaned and reweighed after testing. Density determinations were made on each alloy and weight losses converted to volume losses. Statistical analysis was then applied to the results to compare the alloys tested (PDRL 163, IN 728 NX, 713C + Cr, 713C + Cr + Y, Mar M 421, 713C, IN-100, Inco 717, GMR 235, Mar M 246). The results are presented in Tables 36.I, 36.II, 36.III, 36-IV, and 36.V, and in Figures 36.1 and 36.2. PDRL 163 and IN 728 NX showed significantly better resistance to hot corrosion than all the other alloys through 1850°F (1010°C). The corrosion severity increases progressively with increasing temperature. The effect of heat-treatment is shown in Figure 36.3: the effect on PDRL (as on most of the alloys) is negligible. Figure 36.4 shows the volume loss as a function of test temperature for as cast and heat-treated PDRL 163. Tables 36-VI through 36-XI list the volume loss data for all the alloys. Figure 36.5 shows the alloy corrosion at the blade tip as a function of test temperature for all the alloys: again PDRL 163 appears to be one of the best alloys. The data are listed in Table 36-XII. Figures 36.5, 36.7 shows an optical evaluation of corrosion severity for all the alloys.

The data were then subjected to a regression analysis in terms of the chemical compositions of the alloys. It was concluded for the as-cast alloys that (1) increasing the weight per cent of Cr or Al in an alloy will reduce the volume loss due to hot corrosion: (2) increasing the weight per cent W or Mo in an alloy will produce greater volume loss; (3) increasing the temperature will increase volume loss. Figure 36.8 shows the effect of Cr, W, Al, and Mo as indicated by the regression analysis. Figure 36.9 shows the comparison of the measured volume loss for PDRL 163 as a function of temperature with the loss predicted by the regression equation: $\log_{10}$ (volume loss) = $5.85238 \times 10^{-9} T^3 - 1.33860 \times 10^{-5} T^2 + 6.32837 \times 10^{-2}$ w/o W + 8.63834×10^{-2} w/o Mo - 6.77702×10^{-2} w/o Cr - 8.982×10^{-2} w/o Al + 11.2807.

For all the alloys metallography suggested that the corrosion area could be divided into three general zones: (1) an outer layer of continuous oxide on the surface which gradually graded into an area of mixed metal and oxide; (2) a layer of depleted metal: (3) globular sulphide particles. These generally formed a line between the depleted zone and the matrix but occasionally a selective grain boundary attack preceded the frontal row of sulphides. Micrographs are shown of 713C and 717, but none of PDRL 163.

J. J. Walters (AVCO/Lycoming Division) Technical Report to the Air Force Materials Laboratory, Wright-Patterson Air Force Base, AFML-TR-67-297 (September 1967).

See B 1900 for summary. PDRL 163 is not one of the alloys studied in the programme, but Figure 10.1 (see 713C) compares the performance of four alloys, including PDRL 163, in a 120h test in the AVCO Lycoming environmental rig with 6 ppm salt and 60 and 90h engine tests with 1ppm salt in the air. The diagram is taken from a paper by F. J. St. John, W.A. Rentz and W. R. Freeman, Jr., presented to the Sixth Annual National Conference on Aircraft and Propulsion Systems, September 1966. PDRL 163 seemed rather better than, but comparable with, 713C.

R. Viswanathan, Corrosion 24 (1968) 359.

See 713C for details. PDRL 163 was one of the best alloys tested, losing only 1.3 mg/cm^2 in 150h at 1500°F (866°C); 97.4% of the alloy was unaffected. Better than Waspalloy or U-500; comparable to GMR 235.

R. Field, D. J. Fisk and H. von E. Doering, Naval Ship Research and Development Centre, Materials Laboratory Research and Development Report 2833 (January 1969).

See 713C.

R. W. Hardt, J. R. Gambino, and P. A. Bergman, Hot Corrosion Problems Associated with Gas Turbines, ASTM Special Technical Publication, STP 421, 1967, 64.

This paper is concerned with a study of the hot corrosion mechanism in relation to the development of alloys for marine service. A small burner rig was used (1% S diesel oil, 200 ppm salt in the air, 100h tests). The two nickel-base commercial alloys SEL and PDRL 163 were included for comparison: At 1675°F (915°C): PDRL 163 was rather worse than SEL, with a maximum penetration of approximately 25 mils and a surface loss of 10 mils. At 1900°F (1038°C): PDRL 163 was appreciably better than SEL, with a maximum penetration of 10 mils and a surface loss of only 2 mils. The principal oxide detected at the lower temperature was NiO, with traces of Cr_2O_3; Na_2SO_4 was alsopresent. At the higher temperature only Cr_2O_3 was present: no Na_2SO_4 was detected.

P. E. Hamilton, K. H. Ryan and E. S. Nichols, Hot Corrosion Problems Associated with Gas Turbines, ASTM Special Technical Publication STP 421, 1967, 188.

See 713C for details. In a cyclic salt-spray hot corrosion test, PDRL 163 was a little better than 713C; but a PDRL 163 with 10% Co was very considerably better.

Rolls-Royce (1971) Ltd.

Hot corrosion data from a small burner rig are shown under X-40.

Data relating to this alloy will also be found in the following Figures:
10.1, 10.67, 10.68, 10.76, 52.28, 52.29.

TABLE 36-I

SIGNIFICANT DIFFERENCES BETWEEN INDIVIDUAL ALLOYS AT 1700°F CYCLIC TEMPERATURE. (RYAN ET AL)

Material	Vol. loss (mm^3)	Mar M246	GMR 235	Inco 717	IN 100	713C	Mar M421	713C Cr+Y	713C +Cr	IN 728NX	PDRL 163
		11.11	4.50	2.67	2.34	2.30	2.06	1.99	1.98	1.11	0.42
PDRL 163	0.42	*26.452	*10.714	*6.357	*5.571	*5.476	*4.904	*4.738	*4.714	*2.642	
IN728NX	1.11	*10.009	* 4.045	*2.405	*2.108	*2.072	*1.855	*1.792	*1.783		
713C+Cr	1.98	* 5.611	* 2.272	1.348	1.181	1.161	1.040	1.005			
713+Cr+ Y	1.99	* 5.582	* 2.261	1.341	1.175	1.155	1.035				
Mar M421	2.06	* 5.393	* 2.184	1.296	1.135	1.116					
713C	2.30	* 4.830	* 1.956	1.160	1.017						
IN100	2.34	* 4.747	* 1.923	1.141							
Inco 717	2.67	* 4.161	* 1.685								
GMR 235	4.50	* 2.468									
Mar M246	11.11										

* Denotes a significant difference at a = 0.05

TABLE 36-II

SIGNIFICANT DIFFERENCES BETWEEN INDIVIDUAL ALLOYS AT 1750°F CYCLIC TEMPERATURE. (RYAN ET AL)

Material	Vol. loss (mm^3)	Mar-M246	GMR-235	IN-100	Inco 717	713C	713C +Cr	713C +Cr+Y	Mar-M421	IN-728 NX	PDRL 163
		42.53	11.72	4.46	4.37	4.02	3.67	3.23	3.23	2.00	1.48
PDRL 163	1.48	*28.736	*7.918	*3.013	*2.952	*2.716	*2.479	*2.182	*2.182	1.351	
IN728NX	2.00	*21.265	*5.860	*2.230	*2.185	*2.010	*1.835	*1.615	*1.615		
Mar M421	3.23	*13.167	*3.628	1.380	1.352	1.244	1.136	1.000			
713+Cr+Y	3.23	*13.167	*3.628	1.380	1.352	1.244	1.136				
713C+Cr	3.67	*11.588	*3.193	1.215	1.100	1.095					
713C	4.02	*10.579	*2.915	1.109	1.087						
Inco 717	4.37	* 9.732	*2.681	1.020							
IN 100	4.46	* 9.535	*2.627								
GMR 235	11.72	* 3.628									
Mar M246	42.53										

* Denotes a significant difference at a = 0.05

TABLE 36-III

SIGNIFICANT DIFFERENCES BETWEEN INDIVIDUAL ALLOYS AT 1800°F CYCLIC TEMPERATURE. (RYAN ET AL)

Material	Vol. loss (mm^3)	Mar-M246	GMR-235	Mar M421	IN-100	713C	Inco 717	713C +Cr	713C +Cr+Y	IN 728 NX	PDRL -63
		85.59	24.53	10.87	10.17	9.27	7.52	7.02	5.98	4.30	3.79
PDRL 163	3.79	*22.583	* 6.472	* 2.868	* 2.683	*2.445	*1.984	*1.852	*1.577	1.134	
IN728NX	4.30	*19.904	* 5.704	* 2.527	* 2.365	*2.155	*1.748	*1.632	*1.390		
713C+Cr+Y	5.98	*14.312	* 4.102	* 1.817	* 1.700	*1.550	1.257	1.173			
713C+Cr	7.02	*12.192	* 3.494	* 1.548	1.448	1.320	1.071				
Inco 717	7.52	*11.381	* 3.261	1.445	1.352	1.232					
713C	9.27	* 9.233	* 2.646	1.172	1.097						
IN 100	10.17	* 8.415	* 2.411	1.068							
Mar M421	10.87	* 7.873	* 2.256								
GMR 235	24.53	* 3.489									
Mar M246	85.59										

* Denotes a significant difference at a = 0.05

TABLE 36-IV

SIGNIFICANT DIFFERENCES BETWEEN INDIVIDUAL ALLOYS AT 1850°F CYCLIC TEMPERATURE. (RYAN ET AL)

Material	Vol. loss (mm^3)	Mar-M246	GMR 235	IN-100	Mar-M421	713C	Inco 717	713C +Cr	713C +Cr+Y	IN 728 NX	PDRL 163
		265.3	68.47	31.61	28.44	27.65	21.70	19.53	19.09	13.46	12.17
PDRL 163	12.17	*21.799*	5.626*	2.597 *	2.336 *	2.271 *	1.783 *	1.604*	1.568	1.105	
IN728NX	13.46	*19.710*	5.086*	2.348 *	2.112 *	2.054 *	1.612 *	1.450*	1.418		
713C+Cr+Y	19.09	*13.897*	3.586*	1.655 *	1.489 *	1.448	1.136	1.023			
713C+Cr	19.53	*13.584*	3.505*	1.618 *	1.456 *	1.415	1.111				
Inco 717	21.70	*12.225*	3.155*	1.456 *	1.310 *	1.274					
713C	27.65	* 9.594*	2.476	1.143	1.028						
Mar M421	28.44	* 9.328*	2.407	1.111							
In 100	31.61	* 8.392*	2.166								
GMR 235	68.47	* 3.874									
Mar M246	265.3										

* Denotes a significant difference at a = 0.05

TABLE 36-V

SIGNIFICANT DIFFERENCES BETWEEN INDIVIDUAL ALLOYS AT 1900°F CYCLIC TEMPERATURE. (RYAN ET AL)

Material	Vol. loss (mm^3)	Mar-M246	GMR-235	Mar-M421	IN-100	Inco 717	713C	IN-728 NX	713C +Cr+Y	713C +Cr	PDRL 163
		1337.25	302.6	170.9	128.4	96.66	95.61	70.63	69.01	68.54	60.16
PDRL 163	60.16	*22.228	*5.029	* 2.840	* 2.134	*1.606	*1.589	1.174	1.147	1.139	
713C+Cr	68.54	*10.510	*4.414	* 2.493	* 1.873	1.410	1.394	1.030	1.006		
713C+Cr+Y	69.01	*19.377	*4.384	* 2.476	* 1.860	1.400	1.385	1.023			
IN728NX	70.63	*18.933	*4.284	* 2.419	* 1.817	1.368	1.353				
713C	95.61	*13.986	*3.164	* 1.787	1.342	1.010					
Inco 717	96.66	*13.834	*3.130	* 1.768	1.328						
IN 100	128.4	*10.414	*2.356	1.330							
Mar M421	170.9	* 7.824	*1.770								
GMR 235	302.6	* 4.419									
Mar M246	1337.25										

* Denotes a significant difference at a = 0.05

TABLE 36-VI

VOLUME LOSSES DURING 500-CYCLE TEST - 1700°F CYCLIC TEMPERATURE. (RYAN ET AL)

Test Number	Volume loss in cubic millimeters S-1	S-2	S-3	S-4	S-5	S-6
As cast						
Alloy						
713C	3.21	1.87	2.12		3.185	
713C (Mod Cr)	2.82	1.80	2.02		2.73	
713C (Mod Cr + Y)	2.90	1.54	2.14		2.59	
Mar-M421	3.04		2.23	1.69	2.63	
Inco 717	4.05	2.78	2.81		3.57	
Mar-M246	18.32		7.70	3.71	10.82	
PDRL 163	3.40		0.27	0.05	0.50	
IN-728 NX	1.40		1.03	0.68	1.53	
GMR-235	9.74		2.72	1.33	3.96	
IN-100	4.28	2.56	1.96		2.98	

Table 36-VI (Continued).

Heat treated						
713C	4.34	2.47		1.83	3.68	
713C (Mod Cr)	3.04	2.19		1.50	3.05	
713C (Mod Cr + Y)	3.28	2.46		1.72	2.68	
Mar-M421		2.38	2.27	1.72		1.81
Inco 717	4.10	2.54		2.19	3.68	
Mar-M246		18.46	18.75	8.22		22.8
PDRL 163		0.46	0.41	0.38		0.84
IN-728 NX		1.08	1.00	1.49		1.64
GMR-235		7.49	5.20	3.92		12.37
IN-100	3.89	2.21		1.94	3.12	

TABLE 36-VII

VOLUME LOSSES DURING 500-cycle test - 1750°F cyclic temperature

(RYAN ET AL)

	Volume loss in cubic millimeters					
Test Number	S-11	S-12	S-13	S-14	S-15	S-16
As cast						
Alloy						
713C	3.24	3.83	5.65		4.42	
713C (Mod Cr)	2.83	3.54	5.79		3.82	
713C (Mod Cr + Y)	3.02	3.47	3.96		3.12	
Mar-M421	3.41		5.88	5.62	4.34	
Inco 717	4.31	4.06	9.00		4.53	
Mar-M246	54.71		70.31	26.13	23.06	
PDRL 163	0.79		5.21	2.59	1.79	
IN-728 NX	1.36		2.81	3.10	2.38	
GMR-235	8.56		34.41	9.21	8.31	
IN-100	4.53	3.88	4.89		4.67	
Heat treated						
713C	3.34	4.04		5.71	5.83	
713C (Mod Cr)	3.02	5.08		4.79	4.15	
713C (Mod Cr + Y)	2.99	3.65		4.44	3.92	
Mar-M421		4.73	7.07	0.69		1.87
Inco 717	3.84	3.89		5.59	4.77	
Mar-M246		61.32	124.78	91.25		21.21
PDRL 163		1.09	2.25	2.44		0.36
IN-728 NX		1.99	2.96	2.68		1.07
GMR-235		8.39	22.02	19.95		7.62
IN-100	4.69	4.01		4.63	4.53	

TABLE 36-VIII

VOLUME LOSSES DURING 500-CYCLE TEST-1800°F CYCLIC TEMPERATURE. (RYAN ET AL)

Test Number	Volume loss in cubic millimeters				
	S-21	S-22	S-23	S-24	S-25
As cast					
Alloy					
713C	8.46	14.16	9.26		12.9
713C (Mod Cr)	6.05	12.99	9.05		11.19
713C (Mod Cr + Y)	5.50	8.61	8.72		9.22
Mar-M421	7.81		9.99	11.03	108.45
Inco 717	7.47	21.30	9.43		11.38
Mar-M246	76.46		74.43	60.51	102.90
PDRL 163	3.08		4.96	5.88	7.48
IN-728 NX	4.72		5.15	5.32	6.93
GMR-235	20.21		23.77	19.73	40.88
IN-100	15.48	1.25	10.31		14.33
Heat treated					
713C	12.19	21.81		12.36	15.26
713C (Mod Cr)	7.71	10.24		9.43	11.34
713C (Mod Cr + Y)	5.71	9.97		9.17	10.85
Mar-M121		10.18	11.99	11.68	
Inco 717	7.67	9.32		8.60	12.88
Mar-M246		147.17	174.44	153.62	
PDRL 163		4.00	5.00	5.19	
IN-728 NX		4.85	5.46	6.71	
GMR-235		54.16	30.90	34.35	
IN-100	10.14	16.19		8.74	14.59

TABLE 36-IX

VOLUME LOSSES DURING 500-CYCLE TEST-1850°F CYCLIC TEMPERATURE. (RYAN ET AL)

Test Number	Volume loss in cubic millimeters					
	S-31	S-32	S-33	S-34	S-35	S-36
As cast						
Alloy						
713C	25.79	39.39	46.59		33.36	
713C (Mod Cr)	17.53	27.75	36.06		27.93	
713C (Mod Cr + Y)	18.09	29.64	34.12		26.94	
Mar-M421	25.02		50.60	23.85	47.69	
Inco 717	17.32	42.77	39.34		31.15	
Mar-M246	229.06		287.29	168.70	206.21	
PDRL 163	8.60		22.59	9.29	18.01	
IN-728 NX	9.37		21.93	10.66	18.62	
GMR-235	88.95		79.31	55.89	56.39	
IN-100	45.49	83.14	62.13		36.30	
Heat treated						
713C	37.85	63.68		26.95	28.53	
713C (Mod Cr)	22.04	43.61		18.41	20.93	
713C (Mod Cr + Y)	17.52	37.46		16.00	23.01	
Mar-M421		51.35	42.71	22.12		12.34
Inco 717	19.61	52.70		17.54	25.60	
Mar-M246		516.11	498.43	359.40		183.83
PDRL 163		25.74	23.38	8.78		5.73
IN-728 NX		20.70	24.32	11.65		9.07
GMR-235		151.30	192.63	70.23		20.01
IN-100	31.70	46.16		24.08	28.38	

TABLE 36-X

VOLUME LOSSES DURING 500-CYCLE TEST-1900°F CYCLIC TEMPERATURE. (RYAN ET AL)

Test Number	Volume loss in cubic millimeters					
	S-41	S-42	S-43	S-44	S-45	S-46
As cast						
Alloy						
713C	106.77	43.76	30.89		22.65	
713C (Mod Cr)	68.78	29.25	18.72		15.56	
713C (Mod Cr + Y)	72.24	28.91	19.35		12.53	
Mar-M421	117.65		32.31	59.64	30.27	
Inco 717	81.62	40.83	33.35		30.17	
Mar-M246	504.03		277.98	314.32	267.79	
PDRL 163	54.19		13.45	24.24	10.81	
IN-728 NX	66.27		16.51	18.86	14.81	
GMR-235	222.07		70.52	91.76	31.46	
IN-100	162.54	63.84	41.09		20.78	
Heat treated						
713C	114.84	39.72		18.62	20.90	
713C (Mod Cr)	81.94	27.25		22.87	13.52	
713C (Mod Cr + Y)	74.29	31.76		21.88	16.33	
Mar-M421		81.43	53.18	60.42		23.68
Inco 717	78.15	37.28		29.27	21.78	
Mar-M246		534.60	443.47	510.34		419.00
PDRL 163		26.20	14.33	20.49		6.83
IN-728 NX		27.76	17.82	23.24		10.38
GMR-235		143.03	120.12	154.95		341.20
IN-100	129.71	59.36		48.21	22.96	

TABLE 36-XI

VOLUME LOSSES DURING 500-CYCLE TEST-2000°F CYCLIC TEMPERATURE. (RYAN ET AL)

As cast	Volume loss (mm^3)
Test No. S-61	
Alloy	
713C	101.2
713C (Mod Cr)	80.35
713C (Mod Cr + Y)	87.12
Mar-M421	109.7
Inco 717	131.2
Mar-M246	357.3
PDRL 163	27.08
IN-728 NX	49.61
GMR-235	162.4
IN-100	114.5

TABLE 36-XII

CORROSION AREAS* AT SECTION D'-D' AFTER 500-CYCLE TEST. (RYAN ET AL)

Cyclic test temperature (°F)	Corrosion area ($in.^2 \times 32^2$)			
Alloy — as-cast	1700	1800	1900	2000
Alloy 713C	0.27	1.10	3.79	7.60
Alloy 713C (Mod Cr)	0.23	0.63	2.40	8.78
Alloy 713C (Mod Cr + Y)	0.45	1.71	1.08	11.30
Mar-M121	0.38	1.30	4.77	13.70
Inco 717	0.50	1.00	2.59	9.09
Mar-M246	1.62	4.10	16.18	13.48
PDRL 163	0.11	0.74	1.72	2.49
IN-728 NX	0.22	0.88	1.28	7.92
GMR-235	0.78	8.80	3.08	8.73
IN-100	0.24	1.25	4.78	12.40

*Corrosion areas were determined by the following method:

1. Test blades were sectioned at airfoil section D'-D', mounted and polished.
2. Metallographic sections were projected on the scope of a Leitz Large Metallograph at 32×.
3. A transparency containing the original profile of section D'-D' was laid over the projected image and the corrosion areas were traced on the transparency.
4. Areas of corrosion were measured with a planimeter.

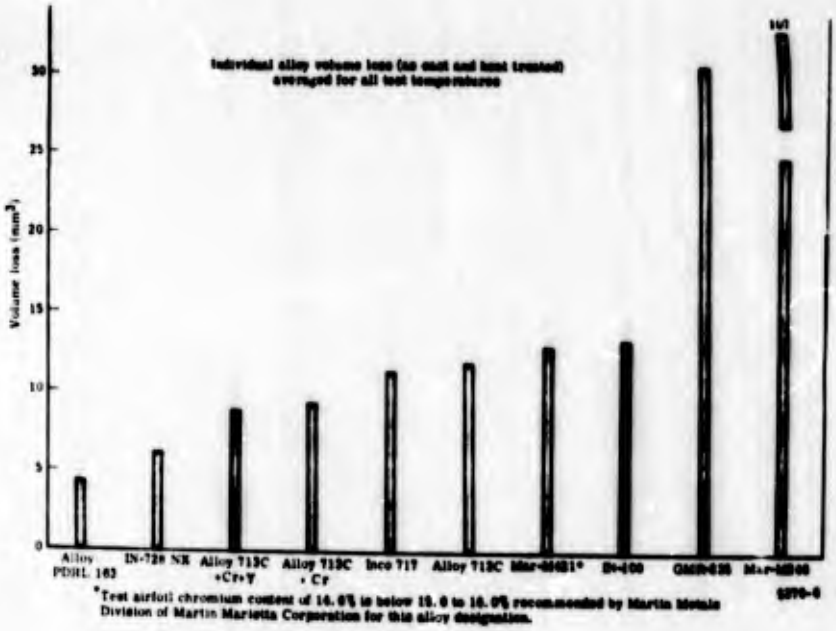

Figure 36.1. Bar graph of individual alloy volume losses averaged over all test temperatures. (Ryan et al).

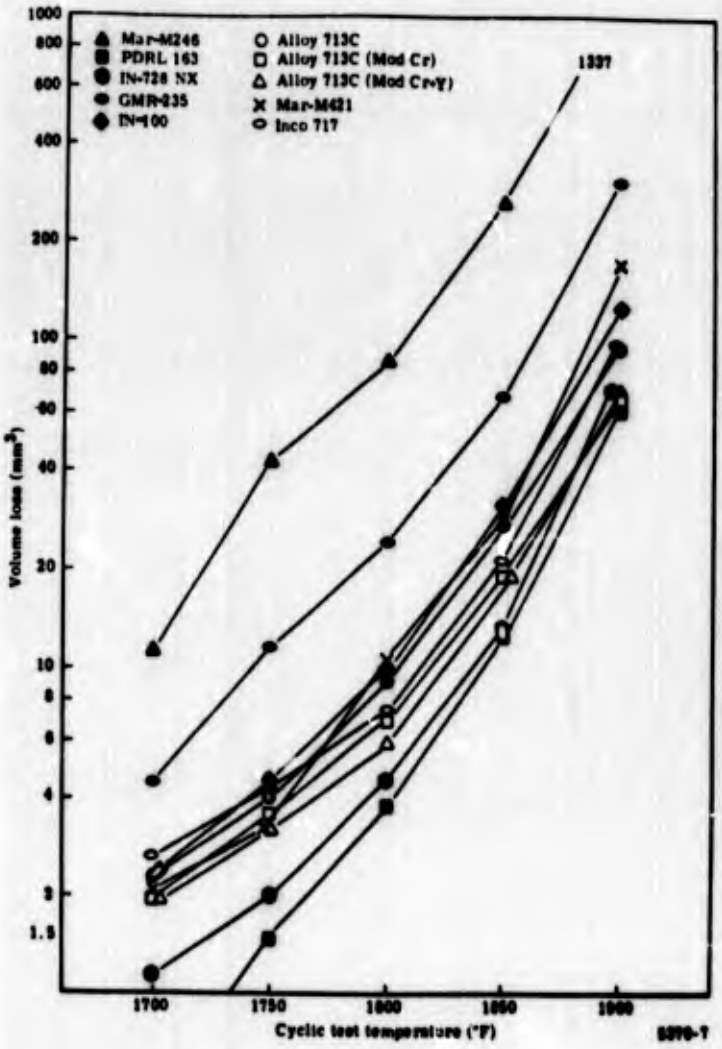

Figure 36.2. Individual alloy volume losses at each test temperature. (Ryan et al).

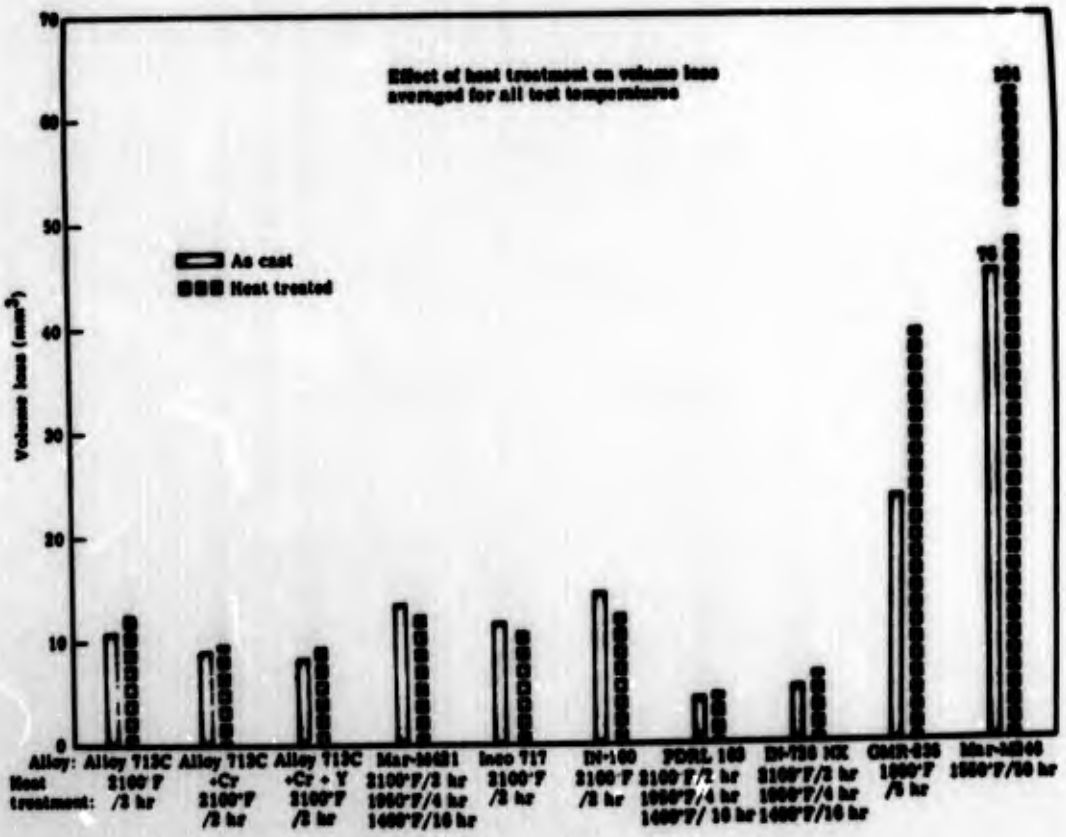

Figure 36.3. Bar graph showing the effect of heat treatment on individual alloy volume losses. (Ryan et al).

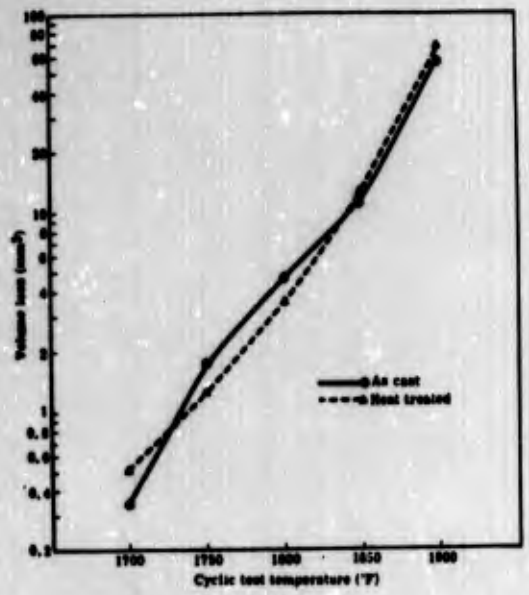

Figure 36.4. As-cast versus heat treated PDRL 163 at each cyclic test temperature. (Ryan et al).

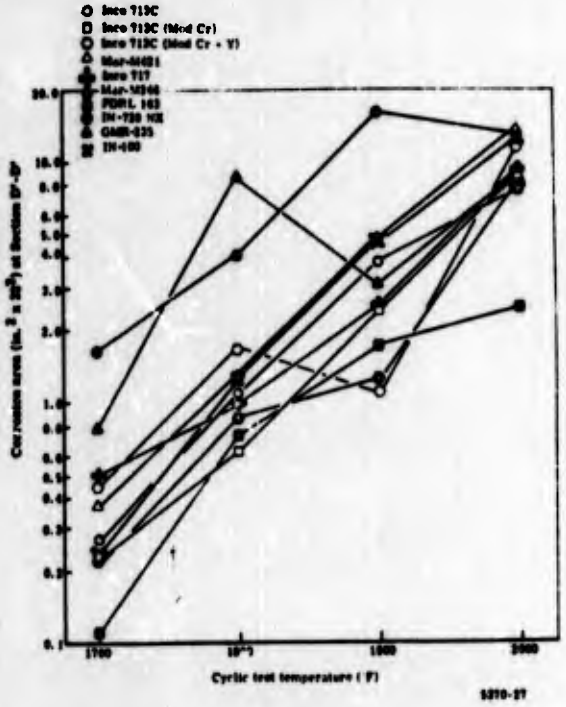

Figure 36.5. Alloy corrosion areas at airfoil section D'-D' versus cyclic test temperature. (Ryan et al).

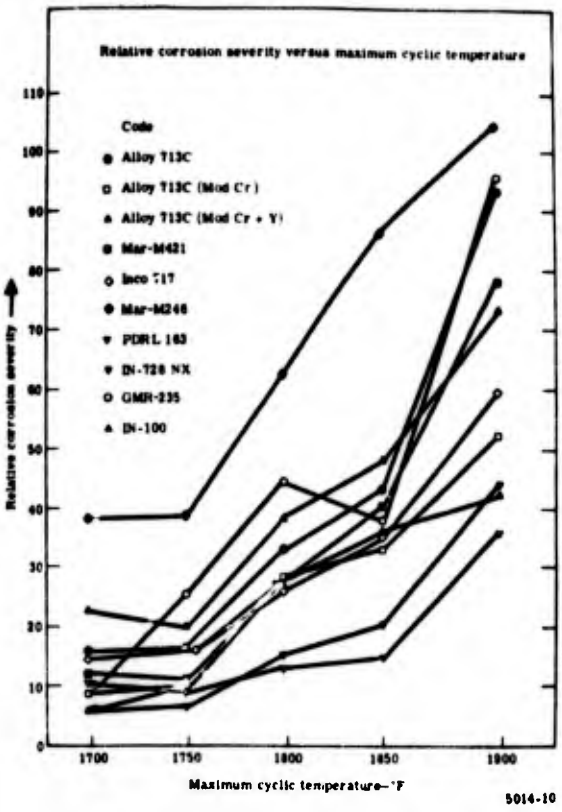

Figure 36.6. Binocular evaluation - leading edge and upper-middle airfoil. (Ryan et al).

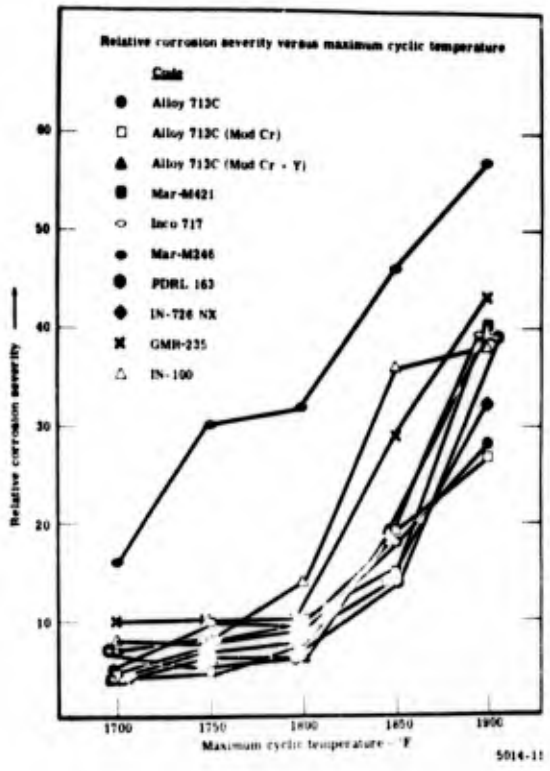

Figure 36.7. Binocular evaluation - stalk and lower airfoil. (Ryan et al).

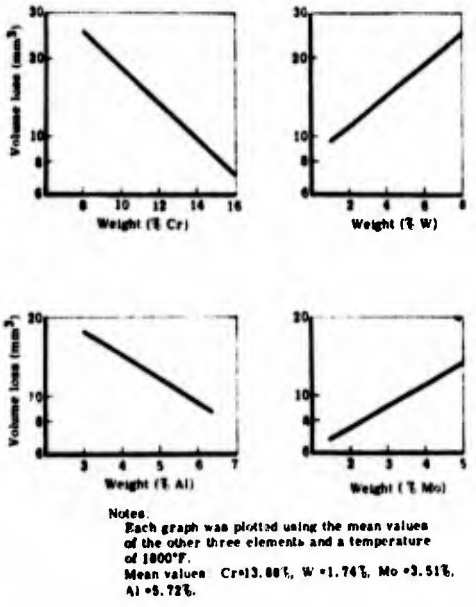

Figure 36.8. The effects of Cr, W, Al, and Mo on volume loss as predicted by the regression equation. (Ryan et al).

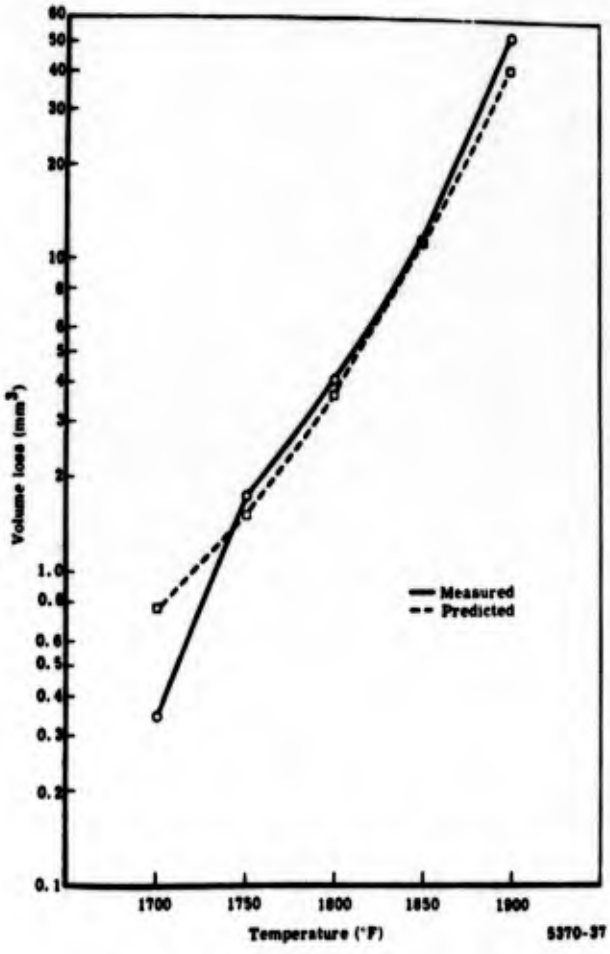

Figure 36.9. Comparison of the measured volume loss and the loss predicted by the regression equation for PDRL 163. (Ryan et al).

RA 333

R. Viswanathan, Corrosion 24 (1968) 359.

See 713C for details. Ra 333 was one of the better alloys tested, similar to PDRL 163 and Waspaloy. After 150h testing at 1500°F (816°C) the specimen had lost 2.0 mg/cm^2 (after descaling); 97.7% of the alloy was unaffected.

F. J. Wall and S. T. Michael, Hot Corrosion Problems Associated with Gas Turbines ASTM Special Technical Publication STP 421, 1967, 223.

See 713C for an extended summary. Several commercial alloys were tested by coating with 50% Na_2SO_4/50% $MgSO_4$ and oxidising in a simulated combustion atmosphere at 1250, 1350 and 1450°F (677, 732 and 788°C) for times up to 1000h. The alloys are identified only by number and approximate composition, but No. 3 appears to be Ra 333. Its corrosion resistance is rated as "excellent", the best of the nickel-base alloys tested, on the basis of a 100h test at 1450°F. Figure 37.1 shows the kinetics of the corrosion: the attack is less at 1450°F than at the two lower temperatures.

S. K. Rhee and A. R. Spencer, Oxid. Metals 7 (1973) 71.

An extension of a programme to select material for porous, transpiration cooled blades (F.W. Cole, J. B. Padden and A. R. Spencer, NASA CR-930, Feb. 1968). Oxidation kinetics studied at 760 - 1100°C. Sheet specimens annealed at 1150°C for 8h in dry hydrogen, polished to 320 grit silicon carbide. Oxidation times up to 600h in static air; all specimens removed at 4, 16, 64, 100, 200, 300, 400, 500 and 600h; one specimen removed at each cycle for examination. Weight gain increased parabolically.

T°C	Rate constant $g^2 cm^{-4} s^{-1}$
760	3.73×10^{-14}
870	2.99×10^{-13}
982	2.70×10^{-12}
1093	1.56×10^{-11}

Activation energy = 51 kcals/mole

These are very similar to those previously reported for Hastelloy X (J. Electrochem. Soc., 119 (1972) 396). Cr_2O_3 was the principal oxide; brown islands of spinel were also observed.

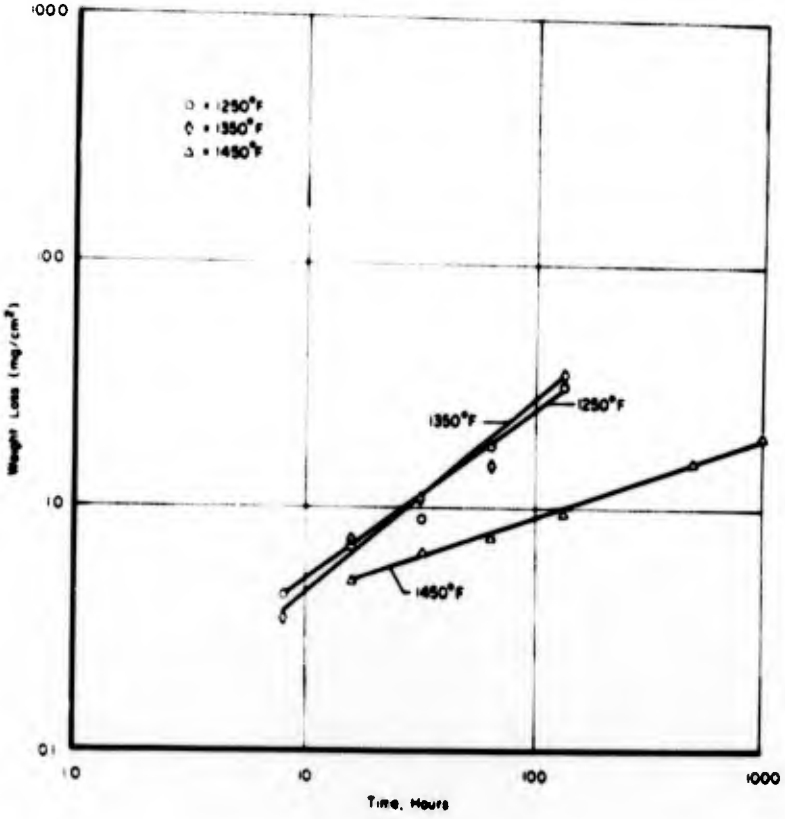

Figure 37.1. Weight loss of Ni-25 Cr alloy after exposure to 1250, 1350, and 1450 F. (Wall and Michael).

Rene 41

R. Field, D. J. Fisk and H. von E. Doering, Naval Ship Research and Development Centre Materials Laboratory Research and Development Report 2833 (January 1969).

See 713C.

V. S. Moore and A. R. Stetson, Final Report on NASC Contract No. N00019-68-C-0532 (Solar Research Division Report RDR -1626-5) December 1970.

See B 1900 for details. Figure 38.1 shows a cross section of a specimen tested for 150h at 1650°F. Rene 41 was one of the better alloys tested, nearly as good as U700 and appreciably better than 713C.

The cumulative weight changes of two specimens tested at 1650°F were:

Weight change, mg.	Spec. 1.	+3.3	+3.7	+ 3.4	+8.0	+3.4	-4.3	-6.3	-4.7	-8.2	-8.0	-6.7	-7.6	-9.3
	Spec. 2.	+2.6	+2.5	+2.7	+7.9	+1.0	-8.2	-10.3	-10.1	-10.4	-9.7	-9.3	-8.4	-11.4
Exposure time, hours		10	20	30	40	50	60	70	80	90	100	110	120	150

Two specimens were also tested at 1800°F:

Exposure time, hours	10	20	30	40	50		70	80
weight change, mg. Spec.1.	-	-16.9	-	-39.0	-55.0		-77.8	-
Spec.2.	-	-16.4	-	-37.0	-52.4		-53.0	-

W. L. Wheatfall, in "High Temperature Corrosion of Aerospace Alloys" J. Stringer, R.I.Jaffee and T.F. Kearns, (eds.) AGARD Conference Proceedings No.120, (March 1973) 235.

See 713C for details

S.T. Wlodek Trans. AIME, 230 (1964) 1078

Continuous weight gain measurements in dry air on specimens ground to 600 grit, electropolished, and lightly etched. Figure 38.2 shows the weight gain data, and Figure 38.3 is the initial linear section. Figure 38.4 is the later parabolic section, and Figure 38.5 is an Arrhenius plot of both the parabolic and linear rate constants. Figure 38.6 is a transmission electron micrograph of a thinoxide film stripped from Rene 41 oxidised for 10 min. at 1600°F (871°C), showing Al_2O_3 growing over the bulk of the grains, but Cr_2O_3 forming at the grain boundaries. Table 38-I lists the phases in the scale. Figure 38-7 shows the alloy depleted layer and the internal oxidation after 100h at 1800°F(982°C) and Figure 38-8 shows that both the internal oxidation and the depleted layer thickness grows in a parabolic fashion. Figure 38-9 is a schematic presentation of the time and temperature conditions required to produce 1.0 mil per side of internal oxidation and 1,2,3 and 4 mils per side of alloy depletion. TiN and Al_2O_3 were identifiedin the internal oxidation and alloy depleted regions.

Figure 38-10 shows the effect of surface preparation on the oxidation of Rene 41. Pronounced surface working increases the amount of subscale oxidation at 1600°F (871°C) and 100h exposure.

Figure 38-11 is a schematic presentation of the major reaction products in the oxidation of Rene 41.

D.M. Royster and W.B. Lisagor. "Effect of High-Temperature Creep and Oxidation on Residual Room-Temperature Properties for Several Thin-Sheet Superalloys" N A S A Technical Note TN D-6893 (November 1972)

This programme is related to primary heat shields and supports in hypersonic aircraft and space shuttle vehicles. Continuous oxidation tests were performed in dry air at 1.0664 kN/m² (8 Torr) in a vertical tube furnace at 1033 and 1256K (760 and 983°C., 1400 and 1800°F). Specimens were exposed for preselected times up to 5000h removed and weighed. Cyclic tests were made in dry air at 0.1333 kN/m² (1 Torr); specimens were left 30 min.at temperature, air cooled to ambient, then cooled to 220K (-53°C,-65°F.) with dry nitrogen, allowed to return to room temperature for 30 minutes. This cycle was repeated until a total time at temperature of 100h had been accumulated.

The microstructures of Rene41 after 100h at 983°C.Haynes 188 after 1000h at 983°C and TD NiCr after 200h at 1205°C in air at 760 torr are shown in Figure 38.12; Figure 38.13 shows sections of specimens exposed at 760°C. Figure 38.14 shows the continuous oxidation results as time to a sheet thickness loss of 0.0508 m.m. which is regarded as the maximum permissible. TD NiCr was very much better than any of the other alloys: Rene 41 was relatively poor. Figure 38.15 shows the sheet thickness loss in continuous cyclic tests at 1256 K(983°C) maximum temperature,100h total time at temperature: again Rene 41 is relatively poor. The results of all the oxidation tests are listed in Table 38-I and II

Data relating to this alloy will also be found in the following figures:

10.51, 10.123, 10.124; and Tables 1 - $\underline{\underline{X}}$, 10 - $\underline{\underline{XXX}}$, 18 - $\underline{\underline{IV}}$

TABLE 38-I

SHEET-THICKNESS LOSS RESULTING FROM OXIDATION OF SPECIMENS EXPOSED CONTINUOUSLY IN AIR PRESSURE OF 1.0664 kN/m^2 (8 torr) (ROYSTER AND LISAGOR)

(a) SI Units (sheet-thickness loss in mm)

Alloy	Sheet thickness, mm	Exposure in hours								
		50	100	200	400	650	1000	2000	3500	5000
Temperature = 1256 K										
René 41	0.254	0.0508	0.0635	0.0787	0.0864	0.1017	0.1170	(a)	(a)	(a)
	.508	.0457	.0610	.0736	.0888	.1017	.1244	0.1830	(a)	(a)
Hastelloy X	.254	.0178	.0254	.0304	.0279	.0330	.0585	(a)	(a)	(a)
	.508	.0152	.0203	.0304	.0254	.0329	.0508	.0584	0.0940	(a)
Inconel 625	.254	.0127	.0152	.0203	.0228	.0304	.0864	.0432	(a)	(a)
	.508	.0127	.0178	.0279	.0304	.0330	.0890	.0457	.0559	0.0711
Inconel 718	.254	.0279	.0406	.0533	.0660	.0761	.0432	.1041	(a)	(a)
	.508	.0279	.0304	.0533	.0610	.0811	.0559	.0889	.1193	.1450
Haynes 25	.254	.0178	.0228	.0304	.0254	.0356	.0534	.0559	(a)	(a)
	.508	.0203	.0279	.0304	.0304	.0482	.0660	.0838	.0965	.7870
Haynes 188	.254	.0127	.0203	.0355	.0508	.0660	.0761	.0889	.0990	(a)
	.508	.0152	.0228	.0406	.0482	.0610	.0635	.0685	.0813	.1017
TD NiCr	.254	(b)	(b)	(b)	(b)	(b)	(b)	(b)	(b)	(b)
	.508	(b)	(b)	(b)	(b)	(b)	(b)	(b)	(b)	(b)
Temperature = 1033 K										
René 41	0.254	(b)	(b)	(b)	(b)	(b)	0.0076	0.0107	0.0178	0.0228
	.508	(b)	(b)	(b)	(b)	(b)	.0076	.0076	.0152	.0203
Hastelloy X	.254	(b)	(b)	(b)	(b)	(b)	.0076	.0076	.0152	.0107
	.508	(b)	(b)	(b)	(b)	(b)	.0076	.0076	.0152	.0076
Inconel 625	.254	(b)	(b)	(b)	(b)	(b)	.0076	.0076	.0152	.0076
	.508	(b)	(b)	(b)	(b)	(b)	.0076	.0076	.0152	.0076
Inconel 718	.254	(b)	(b)	(b)	(b)	(b)	.0076	.0076	.0076	.0076
	.508	(b)	(b)	(b)	(b)	(b)	.0076	.0076	(b)	.0076
Haynes 25	.254	(b)	(b)	(b)	(b)	(b)	.0076	.0051	.0107	.0107
	.508	(b)	(b)	(b)	(b)	(b)	.0076	(b)	.0127	.0127
Haynes 188	.254	(b)	(b)	0.0076	0.0076	0.0076	(c)	(c)	(c)	(c)
	.508	(b)	(b)	.0076	.0076	.0107	(c)	(c)	(c)	(c)
TD NiCr	.254	(b)	(b)	(b)	(b)	(b)	(b)	(b)	(b)	(b)
	.508	(b)	(b)	(b)	(b)	(b)	(b)	(b)	(b)	(b)

[a] Oxidation penetrates entire cross section.
[b] No measurable sheet-thickness loss.
[c] Data not obtained.

(b) U.S. Customary Units (sheet-thickness loss in inches)

Alloy	Sheet thickness, in.	Exposure in hours								
		50	100	200	400	650	1000	2000	3500	5000
Temperature = 1800° F										
René 41	0.010	0.0020	0.0025	0.0031	0.0034	0.0040	0.0046	(a)	(a)	(a)
	.020	.0018	.0024	.0029	.0035	.0040	.0049	0.0072	(a)	(a)
Hastelloy X	.010	.0007	.0010	.0012	.0011	.0013	.0023	(a)	(a)	(a)
	.020	.0006	.0008	.0012	.0010	.0013	.0020	.0023	0.0037	(a)
Inconel 625	.010	.0005	.0006	.0008	.0009	.0012	.0034	.0017	(a)	(a)
	.020	.0005	.0007	.0011	.0012	.0013	.0035	.0018	.0022	0.0028
Inconel 718	.010	.0011	.0016	.0021	.0026	.0030	.0017	.0041	(a)	(a)
	.020	.0011	.0012	.0021	.0024	.0032	.0022	.0035	.0047	.0057
Haynes 25	.010	.0007	.0009	.0012	.0010	.0014	.0021	.0022	(a)	(a)
	.020	.0008	.0011	.0012	.0012	.0019	.0026	.0033	.0038	.0310
Haynes 188	.010	.0005	.0008	.0014	.0020	.0026	.0030	.0035	.0039	(a)
	.020	.0006	.0009	.0016	.0019	.0024	.0025	.0027	.0032	.0040
TD NiCr	.010	(b)	(b)	(b)	(b)	(b)	(b)	(b)	(b)	(b)
	.020	(b)	(b)	(b)	(b)	(b)	(b)	(b)	(b)	(b)
Temperature = 1400° F										
René 41	0.010	(b)	(b)	(b)	(b)	(b)	0.0003	0.0004	0.0007	0.0009
	.020	(b)	(b)	(b)	(b)	(b)	.0003	.0003	.0006	.0008
Hastelloy X	.010	(b)	(b)	(b)	(b)	(b)	.0003	.0003	.0006	.0004
	.020	(b)	(b)	(b)	(b)	(b)	.0003	.0003	.0006	.0008
Inconel 625	.010	(b)	(b)	(b)	(b)	(b)	.0003	.0003	.0006	.0003
	.020	(b)	(b)	(b)	(b)	(b)	.0003	.0003	.0006	.0003
Inconel 718	.010	(b)	(b)	(b)	(b)	(b)	.0003	.0003	.0003	.0003
	.020	(b)	(b)	(b)	(b)	(b)	.0003	.0003	2.0000	.0003
Haynes 25	.010	(b)	(b)	(b)	(b)	(b)	.0003	.0002	.0004	.0004
	.020	(b)	(b)	(b)	(b)	(b)	.0003	(b)	.0005	.0006
Haynes 188	.010	(b)	(b)	0.0003	0.0003	0.0003	(c)	(c)	(c)	(c)
	.020	(b)	(b)	.0003	.0003	.0004	(c)	(c)	(c)	(c)
TD NiCr	.010	(b)	(b)	(b)	(b)	(b)	(b)	(b)	(b)	(b)
	.020	(b)	(b)	(b)	(b)	(b)	(b)	(b)	(b)	(b)

[a] Oxidation penetrates entire cross section.
[b] No measurable sheet-thickness loss.
[c] Data not obtained.

TABLE 38-II.

SHEET-THICKNESS LOSS RESULTING FROM OXIDATION OF SPECIMENS EXPOSED CYCLICALLY AND CONTINUOUSLY IN AIR PRESSURE OF 0.1333 kN/m^2 (1 torr) AT 1256 K (1800°F)

(ROYSTER AND LISAGOR)

(a) SI Units (sheet-thickness loss in mm)

Alloy	Sheet thickness, mm	Exposure in hours						
		10	25	50	100	25	50	100
		Number of cycles				(Continuous exposure)		
		20	50	100	200			
René 41	0.254	0.0356	0.0457	0.0533	0.0635	0.0406	0.0508	0.0610
	.508	.0330	.0457	.0533	.0710	.0406	.0508	.0585
Hastelloy X	.254	(a)	(a)	(a)	.0152	(a)	.0152	.0178
	.508	(a)	(a)	(a)	.0120	(a)	(a)	.0203
Haynes 25	.254	(a)	.0228	.0254	.0356	(a)	.0228	.0254
	.508	(a)	.0178	.0356	.0406	(a)	.0279	.0305
Haynes 188	.254	(a)	(a)	.0228	.0305	(a)	.0203	.0178
	.508	(a)	(a)	.0203	.0305	(a)	.0178	.0228
TD NiCr	.254	(a)	(a)	(a)	(a)	(a)	(a)	(a)
	.508	(a)	(a)	(a)	(a)	(a)	(a)	(a)

Alloy	Sheet thickness, in.	Exposure in hours						
		10	25	50	100	25	50	100
		Number of cycles				(Continuous exposure)		
		20	50	100	200			
René 41	0.010	0.0014	0.0018	0.0021	0.0025	0.0016	0.0020	0.0024
	.020	.0013	.0018	.0021	.0028	.0016	.0020	.0023
Hastelloy X	.010	(a)	(a)	(a)	.0006	(a)	.0006	.0007
	.020	(a)	(a)	(a)	.0005	(a)	(a)	.0008
Haynes 25	.010	(a)	.0009	.0010	.0014	(a)	.0009	.0010
	.020	(a)	.0007	.0014	.0016	(a)	.0011	.0012
Haynes 188	.010	(a)	(a)	.0009	.0012	(a)	.0006	.0007
	.020	(a)	(a)	.0008	.0012	(a)	.0007	.0009
TD NiCr	.010	(a)	(a)	(a)	(a)	(a)	(a)	(a)
	.020	(a)	(a)	(a)	(a)	(a)	(a)	(a)

[a] No measurable sheet-thickness loss.

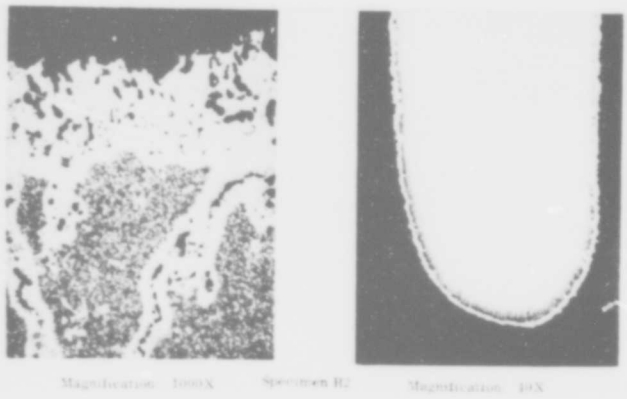

Figure 38.1. Microstructure of uncoated Rene 41 after hot corrosion tests at 1650°F for 150 hours. (Moore and Stetson).

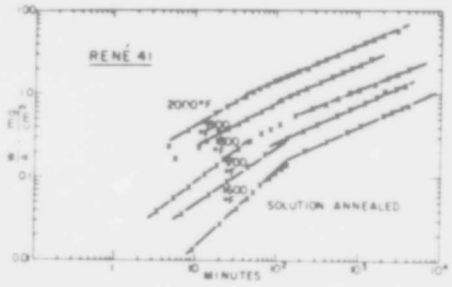

Figure 38.2. Log-log plot of weight gain against time for the oxidation of Rene 41. Note initial linear rate (slope = 1) at 1600°, 1700°, and 1800°F followed, and at higher temperatures replaced, by parabolic oxidation (slope = $\frac{1}{2}$). All data for Heat A. (Wlodek).

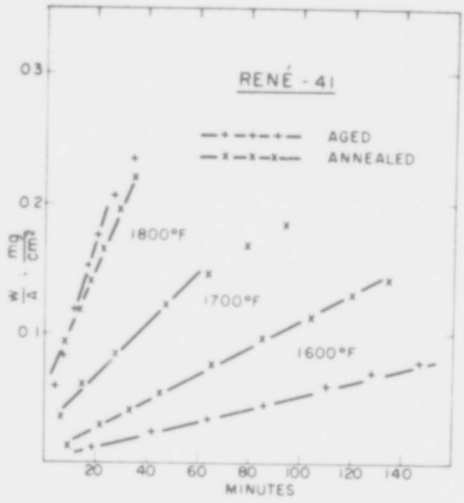

Figure 38.3. Linear oxidation of Rene 41 for specimens in the aged or annealed condition. All data for Heat A. (Wlodek).

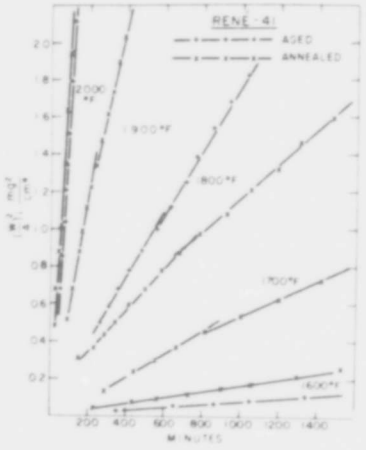

Figure 38.4. Parabolic oxidation kinetics as exhibited by Heat A of Rene 41. Note presence of two rate constants at 1700°, 1800°, 1900°, and 2000°F. (Wlodek).

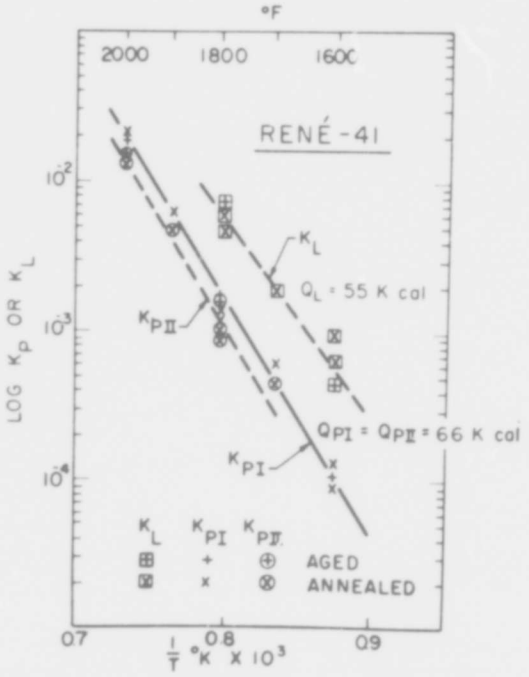

Figure 38.5. Arrhenius plot of the linear and parabolic rate constants observed for Rene 41 (Heats A and B) initially in the aged or solution-annealed condition. Activation energies of 66 kcal per mole can be ascribed to either parabolic rate, while the linear rate constants reflect an activation energy of 55 kcal per mole. (Wlodek).

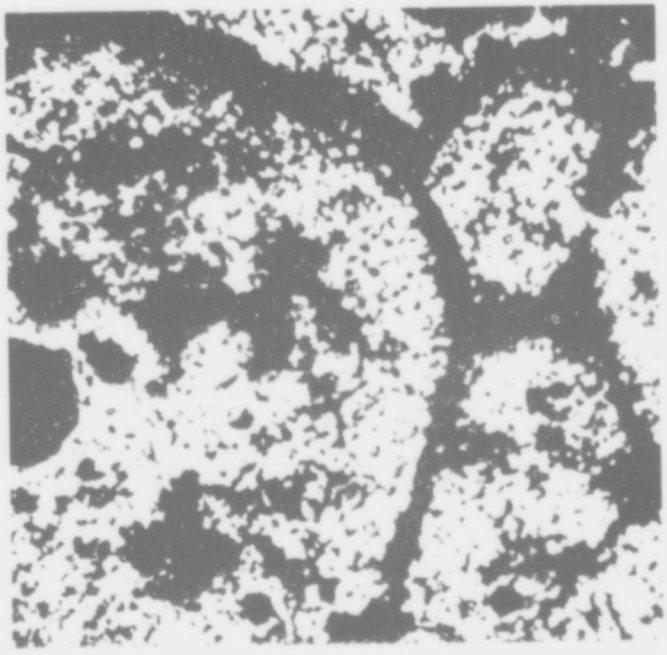

Figure 38.6. Oxide film stripped from Rene 41 oxidized 10 min at 1600°F as viewed directly in the electron microscope, X4000. Transmission electron diffraction identified the thin, continuous oxide as α Al_2O_3 and the dark, thicker overgrowth along grain boundaries as Cr_2O_3. Enlarged approximately 39% for reproduction. (Wlodek).

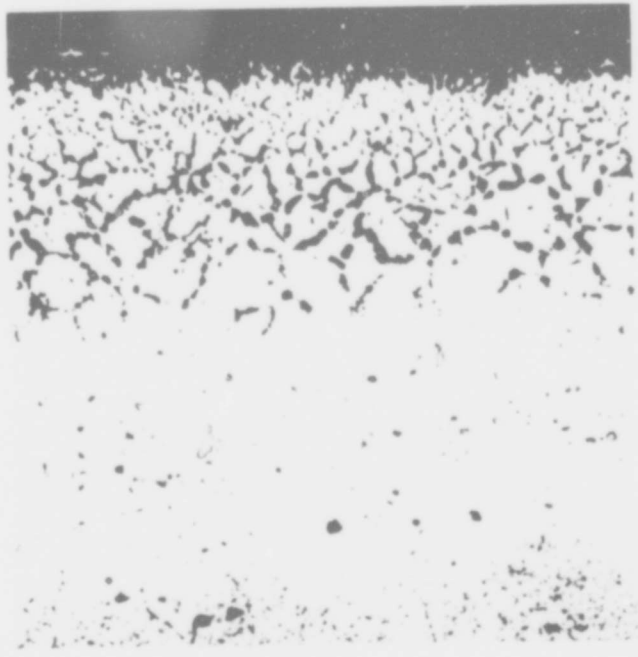

Figure 38.7. Subscale oxidation in Rene 41 after 100 hr at 1800°F. Scale (top) not continuous with internally oxidized zone. Note acicular constituent in alloy-depleted region immediately above unaffected base alloy (bottom). Etched in mixed acids. Taper X4. Magnification X250. Enlarged approximately 44% for reproduction. (Wlodek).

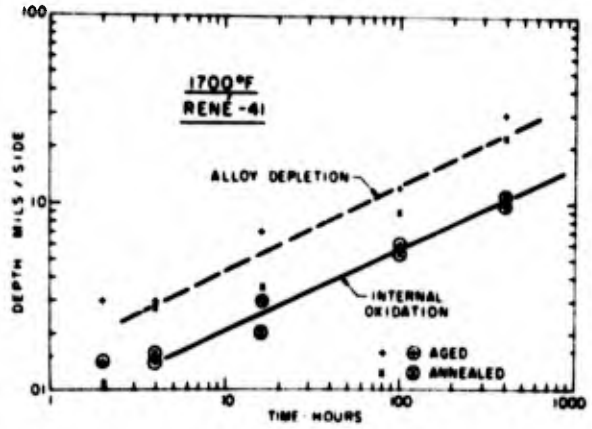

Figure 38.8. Parabolic nature of alloy-depletion and internal-oxidation processes for Rene 41 revealed by slope of logarithmic plot for these processes at 1700°F. (Wlodek).

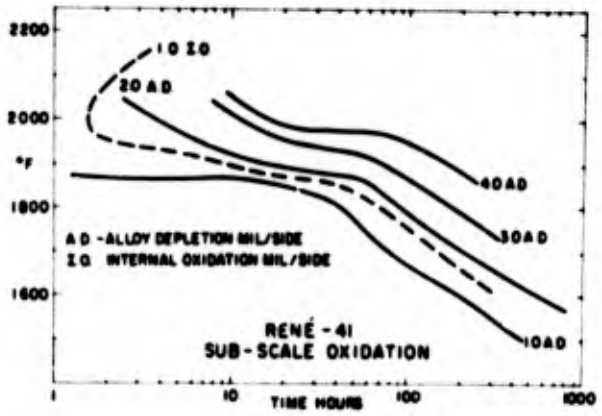

Figure 38.9. Qualitative portrayal of time and temperature conditions required to produce 1.0 mil per side of internal oxidation and 1, 2, 3, and 4 mils per side of alloy depletion of Rene 41. (Wlodek).

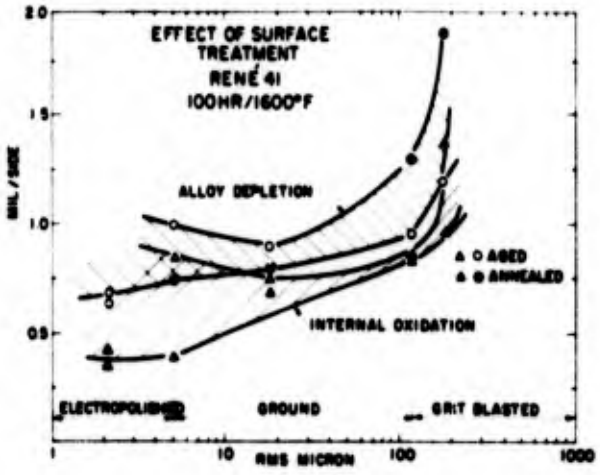

Figure 38.10. Effect of surface preparation: electropolishing, mechanical polishing, fine and coarse grinding, and grit blasting plotted in terms of rms of the resultant surface finish. Pronounced surface working increases the amount of subscale oxidation for Rene 41 at 1600°F and 100 hr exposure. (Wlodek).

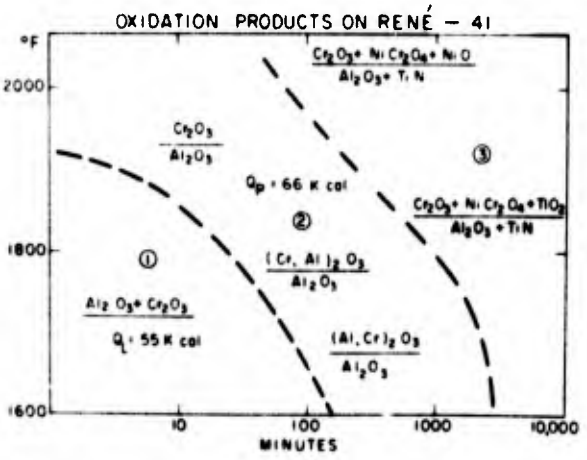

Figure 38.11. Schematic presentation of the major reaction products that can form during the oxidation of Rene 41 and the associated kinetic regions: 1, linear; 2 and 3, parabolic. The phases present in the numerator are the scale constituents, those in the denominator are the products of internal oxidation. (Wlodek).

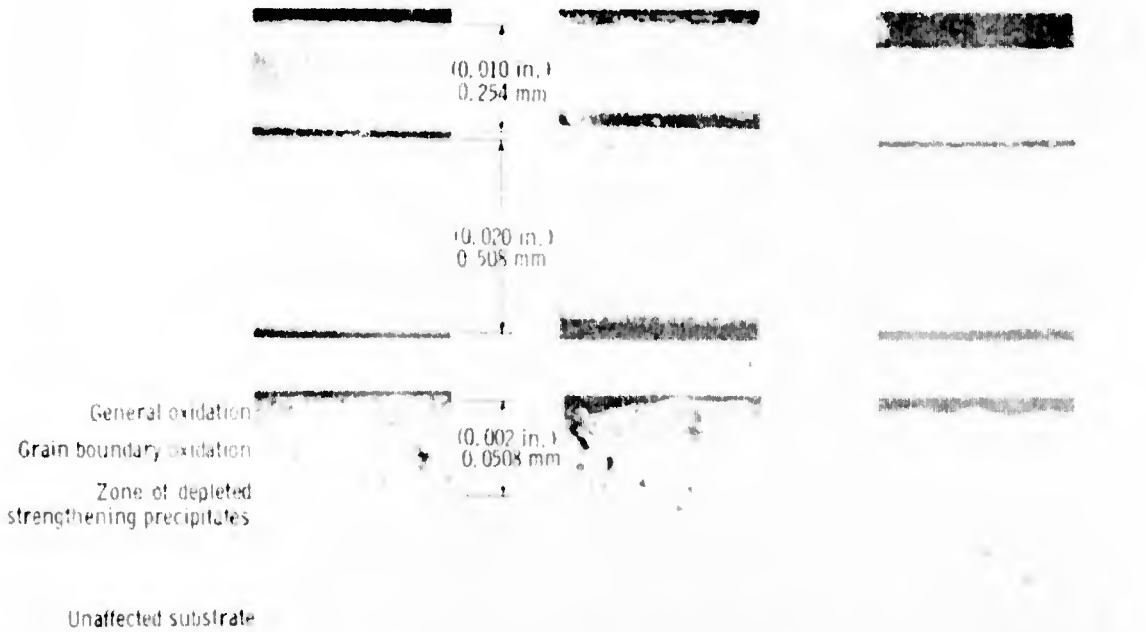

Figure 2.- Microstructure of oxidation specimens after exposure.

Figure 38.12. Microstructure of oxidation specimens after exposure. (Royster and Lisagor).

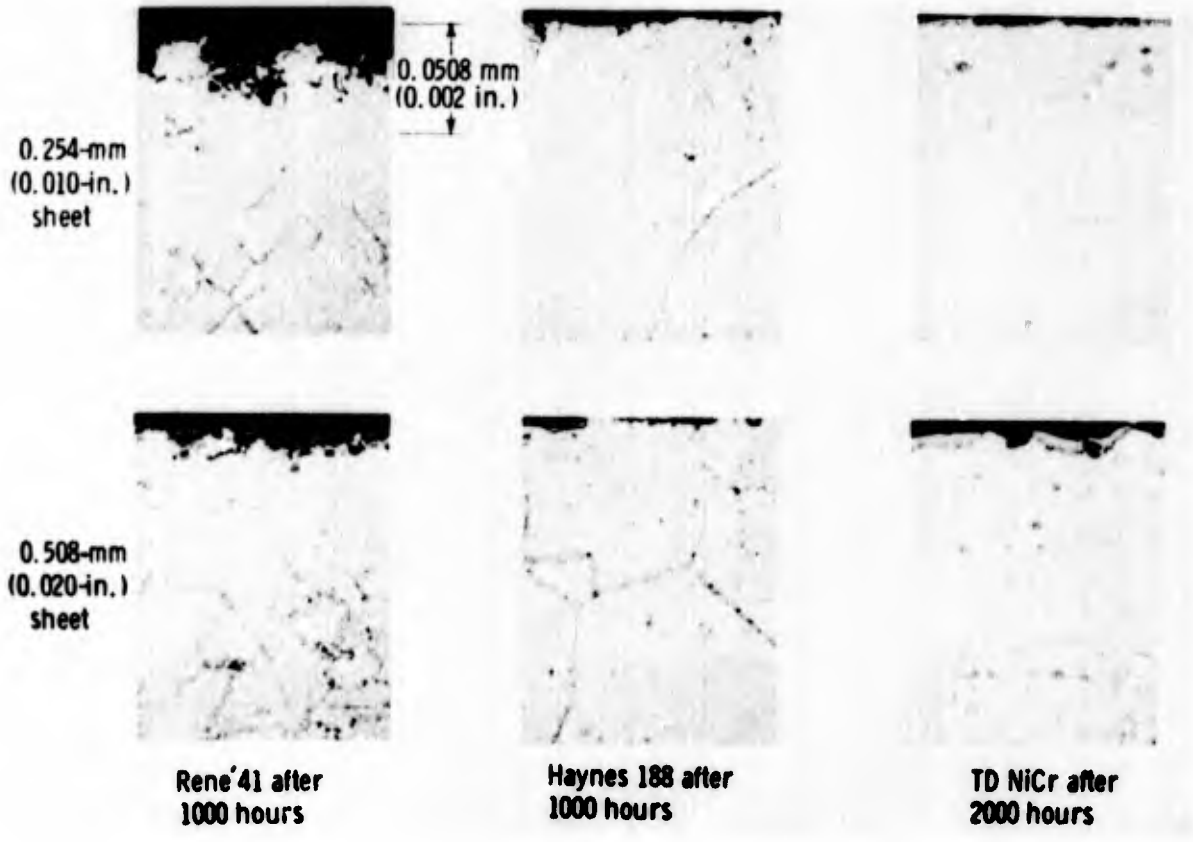

Figure 38.13. Microstructure of oxidation specimens after exposure at 1033K (1400°F), 1.0664 kN/m² (8 torr). (Royster and Lisagor).

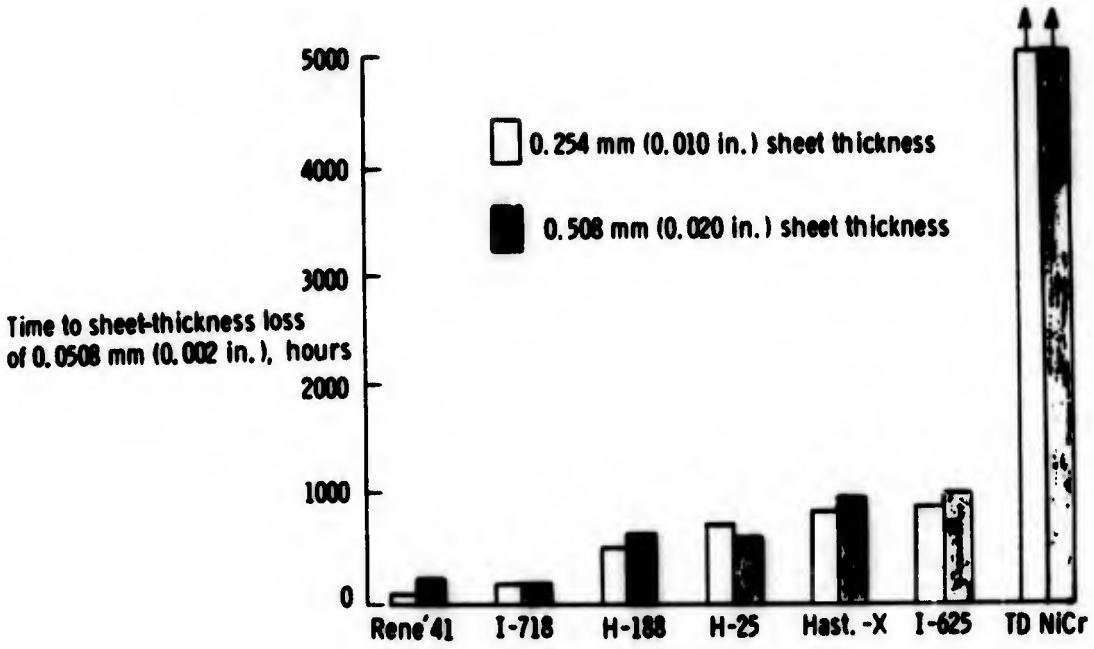

Figure 38.14. Continuous oxidation tests at 1256 K (1800°F) and 1.0664 kN/m^2 (8 torr). (Royster and Lisagor).

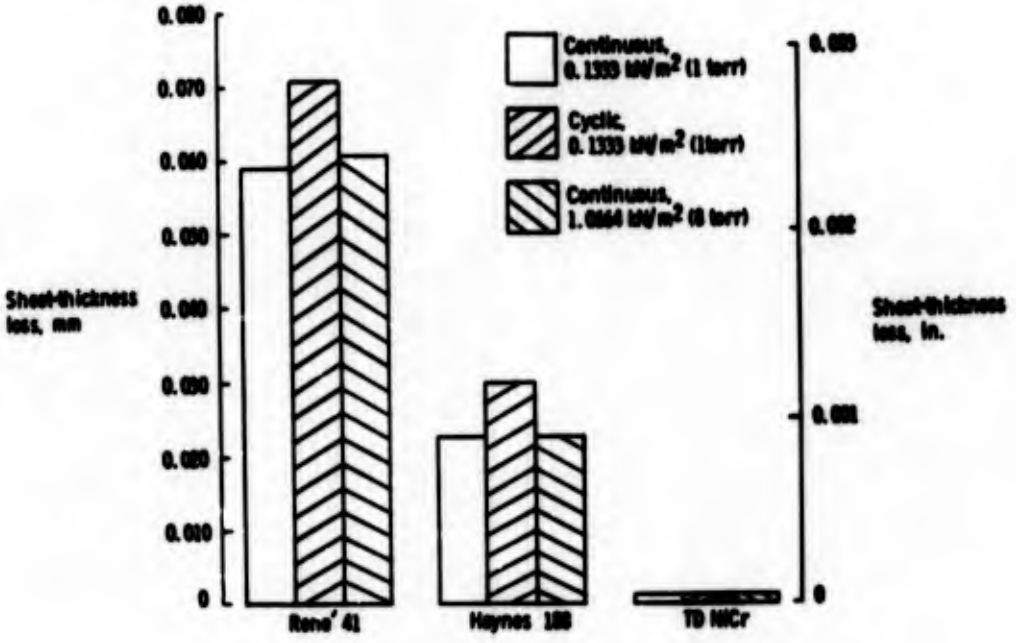

Figure 38.15. Results of 100-hour cumulative exposure at 1256K (1800°F) on 0.508 mm (0.020 in.) thick oxidation specimens subjected to continuous and half-hour cyclic exposures. (Royster and Lisagor).

Rene 80

I.I. Bessen and R.E. Fryxell, General Electric Technical Information Series Report No. R72 AEG 317 (Nov. 1972). Paper presented at Gas Turbine Materials Conference, Naval Ship Engineering Center (Oct. 1972). 73.

After a general discussion of corrosion of coated alloys in shipboard turbines, the importance of the deposition of Na_2SO_4 and the possible role of the presence of a reducing agent in the form of carbon deposits is emphasized. Experiments were conducted with sodium sulphate in air, argon, or in argon with a carbon deposit, using either half-immersed pins in a crucible test at 1650°F (899°C) or dip-coated specimens, coated at 1650°F and then exposed at 1400 or 1500°F (760 or 816°C) (i.e. the salt coating was solid during the exposure). Table 39-I lists the results for U 500, Rene 77, Rene 80 and IN 738; the accelerating effect of the reducing environment on the depth of penetration of the corrosion is apparent. Analysis of the salt showed the presence of Na_2S excess in the salts in the reducing environments, as high as 1.8 mole % in the argon + carbon experiments. Figure 39-I shows flame tunnel data for Rene 80 and Rene 77, confirming the relative order found in the crucible tests, and the authors comment that this is also consistent with shipboard experience: Figure 39.2 shows the penetration of blades in a LM 2500 engine, both coated with BC 21 coating, and run in the same engine for 3600h: the coating thickness ranged from 0.001 to 0.0035 in to allow penetration at different times.

The authors also report that a T58 helicopter engine ingests large and variable amounts of salt and particulates in Navy service. In a 146h Navy engine test with 250 ppb (parts per billion) sea salt using JP-5R fuel, an aluminide-coated 713 nozzle showed some corrosion blistering and attack to the base metal. A cobalt-base X-40 vane included in the test was not corroded. Aluminide coated blades of SEL and Rene 80 were compared, the latter being slightly more resistant. Again, this ranking corroborated flame-tunnel tests.

TABLE 39-I

EFFECT OF REDUCING ENVIRONMENT IN Na_2SO_4 HOT CORROSION (BESSON AND FRYXELL)

Alloy	Temperature °F	Hours	Maximum Affected Depth, mils		
			Air	Argon	Argon + Carbon
U500	1400	500		0.4	6.9
Rene' 77	1400	500		0.5	7.8
U500	1500	500		2.4	>5.4
Rene' 77	1500	285		1.0	>7.0
Rene' 80	1500	500		2.2	>4.7
U500	1650	100	0.7	>20.	53.
Rene' 77	1650	72	32.		66.
Rene' 80	1650	100	2.1	>15.	36.
Inco 738	1650	100	1.0		19.

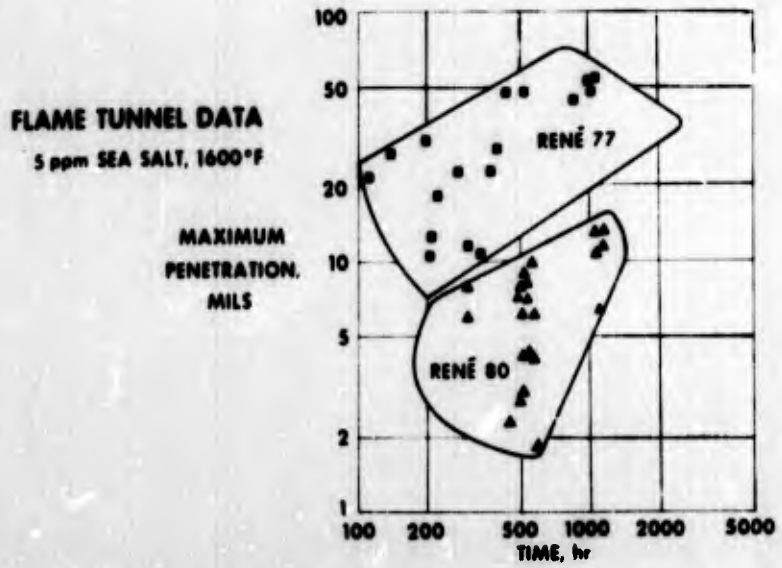

Figure 39.1. Flame tunnel data for Rene 77 and Rene 80 at 1600 F (871°C) with 5 ppm sea salt (Bessen and Fryxell).

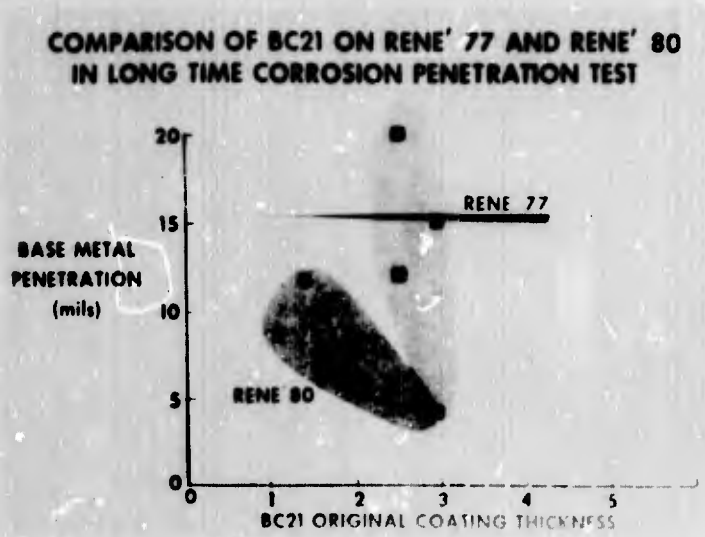

Figure 39.2.

S 816

B.O. Buckland , A.D. Foster and J.J. Treanor, presented at National Association of Corrosion Engineers, Annual Meeting (April 21, 1966) Miami, Florida.

See U-500 for a summary of the paper. S 81 seems rather poorer than the other alloys (X-45, U 500, M252). Several parts from actual engines were examined; of which the following were of S 816.

Bucket B4 from turbine operating on crude oil, removed after 15,000h operation; shutdown on average 0.4 times every 100h. Calculated metal temperature was 1330°F (721°C) and the corrosion was 6 mils, which is what would be expected in this time at a temperature of 1560°F (849°C) on the basis of the small burner tests.

Bucket B9: residual oil, 13,000h. 29 shutdowns per 100h, 1280°F (693°C), 4 mils, 1530°F (832°C).

Bucket B10: crude oil, 7,000h, 0.4 shutdowns per 100h. 1320°F (716°C), 4 mils, 1580°F (860°C).

A.M. Beltran, Cobalt, No. 46, 1970, 3.

See X-40 for details. The oxidation resistance of a number of Co-base alloys at 1600, 1800 and 2000°F (871, 982 and 1093°C) is compared. S-816 is worst of those tested (differences not very great). In a burner rig test using 3% S residual oil containing 325 ppm NaCl (= 5 ppm salt in the air), 600h tests at 1600°F (871°C), the maximum penetration for S 816 was 0.06 mm per side, which is quite good, better than Mar-M 509, nearly as good as FSX 414.

Data relating to this alloy will also be found in Tables 45.I, 45.II and 45.III.

SEL

P.A. Bergman, C.T. Sims and A.N. Beltran, Hot Corrosion Problems Associated with Gas Turbines; ASTM Special Technical Publication, STP 421, 1967, 38.

See 713C for details. Attack at 1750°F (954°C) in burner rig, 100h, 200 ppm salt produced a surface loss of about 44 mils (on diameter) and a maximum penetration of about 66 mils. At 1600°F (871°C) there was very little attack. At 1900°F (1039°C) the attack was again less than that at 1750°F: surface loss was about 15 mils, maximum penetration was about 34 mils. Some scatter in results at 1750F, because two specimens had deep but localised attack. Range of maximum penetration was 34 - 115 mils in 7 tests.

R.W. Hardt, J.R. Gambino and P.A. Bergman, Hot Corrosion Problems Associated with Gas Turbines: ASTM Special Technical Publication, STP 421, 1967, 65.

Presents bar diagrams to show attack at 915 and 955°C, 1040°C, in burner rig, 200 ppm salt, 100h tests. Loss in diameter due to (a) surface loss; (b) maximum penetration. 915°C: (a) 2 mils; (b) 15 mils; 955°C: (a) 20 mils; (b) 30 mils. 1040°C: (a) 18 mils; (b) 33 mils.

Oxides formed: 915°C: a little Cr_2O_3, a little NiO: mainly a spinel with spacing 8.26 Å.

1040°C: In one case, moderate NiO, moderate spinel 8.22 A. In a second case, moderate CoO, (Ni, Cr)O, moderate spinel 8.33 A.

P.A. Bergman, Corrosion 23 (1967) 72.

Tested alloys in low velocity, low pressure burner rig - early version of G.E. small burner rig. J.P.-5 referee fuel with 0.25 wt % S, air/fuel ratio 30/1. Sea salt (both natural and synthetic) sprayed in aqueous solution into air, maximum 200 ppm. All tests 50h. Specimens cylindrical pins 0.8 in long by 0.125 in diameter. Metallographic evaluation used principally: author felt that weight loss measurements could be highly misleading. Figure 41.1 shows the loss in diameter for 713, SEL, SEL-15, and X-40 for tests on the temperature range 1600 - 2000F (871 - 1093°C) with 0 and 2 ppm salt: Figure 41.2 shows the loss in diameter for these four alloys and IN-100, Hastelloy X, K2 and L605, tested at 200 ppm salt. At the lower salt concentrations, the attack on all four alloys was slight: SEL-15 was a little poorer than the others, but the remainder showed no differences at all. The attack at 200 ppm salt was much greater: SEL was relatively poor, the attack reaching a maximum at about 1020°C. 713 was rather worse, particularly at 920°C, and SEL-15 IN-100 and (at 1020°C) L605 were very much worse.

All the nickel-base alloys studies at 913 - 1093°C with 200 ppm salt formed nickel oxide and spinels with lattice parameters in the range 8.16 - 8.34 Å and usually in the range 8.28 - 8.34 Å; these latter were identified as $NiCr_2O_4$. Figure 41.3 shows a cross-section of a SEL specimen (200 ppm salt: test temperature not given) showing severe grain boundary attack and penetration of small globular particles along the grain boundaries. At high salt and sulphur concentrations (200 ppm salt, 0.25% S) large grey phases and golden coloured areas were apparent in the depleted zones in the metal beneath the scale/metal interface. Figure 41.4 shows such a structure produced at 913°C: for comparison, Figure 41.5 shows a specimen tested with no sea salt present. Table 41-I contains the electron microprobe analysis of these two structures. For the oxidised specimen, the outer oxide was chromium and titanium rich. The subsurface oxide was aluminium and molybdenum rich, and in the metal near the surface there was an increase in nickel and cobalt and a decrease in chromium, aluminium, titanium and molybdenum. In the corroded specimen the grey phases appeared to be essentially chromium-rich M_2S_3 sulphides, with the angular phase being $(Cr, Co, Ni, Mo, Al)_2S_3$ and the globular phase being $(Cr, Co, Ni)_2S_3$. The gold-coloured area (appearing light-grey in the micfographs) was predominantly nickel sulphide containing some cobalt: apparently the eutectic of Ni_3S_2 and Ni. The affected zone between the sulphides and the surface was depleted of all titanium, some aluminium and most of the chromium. Nickel was considerably higher, molybdenum slightly lower, and cobalt lower than the matrix.

200 ppm NaOH gave effects similar to sea salt at 913 and 982°C. So did LiOH: at 1675F and 1800F (913 and 982°C) a deposit of Li_2SO_4 was formed which led to severe hot corrosion. $CaSO_4$ was not noticeably aggresive however. The hot corrosion at three sulphur levels, 88, 2.0 and 0.07 ppm with 200 ppm sea salt or NaCl was determined, the sulphur being the total in the fuel and the salt. The results for four alloys, including SEL at 913 and 982°C are shown in Figures 41.6 and 41.7. Also included are the results for 83 ppm sulphur and no salt: the rate of attack on all the alloys is very small.

A.U. Seybolt, AIME, 242 (1968) 1955.

Reports analysis of sulphides formed during corrosion of SEL in a "burner rig" (presumably the G.E. small burner rig) for 100h at 1000 - 1750°F (871 - 955°C) burning jet fuel with injected sea salt. Some sulphide particles were as large as 30 μm. The results for three samples are shown below:

	Temp. °F	S	Ni	Cr,	Co(all at %)	Formula
SEL-1	1750	59.5	3.3	34.2	3.2	$MS_{1.46}$
2	1750	55.6	8.0	34.3	2.1	$MS_{1.62}$
3	1600	60.6	7.6	24.5	7.2	$MS_{1.54}$

H. von E. Doering and P.A. Bergman, Naval Ship Research and Development Centre, Materials Laboratory Research and Development Report No. 2844 (March 1969)

See 713C for details. In a 100h at 1750°F (955°C) with 200 ppm salt the surface loss was 15.9 mils and the maximum penetration 26.4 mils; about the same as L605. rather better than SM 200 and a lot worse than U 500. In a 1000h test with 5 ppm salt the figures were 31.5 and 51.8 mils respectively; again worse than U 500, a little better than 713C.

R. Field, D.J. Fisk and H. von E. Doering, Naval Ship Research and Development Centre, Materials Laboratory, Research and Development Report 2833 (January 1969)

See 713C.

M. Kaufman, Trans. ASM 62 (1969) 590.

1/8 in diameter pins in 3/4 in length, tested in the small burner rig described in the paper by Bergman. JP-5 fuel containing 0.34% S at an air/fuel ratio of 30/1 at atmospheric pressure. 0 or 200 ppm synthetic sea salt in the air. 1/4 - 100h exposure at 1675 and 1800°F (913 and 982°C) and also at 2000°F (1093°C) for the cobalt-base alloys tested. Loss of section and maximum penetration was evaluated metallographically.

Figure 41.8 shows the appearance of SEL, oxidised without salt for 100h at 1675°F; fine oxide fingers penetrate into the metal. Figure 41.9 shows the corrosion of SEL in 200 ppm salt at 1675 and 1800°F as a function of time: after approximately 2h at the higher temperature, the rate becomes linear. This Figure also shows the oxidation rate without salt: the rate becomes linear after approximately 20h at 1675°F, but does not seem to become linear at 1800°F.

Na_2SO_4 was found on every specimen, but NaCl was never detected (by X-ray diffraction). The external scale products in 200 ppm salt tests were determined, some NiO was present at both 1675 and 1800°F, a small amount of Cr_2O_3 and a "high parameter" spinel (a_o = 8.27 - 8.33 Å). In no-salt tests NiO was possibly present in small amounts, together with higher parameter spinel at 1800°F. The subsurface sulphide particles in the 200 ppm salt test were mainly CrS with some Al, Ti and Ni.

W.L. Wheatfall, in "High Temperature Corrosion of Aerospace Alloys" J. Stringer, R.I. Jaffee and T.F. Kearns (eds.), AGARD Conference Proceedings No. 120, (March 1973) 235.

See 713C for details.

Data relating to this alloy will also be found in the following Figures :
10.58, 10.105, 10.106.
and Tables,
10-VIII, 10-XXX.

TABLE 41-I

ELECTRON MICROPROBE RESULTS FOR SEL (BERGMAN)

Test Condition	Fig.No.	Location Area	Composition (w/o)						
			Ni	Co	Cr	Mo	Al	Ti	S
1675 F (913 C)	41.5	1 - Surface oxide			Ti, Cr-rich				
		2 - Metal between oxides	51.0	30.0	8.8	3.7	4.5	0.5	
0 ppm Sea Salt		3 - Sub-surface oxide			Al, Mo-rich				
		4 - Metal	50.3	27.2	11.0	3.9	4.8	1.8	-
		5 - Metal	48.4	26.7	12.8	4.3	5.6	1.7	-
		6 - Base composition	46.0	26.3	15.5	4.3	5.6	1.8	-
1675 F (913 C)	41.4	1 - Large grey angular phase	12.6	4.9	29.4	3.7	3.5	-	46.5
200 ppm Sea Salt		2 - Large grey globular phase	8.8	7.1	37.2	-	-	-	47.0
		3 - Golden-colored phase	71.0	5.7	-	-	-	-	23.5
		4 - Metal	73.1	20.2	0.5	3.7	1.7	-	-
		5 - Metal	76.1	17.1	0.4	3.7	1.9	-	-
		6 - Metal	75.2	20.3	0.4	3.7	1.0	-	-
		7 - Base composition	46.0	26.3	15.5	4.3	5.6	1.8	-

Figure 41.3. An SEL specimen showing a grain boundary penetration of the small globular particles. Marble's Reagent. 500X. (Bergman).

Figure 41.4. An SEL specimen tested at 1675 F (913 C) with a 200 ppm sea salt concentration. Electron microprobe analyses were made in the designated areas as shown in Table 4. Marble's Reagent. 600X. (Bergman).

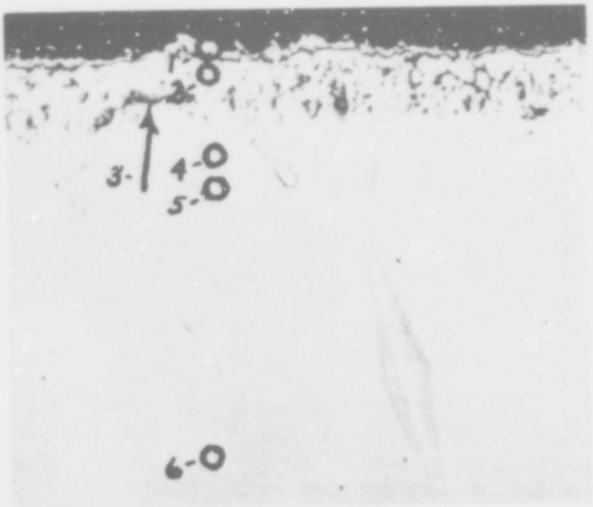

Figure 41.5. An SEL specimen tested at 1675 F (913 C) with no sea salt. Electron microprobe analyses were made in the designated areas. Marble's Reagent. (600X) (Bergman).

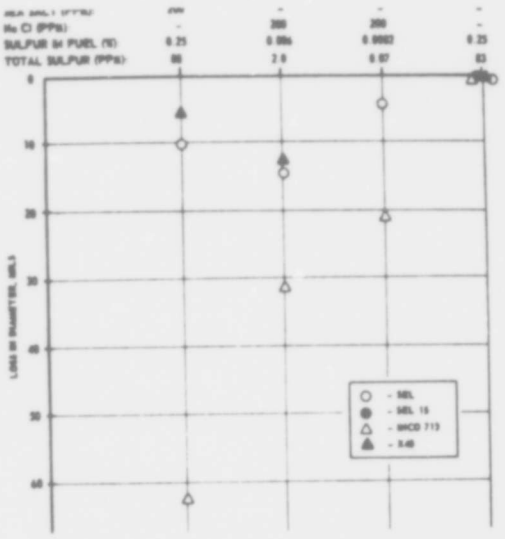

Figure 41.6. Sulphur effect at 1675 F (913 C). 200 ppm salt and 50 hours. Results on the right at a high sulphur concentration and no salt are included for comparison purposes. (Bergman).

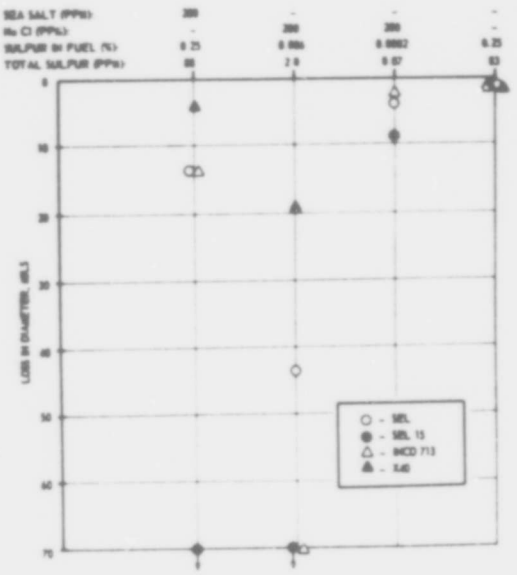

Figure 41.7. Effect of sulphur at 1800 F (982 C). 200 ppm salt and 50 hours. Results on the right for a high sulphur content and no salt are included for comparison. (Bergman).

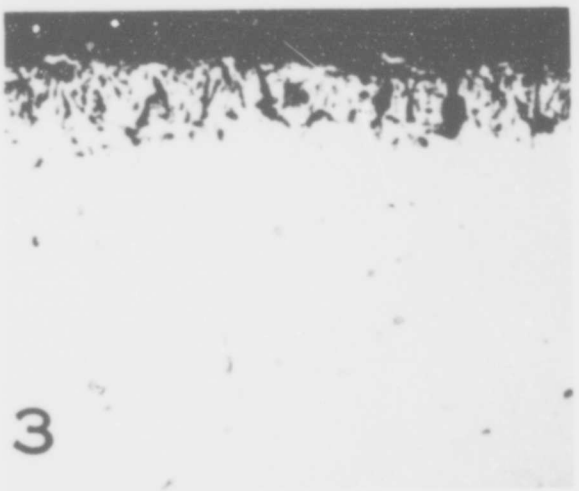

Figure 41.8. SEL oxidised at 1675^{O}F (913^{O}C) for 100h with no salt, showing fine subsurface oxide fingers (X400). (Kaufman).

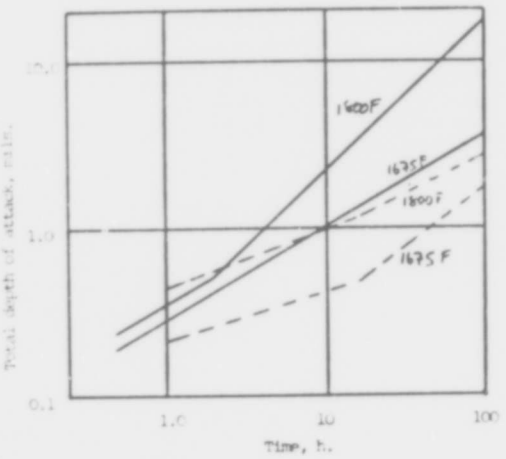

Figure 41.9. Corrosion of SEL. Full lines, with 200 ppm sea salt in air; dashed lines, with no salt. (Kaufman).

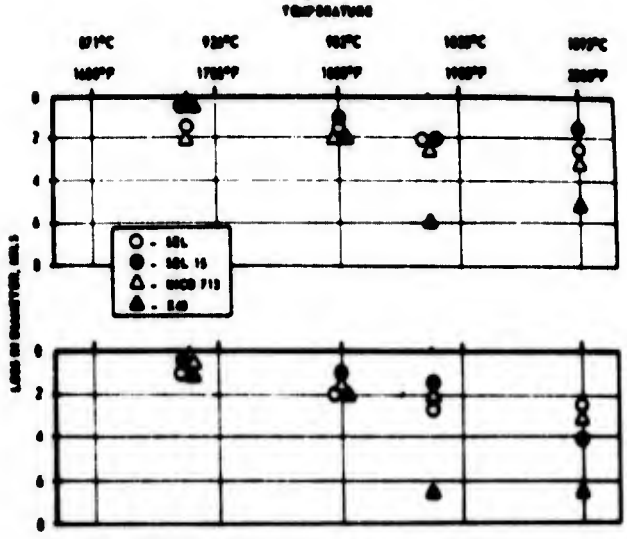

Figure 41.1. The top graph shows the effects of 50 hours with no sea salt and the bottom graph is for 50 hours at 2 ppm sea salt. (Bergman).

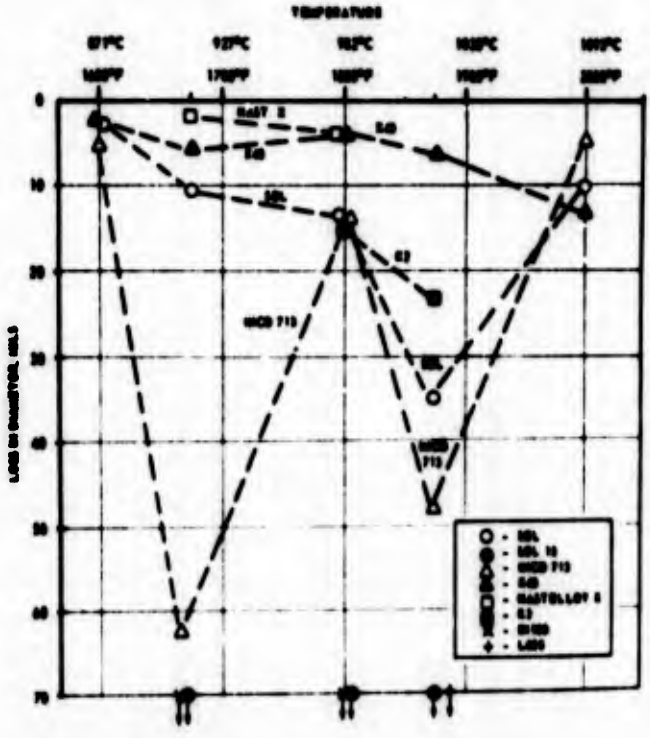

Figure 41.2. Hot corrosion results for 50 hours at 200 ppm sea salt. (Bergman).

SEL 15

P.A. Bergman, Corrosion 23 (1967) 72.

See SEL for a summary of the method. With no salt, SEL 15 was the most resistant of the alloys (the others were SEL, 713, X-40) and about the same as the others with 2 ppm salt (all were however quite resistant under these conditions). With 200 ppm salt the corrosion of SEL 15 was very severe: it and IN 100 were the worst alloys tested. With high sulphur (88 ppm) and no salt, the attack was very small: with 200 ppm sea salt and 0.25% S in the fuel the attack was very rapid at 982°C; and with 200 ppm NaCl and 0.0002% S the attack was slight. However, at 913°C the alloy was severely attacked at all three sulphur levels with salt.

H. von E. Doering and P.A. Bergman, Naval Ship Research and Development Centre Materials Laboratory Research and Development Report No. 2844 (March 1969).

See 713C for details. In a 100h test at 1750°F (955°C) with 200 ppm salt and in a 1000h test with 5 ppm salt the specimen was completely destroyed. IN 100 wasas bad, 713C rather better.

R. Field, D.J. Fisk and H. von E. Doering, Naval Ship Research and Development Centre, Materials Laboratory Research and Development Report 2833 (January 1969).

See 713C.

V.S. Moore and A.R. Stetson, Final Report on NASC Contract No. N00019-68-C-0532 (Solar Research Division Report RDR 1626-5) December 1970.

See B 1900 for details. The corrosion resistance was very poor, comparable with B 1900 and IN 100.

For SEL 15 two specimens were tested for 10h at 1650°F: the weight changes were -0.4 and -7.2 mg (however, note that the specimens had failed at this time, so weight gain due to oxidation must have more or less balanced weight loss due to spallation etc.). After 20h at 1800°F, the changes were -4895 and -3673 mg.

W.L. Wheatfall, in "High Temperature Corrosion of Aerospace Alloys" J. Stringer, R.I. Jaffee and T.F. Kearns (eds.), AGARD Conference Proceedings No. 120, (March 1973) 235.

See 713C for details.

Data relating to this alloy will also be found in the following Figures :
10.105, 10.106, 10.123, 10.124, 41.1, 41.2, 41.6, 41.7;
and Tables :
1-X, 10-VIII, 10-XXX.

TRW 1800

J.J. Walters (AVCO/Lycoming Division) Technical Report to the Air Force Materials Laboratory, Wright-Patterson Air Force Base AFML-TR-67-297 (Sept. 1967).

Extended summary in B 1900. TRW 1800 was one of a group of alloys described as having "relatively good resistance to attack" - the others in this group were U700 and IN728X. For TRW 1800 the threshold and terminal temperatures after 120 and 360h testing with JP-4 fuel and 4 ppm salt in the air were 1500 and 1600°F; and 1475 and 1635°F (816 and 871°C; 802 and 891°C). X-ray analysis of corrosion products found on the trailing edge after 40h rig testing detected in order of predominance a spinel with a_o = 8.24 Å, NiO, a trace of $NiWO_4$ and a trace of Al_2O_3. After 120h testing they were the same as at the shorter time. The corrosion products detected in powder removed from an area which had undergone sulphidation corrosion in a 120h test were a spinel with a_o = 8.20 Å, NiO and $NiWO_4$. A microprobe analysis of the depleted metal zone was 90.5% Ni, 0.5% Cr, 2.8% Al, 0.08% Ti, 1.0% Mo and 4.6% W.

Figure 43.1 shows the corrosion of TRW 1800 tested using JP-4 fuel and a salt -to-air ratio of 8 ppm as a function of temperature. Figure 43.2; JP-4 4 ppm salt. Figure 43.3; JP-4R, 8 ppm salt. Figure 43.4; JP-4R, 4 ppm salt. Figure 43.5; JP-5, 8 ppm salt. Figure 43.6 shows the corrosion as a function of temperature for three different testing times - 120, 240, and 360h using JP-4 fuel, 4 ppm salt.

Although TRW-1800 seems quite good at the shortest time, its long-term resistance does not seem as good as the other resistant alloys, U 700 and IN 728X.

Data relating to this alloy will also be found in the following Figures :
1.1, 1.7, 1.8, 10.13, 10.14:
and Tables :
1-I, 1-II, 1-IV, 1-V, 1-VI, 1-VII, 1-VIII, 1-IX.

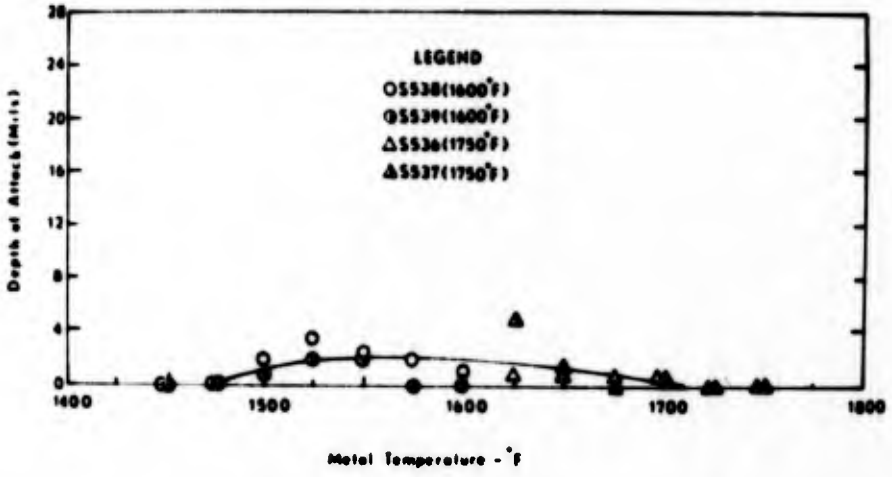

Figure 43.1. Corrosion as a function of temperature for TRW 1800 tested using JP-4 fuel with a Salt/Air Ratio of 8 ppm. (Walters).

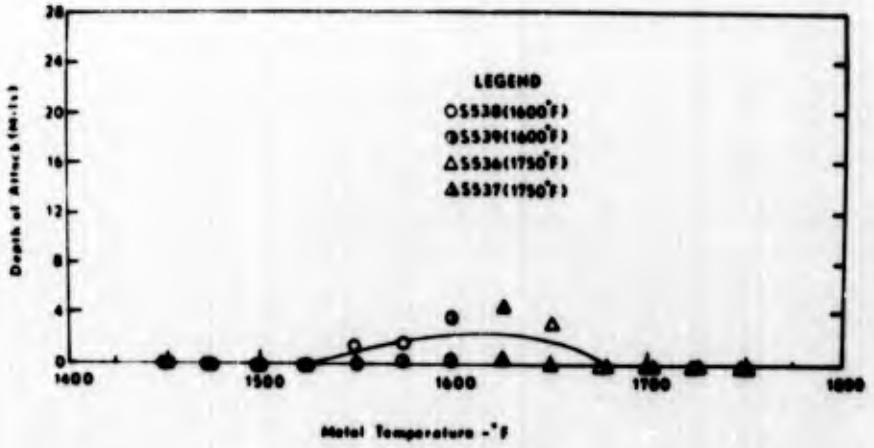

Figure 43.2. Corrosion as a function of temperature for TRW 1800 tested using JP-4 fuel with a Salt/Air Ratio of 4 ppm. (Walters).

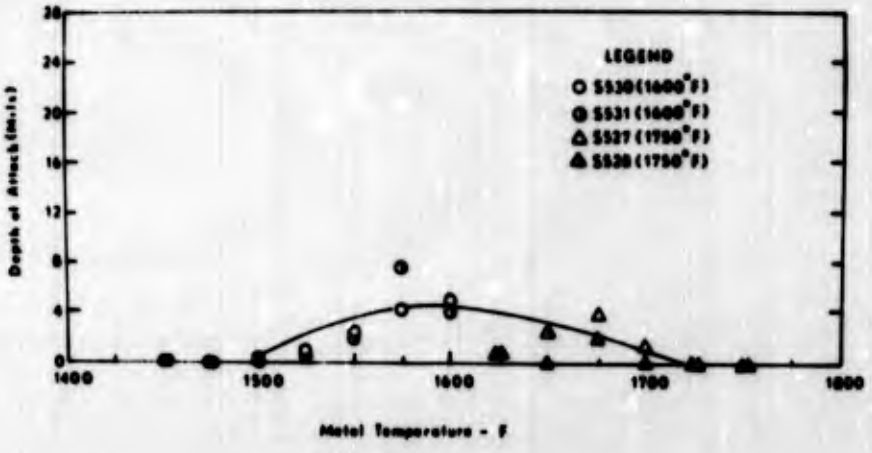

Figure 43.3. Corrosion as a function of temperature for TRW 1800 using JP-4R fuel with a Salt/Air Ratio of 8 ppm. (Walters).

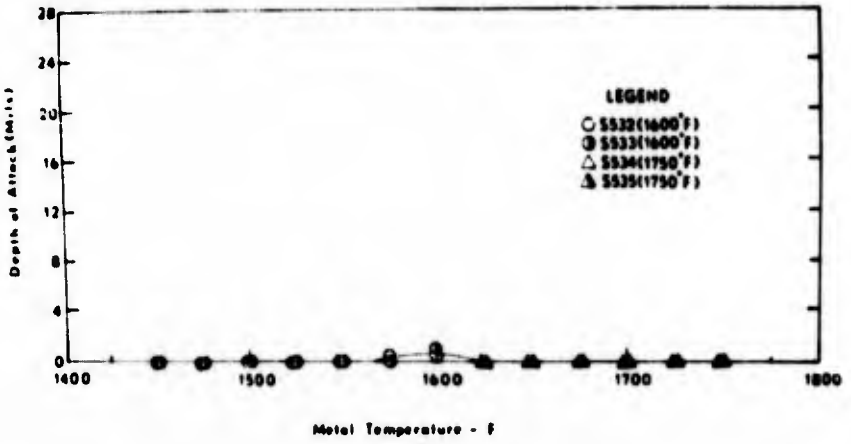

Figure 43.4. Corrosion as a function of temperature for TRW 1800 using JP-4R fuel with a Salt/Air Ratio of 4 ppm. (Walters).

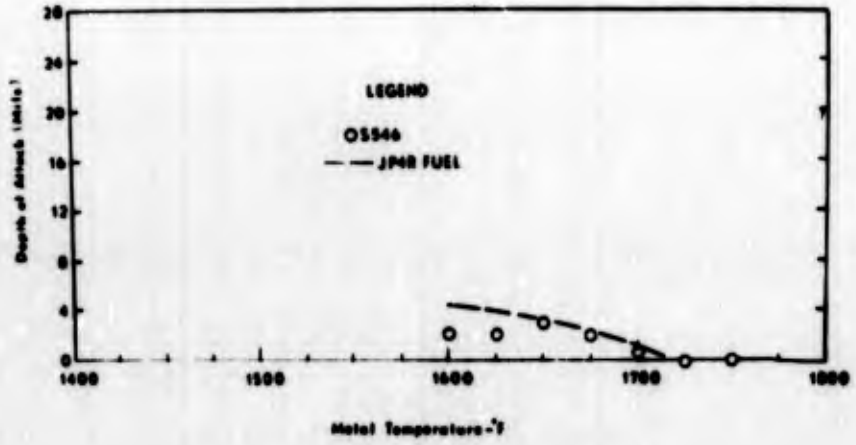

Figure 43.5. Corrosion as a function of temperature for TRW 1800 tested using JP-5 fuel (0.16%S) with a Salt/Air Ratio of 8 ppm. (Walters).

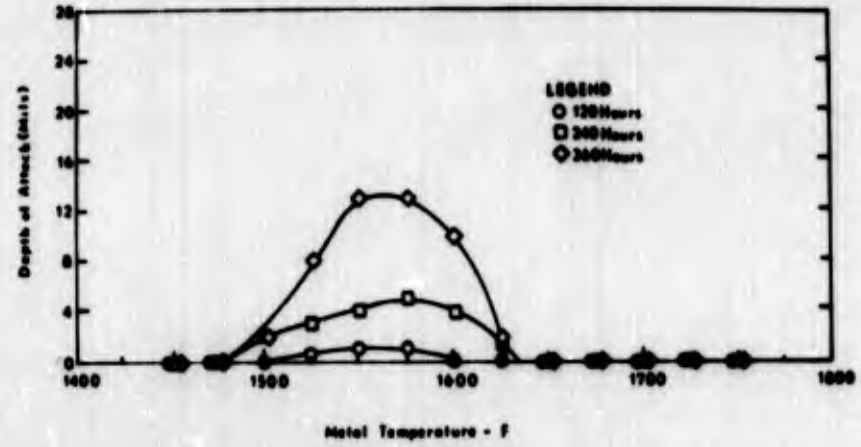

Figure 43.6. Corrosion as a function of temperature for TRW 1800 tested using JP-4 fuel with a Salt/Air Ratio of 4 ppm. (Walters).

TRW 1900

L.D. Graham, J.D. Gadd and R.J. Quigg, Hot Corrosion Problems Associated with Gas Turbines, ASTM Special Technical Publication, STP 421, 1967, 105.

See 713C for details. TRW 1900 was one of the worst alloys tested - only MM 302 was worse. B 1900, MM 200 about the same.

P.E. Hamilton, K.H. Ryan and E.S. Nichols, Hot Corrosion Problems Associated with Gas Turbines, ASTM Special Technical Publication STP 421, 1967, 188.

See 713C for details. Without salt injection, TRW 1900 is better than Mar-M 200 and 713C; with salt injection TRW 1900 together with IN 100 were the worst alloys tested.

Data relating to this alloy will also be found in Figures :
10.68, 10.74 and 10.75.

Udimet 500

P.A. Bergman, C.T. Sims and A.N. Beltran, Hot Corrosion Problems Associated with Gas Turbines; ASTM Special Technical Publication STP 421, 1967, 38.

See 713C for details. 200 ppm salt at 1750F (954°C). Surface loss in burner rig, 100h, approx 2 mls on diameter: maximum penetration about 10 mils. This is very good. Figure 45.1 shows intergranular attack. Commercial experience shows this to be a good, hot-corrosion resistant alloy.

B.O. Buckland, A.D. Foster and J.J. Treanor, Presented at National Association of Corrosion Engineers Annual Meeting (April 21, 1966) Miami, Florida.

Used "small burner test" in range 100 - 6000h, 1400 - 2000°F (760 - 1093°C), variety of fuels and contaminants= assessed corrosion metallographically. Found could describe attack as

$$\text{corrosion} \propto (\text{time})^n$$

where the exponent n increases with temperature, from 1/3 to 1. Depends on alloy, but usually about 1/3 for 1100 - 1400F (593 - 760°C), about ½ for 1400 - 1700F (760 - 927°C) and approx. 1 at 1900 and 2000°F (1038 and 1093°C). Tests up to 5000h necessary to extrapolate to times of 30,000 to 100,000h. U500 suffered somewhat higher corrosion in distillate gas oils containing 5 ppm sodium than in natural gas. As much as 2.35% S in the fuel seemed to make little difference. 5 ppm sodium and 2 ppm vanadium in the gas oil produced corrosion. Corrosion with fuels containing appreciable quantities of alkalis characteristically exhibited a delayed reaction in which the initial corrosion rate was no different from that with natural gas; however, after a certain time depending on the alloy and the alkali concentration, the corrosion rate may increase greatly. Figure 45.2 shows a graph of total corrosion with natural gas at a number of temperatures as a function of time. Table 45-I shows total corrosion for five different fuels for various temperatures and times, and Table 45-II shows corrosion with residual fuels. General U 500 seemed fairly resistant - comparable with X-45. In addition, some actual gas turbine components were studied after service: one of these was of U 500 (part B11 - see Table 45-III) from 20,730 h in a turbine burning natural gas. The shutdown frequency was 0.25 stops per 100h. The calculated metal temperature was 1330°F (721°C); the corrosion was 1 mil, which is equivalent to the corrosion rate at a "small burner" test temperature of 1410°F (766°C). It was concluded that there were four important variables: shutdown frequency (30 shutdown per 100h gives an apparent tem. 25°F higher than the actual); fuel (apparent temperature 60°F higher with treated crude or residual fuels than with natural gas); service rating (poor service 70°F worse than good service); turbine part (buckets 110F higher than nozzles - possibly due to stress effects or erosion, but seemed unreasonably higher). Pressure seemed to have no systematic effect. The general idea is, one assesses these four factors for a given part from an engine, and hence get an apparent enhancement temperature - add this to the actual temperature to give the "apparent temperature" - then the small burner test graph should give the corrosion rate. Table 45-IV shows the correlations obtained.

R.M. Schirmer and H.T. Quigg, Progress Report No. 3 for NASC Contract NO_w65-0310-d; Phillips Petroleum Company Research Division Report 4370-66R (June 15, 1966).

See 713C for details.

U-500 suffers heavy attack at 1400 and 1600°C at 10 ppm salt with 0.002 and 0.04% S in the fuel. Otherwise, the alloy was fairly resistant. U-500 seems quite good, but not all that much better than 713C. Figure 45.3 shows the effect of fuel sulphur, sea salt in the air and gas temperature on the weight loss. Figure 45.4 shows a detail of the interface of U-500 specimen tested for 5h at 2200°F, 10 ppm sea salt in the air and 0.0002 wt % S in the fuel showing a very irregular metal interface.

At 2000°F, with 0.040 wt % S in the fuel and 10.0 ppm salt in the air, the weight loss corresponds to a penetration of 0.6 mils in 5h; the measured sulphide penetration was 10.6 mils. The metal durability in terms of penetration from the cross-sectional area was compared: U-500 and IN 713 C are the best alloys and are fairly comparable. In terms of weight loss the results are the same, but U-500 looks a little better than 713C.

Increasing the temperature from 1400 to 1600°F decreased the metal weight loss with 0.40 wt % S in the fuel, and had no effect at lower sulphur levels. An increase from 1800 to 2000°F and from 2000 to 2200°F increased the weight loss at 10.0 ppm sea salt but had no effect at lower levels of sea salt. Increasing the temperature from 1800° to 2200°F increased metal loss at all three levels of sea salt. Increasing the sea salt increased metal loss at lower temperatures, and in the majority of cases at high temperatures. Sulphur content had very little effect at low temperatures and none at high temperatures.

U-500 suffers from only limited oxidation attack (Fig. 45.5) and only restricted penetration of sulphur in low salt, high sulphur test (Fig. 45.6). Figure 45.5 shows the cross-section of U-500 after 5h at 2200°F with no sea salt and 0.0002 wt % S in the fuel. Figure 45.6 shows a section after 5h at 1400°F with no sea salt with 0.40 wt % S in fuel. Figure 45.7 shows a section after 5h at 1600°F with 10 ppm sea salt in the air and 0.0002 wt % S in the fuel: there is heavy sulphide penetration and "interdendritic" oxidation apparently following the sulphide penetration. Figure 45.8 shows a section after 5h at 1800°F, 10.0 ppm salt, 0.0002 wt % S. Figure 45.9, a section after 5h at 2200°F, 10 ppm salt, 0.0002 wt % S. Figure 45.10 5h, 1600°F, 10 ppm salt, 0.40 wt % S.

H.T. Quigg and R.M. Schirmer Progress Report No.3 on NASC Contract NO_w66-0263-d; Phillips Petroleum Company Research Division Report 4706-67R, April 1967.

See 713C for details. Figure 45.11 shows a cross-section of the surface of the convex side of a first stage turbine blade that had completed 1800h in domestic air-line service since overhaul.

H.T. Quigg and R.M. Schirmer Progress Report No. 4 on NASC Contract NO_w65-0310-d; Phillips Petroleum Company Report 4411-66R August 1966.

See 713C for details.

R. Viswanathan Corrosion 24 (1968)359.

See 713C for details. U 500 was one of the better alloys tested, losing 2.6 mg/cm^2 in 150 h at 1500°F (816°C); 96.0% of the alloy was unaffected. Waspalloy was much the same, as was GMR 235. Figure 45.12 shows the essentially uniform attack on U-500.

U-500 was modified by adding 0.1 - 0.3% of lanthanum and yttrium; the scale contained Cr_2O_3, Al_2O_3 (MgO) $(TiO_2)_y$ and the affected alloy contained CrS_x, TiS_x and LaS_x. No further details are given.

The effect of two different sulphur trioxide levels in the gas stream was tested: 6 ppm and 150 ppm for U-500 the weight losses in a 150h test at 1500°F (816°C) were 1.60 and 2.6 mg/cm^2 respectively. U-500 was less sensitive to the sulphur trioxide level than alloys such as U-700, 713 C and Inco 700.

A.U. Seybolt, Trans AIME, 242, (1968) 1955.

Figure 45.13 shows the hot corrosion morphology of U-500 after 616h at 1600°F (871°C) in a combusted 2.9% S distillate oil containing 125 ppm sodium as NaCl. This alloy was then subjected to electron probe micro-analysis for Cr along a traverse from a chromium sulphide inclusion through the matrix; the result is shown in Figure 45.14. There is a considerable chromium depletion in the matrix adjacent to the particle: it was then shown that U-500 with only 7% Cr would suffer rapid oxidation, implying that the depleted metal adjacent to the sulphide is oxidised rapidly in hot corrosion. Figure 45.15 shows the oxidation of U-500 after 3 days at 1000°C in air. Figure 45.16 shows the 7% Cr alloy after the same treatment.

Figure 45.17 shows a section of cast U-500 tested for 1000h in a hot corrosion rig (presumably the GE rig described by Bergman) at 1750°F (955°C), using 1% S diesel fuel with 5 ppm sea salt (not clear whether in fuel or air). The penetration recorded for this test was 0.023 in in one case and 0.058 in in another. An alloy containing 0.5% Ce was prepared: the penetration in a similar test was 0.012 in; the microstructure is shown in Figure 45.18.

H. von E. Doering and P. A. Bergman, Naval Ship Research and Development Centre Materials Laboratory and Development Report No. 2844 (March 1969)

See 713C for details. In a 100h test at 1750°F (955°C) with 200 ppm salt, U-500 was the best of the alloys tested: the surface loss was 1.1 mils, and the maximum penetration was 7.0 mils. In a 1000h test with 5ppm salt the corresponding values were 8.8 and 31.7 mils, still much better than SEL, the next best of the nickel base alloys tested, but not as good as the cobalt-based alloys X-40 and L605.

H. von E. Doering and P. A. Bergman, Naval Ship Research and Development Centre, Materials Laboratory Research and Development Report 2833 (January 1969).

See 713C.

H. T. Quigg and R. M. Schirmer, Progress Report No. 3 on NASC Contract No. N00019-68-C-0252 (Phillips Petroleum Company Research and Development Report 5423-69) July 1969.

See 713C for details. This report is primarily concerned with testing the ASTM "Round Robin" group of alloys in the Phillips Turbine Environmental Simulator using a cyclic test in which the specimen is heated to 1600, 1800 or 2000°F (871, 982 or 1093°C) maximum temperature for 8 min following a cooling to 1000°F (538°C) for 2 min, producing an attack approximately six times more severe than the isothermal routine used in their earlier tests. After 44h at 2000°F maximum, the weight loss was 56 mg/cm^2, the surface loss was 2 mils and the maximum attack was 8 mils. This was by far the best of the alloys tested, much better than IN 738. It was estimated that it would take 81h for the specimen to lose 127 mg/cm^2. Figure 45.19 shows a U-500 specimen after 143h in a 2000°F test.

The data are presented in tables and graphs (see 713C).

ASTM Round Robin Test organised by the Hot Corrosion Task Force of the Gas Turbine Panel, 1970.

See 713C for details. U-500 was one of the best two alloys tested; the other was IN 738. Figure 45.20 shows the metal loss data reported by the participants.

W. L. Wheatfall, H. Doering and G. J. Danek, Jr., Hot Corrosion Problems Associated with Gas Turbines, ASTM Special Technical Publication STP 421, 1967, 206.

See 713C for details. The paper is concerned with the effect of molten salts at 1650°F (899°C) on two alloys, one of which designated AMS 5384, is clearly U-500. Figure 45.21 shows the change in potential of the cell as a function of time. Figure 45.22 shows sections of the alloy corroded under different circumstances. Figure 45.23 shows the maximum oxide penetration as a function of time in air, and in molten Na_2SO_4 under air and in argon respectively. Figure 45.24 shows sections of specimens preoxidised before immersion in molten Na_2SO_4-5% NaCl. Whereas 713C was attacked by both Na_2SO_4 and Na_2SO_4-NaCl mixtures, U-500 was attacked only by the mixed salt.

F. J. Wall and S. T. Michael, Hot Corrosion Problems Associated with Gas Turbines, ASTM Special Technical Publication STP 421, 1967, 223.

See 713C for an extended summary. A number of alloys tested in a simulated combustion gas at 1450°F (788°C), coated with 50% Na_2 50% Na_2SO_4/50% $MgSO_4$, for 100h. Alloys designated by number only, and approximate compositions given: No. 13 appears to be U-500. There was very little attack after either 100 or 200h. Tests were also run on this alloy at 1250, 1350 and 1450F (677, 732 and 788°C). The attack was greater at the two lower temperatures. (Figure 45.25).

Corroded specimens were examined by electron probe micro-analysis: Figure 45.26 shows the results.

R. M. Schirmer and H. T. Quigg, Hot Corrosion Problems Associated with Gas Turbines, ASTM Special Technical Publication STP 421, 1967, 270.

See 713C for details. This paper is drawn from reports abstracted above, and describes experiments in the Phillips Environmental Simulator at temperatures in the range 1400 - 2200°F (760 -1204°C) with 0.0002, 0.040 and 0.40% S in JP-5 fuel. 0, 1.0 and 10.0 ppm sea salt in the air. Figure 45.27 shows the weight loss for U-500 as a function of time and test conditions. U-500 was the best of the group tested, a little better than 713C (but not a very marked difference). MDC-1 coated 713C was better than either.

In discussion, A. U. Seybolt remarked that experiments at General Electric Research and Development Center had shown that U-500 can be hot corroded by Na_2SO_4 in the absence of NaCl (typically at 1000°C, 24h). Schirmer and Quigg replied that on other alloys (713C and SM-200) corrosion had been produced by sea salt, NaCl and NaOH in the virtual absence of fuel sulphur: they felt the sodium was important rather than the sulphur.

C. S. Wukusick, Paper no. 12 in Reactions Between Gasses and Solids, AGARD Conference Proceedings No. 52, 1969.

Figure 45.27(a) shows oxidation of U-500 turbine blades during service.

S. Y. Lee and W. E. Young in Combustion and Heat Transfer in Gas Turbine Systems: Cranfield Symposium No. 11, E. R. Norster (ed.) (Pergamon, Oxford 1971) 253.

See 713C for details and the principal results. Figure 45.28 shows the effect of specimen cooling on the oxidation rate.

S. Y. Lee, S. M. DeCorso and W. E. Young, J. Eng. for Power (Trans. ASME) July 1971, 313.

Description of test facilities similar to paper above. The test specimen geometries include ¼ in diameter pins, airfoil shaped paddles, and cylinders with holes in the walls for thermocouples: these last can be cooled by passing air up the centre. Figure 45.29 shows oxidation of U-500 and X-45 as a function of time at 1800°F both as removed and descaled. The scale appeared to spall continuously from U-500, but appeared tightly adherent to X-45, in spite of the 1 h cycles in the test. Metallographic examination showed that X-45 suffered less subscale oxidation than U-500. The scale on X-45 was much thicker, confirming its adherent nature.

However, X-45 shows a greater degree of oxidation than U-500 in the pressurised test rig. Figure 45.30 shows the effect of gas velocity on the oxidation. Figure 45.31 shows the oxidation rate at 1600°F (871°C) and 3 atm pressure as a function of time up to 500h: oxidation is relatively rapid up to about 200h, but thereafter the rate decreases. The oxidation of the two alloys is approximately the same up to 100h or so: thereafter U-500 oxidises rather more slowly. However, the difference is not great. The correlation between the pressurised passage oxidation and that in practice seems quite good: U-500 blades removed from the turbine after 20,000h service had lost approximately 4 mils (see C. J. Spengler et al, Metals Eng. Quart., 10 (1970)), which is closely similar to the value found by extrapolating a pressurised passage test at a similar temperature and contaminant condition.

Figure 45.32 shows results of 50h tests using the specification limit of 5 ppm sodium in the ASTM 3-GT fuel. The two alloys are very similar at 1450°F (788°C) but X-45 is rather better at 1800°F (982°C). The loss was some ten times greater at the higher temperature.

Figure 45.33 shows the results at 1500°F (816°C) for 150h at 3 atm pressure burning fuel containing no sodium but 0, 2 and 10 ppm vanadium for several superalloys. With the higher vanadium content X-45 was the worst of the alloys tested (the others were U-500, U-710, M-421, 738X, and 713C, in order of increasing resistance to attack). Figure 45.34 compares X-45 and U-500 with 2 ppm vanadium, no sodium, at 1500°F, 3 atm pressure as a function of time up to 500h. Up to 150h, X-45 is less attacked, but thereafter U-500 is better. The authors comment that, at this level, extrapolation indicates that there will be no serious problem at 1500°F, in agreement with field experience that "minor corrosion will take place at a vanadium level of 2ppm and a sodium level of less than 1 ppm, but not to the catastrophic degree seen previously at higher contaminant levels". (C. E. Hussey and K. W. Johnson, ASME paper No. 68-GT-28. 1968).

Figure 45.35 shows the corrosion of a number of alloys at 1500°F at 3 atm pressure for 150h with 2 ppm vanadium and 0, 2 and 5 ppm sodium in the fuel. In these tests, 713C was the worst at all sodium levels, the other alloys (X-45, U-500, U-710, IN-738X and Mar-M 421) were essentially similar to each other: the loss of metal was some five times as great with 5 ppm sodium as with no sodium. In addition there was significant sub-scale sulphidation of the alloys. Examination of specimens tested with 2 ppm vanadium and 5 ppm sodium showed catastrophic attack on 713C, intolerable penetrations of 10 mils on U-500, and 6 mils on X-45 in 150h.

S. Y. Lee, W. E. Young and C. E. Hussey, J. Eng. for Power, Trans. ASME (April 1972) 149.

An extension of the 1971 paper summarised above, in particular reporting data on cooled specimens (Figure 45.35 includes two points from this work). Figure 45.36 shows the effect of gas and metal temperature on the corrosion of U-500. Figure 45.37 compares the corrosion rate of several alloys when burning 3-GT fuel with 5ppm Na and 3ppm V as compared to normal oxidation.

C. J. Spengler, S. Y. Lee and W. E. Young, in "Deposition and Corrosion in Gas Turbines" A. B. Hart and A. J. B. Cutler (eds.) (Applied Science Publishers, London, 1973) 294.

This paper describes the use of the Westinghouse pressurised passage rig, burning a variety of fuels under a variety of conditions, with either ¼" dia. pins, airfoil shaped paddles, or cylinders for internally cooled test. In addition the use of a "corrosion dipstick" in actual operating turbines is described. Figure 45.38 compares the dipstick and laboratory turbine simulator tests for U-500 and IN-700; for a fuel containing 2 ppm V and 0.8 ppm Na. The correlation between the two tests was only fair, but corrosion rates in both cases were very small. Table 45-V lists the metal loss for a number of alloys in the two tests. There are some differences in the corrosion products in the two tests. For U-500 and X-45, the specimens from the turbine simulator showed the presence of vanadium-containing spinel scales and sodium-magnesium salts. There was little Cr_2O_3 present and very limited subscale sulphidation or oxidation. The specimens of the same alloys from the monitor show normal Cr_2O_3 scales and no subscale sulphidation; there is a (Ni,Co) vanadate present on the surface but no detectable sodium-containing salts. The authors comment that whereas in the simulator the specimens were hot corroded all over, in the monitor they were irregularly attacked, with normal oxidation in some places and hot corrosion in others, indicating localised deposition of alkali metal salts which produced in alloys like IN 700 and 713C local catastrophic attack.

Part of the programme studied the effect of various additives on the deposits formed when burning 3-GT fuel. Table 45-VI shows the effect of the additives on the corrosion of U-500, X-45, U-710 and 713C.

Another section was concerned with the evaluation of various coatings on U-500 and X-45 using both a small burner "spinning rig" and the pressurised passage turbine simulator. Figure 45.39 shows the behaviour of uncoated U-500, slurry coating type NC-301, uncoated X-45 and uncoated U-710 in a spinning rig test. Figure 45.40 shows the behaviour of U-500 and X-45 both uncoated and with a variety of coatings in the simulator. Figure 45.41 shows the localised penetration determined metallographically at different sections of the specimens. A is near the tip, and D near the root. Figure 45.42 shows metallographic cross-section of a U-500 specimen from the spinning rig; Figure 45.43 shows sections from turbine simulator specimens. Figure 45.44 shows the average penetration rates at the different cross-sections for U-500 and X-45, coated and uncoated, in the spinning rig and the simulator at 1650°F (899°C).

W. L. Wheatfall, in "High Temperature Corrosion of Aerospace Alloys", J. Stringer, R. I. Jaffee and T. F. Kearns (eds.), AGARD Conference Proceedings No. 120 (March 1973) 235.

See 713C and In-738 for details.

C. E. Hussey, S. Y. Lee and W. E. Young, presented to ASTM Annual Meeting Symposium on Gas Turbine Fuel Requirements, Handling and Quality Control, June 1972.

This paper describes experience with two Westinghouse W171 gas turbines installed at the Miraflores station of the Panama Canal Co. overhauled and put in to service in 1965 burning a fuel containing less than 10 ppm Na, less than 4 ppm V, less than 10 ppm Ca and less than 1.8% S. Although some corrosion was expected, even at the reduced turbine inlet temperature of 1375°F (746°C), the corrosion after 6375h operation was extensive. The turbines were overhauled and put back into service in 1966 using the same fuel, but in a treated state, with the vanadium averaging 2.5 ppm and the sodium 0.5 ppm. After nearly 5000h, inspection showed only minor acceptable corrosion. Laboratory tests using a pressurised passage rig, and a "corrosion dipstick" monitor in the actual turbine, supplemented the practical observations. It was shown that 5 ppm V, 2 ppm Na, metal surface temperature 1500°F (816°C) would result in an extensive amount of attack.

The first and second stage vanes were U500. The first stage blades were U520 in one of the turbines, and IN700 in the other.

Extensive damage of the first stage U500 vanes had occurred after 6375h; the second stage vanes showed heavy surface corrosion similar to the first stage, but less severe. Both the first and second row blades showed heavy oxidation scale with evidence of surface corrosion. Figure 45.45 shows the first stage U-500 vanes. Metallographic examination showed the presence of grey islands of CrS_x in the affected layer of the alloy beneath the corrosion interface. Table 45 - VII lists the composition found in the turbine blade path: they include sodium sulphate, nickel oxide, and various vanadium and sodium/vandium oxides.

Figure 45.46 shows the pressure side of U500 stator blades after using the treated fuel; the suction (convex) side showed no visible attack. The deposit level was much less, and the components identified by X-ray diffraction are listed in Table 45 - VIII: they include nickel iron oxide, nickel vanadates, nickel oxide, cobalt sulphate, cobalt vanadate, and sodium magnesium sulphate, $Na_2Mg(SO_4)_2.4H_2O$. This is the product of a 50/50 molar mixture of sodium and magnesium sulphates heated to the melting point, which is at 1250°F(621°C): the authors believe this is an important corrosive constituent in the deposit.

S. K. Rhee and A. R. Spencer, Oxid. Metals 8 (1973) 11.

See RA 333. Sheet specimens, annealed 8h in dry hydrogen at 1150°C, ground to 320 grit, oxidised in static air over the temperature range 760 - 1200°C. All specimens withdrawn and cooled at 4, 16, 64, 100, 200, 300, 400, 500 and 600h, one removed each cycle for examination. Parabolic weight gain.

T°C.	Rate constants $g^2cm^{-4}s^{-1}$	Total time, h.
760	4.63×10^{-14}	600
870	9.01×10^{-13}	600
982	9.08×10^{-12}	400
1093	1.56×10^{-11}	200
1150	1.16×10^{-10}	500
1204	2.78×10^{-10}	100

Activation energy = 58.8 kcals/mole

Major phase in outer scale was Cr_2O_3, probably with $Ni(Al,Cr)_2O_4$ spinel dispersed in it. Internal oxide phase was Al_2O_3, which became continuous at 1093°C.

W. L. Wheatfall, S. J. Dapkunas and J. Sydavar, Naval Ship Research and Development Center, Materials Department, Research and Development Report 8-868 (August 1971).

Samples of U 500, IN 738 and Mar-M 432 were oxidised in flowing oxygen for 210h at 1650°F (899°C) and 235h at 1750°F (954°C). The extent of oxidation was measured in terms of oxide thickness, general penetration, and maximum depth of oxide penetration. For U 500 the results were

	Surface oxide.	General penetration.	Maximum penetration (all mils)
210h at 899°C	1.0	1.5	3.0
235h at 954°C	1.1	2.2	3.1

U-500 was the most deeply oxidised alloy at 899°C, but had the lowest depth of attack at 954°C. The oxide scale on U 500 at 899°C was twice as thick as that on IN 738 and Mar-M 432. Surface scales on U 500 were rough and uneven at both temperatures.

I. I. Bessen and R. E. Fryxell, Gas Turbine Materials Conference Proceedings, Naval Air Systems Command, Washington (1972) 73.

Describes tests in which specimens were half-immersed in (a) Na_2SO_4 in air, (b) Na_2SO_4 in argon, (c) Na_2SO_4 plus carbon in argon, all at 1650°F (899°C); or alternatively were coated by dipping at 1650°F and then exposed at 1400 or 1500°F (760 and 816°C). See Rene 80 for details. In the argon tests small amounts of Na_2S were detected in the salt; with carbon also present as much as 1.8 mole % was observed.

Data relating to this alloy will also be found in the following Figures 10.51, 10.53, 10.54, 10.58, 10.83, 10.105, 10.122, 14.11, 52.14;
and Tables:
10.1, 10.V, 10-V111, 10-X1, 10-XV, 10-XV1, 10-XX1, 10-XX11, 10-XX111, 10-XX1V, 10-XXX, 39-1.

TABLE 45-I

CORROSION WITH DISTILLATE AND GAS FUELS, MEASURED BY SMALL BURNER TEST (BUCKLAND ET AL)

Fuel (See Table 2)	Temp. F	Time Hrs.	Total Corrosion Mils Alloys 310	314	446	X45	S816	M252	U500
2	2000	600	7.8		6.4	15.5			5.5
2	1800	1000	6.5 2.9		1.8	3.9	7.1	5.9	6.7
2	1600	1000	3.1		0.6	1.5	0.58	3.1	2.9
3	2000	600	7.4 6.8 5.5		4.4	14.0	23.0	10.5	5.1
3	1800	1000	3.9 3.4		2.1	5.2	12.0	3.6	3.6
4	2000	600	8.9	4.5				12.0	6.2
4	2000	500				13.0			
4	1800	600	2.0 1.9	2.5		3.4			4.6
5	2000	600	7.9 8.5	5.5					
5	2000	500						11.5	
5	2000	400				10.0			
5	2000	475							7.0
5	1800	1000	5.5 3.2	4.9		5.0			6.0
5	1600	600			0.62				
5	1600	1000	1.1	1.4		2.5			4.1
6	2000	600				13.0			
6	2000	1000	11.5		6.4				15.0
6	2000	1400	16.0						18.0
6	2000	1600			15.0			24.0	
6	2000	1750	16.5						
6	1800	1000	7.5 9.2			8.0			9.0
6	1800	1600					25.6		
6	1800	2500				18.0			
6	1800	3500	20.0 18.0		4.5			23.0	29.0
6	1600	1000	3.8		2.2	2.9		3.2	3.7
6	1600	3000	3.8 2.9		2.6	3.4	3.0	5.1	4.9

TABLE 45-II

CORROSION WITH RESIDUAL FUELS, MEASURED BY SMALL BURNER TESTS (BUCKLAND ET AL)

NOTE:

(1) Cr 28.5%, Ni 10.2%, Fe 44%, C 49%, Si 65%, Mn 12%, W 8.58%, Co Balance.

Fuel	Temp. F	Time Hrs.	Total Corrosion Mils Alloys 310	446	X45	Mod. (1) X-40	S816	M252	U500
7	1800	370	2.1 1.8	2.4	2.4		1.9	5.3	4.1
7	1600	250	0.19 0.51	-	-	0.32 0.34	0.49	1.3	-
7	1600	556	0.24	-	-	1.46	-	-	-
7	1600	600	2.0	-	-	1.6	0.25	1.19	-
7	1500	250	0.49	-	-	0.09	0.17	0.15	-
7	1500	600	0.39	-	-	1.11	-	-	-
7	1400	250	0.23			0.29	0.14	0.41	
7	1400	600	1.0			0.33			

TABLE 45-III

OBSERVATIONS ON PARTS EXAMINED AFTER GAS TURBINE SERVICE (BUCKLAND ET AL)

NOTES

(1) Buckets are coded "B", nozzle partitions are coded "N".
(2) Residual and Crude Oils nominally treated in accordance with ASTM Committee D-2 "Proposed Specification for Gas Turbine Fuel Oils", 1965, Fuel, No. 4-GT.
(3) Time at Calculated Metal Temperature.
(4) Assigned to weight data in favor of parts on which corrosion history could be established with most certainty.
(5) B Best, F Fair, P Poorest. Refers to relative quality of maintenance of turbine and fuel.
(6) Small Burner test temperature producing the indicated corrosion at the stated time for that particular alloy.
(7) Difference between the Apparent and the Calculated Metal Temperatures.

Identification(1)	Fuel(2)	Material	Time Hours(3)	Shutdown Frequency Stops 100 Hrs.	Reliability Rating(4)	Service Rating(5)	Calculated Metal Temp. °F	Measured Corrosion Mils	Apparent Temp. °F (6)	Temperature Differential °F (7)
B-1	Residual Oil	M-252	12,700	29	2	F	1280	6	1570	+290
B-2	Residual Oil	S-590	14,483	16	3	F	1430	5.5	1560	+130
B-3	Crude Oil	M-252	15,937	0.4	1	P	1330	6	1550	+220
B-4	Crude Oil	S-816	15,000	0.4	1	P	1330	6	1560	+230
B-5	Natural Gas	M-252	32,500	0.2	3	B	1260	0.75	1370	+110
B-6	Natural Gas	M-252	9,000	0.2	3	B	1340	1	1430	+90
B-7	Natural Gas	N80A	60,836	0.2	3	B	1350	2	1420	+70
B-8	Natural Gas	N80A	32,850	0.2	3	B	1320	2	1440	+120
B-9	Residual Oil	S-816	13,000	29	2	B	1280	4	1530	+250
B-10	Crude Oil	S-816	7,000	0.4	2	F	1320	4	1580	+250
B-11	Natural Gas	U-500	20,730	0.25	3	B	1330	1	1410	+80
B-12	Natural Gas	M-252	21,000	0.2	3	B	1340	1.5	1430	+90
B-13	Natural Gas	N80A	40,000	0.2	3	B	1320	1	1390	+70
N-1	Residual Oil	314	9,690	1	5	B	1530	7	1600	+70
N-2	Residual Oil	X45	5,200	29	4	F	1590	11.6	1720	+130
N-3	Residual Oil	X40	4,900	29	3	F	1590	20	1750	+160
N-4	Residual Oil	X40	9,020	29	3	F	1590	40	1770	+180
N-5	Residual Oil	X40	2,860	29	3	P	1760	130	1960	+200
N-6	Residual Oil	446	2,860	29	3	P	1760	22	1980	+220
N-7	Residual Oil	446	4,410	16	4	B	1780	8	1860	+80
N-8	Crude Oil	310	8,000	0.4	2	P	1670	31	1830	+160
N-9	Residual Oil	310	340	29	3	F	1760	2	1800	+40
N-10	Residual Oil	446	340	29	3	F	1760	1	1760	0
N-11	Residual Oil	446	680	29	3	F	1760	2	1820	+60
N-13	Natural Gas	310	6,600	0.2	5	B	1750	25+	1850	+100
N-14	Natural Gas	310	6,600	0.2	5	B	1650	8	1650	0
N-15	Natural Gas	X40	8,000	27	2	P	1750	50	1790	+40
N-16	Natural Gas	X40	18,500	0.2	3	B	1475	1.5	1400	-75
N-18	Natural Gas	314	20,730	0.2	4	B	1700	20	1720	+20
N-19	Residual Oil	X45	16,700	29	4	F	1590	4	1530	-60
N-20	Natural Gas	314	3,000	4	4	F	1640	7	1720	+80
N-21	Natural Gas	310	69,847	0.2	4	B	1620	13	1540	-80
N-22	Natural Gas	314	9,000	27	2	P	1690	6	1580	-110
N-23	Natural Gas	X45	22,859	0.2	4	F	1630	5	1550	-80
N-24	Natural Gas	X45	8,000	15	3	F	1690	10	1670	-20
N-25	Residual Oil	X40	11,700	29	3	F	1590	13	1660	+70
N-26	Natural Gas	X40	44,905	0.2	4	F	1530	5	1530	0
N-27	Residual Oil	X45	5,600	1	3	B	1640	<4	1580	-60
N-28	Natural Gas	X45	14,000	15	3	F	1690	<6	1580	-110

TABLE 45-IV

CORRELATION BETWEEN LABORATORY AND FIELD DATA (BUCKLAND ET AL)

NOTES:
1. Refer to Table 45-III
2. Following corrections applied: -6OF for residual or crude oil
   - 1F for each shutdown per 100 hours operation
   -7OF for poorest service factor (see Table 5)
   -11OF for buckets over the 1260-1430 F temperature range.
3. Deviation of corrected temperature differential from the over-all average of -15 F.

Identification (1)	Temperature Differential		Deviation From Average(3)
	Original(1)	Corrected(2)	
B1	-290	- 95	-110
B2	-130	- 50	- 35
B3	-220	- 20	- 5
B4	-230	- 20	- 5
B5	-110	- 25	- 10
B6	- 90	- 20	- 5
B7	- 70	- 40	- 15
B8	-120	- 10	- 25
B9	-250	- 55	- 70
B10	-250	0	- 15
B11	- 80	- 30	- 15
B12	- 90	- 20	- 5
B13	- 70	- 40	- 25
N1	- 70	- 15	0
N2	-130	- 45	- 60
N3	-160	- 75	- 90
N4	-180	- 95	-110
N5	-200	- 45	- 60
N6	-220	- 65	- 80
N7	- 80	- 5	- 20
N8	-160	- 30	- 45

Identification (1)	Temperature Differential		Deviation From Average(3)
	Original(1)	Corrected(2)	
N9	- 40	- 45	- 30
N10	0	- 85	- 70
N11	- 60	- 25	- 10
N13	-100	-100	-115
N14	0	0	- 15
N15	- 40	- 30	- 45
N16	- 75	- 75	- 60
N18	- 20	- 20	- 35
N19	- 60	-145	-130
N20	- 80	- 80	- 95
N21	- 80	- 80	- 65
N22	-110	-120	-105
N23	- 80	- 80	- 65
N24	- 30	- 30	- 15
N25	- 70	- 15	0
N26	0	0	- 15
N27	- 80	-120	-105
N28	-110	-120	-105

Data Points Analyzed	Temperature Differential °F	
	Average	Standard Deviation
Base Load Units, Nat. Gas Fuel (No Corrections Required)	-15	40
All Data	-15	70

TABLE 45-V

METAL LOSS (cms) (SPENGLER, LEE AND YOUNG)

Alloy hours	U-500	U-520	In-700	X-45	In-713C
			Turbine simulator		
101	0·001 6	0·002 8	0·002 7	0·002 0	0·001 9
200	0·003 9	0·004 3	0·004 2	0·005 0	0·004 6
248	0·003 3	0·005 8	0·003 7	0·003 2	0·004 0
300	0·004 2	0·004 0	0·003 4	0·004 3	0·004 0
			Corrosion monitor		
3 007					
A	0·002 5	0·007 6			
B	0·002 5	0·005 1	0·002 0	0·001 5	0·011 7
7 306					
A	0·004 6	0·003 6	0·010 0	0·002 5	0·005 2
B	0·002 0	0·003 6	0·001 8	0·001 5	0·050 0

TABLE 45-VI

50 HOUR TURBINE SIMULATOR CORROSION TEST RESULTS WITH VARIOUS ADDITIVES (SPENGLER, LEE AND YOUNG).

Contaminant in fuel	*None (oxidation)*		0·5% *S*	5 *ppm Na*	2 *ppm V*	
Additive	None	None	Mg & Si Si/Mg = 1	Mg & Si Si/Mg = 2	Mg & Si Si/Mg = 4	Mg & Al
U-500	2·7	18·8	8·6	5·2	2·8	1·4
Weight loss X-45	1·9	12·0	10·6	6·1	8·8	6·0
mg/cm² U-710	—	14·3	9·9	6·2	3·1	1·8
In 713 C	1·2	72·1	12·7	8·1	6·9	2·1
Sintering temp. F	—	—	1 674	1 562	1 953	—
Initial melt temp. F	—	—	2 032	2 033	2 090	—
Deposit	—	—	Hard ~27 mg/cm²	Soft 21 mg/cm²	Soft 30 mg/cm²	Soft 20 mg/cm²

TABLE 45-VII

COMPOUNDS IDENTIFIED BY X-RAY DIFFRACTION IN DEPOSIT IN THE TURBINE BLADE PATH AFTER 1 YEAR IN OPERATION ON LOW-VANADIUM FUEL (HUSSEY ET AL)

Na_2SO_4	Sodium sulfate
$Na_2Mg(SO_4)_2 \cdot 4H_2O$	Sodium magnesium sulfate tetrahydrate
$MgSO_4$	Magnesium sulfate
$Na_2O \cdot V_2O_4 \cdot 5V_2O_5$	Sodium vanadyl vanadate
$Na_2O \cdot V_2O_5$	Sodium metavanadate
V_2O_5	Vanadium pentoxide
$(VO)_2SO_4 \cdot 16H_2O$	Vanadyl sulfate-hexadecahydrate
$V_{12}O_{26}(2V_2O_4 \cdot V_2O_5)$	Vanadyl vanadate
NiO	Nickel oxide

TABLE 45-VIII

CONSTITUTES THE DEPOSITS FORMED AFTER A ROUND YEAR'S OPERATION FOLLOWING OVERHAUL (HUSSEY ET AL)

$NiFe_2O_4$	Nickel iron oxide
$3\ NiO \cdot V_2O_5$	Nickel orthovanadate
Fe_2O_3	Iron oxide
$Ni(VO_3)_2$	Nickel vanadate
NiO	Nickel oxide
V_2O_5	Vanadium pentoxide
V_2O_4	Vanadium tetroxide
$Na_2Mg(SO_4)_2 \cdot 4H_2O$	Sodium magnesium sulfate tetrahydrate
$CoSO_4 \cdot 6H_2O$	Cobalt sulfate
$3\ CoV_2O_5$	Cobalt orthovanadate

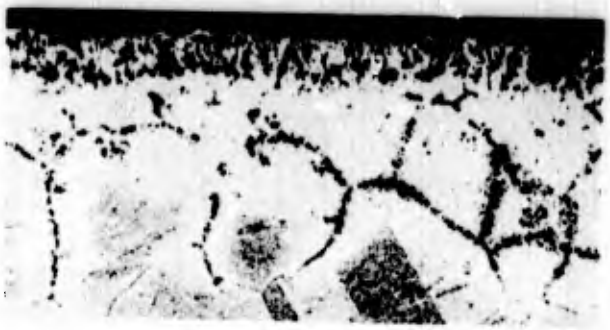

Figure 45.1. Subsurface intergranular attack of U 500 tested at 1750°F (954°C) (X250). (Bergman et al).

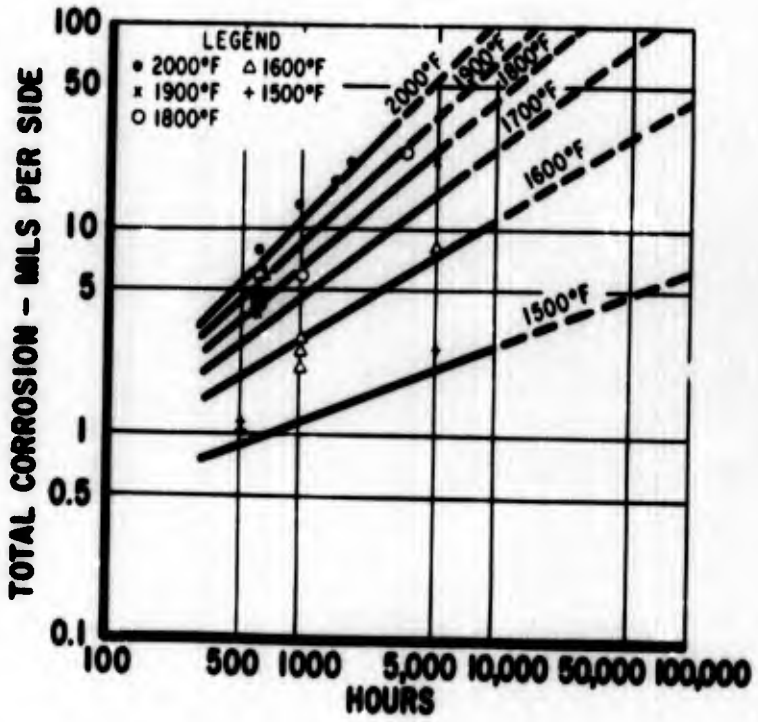

Figure 45.2. Total corrosion of alloy U 500 with natural gas fuel as measured by the small burner test. (Buckland et al).

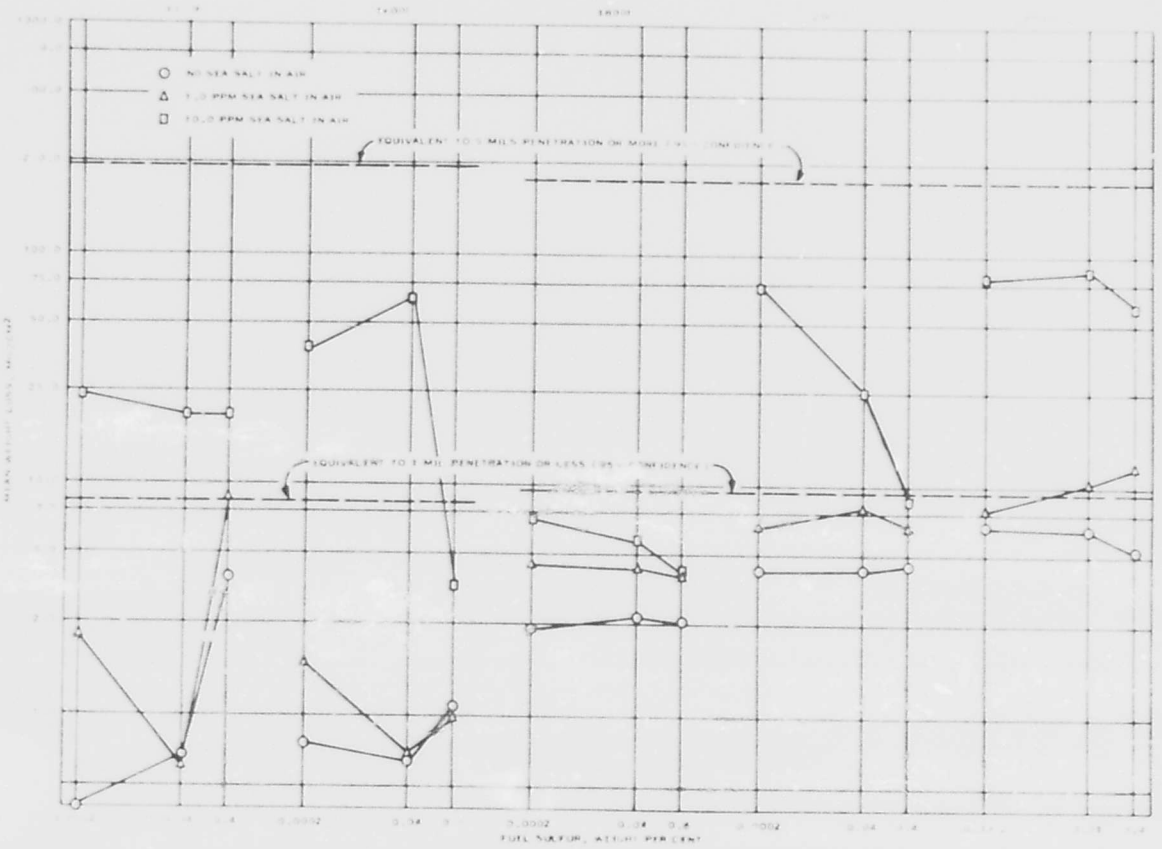

Figure 45.3. Effect of fuel sulphur, sea salt in air and gas temperature on metal loss of Udimet 500 test specimens (Schirmer and Quigg).

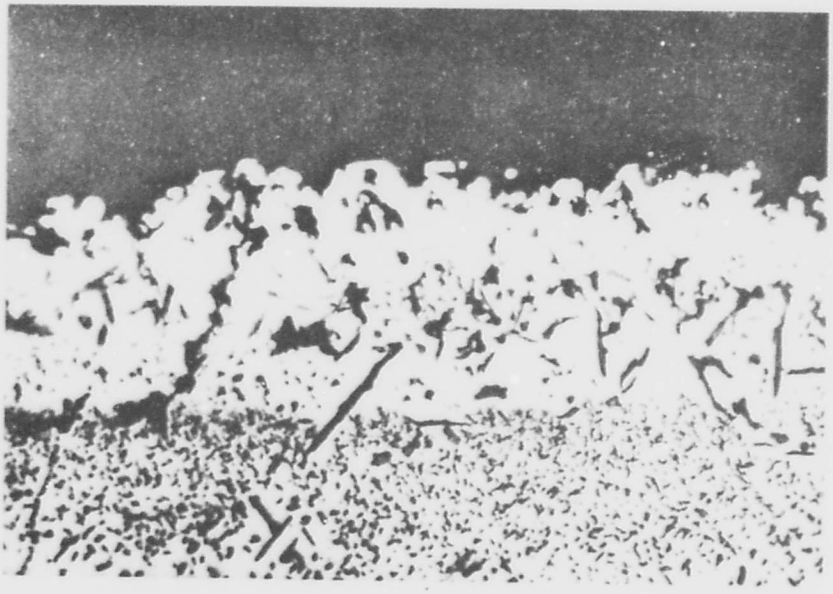

POLISHED ETCHED SECTION X1000

Figure 45.4. Photomicrograph of edge of test specimen showing surface roughened by severe oxidation (2200°F, 10 ppm sea salt in air, 0.0002 wt%S in fuel) (Schirmer and Quigg).

SLIGHT UNIFORM
SURFACE ATTACK

BASE METAL
UNETCHED
200X

INTERDENDRITIC OXIDATION

BASE METAL
UNETCHED
2000X

Figure 45.5. Oxidation of Udimet 500 in Phillips Rig. (Schirmer and Quigg).

5 hours exposure at 2200 F test condition with no sea salt in air and 0.0002 wt % sulphur in fuel.

SLIGHT VARIABLE
SURFACE ATTACK

BASE METAL
UNETCHED
200X

SULFIDE PENETRATION

BASE METAL
UNETCHED
2000X

Figure 45.6. Sulphidation of Udimet 500 in Phillips rig. (Schirmer and Quigg).

5 hours exposure at 1400 F test condition with no sea salt in air and 0.40 wt % sulphur in fuel.

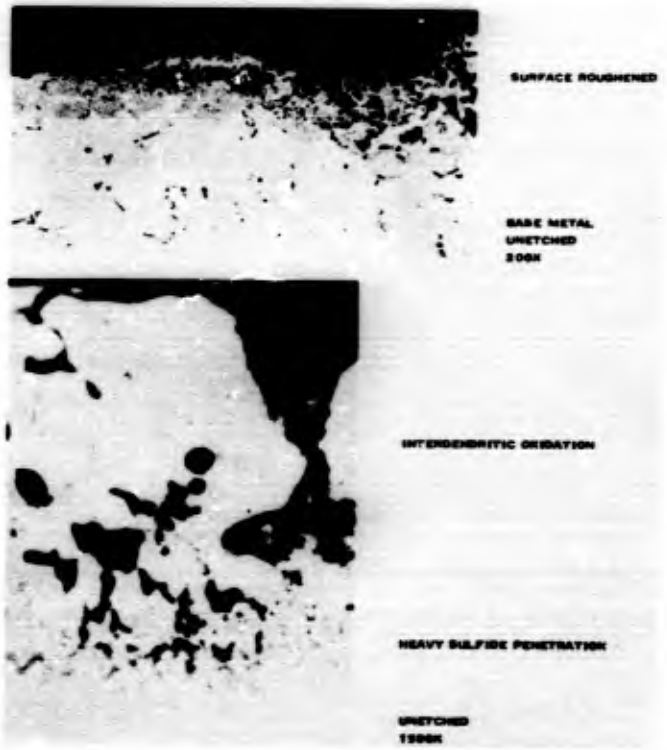

Figure 45.7. Hot corrosion of Udimet 500 in Phillips Rig. (Schirmer and Quigg).

5 hours exposure at 1600 F test condition with 10 ppm sea salt in air and 0.0002 wt % sulphur in fuel.

Figure 45.8. Hot corrosion of Udimet 500 in Phillips Rig. (Schirmer and Quigg).

5 hours exposure at 1800 F test condition with 10 ppm sea salt in air and 0.0002 wt % sulphur in fuel.

SURFACE ROUGHENED

BASE METAL
UNETCHED
200X

HEAVY SULFIDE PENETRATION
PRECEDING OXIDATION

UNETCHED
1500X

Figure 45.9. Hot corrosion of Udimet 500 in Phillips Rig. (Schirmer and Quigg).

5 hours exposure at 2200 F test condition with 10 ppm sea salt in air and 0.0002 wt % sulphur in fuel.

SURFACE ROUGHENED

BASE METAL
UNETCHED
2000X

SULFIDE PENETRATION

BASE METAL
UNETCHED
2000X

Figure 45.10. Hot corrosion of Udimet 500 in Phillips Rig. (Schirmer and Quigg).

5 hours exposure at 1600 F test condition with 10 ppm sea salt in air and 0.40 wt % sulphur in fuel.

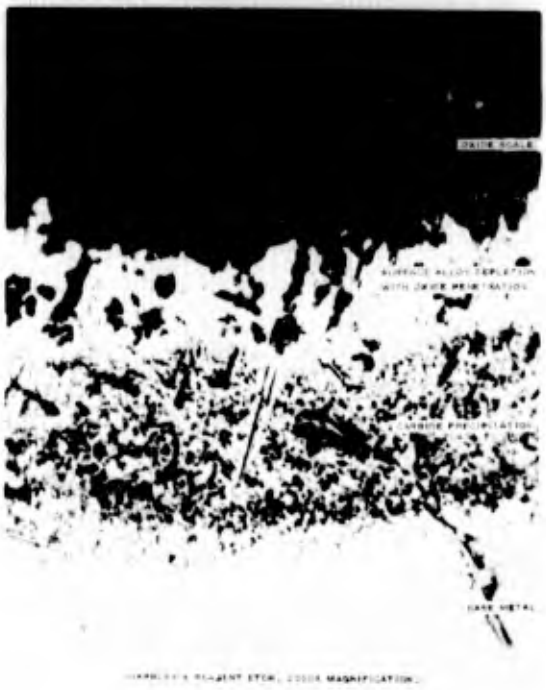

Figure 45.11. Oxidation of Udimet 500 turbine blade. (Quigg and Schirmer).

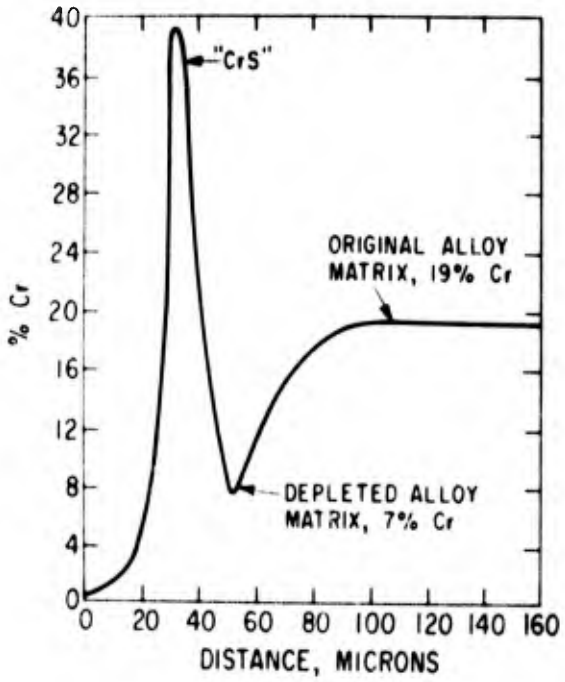

Figure 45.14. Electron probe trace for chromium in Udimet 500 alloy from sulphide particle into marks. (Seybolt).

Figure 45.12. Udimet 500 after 150 hours of corrosion testing. 500X. (Viswanathan).

Figure 45.15. Regular Udimet 500 sample after oxidation for 3 days at 1000°C in air. Magnification 460X. (Seybolt).

Figure 45.13. Udimet 500 nickel-base alloy subjected to hot corrosion atmosphere 616 hr, 1600°F. Magnification 680X. (Seybolt).

Figure 45.16. Udimet 500 with only 7% Cr after oxidation for 3 days at 1000°C in air. Magnification 460X. (Seybolt).

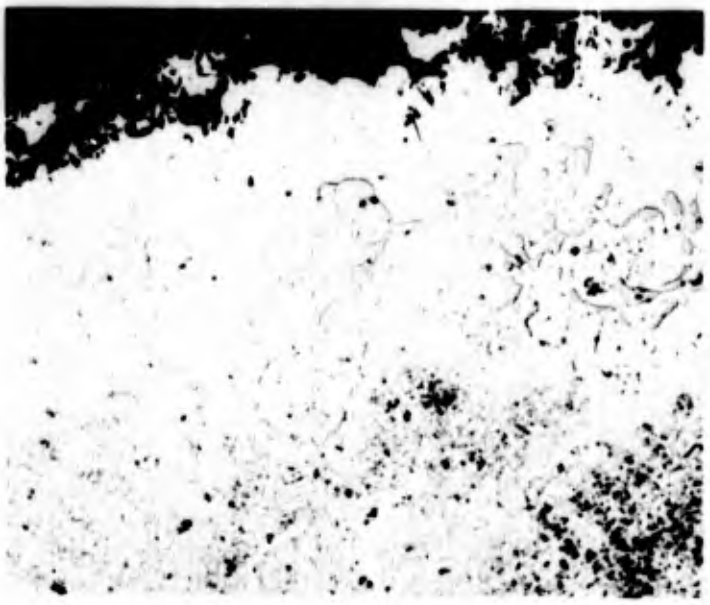

Figure 45.17. Cast Udimet 500, tested for 1000 hr in hot corrosion rig at 1750°F. Magnification 240X. (Seybolt).

Figure 45.18. Cast Udimet 500 + 0.5 Ce tested for 1000 hr in hot corrosion rig at 1750°F. Magnification 240X. (Seybolt).

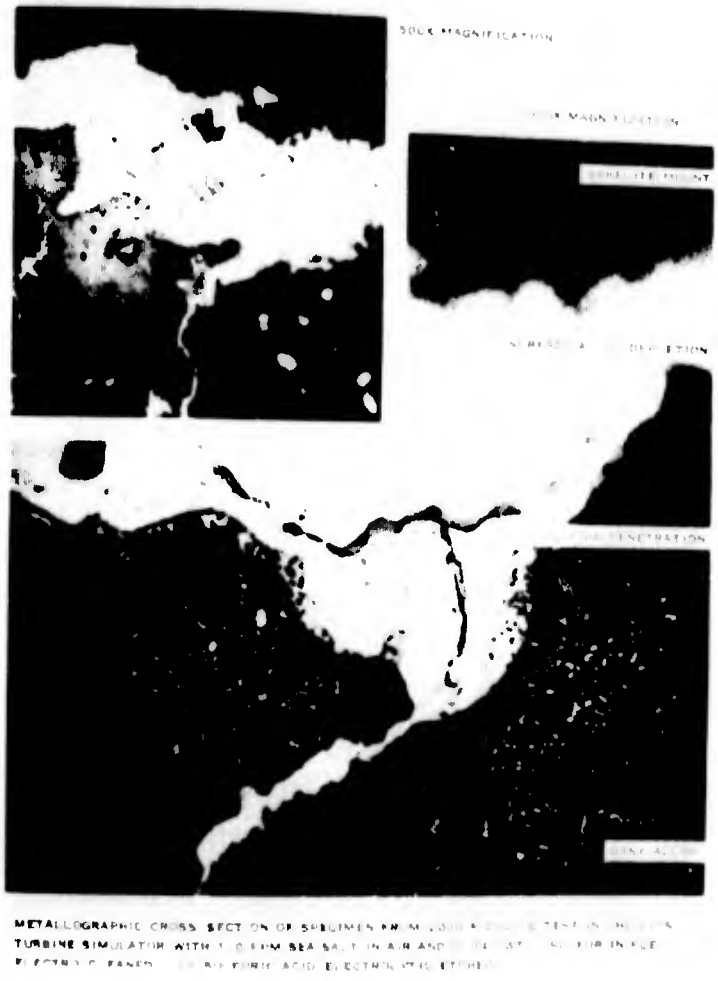

Figure 45.19. Accelerated surface oxidation of Udimet 500 specimen after 143 hours. (Quigg and Schirmer).

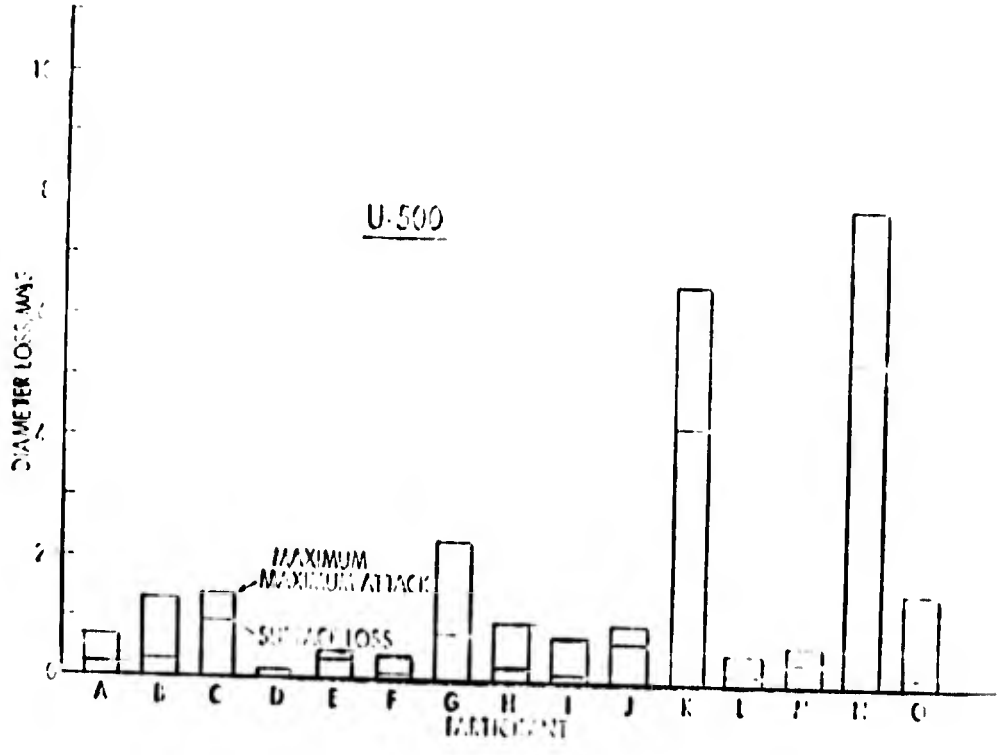

Figure 45.20. Results of the ASTM Round Robin test for U-500.

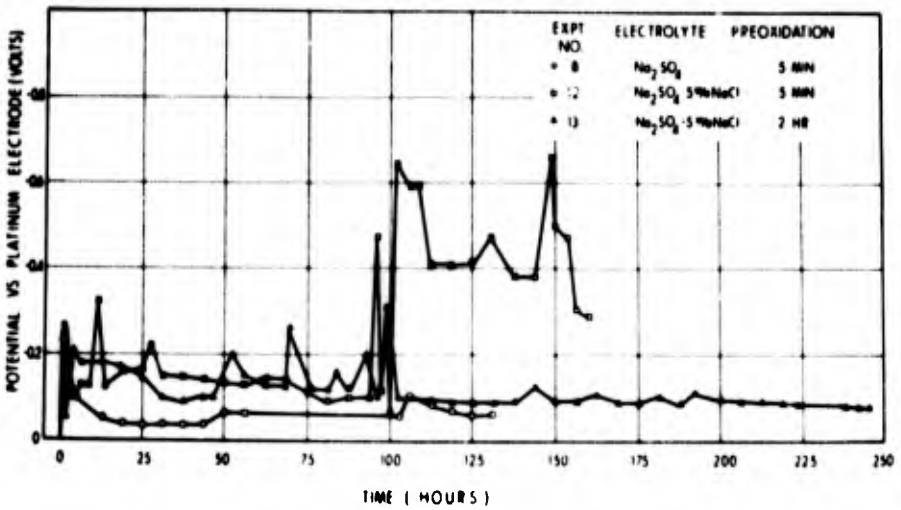

Figure 45.21. Potential-time curves of Alloy B (AMS 5384) at 1640 F in molten salts under air. (Wheatfall et al).

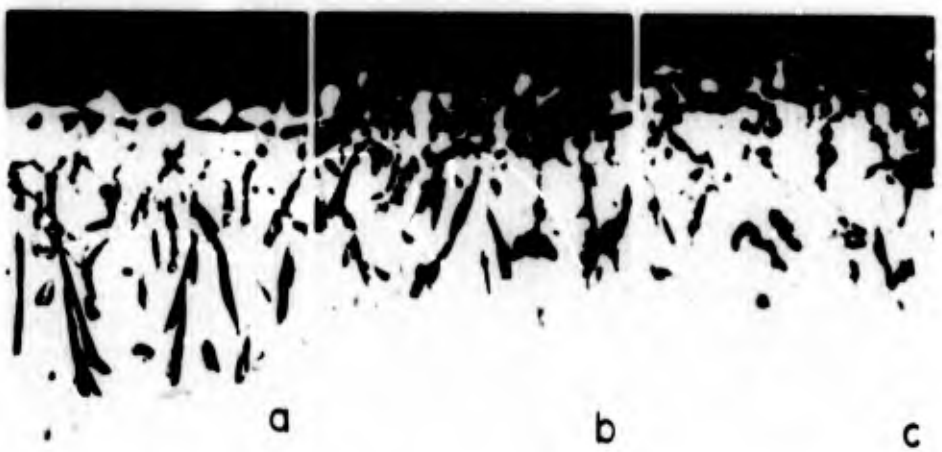

(a) Oxidized in air for 250 hr at 1650 F.
(b) Preoxidized 2 hr and immersed in Na_2SO_4 for 328 hr at 1650 F under air (Experiment 9, Table 10-XX).
(c) Preoxidized 2 hr and immersed in Na_2SO_4 for 238 hr under argon (Experiment 11, Table 10-Y).

Figur: 45.22. Micrograph of Alloy B (AMS 5374) (X2100) (Whea fall et al).

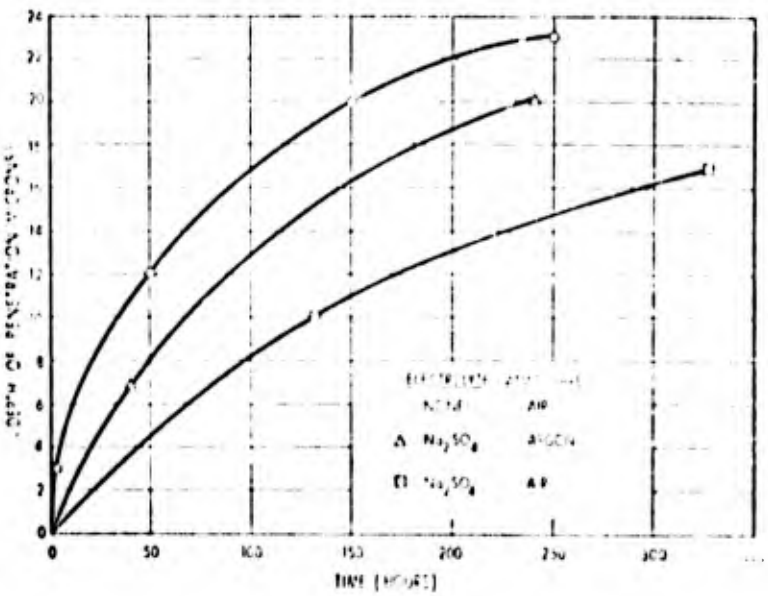

Figure 45.23. Maximum oxide penetration in Alloy B (AMS 5384) in air and molten Na_2SO_4 at 1650F under air and argon as indicated. (Wheatfall et al).

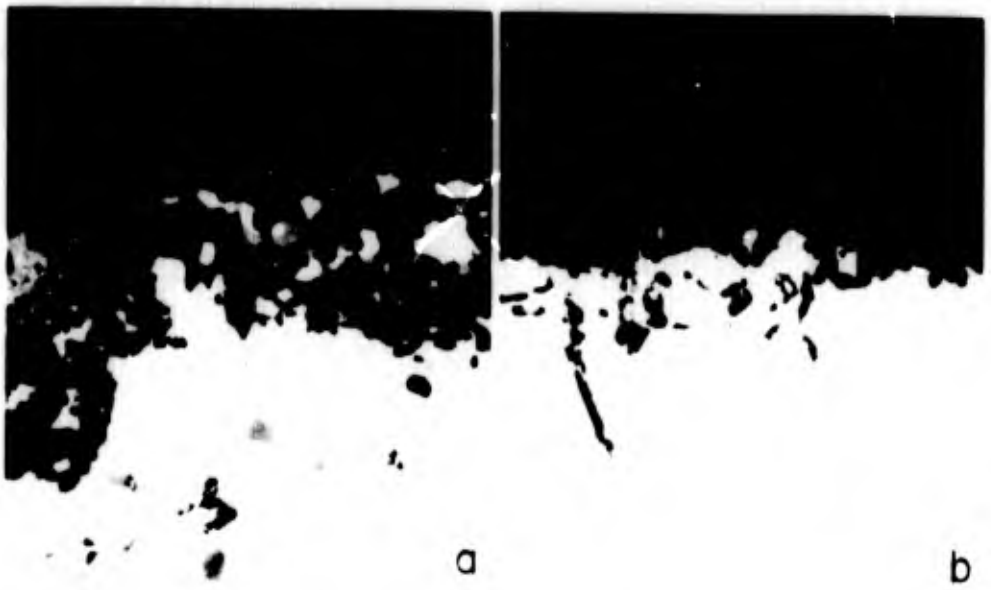

(a) Preoxidized 5 min and immersed in Na_2SO_4-5 weight % NaCl for 160 hr 1650 F under air (Experiment 12, Table 10-XX).
(b) Preoxidized 2 hr and immersed in Na_2SO_4-5 weight % NaCl for 245 hr at 1650 F under air (Experiment 13, Table 10-XX).

Figure 45.24. Micrograph of Alloy B (AMS 5384) (X2100). (Wheatfall et al).

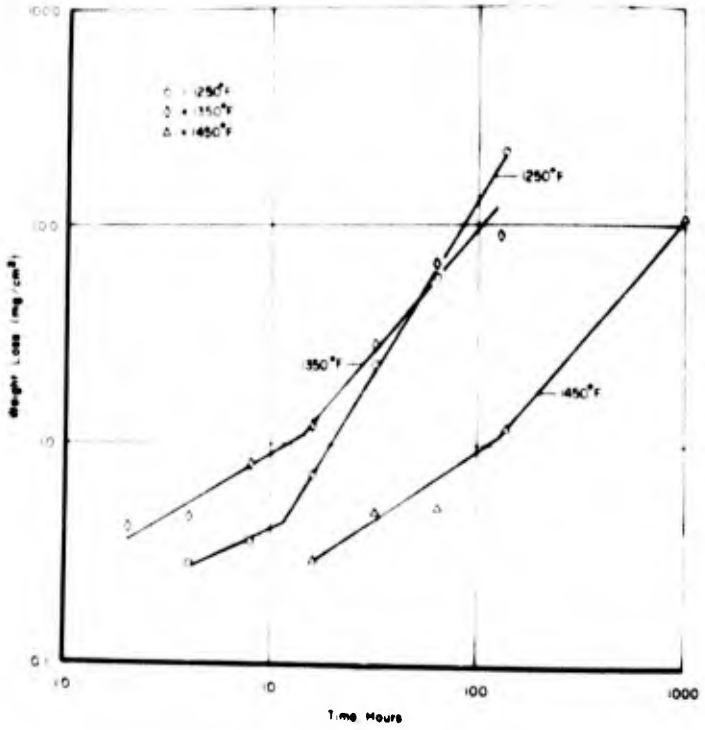

Figure 45.25. Weight loss of Ni-19 Cr-3 Al alloy after exposure to 1250, 1350, and 1450 F. (Wall and Michael).

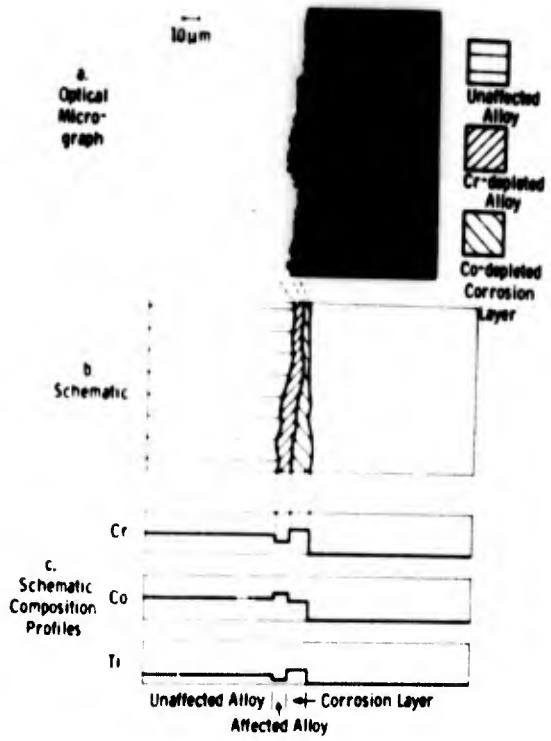

Figure 45.26. Composition profile of Ni-19 Cr-3 Al alloy exposed 200 hr at 1450 F. (Wall and Michael).

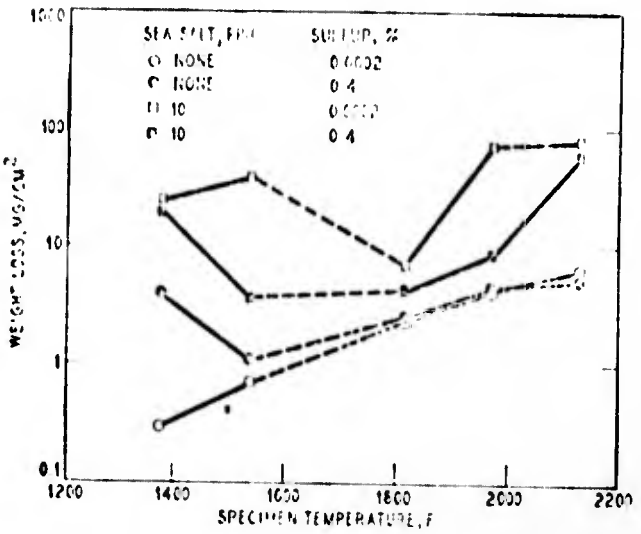

Figure 45.27. Hot corrosion of Udimet 500. (Quigg and Schirmer).

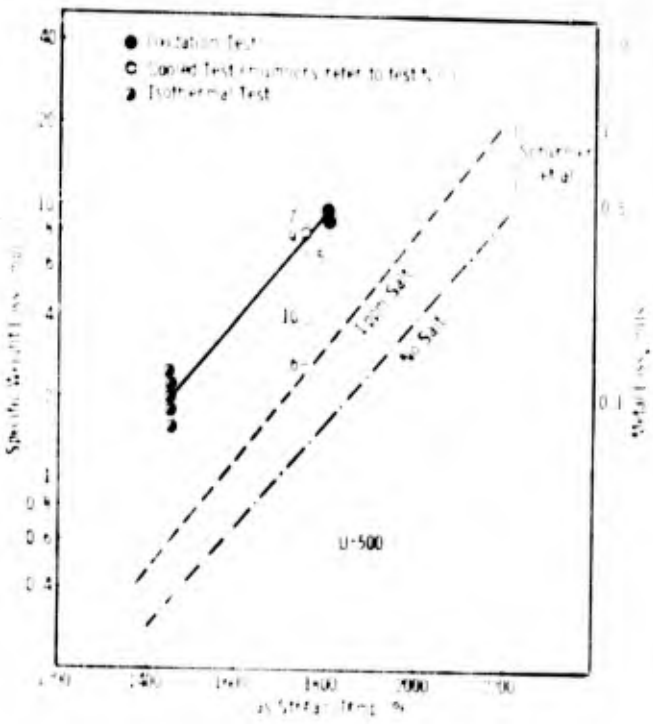

Figure 45.28. Effect of specimen cooling (U-500). (Lee and Young).

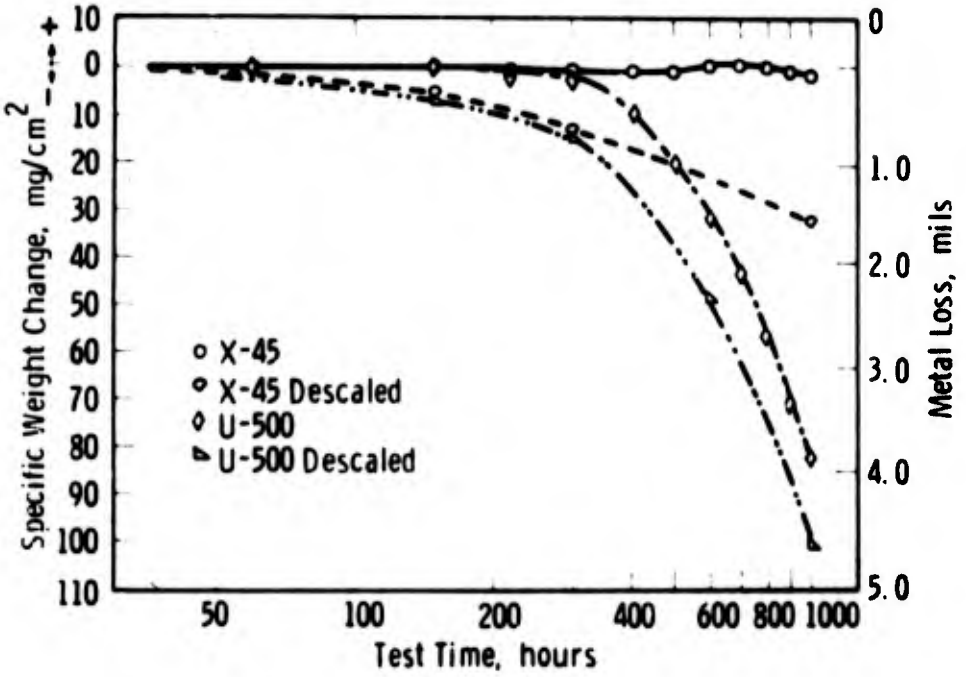

Figure 45.29. Weight change of U-500 and X-45 alloys oxidation tested at 1800°F in the cyclic furnace. (Lee et al).

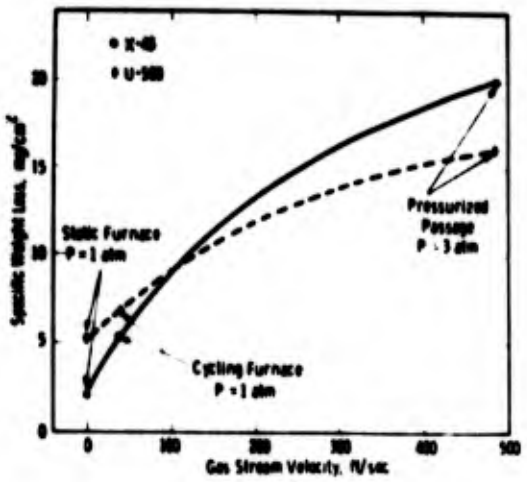

Figure 45.30. Effect of gas stream velocity on oxidation rate of X-45 and U-500 tested at 1800°F for 150 hr. (Lee et al).

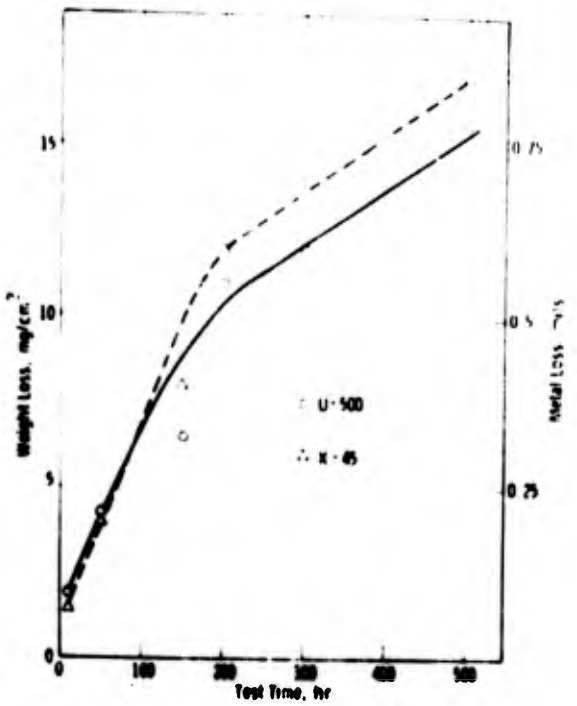

Figure 45.31. Oxidation rate of X-45 and U-500 tested in the pressurized passage of 1600°F gas temperature and 3 atm pressure. (Lee et al).

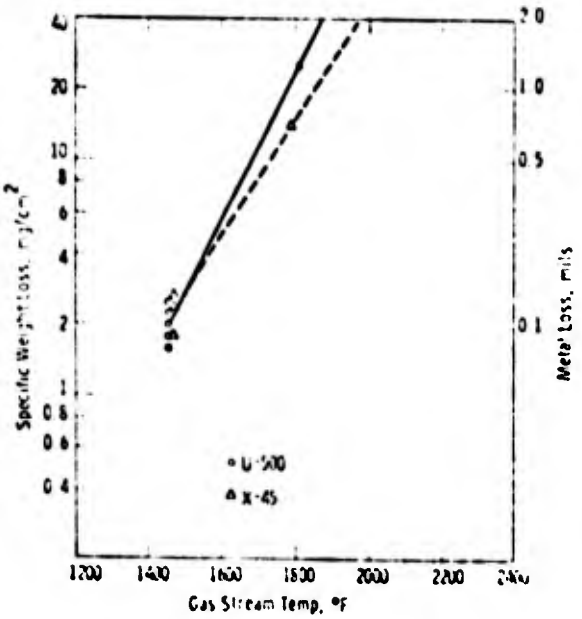

Figure 45.32. Effect of gas temperature on hot corrosion characteristics of X-45 and U-500 specimens tested for 50 hr at 3 atm pressure. (Lee et al).

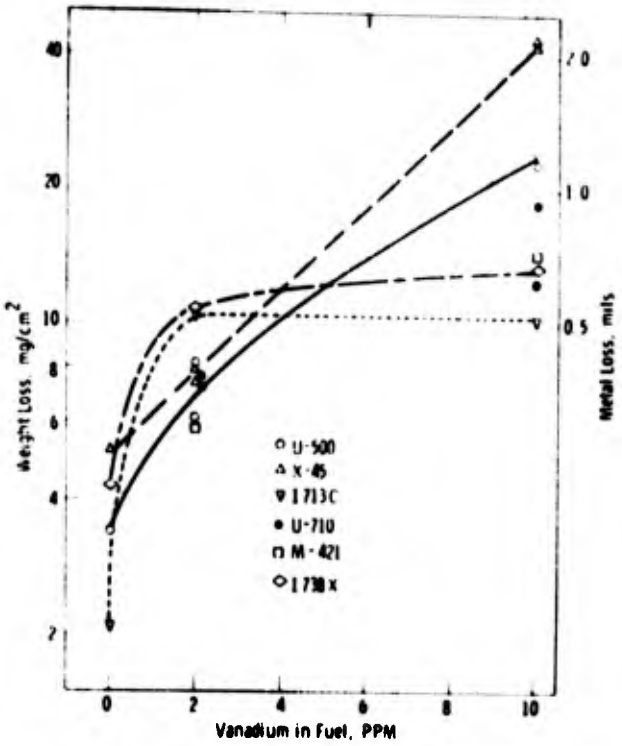

Figure 45.33. Effect of vanadium (with no sodium) on various alloys tested in the pressurized passage at 1500°F metal temperature and 3 atm pressure for 150 hr. (Lee et al).

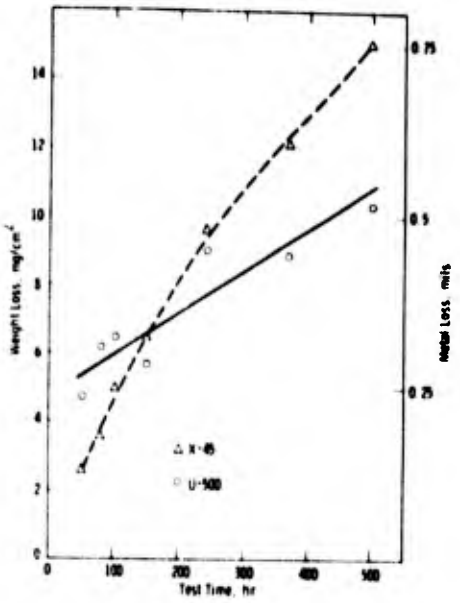

Figure 45.34. Corrosion rates of X-45 and U-500 tested in the passage with 2 ppm vanadium and no sodium at 1500°F and 3 atm pressure. (Lee et al).

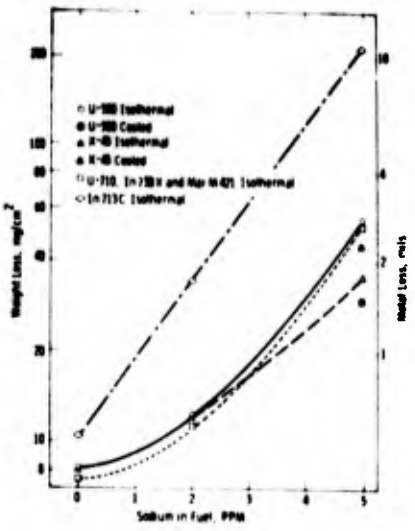

Figure 45.35. Effect of sodium (with 2 ppm vanadium) on various alloys tested in the pressurized passage at 1500°F metal temperature and 3 atm pressure for 150 hr. (Lee et al).

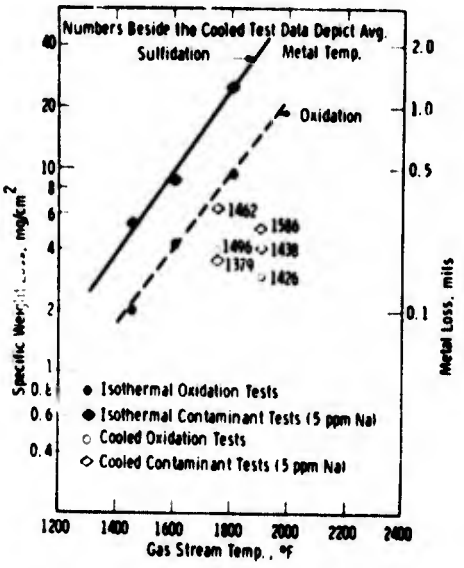

Figure 45.36. Effect of gas and metal temperature on hot corrosion characteristics for cooled and isothermal U-500 specimens tested for 50 hr at 3 atm pressure. (Lee et al).

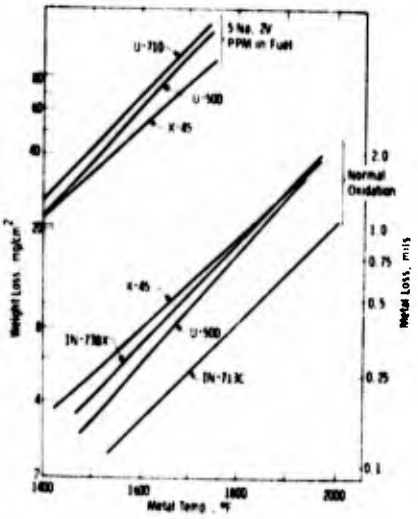

Figure 45.37. Corrosion rate of several alloys when burning 3-GT fuel compared to normal oxidation (Lee et al).

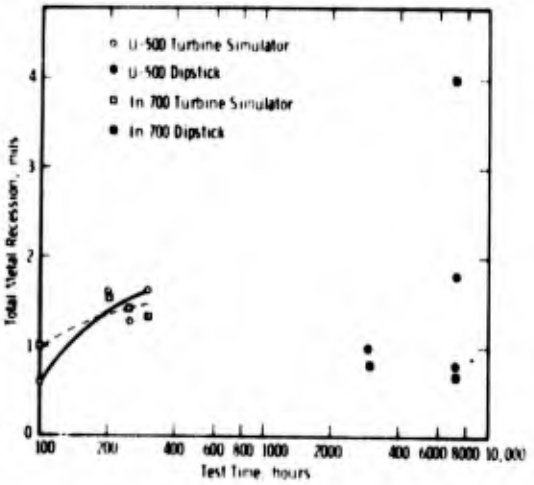

Figure 45.38. Turbine simulator and dipstick test data with fuel containing 2 ppm V and 0.8 ppm Na at 1370°F (Lee et al).

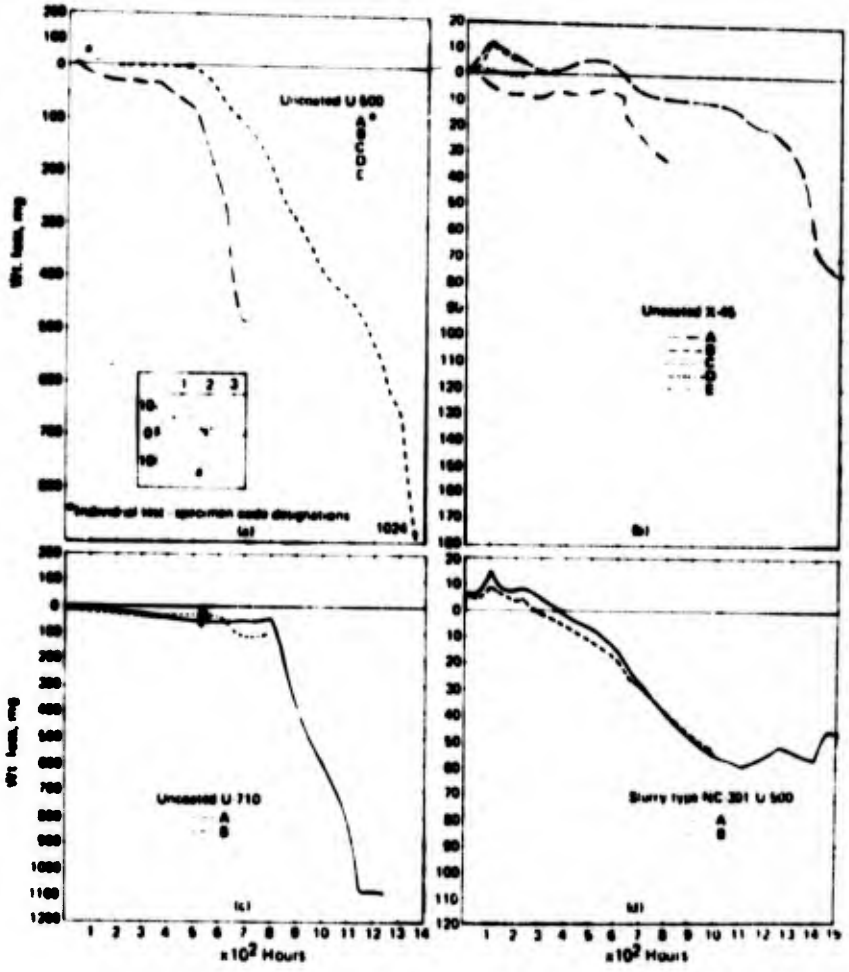

Figure 45.39. Weight change curves from spinning rig test No. 1. (Spengler et al).

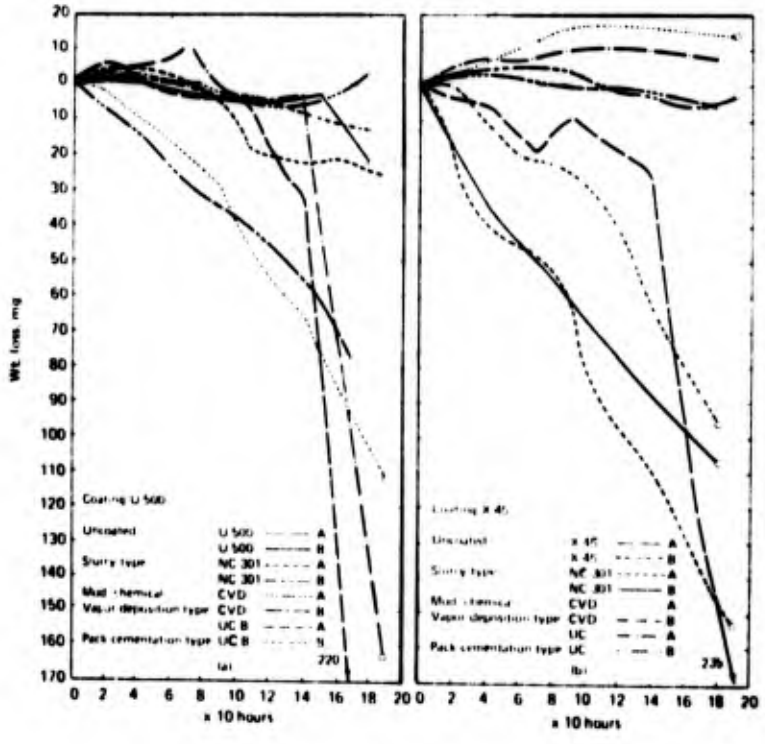

Figure 45.40. Weight change curves from turbine simulator test No. 1. (Spengler et al).

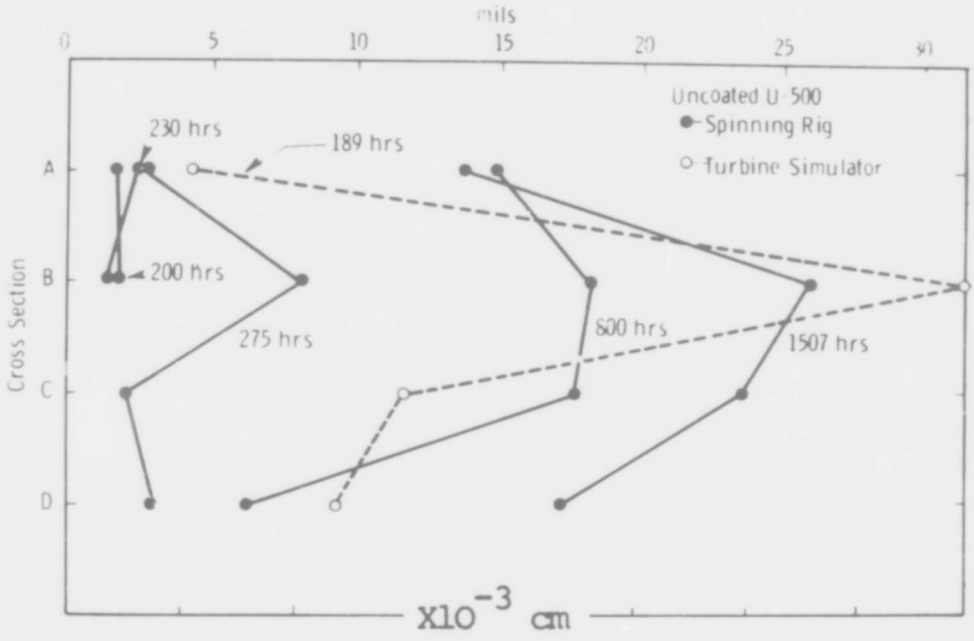

Figure 45.41. Penetration determined metallographically at different sections of U500 specimens: A is near the tip and D near the root. (Spengler et al).

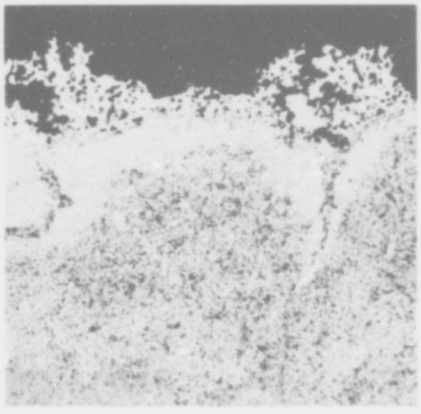

Figure 45.42. Section B, leading edge. Spinning rig at 1650°F, 1507 h (X120). (Spengler et al).

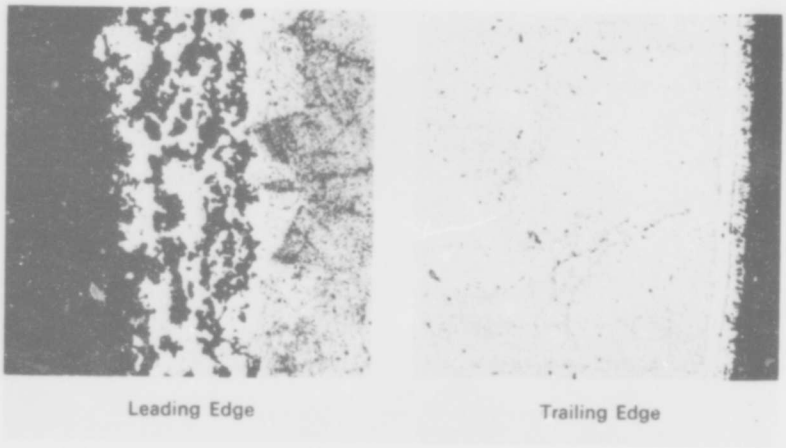

Figure 45.43. Section B. Turbine simulator at 1650°F, 189 h (X120). (Spengler et al).

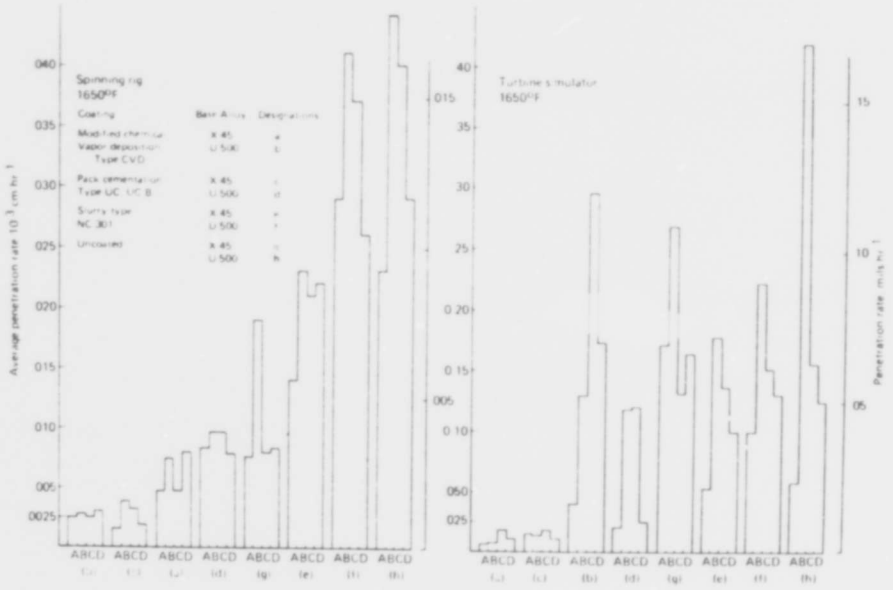

Figure 45.44. Long-term average penetration rates. Variation by cross-section. (Spengler et al).

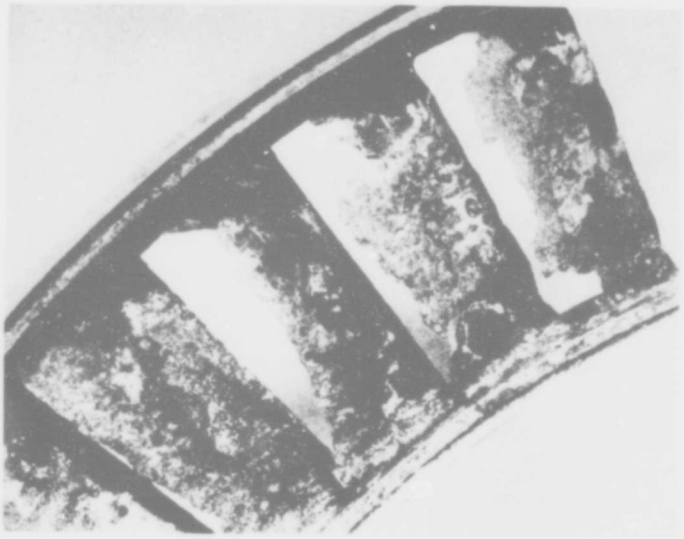

Figure 45.45. First-stage Udimet 500 stator, 1965-66. (Hussey et al)

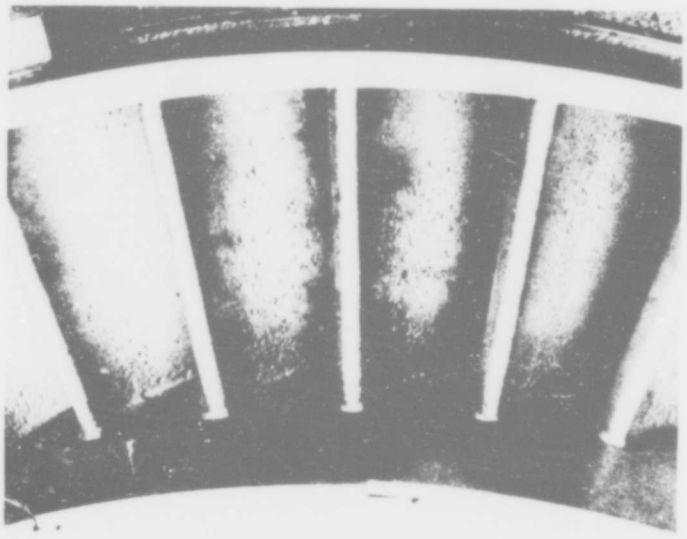

Figure 45.46. First-stage Udimet 500 stator pressure side, 1966-67.

Udimet 520

R. Viswanathan, Corrosion 24 (1968) 359.

See 713C for details. U-520 was one of the better alloys, very similar to U-500, Hastelloy X and Waspaloy. After 150h at 1500°F (816°C) it had lost 2.9 mg/cm^2 (after descaling). 96.0% of the metal was unaffected. Figure 46.1 shows the essentially uniform attack on the alloy.

The alloy was modified by the addition of 0.1 - 0.3% La and Y. With 0.2% La, the scale after 150h corrosion at 1500°F (816°C) contained $(Cr,Ti)_2O_3$, $CoCr_2O_4$, and Al_2O_3. The affected alloy contained CrS_x, TiS_x and LaS_x. No other details are given.

The effect of two different sulphur trioxide levels in the gas stream was tested: 6 ppm and 150 ppm. The weight losses in a 150h test at 1500°F (816°C) were 2.90 and 2.9 mg/cm^2 respectively. Some alloys - U-700, 713C, and Inco 700 - were very sensitive to the amount of So_3.

C. E. Hussey, S. Y. Lee and W. E. Young, paper presented to the ASTM Annual Meeting, Symposium on Gas Turbine Fuel Requirements, Handling and Quality Control, June 1972.

See U-500 for extended summary.

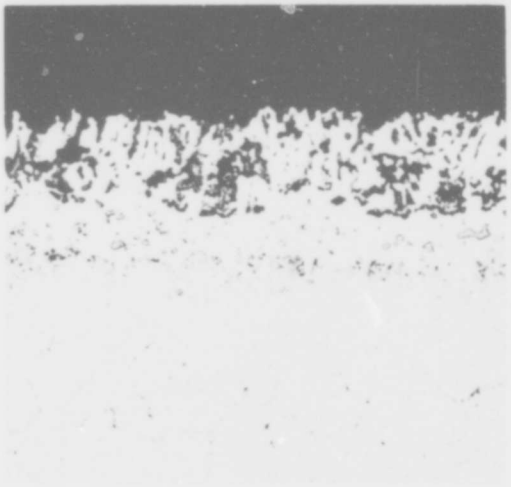

Figure 46.1. Udimet 520 after 150 hours of corrosion testing. 500X. (Viswanathan).

Udimet 700

P. A. Bergman, G. T. Sims, and A. N. Baltran, Hot Corrosion Problems Associated with Gas Turbines; ASTM Special Technical Publication, STP 421, 1967, 38.

See 713C for details.In burner rig.test,100h 200 ppm salt, 1750°F(954°C), the surface loss was 75.6 mils (loss in diameter); the maximum penetration was 92.4 mils. Very poor. The authors note that this is surprising, since the alloy has served most reliably in aircraft jet engines, whereas 713 has been subject to severe hot corrosion (comes out better in this test). This heat of U-700 was low in chromium (13.6 versus nominal 15%). Also, U-700 shows a "reversal" at 1600°F (871°C) where behaviour is acceptable. So test may be misleading in this respect.

L. D. Graham, J. D. Gadd, and R. J. Quigg, Hot Corrosion Problems Associated with Gas Turbines, ASTM Special Technical Publication, STP 421, 1967, 105.

See 713C for details. Very little attack in either the PWA rig test or the crucible test. U-700 is listed as one of the better "intermediate" alloys: W1-52 (!) is about the same, IN 100 a little worse.

J. J. Walters (AVCO/Lycoming Division) Technical Report to the Air Force Materials Laboratory, Wright-Patterson Air Force Base AFML-TR-67-297 (September 1967).

Extended summary in B 1900. U-700 is one of a group of alloys stated to have "relatively good resistance to attack" (the others are IN 728X, and TRW 1800). Threshold and terminal temperatures after 120 and 360h in JP-4 with 4 ppm salt are 1625 and 1750°F in 120h, 1600 and 1750°F in 360h (885 and 953; 871 and 953°C). The corrosion products on trailing edge after 40h of rig testing are NiO + spinel with spacing 8.32 Å ; after 120h, the same and the same in powders removed from an area which had undergone sulphidation corrosion in 120h test. Microprobe analysis of the depletion layer in the alloy: 76.2% Ni, 0.9% Cr, 3.6% Mo, 2.3% Al, 0.12% Ti, 19.0% Co. Figure 47.1 shows the corrosion as a function of temperature for U-700, JP-4 fuel, 8 ppm salt. Figure 47.2 - JP - 4, 4ppm salt. Figure 47.3 - JP - 4; 8 ppm salt. Figure 47.4 - JP - 4R fuel, 4 ppm salt. Figure 47.5 - JP-5 fuel, 8 ppm salt. Figure 47.6 - corrosion as a function of temperature for U-700 tested using JP-4 fuel with 4 ppm salt in 120, 240 and 360h. Figure 47.7 shows a section of the oxidised surface after 360h at 1700°F (927°C).

R. Viswanathan, Corrosion 24 (1968) 359.

See 713C for details. U-700 was one of the worst alloys tested: only Inco 700 was as bad. The weight loss after 10h at 1500°F (816°C) was 0.6 mg/cm^2; after 150h it was 275 mg/cm^2 (this suggests the existance of an incubation period). After the 150h test, none of the specimen was unaffected by the corrosion. The attack was very irregular: some regions showed little attack, others were completely penetrated. Figure 47.8 shows the cross-section of a specimen corroded for 150h; it appears that there is preferential oxidation along grey sulphides.

The alloy was modified by the addition of 0.1 - 0.3% La or Y.

Figure 47.9 shows the attack in a 200h test at 1500°F as a function of rare earth content: La seems more effective than Y; the optimum level seems to be 0.2% in both cases. While the unmodified alloy was severely attacked, the modified alloys seemed to be totally unattacked. Figure 47.10 shows a cross-section of the 0.2% La alloy after 200h at 1500°F. The alloy contained Cr_2O_3, Al_2O_3, CoO and TiO_2 in the scale: (Cr, Ti, Mo) S_x, CrS_x, TiS_x and LaS_x in the affected alloy. Figure 47.11 sketches the general distribution of the phases.

The effect of two different sulphur trioxide levels in the gas stream was tested: 6 ppm and 150 ppm. In 150h at 1500°F the weight losses were 3.40 and 275 mg/cm^2 respectively. The author considers that the sulphur trioxide stabilises the sulphate coating of the specimen.

R. Field, D. J. Fisk and H. von E. Doering, Naval Ship Research and Development Centre, Materials laboratory Research and Development Report 2833 (January 1969).

See 713C.

V. S. Moore and A. R. Stetson, Final Report on NASC Contract No. N00019-68-C-0532 (Solar Research Division Report RDR 1626-5) December 1970.

See B1900 for details. Figure 47.12 shows the microstructure of uncoated U-700 after 110h at 1650°F (899°C). The alloy was quite resistant, but failed after 110h at 1650°F. There was no severe intergranular oxidation. Hot corrosion testing resulted in decarburisation and the formation of an alloy depletion layer. U 700 was one of the best tested, exceeded only by U 710; better than Rene 41.

At 1650°F two specimens were tested, with cumulative weight change as shown : Table 47-I.

Table 47-I Cumulative weight changes in Hot Corrosion Tests and U 700 (Moore and Stetson)

Exposure time, hrs.		10	20	30	40	50	60	70	80	90	100	110
Cumulative weight change, mg.	Spec. 1.	+7.4	+10.6	+11.0	+20.4	·19.4	+19.7	+19.8	+22.1	+20.0	+12.9	+10.6
	Spec. 2.	+8.1	+8.9	+9.5	+23.7	+19.5	+20.7	+20.9	+22.5	+21.4	+23.2	+3.2

At 1800°F two specimens were tested :-

Spec. 1.	+15.2	+14.4	+20.8	+20.4	+20.7	+25.1	+19.0	+18.9	+24.4	+25.2	+25.0
Spec. 2.	+5.3	+21.8	+42.4	+43.2	+24.4	+21.9	+17.6	+17.6	+17.4	+12.0	+35.7
Time, h.	10	20	30	40	50	70	80	100	120	140	150

H. T. Quigg and R. M. Schirmer, Progress Report No.3 on NASC Contract No. N00019-68-C-0252 (Phillips Petroleum Company Research and Development Report 5423-60) July 1969.

See 713C for details. This report is primarily concerned with testing the ASTM "Round Robin" group of alloys in the Phillips Turbine Enviromental Simulator using a cyclic test in which the specimen is heated to 1600, 1800 or 2000°F (871, 982 or 1093°C) maximum temperature for 8 min following a cooling to 1000°F (538°C) for 2 min, producing an attack approximately six times more severe than the isothermal routine used in their earlier tests. After 44h at 2000°F maximum, the weight loss was 164 mg/cm^2 , the surface loss was 20 mils and the maximum attack was 21 mils: a little worse than Mar-M 421 but a great deal better than 713C. It was estimated that it would take 35h to lose 127 mg/cm^2 at 2000°F.

ASTM Round Robin Test organised by the Hot Corrosion Task Force of the Gas Turbine Panel, 1970.

See 713C for details. U-700 was one of two alloys of intermediate corrosion resistance, being rather worse than the other, Mar-M 421, but significantly better than 713C. Figure 47.13 shows the metal loss data reported by the participants.

H. T. Quigg, R. M. Schirmer and L. Bagnetto, Final Report to NASC on Contract No. N00019-69-C-0221 (Phillips Petroleum Company Research and Development Report 5732-70) July 1970.

See 713C for details.

M. J. Donachie, Jr., R. A. Sprague, R. N. Russell, K. G. Boll and E. F. Bradley, Hot Corrosion Problems Associated with Gas Turbines, ASTM Special Technical Publication STP 421, 1967, 85.

See 713C for details and to principal results U-700 was tested in both wrought and cast conditions; U 700 (wrought) behaves almost exactly the same as 713, with little corrosion at 7 ppm salt, but considerable attack with 35 ppm in 50h tests at 1650F (899°C). In tests at 1650F with JP-5R fuel and 3.5 ppm salt as a function of time the cast alloy behaves like 713, but the wrought alloy is significantly better, comparable with Waspaloy. In a 50h, 35 ppm salt test U 700 was comparable to 713, and significantly worse than X-40 or Mar-M 302; but in a 500h, 3.5 ppm salt test at 1650°F, it was comparable to the cobalt base alloys and much superior to 713.

Some crucible tests are briefly mentioned: U 700 was severely attacked by a 90/10 Na_2SO_4/NaCl mixture at 1650F in still air, whereas Waspaloy was unattacked.

Figure 47.14 shows a first stage U 700 turbine blade from a marine engine after 1100h, showing severe hot corrosion of the airfoil surface.

The authors comment that in aircraft engines operated in areas where sporadic salt ingestion occurs, slight distress due to hot corrosion of 713 has occured while U 700 operated under the same conditions has been free from hot corrosion attack.

H. T. Quigg, R. M. Schirmer and L. Bagnetto, Final Report to Naval Air Systems Command on Contract N00019-70-C-0293 (Phillips Petroleum Company Research and Development Report 5903-71) Jan. 1971.

See 713C for details. Uncoated U 700 seems intermediate between 713C and IN 738, which is about the same as U 710.

K. Page and R. J. Taylor, in "Deposition and Corrosion in Gas Turbines" A. B. Hart and A.J.B. Cutler (eds.), (Applied Science Publishers, London, 1973) 350.

See Nimonic 105 for details.

W.L. Wheatfall, in "High Temperature Corrosion of Aerospace Alloys" J. Stringer, R. I. Jaffee and T. F. Kearns (eds.), AGARD Conference Proceedings No. 120, (March 1973) 235.

See 713C for details.

S. T. Wlodek, Trans. AIME, 230 (1964) 1078.

See also Rene 41. Specimen were tested in dry air with surfaces abraded through 600 grit, electropolished and lightly etched. Figure 47.18 shows the weight gains as a function of time for temperatures in the range 1600 - 2000°F (871 - 1093°C); the initial stages can be reasonably fitted by a linear rate law, the later stages by a parabolic rate law, although at 1900°F the rate of reaction slows down more rapidly than this; the shape of the rate curve at 1900°F was reproduced three times. Figure 47.19 shows the initial linear reaction rate, and Figure 47.20 shows a parabolic plot of later stages; there is some indication of a rate transition from a fast parabolic rate to a slower one. The various rate constants are presented in Table 47.I. The reaction products were identified by X-ray diffraction and tabulated (see Rene 41).

Figure 47.21 sumarises the conditions required to produce 1.0 or 2.0 mls of damage, either by alloy depletion (AD) or by internal oxidation (IO) Figure 47.22 (a) shows a sample oxidised 100h at 1800°F: there has been internal oxidation, but at 1900°F, the internal oxidation is absent (47.22b).

The phases produced during internal oxidation were determined by electron diffraction from extraction replicas. Figure 47.23 presents the results schematically for U-700. Table 47.II shows the surface oxides identified on U 700 after 100h at 1800°F (982°C) Figure 47.24 shows the effect of surface preparation on the oxidation - the trend seems to be the reverse of that for Rene 41.

Figure 47.25 presents a summary of the principal stages of oxidation of U-700. The "passivation" at 1900°F is attributed to the formation of an Al_2O_3 scale, reducing the oxygen activity at the metal surface to the point at which internal oxidation cannot take place.

Data relating to this alloy will also be found in the following figures :

1.1, 1.7, 1.8, 10.13, 10.51, 10.53, 10.58, 10.62, 10.65, 10.66, 10.67, 10.68, 10.84, 10.105, 10.106, 10.119, 10.123, 10.124, 32.17, 32.18, 32.19, 32.20;

and Tables :

1-1, 1-11, 1-IV, 1-V, 1-V1, 1-V11, 1-V111, 1-1X, 1-X, 10-X1, 10-X111, 10-XV, 10-XV1, 10-XV111, 10-X1X, 10-XXV, 10-XXV1, 10-XXX, 18-1V.

TABLE 47-I

SUMMARY OF UDIMET 700 RATE CONSTANTS (WLODEK)

Temp., F	Condition	Operating Rate Constants and Time of Duration
1600	S.A.	A_{I} $1.97 \cdot 10^{-1}$ (t 30), $A_{I\,II}$ $5.00 \cdot 10^{-4}$ (200 t 30), A_{II} $3.89 \cdot 10^{-5}$ (t 200)
1600	Aged	A_{I} $1.72 \cdot 10^{-1}$ (t 25), $A_{I\,II}$ $5.36 \cdot 10^{-4}$ (200 t 25), A_{II} $5.25 \cdot 10^{-5}$ (t 200)
1700	S.A	A_{I} $3.46 \cdot 10^{-1}$ (100 t 10), $A_{I\,II}$ $1.15 \cdot 10^{-3}$ (200 t 100), A_{II} $7.50 \cdot 10^{-6}$ (t 200)
1800	S.A	A_{I} $1.95 \cdot 10^{-1}$ (t 10), $A_{I\,II}$ $3.32 \cdot 10^{-3}$ (300 t 10), A_{II} $1.28 \cdot 10^{-3}$ (t 300)
1800	Aged	A_{I} $1.57 \cdot 10^{-1}$ (t 10), $A_{I\,II}$ $1.25 \cdot 10^{-3}$ (500 t 10), A_{II} $7.87 \cdot 10^{-5}$ (t 500)
1900	S.A.	A_{I} $2.18 \cdot 10^{-1}$ (t 10), $A_{I\,II}$ $1.97 \cdot 10^{-3}$ (350 t 10), A_{II} $1.17 \cdot 10^{-5}$ (t 350)
1900	S.A.	A_{I} $2.32 \cdot 10^{-1}$ (t 10), $A_{I\,II}$ $5.64 \cdot 10^{-4}$ (200 t 10), A_{II} $1.32 \cdot 10^{-5}$ (t 200)
2000	S.A.	A_{I} $4.70 \cdot 10^{-1}$ (t 10), $A_{I\,II}$ $3.65 \cdot 10^{-4}$ (t 10)
2000	Aged	A_{I} $1.44 \cdot 10^{-1}$ (t 5), $A_{I\,II}$ $5.65 \cdot 10^{-4}$ (t 5)

A_{I} mg per sq cm per min, A_{II} sq mg per cm^4 per sq min. Values in parentheses indicate time in minutes during which each rate constant is operative.

TABLE 47-II

X-RAY DIFFRACTION ON SURFACE OXIDES FORMED ON UDIMET 700 AFTER 100 Hr/1800°F (WLODEK)

Electropolished before Exposure					Grit-Blasted before Exposure		
d, Å	I	$NiCr_2O_4$, Cubic, a_o=8.31Å	Cr_2O_3, Rhombohedral, a = 55.40°, a_o = 5.37Å	TiO_2, Tetragonal, a_o = 4.6Å, c_o = 2.9Å	d, Å	I	$NiCr_2O_4$, Cubic, a_o = 8.29Å
4.80	VW	(111)	-	-	4.80*	VW	(111)
3.65	VW	-	(012)	-	4.50*	VW	-
3.27	VW	-	-	(110)	3.30	W	-
2.93	M	(220)	-	-	2.95	M	(220)
					2.51*	S	(311)
2.67	W	-	(104)	-	2.40*	VW	-
2.51	S	(311)	-	(101)	2.33	VW	-
2.48	VW	-	(110)	-	2.07	M	(400)
2.33	VW	-	-	(220)	1.75*	VW	-
2.19	VW	-	-	(111)	1.71	VW	-
1.07	M	(400)	-	-	1.70*	VW	(422)
1.81	VW	-	(024)	(211)	1.65	W	-
1.69	VW	(422)	-	-	1.60	M	(511), (353)
1.67	VW	-	(116)	-	1.47*	M	(440)
1.60	M	(511), (333)	-	-	1.38	W	-
1.465	M	(440)	-	-	1.265*	W	(533)
1.310	VW	(620)	-	-	1.100	VW	-
1.269	VW	(533)	-	-	1.080*	VW	(731), (553)
1.250	VW	-	(220)	-	1.060*	VW	-
1.200	VW	(444)	-	-	1.040	VW	-

*Unidentified. Most if not all of these weak reflections could be associated with traces of TiO_2, TiO, and NiO.

D & S film patterns on surface oxides scrapped from specimens. Filtered Cu radiation. All samples Heat B fully aged.

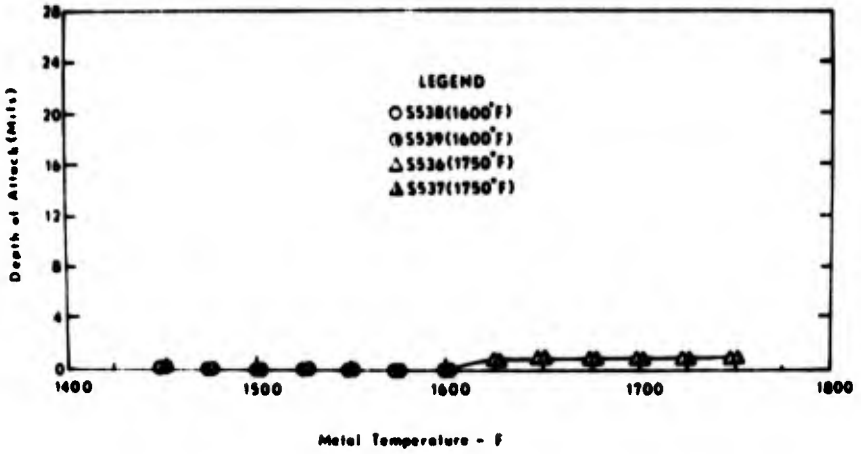

Figure 47.1. Corrosion as a function of temperature for U700 tested using JP-4 fuel with a Salt/air ratio of 8 ppm. (Walters).

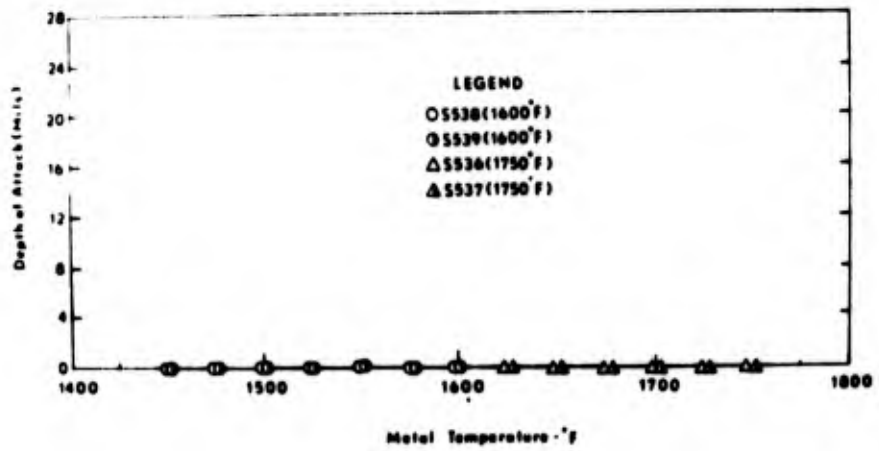

Figure 47.2. Corrosion as a function of temperature for U700 tested using JP-4 fuel with a Salt/Air Ratio of 4 ppm. (Walters).

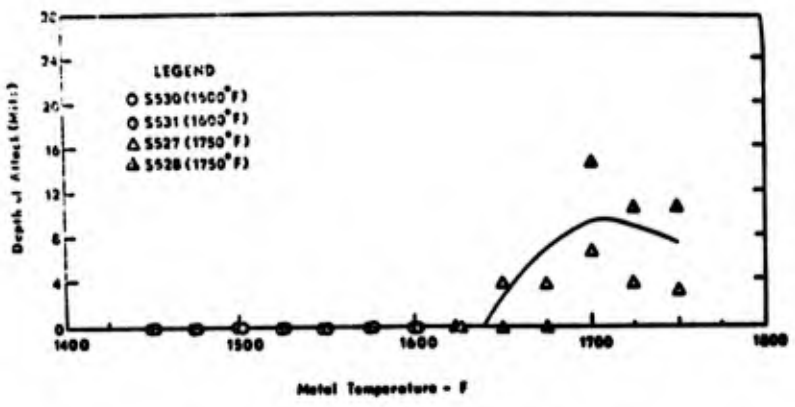

Figure 47.3. Corrosion as a function of temperature for U700 using a JP-4R fuel with a Salt/Air Ratio of 8 ppm. (Walters).

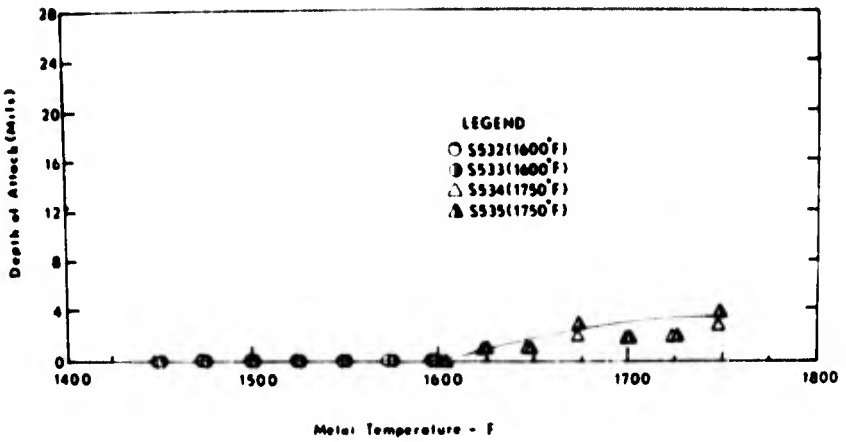

Figure 47.4. Corrosion as a function of temperature for U700 using JP-4R fuel with a Salt/Air Ratio of 4 ppm. (Walters).

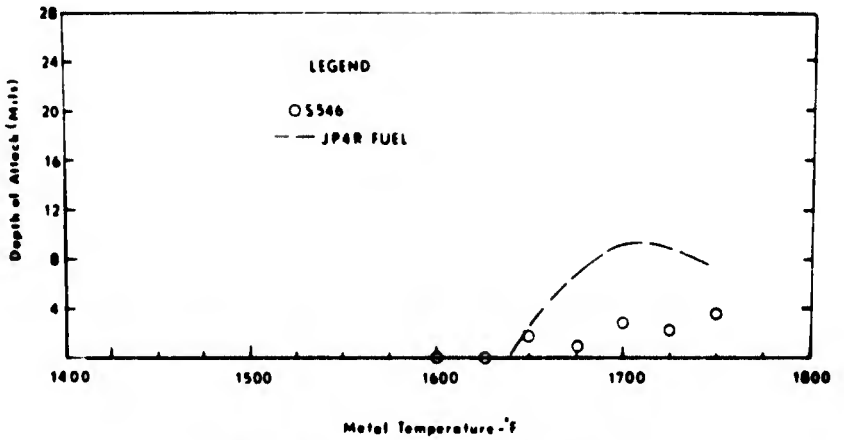

Figure 47.5. Corrosion as a function of temperature for U700 tested using JP-5 fuel (0.16%S) with a Salt/Air Ratio of 8 ppm. (Walters).

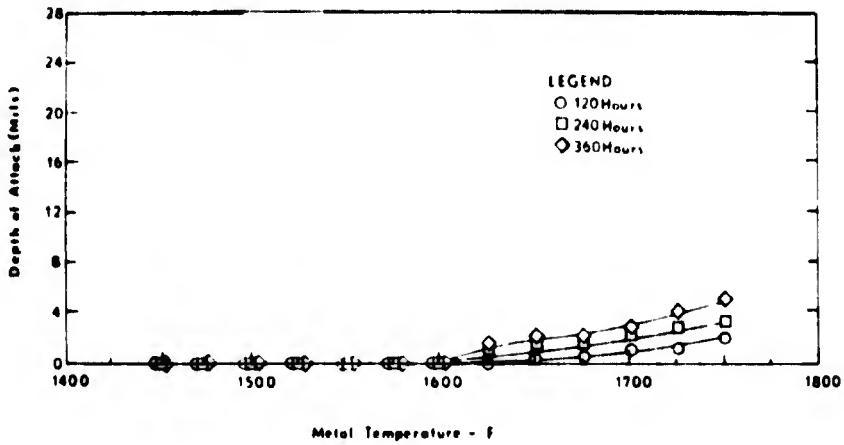

Figure 47.6. Corrosion as a function of temperature for U700 tested using JP-4 fuel with a Salt/air Ratio of 4 ppm. (Walters).

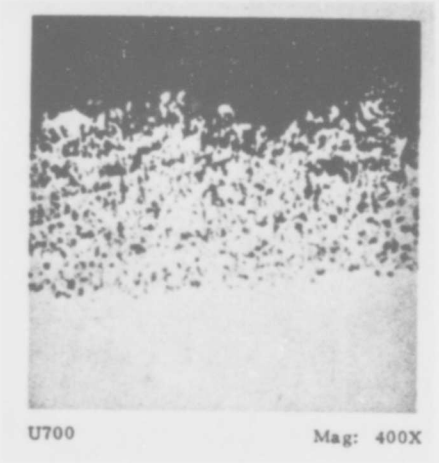

Figure 47.7. Oxidised surface of U700 after 360h testing at 1700°F. (Walters).

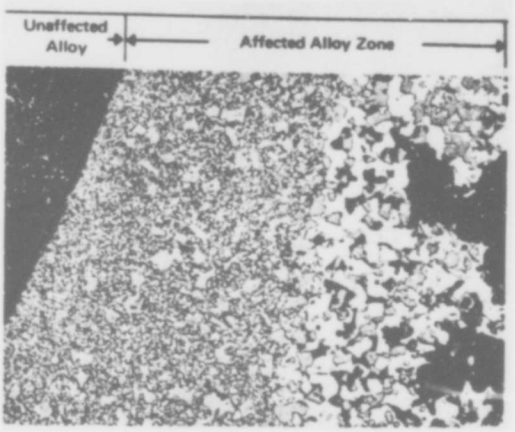

Figure 47.8. Udimet 700 after 150 hours of testing at 1500 F. 142X. (Viswanathan).

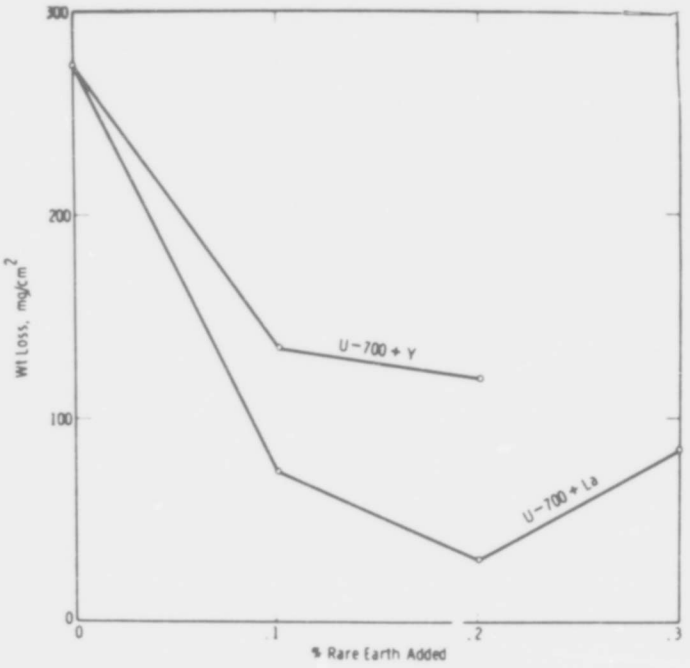

Figure 47.9. Weight loss vs % rare earth addition for samples tested at 1500 F for 200 hours. (Viswanathan).

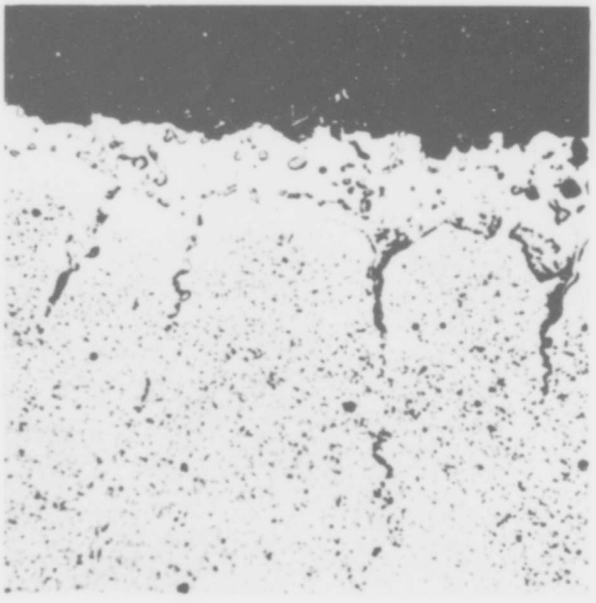

Figure 47.10. Udimet 700 + 0.2 La corroded at 1500 F for 200 hours. 500X. (Viswanathan).

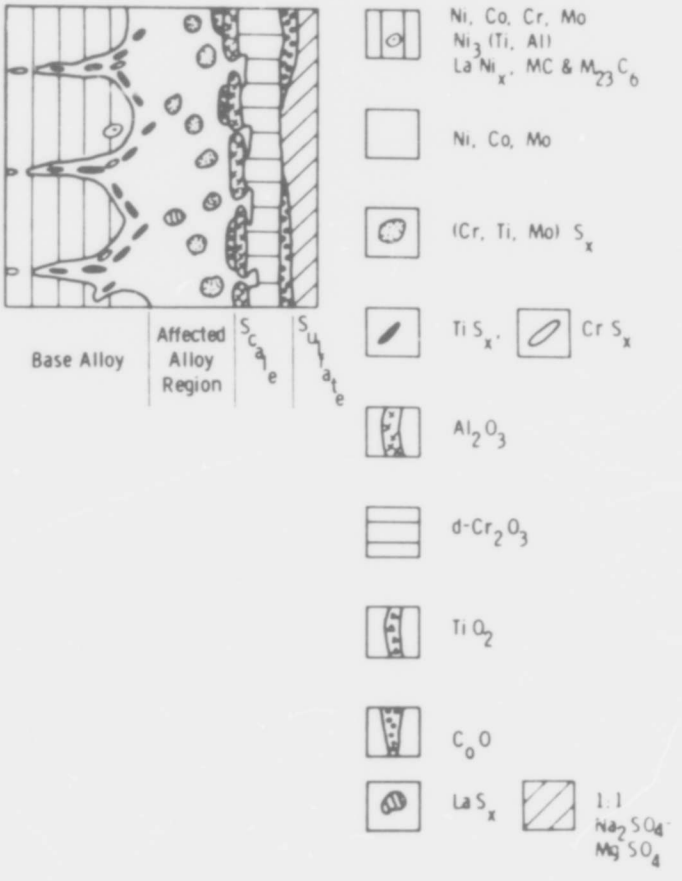

Figure 47.11. Udimet 700 + 0.2 La at 1500 for 150 hours. The schematic represents corrosion layers. (Viswanathan).

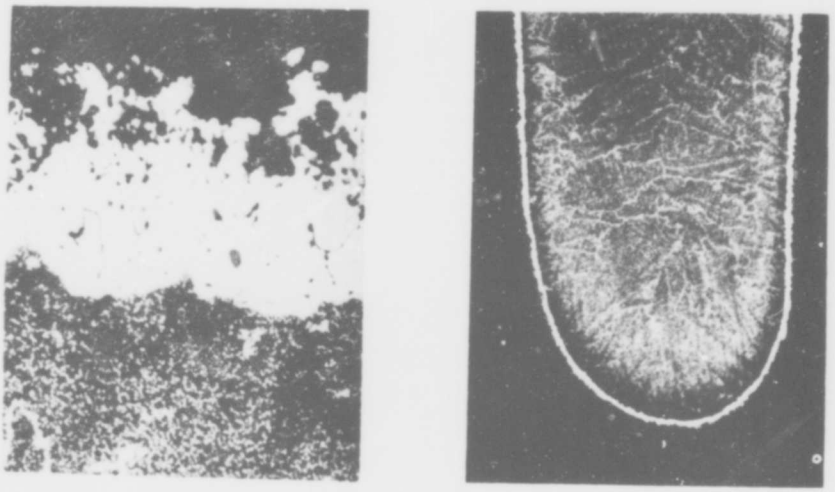

Magnification: 1000X Specimen U2 Magnification: 10X

Figure 47.12. Microstructure of uncoated U-700 alloy after hot corrosion tests at 1650°F for 110 hours. (Moore and Stetson).

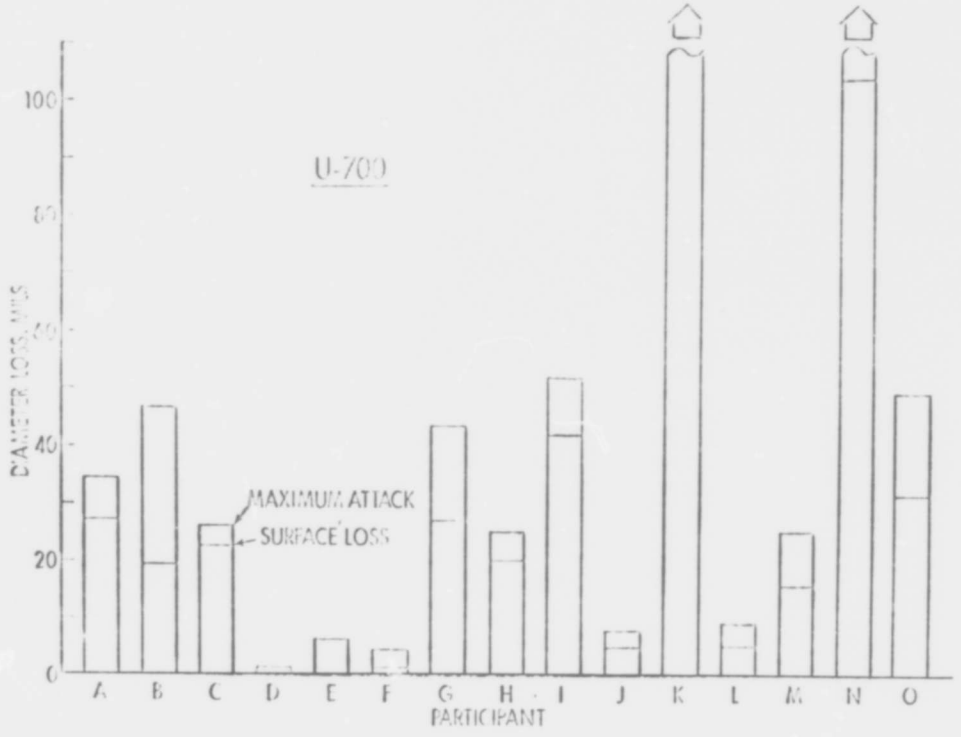

Figure 47.13. Results of the ASTM Round Robin test for U 700.

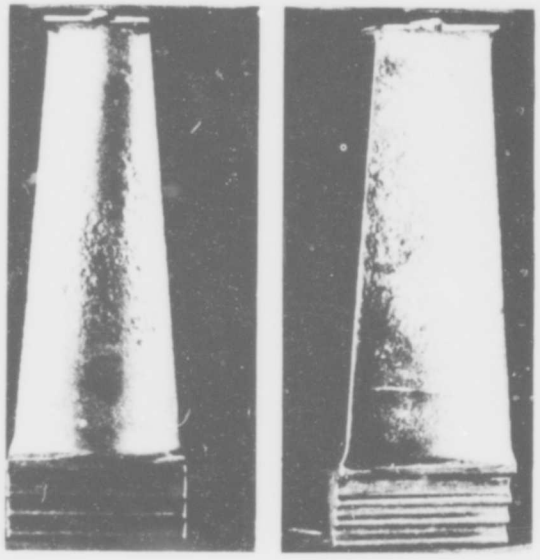

Figure 47.14. First stage U 700 turbine blade from marine engine after approximately 1100 hr showing severe sulphidation corrosion of airfoil surface. (Donachie et al).

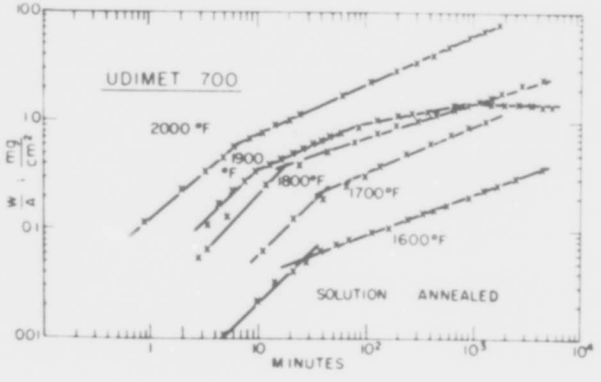

Figure 47.18. Logarithmic weight-gain plot for Udimet 700 indicating initial linear and subsequent parabolic behaviour and a complete cessation of weight gain at 1900°F after 1000 min. (Wlodek).

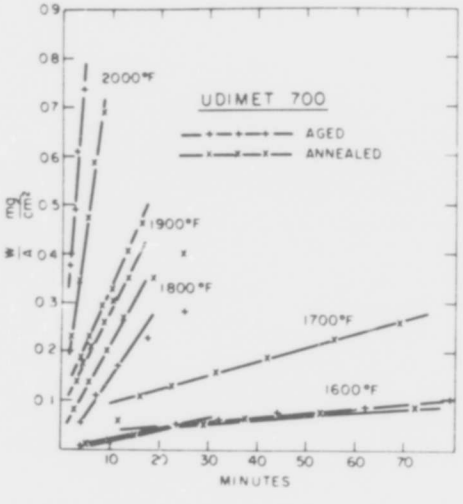

Figure 47.19. Linear plot of weight gain during initial oxidation of Udimet 700. (Wlodek).

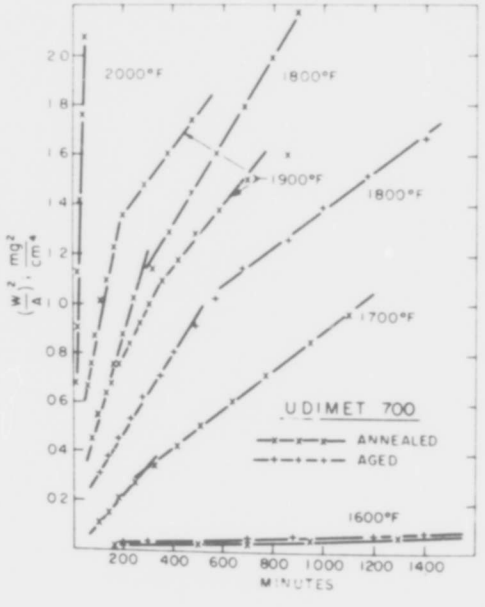

Figure 47.20. Parabolic oxidation kinetics for Udimet 700 reflect the instability of behaviour at 1900°F. (Wlodek).

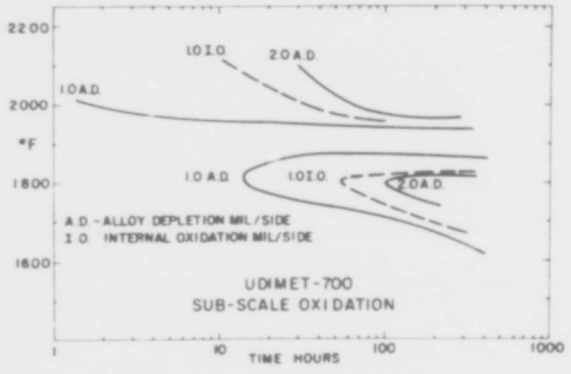

Figure 47.21. Isoreactivity plots for constant amount of subscale damage in Udimet 700. Note complete reversal of behaviour at 1900°F and absence of internal oxidation at this temperature. (Wlodek).

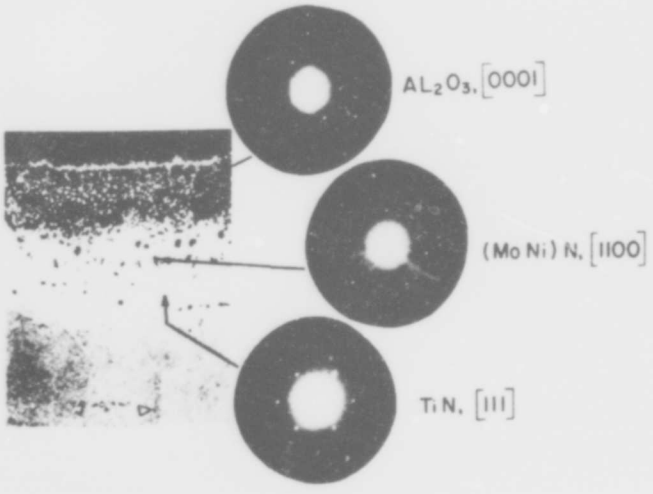

Figure 47.23. Identification of subscale reaction products by electron-diffraction and extraction-replica techniques on a specimen oxidized 400 hr at 1700°F. Photomicrograph on tapered section (X3), X250. Reduced approximately 42% for reproduction. (Wlodek).

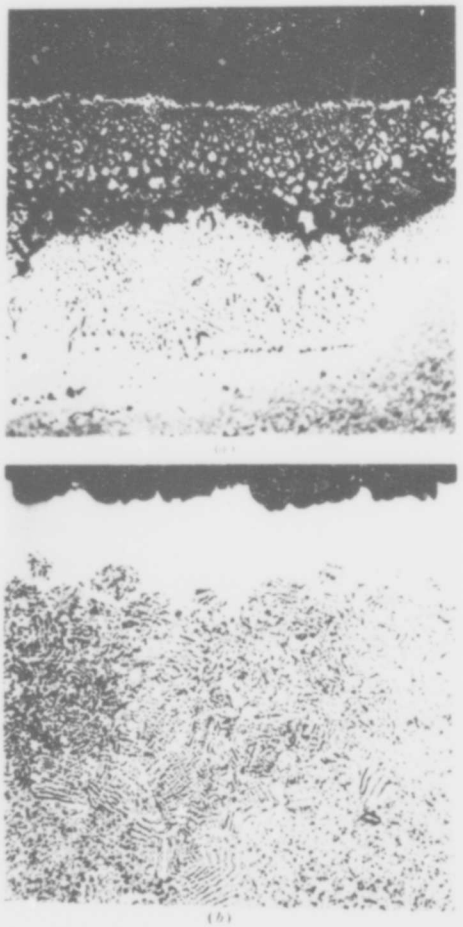

Figure 47.22. Subscale reactions in Udimet 700. (a) Oxidized 100 hr at 1800°F; note extensive internal oxidation. X250. Taper X3. (b) Oxidized 100 hr at 1900°F; note complete absence of internal oxidation, small amount of alloy depletion next to oxide/metal interface, and coarse, degenerate γ' next to alloy-depleted zone. X250. Taper X3. Enlarged approximately 52% for reproduction. (Wlodek).

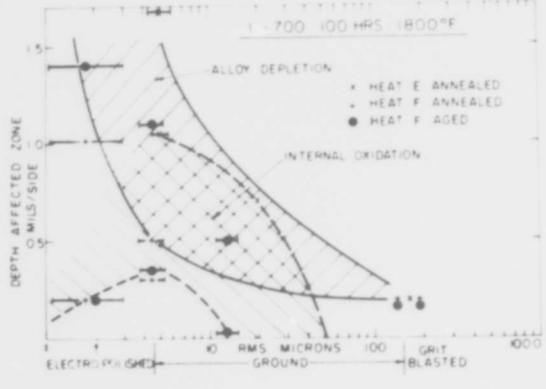

Figure 47.24. Subscale reactions in Udimet 700 can be completely eliminated by extensive surface working prior to exposure for 100 hr at 1800°F. Data for two heats (E and F) in the solution-annealed or aged condition. (Wlodek).

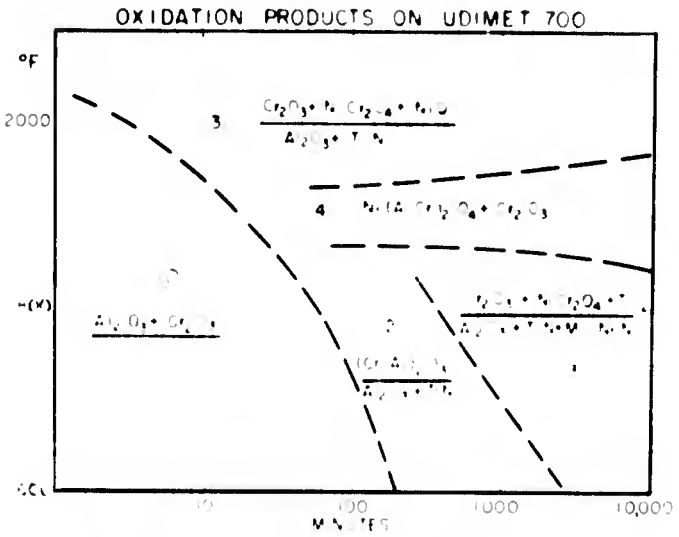

Figure 47.25. Simplified summary of the four main phenomenological stages of oxidation encountered by Udimet 700. Subscale and scale reaction products expressed as numerator and denominator of a quotient which identifies the reaction species in each region. Note absence of internal oxidation in Regions 1 and 4. Scaling kinetics linear in Region 1, parabolic in others except 4, where weight gain reaches a constant value in some 1000 min. (Wlodek).

Udimet 710

V. S. Moore and A. R. Stetson, Final Report on NASC Contract No. N00019-68-C-0532 (Solar Research Division Report RDR 1626-5). December 1970.

See B$_0$1900 for details. Figure 48.1 shows the microstructure of a U-710 specimen after 160h at 1650°F (899 C). U-710 was the most corrosion resistant of the alloys tested, better than U-700. Table 48.1 presents cumulative weight loss data for the alloys.

H. T. Quigg, R. M. Schirmer and L. Bagnetto, Final Report to NASC on Contract No. N00019-60-C-0221 (Phillips Petroleum Company Research and Development Report 5903-71) Jan. 1971.

See 713C for details. Figure 48.2 shows a U-710 specimen exposed for 60h to a 2000F (1093°C) cyclic test with 1 ppm salt and 0.04 wt %S in the fuel.Figure 48.3 shows a similar specimen tested with 0.0004 wt %S in the fuel.

H. T. Quigg, R. M. Schirmer and L. Bagnetto, Final Report to Naval Air Systems Command on Contract N00019-70-C-0293 (Phillips Petroleum Company Research and Development Report 5903-71) Jan. 1971.

See 713C for details. Uncoated U-710 is comparable with IN 738, and in most situations rather better.

C. J. Spengler, S. Y. Lee and W. E. Young, in "Deposition and Corrosion in Gas Turbines" A. B. Hart and A. J. B. Cutler (eds.) (Applied Science Publishers, London, 1973) 294.

See U-500 for details.

L. M. Maas and C. L. Miller, ASME Paper No. 72-GT-77, presented to the Gas Turbine and Fluids Engineering Conference and Products Show, March. 1972.

See 713C for details.

Data relating to this alloy will also be found in the following figures :

10-51, 10-84, 10-123, 10-124, 45-33, 45-35, 45-37, 45-39;

and Tables :

1-X, 10-XXV, 10-XXVI.

TABLE 48-I

WEIGHT CHANGE DURING HOT-CORROSION TESTS

1650°F MAXIMUM TEST TEMPERATURE (MOORE AND STETSON)

35 ppm SEA SALT

U-710 ALLOY

Exposure Time (Hours)	Cumulative Weight Change (mg)							
	Specimen Number							
	DA1	DA2	DG1	DG2	DJ1	DJ2	D1	D2
20	-	-	- 1.9	-4.5	+ 7.1	+ 5.7	+ 4.2	+ 2.5
30	+2.7	+3.2	-	-	-	-	-	-
40	-	-	+ 5.7	+4.2	+13.1	+ 6.1	+ 5.7	+ 4.3
60	+5.1	+5.5	+ 2.4	+2.2	+18.1	+26.9	+10.3	+ 8.2
80	-	-	+ 4.9	-0.6	+16.6	+15.8	+13.6	+12.6
90	+6.4	+5.7	-	-	-	-	-	-
100	-	-	+11.5	+4.3	+17.7	+16.2	+18.8	+22.2
120	+7.0	+7.6	+16.1	+8.3	+20.9	+20.5	+18.2	+16.6
150	+7.6	+7.5	+14.5	+9.9	+26.5	+28.5	+26.0	+22.5

Note: - denotes weight loss

WEIGHT CHANGE DURING HOT-CORROSION TESTS

1800°F MAXIMUM TEST TEMPERATURE

35 ppm SEA SALT

U-710 ALLOY

Exposure Time (Hours)	Cumulative Weight Change (mg)							
	Specimen Number							
	D4	D5	DA3	DA4	DG4	DG5	DJ4	DJ5
20	+11.4	+ 7.2	-	-	-	-	-	-
30	-	-	+ 5.8	+ 5.5	+ 8.4	+ 6.8	+12.2	+16.2
40	+14.3	+10.4	-	-	-	-	-	-
60	+11.9	+16.6	+ 9.7	+ 8.1	+13.2	+12.2	+12.4	+15.0
80	+12.2	+19.4	-	-	-	-	-	-
90	-	-	+12.6	+11.1	+13.9	+12.9	+20.0	+22.2
100	+13.4	+25.0	-	-	-	-	-	-
120	+ 9.9	+13.7	+16.3	+13.8	+18.9	+16.7	+20.4	+22.3
150	+ 5.2	+ 8.9	+19.8	+16.4	+21.2	+19.6	+23.3	+25.3

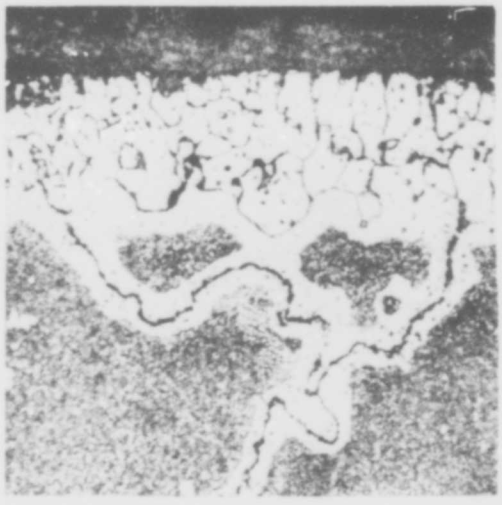

Magnification: 1000X

Specimen D2

Magnification: 40X

Figure 48.1. Microstructure of uncoated U-710 after hot corrosion tests at 1650°F for 160 hours. (Moore and Stetson).

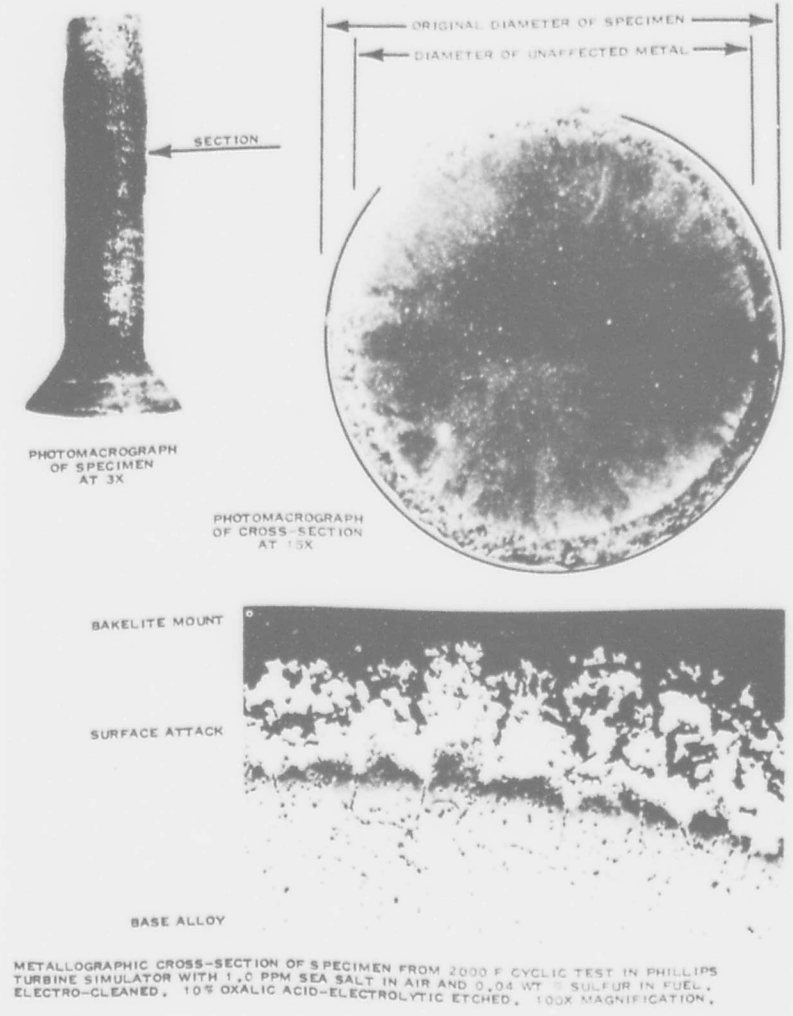

Figure 48.2. Hot corrosion of Udimet 710 specimen after 60 hrs. with high-sulphur fuel (Quigg et al).

Figure 48.2. (continued).

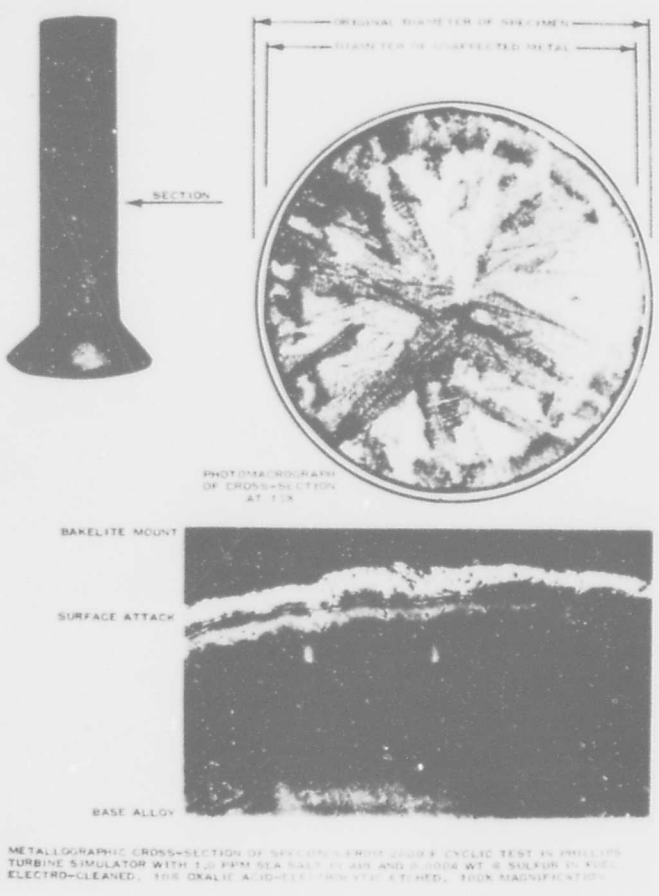

Figure 48.3. Hot corrosion of Udimet 710 after 60 hrs. with low-sulphur fuel (Quigg et al).

Unitemp 1753

R. Viswanathan, Corrosion 24 (1968) 359.

See 713C for details. Unitemp 1753 was one of the best alloys tested. After 150h testing at 1500°F (816°C) the specimen had lost 2.6 mg/cm^2. 98.5% of the alloy was unaffected. GMR-235, Ra 333 and PDRL 163 were comparable.

Waspaloy

M. J. Donachie, R. A. Sprague, R. N. Russell, K. G. Boll and E. F. Bradley, Hot Corrosion Problems Associated with Gas Turbines, ASTM Special Technical Publication, STP 421, 1967, 85.

See 713C for details. Waspaloy seems very resistant - MM302 is better, AMS 5382 (X40?) is comparable. However, 713 doesn't look bad either in these tests.

L. D. Graham, J. D. Gadd and R. J. Quigg, Hot Corrosion Problems Associated with Gas Turbines, ASTM Special Technical Publication, STP 421, 1967, 105.

See 713C for details. Ranking shows Waspaloy very resistant alloy - best of those tested, with negligible attack at 1800F.

R. Viswanathan, Corrosion 24 (1968) 359.

See 713C for details. Waspaloy was one of the better alloys tested, closely comparable to U-500. After 150h test at 1500°F (816°C) the specimen had lost 2.5 mg/cm^2 (after descaling); 96.4% of the alloy was unaffected.

P. E. Hamilton, K. H. Ryan, and E. S. Nicholls, Hot Corrosion Problems Associated with Gas Turbines, ASTM Special Technical Publication STP 421, 1967, 188.

See 713C for details. The authors remark that they have observed isolated cases of hot-corrosion of Waspaloy after long time service at temperatures which should have been below 1400°F (760°C).

Additional data relating to the alloy will be found in Figure 10.68 and in Tables 10-XVIII and 10-XIX.

WI 52

H. T. Quigg and R. M. Schirmer (Phillips Petroleum Company, Research Division) Progress Report No. 4 Naval Air Systems Command Contract NO_w65-0310-d (August 1966) Phillips Petroleum Company Report 4411-66R.

See 713C for details.

R. M. Schirmer and H. T. Quigg, Progress Report on NASC Contract NO_w65-0310-d. Phillips Petroleum Company Research Division Report 4370-66R (June 1966).

See 713C for details. Figure 51.1 shows the effect of sulphur, sea salt and temperature on the metal loss of Wl-52. Wl-52 was relatively poor, considerably worse than IN-100 and only slightly better than SM-200. The measured sulphide penetration and the penetration calculated from the weight loss were compared. For Wl-52 tested at 2000°F (1093°C) with 0.040 wt % S in the fuel and 10.0 ppm salt in the air the figures were 15.0 and 3.0 mils in the 5h test, respectively. Increasing the temperature from 1800 to 2000 to 2200°F significantly increased the weight loss of Wl-52. Decreasing sea salt from 10 ppm to 1.0 ppm decreased metal loss at 1400 and 1600°F at 0.0002 and 0.040 wt % S. Decreasing salt for 1.0 to 0 ppm decreased metal loss at 0.0002 wt % S. At higher temperatures decreasing the sea salt decreased the metal loss. Decreasing the sulphur from 0.40 to 0.040 wt % S decreased metal loss at 1400 and 1600°F at 0 and 1.0 ppm sea salt, no effect at 10 ppm. Decreasing sulphur from 0.04 to 0.0002 wt % decreased metal loss at 1.0 ppm salt, no effect at other salt concentrations. No effect of sulphur at higher temperatures.

Figure 51.2 shows oxidation after 5h at 2200°F (1204°C), no sea salt, 0.0002 wt % S. Figure 51.3 shows sulphidation after 5h at 1400°F (760°C), no sea salt, 0.40 wt % S. Figure 51.4 shows hot corrosion after 5h at 1600°F (871°C), 10ppm sea salt, 0.0002 wt % S. Figure 51.5 shows hot corrosion after 5h at 1800°F (982°C), 10 ppm sea salt, 0.0002 wt % S. Figure 51.6 shows hot corrosion after 5h at 2200°F (1204°C), 10 ppm sea salt, 0.0002 wt % S.

J. R. Johnston and R. L. Ashbrook, NASA Technical Note TN-D-5376 (August 1969).

See B 1900 for details and for a list of the general tables and figures. The weight losses in 50h tests at 2000°F (1093°C) in the high gas-velocity cyclic tests (381 mg/cm^2) and in a static oxidation test (18 mg/cm^2 are compared: Wl-52 was the worst of the seven alloys tested in this section, and the most affected by the high velocity, cyclic conditions. The oxides detected by X-ray diffraction after high gas-velocity cyclic tests are listed: at 1800°F (982°C), 100h: Cr_2O_3, monoxide (CoO), spinel, and $CoWO_4$; 1900°F (1038°C), 100h: Cr_2O_3, CoO, spinel with a_o = 8.30 Å, and $CoWO_4$; 2000°F (1093°C): 20h, Cr_2O_3, CoO, a spinel with a_o = 8.05 Å, a spinel with a_o = 8.35 Å, and $CoWO_4$; 60h, Cr_2O_3, CoO, a spinel with a_o = 8.10 Å, a spinel with a_o = 8.35 Å, and $CoWO_4$; 100h, Cr_2O_3, CoO, spinel and $CoWO_4$.

The average weight loss of Wl-52 in 100h tests at 1093°C was 23,700 mg - by far the worst of the alloys tested.

V. S. Moore and A. R. Stetson, Final Report on NASC Contract No. N00019-68-C-0532 (Solar Research Division Report RDR 1626-5) December 1970.

See B 1900 for details. The cumulative weight gains are listed at 1800°F (982°C) after 10h the weight change of two specimens was -305 and -324 mg: after 17h it was -484 and -511 mg. At 2000°F (1093°C) after 10h the weight change was -1251 and -1434 mg.

A. R. Cox and R. J. Hecht (Pratt and Whitney Aircraft, Florida Research and Development Center) Technical Report to the Air Force Materials Laboratory, Wright-Patterson AFB, AFML-TR-70-273. (December 1970).

The report is principally concerned with the evaluation of two experimental TD Cobalt-base alloys (Co-20 Ni-18 Cr-2 ThO_2 and Co-20 Ni-30 Cr-2 ThO_2) but other cobalt-base alloys were included for comparison. The tests used were:

(1) 2000° and 2200°F (1093 and 1204°C) isothermal oxidation-erosion tests;

(2) 2100°F (1149°C) cyclic hot corrosion, and

(3) Accelerated cyclic hot corrosion.

The dynamic isothermal oxidation/erosion test apparatus consisted of a flame tube, burning JP-5 fuel, providing a gas velocity of 400 - 700 ft/sec. The samples were rotated at 1750 rpm in this gas stream. Sample inspection and weight change recording were performed at regular intervals. The results for all the alloys tested at 2200°F (1204°C) are shown in Figure 51.7, from which it is apparent that Wl-52 was much the worst of the commercial alloys tested (the others were Mar-M 302 and Mar-M 509). The microstructure of the specimens is shown in Figure 51.8 after 225h at 2200°F.

The cyclic hot corrosion test consisted of 10 min at 1050°F (565°C) with 0.02 ppm synthetic sea salt in the combusted fuel, followed by a ten-minute heating cycle with 0.2 ppm salt, the maximum temperature being 2100°F (1149°C). This temperature was attained in about 1 min of the heating cycle. Three repetitions (at a total time of 1h) constituted one cycle. The apparatus was the same as that for the dynamic oxidation test, except that a salt-injection facility was added; the specimens were again spun at 1750 rpm. Samples were run for 670h; the commercial alloys were not apparently included in this test.

The accelerated test consisted of 2 min at 1250°F (676°C) 2 min at 1750°F (955°C) and 2 min at 2050°F (1121°C). Including heating and cooling times, the total cycle time was 7 min. The salt concentration was constant throughout. Figure 51.9 shows the weight loss in 70h tests with 35 ppm salt: again, Wl-52 was very much the worst of the alloys examined. The cross-sections of the corroded specimens are shown in Figure 51.10. Figure 51.11 shows the results of 220h tests with 3.5 ppm salt; again Wl-52 is the worst, but the difference is not as great. MM-509 seems rather worse than MM-302. Figure 51.12 shows the appearance and cross-section of the corroded samples: the Wl-52 shows very extensive internal oxidation along the carbide network.

The corrosion behaviour of all the alloys was also studied coated, with a CoCrAlY coating on the TD alloys, and pack cementation coatings on the commercial alloys.

The TD alloys and Mar-M 302 were compared as first stage turbine vanes in a TF 30 engine. The maximum metal temperature were 2000 and 2100°F (1093 and 1149°C). The engine test was run for 150h under simulated flight conditions. No salt additive was used; JP-4 fuel was burnt. The 150h test consisted of 25 x 6h cycles. Some oxidation results are reported for the uncoated TD alloys.

N. T. Wagenheim, Cobalt, No. 48, 1970, 129.

See X-40 for details. Corrosion data at the 5 ppm salt level given in Table V: After 500h at 1650°F (871°C) the surface loss was 15.6 mils, and the maximum penetration was 21.4 mils. 1000h at 1750°F (955°C): 6.6 and 18.2 mils. 1000h at 1900°F (1038°C): 63.4 and 73.9 mils. Much worse than X-40 or Mar-M 302.

A. M. Beltran, Cobalt, No. 46, 1970, 3.

See X-40 for details and for the principal results. The internal oxidation is shown of Wl-52 hot corroded at 1900°F (1038°C) in GE burner rig burning 1% S diesel oil, with 5 ppm sea salt in the air; showing very extensive attack of the internal carbides.

H. T. Quigg, R. M. Schirmer and L. Bagnetto, Final Report to NASC on Contract No. N00019-69-C-0221 (Phillips Petroleum Company Research and Development Report 5732-70) July 1970.

See 713C for details.

P. A. Bergman, C. T. Sims and A. N. Beltran, Hot Corrosion Problems Associated with Gas Turbines; ASTM Special Technical Publication STP 421, 1967, 38.

See 713C for details. Three commercial cobalt-base alloys (Wl-52, X-45, SM 302) tested in a small burner rig (1% S diesel fuel, 200 ppm salt in the air, 100h tests, 1750 and 1900°F (955 and 1038°C)). Wl-52 was quite resistant at 1750°F, but was severely attacked at 1900°F. Figure 51.13 shows a cross-section of a specimen tested at 1900°F: there is considerable internal attack,apparently along the carbide networks.

M. J. Donachie, Jr., R. A. Sprague, R. N. Russell, K. G. Boll and E. F. Bradley, Hot Corrosion Problems Associated with Gas Turbines, ASTM Special Technical Publications STP 421, 1967, 85.

See 713C for details.

L. D. Graham, J. D. Gadd and R. J. Quigg. Hot Corrosion Problems Associated with Gas Turbines, ASTM Special Technical Publication STP 421, 1967, 105.

See 713C for details. The ranking of several alloys is compared in a 1h crucible test at 1800°F (982°C) in 1% NaCl, 99% Na_2SO_4. Wl-52 is one of the better alloys, comparable to U-700, much better than 713C. (Mar-M 302 was one of the worst alloys tested).

R. M. Schirmer and H. T. Quigg, Hot Corrosion Problems Associated with Gas Turbines, ASTM Special Technical Publication STP 421, 1967, 270.

See 713C for details. This paper is based on reports abstracted above, and describes tests in the Phillips Environmental Simulator in the temperature range 1400 - 2200°F (760 - 1204°C); 0.0002, 0.040 and 0.40% S in JP-5; 0, 1.0, and 10.0 ppm sea salt in the air. The corrosion of Wl-52 is shown in Fig. 51.14 as a function of temperature and test conditions. The relative durability of the alloys is compared : Wl-52 was poor, comparable with IN 100 and SM 200.

D. L. Deadmore, NASA Technical Memorandum TM X-2195 March 1971 (Lewis Research Center).

See IN 100 for details. Figure 51.15 shows a typical micrograph of W1-52 oxidised at 1900°F (1038°C), 302hcycles. The weight change data for W1-52 tested under isothermal and cyclic conditions at 1900 and 2000°F (1038 and 1093°C) are presented in Figures 51.16 - 51.21. The isothermal weight change data are presented in Figures 51.16 and 51.17. At 1038°C W1-52 gains weight approximately linearly with time (0.05 mg/cm^2/hr). Considerable spalling of the oxide scale occurred on cooling the specimen at the end of the run. At 1093°C the weight gain is again approximately linear (0.075 mg/cm^2/h). Again, there was heavy spalling at the end of the run. Figure 51.17 compares the present isothermal data with that from C.E. Lowell and I. L. Drell, NASA TN D-6148, 1970 and C. H. Lund and H. T. Wagner DMIC Rept. 214, Mar. 1, 1965. The former are about the same as the present study, but the latter concerned specimens in the as-cast condition, which oxidised faster (0.34 mg/cm^2/hr).

Cyclic oxidation weight change data are also included in Figs. 51.16 and 51.17. Initially there is a weight gain and little spalling: once a peak weight gain of 1 to 2 mg/cm^2 is reached spallation increased and a few cycles beyond this peak the specimens showed a net weight loss. Soon the loss was linear with time at all cycle frequencies. Spallation of the oxide scale was extensive and often explosive in nature in this linear weight loss region. Spallation increased with increasing cycle frequency and with increasing temperature. Figure 51.18 plots the time required for a weight loss of 80 mg/cm^2 versus the cycle frequency.

The weight gains at the test temperature for the 2, 5 and 20h cycles were continuously recorded and are plotted in Figures 51.19 to 51.21. Figure 51.22 shows the change in metal thickness as a function of time at both temperatures.

After each 20h cycle at 1093°C the insitu surface scale on ground and lapped and ground and polished specimens was found to contain Cr_2O_3, $CoWO_4$, $CoCr_2O_4$ and CoO. The spalled material was predominantly $CoCr_2O_4$ and CoO with lesser amounts of Cr_2O_3 and $CoWO_4$. Table 51-I shows the data.

H. T. Quigg, R. M. Schirmer and L. Bagnetto, Final Report to Naval Air Systems Command on Contract N00019-70-C-0293 (Phillips Petroleum Company Research and Development Report 5903-71) Jan. 1971.

See 713C for details. WI-52 was the most heavily corroded of the cobalt-base alloys under all test conditions. (The others were X-40, Mar-M 509 and Mar-M 302).

W. L. Wheatfall, in "High Temperature Corrosion of Aerospace Alloys" J. Stringer, R.I. Jaffee and T. F. Kearns (eds.) AGARD Conference Proceedings No. 120, (March 1973) 235.

See 713C for details.

Additional data relating to this alloy will be found in the following Figures:
1.9, 1.10, 1.11,1.12,1.13,10.58, 10.68, 10.105, 10.123, 10.124, 52.8, 52.9, 52.11, 52.12, 52.13, and Tables:
10-I, 10-VI, 10-XVIII, 10-XIX, 10-XXI, 10-XXV, 10-XXVI, 10-XXX, 31-I.

TABLE 51-I

QUANTITATIVE SPALL COMPOSITION BY

X-RAY DIFFRACTION FOR 2000° F (1093°C) TESTS

(Total exposure in each test, 60 hr.)

Surface condition and cycle	Phase content of spall, wt %			
	Cr_2O_3	$CoCr_2O_4$	CoO	[a]$CoWO_4$
Ground-lapped				
20-hr cycles (3rd cycle)	4	50	35	11
5-hr cycles (12th cycle)	2	46	32	20
2-hr cycles (30th cycle)	[b]ND	40	33	27
Ground-polished				
20-hr cycles (3rd cycle)	4	21	56	19

[a]By difference.

[b]Not detected.

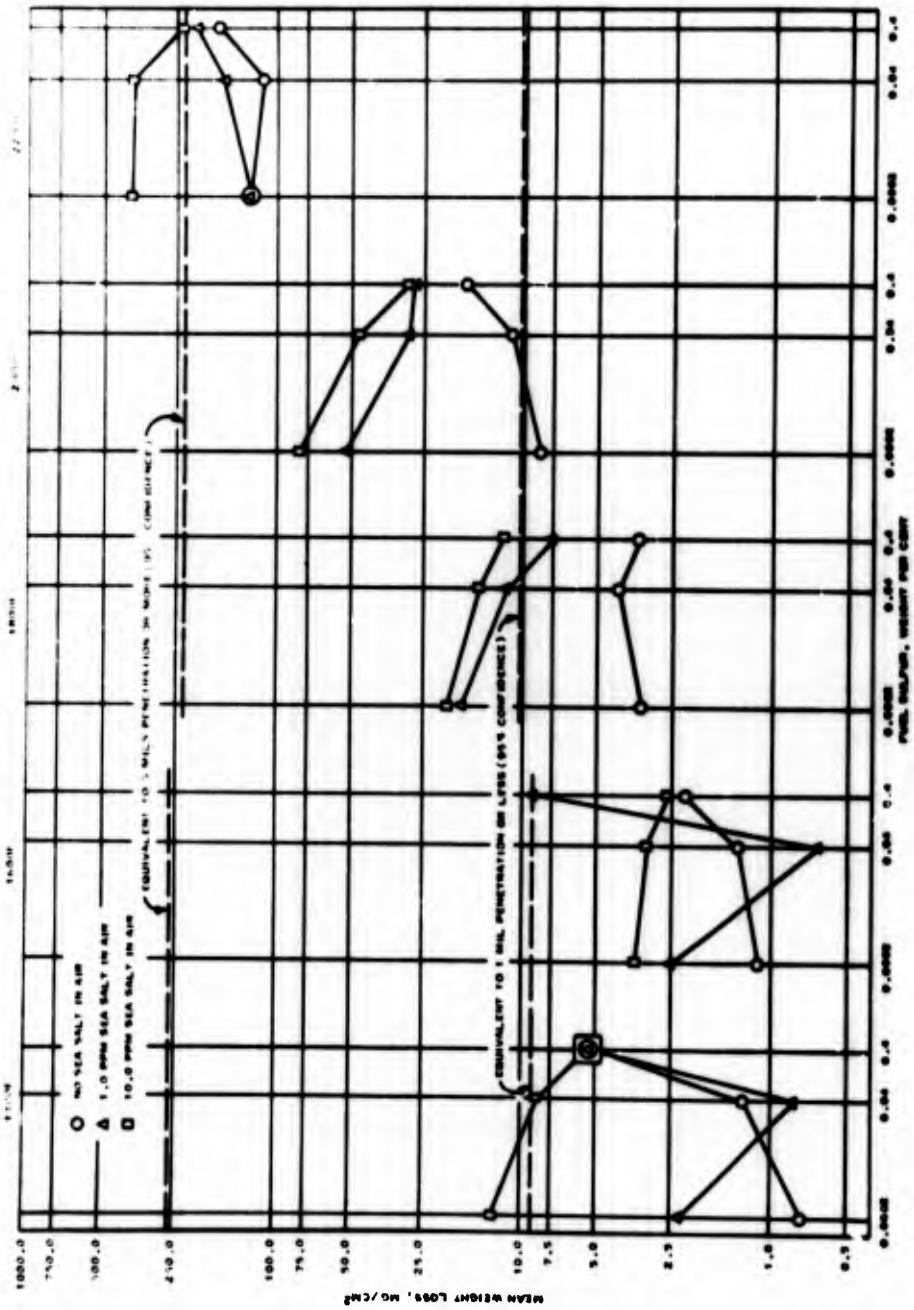

Figure 51.1. Effect of fuel sulphur and salt in air and gas temperature on metal loss of VI-52 test specimens (Schirmer and Quigg).

HEAVY VARIABLE
SURFACE ATTACK

BASE METAL
UNETCHED
200X

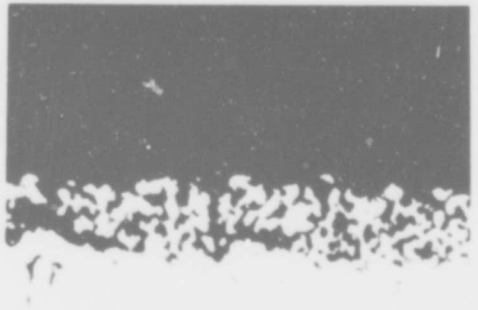

GROSS OXIDATION

BASE METAL
UNETCHED
2000X

Figure 51.2. Oxidation of WI-52 in Phillips rig. (Schirmer and Quigg).

5 hours exposure at 2200 F test condition with no sea salt in air and 0.0002 wt % sulphur in fuel.

VARIABLE
SURFACE ATTACK

BASE METAL
UNETCHED
2000X

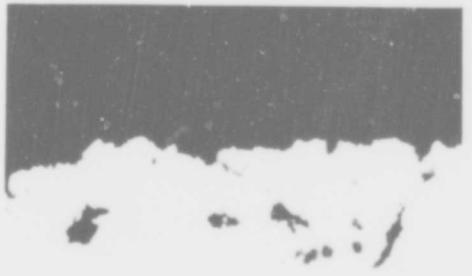

SULFIDE PENETRATION

BASE METAL
UNETCHED
2000X

Figure 51.3. Sulphidation of WI-52 in Phillips rig. (Schirmer and Quigg).

5 hours exposure at 1400 F test condition with no sea salt in air and 0.40 wt % sulphur in fuel.

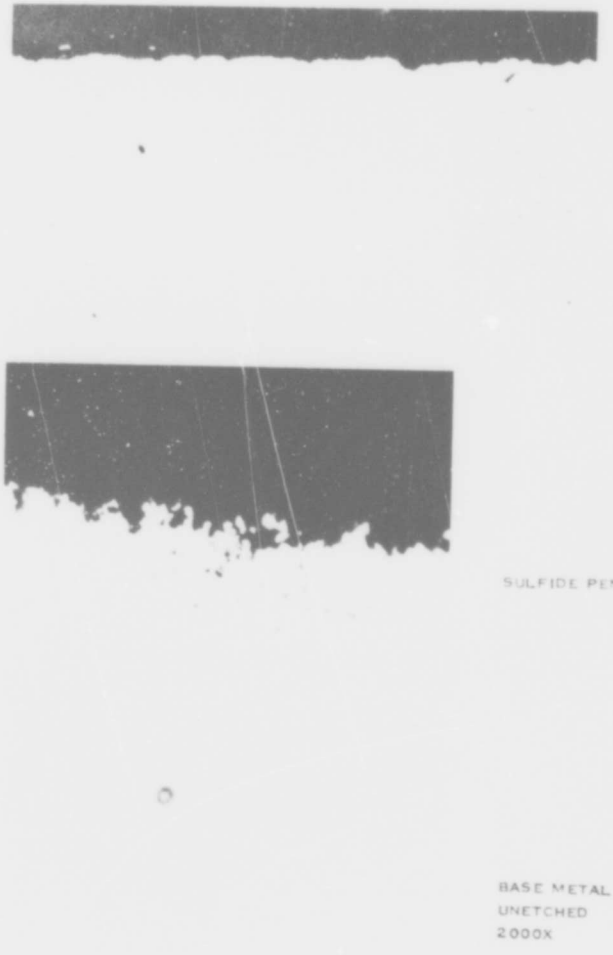

Figure 51.4. Hot corrosion of WI-52 in Phillips rig. (Schirmer and Quigg).

5 hours exposure at 1600 F test condition with 10 ppm sea salt in air and 0.0002 wt % sulphur in fuel.

Figure 51.5. Hot corrosion of WI-52 in Phillips rig.

5 hours exposure at 1800F test condition with 10 ppm sea salt in air and 0.0002 wt % sulphur in fuel. (Schirmer and Quigg).

Figure 51.6. Hot corrosion of WI-52 in Phillips Rig. (Schirmer and Quigg).

5 hours exposure at 2200 F test condition with 10 ppm sea salt in air and 0.0002 wt % sulphur in fuel.

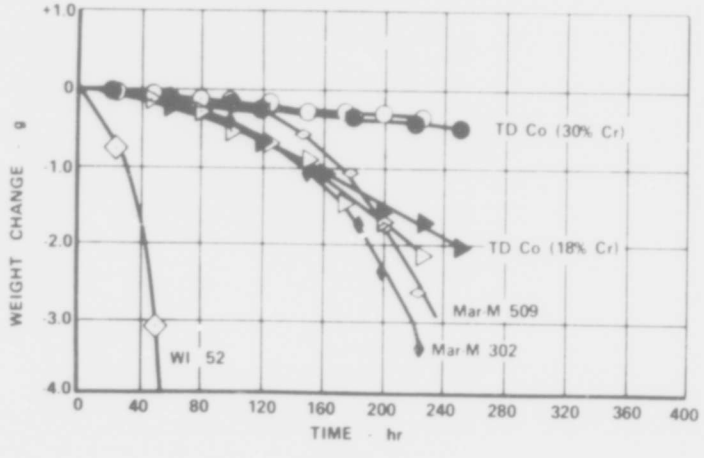

Figure 51.7. 2200°F dynamic isothermal oxidation erosion test results. (Cox and Hecht).

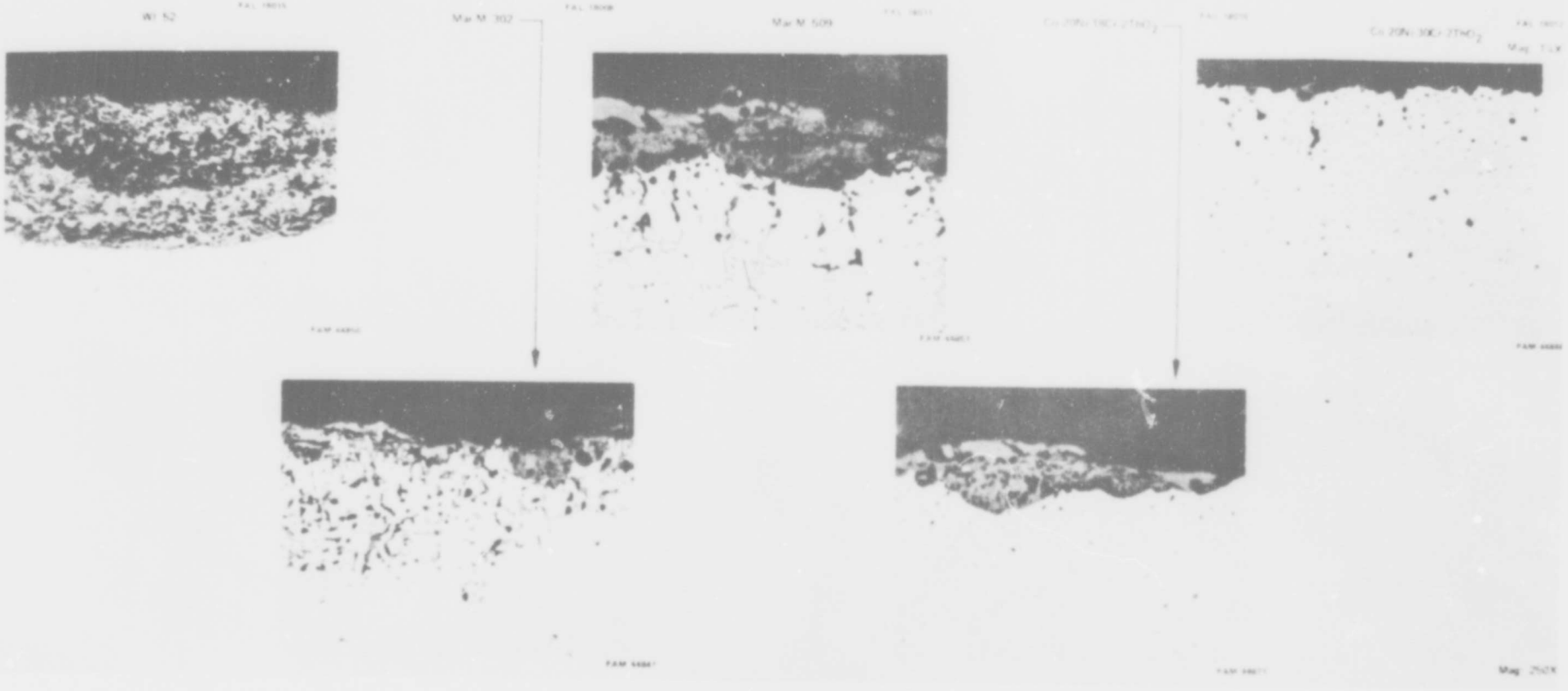

Figure 51.8. Surface microstructure after 225h in 2200°F (1204°C) dynamic isothermal oxidation erosion test. (Cox and Hecht).

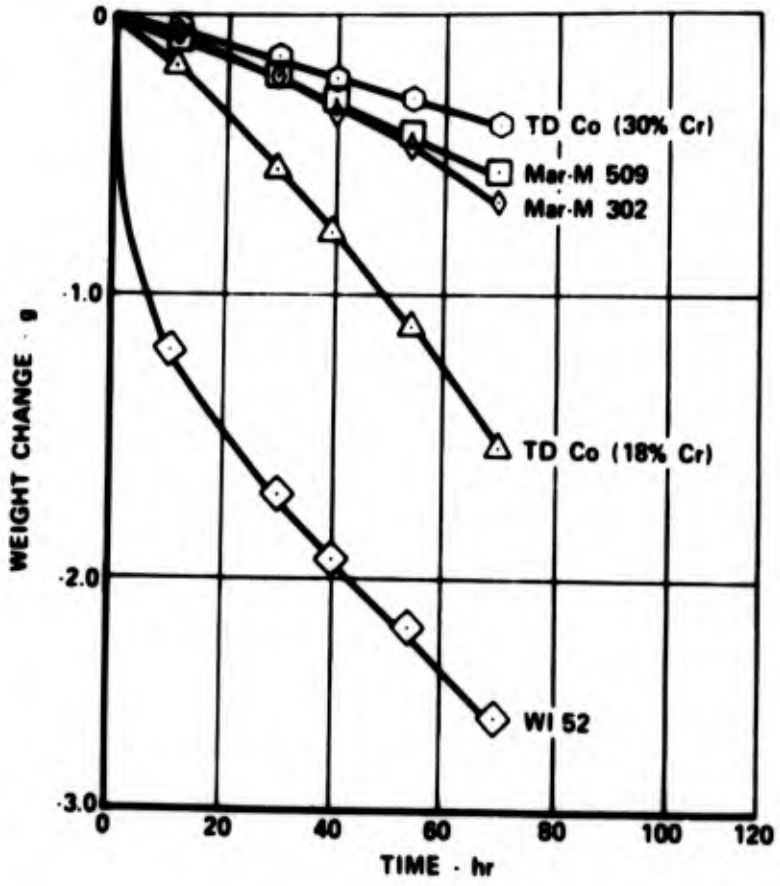

Figure 51.9. Accelerated cyclic hot corrosion test results (35 ppm salt injection) after 70 hours. (Cox and Hecht).

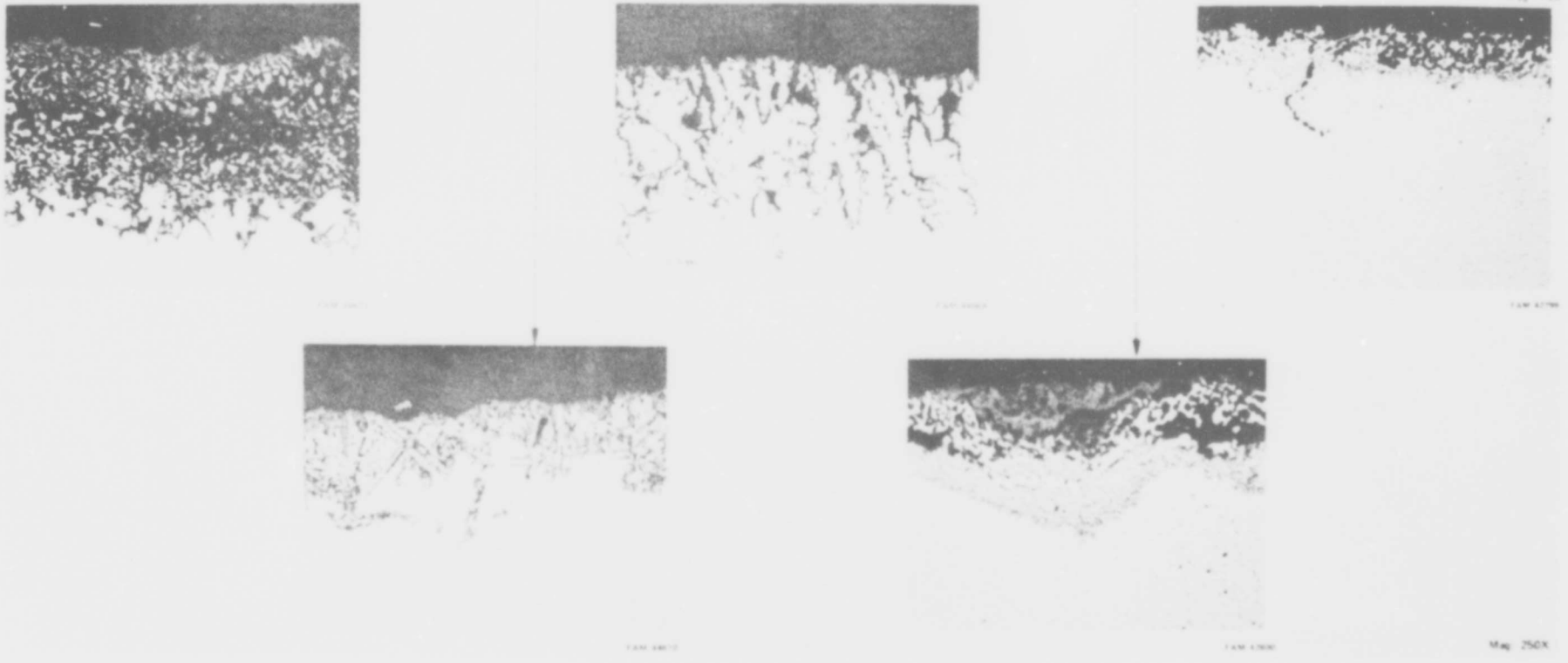

Figure 51.10. Surface microstructure of samples tested in 35 ppm salt accelerated hot corrosion test for 70 h (Cox and Hecht).

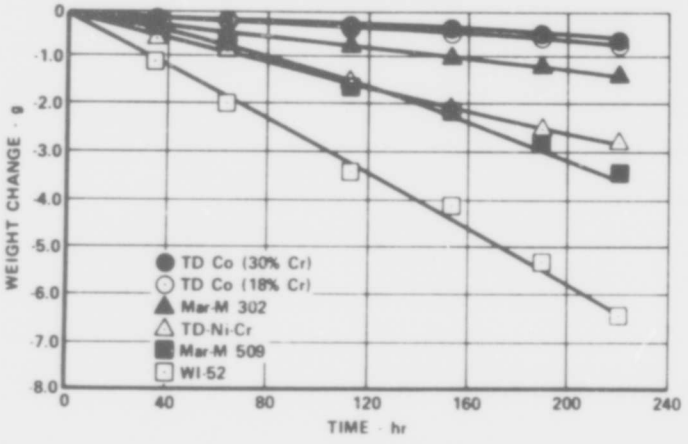

Figure 51.11. Accelerated hot corrosion test results (3.5 ppm salt injection) after 220 hrs. (Cox and Hecht).

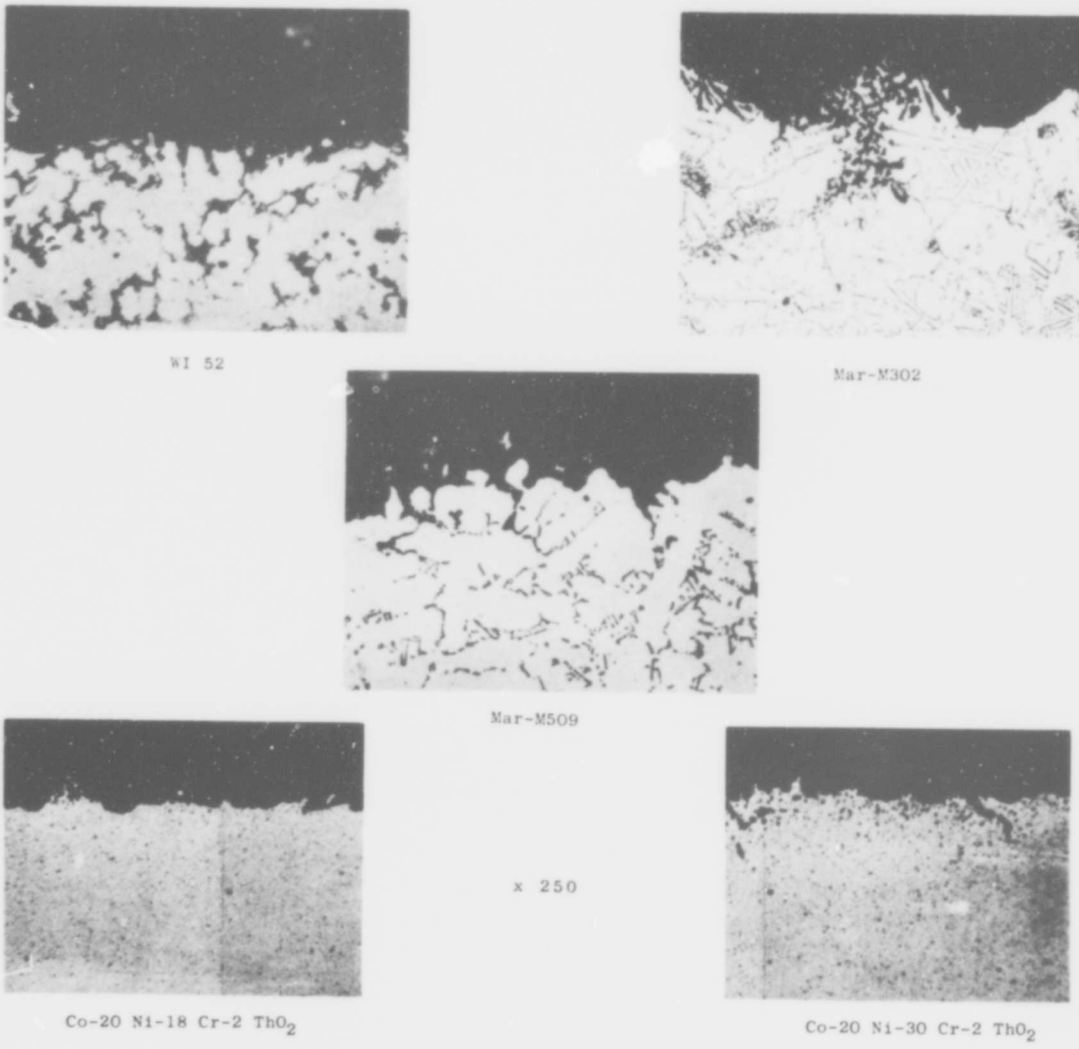

Figure 51.12. Surface microstructure of samples after 220 h in 3.5 ppm salt hot corrosion test. (Cox and Hecht).

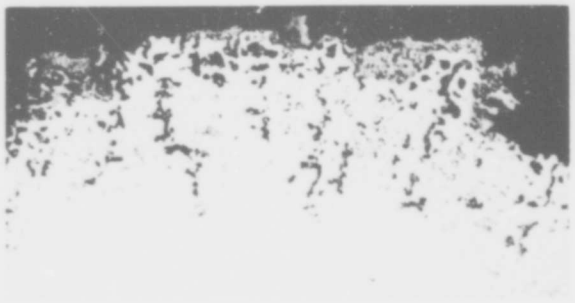

Figure 51.13. Subsurface oxides (dark gray) and chromium-rich sulphides (medium gray) in WI-52 tested in G.E. small burner rig at 1900°F (1038°C). (Bergman et al).

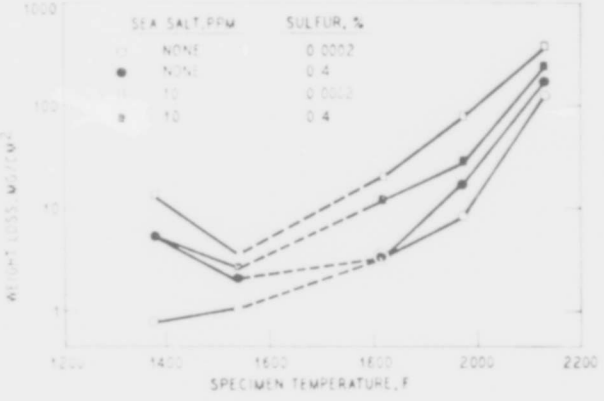

Figure 51.14. Hot corrosion of WI-52 (Schirmer and Quigg).

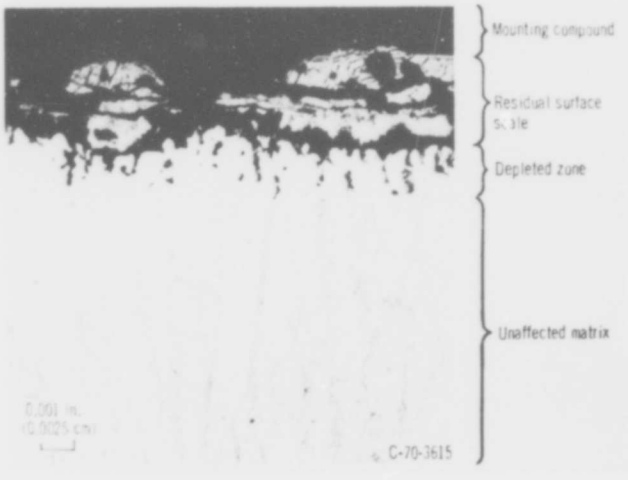

Figure 51.15. WI-52 after thirty 2-hour cycles at 1900°F (1038°C). X250. (Deadmore).

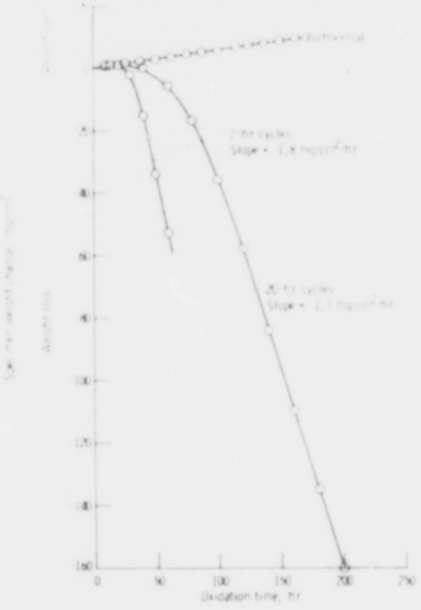

Figure 51.16. Weight change of ground-lapped WI-52 specimens during isothermal and cyclic oxidation at 1900°F (1038°C). (Deadmore).

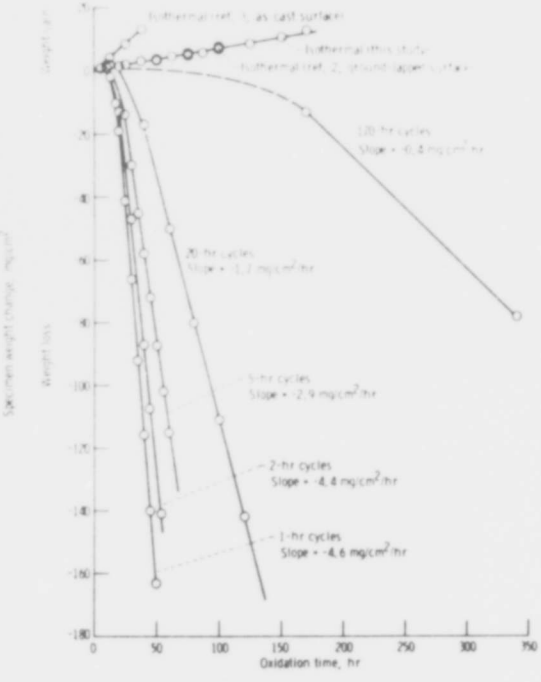

Figure 51.17. Weight change of ground-lapped WI-52 specimens during isothermal and cyclic oxidation at 2000°F (1093°C). (Deadmore).

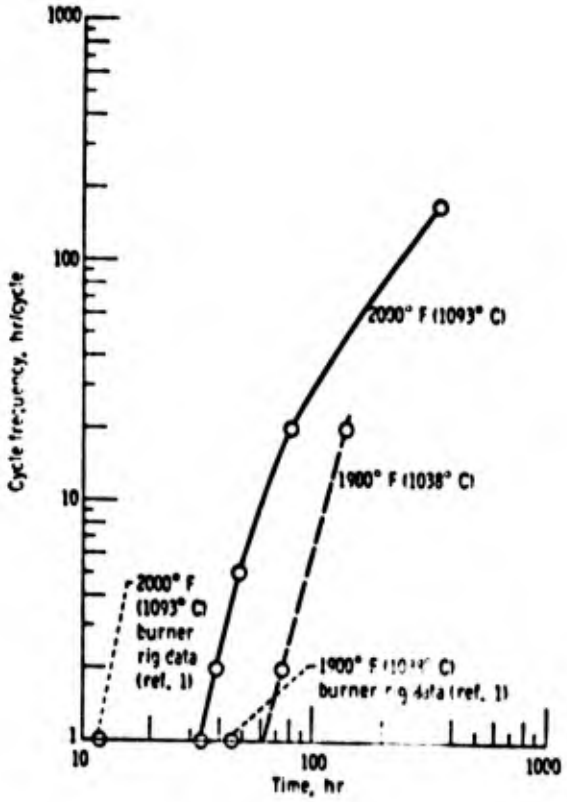

Figure 51.18. Relation between cycle frequency and time to loss of 80 milligrams per square centimetre for WI-52. Ground-lapped specimens (Deadmore).

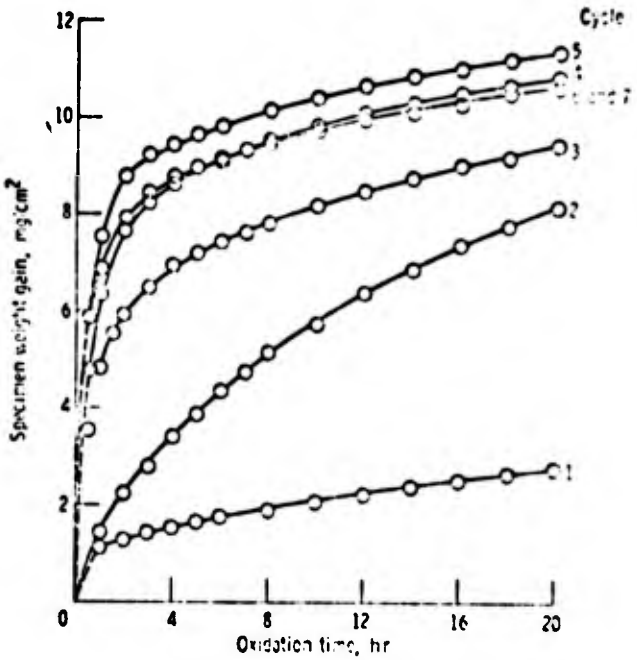

Figure 51.19. Weight gain of WI-52 during heating portion of each 20-hour cycle at 2000°F (1093°C) ground-lapped specimen. (Deadmore).

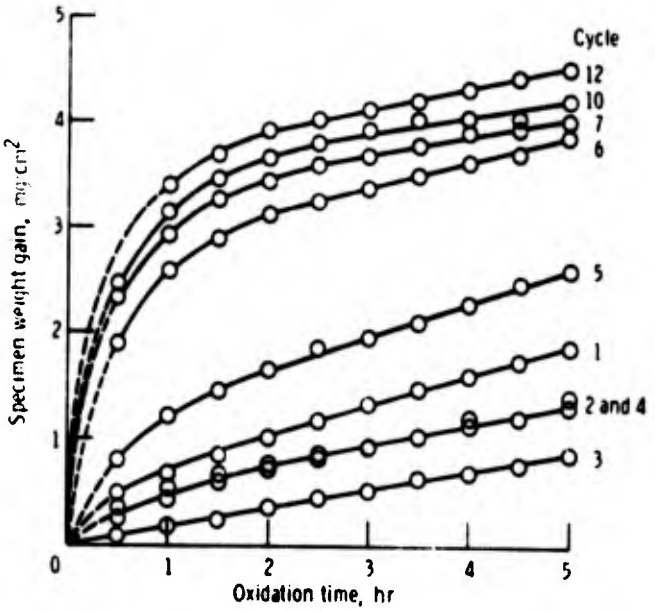

Figure 51.20. Weight gain of WI-52 at 2000° F (1093°C) during heating portion of successive 5-hour cycles for ground-lapped specimen. (Deadmore).

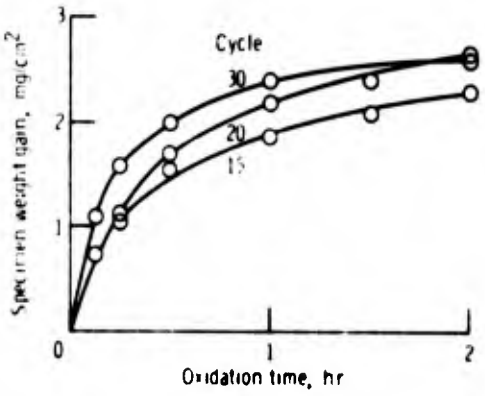

Figure 51.21. Weight gain during heating portion of several 2-hour cycles for WI-52 at 2000°F (1093°C) for ground-lapped specimen. (Deadmore).

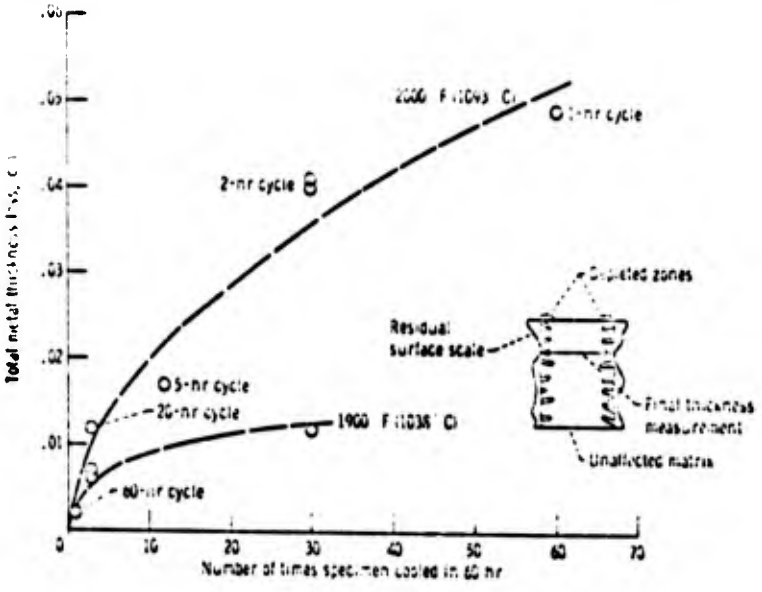

Figure 51.22. Effect of cyclic oxidation on total metal thickness loss of WI-52 at 1900° and 2000°F (1038° and 1093°C) for ground-lapped specimens. Original metal thickness, 0.25 centimetre. (Deadmore).

X-40 and X-45

P. A. Bergman Corrosion 23 (1967) 72.

See SEL for a summary of the method and some of the general results. The loss in diameter of some alloys in 50h in the temperature range 900 - 1093°C in 0.25% S fuel with 0, 2 and 200 ppm sea salt in the air is shown. With no salt, the oxidation of X-40 was rather greater than that of the nickel-base alloys, SEL, SEL 15 and 713 at 1020 and 1093°C, but the corrosion was not great. With 200 ppm salt the alloy was relatively resistant by comparison with a large range of alloys: indeed, the corrosion rate was only slightly affected by the presence of the salt. Metallographic examination showed that the carbide network in the alloy was attacked. A grey phase consumed the carbides and was, in its own turn, oxidised.

The effect of sulphur and salt in the attack at 913 and 982°C for X-40, SEL, SEL 15 and 713 is shown. X-40 was the most resistant under all circumstances: it was most heavily attacked by 200 ppm NaCl, 0.006% S; 200 ppm sea salt + 0.25% S was less aggressive.

J.J. Walters (AVCO/Lycoming Division) Technical Report to the Air Force Materials Laboratory, Wright-Patterson Air Force Base AFML-TR-67-297 (September 1967).

Extended summary in B1900, X-40 was the best alloy tested, showing no corrosion under any conditions - JP-4, JP-4R fuel with 4 ppm or 8 ppm salt in the air; JP-5 fuel with 8 ppm salt, in the temperature range 1450 - 1750°F (788 - 954°C).

B. O. Buckland, A. D. Foster and J. J. Treanor. Paper presented to the Annual Meeting of the National Association of Corrosion Engineers, Miami, Florida (April 1966).

See U500 for details.

Discusses the G.E. small burner test, its use in predicting practical lifetimes, and the effect of service variables on the expected life. Tests are commonly run from 100 to 6000h at temperatures in the range 1400 - 2000°F (760 - 1093°C). Metallographic method of evaluation of corrosion. Empirical expression; corrosion varies as $(\text{time})^n$, where the index n varies with temperature, is used for extrapolation: graphs plotted as log corrosion versus log time. At temperatures in the range 1100 - 1400°F (593 - 760°C), n is approximately 1/3; 1400 - 1700°F (760 - 927°C), $n \sim \frac{1}{2}$; 1900 and 2000F (1038 and 1093°C), $n \sim 1$. Testing up to at least 5000h was felt to be necessary if extrapolations to 30,000 or 100000h were to be made. Figure 52.1 shows the corrosion of X-45 as determined by the small burner rig. Table 45-III lists observations on parts examined after gas turbine service. Nozzle N2 was of X45 which had run using residual oil for a total of 5,200h stopping an average 29 times every 100h. The running temperature was 1590°F, and the corrosion was 11.6 mils. The small burner test would produce this amount of corrosion in this time at a temperature of 1720°F. Nozzle N3 was of X-40; 4,900h; 29 stops per 100h; 1590°F; 20 mils corrosion; small burner temperature 1750°F. Nozzle N4; X40; 9,020h; 29 stops/100h; 1590°F; 40 mils corrosion; 1770°F. Nozzle N5; 2860h; 29 stops/100h: 1760°F; 130 mils corrosion; 1960°F.etc. (9 other examples listed). The authors discuss various factors which alter the apparent temperature; use of residual or crude oil (-60°F); shutdown frequency (-1°F for each shut-down per 100h operation); service factor (-70°F for the poorest service); and a differential to account for the more severe conditions encountered by blades as opposed to vanes (-110F for blades over the 1260 - 1430°F temperature range).

A. U. Seybolt, Trans. AIME, 242 (1968) 1955.

Figure 52.2 shows an X-45 specimen subjected to 616h, at 1600°F (871°C) in a combusted 2.9% S distillate oil containing 125 ppm sodium as NaCl (see U 500).

H. von E. Doering and P. A. Bergman, Naval Ship Research and Development Centre Materials Laboratory Research and Development Report No. 2844 (March 1969).

See 713 C for details. In a 100h test at 1750°F (955°C) with 200 ppm salt the surface loss was 0.6 mils and the maximum penetration was 9.2 mils; in a 1000h test with 5 ppm salt the corresponding figures were 1.0 and 11.6 mils. At the high salt content U-500 was a little better, although the difference was not great- at the lower salt content, which the authors regard as the more realistic, X-40 was clearly the best of the alloys tested - the next was L605.

J. R. Johnston and R. L. Ashbrook NASA Technical Note TN D-5376 (August 1969).

See B1900 for details, and for a list of the general tables and graphs. The weight loss in 50h tests in the high velocity cyclic tests (18 mg/cm^2) and in static oxidation tests (4.5 mg/cm^2) at 2000°F (1093°C) is compared: X-40 stood up to the cyclic tests rather better than most.

The oxides determined by X-rays after high gas-velocity cyclic testing are listed. 1800°F (982°C): 20h and 60h, Cr_2O_3 and a spinel with a_o = 8.30 Å; 100h, Cr_2O_3 only. 1900°F (1038°C): 20h, Cr_2O_3 and a spinel with a_o = 8.35 Å; 60h and 100h, Cr_2O_3, monoxide (CoO), a spinel and $CoWO_4$. 2000°F (1093°C): 20h, Cr_2O_3, CoO, spinel; 60h, Cr_2O_3, CoO, spinel; $CoWO_4$; 100h, CoO and a spinel with a_o = 8.30Å.

On average, X-40 specimens lost 1240 mg after 100h testing at 2000°F (1093°C), a little better than Hastelloy X or Mar M 200.

V.S. Moore and A. R. Stetson, Final Report on NASC Contract No. N00019-68-C-0532 (Solar Research Division Report RDR 1626-5) December 1970.

See B 1900 for details. The tests were terminated after 17h at 1800°F because of the extremely rapid hot corrosion which was nevertheless not as bad as 713 C No metallographs of the attack are shown.

Tables of cumulative weight changes during testing are shown. At 1800°F:

Exposure Time, hours	10	17	
weight change, mg.	-174	-328	specimen 1.
	-194	-311	specimen 2.

At 2000°F:

Exposure Time, hours	10	20	30	40	50	
weight change, mg.	-385	-710	-1124	-	-2006	specimen 1
	-421	-784	-1215	-	-2087	specimen 2

M. Kaufman, Trans. ASM 62 (1969) 590.

See SEL for details. The scales on the cobalt-base alloys tended to spall, although this tendency was rather less in X-40 than in the experimental CEDO alloys. Figure 52.3 shows the corrosion attack, with and without 200 ppm salttests at 1675, 1800 and 2000°F (913, 982 and 1093°C). The salt seemed to have relatively little effect at 2000°F but produced a significant acceleration at 1675°F.

The external scale products in the 200 ppm salt tests were identified by X-ray diffraction: Na_2SO_4 was found on all specimens at 1675 and 1800, but not at 2000°F. Two forms of CoO were observed, one with a normal lattice parameter and one with a lower parameter, probably containing nickel. The amount of this diminished with increasing temperature. Cr_2O_3 was present at the start, but the amount diminished after the first few hours, virtually disappearing. A Co-Cr spinel was present at all temperatures and times. In oxidation tests without salt, only small amounts of CoO were present at early times at 2000°F, none at lower temperatures. Small amounts of Cr_2O_3, and small amounts of spinel, increasing to moderate amounts at longer times and higher temperatures, were present.

At 2000°F sulphides were rarely seen and only at longer times. In the no-salt tests the carbides were attacked: after 16h at 2000°F X-40 had a surface layer depleted of all carbides.

S. T. Wlodek, Paper presented at the Atlantic City Meeting of the Electrochemical Society, October 1970.

See L605 for details. Specimens were abraded through 600 paper and electropolished. Figure 52.4 shows weight gain versus time on log scale: the curves were erratic and irreproducible. Areas of very localised attack which may have been associated with liquid reaction products were noted after testing at 2000°F (1093°C) and above. On cooling, the scale on all X-40 specimens cracked and exfoliated usually along the metal/oxide interface. The major source for the erratic data appeared to be the preferential oxidation of the high tungsten M_6C type carbide phases and other compositional heterogeneities.

Figure 52.5 shows the appearance of the sub-surface oxidation after 100 at 1800°F (982°C). Figure 52.6 shows the extent of internal oxidation for times up to 400h at 1600, 1800 and 2000°F (871, 982 and 1093°C) and 100h at 2200°F (1204°C). Figure 52.7 shows the sort of localised catastrophic oxidation encountered after 100h at 2000°F (1093°C). Table 52-I shows the surface reaction products identified by X-ray diffraction. At long times and high temperatures the principal product was a spinel, probably $CoCr_2O_4$, with $a_o \sim 8.29 - 8.43$ Å. At shorter times at the lower temperatures Cr_2O_3 predominates. Table 52-II shows the sub-scale products obtained by X-ray diffraction of an extraction residue. After 400h at both 1800 and 2000°F, the residues were Cr_2O_3 and α - cristobalite.

N. T. Wagenheim, Cobalt, 48 (1970) 129.

This paper reports work designed to develop cobalt-base alloys for service as a vane material in a typical marine gas turbine having a firing temperature of 1750F (955°C) and a 5000h life between overhauls. The first stage vane metal temperature may approach 1900°F (1038°C). Aimed at strength at 1900°F comparable to WI-52 and hot corrosion resistance superior to that of X40/X45. The experimental alloys were designated MELCO, and were modifications of the X-45 composition. The commercial alloys X45, WI 52 and Mar-M 302 were included for comparison. In addition, a series of experimental alloys (DISCO) were developed as a basis for dispersion-strengthened alloys. The hot-corrosion resistance was tested in the GE Small Burner Rig, described by Bergman, using a 1% S diesel fuel, with between 5 and 200 ppm sea salt added to the combustion gases. 100 - 1000h at temperatures in the range 1600°-2050°F (871° -1121°C), specimens were cycled every 50h to room temperature by air blasting. The specimens were pins, 0.125" diameter: the corrosion was evaluated metallographically in terms of the surface loss and the maximum penetration.

At 5 ppm salt level, the attack of X40 is: at 1600°F (871°C), 500 h 0.6 mils surface loss, 4.2 mils maximum penetration; 1750°F (955°C), 1000h, 1.0 and 11.6 mils; 1900°F (1038°C), 1000h, 3.8 and 18.5 mils. After 500h at 1600°F, there is internal oxidation of the carbides, some small amounts of sulphides just under the interface, but really relatively little attack.

A. M. Beltran, Cobalt No. 46, 1970, 3.

Figure 52.8 shows the static oxidation of WI 52, X45, Mar M. 509, Mar M-302, and FSX 414 at 2000°F (1093°C), mostly taken from H.L. Wheaton, Cobalt, No. 29, 1965, 163. WI-52 and X-45 oxidise very rapidly, although the X-45 curve only extends to 20h, and the rate is diminishing. Mar-M 509 and 302 are almost the same, FSX-414 is much slower.

Figure 52.9 shows the relative oxidation resistance of a number of cobalt-base alloys as determined in the G.E. small burner rig, operating with natural gas and no salt. Data are shown for X-45, FSX-414, FSX-418, Mar-M 302, Mar-M 509 and S816 at 1600°F (871°C) (air:fuel 70:1); 1800°F (982°C) (air:fuel 60:1) and 2000°F (1093°C) (air:fuel 50:1); gas velocity 70 fps (21 m/sec). The standard test is of 600h, but some have extended to 10,000h. The ranking at 2000°F is: FSX 418 test, then FSX 414, Mar M 302, Mar M 509 and X-45 about the same, and finally S.816. The orders at the lower temperatures are not so clear, but at long times it seems to be about the same as this.

Figure 52.10(a) shows the microstructure of X-45 after 1000h at 2000°F (1093°C), local regions of heavy attack (similar to those shown by Wlodek) are separated by regions where there is little attack. The author concludes that increasing the Cr content improves oxidation resistance; niobium is "clearly harmful", tungsten is innocuous at intermediate temperatures but deleterious at high temperatures, and tantalum is somewhat beneficial. Molybdenum is present in S 816, and possibly it also may be deleterious at high temperatures.

Figure 52.11 shows the relative hot-corrosion resistance of cobalt-base alloys tested in the GE burner rig, using 3% S residual oil. 325 ppm NaCl in the fuel, equivalent to 5 ppm in the air, 600h tests at 1600F (871°C). In this, X-45 was the poorest, Mar-M 302 about the same; Mar M-509 rather better, S 816 better again, and FSX 414 and 418 still better. Figure 52.12 shows the relative resistance as a function of temperature, of a number of alloys: in 1% S Diesel oil, 5 ppm sea salt in the air; generally WI-52 is worst, L-605 next, Mar-M 509 next, then Mar-M 302 and X-40 about the same. Figure 52.13 shows the appearance of X-40 and WI-52 after 1000h at 1900°F (1038°C). Internal oxidation of the carbides had taken place.

The sulphides found in the hot corroded alloys were generally CrS_x, and it was stated that the alloy oxidation was relatively unharmed by its presence, although "some chromium is used up in the process". In no case has the formation of the liquid Co_4S_3/Co eutectic been found in the hot corrosion of commercial cobalt-base alloys.

Figure 52.14 compares the oxidation resistance of Co-base and Ni-base commercial alloys: at temperatures above 1800°F FSX 414 and 418 are better than U 500 and comparable with Rene 77. X-45 appreciably worse.

Figure 52.15 shows hot corrosion of an X-45 vane after 33,000 h of service in an industrial gas turbine, and compares it with a 713C vane.

H. T. Quigg, R. M. Schirmer and L. Bagnetto, Final Report to NASC on Contract No. N00019-69-C-0221 (Phillips Petroleum Company Research and Development Report 5732-70) July 1970.

See 713C for details. Figure 52.16 shows a specimen exposed to a 85h cyclic test at 2000°F (1093°C) with 1.0 ppm sea salt in the air, and 0.04 wt % S in the fuel. Figure 52.17 shows a similar specimen tested with 0.0004% S in the fuel.

P. A. Bergman, C. T. Sims and A. N. Beltran, Hot Corrosion ProblemsAssociated with Gas Turbines; ASTM Special Technical Publication STP 421, 1967, 38.

See 713C for details. Three cobalt-base commercial alloys (X-45 SM 302 and WI 52) tested in small burner rig (100h tests, 200 ppm salt, 1% S diesel fuel) at 1750 and 1900°F (955 and 1038°C) as a basis for comparison with a series of experimental alloys. X-40 was very resistant: maximum penetration less than 10 mils at either temperature.

R. W. Hardt, J. R. Gambino and P. A. Bergman, Hot Corrosion Problems Associated with Gas Turbines, ASTM Special Technical Publication STP 421, 1967, 64.

X-40 was included for comparison in a programme designed to study the mechanism of corrosion in experimental alloys for marine applications. A small burner rig was used with 1% diesel fuel, 200 ppm sea salt in the air, 100h exposure. At 1675°F (913°C), X-40 was very resistant, with the surface loss being almost undetectable and the maximum penetration only 3 mils. The results at 1750°F (955°C)were virtually the same. The principal oxide formed at 1675°F was a spinel with a_o = 8.28 Å, with traces of NiO (sic) and Cr_2O_3.

M. J. Donachie, Jr., R. A. Sprague, R. N. Russell, K. G. Boll and E. F. Bradley. Hot Corrosion Problems Associated with Gas Turbines, ASTM Special Technical Publications STP 421, 1967, 85.

See 713C for details. Among the alloys tested was "AMS-5382" which from the composition is identical with X-40. The weight loss is compared with Mar-M 302 and 713: all seem comparable. The alloy is not very sensitive to salt concentrations. The corrosion in a 50h test with 35 ppm salt and that in a 500h test with 3.5 ppm salt, both at 1650°F, is compared. X-40 is very good in the shorter test, comparable with Mar-M 302 and U 700 in the longer test.

F. J. Wall and S. T. Michael, Hot Corrosion Problems Associated with Gas Turbines ASTM Special Technical Publication STP 421, 1967, 223.

See 713C for an extended summary. Specimens of several commercial alloys were tested by coating with 50% Na_2SO_4/50% $MgSO_4$ and oxidising in a simulated combustion gas at 1250, 1350, and 1450°F (677, 732 and 788°C) for times up to 1000h. The alloys are identified only by number and by approximate compositions, but No. 2 appears to be X-40. On the basis of a 100h test at 1450°F, the alloy is rated excellent, the same as a 20 Ni-25 Cr steel and Ra 333 (the authors comment that the chromium content, rather than the base metal, is the significant factor). Figure 52.18 shows the kinetics of the corrosion: the attack is significantly greater at 1250°F than at the higher two temperatures.

S. Y. Lee and W. E. Young, in Combustion and Heat Transfer in Gas Turbine Systems: Cranfield Symposium No. 11, E. R. Norster (ed.) (Pergamon, Oxford 1971) 253.

See 713C for details. The effect of pressure on oxidation is shown: the rate for X45 is nearly quadrupled on going from 1 atm to 3 atm pressure. The rate of oxidation at both pressures is similar for IN 738 and U500. 713C is the same at the lower pressure, but the rate only doubles at the higher pressure. Figure 52.19 shows the effect of specimen cooling on the oxidation rate.

S. Y. Lee, S. M. DeCorso and W. E. Young, J. Engineering for Power, (Trans. ASME) July 1971, 313.

Series of tests comparing U 500 and X-45, described in detail under U500. Under most circumstances the two alloys do not appear to be significantly different: X-45 seems to have rather better resistance at higher sodium plus vanadium levels.

H. T. Quigg, R. M. Schirmer and L. Bagnetto, Final Report to Naval Air Systems Command on Contract N00019-70-C-0293 (Phillips Petroleum Company Research and Development Report 5903-71) Jan. 1971.

See 713C for details. Figures 52.20 and 52.21 show details of the corrosion interface for X-40 specimens corroded for 85h with sulphur contents in the fuel of 0.0040 and 0.0004 wt %.

A. J. B. Cutler and C. J. Grant in "Deposition and Corrosion in Gas Turbines" A. B. Hart and A. J. B. Cutler (eds.), (Applied Science Publishers, London 1973) 178.

See IN 738 for details. X-40 corrodes more slowly than Nimonic 105, but not as slowly as IN 738, in molten Li/Na/K sulphate at 727°C in 1 atm O_2, 3.23×10^{-4} atm SO_3. After corrosion, the molten sulphate had an intense blue coloration due to the presence of an appreciable concentration of Co^{++} ions dissolved in the melt. The concentrations of Co^{++} and Ni^{++} ion dissolved in the molten sulphate after the alloy electrode had been removed were derived from the experimental values obtained for the reversible metal/metal ion potentials at 600°C using pure cobalt and pure nickel electrodes, relative to the standard metal/metal ion potentials at this temperature derived by the authors (unpublished work). The concentration of Co^{++} was $7.0 \pm 1.5 \times 10^{-4}$ molal, and the charge transfer required to form this concentration from the alloy is 5.4 coulombs. For Ni^{++} the corresponding figures were $9.0 \pm 2.5 \times 10^{-5}$ molal, 0.7 coulomb. The total charge transfer corresponding to the integration of the corrosion current data for X-40 in Figure 4 (see In 738) is 7.5 coulombs. The concentrations of the dissolved metal ions thus corresponds to almost complete dissolution of the cobalt and nickel corrosion products if the alloy components are oxidised in proportion to their concentration in the alloy. The solubility of the cobalt and nickel ions in the molten sulphate is consistent with the values of the equilibrium constants for the metal oxide/metal sulphate equilibria. The corresponding equilibrium constant for $Cr_2(SO_4)_3$ indicates that the solubility of chromium oxide will be relatively small. The difference in the charge transfer from the corrosion current and that corresponding to the dissolved nickel and cobalt ion is consistent with the thin (5ppm) oxide layer formed on the surface of the metal.

Electron microprobe analysis did not show any significant sulphide concentration.

J. F. G. Conde and G. C. Booth, in "Deposition and Corrosion in Gas Turbines" A. B. Hart and A. J. B. Cutler (eds.) (Applied Science Publishers, London 1973) 278.

See Nimonic 105 for details. Tests in the AML low-pressure rig, principally at 750 and 830°C with 0.1 ppm salt for 200h are described. Overall, X-40 is the best alloy tested.

C. J. Spengler, S. Y. Lee and W. E. Young in "Deposition and Corrosion in Gas Turbines" A. B. Hart and A. J. B. Cutler (eds.) (Applied Science Publishers, London 1973) 294.

See U 500 for details and the principal results. The paper reports a number of tests, using U 500 and X-45 as the principal alloys. Figure 52.22 shows the effect of gas and metal temperature on the oxidation and hot corrosion of X-45 in a pressurised passage turbine simulator operated at 3 atm pressure, the test time being 50h. For the hot corrosion tests the fuel contained 5 ppm sodium.

K. Page and R. J. Taylor in "Deposition and Corrosion in Gas Turbines" A. B. Hart and A. J. B. Cutler (eds.) (Applied Science Publishers, London 1973) 350.

See Nimonic 105 for details. Several photographs compare Nimonic 105 and X-40 blades from hovercraft Proteus engines: X-40 seems significantly better. Figure 52.23 shows the first stage nozzle guide vanes from a marine Proteus after 1525h in a hovercraft, the vane metal temperature being approx. 900°C. Without pack aluminising the vanes are catastrophically attacked; the pack aluminised vanes show relatively minor hot corrosion.

W. L. Wheatfall, in "High Temperature Corrosion of Aerospace Alloys" J. Stringer, R. I. Jaffee and T. F. Kearns (eds.), AGARD Conference Proceedings No. 120 (March 1973) 235.

See 713C and IN 738 for details.

L. M. Maas and C. L. Miller, ASME Paper No. 72-GT-77, presented to the Gas Turbine and Fluids Engineering Conference Products Show, March, 1972.

See 713C for details.

I. I. Bessen and R. E. Fryxell, General Electric Technical Information Report R72AEG317, (Nov. 1972); paper presented at the Gas Turbine Materials Conference, Naval Ship Engineering Center, Oct. 1972.

See Rene 80 for details.

E. G. Roberts, Rolls-Royce Laboratory Report No. LE 72/83 (March 1972)

Reports a comparison of aluminised and non-aluminised X-40 nozzle segments from a Proteus marine engine after 1525h running with excessive salt ingestions (on hovercraft SRN 4). The non-aluminised segments showed very considerable attack: the aluminised very little (Fig. 52.24 and 52.25). The metallography of the attack on the heavily corroded vanes (Figure 52.26) showed the presence of a sulphide layer (stated to be chromium sulphide) and attendance scale layering, of the sort experienced with the more susceptible nickel-base alloys (e.g. Nimonic 105) but not hitherto with X-40. The adjacent X-40 rotor blades were in excellent condition, and the author comments that the superior resistance of X-40 compared to Nimonic 105 may have masked the fact that the stator segments do experience a more aggressive environment than the rotor blades.

E.G. Roberts, Rolls-Royce Laboratory Report LE 71/11 (April 1971)

See Nimonic 105 for details. Test bed running of Proteus marine engine for 692h with salt in fuel. Little attack of P.A.X. -40 stator segments, except for selective oxidation of carbides when the aluminised layer had gone (Figure 52.27).

Rolls-Royce (1971) Ltd.

Figures 52.28 and 52.29 show hot corrosion data from a small burner rig with 4 ppm salt in the air at 870°C and 1050°C respectively, for X-40 (Haynes Stellite 31), PDRL 163 and IN 728.

Data relating to the alloy will also be found in the following Figures:

1.7, 1.9, 1.10, 1.11, 1.12, 1.13, 10.58, 10.61, 10.62, 10.65, 10.66, 10.83, 10.105, 10.123, 10.124, 14.6, 14.11, 30.1, 32.9, 32.10, 32.11, 32.12, 32.19, 32.20, 41.1, 41.2, 41.6, 41.7, 45.30, 45.31, 45.32, 45.33, 45.34, 45.35, 45.37, 45.39, 45.40, 45.44;

and Tables:

1-I, 1-II, 1-V, 1-VI, 1-VII, 1-VIII, 1-IX, 10-VIII, 10-XVIII, 10-XIX, 10-XX, 10-XXII, 10-XXIII, 10-XXIV, 10-XXV, 10-XXVI, 10-XXX, 18-III, 18-IV, 31-I, 45-I, 45-II, 45-III.

TABLE 52-I

SURFACE REACTION PRODUCTS ON X-40 (WLODEK)

Exposure Temp °F	Hr.	Phases Identified
1600	100	Cr_2O_3 + $CoCr_2O_4$ (a_o = 8.34Å)
1600	400	$CoCr_2O_4$ (a_o = 8.29Å) + Cr_2O_3 + CoO (a_o = 4.32Å)
1800	100	Cr_2O_3 + $CoCr_2O_4$ (a_o = 8.32Å)
1800	400	$CoCr_2O_4$ (a_o = 8.43Å) + Cr_2O_3
2000	24	$CoCr_2O_4$ (a_o = 8.29Å) + Cr_2O_3 + Co_3O_4 (a_o = 8.06Å)
2000	100	$CoCr_2O_4$ (a_o = 8.34Å) + Cr_2O_3 + CoO (a_o = 4.20Å)
2000	400	$CoCr_2O_4$ (a_o = 8.30Å) + CoO (a_o = 4.24Å) + Cr_2O_3

All identifications obtained by in-situ x-ray diffraction

Lattice parameters of pure phases are:

CoO, a_o = 4.26Å
Co_3O_4 a_o = 8.04Å
$CoCr_2O_4$ a_o = 8.34Å

TABLE 52-II

IDENTIFICATION OF INTERNAL OXIDATION* PRODUCTS IN X-40 (WLODEK)

d Å	I	Cr_2O_3 h,k,l	SiO_2 α-Cristobalite Tetragonal a_o = 4.97Å c_o = 6.93 Å h,k,l
4.05	S		101
3.63	M	012	
3.15	W		111
2.85	M		102
2.67	M	104	
2.56	W		
2.48	S	110	200
2.39	VW		
2.18	W	113	
2.09	W		202
1.93	VW		113
1.87	VW		212
1.82	W	024	
1.69	VW		203
1.67	S	116	
1.62	W		301
1.61	W		213
1.54	VW		311
1.468	W	214	
1.435	M	300	
1.405	VW		223
1.380	VW		214
1.370	VW		
1.335	VW		105
1.297	VW	1.01.0	

Oxidized 400 hours 2000°F. Surface oxide removed by grinding and 2 to 3 miles of internally oxidized zone removed by electrolytic etching.

Film pattern (CrKα) on resultant residue

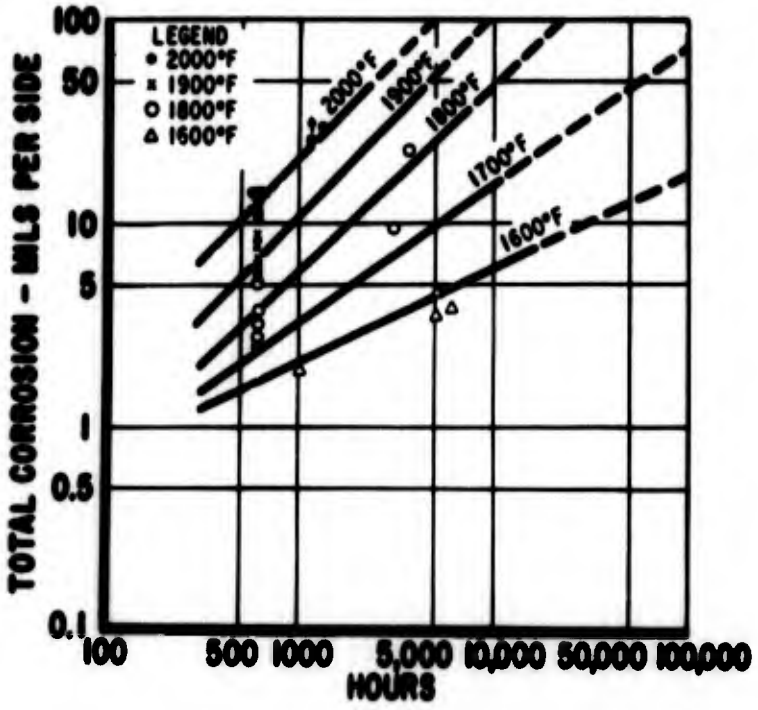

Figure 52.1. Total corrosion of alloy X45 with natural gas fuel as measured by the small burner test. (Buckland et al).

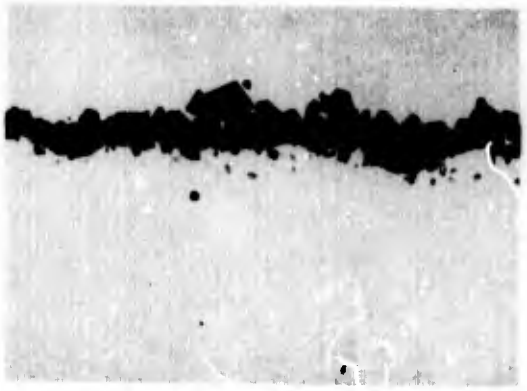

Figure 52.2. X-45 cobalt-base alloy subjected to hot corrosion atmosphere 616 hr, 1600°F. Magnification 680 times. (Seybolt).

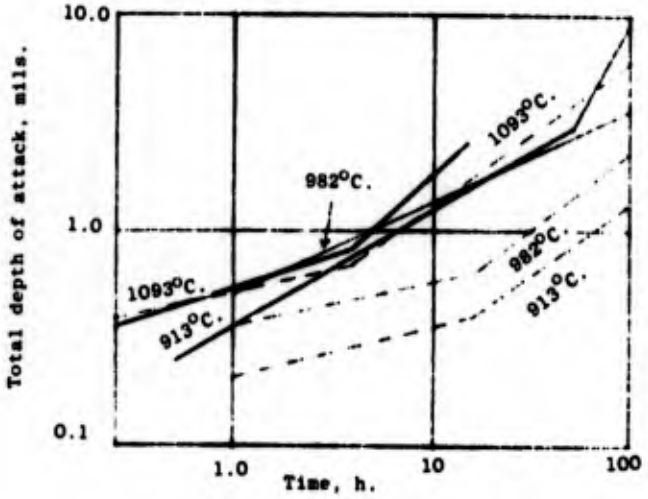

Figure 52.3. Corrosion of X-40: full lines, with 200 ppm salt; dashed lines, no salt. (Kaufman).

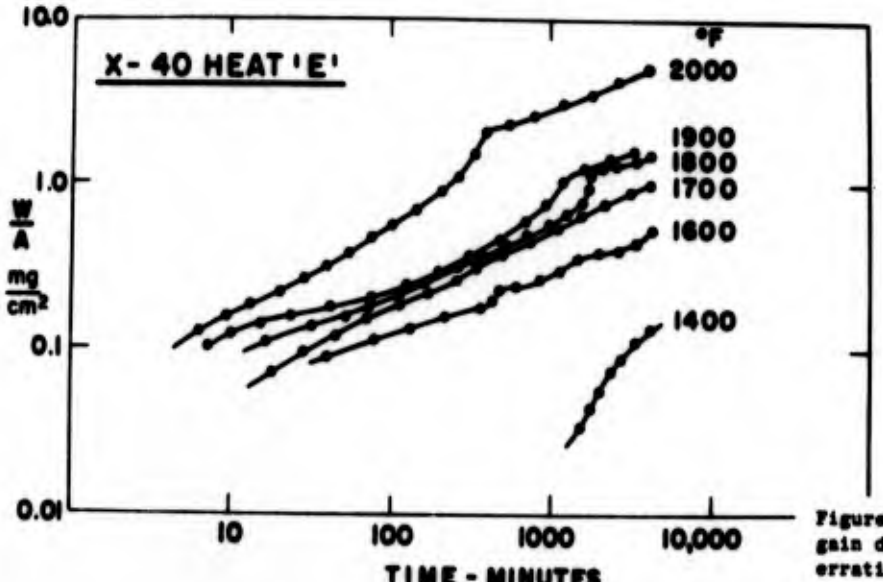

Figure 52.4. Log-log plot of weight gain data for X-40 (Heat E) showing erratic and irreproducible behaviour over whole temperature range. (Wlodek).

Figure 52.5. The extent of the internal oxidation of X-40 after 100h at 1800°F (982°C). X500, taper section x3.5. (Wlodek).

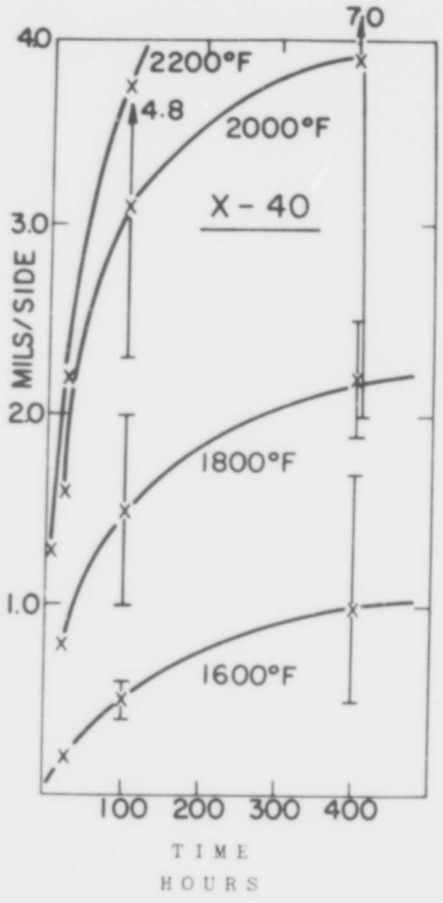

Figure 52.6. Extent of internal oxidation in X-40. Results reflect three specimens and two heats. (Wlodek).

Figure 52.7. Localized catastrophic oxidation in X-40 after 100 hours at 2000°F. (Wlodek). Unetched X100.

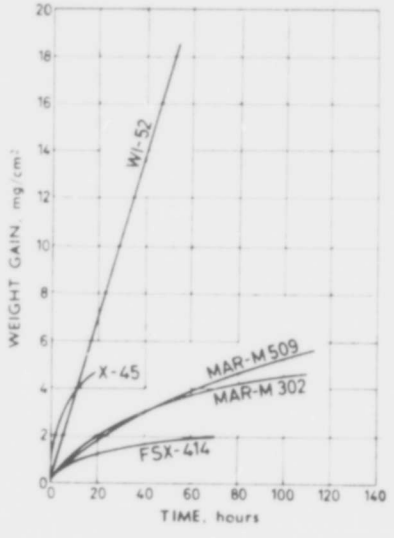

Figure 52.8. Static oxidation of selected Co-base alloys at 2000 F (1093°C). (Beltran, after Wheaton).

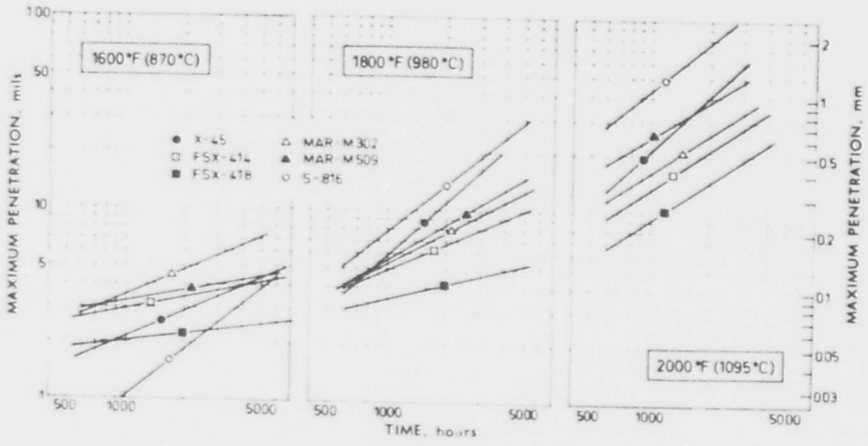

Figure 52.9. Relative oxidation resistance of complex cobalt-base alloys - natural gas burner rig data: air:fuel mixtures of 70:1 at 1600°F, 60:1 at 1800°F, and 50:1 at 2000°F; gas velocity: 70 fps (21 m/sec). (Beltran).

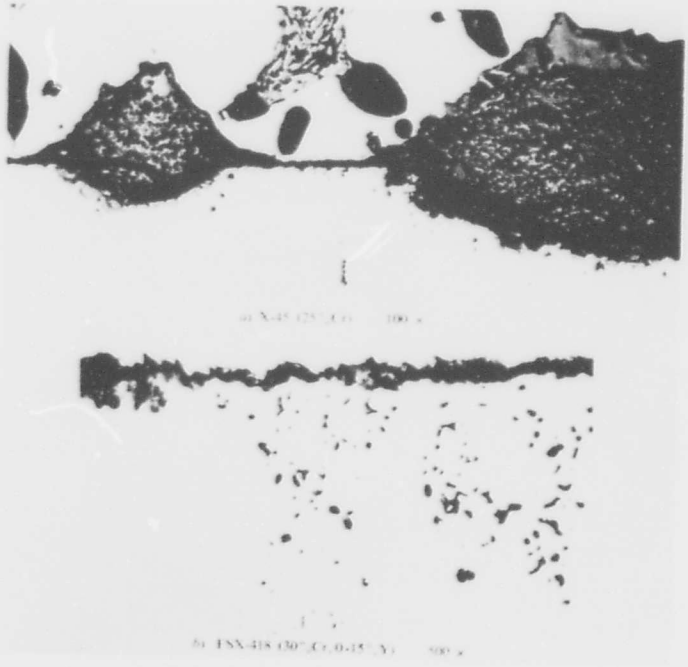

Figure 52.10. Effect of raising the chromium content from 25 to 30% and adding 0.15% yttrium on oxidation resistance at 2000°F (1093°C) in still air (exposure time : 1000 h). (Beltran).

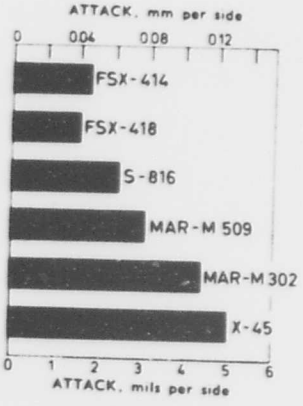

Figure 52.11. Relative hot-corrosion resistance of complex cobalt-base alloys - GE Schenectady burner rig data: 3%S residual oil. 325 ppm NaCl in fuel, 600-hour tests at 1600°F (871°C). (Beltran).

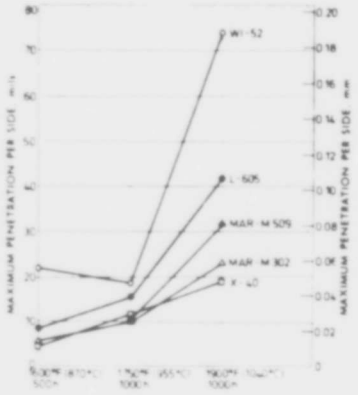

Figure 52.12. Relative hot-corrosion resistance of complex cobalt-base superalloys - GE-Lynn burner rig data: 1%S Diesel oil, 5 ppm sea salt in air. (Beltran).

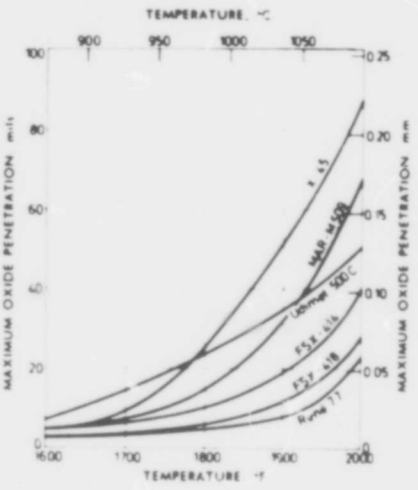

Figure 52.14. Oxidation behaviour of selected alloys. (GE-Schenectady rig data; natural gas; 5000 hour tests).

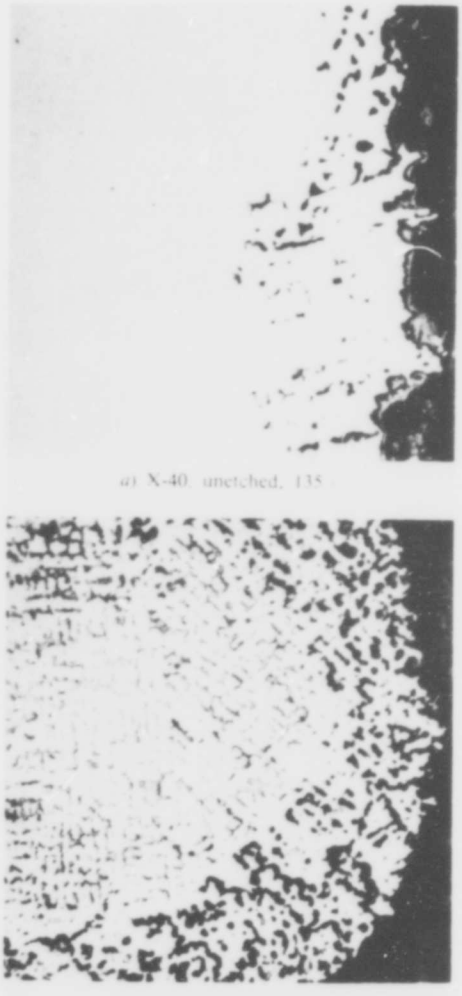

a) X-40, unetched, 135 ×

b) WI-52, unetched, 135 ×

Figure 52.13. Internal sulphidation of X-40 and WI-52 after exposure for 1000 h at 1900 F (1038°C) in GE-Lynn rig (conditions as in Fig. 52.12). (Beltran).

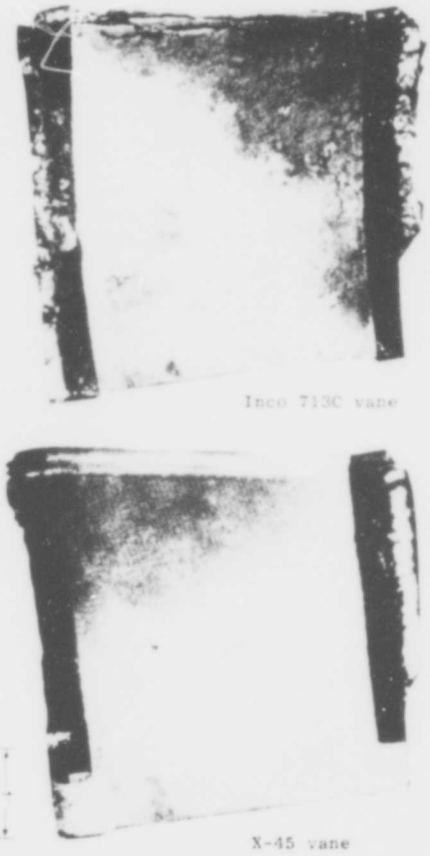

Inco 713C vane

X-45 vane

Figure 52.15. Hot-corrosion attack of Inco 713C and X-45 vanes after 33,000 hours of service in an industrial gas turbine. (Beltran).

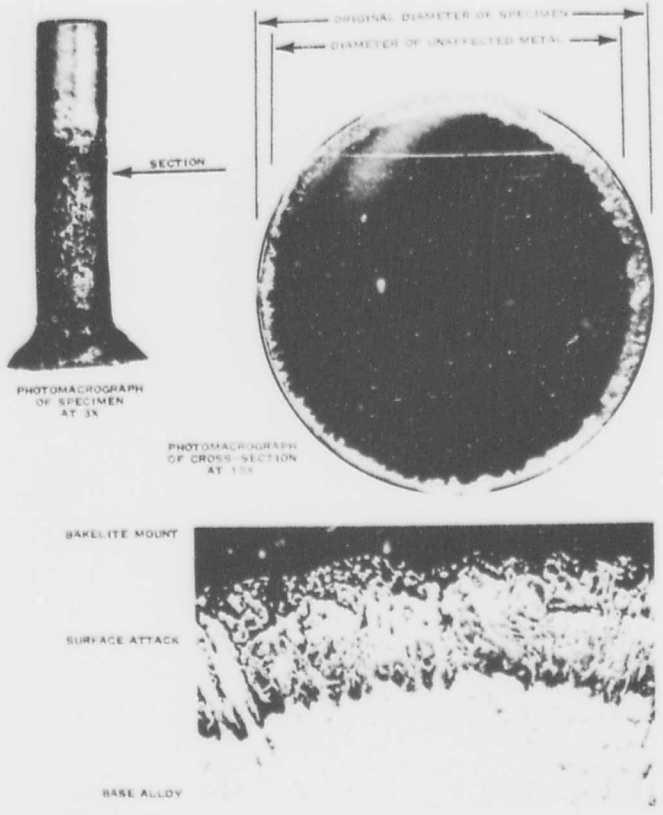

Figure 52.16. Hot corrosion of X-40 specimen after 85 hours with high-sulphur fuel (Quigg et al).

Figure 52.16. (continued)

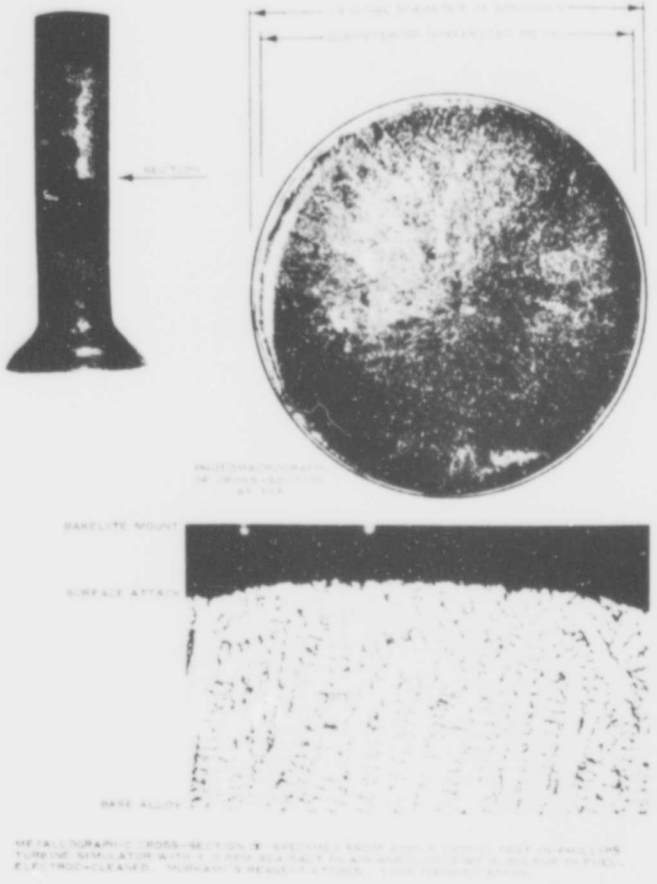

Figure 52.17. Hot corrosion of X-40 after 85 hours with low-sulphur fuel. (Quigg et al).

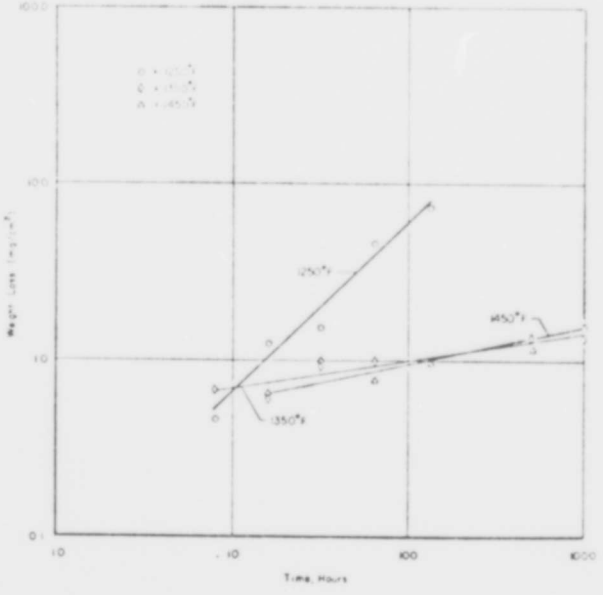

Figure 52.18. Weight loss of Co-26 Cr alloy after exposure to 1250, 1350, and 1450 F. (Wall and Michael).

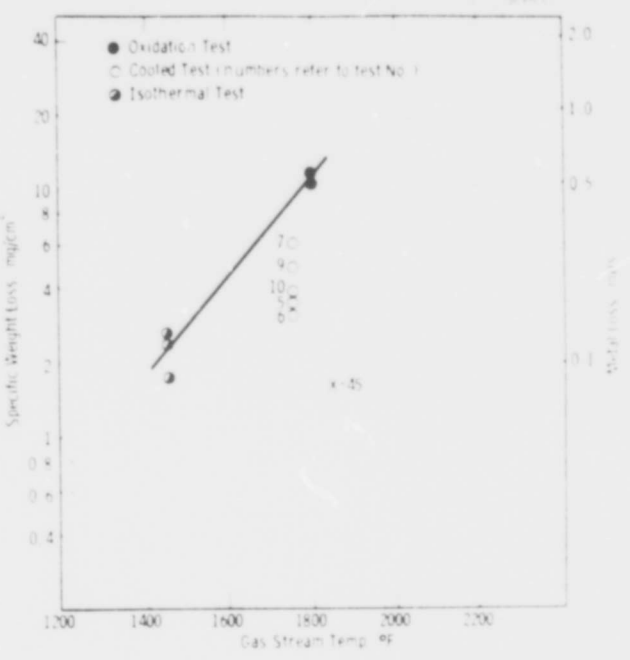

Figure 52.19. Effect of specimen cooling (X-45) (Lee and Young).

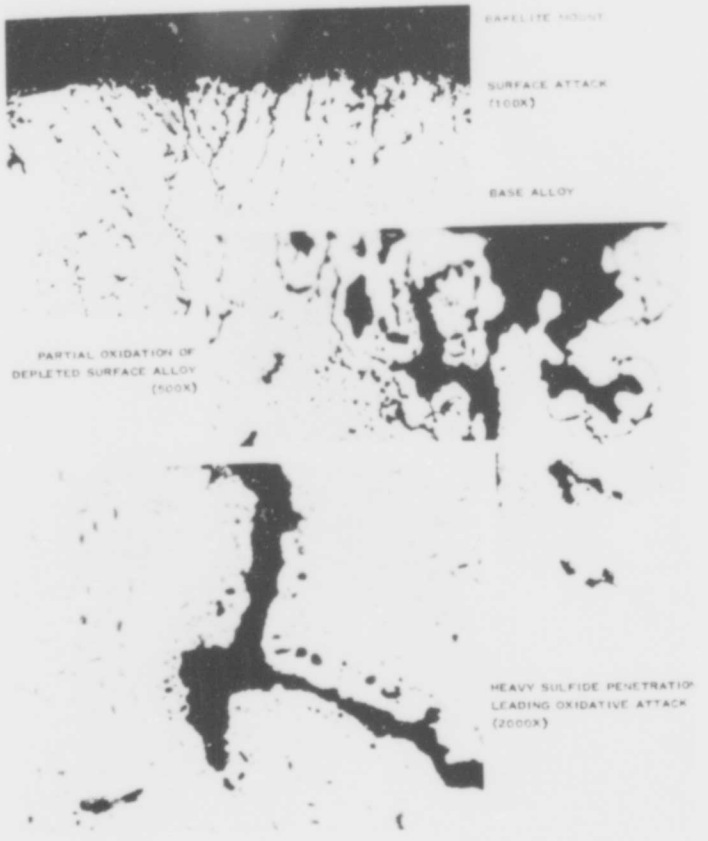

METALLOGRAPHIC CROSS-SECTION OF SPECIMEN FROM 2000 F CYCLIC TEST IN PHILLIPS TURBINE SIMULATOR WITH 1.0 PPM SEA SALT IN AIR AND 0.0040 WT % SULFUR IN FUEL. ELECTRO-CLEANED, MURKAMI'S REAGENT ETCHED.

Figure 52.20. Hot corrosion of bare X-40 specimen after 85 hours (low sulphur fuel).

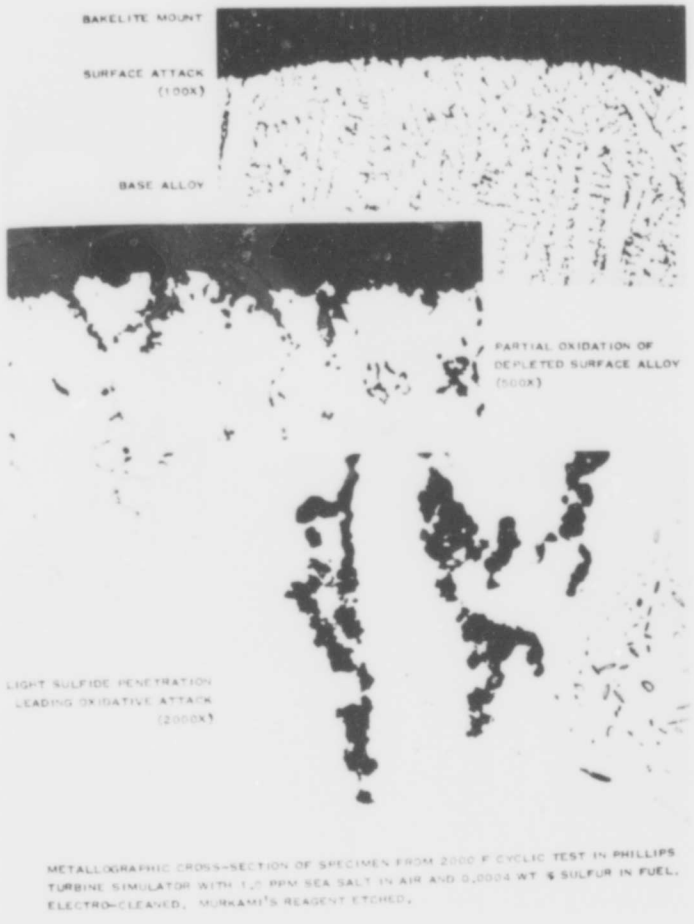

Figure 52.21. Hot corrosion of bare X-40 specimen after 85 hours (very low sulphur fuel).

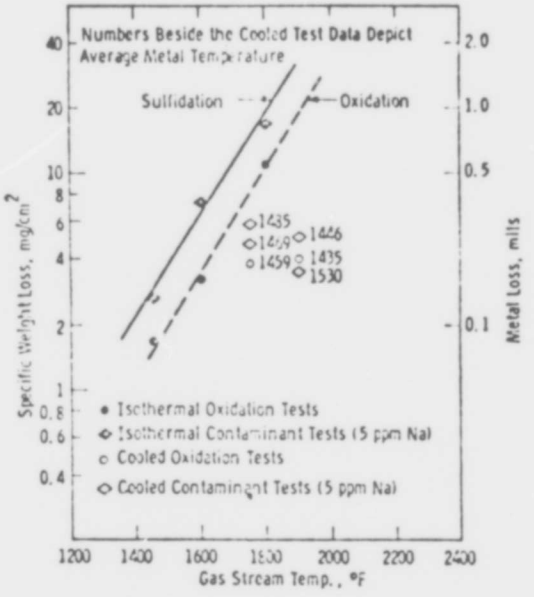

Figure 52.22. Effect of gas and metal temperatures on hot corrosion characteristics for cooled and isothermal X-45 specimens tested for 50 hr at 3 atm pressure. (Spengler et al).

a. X 40 uncoated H.P. vanes—showing catastrophic hot corrosion attack.

b. X 40 pack aluminised H.P. vanes—showing characteristic hot corrosion attack.

Figure 52.23. Proteus engine - HP nozzles in X-40 with and without pack aluminising - 1500 h - Hovercraft operation - maximum turbine entry temperature 1145oK. (Page and Taylor).

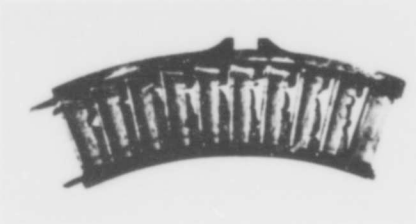

Figure 52.24. X-40 stator segment from a marine Proteus engine after 1525h field trials with excessive salt ingestion. (Roberts).

Figure 52.25. Opposite side of the segment shown in Figure 52.24.

Figure 52.26. A pack aluminised X-40 stator segment from the same test as that shown in Figure 52.24.

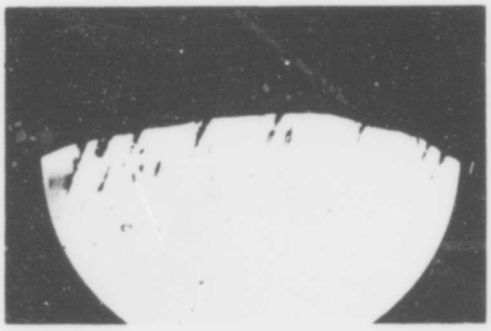

Figure 52.27. A section at the leading edge of a pack-aluminised X-40 stator segment from a marine Proteus engine after 692h with salt in the fuel. The pack aluminised layer has been completely lost and there has been selective oxidation of the carbides. (X70). (Roberts).

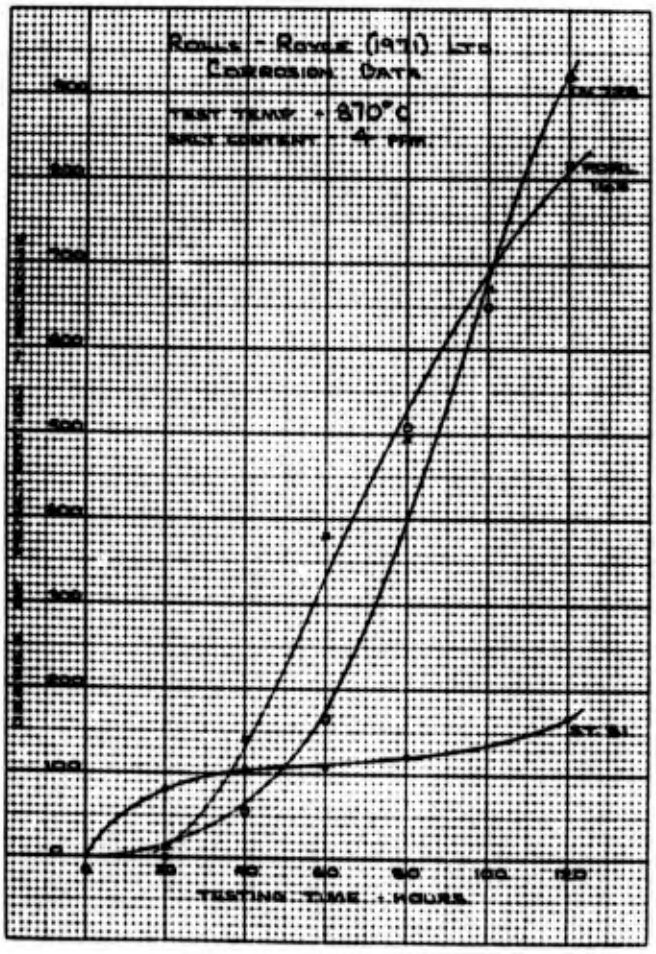

Figure 52.28. Hot corrosion data from Rolls-Royce (1971) Ltd.

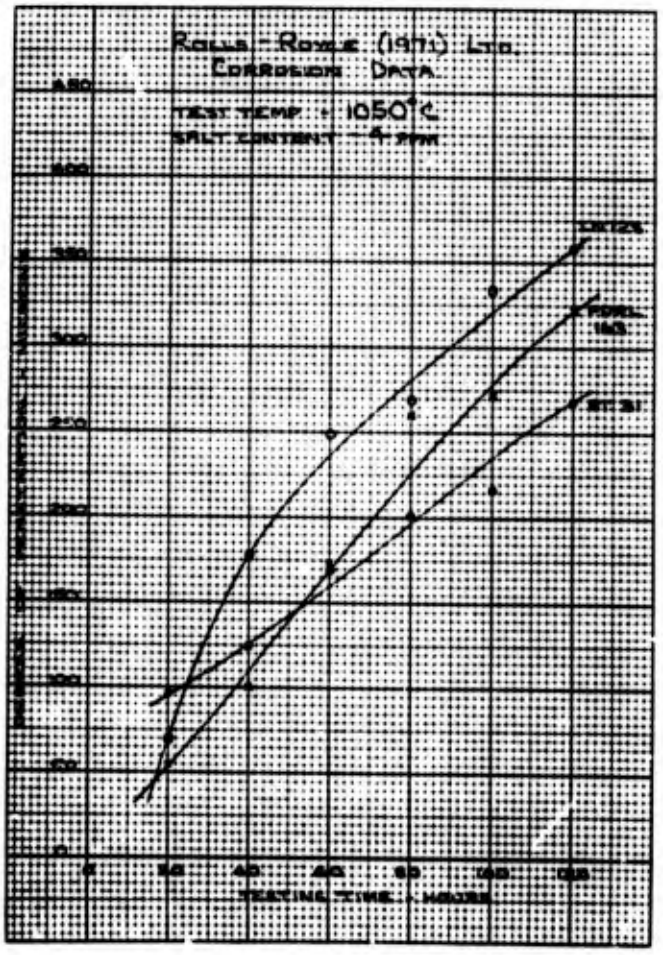

Figure 52.29. Hot corrosion data from Rolls-Royce (1971) Ltd.

Part 3. The Refractory Metals

Part 3. The Refractory Metals

The four metals niobium, tantalum, molybdenum and tungsten, commonly referred to as the refractory metals, all have attractive properties in advanced aerospace applications. They have high melting points and retain excellent mechanical strength to elevated temperatures; in addition, niobium and tantalum have very good ductility at low temperatures. Unfortunately, all four metals oxidize very readily at moderate temperatures. Figure 0.1, taken from Michael[1] compares the metal recession rates of the four metals at 2000°F (1093°C). During the latter part of the 1950's it became clear that materials with superior high temperature properties would be required for space vehicles and for advanced gas turbines, and many programs of research were initiated to develop alloys with improved mechanical and oxidation properties. Although there was considerable success in improving the mechanical properties, the only alloys developed with significant oxidation resistance were based on intermetallic compounds and were extremely brittle.

As a result, in the early 1960's attention shifted almost entirely to the development of coatings, which lies outside the scope of this Handbook. However, although satisfactory coatings--notably those based on the silicides--were developed, local coating failures could not be entirely avoided, and furthermore at the highest temperatures degradation of the coating due to interdiffusion with the substrate became a problem.

Some of the urgency had been removed by engineering advances. In the case of aerospace vehicles, the development of ablative heat shields and in the case of gas turbines the development of blade cooling techniques reduced the requirements for high temperature materials. However, once again technology has advanced to a point where the relaxation achieved in these ways has been exhausted. In the case of space vehicles, the concept of the reusable space shuttle has led to renewed interest in coated refractory metal systems, although they are still not prime materials candidates: the overall materials situation for the shuttle has recently been reviewed by Deutsch[2]. In the case of gas turbines there are two possibilities: the first is the need for small high power-to-weight ratio engines with short lifetimes for various purposes including direct lift for VSTOL aircraft; and the second is the need to increase still further the turbine entry temperature in conventional aircraft engines, in which case it will be necessary to achieve long lives and high dependability.

In the case of material for the gas turbine, a possible method is to use a composite, of which two different types have been proposed: in the first, the large part of the blade is made from a high-strength alloy, which is then clad with a relatively thin layer (0.5 mm or so) of a relatively oxidation resistant, relatively ductile alloy; finally a coating is applied to the outside of this. The idea is that the cladding provides both a diffusion barrier, preventing degration of the strong core, and a back-up in the event of coating failure. The second type involves the strengthening of a relatively weak, oxidation resistant alloy with strong fibres--for example, tungsten wires--the whole again being coated.

As a result of these developments there has recently been a renewed interest in the study of the oxidation behavior of refractory metal alloys, although the total effort is still very limited in comparison with that of the late 1950's and early 1960's. For a number of reasons the major effort has been concerned with niobium (columbium) based systems. There seems little hope that competitive oxidation resistant alloys can be developed on the base of tungsten or molybdenum, and at the highest temperatures, where the use of these metals is mandatory, the extreme volatility of these oxides means that alloying for oxidation protection is virtually impossible. The problem is essentially the development of a coating system. Tantalum seems to respond worse than niobium to alloying for oxidation resistance for reasons which are not clear; but because of its greater density there has been much less interest in this metal.

In addition to the alloy development programs there has been a continuing study of the mechanisms of the oxidation of the refractory metals and their simpler alloys. The oxidation of niobium, tantalum and tungsten has been discussed by Kofstad[3], and all four metals and their alloys have been reviewed by Kubaschewski and Hopkins[4]. The oxidation of tantalum and its alloys has been reviewed in detail recently by Stringer[5]. In this Handbook, only the main points about the oxidation of the pure metals will be summarized; little of the detailed mechanistic discussion and the experiments designed principally to evaluate mechanisms will be presented. However, since the development of oxidation-resistant alloys is at a very early stage, data relating to simple systems will be presented, in contrast to its omission from the part concerned with superalloys.

Section 1 Niobium and Niobium Alloys

Niobium forms three stable oxides, NbO, NbO_2 and Nb_2O_5, and a number of metastable lower oxides whose composition is uncertain. The pentoxide apparently exists in a number of modifications, but there is some argument about the equilibrium nature of some of the modifications. The most common notation is that of Brauer[6] who identified a low-temperature form, T-Nb_2O_5, stable up to approximately 900°C; an intermediate form, M-Nb_2O_5, stable between 900 and 1100°C; and a high temperature form, H-Nb_2O_5, stable above 1100°C. Later authors have questioned the separate existence of M-Nb_2O_5; the powder diffraction pattern is similar to the H form, and M was probably an incompletely crystallized form of H. It seems probable that Nb_2O_5 has a limited range of stoichiometry: oxygen-deficient material can be produced, which is black in color; but at large deviations a succession of closely-related berthollide structures with the general formula $Nb_{3n+1}O_{8n-2}$ appear, due to different ways of stacking NbO_3 octahedran. The oxygen-deficient Nb_2O_5 appears to be an oxygen vacancy, n-type semiconductor, although there is some disagreement. The situation has been reviewed by Kofstad[7].

When a clean niobium surface is exposed to oxygen, oxygen initially dissolves in the metal before a distinct oxide phase is nucleated. The length of the period before the nucleation of an oxide depends on the temperature and the gas pressure. Eventually a distinct oxide is formed. At temperatures up to 400°C the first-formed oxide is a tetragonal phase labelled NbO_x[8]. Above 400°C a second suboxide, NbO_z is formed. Norman, et. al.[9] show a specimen of niobium oxidized for 1300 minutes at 500°C in oxygen at 10^{-2} torr. The only phases present were niobium containing

dissolved oxygen and NbO_z, which formed as platelets within the metal. Eventually, a superficial layer of Nb_2O_5 nucleates and spreads over the metal surface. At high oxygen pressures these processes occur much more rapidly.

Above 600°C the metastable lower oxides do not appear to form, and beneath the outer pentoxide layer there are small amounts of the stable lower oxides NbO and NbO_2; these do not seem to form a complete layer, at least so far as can be detected by metallography.

The pentoxide is formed under very considerable compressive growth stresses, and eventually fails, allowing the penetration of oxygen to the metal surface. This process repeats with the development of a thick porous outer scale.

As a result of these sequences of events, the kinetics of the reaction are quite complex; during the solution of oxygen without the formation of an oxide the weight gain is parabolic. It is also parabolic during the formation of the pentoxide before its fracture; once the repeated fracturing process is established the rate law becomes effectively linear. There is a considerable evolution of heat in the oxidation, which can lead to initial non-steady state reaction when oxygen is first admitted to the metal surface, which can last several minutes. Eventually a temperature is reached where the whole process accelerates and the metal burns; this ignition temperature depends on the specimen size and the atmosphere, but for oxygen at 1 atm and 0.5 mm metal sheet it is probably of the order of 1100-1200°C.

Most kinetic studies have been concerned with the approximately linear rate during which the porous oxide is formed. Figure 1.1 shows Kofstad's[3] representation of the temperature dependence of the rate constant. Figure 1.2 shows a different representation of essentially the same data taken from Stringer[10] and divided up according to a scheme due to McLintock[11]. Region A is an early stage of the reaction at lower temperatures when a fairly uniform egg-shell like oxide forms on the metal surface. After a time, a breakaway occurs at local points on the metal surface, a powdery oxide breaking through the continous layer, and gradually spreading over the surface. A faster linear rate is eventually established: this post-breakaway linear rate is Region B. At 600°C there is an abrupt reduction in the rate which appears to be associated with the disappearance of the metastable NbO_z platelets as a dynamic feature of the oxidation process. In Region C a laminar scale forms, the lamination thickness increasing with temperature as the scale appears to become more plastic. The change in temperature dependence between Region C and Region D appears to be associated with the change in the pentoxide scale from T-Nb_2O_5 to H-Nb_2O_5.

Stringer[10] suggests that the NbO_z platelets act as crack initiators in the scale, and this is why the rate falls abruptly at 600°C. There are other views, but it would seem desirable to suppress the formation of the platelet phase and encourage the formation of the stable lower oxides NbO and NbO_2.

The oxidation rate shows a marked pressure dependence as is indicated by Figure 1.1. At a fixed temperature, the pressure dependence is fitted well by a Langmuir isotherm, at least at the lower temperatures, suggesting that adsorption of oxygen at some interface is involved in the reaction, but again there is no general agreement about the mechanism.

The data in Figures 1.1 and 1.2 come from a variety of sources[10-17] and there is general agreement on the overall rates of oxidation. One problem in interpreting the kinetic data is that the oxidation rate is not uniform over the surface of the specimen. In the case of the usual coupon-shaped specimens, the edges and corners oxidize very much more rapidly (sometimes by a factor of 10 or more) than the broad faces, and the nominal weight gain figure isthus a rather ill-defined average rate.

Kling[18] noted that the oxidation involved the repeated fracturing of the pentoxide scale, and suggested that first, alloy additions might be made in accordance with the well-known Wagner model, thus reducing the rate at which the initial oxide film grows prior to fracturing. Secondly, alloy additions might be made to alter the mechanical properties of the scale, either by increasing the fracture strength or decreasing the creep strength, so that the growth stresses could be relaxed by creep. Finally, alloy additions might be made which would stabilize the lower oxides, which might have better transport properties and lower growth stresses. On the basis of his experiments, in which Ti, V, and Mo were all shown to have good effects at moderate concentrations, he suggested that a change in the mechanical properties and in particular an increase in the creep rate of the oxide, was the most important effect.

Clauss and Barrett[19] suggested that alloy elements capable of forming 3+ ions with a size similar to that of the Nb^{5+} ion appeared to give good results. Klopp[20] suggested on the basis of a large number of binary and ternary alloys that the size effect was more important than the valence effect, with smaller ions than Nb^{5+} apparently contracting the scale and thus reducing the growth stresses in the scale. Many authors have concluded that simply modifying the Nb_2O_5 scale is not enough; either sufficient alloy element must be added to form its own protective oxide, by analogy with chromium or aluminum in nickel-base alloys, or an element capable of entering with niobium into a complex oxide more stable (and, of course, slower growing) than Nb_2O_5 must be added.

In addition to the problem of metal removal by oxidation, niobium has a fairly large solubility for oxygen, of the order of 2-3 at %O at 1000°C, and the inward diffusion of oxygen degrades the mechanical properties of the core. Figure 1.3 shows the contamination rate of niobium at various temperatures. In the development of an oxidation resistant alloy, both the contamination and the scaling must be considered.

A number of investigators have conducted screening tests on wide ranges of alloys. Because of the different methods used a direct comparison is not always possible, and therefore they will be presented here separately, more or less in chronological order. In some cases commercial designations are used for alloys, and it is also useful to see how the compositions of the simpler alloys relate to the commercial systems. Table 1-I is a listing of a number of alloys, taken from Frank[21]. A notable omission from the listing is the oxidation resistant alloy WC-3015, introduced by Wah Chang Albany in 1969. The composition can be varied within the following limits to meet particular requirements: HF, 28-30%; Zr, 1-2%; Ti, 0-5%; Ta, 0-4%; W, 13-16%; and C, 0.07-0.33%. The optimum oxidation resistance (oxide penetration to a depth of about 0.030 in. in 24 hour exposure to static air at 2400°F) is achieved by adding 5% Ti at the expense of some reduction in hot strength above 1500°F.

Table 1-II is taken from Klopp[20] and includes virtually all the data available at the time. Figures 1-4 and 1-5 present some of the data of Klopp, et. al.[25] in graphical form. Figures 1-6 and 1-7 present the data of Michael[1] in terms of metal recession. Figures 1-8, 1-9 and 1-10 relate to Nb-Ta and modified Nb-Ta alloys, again from Michael. Table 1-III shows the variation in the oxide structure with temperature for the Nb-20Ta alloy, and Figure 1-11 shows the air oxidation of a number of Nb-base alloys. Figure 1-12 shows the oxidation behavior of a number of Nb-Cr alloys, from Barrett and Clauss[27]. At chromium concentrations greater than about 4 at.%Cr, the formation of H-Nb_2O_5 was promoted. Figure 1-13 is taken from Klopp[20] and shows the effect of chromium on the oxidation. It is not entirely clear whose data these are, but they are probably those of Klopp, et. al.[24]. Figure 1-14 shows the effect of molybdenum. Again the original source is probably Klopp, et. al.[24] Figures 1-15-1-18 similarly show data for Nb-Ti, Nb-V, Nb-W and Nb-Zr alloys.

Table 1-IV shows the contamination rates for some binary alloys, from Sims, et. al.[22], and Figure 1-19 compares the hardening of unalloyed Nb with that of two alloys.

Table 1-V, also from Klopp[20] lists data for the oxidation of complex niobium alloys in air. Figure 1-20 to 1-30 present the data for a number of ternary systems in diagrammatic form. Figure 1-21 compares the oxidation of a number of niobium alloys with that of FeCrAl in air at 1000°C.

Wlodek[37] conducted a most detailed study of the oxidation of Nb-W-Ti alloys, the results of which are presented in Figures 1-31 to 1-42 and Table 1-VI to 1-VIII. Wlodek notes that the oxidation resistance that occurs within a critical region in the Nb-Ti-W ternary system suggests the formation of a protective compound oxide, which appears to be a ternary niobate with a wide stability range, which appears to be miscible with $Nb_2O_5WO_3$. The solution of TiO_2 in this prevents spalling by increasing the mechanical stability of the niobate, but if the titanium content is too high, the phase $Nb_2O_5 \cdot TiO_2$ appears at high tungsten levels and the phases Nb_2O_5-TiO_2 and TiO_2 at low tungsten levels. These are less desirable. At 800°C the scale exfoliates and contains flakes of oxygen-contaminated metal bounded by (110) faces suggesting that the exfoliation is due to cracking in the metal rather than in the oxide or at the oxide/metal interface. Molybdenum and vanadium additions reduce this exfoliation, apparently by reducing the oxygen contamination of the metal. Vanadium is the more effective, but unfortunately also reduces the melting point of the reaction products.

Wlodek[38] also conducted a similar detailed study of the oxidation of Nb-Al-V alloys. The results are presented in Figures 1-43 to 1-53 and Tables 1-IX to 1-XI. Small amounts of Al in V improve the oxidation resistance of niobium, apparently by stabilizing a protective layer of NbO. As little as 3% Al and 3% V produces a fifty to one hundred fold improvement over the oxidation resistance of pure niobium in the temperature range 800-1200°C. Further improvements are possible with Ti, Cr, Ni and Fe. The ternary alloys exhibit good resistance to oxygen contamination; Ti and Zr increase the depth and rate of contamination.

Jahnke[39] compared the oxidation and contamination of a number of commercial niobium base alloys with nickel-base alloys and molybdenum alloys as shown in Figure 1-54.

Miller and Cox[40] oxidized a number of binary niobium alloys, Nb-W-Ti and Nb-W-V alloys, and quaternary alloys based on Nb-20 at.% W to 20 at.% Ti. The results are presented in Figures 1-55 and 1-56 and in Tables 1-XII to 1-XIV.

Mayo, et. al.[41] examined the possibility of forming a protective double oxide on a niobium alloy, and concluded on the basis of thermal expansion, volume ratio and structure that the most likely candidate was $CrNbO_4$, and accordingly the oxidation of alloys in the range 25 to 50% Cr was studied at 1100°C. The results are shown in Figure 1-57. Interestingly, an alloy of Nb-35%Cr oxidized more rapidly in air than in oxygen (Figure 1-58).

Smith[42] reported results on the oxidation of ternary and quaternary alloys based on Nb-Ti. The results are shown in Figures 1-59 to 1-64 and Tables 1-XV to 1-XVII.

Argent and Phelps[43] studied the oxidation of Nb-Ti and Nb-Mo alloys. The results are shown in Figures 1-65 to 1-69 and Tables 1-XVIII to 1-XXI. In Table 1-XXI, α Nb_2O_5 is the same as T-Nb_2O_5 in Brauer's notation, and β Nb_2O_5 is the same as H-Nb_2O_5.

Bacon and Moanfeldt[44] reviewed the reaction of niobium and niobium-based alloys with oxygen in some detail, presenting data on oxidation rates, most of which has been presented above. However, they include unpublished data by Wlodek, et. al.[65] and this is listed in Table 1-XXII. Data for more complex Nb-Ti base alloys from the same source is shown in Table 1-XXV.

Babitzke and co-workers have been conducting a development program for niobium and tantalum base alloys for several years. Table 1-XXVI and Figure 1-70 relate to Nb-V alloys[46]. Figure 1-71 shows results for Nb-Hf alloys[47]. Figure 1-72 shows further weight gain data for several Nb-V alloys, together with data for Ta-Hf and Ta-V alloys[48]. The oxidation rates for the Nb-V alloys are shown in Table 1-XXVII. Figure 1-73 shows data for Nb-10 wt.% Ti alloys with additions of oxide, borides or carbides[48]. Table 1-XXVIII expresses the results as oxidation rates. Table 1-XXIX lists results for a number of more complex niobium alloys. Some tantalum alloy results are also included[49]. Figure 1-74 compares the oxidation rates of one or two of the better alloys with the pure metals. Table 1-XXX lists further data[50] and Figures 1-75 and 1-76 show the oxidation of a further group of alloys[51]. Table 1-XXXI shows oxidation weight gains for a group of complex alloys in 1 hour tests at 1000°C in air[52]. Table XXXII shows the oxidation behvior of another group of niobium and tantalum base alloys in 2 hour tests at 800 and 1000°C in air[53]. Table 1-XXXIII lists the composition and Figure 1-77 shows the oxidation behavior of another group of alloys[54]. Table 1-XXXIV and Figures 1-78 to 1-81 show the effect of boron on the oxidation behavior of a group of Nb-W-Hf alloys[55].

Chang[56] conducted a study of the oxidation behavior of two niobium base alloys, designated Cb-1 (Nb-30W-1Zr-0.1C) and Cb-2 (Nb-30W-2Ti-1Zr-0.1C). The nominal composition of Cb-2 actually included 5% Ti, but analysis showed there to be only 2% present. The carbon content of both alloys is also a little smaller than specified, at around 0.06%, and they both contain approximately 0.04%N and 0.01%O. Table 1-XXXV and Figures 1.82 to 1.84 present the data.

Begley, et. al.[57] has reported results for the oxidation of a group of niobium base alloys. Their data are shown in Table 1-XXXVI.

Figure I-85 shows some data for the oxidation and contamination of a group of commercial Nb-base alloys, taken from Frank[21].

Metcalfe and Stetson[58] reviewed the development of refractory metal components for use at elevated temperatures, discussing the various aspects of coating and cladding. Figure I-86 shows the oxidation rates of a number of uncoated substrate alloys at 1600°F (871°C) and Figure I-87 shows the oxidation behavior of the most oxidation resistant ductile niobium alloys at the same temperature. Figure I-88 presents oxidation curves for a Nb-27Ti-5Al alloy.

Cornie and Goodspeed[59] conducted an extensive program designed to develop a fabricable, moderately oxidation resistant alloy for application as a cladding or a back-up for primary protective coatings for high-strength niobium alloy turbine blades. The target time was up to 50 hr at temperatures of 2200 F (1204 C). An analysis suggested that the maximum permissible oxidation rates at 2000 and 2200°F (1093 and 1206°C) were 5.6 and 4.0 mils/hour$^{1/2}$, respectively. The best oxidation resistance was demonstrated for Nb-15Ti-10Ta-10W-2Hf-3Al alloy, designated B-1, with surface recession rate of roughly 2.5 and 1.5 mils/hour$^{1/2}$ at 2200 and 2000°F, respectively. The surface oxide formed in flowing air at temperatures through 2400°F (1316°C) was quite adherent although some spalling occurred on cooling below 1500°F (816°C). Figure I-89 shows the oxidation of B-1 at various temperatures, and Figure I-90 shows the oxygen penetration and surface recession rates at 2000 and 2200°F. Figure I-91 compares the oxidation of B-1 with that of pure Nb and B-88 type alloys.

Table I-XXXVII lists the compositions of the first series of experimental alloys, and Table I-XXXVIII gives their oxidation behavior at 2200°F. Figures I-92 through I-101 present the data in graphical form. Table I-XXXIX shows the calculated rate constants and Figures I-102 and I-103 compare the weight gain and surface recession data for the alloys.

The scale on all these alloys consisted of two layers--an outer yellow to brown porous layer which spalled on cooling, and a darker, denser and strongly adherent inner scale. Both gave similar X-ray patterns, which were identified as $Nb_2O_5 \cdot TiO_2$ with a small amount of NbO and NbO_2 present.

Table I-XL shows the composition of the second series of alloys, and Table I-XLI lists the oxidation data. Table I-XLII lists the kinetic rate constants. Figure I-104 and I-105 show the weight gain and surface recession of these alloys at 2200°F. Table I-XLIII and Figure I-106 show the effect of a 1 hour preoxidation on the weight gain behavior. Finally, Figure I-107 compares the weight gain data for the B-1 alloy with several modifications of WC-3015.

Kolski[60] studied the oxidation of Nb-10Ti in the temperature range 500-1200°C for times of the order of 25-200 hours. At 700°C the reaction is relatively slow for 15-20 hours, but then accelerates to a rapid rate. At 600°C there is a relatively mild breakaway after approximately 70 hours. The scales formed at 800°C or higher consisted of a solid solution of TiO_2 in Nb_2O_5. Figures I-108 to I-110 show the kinetics.

Felten[61] studied the oxidation of Nb-25wt.%Ti (39at.%Ti) in oxygen and air. At 1000°C, the kinetics were linear in air, the rate constant depending on pressure to the power 0.4; in oxygen the kinetics were parabolic after 8 hours, and were less dependent on the oxygen pressure. The external oxide layer at the oxide/metal interface

consisted of TiO_2 and $2TiO_2 \cdot 5Nb_2O_5$; at the oxide/oxygen interface $TiO_2 \cdot Nb_2O_5$ was present, having been formed by the solid state reaction of the other two phases. In a second paper[62] the oxidation of the alloy was studied at temperatures between 650 and 1000°C. Below 800°C the rate was parabolic in either air or oxygen. Figures 1-111 to 1-114 show the kinetic results.

Kolski[63] also studied the oxidation of Nb-10%Mo in the temperature range 400 to 1200°C in oxygen at 1 atm for times ranging from 1 to 200 hours. In the range 450 to 550°C there is a breakaway to a catastrophic oxidation rate, as for pure Nb. Figures 1-115 to 1-118 present the results.

Taylor and Stringer[64] oxidized Nb-5.5at.%Mo single crystals in the temperature range 530-1100 C. Figure 1-119 compares the rates in their investigation with those of Kolski[63] and Phelps[43]. At 750 C severe cracking of the metal was encountered, along (100) planes and apparently associated with NbO_2 suboxide platelets.

Brentnall, et. al.[65] have attempted to develop ductile, relatively oxidation-resistant niobium-base alloys which may then be strengthened by tungsten wires; the composite is finally coated. The program goal was 200 hours at 2200°F (1204°C) and tests were conducted up to 2400°F (1316°C) for 16 hours. Figure 1-120 shows the general oxidation behavior of a number of niobium-base alloys. Table 1-XLIV summarizes the oxidation rate of a number of oxidation-resistant niobium alloys. In addition to oxidation tests, some specimens were hot-corrosion tested in a crucible containing 95% Na_2SO_4, 5% NaCl at 1650°F (899°C) for 18 hours. Table 1-XLV shows the alloys tested in the program. The alloys designated S and T are titanium-modified versions of WC-3015. Tables L-XLV to 1-L summarize the results of the oxidation tests and these are also presented in Figure 1-121. Table 1-LI summarizes the results of the crucible tests.

In a later report on the same contract, Klein, et. al.[66] studied the oxidation of a composite of the J-alloy with tungsten wires, observing the time taken for the first oxidation of one of the wires to take place. The results are shown in Figure 1-122, and the estimated oxidation life of the composite is shown in Figure 1-123.

Scheirer[67] also reported results of an investigation aimed at developing an oxidation-resistant cladding material for use over a strong core, the whole being coated. The core material selected was Cb-132M (Nb-20Ta-15W-5Mo-1.5Zr-0.1210WC) Two cladding alloys were selected on the basis of preliminary testing of oxidation resistance and fabricability of ten candidates: Nb-15Ti-10Ta-10W-2Hf-3Al (Alloy 7M) and Nb-5W-30Hf-3Ti-3Re (Alloy 10). Both of these alloys were capable of preventing rapid oxidation of the core alloy at 2200°F (1206°C) for times in excess of 64 hours. Table 1-LII lists the candidate alloys, and Table 1-LIII the oxidation data.

Roche and Graham[68] attempted to develop alloys having good strength and oxidation resistance for use as blading alloys. The aim was to produce an alloy with oxidation resistance equivalent to that of TD Nickel at 2000°F (1097°C), i.e., about 1 to 2-mils loss per side in 100 hours. Two alloy systems were selected for study: Nb-10-25%W-15-30%Ta, and Nb-10-25%W-2-35%Hf. The Nb-W-Ta alloys were heavily oxidized, a 0.10-inch-thick specimen being completely penetrated within 20 hours at 2000°F. However, the Nb-W-Hf alloys with moderate amounts of tungsten and fairly large amounts of hafnium were much better, containing unaffected metal even after 65 hours in flowing air at 2000°F. A base of Nb-15W-35Hf was

selected and the effect of further additions studied. Ti, Cr, Al, and V all enhanced the oxidation resistance, but at the expense of other properties. The data are presented in Figures 1-124 to 1-126 and in Tables 1-LIV to 1-LIX.

Vasilyeva and Prokoshkin[69] studied the oxidation of ternary Nb-Ta-Mo alloys at 1000, 1100 and 1200°C. Table 1-LX shows the results; the high temperature form of Nb_2O_5 was the only oxide detected.

Rapp and Goldberg[70] studied the oxidation of Nb-Zr and Nb-Zr-Re alloys in oxygen at 1000°C. For alloys with 10 at.% Zr, the high temperature form of Nb_2O_5 was the only oxide detected, for alloys with 20, 30 and 40 at.% Zr, ZrO_2, Nb_2O_5 and $NbO_5 \cdot 6ZrO_2$ were identified. These alloys also showed evidence of internal oxidation of the zirconium to form ZrO_2. Rhenium additions of 5 at.% Re resulted in improved scale adhesion and a decrease in scaling rate.

Sikka and Rosa[71] studied the oxidation of Nb-10 at.% W in the temperature range 900-1200°C. 10% W reduces the oxidation rate at 1000 to 1200°C (see Table 1-LXI) but at 900°C the oxidation is catastrophic.

Rosa and Chen[72] oxidized Nb-10 at.% Cr in the temperature range 900-1100°C. The rate is less than pure Nb at 1000 and 1100°C, but faster at 900°C (Table 1-LXII).

Felten[73] has conducted a detailed study of the oxidation of the commercial alloy Cb-132 (Nb-20Ta-15W-5Mo) in the temperature range 550-1316°C. Between 550 and 650°C dissolution of oxygen without the formation of a significant amount of surface scale was observed. Between 650 and 900°C there is an initial slow reaction followed by a more rapid linear rate. Above 900°C the oxidation curves are parabolic over a substantial part of their length, and the outer scale is dense and adherent. Figures 1-127 to 1-130 and Tables 1-LXIII to 1-LXV present the results.

Tavassoli[74] examined the oxidation of WC3015 containing 4.6% Ti at 2400°F (1316°C) and compared it to Cb752. WC3015 oxidized in a parabolic manner, but for the first 30 minutes it oxidized more quickly than Cb752. Although in the long term, the oxidation would be slower, this was not useful for re-entry vehicles or for thin sheet components. Elkington and McDonald[75] disagreed with this observation, noting that in a 5-min exposure at 2600°F a 20-mil sheet specimen of Cb752 was completely oxygen-contaminated, whereas oxygen had only penetrated about halfway into the WC3015 sheet.

Table 1.I. Nominal Chemical Composition of Columbium Alloys. (from Frank (21)).

Alloy Designation	Original Investigator	Nominal Composition w/o Cb	W	Mo	Ta	V	Hf	Zr	Ti	C	ppm O	ppm N	Status[a]
USA													
Cb-1Zr	-	Bal	-	-	-	-	-	1	-	0.005	100	50	C
SCb-291	Fansteel	Bal	10	-	10	-	-	-	-	0.006	100	100	C
FS-85	Fansteel	Bal	10	-	28	-	-	1	-	0.004	60	50	C
Cb-752	Union Carbide	Bal	10	-	-	-	-	2.5	-	0.004	60	80	C
Cb-753	Union Carbide	Bal	-	-	-	5	-	1.25	-	0.005	100	75	C
C-103	Wah Chang/Boeing	Bal	-	-	-	-	10	0.7	1	0.015	225	150	C
C-129Y	Wah Chang/Boeing	Bal	10	-	-	-	10	-	(0.2Y)	0.015	225	150	C
B-33	Westinghouse	Bal	-	-	-	5	-	-	-	0.006	120	60	C
B-66	Westinghouse	Bal	-	5	-	5	-	1	-	0.006	120	60	C
D-14	DuPont	Bal	-	-	-	-	-	5	-	0.006	100	40	C
D-36	DuPont	Bal	-	-	-	-	-	5	10	0.006	100	40	C
D-43	DuPont	Bal	10	-	-	-	-	1	-	0.1	100	40	C
F-48	General Electric	Bal	15	5	-	-	-	1	-	0.05/0.1	300	100	PP
PWC-11	Pratt & Whitney	Bal	-	-	-	-	-	1	-	0.1	150	100	PP
AS-30	General Electric	Bal	20	-	-	-	-	1	-	0.1	100	100	D
AS-55	General Electric	Bal	5	-	-	-	-	1	(0.2Y)	0.06	200	250	D
Cb-1	General Electric	Bal	30	-	-	-	-	1	-	0.06	100	300	D
Cb-2	General Electric	Bal	30	-	-	-	-	1	5	0.06	100	300	D
B-88	Westinghouse	Bal	28	-	-	-	2	-	-	0.067	30	40	D
VAN-79	Westinghouse	Bal	22	-	-	-	2	-	-	0.067	50	50	D
Cb-132	Pratt & Whitney	Bal	15	5	20	-	-	-	-	0.004	100	40	D
Cb-132M	Pratt & Whitney	Bal	15	5	20	-	-	2.5	-	0.13	60	40	D
UK													
SU-16	Imperial Metal Ind.	Bal	11	3	-	-	2.0	-	-	0.08	-	-	PP
SU-31	Imperial Metal Ind.	Bal	17	-	-	-	3.5	-	-	0.1	-	-	D
USSR													
RN-5	-	Bal	10	-	-	-	-	1.2	-	0.034	250	-	-
RN-6	-	Bal	5	5	-	-	-	1.2	-	0.026	280	-	-
-	-	Bal	16.5	-	-	-	-	0.5	-	0.1	-	-	-

(a) C indicates commercial; PP, pilot production; D, development.

Table 1.II. Oxidation rates of columbium and columbium binary alloys in air. (Klopp (20)).

Alloy Composition, Balance Columbium[a] At. %	Wt %	Oxidation Rate, mg/cm²/hr 600 C (1110 F)	800 C (1470 F)	1000 C (1830 F)	1090 C (2000 F)[b]	1200 C (2190 F)	Reference
100 Cb	--	7.2	27.7	58.4	44	74	1
0.2 Al	--	7.5	39.2	19.8	--	--	22
1.0	--	8.0	37.2	22.5	--	--	22
5.0[c]	--	7.1	44.2	19.4	--	--	22
2	--	--	--	--	<44	--	1
5	--	--	--	--	41	--	1
20	--	--	--	--	4.5	--	1
0.27[d]	--	--	--	19.1	--	100	19
1.03[d]	--	--	--	20	--	95	19
3.80[d]	--	--	--	19.7	--	90	19
7.00[d]	--	--	--	22	--	86	19
16.6[d]	--	--	--	27	--	76	19
15.36	5	--	--	51	--	--	23
0.2 B	--	5.8	39.3	19.9	--	--	22
1.0	--	3.8	27.8	20.2	--	--	22
5.0	--	3.0	10.3	15.1	--	--	22
0.2 Be	--	5.7	27.6	24.0	--	--	22
1.0	--	6.9	31.1	21.5	--	--	22
5.0[e]	--	6.5	40.6	18.0	--	--	22

Table 1.II. (Continued).

Alloy Composition, Balance Columbium[a]		Oxidation Rate, mg/cm^2/hr					
At. %	Wt %	600 C (1110 F)	800 C (1470 F)	1000 C (1830 F)	1090 C (2000 F)[b]	1200 C (2190 F)	Reference
1 Cr	--	3.4	29.8	33.1	--	--	22
2.9[d]	--	3.5	24.2	28.1	--	--	22
5[f]	--	1.3	24.4	26.2	--	--	22
15.7[d]	--	0.5	5.1	6.1	--	--	22
20[f]	--	0.1	0.4	22.3	--	--	22
23[f]	--	--	--	150	--	70[g]	24
7	--	--	--	--	>45	--	1
10	--	--	--	--	9.2	--	1
20	--	--	--	--	5.8	--	1
0.48[d]	--	--	--	18.1	--	69	19
1.10[d]	--	--	--	17.4	--	84	19
2.01[d]	--	--	--	19.5	--	97	19
3.17[d]	--	--	--	34	--	86	19
5.10[d]	--	--	--	32	--	80	19
8.6	5	--	--	36.5	--	--	23
1 Cu	--	--	--	58	--	98	19
2	--	--	--	43	--	80	19
2.98[d]	--	--	--	34	--	56	19
0.2 Co	--	5.2	40.8	43.8	--	--	22
1.0	--	3.7	41.9	37.6	--	--	22
5.0	--	4.1	39.2	38.5	--	--	22
10	--	--	--	--	>45	--	1
20 Co	--	--	--	--	>45	--	1
1	--	--	--	47	--	103	19
2	--	--	--	28	--	77	19
4.3[d]	--	--	--	27	--	52	19
<0.1 Fe[d]	--	6.6	32.0	35.6	--	--	22
0.4[d]	--	7.0	40.5	25.0	--	--	22
1.9[d]	--	5.5	22.0	25.0	--	--	22
30	--	--	--	--	>45	--	1
1	--	--	--	47	--	105	19
2	--	--	--	40	--	100	19
3.84[d]	--	--	--	28	--	40	19
7.68	5	--	--	36.2	--	--	23
1 Ge	--	--	--	55	--	120	19
2	--	--	--	54	--	152	19
5	--	--	--	49	--	125	19
10.4[d]	--	--	--	62	--	93	19
1 Ir	--	--	--	54	--	101	19
2	--	--	--	57	--	111	19
5	--	--	--	56	--	92	19
10	--	--	--	51	--	82	19
28.1[d]	--	--	--	43	--	58	19
0.2 Mn	--	7.8	40.0	21.8	--	--	22
1	--	4.3	38.0	22.1	--	--	22
5[h]	--	4.5	39.3	23.9	--	--	22
1 Mo	--	1.7	12.0	13.2	--	--	22
2.5	--	--	--	6.6	--	31.5	25
5	--	0.3	2.1	5.0	--	21.5	25
7.5	--	--	--	3.0	--	18.5	25
10	--	0.4	1.9	4.6	--	14.5	25
25	--	2.0	3.8	42.5	--	--	22
3	--	--	--	--	24	--	1
10	--	--	--	--	4.0	--	1
30	--	--	--	--	>44	--	1
1	--	--	--	54	--	99	19
2	--	--	--	35	--	104	19
5	--	--	--	44	--	103	19
10	--	--	--	58	--	89[g]	19
24.5[d]	--	--	--	24[g]	--	46[g]	19
4.85	5	--	--	8.2	--	--	23
<0.1 Ni[d]	--	7.2	27.3	30.3	--	--	22
0.5[d]	--	5.2	26.5	58.5	--	--	22
2.3[d]	--	5.1	31.5	46.3	--	--	22

Table 1.II. (Continued).

Alloy Composition, Balance Columbium[a]		Oxidation Rate, mg/cm²/hr					
		600 C	800 C	1000 C	1090 C	1200 C	
At. %	Wt %	(1110 F)	(1470 F)	(1830 F)	(2000 F)[b]	(2190 F)	Reference
10 Ni	--	--	--	--	>45	--	1
30	--	--	--	--	>45	--	1
1	--	--	--	51	--	86	19
1.62[d]	--	--	--	39.4	--	108	19
7.65	5	--	--	52.4	--	--	
5 Re	--	--	--	76[g]	--	65[g]	24
1	--	--	--	31[g]	--	24[g]	19
2	--	--	--	34[g]	--	31[g]	19
5	--	--	--	34[g]	--	26[g]	19
10	--	--	--	24[g]	--	19.5[g]	19
19.7[d]	--	--	--	(i)	--	(i)	19
1 Se	--	--	--	34	--	34	19
2	--	--	--	43	--	36	19
5	--	--	--	40	--	44	19
10[j]	--	--	--	24	--	47	19
0.1 Si[d]	--	6.9	52.0	21.4	--	--	22
0.7[d]	--	6.1	53.3	46.5	--	--	22
3.7[d]	--	10.3	67.0	103.8	--	--	22
2	--	-	--	--	42	--	1
7	--	--	--	--	31	--	1
20	--	--	--	--	4.5	--	1
1	--	--	--	51	--	109	19
2	--	--	--	50	--	113	19
5	--	--	--	51	--	80	19
10	--	--	--	50	--	53	19
24.5[d]	--	--	--	31	--	--	19
1 Ta	--	6.2	29.0	68.2	--	--	22
5	--	8.4	34.7	25.5	--	--	22
10	--	7.5	39.7	20.3	--	--	22
25	--	2.0	26.3	61.3	--	--	22
1	--	--	--	--	28	--	1
5	--	--	--	--	16	--	1
10	--	--	--	--	10	--	1
15	--	--	--	--	3.8	--	1
20	--	--	--	--	1.9	--	1
25	--	--	--	--	2.5	--	1
30	--	--	--	--	4.2	--	1
35	--	--	--	--	5.5	--	1
40	--	--	--	--	10	--	1
50	--	--	--	--	18	--	1
60	--	--	--	--	27	--	1
80	--	--	--	--	36	--	1
90 Ta	--	--	--	--	32	--	1
99	--	--	--	--	25	--	1
1	--	--	--	38	--	102	19
2	--	--	--	35	--	87	19
5	--	--	--	32	--	84	19
10	--	--	--	40	--	71	19
24.1[d]	--	--	--	45	--	99	19
2.70	5	--	--	57.1	--	--	23
1 Ti	--	5.8	21.6	26.0	--	--	22
5	--	4.7	21.0	15.7	--	--	22
10	--	0.2	7.5	12.2	--	45.5	25
20	--	--	--	4.8	--	26.5	24
25	--	0.1	0.6	3.4	--	13.5	25
30	--	--	--	5.0	--	13.5	24
35	--	0.2	0.7	6.0	--	19.5	25
3	--	--	--	--	>44	--	1
14	--	--	--	--	>44	--	1
33	--	--	--	--	41	--	1
57	--	--	--	--	22	--	1
1	--	--	--	46	--	90	19
2	--	--	--	34	--	100	19
5	--	--	--	36	--	84	19
10	--	--	--	34	--	80	19
20.2[d]	--	--	--	23	--	46	19

Table 1.II. (Continued).

Alloy Composition, Balance Columbium[a] At. %	Wt %	Oxidation Rate, mg/cm^2/hr 600 C (1110 F)	800 C (1470 F)	1000 C (1830 F)	1090 C (2000 F)[b]	1200 C (2190 F)	Reference
1 V	--	3.6	6.3	13.8	--	--	22
5	--	0.9	1.4	5.4	--	22	25
7.5	--	--	--	4.4	--	21.5	24
10	--	0.1	0.7	3.4	--	18	25
12.5	--	--	--	3.0	--	18.5	24
15	--	--	--	4.4	--	28.5	24
17.5	--	--	--	6.6	--	57.5	24
25	--	0.2	6.1	(266)[h]	--	(200)[h]	25
3	--	--		--	30	--	1
10	--	--		--	24	--	1
30	--	--		--	>44	--	1
1	--	--	--	20	--	70	19
2	--	--	--	12.5	--	93	19
5	--	--	--	9.8	--	71	19
10	--	--	--	11.2	--	54	19
23.6[d]	--	--	--	64	--	86	19
8.24	5	--	--	8.2	--	--	23
1 W	--	6.1	41.0	27.2	--	70	25
5	--	3.1	12.3	30	--	22.5	25
10	--	2.9	17.0	21.2	--	17.5	25
12.5 W	--	--	--	34.0	--	19.5	24
25	--	8.3	31.0	94.0	--	--	22
3	--	--	--	--	7.3	--	1
10	--	--	--	--	5.6	--	1
20	--	--	--	--	2.2	--	1
30	--	--	--	--	2.2	--	1
1	--	--	--	58	--	130	19
2	--	--	--	52	--	97	19
5	--	--	--	51	--	102	19
10	--	--	--	50	--	104	19
28.7[d]	--	--	--	41	--	80	19
2.61	5	--	--	68	--	--	23
1 Zr	--	7.1	64.8	71.0	--	--	22
5	--	3.8	41.2	135	--	--	22
10	--	0.3	25.2	62	--	48.5	25
25	--	4.7	10.7	27	--	40	25
35	--	0.2	2.2	15.6	--	35.5	25
45	--	--	--	9.6	--	26	24
3	--	--	--	--	>44	--	1
10	--	--	--	--	>44	--	1
30	--	--	--	--	30	--	1
1	--	--	--	41	--	97	19
2	--	--	--	37	--	70	19
5	--	--	--	37	--	91	19
10	--	--	--	54	--	91	19
24.8[d]	--	--	--	54	--	94	19
35	--	--	4.8	--	--	--	26
40	--	--	3.3	--	--	--	26
45	--	--	3.1	--	--	--	26
47	--	--	--	10.7	--	--	26
65	--	--	--	9.5	--	--	26
5.10	5	--	--	106.8	--	--	23

(a) Compositions are nominal except where noted. Compositions given originally in wt % are converted to at. %.
(b) Weight-gain data at 1090 C are entirely from Reference 43 and were converted from metal-loss data using the conversion 0.1 cm metal loss equals 400 mg/cm^2 weight gain.
(c) Analyzed <0.7 at. % Al.
(d) Analyzed composition is given.
(e) Analyzed <0.1 at. % Be.
(f) Estimated composition is given.
(g) Volatile oxide was noted; weight-gain data probably low.
(h) Analyzed 0.7 at. % Mn.
(i) Negative weight gain noted resulting from volatile oxide.
(j) Analyzed 2.12 at. % Se.

Table 1.III. Data on the Structures of the oxides on columbium, tantalum, and a Cb-20% Ta alloy. (Michael [1]).

Oxidation temperature, °F	Columbium	Tantalum	Cb-20 pct Ta alloy
1000	T	T	T
1200	T	T	T
1400	T	T	T
1600	H	T	T
1800	H	T	T + H
2000	H	T	H
2200	H	T	H

*Structures of the outer scales after cooling to room temperature. Specimens were oxidized for 16 hr in air.

Table 1.IV. Contamination rates in binary columbium alloys [22].

Alloy Addition (Balance Columbium), at.%		Contamination Rate, 10^{-4} cm^2 per sec, at Indicated Temperature			Alloy Addition (Balance Columbium), at.%		Contamination Rate, 10^{-4} cm^2 per sec, at Indicated Temperature		
Nominal	Adjusted	600 C	800 C	1000 C	Nominal	Adjusted	600 C	800 C	1000 C
100 Cb		0.0865	1.26	7.56	1 W	--	0.12	1.8	8.4
					5 W	--	0.12	1.8	8.0
1 Ti	0.9 Ti	0.068	3.0	9.4	10 W	--	0.09	2.0	(0.71)
5 Ti	4.5 Ti	0.013	0.50	1.6	25 W	--	0.0	2.0	5.1
10 Ti	9.0 Ti	0.0062	0.29	0.71					
15 Ti	14.0 Ti	--	--	--	1 Ta	--	0.022	1.1	11.0
20 Ti	18.5 Ti	--	--	--	5 Ta	--	0.025	1.1	(3.4)
25 Ti	23.0 Ti	0.0052	0.03	0.24	10 Ta	--	0.57	1.0	(1.3)
30 Ti	28.0 Ti	--	--	--	25 Ta	--	0.12	1.3	6.4
35 Ti	32.5 Ti	0.0058	0.024	0.49					
					0.2 Mn	--	0.20	1.3	(11)
1 Mo	0.9 Mo	0.085	1.9	4.7	1 Mn	--	0.13	1.7	(5.7)
2.5 Mo	2.0 Mo	--	--	--	5 Mn	0.7 Mn	0.10	1.6	(6.0)
5 Mo	4.5 Mo	0.14	2.0	(0.029)[a]					
7.5 Mo	6.5 Mo	--	--	--	0.2 Fe	<0.1 Fe	0.16	1.5	(13)
10 Mo	9.0 Mo	0.15	1.5	--	1 Fe	0.4 Fe	0.099	2.1	(7.3)
25 Mo	22.0 Mo	0.025	0.33	--	5 Fe	1.9 Fe	0.041	1.7	(3.0)
1 Cr	0.6 Cr	0.16	1.5	8.0	0.2 Co	--	0.12	2.0	(12)
5 Cr	3.0 Cr	0.19	1.5	9.2	1 Co	--	0.17	1.1	(3.2)
10 Cr	6.0 Cr	0.038	0.9	6.1	5 Co	--	0.16	(0.1)	(1.8)
20 Cr	11.5 Cr	--	--	--					
25 Cr	14.5 Cr	1.1	0.15	0.92	0.2 Ni	<0.1 Ni	0.059	0.73	(6.5)
30 Cr	17.5 Cr	--	--	--	1 Ni	0.5 Ni	0.022	0.39	(0.35)
35 Cr	20.5 Cr	0.09	(0.56)	0.045	5 Ni	2.3 Ni	0.11	0.78	(2.0)
1 V	0.9 V	0.022	0.99	6.7	0.2 Al	--	0.15	2.8	(14)
5 V	4.5 V	0.012	0.51	4.2	1 Al	--	0.13	2.9	(1.2)
7.5 V	6.5 V	--	--	--	5 Al	<0.7 Al	0.10	0.79	(8.2)
10 V	8.5 V	0.011	0.34	2.2					
12.5 V	11.0 V	--	--	--	0.2 Si	0.1 Si	0.04	0.61	0.41
25 V	21.5 V	0.079	0.080	0.13	1 Si	0.7 Si	0.034	3.2	20
					5 Si	3.7 Si	0.56	3.8	18
1 Zr	--	0.048	0.38	3.4					
5 Zr	--	0.027	0.064	--					
10 Zr	--	0.035	0.023	0.012					
25 Zr	--	0.087	0.064	0.066					
35 Zr	--	0.0	0.0	0.012					

(a) Contamination rates in parentheses are estimated; oxygen diffused through the centers of these samples.

Table 1.V. Oxidation rates of columbium and complex columbium alloys in air.

Alloy Composition[a], Balance Columbium		Oxidation Rate, mg/cm²/hr							
At. %	Wt %	600 C (1110 F)	800 C (1470 F)	900 C (1650 F)	1000 C (1830 F)	1090 C (2000 F)	1200 C (2190 F)	1260 C (2300 F)	Reference
100Cb	100Cb	7.2	27.7	--	58.4	44[d]	74	--	1
Columbium-Titanium-Base Alloys									
25Ti	--	0.1	0.6	--	3.4	--	13.5	--	25
11.1Ti-9.1Al	7Ti-3Al	--	--	--	2.7[b]	--	--	--	28
15.2Ti-14.2Al	9.5Ti-5Al	--	--	--	12.5	--	--	--	23
25Ti-1Al	--	0.16	1.0	--	4.0	--	--	--	22
28.4Ti-13.2Al	19Ti-5Al	--	--	--	15.2	--	--	--	23
27.1Ti-24Al	20Ti-10Al	--	--	--	1.9	--	--	--	28
31.3Ti-8.1Al-2.9Co	20Ti-3Al-2Co	--	--	--	2.8[b]	--	--	--	28
53.5Ti-9.0Al-4.7Cr	42Ti-4Al-4Cr	--	--	--	0.45	--	2.0	--	29
23.1Ti-13.7Al-11.5Mo	15Ti-5Al-15Mo	--	--	--	2.4[b]	--	--	--	28
21.5Ti-8.49Al-2.39Mo-3.42Fe	13.5Ti-3Al-3Mo-2.5Fe	--	--	--	2.4[b]	--	--	--	28
20.2Ti-8.94Al-3.14Mo-2.18Fe-20.1Be	16Ti-4Al-5Mo-2Fe-3Be	--	--	--	2.0[b]	--	--	--	28
42.3Ti-2.59Al-7.27Mo-6.39Mn	29Ti-1Al-10Mo-5Mn	--	--	--	1.4[b]	--	--	--	28
14.9Ti-15.8Al-6.5Mo-11.2V	10Ti-6Al-6Mo-8V	--	--	--	1.7[b]	--	--	--	28
23.05Ti-10.9Al-2.62Si	15Ti-4Al-1Si	--	--	--	2.2[b]	--	--	--	28
25Ti-2Co	--	0.083	0.72	--	3.7	--	--	--	24
5.2Ti-4.1Cr[c]	--	0.08	5.4	--	3.3	--	--	--	24
9.1Ti-1.0Cr[c]	--	0.09	4.5	--	5.0	--	--	--	24
10Ti-17Cr[c]	--	--	--	2.4	(2.8)[1]	--	--	--	26
10Ti-29Cr[c]	--	--	--	4.2	(4.8)[1]	--	--	--	26
12Ti-1.5Cr[c]	--	--	--	--	6.1	--	26.8	--	25
12.3Ti-4.3Cr[c]	--	0.24	2.0	--	3.9	--	--	--	24
16Ti-7Cr[c]	--	--	--	1.0	(1.2)[1]	--	--	--	26
16.3Ti-7.9Cr	9.5Ti-5Cr	--	--	--	5.0	--	--	--	23
18.2Ti-2.4Cr[c]	--	0.29	1.3	--	2.5	--	--	--	24
20Ti-2Cr[c]	--	--	--	--	2.7	--	19.8	--	25
21Ti-8Cr[c]	--	--	--	1.0	(1.2)[1]	--	--	--	26
28Ti-6Cr[c]	--	--	--	--	2.5	--	15.8	--	25
30.2Ti-7.3Cr	19Ti-5Cr	--	--	--	4.9	--	--	--	23
31Ti-8Cr	--	--	--	1.2	(1.4)[1]	--	--	--	26
32Ti-15Cr	--	--	--	3.5	(4.0)[1]	--	--	--	26
41Ti-9Cr	--	--	--	0.8	(0.9)[1]	--	--	--	26
23Ti-2Fe	--	0.10	0.83	--	3.7	--	--	--	24
16.4Ti-7.4Fe	9.5Ti-5Fe	--	--	--	7.8	--	--	--	23
30.4Ti-6.85Fe	19Ti-5Fe	--	--	--	6.8	--	--	--	23
5Ti-5Mo	--	0.11	9.7	--	7.1	--	--	--	24
10Ti-3Mo	--	--	--	--	3.0	--	--	--	29
10Ti-5Mo	--	0.10	7.3	--	3.9	--	--	--	24
10Ti-10Mo	--	0.16	7.1	--	3.4	--	--	--	24
12Ti-4Mo	--	--	--	--	3.7	--	20	--	25
15Ti-5Mo	--	0.11	3.5	--	3.1	--	--	--	24
17Ti-11.47Mo	9.5Ti-5Mo	--	--	--	8.5	--	--	--	23
17.5Ti-6Mo	--	--	--	--	3.2	--	19.7	--	25
17.8Ti-8.9Mo	10Ti-10Mo	--	--	--	2.4	--	8.5	--	29
20Ti-5Mo	--	0.20	1.7	--	2.7	--	--	--	24
23Ti-8Mo	--	--	--	--	3.1	--	15.2	--	25
31.3Ti-4.1Mo	19Ti-5Mo	--	--	--	8.2	--	--	--	23
16.4Ti-7.1Ni	9.5Ti-5Ni	--	--	--	16.0	--	--	--	23
23Ti-2Ni	--	0.22	1.1	--	7.6	--	--	--	24
25Ti-5Ni	--	0.10	0.68	--	3.0	--	--	--	24
30.5Ti-6.5Ni	19Ti-5Ni	--	--	--	12.5	--	--	--	23
24Ti-1Si	--	0.18	1.0	--	3.8	--	--	--	24
12.5Ti-12.5Ta	--	0.10	5.8	--	7.9	--	--	--	24
17.35Ti-2.4Ta	9.5Ti-5Ta	--	--	--	8.2	--	--	--	23
31.9Ti-2.2Ta	19Ti-5Ta	--	--	--	7.3	--	--	--	23
2.5Ti-7.5V	--	0.11	1.6	--	4.3	--	--	--	24
5Ti-5V	--	0.10	2.2	--	5.5	--	--	--	24
10Ti-5V	--	0.16	3.5	--	4.0	--	--	--	24
10.5Ti-5V	--	--	--	--	4.1	--	22	--	25
15Ti-5V	--	0.12	1.5	--	3.3	--	--	--	24
16Ti-8.5V	--	--	--	--	3.1	--	13.6	--	25
16.3Ti-8.1V	9.5Ti-5V	--	--	--	6.7	--	--	--	23
17.5Ti-2.5V	--	0.11	1.4	--	3.4	--	--	--	24
20Ti-5V	--	0.10	0.94	--	2.8	--	--	--	24
22.5Ti-11V	--	--	--	--	9.3	--	21.6	--	25
30.2Ti-7.45V	19Ti-5V	--	--	--	14.2	--	--	--	23
10Ti-4W	--	--	--	--	--	4[d]	--	--	1
17.3Ti-2.4W	9.5Ti-5W	--	--	--	8.4	--	--	--	23
20Ti-10W	--	0.11	1.8	--	2.8	--	--	--	24
23Ti-10W	--	--	--	--	--	9.6[d]	--	--	1
27Ti-5W	--	--	--	--	--	24[d]	--	--	1
31.9Ti-2.2W	19Ti-5W	--	--	--	12.0	--	--	--	23
16.85Ti-4.67Zr	9.5Ti-5Zr	--	--	--	25.7	--	--	--	23
28.9Ti-4Zr	19Ti-5Zr	--	--	--	10.9	--	--	--	23

Table 1.V. (Continued).

Alloy Composition[a], Balance Columbium		Oxidation Rate, mg/cm²/hr							
At. %	Wt %	600 C (1110 F)	800 C (1470 F)	900 C (1650 F)	1000 C (1830 F)	1090 C (2000 F)	1200 C (2190 F)	1260 C (2300 F)	Reference
Columbium-Chromium-Base Alloys									
18.2Cr[c]	--	0.5	5.1	--	6.1	--	--	--	24
19.7Cr-0.5Al[c]	--	0.61	1.4	--	10.8	--	--	--	24
12.4Cr-35.8Al	10Cr-15Al	--	--	--	0.05	--	--	--	30
16.7Cr-42.9Al	15Cr-20Al	--	--	--	0.03	--	--	--	30
39.5Cr-12.7Al	30Cr-5Al	--	--	--	0.15	--	0.26	--	30
23.5Cr-36.1Al-0.9Ce	20Cr-15Al-2Ce	--	--	--	0.05	--	0.14	--	30
22.3Cr-4.17Al-11.7Co	15Cr-2Al-9Co	--	--	--	--	3.9[d]	--	--	1
23Cr-23.3Al-15.7Co	19Cr-10Al-15Co	--	--	--	0.01	--	0.06	--	30
36.7Cr-12.9Al-2.4Ni	26Cr-5Al-2Ni	--	--	--	0.05	--	0.16	--	30
12.9Cr-24.9Al-16.9Ni-1.5W-0.9Ce	10Cr-10Al-15Ni-4W-2Ce	--	--	--	0.02	--	0.05	--	30
4.6Cr-17.2Al-4.7V	3Cr-8Al-3V	--	--	--	--	(1-0.1)[m]	--	--	31
14Cr-15.7Al-14.3V	10Cr-8Al-10V	--	--	--	--	(1-0.1)[m]	--	--	31
21.8Cr-6.4Al-5.9V	15Cr-3Al-4V	--	--	--	--	(0.1)[m]	--	--	31
28.5Cr-4Al-11.7V	20Cr-2Al-8V	--	--	--	--	(1-0.1)[m]	--	--	31
14.7Cr-8.5Al-4.5V-6.9Fe	10Cr-3Al-3V-5Fe	--	--	--	--	(1-0.1)[m]	--	--	31
21.2Cr-11.9Al-8.7V-2.64Fe-0.8W	15Cr-6Al-6V-2Fe-2W	--	--	--	--	(1-0.1)[m]	--	--	31
16Cr-9.2Al-4.9V-4.6W	10Cr-3Al-3V-10W	--	--	--	--	(1-0.1)[m]	--	--	31
23.4Cr-9Al-7.9V-2.2W-1.5Fe	15Cr-6Al-5V-5W-1Fe	--	--	--	--	(0.1)[m]	--	--	31
23.5Cr-13.2Al-10.1Ta-8V	15Cr-6Al-22.5Ta-5V	--	--	--	--	(0.1)[m]	--	--	31
23.8Cr-13.4Al-10.3Ta-8.12V-2.3W-1.5Fe	15Cr-6Al-22.5Ta-5V-5W-1Fe	--	--	--	--	(0.1)[m]	--	--	31
13.7Cr-26.4Al-1.5W	10Cr-10Al-4W	--	--	--	0.05	--	0.17	--	30
2Cr-6Co	--	--	--	--	--	>44[d]	--	--	1
3Cr-2Co	--	--	--	--	--	>44[d]	--	--	1
5Cr-17Co	--	--	--	--	--	11.0[d]	--	--	1
9Cr-6Co	--	--	--	--	--	5.1[d]	--	--	1
10Cr-25Co	--	--	--	--	--	1.1[e]	--	--	1
12Cr-8Co	--	--	--	--	--	2.5[d]	--	--	1
15Cr-9Co	--	--	--	--	--	2.5[d]	--	--	1
15Cr-25Co	--	--	--	--	--	4.5[d]	--	--	1
20Cr-12Co	--	--	--	--	--	2.5[d]	--	--	1
15Cr-10Co-10Mo	--	--	--	--	--	38[d]	--	--	1
15Cr-10Co-5Mo-5W	--	--	--	--	--	16[d]	--	--	1
15Cr-9Co-2Si	--	--	--	--	--	5.2[d]	--	--	1
15Cr-9Co-10W	--	--	--	--	--	3.9[d]	--	--	1
2Cr-6Ni	--	--	--	--	--	>44[d]	--	--	1
3Cr-2Ni	--	--	--	--	--	>44[d]	--	--	1
5Cr-17Ni	--	--	--	--	--	8.3[d]	--	--	1
7.8Cr-0.04Ni[c]	--	1.5	35.8	--	23.0	--	--	--	24
10Cr-25Ni	--	--	--	--	--	3.2[d]	--	--	1
15Cr-9Ni	--	--	--	--	--	5.7[d]	--	--	1
20Cr-12Ni	--	--	--	--	--	3.2[d]	--	--	1
18.4Cr-0.8Si[c]	--	0.72	9.3	--	23.6	--	--	--	24
8.0Cr-12.6Ta[c]	--	0.86	6.6	--	36.0	--	--	--	24
8.9Cr-5.3W[c]	--	0.12	8.4	--	10.2	--	--	--	24
20Cr-10W	--	--	--	--	--	>44[d]	--	--	1
Columbium-Molybdenum-Base Alloys									
5Mo	--	0.3	2.1	--	5.0	--	--	--	24
5Mo-1Al	--	0.19	1.9	--	3.6	--	--	--	24
8.0Mo-24.2Al	10Mo-10Al	--	--	--	0.02	--	--	--	24
14.1Mo-41.9Al	20Mo-20Al	--	--	--	0.08	--	0.62	--	32
10.7Mo-38.1Al-1Ce	15Mo-15Al-2Ce	--	--	--	0.05	--	0.45	--	32
7.4Mo-22Al-20.6Cr	10Mo-10Al-15Cr	--	--	--	0.24	--	0.95	--	32
14.5Mo-38.6Al-1.9W	20Mo-15Al-5W	--	--	--	0.40	--	--	--	32
10.4Mo-34.5Al-7.3Zr-1.45W-6.14B	15Mo-14Al-10Zr-4W-1B	--	--	--	0.12	--	0.32	--	32
2.1Mo-2.5Cr[c]	--	0.18	2.4	--	4.1	--	--	--	32
4.2Mo-1.5Cr[c]	--	0.16	1.8	--	4.6	--	--	--	24
6.2Mo-2.3Cr[c]	--	0.13	1.7	--	6.5	--	--	--	24
4.7Mo-10.6Cr[c]	--	0.10	4.1	--	1.7	--	--	--	24
7.5Mo-10.5Cr[c]	--	--	--	--	2.4	--	9.6	--	24
5Mo-5Ni	--	0.45	3.2	--	7.2	--	--	--	25
5Mo-1Si	--	0.09	9.8	--	15.4	--	--	--	24
5Mo-12.5Ta	--	0.10	7.6	--	4.4	--	--	--	24
15Mo-15W	--	--	--	--	--	>44[d]	--	--	24
Columbium-Vanadium-Base Alloys									1
10V	--	0.1	0.7	--	3.4	--	1.8	--	25
5V-9.4Al	3V-3Al	--	0.3[f]	--	1.2[f]	--	3[f]	--	33
2V-0.4Cr[c]	--	0.43	8.7	--	15.4	--	--	--	24
2.1V-1.7Cr[c]	--	0.1[e]	7.7	--	7.5	--	--	--	24
3.8V-0.4Cr[c]	--	0.12	3.6	--	8.7	--	--	--	24
3.8V-0.7Cr[c]	--	0.22	2.8	--	8.2	--	--	--	24
4.8V-14.2Cr[c]	--	0.05	0.56	--	5.8	--	--	--	24

Table 1.V. (Continued).

Alloy Composition[a], Balance Columbium		Oxidation Rate, mg/cm²/hr							
At. %	Wt %	600 C (1110 F)	800 C (1470 F)	900 C (1650 F)	1000 C (1830 F)	1090 C (2000 F)	1200 C (2190 F)	1260 C (2300 F)	Reference
12V-26Co	--	--	--	--	--	>44[d]	--	--	1
27V-12Co	--	--	--	--	--	>44[d]	--	--	1
2.5V-2.5Mo	--	0.21	1.5	--	4.1	--	--	--	24
2.5V-5Mo	--	0.15	2.4	--	4.1	--	--	--	24
5V-2.5Mo	--	0.19	1.6	--	4.3	--	--	--	24
5V-5Mo	--	0.12	2.8	--	3.2	--	--	--	24
8V-5.5Mo	--	--	--	--	2.8	--	13.3	--	25
8V-18Ni	--	--	--	--	--	>44[d]	--	--	1
10V-5Ni	--	0.15	1.1	--	4.1	--	--	--	24
12V-26Ni	--	--	--	--	--	>44[d]	--	--	1
27V-12Ni	--	--	--	--	--	>44[d]	--	--	1
5V-5Ta	--	0.09	7.3	--	16.2	--	--	--	24
5V-5W	--	0.36	9.8	--	36.3	--	--	--	24
Columbium-Tungsten-Base Alloys									
10W	--	2.9	17.0	--	21.2	--	17.5	--	25
20W-2Al	--	--	--	--	--	38[d]	--	--	1
5W-5Mo	--	0.13	13.4	--	22.0	--	--	--	24
8.2W-5.2Mo-1Zr	15W-5Mo-1Zr	--	--	--	--	9[g]	--	30[g]	34
7.4W-4.7Mo-1Zr-0.6Ti	15W-5Mo-1Zr-0.5Ti	--	--	--	--	4[g]	--	19[g]	34
20W-2Si	--	--	--	--	--	62[d]	--	--	1
20W-7Si	--	--	--	--	--	6.5[d]	--	--	1
Columbium-Zirconium-Base Alloys									
35Zr	--	0.2	2.2	--	15.6	--	35.5	--	25
12.1Zr-8.8Cr[c]	--	3.2	5.9	--	37.0	--	--	--	24
43Zr-10Ti	--	--	--	--	2.0	--	--	--	26
50Zr-5Ti	--	--	--	1.4	2.1	2.9[h]	--	--	26
20Zr-5V	--	0.68	7.8	--	20.1	--	--	--	24
Columbium-Iron-Base Alloys									
10.9Fe-43Al	10Fe-19Al	--	--	--	0.03	--	0.09	--	35
25Fe-23Al	20Fe-9Al	--	--	--	0.08	--	0.20	--	35
24Fe-42Al	24Fe-20Al	--	--	--	0.04	--	0.08	--	35
12.2Fe-15.1Al-12.6B	10Fe-6Al-2B	--	--	--	0.09	--	0.34	--	35
22.2Fe-36.5Al-5.2Mo	20Fe-15Al-5Mo	--	--	--	0.08	--	--	--	35
11.15Fe-32.3Al-2.6Mo-15.9Co-0.4Ce	10Fe-14Al-4Mo-15Co-1Ce	--	--	--	0.01	--	0.05	--	35
6.2Fe-25.8Al-11.9Ni	5Fe-10Al-10Ni	--	--	--	0.09	--	0.15	--	35
10.3Fe-23.7Al-27.3Ni	9Fe-10Al-25Ni	--	--	--	0.01	--	0.04	--	35
8Fe-16Co	--	--	--	--	--	20[d]	--	--	1
12Fe-27Co	--	--	--	--	--	3.6[d]	--	--	1
25Fe-12Co	--	--	--	--	--	2.1[d]	--	--	1
25Fe-12Ni	--	--	--	--	--	4.1[d]	--	--	1
Miscellaneous Columbium-Base Alloys[k]									
12.0Al-0.3Ce	3.8Al-0.36Ce[j]	--	--	--	E	--	G	--	36
12.2Al-1.1Ca	3.9Al-0.5Ca[j]	--	--	--	E	--	E	--	36
7.0Cr-1.7Ca	4.1Cr-0.76Ca[j]	--	--	--	E	--	G	--	36
11.3Si-0.3La	3.7Si-0.47La[j]	--	--	--	E	--	G	--	36
3.4Zr-0.7Sn	3.4Zr-0.8Sn[j]	--	--	--	E	--	F	--	36
4.1Zr-0.3Th	4.0Zr-0.6Th[j]	--	--	--	E	--	G	--	36

(a) Compositions given are nominal except where otherwise indicated. Where both at. % and wt % compositions are given, original composition was reported in wt %.
(b) Rates converted from percentage weight gains in original reference.
(c) Estimated composition based on weight loss during melting.
(d) Rates converted from 16-hour metal loss data in original reference.
(e) Rate converted from 200-hour metal loss data in original reference.
(f) Rates based on percentage weight gains after 100-hour exposure in pure oxygen as compared to unalloyed columbium.
(g) Rate estimated from 10-hour metal loss data in original reference.
(h) Oxidation temperature was 1100 C (2010 F) rather than 1090 C (2000 F).
(j) Analyzed composition.
(k) Rates are qualitative. E = excellent, G = good, F = fair.
(l) Rate at 1000 C estimated on basis of 900 C data.
(m) Rates are estimated order of magnitude.

Table I.VI. Metal loss and contamination behaviour. (Wlodek (37)).

Temperature °C	Temperature °F	Time, hr	65Cb-7Ti-28W, mil/side Metal loss	65Cb-7Ti-28W, mil/side Depth cont	67Cb-10Ti-20W-3V, mil/side Metal loss[b]	67Cb-10Ti-20W-3V, mil/side Depth cont[b]	65Cb-10Ti-20W-3V-2Zr, mil/side Metal loss[b]	65Cb-10Ti-20W-3V-2Zr, mil/side Depth cont[b]	70Cb-7Ti-20W-3Mo, mil/side Metal loss[b]	70Cb-7Ti-20W-3Mo, mil/side Depth cont[b]	69Cb-7Ti-20W-3Mo-1Zr, mil/side Metal loss[b]	69Cb-7Ti-20W-3Mo-1Zr, mil/side Depth cont[b]
1093	2000	5.0	—	—	1.0	4.1	None[c]	6.0	—	—	—	—
		24.0	—	—	5.0	7.0	3.5	13.5	1.0	16.0	None[c]	13.0
1204	2200	5.0	1.0	11.0	1.5	4.0	1.0	4.7	—	—	—	—
		24.0	3.5	28.0	6.0	6.5	4.5	12.0	3.0	23.0	2.5	20.0
1288	2400	5.0	—	—	1.0	2.5	—	—	—	—	—	—
		24.0	—	—	14.0	9.7	—	—	—	—	—	—
1310	2400	5.0	4.5	19.5	*L*	*L*	*L*	*L*	2.0	15.0	—	—
		24.0	22.0	—	*L*	*L*	*L*	*L*	12.5	28.0	14.0	25.0
1427	2600	2.0	1.0	2.5	*L*	*L*	*L*	*L*	*L*	*L*	*L*	*L*
		5.0	4.5	8.0	*L*	*L*	*L*	*L*	*L*	*L*	*L*	*L*

[a] For unalloyed columbium the rate of metal loss at 2000, 2200, 2400, and 2600°F is about 4.5, 11.0, 30.0, and 11.5 mils/hour.
[b] Here, *L* indicates liquid oxidation products.
[c] A slight expansion, probably due to the solution of oxygen in the contaminated zone was actually measured.

Table I.VII. Identification of oxide phases. (Wlodek (37)).

Nominal and analyzed alloy composition, wt-% Cb	Ti	W	Other	Test temp, °C	100 hr wt gain, mg cm^{-2}	Phases identified[a] Inner oxide[b]	Outer oxide[b]	Alloying elements in outer oxide, wt-% Cb	Ti	W	Other
85.0	10.0	5.0	—	800	Spalling	x	x + Cb_2O_5, TiO_2				
	10.02	5.65	—	1000	338	x	Cb_2O_5, TiO_2	58.2	6.7	3.9	
				1200	1120	x + Cb_2O_5, TiO_2	CbO_2 + Cb_2O_5, TiO_2	58.5	6.9	3.9	
								58.5	6.9	3.7	
70.0	10.b	20.0	—	800	Spalling	x + Cb	x + Cb	—	—	—	
	9.7	19.7	—	1000	122	x	x	48.2	6.9	14.6	
				1200	456	x + Cb_2O_5, TiO_2	Cb_2O_5, TiO_2	47.9	6.8	14.8	
65.0	7.0	28.0	—	800	Spalling	x + Cb	x + Cb	—	—	—	
	7.0	27.9	—	1000	118	x + CbO_2	CbO + CbO_2	50.3	3.4	17.1	
				1200	208	x	x + CbO(?)	52.4	3.2	15.2	
60.0	20.0	20.0	—	800	12.3	x +	x +	—	—	—	
	20.3	21.7	—	1000	204	x + Cb_2O_5, TiO_2	Cb_2O_5, TiO_2	41.2	14.2	14.0	
				1200	1860	Cb_2O_5, TiO_2	Cb_2O_5, TiO_2	41.0	14.4	14.0	
67.0	10.0	20.0	3.0 Mo	800	43.9	x	x	—	—	—	
	10.7	20.8	2.97 Mo	1000	107	x	x	—	—	—	
				1200	249	CbO	x	47.2	7.2	14.2	1.7 Mo
67.0	10.0	20.0	3.0 V	800	20.9	x	x	—	—		
	9.2	21.6	2.9 V	1000	185	x + CbO + CbO_2(?)	x	46.1	6.5	15.2	2.5 V
				1200	376	x + CbO(?)	x	45.9	6.4	15.2	1.8 V
62.0	10.0	20.0	3.0 V, 3.0 Fe, 2.0 Ni	800	15.8	x[1]	x[1]	—	—	—	
	9.8	20.3	2.9 V, 1.6 Fe, 0.9 Ni	1000	47.5	x[1]	x[1]	—	—	—	
				1200	221	CbO	Cb_2O_5 + x	43.2	7.5	11.4	2.0 V, 2.0 Fe, 0.56 Ni.

[a] Order signifies abundance.
[b] Here, x is the compound of the variable composition that ranges at least from $2Cb_2O_5 \cdot TiO_2 \cdot WO_3$ to $Cb_2O_5 \cdot TiO_2 \cdot 2WO_3$, generally referred to as $Cb_2O_5 \cdot TiO_2 \cdot WO_3$. x^1 is similar to x but not identical. All are isomorphous with $Cb_2O_5 \cdot WO_3$.

Table I.VIII. Oxidation kinetics of Cb-Ti-W alloys. (Wlodek (37)).

Cb	Ti	W	Other	Test temp, °C	100 hr wt gain mg cm^{-2}	Predominant kinetic relationships	Rate constants[a] K_L = mg^2/cm^4 sec K_p = mg^2/cm^4/sec	
85	10	5		800	S	Spalling	—	
				1000	338	P(t < 4.0 hr) P(t > 4.0 hr)	K_{p_2} = 2.96 × 10^{-9}	K_{p_1} = 1.64 × 10^{-8}
				1200	1120	P(t < 3.0 hr)	K_p = 1.15 × 10^{-8}	K_L = 2.88 × 10^{-8}
70	10	20		800	S	Spalling	—	
				1000	122	P	K_p = 1.51 × 10^{-9}	
				1200	456	P	K_p = 1.16 × 10^{-8}	
65	7	28		800	S	Spalling	—	
				1000	118	P	K_p = 1.08 × 10^{-9}	
				1200	208	P	K_p = 9.94 × 10^{-9}	
60	20	20		800	12.3	P	K_p = 2.70 × 10^{-9}	
				1000	204	P	K_p = 1.96 × 10^{-8}	
				1200	1860	L	K_L = 5.10 × 10^{-8}	
67	10	20	3 Mo	800	43.9	P	K_p = 1.98 × 10^{-9}	
				1000	107	P	K_p = 1.49 × 10^{-9}	
				1200	249	P	K_p = 7.75 × 10^{-9}	
67	10	20	3 V	800	20.9	P	K_p = 8.80 × 10^{-9}	
				1000	185	P(t < 5.0 hr) L(t > 5.0 hr)	K_p = 8.65 × 10^{-9}	K_L = 4.95 × 10^{-8}
				1200	376	P(t < 3.0 hr) L(t > 3.0 hr)	K_p = 6.65 × 10^{-9}	K_L = 1.00 × 10^{-8}
62	10	20	3 V, 3 Fe, 2 Ni	800	15.8	P	K_p = 6.75 × 10^{-9}	
				1000	47.5	P	K_p = 3.98 × 10^{-9}	
				1200	221	P	K_p = 6.60 × 10^{-9}	

[a] Flowing oxygen (23.4 L/hr)
[b] Linear (L) – W/A = $K_L t$; parabolic (P) – (W/A)^2 = $K_p t$

Table 1.IX. Structure and composition of oxide phases on Cb-Al-V alloys. (Wlodek [38]).

Nominal and analyzed alloy composition, wt-%					Test temp., °C	100 hr wt gain, mg cm²	Phases identified[a]		Alloying elements in outer oxide,[b] wt %			
Cb	Al	V	Ti	Other			Inner oxide	Outer oxide	Al	V	Ti	Other
98.0	1.0	1.0	—	—	800	12.8	$CbO + Cb_2O_5$	Cb_2O_5	<1.0	0.8	—	—
—	0.88	0.89	—	—	1000	33.0	CbO	$CbO + CbO_2$	<1.0	0.9	—	—
					1200	512.0	$Cb_2O_5 + CbO$	Cb_2O_5	<1.0	0.9	—	—
95.5	2.0	2.50	—	—	800	47.8	CbO	$CbO + Cb_2O_5$	<2.0	2.1	—	—
—	2.02	2.50	—	—	1000	180	CbO	$CbO + Cb_2O_5$	<2.0	2.2	—	—
					1200	904	$CbO + CbO_2$	Cb_2O_5	1.44	2.2	—	—
94.0	3.0	3.0	—	—	800	47.8	CbO	$CbO + Cb_2O_5$	2.04	1.66	—	—
—	3.1	2.2	—	—	1000	139	CbO	$CbO + Cb_2O_5$	2.16	1.75	—	—
					1200	675	CbO	$Cb_2O_5 + CbO$	2.03	1.72	—	—
93.0	3.0	4.0	—	—	800	27.9	CbO	$CbO + Cb_2O_5$	3.0	3.4	—	—
—	3.0	4.3	—	—	1000	104	$CbO + CbO_2$	$CbO + CbO + Cb_2O_5$	2.9	2.9	—	—
					1200	738	CbO	$Cb_2O_5 + CbO + CbO_2$	2.1	2.8	—	—
84.0	3.0	3.0	10.0	—	800	30.3	CbO	Cb_2O_5, TiO	*	*	*	—
—	2.7	2.9	10.0	—	1000	154	$CbO + CbO_2$	Cb_2O_5, TiO	<2.7	5.2	13.2	—
					1200	397	CbO	Cb_2O_5, TiO + $CbO + Cb_2O_5$	2.12	2.6	6.9	—
71.0	3.0	4.0	10.0	12.0 Cr	800	7.6	$CbO + CbO_2$	$CbO + CbO_2$	*	*	*	*
—	2.95	3.9	9.9	11.1 Cr	1000	73.2	$CbO + CbO_2$	$CbO + CbO_2$	*	*	*	*
					1200	573	$CbO + CbO_2 + Cb_2O_5$, TiO	Cb_2O_5, TiO + Cb_2O_5	*	*	*	*

[a] Order signifies abundance. [b] Aluminum by wet analysis, other elements by x-ray fluorescence. * Oxidation products too adherent to allow removal and analysis.

Table 1.X. Kinetics of Oxidation. (Wlodek [38]).

Alloy composition, wt %					Test temp., °C	100-hr wt gain mg cm²	Observable kinetic relationships during first 24 hr	Corresponding[a] rate constant for first 24 hr
Cb	Al	V	Ti	Other				
98.0	1.0	1.0	—	—	800	12.8	P	$K_P = 8.45 \times 10^{-9}$
					1000	33.0	L	$K_L = 9.72 \times 10^{-2}$
					1200	512.0	L	$K_L = 1.08 \times 10^{-1}$
95.5	2.0	2.5	—	—	800	47.8	P	$K_P = 6.25 \times 10^{-9}$
					1000	180	P_1 ($t < 1.5$ hr)	$K_{P_1} = 1.42 \times 10^{-8}$
							P_2 ($t > 1.5$ hr)	$K_{P_2} = 4.62 \times 10^{-9}$
					1200	904	P ($t < 10$ hr)	$K_P = 7.4 \times 10^{-8}$
							L ($t > 10$ hr)	$K_L = 2.5 \times 10^{-4}$
94.0	3.0	3.0	—	—	800	47.8	P	$K_P = 2.05 \times 10^{-8}$
					1000	139	P_1 ($t < 3.0$ hr)	$K_{P_1} = 2.22 \times 10^{-8}$
							P_2 ($t > 4.0$ hr)	$K_{P_2} = 5.00 \times 10^{-9}$
					1200	675	P_1 ($t < 0.5$ hr)	$K_{P_1} = 2.22 \times 10^{-8}$
							P_2 ($t > 0.5$ hr)	$K_{P_2} = 5.00 \times 10^{-9}$
94.0	3.0	4.0	—	—	800	25.9	P	$K_P = 2.3 \times 10^{-8}$
					1000	104	P_1 ($t < 5.0$ hr)	$K_{P_1} = 9.6 \times 10^{-9}$
							P_2 ($t > 5.0$ hr)	$K_{P_2} = 2.54 \times 10^{-9}$
					1200	738	P_1 ($t < 20$ hr + L ($t > 20.0$ hr)	$K_P = 4.22 \times 10^{-1}$
								$K_L = 1.94 \times 10^{-4}$
84.0	3.0	3.0	10.0	—	800	30.3	P_1 ($t < 3.0$ hr)	$K_{P_1} = 1.44 \times 10^{-8}$
							P_2 ($t > 3.0$ hr)	$K_{P_2} = 1.95 \times 10^{-9}$
					1000	154	P	$K_P = 7.15 \times 10^{-9}$
					1200	397	P	$K_P = 2.94 \times 10^{-8}$
71.0	3.0	4.0	10.0	12.0 Cr	800	7.6	P	$K_P = 2.16 \times 10^{-9}$
					1000	73.2	P	$K_P = 5.97 \times 10^{-9}$
					1200	573	P	$K_P = 8.82 \times 10^{-8}$

[a] Flowing pure oxygen, flow rate 22.4 liters/hr. [b] Units: K_L in mg cm⁻² sec⁻¹ and K_P in mg² cm⁻⁴ sec⁻¹. The symbols P_1 and P_2 are used to signify two succeeding parabolic rate laws each effective over the time interval denoted in brackets.

Table 1.XI. (Wlodek [38]).

Alloy composition, %				K_P mg²/cm⁴/sec at:		
Al	V	Ti	Cr	800°C	1000°C	1200°C
2.0	2.5	—	—	6.25×10^{-9}	1.42×10^{-8}	7.40×10^{-8}
3.0	4.0	—	—	2.30×10^{-9}	2.54×10^{-9}	1.22×10^{-8}
3.0	3.0	10.0	—	1.97×10^{-9}	7.15×10^{-9}	2.94×10^{-8}
3.0	4.0	10.0	12.0	2.16×10^{-9}	5.97×10^{-9}	8.82×10^{-8}

Table 1.XII. Nominal composition and oxidation test data for binary niobium alloys. (Miller and Cox[40]).

Alloy No.	Element added	Nominal composition		[illegible]
		Atomic %	Weight %	
13/1	Unalloyed niobium	100	100	98. 95
13/2		—	—	118. 93
13/3		—	—	96. 98. 117
16/9		—	—	94. 91
23/1	Beryllium	1	0·10	73. 78
23/2		5	0·51	89. 100
23/3		20	2·4	114. 92
24/4		40	6·1	16. 81
63/1	Aluminium	1	0·29	63. 74
63/2		5	1·5	96. 105
63/3		20	6·8	92. 92
7/1	Titanium	1	0·52	71. 72
7/2		5	2·6	80. 84
7/3		20	11·4	25. 18
3/1	Zirconium	1	0·98	120. 116
3/2		5	4·9	173. 196
3/3		20	19·7	50. 64
11/1	Silicon	1	0·30	187. 214
11/2		5	1·6	284. 285
11/3		20	7·0	115
17/1	Tantalum	1	1·9	98. 105
17/2		5	9·3	102. 107
17/3		20	34·7	103. 105
19/1	Chromium	1	0·56	60. 73
19/2		5	2·9	74. 69
19/3		20	12·3	47. 56
18/1	Molybdenum	1	1·0	60. 59
18/2		5	5·2	32. 22
18/3		20	20·5	103. 157
21/1	Tungsten	1	2·0	130. 158
21/2		5	9·4	131. 115
21/3		20	33·1	169. 177
12/1	Iron	1	0·6	83. 76
12/2		5	3·1	78. 72
12/3		20	13·1	80. 76
8/1	Cobalt	1	0·64	96. 90
8/2		5	3·2	105. 124
27/1		20	13·7	64. 68
9/1	Nickel	1	0·61	92. 100
9/2		5	3·1	98. 113
9/3		20	13·2	96. 96
20/1	Rare earth	—	1	89. 96
20/2	elements added	—	5	167. 123
20/3	as Mischmetall	—	20	433. 346

Table 1.XIII. Composition and oxidation rates in air at 1,200°C of niobium-tungsten-titanium and niobium-tungsten-vanadium alloys. (Miller and Cox [40]).

Alloy No.	Composition						Oxidation conditions at 1,200°C	Test period hours	Test piece surface area (cm²)	Oxidation rate (mg/cm²/h)		Remarks
	Atomic %			Weight %						Gain	Loss	
	Nb	W	Ti	Nb	W	Ti						
204	60	20	20	54·6	36·0	9·4	Moist air at 4 l/min	3	3·58	10·6	16·2	Scale spalls
								3	4·51	12·1	18·9	
204R	60	20	20	54·6	36·0	9·4		3	3·56	11·4	16·5	
								3	3·74	10·3	15·9	
205	60	25	15	51·2	42·2	6·6	..	3	3·44	> 60	—	Test pieces almost completely consumed
								3	3·37			
206	60	15	25	58·4	29·0	12·6	..	3	3·92	13·3	21·5	Scale spalls
								3	4·09	15·4	22·0	
221	50	25	25	44·5	44·0	11·5	..	3	—	11·6	—	Partly adherent scale
								3	—	13·3	—	
222	70	15	15	65·2	27·6	7·2	..	3	—	24·4	—	Partly adherent scale
	Nb	W	V	Nb	W	V						
230	70	20	10	60·8	34·4	4·8	..	1	2·34	> 250	—	Test piece completely consumed
231	70	10	20	69·4	19·7	10·9	..	1	3·75	> 250	—	Test piece completely consumed
232	60	20	20	54·3	35·8	9·9	..	1	2·67	> 250	—	Test piece completely consumed
233	80	10	10	76·0	18·8	5·2	..	3	3·34	> 150	—	Test pieces almost completely consumed
								3	3·62	> 150	—	

Table 1.XIV. Composition and 3-hour oxidation rates at 1,200°C in air saturated at room temperature of 60 : 20 : 20 atomic % Nb-W-Ti alloy with addition of other elements. (Miller and Cox [40]).

Composition: Atomic % Nb	W	Ti		Weight % Nb	W	Ti		Oxidation rate gain in weight mg/cm²/h	Remarks
60	17.5	17.5	Co 5.0	56.2	32.4	8.4	Co 3.0	7.7	Partly adherent scale
60	17.5	17.5	Si 5.0	57.1	32.9	8.6	Si 1.4	9.0	—
60	17.5	17.5	Al 5.0	57.1	33.0	8.6	Al 1.4	11.0	—
60	17.5	17.5	V 5.0	56.4	32.6	8.5	V 2.6	43.9	—
60	17.5	17.5	Fe 5.0	56.2	32.5	8.5	Fe 2.8	7.5	Partly adherent scale
60	17.5	17.5	Ni 5.0	56.2	32.5	8.4	Ni	8.2	"
60	17.5	17.5	Cr 5.0	56.4	32.5	8.5	Cr 2.6	14.4	—
60	17.5	17.5	Zr 5.0	55.4	31.9	8.4	Zr 4.3	14.7	—
60	17.5	17.5	Mn 5.0	56.4	32.5	8.5	Mn 2.5	12.1	—
60	17.5	17.5	Mg 5.0	57.2	33.0	8.6	Mg 1.25	9.7	—
60	17.5	17.5	Zn 5.0	56.0	32.4	8.4	Zn 3.3	15.5	Scale partly adherent
60	17.5	17.5	Ag 5.0	54.5	31.7	8.2	Ag 5.3	14.4	—
60	17.5	17.5	Be 5.0	57.6	33.2	8.7	Be 0.5	>150	Test pieces almost completely consumed
60	17.5	17.5	B 5.0	57.6	33.2	8.7	B 0.6	10.6	—
60	17.5	17.5	Cd 5.0	56.7	32.7	8.5	Cd 2.2	11.0	—
60	17.5	17.5	Cu 5.0	56.0	32.4	8.4	Cu 3.2	150	Test pieces almost completely consumed
60	17.5	17.5	Mo 5.0	55.1	31.8	8.3	Mo 4.75	10.6	—
60	17.5	17.5	Ta 5.0	52.9	30.6	8.0	Ta 8.6	8.8	—
60	17.5	17.5	Re 5.0	52.8	30.5	7.9	Re 8.8	9.0	—
60	17.5	17.5	Pt 5.0	52.6	7.9	30.4	Pt 9.2	7.6	Scale partly adherent
60	17.5	17.5	C 5.0	52.5	8.6	33.2	C 0.62	13.4	"
60	20	20 + 5 wt % Mischmetall						>250	Test pieces completely consumed
50	16.7	16.7	Co 16.7	48.9	32.3	8.4	Co 10.35	>100	Almost completely consumed
50	16.7	16.7	Fe 16.7	49.2	32.5	8.5	Fe 9.9	20.8	Partly adherent scale
50	16.7	16.7	Ni 16.7	49.1	32.4	8.5	Ni 10.0	26.3	—
50	16.7	16.7	Si 16.7	51.7	34.2	8.9	Si 5.2	21.5	Partly adherent scale

Table 1.XV. Degree of oxidation of ternary niobium alloys. (Smith [42]).

Nominal alloy composition (atomic %)	Time and temperature of exposure: 1 h 1,100°C	5 h 1,100°C	100 h 1,100°C	1,200°C
Pure niobium	45.8			
Nb – 18 Ti	7.7			
– 18 Ti – 3 Mo	22.0			
– 18 Ti – 6 Mo	19.0			
– 18 Ti – 9 Mo	4.2	63.2		
– 18 Ti – 18 Mo	18.0			
– 18 Ti – 9 W	3.3	11.0	244.9*	
– 18 Ti – 18 W	2.0	16.8		27.0 (5 h)
– 25 Ti – 18 W	8.1			
– 18 Ti – 12 W			149.0*	
– 18 Ti – 9 Ta	5.0			
– 18 Ti – 18 Ta	7.4	29.2		
– 18 Ti – 3 V	17.0			
– 18 Ti – 6 V	16.8			
– 18 Ti – 9 V	14.0			
– 18 Ti – 18 V	52.0	c.o.		c.o. (5 h)
– 9 Ti – 6 Cr	10.8			
– 9 Ti – 9 Cr	12.0			
– 9 Ti – 18 Cr	11.0			
– 18 Ti – 6 Cr	5.8			123.0 (25 h)
– 18 Ti – 10 Cr	1.4	7.0		29.9 (5 h)
– 18 Ti – 12 Cr	0.7			47.2 (5 h)
– 18 Ti – 18 Cr	6.0			
– 25 Ti – 9 Cr	2.0		270.2*	c.o. (18 h)
– 9 Ti – 6 Zr	32.0			
– 9 Ti – 9 Zr	22.0	c.o.		
– 18 Ti – 6 Zr				101.8 (5 h)
– 18 Ti – 9 Zr	7.0	31.0		
– 18 Ti – 18 Zr	19.0			
– 18 Ti – 3 Ni	5.5	17.6		
– 18 Ti – 6 Ni	1.8			
– 18 Ti – 9 Ni	8.5	22.5		
– 18 Ti – 3 Fe	6.0			
– 18 Ti – 6 Fe*	0.6, 0.75, 2.3 } Mean 1.22			c.o. (25 h)
– 18 Ti – 9 Fe	8.3, 7.7 } Mean 8.0			
– 18 Ti – 6 Co	9.0			
– 18 Ti – 6 Mn	10.0			

2 g specimens denoted by *

c.o. = complete oxidation

Table 1.XVI. Degree of oxidation of ternary and quaternary alloys. (Smith [42]).

(Total weight gain in mg/cm² on 2 g and 1 g* rectangular specimens)

Nominal alloy composition (atoms %)	Time and temperature of exposure			
	2 h/ 1,100°C	20 h/ 1,100°C	100 h/ 1,100°C	16 h/ 1,180°C
Nb – 18 Ti	13 1		320 (M)	
– 25 Ti – 9 W	4 7			98 9
– 22 Ti – 9 W	3 0			79 3
– 22 Ti – 18 W	12 1			148 7
– 18 Ti – 9 W – 3 Cr	1 4*			
– 18 Ti – 9 W – 6 Cr	1 5*			
– 25 Ti – 9 W – 6 Cr	16 4		321 6(M)	
– 18 Ti – 10 Cr – 2 Ce	16 2		284 9(M)	
– 30 Ti – 12 Cr	22 1			
– 18 Ti – 9 W – 6 Ni	0 8*			
– 18 Ti – 9 W – 3 Ni			161 8(M)	
– 18 Ti – 9 W – 3 V	15 0	c o		
– 18 Ti – 9 W – 6 V	15 3	219 7		
– 18 Ti – 9 W – 3 Ta	11 2	66 6		
– 18 Ti – 9 W – 6 Ta	17 5	113 7		
– 18 Ti – 6 Ce	c o*			
– 18 Ti – 6 Al	6 6*			
– 18 Ti – 6 Si	13 6*			
– 18 Ti – 6 Re	8 0*			
– 18 Ti – 1 B	18 5*			
– 18 Ti – 2 B	21 0			
– 18 Ti – 15 W – 2 Ce	14 6		213 8(M)	
– 33 Ti – 33 Cr	0 6*			20 (20 h)*
– 50 Ti – 10 Zr	23 0*			

1 g specimens denoted by *
(M) = The mean of the original and final surface areas used
c o = complete oxidation

Table 1.XVII. Oxidation rate of some complex niobium alloys. (Smith [42]).

(Weight gain/loss in mg/cm²/h on 1 g spherical specimens)

Nominal alloy composition (atoms %)	Time and temperature of exposure		
	20 h 1,000°C	20 h 1,100°C	20 h 1,140°C
Nb – 20 Ti – 6 W	1 5		
– 20 Ti – 6 W – 1 Zr	2 4		
– 20 Ti – 8 W			2 8
– 20 Ti – 6 W – 3 Cr			3 3
– 20 Ti – 6 W – 3 Co			4 6
– 20 Ti – 6 W – 3 Co – 3 Cr			3 1
– 20 Ti – 10 W		2 0	
– 20 Ti – 10 W – 1 Zr		4 4	
		2 8	
– 20 Ti – 10 W – 4 Ni		1 4	
– 20 Ti – 10 W – 4 Ni – 5 Al		1 7	
– 20 Ti – 10 W – 3 Ni – 3 Cr			11 8
– 20 Ti – 10 W – 3 Ni – 2 Cu		1 6	
– 20 Ti – 10 W – 3 Ni – 2 Mn		1 9	

Spherical 1 g specimens used, and oxidation rate calculated from the mean of original and final surface area

Table 1.XVIII. Oxidation rates for niobium alloys exposed in moist air. (Argent and Phelps [43]).

Alloy at %	Oxidation rate, mg/cm²/h			
	55°C	700°C	800°C	1,050°C
Pure Niobium	3 7	7 4	22.8	38 0
1 Tantalum	5 6	6 1	28 3	14.6
5 Tantalum	5 6	6 1	28 3	14 6
10 Tantalum	3 7	6 7	28.3	25.6
20 Tantalum	5 6	5 6	19 5	36 0
1 Vanadium	3 4	7 0	32.0	9.9
5 Vanadium	1 4	1 0	3 7	7.0
1.7 Chromium	—	13 7	27.4	35.0
5 Molybdenum	—	—	0.9	4.3
1 Tungsten	3 3	—	6.0	17.7
1 Titanium	3 0	—	2.7	37.3
10 Titanium	1.0	0.7	2.1	13.7
20 Titanium	—	1.0	0.8	3.3
46 Titanium	—	—	1.0	9 2
1 Zirconium	—	8.4	33 8	50 0

Table 1.XIX. Oxide characteristics of niobium-titanium alloys. (Argent and Phelps [43]).

Temp °C	1-5 at %	5-10 at %	10-20 at %
400–500	400: Thin black adherent film 450: Cream oxide which spalls on cooling, leaving some oxide on metal surface		
500–700	Oxide goes from powdery cream to coherent yellow with increased Ti and temperature	Oxide goes from powdery cream through grey to a black adherent scale with increased Ti and temperature	Adherent black layer
700–1,100	A yellowish adherent scale changing to a thin grey film overlaying black surface. Above the allotropic change temp a creamy crystalline oxide which spalls cleanly on cooling	Black adherent scale changing to a greyish powdery scale with increasing temp for the low Ti alloys. Above the change point a creamy oxide cleanly spalling on cooling.	Dark grey oxide showing slight spalling at lower temperatures. Above allotropic point a creamy oxide which cleanly spalls on cooling

Table 1.XX. Oxide characteristics of niobium-molybdenum alloys. (Argent and Phelps [43]).

Temp °C	0-1 at %	1-3 at %
400-500	400 Adherent greyish yellow oxide 450 Powdery yellow oxide	400 Adherent yellowish grey 450 Slight formation of powdery yellow oxide
500-700	Yellow powdery oxide becoming more grey and coherent with increased Mo and temperature	A powdery yellow grey oxide changing to a light black adherent oxide at higher temperatures and molybdenum contents
700-900	Black adherent oxide becoming covered by a thin grey film at higher temp. Green oxide above change point	Black adherent oxide. Above change point a grey-cream oxide retained on cooling

Table 1. XXI. X-ray examination of scales. (Argent and Phelps [43]).

Composition	at % Titanium			at % Molybdenum		
Temp °C	1 %	3 %	6 %	1	2 %	3 4
900	βNb_2O_5	βNb_2O_5	βNb_2O_5 + trace cpd	βNb_2O_5	βNb_2O_5	βNb_2O_5
850				αNb_2O_5 + βNb_2O_5		
800				αNb_2O_5	αNb_2O_5 + βNb_2O_5	
750	αNb_2O_5		αNb_2O_5 + cpd	βNb_2O_5		βNb_2O_5
700	αNb_2O_5		αNb_2O_5 + cpd			
680					αNb_2O_5	
650						αNb_2O_5
600	αNb_2O_5	αNb_2O_5	αNb_2O_5 + cpd			
550	αNb_2O_5		αNb_2O_5 + cpd	αNb_2O_5	αNb_2O_5	αNb_2O_5

cpd = $TiO_2 \cdot 3\ Nb_2O_5$

Table 1-XXII. Oxidation rates of binary Nb alloys. (Wlodek et al[45]).

Alloy addition, at %.	Oxidation rate, mg/cm²/hr. 800	1000	1200°C.
1.0 Al	44.1	-	-
5.0 Al	39.9	-	-
12.5 Al	5.9	-	-
18.0 Al	1.9	-	-
75.0 Al	2.05	-	-
8.6 Cr	11.2	5.0	28.2
10.0 Cr	18.1	-	-
16.6 Cr	5.0	1.21	30.0
24.0 Cr	0.25	0.74	11.2
31.0 Cr	0.20	0.23	5.1
37.3 Cr	0.07	-	6.2
44.4 Cr	0.05	0.12	0.16
66.7 Cr	0.30	-	-
1.6 Co	53.4	-	-
7.6 Co	26.5	-	-
14.9 Co	22.6	-	-
2.9 Cu	35.5	-	-
7.7 Fe	34.4	36.9	-
15.6 Fe	-	39.7	46.5
35.0 Fe	0.12	1.71	3.23

Table 1-XXII. (Continued).

Alloy addition at %.	Oxidation rate, mg/cm²/hr. 800	1000	1200
5.0 Mn	-	53.11	-
1.6 Ni	58.6	-	-
7.8 Ni	22.0	-	-
15.2 Ni	11.7	-	-
28.8 Ni	2.8	-	-
1.6 Si	>156	-	-
10.0 Si	396	-	-
2.5 Ta	74.5	88	78.4
5.4 Ta	88.4	79	65.3
11.4 Ta	90.6	103	48.2
18.0 Ta	66.8	5	23.4
33.8 Ta	-	12.9	exothermic
53.0 Ta	21.6	18.8	-
10.0 Ti	4.8	-	-
17.6 Ti	0.67	2.91	22.6
25.5 Ti	0.31	2.23	33.9
37.7 Ti	0.42	3.03	22.6
40.0 Ti	0.21	-	28.5
44.1 Ti	0.28	5.68	23.8
51.0 Ti	0.24	6.35	26.1
61.3 Ti	0.18	5.03	22.9
66.0 Ti	0.30	-	22.6
20 W	5	-	-
0.4 Th	104	-	-
10.0 Th	0.43	-	-
12.1 V	10.8	-	-
24.8 V	33.8	-	-
5.7 Zr	44.5	-	-
10.3 Zr	46	-	-
20.3 Zr	5	15.4	-
50.5Zr	5	3.9	15.3

Weight %	800°C	1000°C	1200°C
2Al-3Si	6.88		
5Al-3Si	13.80		
10Al-3Si	7.21		
10Al-5Si	0.810		
9Co-5Al	17.30	20.50	12.50
9Ni-3Al	41.40	*	42.10
9Ni-5Al	29.10	25.90	35.90
10Ta-5W	26.90	34.20	19.90
10Ta-10W	17.00	27.90	9.83
10Ta-15W	*	*	6.03
10Ta-25W	*	*	4.45
20Ta-5W	28.00	30.50	18.30
20Ta-10W	*	7.68*	4.75
20Ta-15W	*	*	5.12
25Ta-10W		1.78	
40Ta-10W		Melted	
20Ta-7Zr			Melted
30Ta-7Zr	*	6.33	Melted
40Ta-7Zr	*	5.70	Rapid
40Ta-2Zr		Exotherme	
40Ta-1Zr		Exotherme	
40Ta-10Zr		Exotherme	

* Scaled

Table 1.XXIII. Oxidation rate ($mg/cm^2/hr$) of columbium-aluminium base, columbium-cobalt base, columbium-nickel base, and columbium-tantalum base alloys. (Wlodek et al (45)).

Table 1.XXIV. Oxidation rate ($mg/cm^2/hr$) of columbium-chromium base alloys. (Wlodek et al [45]).

Atomic %	600°C	800°C	1000°C	1000°C	1200°C
6Cr-5Al		0.398	1.26		
9Cr-3Al		2.77	2.25		13.50
9Cr-4Al		2.51	2.38		13.10
9Cr-5Al		0.199	1.55		15.50
12Cr-2Al		1.23	2.49		15.10
12Cr-3Al		0.236	1.13		18.20
12Cr-4Al		0.731	1.08		13.70
12Cr-5Al		0.121	1.27		
30Cr-10W			0.153		
30Cr-15W			0.588		
30Cr-20W			0.544		
30Cr-25W			0.525		
30Cr-30W			0.652		

Table 1. XXVI. Oxidation rates of columbium alloys. (Babitzke et al [46]).

Alloy composition, atomic percent	Weight gain per hour, milligrams per square centimeter		
	600° C.	800° C.	1,000° C.
100 Cb	9	22	-
100 Cb[1]	5.7	33.7	24.2
99 Cb-1 V	7	14	-
99 Cb-1 V[1]	3.6	6.3	13.8
98 Cb-2 V	1.0	12	-
95 Cb-5 V	.3	7	7
95 Cb-5 V[1]	.9	1.4	4.6
90 Cb-10 V	.3	1.9	4.2
90 Cb-10 V[1]	.1	.7	3.5
75 Cb-25 V	.7	11	-
75 Cb-25 V[1]	.2	6.1	19.3
50 Cb-50 V	.8	34	-
75 V-25 Cb	.9	46	-
90 V-10 Cb	.4	-	-
95 V- 5 Cb	.3	-	-
98 V- 2 Cb	.3	-	-
99 V- 1 Cb	.4	-	-
100 V	1.1	-	-
Zirconium	.4	1.0	15.4
Zircaloy-2	.3	1.1	28.6

[1]Value reported by Sims, Klopp, and Jaffee (22).

Table XXV. Oxidation rate ($mg/cm^2/hr$) of Nb-Ti base alloys. (Wlodek et al (45)).

Composition	600°C	800°C	900°C	1000°C	1100°C	1200°C
Weight %						
10Ti-4Al		0.512		1.14		9.42
15Ti-3Al		0.411		1.22		13.50
15Ti-5Al		0.606		1.40		8.9
20Ti-10Al		0.280		0.602		3.82
25Ti-5Al		0.245		1.12		10.80
20Ti-5Cr		0.280				28.50
20Ti-10Cr		0.368		0.862		15.80
20Ti-20Cr		0.182		0.477 *		6.82
30Ti-10Cr		0.108		0.751		12.70 *
10Ti-30Cr		0.073		0.251		0.861
10Ti-40Cr		0.062		0.031		0.061
15Ti-10Cr		0.18 *		1.815		20.30
20Ti-5Cr		0.262		1.900		27.40
20Ti-10Cr		0.195		2.58		16.61
20Ti-15Cr				1.28		
20Ti-20Cr		0.226		0.551		1.74 *
20Ti-30Cr				0.581		
30Ti-10Cr		0.179		1.33		7.94
30Ti-20Cr				4.45		
40Ti-10Cr		*		0.262		5.65
10Ti-5Fe		0.214		2.74		27.30
20Ti-5Fe		0.964				
21Ti-5.5Fe		0.160		6.06		19.00
15Ti-10Fe		0.365		2.18		
20Ti-10Fe		0.234		2.03		35.60
25Ti-10Fe		0.162		1.74		28.50
30Ti-10Fe		0.179		2.12 *		
40Ti-10Fe		0.189		1.70		10.30
12.8Ti-16.5Fe		0.178		1.25		16.70
18Ti-16.5Fe		0.144		0.856		21.30
23.5Ti-16.5Fe		0.070				
10Ti-20Fe		0.129		0.447		4.64
20Ti-20Fe		0.063		0.412		
12.8Ti-25Fe		0.13		0.352		3.15
20Ti-5Ni		0.197		0.725		3.85
10Ti-10Ni		10.60		16.60 *		45.00
20Ti-10Ni		1.51		0.903 *		16.70
30Ti-10Ni		0.45		1.31		14.00
10Ti-20Ni		1.94		25.10		43.20
20Ti-20Ni		0.21		0.889		25.30
10Ti-2.5Si				32.60		
20Ti-2.5Si		0.207		5.39		10.20
10Ti-5Si				38.60		
20Ti-5Si				7.04		
30Ti-5Si		0.272		3.12		7.48
20Ti-10Si				2.55		
10Ti-10Ta		1.07		2.53		12.60
25Ti-10Ta		0.401		2.21		21.50
40Ti-10Ta		0.252				23.70
10Ti-25Ta		0.496		1.25		6.15
25Ti-25Ta		0.736		3.58		17.70
40Ti-40Ta		1.97 *		1.28		10.60 *
20Ti-5V		0.243		2.69		8.21
30Ti-5V		0.209		2.68		9.78
10Ti-10V		0.782		53.30		Exothermic
20Ti-10V		0.758		42.40		48.56
30Ti-10V		0.327		38.00		41.40
40Ti-10V		3.871		21.54		4.74 *
20Ti-20V		64.60 *		Very rapid		Very rapid
5Ti-3W		*		27.60		34.00
5Ti-5W				22.70		26.10
10Ti-5W		*		3.38		11.20
15Ti-5W		0.769		1.51		12.20
20Ti-5W		0.237		2.73		23.20
30Ti-5W		0.221		2.53		25.60
5Ti-10W		*		24.60		25.40
5Ti-20W		0.259		5.46		21.70
20Ti-20W		0.123				18.60
10Ti-10Zr		1.74		7.86		24.70
20Ti-10Zr				2.68		
30Ti-10Zr		1.18 *		3.18		27.00
10Ti-20Zr		*		3.48		15.20
20Ti-20Zr		*		2.84		11.70
10Ti-30Zr		*		1.49		4.34

* Spalled

Table 1.XXVII. Oxidation rates for Nb-V alloys. (Babitzke et al [48]).

Alloy Composition at %.	weight gain per hour, mg/cm^2* 600°C.	800°C.	1000°C.
100 Nb	10.1	18.1	-
Nb-5V	0.3	7	7
Nb-8V	undetectable	3.1	5.0
Nb-10V	0.3	1.9	4.2
Nb-12V	undetectable	1.7	4.1
Nb-15V	0.1	2.2	5.5
Nb-20V	0.2	5.0	53.9

* average taken over a 3 hr. period.

Table 1.XXVIII. Oxidation rates of columbium-10 wt % titanium with oxides, borides, or carbides. (Babitzke et al[48]).

Cb-10 wt pct Ti plus impurity in mole-percent	Weight gain per hour, mg/cm^2 † 800° C	1,000° C
0	1.3	4.9
0.1 ZrO_2	1.4	4.8
0.5 ZrO_2	1.3	4.9
2.0 ZrO_2	1.5	4.8
5.0 ZrO_2	1.9	6.2
0.1 TiO_2	1.6	5.1
0.5 TiO_2	1.2	5.6
1.0 TiO_2	1.4	6.6
0.1 ZrB_2	1.5	6.1
0.5 ZrB_2	1.6	6.5
1.0 ZrB_2	1.8	6.0
2.0 ZrB_2	1.1	7.0
0.1 TiB_2	1.5	4.8
0.5 TiB_2	1.4	5.1
1.0 TiB_2	1.8	5.4
2.0 TiB_2	1.5	7.9
0.1 ZrC	1.3	4.3
0.5 ZrC	1.3	4.0
1.0 ZrC	1.4	5.0
2.0 ZrC	1.6	6.0
0.1 TiC	1.5	5.3
0.5 TiC	1.3	4.4
1.0 TiC	1.4	4.4
2.0 TiC	1.4	5.0

†Average was taken on a 4-hour testing period.

Table 1.XXIX. Oxidation results of columbium and tantalum alloys. (Babitzke et al [48]).

Alloy composition, atomic percent	Average weight loss, mg/cm²/hr		Alloy composition, atomic percent	Average weight loss, mg/cm²/hr	
	At 800° C	At 1,000° C		At 800° C	At 1,000° C
100 Cb.....	52	85	Cb-5V-10W-2Ti.....	3	14
Cb-5Hf-5W.....	76	236	Cb-5V-10W-10Ti....	8	22
Cb-5Hf-10W.....	-	156	Cb-5V-10W-2Zr.....	9	78
Cb-5Hf-15W.....	-	185	Cb-5V-10W-5Ti-5Zr.	14	44
Cb-10Hf-5W.....	-	196			
Cb-10Hf-10W.....	21	178	Cb-10V-5W-2Ti.....	2	28
Cb-10Hf-15W.....	-	161	Cb-10V-5W-5Ti.....	4	19
Cb-15Hf-5W.....	-		Cb-10V-5W-10Ti....	4	10
Cb-15Hf-10W.....	-	1[illegible]	Cb-10V-5W-2Zr.....	34	50
Cb-15Hf-15W.....	-	128	Cb-10V-5W-5Zr.....	19	99
			Cb-10V-5W-5Ti-5Zr.	-	45
Cb-15Hf-5W-2Ti....	3	13			
Cb-15Hf-5W-5Ti....	2	11	Cb-10V-10W-2Ti....	-	17
Cb-15Hf-5W-10Ti...	4	7	Cb-10V-10W-5Ti....	-	24
Cb-15Hf-5W-2Zr....	4	30	Cb-10V-10W-2Zr....	8	53
Cb-15Hf-5W-5Zr....	3	27			
Cb-15Hf-5W-10Zr...	6	20	100 Ta.....	51	223
Cb-15Hf-5W-5Ti-5Zr	4	20	Ta-20V.....	-	70
			Ta-30V.....	-	43
Cb-15Hf-10W-2Ti...	7	31	Ta-40V.....	6	112
Cb-15Hf-10W-5Ti...	5	28	Ta-50V.....	-	113
Cb-15Hf-10W-10Ti..	5	8			
Cb-15Hf-10W-5Zr...	6	53	Ta-20Hf.....	29	66
Cb-15Hf-10W-10Zr..	9	30	Ta-25Hf.....	13	41
			Ta-30Hf.....	-	37
Cb-5V-5W.....	-	50	Ta-33Hf.....	-	29
Cb-5V-10W.....	-	41			
Cb-5V-15W.....	-	76	Ta-20Hf-0.007C....	24	57
Cb-10V-5W.....	7	30-42	Ta-25Hf-0.007C....	10	35
Cb-10V-10W.....	-	27	Ta-30Hf-0.007C....	-	24
Cb-10V-15W.....	-	48	Ta-33Hf-0.007C....	-	26
Cb-15V-5W.....	-	42			
Cb-15V-10W.....	-	55	Ta-20Hf-0.014C....	26	45-51
Cb-15V-15W.....	-	58	Ta-25Hf-0.014C....	-	33
			Ta-30Hf-0.014C....	-	23
			Ta-33Hf-0.014C....	-	25

Table 1.XXX. Oxidation data at 1,000°C for columbium and tantalum alloys. (Babitzke et al [50]).

Alloy	Alloy composition	Weight gain, mg/cm²/hr		Remarks
		Sample 1	Sample 2	
1...	Cb-50[illegible].....	25.6	19.0	Linear weight gain.
2...	Cb-20Hf.....	49.7	25.5	Do.
3...	Cb-33Hf.....	33.7	18.7	Do.
4...	Cb-75Hf.....	6.4	13.1	Do.
5...	Cb-10W.....	22.9	9.1	Do.
7...	Cb-20Hf-5W.....	19.7	-50	Weight loss and spalling of oxide for 2d sample.
8...	Cb-20Hf-5W-10Ti	6.0	7.7	Linear weight gain.
9...	Cb-33Hf-5W.....	11.2	11.5	Do.
10...	Cb-33Hf-10W....	6.7	7.2	Do.
11...	Cb-33Hf-5W-10Ti	6.5	6.7	Do.
12...	Cb-33Hf-10V....	7.0	14.3	Do.
13...	Ta-20Hf.....	-19.9	13.9	Weight loss for 1st sample and linear weight gain for 2d sample.
14...	Ta-33Hf.....	4.4	13.0	Linear weight gain.
15...	Ta-75Hf.....	22.5	24.4	Do.
16...	Ta-10W.....	9.6	41.1	Oxide spalled last 15 minutes for 2d sample.
17...	Ta-20Hf-5W.....	-15.4	13.1	Weight loss for 1st sample and linear weight gain for 2d sample.
18...	Ta-20Hf-5W-10Ti	-12.2	11.7	Do.
22...	Ta-33Hf-5Zr....	9.2	11.0	Linear weight gain.
23...	Ta-8W-2Hf.....	16.5	-	Do.

Table 1.XXXI. Oxidation results for niobium-base alloys in air at 1000°C (Yoda et al (52)).

Composition, at %	weight gain, mg/cm²/hr.
Nb-15Hf-5W-9Ti-1Zr	22.2
Nb-15Hf-5W-8Ti-2Zr	21.2
Nb-15Hf-5W-2Zr-2Al	23.0
Nb-15Hf-5W-1Zr-4Al	24.6
Nb-15Hf-5W-0.5Zr-6Al	20.8
Nb-15Hf-5W-8Al	21.5
Nb-15Hf-5W-8Ti-1Zr-4Cr	15.5
Nb-15Hf-5W-8Ti-4Cr	15.9
Nb-15Hf-5W-8Ti-2Zr-4Cr	13.8
Nb-15Hf-5W-10Ti-2Zr	21.6
Nb-15Hf-5W-10Ti-2Zr-1Cr	17.1
Nb-15Hf-5W-10Ti-2Zr-2Cr	20 0
Nb-15Hf-5W-10Ti-2Zr-3Cr	24.7
Nb-15Hf-5W-2Zr-10Al	16.1
Nb-15Hf-5W-10Ti-2Zr-10Al	11.3
Nb-7.9Hf-2.5W-17.6Ti-1.0Zr	18.0
Nb-7.9Hf-2.6W-15.8Ti-2.1Zr	18.7
Nb-8.5Hf-2.8W-2.2Zr-1.9Al	37.9
Nb-10Ta-10Hf-5W-5Mo-10Ti-2Zr	15.7
Nb-10Ta-10Hf-5W-5Mo-10Ti-2Zr-0.5C	10.9
Nb-10Ta-10Hf-5W-5Mo-10Ti-2Zr-1.5C	8.4
Nb-10Ta-10Hf-5W-5Mo-10Ti-2Zr-2.5C	11.9
Nb-10Ta-10Hf-5W-5Mo-10Ti-2Zr-3.5C	-
Nb-10Ta-10Hf-5W-5Mo-10Ti-2Zr-2V	12.5
Nb-10Ta-10Hf-5W-5Mo-10Ti-2Zr-2V-0.5C	12.0
Nb-10Ta-10Hf-5W-5Mo-10Ti-2Zr-2V-1.5C	10.6
Nb-10Ta-10Hf-5W-5Mo-10Ti-2Zr-2V-2.5C	11.9
Nb-10Ta-10Hf-5W-5Mo-10Ti-2Zr-2V-3.5C	-

Table 1.XXXII. Columbium and tantalum alloys, oxidation data. (Habitzke and Croeni (53)).

Alloy sample No.	Alloy composition, atomic percent	Weight gain, mg/cm² at 1,000° C		Weight gain, mg/cm² at 800° C	
		End of 1st hour	End of 2d hour	End of 1st hour	End of 2d hour
Group 1:					
66- 1	Cb-15Hf-5W-1Zr-4Al	11	WL[1]	WL	WL
66- 3	Cb-15Hf-5W-2Zr-4Al	18	28	WL	WL
66- 4	Cb-15Hf-5W-2Zr-5Al	14	20	WL	WL
66- 5	Cb-15Hf-5W-1Zr-4Al-4Ti	9	13	WL	WL
66- 7	Cb-15Hf-5W-2Zr-4Al-4Ti	8	13	WL	WL
66- 8	Cb-15Hf-5W-2Zr-4Al-6Ti	8	12	WL	WL
66- 9	Cb-15Hf-5W-2Zr-4Al-1N	13	21	WL	WL
66-11	Cb-15Hf-5W-2Zr-4Al-4Ti-1N	6	9	2	WL
66-12	Cb-15Hf-5W-2Zr-4Al-4Ti-2N	7	10	2	3
66-13	Cb-15Hf-5W-2Zr-4Al-1N-1C	14	22	3	3
66-14	Cb-15Hf-5W-2Zr-4Ti-2N-1C	18	26	2	3
Group 2:					
66-18	Cb-15Hf-10W-10Ti-4Al	9	15	3	3
66-19	Cb-15Hf-10W-4Al	WL	WL	3	WL
66-20	Cb-15Hf-5W-5Zr	21	31	WL	WL
66-21	Cb-15Hf-5W-5Zr-4Al	17	25	WL	WL
66-26	Cb-15Hf-5V-4Al-1C	7	12	2	2
66-27	Cb-5W-4Al	48	89	24	38
66-28	Cb-5V-4Al	11	15	11	13
66-29	Cb-5V-4Al-1C	9	15	10	14
66-30	Cb-5V-5W-4Al	21	34	8	9
66-33	Cb-2Ti-2Al-2Mo-2Cr-1C-2Re	42	69	-	-
Group 3:					
66-35	Cb-16.9Ti-4.4Zr-3.9W-0.9Re	9	14	7	8
66-36	Cb-17.2Ti-4.5Zr-3.1Al	10	14	6	7
66-37	Cb-16.5Ti-4.3Zr-3.8W-1.2Al	7	14	7	11
66-44	Cb-16.7Ti-4.4Zr-2.8Ni-3.0Al	16	25	6	9
66-45	Cb-15.3Ti-4.1Zr-13.7Hf	16	16	WL	WL
66-46	Cb-14.4Ti-3.8Zr-14.4Hf-4.5W	8	10	4	7
66-47	Cb-13.8Ti-3.6Zr-14.0Hf-4.4W-3.7Al	6	9	WL	WL
66-48	Cb-14.7Ti-3.9Zr-13.3Hf-3.5Al	16	20	2	3
66-49	Cb-14.3Ti-3.7Zr-13.4Hf-5.6V	11	13	WL	WL
66-50	Cb-16.2Ti-4.2Zr-5.1V-3.8W	5	7	2	3
66-56	Cb-17.7Ti-4.7Zr	6	13	27	36
Group 4:					
66-51	Ta-20Hf-4Al	WL	WL	WL	WL
66-52	Ta-30Hf-4Al	6	8	6	8
66-53	Ta-20Hf-5W	WL	WL	WL	WL
66-54	Ta-20Hf-5W-4Al	WL	WL	WL	WL
66-55	Ta-20Hf-5V-4Al	WL	WL	WL	WL

[1] WL = Weight loss.

Table 1-XXXIII. Compositions of the alloys whose oxidation behaviour is shown in Figure 1.77 (Babitzke et al [54]).

(Alloy composition in atomic percent).

Alloy	Composition
Group 1:	
1.....	Cb-1N-5W-3V-5Hf
2.....	Cb-1N-5W-5V-5Hf
3.....	Cb-1N-5W-3V-10Hf
4.....	Cb-1N-5W-5V-10Hf
5.....	Cb-1N-5W-3Si-5Hf
6.....	Cb-1N-5W-3Cr-5Hf
7.....	Cb-15Hf-5W-4Si
8.....	Cb-15Hf-5W-4Si-1N
9.....	Cb-15Hf-5W-2Si-2Al
10.....	Cb-15Hf-5W-2Zr-4Al-1C
11.....	Cb-15Hf-5W-2Zr-1C
12.....	Cb-15Hf-2Zr-4V-1C
13.....	Cb-10Ti-4Al-0.1Cu-2W
14.....	Cb-14.6Ti-3.9Zr-13.3Hf-3.5Al-0.7N
15.....	Cb-14.8Ti-3.9Zr-13.4Hf-3.4Si
18.....	Cb-69Fe
Group 2:	
19.....	Cb-5Zr-5W
20.....	Cb-10Zr-5W
21.....	Cb-15Zr-5W
22.....	Cb-20Zr-5W
23.....	Cb-33Zr-5W
Group 3:	
13a.....	Cb-15Hf-5W
24.....	Cb-15Hf-5W-0.1C
25.....	Cb-15Hf-5W-0.5C
26.....	Cb-15Hf-5W-1.0C
27.....	Cb-15Hf-5W-0.1N
28.....	Cb-15Hf-5W-0.5N
29.....	Cb-15Hf-5W-1.0N
30.....	Cb-15Hf-5W-0.1B
31.....	Cb-15Hf-5W-0.5B
32.....	Cb-15Hf-5W-1.0B
Group 4:	
16.....	Ta-5W-5Mo
17.....	Ta-15Hf-5W-2Re

Nominal values are used throughout the paper.

Table 1.XXXIV. Tables of a significant means from oxidation data. (Babitzke et al [55]).

	0Hf	7.5Hf	15Hf	Overall
Boron, at pct:				
0.....	46.2500	45.4583	42.2083	44.6388
2.....	52.7083	48.9167	40.6250	47.4166
5.....	65.7500	75.2083	61.1667	67.3750
10.....	81.4167	86.4583	61.9583	76.6111
Overall.....	61.5312	64.0104	51.4895	59.0103
Temp, ° C:				
1,000.....	41.4167	43.5417	35.8958	40.2847
1,200.....	81.6458	84.4792	67.0833	77.7361
Overall.....	61.5312	64.0104	51.4895	59.0104
	0B	2B	5B	10B	Overall
Temp, ° C:					
1,000.....	36.8056	34.7778	43.0556	46.5000	40.2847
1,200.....	52.4722	60.0556	91.6944	106.7222	77.7361
Overall.....	44.6388	47.4166	67.3750	76.6111	59.0103
Time, min:					
30.....	23.8889	25.1667	34.6111	36.3333	29.9999
60.....	38.6667	41.2222	59.0556	65.5556	51.1250
90.....	51.9444	55.2778	79.7778	91.5556	69.6388
120.....	64.0556	68.0000	96.0556	113.0000	85.2777
Overall.....	44.6388	47.4166	67.3750	76.6111	59.0103
	0W	5W	10W	Overall
Boron, at pct:				
0.....	70.2500	32.3750	31.2917	44.6388
2.....	72.8333	38.4583	30.9583	47.4166
5.....	102.7917	55.5833	43.7500	67.3750
10.....	112.0000	60.2500	57.5833	76.6111
Overall.....	89.4687	46.6666	40.8958	59.0103
Temp, ° C:				
1,000.....	79.1250	24.5625	17.1666	40.2847
1,200.....	99.8124	22.1041	23.7292	77.7361
Overall.....	89.4687	46.6666	40.8958	59.0104
Time, min:				
30.....	44.7083	23.8333	21.4583	29.9999
60.....	77.5000	40.2083	35.6667	51.1250
90.....	105.8333	54.6250	48.4583	68.6388
120.....	129.8333	68.0000	58.0000	85.2777
Overall.....	89.4687	46.6656	40.8958	59.0103
	30 min	60 min	90 min	120 min	Overall
Temp, ° C:					
1,000.....	22.0278	35.1667	46.7500	57.1944	40.2847
1,200.....	37.9722	67.0833	92.5278	113.3611	77.7361
Overall.....	29.9999	51.1250	69.6388	85.2777	59.0104

Table 1.XXXV. Oxidation data of Cb-base Alloys. (Chang [56]).

Temp °F	Time Hrs.	Weight Gain mg/cm² Cb-1	Weight Gain mg/cm² Cb-2	Depth of Hardening Mils/Side Cb-1	Depth of Hardening Mils/Side Cb-2	Metal Loss Mils/Side Cb-1	Metal Loss Mils/Side Cb-2
1800	1	6.0	3.2	17	9	0.3	0
	3	23.5	8.2	25	15	1.4	0
	8	83.1	18.6	32	17	7.2	1
	16	201.4	25.8	36	20	28.5	1.5
	16	213.8	28.8	-	-	-	-
	24	300.0	28.6	35	20	52.5	1.9
	24	-	30.3	-	-	-	-
2100	1	15.6	12.3	25	12	1.3	0.13
	3	27.5	19.1	33	15	3.9	1.0
	8	49.6	34.5	40	21	4.2	2.0
	16	74.8	46.9	53	28	6.6	3.3
	24	96.7	60.4	65	32	9.0	4.0
	50	160.2	89.5	> 97	51	17.6	7.1
	100	250.1	133.5	> 88	67	27.0	10.9
2400	1	32.4	28.0	30	15	2.8	1.6
	3	67.4	51.9	46	25	6.2	3.4
	8	137.2	115.4	70	35	12.9	6.3
	16	230.0	146.5	> 91	45	24.4	11.3
	24	312.9	196.0	> 75	55	40.0	18.4

Table 1.XXXVI. Weight gain data for Cb alloys oxidized at 1093°C. (2000°F). (Begley et al [57]).

Alloy	Composition w/o	Cumulative Weight Gain (mg/cm^2) Time at Temperature (Hrs.) 0.5	1	1.5	2	2.5	3
VAM-76	76Cb-22W-2Hf	10.87	17.76	29.56	43.20	55.31	65.68
VAM-77	80Cb-18W-2Hf	11.66	21.50	36.25	52.50	69.78	82.32
VAM-78	76Cb-22W-2Hf-.13C	13.98	23.00	31.85	40.01	48.25	56.51
VAM-79	76Cb-22W-2Hf-.067C	13.22	21.08	27.95	35.60	42.75	52.25
VAM-80	70Cb-28W-2Hf-.067C	--	148.80	--	--	--	--
VAM-81	76Cb-22W-2Hf-.167C	--	58.80	--	--	--	--
VAM-82	76Cb-22W-2Hf-.034C-.039N	12.38	17.62	24.22	30.88	36.31	41.14
VAM-83	76Cb-20W-2Hf-2Re-.133C	15.74	25.06	33.81	41.09	51.15	60.29
VAM-84	70Cb-22W-2Hf-6Ta-.13C	15.30	21.45	27.66	34.36	38.77	43.54
VAM-85	77Cb-22W-1Hf-.067C	14.65	22.61	29.82	37.74	43.34	48.76
VAM-86	68Cb-26W-4Re-2Hf-.067C	13.58	21.70	28.48	33.00	38.30	41.95

Table 1.XXXVII. Nominal composition of series A Cb Alloys. (w/o). (Cornie and Goodspeed [59]).

Alloy No.	Cb	W	Ta	Ti	Hf	Mo	V	Al	Cr	Y	B	Re	Be	U
A	Bal.	10	10	10	1.8	--	--	--	--	--	--	--	--	--
A-1	Bal.	10	10	15	1.8	--	--	--	--	--	--	--	--	--
A-2	Bal.	10	10	10	1.8	5	--	--	--	--	--	--	--	--
A-3	Bal.	10	10	10	1.8	--	3	--	--	--	--	--	--	--
A-4	Bal.	10	10	10	1.8	--	--	3	--	--	--	--	--	--
A-5	Bal.	10	10	10	1.8	--	--	--	3	--	--	--	--	--
A-6	Bal.	10	10	10	1.8	--	--	--	--	0.1	--	--	--	--
A-7	Bal.	10	10	10	1.8	--	--	--	--	--	0.2	--	--	--
A-8	Bal.	10	10	10	1.8	--	--	--	--	--	--	3	--	--
A-9	Bal.	10	10	10	1.8	--	--	--	--	--	--	--	0.2	
A-10	Bal.	10	10	10	1.8	--	--	--	--	--	--	--	--	5

Table 1.XXXVIII. Oxidation data for series A Alloys at 2200°F. (Cornie and Goodspeed [59]).

Alloy No. (Comp.)	Weight gain (mg/cm^2)				Surface Recession (mils)				Oxygen Penetration (mils)			
	1 hr.	4 hrs.	20 hrs.	66 hrs.	1 hr.	4 hrs.	20 hrs.	66 hrs.	1 hrs.	4 hrs.	20 hrs.	66 hrs.
A (Base)	17.1	40.7	231.0	--	1.7	3.2	6.2	--	--	--	--	--
A-1(Base+5Ti)	15.3	30.6	82.5	179.0	1.0	2.0	6.7	12.3	6	10.3/30°	21	22
A-2(Base+5Mo)	14.6	30.9	76.5	173.9	2.5	2.5	11.0	23.0	7.5	16/30°	33	--
A-3(Base+3V)	15.3	37.7	105.5	218.5	0.7	2.5	9.8	17.0	7.5	15	27	35
A-4(Base+3Al)	10.4	25.2	69.5	131.6	1.0	1.3	3.8	9.3	6/12	7/18°	27/20°	45/27°
A-5(Base+3Cr)	14.5	33.3	92.7	174.3	0.5	2.0	6.5	29.5	7	14/30°	25	43
A-6(Base+.1Y)	18.5	42.8	108.5	220.0	1.0	2.3	7.0	19.0	6	15	27	--
A-7(Base+.2B)	21.3	47.8	223.5	--	0.5	2.3	7.3	--	10	23	36	--
A-8(Base+3Re)	14.0	34.5	89.1	172.7	--	--	--	13.0	--	13	2[illegible]	25
A-9(Base+.2Be)	20.7	36.9	184.4	--	1.0	3.0	6.0	--	8	18	35	--
A-10(Base+5U)	18.6	46.4	110.3	376.6	1.0	2.5	10.0	--	9	14	35	--
B-66(Cb-5Mo-5V-1Zr)	33.3	193.0	248.5	--	--	--	--	--	--	--	--	--

Table 1.XXXIX. Kinetic rate constant for oxidation (2200°F) of series A columbium alloys. (Cornie and Goodspeed (59)).

Alloy	$K_{\Delta Wt}$*			K_{SR}*			K_{OP}*		
	4 Hrs.	20 Hrs.	66 Hrs.	4 Hrs.	20 Hrs.	66 Hrs.	4 Hrs.	20 Hrs.	66 Hrs.
A (Base)**	20.3	51.6	----	1.6	1.6	----			
A-1 (Base+5Ti)	15.3	18.5	22.0	1.0	1.5	1.5	5.0	4.7	2.7
A-2 (Base+5Mo)	15.5	17.1	21.4	1.3	2.5	2.8			
A-3 (Base+3V)	18.9	23.6	26.9	1.3	2.2	2.1	7.5	6.0	4.3
A-4 (Base+3Al)	12.6	15.5	16.2	0.7	0.9	1.1	3.5	4.0	5.6
A-5 (Base+3Cr)	16.7	20.7	21.4	1.0	1.5	3.6	7.0	5.6	5.3
A-6 (Base+0.1Y)	21.4	24.2	27.2	1.2	1.6	2.3			
A-7 (Base+0.2B)	23.9	50.0	----	1.2	1.6	----			
A-8 (Base+3Re)	17.3	19.9	21.2	----	----	1.6	6.5	4.5	3.1
A-9 (Base+0.2Be)	18.5	41.1	----	1.5	1.3	----			
A-10 (Base+5U)	23.2	24.6	46.5	1.3	2.2	----			

* $K_{\Delta Wt}$ = Parabolic weight gain rate constant, $mg\text{-}cm^{-2}\text{-}hr^{-1/2}$

K_{SR} = Parabolic surface recession rate constant, $mils\text{-}hr^{-1/2}$

K_{OP} = Parabolic oxygen penetration rate constant, $mils\text{-}hr^{-1/2}$

** Base composition is Cb-10W-10Ta-10Ti-1.8Hf

Table 1.XL. Nominal compositions of series B columbium alloys. (Cornie and Goodspeed (59)).

Alloy No.	Analysis (w/o)											
	Cb	W	Ta	Ti	Hf	Al	V	Mo	Re	Cr	Y	U
B-1 (base)	Bal.	10	10	15	2	3	--	--	--	--	--	--
B-2	Bal.	10	10	15	2	3	5	--	--	--	--	--
B-3	Bal.	10	10	15	2	3	--	5	--	--	--	--
B-4	Bal.	10	10	15	2	3	--	--	3	--	--	--
B-5	Bal.	10	10	15	2	3	--	--	--	3	--	--
B-6	Bal.	10	10	25	2	3	--	--	--	--	--	--
B-7	Bal.	10	10	15	2	3	--	--	--	--	0.1	--
B-8*	Bal.	10	--	40	2	3	--	--	--	--	--	--
B-9*	Bal.	10	10	15	2	3	--	--	3	--	--	5

*These 3" diameter buttons were not remelted into rectangular molds.

Table XLI. Oxidation data for series "B" alloys at 2200°F. (Cornie and Goodspeed [59]).

Alloy No. Composition	Weight Gain (mg/cm^2)				Surface Recession (mils)				Oxygen Penetration**(mils)			
	1 Hr.	4 Hrs.	20 Hrs.	66 Hrs.	1 Hr.	4 Hrs.	20 Hrs.	66 Hrs.	1 Hr.	4 Hrs.	20 Hrs.	66 Hrs.
B-1 Base (Cb-15Ti-10W-10Ta-2Hf-3Al)	13.1	27.9	78.6	126.3	---	8	11.5	15	9	16	>48***	---
B-3 Base + 5Mo	9.7	13.1	96.3	112.0	---	8	19.5	23	6	9	19	>30***
B-4 Base + 3Re	13.7	29.0	85.5	157.4	5	6	11.5	20.5	7	14	25	55
B-5 Base + 3Cr	12.9	24.1	52.2	99.2	3	7	7.0	15.5	4	6	19	>49***
B-6 Base + 10Ti	10.5	46.0	182.3	295.2*	10	14	23	---*	3	11	>29***	---*
B-7 Base + 0.1Y	11.5	29.2	68.3	178.2	2	---	10.5	15.5	6	17	---	28
B-8 Cb-40Ti-10W-2Hf-3Al	9.8	36.2	175.7	277.6*	2	9	19	---*	3	13	>25***	---*
B-9 Base + 3Re + 5U	---	---	---	289.0	---	---	15	30	---	---	21	25

* Substrate completely consumed.
** Penetration data represents depth of visible oxide precipitation at 100X.
*** Indicates penetration through specimen thickness.

Table 1.XLII. Kinetic rate constants for oxidation (2200°F) of series B columbium alloys. (Cornie and Goodspeed (59)).

Alloy	$K_{\Delta Wt}$*			K_{SR}*			K_{OP}*		
	4 Hrs.	20 Hrs.	66 Hrs.	4 Hrs.	20 Hrs.	66 Hrs.	4 Hrs.	20 Hrs.	66 Hrs.
B-1 (Base)**	14.0	17.6	15.6	4.0	2.4	1.9	8.0	>10.7	----
B-3 (Base + 5Mo)	6.6	21.5	13.8	4.0	4.4	2.9	4.5	4.2	6.2
B-4 (Base + 3Re)	14.5	19.1	19.4	3.0	2.6	2.5	7.0	5.6	6.8
B-5 (Base + 3Cr)	12.1	11.7	12.2	3.5	1.6	1.9	3.0	4.2	>8.5
B-6 (Base + 10Ti)	23.0	40.8	36.3	7.0	5.2***	----	5.5	>6.5	----
B-7 (Base + 0.1Y)	14.6	15.3	21.9	----	2.4	1.9	8.5	----	3.5
B-8 (Cb-40Ti-10W-2Hf-3Al)	18.1	39.3	34.2	4.5	4.3	----	6.5	>5.6	----
B-9 (Base + 3Re+5U)	----	----	35.6	----	3.4	3.7	----	4.7	3.1

* $K_{\Delta Wt}$ = Parabolic weight gain rate constant, $mg\text{-}cm^{-2}\text{-}hr^{-1/2}$
K_{SR} = Parabolic surface recession rate constant, $mils\text{-}hr^{-1/2}$
K_{OP} = Parabolic oxygen penetration rate constant, $mils\text{-}hr^{-1/2}$
** Base composition is Cb-15Ti-10W-10Ta-2Hf-3Al
*** Data may be invalid because of almost complete oxidation of substrate

Table 1.XLIII. Effect of 2400°F exposures on weight increase (1) of alloy B-1 at 1800, 2000, and 2200°F in air. (Cornie and Goodspeed (59)).

Test Temperature (°F)	Weight Increase at Temp. (mg)		Improvement Factor	
	4 Hr. Period Before/After	40 Hr. Period Before/After	4 Hrs.	40 Hrs.
1800(2)	10/5	127/40	2.0	3.2
2000(2)	22/4	----	5.5	---
2200(3)	59/28	703/385	2.1	1.8

(1) Thermobalance Data

(2) Specimens annealed 1 hour at 2400°F

(3) Specimen annealed 1 hour at 3090°F

Table 1-XLIV. Oxidation-resistant columbium alloys and oxidation rates. (Brentnall et al (65)).

Alloy	Extrapolated Oxidation Rate at 2400 F ($mg/cm^2/hr$)	Remarks
Cb-30Cr-5Al	0.33	U.S. Patent No. 2,838,396 duPont, 10 June 1958
Cb-20Cr-15Al-2Ce	0.20	
Cb-19Cr-10Al-15Co	0.09	
Cb-26Cr-5Al-2Ni	0.23	
Cb-10Cr-10Al-15Ni-4W-2Ce	0.07	
Cb-10Cr-10Al-4W	0.17	
Cb-20Mo-20Al	0.80	U.S. Patent No. 2,881,069 duPont, 7 April 1959
Cb-15Mo-15Al-2Ce	0.69	
Cb-15Mo-14Al-10Zr-4W-1B	0.44	
Cb-10Fe-19Al	0.13	U.S. Patent No. 2,838,396 duPont, 10 June 1958
Cb-20Fe-9Al	0.28	
Cb-24Fe-20Al	0.10	
Cb-10Fe-6Al-2B	0.80	
Cb-10Fe-14Al-4Mo-15Cr-1Ce	0.08	
Cb-5Fe-10Al-10Ni	0.19	
Cb-9Fe-10Al-25Ni	0.06	

Table 1-XLV. Columbium alloy compositions for oxidation tests. (Brentnall et al [65]).

Alloy Designation	Composition Wt.%	Reported Oxidation Rate at 2190°F (1200°C) Mg/cm²/hr*	Appearance After Arc Melting	Ductility in Rolling
A	Cb-50Ti-10Al-10Mo	–	No cracks	Poor
B	Cb-42Ti-4Cr-4Al	2.0	No cracks	Excellent
C	Cb-40Ti-5Al-10Mo	–	No cracks	Good
D	Cb-19Cr-10Al-15Co	0.06	Disintegrated	–
E	Cb-10Cr-10Al-4W	0.17	Badly cracked	Very poor
F	Cb-15Mo-14Al-10Zr-4W-1B	0.32	Disintegrated	–
G	Cb-10Cr-10Al-15Ni-4W-2Ce	0.05	Surface cracks	Very poor
H	Cb-9Fe-10Al-10Ni	–	Badly cracked	Very poor
I	Cb-5Fe-10Al-10Ni	0.15	Disintegrated	–
J	Cb-40Ti-10Cr-5Al	–	No cracks	Moderate
K	Cb-20Mo-15Al-4W	–	Disintegrated	Very poor
L	Cb-20Mo-20Al	0.62	Disintegrated	Very poor
M	Cb-20Mo-10Al	–	Surface cracks	Very poor
N	Cb-20Mo-5Al	–	No cracks	Poor
P	Cb-50Zr-5Ti	–	No cracks	Fair
R	Cb-40Zr-10Ti-4Al	–	No cracks	Fair
S	Cb-10W-29Hf-1Zr-5Ti	–	No cracks	Not rolled
T	Cb-10W-29Hf-1Zr-10Ti	–	No cracks	Not rolled

* Data from Reference 9 reported in mg/cm²/hr from 100 or 200 hour oxidation

Table 1-XLVI. Oxidation of columbium alloys. Exposed 16 hours at 1600°F. (Brentnall et al [65]).

Alloy	Appearance	Weight Change Mg/cm²	Scale Thickness* Inch
B	Orange-Brown	4.13	0.0008
E	Completely oxidized	–	–
G	Black	+0.2%	
H	Black	+0.75	
J	Smooth Brown	6.22	0.0006
N	Completely oxidized	–	–
P	Gray-White-spalled	-153.7	N.D.
R	Gray, spalled	34.20	0.020
S	Gray, spalled	86.16	N.D.
T	Gray, spalled	63.7%	N.D.
WC3015 Heat 590078	White, slight spalling	4.51	0.010

* Including continuous subscale
ND Not determined

Table 1-XLVII. Oxidation of columbium alloys. Exposed 16 hours at 2000°F. (Brentnall et al [65]).

Alloy	Appearance	Weight Change Mg/cm²	Scale Thickness* Inch
B	Orange-Brown, Smooth	15.81	0.005
E	Dark Green	+5.1%	ND
G	Brown	+0.72%	ND
H	Black	+4.1%	ND
J	Orange-Black	5.62	0.003
N	Yellow-Black, Spalled	-135.36	ND
P	White	139.06	0.034
R	White	68.16	0.025
S	Yellow, Spalled	-30.5	0.012
T	Yellow, Spalled	8.92	0.018
WC3015 Heat 590078	Yellow, Spalled	23.02	0.017

* Including continuous subscale
ND Not Determined

Table 1-XLVIII. Oxidation of columbium alloys. Exposed 16 hours at 2400°F. (Brentnall et al [65]).

Alloy	Appearance	Weight Change Mg/cm² or %	Scale Thickness Inch
B	Brown-Yellow, Slight Spalling	66.30	0.004
E	Dark Green	6.1%	ND
G	Completely oxidized	–	–
H	Completely oxidized	–	–
J	Black, Spalled	-19.83	0.003
N	Yellow, Spalled	133.56	ND
P	Brown, Spalled	166.21	ND
R	Brown, Spalled	165.57	ND
S	Yellow, Spalled	150.91	ND
T	Yellow, Spalled	172.22	ND
WC3015 Heat 590078	Brown, Spalled	164.71	ND

+ Including continuous subscale
ND Not Determined

Table 1.XLIX. Columbium alloy oxidation. (Brentnall et al [65]).

Alloy	Appearance	Weight Change Mg/cm²	Scale Thickness+ Inch
B	Orange-Brown	8.21	0.002
J	Dark Brown	4.86	0.001
R	Gray	49.49	0.011
S	White-Black Speckled, Spalled	-68.39	0.012
T	White, Spalled	29.52	0.008
WC3015M Heat 590078	Gray, Spalled	-20.30	0.010

Table L . Columbium alloy oxidation (Brentnall et al [65]).

Alloy	Appearance	Weight Change Mg/cm²	Scale Thickness+ Inch
B	Brown	21.54	0.006
J	Gray-Black; loose,powdery oxide	3.61	No adherent scale
R	White	152.85	>0.030
S	Yellow, Heavy Scale	37.78	0.006
T	Yellow, Heavy Scale spalling	-23.29	0.004
WC3015M Heat 590078	Yellow-White, Some spalling	-87.36	0.030

+ Including continuous subscale

Table 1-LI Crucible sulphidation test results. (Brentnall et al [65]).

Alloy	Initial Button Weight (gms) (approx. 2cc vol.)	Appearance	Weight Loss (%)
B	11.2907	Adherent orange/brown scale	4.2
J	11.7729	Adherent brown scale plus fine powder	3.4
N	16.2089	Heavy white oxide, completely oxidized	--
P	16.2457	Orange/white scale	14.4
R	13.2921	Orange/brown loose scale	50.9
S	18.1400	Orange/brown, completely oxidized	--
T	18.0870	Orange/white scale	25.5
WC3015 (Heat 590066)	13.1653*	White, completely oxidized	--
WC3015M (Heat 590075)	20.1334	Yellow/white scale	8.6
TD Nickel Chromium	3.9199 (0.040-inch sheet)	Dark green	0.25

* Smaller button due to material availability.

Table 1-LII. Chemical analysis of arc cast alloys selected for cladding alloy* (Scheirer [67]).

Alloy No.	Density ◆	Cb	Ti	W	Al	Ta	Hf	Mo	V	Cr	Re	Ni	Si	Co	Fe	O_2 (ppm)
1.	0.216	Bal.	40	-	5	-	-	10	-	-	-	-	-	-	-	-
	5.97	Bal.	39.2	-	4.75	-	-	10.1	-	-	-	-	-	-	0.020	1020
2.	0.189	Bal.	50	-	10	-	-	-	-	-	-	-	-	-	-	-
	5.24	Bal.	51.4	<0.3	10.4	-	-	-	-	-	-	-	-	-	0.020	630
3.	0.236	Bal.	27	-	3	-	-	-	5	-	-	-	-	-	-	-
	6.53	Bal.	29.0	<0.3	2.90	-	-	-	4.6	-	-	-	-	-	0.030	525
4. (Cb 16)	0.318	Bal.	10	20	-	-	-	-	3	-	-	-	-	-	-	-
	8.81	Bal.	9.6	21.3	-	-	-	-	2.8	-	-	-	-	-	0.021	330
5. (Cb 7)	0.350	Bal.	7	28	-	-	-	-	-	-	-	-	-	-	-	-
	9.69	Bal.	6.8	28.8	-	-	-	-	-	-	-	-	-	-	<0.001	250
6.	0.476	-	-	-	1.1	25	Bal.	-	-	0.6	-	-	-	-	-	-
	13.16	-	-	0.3	1.6	25.5	Bal.	-	-	0.15	-	-	-	-	0.013	470
7.	0.320	Bal.	10	10	-	10	1.8	-	-	-	-	-	-	-	-	-
	8.85	Bal.	9.8	10.5	-	12.0	1.9	-	-	-	-	-	-	-	0.004	325
8.	0.323	Bal.	10	10	-	10	1.8	3	-	2	2	-	-	-	-	-
	8.93	Bal.	10.4	10.1	-	10.3	2.0	2.9	-	2.3	1.85	-	-	-	0.005	300
9.	0.253	Bal.	20	3	3	3	-	-	3	3	-	3	1	3	2	-
	7.01	Bal.	21.2	3.1	3.2	4.0	-	-	3.0	3.5	-	3.0	0.48	3.1	2.0	260
10.	0.347	Bal.	5	5	-	-	30	-	-	-	3	-	-	-	-	-
	9.61	Bal.	5.3	5.1	-	-	29.2	-	-	-	2.2	-	-	-	0.053	240

* Analysis supplied by Battelle Memorial Institute.

** Nominal compositions shown in first line.

◆ First figure in lbs/in^3
Second figure in gms/cm^3

Table 1-LIII. Oxidation test data (2200°F) for potential cladding alloys [a] (Scheirer [67]).

Alloy No.	Weight Gain (mg/cm²)				Surface Recession (mils)				Oxygen Substrate Penetration (mils)**			
	1 hr	4 hrs	20 hrs	64 hrs	1 hr	4 hrs	20 hrs	64 hrs	1 hr	4 hrs	20 hrs	64 hrs
1	5.5	14.3	36.4	246.7*	1.0	1.0	28.5	47.5*	3/22	5/36	19+/19+	
2	1.6	1.9	6.2	19.9	0.5	0.5	2.0	4.5	15/38	45/41	46+/46+	43.5+/43.5
3	10.6	21.9	69.7	162.2	1.0	2.5	8.0	18.5	5/40	9/47+	41.5+/41.5+	31.5+/31.5
4	11.9	34.5	52.3	133.5	1.0	3.5	10.5	15.0	6/12	10/20	26/45	45.5+/45.5
5	0.5	24.5	29.9	59.1	3.5	1.0	4.0	8.0	9/13	14/15	30/25	46/43
6	12.9	12.5	23.5	171.3	2.5	4.0	6.5	11.0	45.5+/45.5+	44+/44+	41.5+/41.5+	37+/37+
7	2.3	3.6	54.5	99.6	1.5	1.5	4.5	13.0	9/15	9/30	26/32	40/40
8	7.2	30.6	43.9	212.6	1.5	3.0	8.5	44.0*	6/7	10/14	21/30	
9	4.8	9.1	21.9	137.3	1.0	1.5	3.0	9.0	5/8	10/-	18/-	30/-
10	20.6	35.5	64.6	144.1	1.5	1.5	2.5	6.5	7/8	13/13	19/20	35/34

* Substrate totally consumed

** Weight gain data probably affected by oxide loss.

\+ Total oxygen penetration.

\+* Penetration determined optically/penetration determined by Knoop microhardness traverse (100 gm load).

[a] Air flow of 2 cu. ft./in. maintained during tests.

Table 1-LIV. Weight gain, metal loss, oxygen contamination, and total penetration data for Cb-W-Ta alloys oxidized in air for 2 and 20 hours at 2200°F. (Roche and Graham[68]).

Alloy No.	Composition (Wt. Percent)
1	Cb-10.5W-15.6Ta
2	Cb-9.6W-20.5Ta
3	Cb-25.1W-15.8Ta
4	Cb-24.6W-31.6Ta
5	Cb-16.9W-25.8Ta

Alloy No.	Weight Gain (mg/cm²)		Metal Loss (mils/radius)		Contamination (mils/radius)		Total Penetration (mils/radius)	
	2 hrs.	20 hrs.	2 hrs.	20 hrs.	2 hrs.	20 hrs.	2 hrs.	20 hrs.
1	32	142	5.5	15.5	≥ 126	≥ 116	≥ 131	≥ 131
2	24	109	5.0	10.0	≥ 130	≥ 125	≥ 133	≥ 133
3	26	140	8.5	41.0	≥ 117	≥ 84	≥ 125	≥ 125
4	84	398	45.5	86.0	≥ 80	≥ 39	≥ 125	≥ 125
5	33	168	5.5	80.5	≥ 96	≥ 79	≥ 99	≥ 99

Notes: Specimens were cylindrical.
Total Penetration = Metal Loss + Contamination.
Specimens were completely penetrated in all tests.

Table 1-LV. Weight gain, metal loss, oxygen contamination, and total penetration data for Cb-W-Ta alloys oxidized in air for 20 hours at 2000°F. (Roche and Graham (68)).

Alloy No.	Composition (Wt. Percent)
1	Cb-10.5W-15.6Ta
2	Cb-9.8-28.3Ta
3	Cb-25.1W-15.8Ta
4	Cb-24.6W-31.6Ta
5	Cb-16.9W-29.8Ta

Alloy No.	Weight Gain (mg/cm^2)	Metal Loss (mils/side)	Contamination (mils/side)	Total Penetration (mils/side)
1	120	20	≥ 30	≥ 50
2	115	18	≥ 30	≥ 48
3	95	17	≥ 32	≥ 49
4	302	≥ 54	-	≥ 54
5	162	8	≥ 42	≥ 50

Notes: Specimens were rectangular.
Total Penetration = Metal Loss + Contamination.
Specimens were completely penetrated in all tests.
Specimen of Alloy No. 4 was completely oxidized.

Table 1-LVI. Weight gain, metal loss, oxygen contamination, and total penetration data for Cb-W-Hf alloys oxidized in air for 2 and 20 hours at 2200°F. (Roche and Graham (68)).

Alloy No.	Composition (Wt. Percent)
6	Cb-9.8W-1.6Hf
7	Cb-10.6W-30.8Hf
8	Cb-24.1W-4.4Hf
9	Cb-25.0W-26.5Hf
10	Cb-14.7W-18.7Hf

Alloy No.	Weight Gain (mg/cm^2)		Metal Loss (mils/side)		Contamination (mils/side)		Total Penetration (mils/side)	
	2 hrs.	20 hrs.	2 hrs.	20 hrs.	2 hrs.	20 hrs.	2 hrs.	20 hrs.
6	69	322	7.5	46	≥ 124	≥ 85	≥ 131	≥ 131
7	33	122	3	11	9	31	12	42
8	39	252	6	46	≥ 119	≥ 79	≥ 125	≥ 125
9	28	73	2	6	6	13	8	19
10	31	127	1	13	14	≥ 36	15	≥ 49

Notes: Specimens of Alloys No. 6 and 8 were cylindrical; therefore, oxidation measurements are mils/radius.
Specimens of Alloys No. 7, 9, and 10 were rectangular.
Total Penetration = Metal loss plus contamination.

Table 1-LVI (Continued).

Alloy No.	Composition (Wt. Percent)	Alloy No.	Composition (Wt. Percent)
12	Cb-6.3W-26.3Hf	30	Cb-14.2W-28.8Hf
13	Cb-4.0W-34.4Hf	31	Cb-15.1W-34.1Hf
14	Cb-8.5W-28.6Hf	32	Cb-20.2W-21.6Hf

Alloy No.	Weight Gain (mg/cm^2)		Metal Loss (mils/side)		Contamination (mils/side)		Total Penetration (mils/side)	
	2 hrs.	20 hrs.	2 hrs.	20 hrs.	2 hrs.	20 hrs.	2 hrs.	20 hrs.
12	39	240	4	22	14	24	18	46
13	53	248	3	12	16	28	19	40
14	39	204	3	14	14	28	17	42
30	28	77	4	8	10	28	14	36
31	30	78	2	2	8	22	10	24
32	29	94	5	3	9	27	14	30

Notes: Specimens were rectangular.
Total Penetration = Metal Loss + Contamination

Table 1-LVII. Weight gain, metal loss, oxygen contamination, and total penetration data for Cb-W-Hf alloys oxidized in air for 20 hours at 2000°F. (Roche and Graham (68)).

Alloy No.	Composition (Wt. Percent)
6	Cb-9.8W-1.6Hf
7	Cb-10.6W-30.8Hf
8	Cb-24.1W-4.4Hf
9	Cb-23.0W-26.5Hf
10	Cb-14.7W-18.7Hf

Alloy No.	Weight Gain (mg/cm^2)	Metal Loss (mils/side)	Contamination (mils/side)	Total Penetration (mils/side)
6	251	29	≥ 25	≥ 54
7	171	3	≥ 48	≥ 51
8	132	5	≥ 46	≥ 51
9	48	2	13	15
10	73	5	≥ 44	≥ 49

Notes: Specimens were rectangular.
Total Penetration = Metal Loss + Contamination.

Table 1-LVII (Continued).

Alloy No.	Composition (Wt. Percent)	Alloy No.	Composition (Wt. Percent)
11	Cb-4.9W-34.9Hf	30	Cb-14.2W-28.8Hf
12	Cb-6.3W-26.3Hf	31	Cb-15.1W-34.1Hf
13	Cb-4.0W-34.4Hf	32	Cb-20.2W-21.6Hf
14	Cb-8.3W-28.6Hf		

Alloy No.	Weight Gain (mg/cm^2)	Metal Loss (mils/side)	Contamination (mils/side)	Total Penetration (mils/side)
11	263	≥ 52	--	≥ 52
12	257	≥ 49	--	≥ 49
13	290	≥ 56	--	≥ 56
14	267	≥ 52	--	≥ 52
30	51	3	≥ 49	≥ 52
31	54	2	15	17
32	66	9	≥ 44	≥ 53

Notes: Specimens were rectangular.
Total Penetration = Metal Loss + Contamination
Specimens of alloys No. 11, 12, 13 and 14 were completely oxidized.

Table 1-LVIII. Weight gain, metal loss, oxygen contamination, and total penetration data for Cb-W-Hf alloys oxidized in air for 20 and 65 hours at 2000°F. (Roche and Graham [68]).

Alloy No.	Composition (Wt. Percent)
21	Cb-14.4W-35.9Hf
22	Cb-12.1W-35.9Hf

Alloy No.	Weight Gain (mg/cm^2)		Metal Loss (mils/side)		Contamination (mils/side)		Total Penetration (mils/side)	
	20 hrs.	65 hrs.	20 hrs.	65 hrs.	20 hrs.	65 hrs.	20 hrs.	65 hrs.
21	98	100	2	3	16	27	18	30
22	59	110	1	2	19	32	20	34

Notes: Specimens were rectangular.
Total Penetration = Metal Loss + Contamination.

Table 1-LIX. Weight gain, metal loss, oxygen contamination, and total penetration data for alloys of nominally Cb-15W-35Hf with additions of rhenium, titanium, cobalt, aluminium, vanadium, carbon, and nitrogen oxidized in air at 2000°F. (Roche and Graham (68)).

Alloy No.	Composition (Wt. Percent)	Alloy No.	Composition (Wt. Percent)
21	Cb-14.4W-35.9Hf	25	Cb-16.7W-35.2Hf-11.0Ti
23	Cb-15.1 W-34.8Hf-1.9Re	27	Cb-15.5W-36.0Hf-6.6Ti-0.048N-0.052C
26	Cb-17.5W-33.5Hf-2.8Co	29	Cb-15.0W-35.6Hf-6.4Ti-0.11C
24	Cb-16.9W-33.2Hf-6.3Ti	28	Cb-15.7W-34.9Hf-5.5Ti-2.2Al-2.0V

Alloy No.	Weight Gain (mg/cm^2)				Metal Loss (mils/side)				Contamination (mils/side)				Total Penetration (mils/side)			
	4	20	65	100	4	20	65	100	4	20	65	100	4	20	65	100
	(hrs)				(hrs)				(hrs)				(hrs)			
21	-	58	100	-	-	2	3	-	-	16	27	-	-	18	30	-
23	-	90	125	-	-	6	11	-	-	14	23	-	-	20	34	-
26	-	62	112	-	-	3	20	-	-	6	8	-	-	9	28	-
24	-	42	82	-	-	3.5	9.5	-	-	9	12	-	-	12.5	21.5	-
25	-	57	116	-	-	7	12	-	-	6	7	-	-	13	19	-
27	21	53	99	134	0.5	3	7.5	10	6	8	11	12	6.5	11	18.5	22
29	21	57	94	116	1	3	5.5	10	7	10	17	17	8	13	22.2	27
28	17	46	116	155	0.5	1	5.5	19.5	3	5	7	5	3.5	6	12.5	24.5

Notes: Specimens were rectangular.

Total Penetration = Metal Loss + Contamination.

Table 1-LX. Oxidation Data for Nb-10% Mo-Ta alloys. (Vasilyeva and Prokoshkin [69]).

% Ta	Increase in weight, mg/cm^2					
	1000°C.		1100°C.		1200°C.	
	1 hr.	21 hr.	1 hr.	21 hr.	1 hr.	21 hr.
0.25	22.0	159.3	23.9	176.0	29.3	261.7
0.5	21.3	151.3	22.6	174.0	28.2	260.0
1.0	18.6	142.8	21.3	154.0	25.9	258.7
2.0	17.2	132.4	20.5	144.0	24.7	254.3
3.0	16.7	122.0	19.8	139.3	21.3	-
4.0	10.4	119.7	16.3	137.1	19.9	243.0
5.0	17.7	134.3	19.9	191.0	21.1	197.8
10.0	17.9	136.7	21.4	196.7	25.7	208.3
15.0	20.0	226.5	25.3	231.6	34.5	301.2
Nb-10Ta-5Mo	5.7	31.9	13.7	96.2	30.5	273.9
Nb	30.0	271.0	36.0	330.0	67.2	388.2

Table 1-LXI. Weight gain after 1 hr for the oxidation of Nb-10 at % W (Sikka and Rosa [71]).

Table 1-LXI. Weight gain after 1 hr. for the oxidation of Nb-10 at % W. (Sikka and Rosa [71]).

oxygen pressure torr	temperature °C.	weight gain in 1 hr. mg/cm^2
100	1000	68*
	1100	43*
	1150	46*
	1200	53*
400	1000	50
	1100	23
	1150	27
	1200	33
760	1000	46
	1100	27
	1150	27
	1200	44

* Note: there is a discrepancy in the presentation of the data in the report, and it is probable that the weight gains at 100 torr should be a factor of 2 smaller.

Table 1-LXII. Weight gain after 1 hr for the oxidation of Nb and Nb-10 at % Cr. (Rosa and Chen[72]).

oxygen pressure torr	temperature °C.	weight gain in 1 hr. mg/cm².	
		Nb	Nb-10at%Cr
100	900	35	54
	1000	40	13
	1100	40	23
400	900	62	100
	1000	70	14
	1100	60	23
760	900	75	60*
	1000	80	25
	1100	72	28

* after 30 minutes.

Table 1-LXIII. Transition time from slow to fast kinetics and linear rate constant for Cb-132 between 650° and 850°C. (Felten [73]).

Temperature (°C)	*Transition time (min)*	*Weight gain at transition time (mg cm⁻²)*	k_L *(g cm⁻² sec⁻¹)*
651	90	1.0	2.37×10^{-7}
	78	1.0	2.76×10^{-7}
676	54	0.65	1.00×10^{-6}
683	40	0.88	1.42×10^{-6}
	39	0.88	1.49×10^{-6}
702	38	0.63	1.60×10^{-6}
	31	0.41	2.00×10^{-6}
726	32	1.7	3.13×10^{-6}
	19.5	1.2	3.42×10^{-6}
750	16	1.1	6.89×10^{-6}
775	13.5	1.4	6.15×10^{-6}
800	9.5	2.0	1.24×10^{-5}
826	8	1.8	1.26×10^{-5}
850	6	2.0	1.46×10^{-5}

Table 1-LXIV. Parabolic rate constants for Cb-132 oxidized between 900° and 1316°C. (Felten [73]).

Temperature (°C)	*Total time (min)*	*Duration of parabolic behavior (min)*	*Parabolic rate constant* k_p *(g² cm⁻⁴ sec⁻¹)*
982	100	0-40	4.08×10^{-8}
982	200	0-80	4.17×10^{-8}
1004	100	0-30	4.44×10^{-8}
1038	100	10-60	8.00×10^{-8}
1093	100	0-25	8.07×10^{-8}
		25-100	4.38×10^{-8}
1198	100	0-100	1.00×10^{-7}
1204	100	0-100	$8.83 \cdot 10^{-8}$
1204[61]	120	0-120	1.71×10^{-7}
1316	100	10-60	1.65×10^{-7}
1371[61]	120	10-70	$8.1 \cdot 10^{-7}$

Table 1-LXV. X-ray diffraction results of Cb-132 oxide products. (Felten [73]).

Heat treatment	*Type*	*Phases found*
140 min at 650°C	A*	α-Nb_2O_5**
100 min at 702°C	A	α-Nb_2O_5
70 min at 752°C	A	α-Nb_2O_5 + weak β-Nb_2O_5
40 min at 800°C	A	α-Nb_2O_5 + strong β-Nb_2O_5
20 min at 826°C	A	α-Nb_2O_5 + strong β-Nb_2O_5
45 min at 848°C	A	β-Nb_2O_5 + strong α-Nb_2O_5
30 min at 876°C	A	β-Nb_2O_5 + α-Nb_2O_5
150 min at 908°C	A	β-Nb_2O_5 + very weak α-Nb_2O_5
100 min at 982°C	A	α + β-Nb_2O_5
100 min at 982°C	B	β-Nb_2O_5 + weak α-Nb_2O_5
100 min at 1039°C	A	α + β-Nb_2O_5
100 min at 1039°C	B	β-Nb_2O_5 + weak α-Nb_2O_5
100 min at 1093°C	A	β-Nb_2O_5 + weak α-Nb_2O_5
100 min at 1204°C	A	β-Nb_2O_5 only
100 min at 1316°C	A	β-Nb_2O_5 only

* A = Spalled, B = adherent oxide

** α-Nb_2O_5 = low temperature modification, β-Nb_2O_5 = high temperature modification

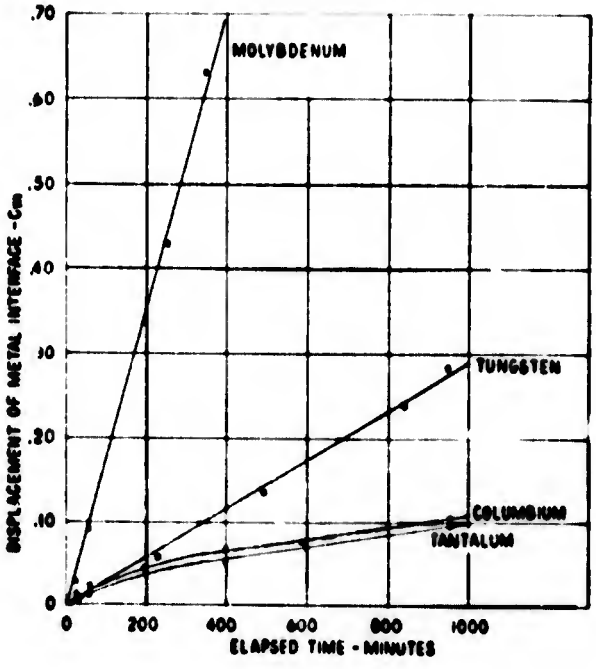

Figure O.1. Scaling of molytdenum, tungsten, tantalum, and columbium. Displacement of the metal interface after various times in air at 2000°F. (Michael).

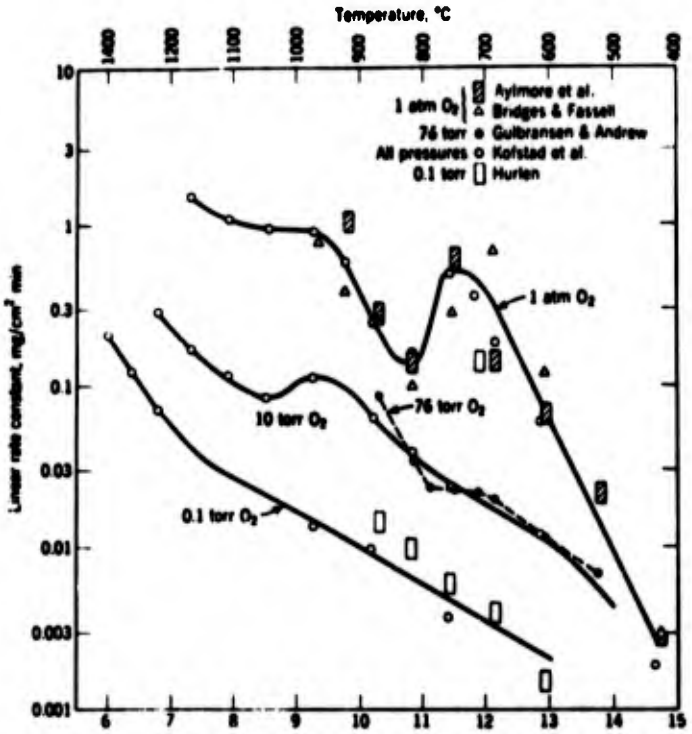

Figure 1.1. Temperature dependence of the linear rate constant of oxidation of niobium (Kofstad[3]).

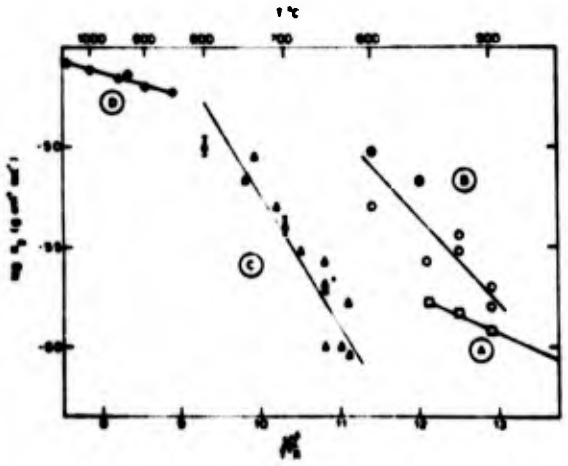

Figure 1.2. The log of the "linear rate constant" vs. the reciprocal of the absolute temperature at an oxygen pressure of 400 torr. The reaction has been divided into separate regions according to the scheme of McLintock (11). (Stringer (10)).

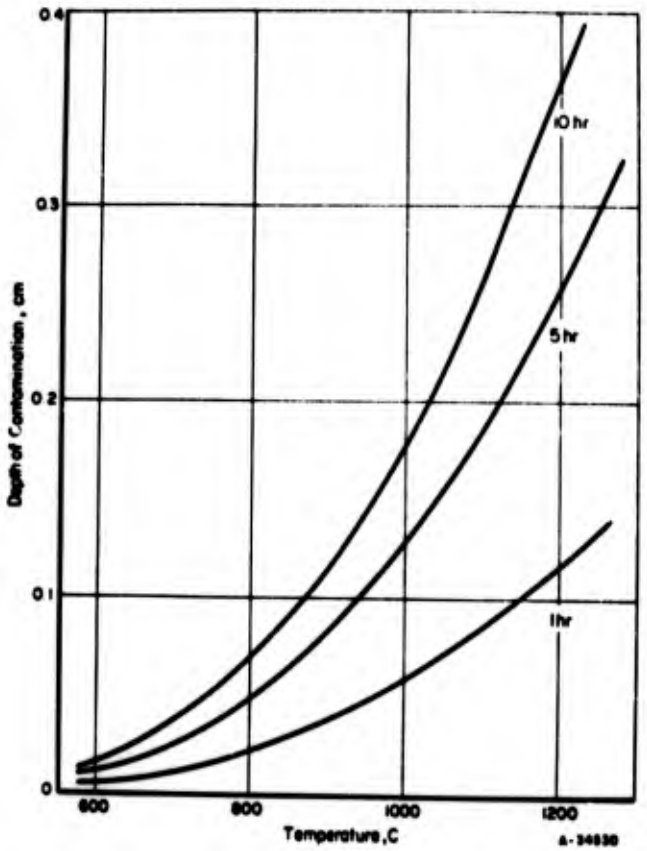

Figure 1.3. Depth of contamination for columbium oxidized for 1, 5, and 10 hr at various temperatures. (25). (Klopp (20)).

The criterion is a hardness increase of 50 Knoop points.

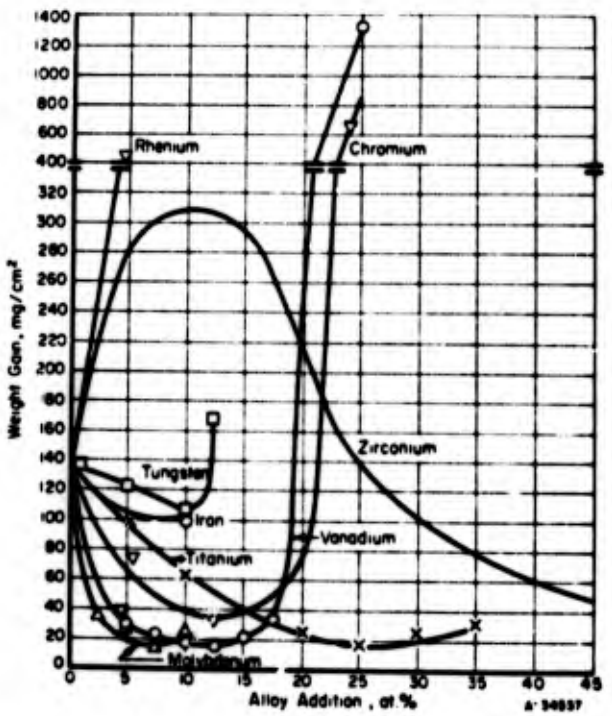

Figure 1.4. Weight gains of columbium alloys exposed 5 hr in dry air at 1000 C (continuous weighing tests) (Klopp et al (25)).

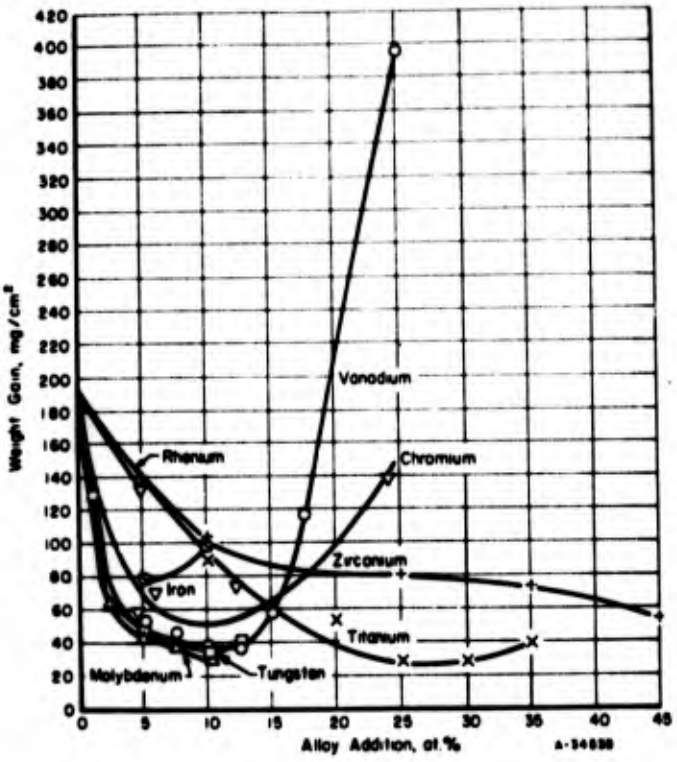

Figure 1.5. Weight gains of columbium alloys exposed 2 hr in dry air at 1200 C (Continuous weighing tests) (Klopp et al (25)).

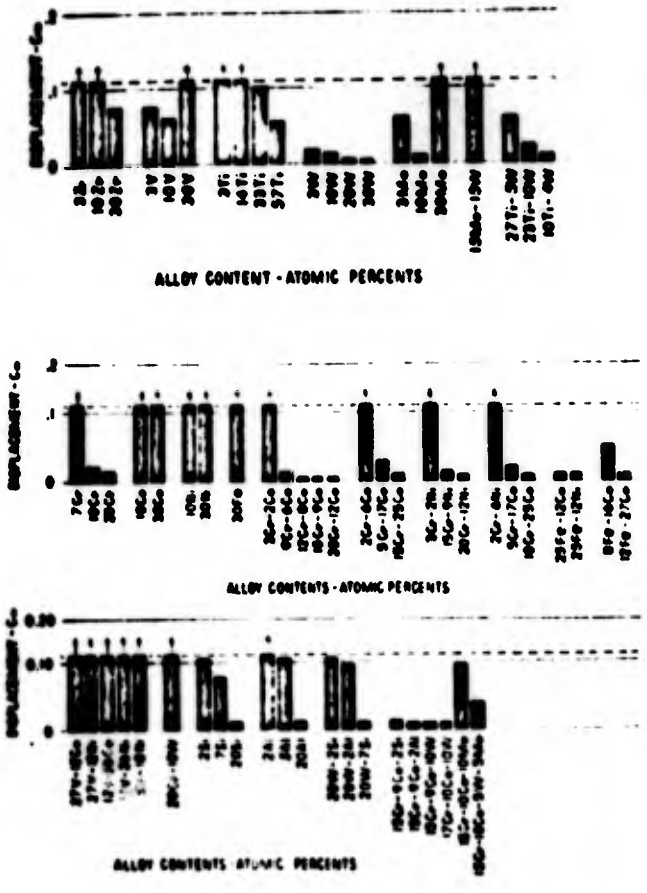

Figure 1.6. Displacement of the metal interface of columbium-base alloys after 16 hr in air at 2000°F. (Michael)

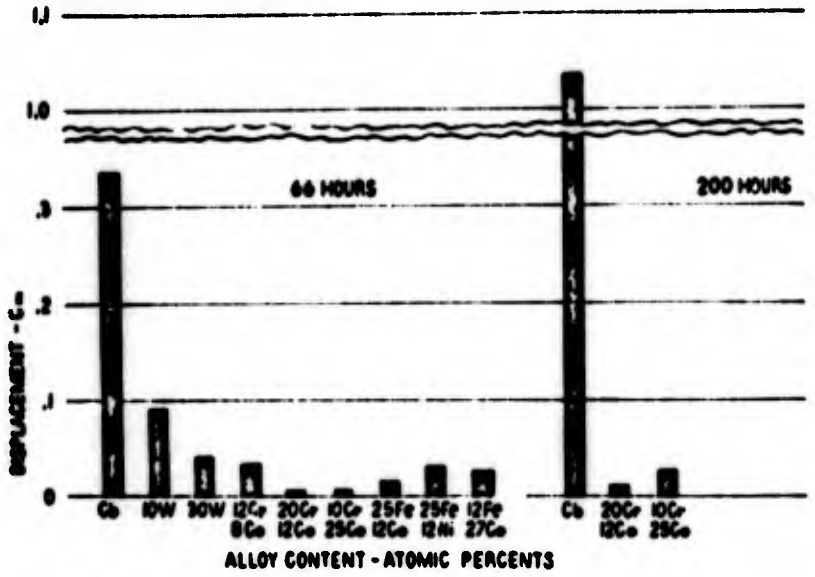

Figure 1.7. Displacement of the metal interface of columbium-base alloys after 66 and 200 hr in air at 2000°F. (Michael).

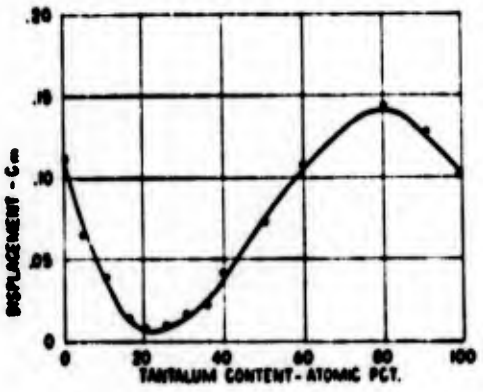

Figure 1.8. Scaling of binary Cb-Ta alloys after 16 hr in air at 2000°F. (Michael).

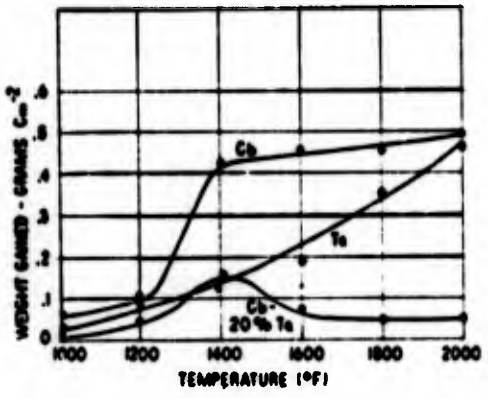

Figure 1.9. Scaling of columbium, tantalum, and a Cb-20% Ta alloy after 16 hr in air at 1000 to 2000°F. Initial sizes of specimens were 0.375 in. diam x 0.500 in. (Michael).

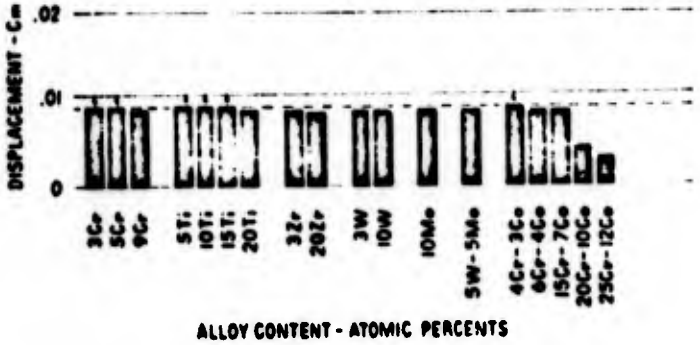

Figure 1.10. Displacement of the metal interface of modified Cb-20% Ta alloys containing the indicated percentages of alloying elements after 16 hr in air at 2000°F. The dashed line refers to the Cb-20% Ta alloy. (Michael).

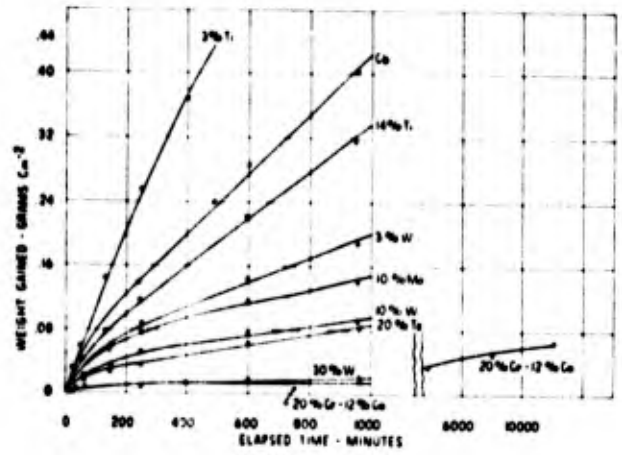

Figure 1.11. Air oxidation of columbium-base alloys at 2000°F. (Michael).

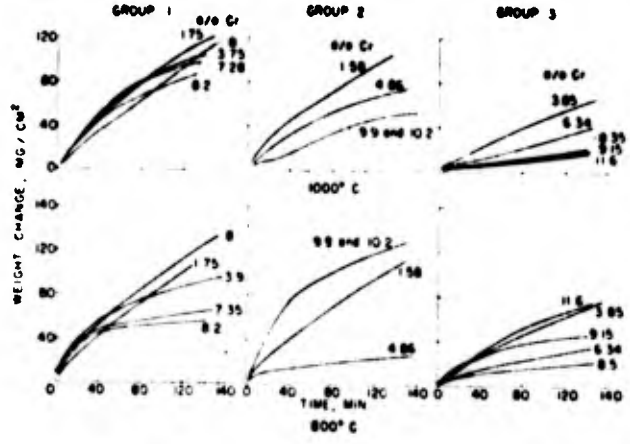

Figure 1.12. Effect of chromium content on oxidation rate for three groups of columbium-chromium alloys at 800° and 1000°C. (Barrett and Clauss[27]).

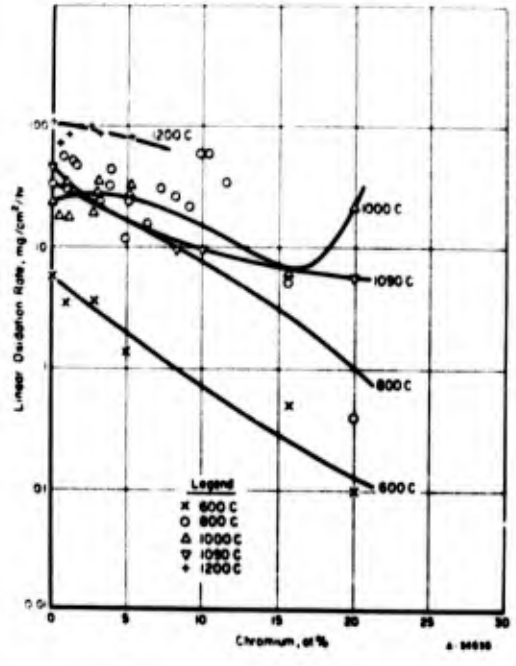

Figure 1.13. Oxidation rates of columbium-chromium alloys in air. (Klopp [2]).

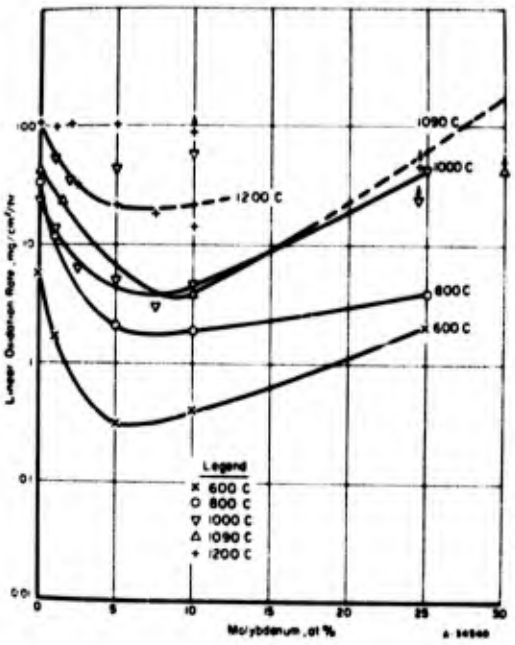

Figure 1.14. Oxidation rates of columbium-molybdenum alloys in air. (Klopp [20]).

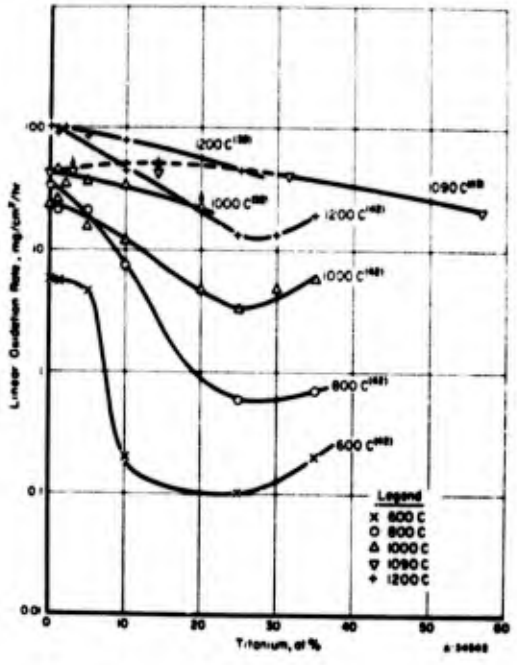

Figure 1.15. Oxidation rates of columbium-titanium alloys ir air. (Klopp [20]).

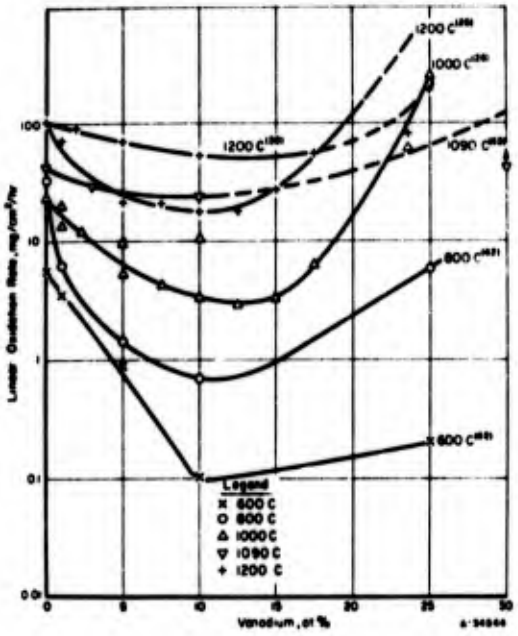

Figure 1.16. Oxidation rates of columbium-vanadium alloys in air. (Klopp (20)).

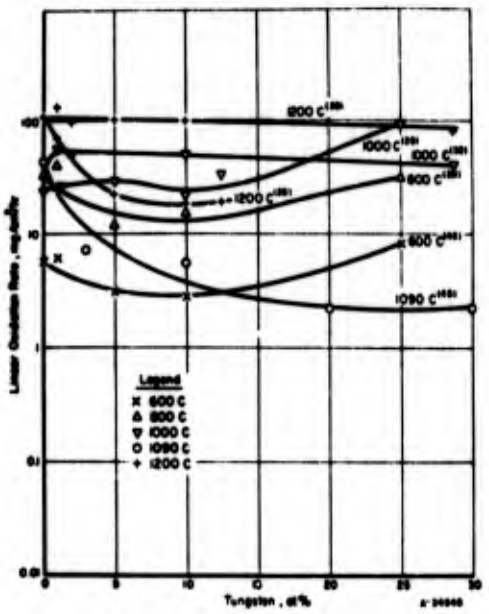

Figure 1.17. Oxidation rates of columbium-tungsten alloys in air. (Klopp (20)).

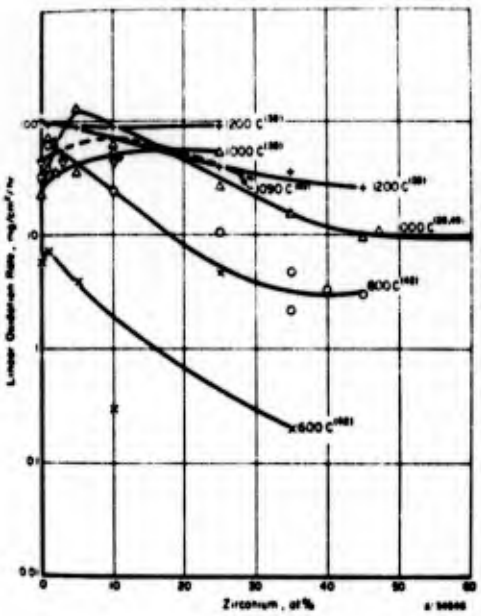

Figure 1.18. Oxidation rates of columbium-zirconium alloys in air. (Klopp (20)).

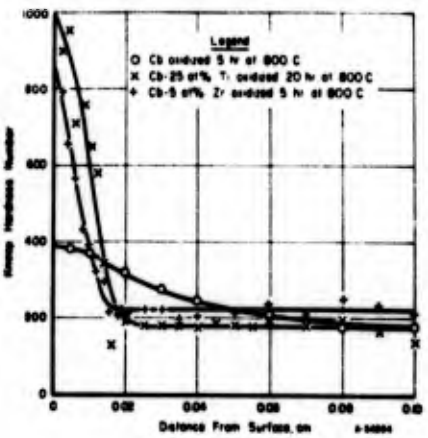

Figure 1.19. Contamination hardening of unalloyed columbium, columbium-25 at % titanium, and columbium-5 at % zirconium after air oxidation at 800 C (22).

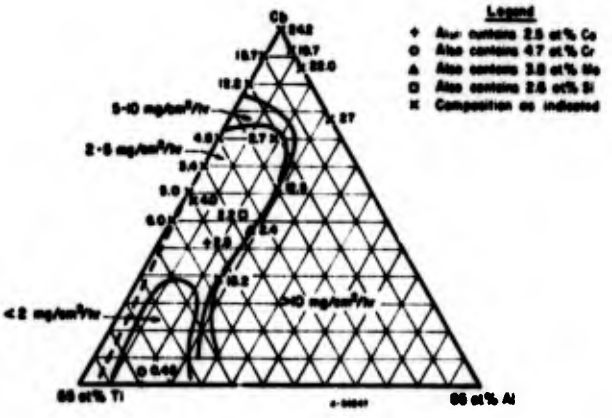

Figure 1.20. Oxidation rates of columbium-titanium-aluminium alloys at 1000 C (1830 F), with estimated constant-rate lines. (Klopp (20)).

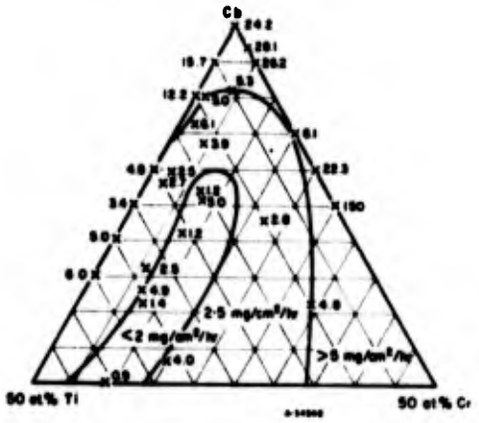

Figure 1.21. Oxidation rates of columbium-titanium-chromium alloys in air at 1000 C (1830 F) with estimated constant-rate lines (Klopp [20]).

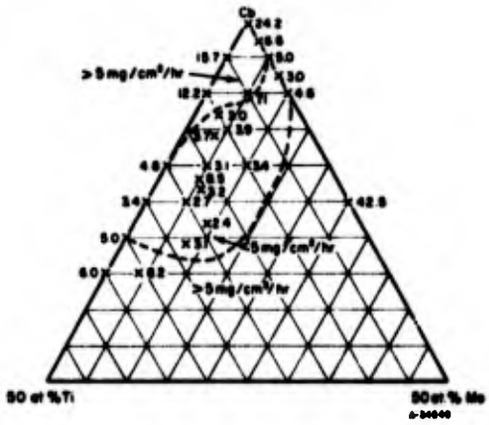

Figure 1.22. Oxidation rates of columbium-titanium-molybdenum alloys in air at 1000 C (1830 F), with estimated constant-rate lines. (Klopp [20]).

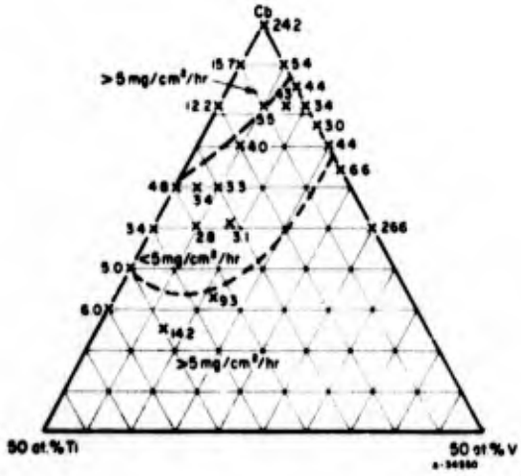

Figure 1.23. Oxidation rates of columbium-titanium-vanadium alloys in air at 1000 C (1830 F), with estimated constant-rate lines. (Klopp [20]).

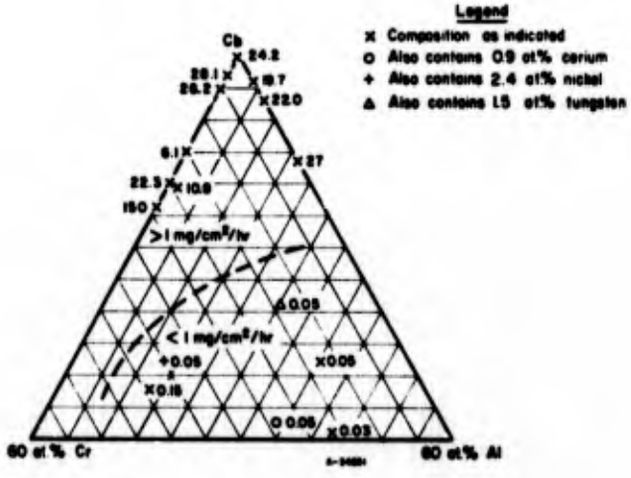

Figure 1.24. Oxidation rates of columbium-chromium-aluminium alloys in air at 1000 C (1830 F), with estimated constant-rate line. (Klopp [20]).

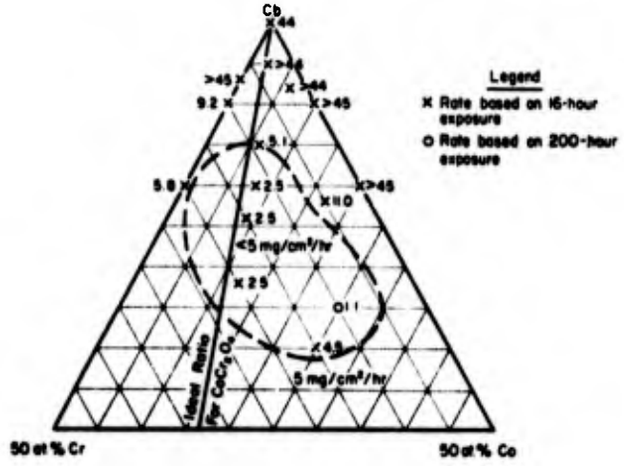

Figure 1.25. Oxidation rates of columbium-chromium-cobalt alloys in air at 1090 C (2000 F), with estimated constant-rate line. (Klopp [20]).

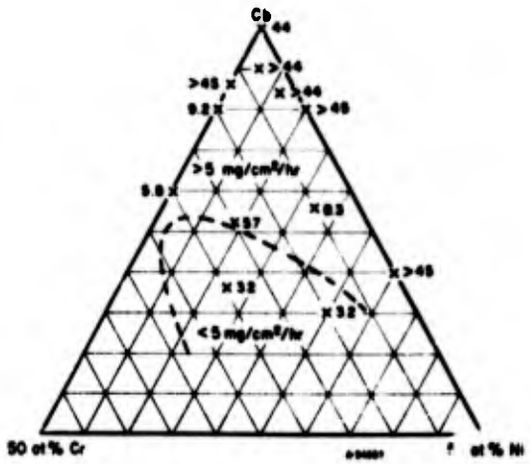

Figure 1.26. Oxidation rates of columbium-chromium-nickel alloys in air at 1090 C (2000 F) with estimated constant-rate line. (Klopp [20]).

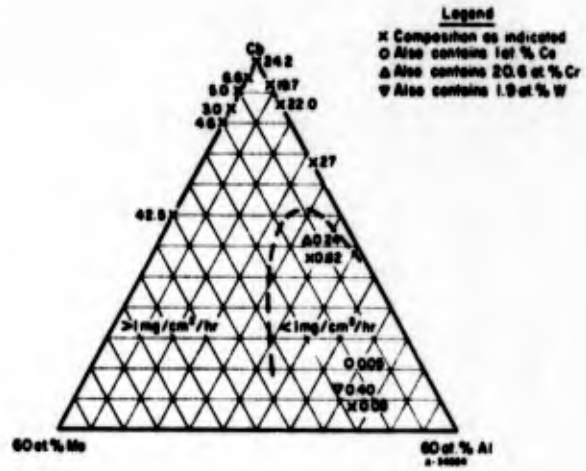

Figure 1.27. Oxidation rates of columbium-molybdenum-aluminium alloys in air at 1000 C (1830 F), with estimated constant-rate line. (Klopp [20]).

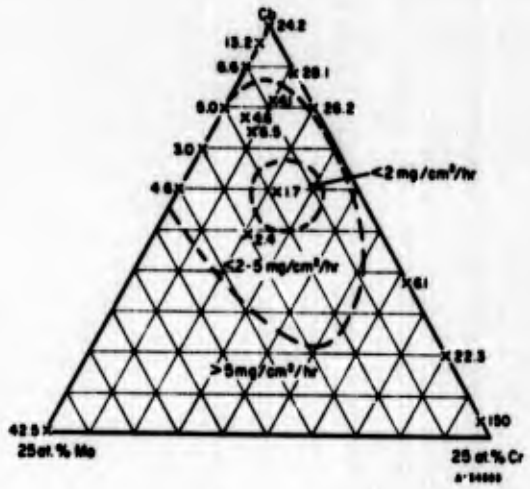

Figure 1.28. Oxidation rates of columbium-molybdenum-chromium alloys in air at 1000 C (1830 F), with estimated constant-rate lines. (Klopp [20]).

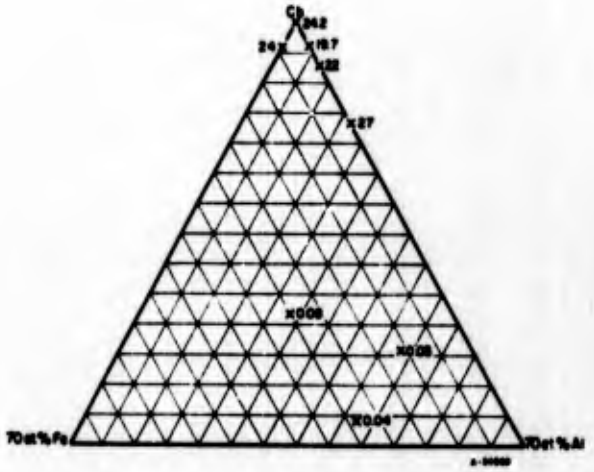

Figure 1.29. Oxidation rates of columbium-iron-aluminium alloys in air at 1000 C (1830 F) (Klopp[20]).

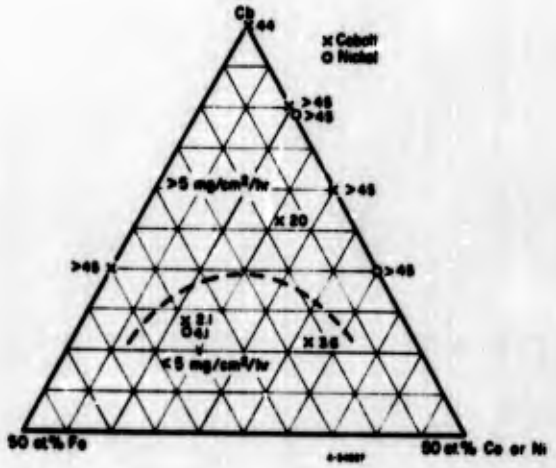

Figure 1.30. Oxidation rates of columbium-iron-cobalt and columbium-iron-nickel alloys at 1090 C (2000 F) in air, with estimated constant-rate line. (Klopp [20]).

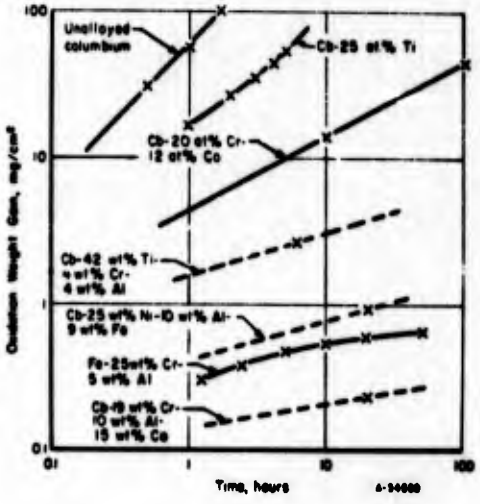

Figure 1.31. Comparison of oxidation behaviour of columbium and selected columbium alloys with FeCrAl in air at 1000 C (1830 F) (Klopp[20])

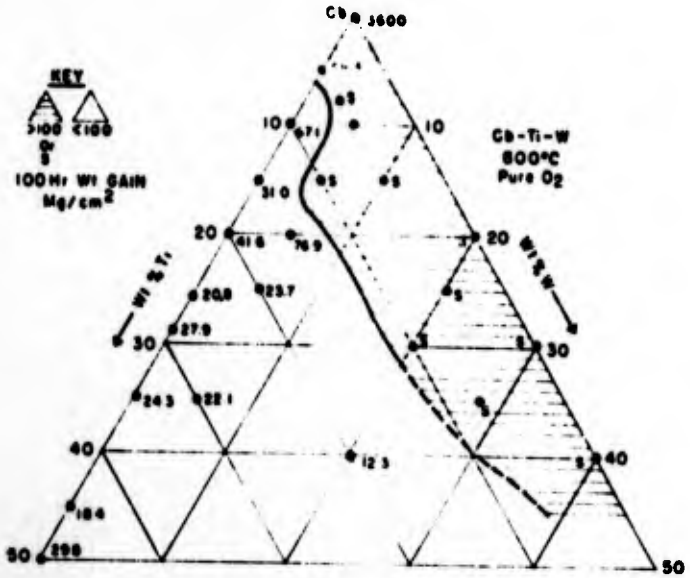

Figure 1.32. Isothermal plot of 100-hr weight gain at 800°C. Spalling (S) denotes a continually exfoliating oxidation product. (Wlodek [37]).

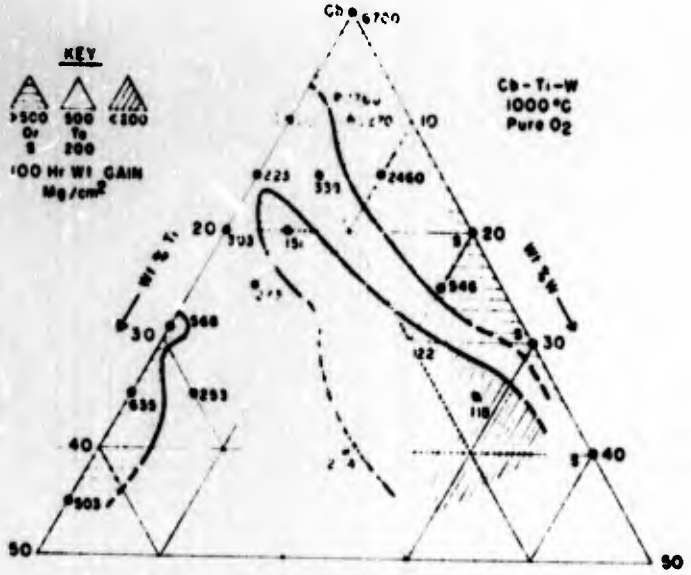

Figure 1.33. Isothermal plot of 100-hr weight gain at 1000°C. Spalling (S) denotes a continually exfoliating oxidation product. (Wlodek [37]).

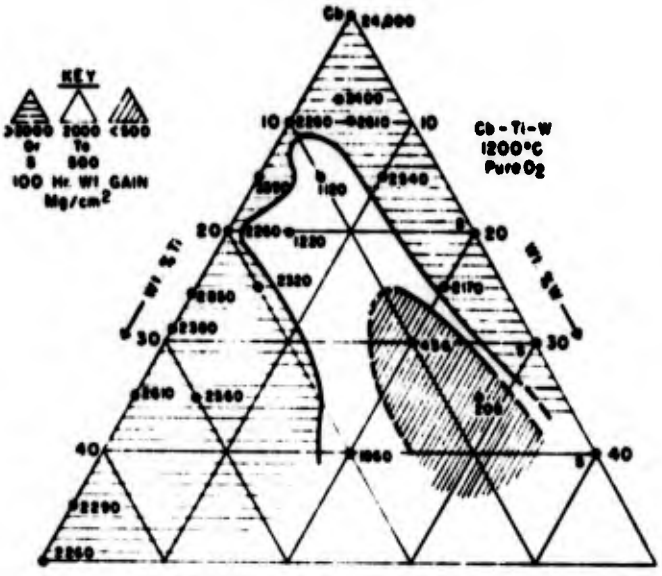

Figure 1.34. Isothermal plot of 100-hr weight gain at 1200°C. Spalling (S) denotes a continually exfoliating oxidation product. (Wlodek [37]).

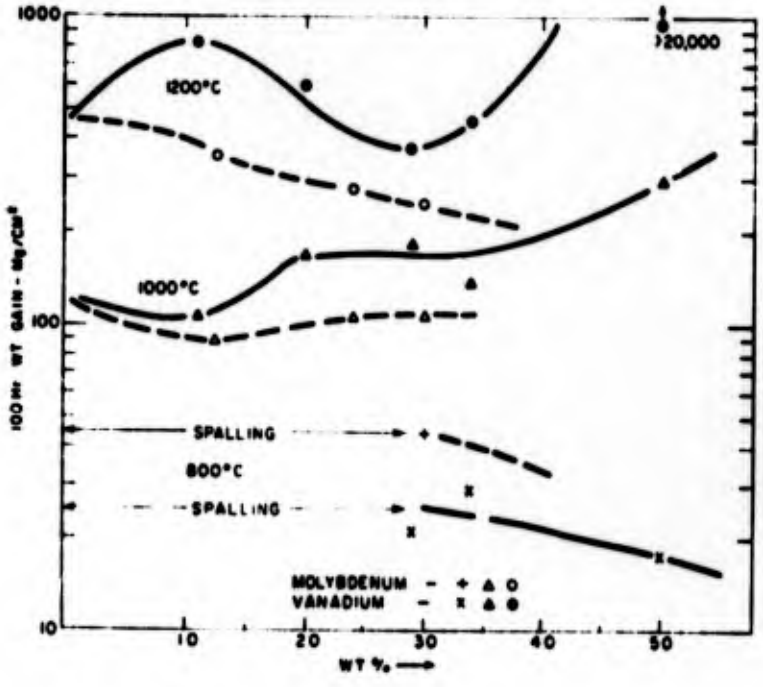

Figure 1.35. Effect of molybdenum and vanadium additions on the 800°C spalling of Cb-Ti-W alloys. (Wlodek [37]).

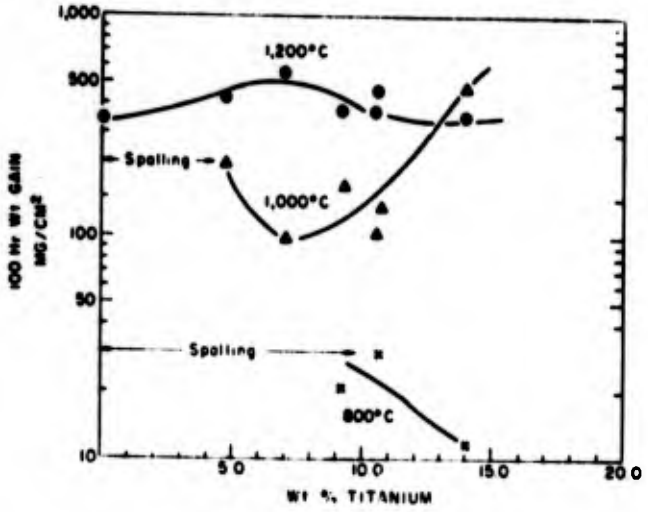

Figure 1.36. Effect of Ti on oxidation of 20W-3V-Cb alloy in O_2. (Wlodek [37]).

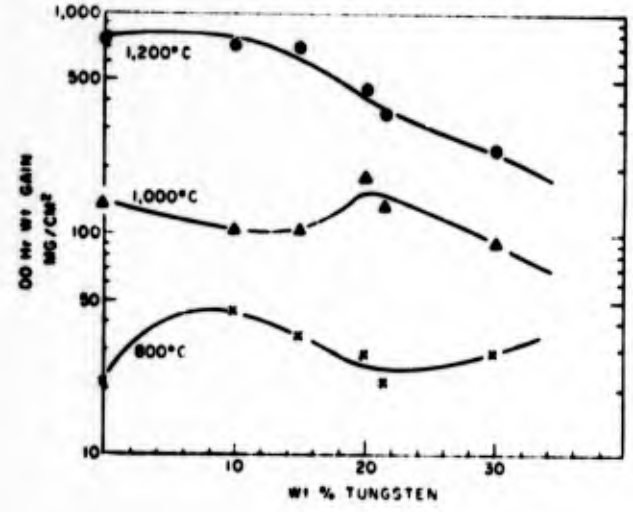

Figure 1.37. Effect of W on oxidation of 10Ti-3V-Cb alloy in O_2. (Wlodek [37]).

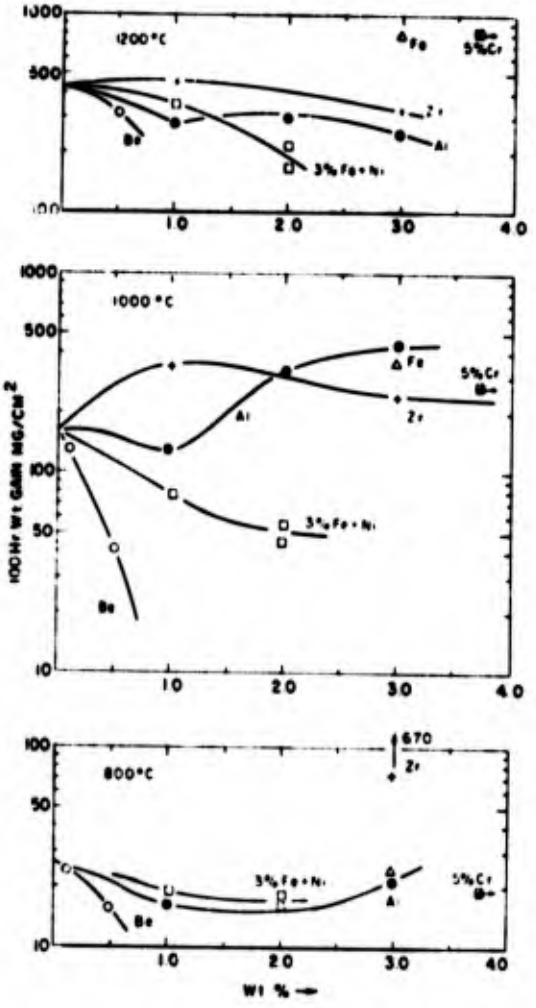

Figure 1.38. Effect of additions on oxidation of 67 Cb-20W-10Ti-3V alloy. (Wlodek [37]).

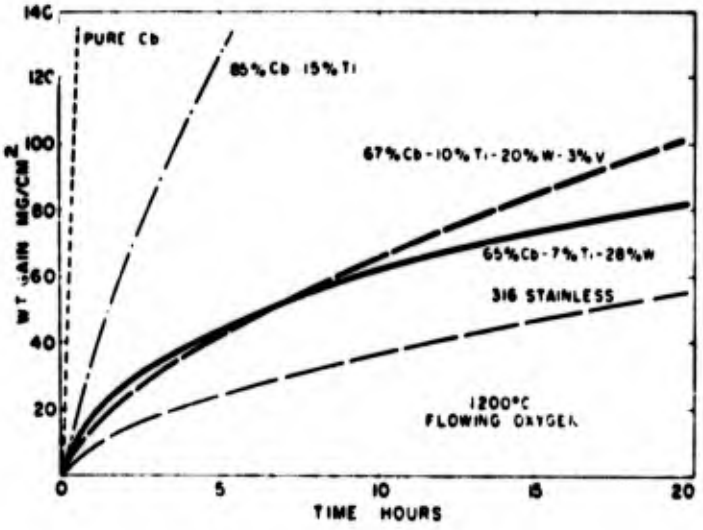

Figure 1.39. Rates of oxidation of Cb-Ti-W alloys compared with unalloyed Cb, an 85% Cb-15% Ti alloy, and 316 stainless steel. (Wlodek [37]).

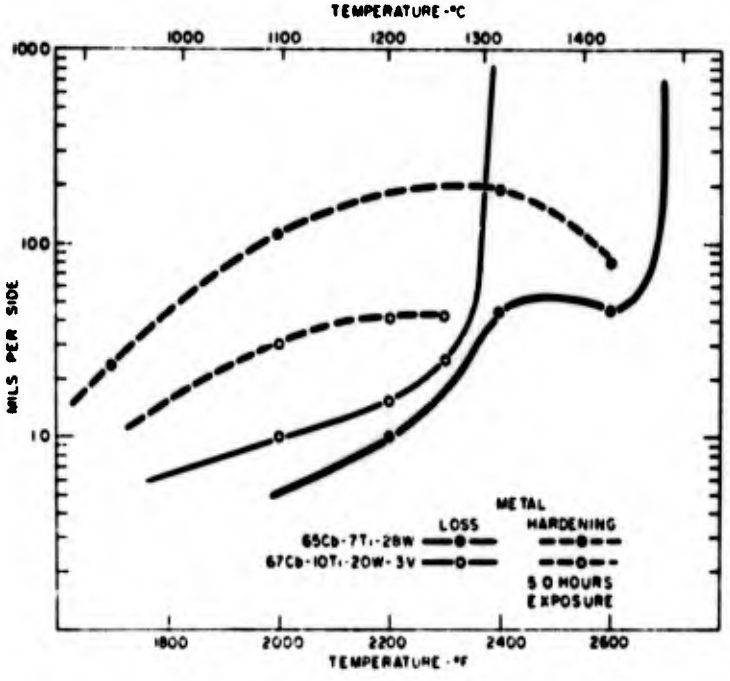

Figure 1.40. Air oxidation of Cb-Ti-W alloys. Effect of temperature on metal loss and internal hardening. (Wlodek [37]).

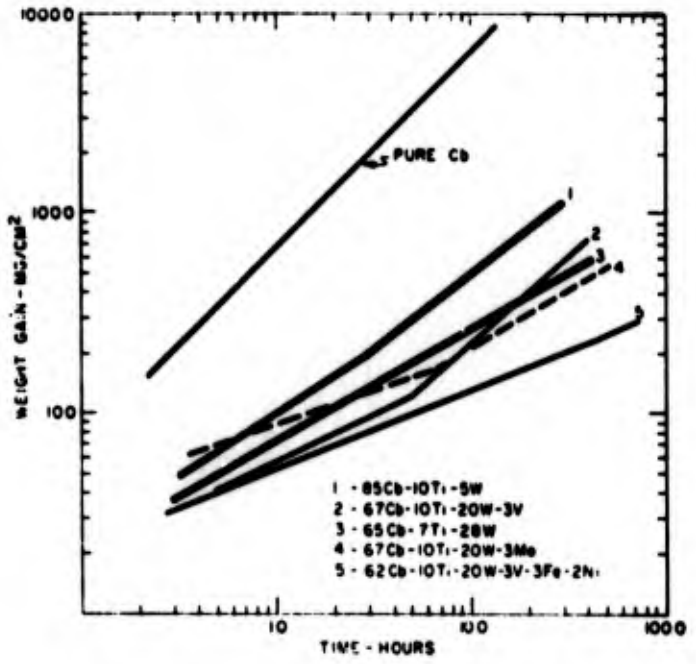

Figure 1.41. Kinetics of reaction at 1000°C. (Wlodek [37]).

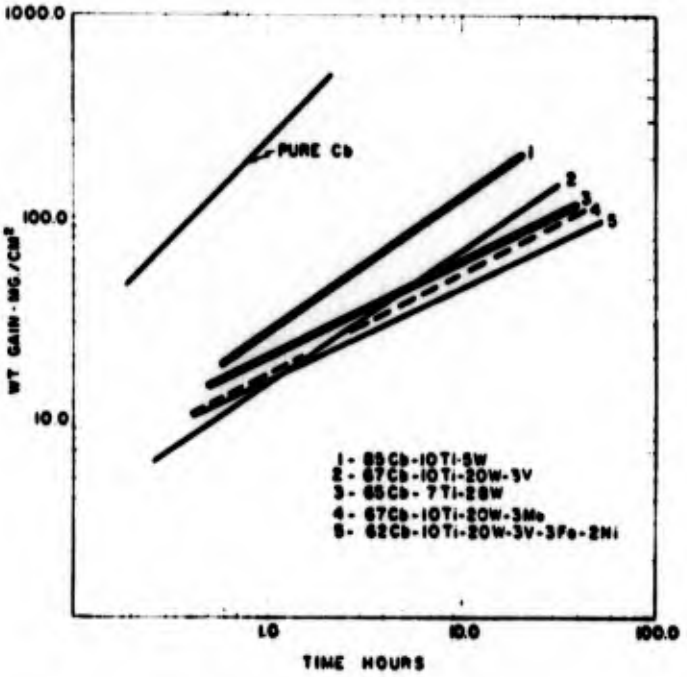

Figure 1.42. Kinetics of reaction at 1200°C. (Wlodek [37]).

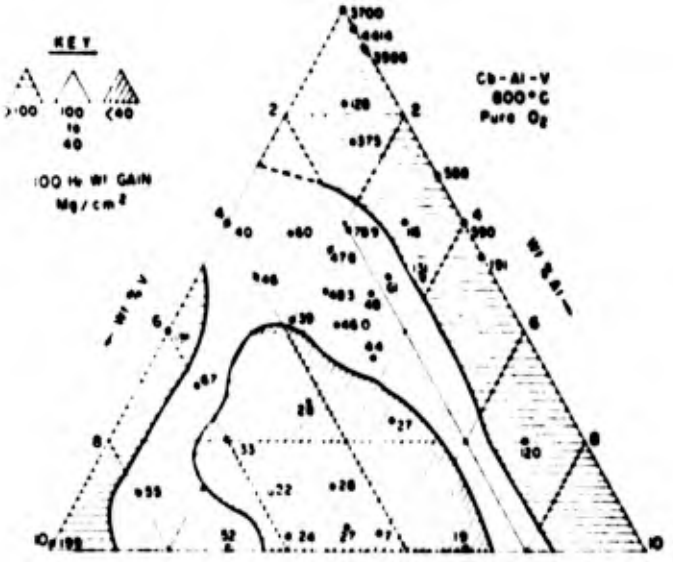

Figure 1.43. Isothermal plot of weight gain (100 hr) at 800°C. (Wlodek (38)).

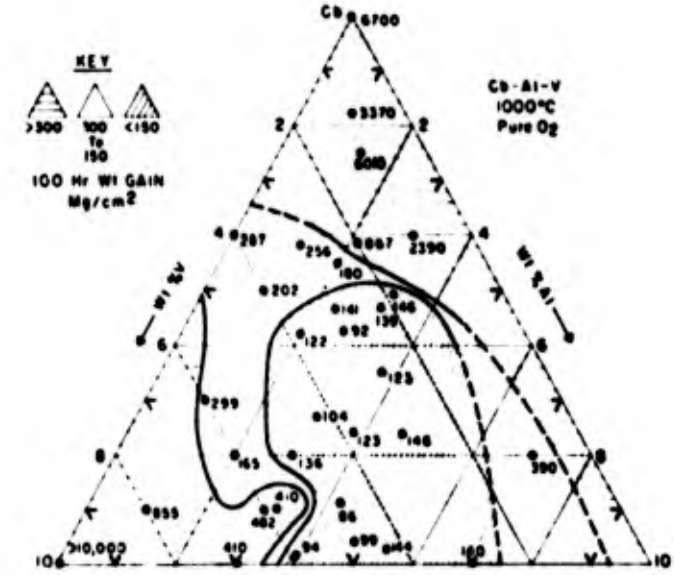

Figure 1.44. Isothermal plot of weight gain (100 hr) at 1000°C. (Wlodek (38)).

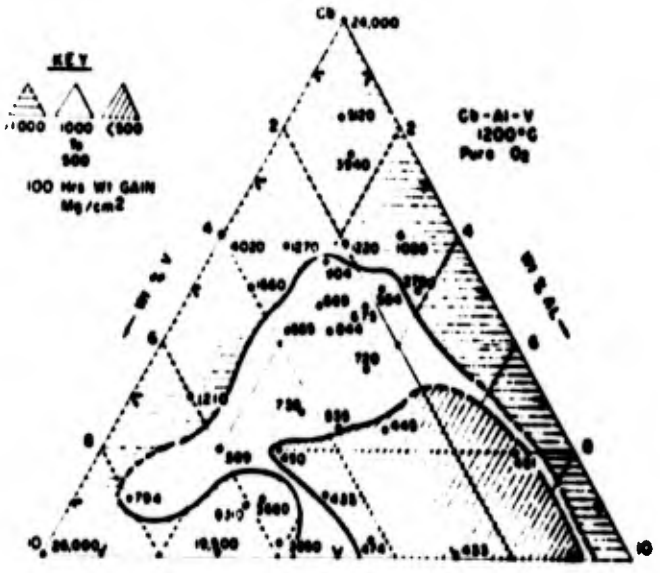

Figure 1.45. Isothermal plot of weight gain (100 hr) at 1200°C. (Wlodek [38]).

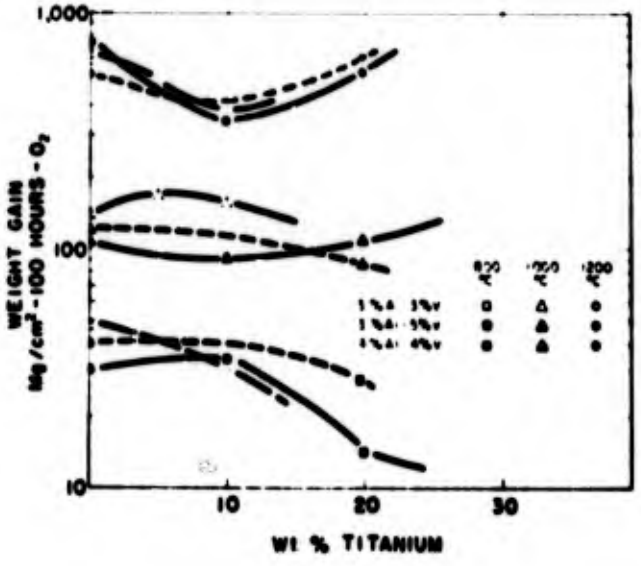

Figure 1.46. Effect of titanium on oxidation of Cb-Al-V alloy. The data for the titanium-free base corresponds to the composition closest to the analyzed quaternary alloys. (Wlodek [38]).

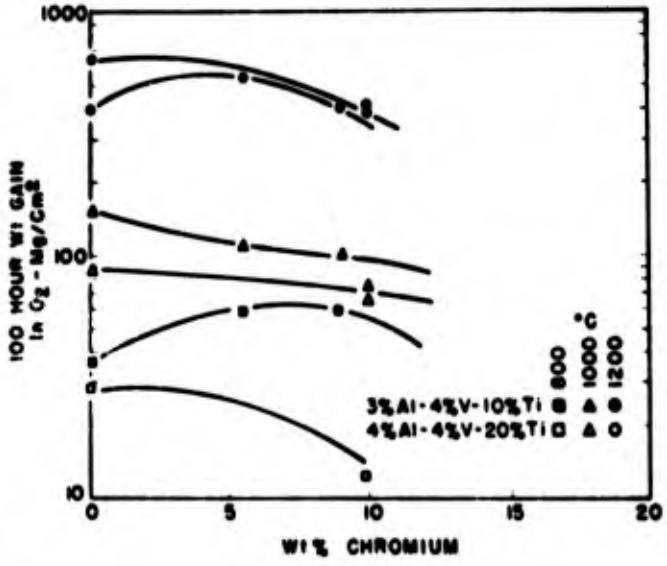

Figure 1.47. Effect of chromium on the oxidation of Cb-Ti-Al-V alloys. (Wlodek [38]).

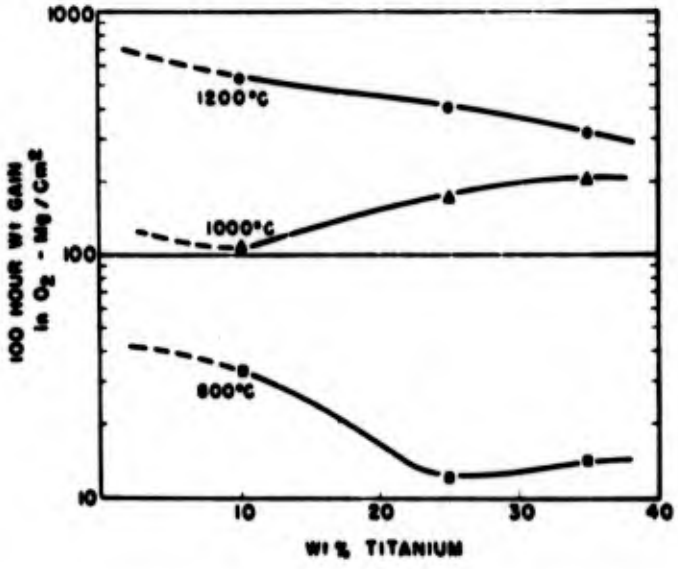

Figure 1.48. Effect of titanium additions on the oxidation of a Cb-8% Cr-3% Al-4% V alloy. (Wlodek [38]).

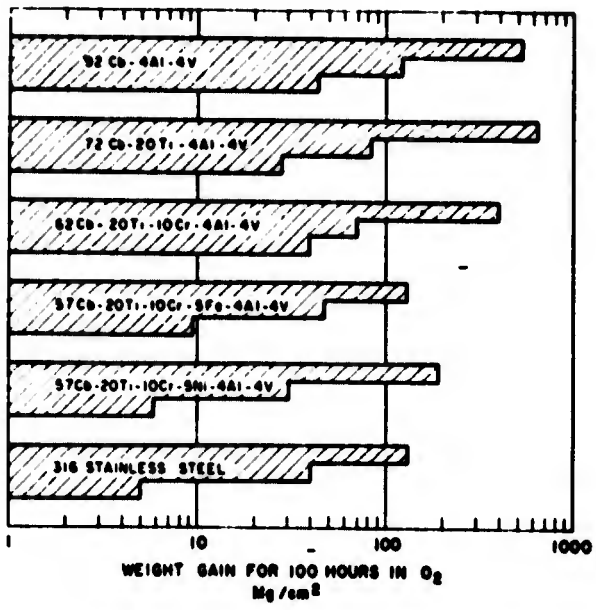

Figure 1.49. Effect of complexing additions on the oxidation of Cb-Al-V alloys. Comparison of oxidation resistance. For each alloy, the three steps in each horizontal bar represent weight-gain values at 1200, 1000, and 800°C, respectively. (Wlodek (38)).

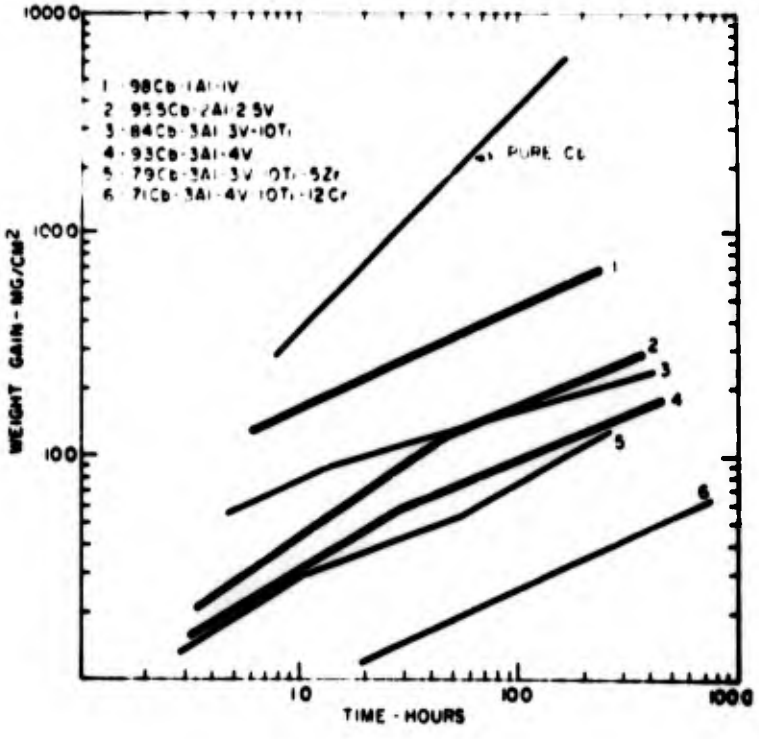

Figure 1.50. Kinetics of oxidation at 800°C. (Wlodek (38)).

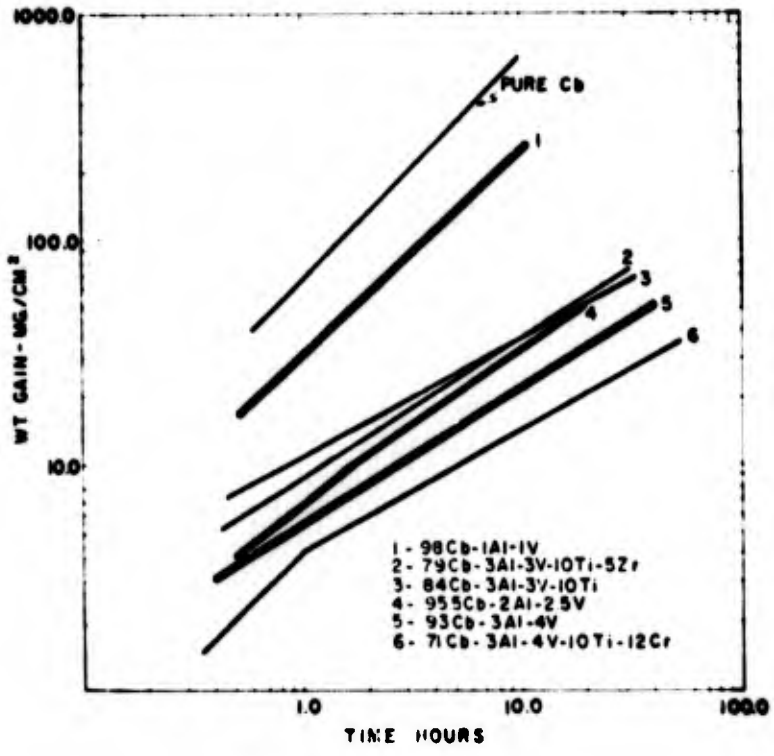

Figure 1.51. Kinetics of oxidation at 1000°C (Wlodek (38)).

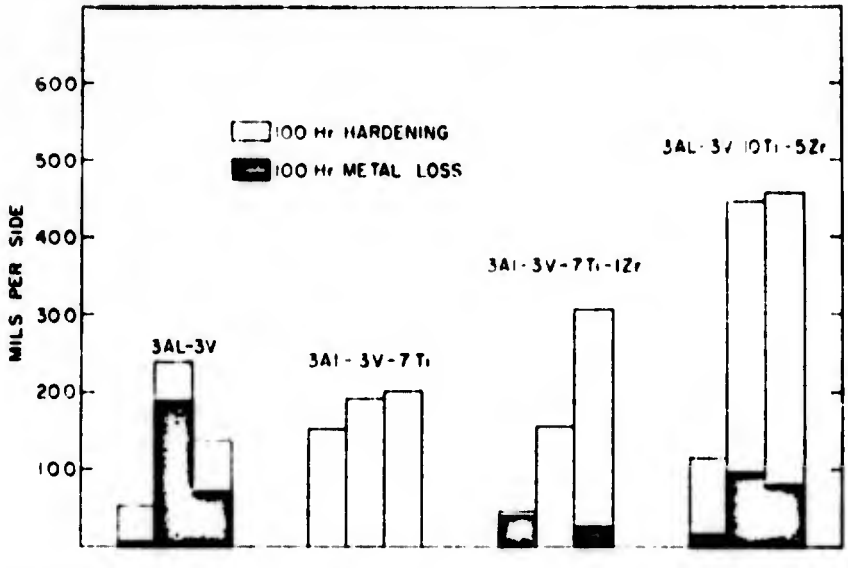

Figure 1.52. For each alloy the three vertical bars indicate the affected zone at 800, 900, and 1000°C, in that order. (Wlodek(38)).

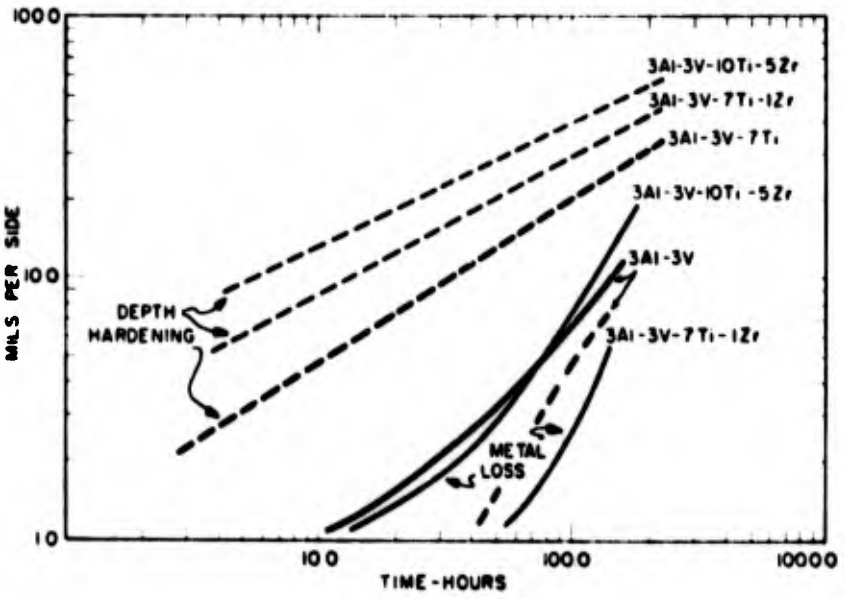

Figure 1.53. Depth of contamination of surface hardening shown by dotted lines. Full lines are used to present the depth of metal loss. (Wlodek [38]).

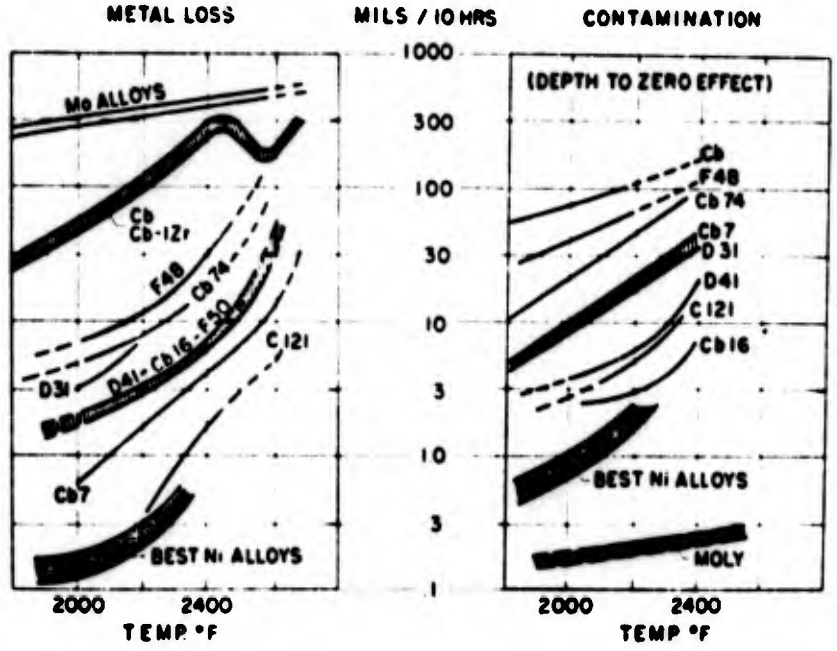

Figure 1.54. Oxidation of current molybdenum and columbium alloys. (Jahnke [39]).

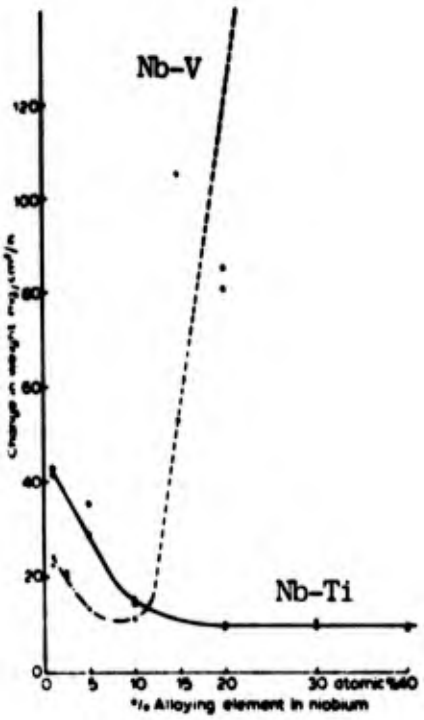

Figure 1.55. Oxidation resistance of niobium/titanium and niobium/vanadium alloys at 1,000°C. Niobium-titanium; niobium-vanadium. (Miller and Cox [40]).

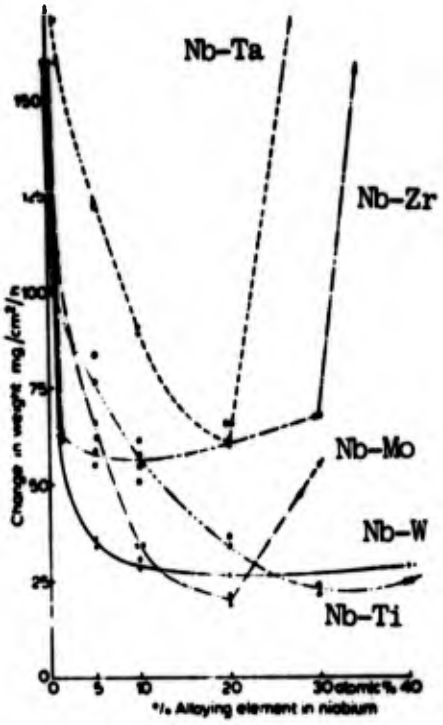

Figure 1.56. Oxidation resistance of binary niobium alloys at 1200°C Niobium-tungsten; niobium-tantalum; niobium-molybdenum; niobium-zirconium; niobium-titanium. (Miller and Cox [40]).

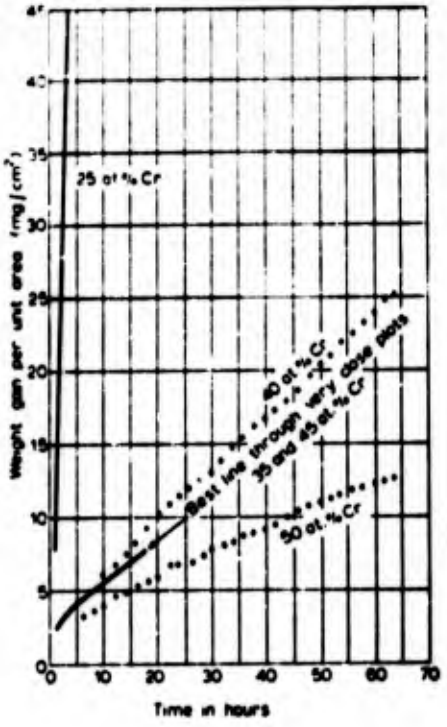

Figure 1.57. Oxidation of various niobium-chromium alloys in oxygen at 1100°C. (Mayo et al [41]).

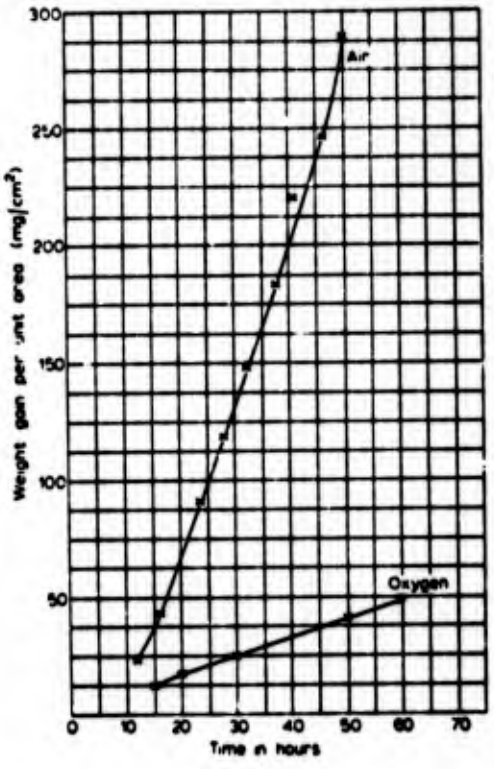

Figure 1.58. Oxidation of a 65-35 at. % niobium-chromium alloy in air and oxygen at 1100°C. (Mayo et al [41]).

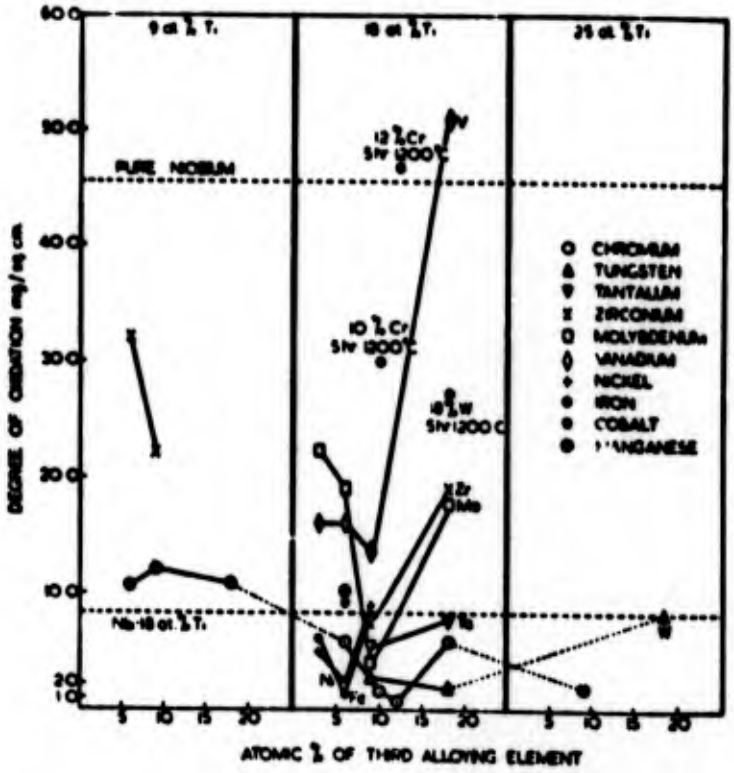

Figure 1.59. Degree of oxidation in air of ternary niobium alloys containing 8.19 at. % titanium after 1 h at 1100°C (1g rectangular specimens). (Smith [42]).

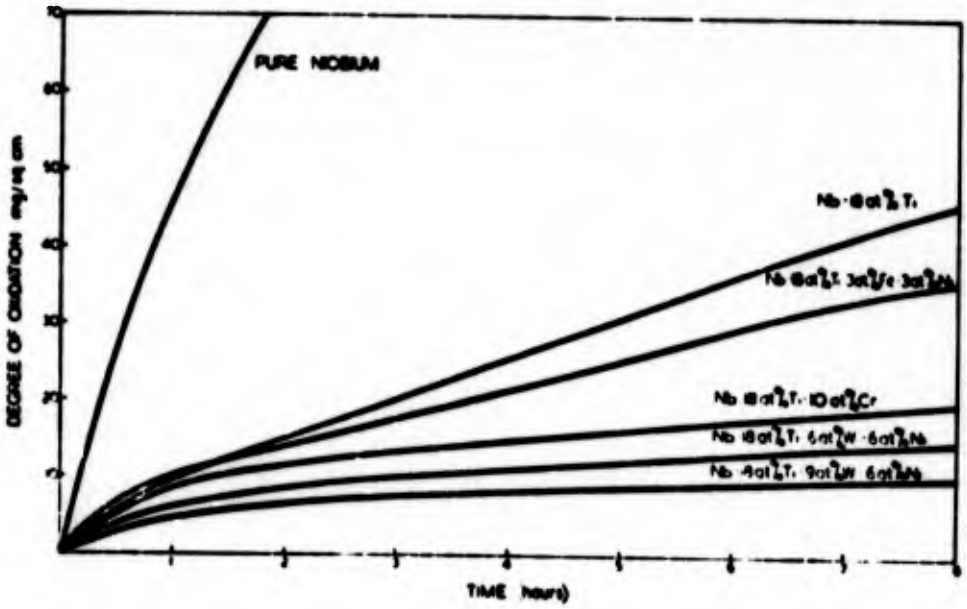

Figure 1.60. Oxidation of some niobium alloys in air at 1100°C. Weight increase continuously recorded by Pyrex spring balance. (Smith[42]).

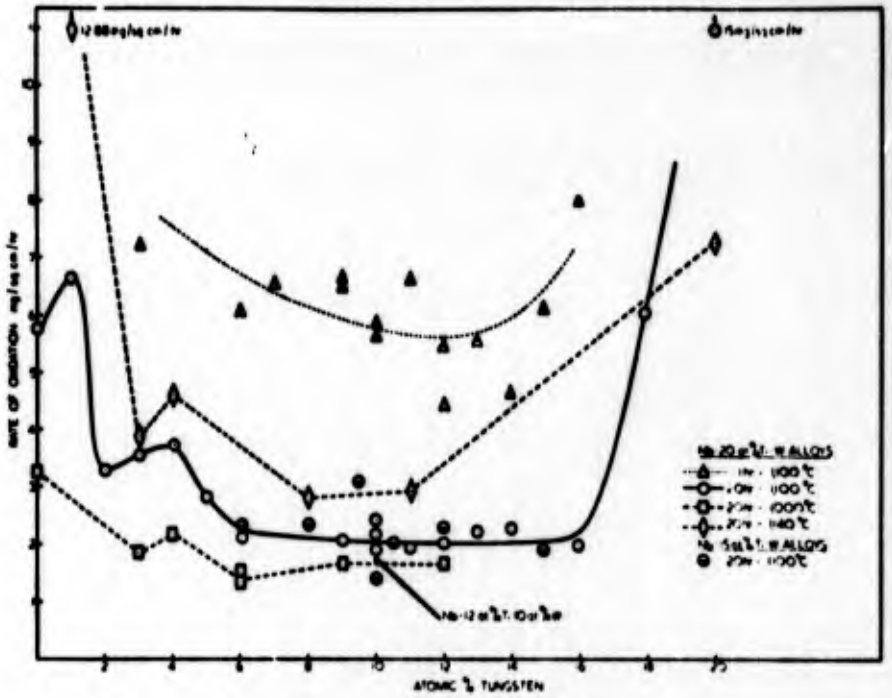

Figure 1.61. Oxidation rates of niobium-20 at.% titanium-tungsten alloys in air at 1000°C, 1100°C and 1140°C. (Smith [42]).

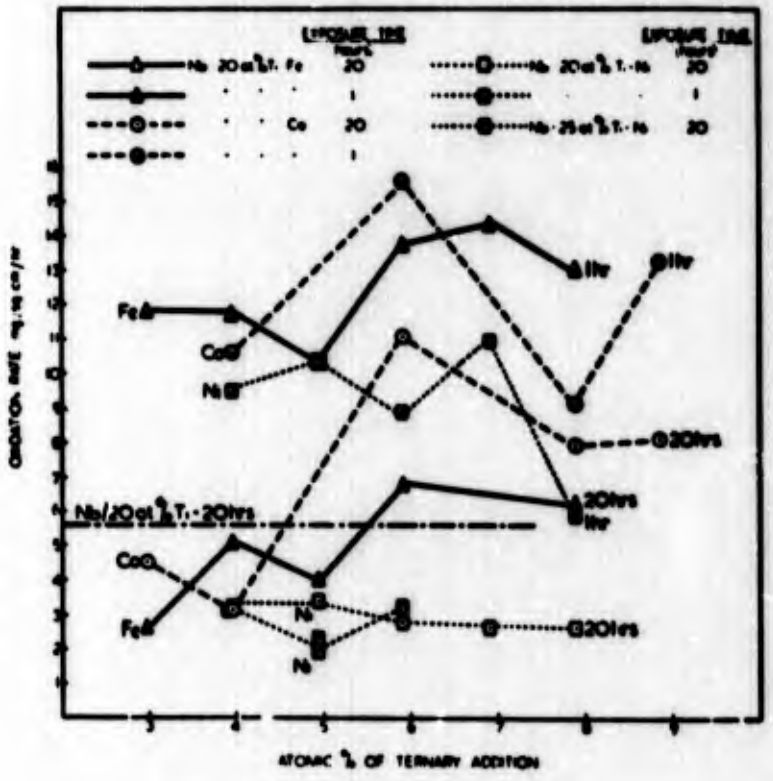

Figure 1.62. Oxidation rates in air at 1100°C of Nb-20 at.% Ti or Nb-25 at.% Ti alloys containing ternary additions of iron, nickel or cobalt. (Smith [42]).

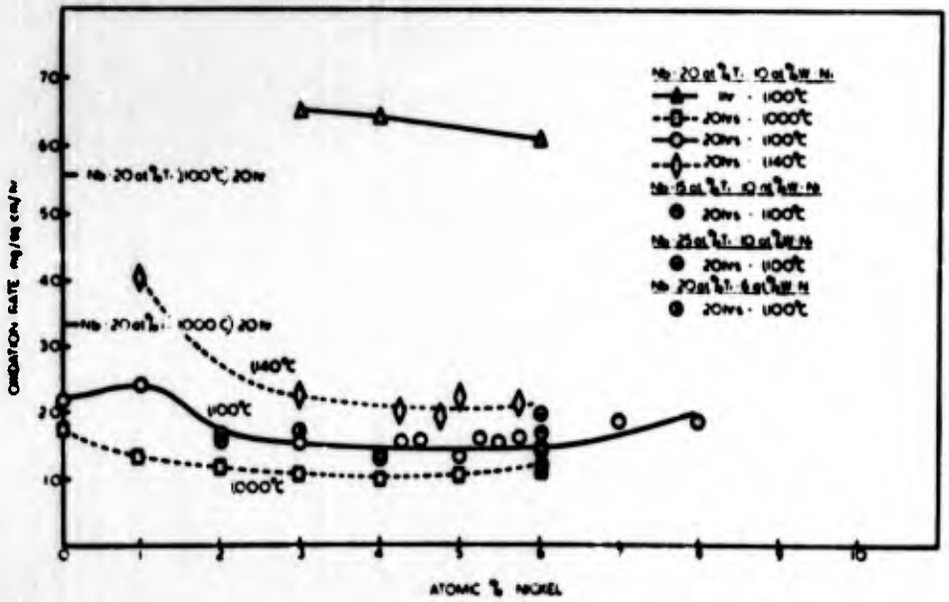

Figure 1.63. Oxidation rates of niobium-titanium-tungsten-nickel alloys in air at 1000°C, 1100°C and 1140°C. (Smith [42]).

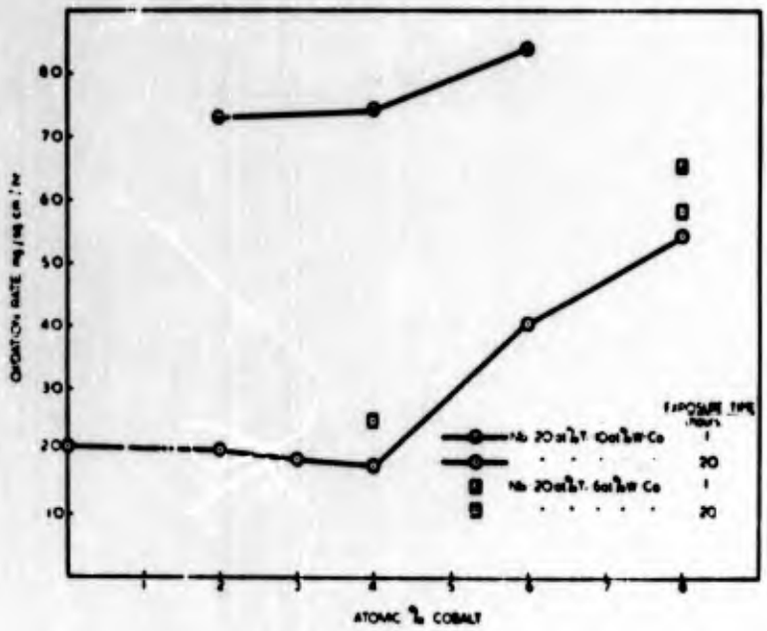

Figure 1.64. Oxidation rates of niobium-20 at.% titanium-tungsten-cobalt alloys in air at 1100°C. (Smith [42]).

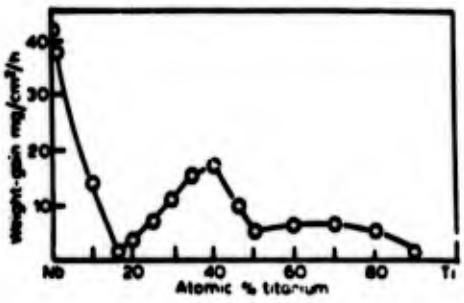

Figure 1.65. Weight-gain oxidation rates for niobium-titanium alloys exposed at 1050°C to moist air (Saturated with water at room temperature.) (Argent and Phelps[43]).

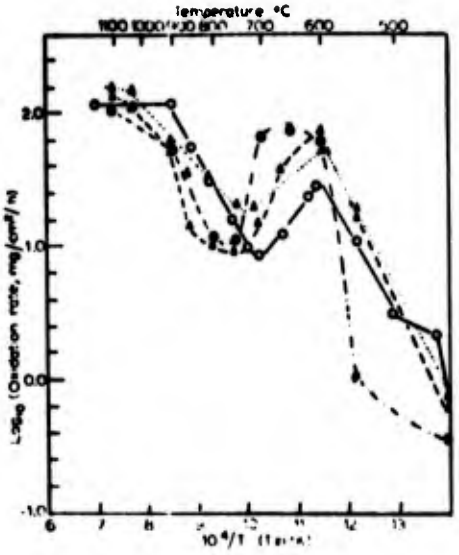

Figure 1.66. Log_{10} (oxidation rate) plotted against 1/T for niobium-titanium alloys exposed to dry oxygen. Pure niobium O; 3.5 at.% titanium ▲ ; 1.6 at.% titanium Δ ; 5.4 at.% titanium ● .
(Argent and Phelps [43]).

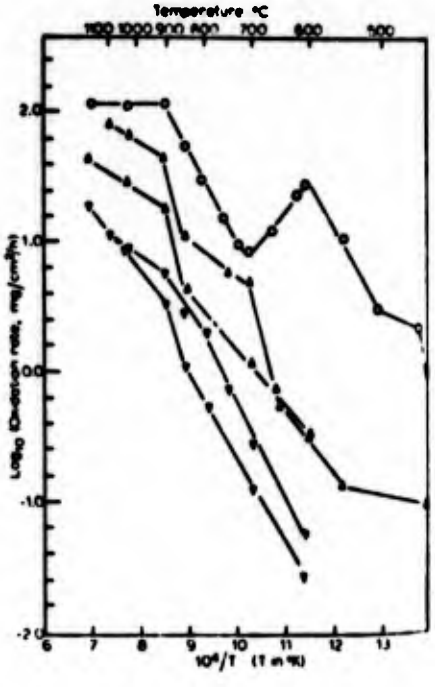

Figure 1.67. Log_{10} (oxidation rate) plotted against 1/T for niobium-titanium alloys exposed to dry oxygen. Pure niobium O; 9.8 at.% titanium ▲ ; 6.6 at.% titanium Δ ; 18.0 at.% titanium ▽ ; 25.0 at.% titanium ▼.
(Argent and Phelps [43]).

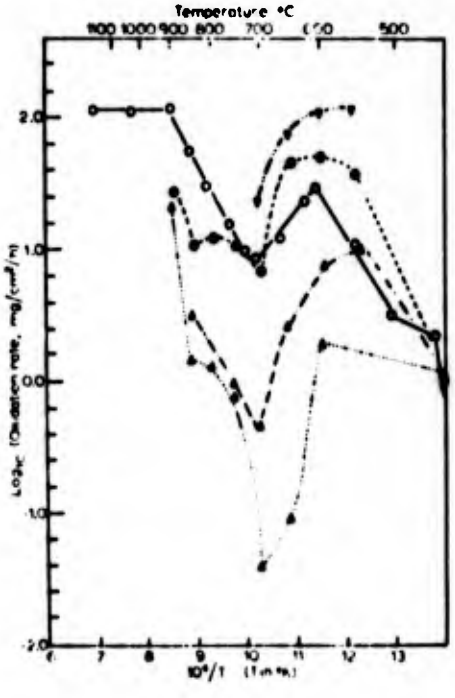

Figure 1.68. Log_{10} (oxidation rate) plotted against 1/T for niobium-molybdenum alloys exposed to dry oxygen. Pure niobium O; 1.0 at.% molybdenum ● ; 0.4 at.% molybdenum ▽ ; 1.9 at.% molybdenum ▲ ; 3.4 at.% molybdenum Δ .
(Argent and Phelps [43]).

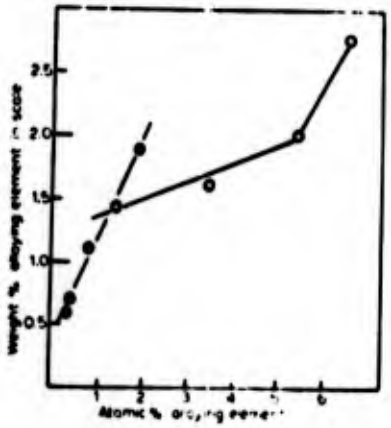

Figure 1.69. The concentration of titanium and molybdenum in scales formed on various alloys at 600°C. O titanium alloys; molybdenum alloys.
(Argent and Phelps [43]).

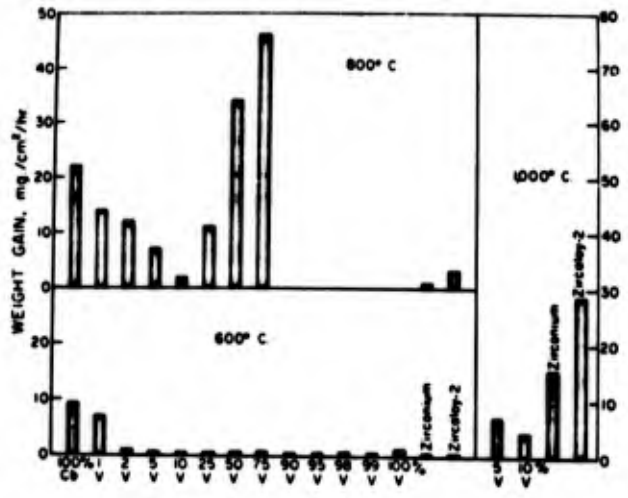

Figure 1.70. Oxidation rates of columbium-vanadium alloys in air.
(Babitzke et al [46]).

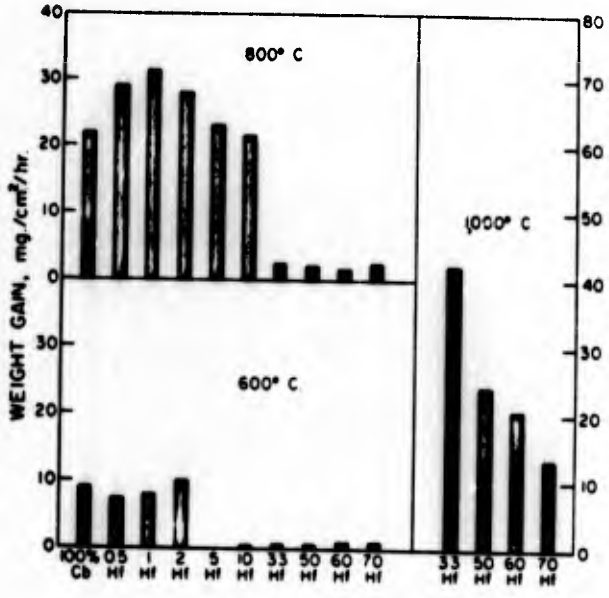

Figure 1.71. Oxidation rates of columbium-hafnium alloys in air.
(Babitzke et al [47]).

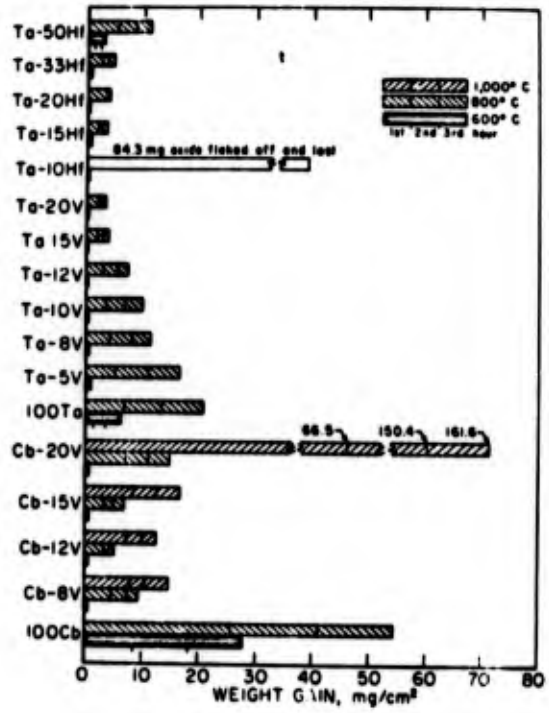

Figure 1.72. Weight gain of columbium-vanadium, tantalum-vanadium, and tantalum-hafnium alloys. (3-hour testing period).
(Babitzke et al [68]).

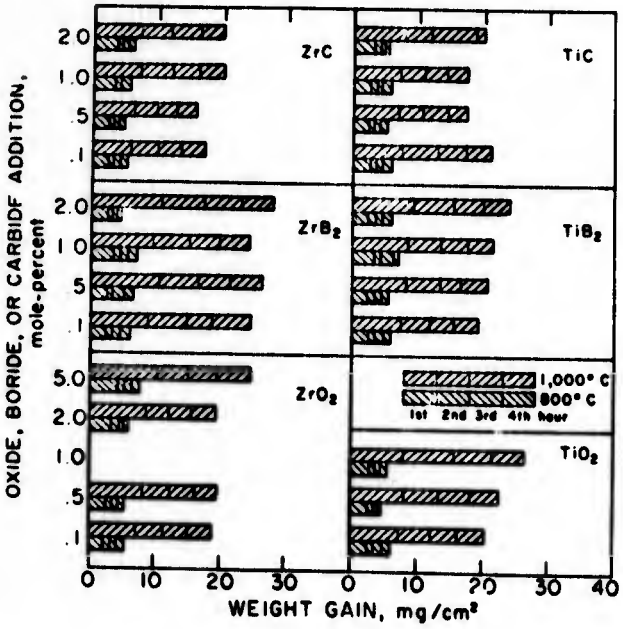

Figure 1.73. Weight gain of columbium-10 weight-percent titanium with additions of oxides, borides, or carbides. (4-hour testing period).
(Babitzke et al [48]).

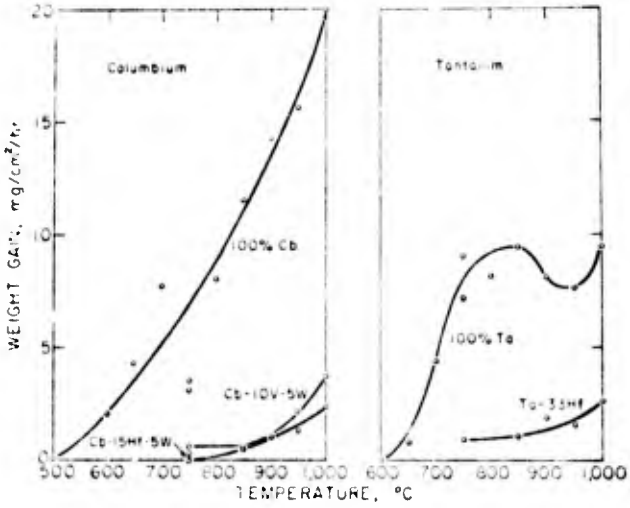

Figure 1.74. Columbium and tantalum alloy oxidation rates. (Babitzke et al, (49)).

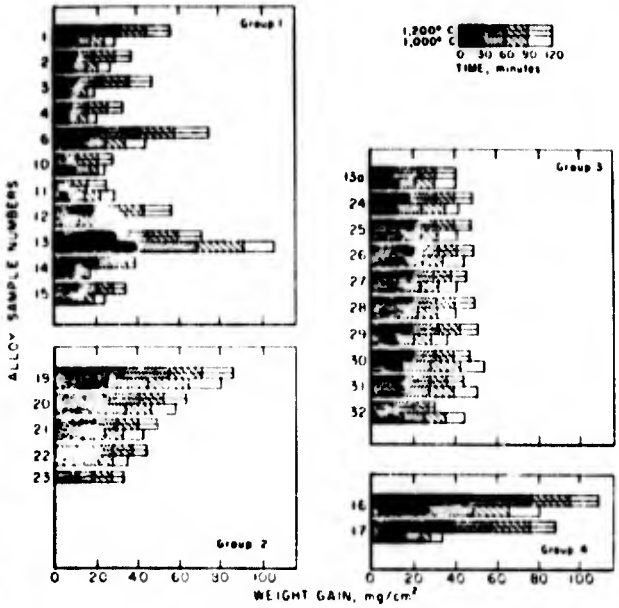

Figure 1.77. Oxidation data for columbium and tantalum alloys. (Babitzke et al (54)).

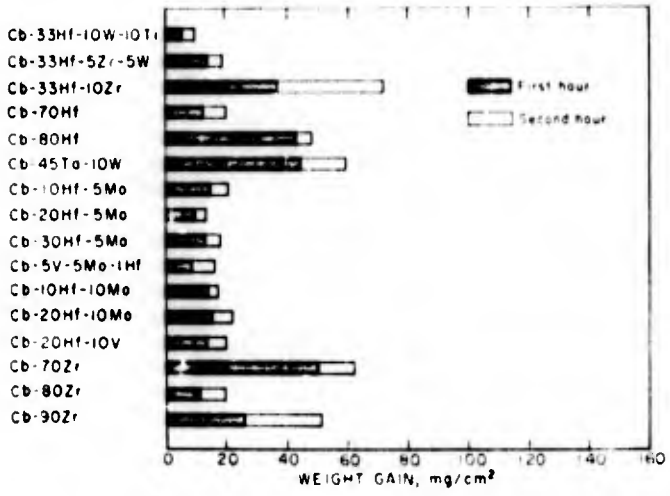

Figure 1.75. Oxidation data for columbium alloys - 1000°C. (Babitzke et al (51)).

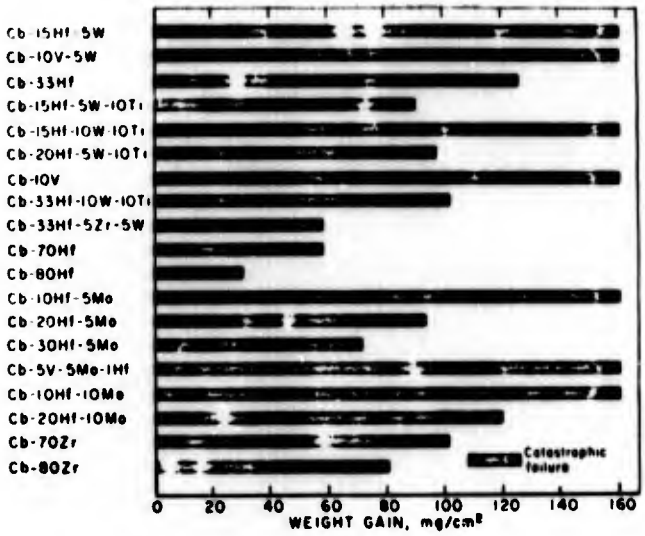

Figure 1.76. Oxidation data for columbium alloys - 1400°C. (Babitzke et al (51)).

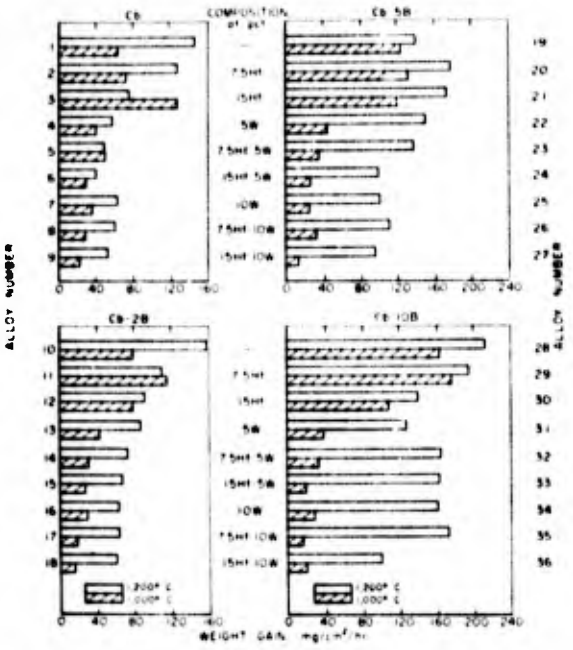

Figure 1.78. Oxidation data for columbium-hafnium-tungsten-boron alloys.
(Babitzke et al [55]).

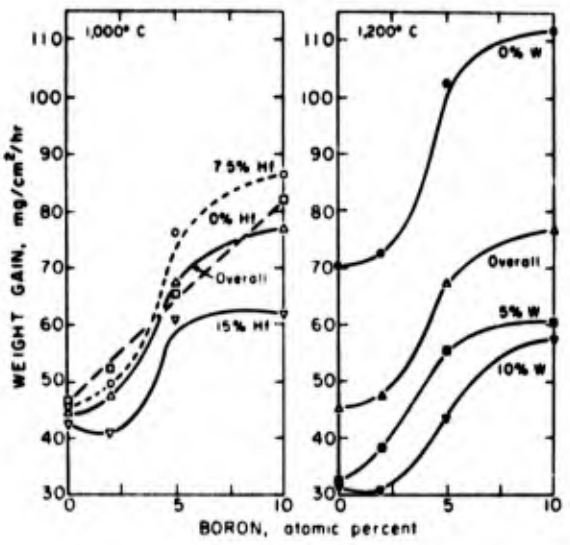

Figure 1.79. Influence of boron on oxidation resistance of columbium-hafnium and columbium-tungsten alloys.
(Babitzke et al [55]).

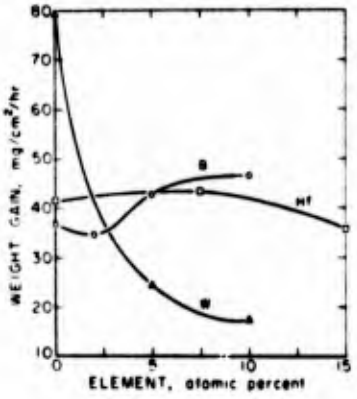

Figure 1.80. Oxidation data - individual influence due to hafnium, tungsten, or boron at 1000°C.
(Babitzke et al [55]).

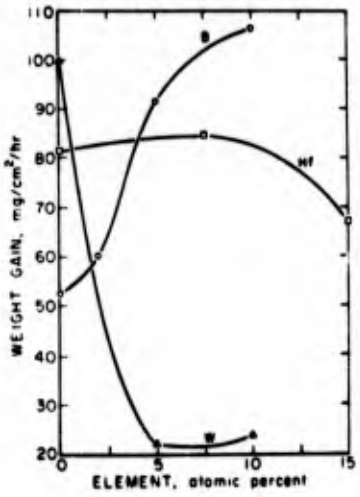

Figure 1.81. Oxidation data - individual influence due to hafnium, tungsten, or boron at 1200°C.
(Babitzke et al [55]).

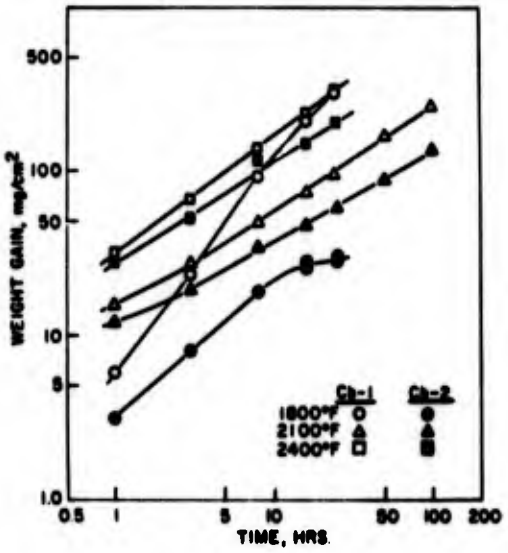

Figure 1.82. Effect of Oxidation time on weight-gain of Cb-base alloys. (Chang [56]).

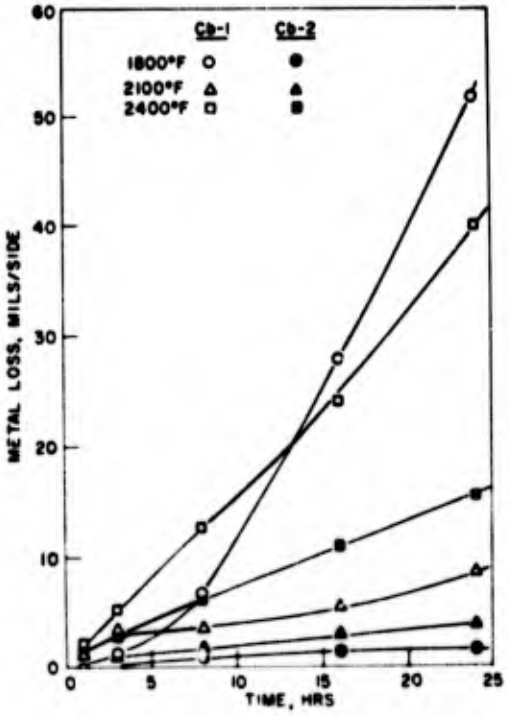

Figure 1.83. Effect of oxidation time on metal loss of Cb-base alloys. (Chang [56]).

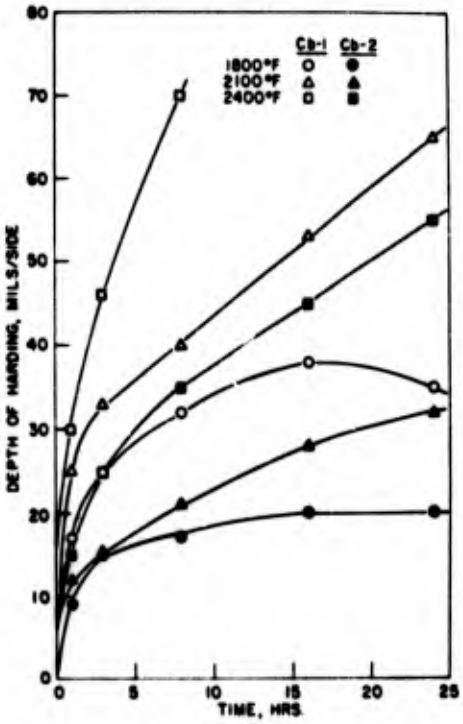

Figure 1.84. Effect of oxidation time on depth of hardening in Cb-base alloys. (Chang [56]).

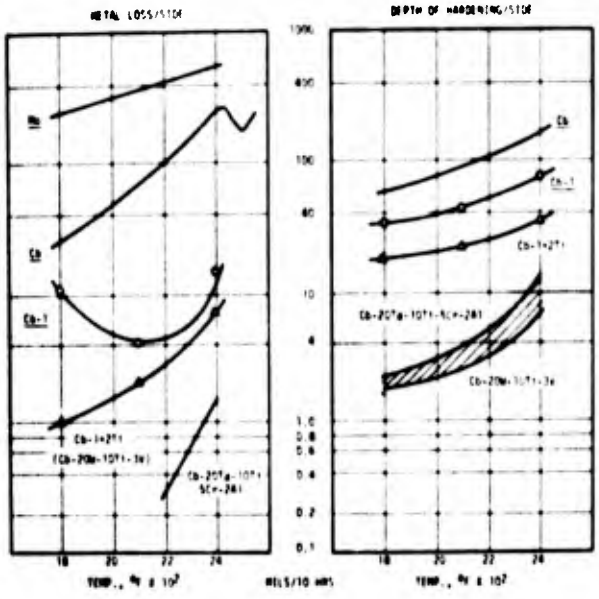

Figure 1.85. Oxidation of columbium alloys. (Frank [21]).

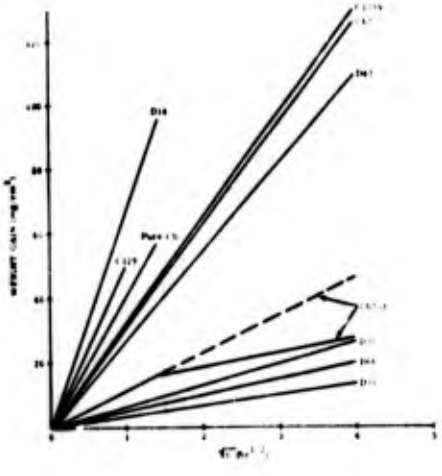

Figure 1.86. Oxidation rate plots of several uncoated substrate alloys; 1600°F. (Metcalfe and Stetson [58]).

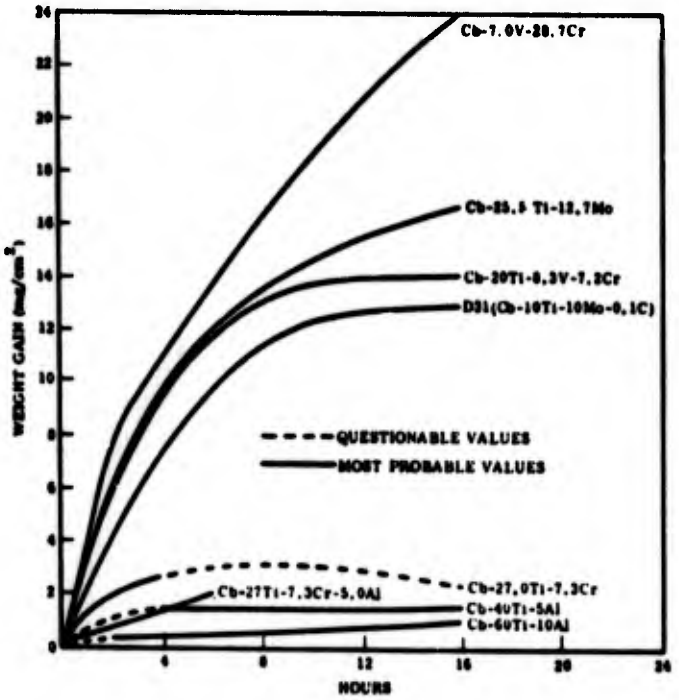

Figure 1.87. Summary of the most oxidation resistant ductile columbium alloy; 1600°F. (Metcalfe and Stetson [58]).

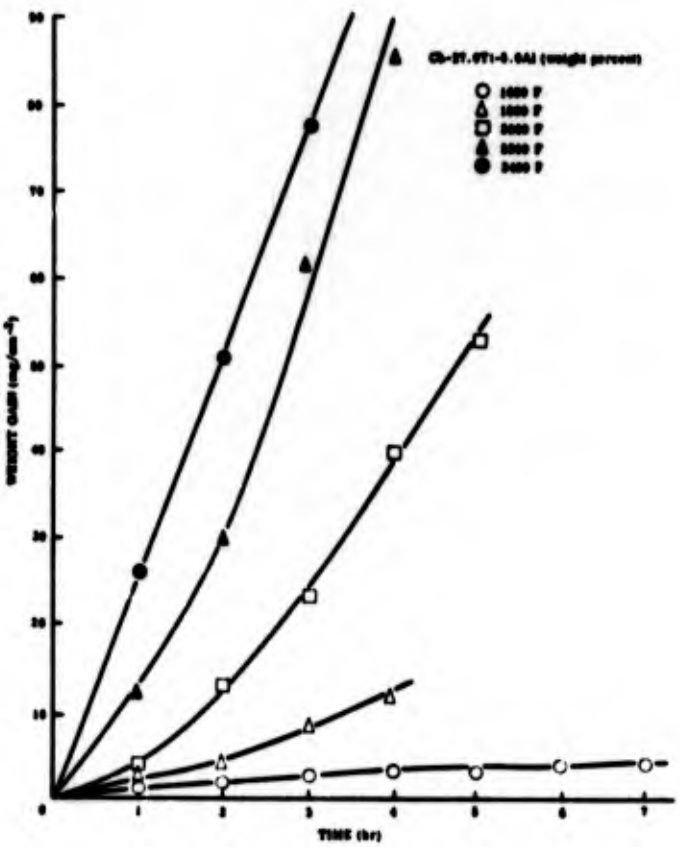

Figure 1.88. Oxidation rate of columbium-titanium-aluminium; one-hour cycles at 1600 to 2400°F. (Metcalfe and Stetson [58]).

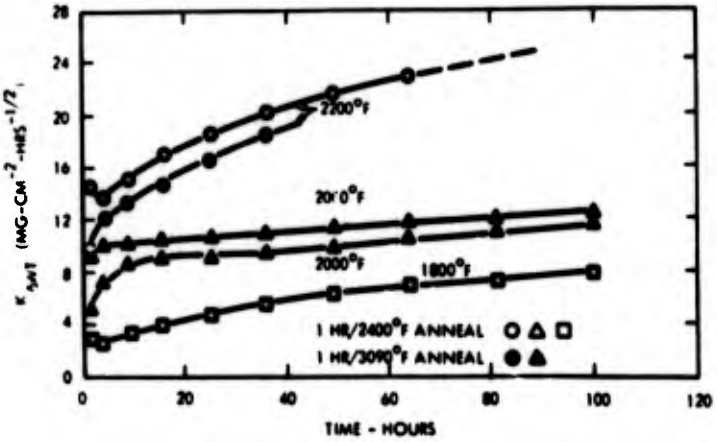

Figure 1.89. Weight gain behaviour of Cb-15 Ti-10 Ta-10 W-2Hf-3Al(B-1) alloy oxidized in flowing air (Cornie and Goodspeed (51)).

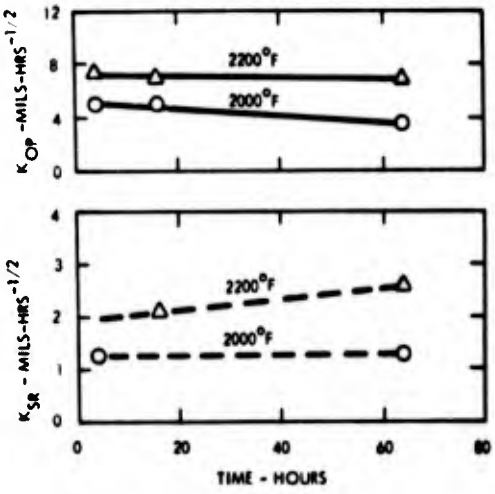

Figure 1.90. Oxygen penetration and surface recession behaviour of Cb-15Ti-10Ta-10W-2Hf-3Al(B-1) alloy oxidized at 2000 and 2200°F in air. (Cornie and Goodspeed (59))

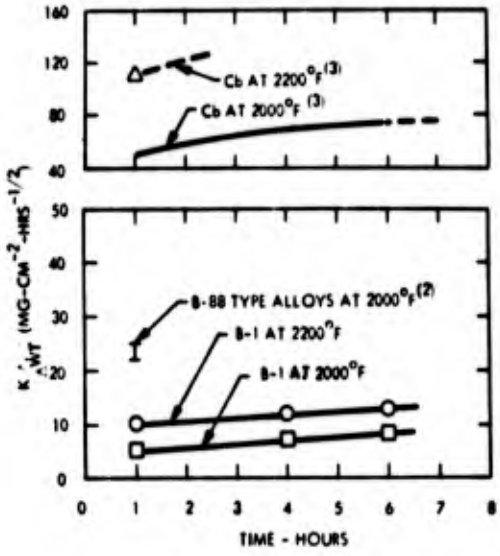

Figure 1.91. Comparison of the oxidation behaviour of pure Cb, high strength Cb alloys, and the oxidation resistant B-1 alloy in air at 2000 and 2200°F. (Cornie and Goodspeed (59)).

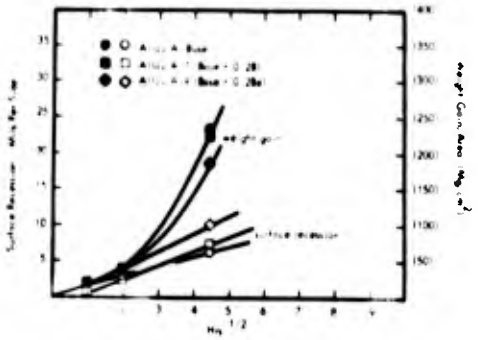

Figure 1.92. Weight gain and surface recession data for alloys A, A-7, and A-9. Exposed to air at 2200°F. (Cornie and Goodspeed (59)).

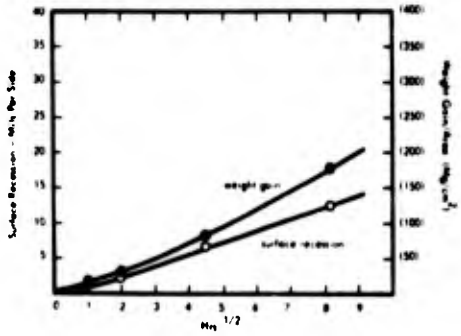

Figure 1.93. Weight gain and surface recession data for alloy A-1 (Base + 5Ti) exposed to air at 2200°F. (Cornie and Goodspeed (59)).

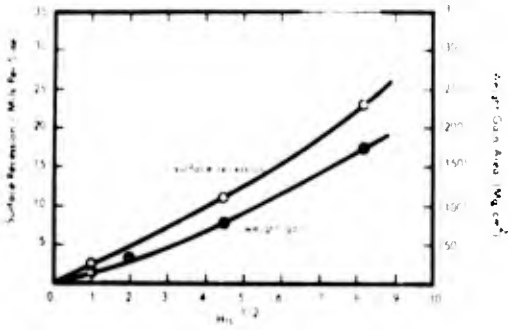

Figure 1.94. Weight gain and surface recession data for alloy A-2 (Base + 5Mo) exposed to air at 2200°F. (Cornie and Goodspeed (59)).

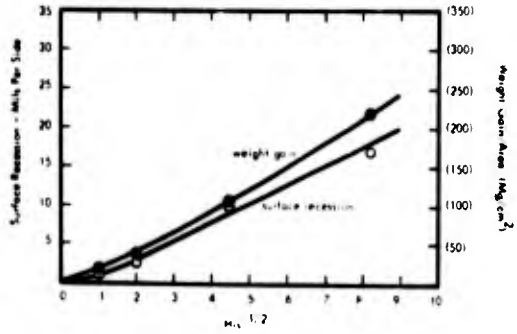

Figure 1.95. Weight gain and surface recession data for alloy A-3 (Base + 3V) exposed to air at 2200°F. (Cornie and Goodspeed (59)).

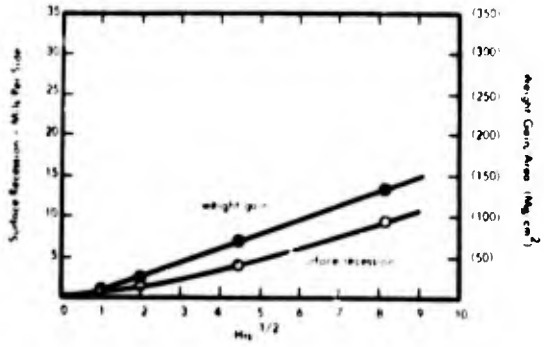

Figure 1.96. Weight gain and surface recession data for alloy A-4 (Base + 3Al) exposed to air at 2200°F. (Cornie and Goodspeed (59)).

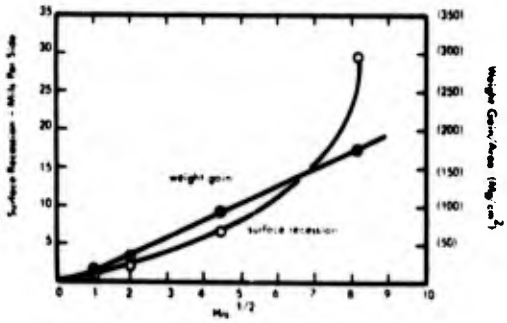

Figure 1.97. Weight gain and surface recession data for alloy A-5 (Base + 3Cr) exposed to air at 2200°F. (Cornie and Goodspeed (59)).

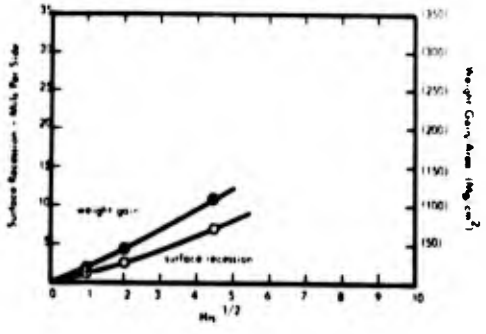

Figure 1.98. Weight gain and surface recession data for alloy A-6 (Base + 0.1Y) exposed to air at 2200°F (Cornie and Goodspeed (59)).

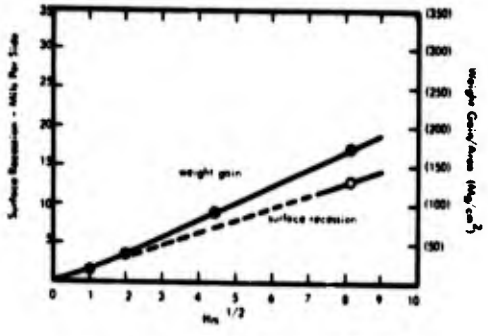

Figure 1.99. Weight gain and surface recession data for alloy A-8 (Base + 3Re) exposed to air at 2200°F. (Cornie and Goodspeed (59)).

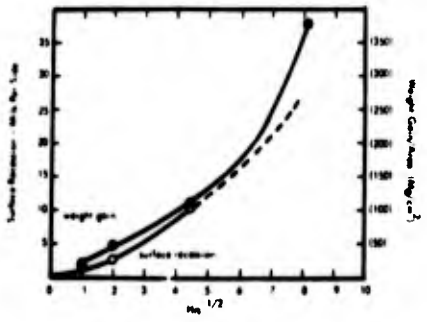

Figure 1.100. Weight gain and surface recession data for alloy A-10 (Base + 5U) exposed to air at 2200°F (Cornie and Goodspeed (59)).

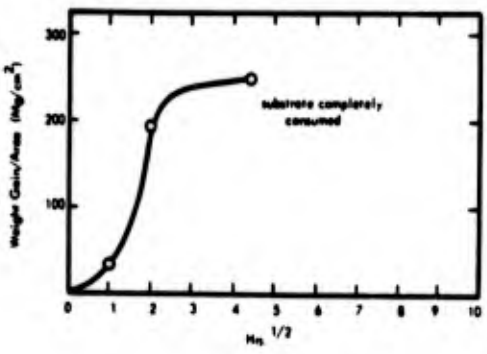

Figure 1.101. Weight gain data for B-66 (Cb-5V-5Mo-1Zr) exposed to air at 2200°F. (Cornie and Goodspeed (59)).

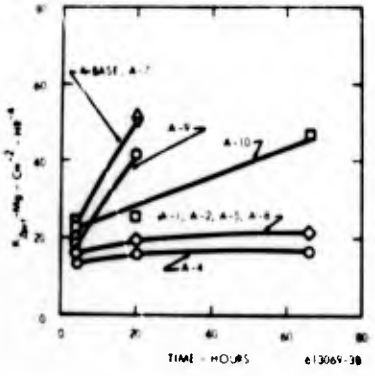

Figure 1.102. Weight gain data for A-series Cb base alloys oxidized in flowing air at 2200°F. (Cornie and Goodspeed (59)).

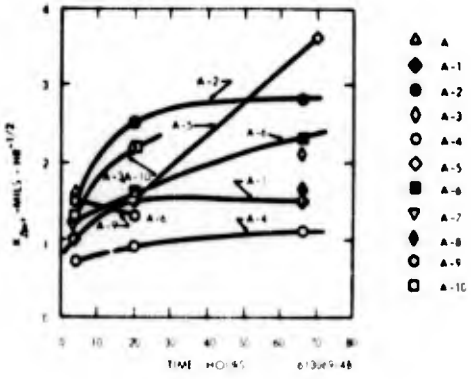

Figure 1.103. Surface recession data for A-series Cb base alloys oxidized in flowing air at 2200°F. (Cornie and Goodspeed (59)).

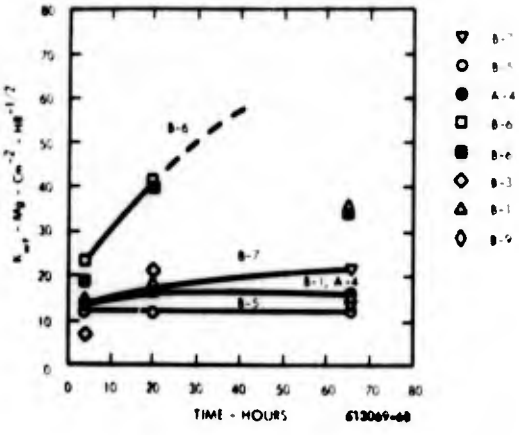

Figure 1.104. Weight gain data for B-Series Cb base alloys oxidized in flowing air at 2200°F. (Cornie and Goodspeed (59)).

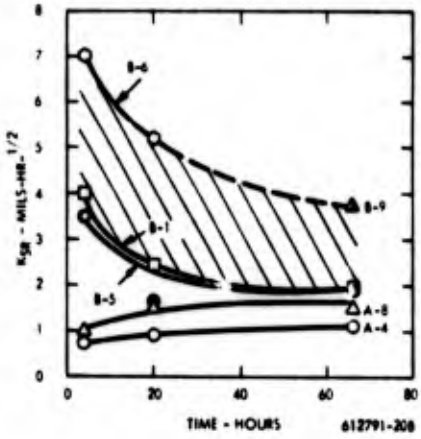

Figure 1.105. Surface recession data for B-Series Cb base alloys oxidized in flowing air at 2200°F. (Cornie and Goodspeed (59)).

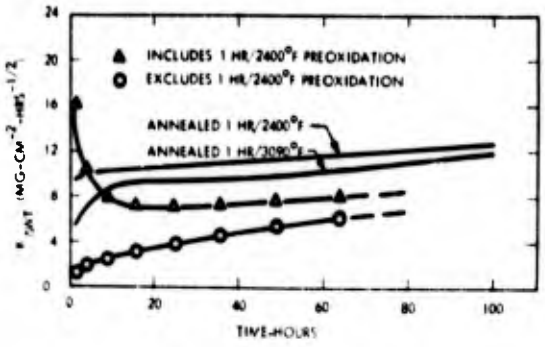

Figure 1.106. Effect of 1 Hour/ 2400°F pre-oxidation treatment on the weight gain behaviour of the B-1 alloy at 2000°F. (Cornie and Goodspeed [59]).

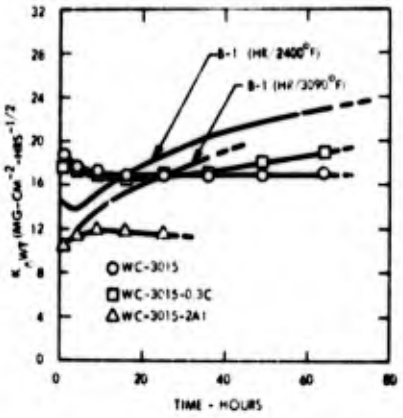

Figure 1.107. Comparison of continuous weight gain data for the B-1 alloy, the high strength Cb-28Hf-15W-4Ta-2Zr-0.1C (WC-3015) alloy, and several of its experimental modifications. (Cornie and Goodspeed [59]).

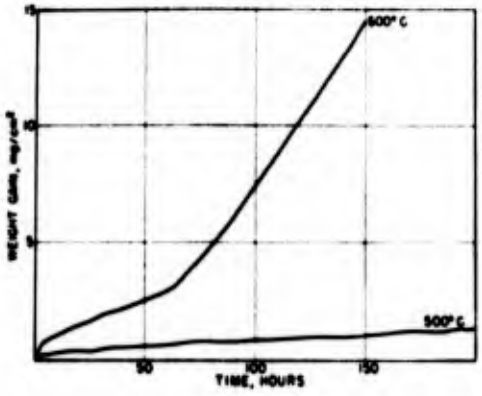

Figure 1.108. Reaction of 90 Cb-10 Ti alloy with oxygen at 1 atm. at 500 and 600°C. (Kolski [60]).

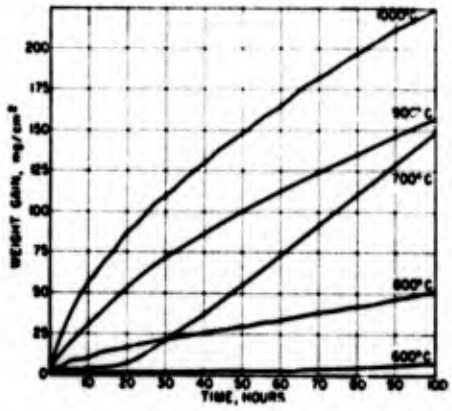

Figure 1.109. Reaction of 90 Cb-10 Ti alloy with oxygen at 1 atm. from 600 to 1000°C. (Kolski [60]).

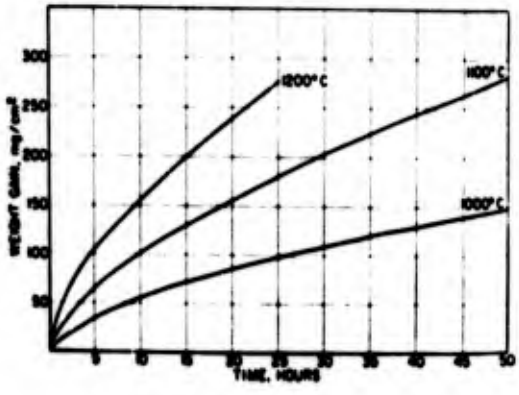

Figure 1.110. Reaction of 90 Cb-10 Ti alloy with oxygen at 1 atm. from 1000 to 1200°C. (Kolski [60]).

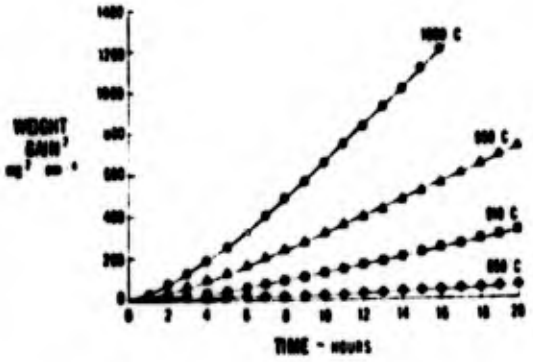

Figure 1.111. Oxidation behaviour of Nb-25 Ti between 850° and 1000°C in 76 mm O_2. (Felten [62]).

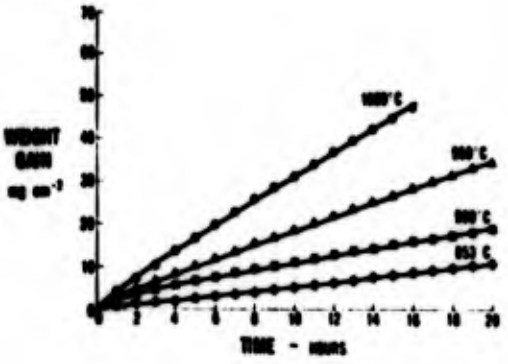

Figure 1.112. Oxidation behaviour of Nb-25 Ti between 650° and 1000°C in 76 mm air. (Felten[62]).

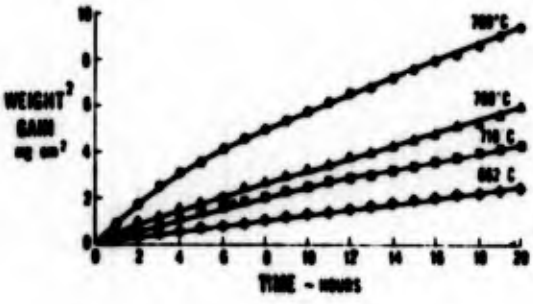

Figure 1.113. Oxidation behaviour of Nb-25 Ti between 660° and 780°C in 76 mm O_2. (Felten [62]).

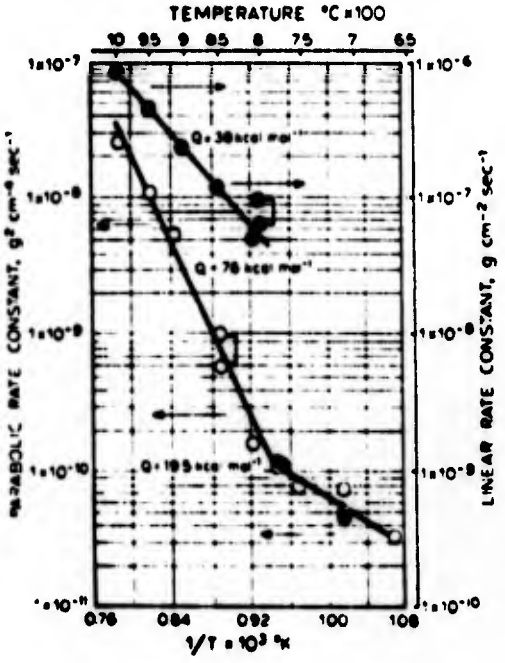

Figure 1.114. Temperature dependence of linear and parabolic rate constants for Nb-25 Ti oxidized in air and oxygen. (Felten [62]).

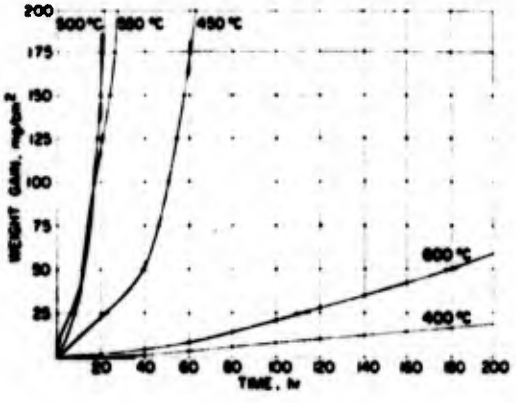

Figure 1.115. Reaction of 90 Cb-10 Mo alloy with oxygen at 1 atm from 400 to 600 C (750 to 1110 F) (Kolski [63]).

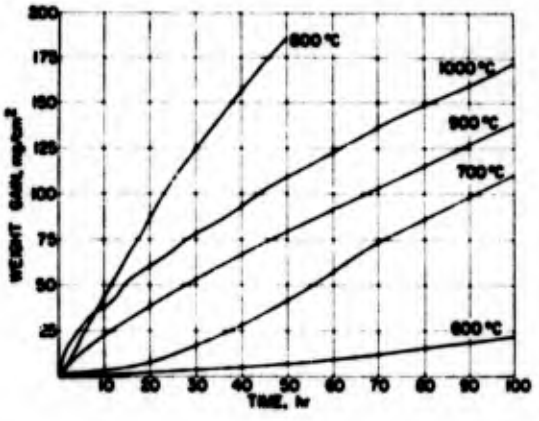

Figure 1.116. Reaction of 90 Cb-10 Mo alloy with oxygen at 1 atm from 600 to 1000 C (1110 to 1830 F). (Kolski [63]).

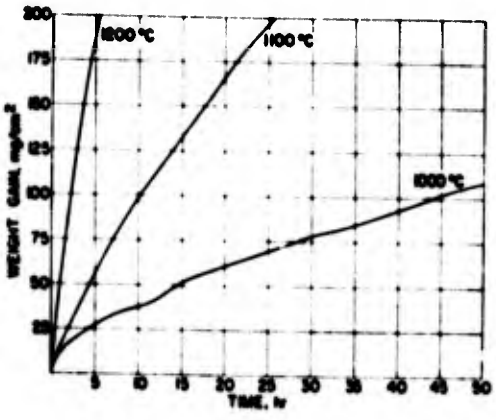

Figure 1.117. Reaction of 90 Cb-10 Mo alloy with oxygen at 1 atm from 1000 to 1200 C (1830 to 2190 F). (Kolski [63]).

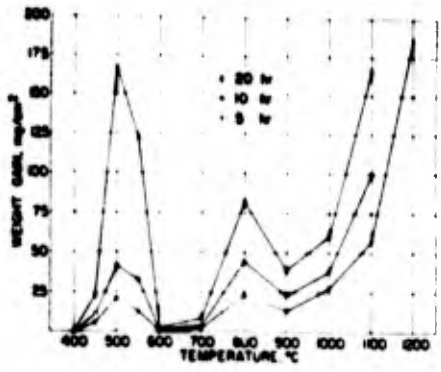

Figure 1.118. Reaction of 90 Cb-10 Mo alloy with oxygen at 1 atm from 400 to 1200 C (750 to 2190 F). Isochronal oxidation levels. (Kolski [63]).

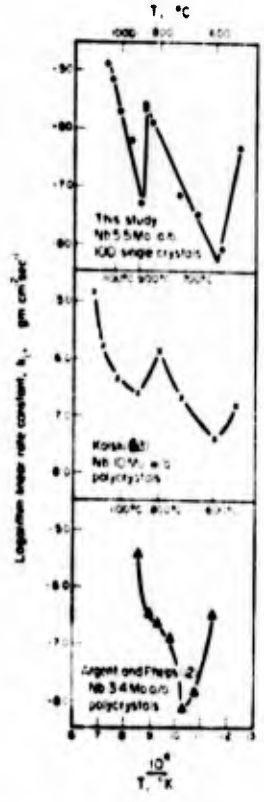

Figure 1.119. A comparison of the kinetic data from this study (using < 100 > Nb.5.5at% Mo single crystals) and those of Kolski (Ref. 63, using polycrystalline Nb-10wt.%Mo alloy) and Argent and Phelps (Ref. 43, using polycrystalline Nb-3.4at.% Mo alloy). (Taylor and Stringer [64]).

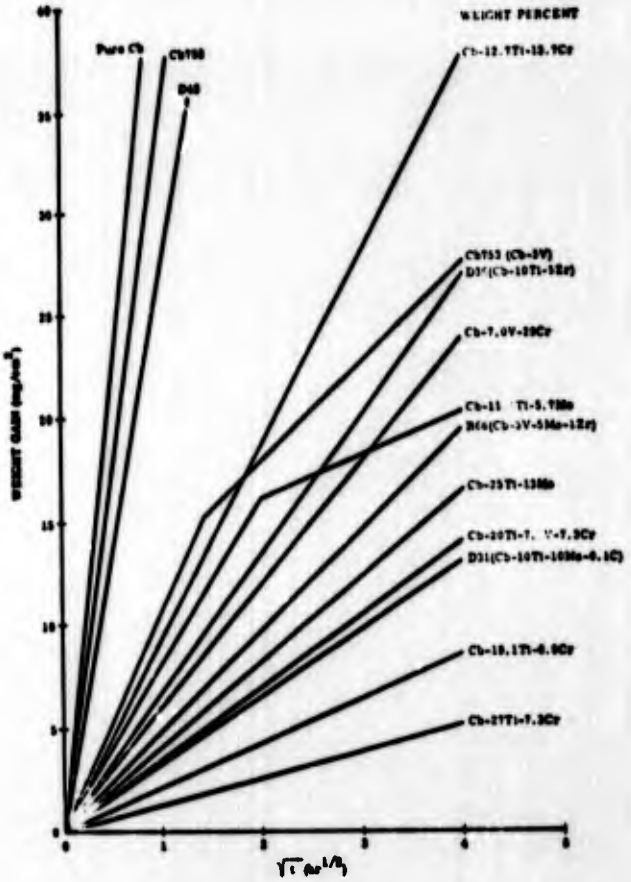

Figure 1.120. Summary plot of oxidation rates at 1600°F at sublayers and substrates. (Brentnall et al (65)).

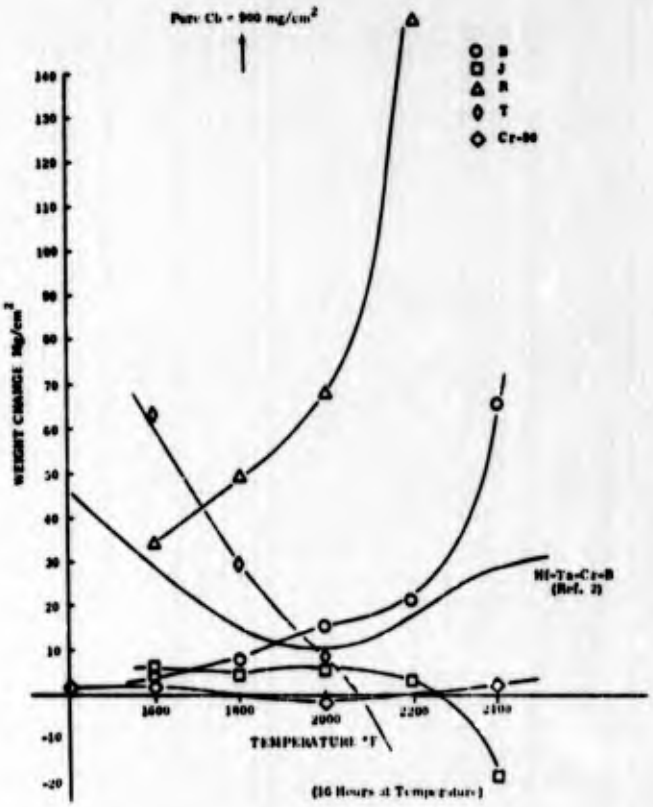

Figure 1.121. Oxidation rates of potential matrix alloys. (Brentnall et al (65)).

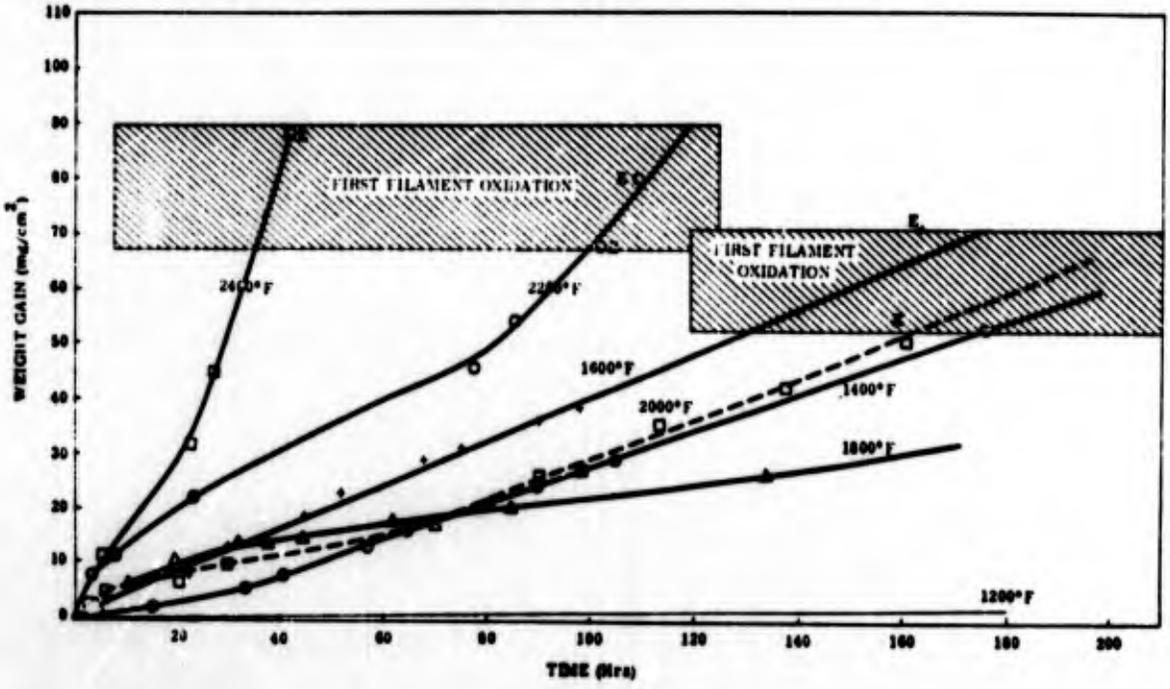

Figure 1.122. Weight gain as a function of oxidation time for J-alloy/W composite; the letter E designates the first observed filament attack and the hatched regions are estimated time-temperature combinations for first filament attack. (Klein et al [66]).

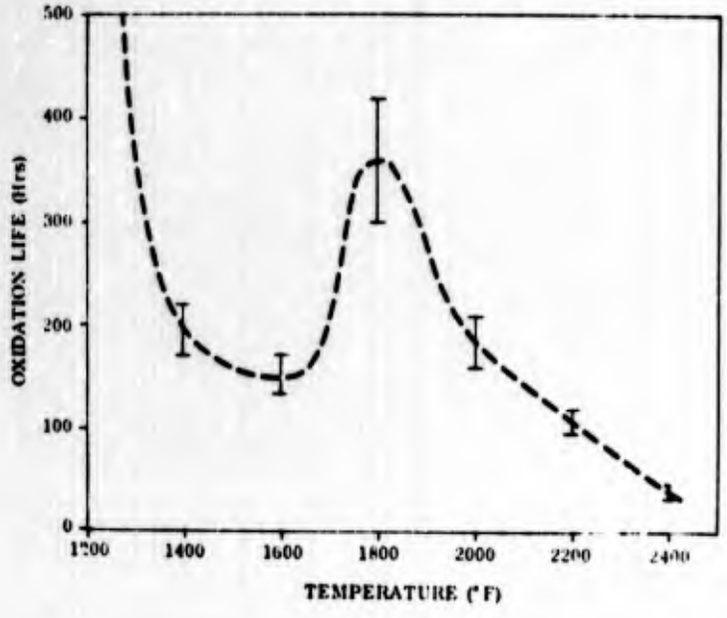

Figure 1.123. Oxidation life of J-alloy/W composite derived from Figure 1.122. (Klein et al [66]).

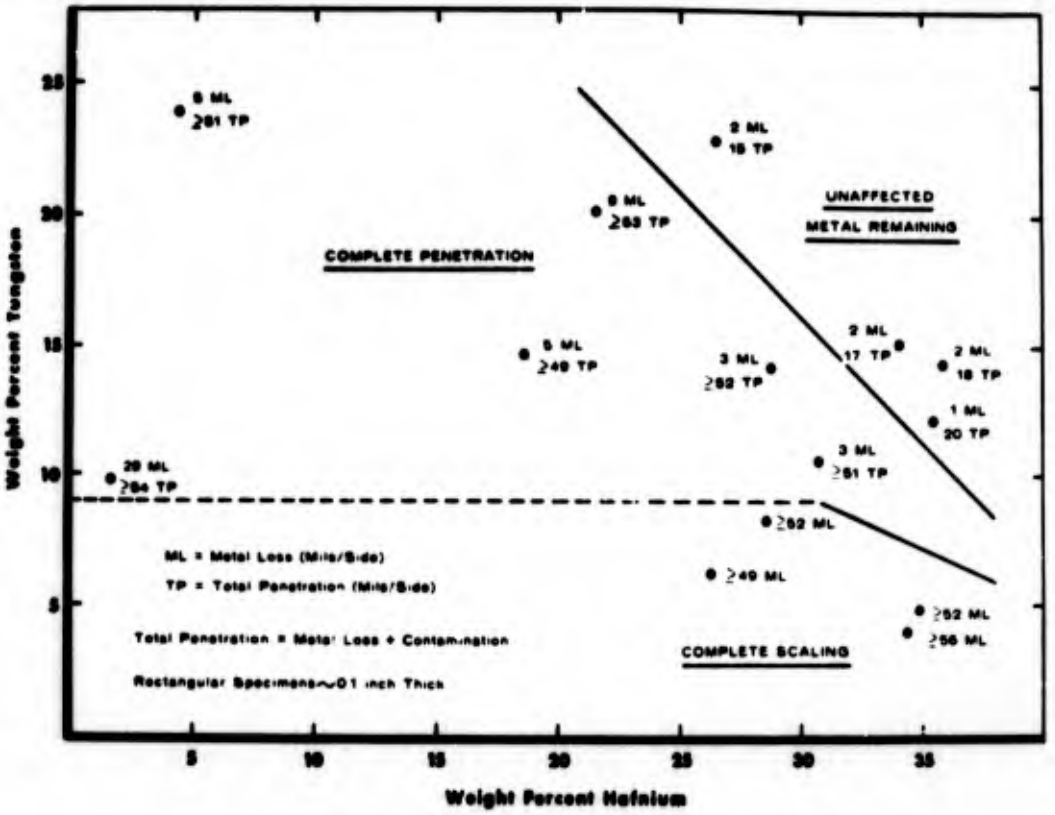

Figure 1.124. Effect of tungsten and hafnium contents on the oxidation behaviour of Cb-W-Hf alloys tested in air for twenty hours at 2000°F. (Roche and Graham (68)).

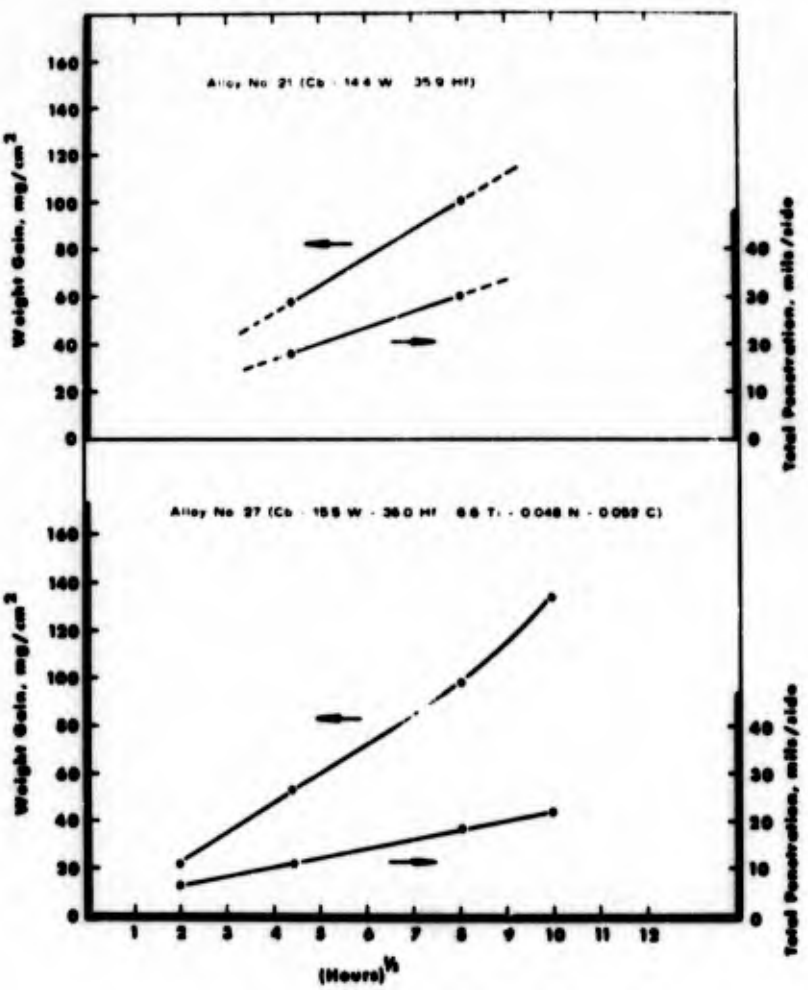

Figure 1.125. Weight gain and total penetration for alloys No. 21 (Cb-14.4W-35.9Hf) and 27 (Cb-15.5W-36.0Hf-6.6Ti-0.048N-0.052C) air-oxidized at 2000°F. (Roche and Graham(68)).

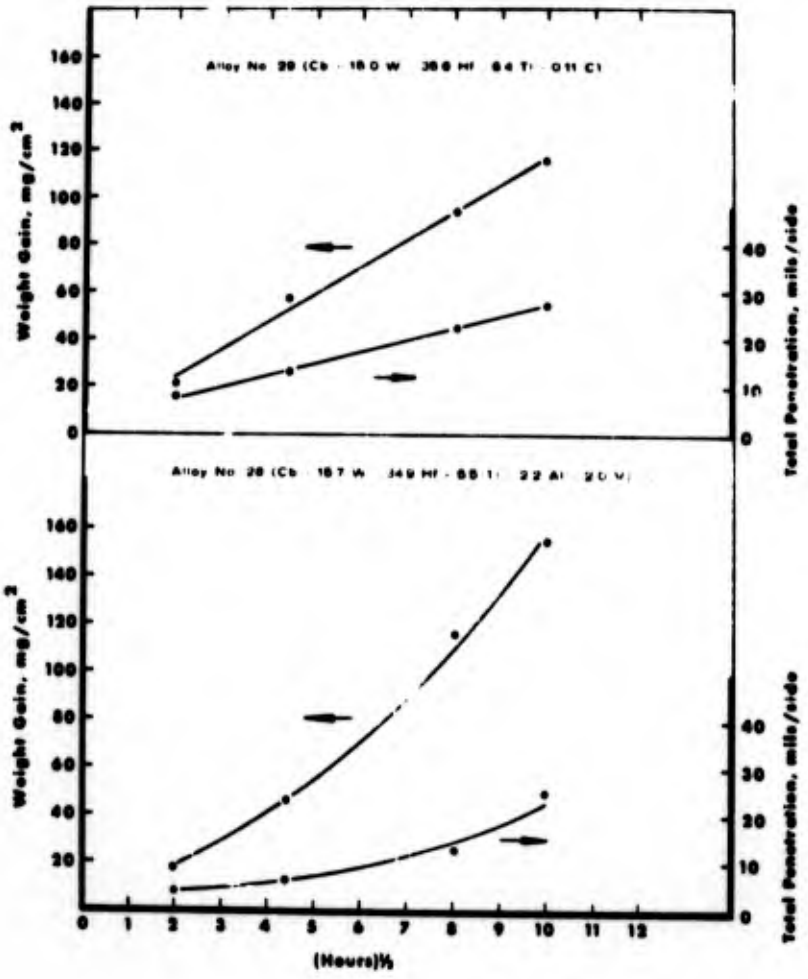

Figure 1.126. Weight gain and total penetration for alloys No. 29 (Cb-15.0W-35.6Hf-6.4Ti-0.11C) and 28 (Cb-15.7W-34.9Hf-5.5Ti-2.2Al-2.0V) air oxidized at 2000°F. (Roche and Graham[68]).

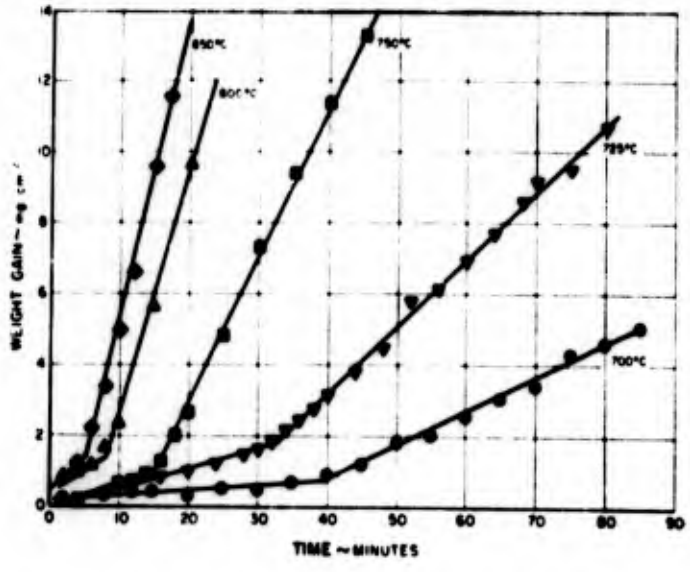

Figure 1.127. Oxidation behaviour of Cb-132 between 700° and 850°C. (Felten [73]).

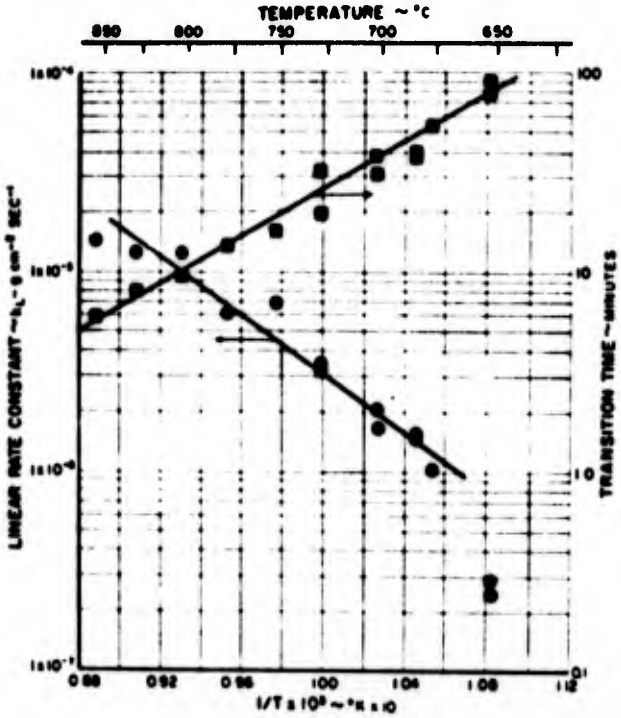

Figure 1.128. Arrhenius plot for transition time and linear rate constant of Cb-132. (Felten [73]).

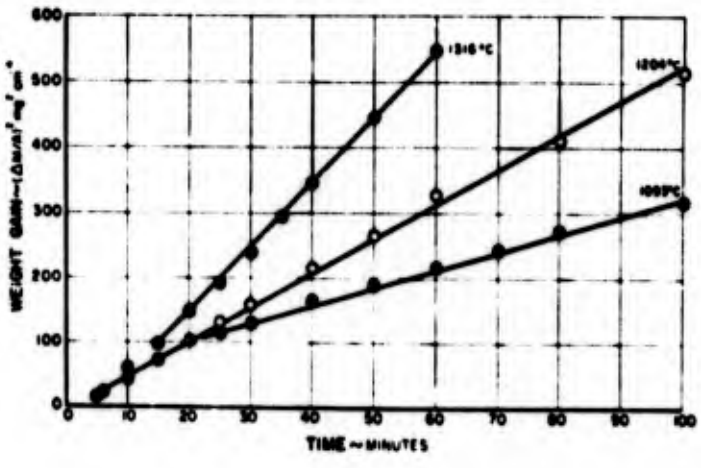

Figure 1.129. Oxidation behaviour of Cb-132 between 1093° and 1316°C. (Felten [73]).

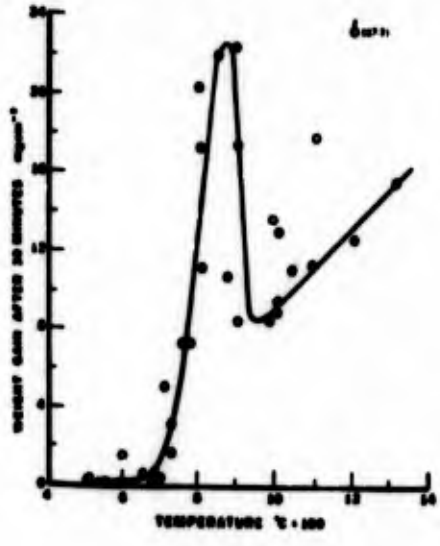

Figure 1.130. Relative oxidation resistance of Cb-132 (closed circles) and columbium (open circles) between 500° and 1300°C. (Felten [73]).

Section 2. Tantalum and Tantalum Alloys

Tantalum forms only one stable oxide, Ta_2O_5, and within the range of concern only one modification, β-Ta_2O_5, exists; although Kofstad[76] suggests that the transition temperature to the high-temperature modification, α-Ta_2O_5 is reduced by reducing the oxygen pressure. At 1250°C the scale formed in oxygen at 0.01 torr consisted of α-Ta_2O_5 plus a little β-Ta_2O_5; at 10 torr the proportions were reversed. Again, the pentoxide appears to be an oxygen-deficit n-type semiconductor. There are again several metastable lower oxides which appear as dynamic features during the oxidation. See Stringer[5] for a detailed discussion of these. In the oxidation context the most important is TaO_z, which appears as optically active platelets penetrating into the metal parallel to $(100)_{Ta}$ planes from the metal/oxide interface. Unlike niobium, these platelets do not cease to be stable at a well-defined temperature, but do become a less obvious feature at temperatures above 1000°C. It is probable that they are wholly absent above 1100°C.

As with niobium, initially oxygen dissolves in the metal without the nucleation of an oxide. A sequence of suboxides appear, their nature depending on the temperature, and finally pentoxide is nucleated. This grows under considerable compressive stresses, and eventually ruptures from the surface, the failure often appearing to be initiated by pores resulting from the presence of the suboxide platelets. The growth and rupture of the pentoxide is repeated resulting in a linear oxidation rate and producing a laminated porous scale. As the temperature increases above 800°C, the pentoxide appears to become more plastic, or possibly the growth stresses diminish; the laminations become thicker and eventually, at temperatures above about 1050°C, the thick, apparently compact pentoxide scales can form. However, the oxidation rate curves, while no longer exactly linear, are far from parabolic, so that it is probable that microfissures exist in much of the outer scale layer. The overall kinetics is often described in terms of a "linear rate constant" even at these temperatures, although it has only qualitative significance. As with niobium, the oxidation of coupon-shaped specimens is much more rapid at the edges and corners. The rate constant is strongly dependent on oxygen pressure, and at temperatures below 800°C this has been interpreted in terms of an "adsorption model". At higher temperatures no wholly satisfactory explanation exists. Figure 2-1 shows the rate constants for the reaction from a number of workers; for an explanation of the theoretical interpretation see Stringer[5]. Figure 2-2 illustrates the dependence on oxygen pressure[3]. The data on both these curves comes from a variety of sources[77-81] and there is general agreement.

In later years there has been very little work done on the oxidation of tantalum alloys. Generally, alloying seems less effective than is the case with niobium, and the high density of tantalum has made the metal less interesting as a potential turbine blade material. The literature up to 1960 is reviewed in detail by Schmidt[82]. Table 2-I lists the weight gain for the oxidation of tantalum alloys at 1200°C. Table 2-II lists weight gain data for alloys oxidized at 1000°C, from Schmidt, et. al.[83]. Figures 2-3 to 2-9 present the oxidation data in graphical form. Table 2-III lists contamination rates, and Figure 2-10 shows the effect of alloying on the contamination rate in air at 1200°C.

Figure 2-11 shows some data for metal recession at 2000°F (1093°C) taken from Michael[1]. Figure 2-12 shows the variation of oxidation rate with composition for Ta-Ti alloys at three temperatures from Klopp, et. al.[85], and Figures 2-13 to 2-15 show the effect of various ternary and quaternary additions on the oxidation of Ta-Ti alloys. Tables 2-IV, 2-V and 2-VI list oxidation behavior of a number of tantalum alloys at three different temperatures, and Table 2-VII lists some data on contamination rates.

It has already been remarked that Babitzke and co-workers included tantulum alloys in their program, and some data has been shown under niobium alloys (see Figures 1-72, 1-74 and 1-77; and Tables 1-XXIX, 1-XXX and 1-XXXII). Figures 2-16 and 2-17 show some results from Babitzke and Kato[51]. Table 2-VIII lists data for the oxidation of Ta-V and Ta-Hf alloys from Babitzke, et.al.[48]

Voitovich[86] reported that additions of up to 10% Ti increased the oxidation of tantalum and over 25% Ti was required to improve the oxidation resistance in the temperature range 500-900°C. Makarova[87] found that below 600°C the addition of Zr had little effect on the oxidation of tantalum and at higher temperatures increased the rate.

Thielemann[88] patented a range of tantalum-base alloys, typically Ta-10-20 wt.% Cr-2-25 wt.% W with small amounts of iron and interstitials, which were claimed to be hot-workable and to have an oxidation resistance at 1093°C 800% better than pure tantalum.

Because of its technical importance, several authors have briefly examined the oxidation of Ta-10% W and similar alloys[89-91]. There is no general agreement on the effect of tungsten on the oxidation rate, but the most significant effect is that during oxidation cracks develop in the metal, and in recrystallized samples extensive separation can occur at the grain boundaries[90]. This appears to be related to a strengthening of the oxide and an improvement of the metal/oxide adhesion, due to a development of pentoxide intrusions into the metal.

Dooley and Stringer have recently conducted some detailed studies of the effect of small binary additions on the oxidation of tantalum single crystals[90,92-95] but these are essentially mechanistic in character and lie outside the scope of the present work.

Table 2.1. Oxidation of tantalum and tantalum alloys in air at 1200 C (2190 F). (Schmidt [82]).

Alloy Composition, weight per cent	Weight Gain, $mg/cm^2/hr$	Appearance of Scale	Reference
100Ta	105.5	Voluminous, porous, white scale	83,84.
Ta-2.9B	138.9	Voluminous, porous, white scale	83
Ta-5.6B	94.3	Voluminous, porous, white scale	83
Ta-7.4B	59.4	Porous white scale	83
Ta-5Cb	50.6	Voluminous, porous, white scale	83
Ta-10Cb	55.8	Voluminous, porous, white-brown scale	83
Ta-30Cb	(a)	Voluminous, porous, white scale	83
Ta-7Co	114.5	Pink, porous scale	83
Ta-4.6Cr	49.3	Tan, porous scale	83
Ta-11.3Cr	33.5	Porous, brown scale	83
Ta-6.2Fe	64.4	Porous, brown scale	83
Ta-8Fe	50.1	Thin, adherent, gray scale	82
Ta-1Hf	154.3	Voluminous, porous, white scale	82
Ta-5Hf	69.9	Adherent, tan scale	83
Ta-10Hf	47.7	Adherent, tan scale	83
Ta-30Hf	28.0	Adherent, tan scale	83
Ta-32Hf	39.0	Dark, adherent scale	84
Ta-50Hf	18.0	Thin, adherent, tan scale	83
Ta-68Hf	10.0	Dark, thin, adherent scale	84
Ta-5Mo	69.9	Porous, gray scale	83
Ta-10Mo	51.5	Porous, gray scale	83
Ta-20Mo	28.8[b]	Porous, gray scale	83
Ta-30Mo	(a)	Porous, gray scale	83
Ta-10Ni	57.0	Adherent, black scale	83
Ta-49.3Ni	18.0	Small amount of black scale	83
Ta-5Re	71.3	Thin, adherent, yellow-white scale	82
Ta-10Re	(a)	Granular, yellow scale	83
Ta-32Re	25.0[c]	Nonadherent, granular, yellow scale	84
Ta-3.3Si	40.7	Porous, white scale	83
Ta-0.5Th	101.8	Voluminous, porous, yellow scale	83
Ta-8Th	168.8	Voluminous, porous, yellow scale	83

Table 2.I. (Continued).

Alloy Composition, weight per cent	Weight Gain, $mg/cm^2/hr$	Appearance of Scale	Reference
Ta-1Ti	104.2	Voluminous, porous, white scale	82
Ta-5Ti	39.1	Yellow, porous scale	83
Ta-10Ti	21.5	Small amount of black scale	83
Ta-27Ti	21.5	Thin, adherent, white scale	83
Ta-5V	55.5	Porous, gray-white scale	83
Ta-10V	68.4	Porous, gray-white scale	83
Ta-20V	159.9	Voluminous, porous, brown scale	82
Ta-30V	96.2	Porous, gray-white scale	83
Ta-5W	57.4	Porous, white scale	83
Ta-10W	61.4	Porous, white scale	83
Ta-30W	45.7	Porous, white scale	83
Ta-32W	59.0(c)	Thick, adherent scale	84
Ta-50W	12.0	Thin, white scale	83
Ta-68W	21.0(c)	Portion granular, non-adherent; thin layer, very adherent, yellowish	84
Ta-0.1Y	90.1	Yellow, porous scale	83
Ta-1Y	82.8	Yellow, porous scale	83
Ta-1Zr	90.6	Voluminous, porous, white scale	82
Ta-5Zr	35.0	Gray, porous scale	83
Ta-10Zr	32.4	Gray, porous scale	83
Ta-20Zr	61.0	Gray, porous scale	83
Ta-30Zr	59.8	Gray, porous scale	83
Ta-10Ti-5Cb	74.7	Tan, thick, adherent scale	82
Ta-10Ti-5W	76.0	Tan, thick, adherent scale	82
Ta-20Ti-5Al	16.7	Thin, yellow-white, adherent scale	82
Ta-20Ti-5Cb	28.9	Thin, adherent, light-yellow scale	82
Ta-20Ti-5Cr	15.5	Thin, adherent, beige scale	82
Ta-20Ti-5Mo	43.1	Thin, adherent, tan scale	82
Ta-20Ti-5V	19.3	Thin, adherent, dark-gray scale	82
Ta-20Ti-5W	39.4	Thin, adherent, light-yellow scale	82
Ta-20Ti-10W	42.1	Thin, adherent, yellow scale	82
Ta-5W-10V	122.0	Voluminous, porous, brown scale	82

Table 2.I. (Continued).

Alloy Composition, weight per cent	Weight Gain, mg/cm^2/hr	Appearance of Scale	Reference
Ta-4W-4Hf	101.0	Voluminous, porous, white scale	84
Ta-5W-10Hf	72.2	Thin, adherent, white scale	82
Ta-8W-8Hf	24.0	Very adherent; whitish portion spalled	84
Ta-8W-16Hf	32.0	Portion spalled; whitish very adherent	84
Ta-26W-5Hf	64.0	Thick, nonadherent, light-yellow scale	84
Ta-33W-33Hf	18.0	Thin, very adherent, whitish scale	84
Ta-48W-4Hf	26.0[c]	Thin, spalled, gray yellow scale	84
Ta-60W-4Hf	7.5[d]	Thin, very adherent, yellow-black scale	84
Ta-33W-33Re	24.0[c]	Granular, nonadherent, with thin white adherent subscale	84

(a) Rate data not available; portion of scale lost at conclusion of test because of crucible fracture.
(b) Sample smoked during test, indicating MoO_2.
(c) Calculated from weight loss after scale removal.
(d) Probably low value because of loss of tungsten oxide by volatilization. Scale could not be removed mechanically, so value could not be calculated from weight loss after scale removal.

Table 2.II. Air-oxidation rates of tantalum and tantalum alloys at 1000 C (1830 F) (83).

Alloy Composition, weight per cent	Parabolic Rate Constant, $(mg/cm^2)^2/hr$	Transition to Linear Behavior, minutes	Linear Rate Constant, mg/cm^2/hr	Slope of Log-Log Plot, n	Weight Gain After Indicated Time, mg/cm^2					
					1 Hour	2 Hours	3 Hours	4 Hours	5 Hours	6 Hours
100Ta	--	--	39.0	0.67	38.8	62.8	(79)[a]	(94)	(107)	(119)
Ta-5Cb	500	30	18.8	0.76	26.2	45.4	63.8	--	--	--
Ta-10Cb	340	60	6.0	0.55	18.6	27.0	34.1	40.7	46.6	52.4
Ta-20Cb	550	(60)	(8.3)	0.55	23.5	34.5	43.0	51.0	--	--
Ta-30Cb	1740	>360	--	0.52	38.6	55.8	70.2	82.7	93.4	102.3
Ta-40Cb	3020	>360	--	0.48	55.6	76.4	91.2	102.0	109.5	--
Ta-50Cb	3000	>360	--	0.56	51.4	75.7	93.5	108.0	119.3	129.0
Ta-5Ti	280	30	16.6	0.75	20.3	38.3	53.8	--	--	--
Ta-10Ti	247	90	6.3	0.63	15.2	23.6	30.4	36.2	41.4	46.7
Ta-20Ti	97	210	2.8	0.69	7.9	12.5	16.0	19.0	21.7	24.6
Ta-30Ti	--	--	4.2	0.80	4.5	11.1	16.8	21.2	25.1	28.6
Ta-40Ti	--	--	2.3→1.6[b]	0.79	2.1	4.3	6.2	7.1	7.9	8.7
Ta-5Hf	--	--	(c)	--	--	--	--	--	--	--
Ta-10Hf	--	--	(c)	--	--	--	--	--	--	--
Ta-20Hf	--	--	(c)	--	--	--	--	--	--	--
Ta-5V	213	60	8.5	0.60	14.4	22.8	31.5	41.8	53.5	67.0
Ta-10V	865	90	14.5	0.61	27.5	43.7	57.5	69.7	--	--
Ta-5Mo	2240	25	(47)	0.82	--	--	--	--	--	--
Ta-10W	(d)	--	--	--	--	--	--	--	--	--
Ta-40Zr	--	--	278	0.59	--	--	--	--	--	--
Ta-10Cb-20Ti	69	>360	--	0.57	7.6	11.2	14.0	16.3	18.3	20.1
Ta-20Cb-10Ti	467	175	6.5	0.58	20.0	30.1	38.1	44.9	51.1	57.1
Ta-10Cb-10Ti	101	>270	--	0.36	11.7	15.2	18.2	20.8	--	--
Ta-10Cb-5V	117	75	5.9	0.42→0.73[e]	11.4	18.0	23.7	29.5	34.9	39.8
Ta-10Cb-10Cr	1336	>120	--	0.50	37.6	51.1	60.2	65.8	69.4	71.7

(a) Values in parentheses are estimated.
(b) Rate decreased from 2.3 to 1.6 mg/cm^2/hr after 3 hours' oxidation.
(c) Data could not be obtained, since sample spalled continuously during test.
(d) Specimen fell from quartz rod into furnace after approximately 12 minutes' exposure.
(e) Slope of log-log plot changed from 0.42 to 0.73 after 75 minutes' exposure. This corresponds to the transition time from parabolic to linear behavior.

Table 2.II. Air-oxidation rates of tantalum and tantalum alloys at 1200 C (2190 F) (83).

Alloy Composition, weight per cent	Parabolic Rate Constant, $(mg\ cm^{-2})^2/hr$	Transition to Linear Behavior, minutes	Linear Rate Constant, $mg/cm^2/hr$	Slope of Log-Log Plot, n	Weight Gain After Indicated Time, mg/cm^2					
					1 Hour	2 Hours	3 Hours	4 Hours	5 Hours	6 Hours
100Ta	--	--	110	0.60	106.0	167.0	211.0	254.0	302.0	--
Ta-5Cb	3350	>180	--	0.58	51.3	76.8	95.8	--	--	--
Ta-10Cb	4000	>210	--	0.56	61.0	90.0	110.0	--	--	--
Ta-20Cb	(a)	--	--	0.25	89.0	110.0	119.0	--	--	--
Ta-30Cb	--	--	(750)[b]	1.06	102.0	117.0	--	--	--	--
Ta-40Cb	--	--	(870)	1.95	--	--	--	--	--	--
Ta-50Cb	--	--	(900)	0.83	--	--	--	--	--	--
Ta-5Ti	--	--	(60)	0.52	69.0	99.0	120.0	--	--	--
Ta-10Ti	1330	60	14.9	0.60	36.1	53.0	67.9	82.7	96.6	106.0
Ta-20Ti	146	150	6.1	0.59	11.6	16.7	20.8	24.8	29.0	33.2
Ta-30Ti	58	45	12.0	1.05	9.8	21.8	33.8	44.8	54.6	--
Ta-40Ti	--	--	9.0	0.91	10.0	18.0	28.0	38.0	47.0	56.0
Ta-5Hf	--	--	(62)	0.67	78.0	126.0	--	--	--	--
Ta-10Hf	--	--	47.0	0.78	62.9	77.4[c]	101.0[c]	--	--	--
Ta-20Hf	1600	180	10.2	0.60	36.4	53.7	67.0	77.8	88.3	97.4
Ta-30Hf	1860	300	9.8	0.47	43.9	61.3	76.8	86.3	96.9	106.7
Ta-5V	4500	50	42.0	0.62	66.2	108.0	141.8	153.8[d]	--	--
Ta-10V	3150	120	16.7	0.55	59.6	80.5	97.5	114.6	131.0	--
Ta-5Mo	6000	>100	--	0.46	78.2	--	--	--	--	--
Ta-5W	8550	>120	--	0.52	92.1	125.6	--	--	--	--
Ta-10W	8275[e]	>60	--	0.56	95.5	122.3	125.1	--	--	--
Ta-20W	7200	>55	--	0.58	77.6	--	--	--	--	--
Ta-5Zr	2670	90	19.6	0.55	50.3	74.0	93.1	111.3	131.9	139.7
Ta-20Zr	(f)	--	--	0.38	85.2	--	--	--	--	--
Ta-30Zr	9300	20	44.0	0.50	67.1	--	--	--	--	--
Ta-40Zr	2550	135	8.0	0.53	47.2	67.0	77.2	83.8	88.5	90.6
Ta-10Cb-20Ti	340	75	8.3	0.65	17.9	28.3	37.3	45.5	53.0	59.8
Ta-20Cb-10Ti	--	--	770	0.98	--	--	--	--	--	--
Ta-30Cb-10Ti	5000	57	46.0	0.47	79.6	--	--	--	--	--
Ta-30Cb-5V	--	--	1110	0.91	--	--	--	--	--	--
[illegible]	--	--	870	0.75	--	--	--	--	--	--
[illegible]	--	--	665	1.00	--	--	--	--	--	--

(a) Curve best described by $w = 90t^{1/4}$.
(b) Values in parentheses are estimated.
(c) Sample spalled.
(d) Furnace failure after 4 hours.
(e) Average of two specimens.
(f) Curve best described by $w = 90t^{1/3}$.

Table 2.II. Air-oxidation rates of tantalum and tantalum alloys at 1400 C (2550 F) (83).

Alloy Composition, weight per cent	Parabolic Rate Constant, $(mg/cm^2)^2/hr$	Transition to Linear Behavior, minutes	Linear Rate Constant, $mg/cm^2/hr$	Slope of Log-Log Plot, n	Weight Gain After Indicated Time, mg/cm^2 1 Hour	2 Hours	3 Hours	4 Hours	5 Hours	6 Hours
100Ta	--	--	(1200)(a)	0.87	--	--	--	--	--	--
Ta-5Cb	--	--	(1000)	0.75	--	--	--	--	--	--
Ta-10Cb	--	--	(b)	--	--	--	--	--	--	--
Ta-20Cb	--	--	(b)	--	--	--	--	--	--	--
Ta-30Cb	--	--	(b)	--	--	--	--	--	--	--
Ta-40Cb	--	--	(1400)	0.68	--	--	--	--	--	--
Ta-50Cb	--	--	1060	0.95	--	--	--	--	--	--
Ta-5Ti	--	--	(1900)	0.73	-	--	--	--	--	--
Ta-10Ti	--	--	950	0.93	--	--	--	--	--	--
Ta-20Ti	--	--	60.0	0.70	63.5	96.4	111.6	--	--	--
Ta-30Ti	--	--	(61)	0.83	60.6	90.0	--	--	--	--
Ta-40Ti	--	--	(39)	0.77	47.0	78.0	100.0	--	--	--
Ta-10Hf	(c)	--	--	0.24	116.9	--	--	--	--	--
Ta-20Hf	4,600	--	-	0.43	70.1	94.5	106.1	--	--	--
Ta-30Hf	--	--	1140	0.74	--	--	--	--	--	--
Ta-5V	--	--	1580	0.72	--	--	--	--	--	--
Ta-10V	68,500(d)	>12	--	0.55	--	--	--	--	--	--
Ta-5Mo	--	--	(2100)	0.66	--	--	--	--	--	--
Ta-5W	--	--	1400	0.72	--	--	--	--	--	--
Ta-10W	--	--	1205(e)	0.79	--	--	--	--	--	--
Ta-20W	--	--	970	0.87	--	--	--	--	--	--
Ta-5Zr	--	--	1360	1.03	--	--	--	--	--	--
Ta-40Zr	(f)	--	--	0.37	57.4	68.3	73.6	77.7	--	--
Ta-10Cb-20Ti	3,500	18	57.0	0.59	67.4	99.0	--	--	--	--
Ta-20Cb-10Ti	--	--	940	0.83	--	--	--	--	--	--
Ta-30Cb-10Ti	--	--	595	0.55	-.9	--	--	--	--	--
Ta-10Cb-5V	--	--	1090	0.98	--	--	--	--	--	--
Ta-10Cb-10Zr	--	--	990	0.83	--	--	--	--	--	--
Ta-10Cb-10W	--	--	860	0.68	--	--	--	--	--	--

(a) Values in parentheses are estimated.
(b) Reaction proceeded too rapidly to allow accurate data.
(c) Curve best described by $w = 117t^{1/4}$.
(d) Curve best described by parabolic equation. Oxidation rate was catastrophic.
(e) Average of two specimens.
(f) Curve best described by $w = 58t^{1/3}$.

Table 2.III. Contamination coefficients of tantalum and tantalum alloys at 1200 C (2190 F)[94]. (Schmidt et al [83]).

Alloy Composition, weight per cent	Contamination Rate, cm^2/sec
100Ta	1.2×10^{-6}
Ta-5Cb	1.5×10^{-6}
Ta-10Cb	1.5×10^{-6}
Ta-5Hf	8.0×10^{-8}
Ta-10Hf	6.0×10^{-8}
Ta-30Hf	6.0×10^{-8}
Ta-50Hf	7.4×10^{-9}
Ta-5Mo	8.8×10^{-7}
Ta-10Mo	5.9×10^{-7}
Ta-10Re	1.7×10^{-7}
Ta-3.34Si	8.4×10^{-8}
Ta-1Th	1.6×10^{-7}
Ta-5V	2.9×10^{-7}
Ta-10V	1.1×10^{-7}
Ta-30V	1.5×10^{-6}
Ta-5W	1.2×10^{-6}
Ta-10W	5.0×10^{-7}
Ta-30W	6.6×10^{-8}
Ta-50W	1.5×10^{-7}
Ta-5Zr	9.0×10^{-8}
Ta-10Zr	5.0×10^{-8}
Ta-30Zr	3.0×10^{-8}

Table 2.IV. Oxidation behaviour of tantalum alloys at 1000°C. (Klopp et al [85]).

Adjusted alloy compn., wt-%[a]	Initial parabolic rate, $(mg/cm^2)^2/hr$	Time for transition to linear behavior, min	Linear rate, $mg/cm^2/hr$	Weight gain in 6 hr mg/cm^2	Thickness of adherent subscale, mils	
					Calc.	Measured
100 Ta	—	—	39	(119)[c]	—	—
Ta-20Ti	97	210	2.8	24.4	—	—
Ta-30Ti	—	—	4.2	28.6	—	—
Ta-40Ti	—	—	(2)	8.7	—	—
Ta-60Ti	5.8	>360	—	5.7	—	—
Ta-80Ti	1.54	>360	—	3	—	—
100Ti	32	400	1	13.7	—	—
Ta-20Ti-1Al	10	40	(1.5)	11.5	—	—
Ta-20Ti-1Cr	8.8	40	(1.7)	12.1	—	—
Ta-20Ti-1Al-2Cr	6.5	200	0.75	7.3	—	—
Ta-20Ti-1Al-1Si	—	—	(2.5)	18.8	—	—
Ta-30Ti-4Al	2.4	>720	—	3.8	1.4	0.5
Ta-30Ti-2Cr	3.9	150	0.55	5.7	0.9	0.15
Ta-30Ti-9Cr	1.4	660	0.21	2.9	0.8	0.15
Ta-30Ti-1Si	27	120	5	18.6	0.7	0.5
Ta-30Ti-1Be	—	—	2.2	14.1	—	0.3
Ta-30Ti-5Al-4Cr	0.19	>900	—	1.21	0.4	0.15
Ta-30Ti-5Al-1Si	0.27	400	0.12	1.30	0.3	0.5
Ta-40Ti-5Al	(3.2)	>900	—	4.6	1.6	0.5
Ta-40Ti-10Al	0.103	>900	—	0.84	0.3	0.2
80Ni-20Cr[b]	0.004	—	—	0.2	—	—

[a] Compositions adjusted for melting losses.

[c] Estimated data in parentheses.

Table 2.V. Oxidation behaviour of tantalum alloys at 1200°C. (Klopp et al [85]).

Adjusted alloy compn., wt-%[a]	Initial parabolic rate, $(mg/cm^2)^2/hr$	Time for transition to linear behavior, min	Linear rate, $mg/cm^2/hr$	Weight gain in 6 hr, mg/cm^2	Thickness of adherent subscale, mils	
					Calc.	Measured
100 Ta	—	—	110	—	—	—
Ta-20Ti	146	150	4.1	33.2	—	—
Ta-30Ti	58	45	12	—	—	—
Ta-40Ti	—	—	9	56	—	—
Ta-60Ti	53	>360	—	17.5	—	—
Ta-80Ti	21	>360	—	11.5	—	—
100Ti	(100)[c]	200	3.8	33.3	—	—
Ta-20Ti-1Al	100	30	6.7	45.6	—	—
Ta-20Ti-1Cr	140	60	8	51.4	—	—
Ta-20Ti-1Al-2Cr	21	60	(4.5)	24.9	—	—
Ta-20Ti-1Al-1Si	42	70	1.5	19.3	—	—
Ta-30Ti-4Al	17	20	4	20.2	0.5	0.2
Ta-30Ti-2Cr	15.5	30	(3.9)	21.7	0.5	0.3
Ta-30Ti-9Cr	5.8	130	0.62	6.15	1.2	0.5
Ta-30Ti-1Si	55	100	3.3	24.3	2.1	0.3
Ta-30Ti-1Be	—	—	13.7	86	—	0.4
Ta-30Ti-5Al-4Cr	4.1	>360	—	5.10	1.3	0.3
Ta-30Ti-5Al-1Si	2.9	320	—	4.33	—	0.5
Ta-40Ti-5Al	14	60	2.3	15.1	0.8	0.2
Ta-40Ti-10Al	3.9	>360	—	4.76	1.6	0.3
80Ni-20Cr	0.13	—	—	1.3	—	—

[a]Composition adjusted for melting losses.

[c]Estimated data in parentheses.

Table 2.VI. Oxidation behaviour of tantalum alloys at 1400°C. (Klopp et al [85]).

Adjusted alloy compn., wt-%[a]	Initial parabolic rate, $(mg/cm^2)^2/hr$	Time for transition to linear behavior, min	Linear rate, $mg/cm^2/hr$	Weight gain in 6 hr, mg/cm^2	Thickness of adherent subscale, mils	
					Calc.	Measured
100Ta			(1200)[c]			
Ta-20Ti			60			
Ta-30Ti			(61)			
Ta-40Ti			(39)			
Ta-60Ti	87	>360		22.9		
Ta-80Ti	383	>360		48.1		
100Ti	(1200)	(100)	(13)			
Ta-20Ti-1Al			(50)			
Ta-20Ti-1Cr			(60)			
Ta-20Ti-1Al-2Cr			(50)			
Ta-20Ti-1Al-1Si			15.2	95.6		
Ta-30Ti-4Al			(14)			0.5
Ta-30Ti-2Cr	(300)	20	32	139	(1.3)	0.2
Ta-30Ti-9Cr	53	110	4.7	25	1.4	
Ta-30Ti-1Si	160	60	11.9	68	1.7	0.1
Ta-30Ti-1Be			(130)			0.2
Ta-30Ti-5Al-4Cr	144	120	5.7	40.3	3.1	0.4
Ta-30Ti-5Al-1Si	32	100	(6)	22.8	(0.7)	0.3 1
Ta-40Ti-5Al	(200)	(20)	8.6	65.8	(3)	0.5
Ta-40Ti-10Al	82	180	2.5	23	4.0	

[a]Compositions adjusted for melting losses.

[c]Estimated data in parentheses.

Table 2.VII. Air-contamination rates of tantalum and tantalum-base alloys at 1000°C. (Klopp et al[85]).

Compn., wt-%	Air-contamination rate, $cm^2/sec \times 10^9$
100Ta	340
Ta-60Ti	18
Ta 80Ti	16
100Ti	8.4
Ta-30Ti-4Al	6.8
Ta-30Ti-2Cr	26
Ta-30Ti-9Cr	21
Ta-30Ti-1Si	3.7
Ta-30Ti-1Be	18
Ta-30Ti-5Al-4Cr	5.3
Ta-30Ti-5Al-1Si	9.8
Ta-40Ti-5Al	4
Ta-40Ti-10Al	1.1

Table 2.VIII. Oxidation rates of Ta-V and Ta-Hf alloys (Babitzke et al [48]).

Alloy Composition, At.%	Weight Gain Per Hour, $mg/cm^2/hr$ 600°C	800°C
100 Ta	2.0	6.9
Ta-5V	0.3	5.5
Ta-8V	I*	3.9
Ta-10V	I	3.3
Ta-12V	I	2.4
Ta-15V	I	1.3
Ta-20V	I	1.1
Ta-30V	--	1.3
Ta-40V	--	2.2
Ta-10HF	I	--
Ta-15HF	0.2	1.1
Ta-20HF	I	1.3
Ta-33HF	0.1	1.5
Ta-50HF	0.9	3.8

* I = insufficient oxide for detection.

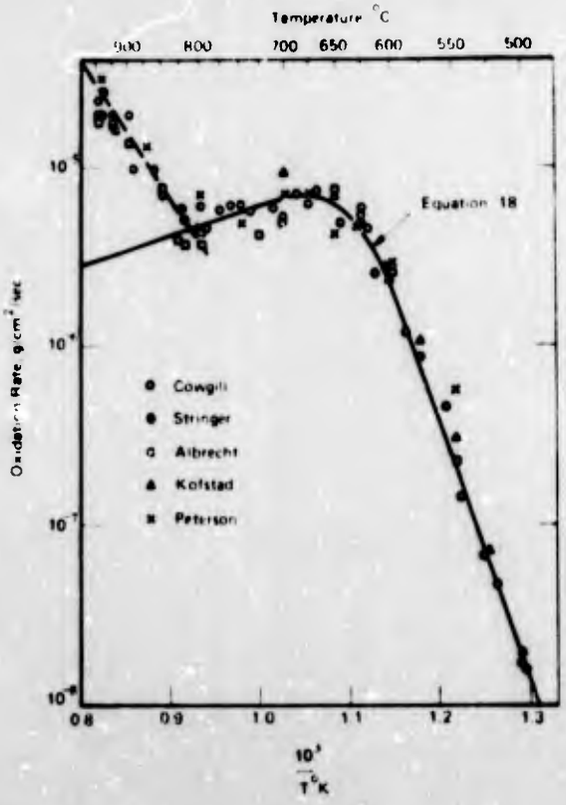

Figure 2.1. The oxidation rate of tantalum at an oxygen pressure of 760 torr as a function of temperature, showing the fit of the adsorption model, from Stringer[5].

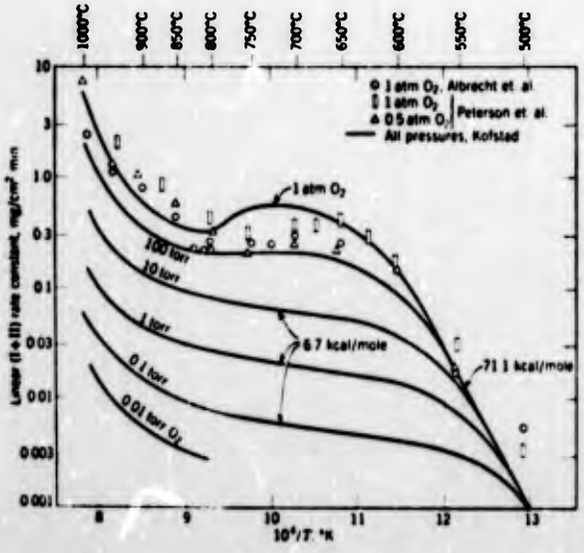

Figure 2.2. The linear rate constant ($k_{lin\ I}$ and $k_{lin\ II}$) for oxidation of tantalum as a function of 1/T. (Kofstad (3)).

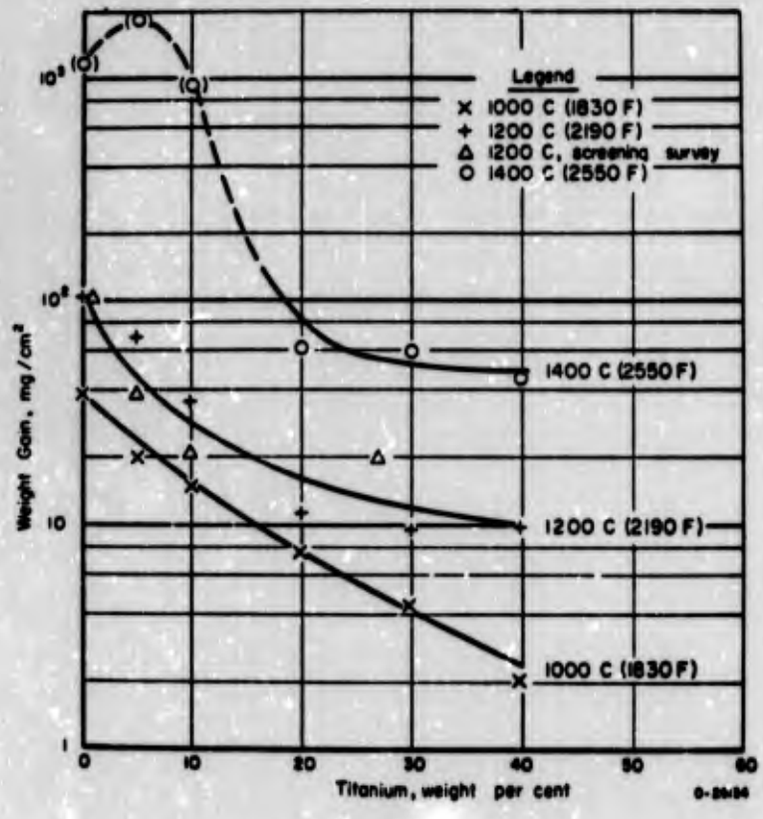

Figure 2.3. 1-hour weight gains of binary tantalum-titanium alloys in air (94,99). (Schmidt (82)).

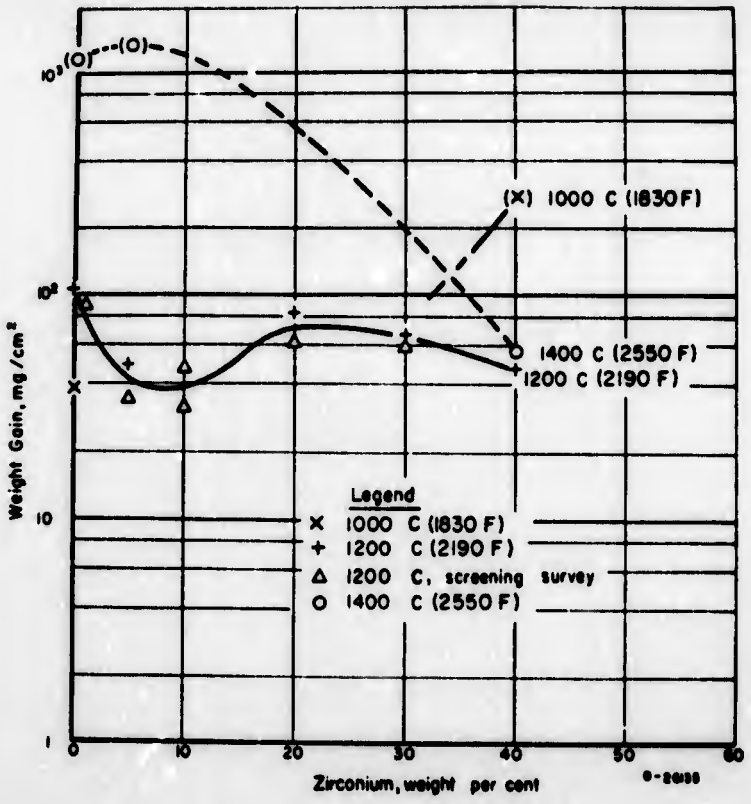

Figure 2.4. 1-hour weight gains of binary tantalum-zirconium alloys in air (94,99). (Schmidt (82).

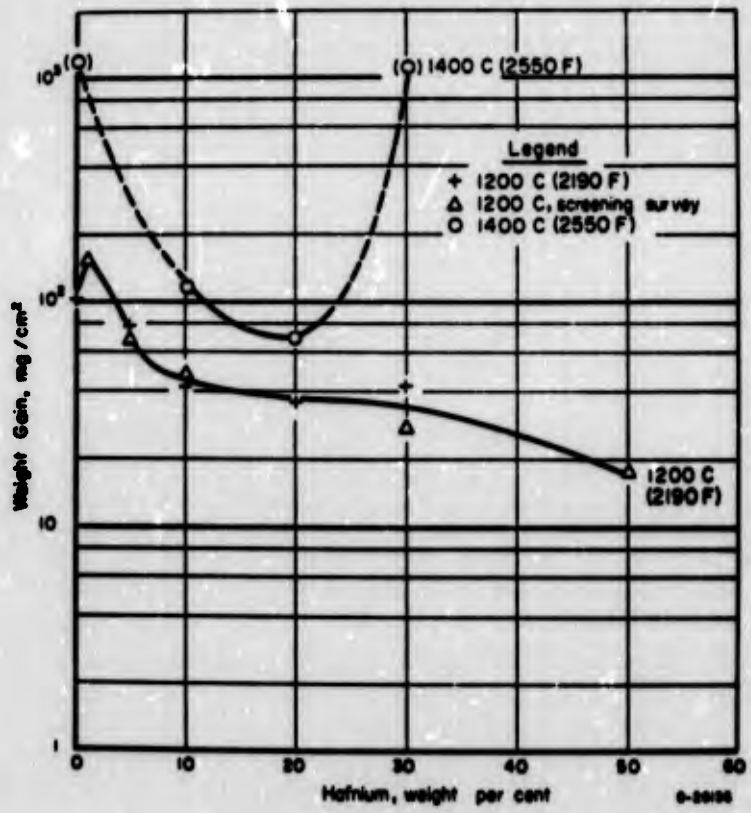

Figure 2.5. 1-hour weight gains of binary tantalum-hafnium alloys in air (94,99). (Schmidt (82).

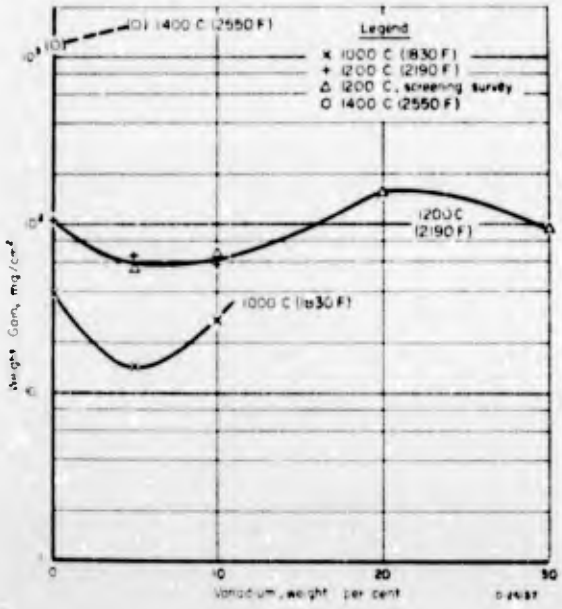

Figure 2.6. 1-hour weight gains of binary tantalum-vanadium alloys in air [94,99]. (Schmidt [82]).

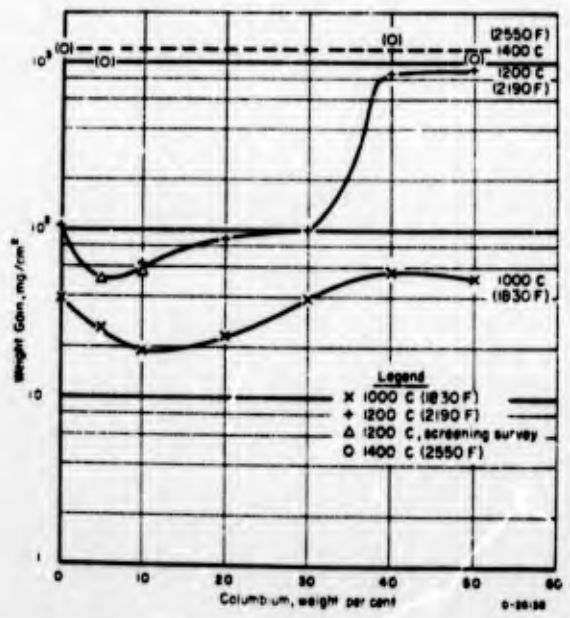

Figure 2.7. 1-hour weight gains of binary tantalum-columbium alloys in air [94]. (Schmidt [82]).

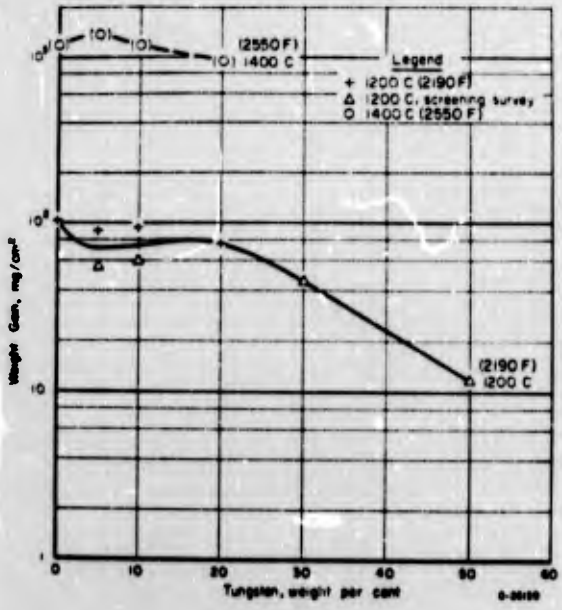

Figure 2.8. 1-hour weight gains of binary tantalum-tungsten alloys in air [94]. (Schmidt [82]).

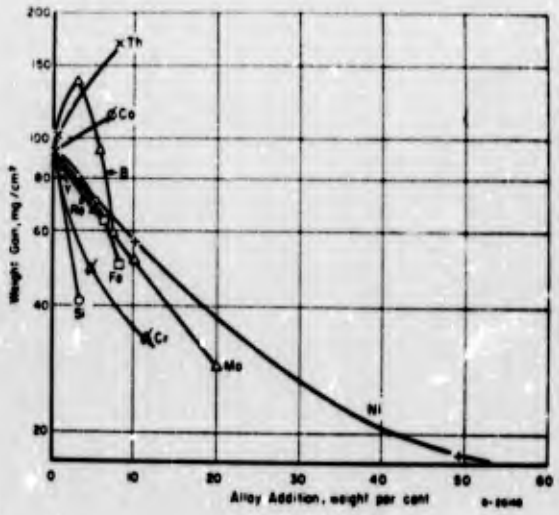

Figure 2.9. 1-hour weight gains of several binary tantalum alloys in air at 1200 C [94,99]. (Schmidt [82]).

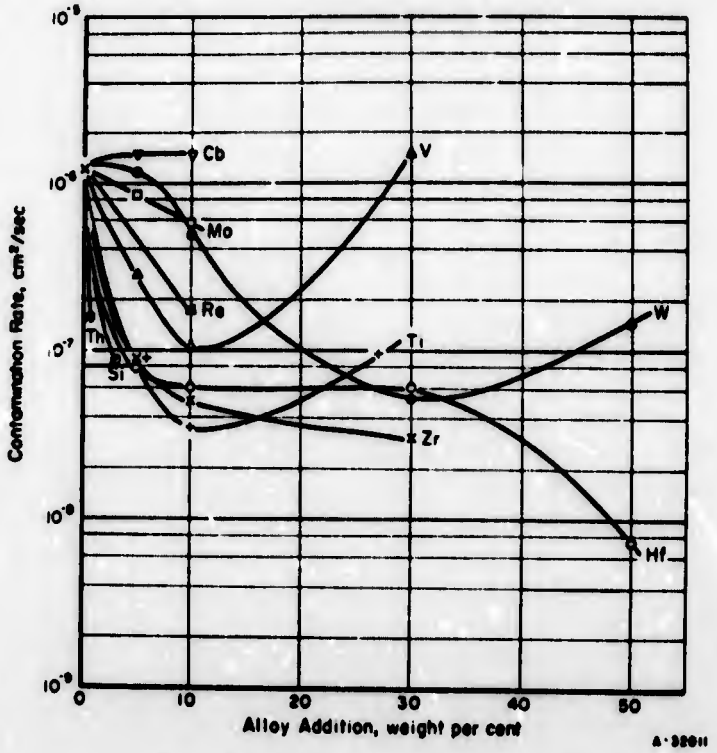

Figure 2.10. Effects of alloying on the contamination rate of tantalum in air (94). (Schmidt et al (83).

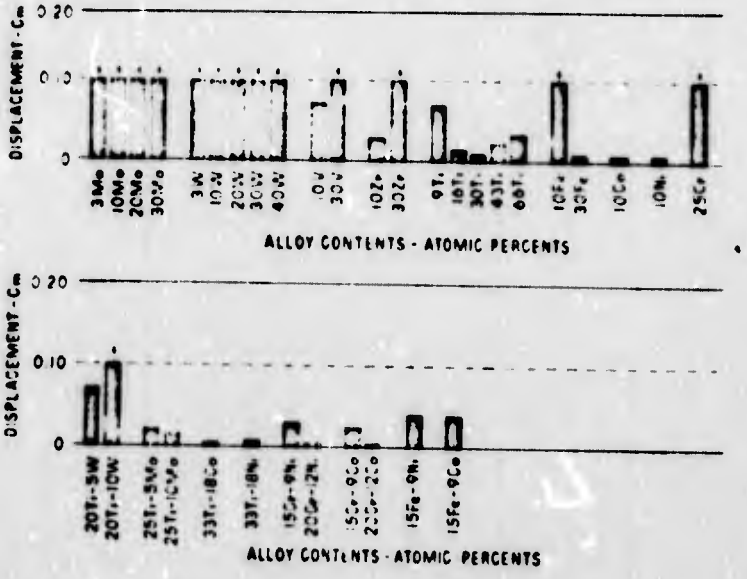

Figure 2.11. Displacement of the metal interface of tantalum-base alloys after 16 hr in air at 2000°F. (Michael)

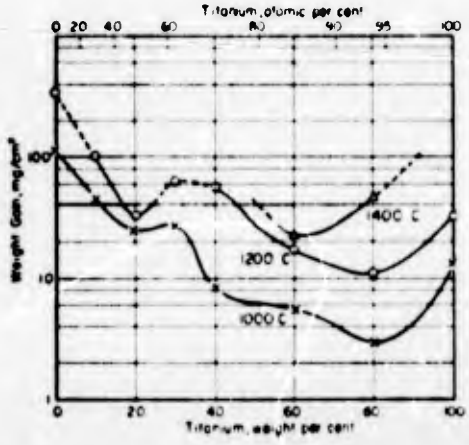

Figure 2.12. Weight gains of tantalum-titanium alloys oxidized for 6 hr in air at 1000, 1200, and 1400°C. (Klopp et al [85]).

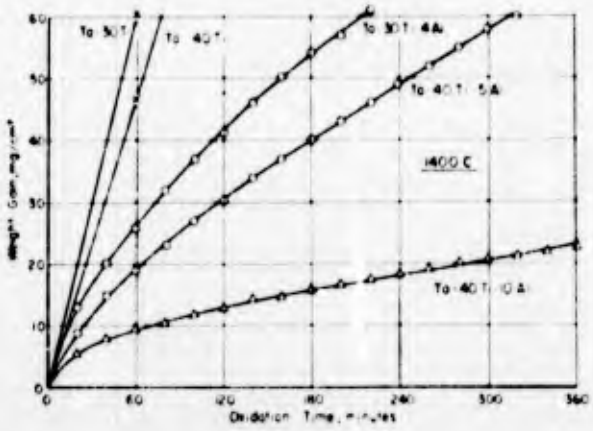

Figure 2.13. Effects of aluminium on the oxidation behaviour of tantalum-titanium alloys at 1400°C. (Klopp et al).

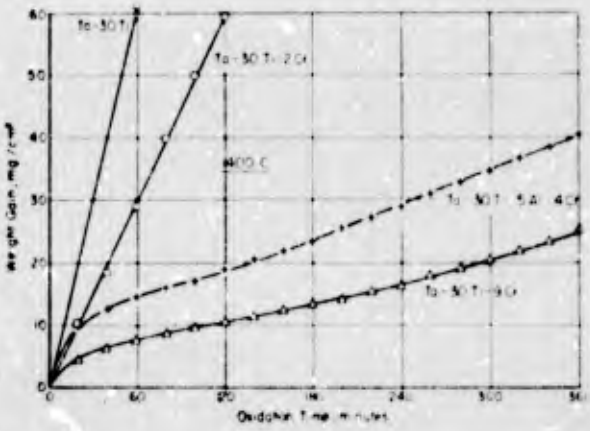

Figure 2.14. Effects of chromium and aluminium-chromium on the oxidation behaviour of tantalum-titanium alloys at 1400°C. (Klopp et al).

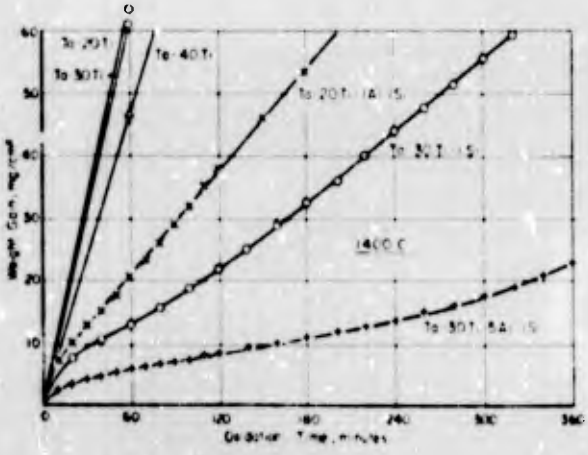

Figure 2.15. Effects of silicon and aluminium-silicon on the oxidation behaviour of tantalum-titanium alloys at 1400°C. (Klopp et al).

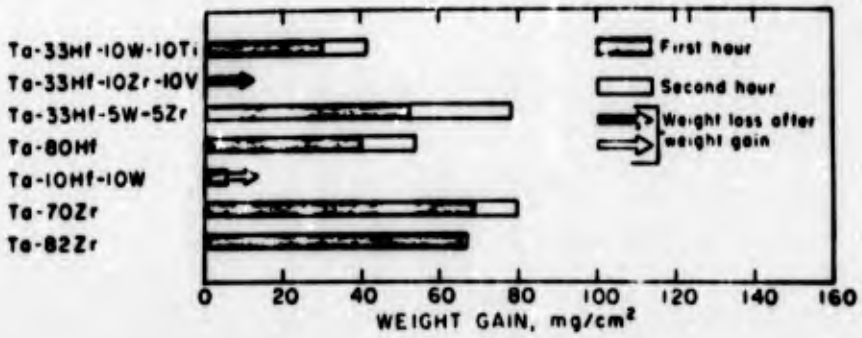

Figure 2.16. Oxidation data for tantalum alloys - 1000°C. (Babitze and Kato [51]).

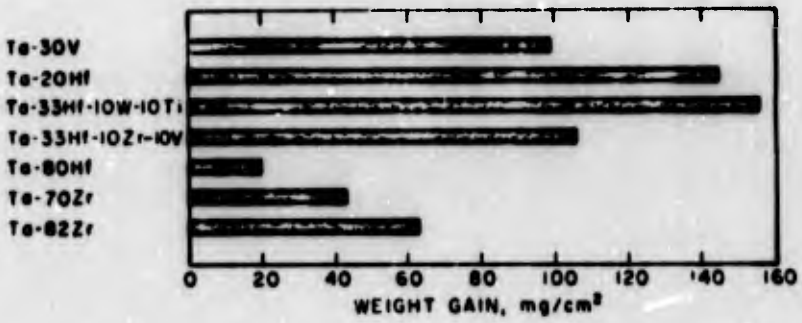

Figure 2.17. Oxidation data for tantalum alloys - 1400°C. (Babitze and Kato [51]).

Section 3. Tungsten and Tungsten Alloys

The early work on tungsten and its alloys has been reviewed in considerable detail by Barth and Rengstorff[96] and other reviews in less detail but including a number of more recent references, will be found in Refs. 3 and 4. Tungsten is relatively oxidation resistant below 700°C or so, but in the range 700-1200°C the oxidation becomes progressively more rapid, with an outer porous yellow layer of WO_3 and a thin inner layer of lower tungsten oxides. Above 1200°C the oxidation becomes catastrophic due to the volatilization of the WO_3.

The rate of oxidation above 700°C or so is most usually described in terms of an "paralinear" model, in which the initial rate is parabolic as a protective oxide builds up, becoming linear as it transforms to a porous non-protective outer layer. The linear rate constant depends on oxygen pressure, the general behavior suggesting a dissociative adsorption step is involved in the reaction. Figures 3-1 to 3-16 and Tables 3-I to 3-V present data from the early investigators.

At elevated temperatures, the overall removal of metal is determined by the evaporation of WO_3, and this appears to involve diffusion through a gaseous boundary layer: the rate is thus highly dependent on gas velocity. Figure 3-17, taken from Reference 3, shows some data, and Figures 3-18 and 3-19 show the evaporation rates of relevant species. Both Perkins[104] and Bartlett and McCamont[109] have noted that the rate of recession of various crystal faces differ, the latter finding that the oxidation rates decreased in the order (100) > (111) > (110). The reaction rate with the (100) surfaces was 6-7 times that with the other two faces. The rate of volatilisation of the oxide species also depends strongly on the water vapor content of the atmosphere as shown in Figures 3-20 to 3-22. There have been recent detailed studies of the thermodynamics of the oxidation process, and of the temperature dependence of the gas phase composition, by Culbransen[110] and by Neumann and Muller[111].

There have been several studies of the oxidation of tungsten at very high temperatures and low oxygen partial pressures in connection with the behavior of lamp filaments. This lies outside the scope of the present Handbook, but for a recent review of the general studies and presentation of much of the data see Batty and Stickney[112]; Figure 3-23 taken from their paper presents most of the kinetic data.

There has been relatively little work on the oxidation of tungsten-base alloys. The early work is again reviewed by Barth and Rengstorff[96]. Semmel[117] found that niobium additions produced a significant improvement in the oxidation resistance of tungsten, as shown in Figures 3-24 and 3-25. Semmel remarked that small additions (5 to 10%) of Co, Ti, Zr, V, Cr, and Mo had little effect on the oxidation resistance; Ta behaved much like Nb in a preliminary test. Prokoshkin, et. al.[118] have also studied the effect of Nb on the oxidation of W, and their results are presented in Table 3-VI. Semchyshen and Barr[119] found little improvement with 1.0% Nb, in agreement with Semmel, but 1.5% Nb produced a noticeable reduction in rate--Figure 3-26. Figures 3-27 and 3-28 show other systems studied in the same program, and Figure 3-29 compares the effect of four alloying elements.

Harmon[120] reported that chromium additions were beneficial; Table 3-VII shows oxidation rates of a number of alloys in hig program, and Table 3-VIII is a later set of results. However, it seems likely that very large chromium contests would be required to produce significant improvements[121].

Table 3-IX is a set of results from Holtz and Van Thyne[122]. Arkharor and Kozmanov[123] investigated the oxidation of W-Fe alloys containing up to 60% W. The 60W-40Fe alloy oxidized slower than Armco iron up to 800°C, forming an oxide of Fe_2O_3, Fe_3O_4 and $FeWO_4$. Above 800 there was an abrupt acceleration in the oxidation rate. Doerr, et. al.[124] have examined the oxidation of W-Co alloys: up to 9.7 wt.% Co a linear rate law is observed at 727 and 827°C. At 9.7 wt.% Co a reduction in rate at 727°C occurs. At 29.3 wt.% Co, the alloy was 17 times more resistant than W in a 2 hour test at 827°C. The principal components of the scale were a Co_3O_4 outer layer, a $CoWO_4$ intermediate zone, and a $W_{18}O_{49}$ inner zone.

Evans[125] has observed that while W-10% Cr alloys do not have particularly good oxidation resistance, the addition of small amounts of palladium produces a dramatic improvement. Tables 3-X and 3-XI report the oxidation life of specimens in the form of 4 mm rods, 15 cm long heated by resistance heating. The specimens all oxidized quite slowly until immediately before failure, when there was a catastrophic collapse. Figure 3-30 shows the oxidation behavior of some as-sintered alloys and Figure 3-31 shows the effect of palladium. If the chromium oxide layer present on the as-sintered material was removed by grinding to produce what Evans referred to as an "untreated" surface, the oxidation rate was in some cases rapid from the start. Figure 3-32 compares the oxidation of as-sintered and untreated specimens.

Andes and Heckel[126] have reported an extended study of a number of ternary tungsten-based systems, using a standard test of 5 hours at 1200°C in flowing air. Following the test, the weight of metal plus oxide was measured, and then the thickness of the metal remaining was measured metallographically. Figures 3-33 and 3-34 show the oxidation behavior of the binary alloys. For the vanadium and zirconium containing alloys, the scales were molten for all the compositions studied, so the alloys were not analyzed: it is probable that considerable losses of Zr and V were obtained on melting. Figures 3-35 to 3-45 show the oxidation behavior of the ternary systems: the best oxidation resistance was in the W-Cr-Ti system.

Wilson and McKinsey[127] studied the tungsten-niobium-tantalum system. Their oxidation results at 2190°F (1199°C) in terms of weight gain in 4 hours in oxygen are shown in Figure 3-47. The shaded areas represent regions where the improvement over the elementary metals is less than tenfold.

Table 3.I. Oxidation of tungsten in 1 hour. (Semmel [100]).

Temperature, F	Yellow and Gray Oxide Thickness per Side, mils	Blue Oxide Thickness per Side, mils	Total Oxide Thickness per Side, mils	Tungsten Loss per Side, mils	Weight Gain, g/cm^2	Weight Gain - Weight Loss x 10^2
1800	10.7	<1	10.7	2.3	0.037	1.6
1800(a)	10.1	<1	10.1	2.0		
1900	17.6	<1	17.6	3.2	0.062	1.9
2000	27.8	<1	27.8	5.3	0.101	1.9
2000	29.0	<1	29.0	5.5		
2100	34.2	<1	34.2	7.0	0.127	1.8
2100(a)	32.8	<1	32.8	7.1		
2200	23.2	<1	23.2	4.8	0.108	2.3
2200(a)	24.5	<1	24.5	5.0		
2300	17.5	1.9	19.4	5.7	0.062	1.1
2300	18.4	2.0	20.4	5.7		
2400	17.2	3.0	20.2	6.8	-0.057	
2500 top oxide	12.2	3.7	15.9			
2500 bottom oxide	7.4	0.2	7.6	11.0	-6.3	
2500(a) top oxide			15.5			
2500(a) bottom oxide			14.5	10.5		

(a) Data for a second batch of 99.95% tungsten.

Table 3.II. Oxidation of tungsten and molybdenum in 1 hour. (Semmel [100]).

Temp. F	Molybdenum Loss per Side, mils	Tungsten Loss per Side, mils	Tungsten Loss per Side, mils, All Pits Removed	Molybdenum Loss ÷ Tungsten Loss	Molybdenum Loss ÷ Tungsten Loss, All Pits Removed
1800	29.7	2.3	3.0	12.9	9.6
1900	30.2	3.2	5.1	9.4	5.9
2000	32.6	5.3	6.9	6.2	4.6
2100	35.0	7.0	8.6	4.9	4.0
2200	37.2	4.8	7.2	7.6	5.1
2300	39.6	5.7	5.7	6.9	6.9
2400	41.8	6.8	6.8	6.1	6.1
2500	44.0	11.0	11.0	4.1	4.1

Table 3.III. Oxidation of unalloyed tungsten in flowing air. (Anthony and Pearl [101]).

Temperature, F	Mass Velocity, lb/ft^2-in.	Thickness Increase, mils/side/hr	Surface Recession, mils/side/hr
1700	500	3.7	.85
1700	1500	4.1	1.0
1700	1500	3.6	.95
1700	4000	4.6	1.3
2000	500	35.8	11.0
2000	1500	34.0	10.9
2000	1500	33.3	10.8
2000	4000	36.8	11.0

Table 3.IV. Oxide thickness versus time, tungsten oxidized at temperatures of 500 to 1150 C, 7.6 cm of oxygen pressure. (Gulbransen et al [98,99]).

Temperature, °C	Weight Gain, μg/cm² at Indicated Time, min					Color	Adherence of Oxide	
	5	10	60	180	360		Surface	Edge
500	9.72	12.2	48.9	103.8	171	Blue black	Stable	Stable
500	19.5	31.0	91.2	180.5	283			
550	36.3	54.0	169	353.5	564	Blue black	Stable	Stable
600	67.4	118.5	473	1,025	1,560	Blue black with green edges	Stable	Stable
600[a]	93.5	143.4	523	1,080	1,620	Blue black	Stable	Split
600[b]	84.8	135.8	496	1,025	1,515	Blue black	Stable	Stable
612.5	90.0	149.0	569	1,272	1,710	Blue black	Stable	Stable
625	129.5	211.0	776	1,615	3,160	Black with yellow spots	Spalled	Split
625	139.7	263	1,342	2,880	4,660			
637.5	152.4	254.5	930	1,815	3,680	Black with yellow spots	Spalled	Split
650.0	228	330	1,130	2,930	8,020	Blue black with yellow covering	Spalled	Split
650.0	230	390	1,304	2,305	4,300	Blue black with yellow covering	Spalled	Stable
700	550	933	2,420	--	--	Black with green edges	Stable	Stable
750	1,048	1,597	3,380	--	--	Black with green edges	Stable	Stable
750	1,180	1,785	4,130	11,800	--	Black with green edges	Stable	Stable
750	1,342	1,740	3,742	--	--	Black with green edges	Stable	Split
775	1,468	2,005	4,980	--	--	Black with green edges	Stable	Split
800	1,593	2,135	8,780	--	--	Black with green edges	Stable	Split
800	1,730	2,310	9,300	--	--	Black with green edges	Stable	Split
825	1,833	2,760	--	--	--	Black with green edges	Stable	Split
850	2,980	4,940	16,090	--	--	Blue black, greenish yellowish edges	Stable	Split
900	2,510	4,000	17,000	--	--	Blue black, greenish yellowish edges	Stable	Split
950	3,020	5,940	--	--	--	Black with green edges	Stable	Split
950	3,950	6,140	--	--	--			
950	4,320	6,540	--	--	--			
1000	7,110	14,480	--	--	--	Black with greenish edges	Stable	Split
1050	13,750	21,650	--	--	--			
1100	10,000	24,350	--	--	--	Yellow-black	Stable	Split
1150	14,700	--	--	--	--			

(a) Heat treated at 1000 C overnight.
(b) Hydrogen treated overnight at 600 C.

Table 3.V. Oxide thickness versus time, tungsten oxidized at temperatures of 600 to 1100 C, varying oxygen pressure. (Gulbransen et al, 98,99).

Temperature C	Oxygen Pressure cm of Hg	Weight Gain, $\mu g/cm^2$ at Indicated Time, min					Color	Adherence of Oxide	
		5	10	60	180	360		Surface	Edges
600	7.6	67.4	118.0	473	1,025	1,560	Green edges Blue black	Stable	Split
600	5.2	65.5	103.5	438	970	1,570	Black	Stable	Stable
600	2.7	71.0	113.0	486	1,000	1,644	Black	Stable	Split
600	1.0	74.8	125.0	492	1,383	2,010	Black	Stable	Split
600	0.36	67.4	100.2	393	862	1,350	Black	Stable	Stable
950	7.6	3,950	6,140	--	--	-			
950	4.6	2,970	4,660	10,050	--	--			Split
950	1.9	2,360	3,700	--	--	--			Split
950	0.9	2,300	3,980	14,700	--	--	Green edges Gray black	Stable	Split
950	0.4	1,550	2,850	11,910	--	--	Green edges Gray black	Stable	Split
950	0.25	1,008	2,035	9,730	19,000	--	Green edges Black	Stable	Split
950	0.10	1,372	2,230	6,640	11,910	14,710	Green edges Gray black	Stable	Split
1000	7.6	7,110	14,450	--	--	--	Green edges Black	Stable	Split
1000	0.90	4,040	6,930	22,500	--	--			Stable
1000	0.25	1,325	2,380	8,150	10,700	--			Stable
1050	10.0	14,000	--	--	--	--			Stable
1050	7.6	13,750	21,850	--	--	--			Stable
1050	5.3	10,100	15,830	23,100	--	--	Yellow edges Yellow gray Surface	Stable	Split
1050	3.9	9,100	15,080	--	--	--			Stable
1050	2.0	7,500	12,170	--	--	--			Stable
1050	0.86	3,820	6,850	--	--	--			Stable
1050	0.50	1,558	2,515	3,700	--	--			Stable
1050	0.25	-535	1,820	-18,750	--	--	Gray black	Stable	Stable
1050	0.10	-907	-2,180	--	--	--	Gray black	Stable	Stable
1100	7.6	16,000	24,950	--	--	--	Yellow black	Stable	Split
1100	3.9	11,580	19,120	--	--	--			
1100	0.2	-4,730	-10,700	--	--	--	Gray black	Stable	Stable

Table 3.VI. The influence of thermal cycling on oxidation life. (Evans [125]).

	Wt.% Nb								
T°C	0	1	5	10	15	20	30	40	50
1000	14.45	--	4.32	3.06	2.21	2.26	1.0	2.06	1.79
1100	73.00	4.17	5.74	3.21	1.87	1.90	1.0	3.00	3.10
1200	13.80	5.32	4.84	4.45	2.36	1.90	1.0	4.49	6.15
1300	16.30	--	--	--	1.32	1.25	1.0	--	--

The figures are the ratio of the increase of weight of the alloys relative to the increase in weight of the alloy with 30% Nb after 4 hr oxidation in air. The weight gains for the W-30% Nb alloy were: 1000°C, 14.2 mg/cm^2; 1100°C, 19.4 mg/cm^2; 1200°C, 27.2 mg/cm^2; and 1300°C, 55.0 mg/cm^2.

Table 3.VII. Oxidation of tungsten binary alloys in dry oxygen. (Harmon [120]).

	Weight Gain, mg/cm^2/hour	
Alloy, %	1200 C	800 C
Unalloyed W	600	
2 Cr	370	
5 Cr	560	
10 Cr	120	
20 Cr	330	
30 Cr	320	
3.67 Si	37	Spalled
0.57 Si	220	
1.65 Si	240	
15 Cb	70	
30 Cb	13	Spalled
35 Cb	15	
40 Cb	Spalled	
25 Ta	7	Spalled
45 Ta	Spalled	
10 Ti	Spalled	
30 Ti	Exothermic	
10 V	Molten oxide	

Table 3.VIII. Oxidation of chromium-tungsten alloys in dry oxygen. (Harmon [120])

Alloy, %	Weight Gain, mg/cm², in., 100 Hr 1200 C	800 C
Unalloyed tungsten	60,000	--
9.0 chromium	45,000	--
26.5 chromium	Spalled	17
42.2 chromium	11	26

Table 3.IX. Oxidation of some tungsten-base alloys in air at 2000 F. (Holtz and Van Thyne [122]).

Composition W	Ni	Fe	Other	Weight Gain in Air, mg/cm²/hr
90	7	3		63
93	4.9	2.1		55
97	1.8	1.2		55
90	7.0	1.5	1.5Al	<100(a)
90	5.25	2.25	2.5Cr	67
90	5.25	2.25	2.5Mo	63
90	5.25	2.25	2.5Cb	60
100	--	--	--	50

(a) Large weight gain may have been related to porosity in the specimen.

Table 3.X. The Oxidation lives of some W-Cr-Pd alloys tested in air in the as-sintered condition. Specimens heated ohmically. (Evans [125]).

Temperature °C.	Oxidation life hrs. 5% Cr 0.1% Pd	5% Cr 1.0% Pd	5% Cr 2.0% Pd	10% Cr 0.1% Pd	10% Cr 1.0% Pd	10% Cr 2.0% Pd	15% Cr 1.0% Pd
1200	417	434	434	—	550	—	—
1300	60.5*	> 68	60*	84*	—	—	> 14
1400	49	22	10	34*	100	—	14
1450	< 1/4	13	10	85	> 94	—	
1500		< 1/4	< 1/4	< 1/4	> 50	—	
1600					7.5*	6*	
1700					1.4*	—	
1800					1.0	1.0*	

Table 3.XI. The influence of thermal cycling on oxidation life. (Evans [125]).

Alloy	Upper cycling temperature °C.	No. of cycles to failure	Cycled life at temperature hr.	Non-cycled life hr.
W- 5% Cr-0.1% Pd	1317	945	31.5	60.5
W- 5% Cr-1% Pd	1317	> 201	> 6.7	47.0
W- 5% Cr-1% Pd	1400	613	20.4	22.0
W-10% Cr-1% Pd	1400	1956	65.2	100.0
W-10% Cr-1% Pd	1500	516	17.2	25.0

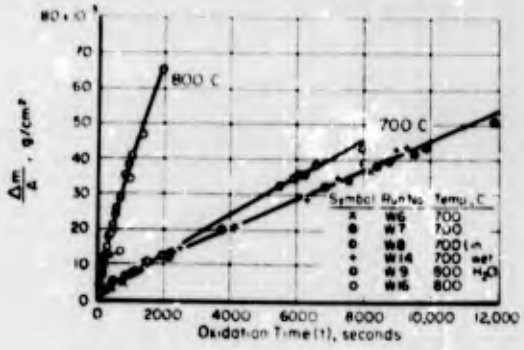

Figure 3.1. Oxidation of tungsten at 700 and 800 C. (Webb et al [97]).

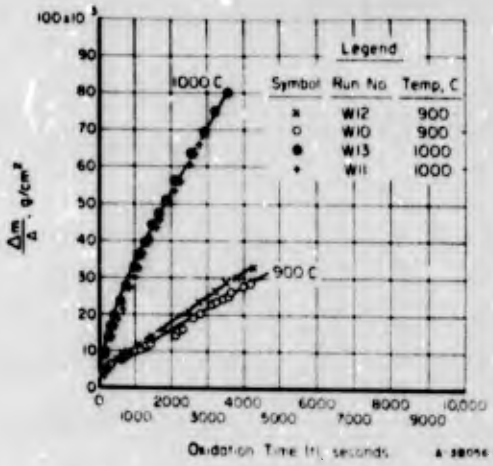

Figure 3.2. Oxidation of tungsten at 900 and 1000. (Webb et al [97]).

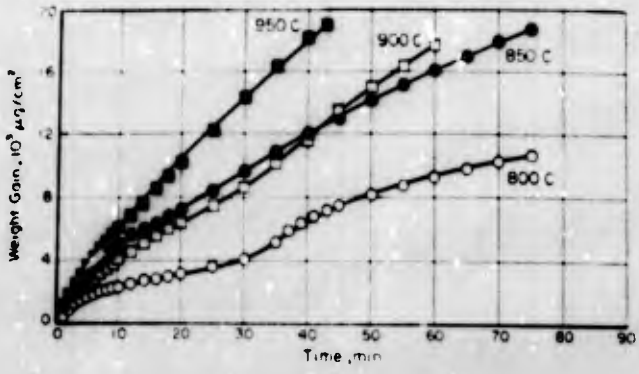

Figure 3.3. Oxidation of tungsten 800 to 950 C, 0.1 atm oxygen. (Gulbransen et al [98,99]).

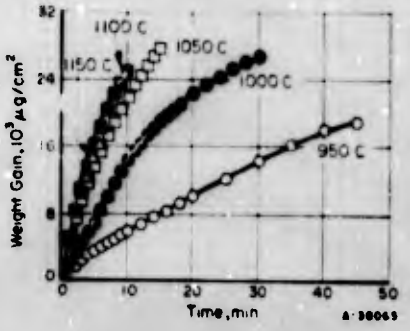

Figure 3.4. Oxidation of tungsten, 950 C to 1150 C, 0.1 atm oxygen. (Gulbransen et al [98,99]).

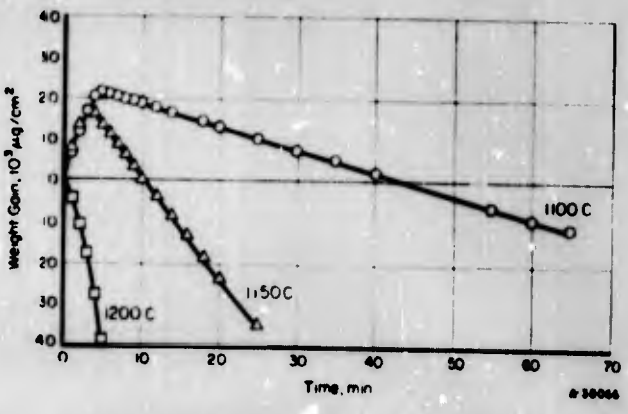

Figure 3.5. Oxidation of tungsten wire sample, 1100 to 1200 C, 0.1 atm oxygen. (Gulbransen et al [98,99]).

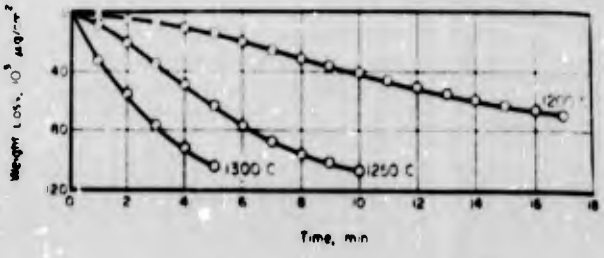

Figure 3.6. Oxidation of tungsten wire sample, 1200 to 1300 C, 0.0013 atm. oxygen [85,86]. (Gulbransen et al [98,99]).

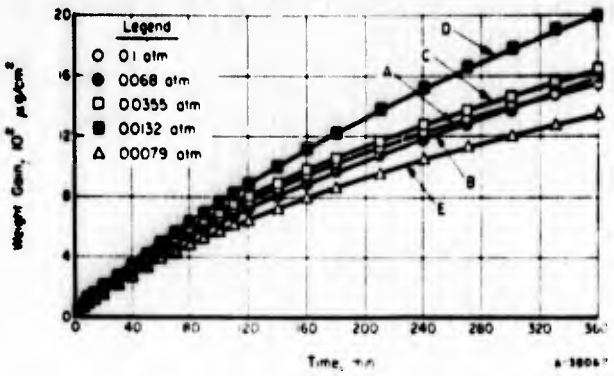

Figure 3.7. Oxidation of tungsten at 800 C, effect of oxygen pressure. (Gulbransen et al [98,99]).

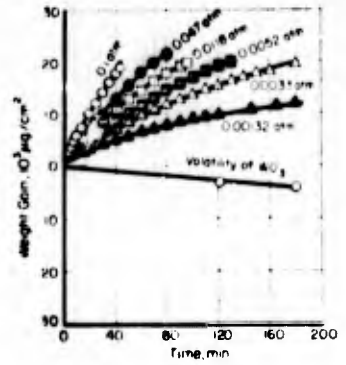

Figure 3.8. Oxidation of tungsten at 950 C, effect of pressure. (Gulbransen et al [98,99]).

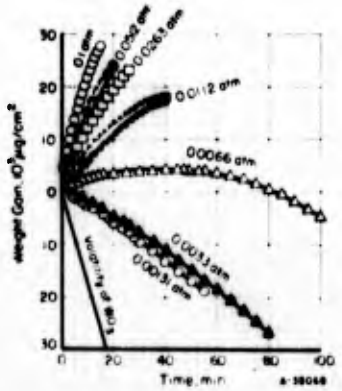

Figure 3.9. Oxidation of tungsten at 1050 C, effect of pressure. (Gulbransen et al [98,99]).

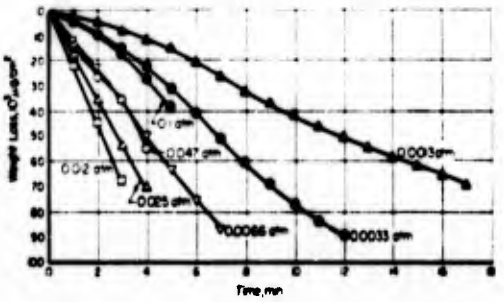

Figure 3.10. Oxidation of tungsten wire sample, at 1200 C, effect of pressure. (Gulbransen et al [98,99]).

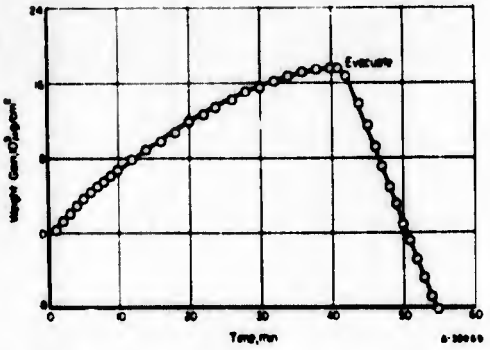

Figure 3.11. Oxidation of tungsten and volatility of oxide formed, 1050 C and 0.0112 atm of oxygen. (Gulbransen et al [98,99]).

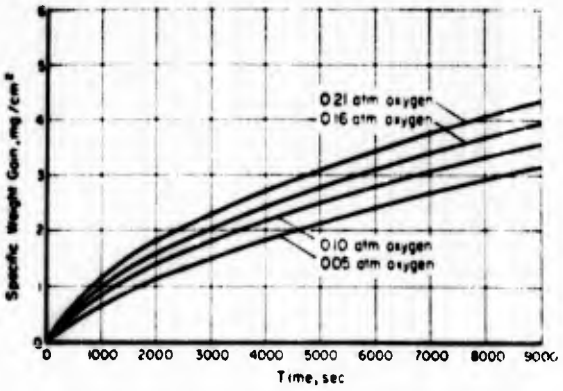

Figure 3.12. Oxidation of tungsten at 600 C (Average values). (Speiser, [102]).

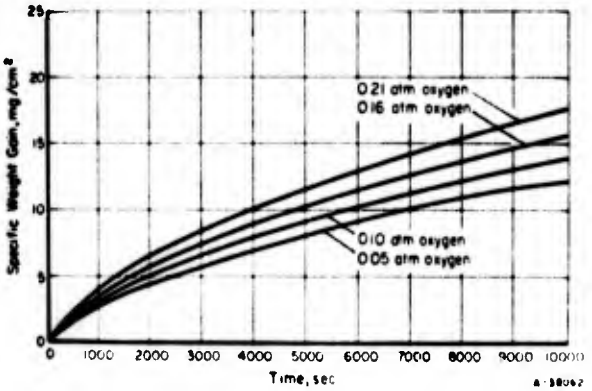

Figure 3.13. Oxidation of tungsten at 800 C(Average values). (Speiser [102]).

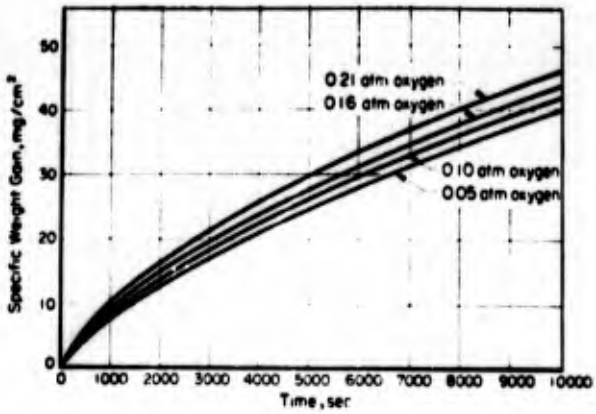

Figure 3.14. Oxidation of tungsten at 950 C (Average values). (Speiser [102]).

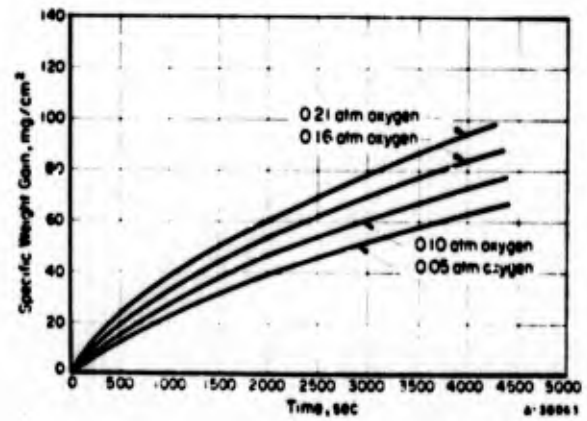

Figure 3.15. Oxidation of tungsten at 1100 C (Average values). (Speiser [102]).

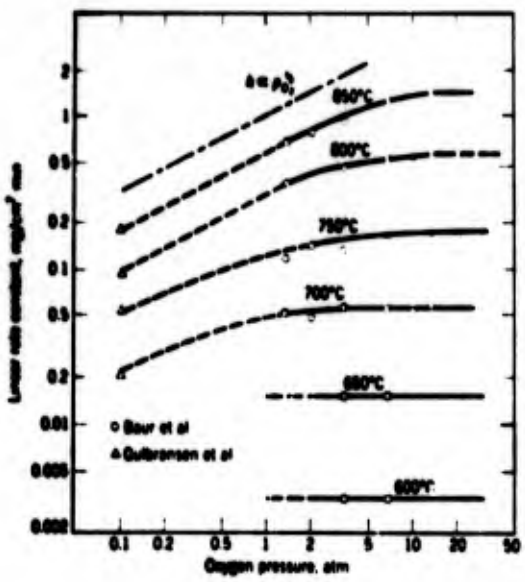

Figure 3.16. Linear rate constant for oxidation of tungsten as a function of oxygen pressure. After Baur et al [103] and Gulbransen et al [98], taken from Kofstad (3).

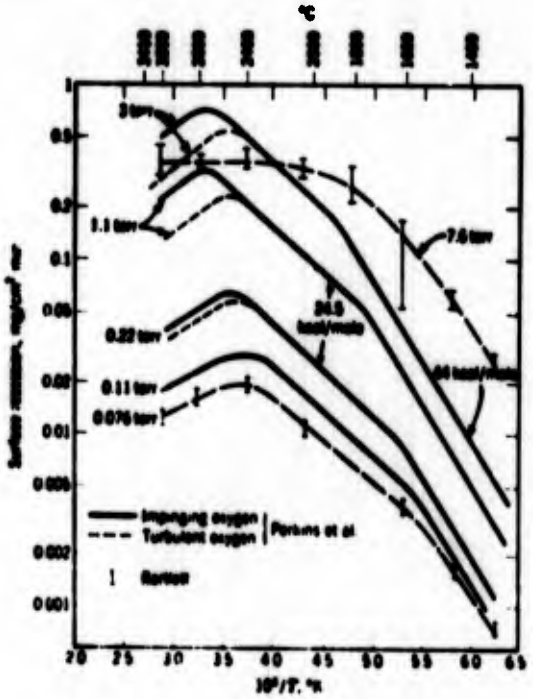

Figure 3.17. Surface recession rates in high-temperature oxidation of tungsten as a function of 1/T. After Perkins et al (104,105) and Bartlett (106); taken from Kofstad(3)

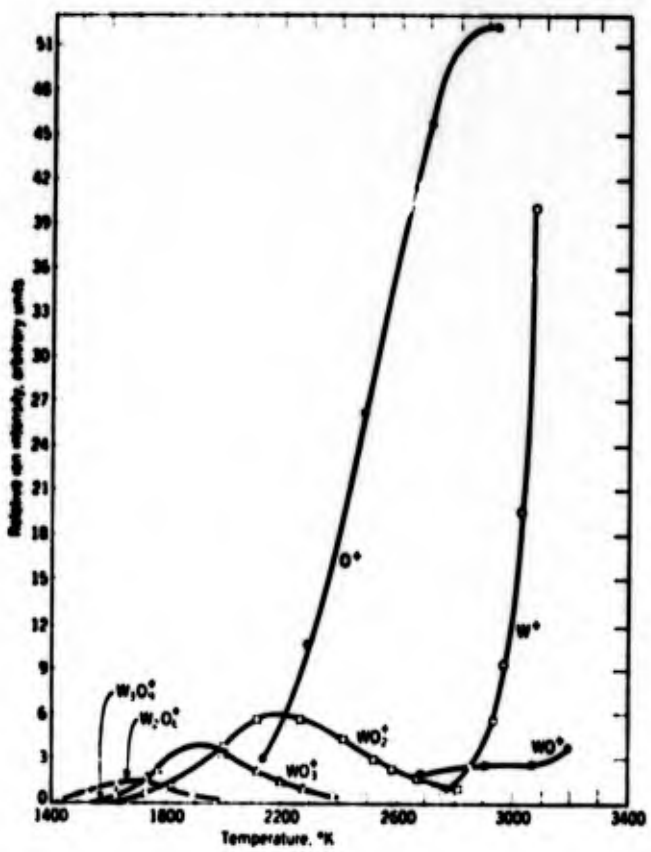

Figure 3.18. Relative evaporation rates of tungsten oxides, oxygen atoms, and tungsten metal as a function of temperature during oxidation of tungsten as 2.1 x 10^{-4} torr O_2. After Schissel and Trulson (106); from Kofstad (3).

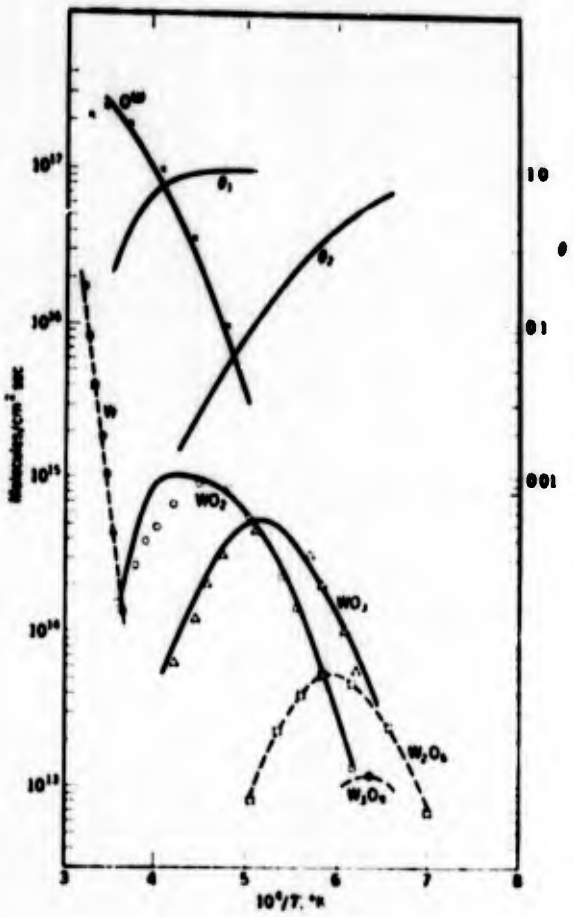

Figure 3.19. Evaporation rates of different gaseous species during oxidation of tungsten at 2 x 10^{-4} torr O_2 as a function of 1/T. Solid lines represent calculated values from the kinetic model. After Schissel and Trulson [108]; from Kofstad [3].

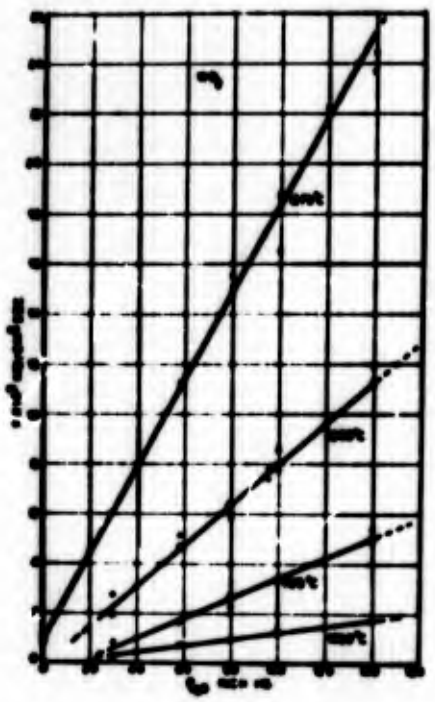

Figure 3.20. Variation of WO_2 volatility rate with water vapour. (Speiser and St. Pierre [107]).

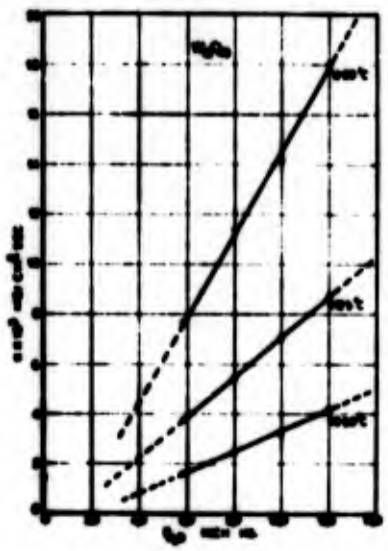

Figure 3.21. Variation of $W_{18}O_{49}$ volatility with the partial pressure of water.
(Speiser and St. Pierre [107]).

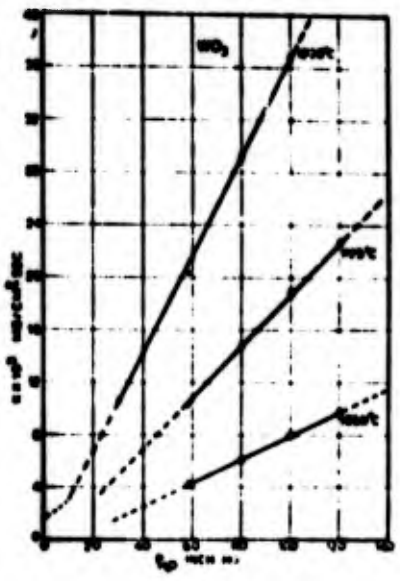

Figure 3.22. Variation of the WO_3 volatility rate constant with the P_{H_2O}. (Speiser and St.Pierre [107]).

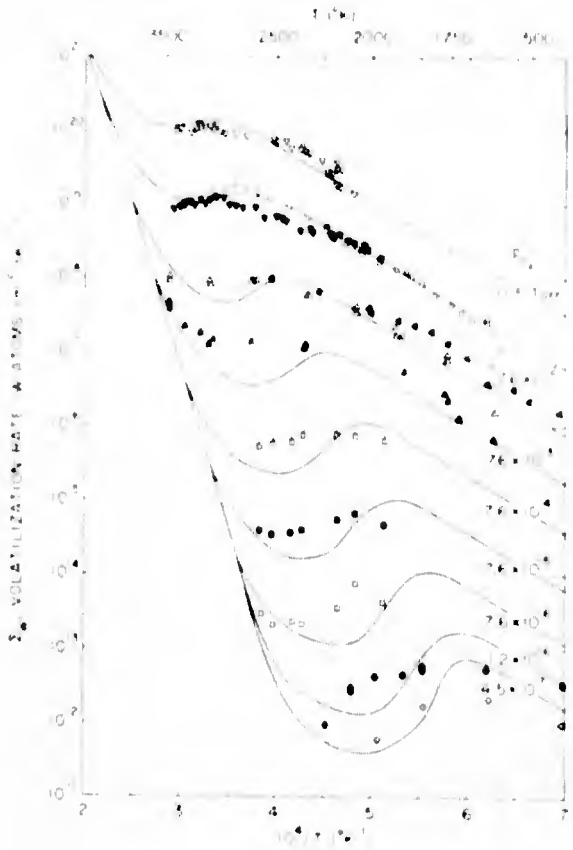

Figure 3.23. Rate of oxidation of tungsten at high temperature ($1400^{\circ} < T < 3500^{\circ}K$) and low pressure ($4.5 \times 10^{-7} < p'O_2 < 11.5$ Torr). The volatilization rate, ε_w, is defined as the number of tungsten atoms removed from the surface per cm^2 per sec by oxidation and by sublimation. (Multiply ε_w by 1.1×10^{-18} to obtain the weight loss in grams per cm^2 per hr.). Experimental data (O_2 partial pressure, $p'O_2$, expressed in Torr): Eisinger,[113] 4.5×10^{-7} (◇) and 1.2×10^{-6} (◆); Anderson,[114] 7.6×10^{-6} (□), 7.6×10^{-5} (■), and 7.6×10^{-4} (▯); Bartlett,[106] 7.6×10^{-3} (▲) and 7.6×10^{-2} (△); Rosner and Allendorf,[115] 7.0×10^{-2} (◀); Perkins et al,[104] 1.1 (○); Walsh et al[116] 1.15 (▼) and 11.5 (▽). The solid curves were computed on the basis of the quasi-equilibrium model for pressures, $p'O_2$, corresponding to the experimental measurements. (Batty and Stickney [112]).

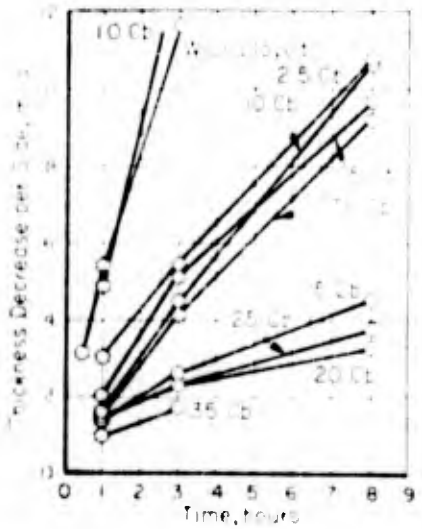

Figure 3.24. The oxidation of tungsten-columbium alloys at 2000 F. (Semmel [117]).

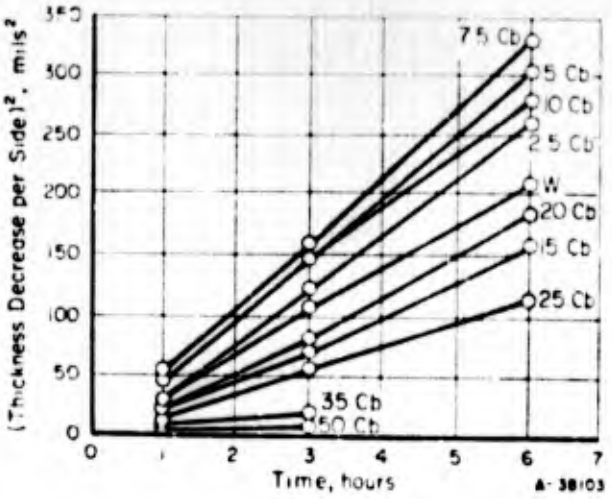

Figure 3.25. The oxidation of alloys at 2300 F. (Semmel [117]).

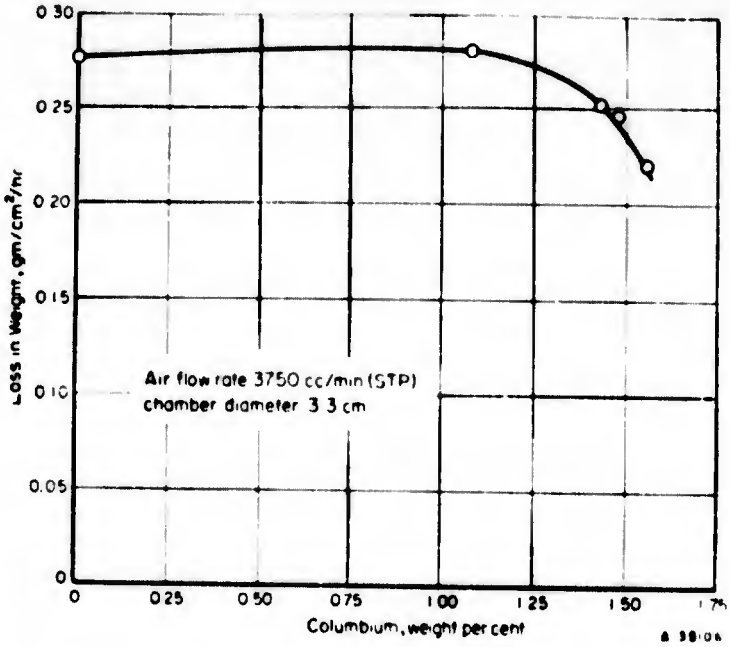

Figure 3.26. Rate of oxidation of arc-cast tungsten-graded columbium alloy at 2000 F in air. (Semchyshen and Barr [118]).

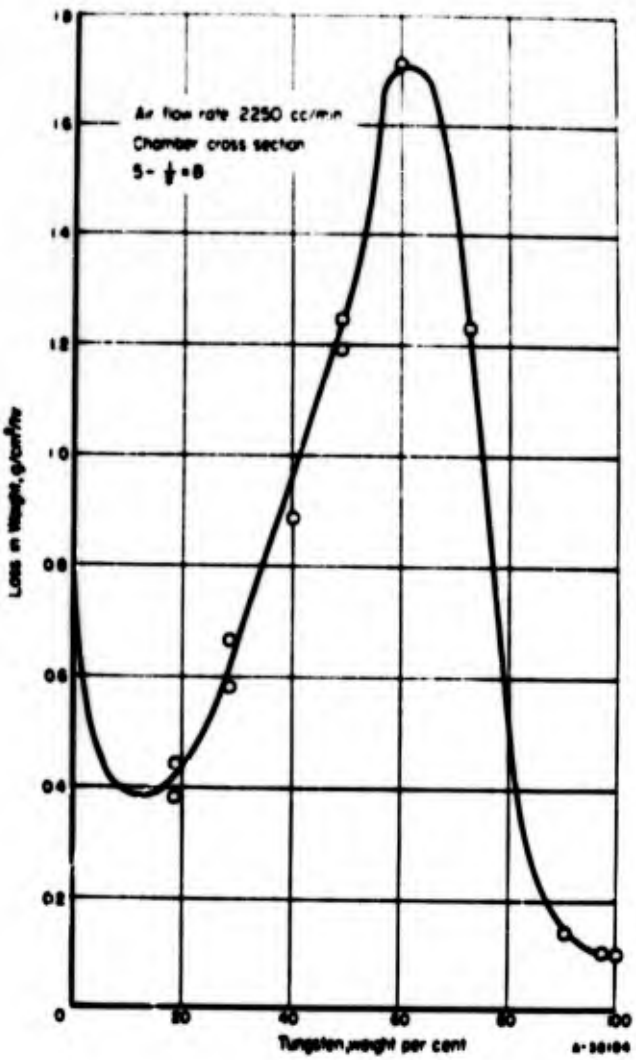

Figure 3.27. Rate of oxidation of arc-cast molybdenum-tungsten alloys at 1750 F in air. (Semchyshen and Barr [118]).

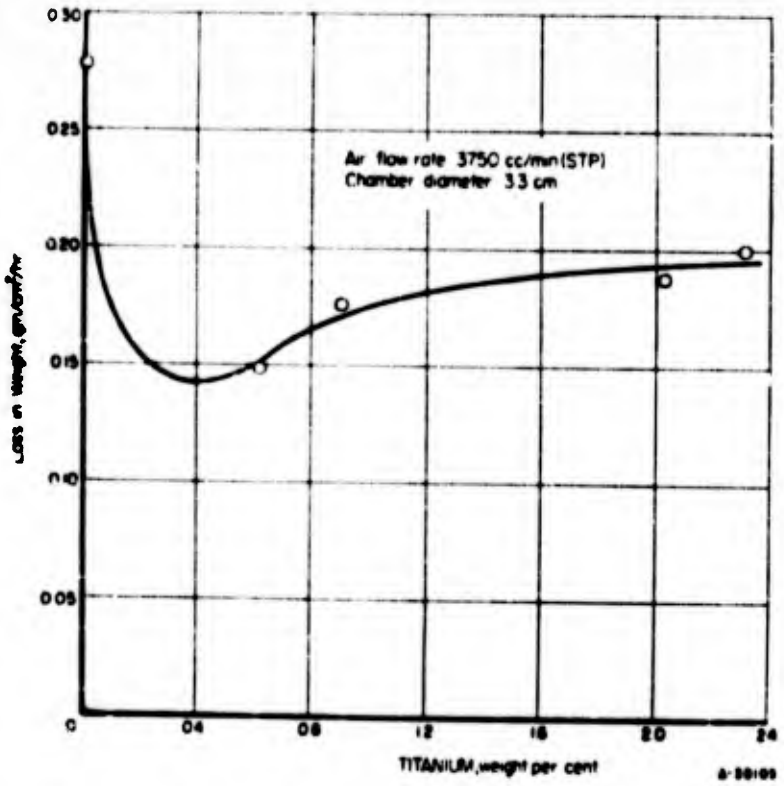

Figure 3.28. Rate of oxidation of arc-cast tungsten-graded titanium alloy at 2000 F in air. (Semchyshen and Barr [118]).

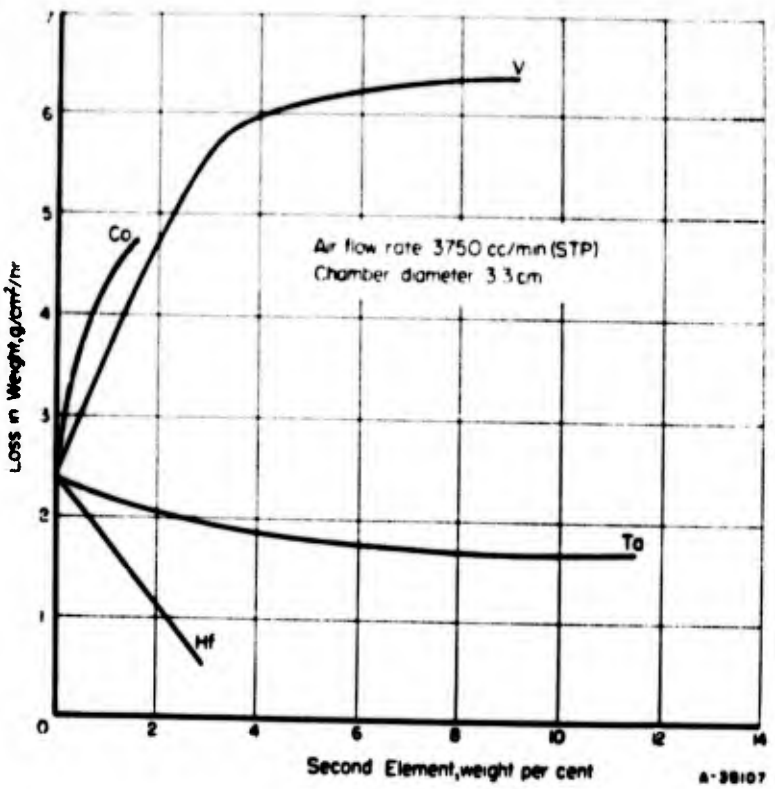

Figure 3.29. Rate of oxidation of arc-cast tungsten-base alloys at 2000 F in dry air. (Semchyshen and Barr [118]).

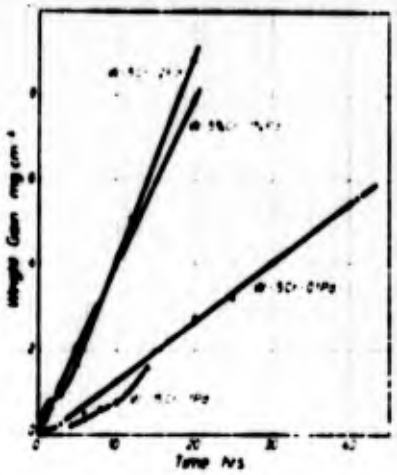

Figure 3.30. Typical weight gains observed in as-sintered W-Cr-Pd alloys at 1300°C .

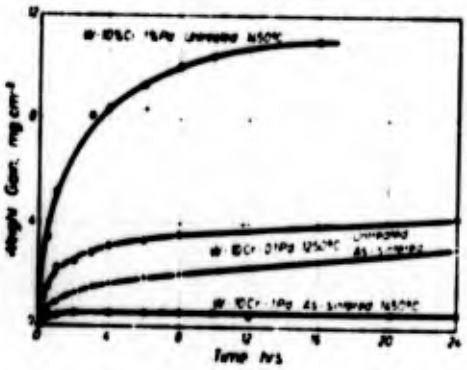

Figure 3.32. Comparison of oxidation curves of untreated and as-sintered alloys. (Evans [125]).

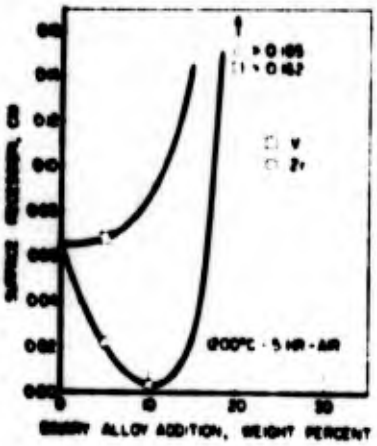

Figure 3.34. Surface recession per side (cm) of tungsten-base binary alloys after 5hr at 1200 C in flowing air. (Nominal compositions). (Andes and Heckel [126]).

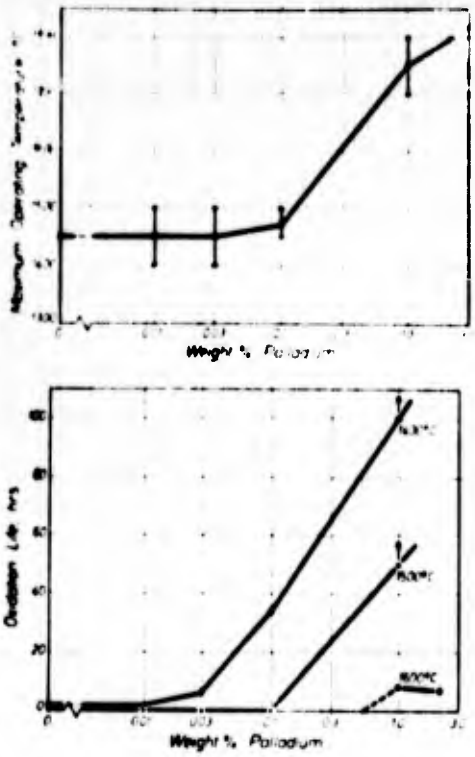

Figure 3.31. The effect of palladium on the oxidation resistance of as-sintered W-10% Cr alloys. (Evans [125]).

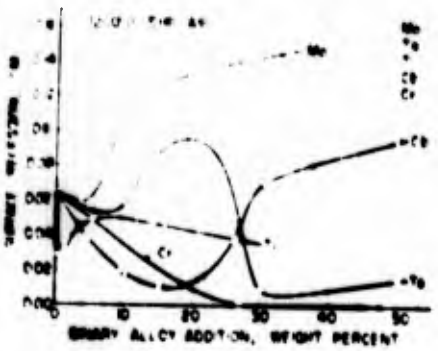

Figure 3.33. Surface recession per side (cm) of tungsten-base binary alloys after 5 hr at 1200 C in flowing air. (Analyzed compositions). (Andes and Heckel [126]).

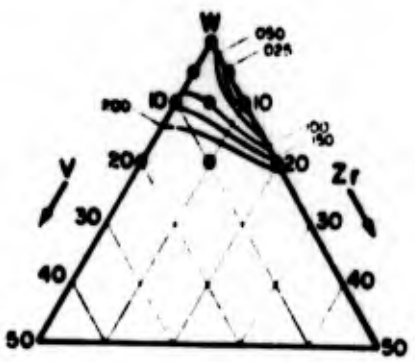

Figure 3.35. Surface recession per side (cm) of tungsten-vanadium-zirconium alloys after 5 hr at 1200 C in flowing air. (Nominal compositions.) (Andes and Heckel [126]).

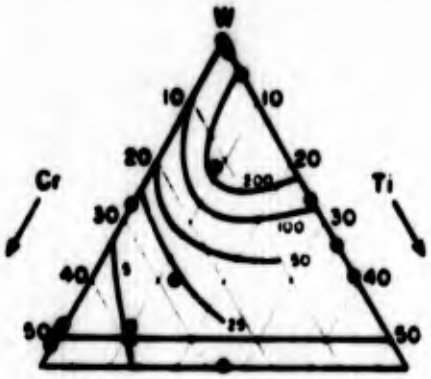

Figure 3.36. Total weight gain per unit area (mg per cm^2) of tungsten-chromium-titanium alloys after 5 hr at 1200 C in flowing air. (Analyzed compositions).
(Andes and Heckel [126]).

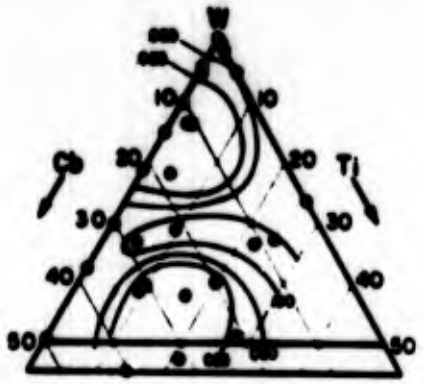

Figure 3.37. Surface recession per side (cm) of tungsten-columbium-titanium alloys after 5 hr at 1200C in flowing air. (Analyzed compositions).
(Andes and Heckel [126]).

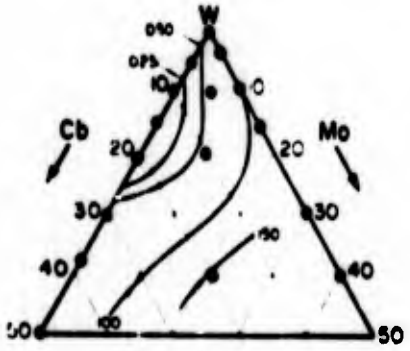

Figure 3.38. Surface recession per side (cm) of tungsten-columbium-molybdenum alloys after 5 hr at 1200 C in flowing air. (Analyzed compositions).
(Andes and Heckel [126]).

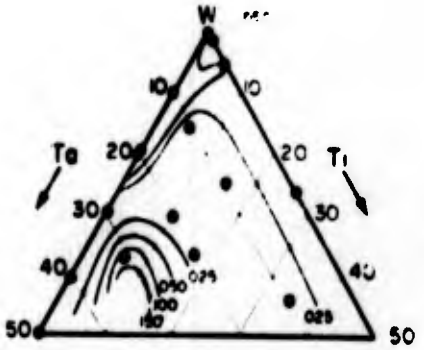

Figure 3.39. Surface recession per side (cm) of tungsten-tantalum-titanium alloys after 5 hr at 1200C in flowing air. (Analyzed compositions).
(Andes and Heckel [126]).

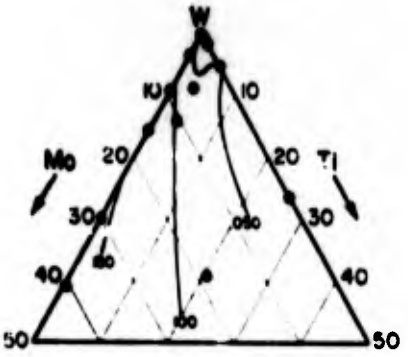

Figure 3.40. Surface recession per side (cm) of tungsten-molybdenum-titanium alloys after 5 hr at 1200C in flowing air. (Analyzed compositions).
(Andes and Heckel [126]).

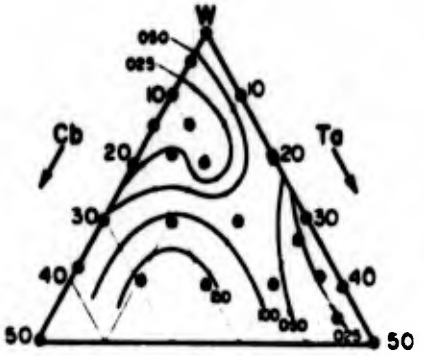

Figure 3.41. Surface recession per side (cm) of tungsten-columbium-tantalum alloys after 5 hr at 1200C in flowing air. (Analyzed compositions).
(Andes and Heckel [126]).

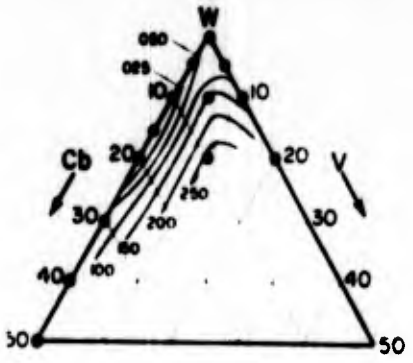

Figure 3.42. Surface recession per side (cm) of tungsten-columbium-vanadium alloys after 5 hr at 1200C in flowing air. (Nominal compositions).
(Andes and Heckel [126]).

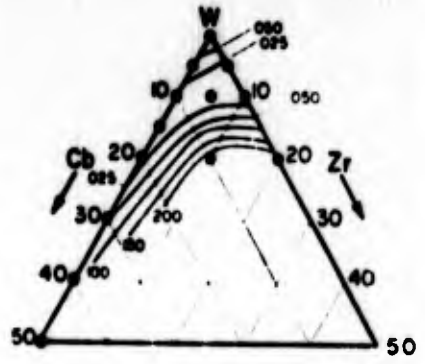

Figure 3.43. Surface recession per side (cm) of tungsten-columbium-zirconium alloys after 5 hr at 1200C in flowing air. (Nominal compositions).
(Andes and Heckel [126]).

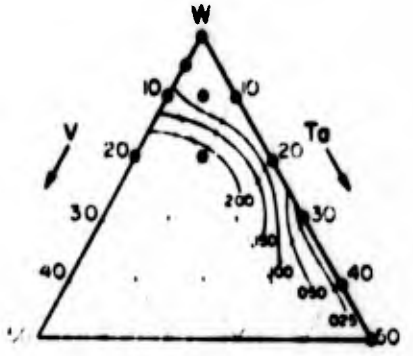

Figure 3.44. Surface recession per side (cm) of tungsten-tantalum-vanadium alloys after 5 hr at 1200C in flowing air. (Nominal compositions).
(Andes and Heckel [126]).

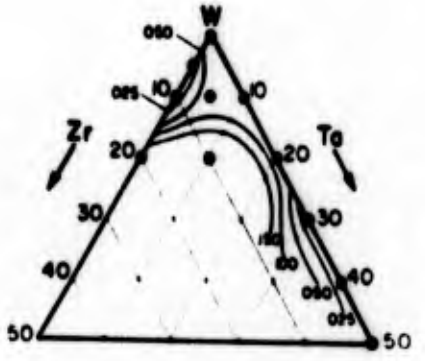

Figure 3.45. Surface recession per side (cm) of tungsten-tantalum-zirconium alloys after 5 hr at 1200C in flowing air. (Nominal compositions).
(Andes and Heckel [126]).

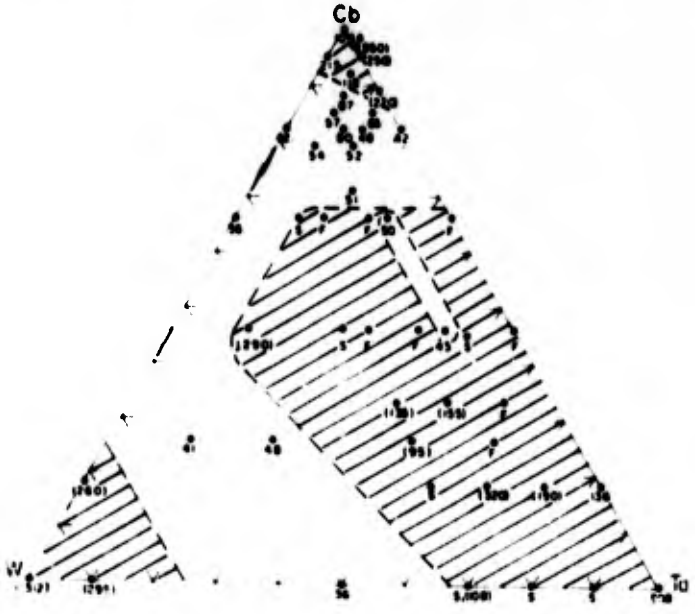

Figure 3.46. Left, weight gain (mg/cm sq) of tungsten-columbium-tantalum alloys after 4 hr in oxygen at 2190°F; ( ) extrapolated data, S spalling, and F very fast rate.
(Wilson and McKinsey [127]).

Section 4. Molybdenum and Molybdenum Alloys

The oxidation of molybdenum resembles that of tungsten, but in general it is much worse, as Table 3-II showed. Gleiser, et. al.[128], concluded that oxidation resistance would require the establishment of a different protective oxide, and examined the possibility of developing alloys which would oxidize to form protective molybdate scales. Table 4-I lists the relevant properties of a number of molybdates; the silicomolybdates were also considered. They concluded that barium, lanthanum, lead, cobalt, and nickel molybdates were potentially interesting; calcium, strontium, cadmium and thorium molybdates might also be possible for moderate temperatures. The nickel and cobalt molybdates turned out to have interesting properties, so most attention was focused on these alloys: some rate curves are shown in Figures 4-1 to 4-3. The relevant molybdates were indeed developed, but spalled on cooling. This was more serious with $NiMoO_4$ than with $CoMoO_4$, and the author attributed it to phase transformations in the oxides; various additives were considered which might stabilize them. The results of simple tests are listed in Table 4-II, from which it appeared that MnO_2 was the best potential stabilizer, and silicon was also a possibility. Initially, a Mo-25 wt.% Co-12 wt.% Si alloy oxidized slowly to form a thin, adherent molybdate scale; but after a certain time the rate accelerated, as shown in Figure 4-4.

Rengstorff[129] conducted a very large screening search for an oxidation-resistant molybdenum-based alloy. He commented that it would be necessary for an alloy to oxidize only 1/5000 as fast as molybdenum itself. The results of the screening tests for oxidation in flowing air at 1800°F (982°C) for 4 hr are shown in Figures 4-5 to 4-14; the black bar represents the oxidation resistance; the cross-hatched bars represent local variation in oxidation rate. If an alloy is represented by a black bar extending up to the zero penetration line, it was completely oxidation resistant. Table 4-III reports some additional tests on a further group of alloys: only the calcium-containing alloy that had not been pre-oxidized was resistant.

Further tests were then conducted on alloys which had proved to be more oxidation resistant. The results are shown in Figures 4-15 and 4-16. The good performance of both the calcium and nickel-containing alloys was attributed to the formation of protective layers of stable molybdates; as in Gleiser's study, the oxide spalled violently from the Mo-Ni alloys during cooling. None of the alloys represented a better than 100-fold reduction in oxidation rate, and Rengstorff comments that the prospects for developing a resistant alloy seem small.

Parfenov and Chuyan[130] examined the Mo-Al system, and were able to produce alloys with good oxidation resistance in the temperature range 700-1200°C, apparently due to the function of a protective layer of $Mo_8Al_2O_{25}$. Approximately 50% Al was required for maximum protection, larger amounts resulting in very rapid oxidation. Both Poole[131] and Guay[132] studied the oxidation or Mo-Hf alloys, pre-oxidizing them to form an internal HfO_2 distribution. Poole found good oxidation resistance in subsequent tests at 725°C over flat surfaces, but over the specimen edges and corners the scale cracked and spalled. Guay also oxidized at 725°C, and found that as MoO_3 formed and evaporated the HfO_2 accumulated at the specimen surface, eventually developing a protective coat.

Wainer[133] suggested that oxidation resistant alloys required the addition of two elements; one with an atomic radius less than molybdenum and a heat of formation for its oxide greater than that for MoO_2, in amounts between 0.5 and 6.0% to form internal oxides and act as a barrier to the ingress of oxygen. The second additive should have an atomic radius greater than that of molybdenum and be present in amounts between 0.1 and 1.0%. The best alloy was Mo-3.98% Al-0.96% Ca, which was "excellent" at both 1093° and 1371°C. On the basis of the other studies reported above, this seems unlikely.

As with tungsten, the high-temperature oxidation rate of molybdenum is largely determined by the volatility of MoO_3. Figures 4-17 and 4-18 show data from Speiser and St. Pierre[107].

Table 4.1. Properties of molybdates. (Gleiser et al[128]).

Formula	Water Solubility[a]	Hygroscopic or Deliquescent Nature[b]	Melting Point, deg Cent	Weight Stability[d]	Specific Gravity[e]	Room Temperature Crystal Structure	Number of Phases, 0 to 1000 C
Li_2MoO_4	S	H	705	NS 1200 C	2.66	Rhombohedral S.G. = $R\bar{3}$ a_c = 8.77Å α = 108°10′	
Na_2MoO_4	S	N	687	NS 1200 C	d_x = 3.63 d = 3.28	Cubic S.G. = Fd3m a_0 = 9.105Å	4
K_2MoO_4	S	D	920	NS 1200 C	2.91		4
Rb_2MoO_4	S	VD	929	NS 1200 C			4
Cs_2MoO_4	S	VH	925	NS 1200 C			4
$CuMoO_4$			<830				
Ag_2MoO_4	SS	N	<690		d_x = 4.61	Cubic, Spinel S.G. = Fd3m a_0 = 9.26Å	
$MgMoO_4$	S	N	>1080	S 1080 C			2
$CaMoO_4$	INS	N	965[c]		d = 4.38 – 4.53 d_x = 4.32	Tetragonal S.G. = $I4_1/a$ a_0 = 5.20Å c_0 = 11.38Å	3
$SrMoO_4$	0.0104 g per l at 17 C	N	≤1040[c]		d = 4.14 d_x = 4.72	Tetragonal S.G. = $I4_1/a$ a_0 = 5.39Å c_0 = 12.00Å	2
$BaMoO_4$	0.0058 g per l at 23 C	N	1480	S 1480 C	d = 4.65 – 4.97 d_x = 5.16	Tetragonal S.G. = $I4_1/a$ a_0 = 5.58Å c_0 = 12.30Å	1
$CdMoO_4$	SS	N	1070	NS 1070 C	d = 5.347 d_x = 6.13	Tetragonal S.G. = $I4_1/a$ a_0 = 5.14Å c_0 = 11.16Å	2
$Al_2(MoO_4)_3$	SS	N	<1000[c]				
$La_2(MoO_4)_3$	INS	N	980	S 1100 C		Tetragonal Pseudo—$I4_1/a$ a_c = 5.356Å c_0 = 11.846Å	1
$Zr(MoO_4)_2$	INS		>910				
$PbMoO_4$	INS	N	1065	S 1000 C NS 1080 C	d = 6.03 – 7.01 d_x = 6.89	Tetragonal S.G. = $I4_1/a$ a_0 = 5.41Å c_0 = 12.08Å	1
$Th(MoO_4)_2$	INS	N	1000[c]			Tetragonal	2
$Cr_2(MoO_4)_3$	INS	N	<1000[c]				
$SeO_2 \cdot MoO_3$			1000[c]				
$Fe_2(MoO_4)_3$	INS	N	1000[c]				
$CoMoO_4$	SS	N	1040	S 1040 C	α = 3.6 β = 4.5 γ = 4.1		3
$NiMoO_4$	INS	N	970	S 970 C	α = 3.5 β = 4.9 γ = ...		3

[a] S = soluble; SS = slightly soluble; INS = insoluble.
[b] H = hygroscopic; VH = very hygroscopic; D = deliquescent; VD = very deliquescent; N = neither hydroscopic nor deliquescent.
[c] Decomposes before melting.
[d] S = stable; NS = nonstable.
[e] d_x = specific gravity determined by X-rays.
d = specific gravity determined by other means.

Table 4.II. Effect of oxide additions on the structure and spalling of cobalt molybdate and nickel molybdate after heating at 1000 to 1100 C. (Gleiser et al[128]).

Added Oxide	Resulting Phases and Effect on Spalling
Cobalt Molybdate	
Al_2O_3	Reacted rapidly to produce $CoAl_2O_4$ spinel plus MoO_3.
Cr_2O_3	Reacted rapidly to produce $CoCr_2O_4$ spinel plus MoO_3.
CuO	Product melted below 1000 C, spalled.
Fe_2O_3	Reacted to produced $CoFe_2O_4$ plus MoO_3.
$MgMoO_4$	Stabilized γ phase by solid solution.
MnO_2	Stabilized γ phase by solid solution.
SiO_2	Apparently stabilized γ phase for about 200 hr, then new phase appeared.
ZnO	Stabilized γ for 44 hr, but product spalled after 120-hr test.
Nickel Molybdate	
Al_2O_3	Reacted to produce $NiAl_2O_4$ spinel plus MoO_3.
$CaMoO_4$	Spalled after less than 16-hr heating, may not spall after 25 hr.
CaO	Product spalled if CaO present in less than 20 molar per cent; no spalling after 18 hr if 50 molar per cent initially present.
Cr_2O_3	Reacted rapidly to form $NiCr_2O_4$ plus MoO_3.
CuO	Product melted below 1000 C, spalled.
Fe_2O_3	Reacted rapidly to form $NiFe_2O_4$ plus MoO_3.
$MgMoO_4$	Stabilized γ phase by solid solution.
MnO_2	When present in concentrations greater than 20 molar per cent, stabilized γ phase by solid solution.
$NiWO_4$	Product spalled in all cases tested.
SiO_2	Results inconclusive; may have stopped spalling temporarily.
TiO_2	Results inconclusive; may have stopped spalling temporarily.
ZnO	Product spalled after 44-hr test.
ZrO_2	Single test showed no spalling after 23-hr test.

Table 4.III. Oxidation at 1800°F of alloys of molybdenum with copper, lead, tin, antimony, zinc, manganese, lithium, magnesium, and calcium. (Rengstorff [129]).

Alloying Element	Estimated Composition, Pct	Pretreatment	Time of Test, Hr	Initial Weight of Sample, G*	Sample Lost by Oxidation, Pct
Copper	9.0	Preoxidized	2	4.8	96
		Not preoxidized	2	4.6	85
Lead	5.4	Preoxidized	2	4.4	91
		Not preoxidized	2	5.2	92
Tin	4.5	Preoxidized	2	4.9	86
		Not preoxidized	2	4.7	83
Antimony	5.9	Preoxidized	2	4.4	94
		Not preoxidized	2	4.8	75
Zinc	7.0	Not preoxidized	2	6.1	80
Manganese	<4.5	Not preoxidized	2	5.6	63
Lithium	Unknown	Preoxidized	2	4.5	100
		Not preoxidized	4	5.1	94
Magnesium	Unknown	Preoxidized	3	6.3	89
		Not preoxidized	4	6.3	78
Calcium	8.7 (analyzed)	Preoxidized	3	6.9	88
		Not preoxidized	4	6.8	None

* All samples were approximately ⅛ in. thick.

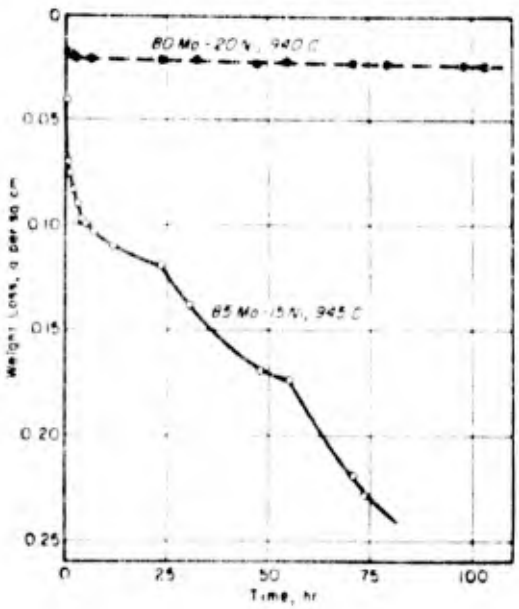

Figure 4.1. Oxidation curves for two molybdenum-nickel alloys. (Gleiser et al [128]).

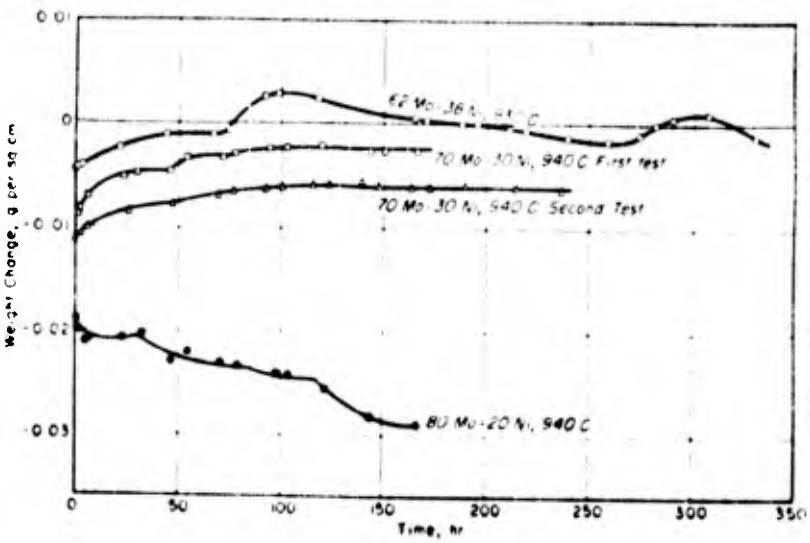

Figure 4.2. Oxidation curves for three molybdenum-nickel alloys. (Gleiser et al [128]).

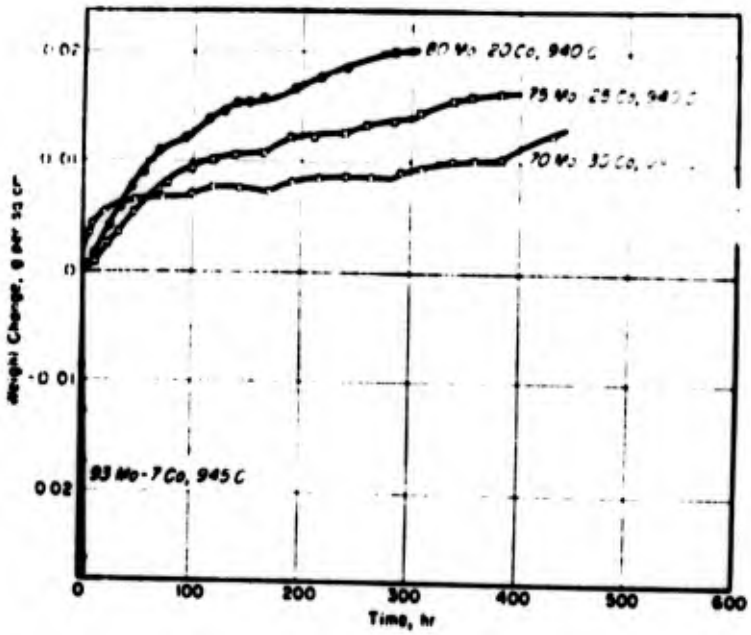

Figure 4.3. Oxidation curves for four molybdenum-cobalt alloys.
(Gleiser et al [118]).

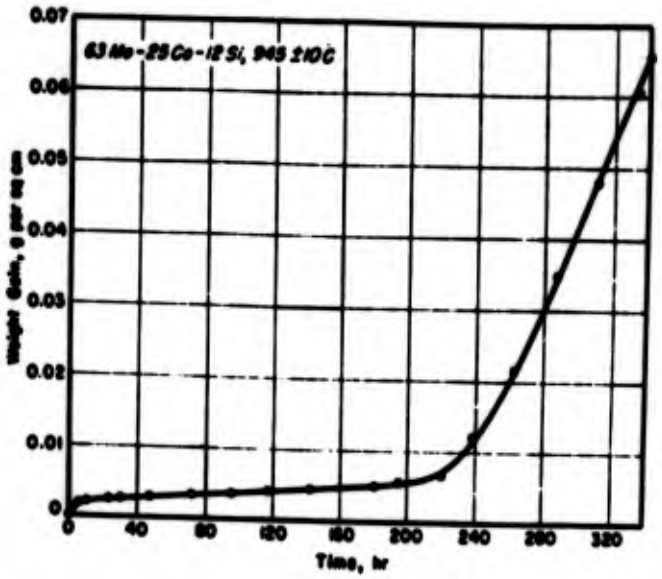

Figure 4.4. Oxidation curve for a 63% molybdenum-25% Cobalt-12% silicon alloy.
(Gleiser et al [128]).

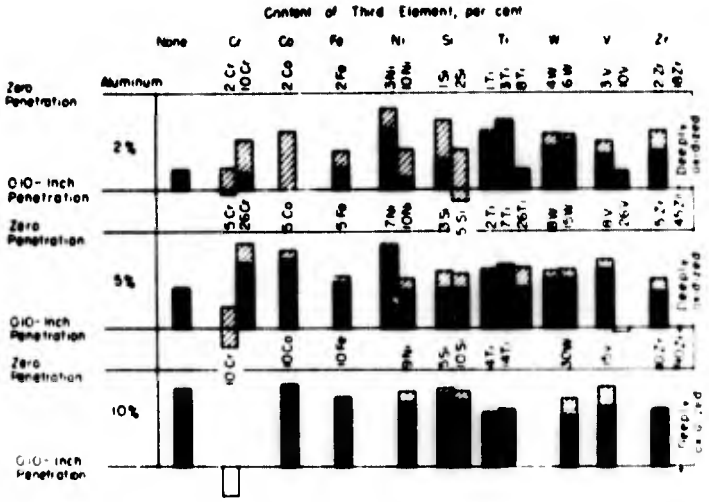

Figure 4.5. Graph shows the oxidation resistance of binary and ternary molybdenum alloys containing aluminium. (Rengstorff [129]).

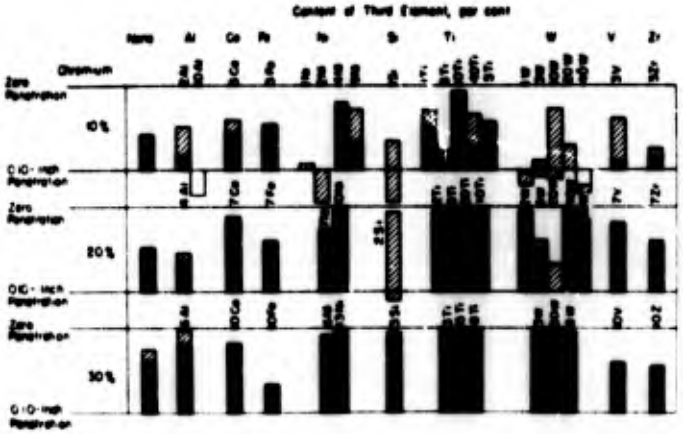

Figure 4.6. Graph shows the oxidation resistance of binary and ternary molybdenum alloys containing chromium. Rengstorff [129]).

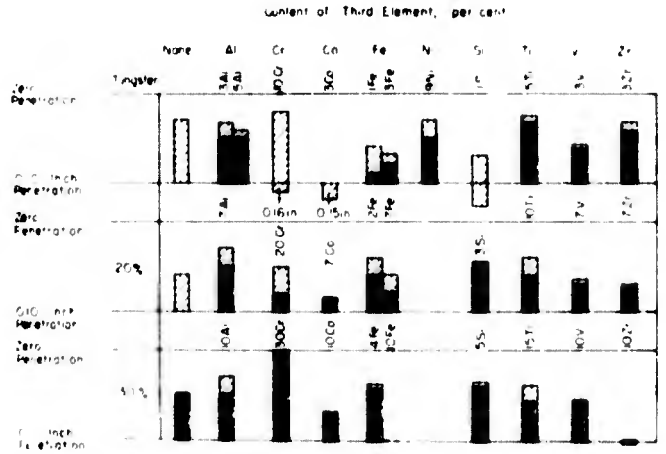

Figure 4.7. Graph shows the oxidation resistance of binary and ternary molybdenum alloys containing cobalt. (Rengstorff [129]).

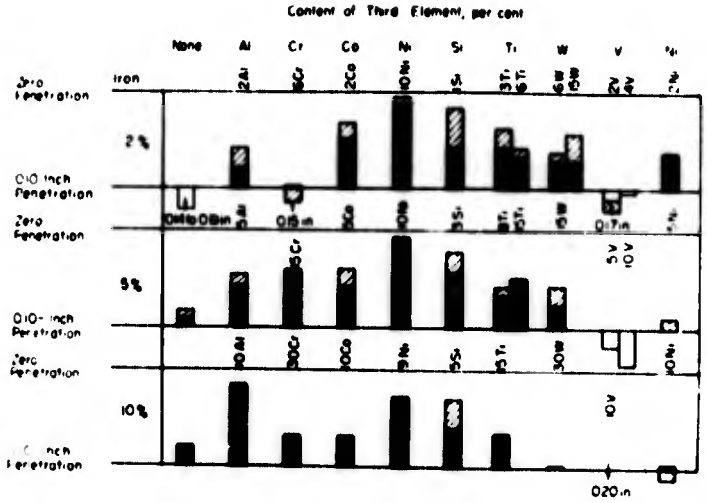

Figure 4.8. Graph shows the oxidation resistance of binary and ternary molybdenum alloys containing iron. (Rengstorff [129]).

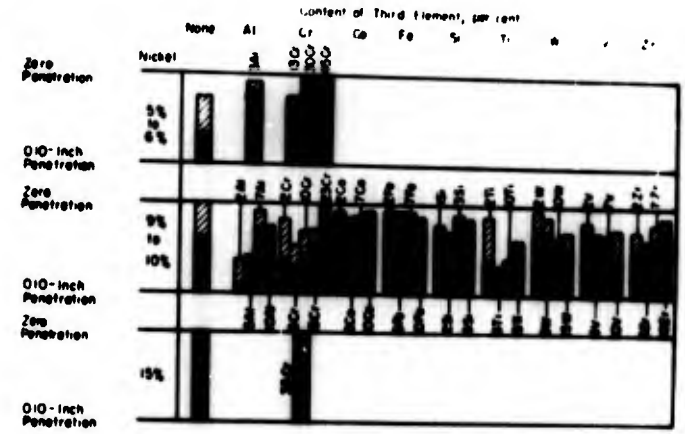

Figure 4.9. Graph shows the oxidation resistance of binary and ternary molybdenum alloys containing nickel. (Rengstorff [129]).

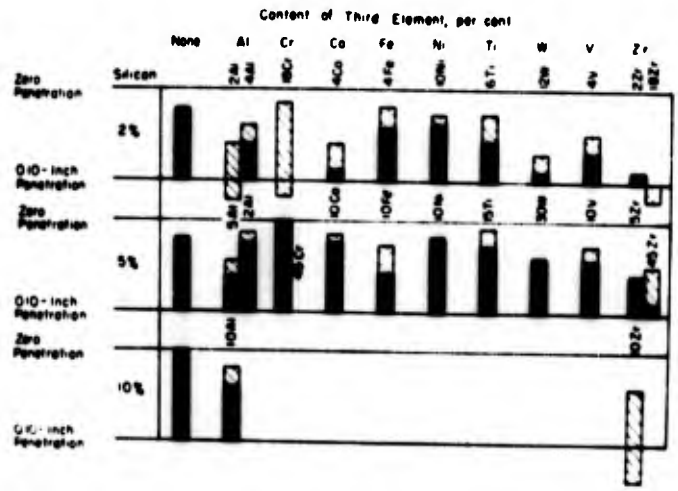

Figure 4.10. Graph shows the oxidation resistance of binary and ternary molybdenum alloys containing silicon. (Rengstorff [129]).

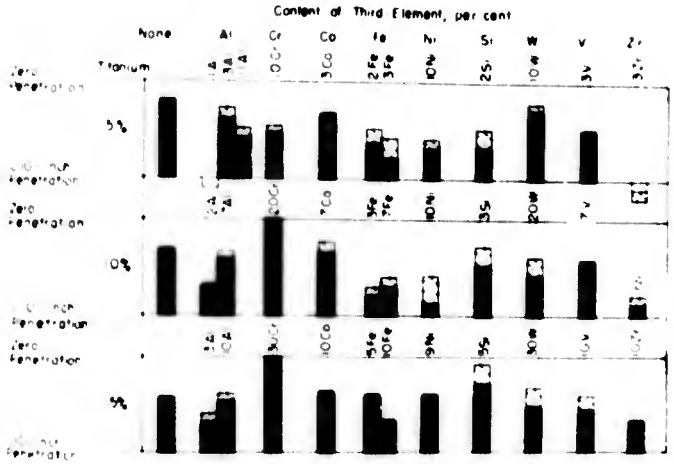

Figure 4.11. Graph shows the oxidation resistance of binary and ternary molybdenum alloys containing titanium.
(Rengstorff [129]).

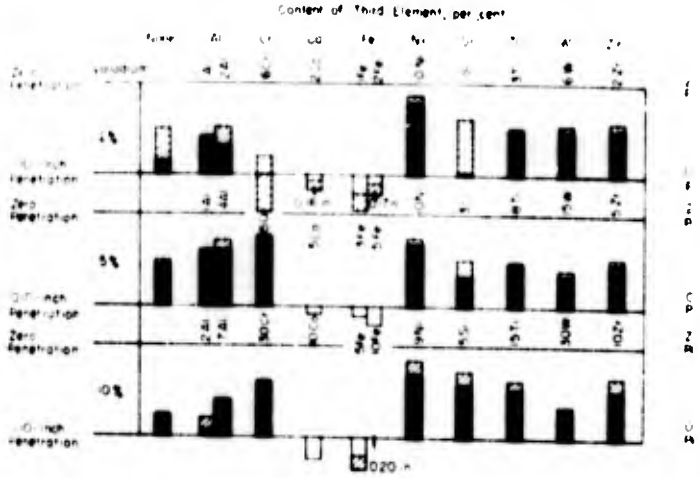

Figure 4.12. Graph shows the oxidation resistance of binary and ternary molybdenum alloys containing tungsten.
(Rengstorff [129]).

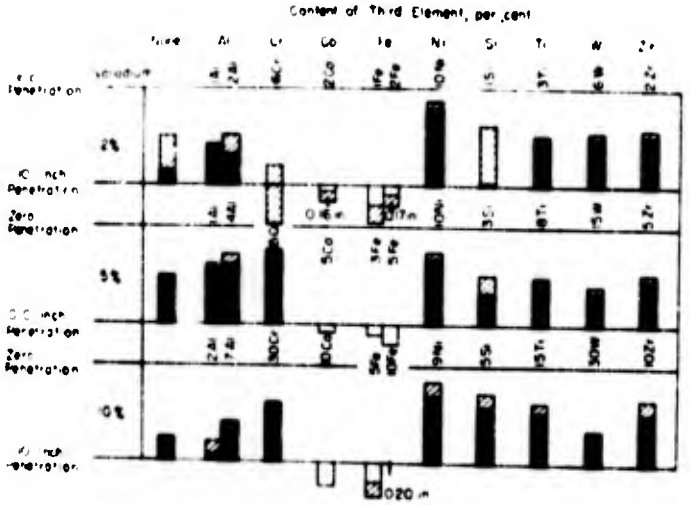

Figure 4.13. Graph shows the oxidation resistance of binary and ternary molybdenum alloys containing vanadium.
(Rengstorff [129])

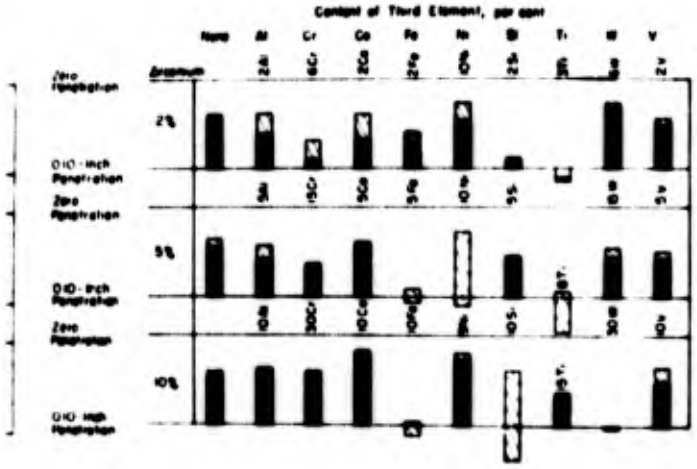

Figure 4.14. Graph shows the oxidation resistance of binary molybdenum alloys containing zirconium. (Rengstorff [129]).

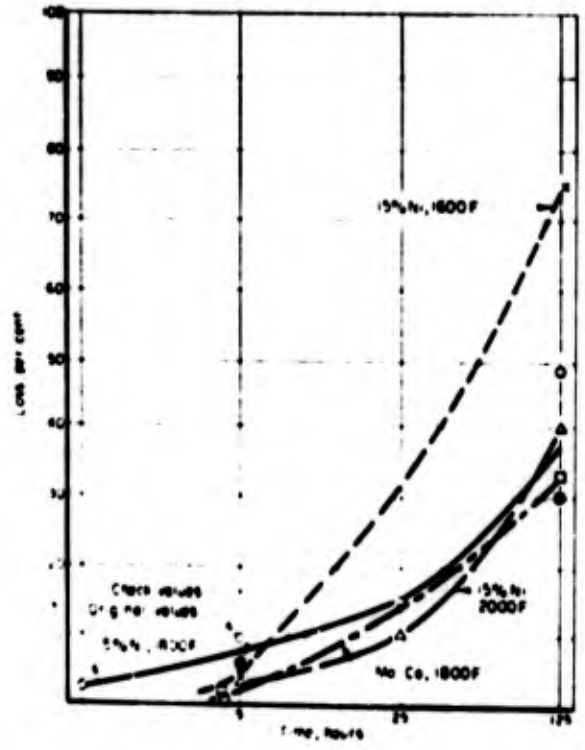

Figure 4.15. Oxidation resistance of 15% Ni-85% Mo alloy as a function of time at 1600°, 1800°, and 2000°F and of an Mo-Ca alloy at 1800°F is charted. (Rengstorff [129]).

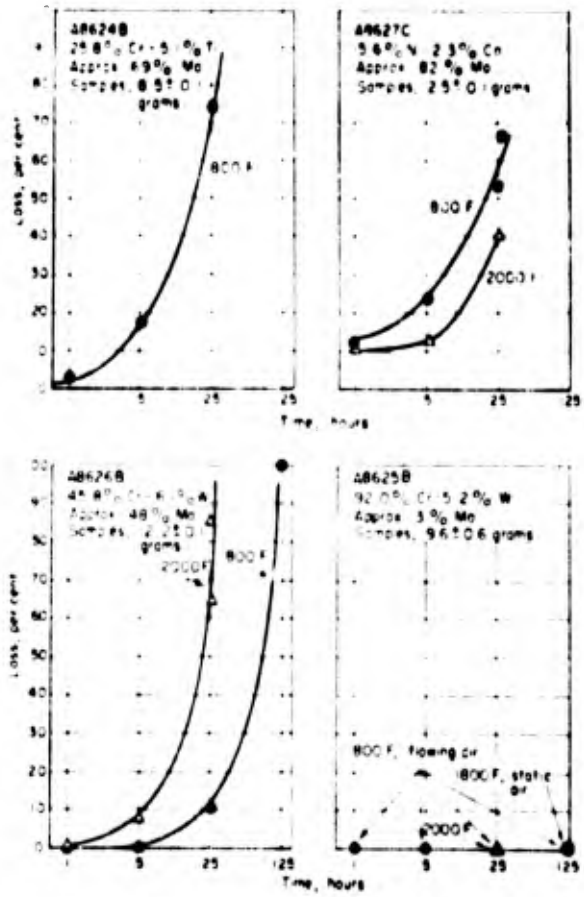

Figure 4.16. Charts show the oxidation rate of various molybdenum alloys containing chromium, titanium, nickel, cobalt, and tungsten at 1800° and 2000°F. (Rengstorff (129)).

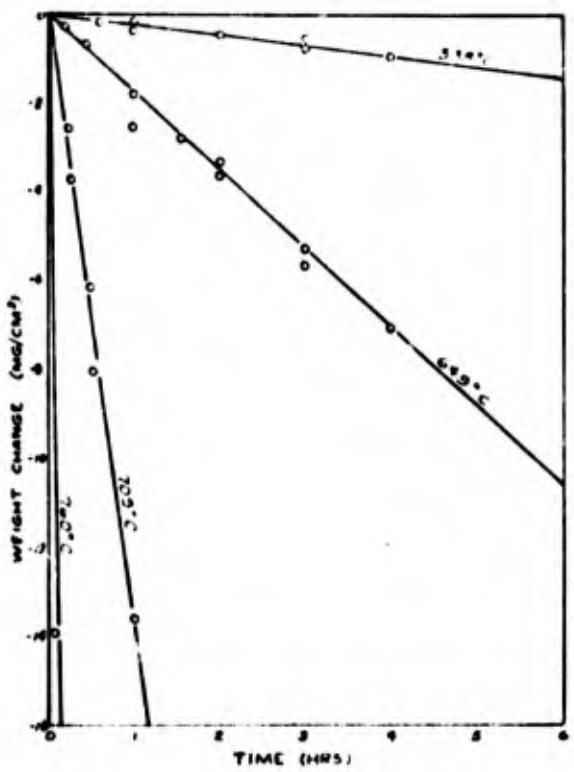

Figure 4.17. Rate of sublimation of MoO_2 at several temperatures. (Speiser and St. Pierre (107)).

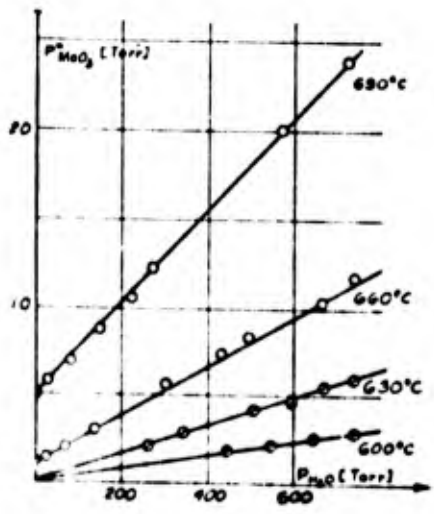

Figure 4.18. Volatility of MoO_3 in the presence of water vapour. (Speiser and St. Pierre (107)).

REFERENCES

1. A. B. Michael, "The Oxidation of Columbium Base and Tantalum Base Alloys", in "Reactive Metals", ed. by W. R. Clough, AIME Metallurgical Society Conferences, Vol. 2, 1958 (Interscience, New York, 1959) 487.

2. G. C. Deutsch, "The Environment and Materials for Glide Re-Entry Vehicles", in "High Temperature Corrosion of Aerospace Alloys", ed. J. Stringer, R. I. Jaffee and T. F. Kearns (AGARD Conf. Proc. No. 120, 1972) 43.

3. P. Kofstad, "High Temperature Oxidation of Metals" (Wiley, New York, 1966).

4. O. Kubaschewski and B. E. Hopkins, "Oxidation of Metals and Alloys", 2nd Edition (Butterworth's, London, 1967).

5. J. Stringer, "The Oxidation of Tantalum and Tantalum Alloys", Reviews on High-Temp. Mat., 1 (1973) 255.

6. G. Brauer, Z. Anorg. Chem., 248 (1941) 1; Naturwiss. 28 (1940) 30.

7. P. Kofstad, "Non-Stoichiometry, Diffusion, and Electrical Conductivity in Binary Metal Oxides" (Wiley, New York, 1972).

8. N. Norman, J. Less Common Metals, 4 (1962) 52.

9. N. Norman, P. Kofstad, and O. J. Krudtaa, J. Less-Common Metals, 4 (1962) 124.

10. J. Stringer, Acta Met., 17 (1969) 1227.

11. C. H. McIntosh and J. Stringer, J. Less-Common Metals, 5 (1963) 278.

12. D. W. Ashmore, S. J. Gregg and W. B. Jepson, J. Electrochem. Soc., 107 (1960) 495.

13. D. W. Bridges and W. M. Fassell, Jr., J. Electrochem. Soc., 103 (1956) 326.

14. E. A. Gulbransen and K. F. Andrew, Trans. AIME, 188 (1950) 586.

15. P. Kofstad and H. Kjollesdal, Trans. AIME, 221 (1961) 285.

16. P. Kofstad and S. Espevik, J. Electrochem. Soc., 112 (1965) 155.

17. T. Hurlen, J. Inst. Metals, 89 (1960-61) 273.

18. H. P. Kling, in "Technology of Columbium (Niobium)" ed. H. M. Conser and E. M. Sherwood (Wiley, New York, 1958) 87.

19. F. J. Clauss and C. A. Barrett, ibid, 92.

20. W. D. Klopp "Oxidation Behavior and Protective Coatings for Columbium and Columbium-Base Alloys", Defense Metals Information Center Report 123, January 1960.

21. R. G. Frank, "Recent Advances in Columbium Alloys", "Refractory Metal Alloys: Metallurgy and Technology", ed. I Machlin, R. I. Begley and E. D. Weisert (Plenum Press, New York, 1968) 325.

22. C. T. Sims, W. D. Klopp and R. I. Jaffee, Trans. ASM, 51 (1959) 256.

23. S. J. Paprocki and J. T. Stacy, "Investigation of Some Niobium-Base Alloys", Battelle Memorial Institute Report BMI-1143 (October 31, 1956).

24. W. D. Klopp, C. T. Sims and R. I. Jaffee, "Effects of Alloying on the Kinetics of Oxidation of Niobium", Proc. Second Intl. Conf. on Peaceful Uses of Atomic Energy, 6 (1958) 293.

25. W. D. Klopp, D. J. Maykuth, C. T. Sims and R. I. Jaffee, "Oxidation and Contamination Reactions of Niobium and Niobium Alloys", Battelle Memorial Institute Report BMI-1317 (February 3, 1959).

26. J. W. Spretnak and R. Speiser, "Protection of Niobium Against Oxidation at Elevated Temperatures", Ohio State University Reports Nos. 467-15, 467-16 and 467-17 (June 15, 1957; March 28, 1958; August 18, 1958).

27. C. A. Barrett and F. J. Clauss, in "Technology of Columbium (Niobium)" Ed. H. M. Gonser and E. M. Sherwood (Wiley, New York, 1958) 98.

REFERENCES (Continued)

28. H. B. Hix, U.S. Patent No. 2,822,268, Assigned to E.I. duPont de Nemours and Company, Inc. (February 4, 1958).

29. Unpublished work performed at Battelle Memorial Institute.

30. T. N. Rhodin, Jr., U.S. Patent No. 2,838,396, assigned to E.I. duPont de Nemours and Company, Inc. (June 10, 1958).

31. R. H. Thieleman, U.S.Patent No. 2,860,970 assigned to Sierra Metals Corporation (November 18, 1958).

32. T. N. Rhodin, Jr., U.S. Patent No. 2,881,069 assigned to E.I. duPont de Nemours and Company, Inc. (April 7, 1959).

33. Private communication from B. F. Boone, Haynes Stellite Corporation, to E. S. Bartlett, Battelle Memorial Institute (October 2, 1959).

34. "Recent Advances in Columbium Alloys", General Electric Flight Propulsion Laboratory Department (July 1959).

35. T. N. Rhodin, Jr., U.S. Patent No. 2,838,395 assigned to E.I. duPont de Nemours and Company, Inc. (June 10, 1958).

36. E. Wainer, U.S. Patent No. 2,833,282 assigned to Horizons, Inc. (April 21, 1959).

37. S. T. Wlodek, "The Properties of Cb-Ti-W Alloys. Part 1 - Oxidation" in "Columbium Metallurgy", AIME Met. Soc. Conf. 10 (1960) ed. D. L. Douglass and F. W. Kunz (Interscience, New York, 1961) 175.

38. S. T. Wlodek, "The Properties of Cb-Al-V Alloys. Part 1 - Oxidation", ibid, 553.

39. L. P. Jahnke, "Review of the Status and Future of Molybdenum and Columbium Alloys", in "High Temperature Materials", AIME Met. Soc. Conf., 18 (1961) ed. G. M. Ault, W. F. Barclay and H. P. Munger (Interscience, New York, 1963) 283.

40. G. L. Miller and F. G. Cox, J. Less-Common Metals, 2 (1960) 207.

41. G.T.J. Mayo, W. H. Shepherd and A. G. Thomas, ibid, 223.

42. R. Smith, ibid 191.

43. B. B. Argent and B. Phelps, ibid, 181.

44. F. E. Bacon and P. M. Moanfeldt, "Reactions with the Common Gases" in "Columbium and Tantalum" ed. F. T. Sisco and E. Epremian (Wiley, New York, 1963) 347.

45. S. T. Wlodek, P. M. Moanfeldt, and E. D. Weisert: unpublished data, Union Carbide Metals Co., quoted in ref. 44.

46. H. R. Babitzke, G. Asai and H. Kato, "Columbium-Vanadium Binary Alloys for High Temperature Service", U.S. Dept. of the Interior, Bureau of Mines Report of Investigation R.I. 5987 (1962).

47. H. R. Babitzke, G. Asai and H. Kato, "Columbium-Hafnium Binary Alloys for Elevated-Temperature Service", U.S. Dept. of the Interior, Bureau of Mines Report of Investigation, R.I. 6101 (1962).

48. H. R. Babitzke, M. D. Carver and H. Kato, "Columbium and Tantalum Alloys Suitable for Use at High Temperatures", U.S. Dept. of the Interior, Bureau of Mines Report of Investigation R.I. 6390 (1964).

49. H. R. Babitzke, R. E. Siemens, G. Asai, and H. Kato, "Development of Columbium and Tantalum Alloys for Elevated Temperature Service", U.S. Dept. of the Interior, Bureau of Mines Report of Investigation R.I. 6558 (1964).

50. H. R. Babitzke, R. E. Siemens and H. Kato, "High Temperature Columbium and Tantalum Alloys", U.S. Dept. of the Interior, Bureau of Mines Report of Investigation R.I. 6777 (1966).

51. H. R. Babitzke and H. Kato, "Columbium and Tantalum Alloy Development", U.S. Dept. of the Interior, Bureau of Mines Report of Investigation R.I. 6964 (1967).

REFERENCES (Continued)

52. K. Yoda, H. R. Babitzke and H. Kato, Trans. Nat. Res. Inst. for Metals, 10 (1968) 13.

53. H. R. Babitzke and J. G. Croeni, "Study of Columbium and Tantalum Alloys", U.S. Dept. of the Interior, Bureau of Mines Report of Investigation R.I. 7116 (1968).

54. H. R. Babitzke, L. L. Oden and H. J. Kelly, "Columbium and Tantalum Alloy Development", U.S. Dept. of the Interior, Bureau of Mines Report of Investigation R.I. 7211 (1968).

55. H. R. Babitzke, L. L. Oden and H. J. Kelly, "Columbium Alloy Development with Boron, Hafnium and Tungsten", U.S. Dept. of the Interior, Bureau of Mines Report of Investigation R.I. 7388 (1970).

56. W. H. Chang, "Influence of Heat Treatment on Microstructure and Properties of Columbium-Base and Chromium-Base Alloys", Technical Documentary Report ASD-TDR-62-711, Part IV to the Air Force Materials Laboratory Research and Technology Division, Wright-Patterson Air Force Base (General Electric Co., Evendale) March 1966.

57. R. T. Begley, J. L. Godshall and D. Harrod, "Development of Columbium Base Alloys", Technical Report AFML-TR-65-385 to Air Force Materials Laboratory, Research and Technology Division, Wright-Patterson Air Force Base (Westinghouse Astronuclear Laboratory).

58. A. G. Metcalfe and A. R. Stetson, "Interaction in Coated Refractory Metal Systems" in "Refractory Metal Alloys: Metallurgy and Technology", ed I. Machlin, R. T. Begley, and E. D. Wiesert (Plenum Press: New York, 1968) 121.

59. J. A. Cornie and R. C. Goodspeed, "Development of Ductile Oxidation Resistant Columbium Alloy", Technical Report AFML-TR-69-64 to Air Force Materials Laboratory, Wright-Patterson Air Force Base (Westinghouse Astronuclear Laboratory) July 1969.

60. T. L. Kolski, Trans. ASM, 56 (1963) 528.

61. E. J. Felten, J. Less-Common Metals, 17 (1969) 185.

62. E. J. Felten, ibid, 199.

63. T. L. Kolski, Trans. ASM, 57 (1964) 690.

64. A. Taylor and J. Stringer, Corr. Sci., 12 (1972) 349.

65. W. D. Brentnall, M. J. Klein and A. G. Metcalfe, "Tungsten Reinforced Oxidation Resistant Columbium Alloys", First Annual Report to Naval Air Systems Command on Contract N00019-69-C-0137 (Solar Division of International Harvester Company, San Diego) January 1970.

66. M. J. Klein, A. G. Metcalfe and R. B. Domes, "Tungsten Reinforced Oxidation Resistant Columbium Alloys", Final Report to Naval Air Systems Command on Contract N00019-69-C-0137, November 1970.

67. S. T. Scheirer, Development of Columbium Alloy Combinations for Gas Turbine Blade Applications", Final Report AFML-TR-70-187 to Air Force Materials Laboratory, Wright-Patterson Air Force Base (TRW Inc.) October 1970.

68. T. E. Roche and D. L. Graham, "Development of Oxidation Resistant High Strength Columbium Base Alloys", Technical Report AFML-TR-69-344 to Air Force Materials Laboratory, Wright-Patterson Air Force Base (Stellite Division, Union Carbide Corporation) January 1970.

69. Ye. V. Vasilyeva and D. A. Prokoshkin, "Properties of Ternary Alloys of Nb with Ta and Mo", Akad. Nauk SSSR Inst. Metal, Issled. Metal. Zhik, Tverd. Sostoyanikch (1964).

70. R. A. Rapp and G. N. Goldberg, Trans. AIME, 236 (1966) 1619.

71. V. K. Sikka and C. J. Rosa, "High Temperature Oxidation of Nb and Nb-10 at.% W Alloy", Project Themis Report No. 70-14 on Contract No. DAHC04-69-C-0016, September 1970.

REFERENCES (Continued)

72. C. J. Rosa and G. C. Chen, "High Temperature Oxidation of Nb-10 at.% Cr Alloy", Project Themis Report No. 71-19 on Contract No. DAHC04-69-C-0016 (February 1971).

73. E. J. Felten, J. Less-Common Metals, 26 (1972) 105.

74. A. A. Tavassoli, Met. Trans., 2 (1971) 1985.

75. W. E. Elkington and W. K. McDonald, Met. Trans., 3 (1972) 1007.

76. P. Kofstad, J. Less-Common Metals, 5 (1963) 158.

77. W. M. Albrecht, W. D. Klopp, B. G. Koehl and R. I. Jaffee, Trans. AIME, 221 (1961) 110.

78. M. G. Cowgill, Ph.D. Thesis, University of Liverpool (1962).

79. P. Kofstad, J. Electrochem. Soc. 109 (1962) 776; 110 (1963) 491.

80. J. Stringer, J. Electrochem. Soc., 112 (1965) 1083.

81. H. C. Peterson, W. M. Fassell and M. E. Wadsworth, J. Metals, 6 (1954) 1038.

82. F. F. Schmidt, "Tantalum and Tantalum Alloys", Defense Metals Information Center Report, DMIC 133 (July 1960).

83. F. F. Schmidt, W. D. Klopp, W. M. Albrecht, F. C. Holden, H. R. Ogden, and R. I. Jaffee, "Investigation of the Properties of Tantalum and its Alloys", WADD TR No. 59-13 (Battelle Memorial Institute) December 1959.

84. L. L. France, "Research and Development in High Strength Heat Resistant Alloys", Report No. 6 on Contract NO as 5882-C (Westinghouse Research Laboratories) August 1959.

85. W. D. Klopp, D. J. Maykuth and H. R. Ogden, "High Temperature Oxidation of Complex Tantalum Alloys" in "High Temperature Material", ed. G. M. Ault, W. F. Barclay and H. P. Munger, AIME Met. Soc. Conf., 18 (1961) (Interscience, New York, 1963).

86. R. F. Voitovich, Fiz. Metal. i Metalloved., 12 (1961) 376.

87. R. F. Voitovich and R. V. Makarova, Izvest. Akad. Nauk, SSSR, Met i Topl., 95 (161).

88. R. H. Thielemann, German Patent 1,096,466, Assigned to Sierra Metals Corporation (December 8, 1960).

89. P. Kofstad, J. Inst. Metals, 91 (1962-63) 411.

90. R. B. Dooley and J. Stringer, J. Less-Common Metals, 25 (1971) 15.

91. J. B. Berkowitz-Mattuck, J. Electrochem. Soc., 116 (1969) 700.

92. J. Stringer and R. B. Dooley, Proc. 4th International Conf. on Metallic Corr., Atlantic City, 1969 (Publ. NACE 1971).

93. R. B. Dooley and J. Stringer, J. Less-Common Metals, 24 (1971) 139.

94. R. B. Dooley and J. Stringer, ibid, 25 (1971) 115.

95. R. B. Dooley and J. Stringer, ibid, 24 (1972) 223.

96. V. D. Barth and G.W.P. Rengstorff, "Oxidation of Tungsten", Defense Metals Information Center Report 155, July 1961.

97. W. W. Webb, J. T. Norton and C. Wagner, J. Electrochem. Soc., 103 (1956), 107.

98. E. A. Gulbransen, K. F. Andrew, P. E. Blackburn, T. P. Copan and A. Merlin, "Oxidation of Tungsten and Tungsten-Based Alloys", Wright Air Development Center Technical Report, WADC TR 59-575 (February 1960).

99. E. A. Gulbransen and K. F. Andrew, J. Electrochem. Soc., 107 (1960) 610.

REFERENCES (Continued)

100. J. W. Semmel, Jr., "The Oxidation of Tungsten and Molybdenum from 1800 to 2500°F", in "High Temperature Materials", ed. R. F. Behemann and G. M. Ault, AIME Met. Soc. Conf., Cleveland, 1957 (Wiley, New York, 1959) 510.

101. F. M. Anthony and H. A. Pearl, "Investigation of Feasibility of Utilizing Available Heat-Resisting Materials for Hypersonic Leading Edge Applications", Bell Aircraft Corporation Report to Wright Air Development Center, WADC-TR 59-744, Vol III on Contract AF33 (616)-6034 (July 1960).

102. R. Speiser, quoted in Reference 96.

103. J. P. Baur, D. W. Bridges and W. M. Fassell, Jr., J. Electrochem. Soc., 103 (1956) 266.

104. R. A. Perkins, W. L. Price, and D. D. Crooks, "Oxidation of Tungsten at Ultrahigh Temperatures", Lockheed Missile and Space Co. Tech. Report 6-90-62-98 (1962); Air Force Materials Laboratory Report ML-TDR-64-162 (1965).

105. R. A. Perkins, quoted in Reference 107.

106. R. W. Bartlett, Trans. AIME 230 (1964) 1097.

107. R. Speiser and G. R. St. Pierre, "Fundamentals of Refractory Metal-Gaseous Environment Interactions", in "The Science and Technology of Selected Refractory Metals", ed. N. E. Promisel (Pergamon, Oxford 1964) 289.

108. P. O. Schissel and O. C. Trulson, J. Chem. Phys., 43 (1965) 737.

109. R. W. Bartlett and J.W. McCamont, J. Electrochem. Soc., 112 (1965) 148.

110. E. A. Gulbransen, Corrosion, 26 (1970) 19.

111. G. M. Neumann and V. Muller, Metall, 26 (1972) 806.

112. J. C. Batty and E. E. Stickney, Oxidation of Metals, 3 (1971) 331.

113. J. Eisinger, J. Chem. Phys., 30 (1959) 412.

114. H. V. Anderson, University of California Lawrence Radiation Laboratory Report UCRL 10135 (1962).

115. D. E. Rosner and H. D. Allendorf, J. Electrochem. Soc., 114 (1967) 305.

116. P. N. Walsh, I. M. Quets and R. A. Graff, J. Chem. Phys., 46 (1967) 1144.

117. J. W. Semmel, Jr., Trans. ASM, 52 (1960) 1015.

118. D. A. Prokoshkin, Ye. V. Vasil'yeva and I. Yu. Lazareva, Akad. Nauk SSSR, Inst. Metal. Issled. Metal. Zhid. Tverd. Sostovaniyakh (1964) 241.

119. M. Semchyshen and R. Q. Barr, quoted by Barth and Rengstorff.

120. E. L. Harmon, "Investigation of the Properties of Tungsten and its Alloys", Union Carbide Metals Co. Final Report on Contract AF33 (616)-5600 (May 1960).

121. O. Fubaschewski and A. Schneider, J. Inst. Metals, 75 (1949) 403.

122. F. C. Holtz and R. J. Van Thyne, "Development and Evaluation of High Temperature Tungsten Alloys", WADC TR-59-19 on Contract AF33 (616)-5218 (April 1960).

123. V. I. Arkharov and Yu. P. Kozmanov, Research on Heat Resistant Alloys, 2 (1957) 131.

124. R. N. Doerr, L. A. Neumeier and J. W. Jensen, "Reaction of Tungsten-Cobalt Alloys with Oxygen at 1000 and 1100 F", U.S. Dept. of the Interior, Bureau of Mines, Report of Investigation R.I. 6998 (August 1967).

REFERENCES (Continued)

125. D. S. Evans, "The Oxidation Characteristics of Tungsten-Chromium-Palladium Alloys" in "High Temperature Materials - 6th Plansee Seminar 1968", ed. F. Benesovsky (Metallwerk Plansee, Reutte, 1969) 42.

126. G. M. Andes and R. W. Heckel, Trans. ASM 55 (1962) 193.

127. J. L. Wilson and C. R. McKinsey, J. Metals, 13 (1961) 494.

128. M. Gleiser, W. L. Larsen, R. Speiser and J. W. Spretnak, "The Properties of Oxidation Resistant Scales Formed on Molybdenum-Base Alloys at Elevated Temperatures", in ASTM Symposium on Basic Effects of Environment on the Strength, Scaling and Embattlement of Metals at High Temperatures, ASTM Special Technical Publication No. 171 (1955) 65.

129. G.W.P. Rengstorff, Trans. AIME, 206 (1956) 171.

130. N. K. Parfenov and A. M. Chuyan, Issled. po Zharoproch. Splavan, Akad. Nauk SSSR, Inst. Met., 10 (1963) 266.

131. H. G. Poole, Reports on Contract NOw 62-0305-d (1962).

132. W. J. Guay, Final Report on Contract NORd-16136, (May 1963).

133. E. Wainer, U.S. Patent No. 2,883,283 (21st April 1959).